SEDHYD 2019

Proceedings of SEDHYD 2019: Conferences on Sedimentation and Hydrologic Modeling

Volume 3

Management & Decision Making Models, Modeling of Major River Systems, Non-Stationary Climate Variability, Physical Sediment Load Measurements, Post Fire Analysis & Restoration, Professional Development & Engineering Ethics, Regional Sediment Management, Remote Sensing & Monitoring, Reservoir Sedimentation & Sustainability, Sediment Properties

Proceedings of SEDHYD 2019: Conferences on Sedimentation and Hydrologic Modeling, 24-28 June 2019 in Reno, NV.

These engineering and scientific proceedings provide much of the latest information on sedimentation and hydrologic modeling (applied research and state of-the-practice) from Federal agencies, universities, and consultants. SEDHYD is the successor to the Federal Interagency Conferences on Sedimentation and Hydrologic Modeling. The Subcommittee on Sedimentation convened the first Federal Interagency Sedimentation Conference (FISC) in 1947. Subsequent FISC conferences were convened in 1963, 1976, 1986, 1991, 1996, and 2001. The Subcommittee on Hydrology convened their first Federal Interagency Workshop, "Hydrologic Modeling Demands for the 90s," in 1993. Subsequent to that workshop, the Subcommittee on Hydrology convened the Federal Interagency Hydrologic Modeling Conferences (FIHMC) in 1998 and 2002. Subsequently, the Subcommittees on Sedimentation and Hydrology began convening the Federal interagency conferences together in 2006 and again in 2010, and 2015. Beginning in 2019, the SEDHYD Conference was hosted by SEDHYD, Inc., a non-profit organization.

Since 1947, the Sedimentation and Hydrologic Modeling Conferences have provided over 3,000 technical papers and extended abstracts and provided engineers and scientists with the opportunity to learn and exchange information about the latest developments and research related to sedimentation and hydrologic modeling. As a continuation of these conferences, SEDHYD provides an interdisciplinary mix of scientists and managers from government agencies, universities, and consultants to present recent accomplishments and progress in research and on technical developments related to sedimentation processes, hydrologic modeling, and the impact of sediment on the environment.

The SEDHYD conference provides a mixed set of formats that include formal technical presentations, poster sessions, field trips, workshops, computer model demonstrations, and a student paper competition. The SEDHYD conference also provides excellent networking opportunities.

The SEDHYD 2019 Conference site was at the Peppermill Hotel and Resort in Reno, Nevada. Reno is situated in a high desert just east of the beautiful Sierra Nevada Mountains. The city lies on the western edge of the Great Basin, at an elevation of 4,400 feet (1,300 meters) above sea level. The Reno downtown area (along with Sparks) occupies a valley informally known as Truckee Meadows. The area offers spectacular desert landscapes and ecosystems, as well as numerous indoor and outdoor recreational opportunities.

Suggested Citation:
In Proceedings of SEDHYD 2019: Conferences on Sedimentation and Hydrologic Modeling, 24-28 June 2019 in Reno, Nevada, USA.

SEDHYD 2019 Planning Committee

Planning Committee Position	Volunteer	Organization
SEDHYD Conference Chair	Jerry Webb	West Consultants
SEDHYD Operations Chair	Jennifer Bountry	Reclamation
SEDHYD Technical Program Chair	Chandra Pathak	USACE
SEDHYD Technical Program Chair (YP)	Will Farmer	USGS
SEDHYD Technical Program	Jerry Bernard	NRCS, retired
Sedimentation Conference Chair	Tim Randle	Reclamation
Sedimentation Program Chair	Eddy Langendoen	ARS
Sedimentation Program Chair (YP)	Joel Sholtes	Mesa State
Hydrologic Modeling Conference Chair	Claudia Hoeft	NRCS
Hydrologic Modeling Program Chair	Jim Barton	USACE, retired
Hydrologic Modeling Program Chair (YP)	Jessica Driscoll	USGS
Student Program Coordinator	Amanda Cox	MWRRC
Proceedings Coordinator	Bob Boyd	BLM
Proceedings Coordinator	Peter Doran	BLM
Poster & Computer Model Demonstration Coordinator	Eddie Brauer	USACE
Short Course Coordinator	Jeff Bradley	ASCE, West Consultants
Short Course Coordinator (YP)	Kevin Denn	USACE, St. Paul Dist.
Field Trip Coordinator	Steve Berris	USGS
Field Trip Coordinator (YP)	Jena Huntington	USGS
Web site Coordinator	Darren Nezamfar	USACE
Registration Coordinator	Penni Baker	USACE
Registration Volunteer	Kathy Randle	
Young Professionals Coordinator	Caroline Ubing	Reclamation
Young Professionals Coordinator	Sara Horgen	Reclamation
Exhibit Coordinator	Molly Wood	USGS
Exhibit Coordinator	Tim Straub	USGS
AV Equipment Coordinator	Jeff Harris	West Consultants
Planning Committee	Jo Johnson	NRCS
Planning Committee	Jon Fripp	NRCS
Planning Committee	Paul Boyd	USACE
Planning Committee	Meg Jonas	USACOE, retired
Planning Committee	Robert R Mason	USGS
Planning Committee	Victor Hom	NOAA

SEDHYD, Inc.

SEDHYD, Inc. Position	Volunteer
SEDHYD President & Board Chair	Jerry Webb
SEDHYD Vice President & Board Member	Jerry Bernard
SEDHYD Treasurer & Board Member	Don Frevert
SEDHYD Secretary & Board Member	Matt Romkens
SEDHYD Board Member	Doug Glysson

Table of Contents

Table of Contents

Table of Contents

Table of Contents

Table of Contents

Table of Contents

Management & Decision Making Models

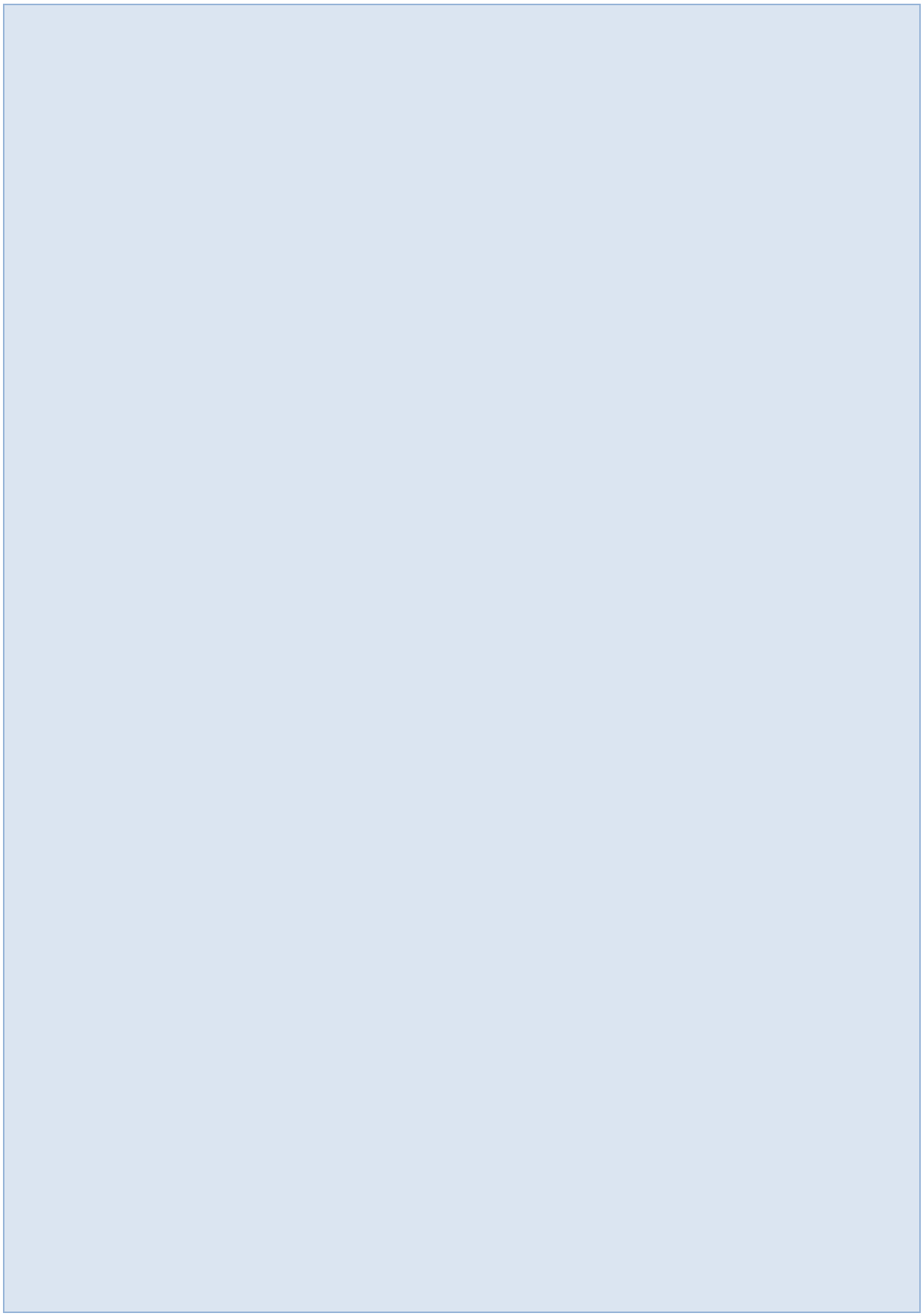

2-D Hydraulic Modeling to Visualize Aquatic Fishery Habitat (Rio Grande Silvery Minnow) with a Suitability Index

Aubrey Harris, Civil Engineer (Hydraulic/Hydrologic), US Army Corps of Engineers, Albuquerque, NM, Aubrey.E.Harris@usace.army.mil

Jennifer Bachus, Biologist (Fisheries), US Bureau of Reclamation, Albuquerque, NM, JBachus@usbr.gov

Eric Gonzales, Biologist (Fisheries), US Bureau of Reclamation, Albuquerque, NM, EGonzales@usbr.gov

Nathan Holste, Civil Engineer, US Bureau of Reclamation, Denver, CO, NHolste@usbr.gov

Abstract

HEC-RAS 5.0 features the ability to perform two-dimensional hydrodynamic routing that produces detailed 2D channel and floodplain analysis (USACE 2016). The hydraulic outputs of velocities and depths were used to evaluate engineering design for the pilot realignment of the Rio Grande channel through the Bosque del Apache National Wildlife Refuge (BDA Pilot Project) in New Mexico. The BDA Pilot Project is also anticipated to create target habitat for the endangered Rio Grande Silvery Minnow (Hybognathus amarus; RGSM). Habitat restoration projects in the Middle Rio Grande river corridor often target habitat for endangered or threatened species affected by water projects.

The primary objective of the BDA Pilot Project is to reconnect this depositional reach of the Rio Grande with its floodplain. This objective improves upon the current perched channel condition that experiences overbanking due to plugging of the river channel, which forces water over to a disconnected floodplain, reducing transport efficiency within the reach. Stranded water reduces effective conveyance and incurs water losses in the river system, and may also cause fish, including the endangered RGSM, to become stranded when the water recedes.

It is hypothesized, from empirical observations, that the BDA Pilot Project will benefit RGSM habitat from the current channel condition by increasing areas of slow-moving, shallow habitat at various discharges, by reducing areas of stranded water. Currently the Rio Grande channel in this area transports water rapidly through a single channel with few slow-moving and shallow areas. To demonstrate the anticipated benefits to RGSM habitat and assist Reclamation with its environmental compliance, a new methodology was developed to model the gains in habitat for RGSM resulting from the BDA Pilot Project.

This paper presents the use of target velocities and depths for the RGSM with HEC-RAS 2-D modeling to map Habitat Suitability Indices (HSI; categorized as unsuitable, suitable and ideal habitat) for RGSM at base flow, the 2-year frequency 14-day spring runoff, and at higher discharges. The HSI modeling results demonstrate the anticipated improvements to aquatic fish habitat resulting from the BDA Pilot Project. AutoCAD Civil 3D was used to develop the design surface and ArcGIS 10 was used for data post-processing and spatial analyses. This hydroecological modeling approach can be supplemented with on-the-ground monitoring data post-project, to evaluate and demonstrate gains in target habitat conditions. It also informs

adaptive management by identifying areas with existing suitable habitat, areas of most likely change, and project design features that may affect success. In turn, this supports improved efficiency and effectiveness in future project designs and ensures that negative environmental impacts to endangered species are minimized.

Introduction

The Rio Grande between San Antonio and San Marcial, NM has perched channel conditions where the floodplain is lower than the active river channel. The Bosque del Apache (BDA) Pilot Project was initiated to reduce sediment plug formation and related complications that are associated with the perched channel at this location. This paper evaluates the expected post-construction effects of channel realignment on habitat suitability for the Rio Grande Silvery Minnow (RGSM).

A habitat suitability index (HSI) was developed and used to evaluate areas where hydraulic parameters are appropriate for the RGSM in the existing channel and compare those conditions to the anticipated condition of the proposed realignment channel post-construction. The HSI uses suitable velocity and depth information for the RGSM larval, juvenile, and adult life stages. Two flow targets were used with 2-dimensional numerical modeling software to estimate areas that would satisfy the identified velocity and depth criteria for each of the life stages of the RGSM. The U.S. Army Corps of Engineers Hydraulic Engineering Center's 2-dimensional model (HEC-RAS 2D version 5.0.3) was used to provide estimates of the hydraulic conditions. ESRI's ArcGIS software (version 10.2.2) was used to identify the habitat that met the identified criteria.

Characterizing the suitability of habitat for RGSM supports federal environmental compliance under the Endangered Species Act as directed by Biological Opinions from the U.S. Fish and Wildlife Service. Modeling habitat suitability informs anticipated project impacts and benefits on RGSM habitat such as changes in river drying, changes in fish stranding events, and availability of target depths and velocities of existing and future conditions. Modeling can also inform adaptive management studies examining changes after project implementation, including extent and duration of habitat suitability conditions.

Aquatic Fisheries Habitat (Suitability Index)

Target values were defined as a range of ideal depths and velocities for egg, larval/juvenile, and adult stages, compiled from information provided by Bovee et al. (2008), Bestgen et al. (2003, 2010), and Dudley and Platania (1997, 1999). RGSM are found in and will use areas outside of these ranges in Table 1, as long as water is present that is connected to the river. Bovee et al. (2008) provides a range of values agreed upon by a group of silvery minnow experts in 2007 to be characteristic of suitable RGSM habitat. This information represents the broadest consensus effort to identify these values to date. For this modeling effort, we assume that free swimming larvae have the same suitable depths and velocities as juveniles, absent other information. Maximum depths for juveniles and adults provided in Bovee et al. (2008) used the U.S. Fish and Wildlife Service's RGSM Recovery Plan for consistency.

Minimum Velocity for drifting life stages (egg, early larval fish) is based on the critical settling velocity for RGSM eggs identified in Dudley and Platania (1999). The eggs are semi-buoyant, so a minimum velocity is needed to prevent eggs from sinking to the riverbed or floodplain ground surface. Maximum Velocity for juveniles and adults represents the maximum reported swimming speed of RGSM over short duration (Bestgen et al. 2003, 2010). Bovee et al. (2008) reported a Maximum Depth value; however, RGSM can use habitat with greater depths. In

deeper waters, the risk of mortality from predation and unsuitability of other habitat features increases with increasing depths beyond the target range. Also, for the drifting life stages (egg, early larvae), risk of downstream transport and potential reduced viability increases at greater depths and velocities without entrainment in suitable nursery habitats off-channel.

In Table 1, the categories identified for modeling RGSM habitat are:

- Ideal Habitat: meets both target ranges for depth and velocity;
- Suitable Habitat: within the maximum limits for depth and velocity;
- Unsuitable Habitat: where wetted areas are disconnected from the river channel (stranding – either off-channel as flows recede, or in-channel during intermittency); where depth is 0; where velocity is 0 for eggs/early larvae stages or exceeds the maximum velocity for adults).

Table 1. Model Categories for RGSM Habitat – Targets for Depth and Velocity for ideal, suitable, and unsuitable habitat.

		Ideal Habitat		Suitable Habitat		Unsuitable
RGSM Life Stage	**Dates**	***Depth Range***	***Velocity Range***	***Maximum Depth***	***Maximum Velocity***	
Egg/Larvae (drifting) [3,1,4]	May-Jun	>0 and <30cm	≥0.93 cm/s	NA - drifting	NA - drifting	• Depth or Velocity of 0 • Disconnected
Larvae/Juvenile (free swimming) [1]	Jul-Sep	5–50 cm	1–30 cm/s	50 cm	Undefined	• Depth of 0 • Velocity > 118 cm/s • Disconnected
Adults (free swimming) [1,2]	Sep+ for YOY	5–50 cm	1–40 cm/s	50 cm	≤118 cm/s for short periods	• Depth of 0 • Disconnected

2-Bestgen et al. (2003; 2010)
3-Dudley and Platania (1997)
4- Dudley and Platania (1999)
YOY: Young of Year

Case Study: Bosque del Apache Realignment

The BDA pilot project consists of relocating the Rio Grande from its current location to the east, the realigned channel is three miles in length and addresses the area where previous sediment plugs had occurred. The project consists of vegetation destabilization in the realignment corridor, excavation, removal of monotypic exotic species outside the corridor, and the conversion of the existing river channel into a floodplain (AuBuchon and Harris, 2017). The HEC-RAS 2-D model was built to represent the current channel condition and the design geometry of the channel realignment after construction. HEC-RAS requires a channel and floodplain geometry, a surface roughness coefficient, and a discharge in order to predict flow paths and the extent of inundation. The ground surface geometry was built based on LiDAR photogrammetry data collected during a low flow condition of approximately 10 cfs (USGS 08355490; Hwy 380 Bridge) around October 1, 2016. To represent the current channel's thalweg on the LiDAR, the surface from a georeferenced 1-D river model of cross-sections was

imprinted over the LiDAR water surface. This surface was used to describe the existing conditions. A second geometry was used to describe the initial realigned condition. This surface used what is expected to be the as-built geometry for the initial channel, including the inlet and outlet excavation and fill of the current channel, as described by the BDA pilot project (AuBuchon and Harris, 2017).

Surface roughness coefficients were based on vegetation types in the area. Vegetation Polygons, from data collected by the Technical Services Center of Reclamation (Reclamation, 2016), were used with Manning's roughness coefficient inferred by type according to Chow (1959). Coefficients were calibrated based on field trips and observations of vegetation density and distribution (see Table 2). For example, roughness coefficients were reduced where there is field evidence that otherwise tall stands of vegetation were bent over, probably due to previous high-water flows. The vegetation being bent rather than standing tall would reduce the resistance created by vegetation to overland flows Vegetation clearing associated with the BDA pilot project was incorporated into the surface roughness mapping for the realigned channel. In the sensitivity analysis during model creation, it was found that time-step and mesh size had a greater effect on the inundation patterns than surface roughness, perhaps due to the topography of the floodplain dictating inundation extents.

Table 2. Roughness coefficients used in the HEC-RAS 2-D model.

Dominant Vegetative Description	**Dominant Vegetative Polygon ID**	**Roughness coefficient (from Chow 1959)**
River channel	Channel	0.017 (Holste, 2016)
Open water	OP	0.035
Salt cedar and willows etc. in shrub sized stands	SC 5	0.05
Salt cedar, dense, young and low growth	SC 6d	0.06
Cottonwood with little or no understory	C 4	0.08
Salt cedar in dense shrub-sized stands or Cottonwood, dense intermediate sized with little to no understory	SC or C 4d-5d	0.1
Coyote willows and others, dense with well-developed understory	CW 3d	0.175*
Vegetation Removal Areas	N/A	0.018

*This Manning's n was reduced from 0.2 due to evidence of blown over brush.

The extent of inundation in the numerical model was visually validated based on field visits (AuBuchon, 2017). The model of the existing channel condition was evaluated for accuracy, in that it showed little to no evidence of overbanking on its western side at discharges near 2000 cfs (USGS 08355490 Rio Grande above US HWY 380 near San Antonio, NM; April 7) and that water accumulates and travels very slowly in the eastern portion of the project area and is confined by a mesa (AuBuchon, 2017). While the model provides a good representation of surface water distribution patterns in the area, the model does not account for sediment transport, infiltration or evaporative losses; therefore, the model results represent a condition immediately post-construction that would be expected to change over time and could vary under different air temperatures or groundwater saturation conditions. Due to the high

sediment loads in the Rio Grande, it would be expected that sediment deposition will change the bed surface elevations surrounding the realignment channel.

The HEC-RAS 2-D model doesn't account for seepage losses, revegetation or sediment deposition, therefore the modeled conditions represent the surface water conditions in the existing river channel and the expected baseline surface water conditions for the realigned channel at the time of implementation, assumes that the water volume is conserved from upstream to downstream, and does not reflect geomorphic changes that occur over time. Therefore, the results from this analysis are best applied to estimating the effects of the project at the time of implementation, and as a guide for future habitat monitoring locations.

Discharges were chosen to simulate flow conditions on the Middle Rio Grande through the Bosque del Apache National Wildlife Refuge that provide a realistic snapshot of the events that occur frequently enough to provide habitat value during the various seasons. A 14-day flow duration with a 2-year return period during the spring snow-melt run-off (1270 cfs) and a baseflow of 500 cfs were set as the two target discharges. The 14-day window is assumed to be sufficient for development of protolarval RGSM to the free-swimming mesolarval stage (e.g., Platania, 1995; Dudley and Planatia, 2007). The 2-year return period was identified as a critical time for the egg drift and larval stages for the RGSM. The 14-day peak run-off period (Figure 1) was identified from daily average hydrographs from the USGS gage at San Acacia (USGS 08354900). The minimum average daily discharge associated with the 14-day peak was chosen for each year between 1992 and 2016, and then fit to a Log-Pearson Type III probability distribution, based on methods described by Bedient and Huber (2001). The 14-day duration, 2-year return was identified as 1270 cfs. The 500 cfs simulation represents a baseflow condition that is exceeded 50% of the time in a given year, based on a flow frequency analysis conducted by Bui (2014) at the USGS San Acacia gage. Bui's analysis looked at average daily flows between 1993 and 2013.

The criteria for suitable habitat was defined as a range of ideal velocities and depths for the egg, larval and adult stages of RGSM. The 2D model was run at the described discharges for 12 hours of simulation. The model results provide both depth and velocity information on the mesh grid based on the existing or design ground surface elevations. These were exported as rasters with 1 square foot cell size. ArcGIS raster math was used to identify areas that are less than or greater than the bounding criteria of suitable velocity and suitable depth. The result shows the area of inundation, as well as whether the areas meet criteria of habitat suitability for the RGSM.

Habitat Suitability Modeled Flows and Results

- "Ideal Habitat" meets the depth and velocity criteria.
- "Suitable" meets only the velocity criteria.
- "Unsuitable" meets neither the depth nor velocity criteria.

It is believed that velocity is the more critical indicator for habitat suitability, because the fish-sampling techniques used in the field may be less effective at higher depths, and velocity has a more direct energy cost to the species than depth. The combination of ideal habitat, not ideal but with suitable velocities, or not ideal with unsuitable velocities, encompass the whole inundation area for the 500 cfs and 1270 cfs simulations.

In addition to the two discharge simulations, a discharge scenario was used to simulate potential stranding conditions that occur after overbanking flows. For this scenario a peak flow condition

of 3,000 cfs (a discharge that has about a 20% chance of being exceeded based on Bui's analysis of flow conditions at San Acacia gage for the period between 1993 and 2013, and one that would exceed bank full capacity in the current channel) was simulated for 3 days and followed by a reduction of flow to 500 cfs. The simulations were run so that the model reaches equilibrium, where inundation patterns remain constant over several "hours" of simulation time. The surface area associated with pools of water that are stranded and will not be effectively conveyed out of the floodplain were then quantified. Stranded water conditions are those that involve isolated pools in the overbank and floodplain area that have the potential to isolate RGSM from the main channel. Disconnected flows, causing stranding, are considered unsuitable habitat features for the RGSM, as it is unlikely the population will survive the drying conditions in the floodplain. For the stranded water situation, the spatial data was inspected to determine areas that reconnect to the river channel at 500 cfs after the flooding event. Disconnected areas were identified as areas with greater than 2 inches of water depth and velocities less than 0.05 fps. The reasoning being that areas of less than 2 inches of water depth would likely infiltrate if the soil is not yet saturated; the low velocities indicate that there is not a flowing surface connection to the main channel.

It was found that the channel realignment for both the baseflow (500 cfs) and 2-year 14-day return period flow (1270 cfs) conditions allowed for more inundation than the existing channel conditions. The current condition of the Rio Grande effectively conveys discharges of water up to at least 2,200 cfs with little overbanking (Bender and Julien, 2011). Therefore, higher velocities and depths would be expected in the existing condition at flows less than 2,200 cfs, not supporting RGSM egg drift or development.

Figures 2 and 3 show baseflow conditions for ideal habitat (meeting both velocity and depth requirements), suitable conditions (meeting only the velocity requirement), and unsuitable conditions (water present, but either too rapid or slow for ideal habitat conditions and does not meet the depth requirements for the life cycle stage). The figures show results for both the existing condition and the realignment channel.

The pilot channel realignment increases the wetted surface area and greatly increases acreage meeting the habitat suitability indices for all RGSM life cycle phases. In addition, the realigned channel improves connectivity on the Rio Grande and is representative of the historical condition with a wide, shallow river channel that frequently migrated across the floodplain.

In the evaluation of the 14-day, 2-year return period, the existing channel effectively conveys the water with little overbanking, therefore the area of potential habitat is not much greater than baseflow condition. Comparing habitat suitability of the realigned channel to the existing channel shows that habitat suitability for the RGSM would be improved (Figure 4 and Figure 5).

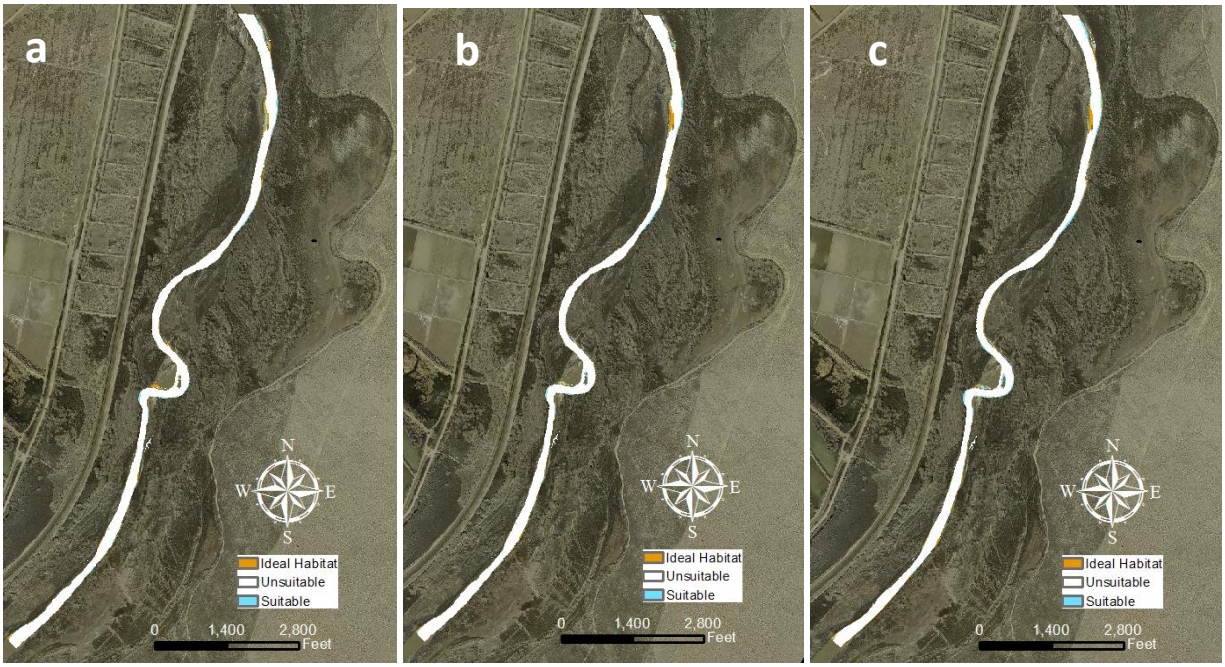

Figure 4. HSI results from the 14-day, 2-year return period (1270 cfs) condition, current channel alignment for the a) egg/larval stage; b) larval/juvenile stage; c) adult RGSM.

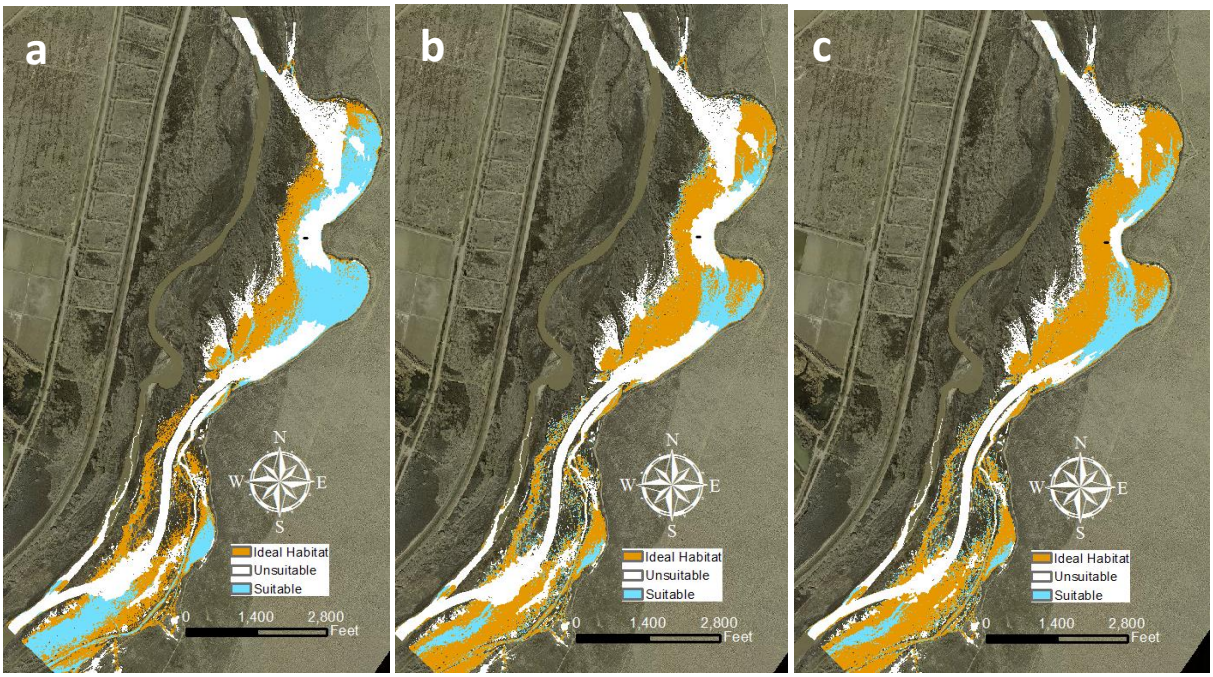

Figure 5. HSI results from the 14-day, 2-year return period (1270 cfs) condition, realigned channel for the a) egg/larval stage; b) larval/juvenile stage; c) adult RGSM.

Tables 3 through 5 provide a summary of the acreage associated with the habitat suitability analysis shown in Figures 2 through 5. The areas were calculated by exporting the output HEC-RAS 2-D rasters containing depth and velocity data to ArcGIS, and after the HSI categories were applied, the area within each habitat category was calculated.

Table 3. Habitat simulation results for the egg/larval life stage of the RGSM. Percentage of the total inundation area shown as well.

	Water Surface Area (acres)	Unsuitable (acres)	Suitable (acres)	Ideal Habitat (acres)
Existing Channel, 500 cfs	53.0	48.0 (90%)	5.0 (10%)	3.4 (6%)
Realignment, 500 cfs	243.1	94.9 (39%)	148.2 (61%)	148.2 (61%)
Existing Channel, 2-year, 14-day return	60.2	55.6 (92%)	4.6 (8%)	2.3 (4%)
Realignment, 2-year, 14-day return	395.1	167.5 (42%)	227.6 (58%)	123.1 (31%)

Table 4. Habitat simulation results for the juvenile life stage of the RGSM. Percentage of the total inundation area shown as well.

	Water Surface Area (acres)	Unsuitable (acres)	Suitable (acres)	Ideal Habitat (acres)
Existing Channel, 500 cfs	53.0	48.0 (91%)	5.0 (9%)	3.5 (7%)
Realignment, 500 cfs	243.1	75.2 (31%)	167.9 (69%)	143.5 (59%)
Existing Channel, 2-year, 14-day return	60.2	55.7 (93%)	4.5 (7%)	2.3 (4%)
Realignment, 2-year, 14-day return	395.1	167.5 (42%)	227.6 (58%)	123.1 (31%)

Table 5. Habitat simulation results for the adult life stage of the RGSM. Percentage of the total inundation area shown as well.

	Water Surface Area (acres)	Unsuitable (acres)	Suitable (acres)	Ideal Habitat (acres)
Existing Channel, 500 cfs	53.0	43.3 (81%)	9.7 (19%)	7.0 (13%)
Realignment, 500 cfs	243.1	58.8 (24%)	184.3 (76%)	157.1 (65%)
Existing Channel, 2-year, 14-day return	60.2	53.4 (89%)	6.8 (11%)	3.2 (5%)
Realignment, 2-year, 14-day return	395.1	126.9 (32%)	268.2 (68%)	197.1 (50%)

The results from the stranded water simulation (first overbank flows of 3000 cfs followed by 500 cfs flows) show areas where water is moving less than 0.05 fps and has a depth greater than 2 inches. The stranded water results show water that was spread on the floodplain but did not

evacuate throughout the simulation. The results show that the realigned condition is anticipated to reduce stranding relative to the existing channel conditions.

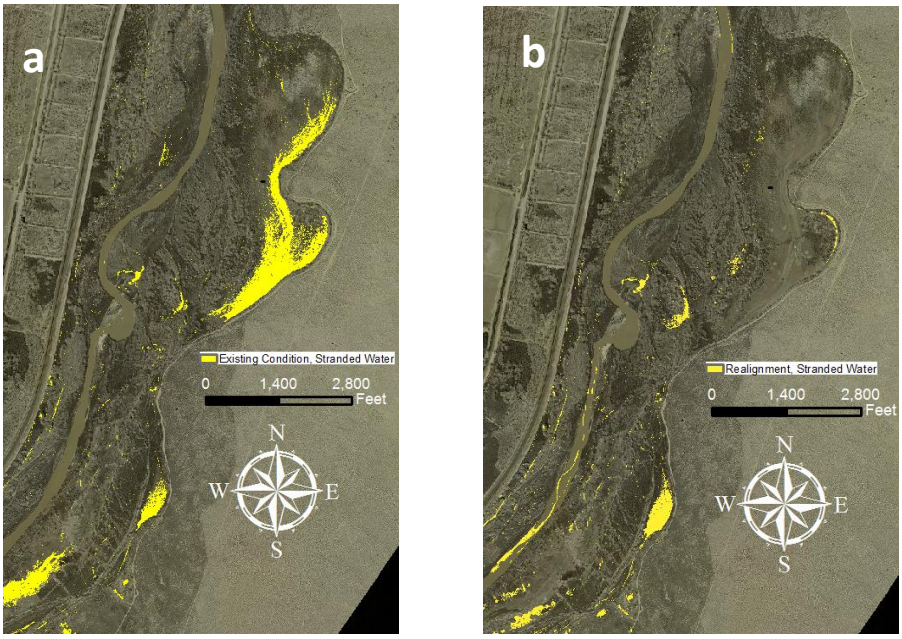

Figure 6. Stranded area results (areas where water is moving less than 0.05 fps and is greater than 2 in in depth) after overbanking flows recede for a) the current and b) the realigned channel.

Table 6. Comparison of Stranded Water for Existing and Realigned Channel

Simulated Area of Stranded Water for the Existing Channel	Simulated Area of Stranded Water in the Realigned Channel
71 acres	37 acres

Because the 2-D modeling does not include seepage or sediment transport, the stranding analysis is best used as a comparative tool between potential scenarios, rather than an exact representation of stranding that would actually occur.

Informing Adaptive Management

The use of adaptive management (AM) promotes flexibility in decision making by addressing scientific uncertainties over time through an iterative process, for both river maintenance projects as well as design features to support RGSM habitat suitability. As a science-based process, AM involves testing hypotheses with observations and data reflecting the system's response and comparing the outcomes to *a priori* predictions (see Williams et al. 2017). Given the inherent uncertainties in the dynamic and complex Middle Rio Grande system, and the need for more flexible decision making for water and species management, there is a renewed emphasis on AM and iterative learning to guide and improve management actions in the Middle Rio Grande, as well as to adjust project implementation in a timely manner to address any concerns and provide valuable lessons learned to projects in the future. The extent of AM used will depend on the level of uncertainty and knowledge gaps for project implementation. The use

of HSI modeling described in this paper provides this *a priori* prediction of the anticipated benefits to RGSM habitat from a selected project, which can be compared post-project with on the ground data collection over time to inform trends in project outcomes such as amount of river drying, stranding events, habitat use patterns, deposition, and revegetation. In turn, this information can support more clearly defined targets for project success and thresholds for action under AM.

To examine likelihood for RGSM stranding, the HSI modeling identifies areas that are isolated, which can be compared with post-project implementation monitoring of flow conditions to identify extent of isolated areas following construction and trends over time. Under adaptive management, this can document improvements in stranding related conditions for RGSM (i.e., improved connectivity of RGSM habitat), as well as identify adaptive management tests as the project site matures. Identifying risks of stranding events focuses primarily on lower flow conditions, which occur in spring, following spring runoff, and during any storm events such as summer monsoons where flows recede after inundation.

Egg and larval monitoring helps inform presence and absence of RGSM eggs in areas considered to be suitable egg/larval habitat. For RGSM, the timing of this monitoring aligns with spring spawning (April to June), during recession of river flows to summer base flow conditions, when both eggs and larvae are present.

Presence and absence in the project area, in both expected and unexpected areas based on the HSI model, allows for ground truthing of model predictions as well as helping to identify adaptive management tests as the project site matures. Sampling should focus on representative areas within the project site, with a recommended distribution of 80% of sampling sites in areas expected to provide suitable egg/larval habitat, and 20% in areas not expected to provide suitable habitat. Assessments of habitat suitability based on presence-absence detections should be used with caution, as the passive drifting nature of these life stages can complicate determinations on habitat suitability.

Monitoring of adult RGSM through fish sampling (e.g., fyke nets, seining, electrofishing) can provide additional data on the presence/absence of RGSM in expected and unexpected habitats based on the HSI modeling anticipated outcomes. Results from this monitoring are also influenced by overall population densities, so results will need to be placed in the context of overall population data, as well as more reach-specific data to provide context.

Evaluating project benefits via reduced river drying can help document enhanced river connectivity, and therefore connectivity and presence of RGSM habitat, as a result of the project. The extent of river drying, timing, and duration should be monitored on the as-built condition to compare and calibrate the HSI modeling, and document habitat improvements resulting from the project. In addition, monitoring the extent, timing, and duration of river drying in the project area will help inform lessons learned for future realignment projects in the vicinity, as well as help identify adaptive management tests as the project site matures.

Depth and velocity measurements are considered primary indicators of habitat suitability for RGSM. Other parameters are relevant for characterizing the suitability of RGSM habitat (e.g., water quality, substrate type, presence of underwater debris, etc.) given the current state of knowledge for this species; however, these additional parameters were not included for

modeling purposes due to the high degree of autocorrelation with depth and velocity. For example, substrate type (from silt to coarse sand in this reach) is dependent on local velocity as finer bed material particle sizes are found in low velocity areas. Under adaptive management, future refinements can be made by adding additional modeling parameters if they would improve the resolution relevant to management decisions.

Representative depths and velocity measurements can be obtained from the as built conditions for the project and compared to the *a priori* predicted outcomes from the HSI modeling. This serves to both calibrate and refine the HSI predictions made for future projects, as well as to identify adaptive management tests as the project site matures.

Conclusions

The BDA Pilot Project was initiated to reduce sediment plug formation and related complications that are associated with the perched channel at this location. The habitat suitability index (HSI) was developed based on 2-dimensional hydraulic modelling results and evaluating the hydraulic parameters appropriate for the RGSM. This paper evaluates the expected post-construction effects of channel realignment on habitat suitability for the RGSM to aid in monitoring and adaptive management for the endangered species. Characterizing the suitability of habitat for RGSM supports federal environmental compliance under the Endangered Species Act as directed by Biological Opinions from the U.S. Fish and Wildlife Service. Post-construction monitoring of fish presence and absence, as well as actual depths and velocities, will help validate the HSI method and improve its applicability to future projects.

References

AuBuchon, J. 2017. BDA Pilot Project April 2017 Site Visit – Trip Report. U.S. Bureau of Reclamation, Albuquerque Area Office, Technical Services Division, Albuquerque, NM. 31 pp.

AuBuchon, J. and Harris, A. 2017. BDA Pilot Project Description. U.S. Bureau of Reclamation, Albuquerque Area Office, Technical Services Division, Albuquerque, NM. 49 pp.

Bachus, J., Gonzales, E. 2017. Technical Note – Habitat targets for BDA Realignment Pilot Modeling Analysis. U.S. Bureau of Reclamation, Albuquerque Area Office, Environment and Lands Division, Albuquerque, NM. 3 p.

Bedient, P., Huber, W. (2001) Hydrology and Floodplain Analysis. Camden, NJ: Pearson. 763 p.

Bender, T., Julien, P. (2011). Bosque Reach, Arroyo de las Canas to South Boundary Bosque del Apache National Wildlife Refuge, Overbank Flow Analysis, 1962-2002. Colorado State University. 175 p.

Bestgen, K.R., B. Mefford, J. Bundy, C. Walford, B. Compton, S. Seal, and T. Sorensen. 2003. Swimming performance of Rio Grande silvery minnow. Final Report to U. S. Bureau of Reclamation, Albuquerque Area Office, New Mexico. Colorado State University, Larval Fish Laboratory Contribution 132, 70p.

Bestgen, K.R., B. Mefford, J.M. Bundy, C.D. Walford, and R.I. Compton. 2010. Swimming Performance and Fishway Model Passage Success of Rio Grande Silvery Minnow. Transactions of the American Fisheries Society 139 (2).

Bovee, K.D., Waddle, T.J., and Spears, J.M., 2008, Streamflow and endangered species habitat in the lower Isleta reach of the middle Rio Grande: U.S. Geological Survey Open-File Report 2008-1323, 177p.

Bui, Chi. 2014, Flow Duration Curve Analysis from Cochiti Dam to Elephant Butte Reservoir. U.S. Bureau of Reclamation, Albuquerque Area Office, Technical Services Division, Albuquerque, NM. 51 pp.

Chow, V.T., 1959. Open-Channel Hydraulics. University of Illinois. McGraw-Hill. 680p.

Dudley, R. K. and S. P. Platania. 1997. Habitat use of Rio Grande silvery minnow. Final Report submitted to New Mexico Department of Game and Fish, Santa Fe, New Mexico, and U.S. Bureau of Reclamation, Albuquerque, New Mexico. 87p.

Dudley, R. K. and S. P. Platania. 1999. Imitating the physical properties of drifting semibuoyant fish (Cyprinidae) eggs with artificial eggs. Journal of Freshwater Ecology 14:423-430.

Dudley, R. K. and S. P. Platania. 2007. Flow regulation and fragmentation imperil pelagic-spawning riverine fishes. Ecological Applications 17(7): 2074-2086.

Fetter, C. W. 1988, Applied Hydrogeology, Macmillan Publishing Company, New York, New York.

Holste, N, 2016 (unpub). BDA Calibration Summary. Middle Rio Grande Project, U.S. Bureau of Reclamation, Technical Services Center, Denver, CO. 8p.

Platania, S. P. 1995. Reproductive biology and early life-history of Rio Grande Silvery Minnow *Hybognathus amarus*. Final report prepared for the U.S. Army Corps of Engineers, Albuquerque District, Albuquerque, New Mexico. 23p.

Richard, Kenneth. 2017. Drying Analysis from River Mile 73 to River Mile 90 based on Flow at USGS 08355490 Gage. Draft Memorandum. U.S. Bureau of Reclamation, Albuquerque Area Office, Water Management Division, Albuquerque, NM, 6 p.

Reclamation, 2016, Southwestern Willow Flycatcher Habitat Suitability (unpub). Middle Rio Grande Project, Technical Services Center, Denver CO.

Williams, K., J. Nichols, and B. Kendall. 2017. Monitoring in Adaptive Management.
Training presentation for ALC3176: Adaptive Management: Structured Decision Making for Recurrent Decisions. U.S. Geological Survey and U.S. Fish and Wildlife Service. National Conservation Training Center (NCTC), Shepherdstown, West Virginia. September 11-15, 2017

Aquifer Characteristics for Predicting Groundwater Table Using van Deemter's Analysis

M.J.M. Römkens, mjmromkens@gmail.com
National Computational Center Hydro-sciences and Engineering

Department of Civil Engineering, University of Mississippi, University, MS 38677

Abstract

Efficient water use on agricultural land requires detailed knowledge of the water needs of the cropping system , the hydrology of the land area concerned, and the effectiveness of water conveyance in the irrigation or drainage system used. Much research has been conducted over the years in these areas of concern. Less is known how variations in the water level of the conveyance system affects the groundwater levels and to have a better basis for determining the required frequency, size, and density of the water conveyance system in order to ensure an adequate water supply for meeting the crop needs everywhere in the field or for the efficient removal of excess groundwater through drainage.

Flow Region and Solution

The historic analysis of van Deemter (1950) allows a precise evaluation of groundwater levels of drainage and sub-irrigation levels in aquifers of land areas between equidistantly placed drains and/or ditches. His analysis was performed for the case of steady state flow with constant and uniform rainfall and/or evapo-transpiration rates using a solution of the Laplace equation for a two-dimensional flow field with an infinitely deep homogeneous and isotropic aquifer intersected to a finite depth with a system of equidistantly placed drains or ditches. Contrary to traditional approximate methods for this fairly simple flow field problem , van Deemter (1950) used the lesser known but potentially the more powerful conformal approach in which the geometric flow field, represented by the complex space variable $z= x + i\cdot y$ and the complex flow potential field ω for this area, represented by the functional relationship $\omega = \phi + i\cdot\psi$, are projected on a complex plane, say t, so that the corresponding vertices of the geometric and potential planes coincide. ϕ and ψ are the pressure and stream flow component potentials, respectively. In van Deemster 's approach, the space variable z and the potential variable ω for the vertices of the flow field are transformed, directly or indirectly, through appropriate relationships onto the upper half of the complex t-plane and co-incide and are located on the real axis of the t-plane. For most flow fields this is a daunting task. One of the earliest published works using this technique on agricultural land was by Muskat and Wyckoff (1937). The technique is more commonly used in groundwater problems involving streams with drop structures, etc. (Harr, 1962; Strack, 1989, and before that by Polybarinova-Kochina, 1921). Römkens (2009) used this method in evaluating seepage and hydraulic potentials near incised ditches in shallow aquifers. More recently, he discussed in detail the work of van Deemter (1950) as it

applies to drainage and infiltration into infinitely deep aquifers with tile lines (Römkens, 2013,and 2017) and incised ditches (Römkens, 2017). In practice, only in simple flow fields with straight line segments described as closed boundaries or curved open boundaries can this procedure be successfully used by utilizing special techniques such as the Schwarz-Christoffel transformation for a flow region where the boundaries are represented by straight line segments or by the Hodograph analysis for the case with open, curved boundaries. Both techniques were employed by van Deemter (1950). This article shows this technique, as used by van Deemter, for the rather simple flow field shown in Fig 1. Briefly, the flow region or aquifer is an infinitely deep strip with parallel vertical boundaries. These boundaries represent streamlines. He considered a drainage situation with a constant, uniform rainfall at the upper, open boundary and with a circular drain on one side that is fully filled with water. This drain ends in a submerged condition in a water conveyance system that is connected to an open water body. The adjoining tracts to this flow field are symmetric images of the tract under consideration. Fig.2 shows the sequence of conformal transformations used for this drainage case and the mathematical formulae used with $t=\sqrt{\sigma}/\lambda$. For details of these transformations, the reader is referred to the article by Römkens (2018) or the original work written in Dutch as a Government document by van Deemter (1950).While it is the objective to obtain z=f(ω), in many situations such a transformation is difficult if not impossible to obtain. In those cases it may be possible to use an intermediary approach in which z=f(t) and ω=g(t) in which t is the common parameter used for both transformations. Much about the analysis involving complex algebra can be learned from textbooks. In this regard, the books by Churchill (1960) and Strack (1989) can be very helpful. The conformal analysis as used by van Deemter (1950), yielded the following relationships for z and ω in terms of t:

$$z = a + i\cdot c + i\cdot\frac{-}{-}\cdot\left(\ln\frac{\quad}{\quad} + \frac{-}{-}\cdot\ln\frac{\quad}{\quad}\right) \qquad (1)$$

and

$$\omega = Kc + i\cdot Na + \frac{-}{-}\cdot[(L - N)\cdot(\ln(t-1) - L\cdot\ln(t-1-\beta) + N\cdot\ln(t+1+\beta) + (L-N)\cdot\frac{\quad}{\quad}\cdot\ln\frac{\quad}{\quad}] \qquad (2)$$

where a, b, and c are the dimensions of the flow region or aquifer under consideration, N and L are the fluxes into (rainfall or seepage) or out of (evaporation or deep drainage) the flow region, and K is the hydraulic conductivity of the soil in the aquifer. Parameters γ and β are respectively defined as:

$$\gamma = \frac{\quad}{\quad} \quad \text{and} \quad \beta = -1 + \exp(\pi\gamma\cdot\frac{\quad}{\quad}) \qquad (3)$$

Physically, γ represents an intrinsic drainage characteristic reflecting the effect of rainfall (input) and transmittance (hydraulic conductivity) of the flow region. β represents the difference in groundwater level at the drain position and the point halfway or midpoint between two parallel drains reduced to unit drain spacing. The drain spacing is represented by 2a. The parameter β is also adjusted by the parameter γ. The origin of the flow region in the geometric plane(z = 0) is located at the vertex P and the corresponding value in the t-plane is given by t(P) = 1 while ω(P) ranges from $-\infty + i\cdot Na$ to $-\infty + i\cdot 0$. Then, for z = 0, relationship (1) becomes:

$$0 = a + i\cdot c + i\cdot\frac{}{} \cdot \left(\ln\frac{}{} + \frac{}{} \cdot \ln\frac{}{}\right)$$

This relationship can be simplified after some algebraic manipulation to yield :

$$\pi\frac{}{} = \ln(1 + \frac{}{}) + \frac{}{} \cdot \ln(1+\frac{}{}) \quad (4)$$

Following the substitution of identity (3) for β in Eqn (4) one obtains:

$$\pi^{\frac{}{}} = \ln(1 + ^{\frac{}{}}) + ^{\frac{}{}} \cdot \ln\left(\frac{}{}\right) \quad (5)$$

Note the complex interdependence between b, c, and β.

Description of Groundwater Table

The location of the groundwater table is determined by a number of factors: (i) the water level in the drainage or conveyance system, (ii) the amount of water entering or leaving the aquifer at the soil surface(rain infiltration or evapo-transpiration) or the bottom of the flow region (seepage, drainage, or deep drainage), (iii) the hydraulic conductivity of the soil material in the aquifer, and (iv) the surface area of the drain or ditch through which groundwater exits or enters the water conveyance system or in other words the geometry of the flow field or of the aquifer. For a drainage flow regime as shown in Fig. 1 with adjoining mirror images of flow, the gradient of the groundwater table is zero above the drain (vertex Q) and halfway between two parallel drains (vertex R). To obtain the relationship for the groundwater table, represented by the open boundary QR in Fig. 1, the following expressions are introduced: (i) Express z in terms of polar coordinates, thus $z = x + i\cdot y = r\cdot\exp(i\cdot(\theta+2\pi k))$, where k is an integer, $r = \sqrt{x^2 + y^2}$, $\frac{}{} = \cos\theta$, and $\frac{}{} = \sin\theta$. (ii) Introduce the identity $t = i\cdot s$, where s is a real number. Note that the groundwater table QR in the complex t-plane (Fig. 2) is represented by the imaginary axis in the complex t-plane and that the value of s varies from 0 at Q to ∞ at R. Then, the following relationship for z is obtained:

$$z = a + i\cdot c + i\cdot\frac{}{}\left[\ln\frac{}{} + \frac{}{} \cdot \ln\frac{}{}\right] \quad (6)$$

The following identities were used to further simplify this relationship in order to obtain explicit expressions for x and y in terms of the parameters β, γ, and the variable s:

$$\ln(i\cdot s - 1 - \beta) = \tfrac{1}{2}\ln[s \quad + \quad] + \pi\cdot i - i\cdot \operatorname{arctg}\frac{}{} \quad (7)$$

$$\ln(i\cdot s + 1 + \beta) = \tfrac{1}{2}\ln[s \quad + \quad] + i\cdot \operatorname{arctg}\frac{}{} \quad (8)$$

$$\ln(i\cdot s + 1) = \tfrac{1}{2}\ln(s \quad + 1) + i\cdot \operatorname{arctg} s \quad (9)$$

Substitution of the relationships (7), (8), and (9) into equation (6) yields:

$$z = x + i\cdot y = \frac{}{} \{\frac{}{} \cdot \text{arctg}\frac{}{} - - \cdot \text{arctg } s \} + i\cdot c + \frac{}{} \ln\frac{}{} \quad (10)$$

This simplified relationship has a real and imaginary part which are associated with x and y, respectively. For a given value of s (a given point on the groundwater open boundary), the following x- and y-values are obtained:

$$- = - \cdot \{ \frac{}{} \cdot \text{arctg}(\frac{}{}) - - \cdot \text{arctg}(s)\} \quad (11)$$

$$- = - + \frac{}{} \cdot \ln(\frac{}{}) \quad (12)$$

Of specific interest are the vertices Q and R, which represent the locations of the groundwater table above the drain (Q) for which s = o and midway between the parallel drains (R) where s = ∞, respectively. The groundwater table at these locations is designated as b and c, respectively. Substitution of s = 0, representing the vertex Q in the t-plane, yields from Eqs. (11) and (12) the coordinates:

$$x = 0 \text{ and } y = c + \frac{}{} \cdot \ln\frac{}{} \text{, which, by definition, is b.} \quad (13)$$

Note, that the second term in the expression for y is a negative number which magnitude depends on the drain spacing and the value of β. The latter value is a quantity greater or equal to 0. Likewise, the vertex R in the t-plane ($t = i\cdot\infty$ and $s = \infty$) yields the coordinates for R in the complex z-plane:

$$x = a \text{ and } y = c \quad (14)$$

The groundwater level c midway between the drain lines can also be determined from the requirement t(P) = 1 for which z = 0 or from Eqn 4.

Groundwater Regime

The groundwater regime in an open aquifer is at all times determined by the interplay between, on one hand, water entering the aquifer, represented by the parameters N and L (precipitation and sub-irrigation via tiles and ditches, seepage upward from deep groundwater sources, etc) and, on the other hand, water leaving the aquifer (evapo-transpiration , drainage, deep drainage). However, it also depends on the ability of the aquifer to hold and transmit water, or in other words on the hydraulic and intrinsic water conductive and storage properties of the soil, represented by the parameter K. The combined effect of these factors is represented by the parameter γ (Eqn 3).

Table 1.The effect (Δ) of β on the groundwater table above the drain and mid-way between drains.

Y	β	c/a	b/a	Δ	y	β	c/a	b/a	Δ
100	100	0.0313	0.0019	0.0294	100	75	0.0316	0.0040	0.0276

100	50	0.0326	0.0084	0.0242	100	25	0.0411	0.0203	0.0208
100	10	0.0694	0.0542	0.0152	100	1	0.3523	0.3478	0.0045
50	50	0.0540	0.0039	0.0501	50	25	0.0576	0.0576	0.0414
50	10	0.0808	0.0503	0.0305	50	1	0.3549	0.3460	0.0089
25	25	0.0908	0.0078	0.0830	25	10	0.1037	0.0426	0.0611
25	1	0.3692	0.3424	0.0168	10	10	0.1721	0.0194	0.1527
10	1	0.3755	0.3314	0.0441	5	1	0.4013	0.3131	0.0882

The complex inter-relationship between the parameters β and γ is clearly indicated upon examination of Eqn(3). While γ only depends on the rainfall intensity and the hydraulic conductivity of the soil in the aquifer, β depends both on the geometry of the wetted part of the aquifer (dimensions a, b, and c) and also on γ. Table. 1 summarizes some numerical values for c/a and b/a for several combinations of β and γ. The parameter Δ, defined as (c/a – b/a), represents the difference between the groundwater table mid-way between drain lines and the groundwater table above the drain line reduced to unit drain spacing. In utilizing Eqs.(4) and (5), one must be aware that the calculated b/a- and c/a-values may yield negative numbers. If so, then the acquired negative numbers suggest that the groundwater table is absent and that the combination of γ and β chosen are by definition inappropriate. The data indicate, that for large values of γ, the difference in the groundwater level between points above the drain and mid-way between the drain lines decreases with decreasing values of β. The groundwater level per se is higher at these points for lower β-values. Also, the groundwater levels are higher for aquifers with small γ-values. Water levels for which β = γ are impossible. As $\beta \sqrt{}$ o, then the solutions for Eqs. (4) and (5) do not exist, because then b and c become $\sqrt{}$.

High values of γ denote, according to Eqn(3), when rewritten as $\gamma\sqrt{\sqrt{}}$ K/N + 1, a high value of the conductivity K or because of a small value of N (precipitation) or both. Then, there will be less water in the aquifer either because of rapid drainage or low precipitation. That means, that there is a larger difference between the ground water level above the drain (vertex Q) and the groundwater level above the mid-point (vertex R) between two parallel drains. In other words, β assumes a large value which can be attributed to both the large value for γ as well as a larger value for the term (b –c), representing the difference in groundwater level between the vertices Q and R. Conversely, low γ-values denote a low hydraulic conductivity or a high precipitation regime. Smaller γ-values also suggests a smaller value of β or a smaller difference between the groundwater level above the drain and that above of the mid-point between parallel drains.

Effect of Water Level in the Conveyance System

Another factor that controls groundwater movement is the aquifer geometry itself such as the length of the flow pathways and the size and location of the water conveyance system in the aquifer. For the case

at hand, in which excess water drains through a fully filled and submerged circular drain into a water conveyance system of ditches and streams, the drain water level also exercises a control on water release from the aquifer. In fact, the water pressure is determined by both the water level in the open water body, h_o, and the drain size and circumference through which drainage takes place. The tile drain is represented by the parameter r_o (the tile radius). Within the fully filled drain, the hydraulic potential is constant and consists of the water pressure, p_o ,at a point in the drain and the gravitational potential or location, h_o ,at that point relative to a known reference. Thus the total potential Φ and the potential function are then, respectively, defined as:

$$\Phi = \frac{}{\rho g} + h_o \quad \text{and} \quad = K\Phi \tag{15}$$

An important point on the drain tile is $z(D) = -i \cdot r_o$ on the drain perimeter below vertex P. In the t-plane, this point is given b by $t = 1 +$ $I + \beta$. The relationship between r_o and δ is given by:

$$-\!\!\!- = a + i \cdot c + i \cdot - [\ \ln\!\!\!- + - \ln\!\!\!- \ ] \tag{16}$$

Upon substitution the values for β and γ, one can determine δ . Also from Eqn(2) one can obtain an expression for φ_o :

$$\varphi_o = Kc + -\cdot[(L-N)\cdot \ln(\delta) - L \cdot \ln(\beta - \delta) + N \cdot \ln(\ 2 + \beta + \delta) + (\ L - N\ ) \cdot \cdot\!\!\!- \cdot \ln(\!\!\!- \ )] \tag{17}$$

With the water level in the drain being $h_o = p_o/\rho g$ and the pressure in the drain being p_o then

$$_o = K\cdot(\ \frac{}{\rho g} - r_o\ ) = K\cdot\ (\ h_o - r_o\ )$$

Van Deemter used the above relationships to calculate δ and came up with the following table:

π—	β	—	
0.0128	9	—0.019	0.10
0.0128	4	0.031	0.028

Another method of determining the effect of water pressure in the conveyance-tile drain system on the groundwater table is the procedure described by Römkens (2009). In this procedure, the center of the drain (vertex P) which has a $-\infty$ pressure potential, is shifted along the imaginary axis of the flow field (towards vertex Q). Then, one can calculate the potential at the bottom of the drain with radius r_o designated as point $z(D_1) = -\ i \cdot r_o$ .Vertex D_1 should have the potential φ_o prevalent in the conveyance system. The flow to the drain in this asymmetrical flow field can then bere-calculated and must yield a

certain value equal to Na. One now calculates the potential at the point $z(D_2) = i \cdot r_o$, which is the upper point of the drain. The potential at this point should be $\sqrt{}_o$ but found to be different due to the asymmetry of the flow field. By systematically changing the location of the vertex P along the imaginary axis y of the z-plane while maintaining the location and the potential at point D_1 one can arrive at potentials at point D_2 equal to $\sqrt{}_o$. Since the value of the drain flow is a fixed quantity Na that does not change, the groundwater level in the aquifer must adjust. This iterative calculation procedure of shifting the location of the vertex P ultimately will lead to a situation of a constant value of the potential around the tile drain perimeter. A different value P(z) where the potential is –infinity, must lead to a flow field that reflects this change. In this manner the potential in the drain is maintained at the level commensurate with that of the real flow field. By using this procedure in this problem case, adjustments in the flow rate is contrary to the condition that q = Na. However the distribution could vary while maintaining the requirement of a total flow of Na. Changes in the flow distribution to the drain tile are then obtained through adjustments in the groundwater table in the aquifer. This particular approach needs further examination.

Summary

The effect of aquifer characteristics on the groundwater table was examined for a steady rainfall regime, The analysis is based on the van Deemster (1950) analytical solution using conformal transformations. His approach offers significant potential to show how drainage flow may be affected by aquifer size and groundwater characteristics which in turn affects the groundwater table regime.

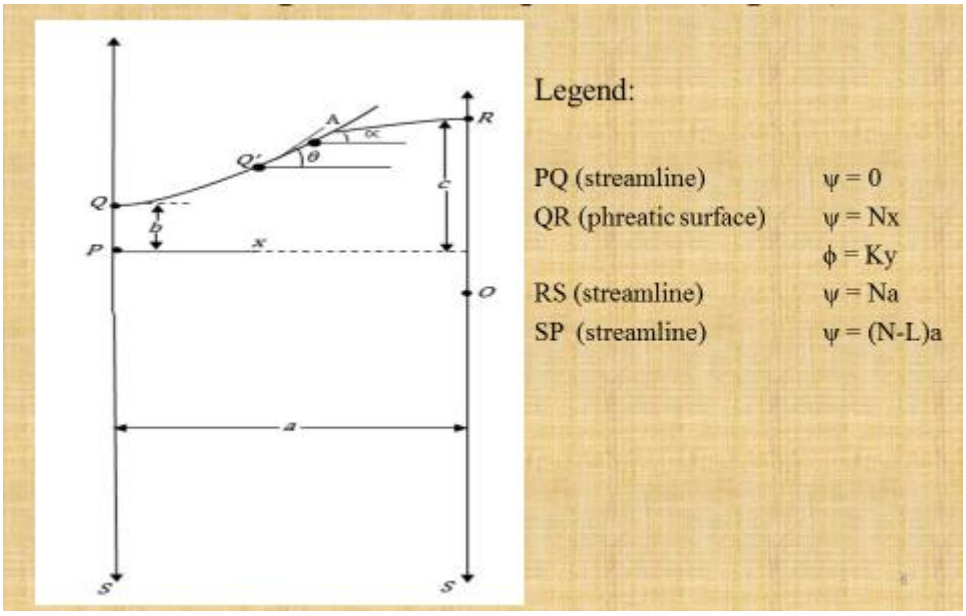

Figure 1. A schematic representation of the flow region with Tile Drain.

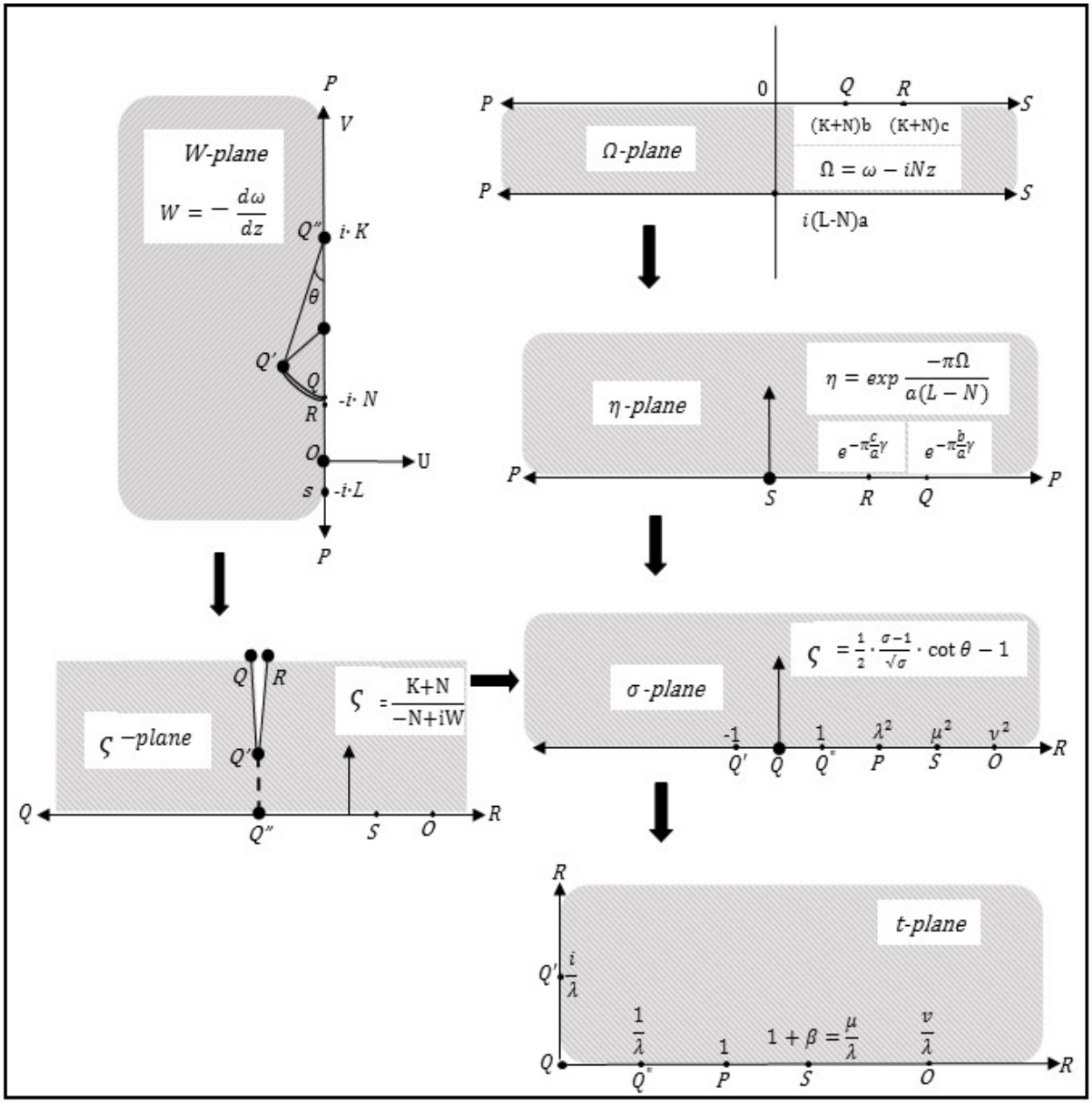

Figure 2. A graphical display of the transformations.

References

Römkens, M.J.M. 2018. A Holistic and Historic Analytical Approach to water management of Flat Land Watersheds with Tile Drains - The van Deemter Analysis. In: Wendroth, O., R.J. Lascano, and L. Ma (Eds) Bridging Among Disciplines by Synthesizing Soil and Plant Processes. Advances in Agricultural Systems Modeling, Volume 8. (Accepted).

Deemter, J.J. van. 1950. Bijdragen ot de kennis van enige natuurkundige grootheden van de grond. No. 11. Theoretische en numerieke behandelingen van ontwaterings en infiltratie stromingsproblemen. (Theoretical and numerical treatment of flow problems connected with drainage and irrigation). Verslagen van Landbouwkundige Onderzoekingen. No 567. Ministerie van Landbouw, Visserij en Voedselvoorziening 's Gravenhagen. The Netherlands. (In Dutch).

Harr, M.E. 1962. Groundwater and Seepage, McGraw-Hill Book Company, Inc., New York.

Römkens, M.J.M. 2009. Estimating seepage and hydraulic potentials near incised ditches in a homogeneous, isotropic aquifer. Earth Surface Processes and Landforms. 34: 1903-1914.

Muskat, M. and R.D. Wyckoff. 1937. The flow of homogeneous fluids through porous media. McGraw-Hill Book Company, Inc., NewYork and London.

Churchill, R.V. 1960. Complex Variables and Applications. McGraw-Hill Book Company, Inc. New York.

Römkens, M.J.M. 2017. Van Deemter's analysis of drainage to incised ditches in lowland areas. In: River Sedimentation. Eds: Wieprecht et al. pp. 77-84, 2017. Taylor and Francis Group. London.

Römkens, M.J.M. 2013. A theoretical treatise of drainage and seepage in bottomland areas adjacent to incised channels: The J.J. van Deemter analysis. In: Advances in River Sediment Research, Des. Fukuoka et al. 249-258. Taylor and Francis Group, London.

Strack, O.D.L. 1989. Groundwater Mechanics. Prentice Hall. Englewood Cliffs. N.J.

Polubarinova-Kochina, P.Ya. 1962. The theory of groundwater research. Princeton Univ. Press, N.J.

CWMS National Implementation Plan

Christopher N. Dunn, Director, P.E., D.WRE, U.S. Army Corps of Engineers, Hydrologic Engineering Center, Davis, CA; christopher.n.dunn@usace.army.mil
Robert C. Winders, Chief, Hydraulics Branch, P.E.,U.S. Army Corps of Engineers, Vicksburg District, Vicksburg, MS; robert.c.winders@usace.army.mil

A primary mission of the U.S. Army Corps of Engineers (USACE, Corps) is to manage the nation's water resources. USACE performs this mission across multiple purposes at the direction of the United States Congress. To satisfactorily meet these sometimes conflicting purposes, both now and in the future, it is critical that the nation's water resources are studied and managed in a holistic and comprehensive approach. The Corps Water Management System or CWMS has been developed to study and manage our nation's water resources from a real-time water management perspective.

CWMS is the USACE Automated Information System (AIS) that supports the USACE Water Management mission. CWMS integrates real-time data acquisition, database storage, flow forecasting, reservoir operation, river profile and inundation modeling, consequence/damage analysis, and information dissemination into a comprehensive suite of software supporting the water management decision processes. CWMS supports the informational needs for USACE water control decisions in its operations of over 700 reservoir and lock-and-dam projects. CWMS retrieves precipitation (rain, snow, and temperature), river stage, gate settings and other data from field sensors, and validates, transforms and stores those measurements in a database. The measurements are used for calibration and adjustment of hydrologic and hydraulic models to reflect current conditions. The gauged precipitation, combined with Quantitative Precipitation Forecasts (QPF) or other future precipitation scenarios, are used by the HEC-HMS (Hydrologic Engineering Center 's (HEC) Hydrologic Modeling System software) to forecast possible snowmelt and future river flows into and downstream of reservoirs. The reservoir operations model, HEC-ResSim (HEC's Reservoir System Simulation software) uses these flow scenarios to provide operational decision guidance for the engineer. The river hydraulics model, HEC-RAS (HEC's River Analysis System software) computes river stages and water surface profiles for these scenarios. An inundation boundary and depth map of water in the floodplain can be calculated from the HEC-RAS results as well. The economic impacts and other consequences of the different flows are then computed by HEC-FIA (HEC's Flood Impact Analysis software). This sequence of modeling software allows engineers to evaluate operational decisions during times of floods or droughts for reservoirs and other control structures, and view and compare hydraulic and economic/consequence impacts for various "what if" scenarios.

While CWMS's data capabilities have been used for years, the modeling capabilities have not been fully implemented by USACE nationwide. CWMS has most, if not all, of the features most water managers needed to perform operational analyses on a daily basis. Still, for a number of reasons, CWMS was not consistently or fully implemented throughout the nation. However, after the devastating floods of 2010 and 2011, USACE leadership asked what could have been done to better prepare and react to these types of system-wide events that require extensive communication, collaboration and modeling. The answer: fully implement CWMS.

Therefore, USACE leadership mandated the implementation of CWMS for the 201 basins where USACE has water management responsibility (Figure 1) and committed to fund the effort. From this direction and funding, the CWMS National Implementation Plan (NIP) was initiated. This plan is the first initiative to fully implement CWMS nationwide which means the suite of models described above would be built and used by Corps water managers to help with operational decisions, communication, and emergency management.

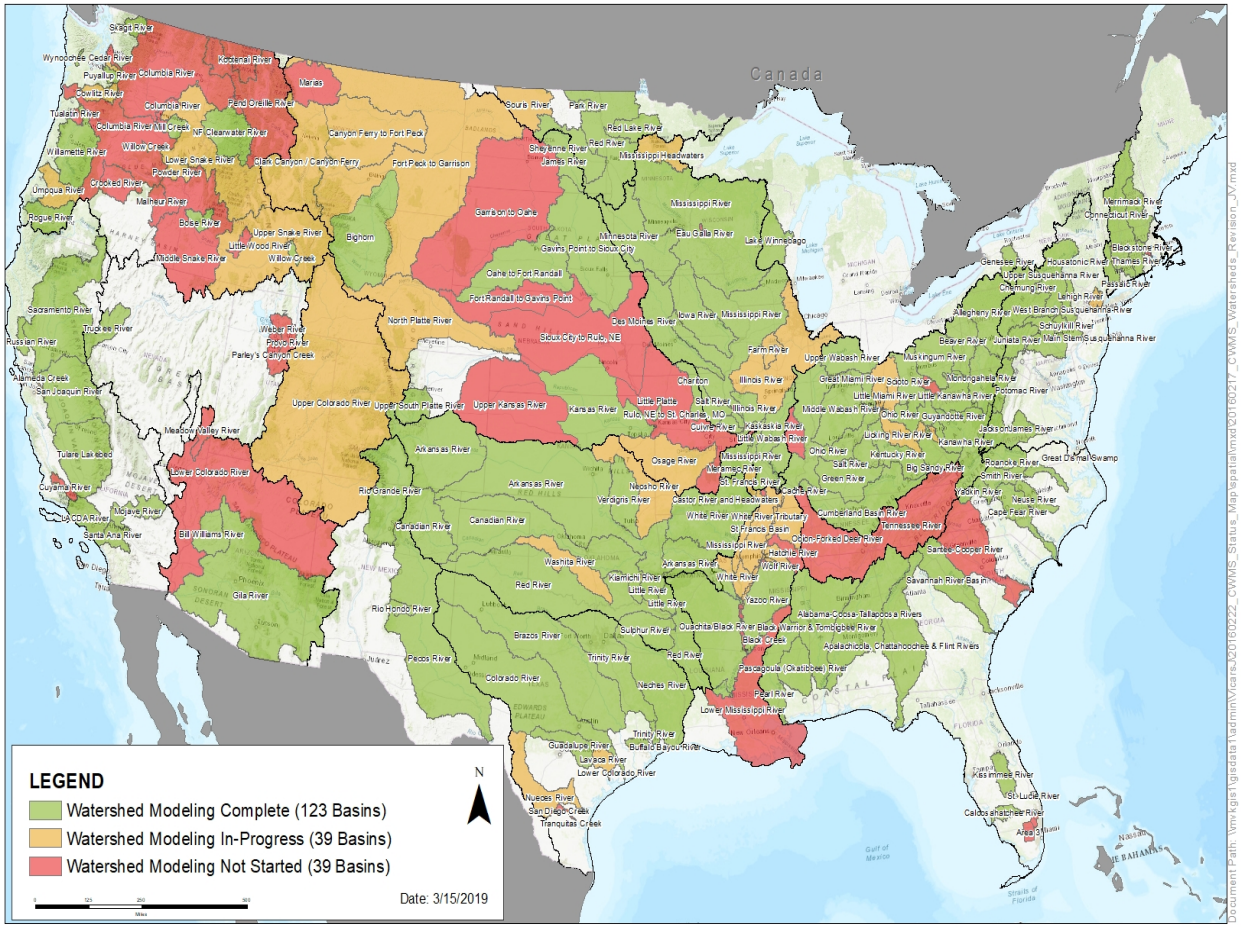

Figure 1. CWMS National Implementation Plan (NIP) Map

Beginning with an implementation plan similar to the one used and documented during the CWMS stimulus initiative (CWMS effort under the American Recovery and Reinvestment Act of 2009 or ARRA), models are being built for every watershed in which USACE has a water management responsibility and the full suite of CWMS software will be employed for each basin. The CWMS NIP is co-led by the USACE Modeling, Mapping and Consequence Center of Expertise (MMC) and CEIWR-HEC. Approximately 342 USACE staff from 37 district and Division offices and additional contractor staff have participated in the development of hydrologic, hydraulic, reservoir and consequence models and integrating them into CWMS. Project teams are composed of local district staff, augmented by staff from other Districts/Divisions when necessary. The models and CWMS implementations are being completed using the Standard Operating Procedures (SOP's) and guidelines written by HEC and MMC. The SOP's, guidelines, and the CWMS software are updated annually to reflect the experiences learned in the previous year of modeling. Upon completion of models, districts work to incorporate them into their daily water management processes. At the writing of this document, 123 of the 201 CWMS basins have been completed and handed over to the host Districts for their daily use (Figure 1). Tiger teams, made up of expert users from other USACE offices, are available to assist the districts on how to incorporate the models into their daily practice. The model development along with the incorporation of the data management, which most districts already used, allows the managers to perform real-time and forecasted operations with CWMS. This effort is expected to take ten years to complete, wrapping up in 2022 - 2024 (per funding).

Initial funding for the NIP came from the USACE Dam Safety program. The USACE Dam Safety program previously conducted evaluations of each USACE dam. Dams were classified within their Dam Safety Action Classification (DSAC) criteria and the dams deemed more vulnerable were listed as DSAC1 or DSAC2. The operation of these dams could influence their risk vulnerability so it was determined that CWMS models would allow water managers to make informed operational decisions that would minimize the risk to the dams and the populations downstream. Therefore, the USACE Dam Safety Program paid for the CWMS implementations for all watersheds that included a DSAC1 or DSAC2 dam. Eventually, the CWMS NIP received its own congressionally approved funding line item for approximately $10 million per year. Now the question was how to prioritize the remaining watersheds for implementation. The CWMS Advisory Group (AG), leaders within the USACE Water Management Community of Practice, were tasked to prioritize the basins for implementation within their area of responsibility. The CWMS AG then created a prioritized list of all the basins within their Division. The CWMS implementations are being completed in this order.

Once complete, the watershed models built for the USACE water management mission could be adapted for many other use cases; essentially these models become a study enabler for many other USACE missions. The CWMS models can be used for dam and levee safety studies that provide information to the USACE Operations Centers which will enhance disaster preparations, and can assist the Critical Infrastructure Protection and Resilience program addressing consequence based screening of the USACE infrastructure portfolio. In addition, the CWMS models can be imported into the HEC's Watershed Analysis Tool (HEC-WAT) software to expedite planning studies. So essentially, the nationwide development of CWMS models is a significant investment into many of the USACE mission areas.

As an extension of the CWMS National Implementation Plan, USACE plans on building a National Model Library where each of the models built for the CWMS National Implementation plan can be stored. These models will then be able to be "checked out" and used for other studies as well. By using the CWMS models as building blocks for other studies, the progress of the other studies can be expedited without losing the fidelity expected of good modeling. As such, the National Model Library will support USACE's new Planning Transformation Initiative. The USACE Planning Transformation Initiative is striving to arrive at planning decisions faster while not sacrificing technical accuracy. The repetitive use of good models will help the modeling teams provide their information quickly to the decision makers who have the ultimate decision. Thus, the CWMS National Implementation Plan with the addition of the National Model Library will support USACE's need to develop comprehensive watershed models that will support the water management, dam and levee safety, emergency operations, and planning missions.

So what about the remaining 96 watersheds (watersheds not influenced by USACE reservoirs) that are not included in the USACE watershed list? While USACE may not have reservoirs in these watersheds, USACE may own or maintain levees along the rivers in these watersheds (48 of these watersheds have Federal levee segments). Therefore, USACE is considering extending the CWMS NIP program to watersheds that include USACE levees. By having CWMS models for these watersheds, USACE will be able to forecast water surface elevations on the levee and thus provide information to emergency managers and other USACE stakeholder/partner personnel. Finally, in areas that have no USACE levees or reservoirs, the MMC has developed a process using HEC-RAS two-dimensional modeling capabilities to quickly model those areas, develop flood inundation maps, and compute consequences. This capability was deployed and flood inundation maps were created on a wide scale basis during Hurricanes Florence and Michael. The trafficability maps that were created were of particular interest as the maps included social media techniques to provide road closure information.

Conclusion

To manage the nation's water resources in a holistic and comprehensive approach while implementing system concepts, USACE has developed CWMS. USACE is currently implementing CWMS nationwide. The models being built for real-time water management purposes are beneficial to other USACE missions as well. CWMS is just one example of how the United States and USACE is trying to study and manage the Nation's water resources in a more coordinated and collaborative manner. This presentation will introduce the CWMS NIP and discuss the benefits to the water management community and other USACE missions. This presentation is to be included as part of the HEC Watershed Systems Decision Tools Session in the Decision Making Models Topic Area.

HEC-WAT: A Planning Tool for Watersheds

Adams, Lea, Chief – Water Resource Systems Division, USACE – Hydrologic Engineering Center, Davis, CA, lea.g.adams@usace.army.mil
Lehman, William, Senior Economist, USACE – Hydrologic Engineering Center, Davis, CA, william.p.lehman@usace.army.mil

Introduction

The USACE Hydrologic Engineering Center (HEC) released Hydrologic Engineering Center-Watershed Analysis Tool (HEC-WAT) Version 1.0 in September 2017. HEC-WAT is a flexible software application designed to support the field of water resources engineering. Because of its flexibility, the mission statement for HEC-WAT is necessarily broad: A water resources tool that integrates engineering and consequence software to support a wide range of USACE applications, including watershed and systems-based risk analysis.

HEC-WAT was developed in response to a series of USACE policy documents stretching back to 2000 that established study guidelines requiring that the planning process "address the Nation's water resources needs in a systems context" (Engineer Regulation 1105-2-100), and apply risk assessment methods (Engineer Regulation 1105-2-101). In short, these and other policy documents required USACE to evaluate projects more comprehensively and with consideration of risk and uncertainty.

Beyond supporting USACE requirements, it's readily apparent that study teams in the field of water resources should take a broad perspective when solving problems. With climate change, population growth and demographic shifts, the demands on our infrastructure to reduce our risk from extreme conditions of drought and flood are increasing. And to meet these demands, we have to more fully embrace integrated water resource management. HEC-WAT is a useful tool for evaluating projects from a more cohesive, watershed-scale perspective.

This discussion focuses on using HEC-WAT as a planning tool at the watershed scale. The three key topics are: 1) integration of software that evaluates various aspects of water resources within a watershed; 2) spatial representation of watershed processes; and 3) incorporation of risk and uncertainty study methods. In addition, results are reviewed and several example project applications are described to illustrate different watershed planning use cases for HEC-WAT.

Integration of Water Resources Software

Currently, HEC-WAT integrates four primary pieces of HEC water resources software: HEC-HMS, HEC-ResSim, HEC-RAS and HEC-FIA. Each of these programs allows users to evaluate a specific aspect of water resources management within a watershed: HEC-HMS (Hydrologic Modeling System) models the rainfall-runoff transformation, HEC-ResSim (Reservoir System Simulation) models reservoir operations, HEC-RAS (River Analysis System) models river hydraulics and HEC-FIA (Flood Impact Analysis) models damage and life loss due to flooding. HEC-WAT integrates these software packages by facilitating the flow of information from one model to the next, eliminating the need for manual handoffs by a modeler. When a study team is evaluating a large number of planning alternatives (especially large-scale or complex

alternatives), creating the data communication pathways inside HEC-WAT can save a tremendous amount of time, as linking models only needs to be done once. Connecting models inside HEC-WAT can also eliminate errors that accidentally occur when users manually transfer data from one model to the next. HEC-WAT allows import of existing HEC models (e.g. HEC-HMS, HEC-RAS, etc.) to efficiently re-use available data, or users can build new individual HEC models within the HEC-WAT framework.

Spatial Representation of Watershed Processes

The spatial component of a watershed-scale water resources study is often key to accomplishing the purpose of the study. One example that illustrates this concept is the application of HEC-WAT to evaluate potential modifications to reservoir operations within the Russian River, California, watershed (Figure 1). In this case, the study team analyzed the changes in flood frequency in the downstream communities of Healdsburg and Guerneville in response to various operational alternatives at Lake Mendocino in the upper watershed. The reservoir is located 50 to 80 miles upstream of the communities of concern, with a number of tributaries joining the Russian River along the way. In this case, the impact locations of concern were spatially distant from the project location within the watershed. The analysis also crossed modeling platforms, using stage-frequency results from HEC-RAS to evaluate flood risk impacts in response to reservoir operation changes modeled in HEC-ResSim. In this way, HEC-WAT supports both the spatial and cross-platform modeling components of watershed evaluations, providing a comprehensive analysis approach.

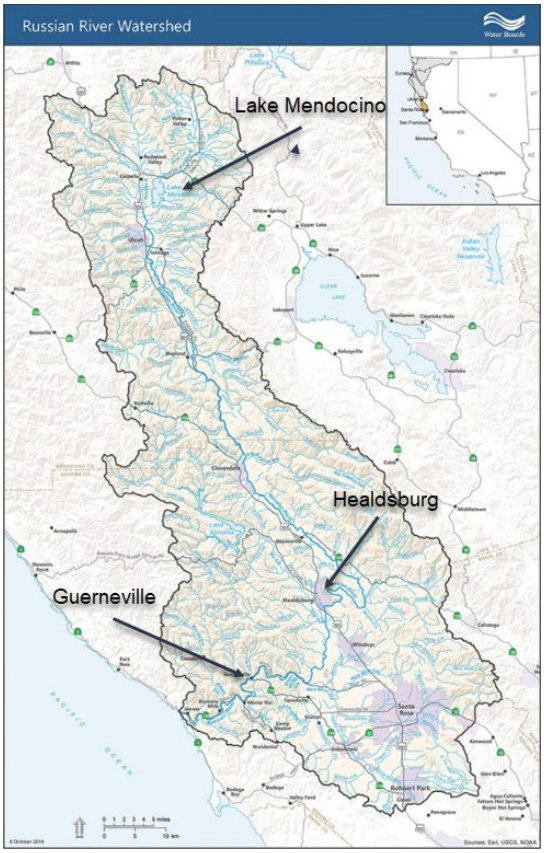

Figure 1. Russian River Watershed

Risk and Uncertainty Methods

The HEC-WAT Flood Risk Analysis (FRA) compute type utilizes a Monte Carlo-style compute to support risk analysis. Hydrologic boundary conditions (precipitation and flow) are typically generated within a tool called the Hydrologic Sampler within HEC-WAT. Uncertainty in initial conditions and parameter values are sampled from uncertainty distributions specified by users within the individual HEC software programs. For example, starting reservoir pool elevations can be sampled within HEC-ResSim, initial loss rates within HEC-HMS, and uncertainty in structure first floor elevations within HEC-FIA. Within a standard FRA compute, hundreds or thousands of events are generated. Each flood event is hydrologically independent, and multiple flood events are organized into groups of events termed 'realizations' (consisting of a minimum of 500 events). Two types of uncertainty are sampled separately within HEC-WAT: knowledge uncertainty and natural variability. Knowledge uncertainty parameters are sampled once per realization, while natural variability parameters are sampled for each flood event within a realization.

Project Results and Example Studies

HEC-WAT users can access standard results from the individual HEC software applications, as well as results specific to an HEC-WAT compute. Results for variables of interest generated during an HEC-WAT FRA compute can be viewed by individual event, or viewed collectively via histograms and frequency curves with uncertainty bounds. Depending on the variable, results can also be displayed spatially.

HEC-WAT has been used on a number of watershed studies to date, including: a climate change evaluation of the Red River basin (North Dakota and Minnesota); a forecast-informed reservoir operations study in the Russian River watershed (California); and a reservoir operations and risk evaluation in support of the Columbia River Treaty (Pacific Northwest and Canada).

Summary

HEC-WAT supports watershed-scale planning studies through: 1) integration of software that evaluates various aspects of water resources within a watershed; 2) spatial representation of watershed processes; and 3) incorporation of risk and uncertainty study methods. It generates standard results from the individual HEC software applications as well as risk analysis results from FRA computes, including spatially distributed results. HEC-WAT has been used to successfully evaluate a range of watershed planning studies, ranging from the effects of climate change to alternative reservoir operations.

References

Engineer Regulation 1105-2-100. 2000. Planning Guidance Notebook. U.S. Army Corps of Engineers.

Engineer Regulation 1105-2-101. 2017. Risk Assessment for Flood Risk Management Studies. U.S. Army Corps of Engineers.

Modeling the Truckee River Operating Agreement as a Basis for Stakeholder Negotiation

Anthony Powell, PE, Project Manager, Precision Water Resources Engineering, Loveland, CO, Tony@precisionwre.com
Thomas Scott, PE, Water Resource Engineer, California Department of Water Resources, West Sacramento, CA, tscott@water.ca.gov

Abstract

The Truckee River Operating Agreement (TROA) is the result of a nearly 30-year process of negotiation and litigation for operations that allow more flexibility for the stakeholders of TROA to use their water. The TROA Operations and the TROA Planning RiverWare© models are used to study the potential benefits and drawbacks of TROA flexibility to stakeholders and their interests. This paper discusses and highlights the outcomes, and the potential benefit of the models that have been vetted by all stakeholders in mitigating disagreements and promoting consensus on operations beneficial to stakeholders. A case study demonstrates how TROA's provision for exchanging credit water in Truckee Basin reservoirs enables a TROA Party to meet environmentally beneficial and recreational preferred flow and storage targets throughout the basin. The case study is based on a Water Year 2016 negotiated operations between three parties in the Truckee basin.

Operations under TROA to establish and exchange of credit water require cooperation between individual TROA Parties and other signatory parties. Some of these operations support other party's goals, while others do not. The operations that do not, potentially require negotiation with the affected party to find an acceptable resolution. TROA provides a basis for these mutually beneficial negotiations, whereas under previous agreements, the negotiations or the operations may not have occurred. When these potentially contentious operations are proposed by a TROA party, the RiverWare© TROA Operations and TROA Planning models can simulate basin conditions with and without the proposed operation action. The RiverWare© models, which are reviewed and available for use by all stakeholder groups, can objectively show the true impacts to a proposed operation, often overcoming preconceived ideas of negative impacts that exist in the absence of this objective information. This may occur when a party is familiar with the broad assumptions and requirements within TROA but may overestimate a potential impact that is disproved with modeling of the river basin. With the basin's TROA Operations and TROA Planning RiverWare© models, parties have the ability to negotiate based on consistent results from a reliable and shared resource.

Introduction

Truckee River Basin

The Truckee River flows from Lake Tahoe through California, into Nevada and terminates into Pyramid Lake. The total length of the river is 120 miles which starts in the Sierra Nevada mountains and terminates in the high desert of Nevada. The total area of the Truckee River Basin is approximately 3,000 square miles. The hydrology of the basin is mainly driven by snow

fall with annual amounts of over 30 inches of precipitation in the mountains, but drier portions of the basin may see less than 5 inches of precipitation during the year.

The headwaters of the Truckee River Basin lie in California and the Truckee River begins in the Lake Tahoe Basin. The Lake Tahoe basin is approximately 500 square miles with the Lake Tahoe comprising approximately 40% of that area. Lake Tahoe is a naturally occurring lake with an outlet on the northwestern portion of the lake with an approximate maximum depth of 1,650 feet and is the 10th deepest lake in the world. A dam exists at the outlet that regulates the outflow of water stored behind the dam. The naturally occurring rim of 6,223.0 feet above sea level is the base of the dam, which rises 6.1 feet and provides a maximum storage capacity of approximately 744,600 acre-feet at an elevation of 6,229.1 feet (Rieker, 2010). When the water surface level is below 6,223.0 feet, no water flows out of the outlet of Lake Tahoe.

Downstream of the Lake Tahoe outlet the Truckee River meets Donner Creek at a confluence near Truckee, California. Downstream of that confluence, the confluence of Martis Creek and Prosser Creek contribute to the river close to the same area. The Little Truckee River confluence is slightly further downstream and from there the river generally flows in an easterly direction, through the town of Floriston, California and into Nevada. The Little Truckee River is the largest sub basin downstream of Lake Tahoe and includes the Independence Creek basin and a trans-basin diversion to the Sierra Valley in a neighboring watershed.

Upon entering Nevada, municipal and agricultural diversions deplete water from the Truckee River through the Truckee Meadows and smaller tributaries add water to the river which includes the effluent from the Truckee Meadows Water Reclamation Facility near the confluence with Steamboat Creek.

The Truckee River flows from the Truckee Meadows and through the Vista Reefs and into Truckee Canyon, until 18 miles downstream of Vista, Derby Dam diverts water from the Truckee River into the Truckee Canal to supply water to the Bureau of Reclamation's Newlands Project. Water in the Truckee Canal is used to supplement water from the Carson River and water flows into Lahontan Reservoir. Water is released from Lahontan Reservoir for downstream use in the Newlands Project, wildlife refuges, and municipal uses.

The Truckee River flows from Derby Dam east and then north where it enters the Pyramid Lake Indian Reservation and passes through several diversion structures before flowing into the delta of Pyramid Lake. The lake terminates in Pyramid Lake, which is home to two native and protected fish species, the Lahontan Cutthroat Trout and Cui-ui.

The Carson River flows from the headwaters through Carson City, the city of Dayton, and into Lahontan Reservoir. A map of the Truckee and Carson Basins is shown in Figure 1.

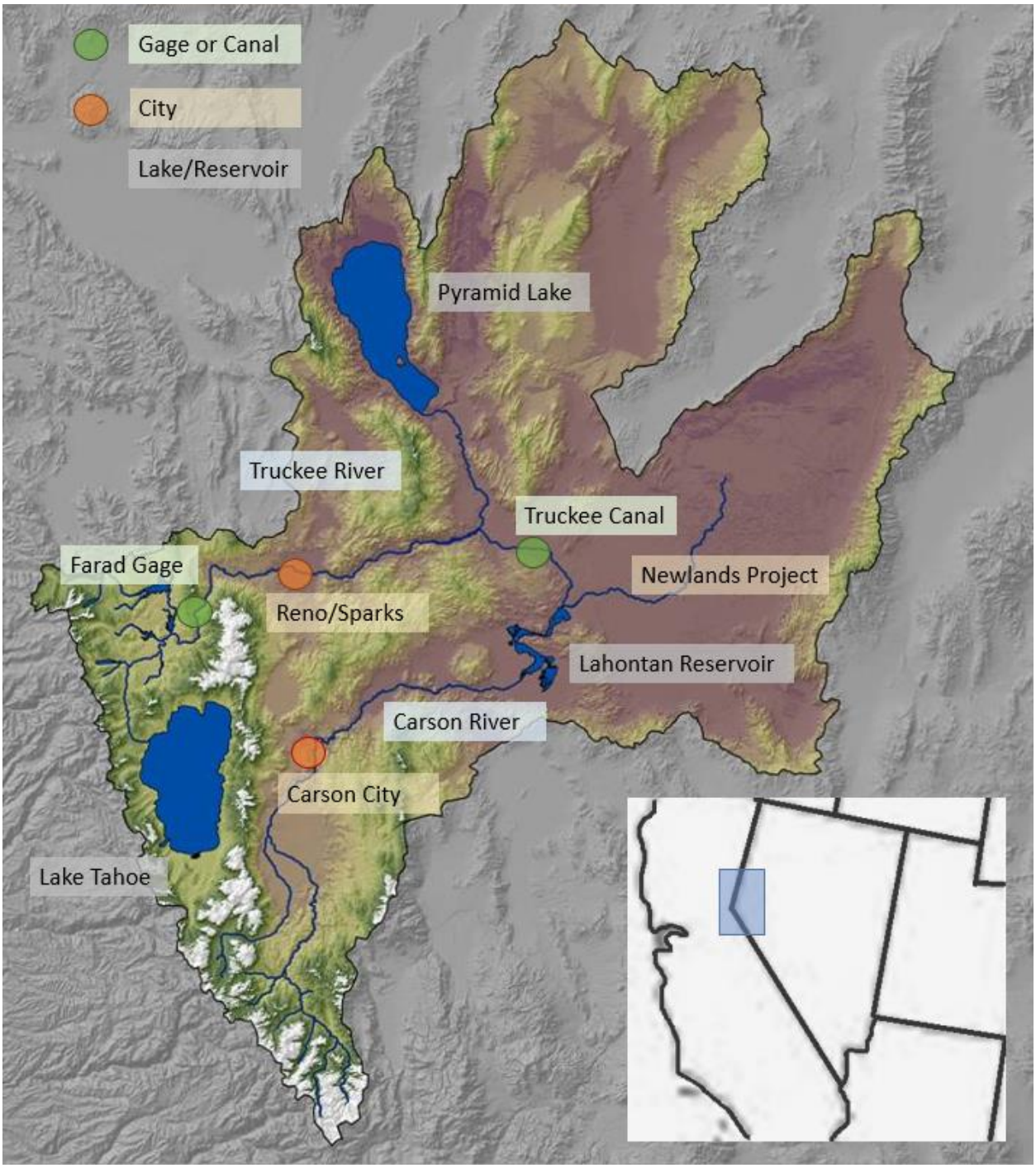

Figure 1. Truckee River Basin

Truckee River Operating Agreement

TROA is the result of years of negotiation and litigation between parties in the Truckee River basin (Basin) and is a result of an assortment of agreements, policies, and regulations that were put in place on the Basin to meet the many conflicts and demands of the limited amounts of water. The following includes a list of agreements and decrees that form the basis of TROA:

- The *Truckee River General Electric Decree* (1915) granted the US Bureau of Reclamation (Reclamation) an easement to operate Lake Tahoe Dam with the requirement that year-round flow (known as Floriston Rate because of the former gage at Floriston California that has been replaced by the Farad Gage) be released for downstream users.
- The *Truckee River Agreement* (1935) is the result of an agreement between Reclamation, the Sierra Pacific Power Company (the predecessor to the Truckee Meadows Water Authority (TMWA)), the Truckee-Carson Irrigation District, the Washoe County Conservation District, and Federal and State of Nevada represented parties to operate reservoirs in the upper Basin to meet modified Floriston Rates for irrigation, municipal, and hydropower uses.
- The *Orr Ditch Decree* (1944) specified the water rights of users in Nevada and ensured that the Federal Water Master enforces the intention of the decree.
- The *Alpine Decree* (1980) specified the Carson River water rights in California and Nevada and defined the specifics of duty and consumptive use for the Newlands Project. The Alpine Decree is also administered by the Federal Water Master.
- *Public Law 101-618*, among other items, required negotiation of new operating agreement which resulted in the TROA. When TROA was implemented in 2015, the Interstate allocation between California, Nevada, and the United States for diversion and use volumes in each state in the Lake Tahoe and Truckee River basins became effective.

TROA is an agreement that was negotiated by all TROA parties to operate the reservoirs in the Basin in a coordinated way that benefits the TROA Parties and is more flexible than the agreements previously put in place. The Mandatory signatory parties for TROA include United States, TMWA, the Pyramid Lake Paiute Tribe (PLPT), and the states of California and Nevada (DOI and State of California 2008). TROA ensures the terms and conditions set forth by the previous agreements in the Basin are met and also provides for flexible and coordinated operations in an effort to meet all of the parties' goals through the benefit of instream flows below reservoirs, improve municipal drought supplies, enhance reservoir levels for use, and improve water quality throughout the main stem of the Truckee River.

TROA was negotiated for better and more efficient coordination between parties in the Basin. Since inception in 2015, parties have more successfully communicated and coordinated on operations and strategies to achieve their own goals. This has become more feasible with the use of technical RiverWare© models of TROA that have been designed for the use by the administrators who distribute the models and any coordinating or signatory party involved with the scheduling. The use of a common model platform for TROA has limited the need for parties to construct or build their own set of technical tools and allowed for discussion about basin policy as opposed to navigating potential arguments over specific party tools. This saves the parties effort and money while allowing for a continual improvement to the tools that are used by all parties.

Models of the Truckee River Operating Agreement

The Truckee Carson TROA Operations and Accounting (TROA Operations Model) and Planning Models (TROA Planning Model) were developed through a collaborative effort of the TROA signatories, including Reclamation, TMWA, PLPT, the Federal Water Master, and the departments of Water Resources of California and Nevada. The models are considered as the operational guidelines for the basin and are available for use by all parties. The TROA

Operations and the TROA Planning RiverWare© models are used to study the potential benefits and drawbacks of TROA flexibility to stakeholders and their interests.

The TROA Operations Model and TROA Planning Model are daily-time step water management simulation models built in the RiverWare© modeling environment. The models simulate Basin water management operations under TROA, including operations of all major dams and reservoirs in the Truckee and Carson River basins: Lake Tahoe, Donner Lake, Independence Lake, Boca Reservoir, Prosser Creek Reservoir, Stampede Reservoir, Derby Diversion Dam, and Lahontan Reservoir. The model also includes all of the major diversions in the system for municipal and industrial uses, as well as agriculture including the Truckee Canal, Lahontan Reservoir, and the Newlands Project. Water is allocated to users with a prioritized water right structure. Current flow and regulatory standards in the basins are included as constraints in the model, including the 1997 Adjusted OCAP, 1935 Truckee River Agreement, 1944 Tahoe Prosser Exchange Agreement, and TROA. The models receive regular review and refinements from regional stakeholders in anticipation of operational changes or their use for future planning studies.

The TROA Operations model is used by the Federal Water Master to model the operations and accounting of the Basin parties with both a forward and backward focus. The backward-looking accounting portion uses real operations to account and charge parties for their use of water based on the policy of the Basin and requests from the parties. The Federal Water Master oversees this process and provides the information to parties through web portals and by distributing the model. The forward-looking operations and accounting use forecasted inputs to the model (hydrology), input scheduled operations requested by parties, and models the Basin for the remainder of the short-term forecast period (up to 15-months).

The TROA Planning model is used for studies and analyses that require a longer than short-term outlook for planning and study purposes. The TROA Planning model can be run for any period of time and is generally limited in length by the historical or generated hydrology to which a party has access. The operational guidelines and scheduling for party operations in the model are determined by logic that consider the Basin conditions and forecast. The logic that determines those guidelines was developed in coordination with individual parties to ensure that operations and forecasts for each party reflect current policy.

Stakeholder Use and Negotiation of the TROA Models

Availability and Use of the TROA Operations and Planning Models

The Truckee River Operations and Planning models are available to all coordinating parties. Parties use the model, and if changes to the model are required as a result of a study to enhance a party's operations, they are documented, and model improvements are made as necessary by the housing agency.

The TROA Operations model is distributed to the coordinating parties on a weekly basis by the Federal Water Master and is available for use by any of the receiving parties. The scheduling inputs to the model for TROA specific operations and guidelines are requested by coordinating parties and input by the Federal Water Master. Parties meet monthly to go over coordinated operational results to review the short-term forecasts.

The TROA Planning model is distributed by Reclamation to all the basin parties, not solely to signatory parties. Parties use the TROA Planning model for studies of their particular operations to evaluate potential future use, future demand, or potential future hydrology for their interests. Parties will use the model to evaluate various operation scenarios to help produce reports that may be distributed to the other parties in the basin.

Basis of Negotiation

The modeling and studies produced by the TROA Operations and Planning models are used by each party in the Basin and can influence discussion on policy guiding the models. Individual parties request specific operations that benefit them in their stored water or instream flow targets. Some of these operations support other party's goals, while some do not. The operations that do not, potentially require negotiation with the affected party to find an acceptable resolution. TROA provides a basis for these mutually beneficial negotiations, whereas under previous agreements, the policy was much more prescriptive allowing little opportunity for collaborative operations. When controversial operations are proposed by a TROA party, which often occurs when a party is familiar with the broad assumptions and requirements within TROA but may overestimate a potential impact, the RiverWare© TROA Operations and Accounting and TROA Planning models can simulate Basin conditions with and without the proposed operation action and to quantify the potential impact assumed by the disputing party. The ability for party discussion to focus on policy and not on the modeling tool itself allows for the parties to have more productive and meaningful discussions that guide the operations of the Basin. This saves on time and money for each of the parties and benefits the operations for the entire Basin. The models, which are reviewed and available for use by all stakeholder groups, can objectively show the impacts to a proposed operation, often overcoming preconceived ideas of negative impacts that exist in the absence of this objective information.

2016 Operations and Party Negotiation

Water Year 2016 was the first Water Year TROA operations were in effect. 2016 followed one of the driest five-year periods in the Truckee Basin. The hydrology in 2016 was considered almost average for flows into the basin but the dry starting conditions meant that by early September 2016, the system would experience a shortage in meeting the Floriston Rate at the Farad Gage near the border of California and Nevada. The Truckee Basin is somewhat unique in that a daily flow target to meet the Floriston Rate is in place and is the basis of daily flow in the Truckee River. The Nevada water rights holders are assumed to be satisfied as long as the Floriston Rate is met each day. In some years, as in 2016, the Floriston Rate storage in the reservoirs plus the inflow hydrology for the year, is not enough to meet the Floriston Rate for the entire year. Not all users that rely on Floriston Rate water would have been satisfied after the Floriston Rate was no longer met in early September 2016.

One of the users that rely on Floriston Rate water is TMWA. TMWA uses Floriston Rate water to meet their daily demand and in times of missed Floriston Rate, can rely on stored sources of water. In 2016, a portion of the storage in Donner Lake, which is part of TMWA's privately owned stored water, was to be used to supplement demand not met by the Floriston Rate. An additional amount of TMWA's water in Donner Lake needed to be exchanged to another reservoir before Floriston Rate were no longer being met. In a normal year, when the storage of Donner Lake is not needed to supplement demand, the Donner Lake water can be exchanged.

Exchanges move water from one reservoir to another by releasing water from one reservoir in lieu of a release from another reservoir, then converting water from the other reservoir to the water released (Figure 2). In 2016, TMWA planned to exchange their Donner stored water, not needed for supplemental Floriston Rate flows, to Boca Reservoir using a Floriston Rate release. Since Floriston Rates were due to not be met after Labor Day, TMWA planned the exchange on Floriston Rate Releases prior to Labor Day, thus lowering the level of Donner Lake in the process.

Donner Lake homeowners have an agreement with TMWA, called the 1943 Donner Lake Indenture Agreement, that requires the level in Donner Lake to remain at a certain storage limit throughout the summer months. The limit that is agreed upon prior to Labor Day is an agreed upon level but is not the preferred limit for many of the homeowners. The Department of Water Resources (DWR) in California has a request to keep Donner Lake higher, at the Preferred level, than the Donner Lake Indenture Agreement level for as long as possible, or until Labor Day, to satisfy the requests of the homeowners on Donner Lake.

The proposal for TMWA to release their water with an exchange to Boca Reservoir prior to Labor Day did not meet the preferred storage of California DWR. California DWR requested that the exchange occur after Labor Day, which was difficult because the exchange with a Floriston Rate release was not possible. The exchange of water out of Donner Lake would be possible as long as it was done with a demanded release, other than Floriston Rate releases.

The Pyramid Lake Paiute Tribe has inflow targets at Pyramid Lake for flows from the Truckee River, measured at the Truckee River at Nixon Gage, and has storage in the Truckee Basin River that can be released to supplement those target flows. In 2016, PLPT had a demand from Prosser Creek Reservoir after Labor Day that was to be used to meet Truckee at Nixon target flows as well as draw Prosser Creek Reservoir down to the winter storage levels that are specified for flood control purposes during the winter. That demand could facilitate the exchange of TMWA's water after Labor Day, but Prosser Creek Reservoir was not a good destination of water for TMWA because of the drawdown that required all stored waters to be released from Prosser by November 1st, meaning TMWA would need to attempt to exchange their water from Prosser to another reservoir before this date to keep it in upstream storage.

To solve the issue, the parties used the TROA Operations Model to simulate various strategies and developed a solution that met downstream flows while allowing TMWA to move the portion of the Donner Lake storage not necessary to supplement for TMWA demand to Boca Reservoir.

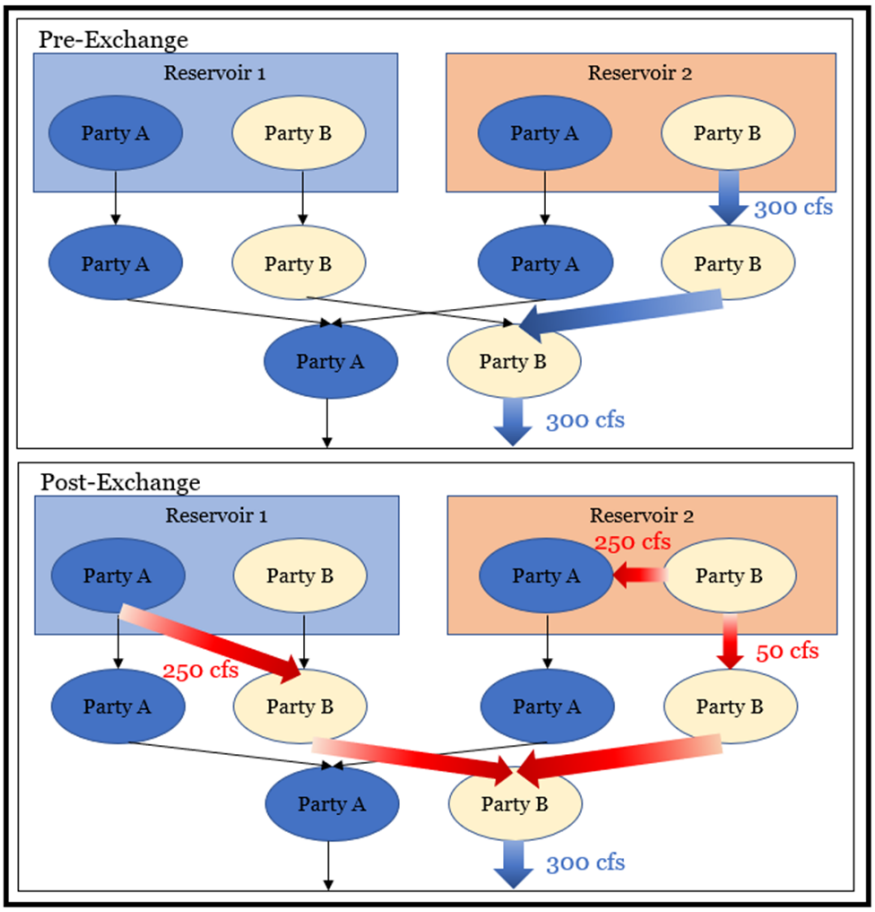

Figure 2. Exchange Example, in 2016 Reservoir 1 would be Prosser Reservoir and Reservoir 2 would be Boca Reservoir, Party A would be TMWA water and Party B would be Floriston Rate

The operation to do this included an exchange of water in Prosser Creek Reservoir that would be used to meet Target Flows at Nixon was exchanged to Boca Reservoir in lieu of a Floriston Rate release prior to Labor Day. This moved the water stored to meet PLPT Targets, from Prosser Creek Reservoir to Boca Reservoir, drawing Prosser Creek Reservoir down prior to when it originally would have. After Labor Day, when the demand of water that would have originally come from Prosser Creek Reservoir to meet target flows in the Truckee River at Nixon, that water was scheduled to be released from Boca Reservoir. TMWA used that demanded release to exchange their water to Boca Reservoir in lieu of the release to meet the Nixon targets and stored their water in Boca.

In the monthly coordination meeting of July 2016 this operation was recognized and negotiations for a coordinated multi-party operational agreement for this commenced. The August 2016 coordination meeting had results of modeling analysis and Figure 3 to Figure 6 show the difference in operations from each of the three reservoirs to accomplish this operation. Each Figure shows the range of future possibilities based on an ensemble of inflow forecasts that are modeled through the TROA Operations model. The ensemble of inflow forecasts is produced by the California Nevada River Forecasting Center (CNRFC).

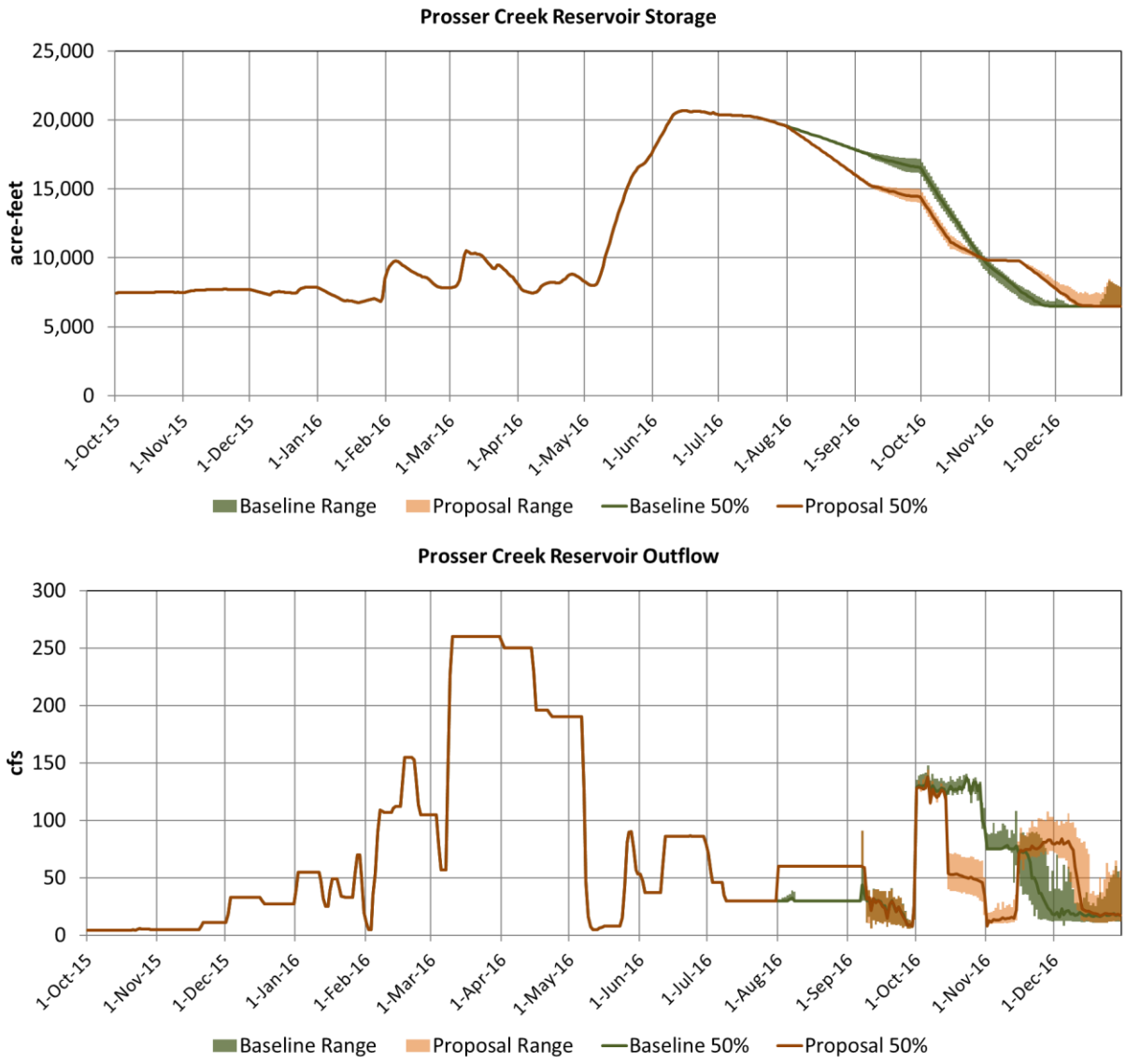

Figure 3. Prosser Creek Reservoir Storage and Outflow Ensemble Operational Comparison from the August 2016 TROA Coordination Meeting. Prosser Creek Reservoir is Proposed to be drawn down prior to the baseline dates with higher outflows in August.

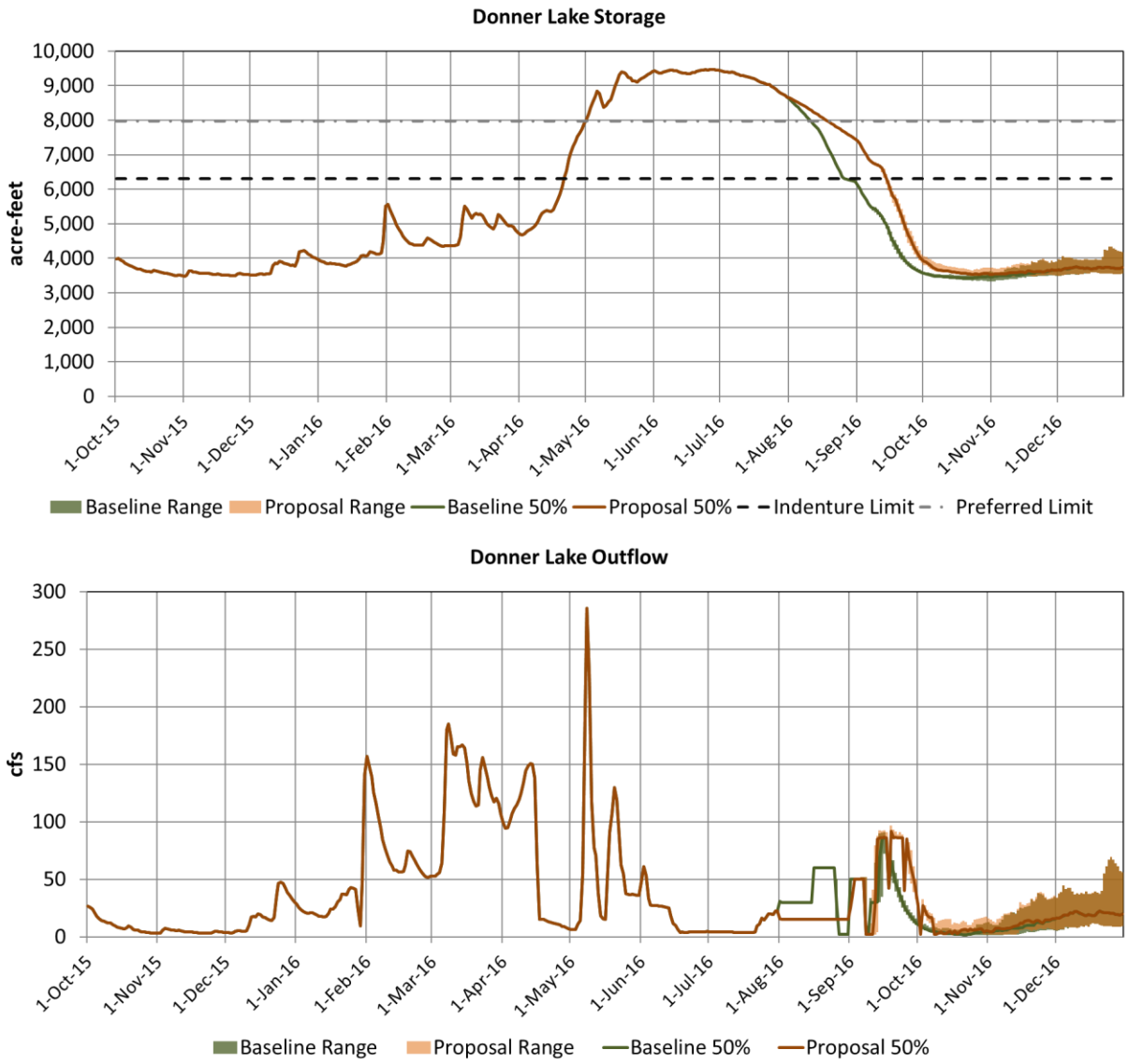

Figure 4. Donner Lake Storage, with Storage Targets, and Outflow Ensemble Operational Comparison from the August 2016 TROA Coordination Meeting. Donner Lake Storage was preserved over the preferred Homeowner Limit for a longer period of time than was originally planned with lower outflows prior to Labor Day.

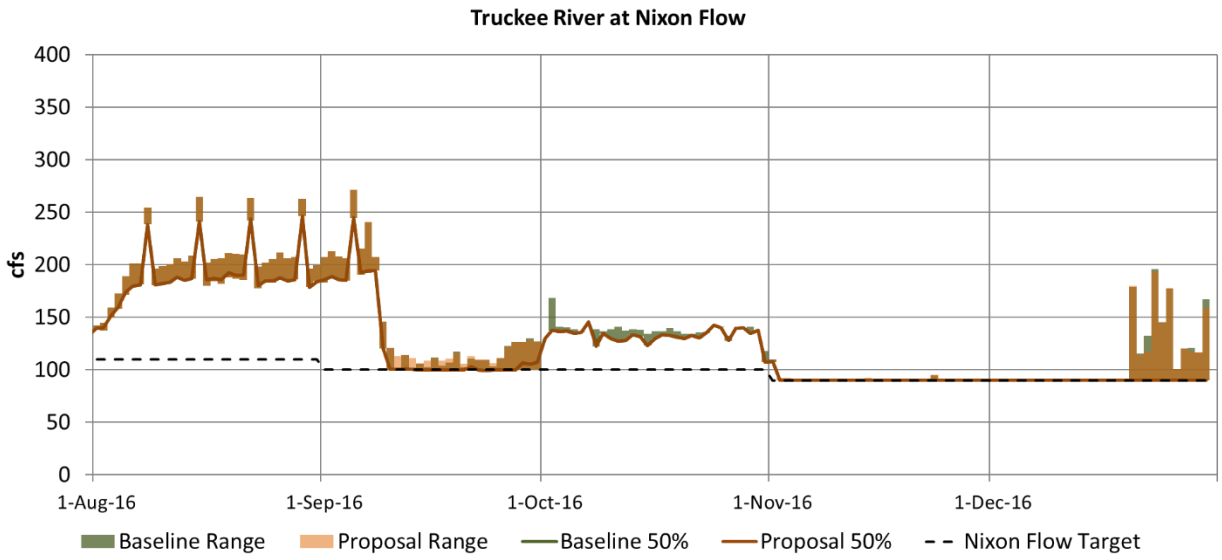

Figure 5. Ensemble Range of Flow at the Truckee River at Nixon Gage Based on Changed Operations from the August 2016 TROA Coordination Meeting. The Range of flows at the Nixon gage were slightly impacted due to the proposed operation but were always above the flow target in the Truckee River at the Nixon Gage.

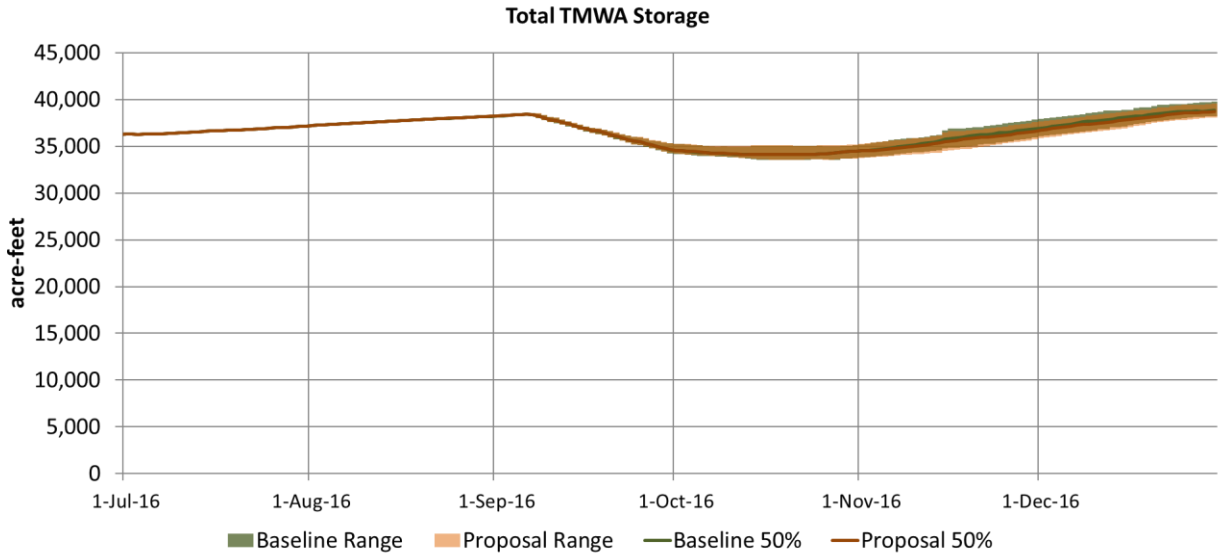

Figure 6. Ensemble Range of Total TMWA Storage Based on Changed Operations from the August 2016 TROA Coordination Meeting.

As a result, the flows in the Truckee River at the Nixon Gage were met for the same period between both operations, Figure 5,and the total stored water for the parties that moved water (TMWA and PLPT) resulted in losses that were modeled to be less than 0.1% of their total stored waters in deterministic modeling results (Table 1).

In the ensemble modeling results that give data for Figure 3 to Figure 6 the range of output showed that the median PLPT storage in the upper Truckee basin resulted in higher storage at the end of the Calendar Year and a decrease in overall TMWA Storage. The maximum

difference in storage from any of the ensemble modeling was a loss of less than 1% of the total storage (Table 2)

Table 1. Results of the Deterministic Model Run between the Baseline and Changed Operation from August 2016

Quantity	Baseline (Acre-Feet)	Proposed (Acre-Feet)	Difference (Acre-Feet)	% Change
Prosser Storage	6,462	6,480	19	0.29%
Donner Storage	3,570	3,571	0	0.00%
Total TMWA Storage	39,391	39,352	-39	-0.10%
Total PLPT Storage	70,296	70,269	-27	-0.04%
Nixon Volume to Date	196,028	196,030	2.0	0.00%

Table 2. Storage Difference and Percent Change of Storage Values for the 60% confidence interval of the ensemble modeling runs from the August 2016 TROA Coordination Meeting

Quantity	Storage Difference (Acre-Feet)			Percent Change (%)		
	80%	50%	20%	80%	50%	20%
Prosser Storage	27	16	63	0.42%	0.24%	0.80%
Donner Storage	0	0	0	0.00%	0.00%	0.01%
Total TMWA Storage	-128	-129	-168	-0.34%	-0.33%	-0.42%
Total PLPT Storage	152	448	-718	0.22%	0.63%	-0.97%
Nixon Volume to Date	-23	-172	787	-0.01%	-0.09%	0.38%

Overall the operation achieved the following results for each party.

- TMWA was able to exchange their water from Donner Lake to Boca Reservoir in the amount that was not necessary to meet the demand that the Floriston Rate could not meet.
- PLPT was able to meet their flow demands in the Truckee River at the Nixon Gage and resulted in a storage in the upstream Truckee basin reservoirs equal to the storage otherwise +/- 1%.
- California DWR was able to guarantee that Donner Lake storage levels would be as high as possible for a longer period of time in 2016 than they would have been otherwise.

All of this is the result of party negotiation that was based on the modeling of the Truckee Basin with regard to the Truckee River Operating Agreement.

Conclusion

The Truckee River Operating Agreement allows for the signatory parties of the agreement to have more flexibility in their operations. The TROA Operations Model and TROA Planning Model are tools for the parties to better understand their flexibility in operations under the agreement to better utilize their water for the benefit of their stakeholders. The common

modeling platform, that has been vetted by each party, allows for party discussion and negotiation over operations that may be complimentary or conflicting. The results of modeling efforts can be discussed with confidence that the use of a common modeling platform represents party interests and saves each party time and money. Through the use of the RiverWare© modeling tools, parties can more easily communicate and collaborate to meet their various complimenting and competing needs and achieve their objectives. The TROA parties have better negotiation and discussion power due to a common modeling platform, which saves time, money, and understanding the policy in the Basin.

In 2016, the first year of TROA implementation, a complex and beneficial operation, that was not possible before TROA implementation, was conducted where three parties negotiated an operation that satisfied each of the party's goals. The result was a satisfactory operation with one party incurring slightly higher evaporative losses as an impact. The operation was the result of parties using a commonly vetted model and coming to an agreement on the operation. This was the first of many operations allowed by TROA, negotiated by parties, and modeled to come to a satisfactory and agreed upon results that may not otherwise occur without a common model and a basin agreement.

References

Nevada Department of Conservation and Natural Resources, Division of Water Planning (DWP). 1999. Nevada State Water Plan Part 1, Section 8: Glossary on Selected Water-Related Decrees, Agreements, and Operating Criteria. pp 317-326.

Rieker, J.D. 2010. Testimony of Jeffrey D. Rieker before the California State Water Resources Control Board at a Hearing regarding Water Right Applications 31487 and 31488 by U.S. Bureau of Reclamation, Change Petition 5169 by Washoe County Water Conservation District, Change Petition 9247 by Truckee Meadows Water Authority, Change Petition 15673 by U.S. Bureau of Reclamation, and Change Petition 18006 by U.S. Bureau of Reclamation. June 29, 2010. 9 pp.

U.S. Department of the Interior and State of California (DOI and California). 2008. Final Environmental Impact Statement/Environmental Impact Report, Truckee River Operating Agreement, Alpine, El Dorado, Nevada, Placer, and Sierra Counties, California, Carson City, Churchill, Douglas, Lyon, Pershing, Storey, and Washoe Counties, Nevada. Prepared by Bureau of Reclamation, Fish and Wildlife Service, Bureau of Indian Affairs, and California Department of Water Resources.

U.S. Bureau of Reclamation (Reclamation). 2015. Truckee Basin Study. Basin Study Report. Sacramento, California. 702 pp.

River and Reservoir Operations using RiverWare within the Corps Water Management System (CWMS)

David Neumann, Senior Research Assistant, Center for Advanced Decision Support for Water and Environmental Systems, University of Colorado, Boulder, CO, david.neumann@colorado.edu
Edith Zagona, Research Professor and Director, Center for Advanced Decision Support for Water and Environmental Systems, University of Colorado, Boulder, CO, zagona@colorado.edu
Jennifer Short, Hydraulic Engineer, U.S. Army Corps of Engineers, Little Rock, AR, Jennifer.R.Short@usace.army.mil
Marc Sidlow, Hydraulic Engineer, U.S. Army Corps of Engineers, Albuquerque, NM, Marc.S.Sidlow@usace.army.mil
Matthew Wunsch, Hydraulic Engineer, U.S. Army Corps of Engineers, Tulsa, OK, Matthew.J.Wunsch@usace.army.mil
John Hunter, Civil Engineer, U.S. Army Corps of Engineers, Fort Worth, TX, John.M.Hunter@usace.army.mil

Abstract

RiverWare, a planning and operations modeling tool, is used by a number of USACE Districts for detailed multi-objective management of river and reservoir systems. For near-real time operations applications, RiverWare models are integrated into the suite of models, analysis and database tools provided by the Corps Water Management System (CWMS) such as HEC-MFP that simulates precipitation, HEC-HMS for modeling rainfall-runoff, HEC-RAS for detailed hydraulic analysis, and HEC-FIA for flood impact analysis. CWMS features a sophisticated control and visualization interface (CAVI) with a GIS integrated with model schematics, allows evaluation of operational alternatives, and manages data inputs, outputs and inter-model data transfers via a database. The CWMS architecture allows additional non-USACE models and customized computational tools to be tightly integrated via plugins; USACE Southwest Division has sponsored the integration of RiverWare into CWMS via this plugin mechanism. The RiverWare plugin allows RiverWare model objects, plots and data to be displayed in the CAVI, RiverWare models to be run in full integration with the other CWMS applications and database, and access to the native RiverWare software if needed.

This paper details the implementation of RiverWare models in the CWMS framework including data connections, data aggregation and disaggregation and the operator interaction with the tools. We will illustrate the features and functionality in a case study of a USACE model, the White River in Arkansas and Missouri, developed by Little Rock District. These models are used in the CWMS framework to assist water managers in making critical decisions on a day-to-day and hour-by-hour basis.

RiverWare is developed by the University of Colorado Center for Advanced Decision Support for Water and Environmental Systems (CU-CADSWES) under sponsorship of the Tennessee Valley Authority (TVA), U.S. Bureau of Reclamation (USBR), and U.S. Army Corps of Engineers (USACE) and distributed by the University of Colorado Office of Technology Transfer.

Introduction

RiverWare, a planning and operations modeling tool, is used by a number of U.S. Army Corps of Engineers (USACE) districts for detailed multi-objective management of river and reservoir systems. RiverWare is developed by the University of Colorado Center for Advanced Decision Support for Water and Environmental Systems (CU-CADSWES) under sponsorship of the Tennessee Valley Authority (TVA), U.S. Bureau of Reclamation (USBR), and USACE, and distributed by the University of Colorado Office of Technology Transfer.

A number of USACE districts have used RiverWare for many years for planning purposes, running period-of record models with proposed facility or operation changes to investigate the impact. Recently, some of these districts have developed near real-time operations models to simulate short term operations, primarily to determine how to schedule releases and movement of water during flood control operations. For near-real time operations applications, RiverWare models are integrated into the suite of models, analysis and database tools provided by the Corps Water Management System (CWMS). This suite consists of multiple models such as the Hydrologic Engineering Center's (HEC) Meteorological Forecast Processor (HEC-MFP) that simulates precipitation, Hydrologic Modeling System (HEC-HMS) for modeling rainfall-runoff, River Analysis System (HEC-RAS) for detailed hydraulic analysis, and Flood Impact Analysis (HEC-FIA) for detailed impacts analysis. CWMS features a sophisticated Control And Visualization Interface (CAVI) with a GIS integration of model schematics, allows evaluation of operational alternatives, and manages data inputs, outputs and inter-model data transfers via a database.

The CWMS architecture allows additional non-USACE models and customized computational tools to be tightly integrated via plugins. USACE Southwest Division has sponsored the integration of RiverWare into CWMS via this plugin mechanism. The RiverWare plugin allows RiverWare model objects, plots and data to be displayed in the CAVI, RiverWare models to be run in full integration with the other CWMS applications and database, and access to the native RiverWare software if needed.

This paper details the implementation of RiverWare models in the CWMS framework including data connections, data aggregation and disaggregation and the operator interaction with the tools.

We will illustrate the features and functionality in the context of the USACE's model of the White River in Arkansas and Missouri, developed by the Little Rock District. This model is used in the CWMS framework to assist water managers in making critical decisions on a day-to-day or hour-by-hour basis.

RiverWare Modeling

Some USACE districts have developed multi-objective RiverWare models of their systems geared toward planning applications. The purpose of these models is to compare a base run against a proposed change in facilities or operating policies with one or more sets of hydrological inputs. Avance (2010) and Daylor (2015) provide a good overview of the approach and the functionality modeled by the Southwestern Division (SWD). In general, the planning models attempt to minimize flooding throughout the network, especially at the key regulation control locations. The system flood evacuation plan calls for releases that evacuate the flood

storage as quickly as possible without causing flooding at downstream control points, while still balancing the system storage and tapering down the flows.

SWD has sponsored development of RiverWare functionality and methods including: disaggregation of local inflows from cumulative values; surcharge releases at reservoirs; regulation discharge computations to determine the available space at downstream control points; a system-wide flood control algorithm that computes flood control releases at all reservoirs while maintaining balanced storages and releasing flood pool water over the forecast period without flooding downstream control points; water supply and minimum flow releases computed to meet targets while balancing reservoir storage; and hydropower releases to meet system load. These simulation methods are each general and can be applied in various applications; but together they constitute a specific USACE modeling approach that can be implemented, in a template-like fashion, on other USACE basins.

The RiverWare modeling described above is geared toward planning studies, especially as implemented in the SWD. The model is typically run over the "Period of Record" consisting of 60-100 years of daily inflows, demands, and other hydrologic data. The rulebased simulation rule logic decides how much water to release on each timestep in the run based on the state of the system and assumed forecasts. There is no operator or user interaction within a run. In addition, many assumptions are made and data is aggregated to simplify the system. These simplifications are reasonable for planning when the purpose of the model is comparing one run to an alternative run. For example, in these planning models, reservoir release gate changes may be made each timestep when in reality, changes may be only made less frequently. These simplifying assumptions are valid over a Period of Record as the outflows will average over time.

Recently, the USACE has determined that the RiverWare models and interfaces could also be useful in short-term operations. In addition, many legacy tools have reached the end of their useful life and replacements are needed. Thus, some districts have converted, re-implemented, or developed sub-daily timestep models (1hr or 6hr) of their systems. Steffen (2015) describes a 6-hr model of the Arkansas River developed by the USACE Tulsa district for operation of the drawdown of reservoirs after a flood. This model implements the USACE approach and methods (like flood control and regulation discharge) but still allows overrides and operator judgement when necessary. Below, we describe another application on the White River in Arkansas and Missouri.

These RiverWare operations models are powerful by themselves, but become even more powerful when integrated with other USACE models that compute the inputs and process the outputs from the RiverWare models. The following section describes the Corps Water Management System, a framework that integrates many USACE models, including RiverWare to provide end-to-end modeling support.

CWMS Integration

The Hydrologic Engineering Center website states, "The Corps Water Management System (CWMS) is the automated information system used by the U.S. Army Corps of Engineers (USACE) to support its water control management mission." The system is "… used to derive the hydrologic response throughout a watershed area, including short-term future reservoir inflows and local uncontrolled downstream flows. The reservoir operation model flows are then processed to provide proposed releases to meet reservoir and downstream operation goals. Then, based on the total expected flows in the river system, river profiles are computed, inundated areas mapped, and flood impacts analyzed." (HEC Website 2018)

Thus, CWMS is a framework that integrates models together, moves data from one model to another, executes runs in order, manages data alternatives, and displays results in an easy to use interface. CWMS uses HEC-DSS as the intermediate data repository but can also extract data from the USACE Oracle database.

CWMS Architecture and Supported Models

The CWMS architecture allows additional non-USACE models and customized computational tools to be tightly integrated via a plugin architecture. Each model is essentially an independent plugin that can be inserted into the framework as needed.

Some of the supported models include:

- HEC-MFP – Precipitation analysis
- HEC-MetVue – Precipitation analysis
- HEC-HMS – Rainfall runoff
- HEC-ResSim – Reservoir Modeling
- RiverWare – River and reservoir modeling
- HEC-RAS – Flood inundation and hydraulic analysis
- HEC-FIA – Flood Impacts Analysis

RiverWare Functionality in CWMS

RiverWare was implemented as a plugin to CWMS through funding from the USACE-SWD. It consists of the "CWMS RiverWare Plugin" that is freely available on the RiverWare.org website. The user copies this set of files into the CWMS installation directory and modifies a few text files indicating that they wish to use this plugin.

Note, CWMS is only available to USACE offices, but the Hydrologic Engineering Center's (HEC) Real Time Simulation (HEC-RTS) software is based on the CWMS software for use by non USACE offices. Below we will reference the HEC-RTS documentation as that is publicly available, whereas the CWMS documentation is not.

CWMS features a sophisticated Control And Visualization Interface (CAVI) with a GIS integration of model schematics, allows evaluation of operational alternatives, and manages data inputs, outputs and inter-model data transfers via a database. All of the CWMS functionality will not be discussed here, as that is provided in the user manual (Real-Time Simulation User's Manual, 2017).

Each model/application implemented in CWMS requires the modeler to do the following:

- Specify the name of the model file to use
- Specify which pieces of data are to be extracted from a database and which will be provided by models earlier in the run sequence
- Specify which pieces of data are to be written to the DSS database for use by models later in the run sequence
- Configure the order of model runs
- Choose a naming convention for the HEC-DSS database

The majority of the RiverWare plugin's functionality is accessed via general mechanisms that apply to all models, as described in the user manual. However, when the modeler imports a

RiverWare model, the plugin presents a dialog to configure how RiverWare will work in the system. The following is the list of configurations:

- Specify the model alternative name
- Select the model file. For rulebased simulation models, the policy (global function sets and ruleset) must be saved within the model file
- Specify the input and output Data Management Interface (DMI) names
- Specify which RiverWare System Control Tables to show
- Specify which RiverWare Plots, Output Canvasses, and Scripts to show
- Choose which RiverWare Policy Language Sets (often the rules) are available from the CAVI

Operator Interactions

Once configured, the RiverWare object icons display in the CAVI map. Based on the configuration, the following RiverWare dialogs are directly accessible from CAVI buttons and right-click context menus:

- RiverWare Policy Language (RPL) editors
- System Control Tables (SCT)
- Plot Page dialogs
- Chart dialogs
- Output Canvas dialogs
- Script Dashboard dialogs
- Open Object dialogs. **Figure 1** shows one sample way to access this dialog from the right-click context menu on the CAVI maps
- Diagnostic Output dialog
- The RiverWare workspace (from which all RiverWare dialogs are available)

As noted in the last bullet, the RiverWare workspace, or standalone model, once opened can then open any other RiverWare dialog. This allows the modeler to easily access the common dialogs, but also access any other dialog as needed.

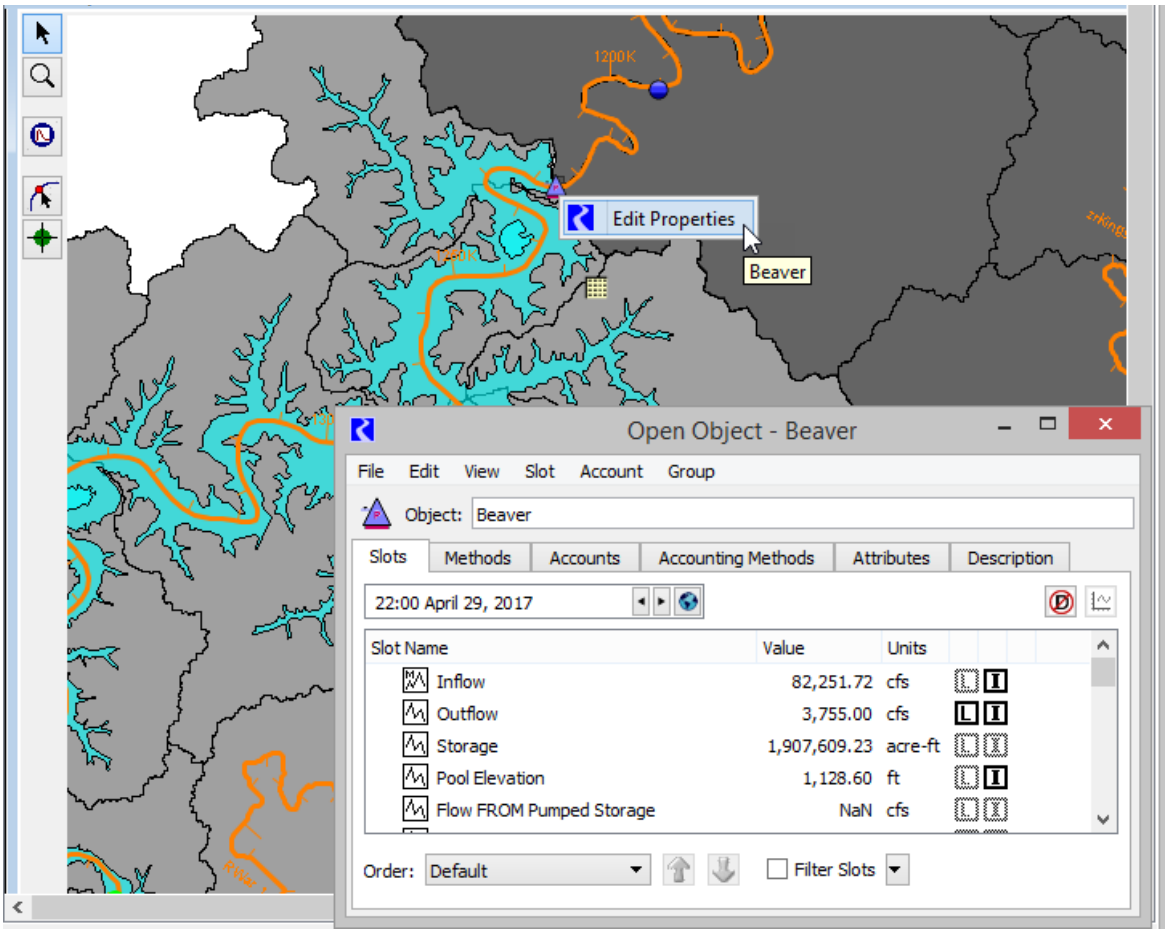

Figure 1. CAVI Setup map showing access to the RiverWare objects

Model Timesteps

Frequently, meteorological and rainfall-runoff modeling is performed at a very small timestep size, often 5 minute, 15 minute or 1 hour, while Reservoir operations are managed and modeled at larger timesteps, often 6 hour or 1 day. Flood hydraulic analysis is often performed at smaller timesteps as well. As a result, the framework must support running RiverWare models at timesteps that are different, often larger, than the other models.

The CAVI instructs RiverWare to start a run by calling the RiverWare plugin. The CAVI provides the run time window which includes the CAVI run timestep, start date and end date. The plugin passes the timestep to RiverWare, which enables RiverWare to check that the timestep is compatible with the RiverWare timestep. The assumption is that CWMS has a smaller timestep which falls on the larger RiverWare model timestep. If the timesteps are compatible, the plugin can then start the run.

Because of the potential timestep mismatch between the CAVI and the RiverWare run, there must be tools to aggregate and disaggregate data between models. In the currently proposed approach, this is performed within the RiverWare model using RiverWare aggregation and disaggregation functions and slot utilities. Time aggregation RPL functions aggregate data from small timestep custom slots to a larger timestep slot on the simulation objects. The run is then made. At the end of the run, recently developed Time Disaggregation Series Slot transform the specified results into the required small timesteps using the desired disaggregation functions,

including a step function or interpolation. These disaggregated values are stored on custom slots which can be exported to the DSS file for use in subsequent models within CWMS.

Case Study

This section describes a case study of CWMS on the White River basin in Arkansas and Missouri that incorporates a RiverWare model.

White River in Arkansas and Missouri

The following section describes the use of CWMS and RiverWare in the White River basin.

Basin Background: The White River consist of five multipurpose reservoirs: Beaver, Table Rock, Bull Shoals, Norfork and Greers Ferry. The operational authorizations are flood control, hydropower, water supply, recreation and environmental stewardship. The CWMS model was primarily developed for the flood control operations. The flood operation of the upper four-lake system, Beaver, Table Rock, Bull Shoals and Norfork, is constrained by regulation points at Batesville and Newport. In addition, Greers Ferry releases flow into the Little Red River and has a regulation point of Judsonia and Georgetown. There is a large uncontrolled drainage area from both the Black and White Rivers to Newport and Georgetown. This means that all of the reservoirs in the system have to hold water for long periods of time and often enter into an induced surcharge operation to maximize flood storage available. The system is operated to prevent flooding at the regulation points and then to evacuate the flood control pool as quickly as possible in a balanced and controlled fashion.

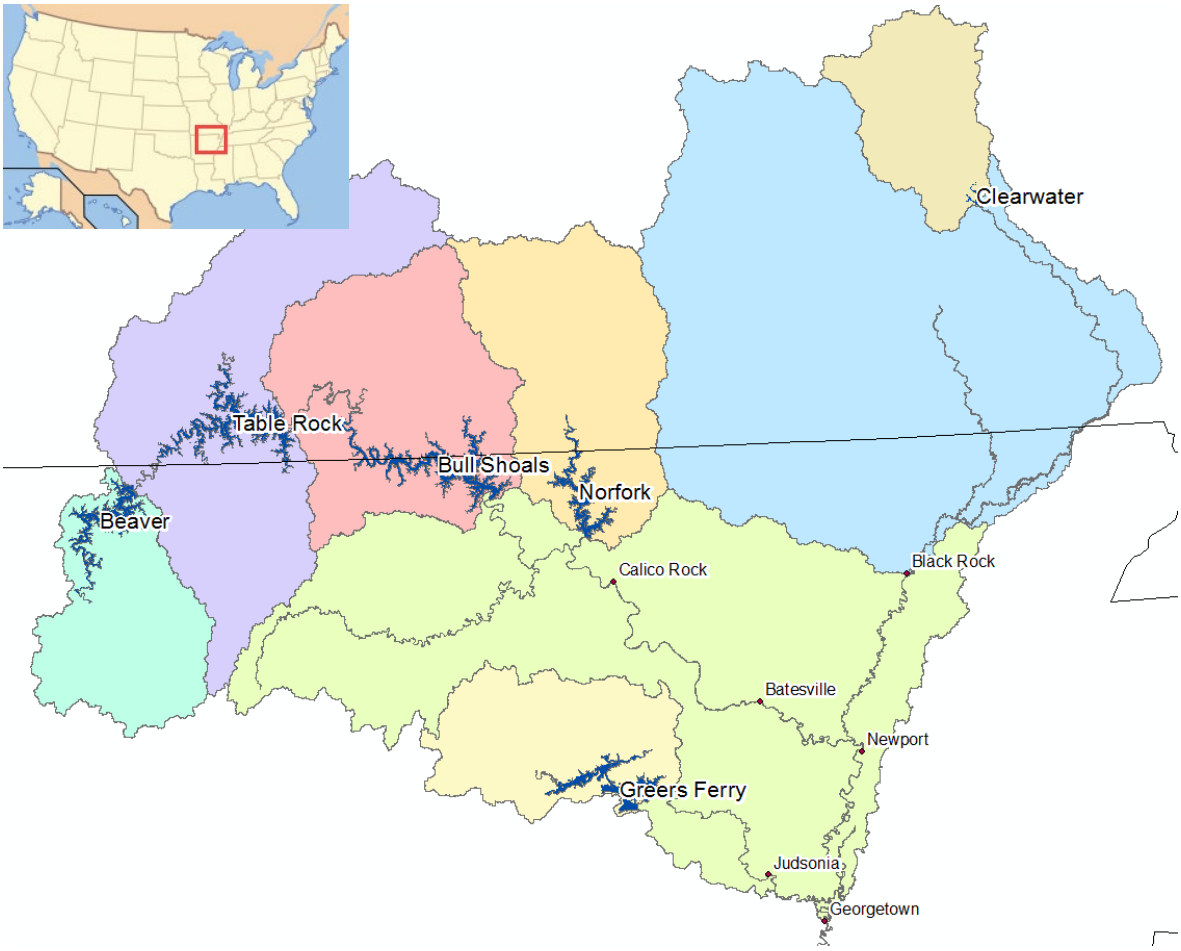

Figure 2. Map of White River Basin

CWMS Implementation: Within the Little Rock District, HEC-MFP or HEC-MetVue is used to view and analyze the rainfall and send it to a rainfall-runoff model HEC-HMS. The HEC-HMS model is then run to forecast the inflows into all of the reservoirs and local areas. The flows are sent into a RiverWare reservoir operation model to determine the release plan. Then the final release plan is sent to HEC-RAS, as needed, to develop water depth and inundation graphs. The results of HEC-RAS can be sent to HEC-FIA for impacts analysis.

The White River basin RiverWare model was developed concurrently with the HEC-HMS and other models implemented in CWMS. As a result, the district had the luxury of developing the RiverWare model to exactly match the layout and naming convention of the other models, particularly the HMS model, in the system. Although there are mapping tools within RiverWare data management interfaces, it is easiest for debugging and comparison between models if the names and locations map directly between models.

Example Operation: This section describes a sample operation to show how the CWMS and RiverWare model was used to operate the system during a sample precipitation event.

During April 28th to May 10th 2017, the White River system had repeated precipitation events ranging from 3 inches to 15 inches throughout the basin, with the majority of the rainfall in the basin averaging 9-10 inches of rain.

To operate the system, the first step in the process is to open CWMS and define a new “forecast” to set up the run ranges for all of the models.

Next, CWMS is run to “Compute all Models”. In order, each model:

1. Runs an “Extract” to import any required timeseries data from the USACE Oracle database.
2. Imports all required data from the CWMS DSS file that was computed by upstream models
3. Simulates
4. Exports specified results to the CWMS DSS file.

Once RiverWare is run, the district operators look at the results in CWMS. This section will focus on the RiverWare results. The operators access the preconfigured plot dialogs, object dialogs, rules, System Control Tables, and other output devices directly from CWMS. **Figure 2** shows a sample view of the White River CAVI with the Modeling tab displayed. Highlighted are the RiverWare actions to open dialogs. The arrows show the dialogs that are opened.

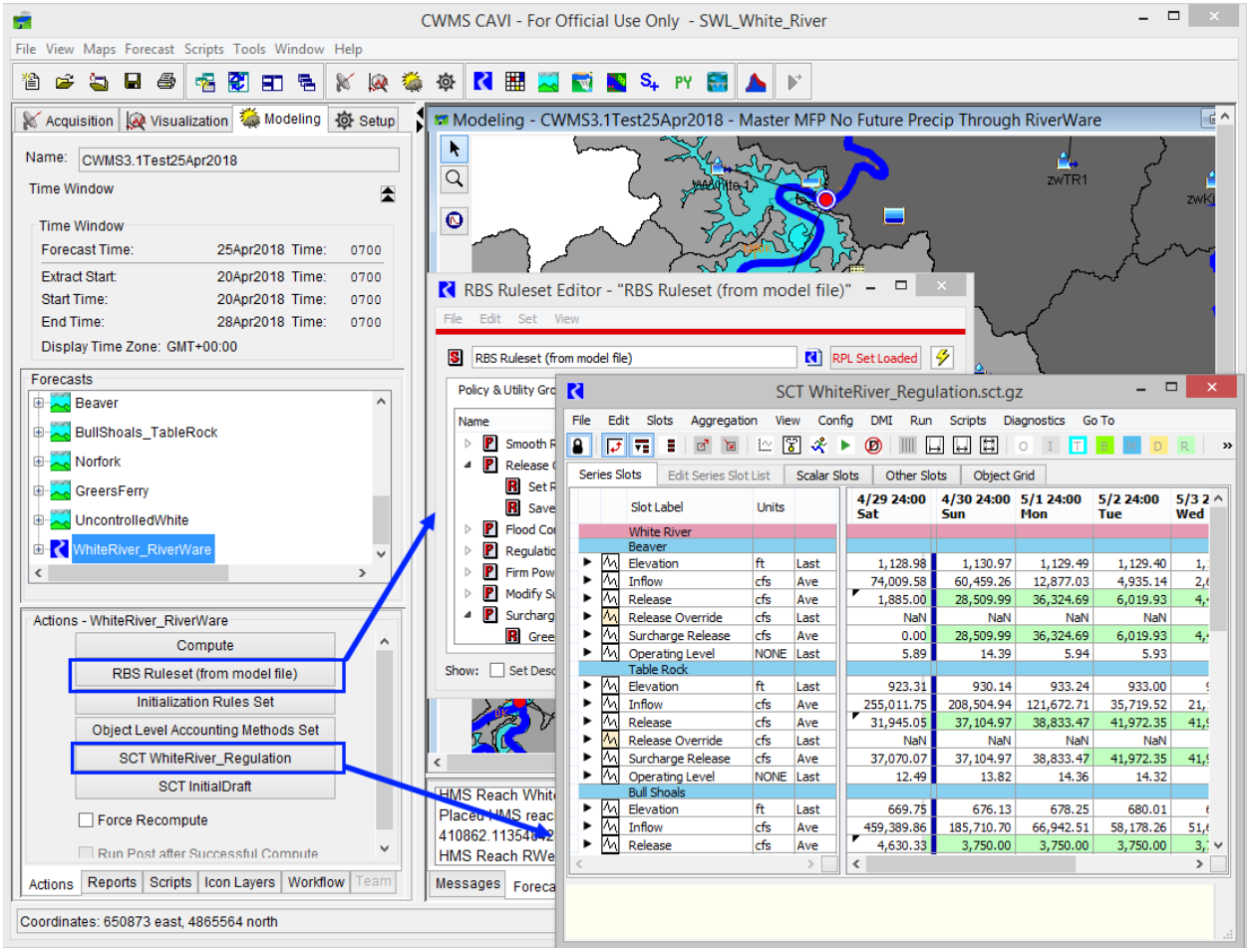

Figure 3. Screenshot of the CAVI modeling tab with RiverWare actions highlighted with their associated dialogs

At this stage, RiverWare has computed an answer, but the model has perfect foresight; it knows the inflows coming into the lake for the next several days, exactly. The real world is imperfect, with inaccuracies and limitations, which is where engineering judgement comes in; operation still requires engineers to regulate the lakes.

The following are tools that have been created to help aid in the process of making changes to the release schedules, and to aid the regulators in making their release decisions.

The regulators can adjust many items including:

- Precipitation forecasts and running the entire suite again
- Changing inflows and re-running just RiverWare
- Changing targets and re-running RiverWare
- Turning on or off rules depending on the situations and rerunning RiverWare
- Changing reservoir releases due to unexpected conditions or requirements and rerunning RiverWare.

For the storm in question shown in **Figure 2**, the black line shows the release that RiverWare developed. The blue line represents the pool elevation. The solid red line shows the top of the flood pool. So this rainfall event raised the pool above the top of the flood pool and into the surcharge pool.

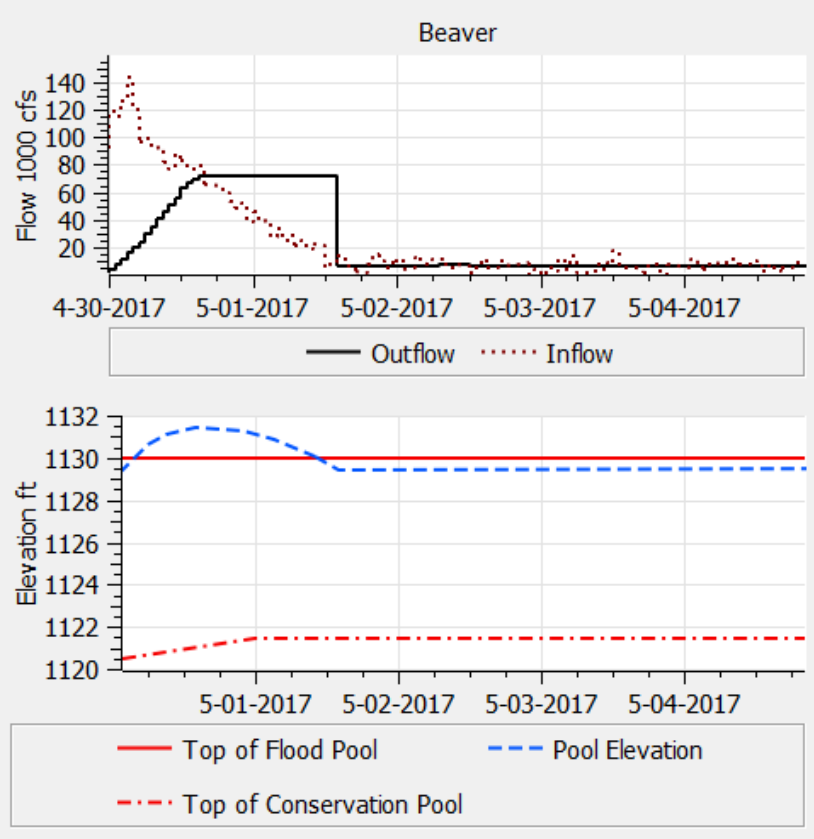

Figure 4. Plot of raw results from RiverWare

Notice, on April 30th, the Outflow changes each timestep as it is ramped up to 70,000 cfs. The project personnel will not appreciate if asked to make a gate change every single hour, unless absolutely necessary. To adjust this, the operator opens a saved System Control Table (SCT) to view and modify data.

The SCT is a customizable view of the data in the RiverWare model. The operator can organize the data as they like and have one or more SCTs open at a time. Operators report that the SCT helps guide them in their engineering decisions; they can quickly see the data they need to see in one place and can color code cells based on the values. **Figure 3** shows a sample SCT displaying an hourly timestep. It can also be configured to show aggregated daily values. Color alerts are

shown in red, indicating that regulations limits downstream at Newport and Georgetown have been exceeded.

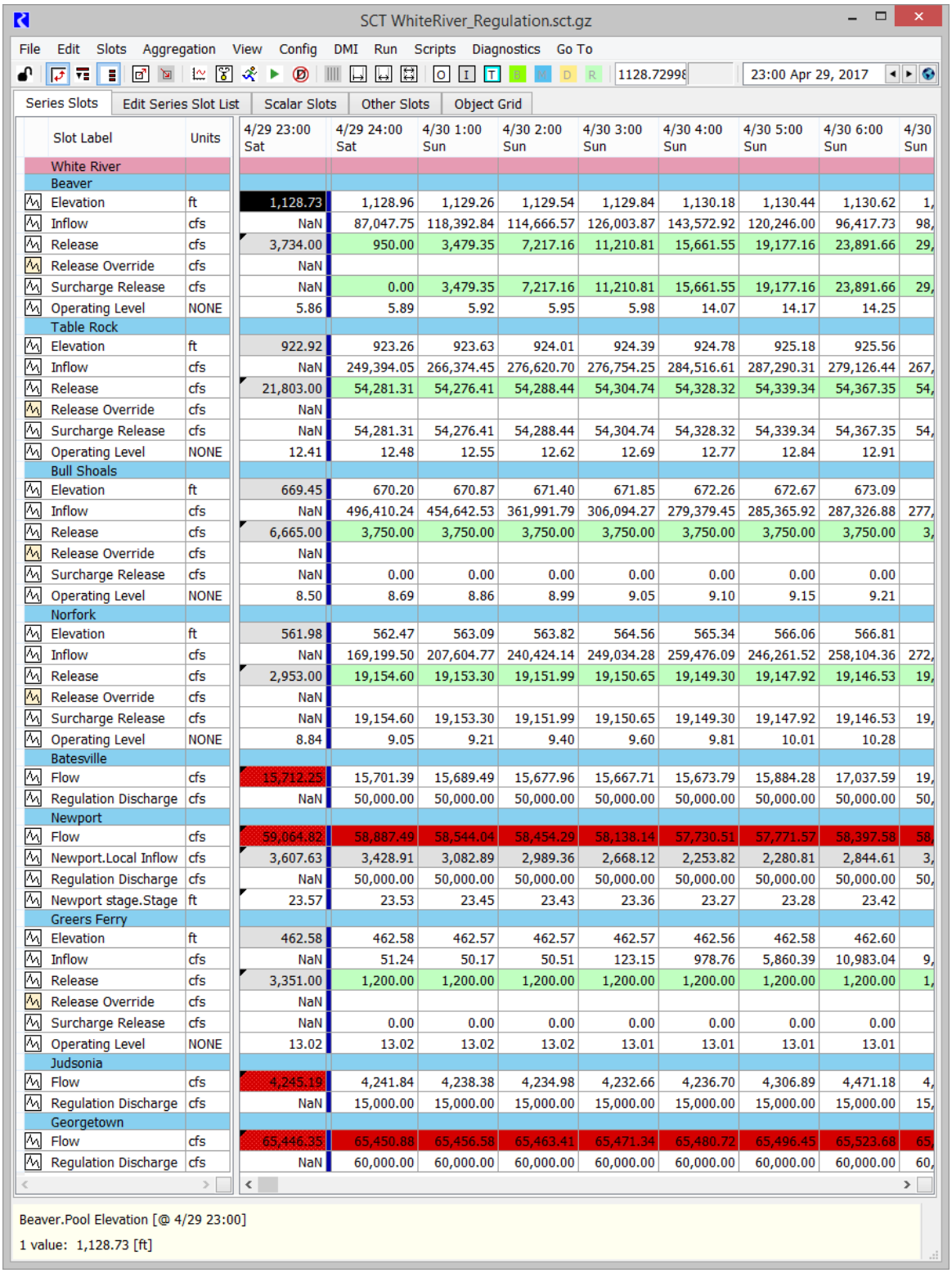

Slot Label	Units	4/29 23:00 Sat	4/29 24:00 Sat	4/30 1:00 Sun	4/30 2:00 Sun	4/30 3:00 Sun	4/30 4:00 Sun	4/30 5:00 Sun	4/30 6:00 Sun	4/30 Sun
White River										
Beaver										
Elevation	ft	1,128.73	1,128.96	1,129.26	1,129.54	1,129.84	1,130.18	1,130.44	1,130.62	1,
Inflow	cfs	NaN	87,047.75	118,392.84	114,666.57	126,003.87	143,572.92	120,246.00	96,417.73	98,
Release	cfs	3,734.00	950.00	3,479.35	7,217.16	11,210.81	15,661.55	19,177.16	23,891.66	29,
Release Override	cfs	NaN								
Surcharge Release	cfs	NaN	0.00	3,479.35	7,217.16	11,210.81	15,661.55	19,177.16	23,891.66	29,
Operating Level	NONE	5.86	5.89	5.92	5.95	5.98	14.07	14.17	14.25	
Table Rock										
Elevation	ft	922.92	923.26	923.63	924.01	924.39	924.78	925.18	925.56	
Inflow	cfs	NaN	249,394.05	266,374.45	276,620.70	276,754.25	284,516.61	287,290.31	279,126.44	267,
Release	cfs	21,803.00	54,281.31	54,276.41	54,288.44	54,304.74	54,328.32	54,339.34	54,367.35	54,
Release Override	cfs	NaN								
Surcharge Release	cfs	NaN	54,281.31	54,276.41	54,288.44	54,304.74	54,328.32	54,339.34	54,367.35	54,
Operating Level	NONE	12.41	12.48	12.55	12.62	12.69	12.77	12.84	12.91	
Bull Shoals										
Elevation	ft	669.45	670.20	670.87	671.40	671.85	672.26	672.67	673.09	
Inflow	cfs	NaN	496,410.24	454,642.53	361,991.79	306,094.27	279,379.45	285,365.92	287,326.88	277,
Release	cfs	6,665.00	3,750.00	3,750.00	3,750.00	3,750.00	3,750.00	3,750.00	3,750.00	3,
Release Override	cfs	NaN								
Surcharge Release	cfs	NaN	0.00	0.00	0.00	0.00	0.00	0.00	0.00	
Operating Level	NONE	8.50	8.69	8.86	8.99	9.05	9.10	9.15	9.21	
Norfork										
Elevation	ft	561.98	562.47	563.09	563.82	564.56	565.34	566.06	566.81	
Inflow	cfs	NaN	169,199.50	207,604.77	240,424.14	249,034.28	259,476.09	246,261.52	258,104.36	272,
Release	cfs	2,953.00	19,154.60	19,153.30	19,151.99	19,150.65	19,149.30	19,147.92	19,146.53	19,
Release Override	cfs	NaN								
Surcharge Release	cfs	NaN	19,154.60	19,153.30	19,151.99	19,150.65	19,149.30	19,147.92	19,146.53	19,
Operating Level	NONE	8.84	9.05	9.21	9.40	9.60	9.81	10.01	10.28	
Batesville										
Flow	cfs	15,712.25	15,701.39	15,689.49	15,677.96	15,667.71	15,673.79	15,884.28	17,037.59	19,
Regulation Discharge	cfs	NaN	50,000.00	50,000.00	50,000.00	50,000.00	50,000.00	50,000.00	50,000.00	50,
Newport										
Flow	cfs	59,064.82	58,887.49	58,544.04	58,454.29	58,138.14	57,730.51	57,771.57	58,397.58	58,
Newport.Local Inflow	cfs	3,607.63	3,428.91	3,082.89	2,989.36	2,668.12	2,253.82	2,280.81	2,844.61	3,
Regulation Discharge	cfs	NaN	50,000.00	50,000.00	50,000.00	50,000.00	50,000.00	50,000.00	50,000.00	50,
Newport stage.Stage	ft	23.57	23.53	23.45	23.43	23.36	23.27	23.28	23.42	
Greers Ferry										
Elevation	ft	462.58	462.58	462.57	462.57	462.57	462.56	462.58	462.60	
Inflow	cfs	NaN	51.24	50.17	50.51	123.15	978.76	5,860.39	10,983.04	9,
Release	cfs	3,351.00	1,200.00	1,200.00	1,200.00	1,200.00	1,200.00	1,200.00	1,200.00	1,
Release Override	cfs	NaN								
Surcharge Release	cfs	NaN	0.00	0.00	0.00	0.00	0.00	0.00	0.00	
Operating Level	NONE	13.02	13.02	13.02	13.02	13.01	13.01	13.01	13.01	
Judsonia										
Flow	cfs	4,245.19	4,241.84	4,238.38	4,234.98	4,232.66	4,236.70	4,306.89	4,471.18	4,
Regulation Discharge	cfs	NaN	15,000.00	15,000.00	15,000.00	15,000.00	15,000.00	15,000.00	15,000.00	15,
Georgetown										
Flow	cfs	65,446.35	65,450.88	65,456.58	65,463.41	65,471.34	65,480.72	65,496.45	65,523.68	65,
Regulation Discharge	cfs	NaN	60,000.00	60,000.00	60,000.00	60,000.00	60,000.00	60,000.00	60,000.00	60,

Figure 5. Sample SCT used to operate the White River

In the sample operation, the operator modifies the release in the "Release Override" slot on Beaver. These values are then applied to the reservoir object's Outflow by a rule. The operators start off with a small gate change and slowly open up in about 3 gate changes to 56,000 cfs. With this override set, the modeler reruns the RiverWare model by clicking "Compute" within the CAVI. The resulting outflow and elevations are shown in **Figure 3**.

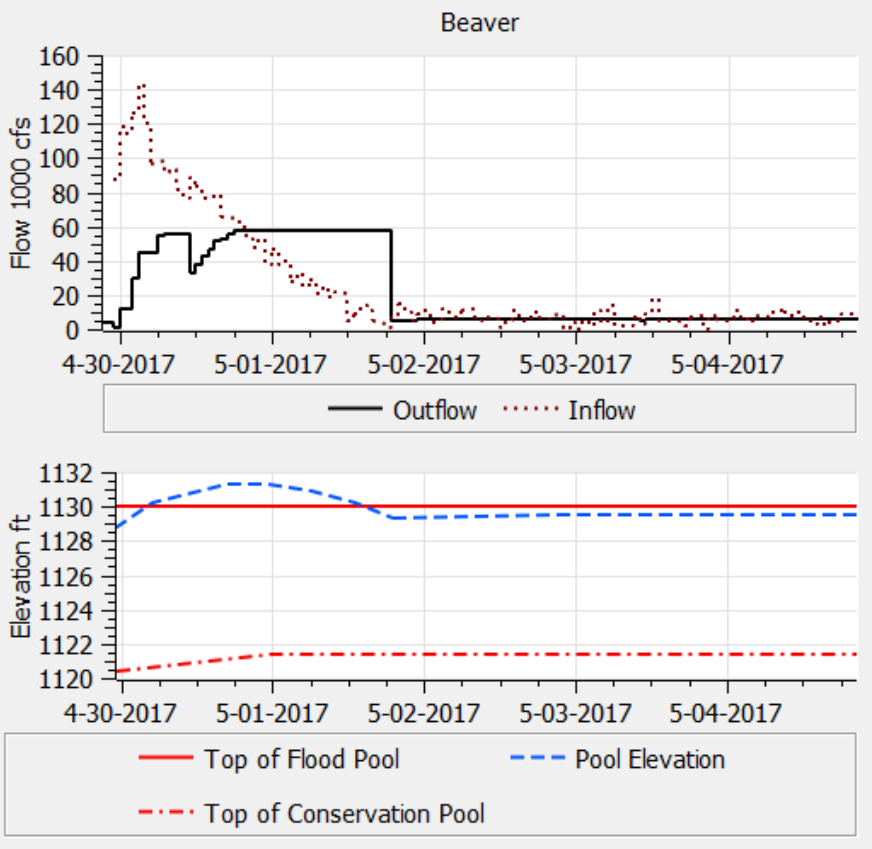

Figure 6. Plot of results from RiverWare after the first set of changes

After the overrides, the RiverWare rules shut back to around 35,000 cfs and then increase outflows back up to 60,000 cfs. This is because there is a rule executing to calculate the induced surcharge curve at Beaver. Part of the purpose for Beaver reservoir is to hold water and keep it out of Table Rock Lake. This reservoir is the last reservoir to empty on the White River and sometimes needs to hold water. The induced surcharge curve represents the flow that has to be released at this elevation. The operators typically like to make releases before this surcharge elevation, which will allow it to cut off the peak release. But the rule results show the operators how long they can hold flows at Beaver and what the peak release will be. In this operation, it is more beneficial to turn this rule off and rerun the model and see the results. **Figure 4** shows the results when turning off the induced surcharge rule and re-running the model.

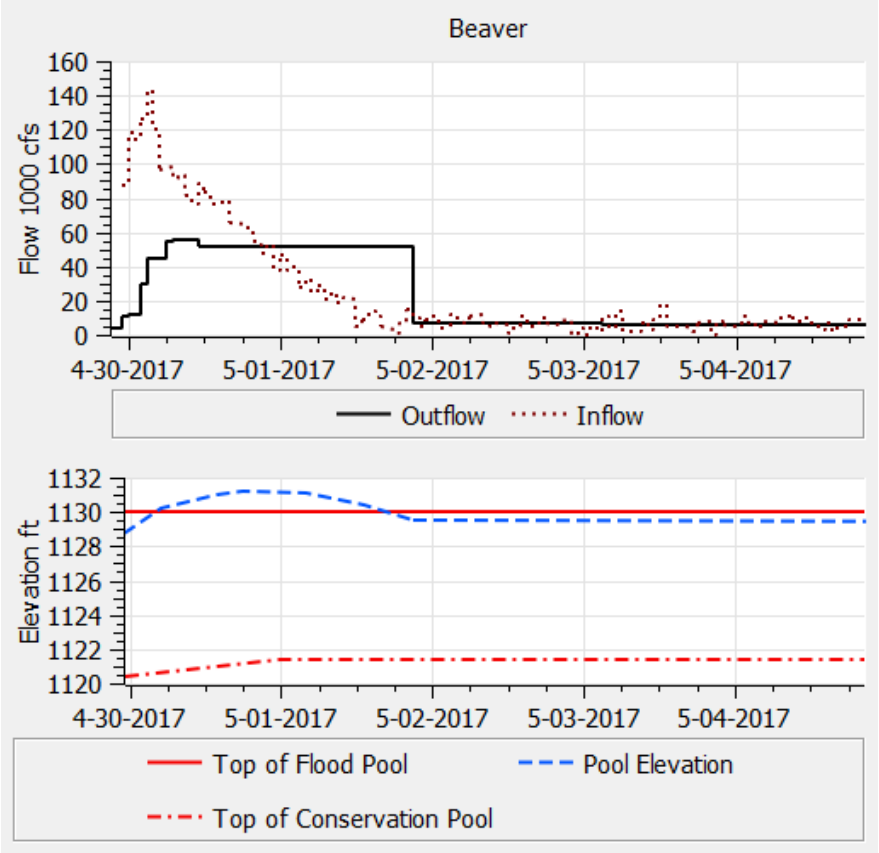

Figure 7. Plot of results from RiverWare after disabling the induced surcharge rule

With the initial opening overrides in place, the operations rules then hold the release until the pool is about 0.5 ft below the top of the flood pool, and then shut backs. This final shut back from 56,000 cfs to 11,500 cfs is still too dramatic. Additional rules were not added to refine the shut back because they are dependent on a variety of variables that engineering judgment is needed to evaluate. The final change is to put in small gate changes. This leads to an operation where the outflow is held at 56,000 cfs and then cut back in two gate changes to 11,500 cfs.

The final results are shown in **Figure 5**. The operations look reasonable and are provided to the dam operators who actually implement the change for the next few timesteps. During an extreme flood, the system is operated on a 24 hr basis, with the model run every few hours and gate changes made as frequently as needed. For smaller floods, the system is monitored and models are updated as necessary.

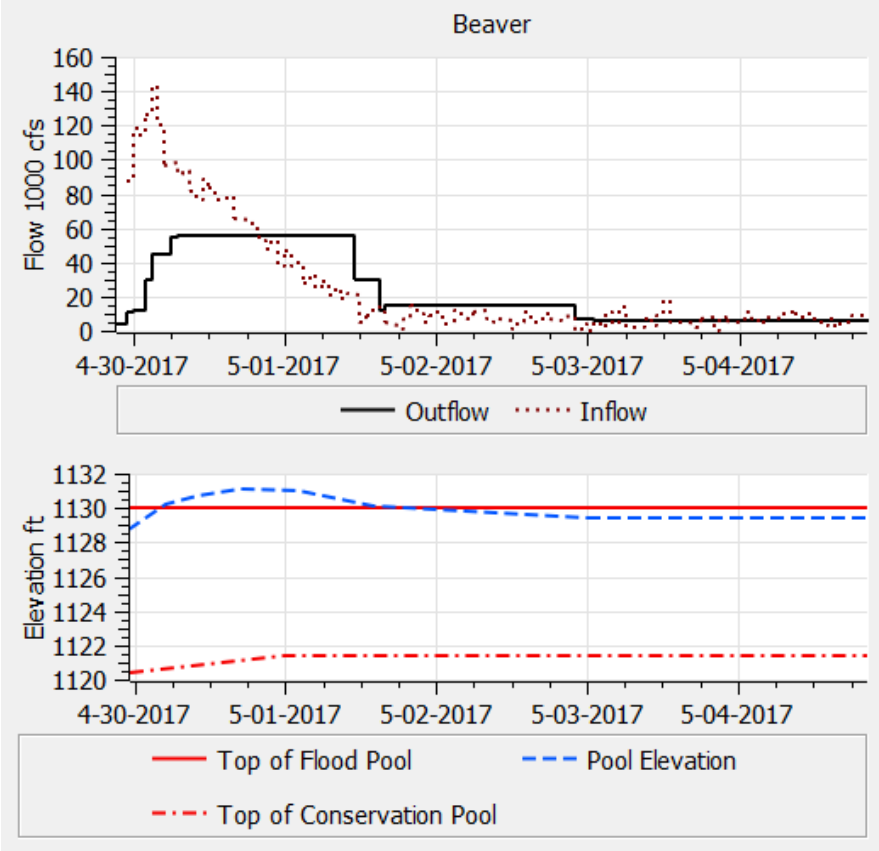

Figure 8. Plot of results from RiverWare after final overrides

Conclusions based on this operation: As we have shown, RiverWare and CWMS are tools to help make decisions. In a real time flood situation, these will never replace the engineering judgment required to operate a complex system like the White River. The benefit of having RiverWare in CWMS is that the operations process is much more automated and easy to use with nice graphical interfaces and stream-lined processes. RiverWare gives regulators a good starting point for a release plan, and reduces the time spent developing the release plan. It also allows them options to quickly compare different general release scenarios by turning rules on or off. With engineering judgment still needed to come up with the final plan. Now the operators can spend time making engineering decisions, not processing data and performing manual manipulation. Instead CWMS has automated many of these steps.

References

Avance, A., J. Daylor, J. Cotter, D. Neumann, and E. Zagona (2010). "Multi-object Modeling in RiverWare for USACE-SWD." In *Proc. of the Fourth Federal Interagency Hydrologic Modeling Conference*, Las Vegas, Jun 27 – Jul 1, 2010

Daylor, J., Neumann, D., Zagona, E., and Steffen, J., (2015). "Multi-objective Modeling in RiverWare for USACE-SWD." In *Proc 3rd Joint Federal Interagency Conference on Sedimentation and Hydrologic Modeling*, April 19-21, 2015, Reno, Nevada, USA.

HEC Website: http://www.hec.usace.army.mil/cwms/cwms.aspx, accessed 12/2018.

Real-Time Simulation (HEC-RTS) User's Manual, (2017), Hydrologic Engineering Center, http://www.hec.usace.army.mil/software/hec-rts/documentation/HEC-RTS_UsersManual_3.0.3.pdf

Steffen, J., Stringer, J., Daylor, J, Neumann, D. and Zagona, E. (2015). "TAPER – A Real-time Decision Support Tool for Balanced Flood Operation of the Arkansas River in Tulsa District." In Proc 3rd Joint Federal Interagency Conference on Sedimentation and Hydrologic Modeling, April 19-21, 2015, Reno, Nevada, USA.

The Arkansas Basin RiverWare Model

Todd Vandegrift, MS, PE, Project Manager, Precision Water Resources Engineering, Loveland, CO, todd@precisionwre.com
Shane Coors, MS, PE, Principal, Precision Water Resources Engineering, Loveland, CO, shane@precisionwre.com

Extended Abstract

A RiverWare® model has been developed that simulates the Arkansas River basin's water resource system from the headwaters near Leadville, Colorado to the Kansas state line on a daily timestep and at a high level of detail. The model can support many potential water management functions for a wide range of stakeholders, ranging from long-term planning, policy development, and water supply evaluations, to short-term operational forecasting, administration support, scheduling, and coordination between parties. Because the basin's policy and operational procedures are complex, contentious, and continuously changing, maintaining flexibility and transparency were key objectives throughout the development of the model. During the presentation, the model will be introduced, the process of validating its results will be surveyed, and the range of water management questions in the Arkansas River basin that this model can help address will be outlined.

The Arkansas basin's native water supplies and several transbasin import projects, including Reclamation's Fryingpan-Arkansas Project, are relied upon by many water users including municipalities such as Colorado Springs and Pueblo, CO, industrial users, and over 400,000 acres of irrigated agriculture. The water resource system is remarkably complex and multifaceted, including integrated operations and detailed accounting throughout many reservoirs, centering on the 357,000-acre-foot Pueblo Reservoir. With limited and highly variable water supplies and growing and changing demands, water is an incredibly valuable resource in the basin. Reliable supply sources, even those yielding relatively small but consistent amounts of water, are worth millions of dollars. In such a water tight system, the ability to appropriately and accurately answer water management questions and estimate the impacts of changes is vital to the continued success of both individual entities and the overall system.

The Arkansas basin's real-world administration and operations demand and depend on an incredibly detailed water accounting and sub-accounting system. Dozens of users with shared and individual water supply sources and demands operate independently and jointly throughout the system. To ensure adequate water supply across variable hydrologic conditions, entities often have multiple water supply sources and storage locations throughout the basin and move their water around the basin with various physical and accounting mechanisms, such as releases, diversions, different types of exchanges, and trades with other entities. Still, other entities don't themselves own direct sources and must instead lease surplus water from others at highly variable costs.

Water supply sources can include collections of direct flow and storage water rights of assorted priorities, transbasin import projects, and reusable return flows that are generated from the delivery of fully consumable water types and recaptured through various mechanisms. The yields of many water supply sources are highly dependent on hydrologic conditions and can vary enormously from one year to the next. Many current water rights have been changed since their

original decree to allow for different uses or alternative diversion or storage locations, however water right change decrees typically contain detailed requirements, limits, and criteria meant to prevent negative impacts to other water rights. These types of complexities necessitate the detailed accounting systems that are used to distinguish and individually track many different classifications of water, or "water types", that may each be subject to unique and dynamic limits, rules, and requirements that have real impacts on individual systems.

While some sources are independently owned and operated, many supply sources, such as a canal company's water rights or a reservoir's storage rights (and storage space), are shared and jointly operated between multiple parties with yields being divided by share ownership percentages. However, these parties may have very different end uses and locations for their share of the yields, different mechanisms for moving water, and/or different other uses for their portion of a storage account's total space.

In a bottom-up manner, the Arkansas basin's overall conditions and operations emerge as the collective result of the many subsystems operating within it according to their own unique objectives, constraints, and rules. Due to these types of complexities, simulating the complex policy, accounting, and operations of the basin in an accurate, detailed, but practicable manner presents numerous challenges and necessitates creative and innovative modeling solutions.

Due to the system's complex and dynamic nature, past modeling efforts in the basin have been relatively limited in scope, applicability, and transferability. Many entities' individual systems span large areas of the basin and are interdependent with other entities' systems, but past models have tended to focus on individual systems alone and have had limited ability to account for the changing operations of others and the ensuing variations in conditions throughout the basin. However, since those changes can have significant impacts on the yields and operational constraints of individual systems, not appropriately accounting for them has presented significant limitations. Additionally, previous models were tied inextricably with historical hydrology, policies, and operations making it difficult to simulate the effects of non-historic hydrology and/or updated policy and operational procedures. Furthermore, other models have generally lacked transparency, obscuring how particular results were reached and limiting the ability for in-depth analysis of why the simulated system acted the way it did and how the effects of various changes can propagate through the system.

The Arkansas Basin RiverWare model is different. The foundation of the Arkansas basin's water supply system is Colorado's prior appropriation water rights system, and thus RiverWare's powerful water rights solver is employed on each timestep to allocate native flow to hundreds of direct flow and storage water rights. Subsequently, the model simulates many operational layers including the Fryingpan-Arkansas Project and other imports, multi-purpose and integrated reservoir operations and storage deliveries, the basin's multi-party Winter Water Storage Program, and numerous exchanges, trades, and accounting transactions. These processes are explicitly and dynamically simulated using customized RiverWare rules that mimic the real world operational decision-making processes. Consequently, the model captures the effects of interdependent operations of various entities under changing basin conditions, as well as subsequent, indirect effects that can propagate throughout the system. Furthermore, this simulation process is very transparent and model results can be traced down to the individual, intuitive calculations and logical decisions made by the model's rules.

Additionally, due to the way that simulated operations are "layered on" by the model's rules, various "mid-timestep" solutions are also created that further enhance model transparency and understanding. The full network initially solves early within each timestep as the model's rules are executed. The first "mid-timestep" solution, referred to as the "native flow solution", is achieved after water right allocation is simulated, water user diversions are set to their allocated direct flow water right supplies only, and reservoir releases are set to their "native passthrough" amounts. This initial, temporary solution represents what the system conditions would look like on that day if no other operations were to occur. Next, the operational rules fire one-by-one and adjust the previously solved network appropriately to reflect their simulated operations. For example, a "deliver from storage" rule will evaluate a water user's total daily diversion demand and their daily water right allocation, and their storage available for delivery from one or more storage sources. If needed, the rule will execute a delivery from storage to supplement native water right diversions and meet its full demand. This delivery is layered on to the previous network solution by increasing the reservoir's release and the water user's diversion by the same amount, as well deducting that amount from the appropriate storage account in the reservoir. After the rule fires, the full network will re-solve based on the changes applied and represent the system with that storage delivery being made, resulting in increased flows in the reaches between the reservoir and water user. Another common operation simulated by the model is an exchange of water from a diversion into a reservoir's storage, which a rule executes by reducing a reservoir release and downstream water user diversion by like amounts, thus "holding back" the water in the reservoir and transferring to the appropriate storage account. When an exchange like this is executed and the network re-solves, it will cause flows to decrease in the reaches between the reservoir and water user. These kinds of exchanges are typically subject to many criteria and limits (e.g., minimum flow requirements) that can be challenging to simulate, however this step-by-step rulebased process allows for transparent "pre-exchange" and "post-exchange" solutions that greatly facilitate the simulation of multiple, complex exchanges.

Managing the simulated level of detail throughout the complex system also presented a significant challenge. To address this, the model was designed to allow for variable levels of detail, allowing for detailed representation where necessary while not requiring it where it is not yet necessary or practicable. The various subsystems and storage accounts and subaccounts of entities are designed in a modular sense to allow for continued refinement and adaptation to meet variable needs. For example, the storage accounting of one water owner may track specific water types in detail though another's may all be simply lumped together, and robust rule logic accounts for the disparity and still allows for interactions or joint operations to be simulated.

Finally, the Arkansas Basin RiverWare model brings state-of-the-art capabilities to the basin water managers because, the model, which simulates the basin's network and operations, is decoupled from the driving hydrology and demand data. The model's network and rules can be altered to represent physical changes to the system and/or operational scenarios, such as proposed reservoir enlargements or changed reservoir operation procedures. Independently, alternative driving data representing varied hydrologic conditions and demand scenarios can be efficiently moved in and out of the model. The model's base naturalized hydrology dataset can be used in historical order, but can also be re-sequenced, sampled, and/or adjusted using various techniques to create novel hydrology scenarios, such as extended drought or flood periods or climate change impacts. This ability to drive the model with alternative hydrology scenarios can help answer many important water management questions relating to how the system might react under conditions very different than those observed in the recent past. On top of that, the ability to combine various system and operational changes with alternative driving data provides the ability to answer complex water management questions in the basin.

The Upper Rio Grande Water Operations Model:

One River, Two Countries, Three States, and Over 20 Years of Multi-Agency Collaboration

Jesse Roach, Tetra Tech, Inc.
Jesse.Roach@TetraTech.com

Marc Sidlow, USACE
Marc.S.Sidlow@usace.army.mil

Nabil Shafike, USACE
Nabil.G.Shafike@usace.army.mil

Carolyn Donnelly, Bureau of Reclamation
CDonnelly@usbr.gov

Extended Abstract

URGWOM Overview:

The Upper Rio Grande Water Operations Model (URGWOM) is a mass balance model of water operations and water accounting in the Rio Grande basin from the headwaters in southern Colorado to Hudspeth County, Texas. URGWOM is built in RiverWare, a generalized river basin modeling environment that can be used to develop an operations model for any hydrologic configuration and to simulate operations to meet needs for flood control, water supply, recreation, water quality, navigation, or any other purpose incorporated into the ruleset. RiverWare is designed to provide river basin managers with a tool for scheduling, forecasting, and planning reservoir operations and includes extensive capabilities for rule-based simulations and water accounting. URGWOM tracks water movement by owner and simulates near and long-term water operations in the multi-state, multi-national Rio Grande basin. URGWOM is collaboratively developed, maintained, and run by multiple Federal and State entities.

URGWOM represents many physical processes including hydrologic travel times, reservoir evaporation and seepage, river channel evaporation, evapotranspiration by riparian and agricultural vegetation, municipal waste water return flows, irrigation return flows, surface water-groundwater interaction including crop percolation, canal leakage, river seepage and drain capture. URGWOM is used by multiple stakeholders for Accounting, Water Operations, and Planning applications.

- Accounting: Water accounting in URGWOM occurs as backward looking, data driven, daily timestep accounting of native and trans-basin (San Juan - Chama) water in the system from the beginning of the calendar year through the previous day. Accounting runs are typically completed daily by the Albuquerque office of the U.S. Bureau of Reclamation (Reclamation).

- Water Operations: Annual operating plans are developed with URGWOM using a forward looking daily timestep, rule-based, real-time (1-2 weeks out) and annual (calendar year) operating plan runs. The annual operating plan runs are typically run 5-6 times per year by the Albuquerque office of the U.S. Army Corps of Engineers (USACE) in conjunction with Reclamation and the New Mexico Interstate Stream Commission (ISC).

- Planning Application - Daily or monthly timestep, rule-based planning runs simulating water operations decades to centuries into the future. These long-term runs are executed as needed depending on planning needs and funding resources allowed by Reclamation, USACE, and ISC.)

History of URGWOM:

In 1996, six federal agencies including USACE, Reclamation, the U.S. Geological Survey (USGS), the U.S. Fish and Wildlife Service (USFWS), the Bureau of Indian Affairs (BIA), and the International Boundary and Water Commission (IBWC) recognized the need for a unified water operations model for the Upper Rio Grande Basin. These agencies entered into a Memorandum of Understanding (MOU) to create URGWOM. During the initial phase of URGWOM development various potential software options were considered. A review of several reservoir and river simulation software packages within the context of the needs of water managers in the basin led to RiverWare being selected as the software package for URGWOM. RiverWare was developed by the Center for Advanced Decision Support for Water and Environmental Systems (CADSWES) at the University of Colorado at Boulder. A new MOU was signed in 2007 designating Reclamation, USACE, and ISC as lead agencies responsible for most funding of model maintenance and development. Contributing agencies including USGS, BIA, IBWC, and CADSWES among others are represented on an Advisory Committee and Technical Team, and provide data and technical review.

Interesting Technical Details of URGWOM:

Geographic Extent

URGWOM started as a model of the Rio Grande in New Mexico upstream of and including Elephant Butte and Caballo Reservoirs. According to the Rio Grande Compact, Colorado delivers water at the Colorado-New Mexico state line, while New Mexico delivers its compact obligation at Elephant Butte Reservoir.

In 2012, the URGWOM Technical Team began development of a Colorado portion of the model which includes large portions of the Rio Grande, Conejos, Los Pinos, and San Antonio Rivers in Colorado. Consistent with management of the Rio Grande system in Colorado, this portion of the model is driven by prior appropriation administration of adjudicated water rights. The Colorado portion of the model was developed to help improve estimates of flows at the Colorado-New Mexico state line. In 2015, the Colorado portion of the model was added to URGWOM. The Lower Rio Grande portion of the model, extending downstream from Caballo Reservoir to Hudspeth County, Texas, was developed over many years and was also added to URGWOM in 2015.

Surface Water – Groundwater Interactions

Surface water – groundwater interactions play a key role in mass balance in the Rio Grande downstream of Cochiti reservoir, particularly when flow in the river is low. URGWOM uses Groundwater Storage Objects to model shallow groundwater levels and resulting surface water – groundwater exchanges downstream of Cochiti Reservoir. Deep aquifer heads associated with each Groundwater Storage Object are extracted from regional groundwater models for use as boundary conditions for the URGWOM representation of the shallow aquifer. This process effectively couples groundwater models built by the USGS and other government agencies with URGWOM. One technical issue associated with this implementation is that the groundwater flow equations are explicit in time, meaning head values at the previous timestep are used to solve for flows between zones in the current timestep. This can and does lead to some numerical instabilities in cases where fluxes between the surface water and groundwater system are relatively large.

Timesteps

URGWOM was initially built and is predominately used as a daily timestep model. High computational intensity and large data input and output requirements associated with decadal or longer daily timestep runs led to the development and implementation of a monthly timestep option in URGWOM. Interestingly, the monthly timestep option is not a separate model, nor is it implemented with a separate ruleset. The model itself can be run at a daily or monthly timestep, and the ruleset was rewritten to generalize logic so that rules could be used at either timestep.

The resulting capability allows URGWOM to be converted to a monthly timestep for the purpose of making many long runs from which a smaller subset may be run at the daily timestep. This timestep generalization has also laid the groundwork for URGWOM to be run at a sub-daily timestep, perhaps 6 hours, which may be helpful when a real-time forecasting application is developed. This real-time application would take precipitation and temperature forecasts several days into the future to run a short-term river system forecast that can be updated daily.

Combined Accounting to Operations or Planning Runs

Originally, the URGWOM accounting, annual operations, and planning models were separate applications. This meant that the up to date historical data available in the accounting model was not readily accessible to the other model types. In 2013, URGWOM was updated to allow all three types of models to be run from a single model file. Specifically, this allows the model to be run in accounting mode from the beginning of the current year through the previous day, and then switched into a rule-based mode to project conditions in the system for the rest of the year or longer starting from the latest available data. Initial conditions for any operations or planning future-cast run are now automatically defined based on the latest observed data as incorporated into the hind-cast accounting run.

Trinity River Basin Dam Safety Analysis with HEC-WAT

Adams, Lea, Chief – Water Resource Systems Division, USACE – Hydrologic Engineering Center, Davis, CA, lea.g.adams@usace.army.mil
Lehman, William, Senior Economist, USACE – Hydrologic Engineering Center, Davis, CA, william.p.lehman@usace.army.mil

Introduction

The Trinity River Basin spans 18,000 square miles in Texas. The basin contains both USACE and non-USACE lakes, with approximately 24% of the watershed area managed by USACE reservoirs. Although the non-USACE lakes do not store floodwaters, they do have an effect on operation of the USACE lakes. Five USACE dams in the Trinity River Basin were classified with a Dam Safety Action Classification of 2 (Urgent) or 3 (High Priority) in the past few years: Grapevine Dam, Benbrook Dam, Lewisville Dam, Ray Roberts, and Joe Pool. HEC-WAT, in conjunction with other HEC software tools, was applied to evaluate extreme hydrologic loading conditions at the dams of interest.

Study Analysis Overview

The USACE Dam Safety Program embraces a risk-informed decision-making process when prioritizing investment decisions. Risk is comprised of both the likelihood of an event occurring and the consequences of that event. USACE identified hydrologic risk drivers at each dam, including overtopping, wave overwash erosion and surface slides. Given the proximity of the dams to the Dallas-Fort Worth metropolitan area downstream, the consequences of a failure at one or more of the dams in the Trinity system could be catastrophic. Estimates range from 1,000 to 10,000 lives lost. This study was intended to evaluate the likelihood portion of the risk equation, with development of stage-frequency hydrologic loading curves at the five USACE dams.

HEC-WAT was well-suited to evaluate the Trinity River watershed as an integrated reservoir system, considering systems operations and coincident flows, and to explicitly consider uncertainty in the analysis as required by USACE policy. Regional precipitation and temperature data were generated using a weather generator program developed specifically for this study. The precipitation was transformed to flow using HEC-HMS and routed through the system reservoirs with HEC-ResSim, all within the HEC-WAT framework.

Model Setup

Trinity Weather Generator

A custom weather generation tool was developed in Python for the Trinity study, and was based on an earlier weather generator created for the USACE evaluation of Herbert Hoover Dike in Florida. The weather generation approach was selected to incorporate a regional precipitation-frequency analysis within a well-developed hydrologic context. Continuous precipitation and

temperature inputs were generated from historical data at a regional scale that considered the various central Texas storm types: local storms, mesoscale storms with embedded convection, mid-latitude cyclones and tropical storm remnants. The computational burden of evaluating enough storm events to reasonably assess extreme hydrologic conditions was initially a concern, and the study team chose a 4-month simulation window instead of an annual simulation window as a balance between accuracy and efficiency in the modeling effort.

The spring season of March 1 to June 30 was chosen as the critical period for reservoir operations because it has the highest background precipitation and highest average reservoir pool stages. The storm typing approach had two main benefits: it works well for larger regions which are subject to different types of storms and it is very useful when trying to evaluate extremely rare events because it retains the probability of each type of event. The final precipitation data set consisted of continuous one-hour data for the 4-month simulation window. The continuous nature of the data sets was important because storm sequencing affected peak reservoir stages. The study team theorized, and eventually the study results confirmed, that multiple smaller storms in sequence could produce more extreme hydrologic conditions than a single large storm.

Another strategy pursued to reduce the computational burden was stratification of the precipitation and temperature data sets. The team planned to evaluate between 400,000 and 1,000,000 events in HEC-WAT. Stratification allowed more events beyond 1xE-06 to be evaluated without a corresponding increase in the number of model simulations, although it is difficult to estimate the frequency of the rarest events because variance is high for those events.

HEC-HMS

The HEC-HMS model used for the Trinity dam safety analysis was originally developed as part of the Corps Water Management System (CWMS) modeling effort. Because compute times are tightly coupled to model setup and application, a number of model adjustments were made to strike a balance between efficiency and accuracy, given the purpose of this particular study:

- Reduced the number of subbasins from 283 to 43, and truncated the watershed footprint at Dallas.
- Changed the routing method in shorter reaches from Muskingum Cunge to Muskingum.
- Removed all modeling features not needed for this particular study, such as observed flows, forecasting information and other extraneous paired data.
- Removed several water supply reservoirs from the HEC-HMS model and added them into the HEC-ResSim model.

Uncertainty in hydrologic parameters, including times of concentration, storage coefficients, loss rates, and recession rates, were evaluated with HEC-HMS as part of this analysis. A new feature in HEC-HMS 4.3, Markov Chain Monte Carlo (MCMC) optimization, was used to generate uncertainty values for the suite of parameters, and the specified values uncertainty method was applied in the model.

HEC-HMS 4.3 was used in the Trinity study because of availability of two new features: the Hamon temperature-only evapotranspiration method, and the specified values sampling uncertainty analysis method (which used results from the MCMC optimization trials). The specified values sampling method is important because it maintains correlation between model

parameters and prevents unrealistic combinations of model parameters. After all the various modeling adjustments and additions were made, the team was able to reduce HEC-HMS runtimes from 90 seconds for a 2.5-month simulation to about 52 seconds for the final 4-month HEC-WAT runs (at a 1-hour timestep).

HEC-ResSim

As with the HEC-HMS model, the original HEC-ResSim model came from the CWMS modeling library. The number of inflow locations in the HEC-ResSim model was reduced to match handoff locations within the simplified HEC-HMS model, and a series of model adjustments were made:

- Fixed broken references in reservoir operating rules.
- Removed redundant operating rules, as well as rules that were unnecessary during flood operations.
- Updated model to correctly account for overtopping flow rates at each dam when experiencing extreme flows.
- Replaced downstream reservoir control rules with maximum release rules.

Uncertainty sampling in HEC-ResSim was limited to sampling starting reservoir pool elevations. The effect of sampled starting pool elevations on seasonal maximum pool elevations was minimal, however, given the long simulation periods.

HEC-ResSim 3.3 beta was used for the Trinity study. The study team was able to reduce HEC-ResSim runtimes from about 6 minutes to 18 seconds for the final 4-month HEC-WAT runs (at a 3-hour timestep).

HEC-WAT

An HEC-WAT model of the Trinity watershed, using HEC-WAT 1.1 beta, was constructed to facilitate modeling hundreds of thousands of hydrologic events. As noted above, precipitation and temperature data were generated externally to HEC-WAT using a study-specific weather generator. This data was imported into HEC-WAT via a plugin called the Stochastic Data Importer, which allows HEC-DSS data sets to be read as inputs to HEC-HMS and HEC-ResSim. The Model Linking Editor in HEC-WAT was used to manage the flow of information between the input data sets and the two study models.

Hydrologic events were organized in the HEC-WAT model by lifecycles and realizations. A lifecycle is the smallest grouping of hydrologic events within HEC-WAT, and is typically 20 to 100 events in length. Lifecycles are then grouped into larger realizations. This structure is typically used to organize the two types of uncertainty sampling within HEC-WAT: natural variability within lifecycles and knowledge uncertainty within realizations. For the Trinity study, the lifecycle-realization structure was further leveraged to organize the compute structure on a distributed compute network, and manage the record keeping for stratification and destratification.

Two custom HEC-WAT plugins were created for this study. The “Trinity” plugin computed critical duration flow and stage averages for various points in the study area, and was run as part of the compute sequence. This added customized study results to the standard set of available

results from the HEC-HMS and HEC-ResSim plugins that summarize Monte Carlo outputs during an HEC-WAT uncertainty simulation. The “Merger” plugin combined several post-processing operations. It gathered all HEC-DSS results files from each compute from across a distributed compute network, organized the files with a numbering scheme, merged them into a master HEC-DSS file and then destratified the results. During the destratification process, convergence criteria were applied to each output to determine whether the results had converged.

Validation and Stress Testing

It was important to ensure that the models were functioning properly over the full range of expected hydrologic conditions prior to launching the study production runs, for purposes of both quality and distributed compute robustness. To this end, the HEC-HMS model was calibrated to one observed event; validation to a second observed event was desirable but constrained by study timelines. The HEC-HMS and HEC-ResSim results were then confirmed to be identical in both standalone and inside the WAT. Uncertainty sampling was turned on and the team ensured that sampling was occurring as expected in both HEC-HMS and HEC-ResSim.

Once the model results were validated, several rare precipitation events created by the Trinity weather generator were applied in HEC-WAT to stress test the HEC-HMS and HEC-ResSim model setups for performance under extreme hydrologic loading conditions. A number of adjustments were made to ensure that the models could pass large flows without failing, as problems in either model could cause a large-scale HEC-WAT compute to fail.

Study Analysis

Distributed Computing

After considering contracting options, the study team chose instead to use an in-house distributed compute network for greater flexibility in performing runs. The compute network consisted of 20 desktop machines managed with several virtual machine (VM) software tools, including Hyper-V, PDQ Inventory and PDQ Deploy. This suite of tools allowed remote access for team members located in different parts of the country to manage the VMs, deploy batch processes and initiate HEC-WAT runs.

The final HEC-WAT compute was structured with 50 events per lifecycle, which met the requirements of stratification scheme, and 20 lifecycles per realization. The production distributed compute network consisted of four grids of 20 compute nodes, plus one master node for storage of aggregated results, but the HEC-WAT model was initially stress tested on a smaller grid to ensure that the distributed compute software was functioning as expected. HEC-WAT supports distribution of computes via either lifecycle or realization. Occasional compute failures were expected to happen due to software or hardware problems, and distribution by lifecycle was chosen to minimize the amount of time needed to re-run a simulation if a failure occurred.

The study plan called for evaluation of up to 1,000,000 events, but initial investigations suggested that results could converge between 600,000 and 800,000 events. The production runs were organized into 100,000 event lifts, with 25,000 events distributed to each VM grid. Convergence looked promising after 400,000 events, but the next compute lift revealed a very

large outlier and additional lifts were required. The unexpected outlier was related to the issue of several more-frequent storms in sequence creating higher peak flows and reservoir stages than a single less-frequent storm. Ultimately the full complement of 1,000,000 events was modeled, and convergence was observed at most but not all study output locations.

Data management was a concern with a study of this size. Dividing the full simulation into 100,000-event lifts, which were further divided into 25,000-event computes across the four VM grids, helped keep data file sizes manageable. The hourly precipitation input data sets resulted in a file size of 14GB for 25,000 events. The HEC-WAT output data set sizes were about 90MB per 25,000 events, or 3.6GB for the full 1,000,000 events.

Study Results

The final HEC-WAT analysis of 1,000,000 events was completed over the course of 14 days, in ten lifts of 100,000 events per run. Stage-frequency results and uncertainty bounds were developed at each of the five dams (Grapevine Dam, Benbrook Dam, Lewisville Dam, Ray Roberts, and Joe Pool) and at the Dallas Floodway for peak inflow, peak inflow volume for the critical duration (2- or 3-day flow) and total inflow volume for the 4-month simulation window. The stage-frequency curve at Grapevine Dam based on 1,000,000 events evaluated in HEC-WAT is shown in Figure 1.

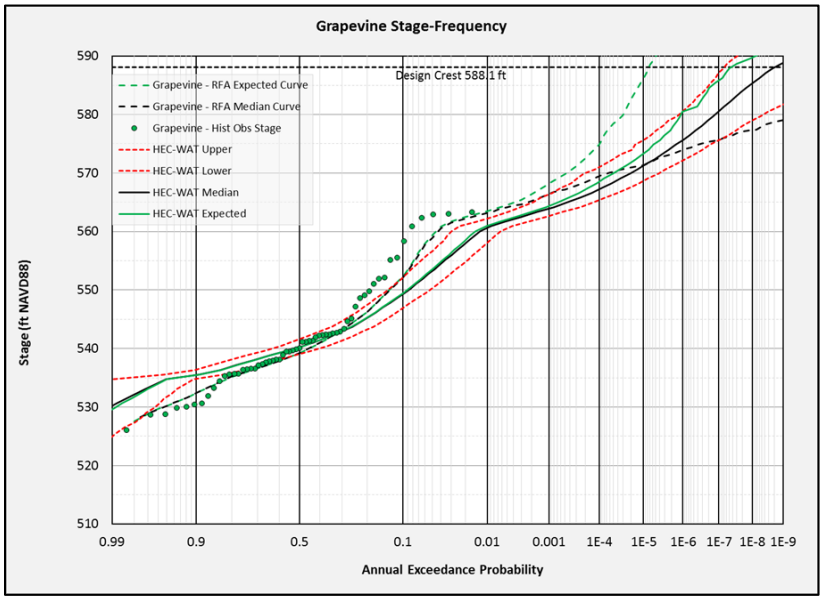

Figure 1. Stage-frequency at Grapevine Dam

Lessons Learned

There were a number of challenges and lessons learned during the Trinity study. The most important items are noted here:

- Questions arose about how to calibrate an HEC-WAT model for an entire watershed. Individual models responsible for one part of the hydrologic process can be calibrated relative to observed events, but it's more difficult to determine where to make

adjustments across three models working in concert with their own intrinsic model errors.

- Runtime failures occurred that were initially attributed to the software, since each program was in active development. After investigations didn't reveal any bugs, it was discovered that the source of the failures was actually extremely large precipitation events that were crashing to the HEC-HMS and HEC-ResSim models, despite the initial stress testing. The study setup effort had focused primarily on the five USACE dams, extending volume-elevation curves at those locations, but it was eventually discovered that the curves needed to be extended further at some of the other dams in the basin. The lesson learned was to investigate the simplest, most obvious source of a problem first, before spending time on the more complex possibility of software bugs.
- Stress testing was performed on the stratification bin with the rarest events, but it was later discovered that several of the most extreme floods actually occurred at more frequent events, driven by multiple smaller events in sequence. There wasn't an easy way to identify these critical stress testing events without running a large number of overall events.
- A 2GB file size limitation on file transfers buried in legacy code caused hours of troubleshooting at the beginning of the production runs. This limitation was missed in stress testing because there were more zero-precipitation hours than during the full production runs and the corresponding stress testing HEC-DSS files compressed into files less than the 2GB limit. Large file sizes also required long transfer times to move data onto the compute network.
- The compute logs for HEC-WAT, HEC-HMS and HEC-ResSim were not originally designed to support troubleshooting for a Monte Carlo-style compute. The model logs capture a large amount of detail to help users find problems, which works well for a small numbers of events. However, the information in model logs can become overwhelming when they are filled with detailed information for thousands of events.
- The original work plan consisted of a smaller set of test runs to confirm model validation, followed by one or two full production runs. When results from the large-scale production runs were reviewed, however, the decision was made to adjust methods in the weather generator to better capture the extreme end of the frequency curve. This required generating new precipitation data, often followed by adjustments to the HEC-HMS and HEC-ResSim models, then re-analysis of the production runs. This review-adjustment-re-analyze cycle occurred several times, and took longer than anticipated because evaluation of the extreme end of the frequency curve required producing hundreds of thousands of events.

Acknowledgments

The following USACE staff made significant contributions to the completion of the Trinity River Basin dam safety analysis with HEC-WAT: Allen Avance, Matt Fleming, John Hunter, Greg Karlovits, Joan Klipsch, Chan Modini, Sara O'Connell, and Haden Smith.

References

Karlovits, G. 2018. Synthetic weather simulation for characterization of uncertainty in extension of stage-frequency curves in a system of flood control dams. Poster presented at: American Geophysical Union Fall Meeting, Washington, D.C.

USACE-Risk Management Center. 2018. “Trinity River Basin Flood Hazard Assessment,” RMC-TR-2018-## (draft).

U.S. Army Corps of Engineers' Corps Water Management System (CWMS) Overview

Chan Modini, Chief Water Management Systems Division, Hydrologic Engineering Center, U.S. Army Corps of Engineers, Davis, CA,
george.c.modini@usace.army.mil

Extended Abstract

The Corps Water Management System (CWMS) serves water managers at District and Division offices of the U.S. Army Corps of Engineers (USACE) by providing real-time data acquisition and hydrologic and hydraulic modeling capabilities. CWMS is a comprehensive data management system and modeling system for water management decision support. Figure 1 shows a picture of CWMS an Automated Information System (AIS).

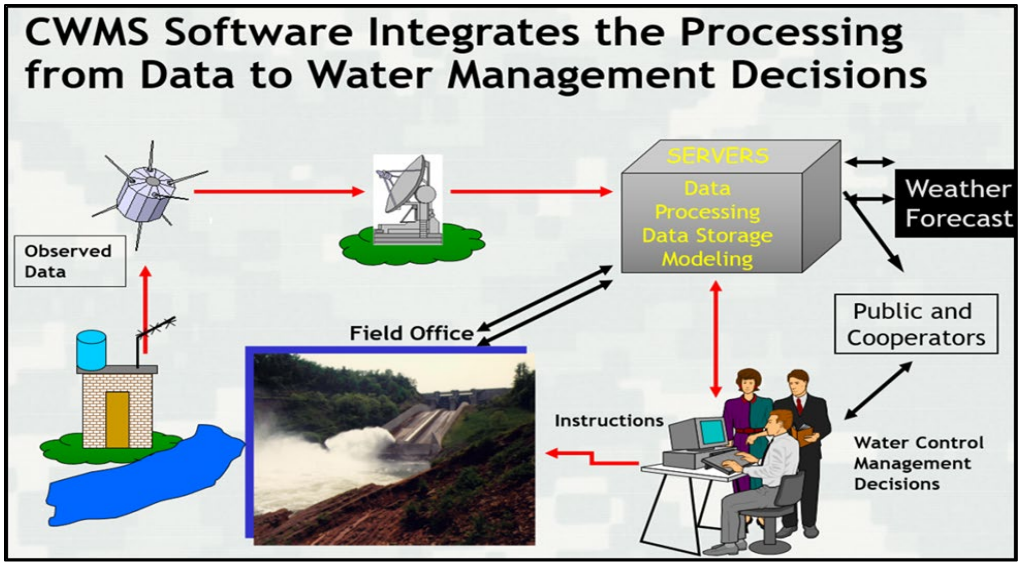

Figure 1. Picture of CWMS an Automated Information System

Through HEC-DSS (Data Storage System), CWMS facilitates the real-time use of observed and forecasted precipitation, observed flows and stages, and other meteorological and hydrologic data. CWMS also allows the integration of HEC-HMS (Hydrologic Modeling System) for forecasting flows throughout a watershed, HEC-ResSim (Reservoir Modeling System) for simulating reservoir operations and release decision, HEC-RAS (River Analysis System) for forecasting river stages and producing flood inundation maps, and HEC-FIA (Flood Impact Analysis) for estimating potential flood impacts on life safety, agriculture, and urban infrastructure. Figure 2 shows the picture of real-time fully integrated hydrologic models.

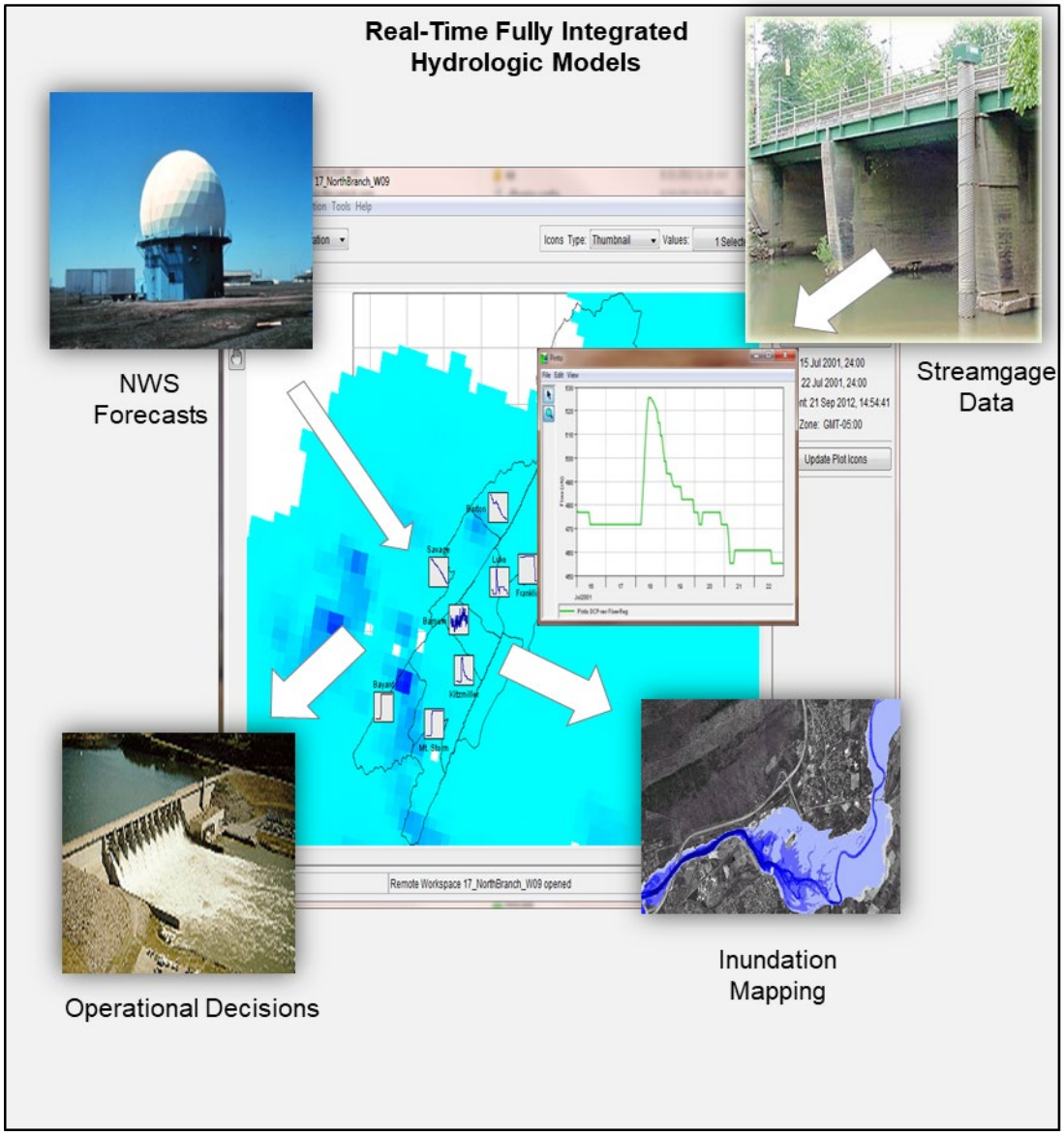

Figure 2. Picture of Real-time Fully Integrated Hydrologic Models

This presentation will provide an overview of the CWMS database component and related utilities and provide an update on the latest enhancements to the CWMS modeling suite and the Control and Visualization Interface (CAVI) including HEC-MetVue. HEC-Metvue is a new tool that will provide the capability to display, verify, manipulate and edit spatial data by interactive visual means. HEC-MetVue will also be part of the modeling suite and can be used in place of the MFP (Meteorolgic Forecast Processor) in the modeling sequence for forecasting purposes. Figure 3 provides a picture of how Storm Editing and Storm Design can be accomplished with HEC-MetVue in order to create a gridded data set for use in modeling studies or forecast simulations.

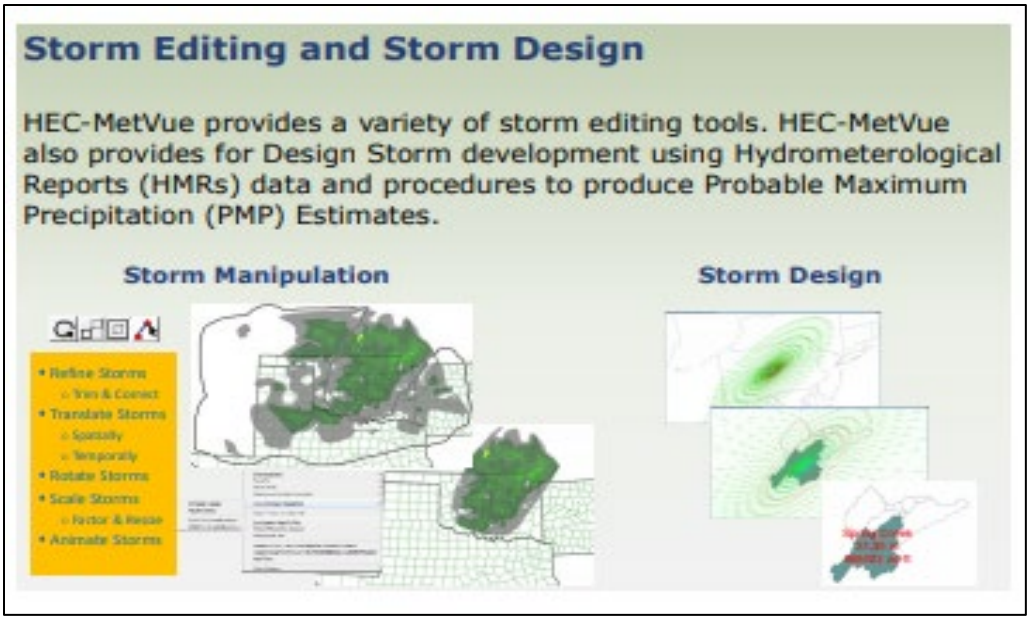

Figure 3. Storm Editing and Storm Design in HEC-MetVue

This presentation will also characterize HEC-RTS, which is the public version of CWMS and how non-USACE entities can implement real-time decision support applications using HEC-RTS. HEC-RTS is PC based and does not include the database component (ORACLE) of CWMS. Time-series data are provided via HEC-DSS (Data Storage System). Enhancements are also planned for development of an API (Application Programming Interface) that will allow linking to MS-Access and other commercial databases.

U.S. Army Corps of Engineers' Corps Water Management System (CWMS) Team Forecasting

Chan Modini, Chief, Water Management Systems Division, Hydrologic Engineering Center, U.S. Army Corps of Engineers, Davis, CA, george.c.modini@usace.army.mil
Fauwaz Hanbali, Senior Hydraulic Engineer, Hydrologic Engineering Center, U.S. Army Corps of Engineers, Davis, CA, fauwaz.hanbali@usace.army.mil

Extended Abstract

Background

The Corps Water Management System (CWMS) is a decision support platform that serves water management personnel at District and Division offices of the US Army Corps of Engineers (USACE) by providing real-time data acquisition and hydrologic and hydraulic modeling capabilities. CWMS is comprised of a database and a modeling framework. CWMS is available for USACE only. For the general population, the publicly available version of CWMS minus the ORACLE database is called HEC-RTS. For CWMS, the main organizing unit is the "Watershed" and the Control and Visualization Interface (CAVI) serves as the main interface. The CAVI provides access to manipulate data and models and includes data acquisition, data visualization, and forecast simulation. Figure 1 shows a screenshot of the CWMS Version 3.1 CAVI.

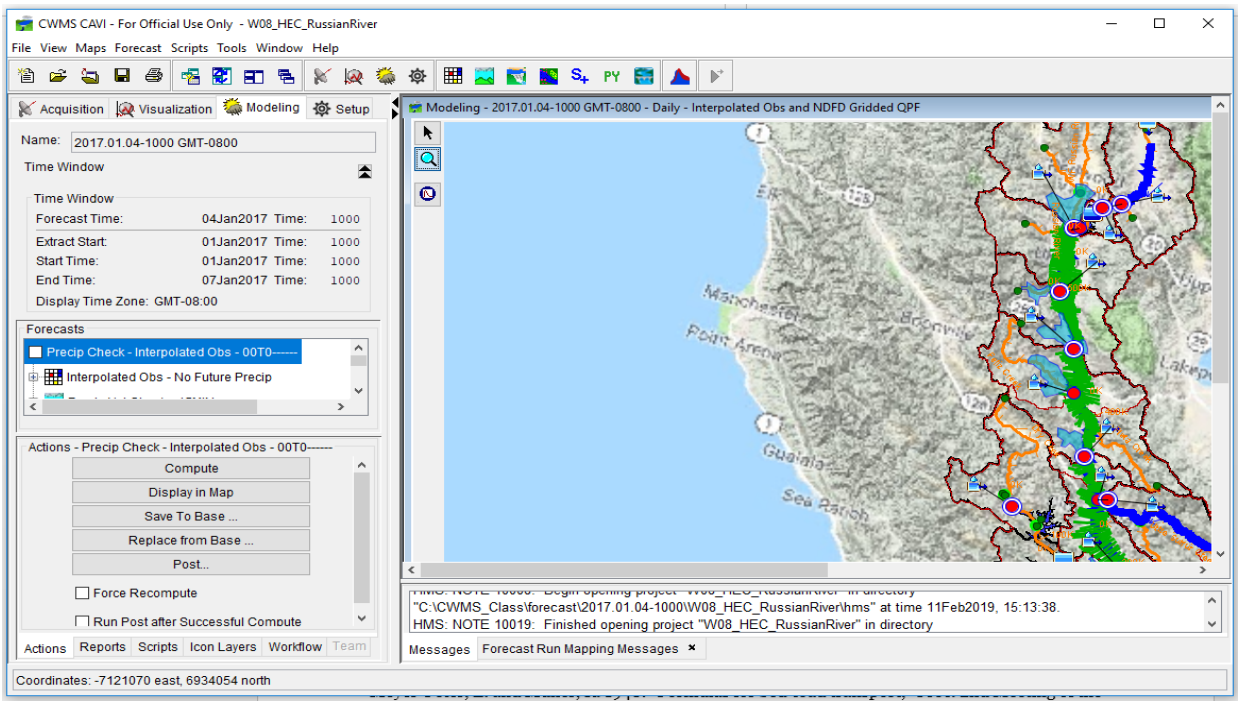

Figure 1. Screenshot of the CWMS Version 3.1 CAVI

A typical forecast simulation includes running the following programs in sequence. These include a Meteorologic Forecast Processor (MFP), Hydrologic Model (HEC-HMS), Reservoir Model (HEC-ResSim), Hydraulics Model (HEC-RAS), and a Flood Impact Analysis Model (HEC-FIA). In this type of scenario, multiple forecast modelers may need to share responsibility across complex watersheds or models, with forecasting responsibility allocated by discipline such as hydrology, reservoir operations, hydraulics, and flood impact analysis. The CWMS Control and Visualization Interface (CAVI) version 3.1 modeling framework supports sharing Watershed configurations and Forecast data sets using either a shared network drive or a CWMS Server.

CWMS Team Forecasting

This sharing concept is called "Team Forecasting". This feature allows a distributed team of collaborators to share Watershed configurations and Forecast models and results using the CAVI. Team modelers sync their own copies of the models and data to a shared Master Watershed. As modelers update working models and generate results, they decide when and which information to upload to the Master Watershed. Figure 2 shows an example of Team Forecasting Workflow.

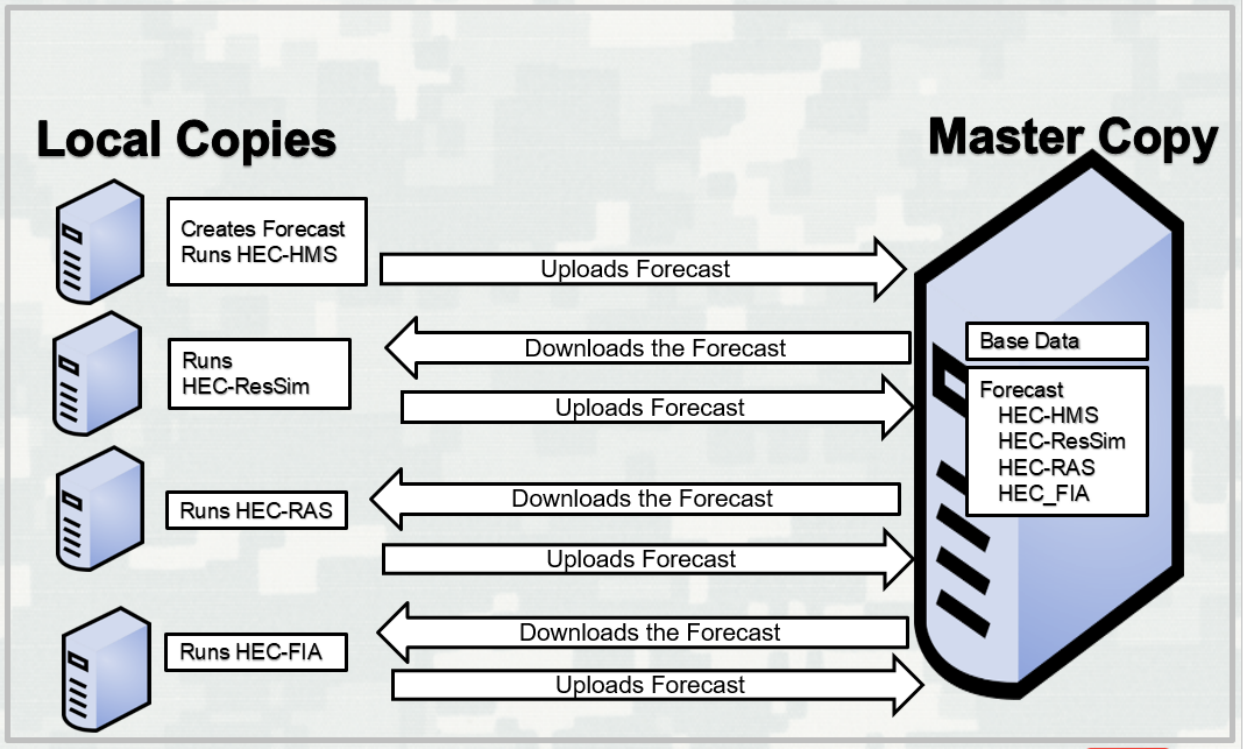

Figure 2. Example of Team Forecasting Workflow

Any CWMS Version 3.0 or later watershed can become a Master Watershed. Figure 3 shows a screenshot of the Watershed Properties Dialog Team tab where a Master Watershed can be created.

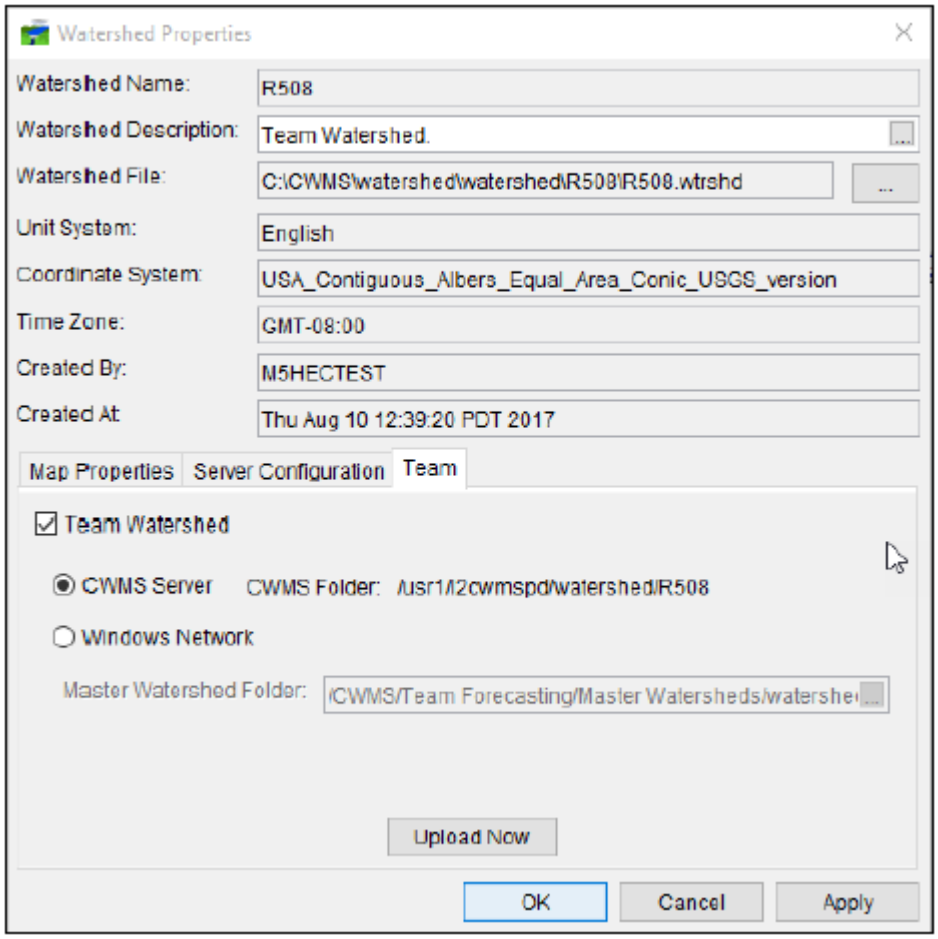

Figure 3. Watershed Properties Dialog Team Tab

The watershed can be uploaded to a CWMS Server or Networked Drive thereby creating a Master Watershed. Once a Master Watershed has been created, modelers can download a copy of the Master Watershed for team modeling purposes. A feature in the CAVI allows team members to be notified of changes to the Master Watershed and prevents file conflicts through read and write locking. Key aspects of this approach to Team Forecasting include the ability to facilitate multiple modelers working within or on a water forecast simultaneously, and the ability to support team members working from remote locations with limited network bandwidth. This presentation will provide an overview of these team forecasting features and future enhancements.

Modeling of Major River Systems

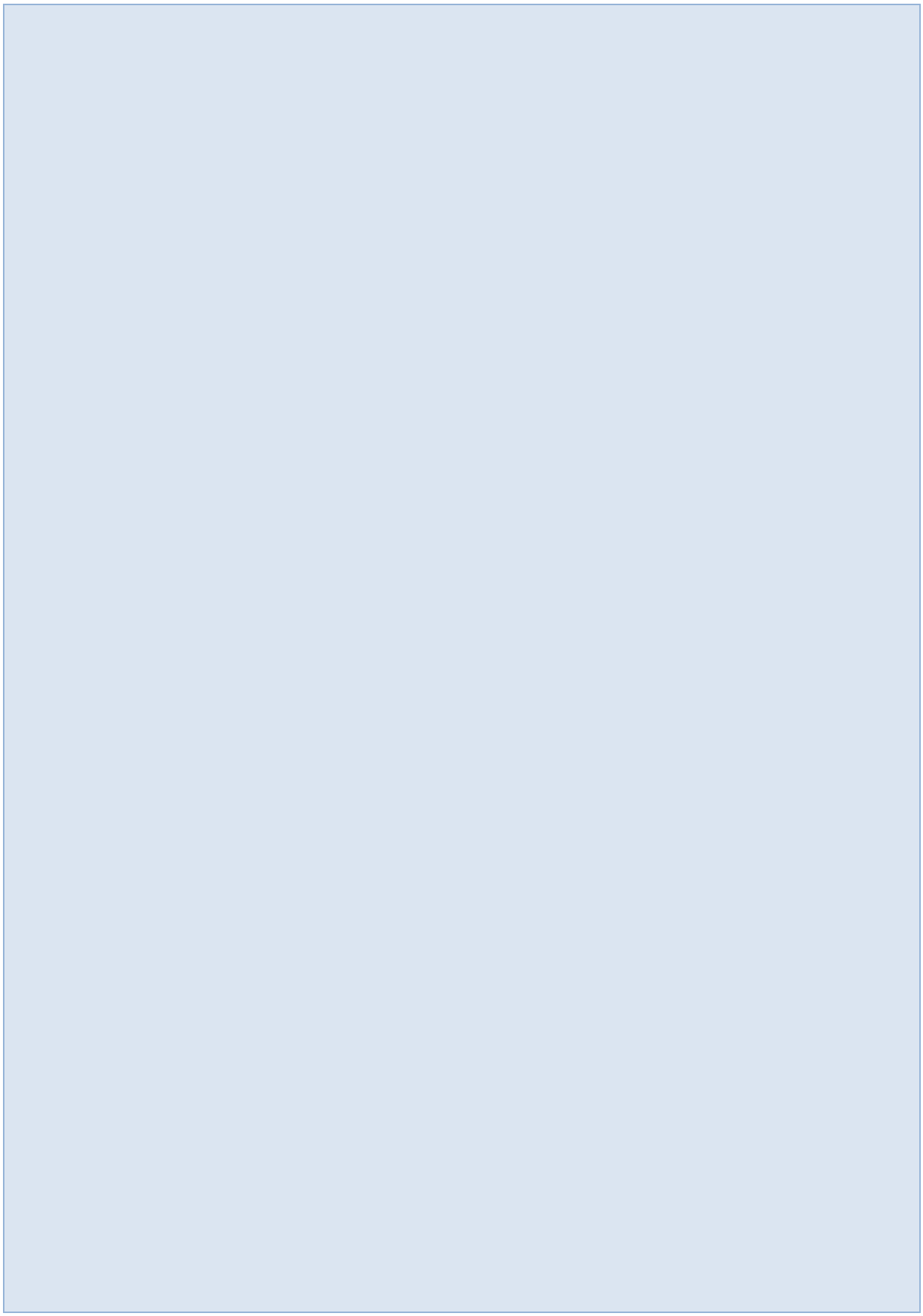

Forecast Informed Reservoir Operations: Developing Best Practices for Enhancing Use of Existing Water Management Infrastructure

F. Martin Ralph, Director, Center for Western Weather and Water Extremes, Scripps Institution of Oceanography, University of California San Diego, La Jolla, CA, mralph@ucsd.edu
Jay Jasperse, Chief Engineer, Sonoma Water, Santa Rosa, CA, jay.jasperse@scwa.ca.gov
Cary A. Talbot, Division Chief, Engineer Research and Development Center, US Army Corps of Engineers, Vicksburg, MS, cary.a.talbot@erdc.dren.mil
Anna M. Wilson, Field Research Manager, Center for Western Weather and Water Extremes, Scripps Institution of Oceanography, University of California San Diego, La Jolla, CA, anna-m-wilson@ucsd.edu

Abstract

Forecast Informed Reservoir Operations (FIRO) is a proposed alternative management strategy that aims to use data from watershed monitoring and state of the art weather and water forecasting to adaptively match available water with available storage to improve water supply reliability while maintaining or enhancing flood protection. This project was guided by the Lake Mendocino FIRO Steering Committee (SC), which consists of water managers and scientists from several federal, state, and local agencies, and universities. An essential component of evaluating and potentially implementing this strategy is to understand and improve prediction of Atmospheric Rivers (ARs), which provide over 50% of the annual precipitation in this watershed. To this end, an extensive data collection campaign has been underway since January 2017 to understand the effect of ARs on watershed management and hydrology. This presentation will provide an overview of the FIRO project and progress to date, with an emphasis on the field data collection program and its role in helping to achieve major FIRO science and management goals.

Introduction

Forecast Informed Reservoir Operations (FIRO) is a proposed alternative management strategy that aims to use data from watershed monitoring and state of the art weather and water forecasting to adaptively match available water with available storage to improve water supply reliability while maintaining or enhancing flood protection. The first testbed for this strategy is Lake Mendocino, which is located in the East Fork of the 1485 mi^2 Russian River Watershed in northern California. This project was guided by the Lake Mendocino FIRO Steering Committee (SC), which consists of water managers and scientists from several federal, state, and local agencies, and universities. The SC shares a vision that operational efficiency can be improved by using monitoring and forecasts to inform decisions about releasing or storing water. Assessment is underway that will consider and recommend FIRO strategies that could be implemented in the near term using current technology and scientific understanding, and identify and develop new science and technologies that can ensure FIRO implementation is safe and successful in the long term.

FIRO would use available reservoir storage in an efficient manner by (1) better forecasting inflow with enhanced technology and monitoring, and (2) adapting operations in real time to meet evolving storage needs. The envisioned FIRO strategy has the potential to simultaneously improve water supply resiliency, flood protection, and ecosystem sustainability through a more efficient use of existing infrastructure while requiring minimal capital improvements in the physical structure of the dam. An essential component of evaluating and potentially implementing this strategy is to understand and improve prediction of Atmospheric Rivers (ARs), which impact not only streamflow but also strongly influence reservoir operations. ARs provide over 50% of the annual precipitation in this watershed, and cause most of the heavy rain and flood events.

To support FIRO, an extensive data collection campaign has been underway since January 2017, with the major science objectives of understanding AR evolution as the AR makes landfall and interacts with terrain, understanding the effect of ARs on watershed management and hydrology, and to form a unique database for model verification. Coastal and inland field sites equipped with multiple ground-based sensors as well as Vaisala radiosonde systems supported these objectives. In the Lake Mendocino sub-watershed, an even more extensive network of in situ sensors was designed and deployed beginning in water year 2018, to support hydrological modeling efforts and process-based understanding. This network includes soil moisture, streamflow, precipitation, and other hydrometeorological information and provides a high density look at how low level water vapor flux brought by ARs moves through the watershed. This preprint will first provide an overview of the FIRO project and progress to date, including the FIRO Steering Committee, the Work Plan and Viability Assessments, and the Major Deviation. It will then describe the field data collection program and its role in helping to achieve major FIRO science and management goals.

FIRO: Project Overview

FIRO Steering Committee

The FIRO Steering Committee (SC; members listed in Table 1) was formed in 2014 in order to investigate potential strategies to modify operating procedures. Proposed modification strategies were designed to maintain or improve flood risk management while more reliably meeting water supply and environmental flow requirements with the Lake Mendocino reservoir. The SC's goal was to leverage improvements in forecasting and monitoring since the original rule curve design in 1959 (with minor updates in 1986). Lake Mendocino is located on the East Fork of the Russian River and has a storage capacity of 122,500 acre-feet. It is owned by the US Army Corps of Engineers and operated according to the rule curve. The local partner, Sonoma Water, controls dam operations when reservoir levels are in the water supply pool. Two catalysts to the SC formation were 1) the major California drought of 2012-2016 and 2) the change in inflow to Lake Mendocino based on the reduction of diversion flows from the Eel River.

FIRO Work Plan and Viability Assessments

The FIRO SC collaboratively developed the framework for assessing FIRO viability. To track milestones and progress, the SC came up with a detailed work plan in order to assess the viability of FIRO for Lake Mendocino (Jasperse et al., 2015). The steps in the work plan are to develop evaluation methodology and criteria, develop evaluation scenarios, identify science needs and carry out relevant research projects, evaluate model results, evaluate FIRO viability

and assess benefits, and develop implementation strategies. As part of the work plan step to evaluate FIRO viability, a Preliminary Viability Assessment (PVA) was completed (Forecast Informed Reservoir Operations Steering Committee, 2017). The PVA found that atmospheric rivers are key drivers of drought and flood in this watershed. It concluded that some elements of FIRO are appropriate for further investigation. Specifically, the PVA found that integrating forecasts into reservoir release decisions does not adversely affect flood risk management, and integrating forecast information also allows operators to more reliably meet water management and environmental flow objectives in the Russian River watershed. However, there are areas for improvement; in particular, significant uncertainty remains in forecasts of timing, landfall location, strength, and duration of landfalling atmospheric rivers. The outcomes of the PVA are guiding the preparation of the Final Viability Assessment and development of appropriate implementation strategies.

Major Deviation

Based on the findings of the PVA, members of the Steering Committee submitted a request for a major deviation from existing reservoir operations to the US Army Corps of Engineers in the fall of 2017. A significant FIRO success was the approval of this request in November 2018. Within the terms of the approved request, a maximum of 11650 acre-feet of additional water may be stored in the reservoir between 1 November and 28 February. This is enough water for a full year's supply for approximately 97000 people. This accomplishment is an example of management changes that can be justified as a result of implementing FIRO.

FIRO: Field Campaign Overview

Science Objectives and Goals

Precipitation from atmospheric rivers (ARs) is the primary source of water supply and the primary cause of flooding in northern California (Gershunov et al., 2017; Ralph et al., 2006). One key component of the investigation of atmospheric rivers is targeted observation and comprehensive monitoring at all relevant spatial and temporal scales. The overarching science objective of the field campaign is to support research that will improve the forecasts of ARs and their impacts in the Russian River watershed, with the goal of determining whether these forecasts are safely useable to inform decision making in reservoir operations, and where and how we can improve them.

Previous research has pointed to a strong correlation between the strength of the AR at landfall and the resulting precipitation and streamflow in the watershed (Ralph et al., 2013). Multiple studies have identified a number of potential avenues for forecast improvement and better fundamental understanding of the AR phenomena. These include the modulation of ARs and their impacts by mesoscale frontal waves (Neiman et al., 2014; Ralph et al., 2011), large scale circulation patterns (Guirguis et al., 2018a,b), the vertical distribution of water vapor, antecedent conditions, aerosol and microphysics, and many others.

Field campaigns were designed and led by the Center for Western Weather and Water Extremes (CW3E) at Scripps Institution of Oceanography, University of California San Diego to thoroughly investigate uncertainties related to atmospheric rivers and are described in more detail next. The field campaigns were designed such that the AR would be sampled at multiple

stages during its life cycle, from its evolution over the Pacific Ocean, through landfall on the California coast, to precipitation on the ground and that precipitation's movement throughout the landscape of the watershed.

Offshore Component: One essential component of the effort to improve forecasts of ARs is to increase sampling efforts upstream in the Pacific Ocean. To this end, CW3E collaborates with multiple other partners to conduct Atmospheric River Reconnaissance during the winter to sample vertical profiles of temperature, moisture, pressure, and winds in transects passing through the core of the AR. Methods to develop optimal flight paths for a given AR include both objective quantitative methods using an adjoint model developed at the Naval Research Laboratory, and physically based methods targeting features of interest such as the AR core (Doyle et al., 2012). These methods generally point at the same features. Research efforts include a quantification of the amount of improvement to the forecast provided by these observations at different lead times, and using the dropsonde measurements to improve our physical understanding of fundamental processes important to AR evolution before landfall (Guan et al., 2018; Lavers et al., 2018).

Radiosonde Component: The primary motivation behind the choice of radiosonde launch sites is to understand how ARs evolve as they move inland from the coast (see locations in Fig. 1). These data will also help to answer questions about the effect of variations in the vertical profile of water vapor and temperature, atmospheric stability, and other factors on precipitation and streamflow produced by atmospheric rivers. The existing dataset available with the Bodega Bay Atmospheric River Observatory provides a profile of winds in the lowest 10 km and one measurement of total integrated water vapor in the atmospheric column (White et al., 2013). The radiosondes provide key additional information on the distribution of water vapor in the vertical. Radiosondes are released during atmospheric river conditions during January – March every 3 hours, increasing to every 1.5 hours during storm peaks. Analysis of data collected so far from over 600 radiosondes total has indicated a 20% reduction on average in the integrated vapor transport (IVT; a measure of the strength of the AR) as the AR moves inland from the coast. However, there is still significant variability that ranges from no decrease in strength at all, to a decrease of more than half.

Hydrometeorological Component: The FIRO field campaign has greatly enhanced the monitoring of soils and streams in the Lake Mendocino watershed (Fig. 1) to support hydrological modeling efforts in the watershed by providing a validation dataset. CW3E and Engineer Research and Development Center (ERDC) scientists are also leading an ongoing effort to conduct hydrograph separation. Hydrograph separation distinguishes between the volume of surface water and groundwater contributing to streamflow. The methodology uses stable isotope and natural geochemical tracers sampled from streams, precipitation, and groundwater springs before, during, and after AR events. Correctly representing these sources of streamwater in ERDC's Gridded Surface Subsurface Hydrologic Analysis (GSSHA) watershed model is expected to improve inflow forecasts to Lake Mendocino.

To support these goals, six stations continuously measuring surface meteorology (temperature, pressure, relative humidity, precipitation) and soil conditions (moisture and temperature) at 6 depths up to 1m below the surface were installed. This instrumentation augments the National Oceanic and Atmospheric Administrations' 14 existing hydrometeorological testbed stations which measure the same parameters. Two of the sites installed by CW3E in the Russian River also include vertically pointing radars, disdrometers that measure size and velocity of

hydrometeors, and GPS-Met sensors that measure the amount of integrated water vapor in the atmospheric column. These two sites support both the radiosonde and the hydrometeorological components of the project. FIRO also sponsored the installation of ten additional stand-alone precipitation gauges and six stream gauges. During the summer of 2018, the six surface meteorology sites were upgraded to also include wind speed and solar radiation sensors. These sensors have provided a high resolution dataset, including more than 20 ARs in the Russian River since installation. Results from hydrograph separation so far show a high groundwater contribution to streamflow, even after the soils are saturated.

Concluding Remarks

First conceptualized by a diverse group of stakeholders in 2014, Forecast Informed Reservoir Operations (FIRO) has made significant progress towards the goals defined in the work plan as of 2019. The Final Viability Assessment for FIRO at Lake Mendocino is expected to be completed on schedule in 2020. During Water Year 2019, Lake Mendocino was operated successfully under the major deviation by the US Army Corps of Engineers, using a decision support system developed for the Russian River.

One key aspect of FIRO is its transferability to other reservoirs in the west whose precipitation inputs are also dominated by atmospheric rivers. For example, a FIRO effort was established this past year on Prado Dam in southern California in a densely populated basin. This effort builds on lessons from Lake Mendocino and is identifying specific challenges unique to Prado. Future plans include working with reservoirs in other areas, with different environmental concerns and hydroclimates, to assess potential FIRO benefits.

Table 1. FIRO Steering Committee Members. Acronyms: USACE- US Army Corps of Engineers; NOAA – National Oceanic and Atmospheric Administration

Member	Agency	Period
Jay Jasperse (co-chair)	Sonoma Water	2014-present
F. Martin Ralph (co-chair)	University of California San Diego Center for Western Weather and Water Extremes	2014-present
Michael Anderson	California Department of Water Resources	2014-present
Levi Brekke	US Bureau of Reclamation	2014-present
Mike Dillabough	USACE San Francisco District	2014-2017
Nick Malasavage	USACE San Francisco District	2017-present
Michael Dettinger	US Geological Survey	2014-present
Rob Hartman	NOAA National Weather Service California Nevada River Forecast Center	2014-2016 (now participating as a consultant)
Alan Haynes	NOAA National Weather Service California Nevada River Forecast Center	2016-present
Christy Jones	USACE Sacramento District	2014-2016
Joe Forbis	USACE Sacramento District	2016-present
Patrick Rutten	NOAA Restoration Center	2014-2018
Natalie Manning	NOAA Restoration Center	2018-present
Cary Talbot	USACE Engineer Research and Development Center	2014-present
Robert Webb	NOAA Earth System Research Lab	2014-present

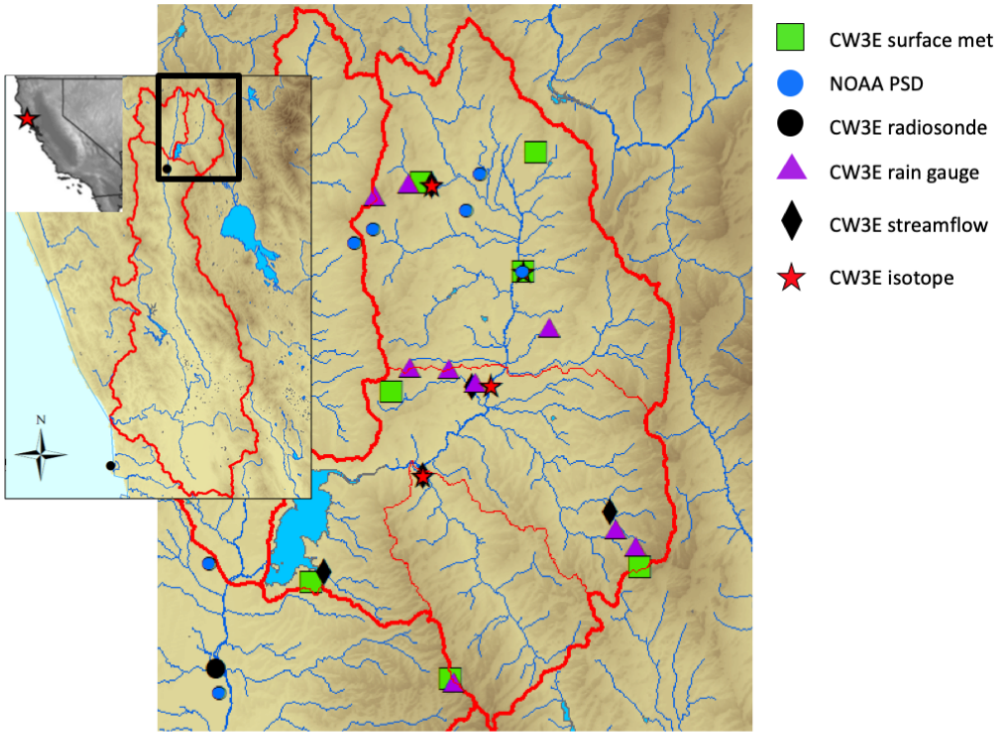

Figure 1. Map of stations located in the Lake Mendocino watershed in the Russian River. NOAA PSD stations are National Oceanic and Atmospheric Administration Physical Science Division run stations installed as part of the Hydrometeorological Testbed. All other stations were installed and are maintained by the Center for Western Weather and Water Extremes at the Scripps Institution of Oceanography, University of California San Diego. CW3E surface met generally includes temperature, precipitation, relative humidity, pressure, and soil moisture and temperature, but two sites also include vertically pointing radars and GPS-Met measuring integrated water vapor. Insets are provided showing the entire Russian River with both radiosonde stations and showing the location of the Russian River watershed in California.

References

Doyle, J.D., Reynolds, C.A., Amerault, C., and Moskaitis, J. 2012. "Adjoint sensitivity and predictability of tropical cyclogenesis," Journal of Atmospheric Science, AMS, 69:3535-3557.

Forecast Informed Reservoir Operations Steering Committee. 2017. "Preliminary viability assessment of Lake Mendocino," Available from: http://escholarship.org/uc/item/66m803p2.

Gershunov, A., Shulgina, T., Ralph, F.M., Lavers, D.A., and Rutz, J.J. 2017. "Assessing the climate scale variability of atmospheric rivers affecting western North America," Geophysical Research Letters, AGU, 44:doi:10.1002/2017GL074175.

Guan, B., Waliser, D., and Ralph, F.M. 2018. "An intercomparison between reanalysis and dropsonde observations of the total water vapor transport in individual atmospheric rivers," Journal of Hydrometeorology, AMS, 19:321-337.

Guirguis, K., Gershunov, A., Clemesha, R.E.S., Shulgina, T., Subramanian, A.C., and Ralph, F.M. 2018a. "Circulation drivers of atmospheric rivers at the North American west coast," Geophysical Research Letters, AGU, 45(22):12576-12584.

Guirguis, K., Gershunov, A., Shulgina, T., Clemesha, R.E.S., and Ralph, F.M. 2018b. "Atmospheric rivers impacting northern California and their modulation by a variable climate," Climate Dynamics, Springer, doi:10.1007/s000382-018-4532-5.

Jasperse, J., Ralph, F.M., Anderson, M., Brekke, L., Dillabough, M., Dettinger, M., Hartman, R., Jones, C., Rutten, P., Talbot, C., Webb, R., Ford, D., O'Donnell, A., and DuBay, A. 2015. "A comprehensive plan to evaluate the viability of forecast informed reservoir operations for Lake Mendocino," Sonoma County Water Agency report, 1-374.

Lavers, D.A., Rodwell, M.J., Richardson, D.S., Ralph, F.M., Doyle, J.D., Reynolds, C.A., Tallapragada, V., and Pappenberger, F. 2018. "The gauging and modeling of rivers in the sky," Geophysical Research Letters, AGU, 45:7828-7834.

Neiman, P.J., Moore, B.J., White, A.B., Wick, G.A., Aikins, J., Jackson, D.L., Spackman, J.R, and Ralph, F.M. 2016. "An airborne and ground-based study of a long-lived and intense atmospheric river with mesoscale frontal waves impacting California during CalWater-2014," Monthly Weather Review, AMS, 144:1115-1144.

Ralph, F.M., Coleman, T., Neiman, P.J., Zamora, R.J., and Dettinger,M.D. 2013. "Observed impacts of duration and seasonality of atmospheric river landfalls on soil moisture and runoff in coastal northern California," Journal of Hydrometeorology, AMS, 14:443-459.

Ralph, F.M., Neiman, P.J., Kiladis, G.N., Weickmann, K., and Reynolds, D.M. 2011. "A multiscale observational case study of Pacific atmospheric river exhibiting tropical-extratropical connections and a mesoscale frontal wave," Monthly Weather Review, AMS, 139:1169-1189.

Ralph, F.M., Neiman, P.J., Wick, G.A., Gutman, S.I., Dettinger, M.D., Cayan, D.R., and White, A.B. 2006. "Flooding on California's Russian River: Role of atmospheric rivers," Geophysical Research Letters, AGU, 33:L13801.

White., A.B., and co-authors. 2013. "A twenty-first century California observing network for monitoring extreme weather events," Journal of Atmospheric and Oceanic Technology, AMS, 30:1585-1603.

HEC-RAS Model Development in RAS Mapper

Cameron T. Ackerman, P.E., D.WRE, Senior Hydraulic Engineer,
Hydrologic Engineering Center, Davis, CA
cameron.ackerman@usace.army.mil
Alex J. Kennedy and **Gary W. Brunner, P.E., D.WRE**,
Hydrologic Engineering Center, Davis, CA

Abstract

HEC-RAS Mapper provides an efficient set of tools for the development of 1D and 2D HEC-RAS river hydraulic models. The hydraulic model development process begins with the development of a terrain model, continues with an interpretation of the land surface and elevations, establishing hydraulic model elements, and enters a cycle of iterating between model simulation, analysis of results, and model refinement. RAS Mapper tools will assist the modeler with the process of creating a terrain model and modifying incorrect elevation data. Visualization of the elevation data along with aerial imagery in HEC-RAS then allows for laying out 1D modeling objects (such as the river network and cross section locations) and creating 2D Flow Areas using the editing tools within RAS Mapper. Mapping of hydraulic results in RAS Mapper allows the modeler to quickly identify model deficiencies for improvement. 2D Flow Area mesh refinement tools and terrain modification capabilities let the hydraulic modeler efficiently improve model geometry and simulation results. This paper will introduce the tools available for developing a river hydraulics model in HEC-RAS for terrain modification, hydraulic elements and refinement, and mapping simulation results.

Introduction

Geospatial editing tools that allow the modeler to fully develop geometric data for a river hydraulics model were introduced in the Hydrologic Engineering Center River Analysis System (HEC-RAS) Version 5.0.4 (HEC 2016a). These vector-based, geospatial editing tools are currently considered to be in Beta condition until the release of HEC-RAS 5.1, when it is envisioned that the full capabilities available from the ArcGIS tool HEC-GeoRAS (HEC 2005) will be available. Editing capabilities have been developed within the RAS Mapper interface, allowing users to work with terrain models, develop geometric data, refine model layout, and visualize results directly within HEC-RAS; thereby, making the process of river hydraulics modeling a much more efficient effort than with previous workflows which required using a GIS pre- and post-porcessor. An example schematic for a combined 1D/2D HEC-RAS model, created within RAS Mapper, is shown in Figure 1.

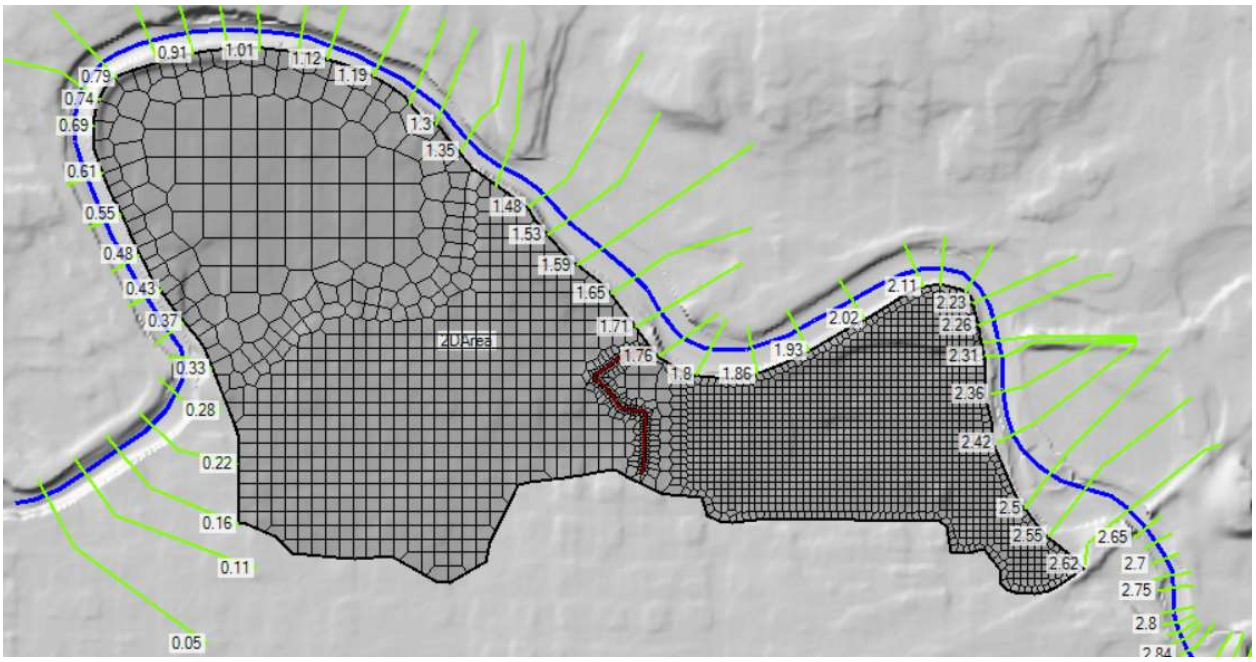

Figure 1. Example schematic of a combined 1D/2D HEC-RAS model domain.

Terrain

The basis for any accurate river hydraulics model is a good representation of ground surface elevations for the area of interest. A good terrain model accurately describes the elevations of the river channel and floodplain by incorporating important features such as the channel bottom and channel banks, and high ground such as roadways and levees that direct flow. If the initial terrain model insufficiently represents the ground surface, HEC-RAS provides tools for improving the terrain data directly in RAS Mapper. Terrain Modification tools in RAS Mapper can be used to improve the terrain by adding channel information, high ground (such as a levee), and features that impede flow (such as piers).

RAS Mapper support many different raster formats; however, you must import your terrain model into HEC-RAS prior to using it in RAS Mapper. The format that RAS Mapper uses for the Terrain layer is based on the GeoTiff file format. The GeoTiff file format supports file compression and pyramiding of the data which allows for smaller file sizes and faster visualization. The RAS Terrain specification allows the user to visualize multiple terrain models as one layer. Therefore, if your study area has multiple terrain models, you select them all in the Import dialog and specify a "priority" level for each. The terrain model tile having the highest priority is used first when evaluating terrain elevations (for extracting elevation data or inundation mapping). An example of the Terrain import dialog is shown in Figure 2.

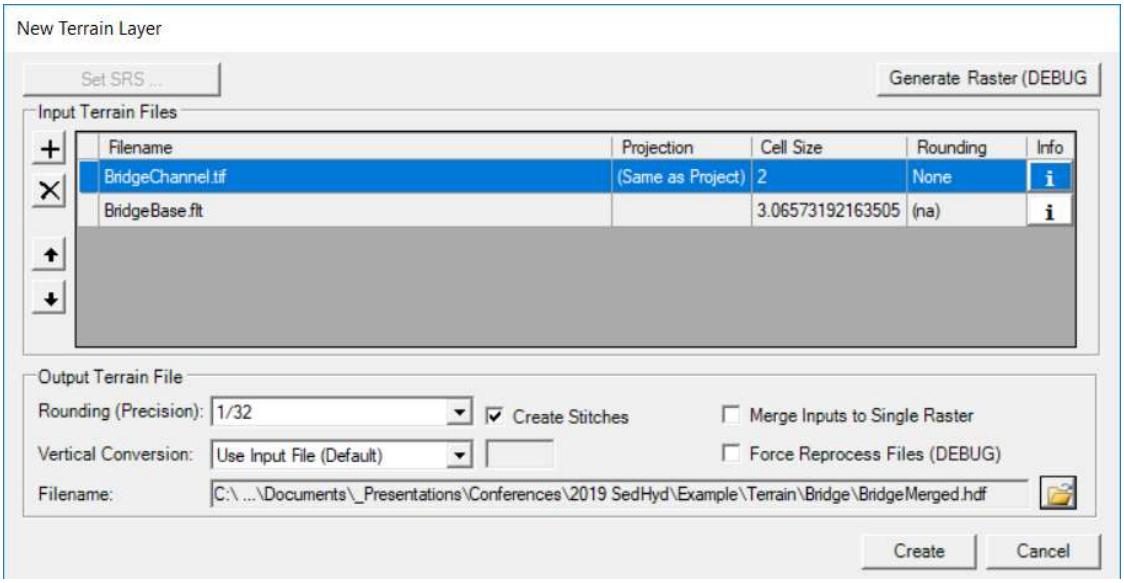

Figure 2. Creating a new Terrain Layer.

Terrain Modifications

Terrain modifications can be performed in HEC-RAS in two different ways. The first set of tools developed in RAS Mapper allows you to use the river centerline, cross sections, and bank lines to develop a surface of the channel or channel and overbank areas. That new surface can then be used to create a new terrain model that combines the channel surface (having top priority) along with other data. A new capability has been added, where the user is not required to create a new terrain model, but rather provide a vector override to the existing data. This means that the user can utilize the geospatial editing tools in RAS Mapper to create features and then apply them to a specific Terrain layer. Different ways to modify a terrain model for adding channel information, high ground, and constant elevations are discussed below.

Channel Information: Adding channel information to a Terrain model in HEC-RAS is accomplished using a river centerline and cross sections. There are work-arounds for missing channel information for a 1-D model by modifying individual cross sections, however, for 2D modeling it is imperative to have proper channel information. If you have an existing 1D model geometry, you can use the cross sections' geometry to "cut" channel information into the terrain. If you do not have an existing set of cross sections, you can create them for the area of interest and apply the cross section elevations to replace information in the channel. An example illustrating the removal of a bridge from the channel is shown in Figure 3.

The steps to include channel information for a specific area of interest (AOI) are provided below.

1. Create a new Geometry
2. Start Editing
3. Create a new River feature for the AOI
4. Create cross sections bounding the AOI
5. Stop Editing
6. Export the Geometry to a new GeoTiff (providing a cell size for the new dataset)
7. Create a new Terrain using the new channel information as the top priority and the old terrain model as the lower priority data

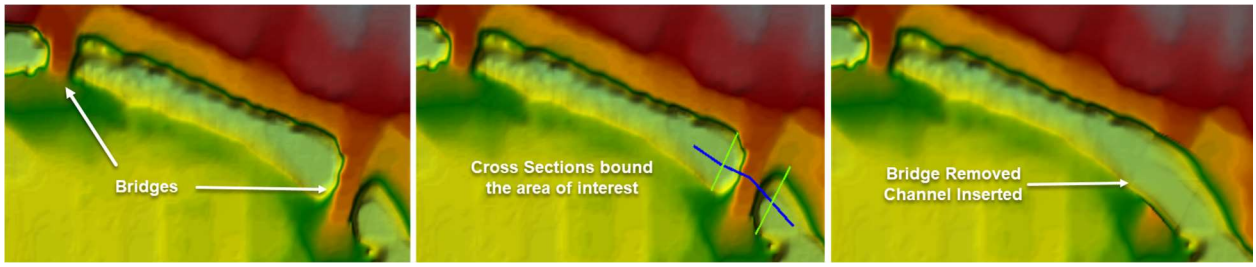

Figure 3. Replacing erroneous bridge data with channel information.

Adding High Ground Features: High ground features such as levees can be modeled in HEC-RAS using a Lateral Structure; however, often you want to modify the terrain model to include the high ground. High ground can be added into a Terrain just like adding channel information (as described above), by turning the cross sections "upside down". An alternate method has been added in RAS Mapper to modify the Terrain using a vector override. With this method, you provide a centerline for the location where the feature will be added and then provide elevation information, top width, and side slope information for the feature. The vector information is then directly added into the Terrain layer. The process for adding high ground into terrain is shown in Figure 4 along with the resulting terrain profile in Figure 5.

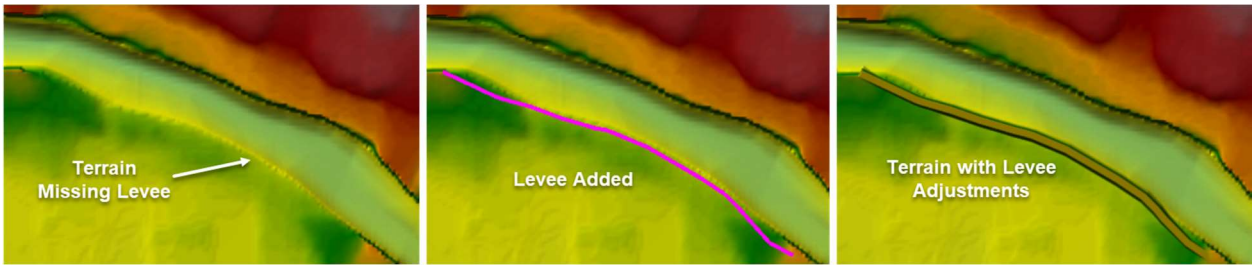

Figure 4. Process of adding high ground into a terrain.

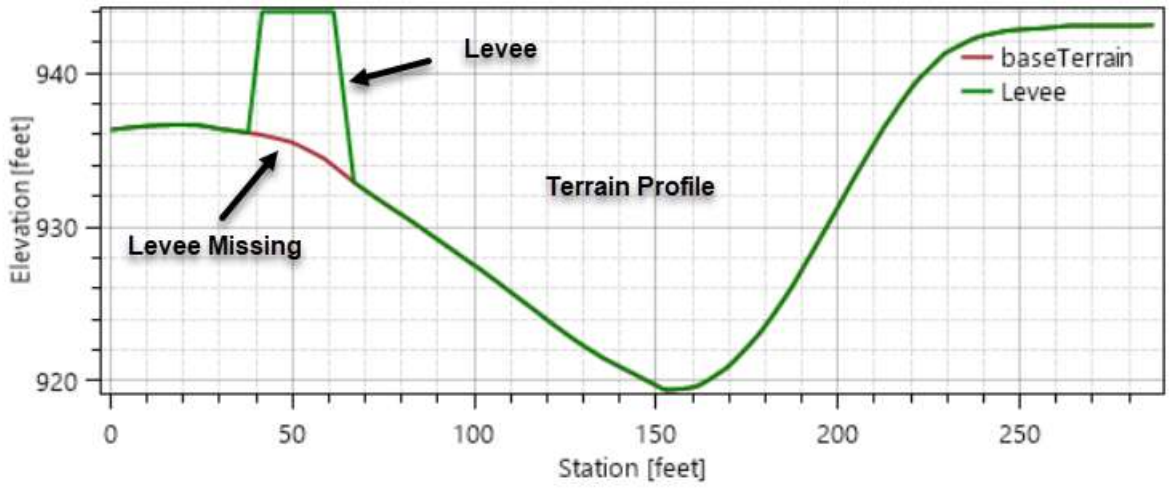

Figure 5. Terrain profile with and without the levee addition.

Constant Height Overrides: The Terrain layer can also be modified using constant height overrides to represent features that obstruct flow or that form storage areas. There are options for adding circles, rectangles, and polygon features. Similar to the high ground option discussed previously, these features are added to the Terrain as vector overrides. An example of adding circular piers at a bridge crossing is shown in Figure 6 and the resulting terrain profile in Figure 7.

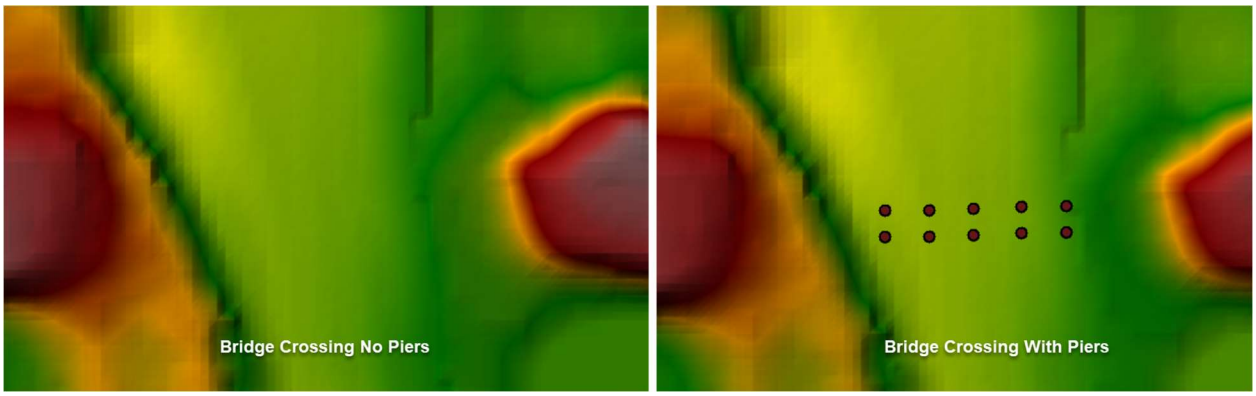

Figure 6. Terrain model with and without piers added.

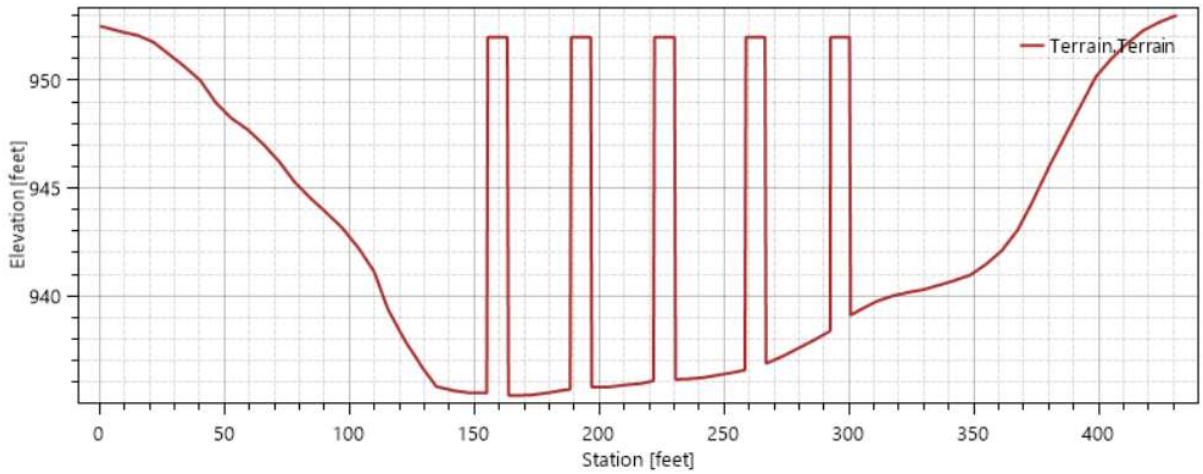

Figure 7. Resultant Terrain profile with piers.

Editing Tools

The RAS Mapper interface has become more than a tool for visualization results from HEC-RAS simulations. You can now manage geometry data by creating a new/empty geometry and then constructing RAS-specific layers (such as the river centerline, cross section locations, and bank lines) using the vector Editing Tools. Once hydraulic objects (such as cross sections) are created, they are used to extract elevation and proximity information for model development. Prior to editing, the user should identify the coordinate system they will be working in and import ground surface elevations into the Terrain layer that will be the basis for elevation computations. A description of the Editing Tools available in HEC-RAS are discussed in the

proceeding sections of this paper. For a more detailed account of how to use RAS Mapper tools, refer to HEC-RAS user's documentation (HEC 2016a, HEC 2016b, HEC 2018).

An edit session is initiated by right-clicking on the Geometry (or any feature layer within a Geometry) and choose the "Edit Geometry" option, as shown in Figure 8. The Geometry (or feature Layer) that is now being edited will show the Edit icon next to it and this will invoke the Edit Tool bar (see Figure 9).

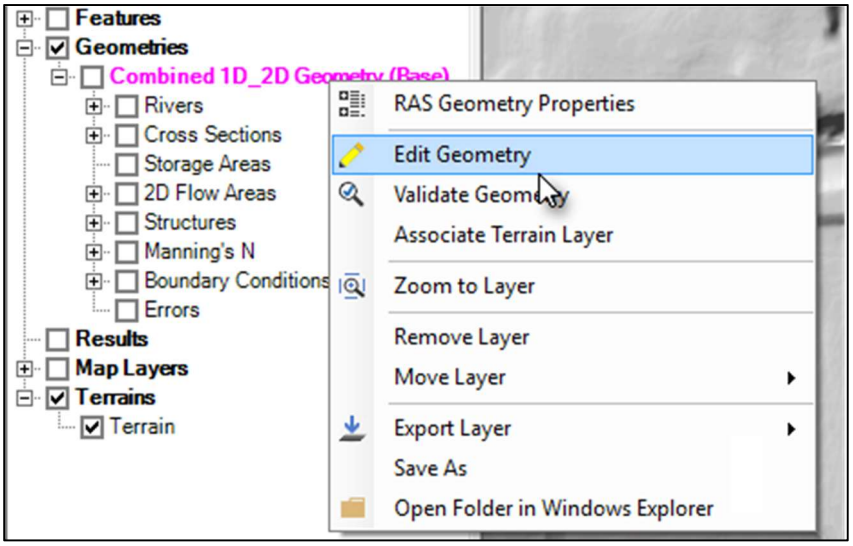

Figure 8. Initiating an edit session.

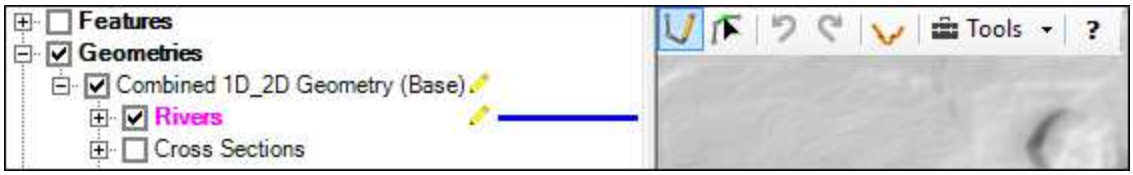

Figure 9. The Edit icon shows the active Edit Layer and the Edit Toolbar is displayed.

While in an edit session, you have access to many features (and will be discussed in proceeding sections); however, Undo Editing will be available to allow you reverse (undo) any digitizing mistakes that may occur along the way! To finish an edit session, you right-click on the Geometry (or Layer) and select "Stop Editing". You will be asked whether you want to save edits or discard the changes.

Edit Toolbar

The **Edit** toolbar (see Figure 10) is active when you are in an edit session and an editable layer is active/selected and the Selection tool is active on the main RAS Mapper toolbar. Tools from the main RAS Mapper toolbar are also available to **Pan** or **Zoom** (to provide the user flexibility);

however, if you switch away from the **Selection** tool, the **Edit** toolbar will no longer be active (make sure you click back to the **Selection** tool!).

Figure 10. The Edit Toolbar.

A focused effort has been made to make the **Edit** tools simple and straight forward. This has been done by concentrating the functionality into very few tools and attempting to provide user-feedback through mouse actions and colors (that change based on the mode you are in) to help you with each editing step. For instance, *Selected* items will be in **magenta** and *Action* items will be colored **chartreuse** (bright green). There are two primary **Edit** tools: the **Add New** tool and **Select/Edit Feature** tool. So you will either be adding a new feature to the Selected layer *or* you will be selecting a feature and then opening the feature for editing.

Add New: Adding new feature is enabled by selecting the **Add New** tool. The RAS Mapper cursor will change to the **Add** cursor indicating that you can start adding a point for feature creation. Click to add a point on the feature; double-click to finish. When completed the feature will remain highlighted allowing you to grab it and move it or delete it. The process of adding a new feature is shown in Figure 11.

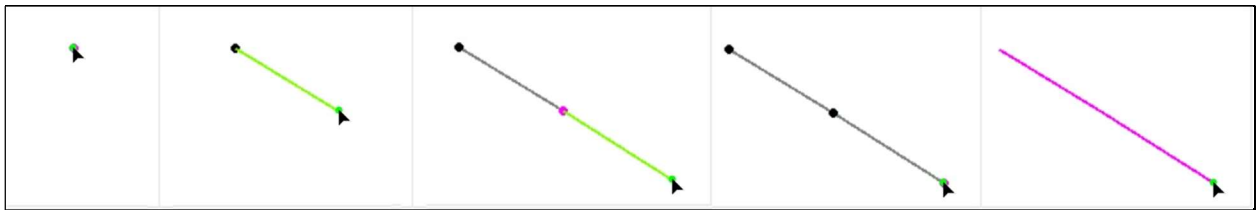

Figure 11. Adding a new line feature in RAS Mapper.

Select/Edit Feature: Selecting an existing feature (to move, edit, delete) and editing are done with the same tool. The workflow allows you to select and interact with features with a single tool. If you don't have any features selected, the tool prompts you to select a feature. Once a feature is selected or opened, a different set of context specific options are provided to the user. Select/edit mode is enabled by selecting the **Select/Edit** tool. The RAS Mapper cursor will change to the **Selection** cursor indicating that you can select a feature for editing. To select a feature, click it or draw a selection box over the features of interest. As shown in Figure 12, as you select a feature the name of the Layer you are selecting from will be written to the screen. Once selected, you can move the feature or double-click to begin editing. The **Hand** cursor is the indication to the user that you can move a feature or a vertex on an open feature. The Add cursor is the indication that you can insert a vertex. As shown in Figure 13, when moving or inserting a point, the graphic will be draw in the Action color – identifying what will result.

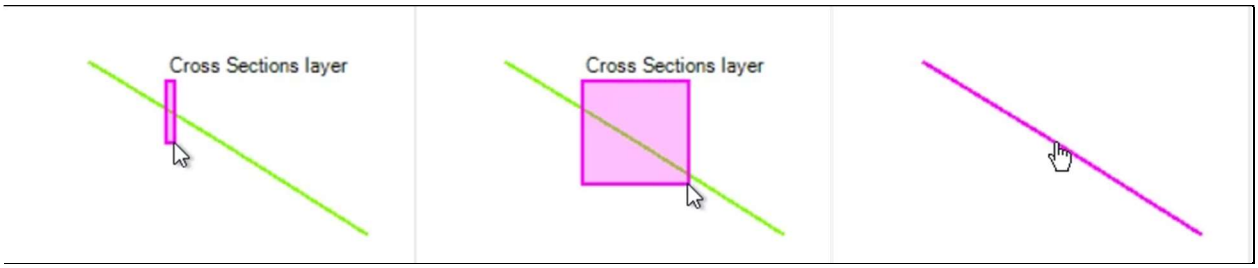

Figure 12. Selecting a feature in RAS Mapper.

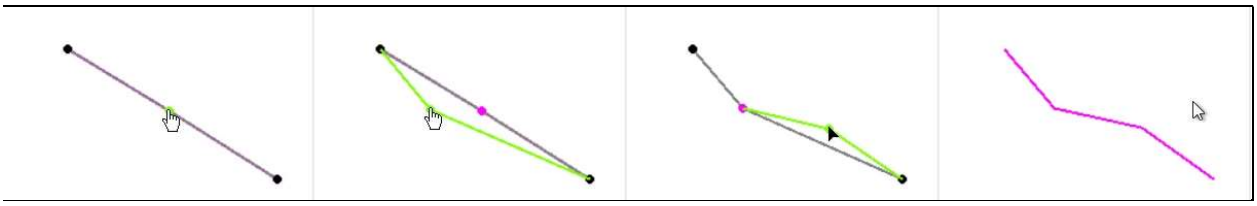

Figure 13. Opening a feature for editing, moving a point, and inserting a point are all done with the same tool in RAS Mapper.

Context menus are available for Selected Features, through a right mouse click. The menu items will be specific to the type of feature that is selected. An example of a context menu is shown in Figure 14.

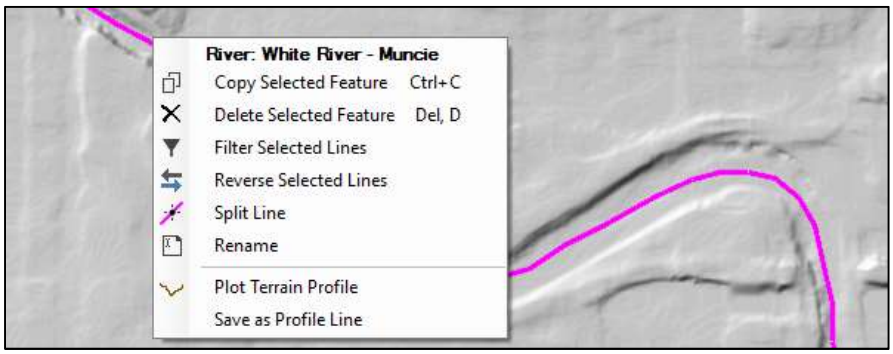

Figure 14. Context menu for a River feature in RAS Mapper.

Undo/Redo: **Undo** and **Redo** capabilities are available from the **Edit** toolbar when mistakes are made while digitizing features. Undo and Redo can also be accessed using Ctrl+Z and Ctrl+Y, respectively, from the keyboard.

Plot Elevations: The **Plot Elevation** button allows for plotting the elevation profile under the selected feature. The profile plot window is active, so as a cross section (or another feature) is modified the plot will automatically update. This is convenient when trying to ensure a cross section extends out to a certain elevation.

Tools: The **Tools** Tools menu item provides access to various feature-specific options. The menu items will automatically reflect options that are available for the feature that is selected, such as Copy, Paste, Merge, Clip, Filter, and Edit/View Points.

Help: The **Help** ? button provides access to an interactive help window to assist new users in getting accustomed to the **Edit** tools. Additionally, it provides some quick tips for interacting with RAS Mapper. For instance, while in an editing session, holding down the Shift key or middle mouse button, allows the user to pan; right-clicking on the map while in Add New mode will automatically re-center the screen; pressing the Tab key will swap between Add New and Select/Edit Feature modes; holding the spacebar down while selecting a feature will change the selected layer.

1D Modeling Layers

A 1D model is appropriate for modeling rivers and floodplains where the direction of flow can be identified prior to creating the hydraulics model. The river network is represented with a River centerline layer, while cross sections are created perpendicular to flow in the main channel and overbank areas. The main purpose of the cross sections is to properly capture the amount of conveyance available in the river floodplain for routing flow downstream. Other RAS Layers are created to compute additional properties. An example 1D model layout with primary RAS Layers is shown in Figure 15.

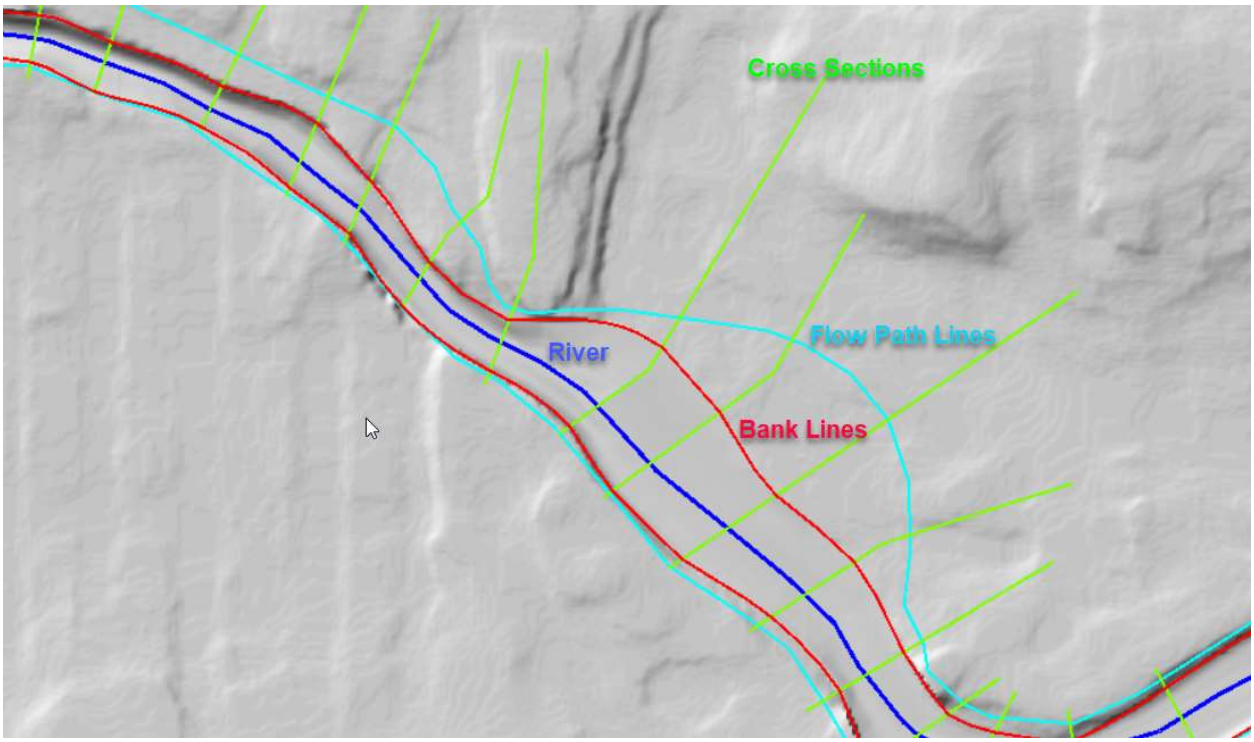

Figure 15. 1D model layout using RAS Layers in RAS Mapper.

RAS Mapper will provide the framework for these geometric layers that need to be constructed. As features are constructed, the user will be prompted to complete information specific to that layer. For instance, when creating a new river line, the user will be prompted to enter a River Name and a Reach Name. A summary of the layers that are available for 1D model construct is provided in Table 1.

Table 1. Summary of 1D modeling layers in RAS Mapper.

Layer	Description	
Rivers	The **Rivers** layer is used to establish the river network. It must be created in the upstream to downstream downstream direction. The **Rivers** layer will be used in concert with the XS Cut Lines layer to establish river stationing for each cross section and compute the main channel reach length between cross sections. The Rivers Layer organizes similar features in the **River Group** that determine how water flows in the river network. The **River Group** includes:	
	Junctions	**Junctions** are automatically created at the confluence of three river reaches.
	Bank Lines	This layer is used to establish the main channel bank stations for the cross sections and should not intersect the **Rivers** lines.
	Flow Paths	**Flow Path** lines are used to compute cross section reach lengths from cross section to cross section in the left and right overbanks. The river centerline will be used to compute the main channel reach length. If the flow paths layer is not specified the main channel reach length will be used in the overbanks.
	River Station Markers	The **River Station Markers** layer is a point layer that can be used to manually assign river stationing along the River Centerline. Values are linearly interpolated between assigned station values.
Cross Sections	**Cross Sections** (XS) are used to establish the spatial location and alignment of cross sections. Cross section elevation profiles will be extracted from the terrain model. Other cross section properties are extracted based on their intersection with other layers. Cross sections must be laid out from left to right while looking downstream The **Cross Sections** layer organizes cross-section specific layers into a **Cross Sections Group**, which includes:	
	Bank Stations	A point layer which identifies the location of the bank station on the cross section.
	Edge Lines	**Edge Lines** are used connect the ends of cross sections. This layer may be edited *between* cross sections; however, the edge line points at the cross section endpoint may not be modified.
	Interpolation Surface	The **Interpolation Surface** is not editable. This layer is constructed from the River Centerline, XS Cut Lines, Bank Lines, and Edge Lines. The interpolation surface is used for mapping HEC-RAS results.
Storage Areas	**Storage Areas** are a set of polygon features that can be used to extract an Elevation-Volume relationship.	
Errors	The **Errors** layer is designed to assist the user in identifying geometric mistakes. For instance, if a cross section is intersected by the river line more than once, and error will be produced.	

The primary 1D modeling layer is the Cross Sections layer. It will be used to extract elevation data and compute additional modeling parameters. By default, the modeling parameters will be automatically recomputed with each feature addition or modification. However, if the data you are working with is an "existing" model, the data updates will only occur when a new feature is added. Therefore, if you modify an existing cross section, you must manually force a re-compute of the information you wish to update. This is done by right-click on the Cross Sections layer and choosing the **Compute** menu item. An example of parameters available for update is shown in Figure 16. Clicking on the Cross Sections layer will update all features; right-clicking on an individual feature will work on the selected set.

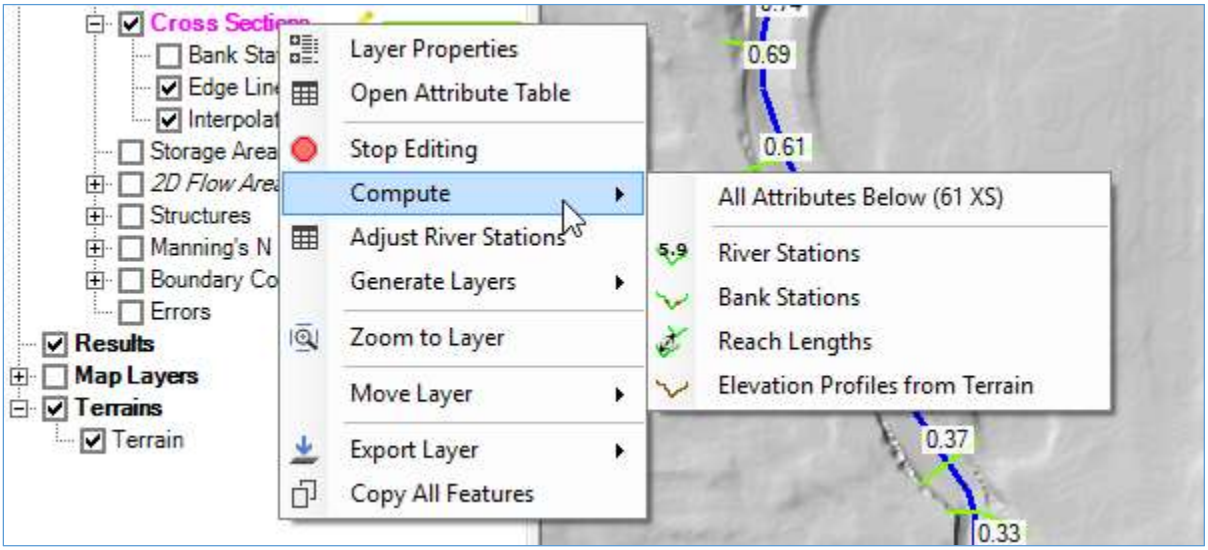

Figure 16. Manual update of Cross Section properties.

2D Modeling Layers

A 2D model is appropriate for modeling rivers and floodplains where the direction of flow is not constrained to one direction that can be identified prior to creating the hydraulics model. A 2D Flow Area in HEC-RAS is represented by computational cells which account for cell volume and direct flow movement via cell faces. RAS Mapper will provide the framework for the geometric layers that are available for creating a 2D Flow Area. A summary of layers used to create a 2D model is shown in Table 2.

Table 2. Summary of 2D modeling layers in RAS Mapper.

Layer	Description	
2D Flow Areas	The 2D Flow Areas layer stores the computed mesh. This Layer also organizes information used to build a 2D Flow Area mesh.	
	Perimeters	A polygon is used to represent the boundary of each 2D Flow Area.
	Computation Points	The "cell centers" are stored in the Computation Points layer.

Layer	Description	
	Break Lines	Breaklines are line features used to enforce cell faces. Each breakline will have a Name and Cell Spacing information.
	Refinement Regions	Refinement Regions are used to modify the cell spacing in a 2D Area. The regions can be used to increase or decrease the density of the computation points. Perimeters are enforced like a breakline.
Manning's N (Group)	This group layer has a raster layer of *n* values used and a vector layer to override base values.	
	Override Regions	The Override Regions layers is a vector layer used to override the base Manning's n value data. The user will specify a description and n value for each polygon in the layer.
	Final *n* values	This layer is a raster composite of base n values and override n values. These are the values used when developing hydraulic property tables for 2D modeling.
Errors	The Error Layer is designed to assist the user in identifying geometric mistakes. For instance, if a 2D cell has too many faces, an error will be produced.	

A 2D Flow Area is comprised of the bounding Perimeter. Computational cells are derived around Computation Points within the bounding Perimeter and are used for the flow calculations. The 2D flow calculations in HEC-RAS are dependent on the location of cell faces (which control the flow of water, much like cross sections). Therefore, the RAS Mapper editing tools provides the ability to add breaklines which allows the user to "enforce" the location of cell faces along high ground. Lastly, a Refinement Regions layer is provided which allows the user to easily increase or decrease the cell sizes within the 2D Flow Area. An example 2D Flow Area with a breakline and refinement regions is shown in Figure 17.

Figure 17. Example 2D model domain with an enforced breakline and refinement regions.

Visualization of Results

Visualization of computed water surface results are directly available in RAS Mapper. The development goal of RAS Mapper visualizations is to be able to quickly see the results from simulations. Therefore, the default method for map creation is what is termed "Dynamic" mapping – maps are generated on-the-fly for the area of interest, at the resolution commensurate with the zoom level and screen size. This allows you to animate water surface profiles without the "down time" of computing unnecessary information (locations you are not looking at) or writing the data to disk.

There are several ways to evaluate computed results in RAS Mapper. Depth, Velocity, and Water Surface Elevation maps are automatically generated for the user; however, more complicated maps using multiple variables such as Depth times Velocity, Courant, Froude, Shear Stress, and Arrival Time are available. The default methods of data query allow the user to animate the maps for a specific water surface profile or time step and then use the mouse hover to report values. For unsteady-flow simulations, you can plot a time series of results for any visible map. You can compare multiple plans by making the results visible and plotting the desired maps. An example map, comparing 2D model results of different cells sizes, is shown in Figure 18.

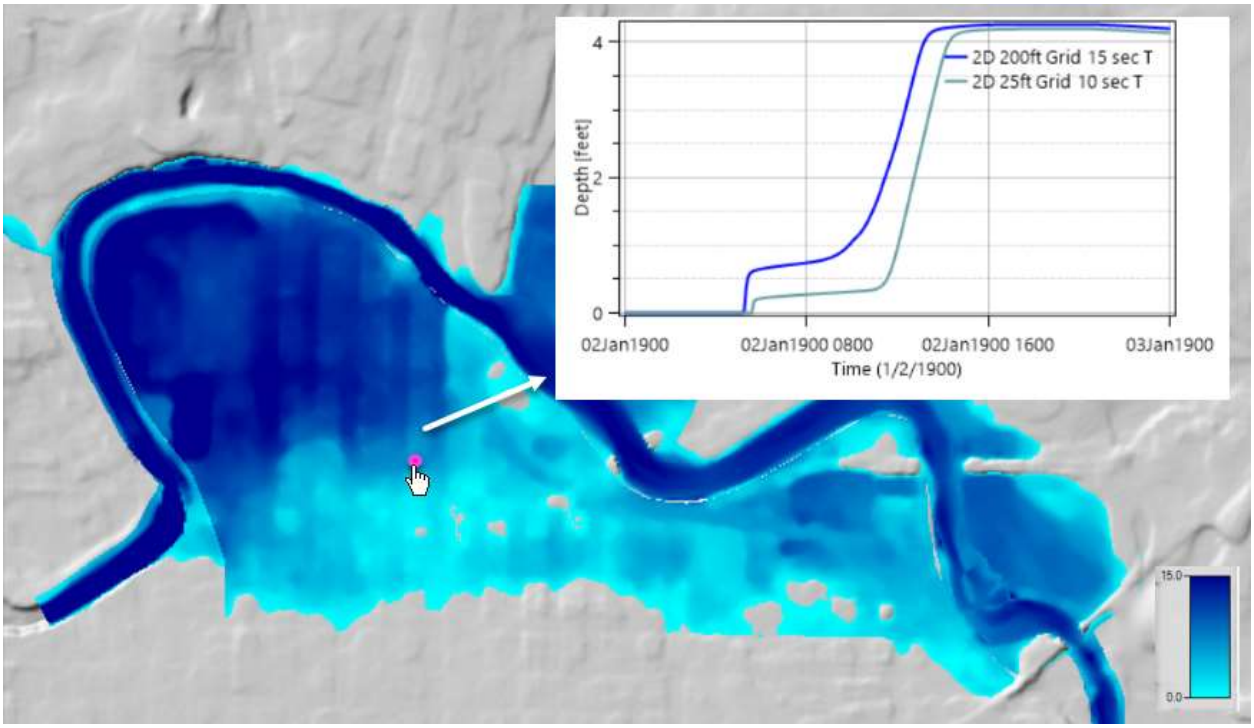

Figure 18. Time series comparison of 2D models with different computation cell sizes.

There are many other ways to provide user feedback on hydraulic computations through different plotting options, changing symbology, querying data and through user-specified profile

line plots. To further assist you in data evaluation, HEC-RAS 5.1 will have a new feature termed the RASter Calculator. The RASter Calculator will allow you to perform operations on raster maps to more easily interpret your data. More specifically, the RASter Calculator has been implemented to allow you to write your own Visual Basic (or C Sharp) scripts to perform mathematical operations, as well as evaluate logical expressions. The resulting output map can then be visualized in RAS Mapper along with all of your other geospatial data. Included with the RASter Calculator is an extensive Help system that will provide numerous examples to assist you in results analysis. An example script which demonstrates a comparison of water surface results for two different 2D model runs is shown in Figure 19. The resulting map from the script, showing the effect of grid cell size on model results, is then shown in Figure 20.

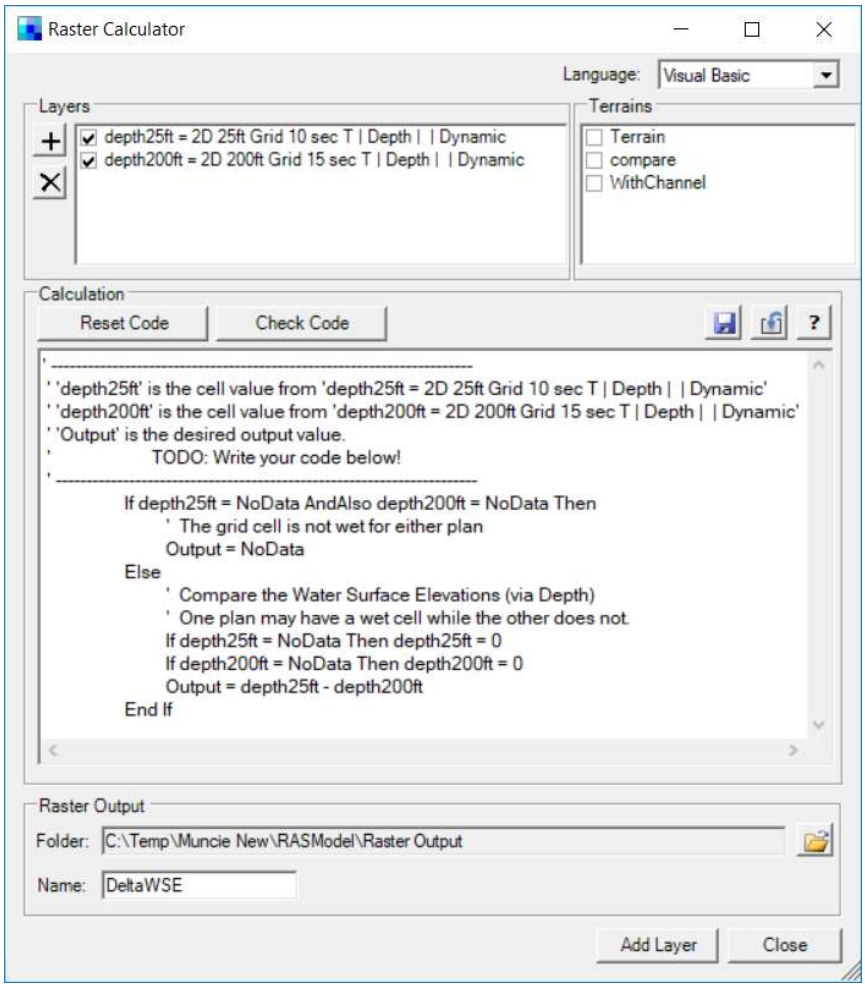

Figure 19. The RASter Calculator with example code to compare two plans.

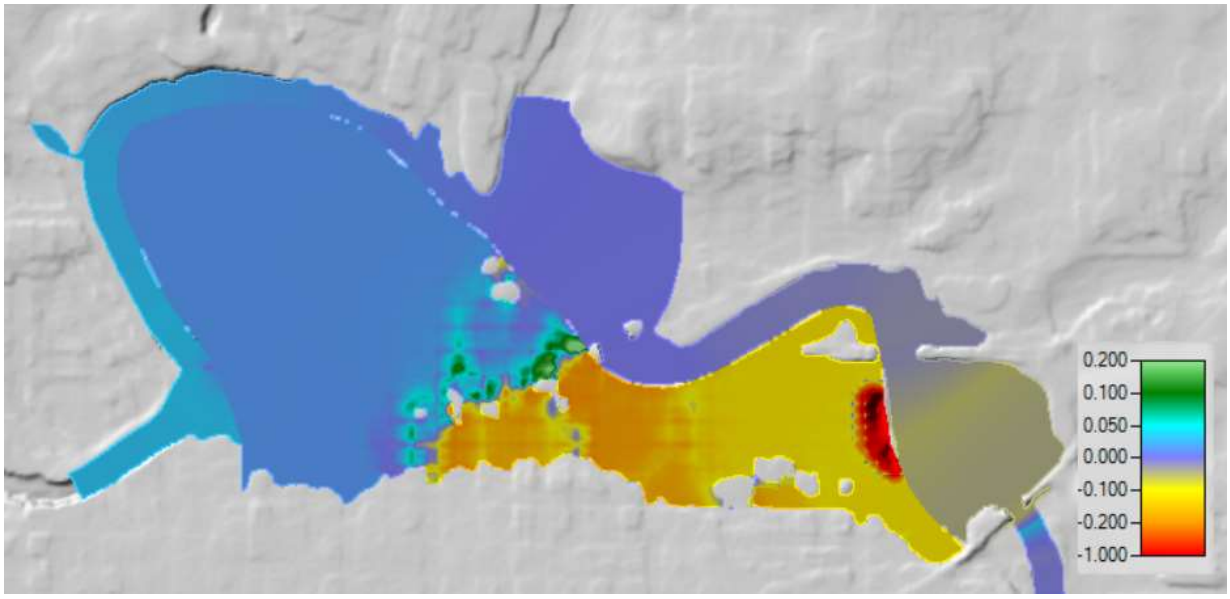

Figure 20. Comparison of a levee breach scenario for two 2D model runs with different grid cell sizes.

The addition of the RASter Calculator to RAS Mapper will allow the user to develop complicated scripts to evaluate HEC-RAS results unique to the modeler and the hydraulic conditions being evaluated. Modelers will not be beholden to a GIS to perform complex math operations for creating visualizations but can do it directly in HEC-RAS to more efficiently gain insight into answering the questions the hydraulic model is intended to solve. One such question might that be answered is what is the likelihood of survival given flood depth and velocity criteria. An example hazard map generated using raster scripting is shown in Figure 21 with the associated script shown in Figure 22.

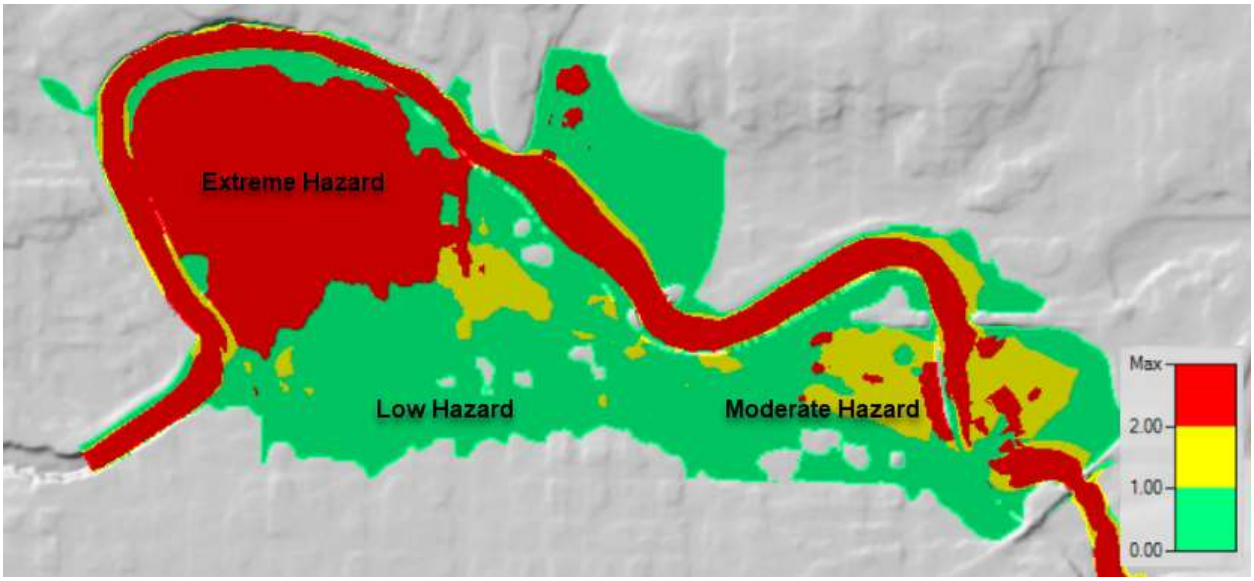

Figure 21. Hazard map generated using the RASter Calculator.
(Red = Extreme, Yellow = Moderate, Green = Low)

```
Const GREEN as Single = 0
Const YELLOW as Single = 1
Const RED as Single = 2

If d = NoData OrElse v = NoData Then
    Output = NoData
Else
    ' Conversion to metric assuming input variables are in feet
    d = d * 0.3048
    v = v * 0.3048
    ' Evaluation of early exits for bounds
    If d > 1.2 Then
        ' Extreme Hazard upper Depth bound
        Output  = RED
    ElseIf v > 3.0 Then
        ' Extreme Hazard upper Velocity bound
        Output  = RED
    ElseIf d < 0.2 Then
        ' Safe/lower bound
        Output  = GREEN
    ElseIf v < 0.5 Then
        ' Safe/lower bound
        Output  = GREEN
    Else
        ' Evaluate potential hazard
        If d * v <= 0.6 Then
            Output  = GREEN
        ElseIf d * v <= 1.2 Then
            Output  = YELLOW
        Else
            Output  = RED
        End If
    End If
End If
```

Figure 22. Example script for creating a flood hazard map where "d" is Depth and "v" is Velocity.

Conclusions

The addition of geospatial editing tools in RAS Mapping provides a major improvement to the HEC-RAS software. It will greatly aid in the efficient creation of model geometry and allow users to quickly make adjustments to refine and improve the model results. Allowing users to modify the input terrain elevations will allow modelers to correct and improve the base elevation data sources that are essential to hydraulic modeling. Terrain modifications with vector additions will allow modelers to represent features that direct the flow and storage of water. With these terrain tools directly available within HEC-RAS, modelers can skip the time-consuming GIS process of creating new terrain models for alternate conditions. Lastly, while there are many improvements to how modelers can visualize and query information in HEC-RAS, the introduction of the RASter Calculator will provide flexibility in combining multiple datasets to help answer questions that arise during the hydraulic modeling process. Further, improved visualization of simulation results with specific map outputs will lead to better communication of modeling results.

References

HEC (2005). *HEC-GeoRAS – An extension for support of HEC-RAS using ArcGIS*, CPD-83, September 2005. Hydrologic Engineering Center, Institute for Water Resources, U.S. Corps of Engineers, Davis, CA.

HEC (2016a). *HEC-RAS River Analysis System, User's Manual, Version 5.0*, CPD-68, February 2016. Hydrologic Engineering Center, Institute for Water Resources, U.S. Army Corps of Engineers, Davis, CA

HEC (2016b). *HEC-RAS River Analysis System, 2D Modeling User's Manual, Version 5.0*, CPD-68A,February 2016. Hydrologic Engineering Center, Institute for Water Resources, U.S. Army Corps of Engineers, Davis, CA

HEC (2018). *HEC-RAS River Analysis System, Supplemental User's Manual, Version 5.0.4*, CPD-68d, April 2018. Hydrologic Engineering Center, Institute for Water Resources, U.S. Army Corps of Engineers, Davis, CA

Ice Jam, Two-Dimensional, and Levee Breach Modeling at Miles City, Montana

Curtis Miller, Hydraulic Engineer, U.S. Army Corps of Engineers, Omaha, NE, Curtis.J.Miller@usace.army.mil

Abstract

Miles City sits at the confluence of the Tongue and Yellowstone Rivers in eastern Montana. Both rivers are largely unregulated and experience ice-affected flooding. The community has a non-accredited levee (i.e. not recognized by FEMA as providing protection from the 1% annual chance exceedance flood) protecting much of the city from both rivers; however, the levee exhibits numerous engineering and maintenance deficiencies including erosion problems, mature trees on the levee, and structural encroachments along the levee toe. Efforts completed for a U.S. Army Corps of Engineers Section 205 Study (a study authorizing small flood risk management projects) include one-dimensional open water and ice jam modeling and two-dimensional levee breach modeling. Difficulties associated with the study include the coincidence of flooding on the two rivers and a high level of uncertainty with respect to ice effects and levee breach parameters. A number of sensitivities were conducted to evaluate the key parameters with respect to flooding in the community. The Hydrologic Engineering Center's River Analysis System (HEC-RAS) was used for both the one-dimensional and two-dimensional modeling. While the highest river stages are typically caused by ice-affected flooding, open water floods can also impact the community. Composite stage-frequency curves were developed from the one-dimensional model based on FEMA guidance. These curves, combined with balanced hydrographs, were transformed into stage-hydrographs which were used as boundary conditions for the two-dimensional model.

Introduction

Miles City sits at the confluence of the Tongue and Yellowstone Rivers in eastern Montana. Both rivers are largely unregulated and experience ice-affected flooding. The community has a non-accredited levee protecting much of the city from both rivers; however, the levee exhibits numerous engineering and maintenance deficiencies including erosion problems, mature trees on the levee, and structural encroachments along the levee toe. Efforts completed for a U.S. Army Corps of Engineers Section 205 Study include one-dimensional open water and ice jam modeling and two-dimensional levee breach modeling.

Several factors contribute to the complexity of the analysis required to evaluate flood damages and potential risk management alternatives at Miles City, MT. Figure 1 shows a general overview of the area. Complicating factors include, but are not limited to, the following:

- Two flooding sources exist (Tongue River and Yellowstone River).
- Ice-affected flooding occurs on both rivers. Both ice-affected and open water modeling was completed, and the results were used to develop composite profiles.
- Flows leaving the Tongue River flow away from the river through town and eventually return to the Yellowstone River.
- The existing levee is not eligible for PL84-99 status, which provides reimbursement for specific damages to levees that result from high-water events. Additionally, its fragility with respect to underseepage, through-seepage, and stability is uncertain due to a lack of knowledge of the materials used for construction, foundation, and maintenance practices. Five locations were selected to evaluate levee breaches (three on the Tongue

River, two on the Yellowstone River). The three breach locations on the Tongue River are the focus of this evaluation since the 205 Study is for the Tongue River. Yellowstone River breach locations must be considered for future alternatives analysis to ensure any protective measures (e.g. levee) would protect against Yellowstone River flooding as well as Tongue River flooding.

- Two railroad embankments run through town essentially splitting the town into three distinct damage areas. While certain floods may overtop the RR embankments, for this analysis, failure of the embankments is not considered in order to simplify the analysis and reduce the potential number of model runs required to evaluate each possible combination of failures.

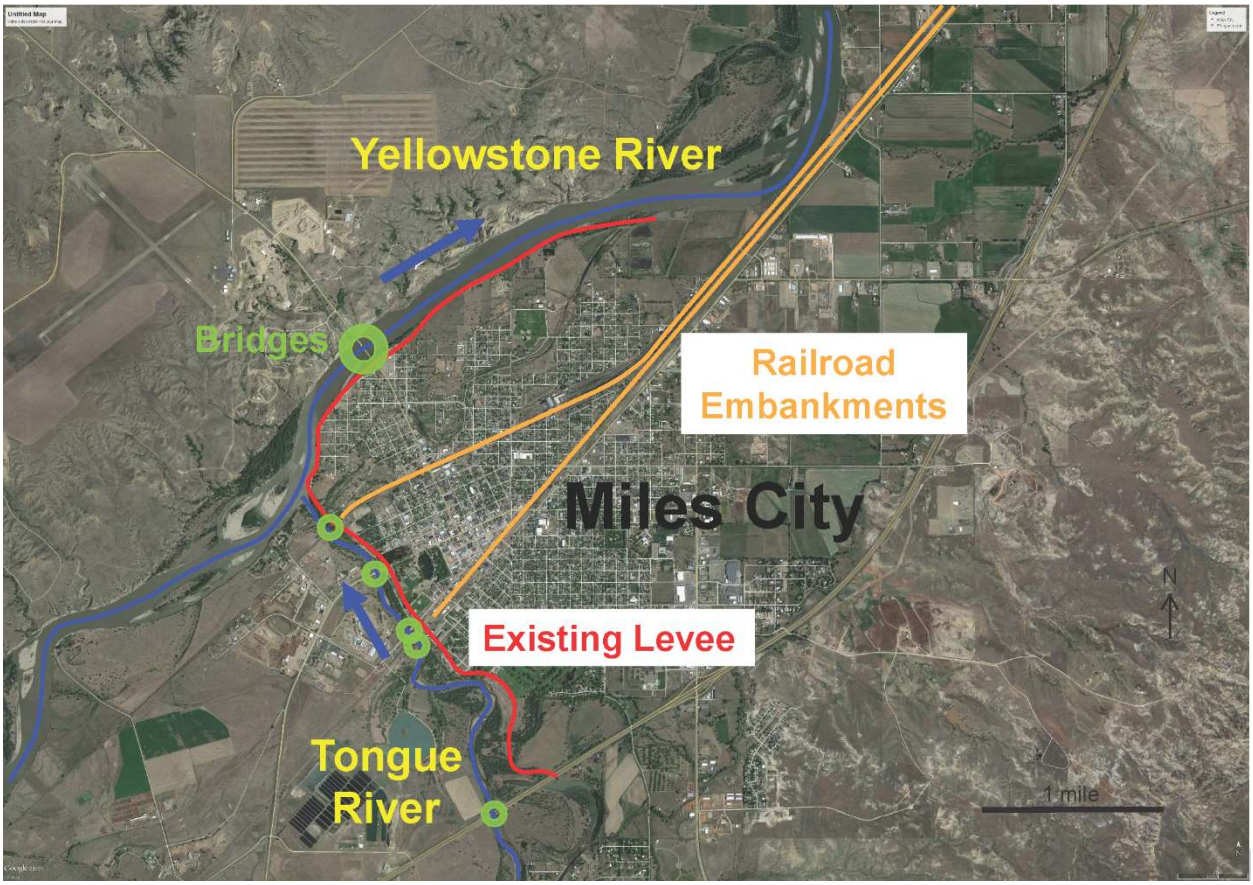

Figure 1. General overview of study area

Analysis

A summary of the overall modeling methodology for the hydraulic analysis is provided below.

1. Model Yellowstone and Tongue Rivers in 1D HEC-RAS for both open water and ice conditions. The 1D model only evaluates the river itself and the left overbank (i.e. cross sections are cut off at the levee on the right overbank).
2. Generate composite stage-frequency data at each cross section using spreadsheet.
3. Convert balanced flow-hydrograph to stage-hydrograph using annual flow values equated to composite stage-frequency developed in step 2. The stage-hydrographs were

developed at each of the breach location cross sections as well as at outflow locations from the 2D area.

4. Apply stage-hydrographs at 2D area boundaries, and evaluate flow through the city due to breaches through internal 2D area connections representing the levee.
5. Combine 2D water surface elevation grids with 1D results to generate a single water surface elevation grid (per event) for use in HEC-FDA (Hydrologic Engineer Center's Flood Damage Reduction Analysis software).

One-Dimensional Open Water and Ice Modeling

A one-dimensional hydraulic model was created to evaluate both open water and ice-affected conditions. The Hydrologic Engineering Center's River Analysis System (HEC-RAS) Version 5.0.3 was used in the analysis (Brunner 2016a). Figure 2 shows the modeled cross sections in green.

Figure 2. One-dimensional HEC-RAS cross sections

The open water modeling at Miles City was generally straightforward and followed accepted practices. The ice-affected modeling required analysis of ice thickness and application of some engineering judgment. The modified Stefan equation as presented in Engineering Manual 1110-2-1612 (USACE 2002) was used to evaluate ice thickness based on the accumulated freezing degree days (AFDD). The computed ice thickness as well as the first and second standard deviations about the mean is shown in Table 1.

Table 1. Computed ice thickness

	$AFDD_{max}$	Computed Ice Thickness (inches)	
		Yellowstone	Tongue
		C=0.7	C=0.5
2 st. dev. above mean	3284	40	29
1 st. dev. above mean	1794	30	21
Mean	**980**	**22**	**16**
1 st. dev. below mean	535	16	12
2 st. dev. below mean	292	12	9

Composite water surface profiles were developed by combining the open water and ice affected results using FEMA guidance (FEMA 2002).

Two-Dimensional Modeling

Model Setup: The two-dimensional (2D) flow area was created based on general knowledge of the Miles City floodplain using HEC-RAS Version 5.0.3 (Brunner 2016b). Terrain data was based on 2.5 meter DEM data created from LiDAR gathered in 2007. Breaklines were added at all major embankments, roads, and other features with hydraulic significance. A land use layer was developed to represent roughness within the 2D flow area. The base land use layer used the 2011 National Land Cover Database (NLCD). The NLCD data was supplemented with polygons representing streets. Selected roughness values, along with high and low sensitivity roughness values, are shown in Table 2.

Table 2. Manning's roughness values

						Sensitivity values		
NLCD Value	Land Cover Definition	Roughness *	NRCS- Kansas **			Low Roughness	**Selected "Base" Value**	High Roughness
			Low	Normal	High			
11	Open Water	0.035	0.025	0.04	0.05	0.02	**0.030**	0.05
21	Developed, Open Space	0.08	0.03	0.04	0.05	0.03	**0.040**	0.1
22	Developed, Low Intensity	0.1	0.08	0.1	0.12	0.06	**0.100**	0.12
23	Developed, Medium Intensity	0.12	0.06	0.08	0.14	0.08	**0.120**	0.14
24	Developed, High Intensity	0.15	0.12	0.15	0.2	0.08	**0.150**	0.2
31	Barren Land	0.04	0.023	0.025	0.03	0.023	**0.030**	0.05
41	Deciduous Forest	0.12	0.1	0.16	0.16	0.1	**0.120**	0.16
42	Evergreen Forest	0.12	0.1	0.16	0.16	0.1	**0.120**	0.16
43	Mixed Forest	0.12	0.1	0.16	0.16	0.075	**0.100**	0.16
52	Shrub/Scrub	0.08	0.07	0.1	0.16	0.07	**0.080**	0.16
71	Grassland/Herbaceous	0.045	0.025	0.035	0.05	0.025	**0.045**	0.055
81	Pasture/Hay	0.06	0.025	0.03	0.05	0.025	**0.050**	0.08
82	Cultivated Crops	0.06	0.025	0.035	0.05	0.025	**0.045**	0.06
90	Woody Wetlands	0.1	0.045	0.12	0.15	0.045	**0.100**	0.15
95	Emergent Herbaceous Wetlands	0.12	0.05	0.07	0.085	0.035	**0.050**	0.1
	Streets					0.013	**0.020**	0.027
	* Values estimated using description of NLCD land covers and "Open-Channel Hydraulics" (Chow, 1959)							
	** "Manning's n Values for Various Land Covers To Use for Dam Breach Analyses by NRCS in Kansas" (NRCS - Kansas, 2016)							

Application of Stage-Hydrographs: The composite water surface elevations developed from the one-dimensional model were used to create balanced stage-hydrographs. Flow hydrographs were developed by USACE (USACE 2018) based on volume-duration analysis using all-seasons daily flow data. The all-seasons flows were equated to composite stages by frequency. The flow hydrographs were then transformed into stage-hydrographs using the all-seasons flow/composite stage relationship.

The stage-hydrographs were applied as exterior boundary conditions on the 2D flow area. The 2D flow area was expanded around the perimeter to extend beyond the existing levee. The levee was then modeled using an internal connection; this allowed modeling of levee breaches. Figure 3 shows one example of the expanded 2D flow area and levee.

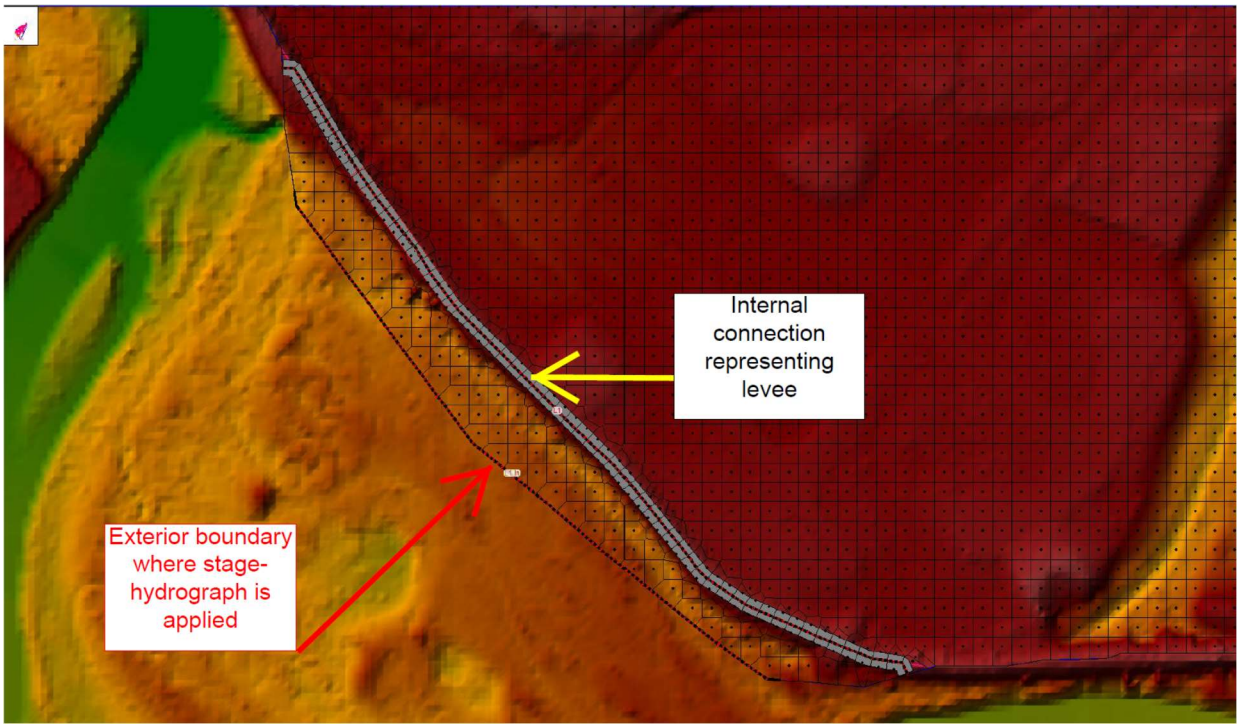

Figure 3. External edge of 2D area showing boundary for application of stage-hydrograph and internal connection

Levee Breach Modeling: The primary challenge for modeling a levee breach is development of breach widths and formation times. The Hydrologic Engineering Center (HEC) has been gathering levee breach data for years, but the information needed to develop regression equations is typically not available. While the breach size is often available, there is very little information pertaining to how high water was at breach initiation, volume of the interior area, levee materials, formation time, etc.

For this analysis, the "base" breach width was estimated based on observed data relating average levee height to breach width as shown in Figure 4 (observed data compiled by HEC). In addition to the "base" breach width, sensitivity analyses were conducted to evaluate small and large breach widths, one-quarter to four times the base breach width, respectively. Table 3 shows the modeled breach widths.

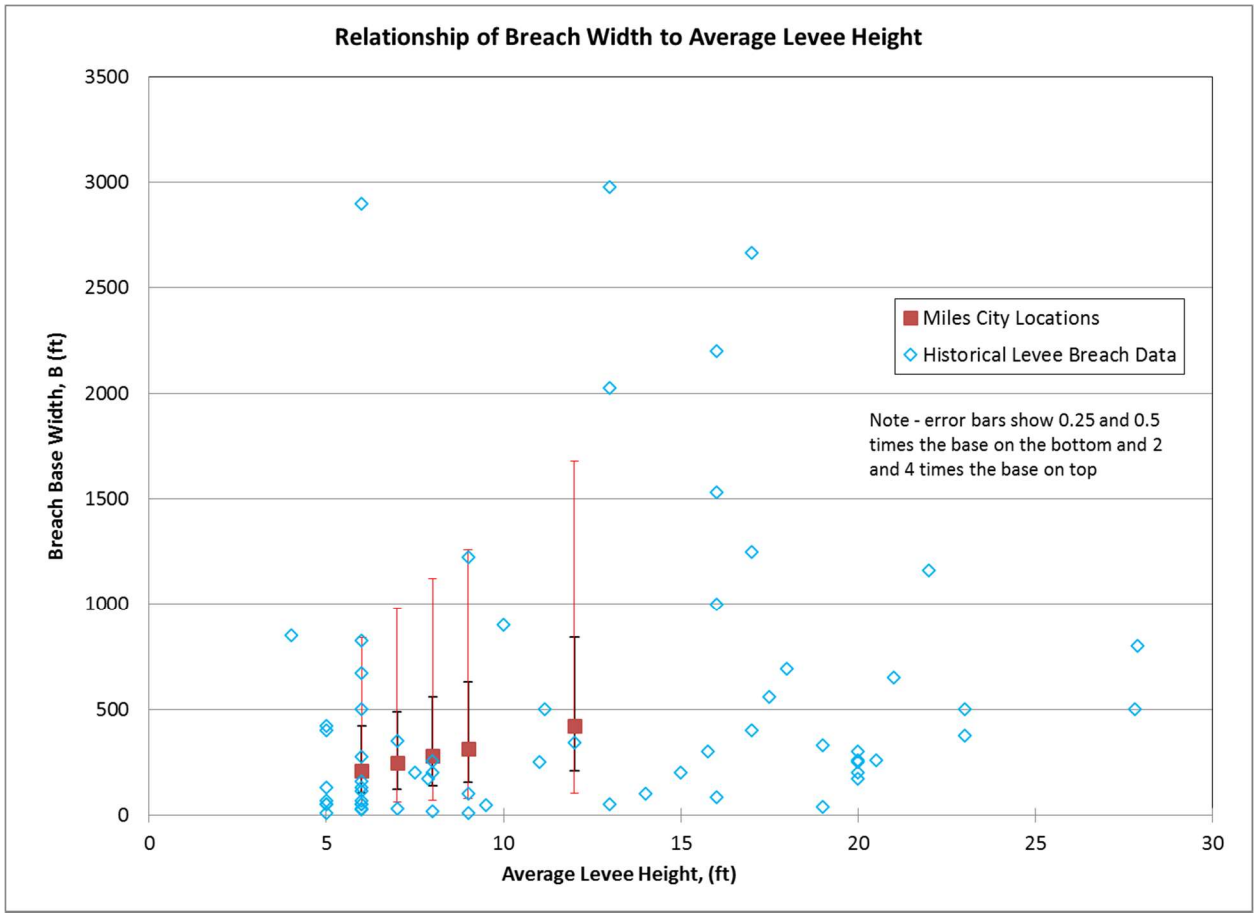

Figure 4. Historical levee breach width vs. levee height compared to modeled values for Miles City

Table 3. Modeled breach widths

					Sensitivity breach width			
Location	River	River Station	Estimated levee height	"Base" breach width	One-quarter	One-half	Double	Quadruple
			(ft)	(ft)	(ft)	(ft)	(ft)	(ft)
1	Tongue	7212	6	210	53	105	420	840
2	Tongue	4029	7	245	61	122.5	490	980
3	Tongue	385	9	315	79	157.5	630	1260
4	Yellowstone	27696	12	420	105	210	840	1680
5	Yellowstone	17794	8	280	70	140	560	1120

Results: The results of the 2D model are used in an HEC-FDA model to evaluate flood damages for a range of events (generally the 50% to 0.2% annual chance exceedance events, commonly referred to as the 2-year to 500-year events). Water surface elevation grids were exported from HEC-RAS for use in the HEC-FDA model. Examples of the results are presented below in Figures 5 and 6.

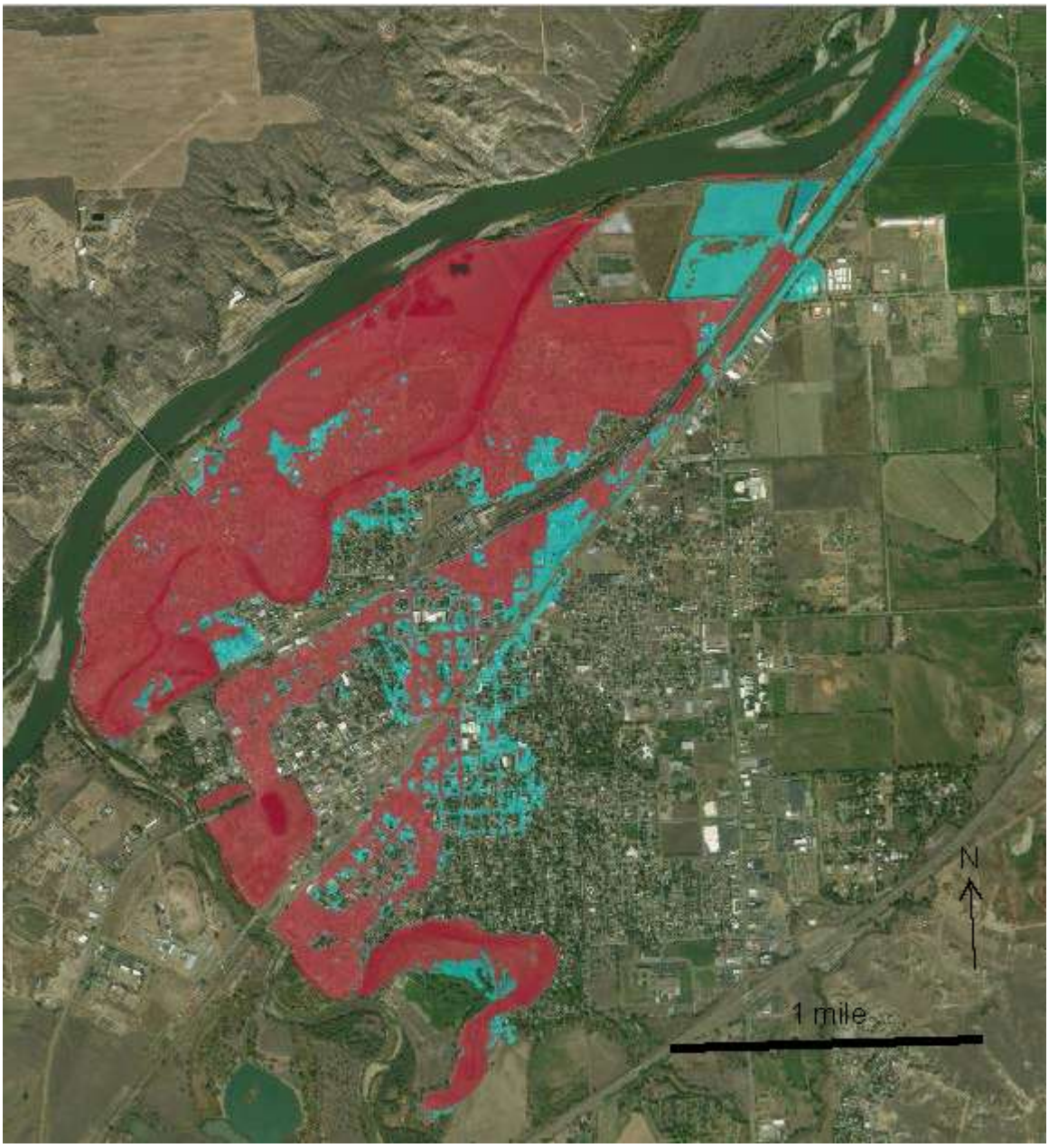

Figure 5. Large vs. small breach inundation for the 1% ACE event (red=small breach, blue=large breach)

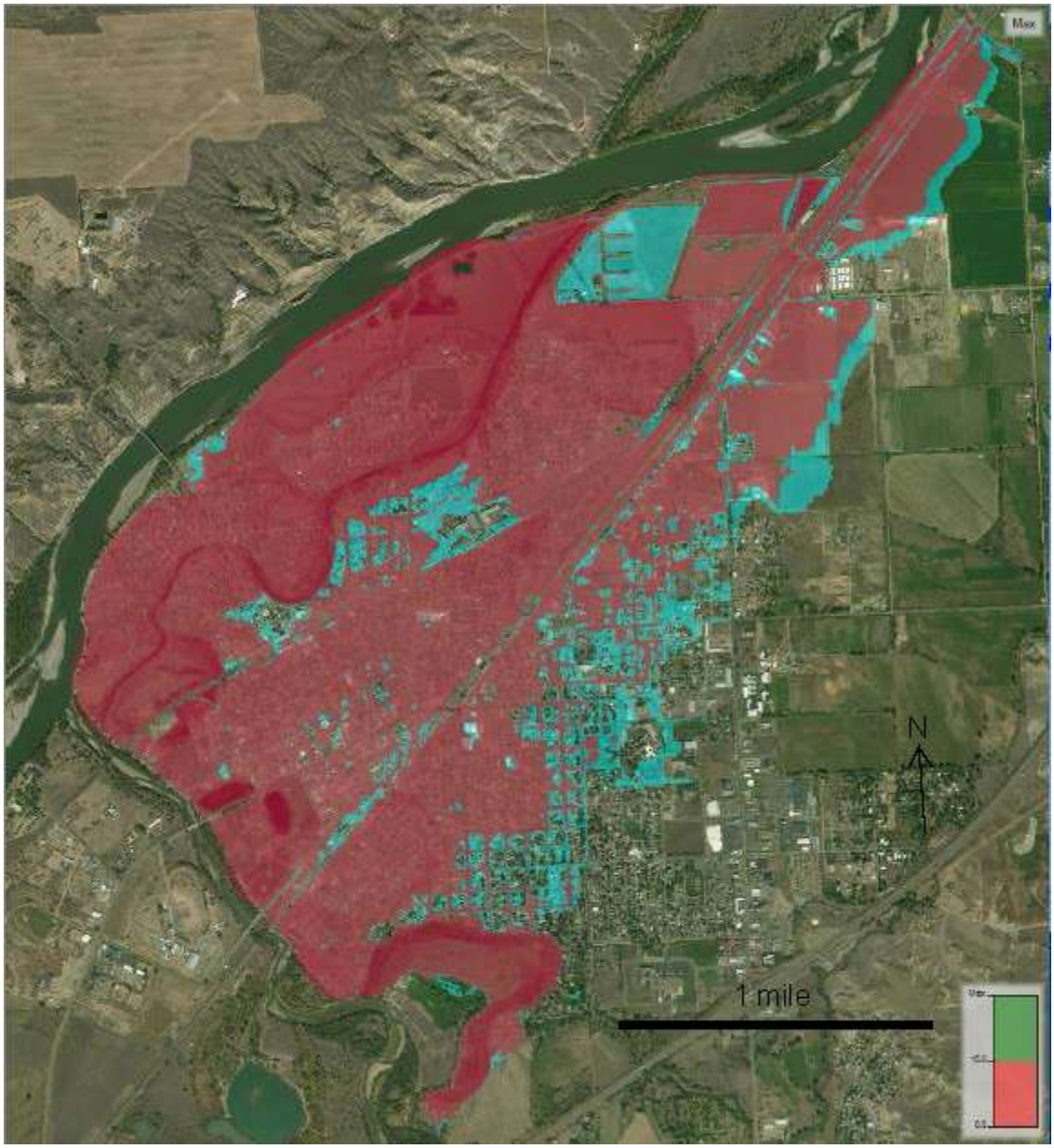

Figure 5. Low vs. high roughness inundation comparison for the 0.2% ACE event (red=high roughness, blue=low roughness)

References

Brunner, G.W. 2016a. HEC-RAS River Analysis System, User's Manual. US Army Corps of Engineers, Institute for Water Resources, Hydrologic Engineering Center.

Brunner, G.W. 2016b. HEC-RAS River Analysis System, 2D Modeling User's Manual, Version 5.0. US Army Corps of Engineers, Institute for Water Resources, Hydrologic Engineering Center.

Chow, V.T. 1959. Open-Channel Hydraulics. McGraw-Hill Book Company, New York, Toronto, London.

FEMA. 2002. Guidelines and Specifications for Flood Hazard Mapping Partners, Appendix F: Guidance for Ice-Jam Analyses and Mapping.

NRCS-Kansas. 2016. Manning's n Values for Various Land Covers to Use for Dam Breach Analyses by NRCS in Kansas.

USACE. 2002. Ice Engineering. EM 1110-2-1612.

USACE. 2018. Miles City, MT, Section 205 Flood Control Project, Hydrologic Analysis (DRAFT).

What's New in HEC-RAS 5.1?

Gary W. Brunner, P.E., M. ASCE, D.WRE, Senior Hydraulic Engineer, Hydrologic Engineering Center, Institute for Water Resources, U.S. Army Corps of Engineers, 609 2nd St., Davis, CA 95616; gary.w.brunner@usace.army.mil

Abstract

HEC-RAS 5.1 will have several significant new features that will dramatically improve the applicability and range of modeling problems that the software can be used to solve. There will be a wide range of new capabilities, such as: spatial precipitation (gridded and point gage options); spatial infiltration; wind forces for 1D and 2D modeling; a new shallow water solution scheme and turbulence modeling; 1D finite volume solution algorithm; pump stations for 2D areas; bridge modeling inside of 2D areas; structure layout in HEC-RAS Mapper; a new 3D viewer for terrain and model results; and calibration tools inside of HEC-RAS Mapper for 1D and 2D regions.

This paper will discuss the details of the new features contained in HEC-RAS 5.1, as well as show real world example applications of their use.

Introduction

HEC-RAS 5.1 will have several significant new features that will dramatically improve the applicability and range of modeling problems that the software can be used to solve. There will be a wide range of new capabilities, such as: spatial precipitation (gridded and point gage options); spatial infiltration; wind forces for 1D and 2D modeling; a new shallow water solution scheme and turbulence modeling; 1D finite volume solution algorithm; pump stations for 2D areas; bridge modeling inside of 2D areas; structure layout in HEC-RAS Mapper; a new 3D viewer for terrain and model results; and calibration tools inside of HEC-RAS Mapper for 1D and 2D regions. This version of HEC-RAS will replace the current version, 5.0.7. At this time there is no scheduled release date for version 5.1.

Spatial Precipitation

The HEC-RAS team has added the ability to apply spatial precipitation as a boundary condition to 2D flow areas and storage areas. The precipitation can be in either a gridded form or based on multiple point gages. Gridded precipitation data can be imported from multiple file formats/sources. Currently, supported gridded precipitation formats include: HEC-DSS; GRIB, and NetCDF. The GRIB and NetCDF formats supported are those precipitation datasets downloadable from the National Weather Service (NWS). GRIB and NetCDF precipitation files from other sources might not be supported as the file format could be different than files from the NWS The HEC-DSS file format has supported gridded datasets for 20 years and HEC has a number of utility programs for converting files in other formats to records inside of a HEC-DSS file. The

software HEC-MetVue can be used to download data, visualize the data, and store it into multiple data formats, including the HEC-DSS file format.

Shown in Figure 1 is a visualization of spatial precipitation being used in HEC-RAS overtop of a 2D Flow Area model. The data shown in Figure 1 is the precipitation that fell in a 1 hour time period.

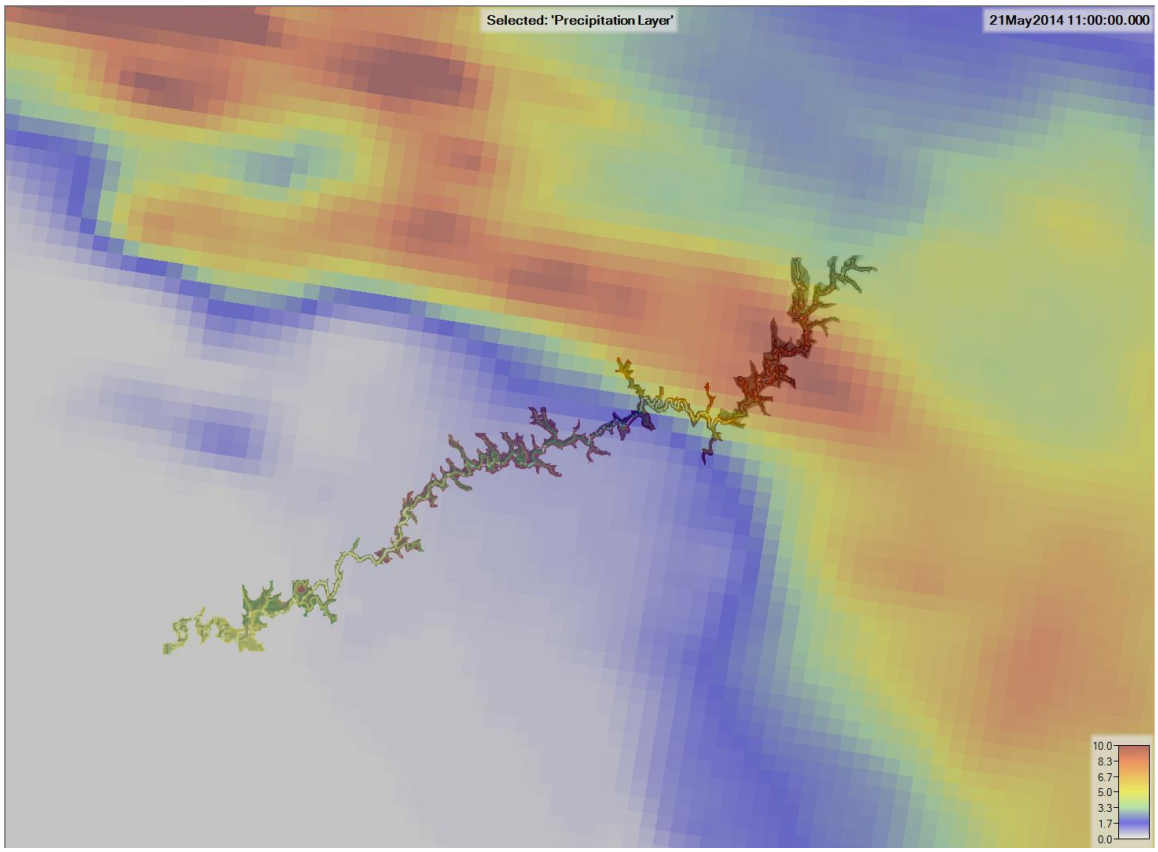

Figure 1. Gridded Spatial Precipitation Boundary Condition for HEC-RAS Modeling.

Spatial Infiltration

The HEC-RAS team has added the option for spatial infiltration to be used along with spatial precipitation. Currently three infiltration methods will be available to users, these are: Deficit/Initial and Constant; Modified SCS Curve Number; and a continuous implementation of the Green and Ampt method. All three infiltration methods work directly from the precipitation hyetograph and do not account for ponding and continuous infiltration on the land surface (that will be in future versions of the software). Additionally, the SCS Curve Number method has several modifications/options. These options include: user specified initial loss (instead of 0.2S); separate Curve Number for pervious only areas, while impervious areas are given a separate curve number (100 by default); the ability to set a minimum infiltration rate, such as the saturated hydraulic conductivity rate (the Curve Number method results in zero infiltration when applied to a precipitation time-series that includes a total

precipitation depth that reaches the curve number's Storage (S) volume); and the option to recover the initial loss once a dry duration has been reached.

Wind forces for 1D and 2D modeling

The option to add in wind forces for both 1D and 2D modeling has also been incorporated into the software for version 5.1. This work has been funded by the Tennessee Valley Authority (TVA). This is only an option for the Full Momentum Equation solution scheme for 1D river reaches and 2D flow areas (i.e. if you are using Diffusion Wave equation solver, no wind forces can be included). Wind data can be included as a boundary condition in both gridded and point gage forms. Gridded data can be in any of the same three formats allowed for precipitation (HEC-DSS, GRIB, and NetCDF). In addition to adding wind surface stresses into the momentum equation as an additional force, user options are available for: computation of the wind drag coefficient; wind height corrections; wind velocity factors; data conversions; and wind hiding factors. An example wind field applied to an HEC-RAS 1D model is shown in Figure 2 below.

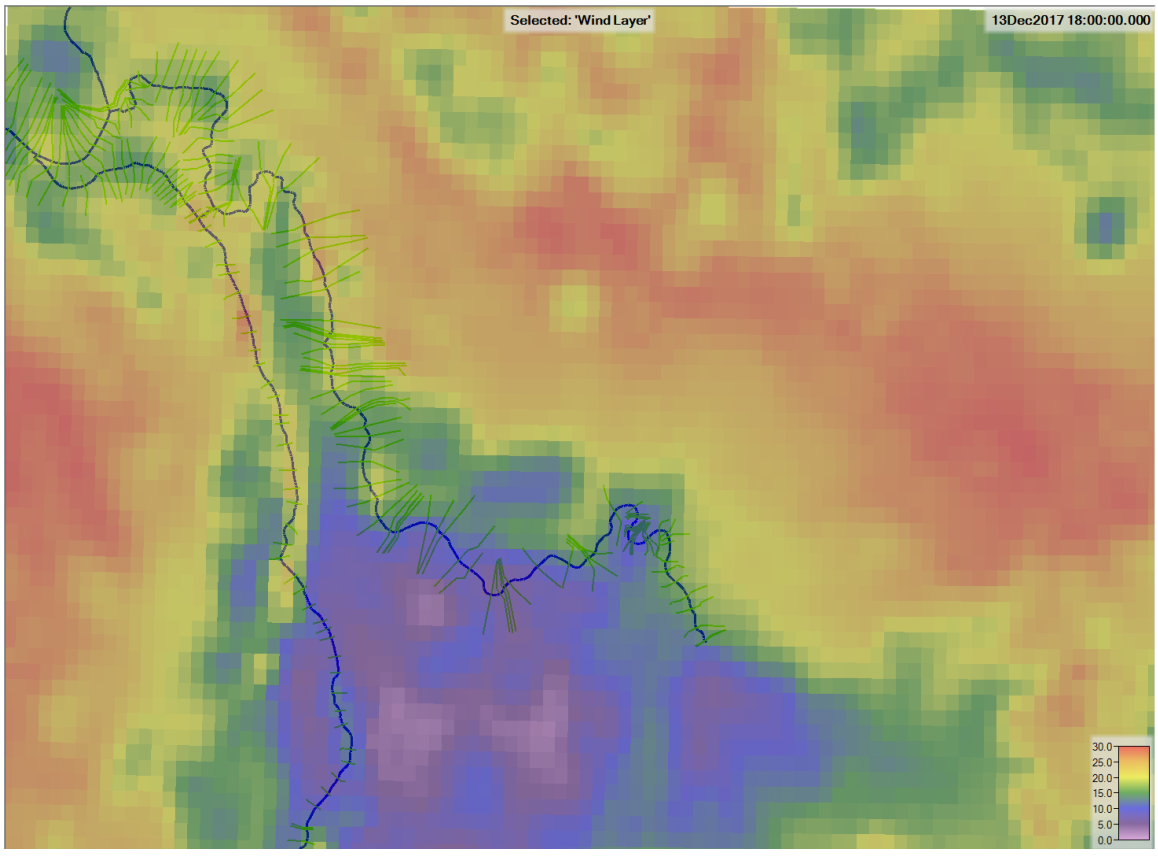

Figure 2. Example Gridded Wind Field Applied to a 1D HEC-RAS Model.

1D Finite Volume Solution Algorithm

A brand new solution algorithm has been developed for 1D modeling. A Finite-Volume solution approach, similar to what was added for 2D modeling is available for 1D modeling in HEC-RAS version 5.1.

The current 1D Finite Difference solution scheme has the following deficiencies:

1. Cannot handle starting or going dry in a XS
2. Low flow model stability issues with irregular XS data.
3. Extremely rapid rising hydrographs can be difficult to get stable
4. Mixed flow regime (i.e. flow transitions) approach is approximate
5. Stream junctions do not transfer momentum

The new 1D Finite Volume approach has the following positive attributes:

1. Can start with channels completely dry, or they can go dry during a simulation (wetting/drying).
2. Very stable for low flow modeling
3. Can handle extremely rapid rising hydrographs without going unstable.
4. Handles subcritical to supercritical flow, and hydraulic jumps better.
5. Junction analysis is performed as a single 2D cell when connecting 1D reaches (continuity and momentum is conserved through the junction).

Additionally, the new 1D Finite Volume approached is solved in the same matrix as the 2D equations. Solving in the same matrix allows for faster 1D/2D model solutions and more accurate flow transfers between 1D and 2D elements. The equations are solved together and all hydraulic connections are updated together on an iteration by iteration approach, rather than separately, as in previous versions of HEC-RAS.

New Shallow Water Solution Scheme and Turbulence Modeling

One of the goals of the HEC-RAS 5.1 software release was to add a third solution scheme for 2D modeling. Previous versions of HEC-RAS had two options for 2D modeling, Diffusion Wave and a Full Momentum (Shallow Water, SW) solution approaches. The current Full Momentum equation solver uses a semi-Lagrangian approach to discretize the acceleration terms in the momentum equation. While this approach has the advantage of being stable for large time steps, in some instances it can create numerical diffusion of momentum. The numerical diffusion can lead to potentially inaccurate results, especially in lab-scale simulations, as well as detailed structure design and analysis, where strict conservation of momentum is important. For this reason, an alternative SW solver option has been developed. The alternative approach utilizes the Eulerian momentum-conservative discretization of the acceleration terms suggested by Kramer and Stelling (2008). However, the tradeoff for more accurate momentum conservation is that the method requires the 2D grid to be strictly orthogonal, and the time step necessary for stability is limited by the Courant condition.

The new Shallow Water solution scheme has been thoroughly tested for several very difficult hydrodynamic problems. One such problem is the sudden dambreak over a completely dry surface. This test is where a wall of water is instantaneously released to a dry downstream reach. A lab study of this problem was performed by the Waterways Experimentation Station (WES, 1960) of the U.S. Army Corps of Engineers. A 400 ft. flume, place on a slope was used to perform this experiment. The details of this experiment can be found in the HEC-RAS Verification and Validation document on the HEC-RAS web page. Shown in Figure 3 are the observed lab data water surface elevations and computed results from the current (version 5.0.7) HEC-RAS Full Momentum solver. As you can see, the current full momentum solver provides an adequate solution to this problem, but it is not able to track the leading edge of the floodwave accurately. This is due to the fact that the method is computing too much numerical diffusion on the wetting front of this extremely dynamic wave problem. Because of the numerical diffusion, the computed wave front is too deep and too slow compared to the observed lab data.

Shown in Figure 4 is the results from the same test with the new Shallow Water Equation solver solution. As you can see, the new solver does extremely well at tracking the wetting front, as well as the negative wave that propagates upstream. The new solver does an excellent job at conserving the momentum and speed of the floodwave as it propagates downstream.

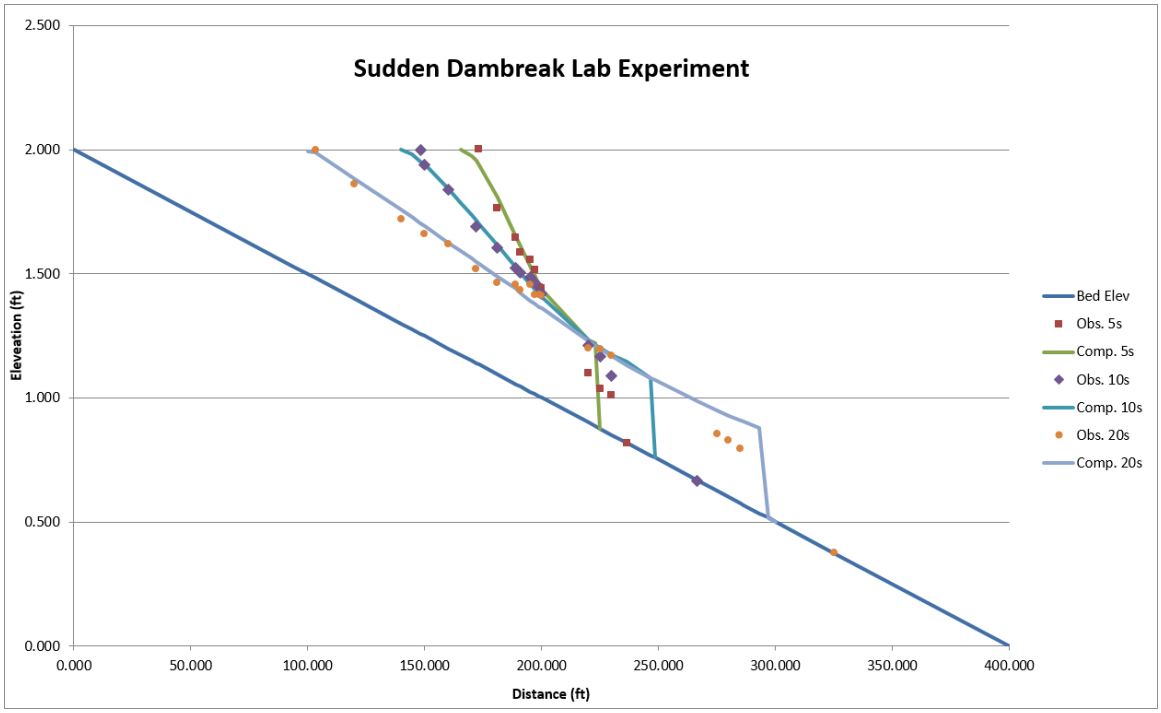

Figure 3. Original Shallow Water Solver vs Lab Results.

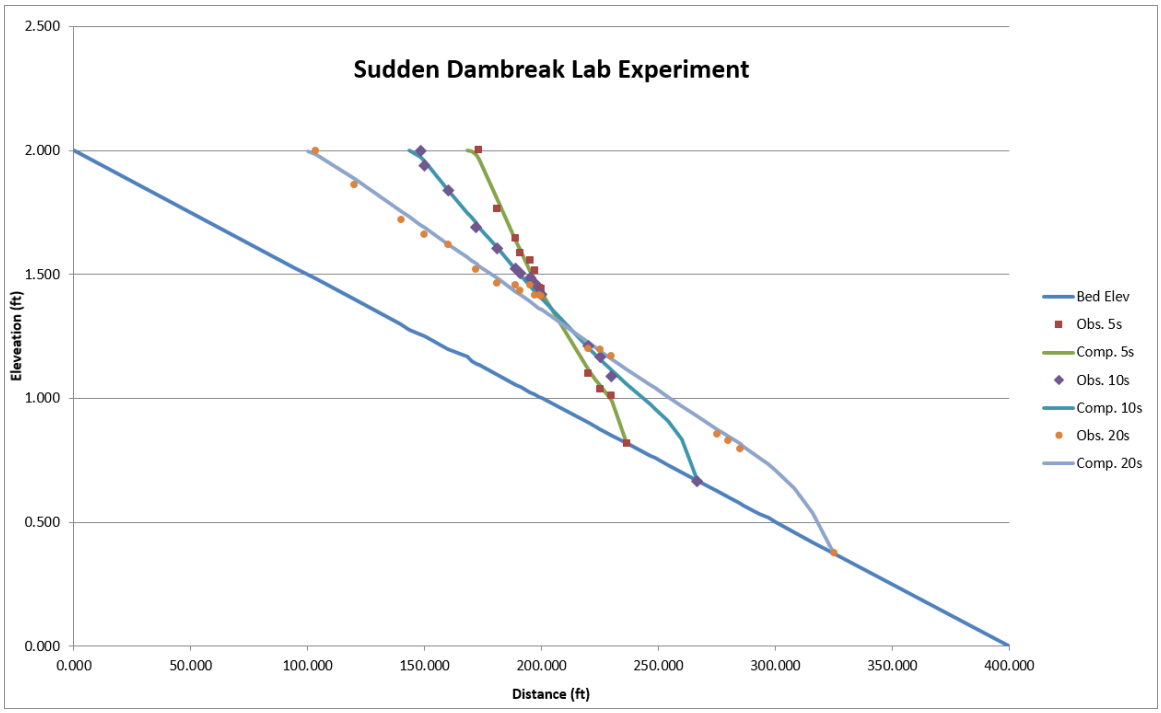

Figure 4. New Shallow Water Equation Solver vs Lab Results.

Pump stations for 2D areas

Previous to HEC-RAS version 5.1, pump stations could not be connected to 2D cells. HEC-RAS version 5.1 allows the user to connect pumps from 1D elements (cross section or storage area) to 2D cells, or 2D cells to another 2D cell. All previous types of pump connections are also still valid (1D to 1D). Each pump can connect to only a single 2D cell; however, users can have multiple pumps at a pump station, and each pump can be explicitly connected to 1D elements and 2D cells. Pump flow is added and extracted with a source/sink type of approach, meaning it is only a flow transfer with no accounting for velocity/momentum.

Bridge modeling inside of 2D areas

Previous to HEC-RAS version 5.1, no direct bridge modeling option (similar to what is in the 1D approach) was available inside of a 2D flow area. Users could model bridge flow in great detail, as long as water depths remained in a low flow condition, and never became either pressurized or pressure flow plus overtopping at the bridge deck. HEC-RAS version 5.1 includes an optional 1D type of bridge modeling approach. Users will be able to put in bridge data (Deck, abutments, piers, etc…) and choose from the full array of 1D solution approaches (Energy, Momentum, Yarnell, WSPRO, Pressure flow, and pressure plus weir flow). A family of rating curves will be developed for the structure, then that family of rating curves is used to solve for the flow and headwater water surface elevations at the structure, for the full range of possible flow regimes.

Additionally, users will have the option to only use the 1D family of bridge curves for the flow going through the bridge opening, while computing any overflow with the full 2D equations. The HEC-RAS team has also developed an approach to account for momentum transfer through the bridge by taking into account, both the velocity and the flow through the bridge opening.

Structure layout in HEC-RAS Mapper

Many new features have been added to HEC-RAS Mapper in order to make a complete set of tools for laying out an HEC-RAS model. The new tools are: ability to layout hydraulic structures spatially (bridges/culverts, inline structures, lateral structures, and SA/2D hydraulic connections); the ability to extract Manning's n values from spatial roughness layers; and the ability to define cross section properties such as ineffective flow areas and blocked obstructions. An example of a model with bridges and lateral structures that were defined in HEC-RAS Mapper is shown in Figure 5 below.

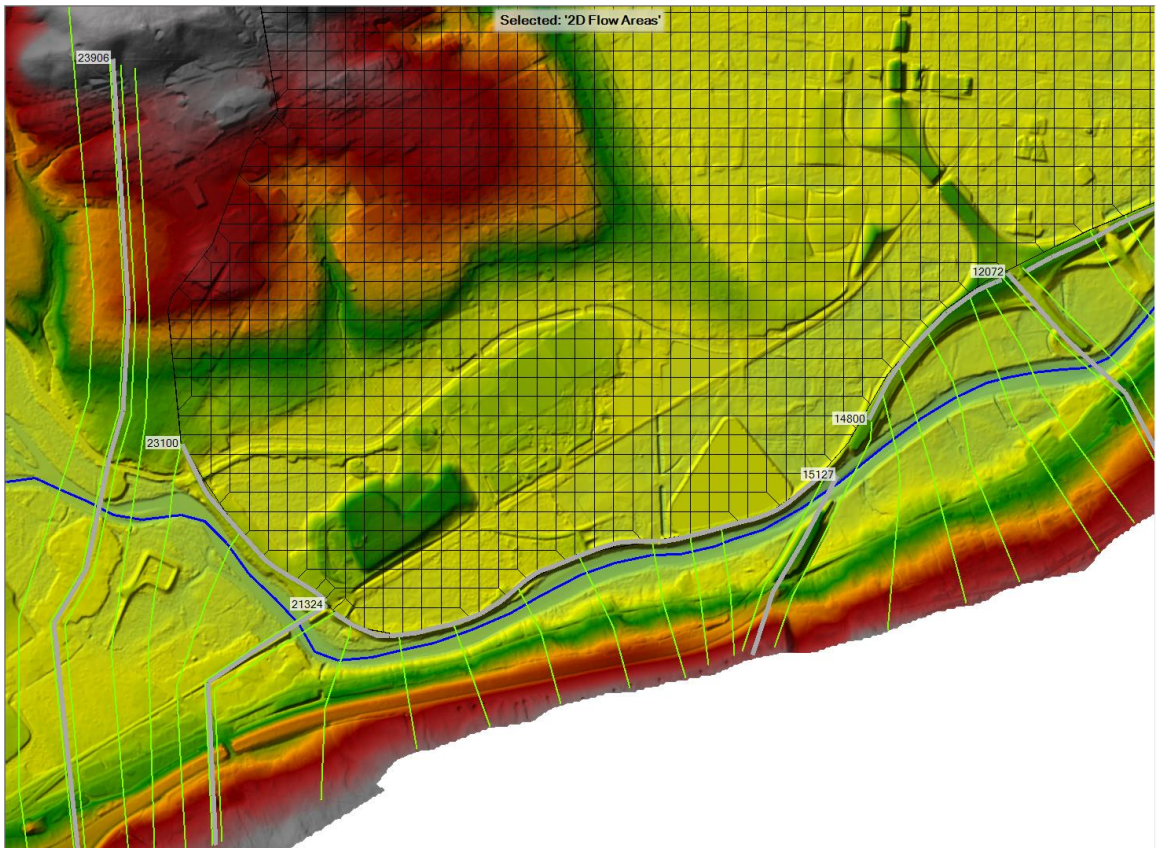

Figure 5. Example Model with Hydraulic Structures laid out in HEC-RAS Mapper.

New 3D viewer for terrain and model results

The HEC-RAS team has developed a new 3D viewer that allows users to visualize the terrain data and model results. The model results can be animated in time and the user can move through the model in a manner similar to a plane flying over an area. Additionally, users will be able to drape various layers over the top of the terrain, such as aerial photography, buildings, and roads. Shown in Figure 6 is a 3D view of Bald Eagle Creek and Sayers Dam, along with the HEC-RAS model results for water depth.

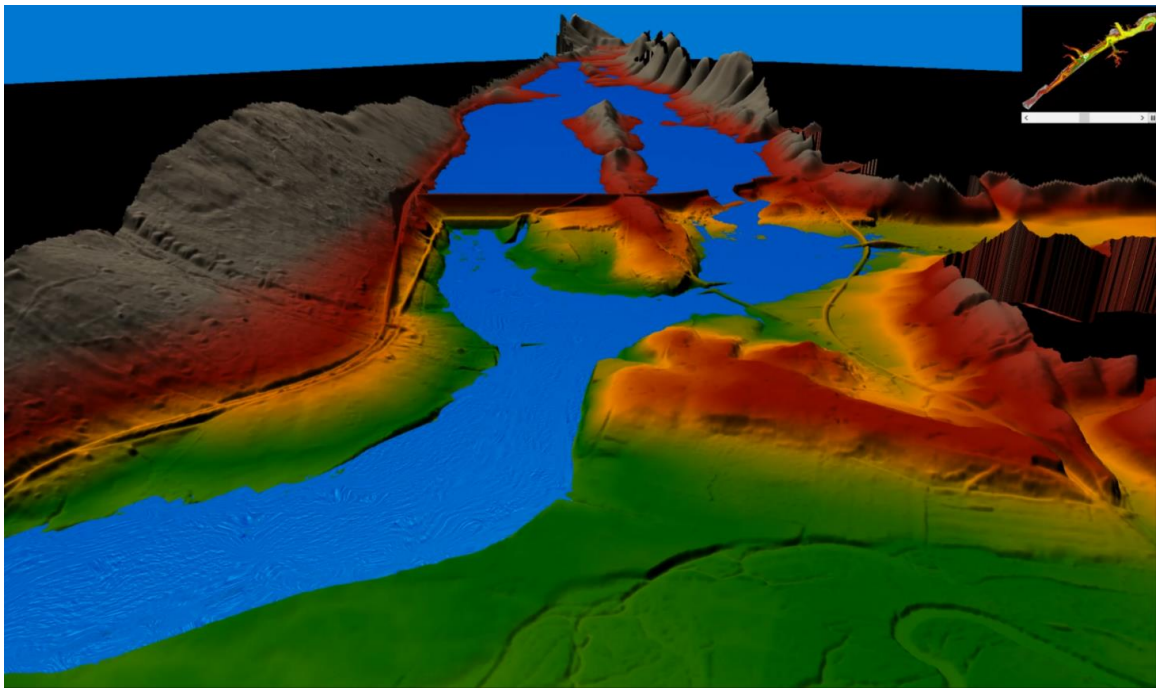

Figure 6. 3D view of Terrain data and HEC-RAS model results.

Calibration tools inside of HEC-RAS Mapper for 1D and 2D regions

The HEC-RAS team has added the ability to display observed data along with computed results from within HEC-RAS Mapper. This will facilitate the model calibration process for 1D and 2D modeling approaches. Users can now plot observed time series data (stage and flow) against HEC-RAS model computed stages and flows at cross sections and user specified profile lines within HEC-RAS Mapper. Users can also plot high water marks against computed results at user defined profile lines. Additionally, observed rating curve data can be entered and compared to computed results at cross sections and user defined profile lines. Figure 7 below shows HEC-RAS Mapper plots for computed stage and observed stage data at two locations in a model.

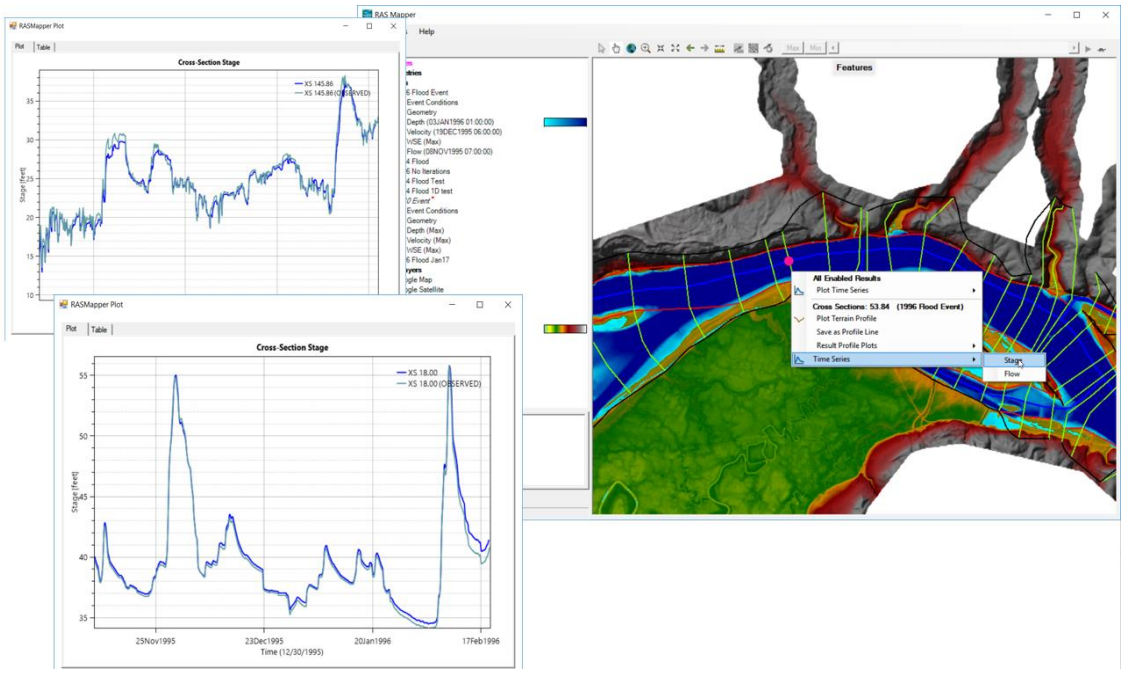

Figure 7. Example of plotting computes and observed data from HEC-RAS Mapper.

References

Kramer, S.C, Stelling, G.S. 2008. A conservative unstructured scheme for rapidly varied flows. International Journal for Numerical Methods in Fluids 58:183-212. DOI: 10.1002/fld.1722.

WES, 1960. Floods Resulting from Suddenly Breached Dams, Conditions of Minimum Resistance. Paper No. 2-374, Report 1. U.S. Army Corps of Engineers, Waterways Experimentation Station, Vicksburg, Mississippi. February 1960.

Non-Stationary Climate Variability

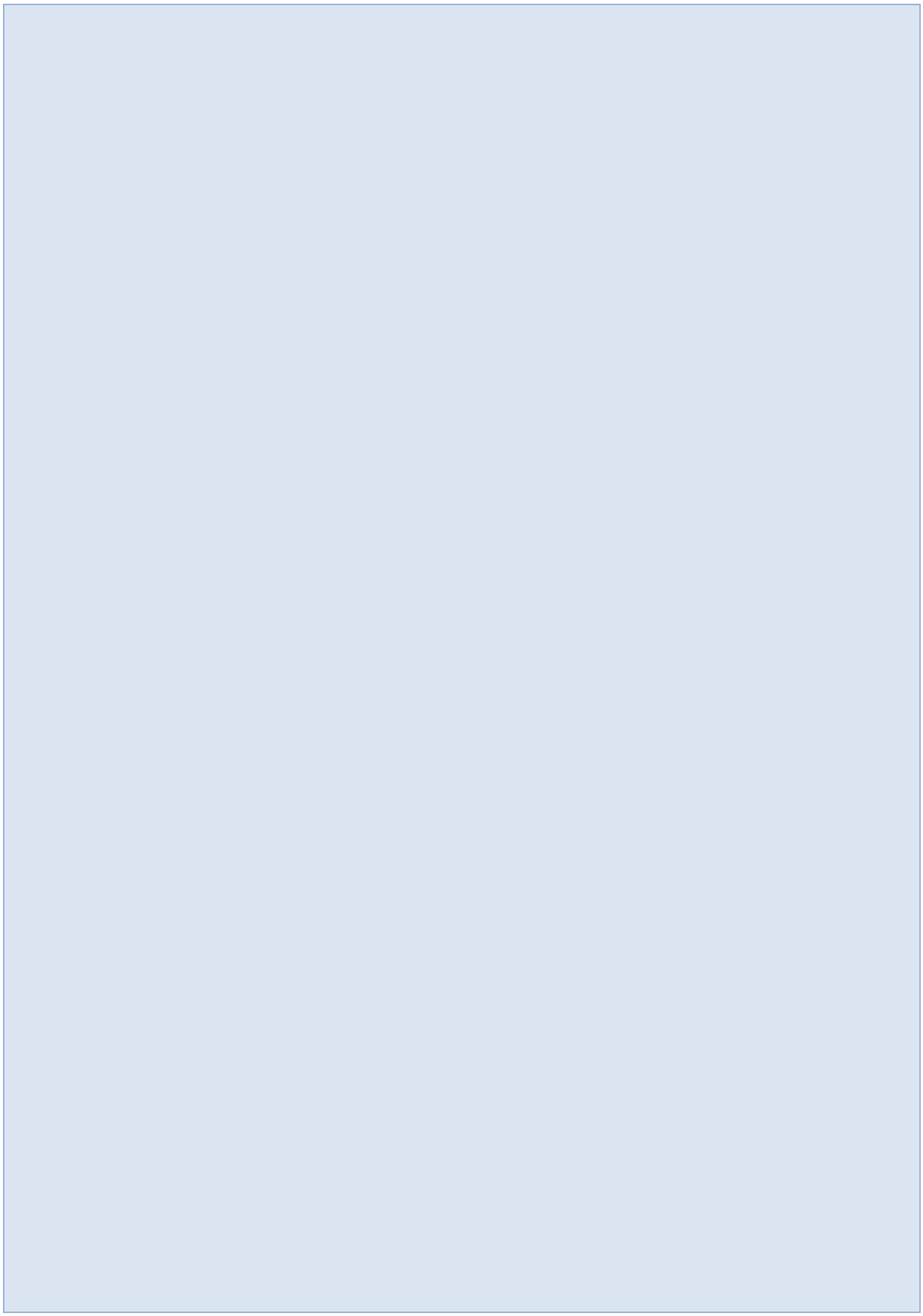

Extremes of Opportunity? A Generalized Approach to Identify Intersections between Changing Hydrology and Water Management.

Erin Towler, Project Scientist, National Center for Atmospheric Research (NCAR), Boulder, CO, towler@ucar.edu
Dagmar Llewellyn, Hydrologist, US Bureau of Reclamation, Albuquerque, NM, dllewellyn@usbr.gov
Lucas Barrett, Hydrologist, US Bureau of Reclamation, Albuquerque, NM, lbarrett@usbr.gov
Rick Young, Hydrologist, US Bureau of Reclamation, Albuquerque, NM, rcyoung@usbr.gov

Abstract

For water managers, changing hydrology can underscore existing vulnerabilities as well as offer new opportunities. The purpose of this paper is to put forth a generalized approach to identify potential intersections between changing hydrology and water management. The generalized approach includes 4 steps: (i) Articulate management vulnerabilities and opportunities, (ii) Quantify current water contributions from sources that may provide the hydrologic opportunity, (iii) Identify key climatic and atmospheric drivers of the hydrologic opportunity, and (iv) Explore the opportunity-management nexus. The framework is demonstrated using a case study example of the Middle Rio Grande Basin of New Mexico and its downstream delivery point, Elephant Butte Reservoir. In Step 1, we articulate how New Mexico's water supplies are vulnerable to decreasing snowpack, but also that the summer monsoon season could offer a potential, currently under-developed, water supply opportunity. In Step 2 we examine historical Elephant Butte Reservoir inflows and find that although monsoon season volumes vary from year-to-year, they are an important contribution to annual water supply. Further, we find that the upper percentile inflows contribute a disproportionately larger fraction of the monsoon volume relative to their frequency of occurrence. Step 3 examines possible climate and atmospheric drivers for different characteristics of monsoon season interannual variability, finding that most monsoon inflow characteristics show a strong association with average precipitation over the contributing watershed and atmospheric precipitable water. In Step 4 we suggest how this information could be integrated into existing planning and operations for the Rio Grande Basin.

1. Introduction

In many river basins in the Western United States, snowmelt provides the primary contribution to water supply (Serreze 1999); hence, most reservoirs are designed to capture snowmelt runoff. However, increasing temperatures (Hayhoe et al. 2018) and decreasing snowpack (Mote et al. 2005, 2018) have already been observed across the Western United States (US), and general circulation models predict that these trends will continue into the future (Collins et al., 2013). Taken together, these changes suggest increasing threats to water storage and availability in these reservoirs (Barnett et al. 2005). It is generally thought that increasing greenhouse gases will lead to an intensification of the hydrologic cycle, with an increase in heavy precipitation, potentially increasing local runoff (Seneviratne et al. 2012). In addition to posing flooding threats, these potentially increasing extreme precipitation events present opportunities to

mitigate the impacts of decreasing snowmelt runoff volumes on water supply. However, the relevance of changing hydrology, including extremes, will depend on the particular water management context. As such, the purpose of this paper is to put forth a generalized approach to identify potential intersections between changing hydrology and water management.

The generalized approach includes 4 steps: (i) Articulate management vulnerabilities and opportunities, (ii) Quantify current water contributions from sources that may provide hydrologic opportunities, (iii) Identify key climatic and atmospheric drivers of the hydrologic opportunity, and (iv) Explore the opportunity-management nexus. In this paper, we first present the generalized framework (Section 2), which is demonstrated using a case study example of a reservoir in the Rio Grande Basin, New Mexico. This is followed by discussion and conclusions (Section 3).

2. Framework to Identify Intersections

2.1 Step 1. Articulate management vulnerabilities and opportunities

The relevance of changing hydrology is dependent on the particular water management context. Articulating local management vulnerabilities and potential opportunities is a critical first step towards adaptation planning. In this step, we provide background information on climate and water resources for New Mexico basins that include projects managed by the US Bureau of Reclamation.

2.1.1. Background: Similar to many water systems in the Western US, one key vulnerability for New Mexico is decreasing snowpack. Snowpack provides the main water source for most of the New Mexico river basins that begin in Colorado, (including the Rio Grande, San Juan, and Chama Rivers) and northern New Mexico (such as the Pecos River) (Gutzler 2013). As such, most of the reservoirs in these river systems are designed to capture snowmelt runoff, with storage located in the headwaters of the basins where temperatures and evaporation rates are lower (Gutzler 2013). Recent work by Chavarria and Gutzler (2018) has shown decreasing snowpack and increasing temperatures in the upper Rio Grande, resulting in slight decreases in snowmelt runoff. Further, they found that small precipitation increases have offset the impact of decreasing snowpack (Chavarria and Gutzler 2018). However, there is growing evidence that runoff efficiencies in the basin are becoming more sensitive to temperature (Lehner et al. 2017).

Rivers that originate further south in the state get a smaller proportion of their flow from snowpack, and warm season precipitation increases in importance. Warm-season precipitation has historically provided a secondary water source in the Western US (Serreze et al., 1999). If the total volume of this secondary supply were to increase in response to increasing ocean and air temperatures, warm-season precipitation could provide a potential water-supply opportunity for New Mexico, which might make up, at least in part, for decreasing supplies from snowmelt runoff. In summer, the central and southern parts of the state are influenced by the North American Monsoon (Gutzler 2013; Adams and Comrie 1997), which result in significant contributions to annual precipitation (Douglas et al. 1993). Tropical cyclones also contribute during this time, though much less (<10%) during the main monsoon period (June 15-Sept 30), and more (up to 80%) in the relatively dry month of October (Wood and Ritchie 2013). For New Mexico, most extreme precipitation occurs in summer, followed by fall (Kunkel et al. 1999), and most flooding has been observed in summer (Villarini, 2016). Pournasiri Poshtiri et al (2018)

examined recent trends in warm season precipitation characteristics, including extremes, and found that negative trends dominate warm season, June, and August, while positive trends dominate July and for some September precipitation characteristics. However, the majority of locations in New Mexico do not exhibit significant trends. The increasing trends for the July indicators show the most potential for water supply, with the location of these significantly positive trends mainly concentrated in the southeastern and eastern part of New Mexico. They also found that trends are more detectable in the frequency of extreme precipitation rather than the magnitude, similar to the findings of Mallakpour & Villarini (2017). As such, for times and locations showing increasing trends, their results suggest that water managers looking to exploit changes in precipitation might not need to plan for larger events, but rather for more frequent events.

The coarse resolution of general circulation models, which are typically used as a basis for projections of future climate and hydrology, limit the ability of these models to resolve monsoonal patterns. Therefore, there is currently low confidence in our ability to project changes in monsoonal patterns as the climate warms (Seneviratene et al. 2012). For parts of the US Southwest, projections for winter and spring seasons at the end of the century (2070-2099) show decreasing precipitation, though changes for this region in all seasons are small and relatively insignificant (Hayhoe et al. 2018). However, some past research (e.g., Asmerom et al., 2013) has suggested a correlation between ocean temperature and monsoon intensity. Seneviratne et al. (2012) recommend that any examination of monsoonal changes should consider large-scale circulation and dynamics, rather than solely examining precipitation. Examining current and future weather patterns, Prein 2018 finds a robust signal for an increase in the frequency of monsoonal circulations in New Mexico, particularly monsoonal patterns that contribute to the majority of monsoon season precipitation, as well as heavy precipitation events.

If Prein's conclusions are correct, there may be opportunities to exploit changes in warm season precipitation for water management (Gutzler, 2013, Llewellyn & Vaddey, 2013), warranting further investigation.

2.2. Step 2. Quantify current water contributions from sources that may provide hydrologic opportunities.

Quantifying the current contribution of water sources that might provide future water supply opportunities provides a critical baseline to which future climate or infrastructure scenarios can be compared. As articulated in Step 1, given decreasing snowpack, a potential opportunity for New Mexico could be moisture from the monsoon season. In this section we provide an example of quantifying current monsoon season contributions to annual water supply.

As a case study, we examine the Middle Rio Grande Basin of New Mexico and its downstream delivery point, Elephant Butte Reservoir, located in the south-central New Mexico (see Figure 1). This reservoir provides significant water storage (up to approximately 2 million acre feet) for both snowmelt runoff and summer precipitation events. The analyses in Step 2 rely on the following dataset and definitions:

- Elephant Butte Reservoir inflows: Data are available from 2000-2017, and are calculated as the sum of the Rio Grande Low Flow Conveyance Channel at San Marcial and the Rio Grande Floodway at San Marcial (URGWOM Technical Team, 2005).

- Monsoon season volume: We define the monsoon season volume as the sum of Elephant Butte Reservoir inflows from July 1 through September 30 (Jul-Sep). Initial analyses also included June 15-June 30, a time period that is often considered to be part of the monsoon season, but here it was found that that these inflows were still influenced by snowmelt.
- Annual volume: We define the annual volume to be the sum of Elephant Butte Reservoir inflows during the calendar year (Jan-Dec).
- Percentile-based indices: The definition of an extreme inflow at a particular location is site-specific; hence, percentile-based indices can be calculated from the historical Elephant Butte Reservoir inflows. We examine several percentiles: P99 is the 99th percentile flow, i.e., the value at which only 1% of daily inflows are higher. Similarly, we examine P95 (the 95th percentile, where only 5% of the daily inflows are higher), P90 (the 90th percentile), P75 (the 75th percentile), and P50 (the 50th percentile, or median daily flow).

In this step, we look at the interannual variability of monsoon season volumes and their contribution to annual inflows to Elephant Butte Reservoir (2.2.1), as well as the relationship between monsoon season volumes and upper percentile thresholds/extremes (2.2.2) and frequency and magnitude characteristics (2.2.3).

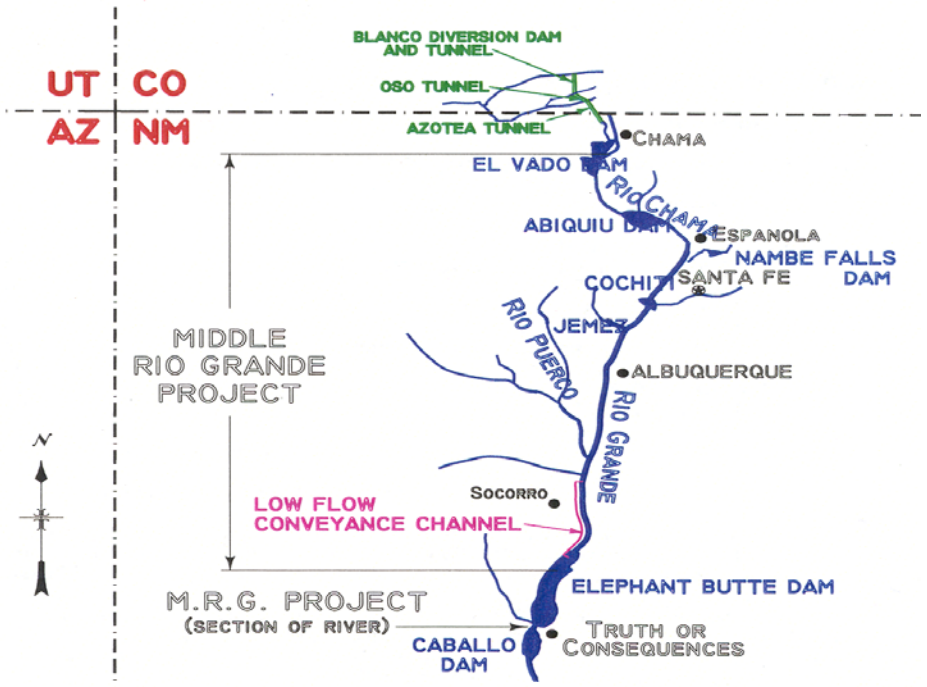

Figure 1. Map of Middle Rio Grande Basin of New Mexico and its downstream delivery point, Elephant Butte Reservoir, New Mexico.

2.2.1. Monsoon season volumes vary from year-to-year, but they are an important contribution to annual water supply:

The interannual variability of Elephant Butte Reservoir inflows and storage volumes play a role in the operations and management decisions in the basin. Figure 2a (left) shows the annual monsoon season volumes for the 2000-to-2017 period analyzed; the average volume is about 68,383 acre-feet (af), the minimum was 16,432 af in 2003 and the maximum was 254,214 af in 2006. It is also useful to look at the contribution of the monsoon volume to annual volume, as in some years, even relatively low volumes may provide critical contributions. Figure 2b (right) shows that on

average, monsoon volumes provide 14.4% of the annual supply, with a minimum of 4.00% in 2017 and a maximum of 43.6% in 2006. There is no statistically significant trend to the contribution, though it is hard to tell with the short sample size (18 years).

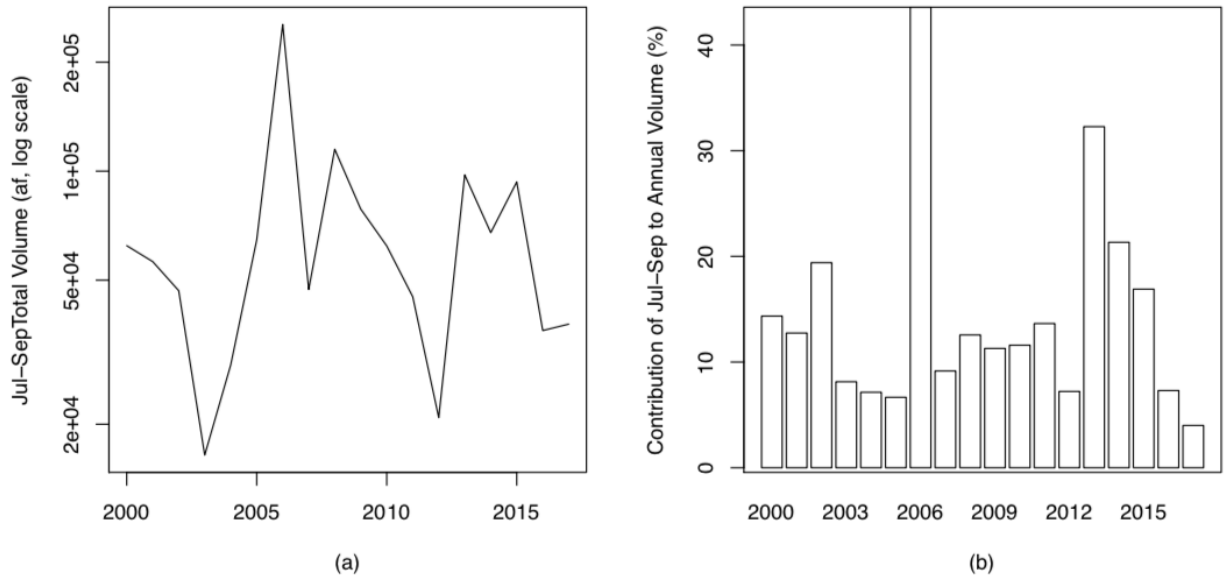

Figure 2. Monsoon (Jul-Sep) total volume in Elephant Butte Reservoir (a) and proportion of annual volume (Jan-Dec) coming from that year's monsoon (Jul-Sep) volume (b).

2.2.2. Inflows from upper percentiles contribute a disproportionately higher proportion of the monsoon volume relative to their occurrence: The percentile indices for the Elephant Butte daily inflows from the monsoon season (i.e., n = 1656 daily inflows) can be seen from the flow duration curve (Figure 3). Figure 3 shows that the upper half of daily inflows span an order of magnitude in volume: the 50th percentile (P50) is 452 acre feet and the 99th percentile (P99) is 5660 acre feet. The maximum daily flow in the analyzed period of record is 11,910 acre feet (in 2006; not shown in Figure 3). We also see that the 75th percentile (P75) for the inflows marks an inflection point: here, the absolute value of the slope starts to increase towards the higher percentiles (moving to the left in Figure 3), indicating a rapid shift towards higher daily inflows. Using these percentiles, we can look at the contribution of daily inflows above each percentile in each monsoon season (Figure 4). In Figure 4, the boxplots are comprised of the annual contributions from each percentile, hence the sample size, N, number of years, decreases; this is as expected, since the exceedance of the higher percentile indices does not occur in every year. As indicated by the median (horizontal line in box plots), the summed volumes from daily flows from the upper half of the distribution (>P50) contribute to 78% of the monsoon reservoir volume. Summed volumes from the top quarter (>P75) of daily inflows contributed 47% of monsoon reservoir volumes; top decile (>P90) of daily inflows contributed 28% of monsoon reservoir volumes. However, there is quite a bit of variability in the contribution from year-to-year for these percentiles (P50-P90). As we move into the higher, more extreme quantiles, these also play a role, but in fewer years. i.e., daily inflows above P99 are contributing disproportionately given their low occurrence, but only in the two years that they occur: this 1% occurrence accounts for 41% in 2006 and 23% in 2013 (resulting in a 32% median). The previously mentioned maximum daily inflow on record (e.g., 11,910 af), which occurred in August of 2006, contributed 5% of that year's monsoon reservoir volume.

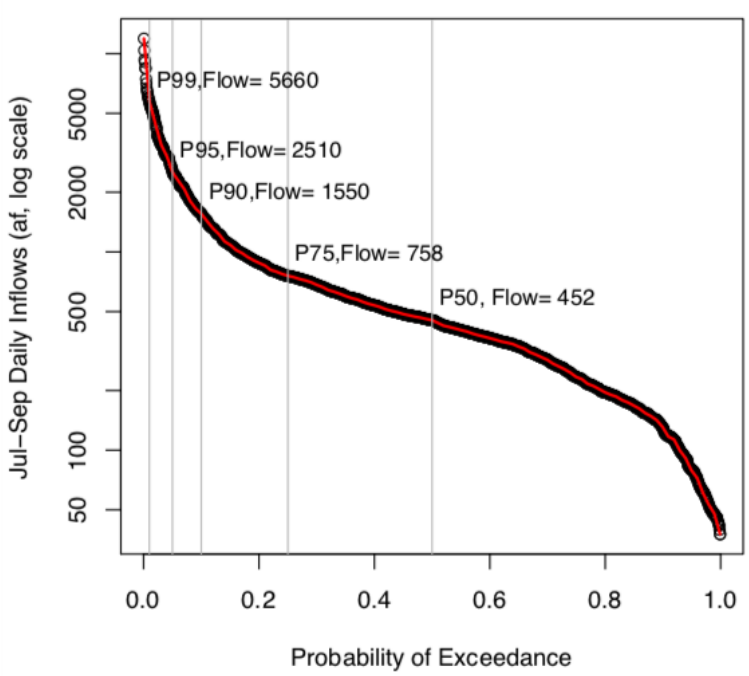

Figure 3. Flow duration curve of monsoon (Jul-Sep) daily inflows in acre feet (af; n=1656 days), with daily values of select percentile-based flow indices (P50, P75, P90, P95, P99), and smoothed spline (red line).

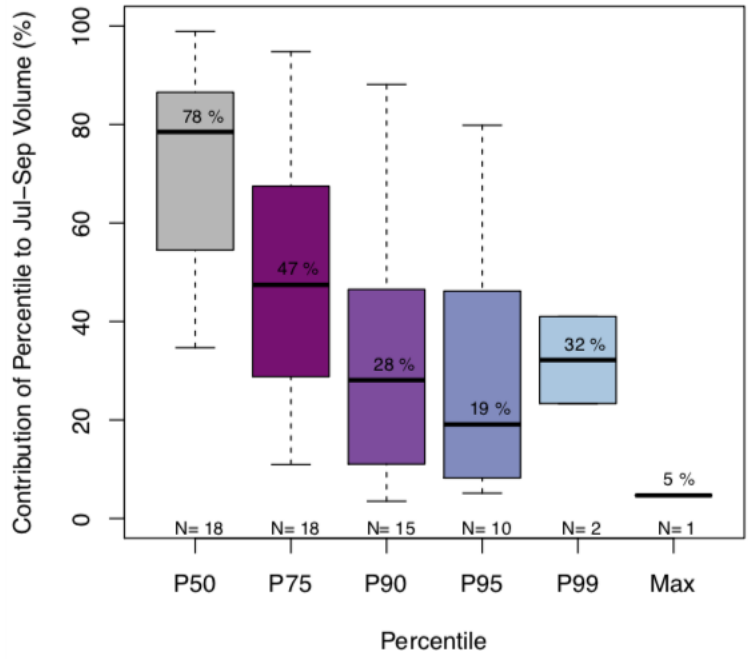

Figure 4. Proportion of monsoon (Jul-Sep) volume coming from daily inflows above each percentile-based flow index; P50 is the 50th percentile, P75th is the 75h percentile, and so on; Max is the maximum daily inflow. N is the number of years from which the daily inflows above the percentiles were observed.

2.2.3. Frequency and magnitude inflow characteristics partially explain interannual monsoon variability: We can also examine how well other inflow characteristics based on the percentile-based indices explain the interannual variability of monsoon reservoir volumes. Here we look at two characteristics: first, the frequency, or the number of days that the daily inflows were above the percentiles during the monsoon season. Figure 5 shows how the number of days above P50, P75, P90, and P95 relates to that year's monsoon reservoir volume. As we would expect, as the number of exceeding days increases, so does the total monsoon inflow volume. We see strong linear correlations, as measured by Pearson's r values, and find that the number of days above P75 has a stronger correlation (r=0.85) than P50 (r=0.62), showing the importance of the count of days in the upper quarter of the inflow distribution to total monsoon season volume. The number of days above P90 and P95 also have high correlations (r = .97 and .96, respectively), but here the linear correlations don't tell the whole story: the scatterplots reveal that there are several years with zero days above these thresholds. This relates to our previous point that these flows can be pivotal, but only in years in which they occur. The second characteristic that we examine is the annual magnitude, i.e., the value of the percentile index calculated annually for each monsoon season. For clarity, these are labeled $P50_{annual}$., $P75_{annual}$, and so on, indicating that these magnitudes are calculated from a flow duration curve like Figure 3, but for each year's monsoon season. The scatterplot in Figure 6 shows the association between the annual percentiles and that year's monsoon reservoir volume. These all exhibit very high linear correlations (r=0.95 to 0.98), indicating that these annual percentiles do a good job at explaining the interannual monsoon variability.

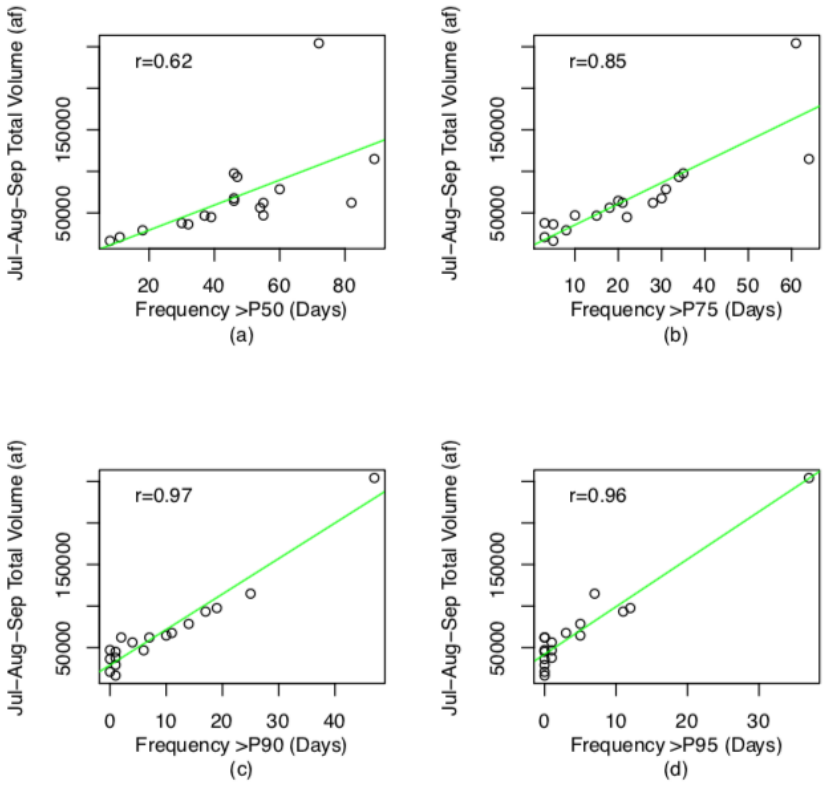

Figure 5. Frequency of days with inflows above select percentile-based indices versus monsoon (Jul-Sep) volumes in acre-feet (af); r is Pearson's linear correlation.

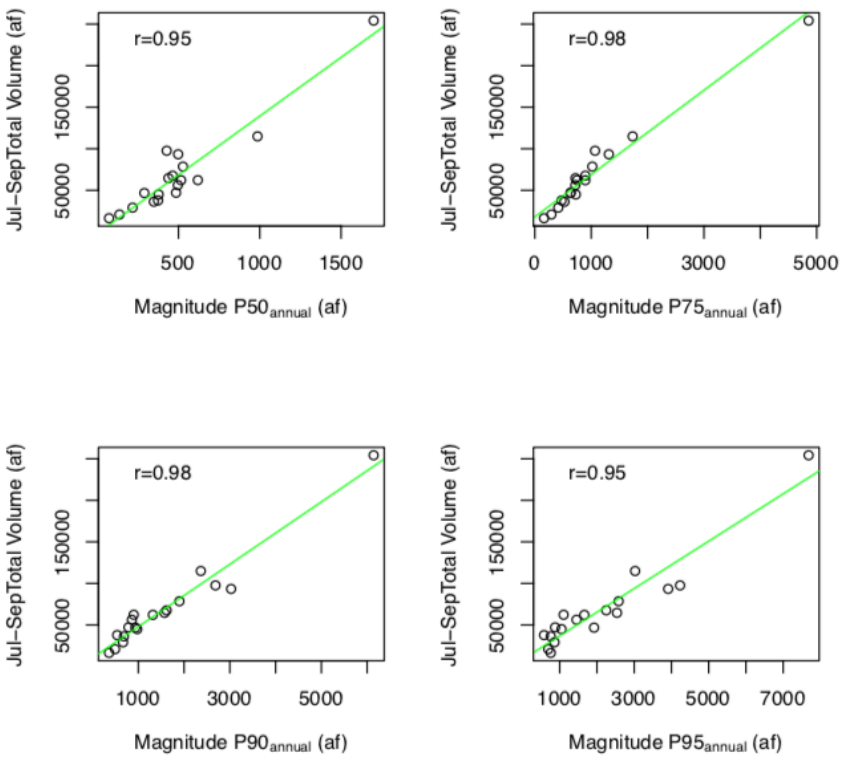

Figure 6. Inflow magnitudes of annual percentile-based indices versus monsoon (Jul-Sep) volumes in acre-feet (af); r is Pearson's linear correlation.

2.3. Step 3. Identify key climatic and atmospheric drivers of the hydrologic opportunity

Understanding the key factors that drive the potential opportunity is critical to understanding its possible role in water management. In step 2, we examined several aspects of the interannual variability of Elephant Butte Reservoir monsoon season volumes. Next we seek to understand the key climate and atmospheric drivers. We recognize that other factors, such as land use and management, are important as well; and though not examined here we discuss this point in the discussion and conclusions. Step 3 analyses rely on several datasets:

- Average precipitation: We use daily precipitation data from PRISM Gridded Climate Data Group (prism.oregonstate.edu), downloadable from http://www.prism.oregonstate.edu/documents/PRISM_downloads_FTP.pdf. Average precipitation is calculated by 1) averaging the daily values over each year's monsoon season (Jul-Sep), and 2) spatially averaging over the Rio Grande watershed contributing to Elephant Butte Reservoir within New Mexico. The data are available through 2014, so the overlapping period with the Elephant Butte Reservoir monsoon volumes is 2000-2014.
- Average large-scale variables: Prein (2018) identifies three potential predictors of monsoon season precipitation anomalies based on weather patterns over New Mexico: sea level pressure, wind speed, and precipitable water; these are from ECMWF's Interim Reanalysis (Dee et al. 2011) (ERA-Interim) Average values are calculated by 1) averaging the daily values over each year's monsoon season (Jul-Sep), and 2) spatially averaging over the entire state of New Mexico.

In this step, we first examine the runoff efficiency of the Elephant Butte Reservoir monsoon volumes with precipitation (2.3.1). Second, we examine the above 4 predictors (basin-average precipitation, sea level pressure, wind speed, and atmospheric precipitable water) and their linear correlation (Pearson's r) with several monsoon inflow characteristics examined in Step 2 (Section 2.3.2).

2.3.1. Runoff efficiency exhibits interannual variability. Runoff efficiency is calculated as the fraction of runoff, here the Middle Rio Grande monsoon volume (measured as the inflow to Elephant Butte Reservoir), divided by precipitation. Then, we normalize the value (i.e., we divide all values by the maximum runoff efficiency). Figure 7 shows the interannual variability of the runoff efficiency: the black line is calculated using the monsoon total precipitation, and shows that 2006 has the highest normalized efficiency within the years analyzed. To get a sense of the efficiency of the upper part of the distribution and extremes, the efficiency is also shown by using two percentile-based indices derived from the precipitation: PR_P75_{annual} and PR_P99_{annual}, corresponding to the magnitude of the 75th and 99th percentiles of daily precipitation in a given year's monsoon season. All three lines show similar patterns, but the PR_P99_{annual} line (purple) is lower for most years, showing that these heavier precipitation events may be less efficient in most years, except in the most extreme years (e.g., 2006). The $P75_{annual}$ line (orange) is above the black line in some years, indicating the relatively higher efficiency of the top quarter of precipitation days, and is just below the black (and purple) lines in 2006, the most extreme year. This underscores the point that when extremes occur, they can be quite efficient, but that more moderate extremes (e.g., P75) contribute more reliably in any given year.

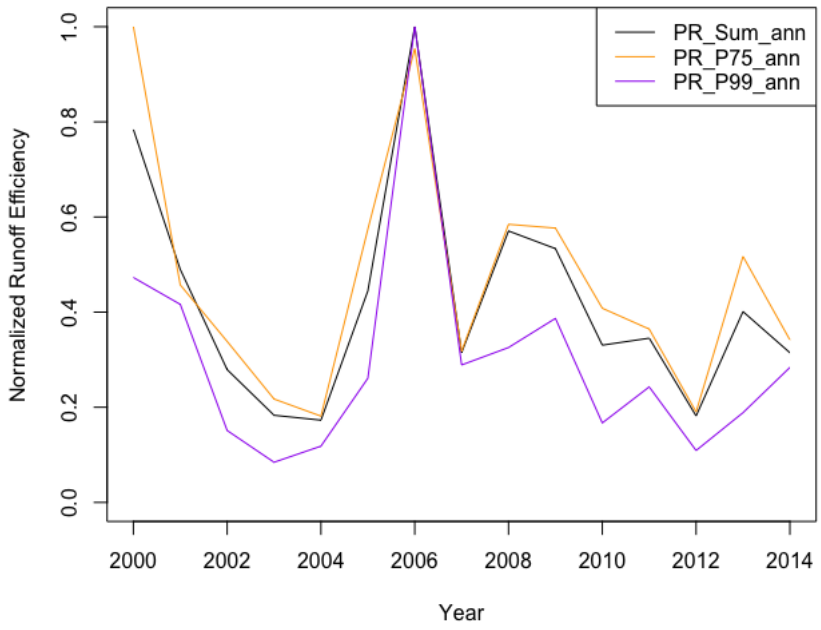

Figure 7. Normalized runoff efficiency of monsoon reservoir volumes using monsoon total precipitation (PR_Sum_ann), and two percentile-based precipitation indices, the magnitude of the year's 75th and 99th percentile precipitation day (PR_P75_ann and PR_P99_ann).

2.3.2. Most monsoon inflow characteristics show strong linear correlations with precipitation and precipitable water. Table 1 shows the linear correlations between the precipitation and large-scale predictors and the monsoon inflow characteristics:

total volume and maximum annual inflows, as well as the percentile-based frequency exceedances and annual magnitudes. Table 1 shows that total volumes are most highly correlated with average precipitation over the contributing watershed (r=0.73), and followed by precipitable water (r=0.61). Annual maximum values are most strongly correlated with higher average wind speeds (r=0.52), followed by precipitable water (r=.43), and not significantly correlated with average precipitation, indicating that predictors for averages versus maximums can be quite different. In terms of the frequency characteristics, average precipitation and precipitable water are both important, though as we get to higher percentiles, precipitable water becomes more important. For the frequency of days above P99, sea level pressure also shows a relatively strong association. These initial diagnostics show predictive promise, and the next step is to develop a statistical model to identify the best combination of significant predictors and the associated predictive skill. The appropriate statistical model that will be explored for each characteristic is shown in the last column of Table 1.

Table 1. Pearson's linear correlations (r) between climate and atmospheric predictors and monsoon inflow characteristic predictants for Elephant Butte (EB) Reservoir, as well as the appropriate statistical model form.

Predictant	Predictors				Appropriate Statistical Model Form
Monsoon EB Inflow Characteristic	AvgPrecip NM Rio Grande	NM Avg Sea Level Pressure	NM Avg Precipitable Water	NM Avg Wind Speed	
Total Volume	**0.73**	0.21	**0.61**	-0.26	Linear Regression
Max Annual Inflow	-0.04	-0.15	0.43	0.52	Generalized Extreme Value
Frequency P50	0.53	0.29	0.50	-0.36	Poisson
Frequency P75	**0.73**	0.46	**0.75**	-0.25	Poisson
Frequency P90	**0.77**	0.52	**0.79**	-0.14	Poisson
Frequency P95	**0.83**	0.32	**0.80**	0.11	Poisson
Frequency P99	-0.10	0.47	**0.66**	0.17	Poisson
Magnitude P50_Annual	**0.66**	0.23	0.59	-0.37	Linear Regression
Magnitude P75_Annual	**0.79**	0.28	**0.69**	-0.25	Linear Regression
Magnitude P90_Annual	**0.78**	0.28	**0.63**	-0.05	Linear Regression
Magnitude P95_Annual	0.59	0.23	**0.60**	0.10	Linear Regression
Magnitude P99_Annual	0.24	0.12	0.47	0.25	Linear Regression

2.4. Step 4. Explore the opportunity-management nexus

The fourth step is to explore the opportunity-management nexus, i.e., to identify quantitative and/or qualitative entry-points to test if and how the changing hydrology could impact management decisions. Managers often use local operations models to understand how changes will affect their water storage and key water operations, which can be used to guide their management decisions. In short, it is critical to collaborate with local water managers to understand their decision and modeling context to explore the potential opportunity-management nexus.

For the Rio Grande of New Mexico, the Upper Rio Grande Water Operations Model (URGWOM) includes reservoirs and operation rules to make hydrologic data relevant to management. URGWOM uses streamflow forecasts to select historical hydrographs to calculate inflows into its reservoirs, include Elephant Butte Reservoir. To date, streamflow forecasts are provided by the

Natural Resources Conservation Services (NRCS), and are based primarily on snowpack measurements, aiming to predict snowmelt runoff. One potential intersection with this framework is to use the understanding gained here as a launching point to predict a suite of monsoon inflow characteristics. It is hoped that these characteristics could be used as guidance for altering the predicted hydrograph during the monsoon season. The tradeoffs between the best predicted monsoon inflow characteristics (such as the total volume versus the magnitude or frequency attributes) and the ability to integrate with and utility for the URGWOM system need to be evaluated. However, even if the information could not be explicitly integrated in the modeling system, even qualitative information on monsoon inflow characteristics may be useful, and would be more than what is currently provided.

3. Discussion and Conclusions

This study offers a 4-step generalized approach to understanding potential opportunities from changing hydrology, including extremes. We provide a specific a case study example of the Middle Rio Grande basin in New Mexico. The goal is to provide both a general approach and a specific example that can be tailored to other watersheds and management systems.

In this investigation, we examined inflows to Elephant Butte Reservoir during the summer monsoon season, as well their association with average basin precipitation and other large-scale variables. However, we note that water resources in the Western US, including New Mexico, are often over-allocated and tightly managed. With full recognition of this fact, we note that we only focus on climate and atmospheric predictors. We recognize a priori that they will only partially explain the variability in the monsoon inflow characteristics, and presumably some of the remaining, unexplained variability would come from groundwater extraction, land-use changes, land surface characteristics, direct management, as well as other factors not examined here. However, we do note that this approach is more suited to looking at the upper percentiles and extremes, as compared to looking at the lower flows of the distribution, where the non-climate signals would likely be more prevalent.

Demonstrating the generalized framework for the Middle Rio Grande basin in New Mexico offers a successful application of the generalized framework, but we note that there could be other applications that yield less useful, though still informative, results. For example, we also stepped-through parts of the framework for the Pecos River basin, New Mexico, which in terms of infrastructure, is already well set-up for collecting extreme precipitation and subsequent runoff along the system. Here, we were interested in not reservoir inflows, but a decision-relevant variable for this watershed, which is the annual allotment to Carlsbad Irrigation District (CID), a Reclamation Project. The CID allotment is the amount of water the farmers are allowed to take per acre of land irrigated. However, when we examined the connections between the CID and Pecos watershed precipitation and the large-scale circulation variables, we did not find strong associations. This indicates that either a) different explanatory variables may need to be examined for the CID allotment, or b) different decision-relevant variables more closely associated with climate could be examined (e.g., reservoir inflows for this basin).

The provocative question posed in this study was “Extremes of Opportunity?” and the results here suggest several conclusions relevant to water managers. First, it depends on what you define as “extreme”. Here, we examine the entire upper half of the flow distribution, and do find that all the upper percentiles contribute a disproportionately higher fraction of the monsoon reservoir volume relative to their occurrence. In the 18-year record examined here, the maximum day contributed 5% of the monsoon flow in that year, and the days that exceeded P99

(or 1% of the days) contributed a median of 32% in the two years that they occurred. Hence, the higher extremes (e.g., maximum and >P99) could certainly provide opportunities in the years they occur. The more moderate extremes (P75-P90) also provide median contributions that are skewed higher than their occurrence, but there is much more variability in these contributions. Nevertheless, we also examined several predictors, including basin-average precipitation and large-scale variables, which showed significant correlations, especially basin-average precipitation and atmospheric precipitable water. These suggest that there is scope for providing outlooks on monsoon inflow characteristics, either from seasonal climate forecasts of the predictor variables, or in terms of downscaling from climate model output. Future work will develop statistical modeling tools to investigate these different applications and to test their ability to integrate with current management in the system.

Acknowledgements

This research was supported by the Bureau of Reclamation Science & Technology award No. 1782: "Detecting, Interpreting, and Modeling Hydrologic Extremes to Support Flexible Water Management and Planning." NCAR is sponsored by the National Science Foundation.

References

Asmerom, Y., Polyak, V.J., Rasmussen, J.B.T., Burns, S.J., and Lachniet, M. 2013. "Multidecadal to multicentury scale collapses of Northern Hemisphere monsoons over the past millennium," PNAS, www.pnas.org/cgi/doi/10.1073/pnas.1214870110

Adams, D.K. and Comrie, A.C. 1997. "The North American monsoon," Bulletin of the American Meteorological Society, 78(10): 2197-2213.

Barnett, T.P., Adam, J.C., and Lettenmaier, D.P. 2005. "Potential impacts of a warming climate on water availability in snow-dominated regions," *Nature*, 438: 303–309.

Chavarria, S. and Gutzler, D.S. 2017. "Observed changes in climate and streamflow in the Upper Rio Grande Basin," Journal of the American Water Works Association, 54(3): 644-659. http://doi.org/10.1111/1752-1688.12640

Collins, M., Knutti, R., Arblaster, J., Dufresne, J.-L., Fichefet, T., Friedlingstein, P., Gao, X., Gutowski, W.J., Johns, T., Krinner, G., Shongwe, M., Tebaldi, C., Weaver, A.J., and Wehner, M. 2013. "Long-term Climate Change: Projections, Commitments and Irreversibility." In: *Climate Change 2013: The Physical Science Basis. Contribution of Working Group I to the Fifth Assessment Report of the Intergovernmental Panel on Climate Change* [Stocker, T.F., Qin, D., Plattner, G.-K., Tignor, M., Allen, S.K., Boschung, J., Nauels, A., Xia, Y., Bex, V., and Midgley, P.M. (eds.)]. Cambridge University Press, Cambridge, UK and New York, NY, USA, pp. 1029-1136.

Dee, D., and Coauthors. 2011. "The ERA-Interim reanalysis: Configuration and performance of the data assimilation system," Quarterly Journal of the Royal Meteorological Society, 137 (656): 553–597.

Douglas, M.W., Maddox, R., Howard, K., and Reyes, S. 1993. "The Mexican monsoon," J. Climate, 6: 1665-1667.

Gutzler, D.S. 2013. "Climate and drought in New Mexico." In: Water Policy in New Mexico [Brookshire, D.S., Gupta, H.V., and Matthews O.P. (eds.)]. RFF Press, New York, 72–86.

Hayhoe, K., Wuebbles, D.J., Easterling, D.R., Fahey, D.W., Doherty, S., Kossin, J., Sweet, W., Vose, R., and Wehner, M. 2018. "Our Changing Climate." In *Impacts, Risks, and Adaptation in the United States: Fourth National Climate Assessment, Volume II* [Reidmiller, D.R., Avery, C.W., Easterling, D.R., Kunkel, K.E., Lewis, K.L.M., Maycock,

T.K., and Stewart, B.C. (eds.)]. U.S. Global Change Research Program, Washington, DC, USA, pp. 72–144. doi: 10.7930/NCA4.2018.CH2

Kunkel, K. E., Andsager, K., and Easterling, D. D. R. 1999. "Long-Term Trends in Extreme Precipitation Events over the Conterminous United States and Canada," Journal of Climate, 12(1998): 2515–2527. https://doi.org/10.1175/1520-0442(1999)012<2515:LTTIEP>2.0.CO;2

Lehner, F., Wahl, E.R., Wood, A.W., Blatchford D.B., and Llewellyn, D. 2017. "Assessing recent declines in Upper Rio Grande River runoff efficiency from a paleoclimate perspective." Geophysical Research Letters, doi:10.1002/2017GL073253.

Mallakpour, I., and Villarini, G. 2017. "Analysis of changes in the magnitude, frequency, and seasonality of heavy precipitation over the contiguous USA," Theoretical and Applied Climatology, 130(1–2): 345–363. http://doi.org/10.1007/s00704-016-1881-z

Mote, P.W., Hamlet, A.F., Clark, M.P. and Lettenmaier, D.P. 2005. "Declining mountain snowpack in western north America," Bulletin of the American Meteorological Society, 86, 39–49.

Mote, P.W., Li, S., Lettenmaier, D.P., Xiao M., and Engel, R. 2018. "Dramatic declines in snowpack in the western US," Npj Climate and Atmospheric Science 1(1), 2, http://doi.org/10.1038/s41612-018-0012-1

Pournasiri Poshtiri, M., Towler, E., Llewellyn, D., and Prein, A.F. 2018. "Extremes of Opportunity: Examining Recent Trends in Warm Season Extreme Precipitation for New Mexico River Basins," 86th Western Snow Conference, Albuquerque, NM, https://westernsnowconference.org/files/PDFs/2018Poshtiri.pdf.

Prein, A. F. 2019. "North American Monsoon Precipitation in New Mexico - The Impact of Monsoonal Flow Characteristics on Historic and Future Water Resources," J. Climate, (in preparation).

Seneviratne, S.I., Nicholls, N., Easterling, D., Goodess, C.M., Kanae, S., Kossin, J., Luo, Y., Marengo, J., McInnes, K., Rahimi, M., Reichstein, M., Sorteberg, A., Vera, C., and Zhang, X. 2012. "Changes in climate extremes and their impacts on the natural physical environment." In: *Managing the Risks of Extreme Events and Disasters to Advance Climate Change Adaptation* [Field, C.B., Barros, V., Stocker, T.F., Qin, D., Dokken, D.J., Ebi, K.L., Mastrandrea, M.D., Mach, K.J., Plattner, G.-K., Allen, S.K., Tignor, M., and Midgley, P.M. (eds.)]. Cambridge University Press, Cambridge, UK, and New York, NY, USA, pp. 109-230.

Serreze, M. C., Clark, M. P., Armstrong, R. L., McGinnis, D. A. and Pulwarty, R. S. 1999. "Characteristics of the western United States snowpack from snowpack telemetry (SNOTEL) data," *Water Resour. Res.*, **35**(7): 2145– 2160.

URGWOM Technical Team. 2005. Draft Upper Rio Grande Water Operations Model Physical Model Documentation: Third Technical Review Committee Draft.

Villarini, G. 2016. "On the seasonality of flooding across the continental United States." *Advances in Water Resources*, *87:* 80–91. http://doi.org/10.1016/j.advwatres.2015.11.009

Wood, K.M. and Ritchie E.A. 2013."An updated climatology of tropical cyclone impacts on the Southwestern United States." Monthly Weather Review, 141: 4322-4336.

Impact of within Storm Intensities trends on Huff Curves

Leili Gordji[1], James V. Bonta[2], and Mustafa S. Altinakar[3]

[1] Ph.D. Candidate, National Center for Computational Hydroscience and Engineering, The University of Mississippi, 327 Brevard Hall, University, MS 38677, USA, lgordji@ncche.olemiss.edu

[2]Research Hydraulic Engineer / Collaborator, USDA - Agricultural Research Service, National Sedimentation Lab, jim.bonta@ars.usda.gov

[3] Director & Research Professor, National Center for Computational Hydroscience and Engineering, The University of Mississippi, 327 Brevard Hall, University, MS 38677, USA, altinakar@ncche.olemiss.edu

Abstract

Increasing air temperatures and extreme precipitation events lead to questions regarding whether climate trends are affecting the temporal distribution of precipitation within storms. This paper investigates whether the storm-intensity patterns expressed through Huff curves (probabilistic representation of storm intensity patterns) are stationary under documented trending air temperature and extreme precipitation. Precipitation data from 4 gauges in the 1,050 acre area of the North Appalachian Experimental Watershed near Coshocton, Ohio (72 years of precipitation data from 1939 through 2010) were divided into eight 9-yr periods. Each period was divided into 4 seasons (winter, spring, summer, and fall). The dimensionless depth with the frequency of 50% (d_{50}) was computed for dimensionless duration verticals of 0.24, 0.50, and 0.74 for each season, each period, and each rain gauge to determine whether there is a shift in the plotting position of the curves through the 8 periods. Spearman rank correlation was utilized to test the trends (rho and p value) for individual gauges and for the averaged of d_{50} for each season and each vertical. The test results showed that only 1 out of 60 cases for d_{50} were significant, suggesting that there is insufficient evidence to reject the null hypothesis of no trends over time in the dimensionless depth of Huff curves. Also, it is visually apparent that Huff curves vary with season throughout a year. The results suggest a promising potential for simplifying and extending the utility of Huff curves in engineering practice under changing climate.

Introduction

Estimation of runoff is needed to design and evaluate-water resource systems for agricultural and urban watershed engineering projects. However, design and other aspects of water-resource management are affected by changing climate (Zahmatkesh, et al., 2015).

The most widely used temporal distributions in engineering practice are the 4 types design storms developed by the Natural Resources Conservation Service (NRCS, 1986). These four types (I, II, III, and IA) are geographically assigned fixed patterns over 24 hours. Huff (1967) introduced a time distribution of rainfall which is expressed as dimensionless cumulative percentages of storm rainfall and storm duration for hydrologic application, and have since become known as “Huff curves”. Bonta (2004) separated storms by month to incorporate the effect of the time of year and developed one plot instead of the four quartiles originally used by Huff. He also showed that summer thunderstorms will have a different pattern of dimensionless precipitation compared to winter storms.

According to Al-Saddi (2002), one of the problems using NRCS distribution is that the distribution is based on 24-hour storms, whereas approximately 75% of Texas storms were shorter than 12 hours. Al-Saadi showed that even though a triangular hyetograph is simpler, Huff curves allow for a better consideration of the rainfall events in Texas. Bonta and Rao (1988) compared four design storms (triangular, mixed rectangular and triangular, mixed triangular, and Huff curves) in mass-curve form and found that among those design storms, Huff curves were the most flexible ones. Bonta (2004) showed that Huff curves visually do not vary over a 644-km distance from Ohio to Illinois; however, they do vary with the season of the year. Because Huff curves are spatially robust, they have the potential to represent short-time increment precipitation intensities over large areas, such as outputs from global circulation models (GCMs).

Huff curves have been suggested for distributing rainfall inputs for watershed modeling (Huff, 1990 and Bonta, 2004), and the National Oceanic and Atmospheric (NOAA) has prepared several regional sets of curves (NOAA, 2017). This study examines the dimensionless distribution of Huff curves and tests whether there are any changes in the position of dimensionless depth at 50% frequency in Huff curves in an area with reported increasing precipitation (Gordji et al., 2016).

Procedure

Study Area and Data

The study site is located at the North Appalachian Experimental Watershed (NAEW) about 16 km northeast of Coshocton, Ohio. Its area is approximately 1,050 acres and includes large lysimeters, small and large experimental watersheds, a weather station, and a network of rain gauges. The average annual precipitation is 959 mm (37.76 in).

The precipitation data used in this study were collected from 4 rain gauges in NAEW-- ry103, rg119, rg113 (rg513), and rg103 (rg503). For two gauges, an alternate ID number starting with digit 5 is given in parentheses. The alternate ID is for those gauges that had missing records and were completed using data from nearby rain gauges. These rain gauges were chosen as representative of NAEW because they are located at four peripheral locations of the NAEW (figure 1).

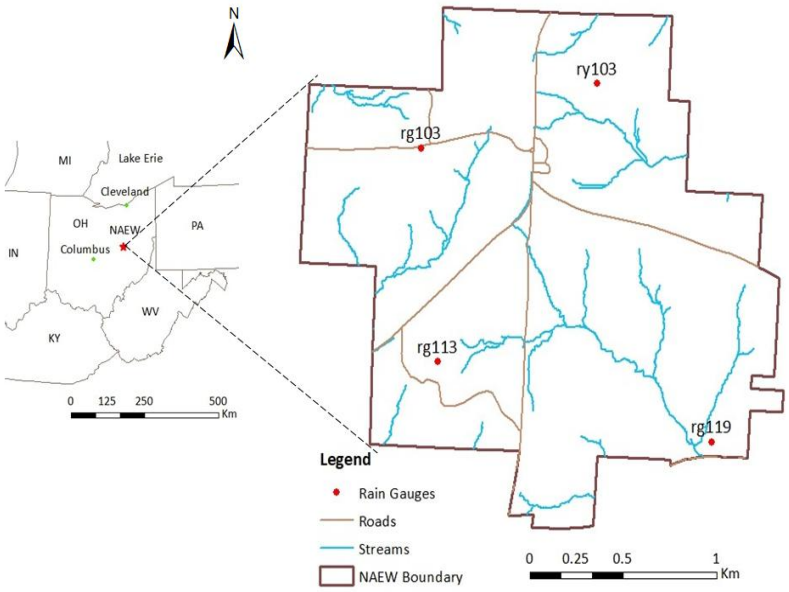

Figure 1. Location of rain gauges on the NAEW

The data used in the present study were obtained over 72 years (1939 through 2010). The 72 years of data were divided into 8 periods. Each period includes 9 consecutive years of data. The data covered in the first period is from 1939 through 1947 and in the second period from 1948 through 1956 and so on. Each period was also divided into 4 seasons: winter (December, January, and February); spring (March, April, and May); summer (June, July, and August); and fall (September, October, and November).

Huff curves

The following steps were taken to construct the Huff curves

1. Calculate the minimum dry period between the storms using the exponential method for each month.
    a. The exponential distribution is given by

(1)

Where f(t) is the probability density function, α is reciprocal of the mean time storms, and t is dry period duration, the random variable.

b. This distribution has equal mean and standard deviation or in other words has a unity coefficient of variation

—— (2)

The “std” and “ave” stand for standard deviation and mean respectively and CV is the coefficient of variation.

   c. CV is calculated for all the time between storms (TBS). If CV is greater than one, then the smallest TBS is removed and then CV is calculated for the remaining TBS. This process is repeated until CV ≤ 1. If CV is less than one then minimum dry period is obtained by interpolation. This process is repeated for each month.
2. Nondimensionalize the depth and duration of each observation point within each storm by dividing those points by the total depth and total duration of that storm respectively.
3. Calculate dimensionless depths for each dimensionless duration from 0.0 to 1.0 with an increment of 0.02 for each season in every period by using linear interpolation. The resulting 51 vertical lines are referred to as "verticals".
4. Add the third dimension (the frequency distributions of dimensionless depth) to determine the percentage of mass-curve intersection at or below assigned percentages of 10% to 90% with an increment of 10% using the following equation

   —— (1)

   Where P is cumulative percentage of dimensionless depth, i is the rank of the observation point, and n is the total number of the observation points.
5. Connect the dimensionless depths with the same frequency along the vertical lines. These nine isopleths of probability constitute "Huff curves".

Quantification of Central Tendency

The dimensionless depth for the 50% isopleth (d_{50}) was computed for dimensionless duration verticals of 0.24, 0.50, and 0.74 for each season for each rain gauge in each period to determine whether there is a shift in the plotting position of the curves through the 8 periods (central tendency).

A significance test for trends in d_{50} would indicate whether a trending precipitation affected the position of 50% curve. Spearman's rank correlation coefficient (rho) and probability value (p) were calculated between d_{50} and the 8 periods in four seasons at three verticals for four rain gauges. Rho gives the strength of the relationship between the independent and dependent variables and is an indication of the direction of the trend (increasing or decreasing) and p is a measure of significance of the trend. The p significance threshold of 0.05 was chosen for testing whether a trend is apparent. By calculating the trends for d_{50}, it can be seen whether there are changes across the periods and four seasons within a storm for shorter time periods (0.24 vertical), central time periods (0.50 vertical), or for longer time periods (0.74 vertical). The statistical analyses were performed using Statistical Analysis System software (SAS, 2019). Also, d_{50} was averaged among 4 gauges in four seasons and three verticals and then the correlation coefficient and p values were obtained for the average of d_{50}. The total number of tests was 60 including four individual gauges and the average values for four seasons at three verticals.

Results and Discussion

Three isopleths of Huff curves (10%, 50%, and 90%) were selected to visually illustrate and to track the changes over three periods of time (2nd, 5th, and 8th) for four seasons - winter (figure 2), spring (figure 3), summer (figure 4), and fall (figure 5). Every season are showing the changes for four gauges - rg119 (figure a in figures 2 through 5), rg113 (figure b in figures 2 through 5), rg103 (figure c in figures 2 through 5), and ry103 (figure d in figures 2 through 5). Each figure of individual gauges consists of 9 plots - 3 isopleths (10%, 50%, and 90%) for three periods (2nd,

5th, and 8th). Therefore in each figure, three periods are visually compared with each other for each isopleth, rain gauge, and season.

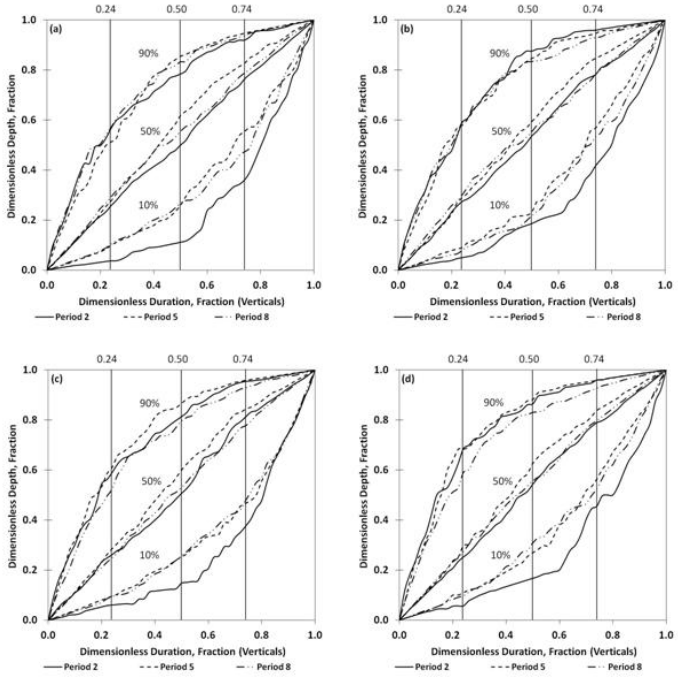

Figure 2. Dimensionless depth versus dimensionless duration for three isopleths for three periods 2nd, 5th, and 8th in winter for four rain gauges: a) rg119, b) rg113, c) rg103, and d) ry103

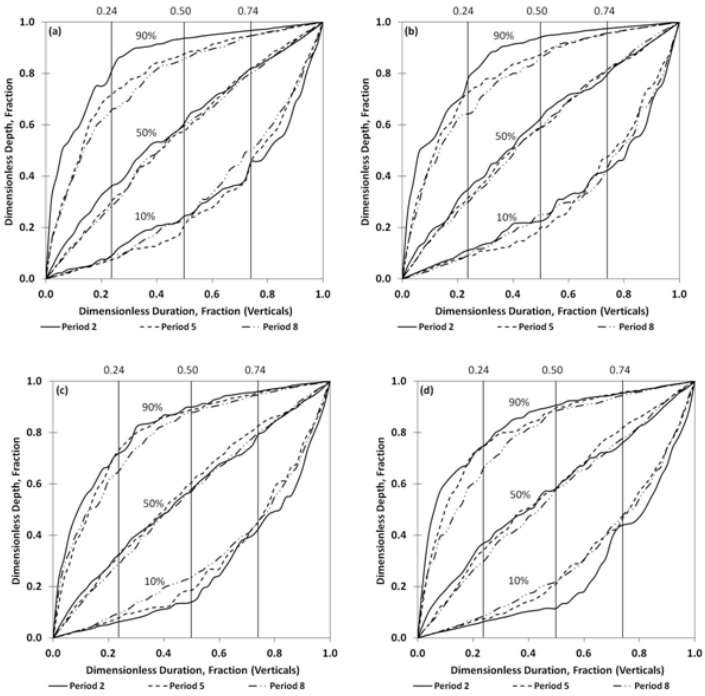

Figure 3. Dimensionless depth versus dimensionless duration for three isopleths for three periods 2nd, 5th, and 8th in spring for four rain gauges: a) rg119, b) rg113, c) rg103, and d) ry103

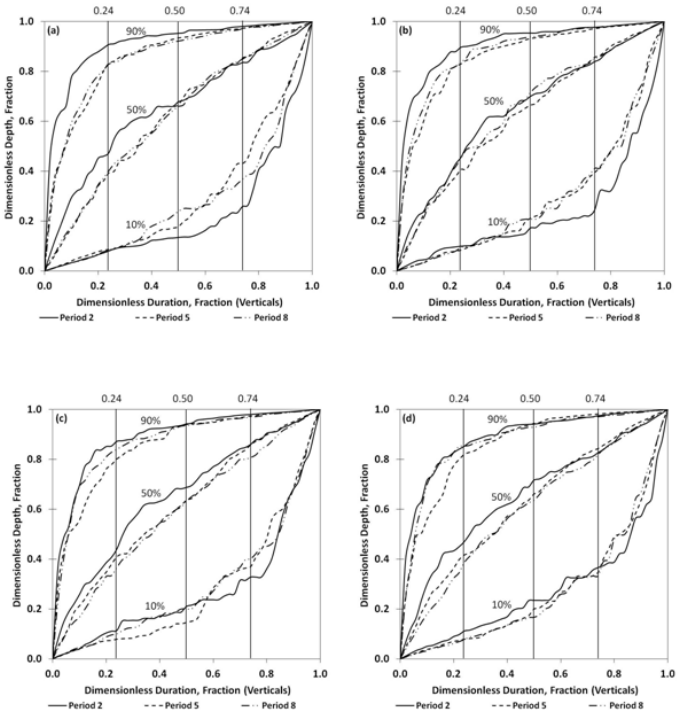

Figure 4. Dimensionless depth versus dimensionless duration for three isopleths for three periods 2nd, 5th, and 8th in summer for four rain gauges: a) rg119, b) rg113, c) rg103, and d) ry103

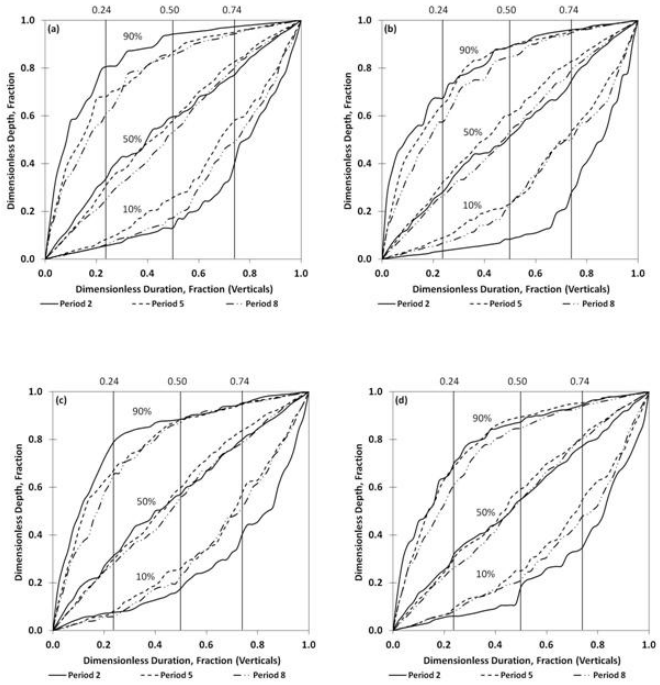

Figure 5. Dimensionless depth versus dimensionless duration for three isopleths for three periods 2nd, 5th, and 8th in summer for four rain gauges: a) rg119, b) rg113, c) rg103, and d) ry103

In winter, for the 10% isopleth the dimensionless depths are generally smaller in period 2 compared to periods 5 and 8 whereas for the 50% and 90% isopleths the dimensionless depths are generally the same for three periods in four rain gauges (figure 2). In spring, the dimensionless depths in period 2 compared to periods 5 and 8 are smaller for the 10% isopleth for ry103 and are larger for the 90% isopleth for rg119 and rg113 whereas for the 50% isopleth the dimensionless depth are generally the same for three periods in four rain gauges (figure 3). In summer, the dimensionless depths in period 2 compared to periods 5 and 8 are smaller for the 10% isopleth for rg119 and rg113 and are larger for the 90% isopleth for rg119 whereas for two other gauges – rg103 and ry103 are approximately the same. The dimensionless depths for the 50% isopleth are larger in period 2 compared to the other periods for rg119 and generally the same for the other three gauges in three periods (figure 4). In fall, the dimensionless depths in period 2 compared to periods 5 and 8 are smaller for the 10% isopleth for rg113 but they are generally the same in three periods (figure 5).

Comparing the four seasons using corresponding Huff curves (figures 2 to 5) visually show that Huff curves vary with season, reflecting seasonal patterns. The difference between the 10% and 90% is largest in summer and smallest in winter (figures 2 to 5). This seasonal effect was also reported by Bonta and Rao (1987) and Bonta (2004).

Figures 2 to 5 illustrate how Huff curves may visually vary for four gauges in three periods for verticals of 0 to 1 with 0.02 increments. The visual observation is also verified by statistical analysis using Spearman rank correlation. Spearman rank correlation coefficients and p values quantify trend results for d_{50} across the 8 periods for three verticals of 0.24, 0.50, and for 0.74 for the four gauges. There are upward trends for winter and generally downward trends for the other seasons for four gauges and for the average d_{50} at the 0.24 vertical (figure 6a). However there are mixed upward and downward trends for four gauges and for the average d_{50} at

verticals of 0.50 and 0.74 (figures 6b and 6c). The statistical significance of individual rain gauges showed only one case out of 60 cases with a significantly increasing trend and one case with a borderline increasing trend – rg113 in winter at 0.24 vertical and in fall at 0.74 vertical respectively (figures 7a, 7b, and 7c).

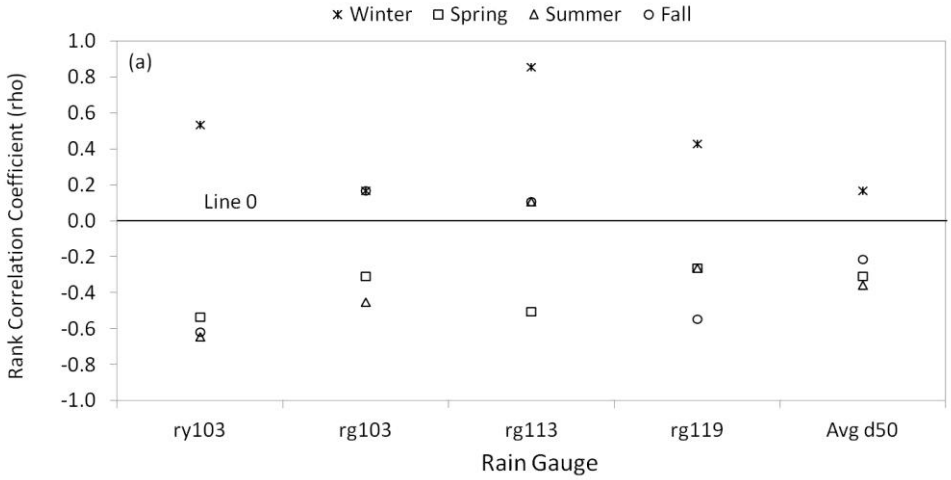

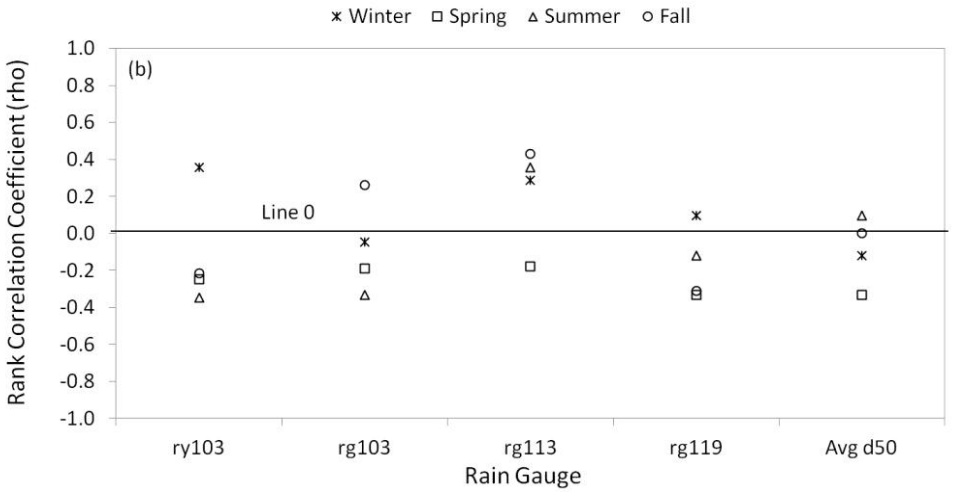

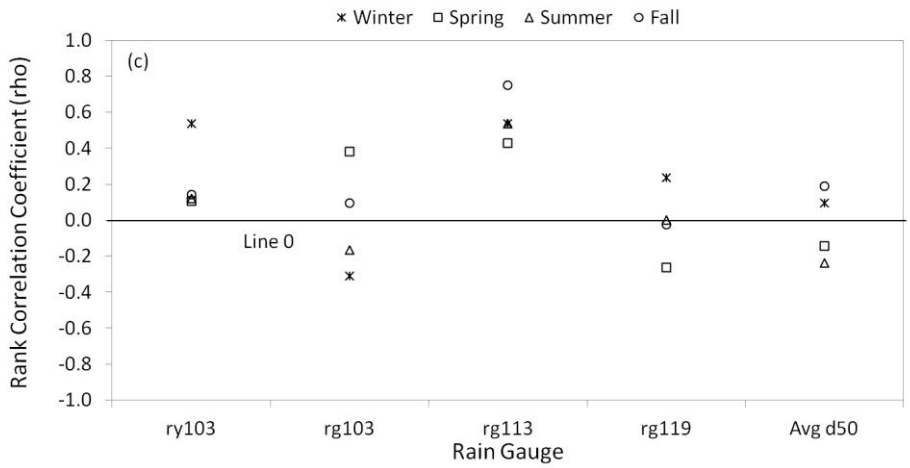

Figure 6. Spearman rank correlation coefficient (rho) of dimensionless depth for 50% isopleth (d_{50}) for 4 rain gauges and for the average of d_{50} over 4 rain gauges versus 8 periods in four seasons at three verticals of a) 0.24, b) 0.50, and c) 0.74

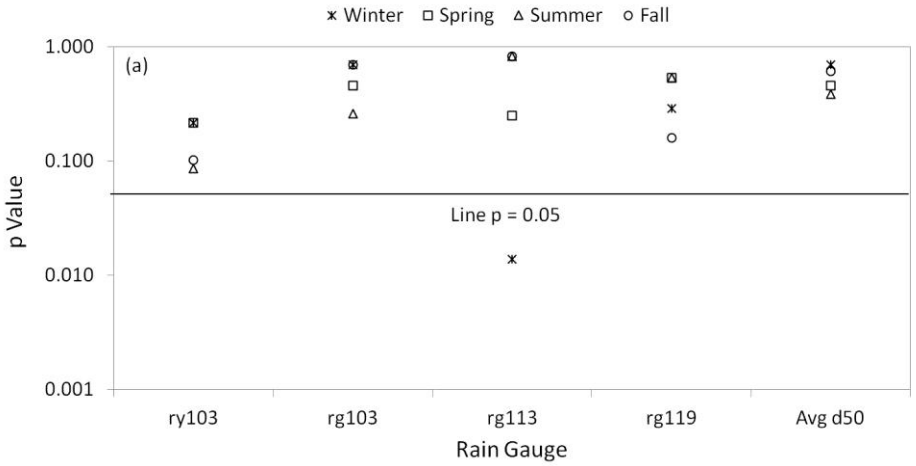

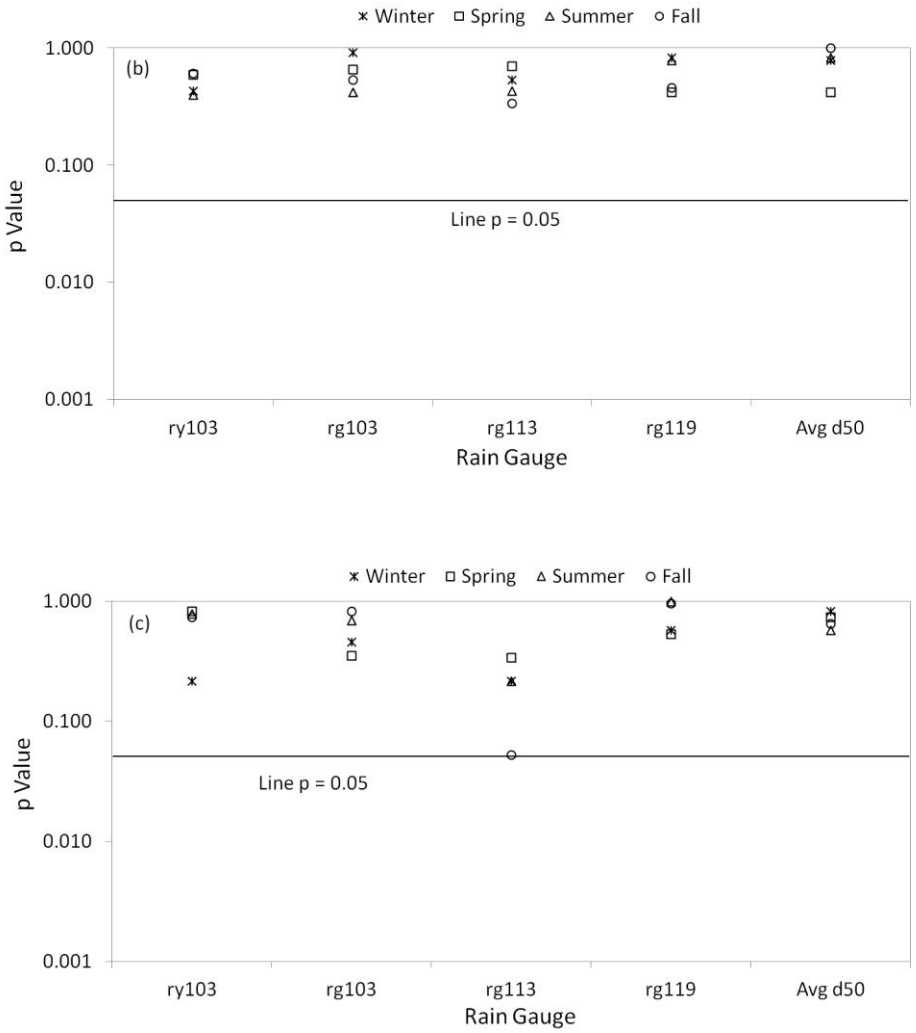

Figure 7. p value of dimensionless depth (d_{50}) for 4 rain gauges and for the average of d_{50} over 4 rain gauges versus 8 periods in four seasons at three dimensionless duration verticals of a) 0.24, b) 0.50, and c) 0.74

Conclusion

The 72 years of precipitation data from four rain gauges at the 1,050 ac area of North Appalachian Experimental Watershed in Coshocton, Ohio were divided into 8 periods. Each period consists of 9 years of precipitation data. After separating the data into 8 periods, the data were further divided into 4 seasons. Huff curves, which are a family of empirical dimensionless storm distribution patterns, were used to identify seasonal trends in the position of the dimensionless depth with frequency of 50% (d_{50}) across the 8 9-yr periods for 4 rain gauges. Data were analyzed using Spearman rank correlation. The statistical results indicate that the position of the 50% curve across Huff curves at the significance level of p=0.05 has not changed, and thus there is no significant trend for the dimensionless depth at three verticals in four seasons for most of the gauges and for the averaged d_{50}. These data do not provide sufficient evidence at the p=0.05 significance level to reject the null hypothesis of unchanging position in the dimensionless depth of the 50% Huff curves in spite of increasing air temperature and

extreme precipitation over the 72-year period. However, our analysis shows that Huff curves vary from season to season and there is greater spacing between summer and lesser spacing between winter curves.

References

Al-Saadi, R. 2002. "Hyetograph estimation for the State of Texas," Texas Tech University, M.S. thesis, 96 pp.

Bonta, J.V. and Rao, A.R. 1988. "Comparison of four design-storm hyetographs," Trans. ASAE, 31(1): 0102-0106. doi:10.13031/2013.30673.

Bonta, J.V. 2004. "Development and utility of Huff curves for disaggregating precipitation amounts," Applied Engineering in Agriculture, 20(5), 641-653.

Gordji, L., Bonta, J.V., and Altinakar, M.S. 2016. "Trends of extreme precipitation at the North Appalachian Experimental Watershed in east-central Ohio." Journal of Soil and Water Conservation 71(5): 430-439.

Huff, F.A. 1967. "Time distribution of rainfall in heavy storms," Water Resources Research, 3 (4), 1007–1019.

Huff, F.A. 1990. "Time distributions of heavy rainstorms in Illinois," Illinois State Water Survey, Circular 173, Champaign, Illinois, USA.

NOAA (National Oceanic and Atmospheric). 2017. NOAA Atlas 14 Temporal distributions for 6-, 12-, 24-, and 96-hour Durations, <http://hdsc.nws.noaa.gov/hdsc/pfds/pfds_temporal.html>.

NRCS (Natural Resources Conservation Service). 1986. "Urban hydrology for small watersheds," Technical Release 55, SCS, U.S. Department of Agriculture, Washington, DC.

SAS (Statistical Analysis Software). 2019. SAS Institute Inc., Cary, NC, USA. <www.sas.com>.

Zahmatkesh , Z., Karamouz, M., Goharian, E., and Burian, S. J. 2015. "Analysis of the effects of climate change on urban storm water runoff using statistically downscaled precipitation data and a change factor approach," Journal of Hydrologic Engineering 2015, 10.1061/(ASCE)HE.1943-5584.0001064.

Bypassing the Uncertainty Question: Using Storylines to Describe Potential Hydrologic Futures for a Basin

Lucas Barrett, Hydrologist, Bureau of Reclamation, Albuquerque, NM, lbarrett@usbr.gov
Dagmar Llewellyn, Hydrologist, Bureau of Reclamation, Albuquerque, NM, dllewellyn@usbr.gov

Introduction

This paper describes an approach for evaluation and modeling of potential responses to future water supply and demand challenges in a way that avoids describing the likelihood of potential future changes, and therefore avoids the need to characterize uncertainty associated with water supply and demand projections. This approach was used by the Bureau of Reclamation, and its partner the New Mexico Interstate Stream Commission (NMISC), for the Pecos River – New Mexico Basin Study

Background

Since the passage of the SECURE Water Act in 2009, the Bureau of Reclamation (Reclamation) has been developing state-of-the art methodologies for characterizing future climate and hydrology within the river basins of the Western US that are served by Reclamation water projects. These methodologies have been developed by Reclamation's West Wide Climate Risk Assessment Team and applied in Reclamation's Basin Studies, which are partnerships with local water-management entities to characterize potential future water supply and demand and develop and model adaptations to the projected system changes. Under the Basin Study Program, Reclamation has developed methodologies for ensembling forecasts of future water supply and demand based on large suites (compiled by the World Climate Research Programme's Coupled Model Intercomparison Project, or CMIP) of Global Climate Model (GCM) simulations, which have been bias-corrected and downscaled, and then run through hydrologic models in an attempt to capture the range of likely future water supply conditions. These ensembling methods are meant to help comprehend the results of the many GCM runs, and the range of variability of these results.

So far, these Basin Studies have primarily relied on two ensembling approaches: Transient Projections and Period-Change Projections. Transient projections are traces of the changes in climatic or hydrologic parameters over time (usually over the course of the 21st century). Transient projections are ensembled through the generation of statistics describing the full suite of these traces that are generated from a suite of GCMs. Period-change projections are projections of the likely range of climate and hydrology parameters at a specific future year. To develop ensemble period-change projections, Reclamation has clustered the hydrologic projections by the degree of change in temperature and precipitation, by the specified year, and then analyzed groups of projections according to their location in the precipitation-temperature

space: central tendency, hot and wet, hot and dry, warm and wet, and warm and dry. Monthly change factors are applied to historic records for each of these groups, generating 5 sets of statistics characterizing the range of variability in the projections for the selected future year.

Both of these methods have in common an attempt to capture the degree of hydrologic change that we can expect in the future, both in terms of means and extremes, as well as the degree of uncertainty in the projection of future conditions, based on the range of variability within the ensembles. However, it is clear, based on the range of uncertainty within these projection sets that they come with considerable uncertainty, especially for precipitation. This uncertainty can complicate planning of adaptation measures by water managers and stakeholders.

In the Pecos Basin in New Mexico, the small portion of the basin's water supply that comes from snowpack, as well as the dominance of groundwater in the water supply, have made the Pecos Basin poorly suited for Reclamation's developed methodologies. Reclamation's Albuquerque Area Office therefore developed an alternative approach utilizing individual projections that tell particular stories about the way that the basin may develop. This approach has the added benefit that it avoids describing the likelihood of potential future changes, and therefore avoids the need to characterize uncertainty associated with water supply and demand projections. It also allowed Reclamation, its study partner, and basin stakeholders to play a game of "what if", which allowed consideration of different ways that the basin might change in the future. For example, we could contrast a future in which snowpack declines, but summer monsoonal precipitation increases with a future in which precipitation declines in both seasons, and another in which the seasonal distribution of precipitation doesn't change significantly. This provided a tool for visioning of different potential futures, which helped with the development of adaptation strategies, and also highlighted the adaptation strategies that are common between the different potential futures.

Methods

Modelling 930 traces (93 GCMs, 2 hydrologic models, and 4 bias-correction techniques plus raw output) takes high-end computing power and a large amount of time and effort for computation and analysis. What if, instead of trying to create a deterministic forecast that shows an envelope of many different traces, a selection of just a few statistically reasonable traces were chosen that describe varying futures for the basin? This is the thought process that was undertaken to narrow down the immense number of possible traces to analyze for the Pecos River Basin Study. The multistep process of narrowing down those 930 traces to a manageable number of storylines is shown in Figure 1.

The process of developing the storylines for the Pecos Basin in New Mexico began with the evaluation of 93 sets of climatic and hydrologic projections developed from the Coupled Model Comparison Project Phase 5 (CMIP5) suite of GCM simulations (https://gdo-dcp.ucllnl.org/downscaled_cmip_projections/). The projections provided on this website have been bias corrected for climate parameters and spatially downscaled to 1/8th degree of

latitude/longitude (through the statistical Bias Correction and Spatial Downscaling process BCSD (Wood et al., 2004)), and processed through two hydrologic modeling codes (the Variable Infiltration Capacity modeling code, or VIC (Liang et al., 1994), and the US Geological Survey's Precipitation Runoff Modeling System, or PRMS (Leavesley et al., 1983)).

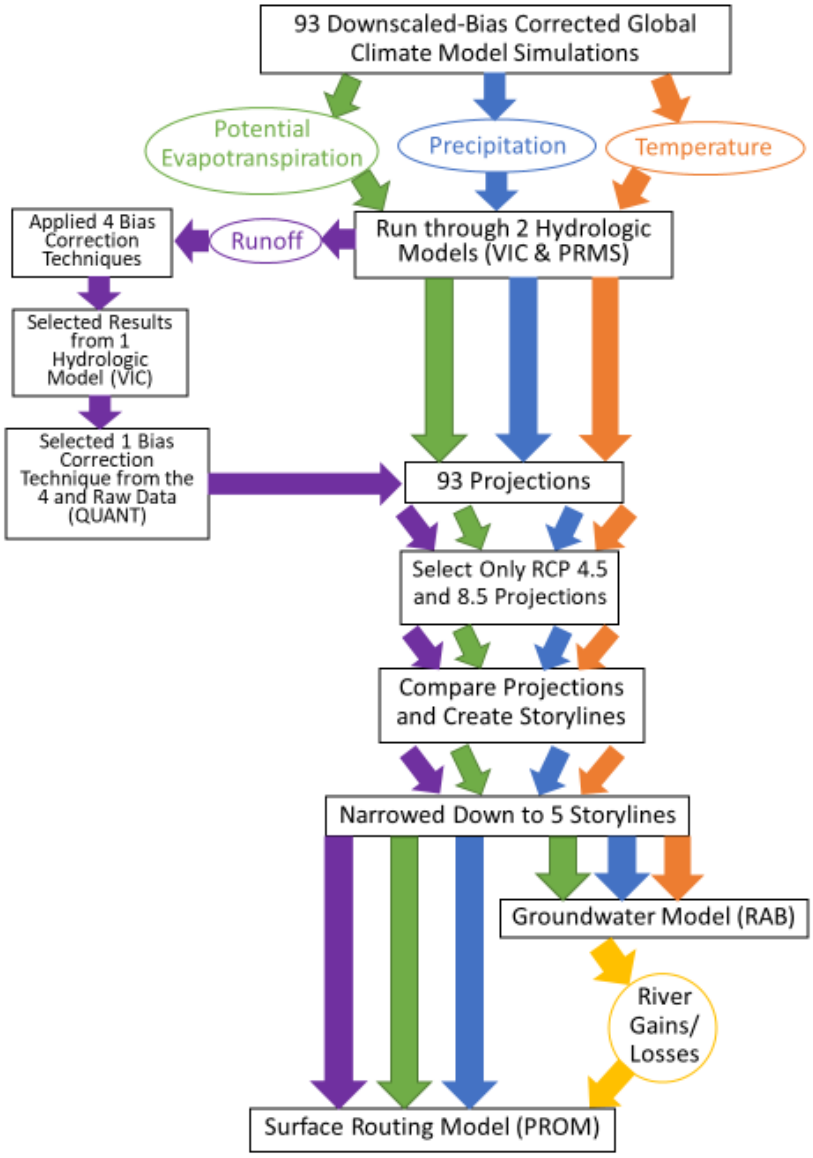

Figure 1. Simplified diagram depicting the steps that were taken to narrow the 930 traces to 5 Storylines.

The resulting hydrologic projections were then routed by the U. S. Army Corps of Engineers (USACE) using a hydrologic routing tool known as mizuRoute (Mizukami, et. al, 2016) to provide projections of streamflow at specific gage locations within the basin. This process provided a more complete projection set for the projections processed through the VIC model code (i.e. it provided hydrologic projections for each of the headwater locations in the operations

model for the Pecos Basin in New Mexico), and for that reason, only projections processed through the VIC model code were carried forward in this study. USACE also performed bias correction on the routed streamflows using four bias correction techniques, and allowed us access to an in-house tool that compared the robustness of the routed streamflows using each technique for hindcast streamflows. Projections processed using the Quant streamflow bias correction technique were deemed the most robust and were carried forward in this study.

The processes described above provided 93 climate and hydrology projection traces for the 21st century. The number of projections under consideration in this study was then reduced through the selection of only the projections based on the greenhouse-gas emissions scenarios referred to as Representative Concentration Pathways 4.5 and 8.5. RCP 8.5 represents a "business as usual" future. In contrast, RCP 4.5 shows what would happen if our global society begins to strongly reduce greenhouse gas emissions. More conservative greenhouse-gas emissions groupings, including RCP 2.6, are broadly outside the projected range of future conditions considered by major climate assessments including those produced by the Intergovernmental Panel on Climate Change (Sun et al., 2015). Further, the Fourth National Climate Assessment (U.S. Global Change Research Program, 2018) which was underway at the time of this study, considers CMIP5 4.5 and CMIP5 8.5 projections only. This process narrowed the number of hydrologic projections under consideration to 48 (28 RCP 8.5 projections, and 30 RCP 4.5 projections).

A detailed comparative analysis was then performed on the remaining projection traces in order to characterize the story that each tells about the projected future climate and hydrology in the basin. Parameters characterized and compared included snowmelt runoff and timing, monsoon intensity, seasonal and spatial precipitation patterns, temperatures, evapotranspiration rates, and total streamflow in the mainstem and key tributaries. The stories were then evaluated by Reclamation and the NMISC, and presented to basin stakeholders as part of a collaborative decision-making process, which resulted in the selection of five stories to be carried forward in the study. Baseline characterizations of potential future conditions in the basin, especially related to the agricultural irrigation districts in the basin, were performed using the Pecos River Operations Model, PROM (Boroughs and Stockton, 2010) developed in RiverWare® (Zagona, et. al., 2001) as well as the Roswell Artesian Basin Groundwater Model (Daniel B. Stephens and Associates, 1995), developed in MODFLOW (Harbaugh, et. al. 2000). The final selected storylines were:

- RCP 8.5 Moderate: a Moderate Storyline that showed a mild amount of drying across the entire basin and was close to the median of all the RCP 8.5s that were analyzed,
- RCP 8.5 Dry: a Dry Storyline that showed extreme drying and increased temperatures across the basin,
- RCP 8.5 High Monsoon, Low Snowpack: a storyline that show an increase to the monsoon intensity great enough to make up for the decrease in snowpack,
- RCP 4.5 Reduced Emissions Increased Monsoon: a storyline that is around the average and median of the 4.5 projections and shows minor increases in monsoon activity and temperature and minor decreases in winter precipitation and snowpack over time,
- RCP 4.5 Reduced Emissions Median: a storyline that is close to the median of the 4.5 projections and shows minor decrease in precipitation and temperature over time.

Implications of this Work

This Storyline approach bypasses concerns about projection uncertainty – each projection is considered equally likely, but none are considered predictions of future conditions. Instead, they provide a picture of the range of variability in basin conditions, from which a variety of possible strategies can be developed. Having these different Storylines, allowed us to model different strategies for improving the basin water management for each of the Storylines and see which strategies worked the best for any specific Storyline, and even more importantly, which strategies worked well in all Storylines. This allowed us to address the stakeholders not only with strategies that will help water resource management in the basin for an average possible future, but from multiple, equally-likely, futures in which the basin's hydroclimate changes in different ways.

References

Boroughs, Craig B. and Stockton, Tomas B., 2010, *Pecos River RiverWare Model Documentation*.

Daniel B. Stephens & Associates, 1995, *Comprehensive Review and Model of the Hydrogeology of the Roswell Basin*. New Mexico State Engineer Office Report.

Harbaugh, A.W., Banta, E.R., Hill, M.C., and McDonald, M.G., 2000, MODFLOW-2000, the U.S. Geological Survey modular ground-water model -- User guide to modularization concepts and the Ground-Water Flow Process: U.S. Geological Survey Open-File Report 00-92, 121 p.

Leavesley, G.H.; Lichty, R.W.; Troutman, B.M.; Saindon, L.G.;, 1983. Precipitationrunoff modeling system--user's manual. U.S. Geological Survey Water Resources Investigations Report 83-4238, , 207.

Liang, X., D. P. Lettenmaier, E. F. Wood, and S. J. Burges, 1994: A Simple hydrologically Based Model of Land Surface Water and Energy Fluxes for GSMs, J. Geophys. Res., 99(D7), 14,415-14,428.

Mizukami, Naoki, Martyn P. Clark, Kevin Sampson, Bart Nijssen, Yizin Mao, Millary McMillan, Roland J. Viger, Stevel L Markstrom, Lauren E. Hay, Ross Woods, Jeffrey R. Arnold, and Levi D. Brekke, 2015; *MizuRoute version 1: a river network routing tool for a continental domain water resources applications*; Geoscientific Model Development 9 (2016)2223-2238; doi:10.5.194/grr:d-92223-20116.

Sun, L., Stevens, L. E., Buddenberg, A., Dobson, J. G., Easterling, D. R., & Easterling, D. R. (2015). Regional surface climate conditions in CMIP3 and CMIP5 for the United States., (July). https://doi.org/10.7289/V5RB72KG

U. S. Global Change Research Program; 2018; *Fourth National Climate Assessment*. November 2018. Doi: 10.7930/NCA4.2018. Available at https://nca2018.globalchange.gov/chapter/front-matter-about/

Wood, A.W., L.R. Leung, V. Sridhar, and D.P. Lettenmaier, 2004. "Hydrologic Implications of Dynamical and Statistical Approaches to Downscaling Climate Model Outputs," Climatic Change, 15(62):189-216.

Zagona, Edith A., Fulp, Terrance J., Shane, Richard, Magee, Timothy, & Goranflo, H. Morgan. 2001 "Riverware: A Generalized Tool For Complex Reservoir System Modeling." *JAWRA Journal of the American Water Resources Association*, vol. 37, no. 4, pp. 913–929., doi:10.1111/j.1752-1688.2001.tb05522.x.

Water Supply Viability of Lake Tahoe Under Modified Climate Conditions

Michael L. Coleman, Project Manager, Precision Water Resources Engineering, Loveland, CO, mike@precisionwre.com
Seshadri Rajagopal, Research Hydrologist, Desert Research Institute – Reno, Reno, NV, Seshadri.Rajagopal@dri.edu
Justin L. Huntington, Research Professor of Hydrology, Desert Research Institute – Reno, Reno, NV, Justin.Huntington@dri.edu
Shane Coors, Principal, Precision Water Resources Engineering, Loveland, CO, shane@precisionwre.com
Greg M. Pohll, Research Professor of Hydrogeology, Desert Research Institute – Reno, Reno, NV, Greg.Pohll@dri.edu
Richard Niswonger, Research Hydrologist, United States Geological Survey, Menlo Park, CA, rniswon@usgs.gov

Abstract

Lake Tahoe is the largest reservoir in the Tahoe/Truckee system and an important water supply source for the Truckee and Carson River basins. However, the presence of a natural rim and the disproportionate importance of evaporation on the lake's water balance lead to some unique challenges for the lake's viability as a water supply. The goal of this study was to assess the likelihood of the lake pool elevation dropping below the rim elevation under the RCP 4.5 and RCP 8.5 future climate scenarios. Results from eight different GCMs under each scenario were first used as forcing for local hydrologic models. The GCM and hydrologic model results were then used as input to a river and reservoir network model that incorporates current operational procedures for the basin under the Truckee River Operating Agreement. Results of the modeling indicate increased average net inflow to Lake Tahoe, along with increased average outflow from the lake, greater outflow variability, and an increased proportion of time for which the Lake Tahoe pool elevation is below the rim elevation.

Introduction

With an average annual release of 235,000 acre-feet, Lake Tahoe is the single largest water supply source in the Tahoe/Truckee system. When the Lake Tahoe pool elevation drops below the lake's rim, and no water can be released from the lake, the basin begins drought operations. So, the importance of Lake Tahoe as a water supply for the downstream users can hardly be overstated. While the overall volume of water contained in Lake Tahoe (~122 million acre-feet) would seem to suggest a stable water supply for years to come, the details of Lake Tahoe's reservoir and water balance suggest otherwise.

Lake Tahoe has a reservoir capacity of 744,600 acre-feet, which is approximately 68% of the total reservoir storage in the Tahoe/Truckee system (1,089,210 acre-feet), and an average annual inflow of 642,000 acre-feet, which is approximately 66% of the average annual inflows to all reservoirs (969,900 acre-feet). However, while Tahoe's average annual release of 235,000 acre-feet is the largest of the system reservoirs, that release represents only 43% of the water supply from the reservoirs.

The importance of the evaporation component to the Lake Tahoe water balance explains why it contributes such a relatively small volume to the water supply. The total impounded volume behind the Tahoe Dam is ~745,000 acre-feet at a height of 6.1 feet over an area of ~120,000 acres. The large surface area, in combination with the surrounding climate, lead to a relatively high annual average evaporation of ~427,000 acre-feet, or 3.6 feet over the lake surface, which represents more than half of the total reservoir capacity.

Evaporation's influence on the Lake Tahoe water balance means that the reservoir is potentially more susceptible than other reservoirs to climate change impacts that may involve decreased inflows and increased evaporation. Additionally, the low height of the dam means that dam operators are limited in their control of the release rate from the lake, and no release is possible if the pool elevation drops below the lake rim. For those reasons, and Tahoe's importance as a water supply, anticipating the effects of climate changes on the Lake Tahoe pool elevation are critical for understanding its future role in water supply projections for the basin.

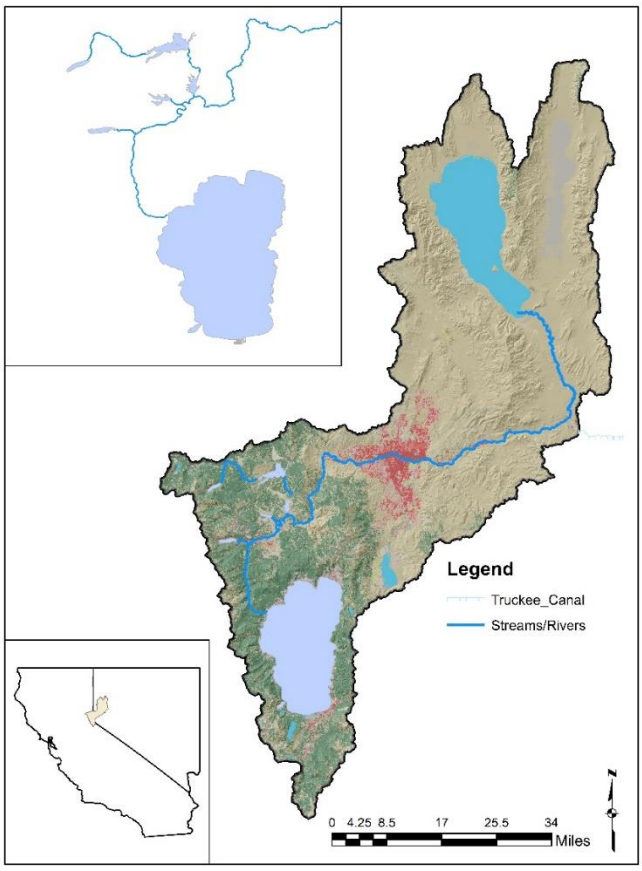

Figure 1. Truckee Basin Map

The major objective of this work is to analyze the effects of plausible future climate scenarios on the likelihood of the Lake Tahoe stage to fall below the lake's natural rim. This objective was pursued through the use of more robust and advanced hydrologic and operations models and climate projections than were previously available or applied to the basin.

Methods

Models and Data

The study was performed by utilizing eight different Global Climate Models (GCMs) (CCSM4, CNRM-CM5, CanESM2, GFDL-ESM2M, HadGEM2-CC, HadGEM2-ES, MIROC5, bcc-csm1-1) under two Representative Concentration Pathway (RCP) scenarios (4.5 and 8.5) (*van Vuuren, 2011*) to generate forcing for PRMS hydrologic models of Lake Tahoe and the Truckee River basin *(Rajagopal et al., 2015)*. In addition, the GCM output was used to calculate open water evaporation for Lake Tahoe with the CRLE model *(Huntington and McEvoy, 2011)*. The GCM precipitation, PRMS streamflows, and CRLE evaporation time series were then used as input to the Truckee River Operating Agreement Planning Model (Planning Model) (*US BOR, 2015)*. The Planning Model was developed on the RiverWare® platform for performing long-range planning scenarios of the Truckee River Basin operating under the Truckee River Operating Agreement (TROA).

Figure 2 indicates how data flows between the models used. The GCMs produce temperature and precipitation series as output. PRMS uses the precipitation and temperature data as input and produces streamflow data as output. The CRLE uses temperature, humidity and insolation as input and produces open water evaporation on Lake Tahoe as output. The Planning Model operates on a daily timestep uses the precipitation, evaporation, and streamflow time series as inputs and produces reservoir outflows and pool elevations as outputs.

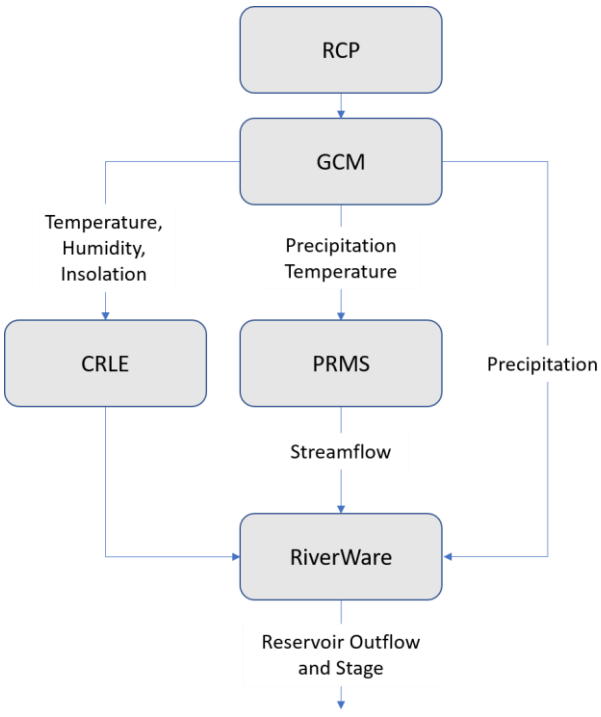

Figure 2. Flow chart showing data flow between the models

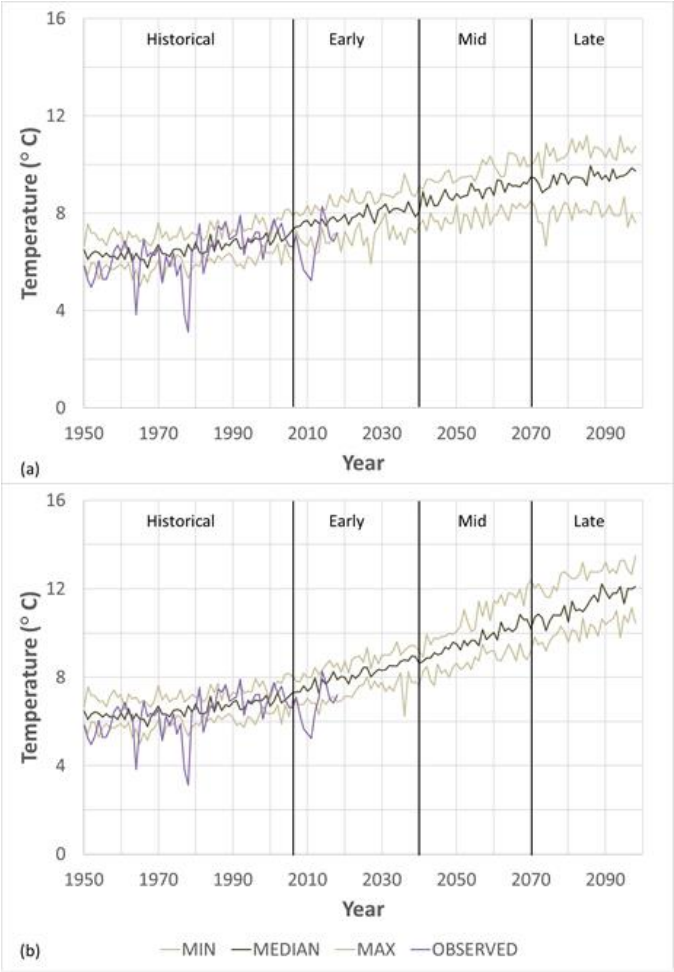

Figure 3. Minimum, Median, and Maximum temperature time series for GCMs under (a) RCP 4.5 and (b) RCP 8.5 scenarios with Historical modeled and observed

Model Calibration/Validation

Two different time series of forcing data were developed from each GCM, for the periods 1951-2005 and 2006-2098. The 1951-2005 series ("Historical") were used for calibration/validation by comparing output from the RiverWare® model forced by the synthetic data with output generated from historical data inputs. Based on those comparisons, the streamflow and precipitation time series for the RCP scenarios were bias-corrected prior to their use as RiverWare® input.

Validation of the GCM-forced hydrologic data was performed by using the PRMS outputs as input to the RiverWare® model and comparing statistically the RiverWare® outputs and historical data. For this purpose, the entire Truckee River basin was divided into three sub-basins corresponding with the individual PRMS models' extents, and referred to as follows: Tahoe, Little Truckee, and Truckee Above Farad. For each GCM, the average of each sub-basin's annual volume and contribution to the overall annual volume was compared to the historical

volume and contributions to the overall volume. While the annual volumes for the Little Truckee and Truckee Above Farad sub-basins were in line with the historical modeled values, the annual volumes for Tahoe were deemed unacceptable. In order to remedy that problem, a multiplicative bias-correction factor was applied to each GCM's Tahoe precipitation and streamflow time series and the factor optimized so that the total Tahoe net inflow volumes over the RiverWare® run period (Oct 31, 1950 to Dec 31, 2005) matched the historical volumes for that period. The optimized factor for each GCM was also applied to the RCP (future) scenarios under the assumption that the bias was the same for those scenarios.

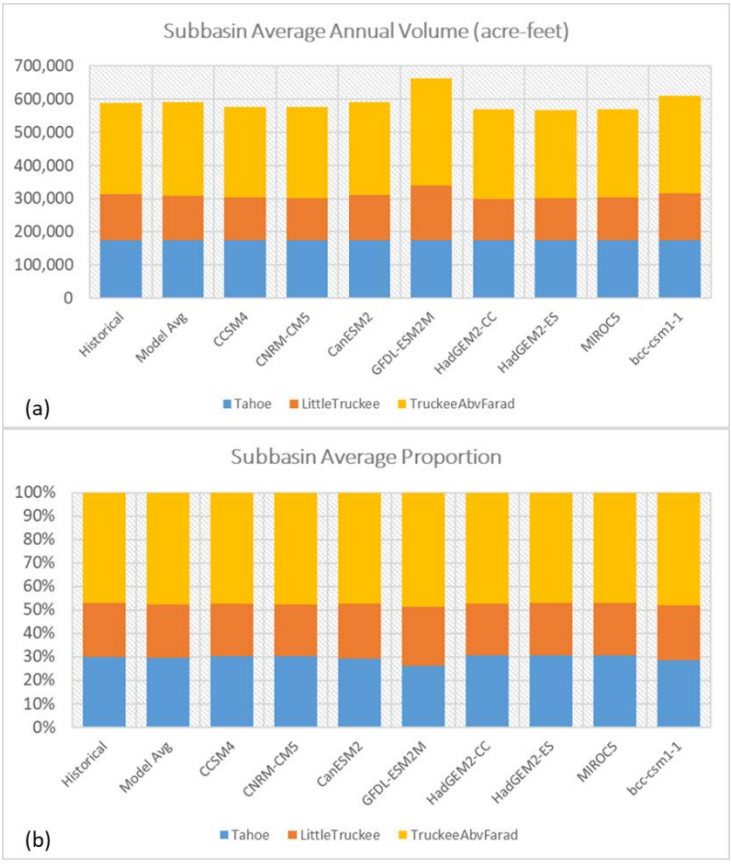

Figure 4. Sub-basin (a) average annual volumes and (b) average annual proportion of total volume after bias correction

Note that the average annual volume for each GCM is not exactly equal to the historical annual average. That discrepancy is due to two factors. First, the optimization was performed based on the total volume and not the annual volumes, and there is a slight amount of shifting of daily volumes based on leap years not being exactly synchronous between the input time series dates and the dates used for the runs in RiverWare® (i.e., a leap year in the input data series is not necessarily counted as a leap year in the RiverWare® run); and second, the annual volumes were calculated based on calendar years, not water years, so the volume for Oct-Dec 1950 is counted as a calendar year when aggregating annually. Nevertheless, the factors bring the annual volumes into what was considered an acceptable margin of discrepancy (<1%) from the historical volumes.

Results

The time series of the minimum, median, and maximum model annual evaporation volumes are shown in Figure 5. The historical period is shown in each figure for comparison, as well as the future period. Observed evaporation is not available for the historical period. From the figure, the modeled median value increases throughout the coming century under both scenarios, more so in the RCP 8.5 scenario than the RCP 4.5 scenario. In the absence of other hydrologic effects of the future scenarios, the increase in evaporation would lead to lower pool elevations and decreased releases for Lake Tahoe; however, the increased evaporation does not occur in isolation, but in conjunction with changes to the lake inflow and precipitation.

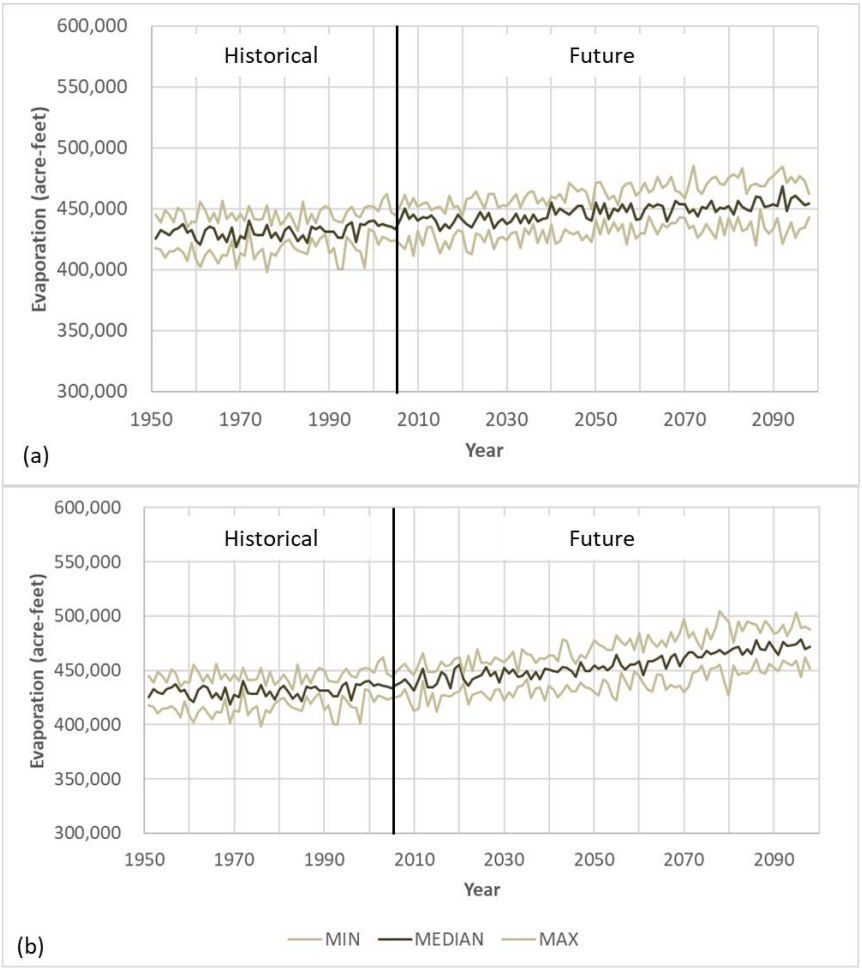

Figure 5. Evaporation time series

The net inflow to the lake contains the combined effects of the climate change scenarios on the hydrologic cycle in the lake watershed. The average annual net inflow to the lake under all three scenarios is presented in Table 1. The model average values for the net inflow under the historical scenario are within approximately 2.5% of the historical values. The individual

models' results under the historical scenario are also relatively consistent, varying between -0.8% and 2.4% difference for the net inflow. However, the average annual values increase substantially under both of the future scenarios, along with greater variability between the models. So, it is clear that the increase in evaporation under the future scenarios is, on average and for the majority of the GCMs, outweighed by increases in inflow and precipitation, albeit with wide variation for the different models.

Table 1. Average annual net inflow (acre-feet) and relative difference from historical observed values

	Historical	**RCP 4.5**	**RCP 8.5**
Observed	175,116		
Model Average	177,502 (1.4%)	214,340 (22.4%)	213,689 (22.0%)
CCSM4	176,772 (0.9%)	201,813 (15.2%)	203,259 (16.1%)
CNRM-CM5	173,791 (-0.8%)	397,013 (126.7%)	379,637 (116.8%)
CanESM2	178,736 (2.1%)	255,411 (45.9%)	277,285 (58.3%)
GFDL-ESM2M	177,288 (1.2%)	194,197 (10.9%)	175,691 (0.3%)
HadGEM2-CC	179,100 (2.3%)	155,702 (-11.1%)	196,670 (12.3%)
HadGEM2-ES	179,378 (2.4%)	164,347 (-6.1%)	199,998 (14.2%)
MIROC5	177,452 (1.3%)	191,329 (9.3%)	141,605 (-19.1%)
bcc-csm1-1	177,497 (1.4%)	154,911 (-11.5%)	135,364 (-22.7%)

Figure 6 contains box and whisker plots depicting the Tahoe pool elevation distributions for the historical, RCP 4.5, and RCP 8.5 scenarios. Distributions for the observed historical and modeled values for each individual GCM are presented in each plot, as well as the distribution for all combined modeled values. The box extents reflect the 20th and 80th percentiles of the values, while the whisker extents reflect the minimum and maximum values. The horizontal line in the plots represents the rim elevation of 6,223 ft MSL. The results for the historical scenario indicate that the models reproduce the middle 60% of the distributions very well, while the minimum and maximum values for some models extend substantially above or below those of the observations. The plots for both the RCP 4.5 and RCP 8.5 scenarios reflect increased variability between the individual GCM results, even with the bias correction that was calculated based on historical period modeling. Those results reflect the varying constructions and interactions within the GCMs, and the varying potential outcomes. The All Models distributions under both future scenarios show greater differences between the minimum and maximum relative to the historical observations, but the 20%-80% ranges are very similar to that of the observations.

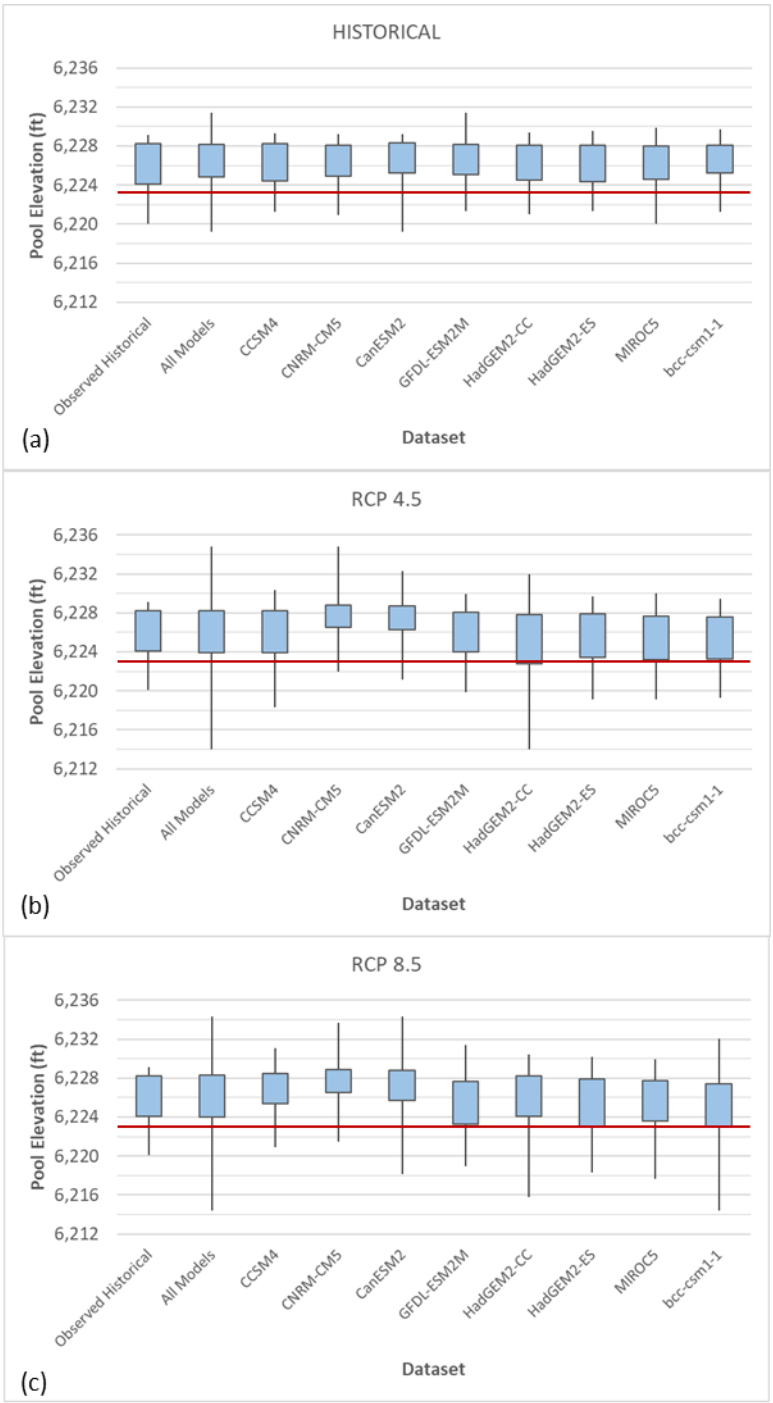

Figure 6. Lake Tahoe pool elevation values with (a) historical input series, (b) RCP 4.5 input series, and (c) RCP 8.5 input series. The red line indicates the natural rim elevation of 6223 ft MSL.

Figure 7 presents box and whisker plots depicting the Tahoe annual outflow volume distributions for the historical, RCP 4.5, and RCP 8.5 scenarios. Distributions for the observed historical and modeled values for each individual GCM are presented in each plot, as well as the distribution for all combined modeled values. The box and whisker extents represent the same quantities as in Figure 6. The historical scenario results indicate that the models reproduce the

middle 60% of the distributions closely, although the individual models exhibit slightly more variation in the 20% and 80% outflow values than they did in the pool elevation distributions. Most, but not all, modeled distributions have a minimum annual outflow volume of 0 acre-feet, indicating that at some point in the run period the pool elevation was below the rim elevation. The All Models distribution shows slightly higher 20% and 80% values than the historical observed values. The results for both the RCP 4.5 and RCP 8.5 scenarios again reflect increased variability between the individual GCM results, with the RCP 8.5 scenario exhibiting a greater increase than the RCP 4.5 scenario. The All Models distributions for both future scenarios show greater minimum-maximum and 20%-80% ranges than the historical observations.

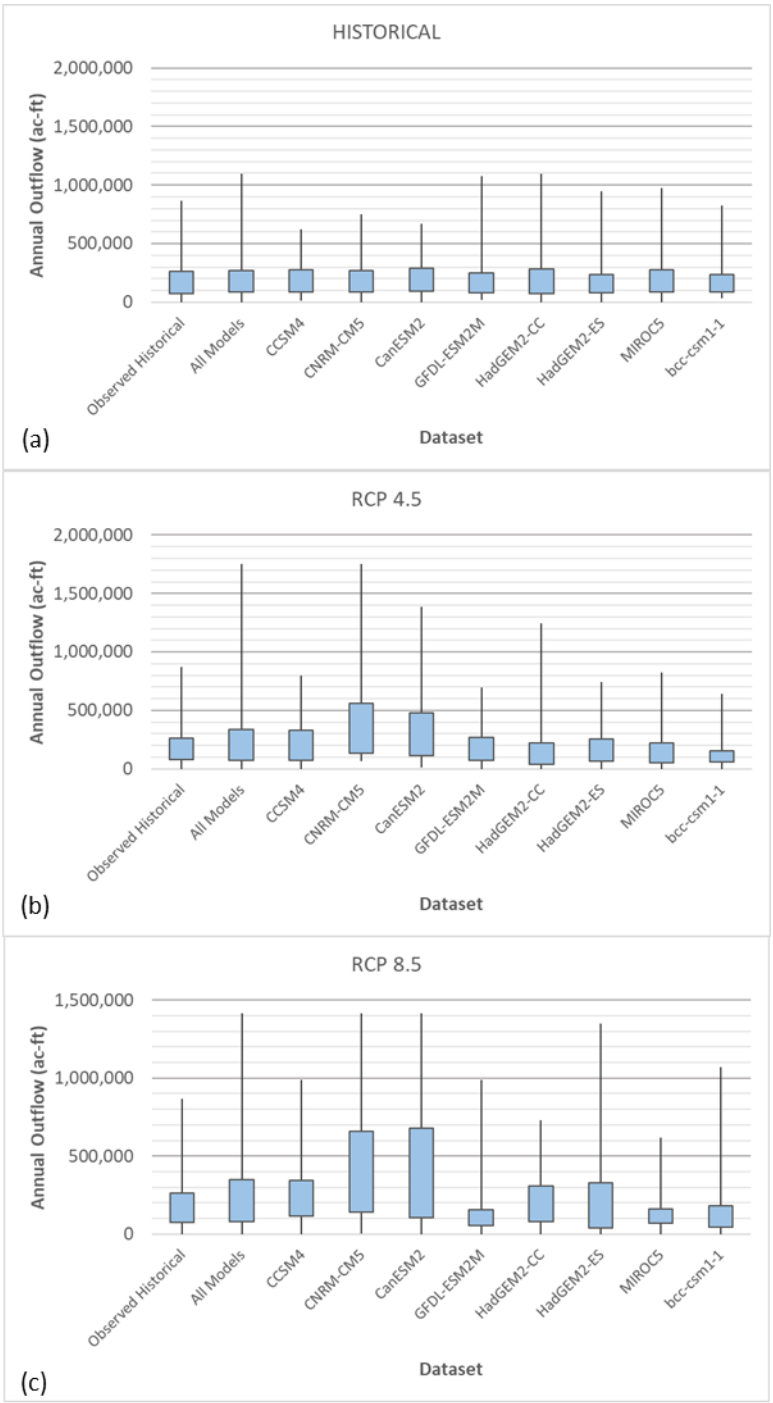

Figure 7. Modeled Lake Tahoe outflow volume distributions with the (a) RCP 4.5 and (b) RCP 8.5 scenarios

Lake Tahoe can only act as a downstream water supply if its pool elevation is greater than the natural rim elevation, 6,223 ft MSL. Therefore, the relative length of time that the pool elevation is below the rim is an important indicator of the lake's water supply viability. The percent of days for which the pool elevation is lower than the rim under each scenario is shown in Table 2. Daily pool elevation readings are only available beginning on October 1, 1957, so the historical

observed and modeled values are based on the time period October 1, 1957 through December 31, 2005. The observed data shows that the daily pool elevation was below the rim for 9.2% of that time period. Under the historical modeled scenarios, the model average was 6.3% of daily values during the time period, with a range of 2.6% (bcc-csm1-1) to 11.6% (HadGEM2-CC). So, the modeled historical periods underestimated the duration of time that the lake was unable to release water downstream. The model average percent days lower than the rim for both the RCP 4.5 (11.8%) and RCP 8.5 (11.7%) scenarios was greater than both the observed historical and modeled historical scenarios. In the RCP 4.5 scenario, all modeled hydrology sets except two (CNRM-CM5 and CanESM2), produced percentages below the rim greater than both the observed and respective modeled historical percentages. Those two hydrology sets produced substantially lower percentages of days below the rim elevation. Under the RCP 8.5 scenario, the percentages of days below the rim for those two models' hydrology increased from the RCP 4.5 scenario but remained lower than the observed and respective modeled historical scenarios. Not all models' RCP 8.5 hydrology produced longer durations below the rim elevation relative to the respective models' RCP 4.5 hydrology sets. Hydrology produced by the CCSM4, HadGEM2-CC, and MIROC5 models led to less time below the rim elevation with the RCP 8.5 scenario than with the RCP 4.5 scenario. This is despite the generally higher temperatures in the RCP 8.5 scenario.

Table 2. Percent of days with pool elevation < 6,223 ft MSL

	Historical*	**RCP 4.5**	**RCP 8.5**
Observed	9.2		
Model Average	6.3	11.8	11.7
CCSM4	6.3	11.9	4.2
CNRM-CM5	5.2	0.5	1.2
CanESM2	8.6	0.6	5.5
GFDL-ESM2M	3.5	9.6	16.6
HadGEM2-CC	11.6	21.7	13.6
HadGEM2-ES	6.6	15.2	19.9
MIROC5	5.7	18.2	13.0
bcc-csm1-1	2.6	16.6	19.3

*Based on USGS daily gage heights from Oct 1, 1957 to Dec 31, 2005, the range of daily observations available on the TROA Information System website

The lake's storage and pool elevation are also dependent on the lake's outflow. The average annual outflow is shown in Table 3, along with the relative difference from the historical observed value. The model average value for the outflow under the historical scenario is within 3% of the historical values. The individual models' results under the historical scenario are also relatively consistent, varying between -2.8% and 1.5% difference for the outflow. However, the average annual values increase substantially under both of the future scenarios, along with greater variability in the individual models' difference from the historical value. While the

annual average values for the outflow provides information regarding the general trends over the modeling periods, the variability is also important to the lake's function as a water supply.

Table 3. Average annual outflow (acre-feet) and relative difference from historical observed value

	Historical	RCP 4.5	RCP 8.5
Observed	184,572		
Model Average	184,451 (-0.1%)	219,293 (18.8%)	217,822 (18.0%)
CCSM4	187,331 (1.5%)	204,801 (11.0%)	203,544 (10.3%)
CNRM-CM5	185,886 (0.7%)	399,007 (116.2%)	381,423 (106.7%)
CanESM2	185,963 (0.8%)	256,036 (38.7%)	276,830 (50.0%)
GFDL-ESM2M	182,809 (-1.0%)	199,359 (8.0%)	182,569 (-1.1%)
HadGEM2-CC	179,431 (-2.8%)	160,196 (-13.2%)	201,917 (9.4%)
HadGEM2-ES	186,691 (1.1%)	178,200 (-3.5%)	210,971 (14.3%)
MIROC5	182,451 (-1.1%)	196,497 (6.5%)	145,557 (-21.1%)
bcc-csm1-1	185,046 (0.3%)	160,246 (-13.2%)	139,765 (-24.3%)

Table 4 provides some illumination into the distribution of annual volumes relative to the observed historical annual average. For each scenario presented, the table indicates the percentage of years with annual volume greater than and less than the historical average, as well as the average volume for those two categories of years. The RCP 4.5 and RCP 8.5 values presented are the averaged values over all individual GCM results. The percentage of years in each scenario greater than and less than the historical average is consistent across all three data sets at ~65% greater than the average and ~35% less than the average, as is the average volume for years that fall below that volume. However, the average volume during the years with a volume greater than the historical average volume are substantially larger for the future climate scenarios than for the historical observed period. So, the wet years are greater in magnitude under the climate change scenarios, while the relatively dry years are roughly the same magnitude.

Table 4. Average annual volumes (acre-feet) and occurrences relative to observed historical annual average volume

	Historical Observed	RCP 4.5	RCP 8.5
Years < Historical Average	66%	66%	65%
Avg Volume for Years < Historical Average	96,273	95,237	98,572
Years > Historical Average	34%	34%	35%
Avg Volume for Years > Historical Average	352,912	419,079	447,218

Conclusions

1. A large degree of variability and uncertainty exists in both the hydrologic variables used as input to the Planning Model, as well as the Lake Tahoe conditions that result from those inputs. As a result, it is not possible to make a definitive statement regarding the direction or magnitude of changes in those conditions from the historical observations.
2. Modeling results from the RCP scenarios indicate that the Lake Tahoe pool elevation will remain below the rim elevation for a greater proportion of time in the future than it has historically, requiring users in the Truckee Basin to employ other water supply sources more frequently.
3. The average net inflow to the lake may increase, even under a generally warmer climate. If the pool elevation is greater than the rim elevation when high net inflows occur, increased outflows may also occur in order to maintain the pool elevation below its maximum.
4. Outflow from Lake Tahoe under the RCP scenarios is likely to exhibit greater variability than historical flows, leading to the need to prepare for high flows as well as more frequent periods requiring the use of alternate water supply sources.
5. The combination of Lake Tahoe remaining below its rim more frequently and greater outflow variability means that water management in the Truckee River watershed is likely to become more challenging in the future.

References

Huntington, J.L. and *D. McEvoy. (2011). Climatological Estimates of Open Water Evaporation from Selected Truckee and Carson River Basin Water Bodies, California and Nevada.Desert Research Institute Publication No. 41254.

Rajagopal, S., Huntington, J. L., Niswonger, R., Pohll, G. M., Gardner, M. A., Morton, C. G., Zhang, Y., Reeves, D. M. (2015). Integrated Surface and Groundwater Modeling of Martis Valley, California, for Assessment of Potential Climate Change Impacts on Basin Scale Water Resources, 54, U.S. Bureau of Reclamation, DRI Report No. 41261

US Bureau of Reclamation (2015). Truckee Basin Study Basin Study Report, 310p.

van Vuuren, D.P., Edmonds, J., Kainuma, M., Riahi, K., Thomson, A., Hibbard, K., Hurtt, G.C., Kram, T., Krey, V., Lamarque, J-F., Masui, T., Meinshausen, M., Nakicenovic, N., Smith, S. J., Rose, S.K. (2011). The representative concentration pathways: an overview. Climatic Change, 109, 5-31. Doi:10.1007/s10584-011-0148-z

Physical Sediment Load Measurements

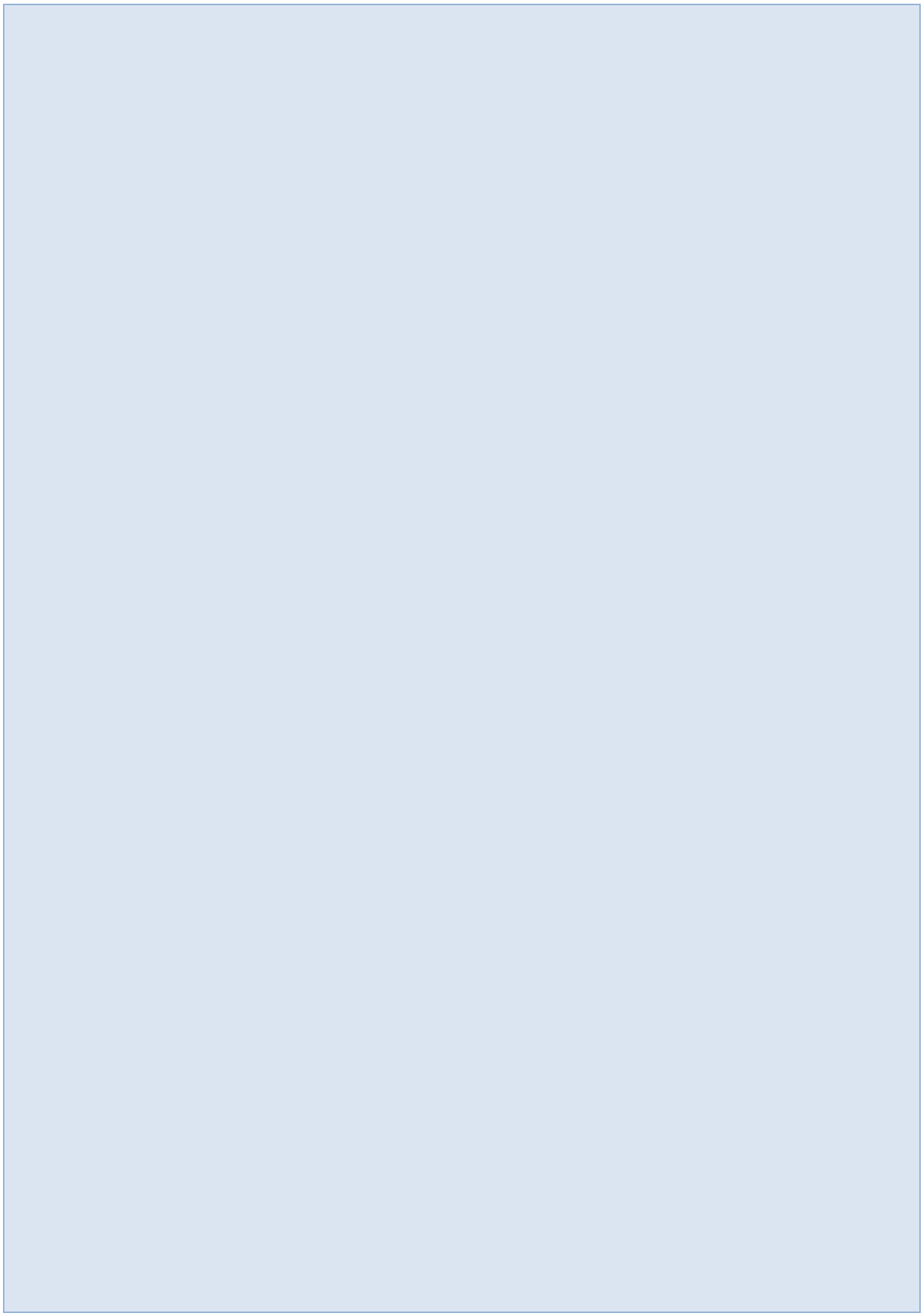

Initial analysis of suspended sediment concentrations during flash floods on the Arroyo de los Piños, NM

Dr. Jonathan B. Laronne, Ben Gurion University of the Negev, Beer Sheva, Israel, john@bgu.ac.il
Kyle Stark, New Mexico Institute of Mining and Technology, Socorro, NM, kyle.stark@student.nmt.edu
Dr. Daniel Cadol, New Mexico Institute of Mining and Technology, Socorro, NM, daniel.cadol@nmt.edu
David Varyu, United States Bureau of Reclamation, Denver, CO, dvaryu@usbr.gov
Madeline Richards, New Mexico Institute of Mining and Technology, Socorro, NM madeline.richards@student.nmt.edu

Abstract

The newly operational Arroyo de los Piños monitoring site includes contemporaneous and automatic sampling of suspended sediment at two depths of flow, at which turbidity is also monitored. Several vertical depth integrated suspended sediment samples were also collected manually. Suspended sediment concentration in the sand-rich monitored catchment is high by global standards due to lack of cover of vegetation, but less than in some semiarid areas rich in loess soils. As the grain size distribution of the suspended sediment is mainly comprised of almost equal amounts of fine sand and silt+clay, there appears to be slight variation in the concentration with depth. This reduces the uncertainty when calculating the average sectional concentration. These suspended sediment data, together with concurrent bedload data (presented elsewhere), are a prerequisite to understand the dynamics of ephemeral flash flood washes and their impact on receiving trunk streams, such as the mid-Rio Grande.

Introduction

Studies of suspended sediment transport in ephemeral channels in arid environments are much less common than in temperate climates, but as sampling of flood water for suspended sediment is not intrusive nor as dangerous as is bedload sampling, the literature on suspended sediment in flashfloods has received more attention than that on bedload. On larger rivers such as the Colorado, Yampa, and Green Rivers accurate acoustic Doppler current profiler (ADCP) measurements of suspended sediment concentration and size can be made when not in flood (Topping et al., 2015). However this acoustic method is inapplicable to sand concentrations above 10,000 mg/L or above 30,000 mg/L for silt and clay (Topping, pers. comm., 2015). However, flash floods in deserts often transport much higher concentrations (Table 2 in Alexandrov et al., 2003) and, moreover, ADCPs cannot be used in flood due to the difficulty in stabilizing them and due to the high cost in the event of damage or loss. Densitometric measurement of suspended sediment concentration is relevant for very high concentrations (Petrovic et al., 2017), but its accuracy decreases as concentration decreases.

Data on both suspended and bedload yields in drylands for a given river are scarce (e.g., Reid & Frostick, 1987). In semiarid areas most of the yield is transported in suspension, as much as 90% (Alexandrov et al., 2009). In arid and hyper-arid areas the ratio of suspended/bedload

yield is lower (Schick, 1977; Alexandrov et al., 2009; Laronne & Wilhelm, 2001). The lengthiest database on suspended sediment concentration (SSC) has been undertaken in the American Southwest at Walnut Gulch (Nichols et al., 2008). Although convective rainfall is common there, median concentrations are most often lower than 2,000 mg/l due to the local vegetation cover at Walnut Gulch (Nearing et al., 2007) - much lower than common in most other studied channels in drylands (Sharma et al., 1984; Lekach & Schick, 1982; Schick & Lekach, 1993; Alexandrov et al., 2003; Reid et al., 1998; Alexandrov et al., 2008). Understanding how ephemeral channels transport sediment is important from a global perspective because of the large number of people affected due to flooding, channel instability and the need for water conveyance and supply. Studying the transport of suspended sediments in drylands allows understanding how and where fines are deposited on banks and floodplains; in upland semi-alluvial rivers it explains the abrasion of bedrock. Flow in these channels can be rare, but sediment production is high (Langbein & Schumm, 1958) promoting rapid reservoir sedimentation (Laronne & Wilhelm, 2001; Tolouie et al., 1993).

Variation of SSC with water discharge (Q) is often hysteretic (e.g., Williams, 1989; Ellis, 2004). As concentrations are typically higher by one order of magnitude relative to those in temperate climates, deviations about a mean concentration are large. The reasons for the wide scatter in the SSC-Q relationships include seasonal depletion of erodible material (Vachtman et al., 2013) and downstream translation of sediment laden water (Alexandrov, 2003). Another important mechanism causing large variations in SSC and a variety of hysteretic responses is the location and direction of motion of discrete convective high intensity storms, particularly evident where vegetation cover is sparse (Alexandrov et al., 2007).

To examine these questions, a new monitoring site to study sediment dynamics and frequency in the American Southwest was planned and deployed on the Arroyo de los Piños (Varyu, 2019). Here, we present initial findings related to suspended sediment concentration in flash floods in 2018. Results on basin-wide runoff (Richards, et al., 2019), monitoring of bedload flux directly (Cadol, et al., 2019), seismically (Dietz et al., 2019) and acoustically by pipe microphones (Stark et al., 2019) and hydrophones (Marineau et al., 2019) are presented elsewhere.

Study Area

The Rio Grande is a perennial channel in the center of the largest semi-arid region in the United States. A crucial part of life in the Southwest U.S., the Rio Grande and other mainstem perennial rivers allow for development in this region. Constant maintenance along such rivers is required to ensure that communities have consistent access to water. These rivers are often modeled to predict changes and allow for effective management. The largest source of uncertainty in modeling these rivers is associated with the sediment influx from ephemeral tributaries.

As a tributary of the Rio Grande, the Piños is typical of many fluvial systems in the southwest. Flash floods carry sediment directly into the Rio Grande causing a localized influx at the confluence. Sediment is easily transported by the Piños not merely due to channel gradient and particle size, but also due to the lack of armoring. Runoff production is highest where intense monsoonal storms cover areas of thin soils and sparse hillslope vegetation in the basin. The geologic setting varies throughout the basin (Cather & Colpitts, 2005). Near the Rio Grande, the channel is anastomosing as it crosses Pliocene and Pleistocene ancestral floodplain and alluvial fan deposits. Further upstream the channels are confined through canyons and valleys eroded

into the more cohesive early Paleozoic sandstones, limestones, and shales. The Abo formation consists of interbedded mudstone, shale, and sandstone; the Bursum formation consists of interbedded dolomitic limestone and sandstone; and the Atrasado Formation of the Madera Group consists of arkosic sandstone and mudstone (Cather & Colpitts, 2005).

The Piños is located at the northern extent of the Chihuahuan Desert. This desert is semi-arid; it has a mild continental climate characterized by low annual precipitation (237 mm), year-round sunshine, and relatively large annual, diurnal temperature changes (DRI, 2013). July and August are the rainiest months; 35% of annual precipitation falls during these 62 days. Summer monsoonal rains occur during brief, but intense storms. Flash flooding occurs locally in these areas because of the intensity of rainfall, sparse vegetation and thin soils.

Prior to completion of the Pinos monitoring facility, floods were monitored using manual sampling techniques (Stark, 2018). During this time, thirty-five suspended sediment samples were collected using a DH-48 sampler. These samples were collected to characterize the nature and size of flood events. The average SSC of these samples was 30,400 mg/L. Analysis of these samples revealed a significant (>50%) fine-sand fraction transported as suspended sediment. SSC was in the range 5,000 - 75,000 mg/L; water discharge predicted suspended sediment concentration only to some extent ($r^2 = 0.43$). During stage rise SSC was generally high and the SSC-Q relationship was scattered, whereas during recession the relation was better defined ($r^2 = 0.72$).

Methods

The sediment monitoring system at the Arroyo de los Piños includes seven different devices and sensors to monitor bedload (detailed in Stark, et al. 2019 and Cadol, et al. 2019). SSC is monitored directly using two bank-located automated pumping water samplers (ISCO 3700). These are connected to telemetering data loggers (Ayyeka), and are activated during storm events by liquid level actuators. The ISCOs begin sampling simultaneously when water level reaches the height at which both of the actuators are activated (Figure 1a). Two high-end turbidity sensors (Confab 950) are actuated by the data logger when water level rises to the level of the vented pressure sensors (Seba DS-22), also located within the stilling well (Figure 1b).

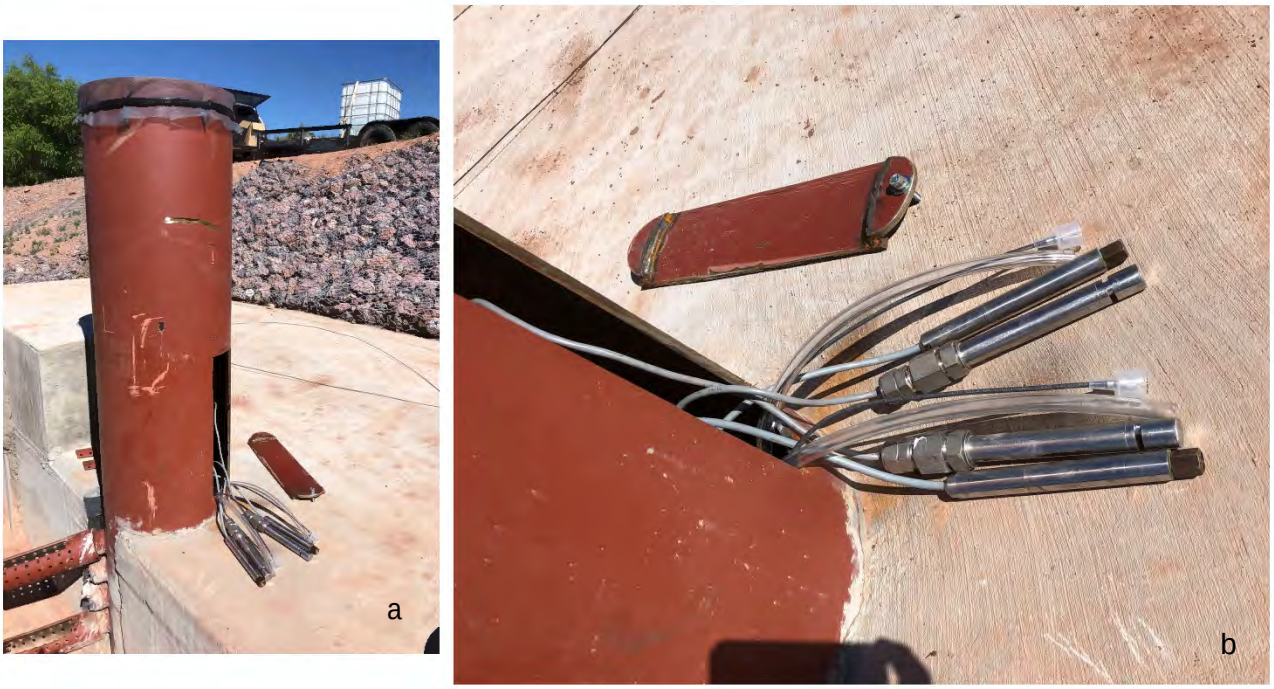

Figure 1: *Stilling well with two perforated pipes attached; their vertical location is changeable. Suspended sediment monitoring includes a pair of the following instruments: intake for water sampler, sampler actuator, turbidity sensor and vented pressure transducer to actuate turbidity monitoring.*

As each intake/turbidity pair is located at different heights (hitherto at 6 and 43 cm above the cement bed), samples are acquired simultaneously only when water depth surpasses the height of the upper pair of sensors; water samples are obtained only from the lower pair at lower depths. As the grain size distribution (GSD) of suspended sediments at the Piños and similar washes contains not merely silt + clay, but also sand, sampling and turbidity measurements at a single depth was assumed to be unrepresentative of the entire depth of flow. Therefore, the advantage of this arrangement is that water samples are obtained simultaneously at two depths, allowing to calculate the variation of SSC with depth (Dey, 2014; Chapter 6), as well as the GSD of suspended sediment at two depths of flow. Sediment size is one of the most important variables affecting the calibration of turbidity with SSC; other factors include particle shape, mineralogic content, color and amount of organic matter in the water column (Gippel, 1995).

Flood water was also sampled manually for SSC when conditions allowed. We used a hand-held DH48 to obtain vertically integrated suspended sediment samples with a 6.35 mm diameter intake to ensure that coarse sand grains in suspension efficiently enter the sampler. The comparison of the grain size distributions of suspended sediment samples and of bedload will eventually allow determination of their variability with water discharge and reach scale shear stress.

The high-end Confab 950 turbidity sensors were calibrated in the lab with respect to carefully sampled sediment from Arroyo de los Piños bank deposits. These contained 39% silt+clay, 58% sand in the range 0.063-0.5 mm; the rest coarse sand. Known volumes of water were added to a concentrated sediment-water mixture. Although lab calibration differs substantially from dynamic (field-based) calibration, the initial results gave us confidence that these sensors will operate well under field conditions.

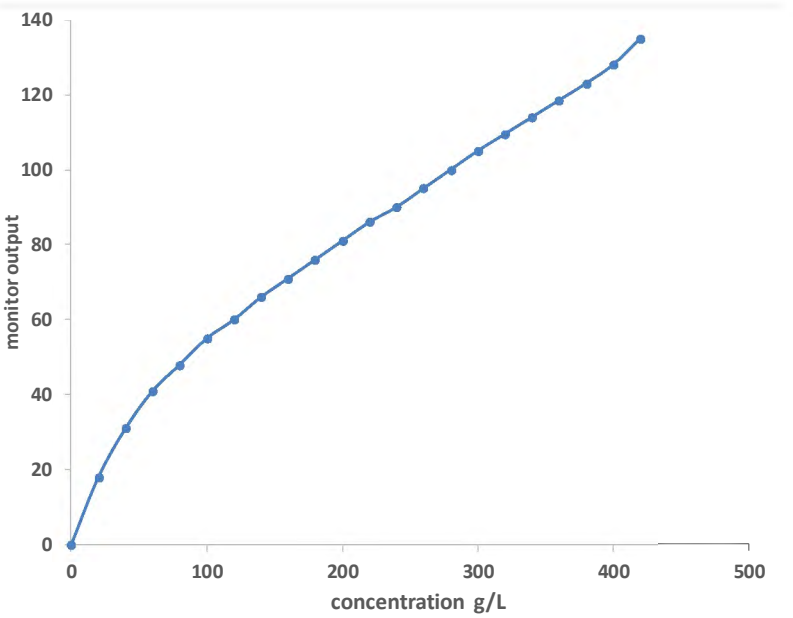

Figure 2: Laboratory calibration of turbidometry data *vs* Arroyo de los Piños sediment concentration.

Results

Five flood events were recorded at the Arroyo de los Piños sediment research station during 2018 (Table 1). Water depth is measured manually and simultaneously with manual suspended sediment samples as well as automatically using pressure transducers. Maximum depth ranged from 15 cm to 161 cm above the fixed cross-stream sill. To date, 60 samples were collected using the automated sampler/sensor tandem pair during the 2018 monsoon season. However, 55 of these were collected from the lower sampler, only 5 from the upper sampler. Additionally, 23 manual samples were collected from a variety of locations along the channel cross-section.

Table 1: Characteristics of the four floods recorded to date at the Piños sediment monitoring facility. They include very shallow events but also large and a very high magnitude flashflood. * denotes values for manual samples.

Flood	*Duration (hour)*	*Maximum Water Depth (cm)*	*Average SSC (mg/L)*	*Maximum SSC (mg/L)*
July 16th	3.00	60	32,300	104,000
July 26th	5.50	161	no samples	no samples
August 9th	1.75	16	14,400	29,600
August 24th	2.75	32	30,500	90,100
September 1st	5.50 (two storms)	15	15,000 20,100*	18,600 34,500*

The average concentration of all samples obtained during the first year of flash floods was 26,200 mg/L. This value must be qualified as no samples were obtained from the very large flashflood that occurred on July 26. The ISCO samplers failed to be actuated due to operator

error – the actuator was aligned vertically, causing air entrapment, so the rise of water level was not sensed.

The GSD of 22 suspended sediment samples sieved hitherto was analyzed by GRADISTAT (Blott & Pye, 2001) and is summarized in Table 2 and shown in Figure 3. Silts and clays represent 40 percent of the suspended sediment. Sediment size fractions 0.063-0.0.125, 0.125-0.25 and 0.25-0.50 mm contain 25, 19 and 10 percent respectively. Only 5% of the suspended sediments are medium and coarse sand (> 0.5 mm). This GSD implies that about two thirds of the suspension is expected to be sufficiently fine-grained to be swept by turbulent eddies, such that the SSC should not vary with depth for that fraction.

Table 2: Average grain size characteristics of selected suspended sediment samples.

	arithmetic	description
	μm	
mean	130	very coarse silt
sorting	171	very poorly sorted
skewness	4.1	very fine skewed
kurtosis	31.5	mesokurtic

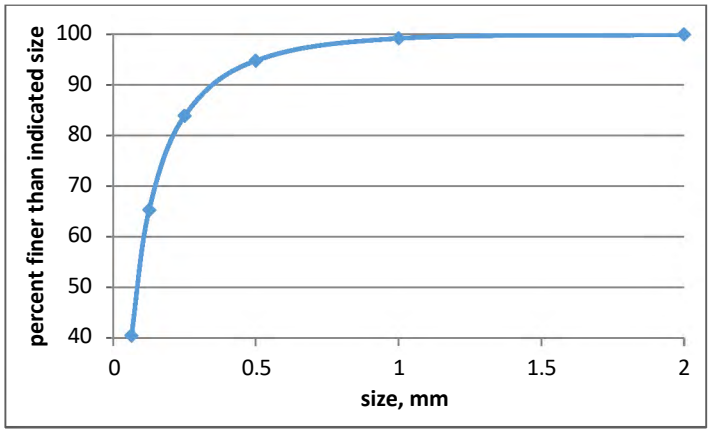

Figure 3: Grain size distribution of selected suspended sediment samples, 2018 floods.

During all flash flood events SSC appears to vary linearly with water depth; it decreased during recessions for all the monitored flow events during 2018 (Figure 4). A similar trend

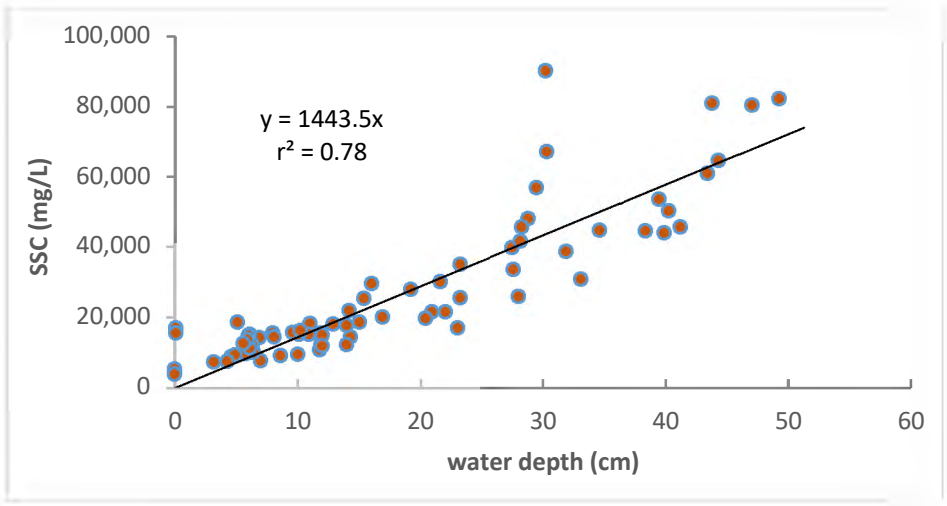

Figure 4. Variation of SSC with water depth for samples obtained manually and automatically during 2018 ; most of the data are from the recession.

characterizes the (35) manually obtained samples during the 2017 monsoon season. Almost no data are available before occurrence of peak flow because stage rise is very fast for the largest floods.

Turbidity was monitored during all the 2018 flash flood events. Throughout most of the events water depth was insufficient to cover the upper turbidity sensor, therefore we present the calibration for the lower sensor (Figure 5). The linear increase in turbidity with increase in SSC is not self-evident, as higher concentrations occurring with higher water depths (Figure 4) are expected to contain larger fractions of coarser sand particles. Outliers such as in Figure 5 may be explained after the GSD of all samples is completed. During the July 16, 2018 flood event samples were contemporaneously obtained from the lower (10 cm) and upper (45 cm above the bed) sampling inlets (Figure 6), demonstrating that SSC did not vary with depth.

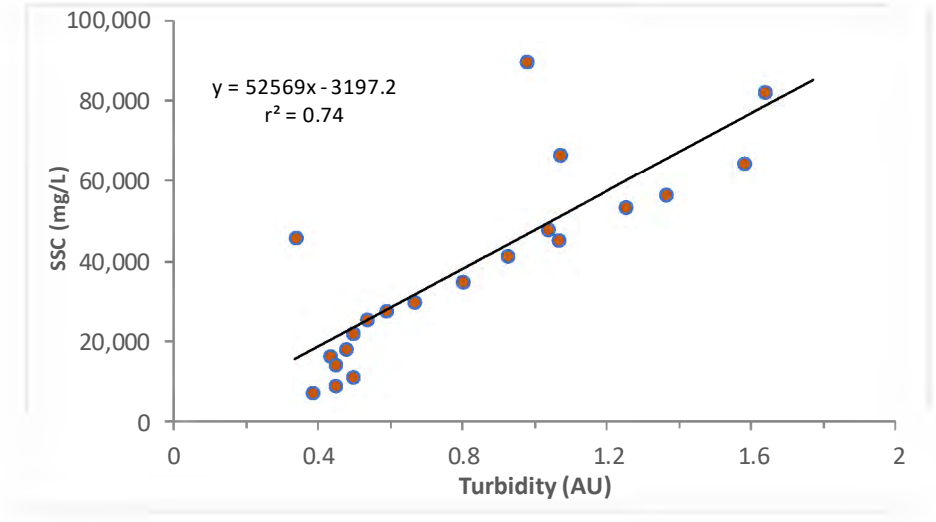

Figure 5. Calibration of suspended sediment concentration vs turbidity based on all samples where turbidity and SSC were simultaneously collected.

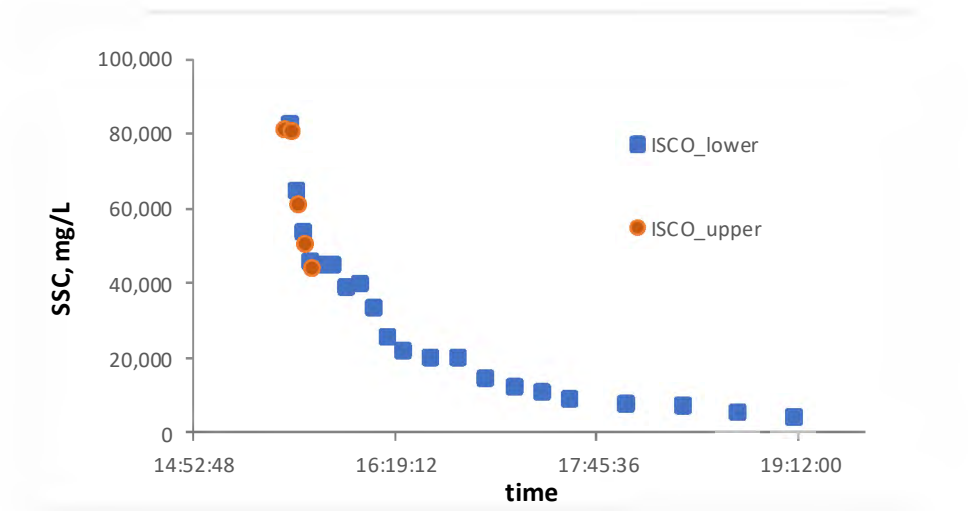

Figure 6. Stage hydrograph and sedigraph for the upper and the lower inlet locations during the July 16 flood event.

Because SSC does not appear to vary considerably with depth based on the comparison of the samples from two heights, we also compared the vertically integrated SSC obtained from manual sampling across the entire cross section with the SSC obtained contemporaneously by

the lower automated sampler (Figure 7). As the slope of the correlation is 0.56, it embodies the fact that as water depth increases (and SSC increases - Fig. 4), so does the near-bed concentration increase relative to the average concentration. If this relationship holds also for higher depths of flow, near-bed samples obtained at the stilling well will be used to determine the average SSC in the water column. We have yet to increase sampling to several locations in the cross section before applying such a relationship to entire flash-flood hydrographs.

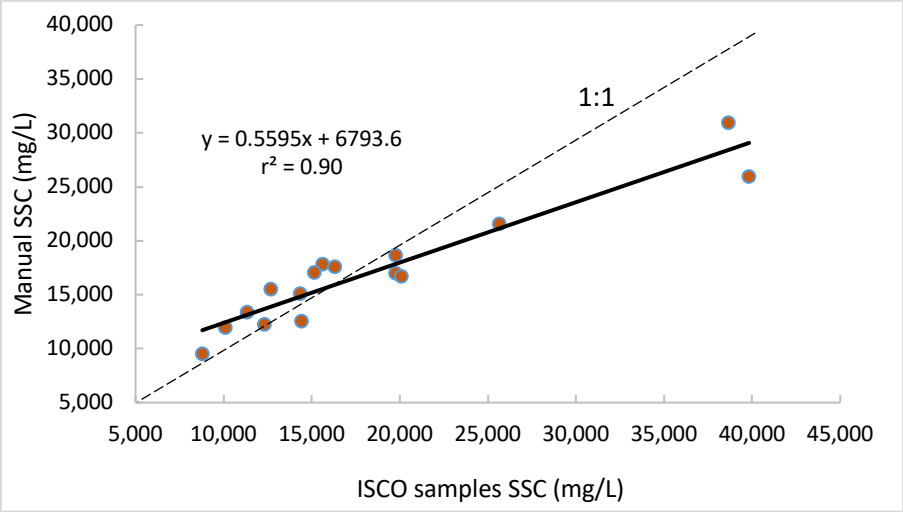

Figure 7. Comparison between depth-integrated SSC obtained manually across the entire cross section and SSC from the automated sampler.

Discussion

The results presented hitherto are preliminary, as they are based on analyses of suspended-related data obtained during the first year of operation of the Arroyo de los Piños sediment monitoring station. As expected, suspended sediment concentrations are on average higher than in temperate regions. However, it was surprising that turbidity in this sand-rich setting can be calibrated against SSC within relatively narrow, well-defined limits. This is based not merely on lab calibration, but also on the similarity of SSC from the few contemporaneously obtained automated samples, signaling that a large portion of the solids carried in suspension are fine grained, as shown by the GSDs comprising silt+clay and fine sand (Figure 3).

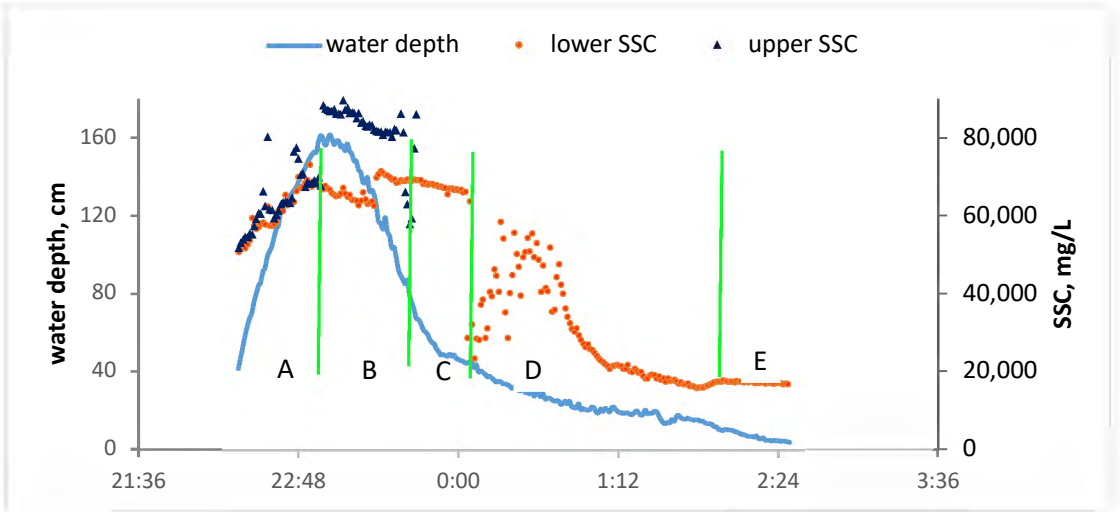

Figure 8. Turbidity-calibrated suspended sediment concentration at the upper and lower monitoring heights during the large July 26 flashflood. See text for explanation of symbols.

The similarity in the concentration of suspended solids at two depths is also demonstrated by the trace of turbidity during the large flood of July 26, 2018. While no suspended sediment samples were collected during the event, turbidity was recorded at both vertical positions. We used the lab-derived SSC-turbidity calibration to derive continuous trends of SSC at two depths (Figure 8). The record of SSC is incomplete; during stage rise both were similar (Figure 8A) until the high SSCs seem to have affected the response of the lower turbidity sensor, as turbidity is expected to be similar or lower in the upper sensor (Figure 8B). The response of the lower sensor later returned to full functionality while the upper sensor ceased to respond when water depth was 80 cm (Figure 8C). This interpretation may be debatable and requires further analyses, among others the extent, if any, of observable sensor clogging. The lower sensor gradually returned to full functionality (Figure 8D) until water depth decreased below its level (Figure 8E). During the rising limb both sensors show comparable concentrations, similar to the results observed in the collected suspended sediment samples. This suggests that, at least for the rising limb of the July 26 event, SSC did not vary with depth.

Conclusions

The average concentration of suspended sediments based on samples obtained in the 2018 floods was 2.6 percent. High by global standards (Figure 9), as expected this is lower than

Figure 9. Suspended sediment samples (red-capped pint bottles, foreground) manually obtained during the June 10, 2017 flash flood. The color of the water indicates the relatively high SSC. View towards the left bank before deployment of the existing monitoring station.

in semiarid settings covered by loessial soils (Alexandrov et al., 2009), but higher than in other nearby sand-rich semiarid areas environments such as Walnut Gulch, where concentrations measured by pump samplers were in the range 0.2-0.3% and o.o6% at the larger channel monitored by a weir (Nearing et al., 2007). The ratio of bedload/suspended load in this setting will be determined when additional data are available. Some flood protection agencies in the southwest assume that suspended sediment concentration is as much as one order of magnitude higher, thereby constructing very expensive flood protection structures to capture the sediment. Our results may be useful to allow planning smaller sediment accumulation sites with relevant lower costs.

Almost half of the suspended sediment transported in flash floods by the Arroyo de los Piños are silts and clays, the rest fine to medium sand. Sand coarser than 0.5 mm is seldom suspended, indicating that this fraction moves mainly by saltation and should be represented in large amounts within the bedload sampler, as it has recently been shown to be (Stark et al. 2019; Cadol et al., 2019). Further sampling will determine whether this clear differentiation occurs at 0.5 mm, or whether it widens according to hydrodynamic conditions.

The strong correlation found between turbidity and suspended sediment concentration indicates that this continuous monitoring method may be used throughout other ephemeral washes in the Southwest.

References

Alexandrov, Y., Laronne, J.B. and Reid, I., 2003. Suspended sediment concentration and its variation with water discharge in a dryland ephemeral channel, northern Negev, Israel. *Journal of Arid Environments*, 53(1), pp 73-84.

Alexandrov, Y., Laronne, J.B. and Reid, I., 2007. Intra-event and inter-seasonal behaviour of suspended sediment in flash floods of the semi-arid northern Negev, Israel. *Geomorphology*, 85, 85-97. doi:10.1016/j.geomorph.2006.03.013.

Alexandrov Y., Balaban, N., Bergman, N., Chocron, M., Krispil, S., Laronne, J.B., Powell, D.M.,

Reid, I. and Wener-Frank, I., 2008. Differentiated suspended sediment transport in headwater basins of the Besor catchment, northern Negev. *Israel Journal of Earth Sciences*, 57, 177-188. doi: 10.1560/IJES.57.3–4.177.

Alexandrov, Y., Cohen, H., Laronne, J.B. and Reid, I., 2009. Total water-borne material losses from a semi-arid drainage basin: a 15-year study of the dynamics of suspended, dissolved and bed loads. *Water Resources Research*, 45, W08408, doi:10.1029/2008WR007314.

Blott, S. J. & Pye, K., 2001. GRADISTAT: A grain size distribution and statistics package for the anlaysis of unconsolidated sediments. *Earth Surf. Process. Landforms* 26, 1237–1248. DOI: 10.1002/esp.261

Cadol, D., Stark, K., Laronne, J.B., Varyu, D. & Richards, M., 2019. Bedload flux and characteristics from flash floods in the Arroyo de los Piños, NM – initial results. SedHyd2019, Federal Interagency Sedimentation and Hydrologic Modeling Conference. June 2019, Reno NV.

Cather, S. M., & Colpitts, R. M. (2005). Geologic Map of the Loma de las Cañas Quadrangle, Socorro County, New Mexico. Socorro, New Mexico.

Dey, S., *Fluvial Hydrodynamics - Hyrodynamic and Sediment Transport Phenomena*. Springer

Dietz, M., Gimbert, F., Turowski, J., Stark, K., Cadol, D. & J.B. Laronne, 2019. The seismic view on sediment laden ephemeral flows – robust inversion of ground motion data for fluid and bedload dynamics in the Arroyo de los Piños. SedHyd2019, Federal Interagency Sedimentation and Hydrologic Modeling Conference. June 2019, Reno NV.

DRI. (2013). Socorro Monthly Climate Summary. Retrieved from https://wrcc.dri.edu/cgi-bin/cliMAIN.pl?nmsoco

Ellis, L.A. 2004. *The morphological representation of channel-forming flow in arroyos*. Unpublished PhD Thesis, University of Nottingham, UK. http://eprints.nottingham.ac.uk/id/eprint/13736

Gippel, C. J., 1995. Potential of turbidity monitoring for measuring the transport of suspended solids in streams. *Hydrological Processes*, 9, 83-97.

Langbein, W. B., & Schumm, S. A. (1958). Yield of sediment in relation to mean annual precipitation. *Transactions, American Geophysical Union*, 39(6), 1076. https://doi.org/10.1029/TR039i006p01076

Laronne, J. B., & Wilhelm, R. (2001). Shifting stage-volume curves: predicting event sedimentation rate based on reservoir stratigraphy. in: *Applying Geomorphology to Environmental Management* (pp. 33–54). Water Resources Publ.

Lekach, J. & Schick, A.P., 1982. Suspended sediments in desert floods in small catchments. I*srael Journal of Earth Science*, 31: 144–156.

Marineau, M.,Wright, S., Gaeuman, D., Curran, C., Stark, K., 2019. Overview of Four Recent Acoustic Bedload Monitoring Field Experiments Using Hydrophones. SedHyd2019, Federal Interagency Sedimentation and Hydrologic Modeling Conference. June 2019, Reno NV.

Nearing, M. A., Nichols, M.H., Stone, J.J., Renard, K.G. & Simanton, J.R., 2007. Sediment yields from unit-source semiarid watersheds at Walnut Gulch. *Water Resources Research*, 43, W06426, doi:10.1029/2006WR005692.

Nichols, M. H., Stone, J.J. & Nearing, M.A., 2008. Sediment database, Walnut Gulch Experimental Watershed, Arizona, United States. *Water Resources Research*, 44, W05S06, doi:10.1029/2006WR005682.

Petrovic, D., Marescaux, A., Vanderborght, J.-P. & Verbanck, M.A. (2017). Densitometric probe based on non-differential pressure: A monitoring technique for high suspended sediment concnetrations. pp 1282-1288 in S. Wieprecht, S. Haun, K. Weber, M. Noak & K. Terheiden (Eds.) *River Sedimentation*. Taylor & Francis.

Reid, I. & Frostick, L.E, 1987. Flow dynamics and suspended sediment properties in arid zone

flash floods. *Hydrological Processes,* 1, 239-252.
Reid, I., Powell, D.M. & Laronne, J.B. 1998. Flood flows, sediment fluxes and reservoir sedimentation in upland desert rivers. pp. 377-386 in I. Reid, H. Wheater and P. Johnson (eds). *Hydrology in a Changing Environment*. John Wiley and Sons, Chichester.
Richards, M., Cadol, D., Laronne, J.B., Varyu, D., Aubuchon, J.S. & Brown, S., 2019. Rainfall-runoff relationships complementing previous sediment transport studies at the Arroyo de los Piños, Socorro New Mexico. SedHyd2019, Federal Interagency Sedimentation and Hydrologic Modeling Conference. June 2019, Reno NV.
Schick, A.P., 1977. A tentative budget for an extremely arid waterdshed in the southern Negev. p.139-163 in D. Doehring (ed.): *Geomorphology in Arid Regions*. Publications in Geomorphology.
Schick, A.P. & Lekach, J., 1993. An evaluation of two ten-year sediment budgets, Nahal Yael, Israel. *Physical Geography*, 14/3: 225–238.
Sharma, K.D., Vangani, N.S. & Choudhari, J.S. (1984). Sediment transport characteristics of desert streams in India. *Journal of Hydrology,* 67: 261–272.
Stark, K., Cadol, D., Laronne, J.B., Varyu, D., Halfi, E., Richards, M., 2019. Initial Calibration of Acoustic Pipe Microphone Sensors to Monitor Bedload During Flash Floods in the Arroyo de los Piños, NM., SedHyd2019, Federal Interagency Sedimentation and Hydrologic Modeling Conference. June 2019, Reno NV.
Stark., K., 2018. *A Two-Year Study of Flash Flood Characteristics in New Mexican and Israeli Ephemeral Channels.* Unpublished M.Sc. thesis, Dept. Earth & Environmental Sciences, New Mexico Institute of Mining & Technology, 52 pp.
Tolouie, E., West, J., & Billam, J., 1993. Sedimentation and desiltation in the Sefid-Rud Reservoir, Iran. In J. McManus & R. W. Duck (eds): *Geomorphology and Sedimentology of Lakes and Reservoirs* (pp. 125–138). Wiley.
Topping, D. J., Wright, S.A., Griffiths, R.E. & Dean, D. J., 2015. Physically based method for measuring suspended-sediment concentration and grain size using multi-frequency arrays of single-frequency acoustic-Doppler profiler. pp. 833-846 in *Proceedings 3rd Joint Federal Interagency Conference on Sedimentation and Hydrologic Modeling*, April 19-23, 2015, Reno, Nevada, USA.
Vachtman, D. , Sandler, A. , Greenbaum, N. & Herut, B., 2013. Dynamics of suspended sediment delivery to the Eastern Mediterranean continental shelf. *Hydrological Processes*, 27: 1105-1116. doi:10.1002/hyp.9265
Varyu, D., Laronne, J.B., Cadol, D., PAdilla, R, Lampert, T., Stark, K., Scissons, S., AuBuchon, J. & Munwes, Y. 2019. Monitoring the transport of sediment in an ephemeral stream. SedHyd2019, Federal Interagency Sedimentation and Hydrologic Modeling Conference. June 2019, Reno NV.
Williams, G.P., 1989. Sediment concentration versus water discharge during single hydrological events in rivers. *Journal of Hydrology*, 111, 89–106.

Application of Dimensionless Sediment Rating Curves to Predict Suspended-Sediment Concentrations and Bedload for Rivers in Minnesota

Christopher A. Ellison, Hydrologist, USGS, Helena, MT, 406.457.5901, cellison@usgs.gov
Joel T. Groten, Hydrologist, USGS, Mounds View, MN, 763.783.3149, jgroten@usgs.gov
Karl S. Koller, Cleanwater Legacy Specialist, Grand Rapids, MN, 218.999.7806, Karl.Koller@state.mn.us

Abstract

The U.S. Geological Survey, in cooperation with the Minnesota Pollution Control Agency and the Minnesota Department of Natural Resources, completed a study to evaluate the use of dimensionless sediment rating curves (DSRCs) to predict suspended-sediment concentrations (SSCs) and bedload for selected rivers and streams in Minnesota based on data collected during 2007 through 2013. This study included the application of DSRC models developed for a small group of streams located in the San Juan River Basin near Pagosa Springs in southwestern Colorado to rivers in Minnesota. Regionally based DSRC models for Minnesota also were developed and compared to DSRC models from Pagosa Springs, Colorado, to evaluate which model provided more accurate predictions of SSCs and bedload in Minnesota.

More than 600 dimensionless ratio values of SSC, bedload, and streamflow were evaluated and delineated according to Pfankuch stream stability categories of “good/fair” and “poor” to develop four Minnesota-based DSRC models. The basis for Pagosa Springs and Minnesota DSRC model effectiveness was founded on measures of goodness-of-fit that included proximity of the model(s) fitted line to the 95-percent confidence intervals of the site-specific model and Nash-Sutcliffe Efficiency values.

Composite plots comparing Pagosa Springs DSRCs, Minnesota DSRCs, site-specific regression models, and measured data indicated that regionally developed DSRCs (Minnesota DSRC models) more closely approximated measured data for nearly every site. Pagosa Springs DSRC models had markedly larger exponents (slopes) when compared to the Minnesota DSRC models and over-represented SSC and bedload at streamflows exceeding bankfull. The Nash-Sutcliffe Efficiency values for the Minnesota DSRC model for suspended-sediment concentrations closely matched Nash-Sutcliffe Efficiency values of the site-specific regression models for 12 of 16 sites. Pagosa Springs DSRC models were less accurate than the mean of the measured data at predicting SSC values for one-half of the good/fair stability sites and one-half of the poor stability sites.

Results of data analyses indicate that DSRC models developed using data collected in Minnesota were more effective at compensating for differences in individual stream characteristics across a variety of basin sizes and flow regimes than DSRC models developed using data collected for Pagosa Springs, Colorado. Minnesota DSRC models retained a substantial portion of the unique sediment signatures for most rivers, although deviations were observed for streams with limited sediment supply and for rivers in southeastern Minnesota, which had markedly larger regression exponents. The results from this study indicated that regionally based DSRCs can be used to estimate reasonably accurate values of SSC and bedload.

Introduction

Beginning in 2007, the U.S. Geological Survey (USGS), in collaboration with the Minnesota Pollution Control Agency (MPCA), identified a group of existing gage stations across Minnesota and began collecting water samples for analyses of suspended-sediment concentrations (SSCs), turbidity, and total suspended-solids (TSS) to improve understanding of fluvial sediment relations and transport processes. In 2012, the USGS, in cooperation with the U.S. Army Corps of Engineers (USACE), the Minnesota Department of Natural Resources (MNDNR), and the Lower Minnesota River Watershed District (LMRWD), expanded sediment sampling from 8 to 22 sites. In addition to collecting SSC samples, the USGS began collecting bedload samples in 2012 to quantify the contribution of bedload to total sediment loads. During this time, hundreds of streamflow measurements and SSC, turbidity, TSS, and bedload samples were collected to develop statistical relations among these constituents (U.S. Geological Survey National Water Information System, http://dx.doi.org/10.5066/F7P55KJN; Ellison and others, 2014).

Mandates to reduce costs, eliminate data gaps, and improve data accuracy have guided Federal and State interests in pursuing alternative methods of measuring and estimating SSCs and bedload. Physically collected samples for analysis of SSCs and bedload remain the most accurate and reliable means for determining sediment loads; however, the specialized equipment, training, and labor required to collect samples are time consuming, expensive, and potentially hazardous in certain conditions.

One alternative to collecting physical sediment samples is the use of dimensionless sediment rating curves (DSRCs) to reduce costs and improve the accuracy of predicting sediment transport (Troendle and others, 2001; Barry and others, 2008; Rosgen, 2006, 2010). Dimensionless rating curves have demonstrated potential to predict constituents of interest by scaling existing data at several regionally representative sites and applying the curves at sites where data are sparse or nonexistent (Leopold and others, 1964; Padmanabhan and Johnson, 2010; Dietrich and others, 1989; Troendle and others, 2001). Anticipated benefits of developing a curve model for SSCs and bedload include (1) improved sediment budgets, (2) reduced costs associated with extensive sediment data collection, (3) ability to identify streams that depart from reference conditions, (4) access to a tool for restoration prioritization, and (5) access to important information for planning river restoration activities.

In 2011, the USGS proposed to the MPCA and MNDNR that DSRCs be evaluated for application in Minnesota Rivers. Subsequently, the USGS, in cooperation with the MPCA and the MNDNR, completed a study to evaluate the use of DSRCs to predict SSCs, bedload, and annual sediment loads for selected rivers and streams in Minnesota based on data collected during 2007 through 2013. This study included the application of DSRCs developed by Rosgen (2010) from data collected from a small group of streams located in the San Juan River Basin near Pagosa Springs in southwestern Colorado to rivers in Minnesota. Regionally based DSRC models also were developed and compared to DSRCs from Pagosa Springs, Colorado, to assess how well Minnesota systems are described by the Pagosa Springs models and to evaluate the improvements gained through the development of a regional model.

Background Information on Dimensionless Sediment Rating Curves

The DSRC method relies on the intrinsic relations among streamflow, SSC, and bedload. Rosgen (2006, 2007, and 2010) continued work by Barry and others (2004) and Troendle and others

(2001) by expanding the application of dimensionless relations to improve predictions of suspended sediment and bedload in rivers. Rosgen's objectives for developing DSRC models were to provide a tool for river restoration planning and design, reduce the error from theoretical sediment prediction models, and help identify rivers that depart from known reference conditions. The Rosgen method (Rosgen, 2010) involves developing dimensionless relations between SSC and streamflow and between bedload and streamflow, and uses bankfull streamflow as a normalization parameter to develop the DSRC models.

Results from Rosgen (2010) indicated that DSRCs developed from a small group of streams located in the San Juan River Basin near Pagosa Springs in southwestern Colorado could be used to estimate sediment transport for geographically far-removed streams with different flow regimes, geology, and climate. Rosgen (2010) developed four reference DSRC model equations delineated by Pfankuch (1975) stream stability categories using data collected from the streams in Colorado. The four DSRC equations developed by Rosgen (2010) for good/fair and poor stability ratings for the Pagosa Springs DSRC models follow:

$$\text{Suspended DSRC (good/fair stability): } SSC = 0.0636 + 0.9326Q^{2.4085} \quad (1)$$

$$\text{Bedload DSRC (good/fair stability): } Qb = -0.0113 + 1.0139Q^{2.1929} \quad (2)$$

$$\text{Suspended DSRC (poor stability): } SSC = 0.0989 + 0.9213Q^{3.659} \quad (3)$$

$$\text{Bedload DSRC (poor stability): } Qb = 0.07176 + 1.02176Q^{2.3772} \quad (4)$$

where

SSC is a dimensionless ratio value of suspended-sediment concentration,
Q is a dimensionless ratio value of streamflow, and
Qb is a dimensionless ratio value of bedload.

Description of Study Area

Minnesota encompasses 86,939 square miles (mi^2) in the upper midwestern United States (Minnesota Department of Natural Resources, 2016a). Minnesota is in a transition zone between the moist eastern United States and the Great Plains (not shown) and has a continental climate with cold winters and warm to hot summers (Minnesota Department of Natural Resources, 2016b). Mean annual precipitation across the State ranges from 35 inches in the southeast to 20 inches in the northwest (Minnesota Department of Natural Resources, 2016b). The six hydrologic unit code (HUC) HUC–level 4 basins (Rainy River, Red River, Western Lake Superior, Mississippi Headwaters, Minnesota, and Upper Mississippi – Black-Root [Minnesota Department of Natural Resources, 2016c; Minnesota Geospatial Information Office, 2016]) selected for this study represent a cross section of basin characteristics present in Minnesota (fig. 1).

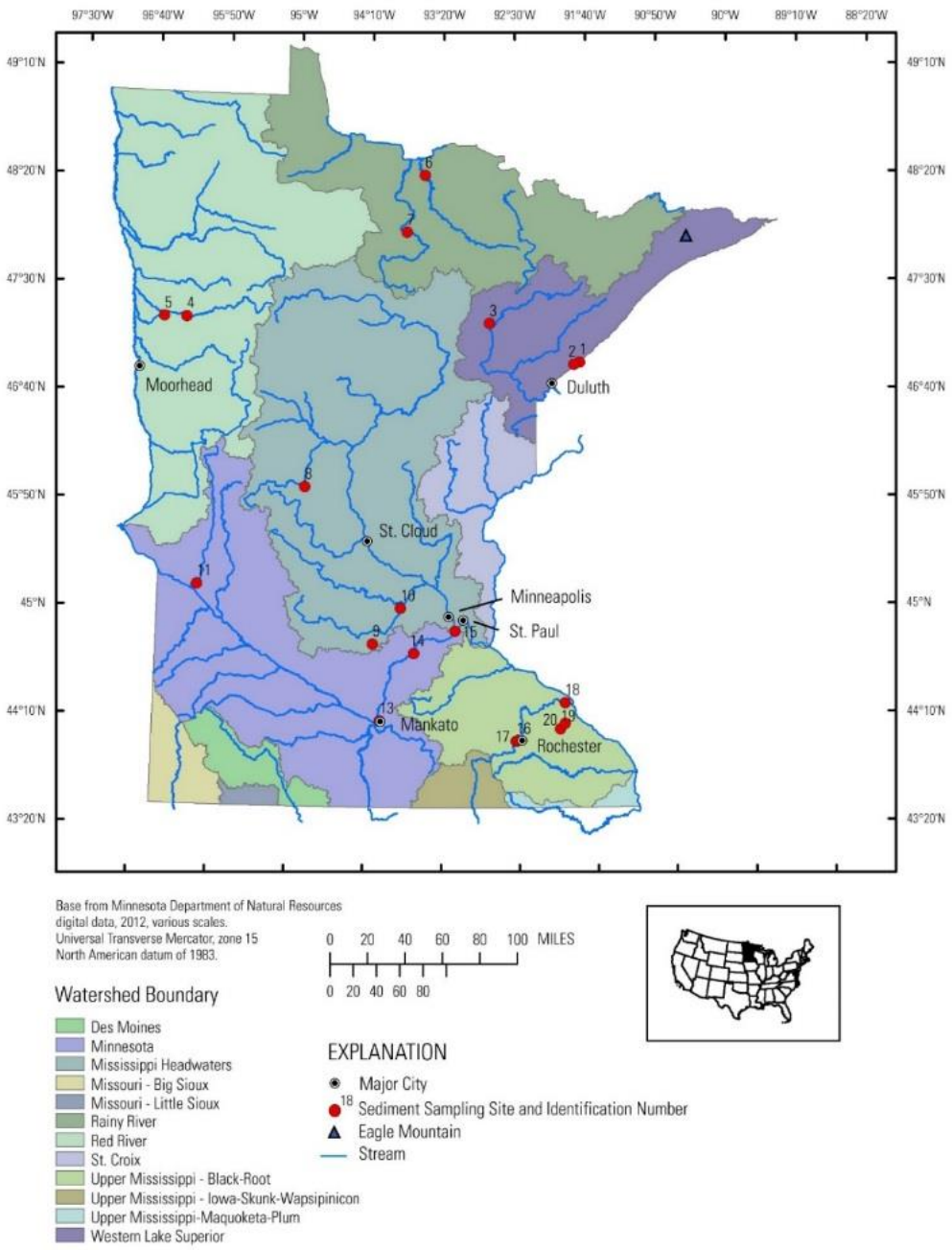

Figure 1. Study area and monitoring sites

Methods of Data Collection and Analysis

Information on sediment sampling sites (that is, site number, USGS station number, station name, position, elevation, drainage area, sampling period, type of streamflow record, and number of samples collected) is available in Ellison and others (2016).

Suspended-Sediment Concentrations

Depth-integrated suspended-sediment samples were collected at equal-width intervals across stream transects using isokinetic samplers according to procedures by Edwards and Glysson (1999). Following collection, samples were transported to the USGS sediment laboratory in Iowa City, Iowa, where they were composited into a single sample and analyzed for SSC and particle-size fraction according to Guy (1969).

Bedload

Two types of USGS-approved pressure-differential bag samplers, the Helley-Smith and the BL-84 sampler (Davis, 2005), were used to collect bedload samples. The single equal-width-increment method of collecting bedload samples according to Edwards and Glysson (1999) was used at all sites and bedload samples were collected concurrently with suspended-sediment samples. Bedload samples were analyzed for nine particle-size distributions (ranging from 0.0625 to 16 mm) using the dry-sieve method (Guy, 1969) at the University of Minnesota Civil Engineering Department by USGS Minnesota Water Science Center (WSC) staff.

Bankfull Streamflow Determination

Bankfull elevations were determined using methods outlined by Leopold and others (1964) and Rosgen (1994, 1996). A combination of field elevation surveys and bankfull field indicators, such as change in slope, changes in vegetation, stain lines, top of point bars, changes in bank material, or bank undercuts along streambanks were used to establish the point on the bank for bankfull stage at each site. For sites with continuous-record streamgages, bankfull elevations were referenced to the wire-weight gage height.

Determining Suspended-Sediment Concentration and Bedload at Bankfull Streamflow

Samples used to determine SSC and bedload at bankfull streamflow were limited to samples collected within the range of one-half to 2 times bankfull streamflow. Samples within this range of streamflow were collected during snowmelt runoff or summer precipitation events and included bankfull stage for at least one sampling event at each site. Based on availability, equal numbers of samples on the ascending and descending limb of the hydrograph were used to minimize disproportionate effects of individual samples from the effects of hysteresis. Once the samples were selected, SSC and bedload were paired with their corresponding instantaneous streamflows, and the mean values of SSC, bedload, and streamflow were calculated. Ratio estimators for SSC and bedload at bankfull streamflow were calculated for each site by dividing each mean SSC and bedload value by the corresponding mean instantaneous streamflow. Site-specific SSC and bedload values at bankfull streamflow were determined by multiplying the ratio estimator and the bankfull streamflow at that site.

Data Analysis

Suspended-sediment concentrations, bedload, and instantaneous and daily mean streamflows were formatted for analysis using S-plus statistical software (TIBCO® Software Inc., 2010) and the R statistical environment (R Development Core Team, 2011). Summary statistics, Kendall's

tau analysis, Nash-Sutcliffe Efficiencies (NSE), weighted nonlinear regression analyses, and simple linear regression analyses composed the analyses. The Pagosa Springs and Minnesota DSRC models were evaluated using measures of goodness-of-fit that included the proximity of the model(s) fitted line to the 95-percent confidence intervals of the site-specific model and NSE values.

Kendall's tau analyses (Kendall, 1938, 1975) were used to test for significance and measure the strength of the relations between SSC and streamflow and between bedload and streamflow at each site; p-values less than 0.05 indicated statistically significant monotonic relations. Data from sites without significant relations among variables (*p*-values of 0.05 or greater) were not used to develop models.

Data collected from rivers in Minnesota were used to develop DSRCs similar to methods described in Rosgen (2010). Minnesota DSRC model prediction efficiency was optimized using a weighted parameter method. More than 600 dimensionless ratio values were calculated using available SSCs, bedload, and streamflow data. Dimensionless ratio values were evaluated and delineated according to Pfankuch stream stability categories of good/fair and poor (Pfankuch, 1975), and selected dimensionless ratio values were used to develop four Minnesota-based DSRC models. Data from sites identified through the Kendall's tau correlation analyses with no relation (that is, *p*-values of 0.05 or greater) between SSC and streamflow or between bedload and streamflow were not used in the development of Minnesota DSRC models.

A weighted nonlinear least squares regression approach (nls function) was used for the analyses in the R statistical environment (R Development Core Team, 2011; Chaterjee and others, 2000).

As part of model development, a framework was incorporated so that the values of the model coefficients ($B1$) and numerical constant ($1 - B1$) ensured that the fitted trendline of the model would pass through the point of interception of the calculated values of SSC and bedload at bankfull with bankfull streamflow. The form of DSRC models for Minnesota was

$$Y_i = (1 - B_1) + B_1 X_i^{B2} + \varepsilon_i \quad (5)$$

where

Yi is a dimensionless ratio value of SSC or bedload,
$(1 - B1)$ is the intercept determined from the data,
B1 is a coefficient determined from the data,
Xi is a dimensionless ratio value of streamflow,
B2 is the slope determined from the data, and
εi is the random error representing the discrepancy in the approximation accounting for the failure of the model to fit the data exactly.

Site-specific simple linear regression (SLR) models were developed for each site for SSC and bedload for use in evaluating the goodness-of-fit of Minnesota and Pagosa Springs DSRC models. The site-specific SLR models were used to construct reference trendlines from which to evaluate the goodness-of-fit of the Minnesota and Pagosa Springs DSRC models.

Nash-Sutcliffe Efficiency values (Nash and Sutcliffe, 1970) were used to evaluate the effectiveness of Pagosa Springs and Minnesota DSRC models to approximate measured SSCs and bedload values. The NSE value is calculated using the measured values of the sampled data, modeled values, and the mean of the measured values. Nash-Sutcliffe Efficiency values can range from negative infinity to 1. An NSE value of 1 indicates that the model matches the

observed values exactly, an NSE value of 0 indicates that the model is predicting values that are no better than the mean of the measured values, and negative values of NSE indicates that the mean of the measured values is better than the model at approximating individual measured values.

Dimensionless Sediment Rating Curves

This section of the report presents DSRCs developed using data collected in Minnesota and provides an assessment of the ability of the Pagosa Springs and Minnesota DSRC models to predict SSC and bedload. Evaluations of DSRC models were based on measures of goodness-of-fit that included proximity of the model(s) fitted line to the 95-percent confidence intervals of the site-specific model and Nash-Sutcliffe Efficiency values.

More than 600 samples were used to develop Minnesota DSRCs for SSC and bedload for good/fair and poor Pfankuch stream stability categories. Four weighted nonlinear regression models were developed using the R statistical environment (nls function; R Development Core Team, 2011). Dimensionless ratio values of streamflow, SSC, and bedload were used to develop the following regression equations:

$$\text{Suspended DSRC (good/fair stability): } SSC = 0.026 + 0.974Q^{0.951} \quad (6)$$

$$\text{Bedload DSRC (good/fair stability): } Qb = -0.054 + 1.054Q^{1.316} \quad (7)$$

$$\text{Suspended DSRC (poor stability): } SSC = 0.066 + 0.934Q^{1.006} \quad (8)$$

$$\text{Bedload DSRC (poor stability): } Qb = 0.012 + 0.988Q^{1.306} \quad (9)$$

where

SSC is a dimensionless ratio value of suspended-sediment concentration,
Q is a dimensionless ratio value of streamflow, and
Qb is a dimensionless ratio value of bedload.

Dimensional values of SSC and bedload are derived from dimensionless ratio values of streamflow using the regression equations 6 through 9 (models). This entails converting streamflow to a dimensionless value by dividing streamflow by the known bankfull streamflow at the selected site. This dimensionless streamflow value is used as the input value in one of the dimensionless regression equations (equations 6 through 9) to calculate a dimensionless SSC or bedload value. Finally, the calculated dimensionless SSC or bedload value is multiplied by the known SSC or bedload value at bankfull streamflow from the site of interest to determine the dimensional SSC or bedload value.

The Pagosa Springs and Minnesota DSRC models for SSC and bedload were evaluated in comparison to site-specific regression models for model ability to predict suspended-sediment concentrations and bedload. As previously mentioned and described in the following subsections, methods used to assess the model effectiveness in predicting SSC and bedload included the comparison of regression trendlines (proximity of the fitted line of the DSRC model to the 95-percent confidence intervals of the site-specific model) and Nash-Sutcliffe Efficiencies.

Regression Trendlines:

Modeled (predicted) values of SSC and bedload using Pagosa Springs and Minnesota DSRC models were compared to measured values of SSC and bedload by plotting the measured values and the regression trendlines of each of the models on a log-log scale. Site-specific model regression trendlines with 95-percent confidence intervals were included to demonstrate the relations between measured SSC and streamflow and measured bedload and streamflow and to examine the level of agreement between DSRC models and site-specific regression models. Pagosa Springs DSRC models, Minnesota DSRC models, and site-specific regression models are presented for Pfankuch stability rating of good/fair in figure 2 for SSC and in figure 3 for bedload for Pfankuch stability rating of poor (SSC models for Pfankuch stability rating of poor and bedload models for Pfankuch stability rating of good/fair are available in Ellison and others [2016]). Pagosa Springs and Minnesota DSRC models were compared to site-specific regression models to evaluate their effectiveness in predicting SSC and bedload. Site-specific regression models are assumed to provide the most accurate predictions of suspended sediment and bedload across a range of streamflow.

Suspended-Sediment Concentrations:

Unique characteristics were observed among sites for the Pagosa Springs DSRC models developed to approximate SSC. Specifically, low sensitivity (little change in slope) at lower streamflows coupled with an identifiable inflection point associated with a marked increase in slope of the fitted trendline was observed for the Pagosa Springs DSRC models (fig. 2).

A notable concern is the disparity in values between regression exponents (slopes) from the Pagosa Springs DSRCs and site-specific regression exponents for rivers in Minnesota. Inspecting each site-specific regression model trendline alongside the regression trendlines for the Pagosa Springs DSRC models at flows near bankfull indicated that Pagosa Springs DSRC models resulted in markedly larger slopes than the site-specific regression models for SSC (fig. 2). For good/fair stability sites, the mean slope of the Pagosa Springs DSRC models for estimating SSC was 3.5 times larger than the mean slope of the site-specific regression models. For poor stability sites, the mean slope of the Pagosa Springs DSRC models (3.66) was 4.7 times larger than the mean slope of the site-specific regression models (0.78) (Ellison and others, 2016). Consequently, predictions of SSC derived from Pagosa Springs DSRC models will overestimate SSC and suspended-sediment loads at streamflows exceeding bankfull compared to the site-specific regression models.

Compared to Pagosa Springs DSRC models, Minnesota DSRC models for SSC more closely approximated the site-specific regression models developed from the measured data (fig. 2). Inspection of the regression trendlines for the Minnesota and Pagosa Springs DSRC models and the site-specific regression models indicate that the regional Minnesota DSRCs are more applicable to rivers in Minnesota. For example, Minnesota DSRC models were more sensitive to variability in streamflow during lower streamflows for SSC, unlike the Pagosa Springs DSRC models, which indicated little response in SSC to changes in streamflow at low streamflows. Also, the regression exponents for the Minnesota DSRC models more closely matched the site-specific regression exponents and were markedly lower than regression exponents from the Pagosa Springs DSRC models. For example, the mean slopes of 0.951 and 1.006 for SSC for the Minnesota DSRC models for good/fair and poor stability streams, respectively, were markedly lower than mean slopes of 2.41 and 3.66, respectively, for the Pagosa Springs DSRC models. Large differences in model slopes indicate that the individual river sediment signatures for

Minnesota's rivers were not as well represented in the Pagosa Springs DSRC models as compared to the Minnesota DSRC models. Overall, the Minnesota DSRC models approximated the site-specific regression models more closely than the Pagosa Springs DSRC models for 14 of 16 sites.

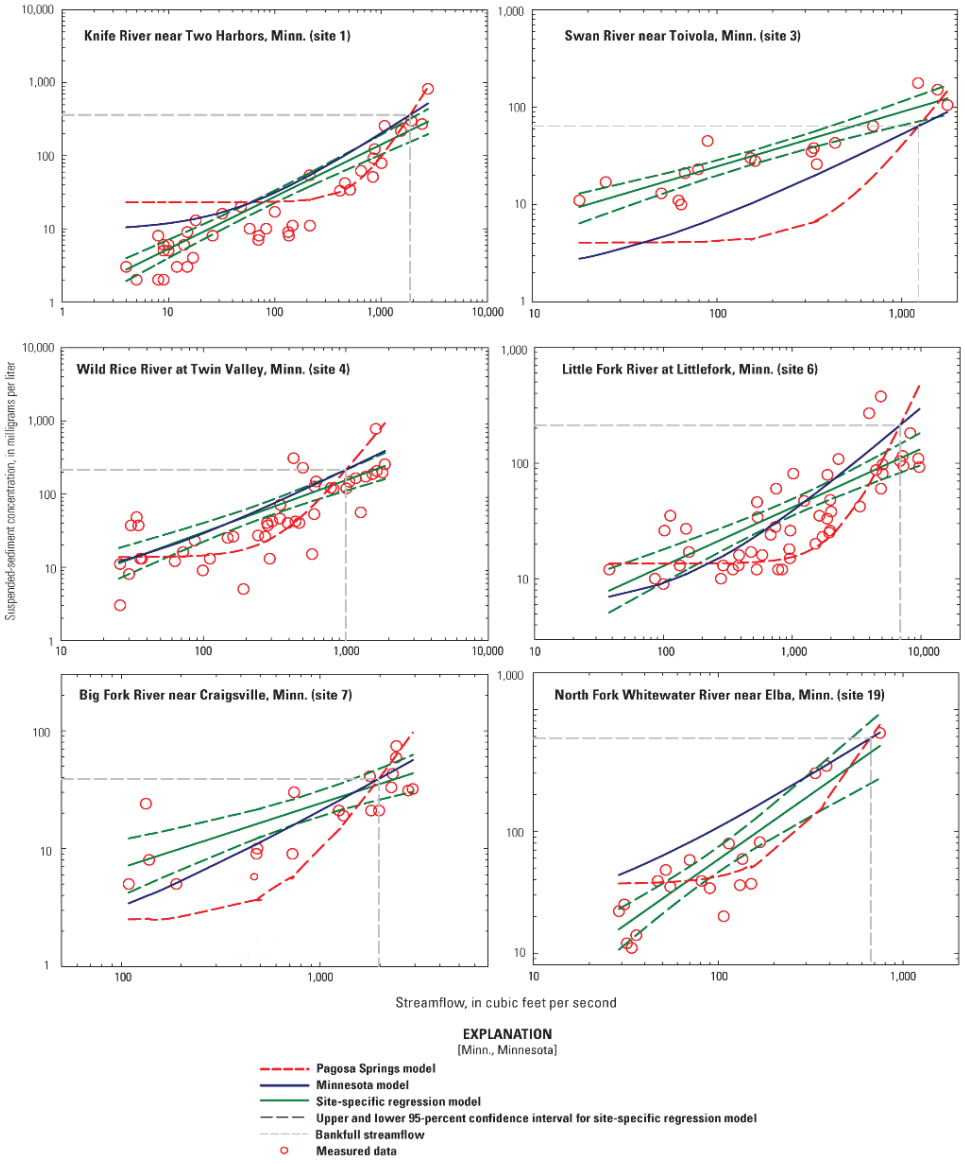

Figure 2. Pagosa Springs and Minnesota dimensionless suspended-sediment rating curves and site-specific regression trendlines for good/fair sites for selected rivers in Minnesota, 2007 through 2013

Bedload:

Regression trendlines for bedload for the Pagosa Springs and Minnesota DSRC models and site-specific regression models for poor stability categories are shown in figure 3 (good/fair stability models available in Ellison and others [2016]). For bedload, Pagosa Springs DSRC models had characteristics similar to those demonstrated by the SSC DSRC models. Similar to the SSC DSRC models, the slopes of the regression trendlines for bedload at streamflows exceeding bankfull were larger for the Pagosa Springs DSRC models than for the Minnesota DSRC and

site-specific regression models for most sites. For example, mean slopes for the Minnesota DSRC models were 1.316 and 1.306 for good/fair and poor stability streams, respectively, compared to mean slopes of 2.19 and 2.38, respectively, for the Pagosa Springs DSRC models (Ellison and others, 2016). In contrast to SSC models, all bedload models nearly intercepted the y-axis at 0 during periods of no streamflow, which corresponds to the expected response of little bedload transport during low streamflows (Bagnold, 1973; Leopold and Emmett, 1976).

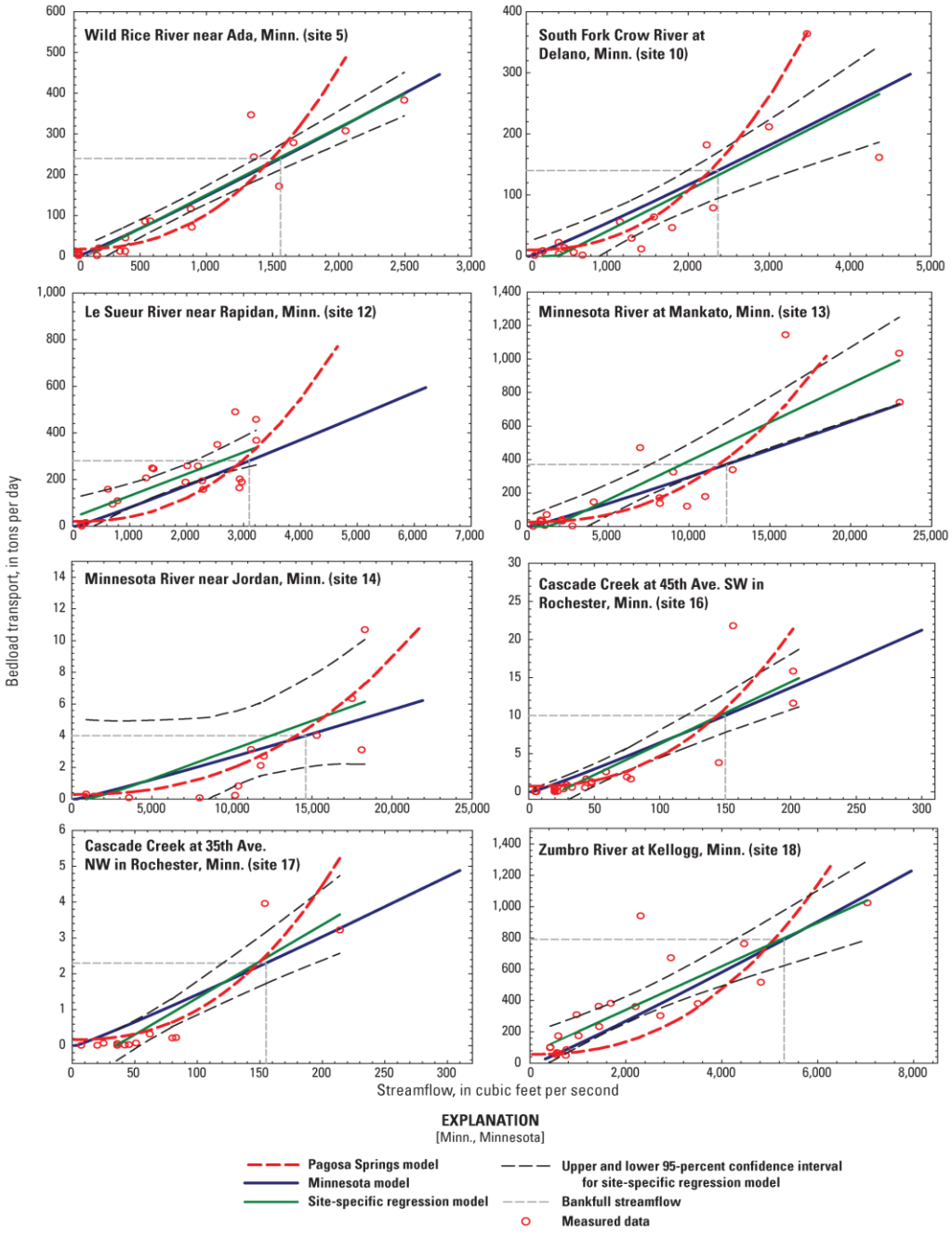

Figure 3. Pagosa Springs and Minnesota dimensionless bedload rating curves and site-specific regression trendlines for Pfankuch stability categories of poor for selected rivers in Minnesota, 2007 through 2013

In general, the predicted values of bedload from the Pagosa Springs and Minnesota DSRC models are contained within the 95-percent confidence intervals of site-specific regression models; however, the Minnesota models more closely approximated the site-specific regression models than did the Pagosa Springs DSRC models for most sites during streamflows near and exceeding bankfull streamflow (fig. 3). At lower streamflows, the Minnesota and Pagosa Springs DSRC models indicate similar fits to the measured data.

Nash-Sutcliffe Model Efficiencies:

Nash-Sutcliffe Efficiency values were determined for the Pagosa Springs DSRC models, Minnesota DSRC models, and site-specific regression models for each of the study sites. The NSE values are presented in figure 4 for SSC and in figure 5 for bedload.

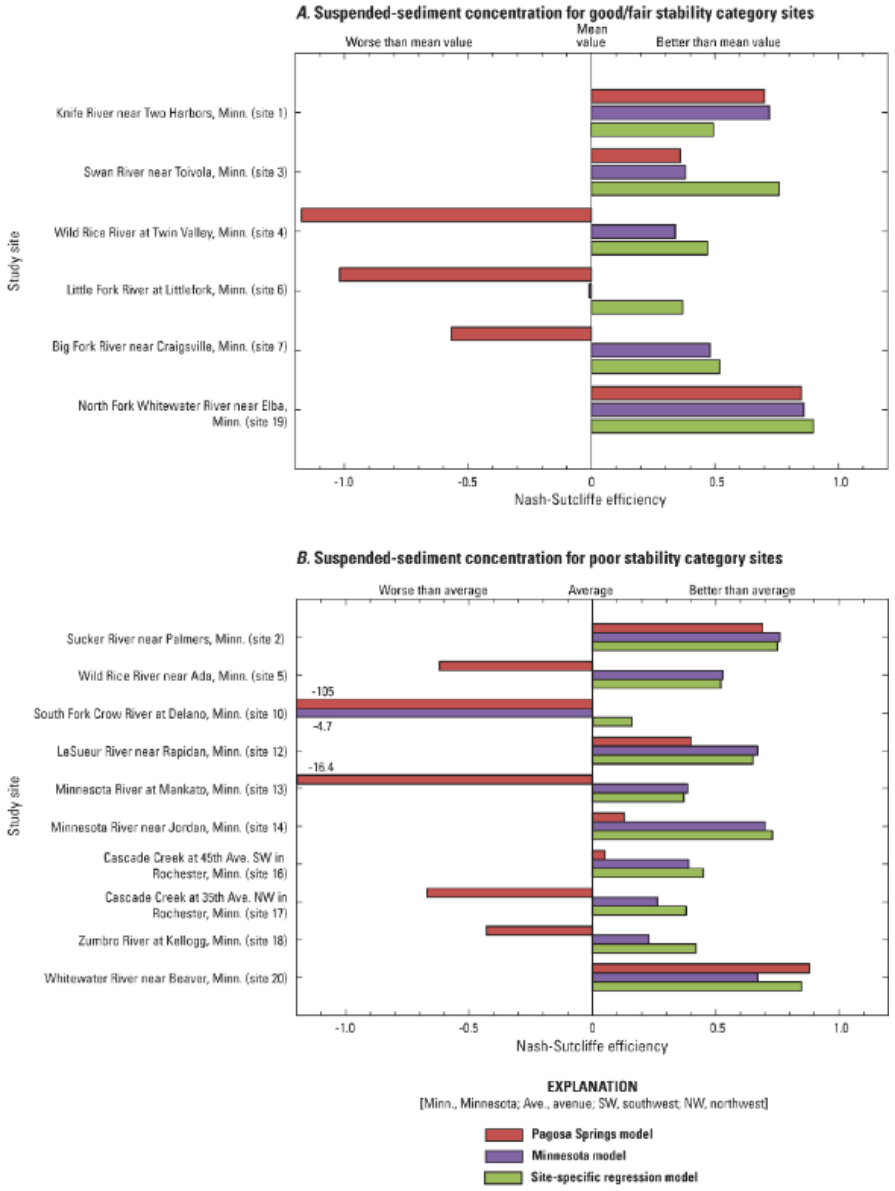

Figure 4. Nash-Sutcliffe Efficiency values for Pagosa Springs and Minnesota dimensionless rating curves and site-specific models for suspended-sediment concentrations for Pfankuch stability categories of good/fair (A) and poor (B) for selected rivers in Minnesota

Among models for SSC, the site-specific regression models provided the overall best fits for 10 of 16 sites (fig. 4) based on the NSE values. For SSC at the good/fair stability sites, the NSE values associated with the Pagosa Springs DSRC model indicated that fits were better than using the mean value of the measured data for 3 of 6 sites (sites 1, 3, and 19) and fits were worse than using the mean value for the remaining 3 sites (sites 4, 6, and 7; fig. 4A).

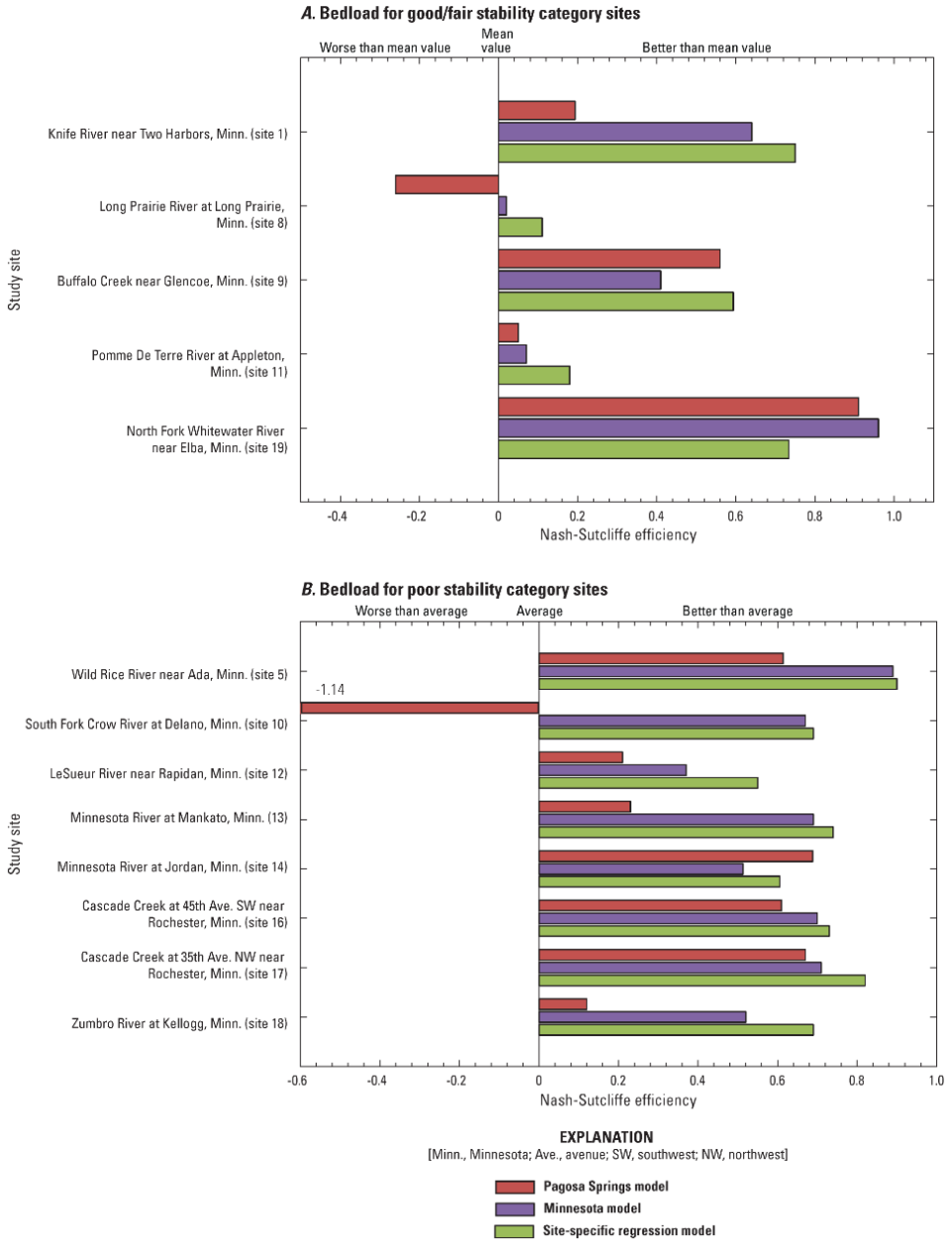

Figure 5. Nash-Sutcliffe Efficiency values for Pagosa Springs and Minnesota dimensionless rating curves and site-specific models for bedload for Pfankuch stability categories of good/fair (A) and poor (B) for selected rivers in Minnesota

Conversely, the Minnesota DSRC models provided a better fit for good/fair stability sites than using the mean value of the measured data for 5 of 6 sites. For poor stability sites for SSC models were similar to those for the good/fair stability sites (fig. 4*B*). The Pagosa Springs DSRC models provided fits that were better than the mean value of the measured data for 3 of 10 sites (sites 2, 12, and 20), slightly better fits than the mean value of the measured data for 2 sites (sites 14 and 16), and worse fits than the mean value for the measured data for the remaining 5 sites. The Minnesota DSRC models provided fits that were better than the mean value of the measured data for 9 of 10 poor stability sites and a worse fit than the mean for one site (site 10). The exceptions were sites 8 and 10, which had negative NSE values of -0.26 and -1.14, respectively. For the 11 sites with positive NSE values using the Pagosa Springs DSRC models, 5 sites (sites 5, 14, 16, 17, and 19) had NSE values that exceeded 0.6, 4 sites had NSE values that ranged between 0.2 and 0.6, and 2 sites (sites 11 and 18), had NSE values (0.05 and 0.12, respectively) that were only slightly better than using the measured samples mean value. The Minnesota bedload DSRC models indicated markedly better NSE values than the Pagosa Springs DSRC models for nearly every site. For the Minnesota DSRC models, all 13 sites had positive NSE values and closely approximated the site-specific regression model results.

Implications of the Model Assessments

Results of data analyses indicate that DSRC models developed using data collected in Minnesota were more effective at compensating for differences in individual stream characteristics across a variety of basin sizes and flow regimes than DSRC models developed using data collected near Pagosa Springs, Colorado. Minnesota DSRC models retained a substantial portion of the unique sediment signatures for most rivers, although deviations were observed for streams with limited sediment supply and for rivers in southeastern Minnesota, which had markedly larger regression exponents. Compared to Pagosa Springs DSRC models, Minnesota DSRC models had regression slopes that more closely matched the slopes of site-specific regression models and had greater Nash-Sutcliffe Efficiency values.

The results presented in this report indicate that regionally based DSRCs can be used to estimate reasonably accurate values of SSC and bedload. Practitioners are cautioned that DSRC reliability is dependent on representative measures of bankfull streamflow, SSCs, and bedload. It is, therefore, important that samples of SSC and bedload, which will be used for estimating SSC and bedload at the bankfull streamflow, are collected over a range of conditions that includes the ascending and descending limbs of the event hydrograph. Applicability of DSRC models may have substantial limitations under certain conditions. For example, DSRC models should not be used to predict SSC and loads for extreme streamflows, such as those that exceed twice the bankfull streamflow value because this constitutes conditions beyond the realm of current (2016) empirical modeling capability. Also, if relations between SSC and streamflow and between bedload and streamflow are not statistically significant, DSRCs should not be used to predict SSC or bedload, as this could result in large errors. For streams that do not violate these conditions, DSRC estimates of SSC and bedload can be used for stream restoration planning and design, and for estimating annual sediment loads for streams where little or no sediment data are available.

References

Bagnold, R.A., 1973, The nature of saltation and of bed-load transport in water: Proceedings of the Royal Society of London, Series A, Mathematical and Physical Sciences, v. 332, no. 1591, p. 473–505.

Barry, J.J., Buffington, J.M., Goodwin, P., King, J.G., and Emmett, W.W., 2008, Performance of bed-load transport equations relative to geomorphic significance––Predicting effective discharge and its transport rate: Journal of Hydraulic Engineering, v. 134, no. 5, p. 601–615. [Also available at http://dx.doi.org/10.1061/(ASCE)0733-9429(2008)134:5(601).]

Barry, J.J., Buffington, J.M., and King, J.G., 2004, A general power equation for predicting bed load transport rates in gravel bed rivers: Water Resources Research, v. 40, W10401, 22 p. [Also available at http://dx.doi.org/10.1029/2004WR003190.]

Chaterjee, Samprit, Hadi, A.S., and Price, Bertram, 2000, Regression analysis by example, (3d ed.): John Wiley and Sons, Inc., New York, 359 p.

Davis, B.E., 2005, A guide to the proper selection and use of federally approved sediment and water-quality samplers: U.S. Geological Survey Open-File Report 2005–1087, 20 p. [Also available at http://pubs.usgs.gov/of/2005/1087/.]

Dietrich, W.E., Kirchner, J.W., Ikeda, H., and Iseya, F., 1989, Sediment supply and the development of the coarse surface layer in gravel-bedded rivers: Macmillan Magazines Limited, 3 p.

Edwards, T.K., and Glysson, G.D., 1999, Field methods for measurement of fluvial sediment: U.S. Geological Survey Techniques of Water-Resources Investigations, book 3, chap. C2, 89 p. [Also available at http://pubs.usgs.gov/twri/twri3-c2/.]

Ellison, C.A., Savage, B.E., and Johnson, G.D., 2014, Suspended-sediment concentrations, loads, total suspended solids, turbidity, and particle-size fractions for selected rivers in Minnesota, 2007 through 2011: U.S. Geological Survey Scientific Investigations Report 2013–5205, 43 p., accessed April 29, 2016, at http://dx.doi.org/10.3133/sir20135205.

Ellison, C.A., Groten, J.T., Lorenz, D.L., and Koller, K.S., 2016, Application of dimensionless sediment rating curves to predict suspended-sediment concentrations, bedload, and annual sediment loads for rivers in Minnesota: U.S. Geological Survey Scientific Investigations Report 2016–5146, 68 p., http://dx.doi.org/10.3133/sir20165146.

Guy, H.P., 1969, Laboratory theory and methods for sediment analysis: U.S. Geological Survey Techniques of Water-Resources Investigations, book 5, chap. C1, 58 p. [Also available at http://pubs.usgs.gov/twri/twri5c1/.]

Kendall, M.G., 1938, A new measure of rank correlation: Biometrika, v. 30, 81–93. [Also available at http://dx.doi.org/10.2307/2332226.]

Kendall, M.G., 1975, Rank correlation methods (4th ed.): London, Charles Griffin, 202 p.

Leopold, L.B., and Emmett, W.W., 1976, Bedload measurements, East Fork River, Wyoming: Proceedings of the National Academy of Sciences, v. 73, no. 4, p. 1000–1004.

Leopold, L.B., Wolman, M.G., and Miller, J.P., 1964, Fluvial processes in geomorphology: San Francisco, California, Freeman, 522 p.

Minnesota Department of Natural Resources, 2016a, Land: accessed March 3, 2016, at http://www.dnr.state.mn.us/faq/mnfacts/land.html.

Minnesota Department of Natural Resources, 2016b, Climate of Minnesota: accessed March 3, 2016, at http://www.dnr.state.mn.us/climate/index.html.

Minnesota Department of Natural Resources, 2016c, Basins of Minnesota: accessed March 3, 2016, at http://www.dnr.state.mn.us/watersheds/basins.html.

Minnesota Geospatial Information Office, 2016, Hydrography standard—watersheds: accessed April 22, 2016, at http://www.mngeo.state.mn.us/committee/hydro/HUC_Names_official.html.

Nash, J.E., and Sutcliffe, J.V., 1970, River flow forecasting through conceptual models part 1––A discussion of principles: Journal of Hydrology, v. 10, no. 3282–3290. [Also available at http://dx.doi.org/10.1016/0022-1694(70)90255-6.]

Padmanabhan, G., and Johnson, B.H., 2010, Regional dimensionless rating curves to estimate design flows and stages: Journal of Spatial Hydrology, v. 10, no. 1, p. 41–75.

Pfankuch, D.J., 1975, Stream reach inventory and channel stability evaluation: Missoula, Montana, U.S. department of Agriculture Forest Service, no. R1-75-002, GPO no. 696-260/200, 26 p.

R Development Core Team, 2011, R Installation and Administration, Version 2.14.1, 2011-12-22, accessed April 29, 2016, at http://streaming.stat.iastate.edu/CRAN/doc/manuals/R-admin.pdf.

Rosgen, D.L., 2006, Flowsed/Powersed––Prediction models for suspended and bedload transport: Proceedings of the Eighth Federal Interagency Sedimentation Conference (8th FISC), April 2–6, 2006, Reno, Nevada, p. 761–769.

Rosgen, D.L., 2007, Watershed Assessment of River Stability and Sediment Supply (WARSS), (2d ed.): Fort Collins, Colorado, Wildland Hydrology, 1933 p.

Rosgen, D.L., 2010, The application and validation of dimensionless sediment rating curves: 2nd Joint Federal Interagency Conference, Las Vegas, Nevada, June 27–July 1, 2010, 11 p.

TIBCO Software Inc., 2010, TIBCO Spotfire S+: Somerville, Massachusetts, accessed November 9, 2012, at http://spotfire.tibco.com/products/s-plus/statistical-analysis-software.aspx.

Troendle, C.A., Rosgen, D.L., Ryan, S., Porth, L., and Nankervis, J., 2001, Developing a 'reference' sediment transport relationship: Proceedings of the Seventh Federal Interagency Sedimentation Conference, Reno, Nevada, March 25–29, p. 73–80.

Bedload traps and Helley-Smith Sampler Collect Different Rates and Particle Sizes of Gravel Bedload

Kristin Bunte, Research Scientist, Department of Civil and Environmental Engineering, Colorado State University, kbunte@engr.colostate.edu
Kurt W. Swingle, Environmental Scientist, Boulder, CO, kskb@ix.netcom.com
Robert Ettema, Prof., Department of Civil and Environmental Engineering, Colorado State University, rettema@engr.colostate.edu
Steven R. Abt, Prof. emer., Department of Civil and Environmental Engineering, Colorado State University, sabt@engr.colostate.edu
Dan A. Cenderelli, Hydrologist, USDA Forest Service, National Stream and Aquatic Ecology Center, Fort Collins, CO, dcenderelli@fs.fed.us

Abstract

Measurements from the commonly used Helley-Smith (HS) sampler can greatly misestimate gravel transport rates and the largest mobile bedload particles in mountain streams, especially when transport is low. Various factors contribute to mismeasurement. To shed light on the relative magnitude of the various factors' contributions, this study compares sampling results between bedload traps and a HS sampler deployed on the bed and on ground plates in mountain streams. Inadvertent pickup of bed material and bedload particles fostered by the HS sampler's high hydraulic efficiency causes the majority of over-sampling (i.e., sampling too much) when the HS sampler is deployed directly on a gravel bed, and transport is low. When the HS sampler is deployed on ground plates, inadvertent particle pickup is prevented, but the high hydraulic efficiency continues to over-sample gravel transport, but under-samples the largest mobile particles. The HS sampler's deployment duration, entrance width, and ambient transport conditions affect sampling results, but transport rates and the largest mobile particle sizes are affected differently.

1. Introduction

A Helley-Smith (HS) sampler (Helley and Smith, 1971) with a 76 mm-by-76 mm opening (often referred to as the 3-by-3-inch HS sampler) is commonly used to measure gravel bedload transport rates and particle sizes in coarse-bedded mountain streams because the sampler is widely available and easy to use. However, the HS sampler is prone to mismeasure gravel transport rates and bedload particle sizes. This paper assesses the reasons causing mismeasurements and offers recommendations for using a HS sampler more effectively.

The HS sampler is a pressure-difference sampler with a highly flared sampler shape (entrance-to-exit ratio of 3.22) (Figure 1, inset). The flared entrance creates a high hydraulic efficiency, meaning that the flow velocity measured at the sampler entrance exceeds the velocity measured when the sampler is absent. The HS sampler was developed following the design of the similarly sized and shaped Dutch "Bedload Transport Meter Arnhem" (BTMA). The BTMA was designed in 1939 for sampling sand and pea gravel bedload in lowland rivers (De Vries, 1979). In that environment, a wide flaring (ratio of 3.28) is desirable to create a high hydraulic efficiency at the sampler's entrance with which to counteract the retardation of flow velocity in the sampler's mesh-wire bag as the mesh pores become clogged with sand during the sampling process. Bedload traps (*see* inset photo at bottom of Figure 1b) are samplers especially designed for capturing low-level gravel transport in coarse-bedded mountain streams (Bunte et al., 2007) (*more*

later) in order to produce accurate measurements of gravel transport rates (Q_B) and the largest transported bedload sizes ($D_{max,QB}$). The writers' previous studies (Bunte et al., 2004, 2008) show that when used in coarse-bedded mountain streams for sampling low rates of gravel transport, the HS sampler over-estimates Q_B by several orders of magnitude and over-estimates $D_{max,QB}$ by a factor of 2-3 when ambient transport is low, but under-estimates Q_B and $D_{max,QB}$ when the rate of gravel transport is high (Figure 1a and b). The cause of these mismeasurements has been attributed to various processes (Bunte et al., 2009). Setting the HS sampler directly onto a gravel bed for deployment may lead to inadvertent capture of particles when the sampler's front edge scoops particles into the opening or when the pressure from holding the sampler onto the bed squeezes small gravels out of their interlock seating. Small gravel particles may also be naturally exposed on the bed or become loosened and/or entrained by turbulent forces exerted onto the bed as the HS sampler is pushed through the water column. The HS sampler's high hydraulic efficiency then pulls the exposed, loosened or entrained small gravels into its opening. Sampling at numerous verticals per cross-section, up to 40 for one sample (e.g., 20 verticals with two traverses or 10 verticals with 4 traverses (Emmett, 1980; Emmett et al., 1996)), considerably multiplies the chance of inadvertent particle capture. The HS sampler's high hydraulic efficiency also causes streamlines to expand in front of the sampler. The expansion funnels flow into the sampler from an area larger than the sampler entrance, thus capturing small gravel particles that travel downstream on a path adjacent to the sampler opening.

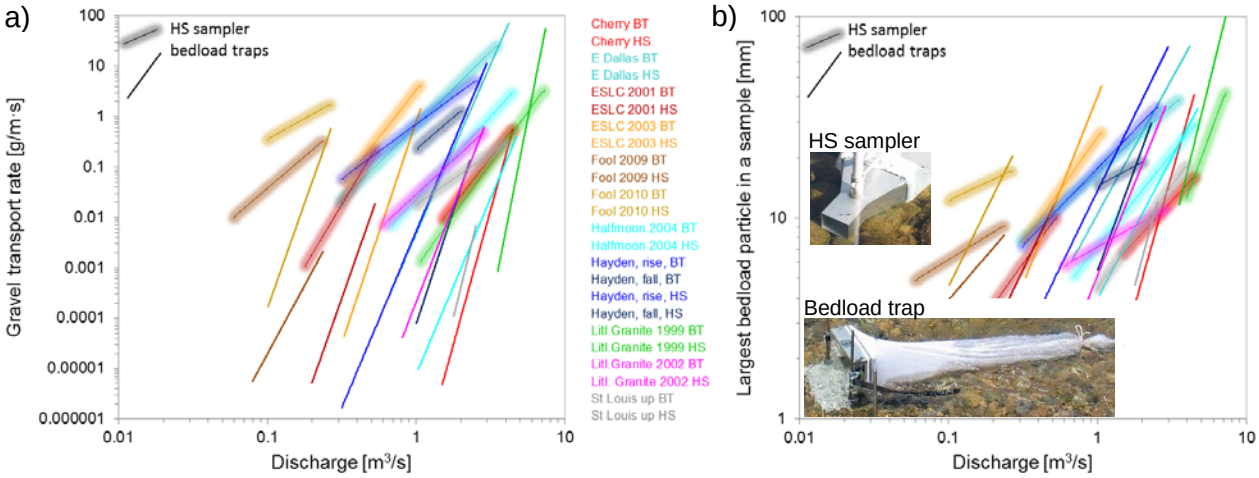

Figure 1. Differences in gravel transport rates (a) and bedload D_{max} sizes (b) collected by the writers using a HS sampler deployed directly on the bed and bedload traps in coarse-bedded, mainly Rocky Mountain streams.

There are also processes that cause the HS sampler to under-sample Q_B and $D_{max,QB}$. If the sampler is set perched onto coarse rocks, small particles can pass beneath or beside the sampler (Camenen et al., 2012). At higher flows, the narrow opening of the HS sampler hinders medium and large gravel from entering, which may exclude them from the sample, and the narrow distance between the sampler walls poses an obstacle to an advancing gravel front. Short sampling duration is likewise known to cause under-sampling of both Q_B and $D_{max,QB}$ (*more in Section 1.2.2*). Practically, though, sampling durations per vertical need to be brief (seconds to minutes) to complete measurements at the 20 or 40 verticals within a time frame for which a near-constant flow can be assumed. Short sampling durations are also needed to prevent overfilling the small HS sampler bag when transport rate is high.

Mismeasurement of Q_B and $D_{max,QB}$ from HS samples has not received much attention. Such mismeasurement, however, poses a problem for individual studies and the research community

at large. Many data sets have been compiled from HS samples in gravel-bed streams (e.g., Leopold and Emmett, 1976, 1977; Williams and Rosgen, 1989; King et al., 2004; Hinton et al., 2017). Those data sets are widely used to make inferences about the functioning of gravel transport, to develop bedload transport equations, to assess watershed bedload export, and to make stream-management decisions.

Presently, the roles and magnitudes of factors contributing to the HS sampler's mismeasurement of gravel transport are not well understood, thereby hampering efforts to correct HS measurements (Bunte et al., 2009, 2010b). This study assesses the relative magnitudes of the various factors contributing to inaccurate measurements when HS samplers are used in gravel-bed streams.

1.2 Background

1.2.1 Bedload-trap design and deployment attributes: The design of bedload traps takes into account the characteristics of gravel bedload in coarse-bedded, mountain streams. Bedload traps have a large entrance 0.3 m wide by 0.2 m high to admit gravel and cobbles. Traps are deployed on ground plates 0.4 m wide and 0.3 m long that are fitted into the bed surface to avoid interaction with the bed. The traps are tied to the stakes that anchor ground plates to the bed. Tying to stakes frees an operator from having to hold bedload traps while sampling and facilitates long sampling durations. Bedload traps have a 1.0-1.4 m long, flexible (knitted) net with a 4-mm-wide mesh that accepts large volumes of bedload, maintains good through-flow while the bag fills, and likewise facilitates long sampling durations (Bunte et al., 2004, 2008, 2010a, 2015). Finally, installing up to 6 or 7 bedload traps, spaced 0.6-1.8 m, covers much of the lateral transport variation per cross-section.

Sampling with bedload traps results in a high sampling intensity, I_s, defined as

$$I_s = t_s \cdot w_s \cdot n_s \qquad \text{(Eq. 1)}$$

where t_s = sampling duration, w_s =sampler width and n_s = number of traps deployed per cross-section. The difference in values of I_s for bedload traps and HS samplers indicate a limitation in measurements obtained with HS samplers. For example, six bedload traps deployed for an hour across a 10 m-wide channel yield an I_s of 110 min·m (60 min · 0.305 m · 6 plates). This intensity amounts to 18% of the total possible $I_{s,tot}$ of 600 min·m which would result from continuously sampling the entire width of the cross-section for an hour. By contrast, I_s for a 76-mm wide HS sampler deployed for 2 minutes on 20 verticals in the same channel reaches only 0.5% of $I_{s,tot}$ which is 2.8% of the I_s obtained when sampling with bedload traps. When the HS sampler is deployed for 2 or for 5 minutes on each of the six bedload trap ground plates, the I_s drops to 0.8 or 2.1% of the bedload trap value.

Owing to their design, deployment mode and high sampling intensity, bedload traps can yield sampling results as accurate as possible for a portable physical sampler in wadeable flow. The close agreement reported by Turowski (pers. comm. 2012) between gravel transport rates measured using bedload traps and rates collected using large baskets placed under an overfall weir in a Swiss mountain stream confirmed that this is the case (Rickenmann et al., 2012).

1.2.2 Effect of sampling duration on Q_B and $D_{max,QB}$: High-resolution records of gravel transport in mountain streams measured using surrogate technologies such as the magnetic tracer technique (e.g., Bunte 1996, 2010; Tunicliffe et al., 2000; Gottesfeld and Tunnicliff, 2003) and impact plates (e.g., Rickenmann, 2018) reveal that transport rates Q_{Bi} and their larg-

est transported sizes ($D_{max,QBi}$) sampled over short durations (i.e., 1-5 minutes) fluctuate rapidly over time. Such fluctuations can introduce measurement errors for short-term measurements.

The largest spikes in Q_{Bi} and similarly in $D_{max,QBi}$ occur rarely, and most measured values of Q_{Bi} are smaller than the mean value ($Q_{Bi,mean}$). The resulting frequency distribution for $Q_{Bi}/Q_{Bi,mean}$ peaks below 1.0 and has a long thin tail signifying $Q_{Bi}>>Q_{Bi,mean}$. Under these conditions, bedload samples collected over 60 minutes integrate over short-term fluctuations and provide a much better chance of including the large, but infrequent, peak values than do 2-minute samples. Hence, short sampling durations under-sample Q_{Bi} and $D_{max,QBi}$ (Figure 2a and b). Empirical evidence for a decrease in sampled Q_B with shorter sampling durations was shown by Bunte and Abt (2005). Fienberg et al. (2010) and Singh et al. (2009) provided mathematical evidence supporting this finding.

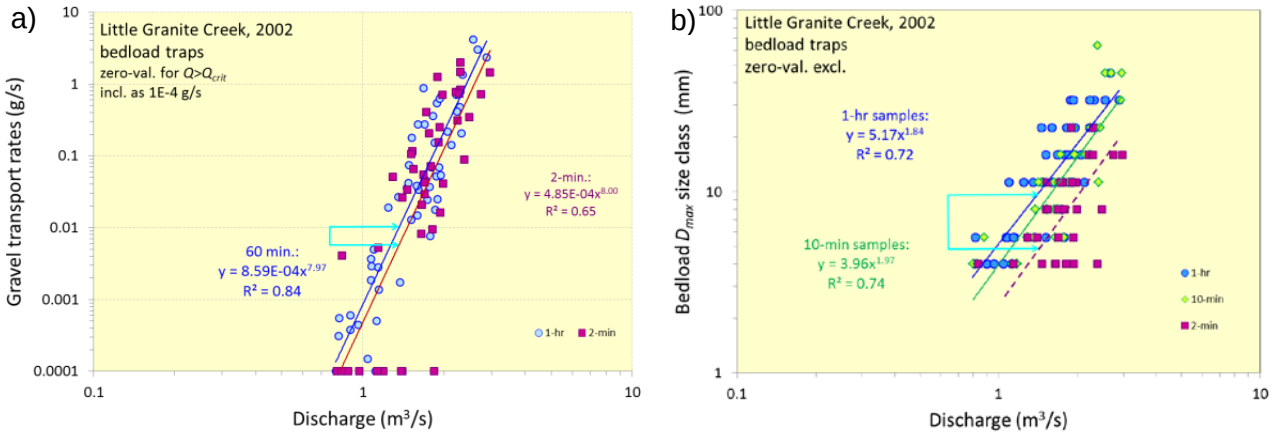

Figure 2. Reducing the bedload trap sampling duration from 60 to 2 minutes decreased sampled Q_B (a; after Bunte and Abt, 2005) and sampled $D_{max,QB}$ (b) each to about one half.

1.3 Study aim and approach

In order to assess the relative magnitudes of factors that cause HS samplers to mismeasure gravel transport rates, this study compared values of Q_B and $D_{max,QB}$ obtained from bedload traps and a HS sampler deployed directly on the bed and on the bedload trap ground plates. The use of ground plates as a physical border between the HS sampler and the bed eliminated a major cause for the HS sampler's over-sampling and, thereby, enabled its effect to be quantified. Comparing sampling results between bedload traps and the HS sampler deployed on the ground plates opened up further possibilities to quantify the degree of how the HS sampler's shape and deployment characteristics affect sampling outcomes, such as mismeasurements caused by low sampling intensity and high hydraulic efficiency. To reveal the effects of sampling duration on Q_B and $D_{max,QB}$ measurements, results from the HS sampler were compared for two and five minute deployments. Finally, we assessed how ambient rates of gravel transport and associated particle sizes influence over-sampling Q_B and under-sampling of $D_{max,QB}$ by the HS sampler, and further examined the roles of hydraulic efficiency, sampler size, and sampling duration on sampling outcomes.

The approach described above is based on bedload transport and flow competence relations fitted to field data. The fitted relations are used to estimate Q_B and $D_{max,QB}$ for the geometric mean of the sampled flow range, and the predicted values of Q_B and $D_{max,QB}$ are then compared between sampler deployments.

2. Methods

Bedload samples for the analyses in this study were collected between 2005 and 2015 during snowmelt runoff in five Rocky Mountain streams (Table 1). In all, 12 data sets were obtained from the five streams, because at some streams, multiple locations were sampled per reach, and at others the seasonal hydrograph was segregated into periods of low and high sediment supply to properly fit transport and flow competence relations. The common arrangement of a sheet-metal version of a HS sampler attached to a wading rod was used; the walls of this sampler are thinner than in the original HS sampler made from ¼-inch aluminum stock and the thin-walled HS sampler tends to collect transport rates about twice as high as those from the thick-walled sampler (Pitlick 1988; Ryan and Port 1999). Bedload traps were used at all sites. Two ground plates were installed across the narrow Fool Creek channel, five at Hayden and N.F. Swan Creek, and six at Halfmoon and East Dallas Creek. At East Dallas Creek, bedload was also sampled at two isolated ground plates. One plate was located on a steep, coarse riffle, the other on a submerged point bar with a loose bed of fine to medium gravel. At Halfmoon Creek, instead of a HS sampler, a 3-by-3 inch opening but lesser-flared BL-84 sampler (Gray et al., 1991) with an entrance-to-exit ratio of 1.4 was deployed on ground plates.

Table 1. Study Site Characteristics

Creek name	A [km²]	$Q_{1.5}$ [m³/s]	$w_{1.5}$ [m]	S_x [m/m]	$d_{1.5}$ [m]	D_{16} [mm]	D_{50} [mm]	D_{84} [mm]	D_{50s} [mm]	HS smpl. duration on bed	HS smpl. duration on plate	Site coordinates	Dominant morphology
Half-moon	61	6.1	8.7	0.012	0.61	19	62	136	22	-	2[1)]	39°10"40.02"N, 106°23"11.63"W	Plane-bed, occ. pool-riffle
East Dallas	34	3.7	7.5	0.017	0.33	16	60	131	21	2	5	38°05'50.31"N 107°48'33.90"W	
NF Swan	16	1.1	5.6	0.030	0.20	7.6; 8.8	39; 54	124; 134	22	-	2	39°50'50.56"N 105°56'26.15"W	Plane-bed w/low steps
Hayden	40	2.0	7.0	0.038	0.26	14; 18	63; 63	163; 172	36	2	5	38°19'54.46"N 105°48'44.12"W	Step-pool
Fool	3	0.30	1.3	0.086	0.17	12	52	122	24	2	5	39°53'28.02"N 105°52'03.58"W	

Notes: A = basin area; $Q_{1.5}$ = 1.5-year recurrence interval flow; $w_{1.5}$ and $d_{1.5}$ = channel width and depth associated with the $Q_{1.5}$ flow; S_x = reach-averaged stream gradient; D_{16}, D_{50} and D_{84} = bed surface particle-sizes of which 16, 50, and 84%, respectively, are finer; D_{50s} = median of subsurface distribution; If two values are given in one cell, the first refers to conditions before and the second to conditions after the high-flow season. [1)]A BL-84 sampler (a lesser-flared variation of the HS sampler) was used.

Bedload traps were typically deployed for one hour per sample. However, deployment sometimes extended over three hours per sample during daily low flows early in the high-flow season, or was as brief as three minutes per sample when bedload was streaming into the traps. To not interrupt the bedload traps' back-to-back sampling arrangement, HS samples on plates were typically collected as the first sample in the morning before bedload traps were deployed and/or as the last sample in the evening after bedload traps had been removed; hence, fewer samples were collected with the HS sampler than with the bedload traps. HS sampling durations varied: they were two minutes per vertical on the bed and five minutes per plate at Hayden, East Dallas, and Fool Creek; but they were two minutes per plate at NF Swan Creek and for the BL-84 sampler used at Halfmoon Creek.

Bedload samples were washed to remove organic debris, bagged, dried, and sieved in 0.5 phi increments. Transport rates (Q_B) and the largest bedload particle size ($D_{max,QB}$) were computed from samples aggregated over all ground plates or all verticals per cross-section. Water discharge Q was computed for all samples. The finest size class sampled in bedload traps was 4 mm. Hence, only transport rates of gravel larger than 4 mm were analyzed in this study.

For data analysis, gravel transport ($Q_B = a\,Q^b$) and flow competence relations ($D_{max,QB} = f\,Q^g$) were fitted to measurements obtained from bedload traps and the HS sampler deployed directly on the bed and on the ground plates at each site; a, b, f and g are empirically fitted coefficients and exponents. Besides a visual comparison of the fitted transport and flow competence relations between samplers, sampling results from the three sampler arrangements were compared using values of Q_B and $D_{max,QB}$ predicted from the fitted transport and flow competence relations for the geometric mean Q between the lower and upper end of the flow range sampled during the high-flow season. Thus, Q_B and $D_{max,QB}$ values compared in this study integrate over many bedload samples and a wide range of Q. When changes in sediment supply during the high-flow season had notably shifted the Q_B-Q and $D_{max,QB}$-Q relations, transport and flow competence relations were fitted to the data ranges before and after the shifts. When the flow range was narrow and data too scattered to yield a reasonable fit to a regression function, the geometric mean of all Q_B measurements within that discharge range was computed. The same approach as described above was used to compute $D_{max,QB}$ values for comparison between bedload traps and the HS sampler on plates and on the bed.

3. Results and Discussion

3.1 Inter-sampler comparison of bedload samples

An overall summary of results is presented in Section 4 of this paper. This section details the causes of HS sampler mismeasurement, and leads to recommendations regarding HS sampler use.

3.1.1 Gravel transport rates Q_B: At all five study sites, the HS sampler deployed on the bed over-estimated Q_B values obtained using the bedload traps by several orders of magnitude at low Q, and hence at low Q_B. But the HS values approached those from the bedload traps at high Q and Q_B (Figure 3). These observations mirror those made in the writers' earlier studies whenever the two samplers were deployed together (Figure 1a) (Bunte et al., 2004, 2008, 2009, 2010b). Compared to HS sampler deployment on the bed, setting the HS sampler on ground plates greatly decreased the degree by which Q_B was over-estimated to an order of magnitude or less (Figure 3). The physical border between the HS sampler and the bed provided by the plates prevented inadvertent pick-up of particles dislodged from the bed. Consequently, such inadvertent pick-up accounts for orders of magnitude of over-estimation by the HS sampler on a bed when gravel transport is low. At the highest flows, the two HS sampler deployments yielded similar results, because inadvertent particle capture from on-bed deployment contributes negligibly, if any, to the overall Q_B when transport is high.

With direct ground contact avoided, the HS sampler deployed for five minutes on the plates still over-estimated the bedload trap Q_B by up to an order of magnitude at low flows and somewhat less at high flows. This outcome is attributed to the effects of two opposing factors. The HS sampler's low sampling intensity (only 2% of the bedload trap sampling intensity) increases the chance that the sampler misses infrequent and dispersed spikes in transport rates. Therefore, taken by itself, low sampling intensity causes the HS sampler to under-estimate Q_B (Section 1.2.2). However, this effect is outweighed by the HS sampler's high hydraulic efficiency, which

funnels particles already traveling as bedload into the sampler, including particles that may be locally entrained by turbulence exerted onto the bed during sampler placement.

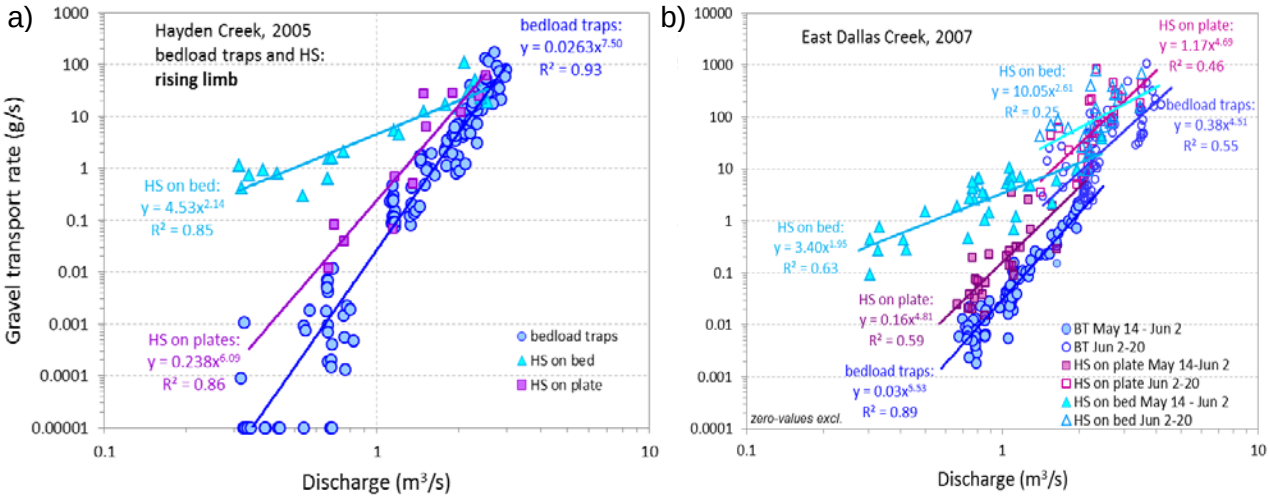

Figure 3. Comparison of gravel bedload transport rates Q_B collected with a HS sampler for 2 minutes on the bed, for 5 minutes on plates, and for about 60 minutes with bedload traps; Example from Hayden Creek, rising limb only, (a) and East Dallas Creek, segregated into the time periods before and after the large increase in sediment supply (a).

3.1.2 Flow competence $D_{max,QB}$: The HS sampler deployed directly on the bed over-estimated the $D_{max,QB}$ collected in bedload traps by about a factor of 3 when flow and gravel transport were low. By contrast, at the highest sampled flows, the on-bed deployment under-estimated $D_{max,QB}$, reaching only about 70% of the bedload trap $D_{max,QB}$ (Figure 4). Results from the five study sites mirror results from all sites where bedload traps and a HS sampler on bed were deployed together (Bunte et al., 2004, 2008, 2009, 2010b) (Figure 1b).

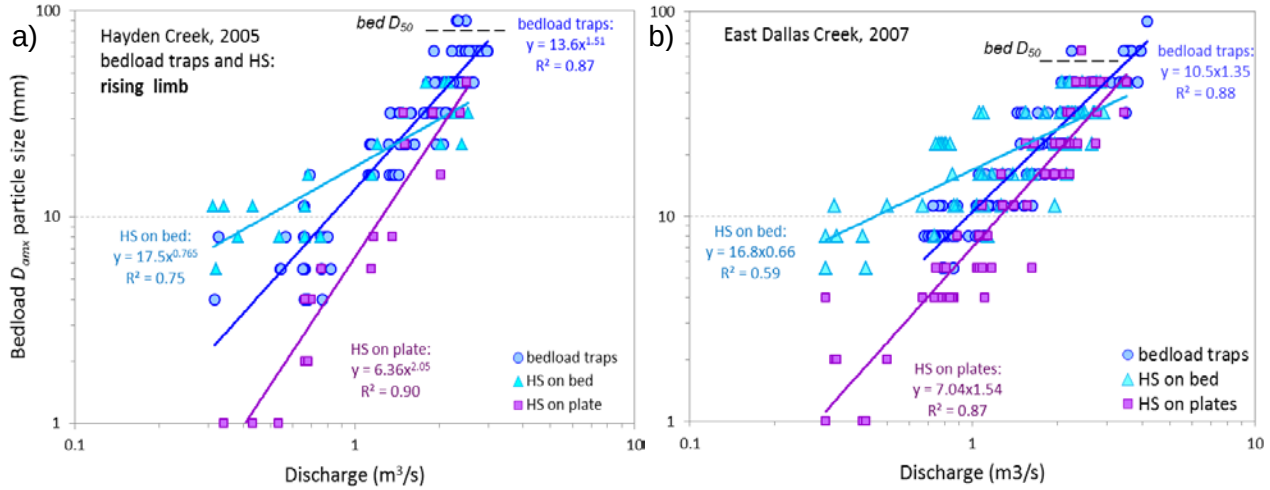

Figure 4. Comparison of gravel bedload $D_{max,QB}$ sizes collected for 2 min. with a HS sampler on bed, for 5 min. with a HS sampler on plates, and for ≅ 60 min. with bedload traps; Example from Hayden Cr., (a) and East Dallas Cr. (b).

At all flows, the HS sampler deployed for 5 minutes on plates collected $D_{max,QB}$ that were only 50-80% of the $D_{max,QB}$ collected in bedload traps (Figure 4). The smaller $D_{max,QB}$ can be attribut-

ed to the HS sampler's low sampling intensity I_s, i.e., the combined effects of the short sampling duration (1/12 of t_s) and sampler narrowness (¼ of w_s) compared to bedload traps. The HS sampler's sampling intensity amounted to only 0.8% of the bedload trap's I_s and greatly reduced the HS sampler's chance to collect the infrequently moving largest bedload particles.

Comparison of $D_{max,QB}$ obtained using the HS sampler deployed on bed and on plates revealed how much the inadvertent particle capture during on-bed deployment increases $D_{max,QB}$ when gravel transport is minimal. Sampling intensity I_s was similarly low for the HS sampler on the bed and on the plates (2% and 0.8%, respectively, of the bedload trap I_s) and decreased $D_{max,QB}$ sizes for both deployments. Hence, inadvertent particle pick-up from the bed during on-bed deployment caused an 8-9 fold increase in $D_{max,QB}$ compared to on-plate deployment, and therefore greatly over-estimated $D_{max,QB}$. At the highest flows, the two HS sampler deployments collected similar $D_{max,QB}$; any additional particle pick-up from the bed during on-bed deployment had negligible effects on sampled $D_{max,QB}$ when transport was high.

3.2 Effects of sampling duration on HS results

To isolate the effect of sampling duration on HS samples, the ratio of results from the HS sampler deployed on plates was compared to results from the bedload traps. The comparison was made between study sites where the HS sampler was deployed for 5 minutes or 2 minutes per plate. The HS sampler deployed for 5 minutes over-measured Q_B values obtained from the bedload traps by 4-10 times, but hardly at all when the HS was deployed for 2 minutes (Figure 5). By contrast, values of $D_{max,QB}$ collected during a 5-minute deployment were about half as large as those from the bedload traps, but only about a third as large when the HS sampler was deployed for 2 minutes. A sketch visually clarifies the observed patterns (Figure 6).

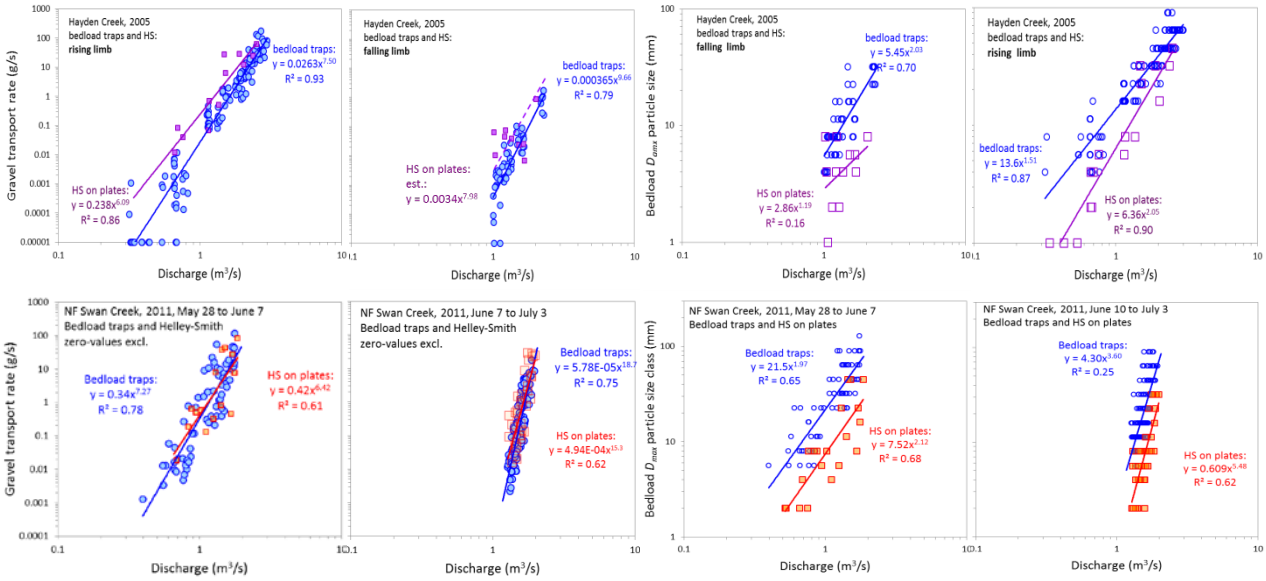

Figure 5. Gravel transport rates (Q_B) and bedload D_{max} sizes ($D_{max,QB}$) compared between bedload traps and a HS sampler deployed on plates for 5 minutes at Hayden Creek (top row) and for 2 minutes at NF Swan Creek (bottom row).

3.2.1 Effects on mismeasurements of gravel transport rates: While a decrease in sampling duration generally reduced Q_B (Section 1.2.2), this study showed that the magnitude of the time effect depends on the sampler's hydraulic efficiency. For bedload traps, a 30-fold

reduction in sampling duration from 60 to 2 minutes halved the Q_B estimate (Figure 2a). The time effect was much larger for the HS sampler deployed on plates: A 2.5-fold reduction in sampling duration from 5 to 2 minutes cut the sampled Q_B to a quarter or a fifth (Figure 6a). The time effect is so much larger for the HS sampler on plates (almost 30 times), because the shortened sampling duration not only reduced the chance of sampling the largest short-term fluctuations of Q_B but also cut the duration during which the HS sampler's high hydraulic efficiency was active and over-sampling bedload. The decrease in sampling duration from 5 to 2 minutes, and consequent decrease in Q_B, almost offset the HS sampler's over-sampling due to its high hydraulic efficiency. Coincidentally, therefore, a sampling duration of slightly under 2 minutes produced a nearly accurate estimate of Q_B from a HS sampler deployed on plates.

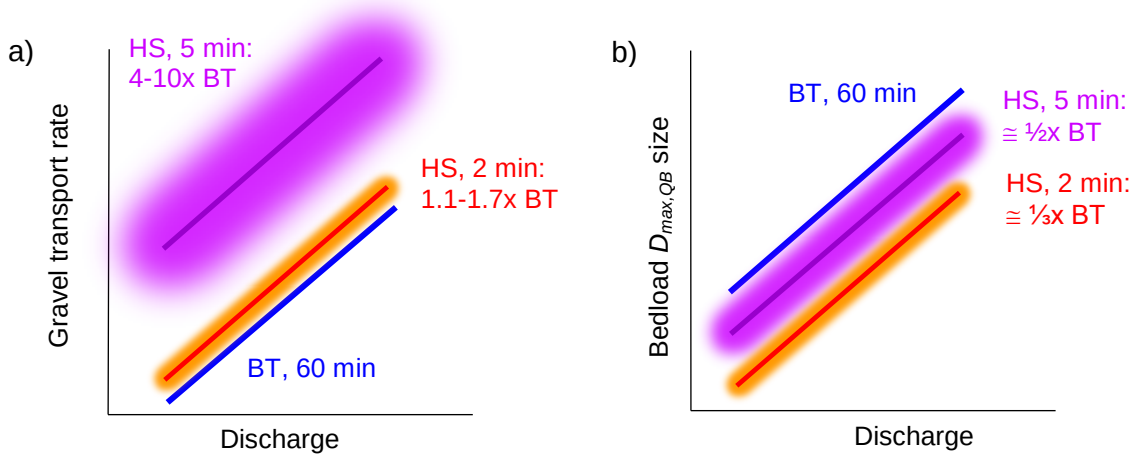

Figure 6. General patterns of difference in sampling results from bedload traps (BT) and a HS sampler deployed on plates for 5 and for 2 minutes: Over-sampling of Q_B (a) and under-sampling of $D_{max,QB}$ (b). The lines' fuzziness reflects variability in the observed sampling results.

3.2.1 Effects on mismeasurement of bedload D_{max} sizes: A decrease in sampling duration likewise reduced $D_{max,QB}$. For bedload traps, a 30-fold reduction in sampling duration from 60 to 2 minutes resulted in roughly halving $D_{max,QB}$ (Figure 2b). Again, the effect is stronger (about 10 times) for a HS sampler deployed on plates: a 2.5 fold reduction in sampling duration from 5 to 2 minutes reduced the sampled $D_{max,QB}$ to about a third of the sizes collected in bedload traps (Figure 6b). A reduction that is larger for Q_B than $D_{max,QB}$ indicates that in an on-plate deployment, the HS sampler's high hydraulic efficiency acts much more on Q_B than on $D_{max,QB}$. Conceivably, a time effect that is greater on Q_B than on $D_{max,QB}$ could also indicate that bedload D_{max} particle sizes fluctuate less over time than do transport rates, but details are not known on this subject.

A 2-minute sampling duration for a HS sampler deployed on plates lead to almost accurate measurement of Q_B, because the over-sampling effects of the HS sampler's high hydraulic efficiency was offset by the under-sampling effect of a short sampling duration (Figure 6). However, the 2-minute sampling duration under-sampled $D_{max,QB}$ more strongly than did the 5-minute duration. To see if there is a suitable sampling duration for accurate measurement of both Q_B and $D_{max,QB}$, the magnitudes of mismeasurements of Q_B and $D_{max,QB}$ (i.e., the ratios of sampling results HS on plate vs. traps) were plotted against deployment duration. Trend lines fitted to scattered data suggest that an approximately 1.5-minute duration provides the most accurate results for measuring gravel Q_B with a HS sampler on ground plates (Figure 7), whereas a sampling durations of more than 40 minutes per plate would be needed to accurately sample

$D_{max,QB}$. This finding indicates that deployment of the HS sampler on ground plates diminishes the problem of over-sampling Q_B, but does not lead to accurate measurements of $D_{max,QB}$. Therefore, no single HS deployment duration can produce accurate estimates of both Q_B and $D_{max,QB}$. Depending on whether a study focuses on accurately measuring Q_B or $D_{max,QB}$, either a short or a long sampling duration needs to be selected for a HS sampler deployed on ground plates.

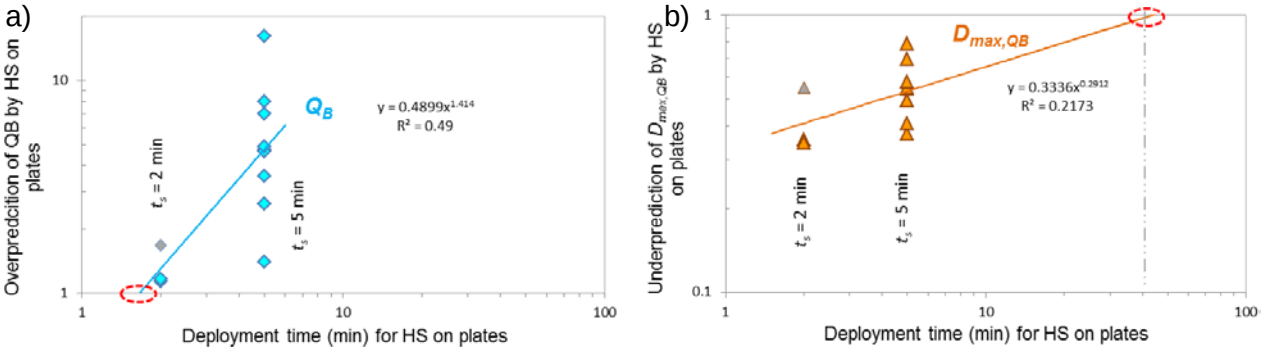

Figure 7. Effect of sampling duration on the degree of over-sampling gravel bedload transport rates (a) and under-sampling gravel bedload $D_{max,QB}$ sizes (b). Accurate sampling result would be obtained for an ordinate value of 1.

3.3 Ambient gravel transport rates and particle sizes affect mismeasurements of Q_B and $D_{max,QB}$ by HS sampler on plates

Comparison of results from bedload trap with those from a HS sampler placed on the bed showed that Q_B and $D_{max,QB}$ were most over-estimated when Q and Q_B were lowest (Figure 1a; Figure 3), mainly due to inadvertent particle pick-up from the bed. The question arises whether the magnitude of ambient Q_B and $D_{max,QB}$ still affect mismeasurement when inadvertent particle pick-up is prevented by deploying the HS sampler on ground plates. Figure 3 and Figure 4 do not give a definitive answer. Hence, the effects of ambient Q_B were analyzed by plotting for each site the extents to which the HS sampler on plate overpredicted the Q_B and underpredicted $D_{max,QB}$ measurements made using the bedload traps (Figure 8).

3.3.1 Effects on mismeasurement of gravel transport rates: As with a HS sampler on the bed, ambient gravel transport rates were found to affect sampling results from the HS sampler on plates. At sites where gravel transport was low (0.0001 g/m·s is just above incipient motion of 4-mm particles), the HS sampler on plates overpredicted Q_B almost 10-fold (Figure 8a), but only 2-3 fold when transport was high (1 to 10 g/m·s). The fineness of bedload sizes—i.e., small ambient $D_{max,QB}$ sizes—also exacerbated the over-estimation of Q_B by the HS sampler on plates (Figure 8, top right). The findings are attributed to the HS sampler's high hydraulic efficiency which causes the streamlines entering a HS sampler to originate from an area larger than the sampler entrance. Streamlines funnel fine gravel moving at low transport into the sampler entrance, but this effect diminishes rapidly as gravel bedload sizes increase during moderate or high rates of transport.

Overall, the study results indicate that inadvertent particle pick-up by a HS sampler deployed on the bed accounts for the vast majority of the over-estimation of Q_B when ambient transport is low and fine-grained. Additionally, the sampler's high hydraulic efficiency causes Q_B to be over-estimated 4-10 fold when transport is low and fine-grained; and, about 2 fold when transport is moderately high (1-10 g/m·s) and comprises gravel larger than about 16 mm. The much lesser

degree of over-estimation of Q_B when sampling duration is short (2 minutes vs. 5 minutes) underscores the prominent influence of high hydraulic efficiency on over-sampling Q_B.

Extrapolation of the fitted trend in Figure 8a suggests that over-estimation of Q_B by the HS sampler deployed for 5 minutes on plates turns into under-estimation once gravel transport exceeds 100 g/m·s, a rate that is very high for Rocky Mountain streams and associated with gravel streaming over the bed at flows notably above $Q_{1.5}$. A shift to under-estimation of Q_B by a HS

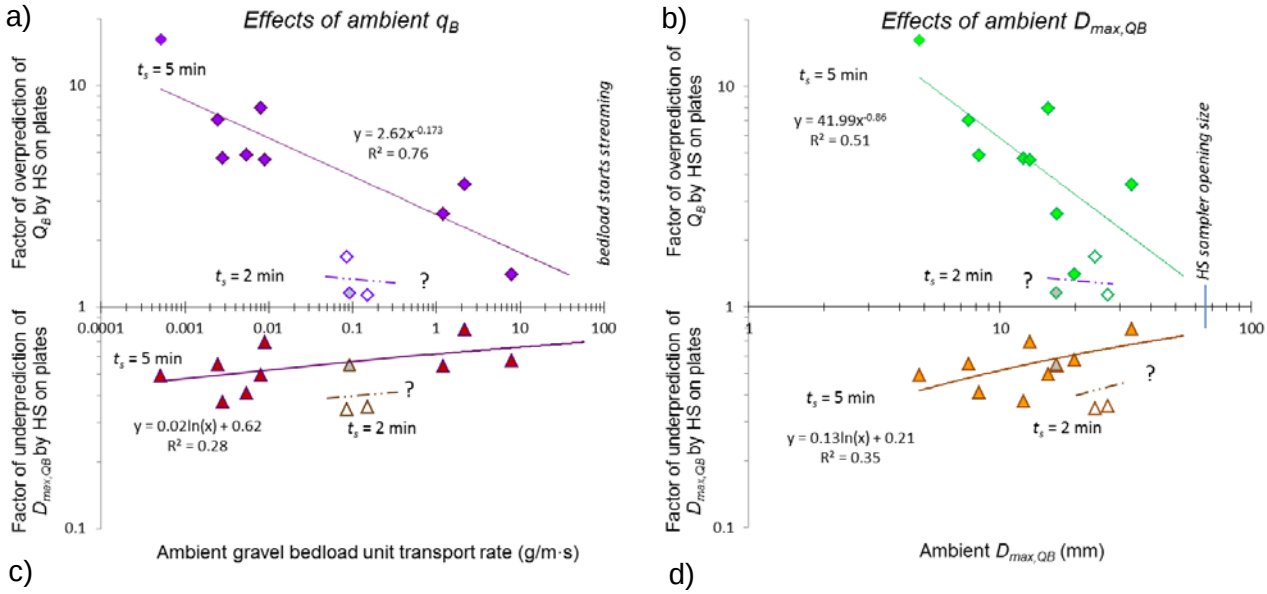

Figure 8. Effects of ambient gravel transport rates (a, c) and ambient bedload sizes (b, d) (both sampled with bedload traps) on the factor of over-sampling and under-sampling by HS sampler deployed on ground plates for 5 and for 2 minutes. The gray-fill data points refer to a BL-84 sampler. Trends for 2-minute samples are estimated. The fact that 2-minute, on-plate deployment of a HS and similarly-sized but a less-flared BL-84 sampler have quite similar results suggests that once direct ground contact is eliminated and sampling duration is short, differences in hydraulic efficiency play a much smaller role.

sampler on plates at high Q_B is attributable to the relatively narrow (76 mm) sampler width that slows gravel particles rolling over each other into the opening and prevents large gravels and cobbles from entering the sampler. Consequently, a HS sampler deployed for 5 minutes per plate has the highest probability of accurately sampling gravel transport when transport rates are high (around 100 g/m·s), but only for medium or finer gravel. Similarly, over-estimation of Q_B turns into under-estimation for coarse gravel, i.e., for sizes that cannot straightforwardly enter the 76-mm wide HS ampler opening (Figure 8b).

3.3.2 Effects on mismeasurement of bedload D_{max} sizes: The under-estimation of $D_{max,QB}$ by the HS sampler on plates was not much affected by ambient gravel transport that was low and fined-grained (Figure 8c and d). Deployment on ground plates effectively prevents inadvertent pick-up of overly large $D_{max,QB}$ from the bed. The HS sampler's high hydraulic efficiency is still active and catching *more* bedload particles by including those particles traveling on a path adjacent to the sampler entrance, but not including *larger* particles. With the influences of inadvertent particle pick-up and high hydraulic efficiency on $D_{max,QB}$ neutralized for the HS sampler deployed on plates, $D_{max,QB}$ is generally under-estimated, because a sampling duration much longer than 5 minutes—probably more than 40 minutes—is needed to accurately collect infrequently moving large particles.

4. Conclusions and Recommendations

Comparison of measurements obtained using three sampler deployments: a HS sampler placed directly on the bed and on the bedload trap ground plates, and bedload traps, explains why a HS sampler over-measures Q_B and under-measures bedload $D_{max,QB}$ size. The following specific conclusions are drawn from the comparison:

- **HS sampler's direct bed contact causes huge over-estimation.** Inadvertent capture of bed and bedload particles from a HS sampler deployed directly on the bed accounts for orders of magnitude of over-estimation of Q_B and up to an order of magnitude over-estimation of $D_{max,QB}$ when the rate of gravel transport is low.

- **A HS sampler attains only low sampling intensity.** Sampling intensity for a 76-mm wide HS sampler deployed for 2 or 5 minutes per ground plate amounts to only 1-2% of the bedload trap sampling intensity. Together, brief sampling duration and narrow width cause a HS sampler to miss infrequently moving large particles and short-term spikes in transport rates.

- **HS generally over-samples Q_B: High hydraulic efficiency outweighs low sampling intensity.** Despite its low sampling intensity, a HS sampler deployed on plates still over-estimates Q_B, because the over-sampling effect of the sampler's high hydraulic efficiency outweighs the under-sampling effects of low sampling intensity.

- **Shifting deployment from the bed to ground plates: over-sampling $D_{max,QB}$ turns into under-sampling.** Once over-sampling of $D_{max,QB}$ from inadvertent pick-up of bed particles is prevented by setting the HS sampler on to ground plates, the HS sampler under-estimates $D_{max,QB}$: Owing to its low sampling intensity, the HS sampler collected $D_{max,QB}$ sizes of only 50-80% of the gravel sizes collected in bedload traps.

- **Shortening sampling duration worse for HS sampler than bedload traps.** Shortening the sampling duration affects HS samples more than bedload trap samples, because sampling briefly limits the duration during which the HS sampler's high hydraulic efficiency can be active and over-sampling bedload.

- **Sampled Q_B more sensitive than $D_{max,QB}$ to shortened sampling duration.** Shortening sampling duration for a HS sampler on plates reduces measured Q_B more than measured $D_{max,QB}$, because limiting the duration of high hydraulic efficiency affects sampled Q_B more strongly than sampled $D_{max,QB}$.

- **Different sampling duration needed for measuring Q_B and $D_{max,QB}$.** A 2-minute deployment of a HS sampler on plates leads to almost accurate estimates of Q_B, because over-sampling due to high hydraulic efficiency is offset by the under-sampling due to short sampling duration. However, a 2-minute deployment is insufficient for quantifying $D_{max,QB}$; More than 40-minute deployment per plate would be needed to accurately sample $D_{max,QB}$ for gravel bedload.

- **Over-sampling Q_B controlled by ambient transport intensity.** A HS sampler deployed for 5 minutes on plates over-estimates Q_B most severely when ambient Q_B and $D_{max,QB}$ are small, because the HS sampler's high hydraulic efficiency, which gathers streamlines from an area larger than the sampler entrance, acts more on fine gravel rather than on coarse gravel bedload. A HS sampler measures Q_B almost accurately when transport approaches 100 g/m·s and involves medium or finer gravel. At higher transport rates and

when coarse gravel or small cobbles are mobile, the narrow width of a HS sampler slows down *en mass* gravel advancement into the opening and prevents coarse particles from entering the sampler and contributing to the sample.

- **Under-sampling of $D_{max,QB}$ barely touched by ambient transport.** Ambient gravel transport does not significantly affect the under-sampling of $D_{max,QB}$ by the HS sampler on a plate. The HS sampler's high hydraulic efficiency mainly acts to catch *more*, but not *larger*, gravel particles.

Recommendations A HS sampler should be deployed on ground plates (or equivalent) in order to prevent inadvertent particle capture that typically occurs when deploying a HS sampler directly on the bed. Deployment on plates is especially important when sampling at low Q_B, but deployment without plates can yield acceptable results when gravel transport rates are high.

Even when deployed on ground plates, a HS sampler should only be used when ambient transport rates are at least moderately high (about 1-100 g/m·s), but not at very low Q_B, and also not when bedload is streaming over the bed or comprises ample coarse gravel.

Sampling duration needs to be adjusted depending on whether the study focus is on accurately measuring Q_B or $D_{max,QB}$. A 1-2 minute sampling duration for a HS deployed on plates during moderate rates of transport yields roughly accurate samples of Q_B, but sampling for more than 40 minutes is needed to accurately collect bedload $D_{max,QB}$ sizes.

Results reported here apply likewise to other pressure-difference samplers (such as the 0.152-by 0.152 m HS sampler, the Toutle River II, the Elwha, and the BL-84 samplers), but the degree of mismeasurement, and how mismeasurements scale with ambient Q_B and sampling duration, depend on the samplers' entrance width and hydraulic efficiencies (e.g., Hubbell et al., 1987; Bunte et al., 2017) which increase with sampler size and flare ratio. Mismeasurements also depend on the sampling intensities attained during deployment and the sampler's sampling efficiencies (Pitlick, 1988; Gray et al., 1991; Ryan and Porth, 1999). Considering the large contribution of hydraulic efficiency to over-sampling Q_B, it may be advisable to use a BL-84 sampler on plates rather than the 3-by-3 inch HS sampler to more accurately determine transport rates for fine and medium gravel bedload.

Acknowledgement We would like to express our thanks to the National Stream and Aquatic Ecology Center (formerly Stream Systems Technology Center) of the U.S.D.A. Forest Service, who funded the many years of field data collection as well as this study.

5. References

Bunte, K., Abt, S.R., Potyondy, J.P., and Ryan, S.E. 2004. "Measurement of coarse gravel and cobble transport using a portable bedload trap," J. Hydraulic Engineering 130(9): 879-893.

Bunte, K. and Abt, S.R. 2005. "Effect of sampling time on measured gravel bed load transport rates in a coarse-bedded stream," Water Resources Research, 41, W11405, doi:10.1029/2004WR003880.

Bunte, K., Abt, S.R., Potyondy, J.P., and Swingle, K.W. 2008. "A comparison of coarse bedload transport measured with bedload traps and Helley-Smith samplers," Geodinamica Acta 21(1/2): 53-66.

Bunte, K., Swingle, K.W., and Abt, S.R. 2007. "Guidelines for using bedload traps in coarse-bedded mountain streams: Construction, installation, operation, and sample processing,"

General Technical Report, RMRS-GTR-191, Fort Collins, CO, U.S.D.A. Forest Service, Rocky Mountain Research Station, 91 pp.

Bunte, K. and Abt, S.R. 2009. "Transport relationships between bedload traps and a 3-inch Helley-Smith sampler in coarse gravel-bed streams and development of adjustment functions," Report submitted to the Federal Interagency Sedimentation Project, Vicksburg, MS, 138 pp. Completion Report 218, Colorado Water Institute, Colorado State University, Fort Collins, CO.

Bunte, K. 2010. "Measurements of gravel transport using the magnetic tracer technique: temporal variability over a highflow season and signal calibration," In: Gray, J.R., Laronne, J.B., and Marr, J.D.G, Bedload-surrogate monitoring technologies: U.S. Geological Survey Scientific Investigations Report 2010-5091, 85-106.

Bunte, K., Swingle, K.W., and Abt, S.R. 2010a. "Necessity and difficulties of field calibration of signals from surrogate techniques in gravel-bed streams: possibilities for bedload trap samples." In: Gray, J.R., Laronne, J.B., and Marr, J.D.G, Bedload-surrogate monitoring technologies: U.S. Geological Survey Scientific Investigations Report 2010-5091, 107-129.

Bunte, K., Abt, S.R., Swingle, K.W., and Potyondy, J.P. 2010b. "Functions to adjust transport rates from a Helley-Smith sampler to bedload traps in coarse gravel-bed streams (rating curve approach)," In: Proceedings of papers presented at the 4th Federal Interagency Hydrologic Modeling Conference and the 9th Federal Interagency Sedimentation Conference Las Vegas, NV, June 27 – July 1, 2010, Session: Fluvial Geomorphology. CD-ROM ISBN 978-0-9779007-3-2.

Bunte, K., Swingle, K.W., Abt, S.R., and Cenderelli, D.A. 2015. "Effect of bedload sampler netting properties on hydraulic and sampling efficiency," In: Proceedings of the 3rd Joint Federal Interagency Conference on Sedimentation and Hydrologic Modeling, April 19-23, 2015, Reno, Nevada, USA, p. 1869-1880.

Bunte, K., Klema, M., Hogan, M., and Thornton, C. 2017. "Testing the Hydraulic Efficiency of Pressure Difference Samplers While Varying Mesh Size and Type," Report submitted to the Technical Committee of the Federal Interagency Sedimentation Project, 116 pp., April 2017.

Camenen, B., Jaballah, M., Geay,T., Belleudy, M., Laronne, J.B., and Laskowski, J.P. 2012. "Tentative measurements of bedload transport in an energetic alpine gravel bed river," River Flow 2012. Murillo (Ed.) Taylor & Francis Group, London, ISBN 978-0-415-62129-8.

De Vries, M. 1979. "Information on the Arnhem Sampler (BTMA)," Internal Report No. 3-79, Delft University of Technology. Department of Civil Engineering, Fluid Mechanics Group.

Emmett, W.W. 1980. "A Field Calibration of the Sediment Trapping Characteristics of the Helley-Smith Bedload Sampler," Geol. Surv. Prof. Paper 1139, Washington, DC.

Emmett, W.W., Burrows, R.L., and Chacho, E.F. 1996. "Coarse-particle transport in a gravel-bed river," International Journal of Sediment Research 11 (2):8-21.

Fienberg, K., Singh, A., Foufoula-Georgiou, E., Jerolmack, D.J., and Marr, J.D.G. 2010. "A theoretical framework for interpreting and quantifying the sampled time dependence in gravel bedload transport rates," U.S.G.S. Scientific Investigations Report 2010-5091, p. 171-184.

Gottesfeld, A.S. and Tunnicliffe, J. 2003. "Bed load measurements with a passive magnetic induction device," In: Erosion and Sediment Transport Measurement in Rivers: Technological and Methodological Advances. J. Bogen, T. Fergus and D.E. Walling (eds.), IAHS-Publication No. 283, p. 211-221.

Gray, J.R., Webb R.H., and Hyndman, D.W. 1991. "Low-flow sediment transport in the Colorado River," Proc. Fifth Federal Interagency Sedimentation Conference, March 18-21, 1991, Las Vegas, Nev., p. 4.63-4.71.

Helley, E.J. and Smith, D.W. 1971. "Development and calibration of a pressure-difference bedload sampler," U.S. Geol. Survey, Water Resources Division, Open File Report, Menlo Park, California, 18pp.

Hinton, D., Hotchkiss, R., and Ames, D.P. 2017. "Comprehensive and quality-controlled bedload transport database," J. Hydraul. Eng., 2017, 143(2): 06016024.

Hubbell, D.W. 1987. "Bed load sampling and Analysis," In: Sediment Transport in Gravel-Bed Rivers. C.R. Thorne, J.C. Bathurst and R.D. Hey (eds.), John Wiley, Chichester, p. 89-118.

Hubbell, D.W. and Stevens Jr., H.H. 1986. "Factors affecting accuracy of bedload sampling," Proc. Fourth Federal Interagency Sedimentation Conference, Las Vegas, Nevada. Vol. I., p. 4.20-4.29.

Leopold, L.B. and Emmett, W.W. 1976. "Bedload measurements, East Fork River, Wyoming," Proc. National Academy of Sciences, USA, 73(4): 1000-1004.

Leopold, L. B. and Emmett, W.W. 1977. "1976 bedload measurements, East Fork River, Wyoming," Proc. National Academy of Sciences, USA, 74(7): 2644-2648.

King, J.G., Emmett, W.W., Whiting, P.J., Kenworthy, R.P., and Barry, J.J. 2004. "Sediment transport data and related Information for Selected Coarse-Bed Streams and Rivers in Idaho," U.S.D.A. Forest Service, Rocky Mountain Research Station, General Technical Report RMRS-GTR 131, 26 pp.

Pitlick, J.C. 1988. "Variability of bed load measurement," Water Resources Research 24(1): 173-177.

Rickenmann, D. 2018. "Variability of bed load transport during six summers of continuous measurements in two Austrian mountain streams (Fischbach and Ruetz)," Water Resources Research, 54, 107–131. doi.org/10.1002/2017WR021376

Rickenmann, D., Turowski, J.M., Fritschi, B., Klaiber, A., and Andreas, L. 2012. "Bedload transport measurements at the Erlenbach stream with geophones and automated basket samplers," Earth Surf. Process. Landforms, 37(9); 1000-1011, DOI: 10.1002/esp.3225

Ryan, S.E. and Porth, L.S. 1999. "A field comparison of three pressure-difference bedload samplers," Geomorphology 30: 307-322.

Singh, A., Fienberg, K. Jerolmack, D.J., Marr, J., and Foufoula-Georgiou, E. 2009. "Experimental evidence for statistical scaling and intermittency in sediment transport rates," J. Geophysical Research 114, F01025,doi:10.1029/2007JF000963.

Tunnicliffe, J., Gottesfeld, A.S., and Mohamed, M. 2000. "High resolution measurements of bedload transport," Hydrological Processes 14: 2631-2643.

Williams, G.P. and Rosgen, D.L. 1989. "Measured total sediment loads (suspended loads and bedloads) for 93 United States streams," U.S. Geol. Survey, Open-File Report 89-67, Denver, Colorado, 128pp.

Comparability of Different River Suspended Sediment Sampling and Laboratory Analysis Methods and the Effect of Sand

Joel Groten, Hydrologist, U.S. Geological Survey, St. Paul, MN, jgroten@usgs.gov
Gregory Johnson, Hydrologist, MPCA, St. Paul, MN, gregory.johnson@state.mn.us

Abstract

Accurate measurements of suspended sediment, a leading water-quality impairment in many rivers, are important for managing and protecting water resources; however, water quality standards for suspended sediment in Minnesota are based on grab field sampling and total suspended solids (TSS) laboratory analysis methods. These methods have underrepresented concentrations of suspended sediment in rivers compared to U.S. Geological Survey equal-width increment or equal-discharge-increment (EWDI) field sampling and suspended-sediment concentration (SSC) laboratory analysis methods. Because of this underrepresentation, the U.S. Geological Survey, in collaboration with the Minnesota Pollution Control Agency, collected concurrent grab and EWDI samples at eight sites to compare results obtained using different combinations of field sampling and laboratory analysis methods.

Study results determined that grab field sampling and TSS laboratory analysis results were biased substantially low compared to EWDI sampling and SSC laboratory analysis results, respectively. Differences in both field sampling and laboratory analysis methods caused grab and TSS methods to be biased substantially low. The difference in laboratory analysis methods was slightly greater than field sampling methods.

Sand-sized particles had a strong effect on the comparability of the field sampling and laboratory analysis methods. These results indicated that grab field sampling and TSS laboratory analysis methods fail to capture most of the sand being transported by the stream. The results indicate there is less of a difference among samples collected with grab field sampling and analyzed for TSS and concentration of fines in SSC. Even though differences are present, the presence of strong correlations between SSC and TSS concentrations provides the opportunity to develop site specific relations to address transport processes not captured by grab field sampling and TSS laboratory analysis methods.

Introduction

Excess suspended sediment can impair rivers by adversely affecting aquatic habitat, degrading water quality, transporting harmful contaminants, diminishing recreational opportunities, and depositing sediment in navigable waterways (U.S. Army Corps of Engineers, 2006; Minnesota Pollution Control Agency [MPCA], 2009). Reliable, consistent suspended-sediment data are imperative to address remediation efforts of river sediment impairments. Currently (2019), the U.S. Environmental Protection Agency and many State water-quality agencies use surface grab samples and the total suspended solids (TSS) laboratory analysis method to compare stream conditions to water-quality standards for suspended sediment (Pat Baskfield, MPCA, oral commun., May 22, 2017). However, previous studies indicated that estimates of suspended

sediment obtained using these protocols substantially underestimated suspended sediment compared to standard U.S. Geological Survey (USGS) equal-width-increment or equal-discharge-increment (EWDI) and suspended-sediment concentration (SSC) laboratory analysis methods (Gray and others, 2000; Ellison and others, 2014). Because previous studies compared data obtained using several protocols that included different field sampling, the same field sampling and subsampling by use of a churn or cone splitter, and different laboratory analysis methods, the exact cause of observed differences could not be determined; therefore, the USGS, in collaboration with the MPCA, completed a study designed using multiple combinations of field sampling and laboratory analysis methods to evaluate how differences in these methods affect suspended sediment results.

Grab samples are typically collected in the centroid of a stream channel, within 1 meter of the water surface. Conversely, water samples collected by USGS methods are collected and composited from multiple locations across the stream using isokinetic samplers and depth-and-width-integration methods, as described by Ward and Harr (1990), Edwards and Glysson (1999), and Davis and the Federal Interagency Sedimentation Project (2005). The use of these data collection methods provides a vertically and laterally discharge-weighted composite sample that is intended to be representative of the entire flow passing through the cross section of a stream.

The TSS laboratory analysis method is commonly used in conjunction with a grab sample. For the TSS laboratory analysis method, a subsample of the original water sample is extracted and filtered to measure the amount of suspended material (Clesceri and others, 1998); however, according to Gray and others (2000), the subsample may not be representative of the whole water sample. Furthermore, if suspended sediment is not homogenous throughout the stream channel, the grab sample likely will not accurately represent the suspended sediment present in the entire stream channel.

In contrast, the SSC laboratory analysis method used by the USGS measures the whole water sample containing the entire amount of suspended material in the original sample (Guy, 1969; American Society for Testing and Material [ASTM], 2000; USGS, variously dated). A study comparing TSS and SSC in Minnesota streams indicated that TSS underestimated SSC median values by about 50 percent (Ellison and others, 2014). In addition, Gray and others (2000) indicated that negative biases in TSS results compared to SSC results are exacerbated when samples consist of more than 25 percent sand-sized particles (Gray and others, 2000). Therefore, additional information is needed to determine the causes and magnitudes of differences between TSS and SSC.

Purpose and Scope

The purpose of this report is to summarize and interpret river suspended-sediment data collected using different field sampling methods (grab and EWDI) and analyzed using different laboratory methods (TSS, SSC, and particle sizes) during water year (WY) 2016 at eight selected sediment monitoring sites (Figure 1) in Minnesota. Specifically, the report (1) quantifies the variation among different combinations of field sampling and laboratory analysis methods, (2) describes the effects of sand-sized particles on field sampling and laboratory analysis methods, and (3) develops relations between field sampling and laboratory analysis methods. A water year is the 12-month period October 1 through September 30 designated by the calendar year in which it ends.

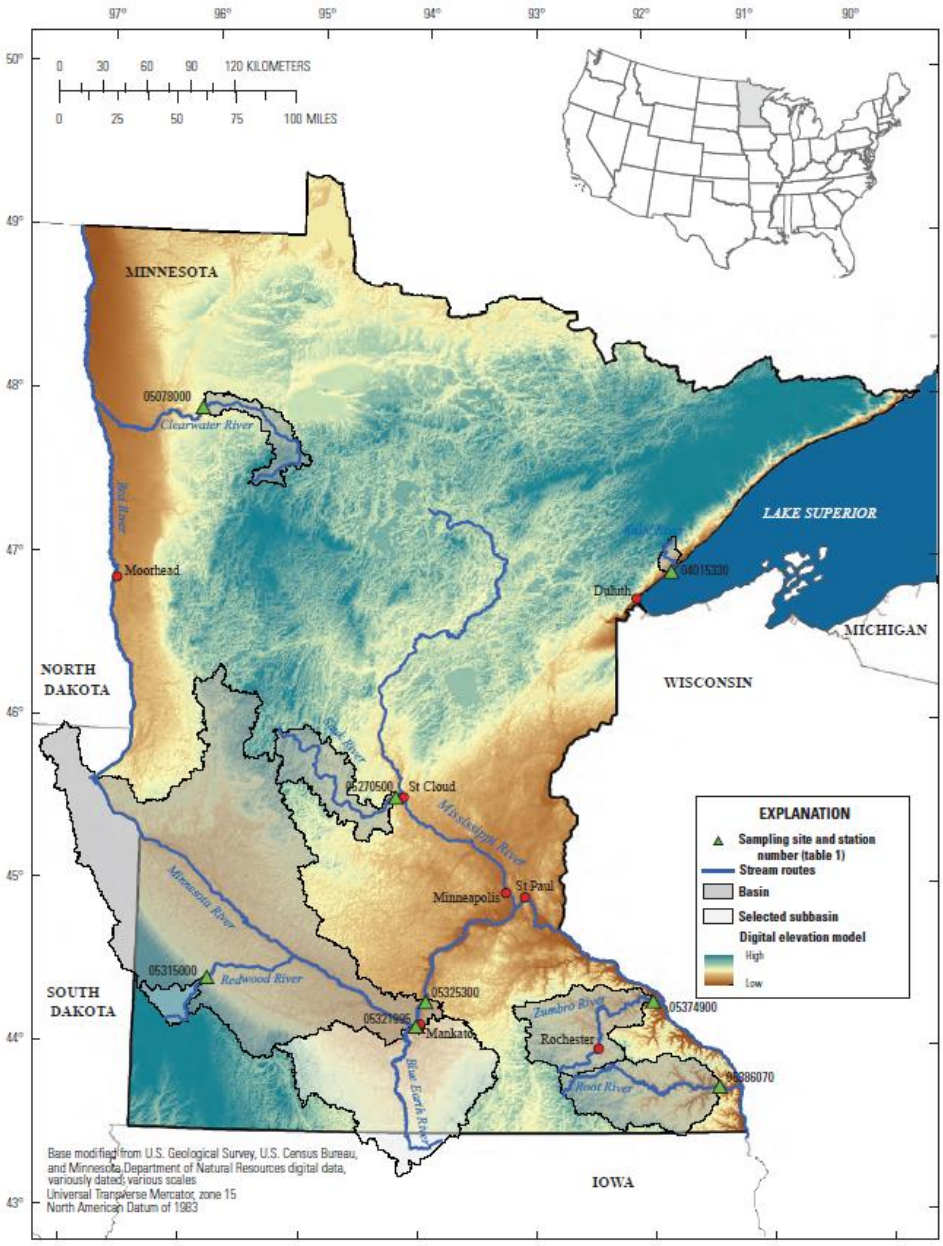

Figure 1. Selected sediment monitoring sites, contributing basins, and hillshade of the landscape relief in Minnesota.

Description of the Study Area

The eight sediment monitoring sites selected for this study represent different basins (Figure 1) in Minnesota. Sediment monitoring sites were collocated at either USGS streamgages, available at https://waterdata.usgs.gov/nwis (USGS, 2019), or the Minnesota Department of Natural Resources (MNDNR) and MPCA cooperative streamgages, available at http://www.dnr.state.mn.us/waters/csg/index.html (MNDNR, 2019).

Methods of Data Collection and Analysis

Water samples were collected for analyses of TSS, SSC, and particle sizes at eight sediment monitoring sites (Figure 1) in WY 2016. All samples were collected during the open-water season (March 1 through September 30). SSC samples were collected over a wide range of streamflow conditions (USGS, 2019; MNDNR, 2019).

The differences attributable to field sampling methods can be determined by concurrently collecting water samples with grab and EWDI field sampling methods and analyzing those two samples with the same laboratory analysis method (SSC or TSS). This isolated the differences caused by field sampling methods. Conversely, differences in laboratory analysis methods were determined by comparing the concurrent water samples that were collected with the same field sampling method (EWDI or grab) and analyzing one sample for TSS and one sample for SSC. This isolated the difference caused by laboratory analysis methods.

Field Sampling Methods

Water samples were collected concurrently using grab and isokinetic, EWDI sampling methods (Edwards and Glysson, 1999) to provide four samples at each sampling visit. Four samples were collected at each sediment monitoring site consisting of two concurrent grab samples and two concurrent EWDI samples.

Grab Field Sampling: A grab sample was collected using a 1-liter high-density polyethylene bottle secured inside of a weighted-bottle sampler (US WBH–96, Rickly Hydrological Co., Inc., Columbus, Ohio; Any use of trade, firm, or product names is for descriptive purposes only and does not imply endorsement by the U.S. Government). The grab sample was collected from the centroid of the river channel at a depth less than 1 meter below the water surface. Two grab samples were collected concurrently at the beginning of EWDI field sampling.

Equal-Width-Increment or Equal-Discharge Increment Field Sampling: Isokinetic and depth-integrated samples were collected at EWDIs (Edwards and Glysson, 1999). Most of the samples were collected using the equal-width-increment field sampling method (Edwards and Glysson, 1999). At each sample point, two separate samples were collected concurrently. Concurrent field sampling was done at each vertical throughout the stream cross section.

Laboratory Analysis Methods

The environmental laboratory at the Minnesota Department of Health (MDH) in Saint Paul, Minnesota, and the USGS Sediment Laboratory in Iowa City, Iowa, were used to analyze collected samples. The two laboratory analysis methods were TSS and SSC.

Total Suspended Solids Laboratory Analysis Method: TSS was analyzed at two laboratories. One grab sample from each sampling event was sent to the MDH Environmental Laboratory and analyzed for TSS following method 2540 D (Clesceri and others, 1998) to determine the concentration of each sample. One EWDI from each sampling event was sent to the USGS Sediment Laboratory and analyzed for TSS following the same method (Julie Nason, USGS, oral commun., May 22, 2016).

Suspended-Sediment Concentration Laboratory Analysis Method: One grab and one EWDI sample from each sampling event were analyzed for SSC following method D3977–97 (Guy, 1969; ASTM, 2000) by the USGS Sediment Laboratory. The percentage of fines (particle sizes less than 0.0625 millimeter [mm]) also was determined for each SSC sample (Guy, 1969) at the same laboratory.

Data Analysis

Field sampling and laboratory analysis method abbreviations will be combined in the following sections of the report to describe the combined field sampling and laboratory analysis methods used for each value or group of values; for example, the field sampling method abbreviation (Grab or EWDI) describes a sample collected in the field by grab or EWDI sampling methods and will come first, followed by an en dash (–), and followed by the laboratory analysis method abbreviation (TSS or SSC), which describes the laboratory analysis method used. EWDI–SSC was considered the most representative field sampling and laboratory analysis method combination, so it was the reference value from which a result obtained from any other method would be compared.

Data analyses included the computation of summary statistics, Wilcoxon signed-rank test (Helsel and Hirsch, 2002), simple linear regression (SLR) analysis, and percent difference (PD; Ellison and others, 2014). Data used in analyses are presented in Table 2 of Groten and Johnson (2018); data also are available at https://waterdata.usgs.gov/nwis (U.S. Geological Survey, 2019) and at https://www.pca.state.mn.us/environmental-data (MPCA, 2019).

Data were normalized with a logarithm transformation (base-10 logarithms) to reduce heteroscedasticity and skewness of the residuals and meet SLR model assumptions (Helsel and Hirsch, 2002). PD provides a measure of the difference between two values when one value is assumed to be more representative of the true value.

Field Sampling and Laboratory Analysis Method Comparison

The study design allowed five sets of comparisons between field sampling and laboratory analysis method combinations. The comparison of EWDI–SSC to Grab–TSS represents the USGS and MPCA field sampling and laboratory analysis methods, respectively. This comparison has been described by Gray and others (2000) and Ellison and others (2014). The two field sampling method comparisons were EWDI–SSC to Grab–SSC and EWDI–TSS to Grab–TSS. The two comparisons for laboratory analysis methods were Grab– SSC to Grab–TSS and EWDI–SSC to EWDI–TSS. Visualizations of the field sampling and laboratory analysis method comparisons used in the following sections are shown in Figure 2.

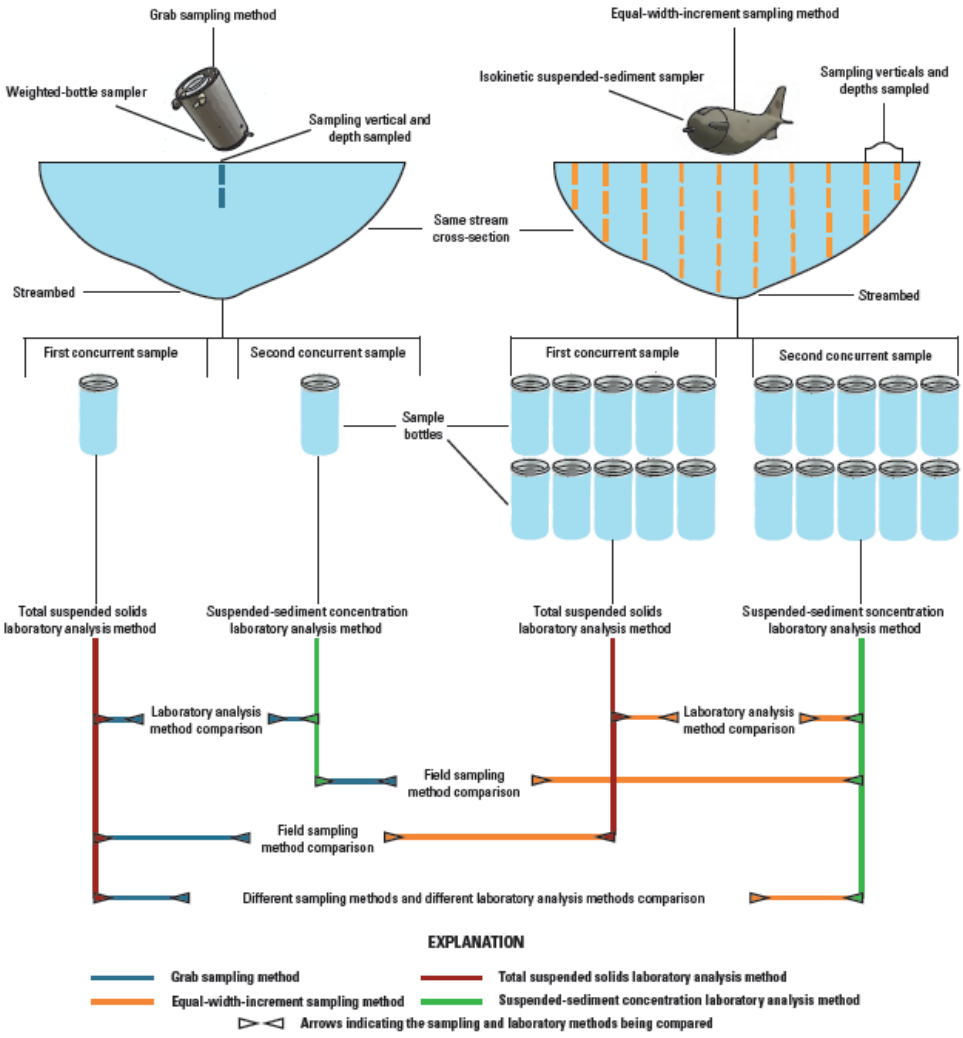

Figure 2. Infographic demonstrating five combinations of field sampling and laboratory analysis methods used to compare differences in sediment concentrations.

The median value of EWDI–SSC was greater than Grab–SSC, EWDI–TSS, and Grab–TSS median values (Table 1). Also, Grab–SSC had a greater median value than EWDI–TSS and Grab–TSS (Table 1).

Table 1. Summary of Wilcoxon signed-rank tests used to evaluate differences between field sampling and laboratory analysis method combinations in Minnesota, water year 2016.

Grab–TSS (mg/L)	Grab–SSC (mg/L)	EWDI–TSS (mg/L)	EWDI–SSC (mg/L)
Median			
69	85	79	116
Method combination comparison	**PD[a]**	**V**	**p–value**
EWDI–SSC to Grab–TSS	41	7	<0.01
Grab–SSC to Grab–TSS	19	158	<0.01
EWDI–SSC to EWDI–TSS	32	151	<0.01
EWDI–TSS to Grab–TSS	13	242	<0.01
EWDI–SSC to Grab–SSC	27	176	<0.01

[a]Calculation of percent difference is $[(x_1 - x_2)/x_1] \times 100$, where x_1 is the median concentration of the first dataset, and x_2 is the median concentration of the second dataset, in milligrams per liter.

[Grab, sample collected with the grab field sampling method; TSS, sample analyzed with the total suspended solids laboratory analysis method; mg/L, milligram per liter; SSC, sample analyzed with the suspended–sediment concentration laboratory analysis method; EWDI, sample collected with the equal–width–increment or equal–discharge–increment field sampling method; PD, percent difference; V, sum of ranks assigned to the differences with a positive sign; p–value, probability value; <, less than]

The Wilcoxon signed-rank test was used to test if differences between concurrent pairs of samples from grab and EWDI field sampling methods and laboratory analysis methods of TSS and SSC median differences were statistically significant (Table 1). Overall, the comparison of EWDI–SSC samples to Grab–TSS samples was statistically significant (probability value [p-value] less than 0.01; Table 1). The PD in this comparison was 41 percent with the EWDI–SSC median value being greater than the Grab–TSS median value (Table 1). For the two field sampling method comparisons (EWDI compared to grab), results indicated that median differences in concentrations for EWDI samples (EWDI–SSC and EWDI–TSS) were statistically significant (p-value less than 0.01) being greater than the corresponding median differences in concentrations for grab samples (Grab–SSC and Grab–TSS), respectively. The PDs between the two field sampling methods were 27 and 13 percent for EWDI–SSC to Grab–SSC and EWDI–TSS to Grab–TSS, respectively (Table 1). The analysis of the two laboratory analysis method comparisons indicated that the median difference in concentrations were statistically significant (p-value less than 0.01) for SSC and TSS. The SSC laboratory analysis method yielded substantially larger median differences in concentrations than the TSS laboratory analysis method. The PDs for the two laboratory analysis methods were 32 and 19 percent for the EWDI– SSC to EWDI–TSS and Grab–SSC to Grab–TSS comparisons, respectively (Table 1).

Scatterplots and SLR best-fit lines are presented to demonstrate the relations between each field sampling and laboratory analysis method combination. The 1:1 and SLR best-fit lines were plotted for each comparison. The 1:1 line indicates perfect agreement between the two concentration datasets being plotted, and the SLR best-fit line indicates the estimated relation

between the two datasets being compared. If the data and SLR best-fit line plots are above the 1:1 line, the response variable (y-axis; Figure 3) is larger than the explanatory variable (x-axis; Figure 3). Conversely, if the explanatory variable is larger than the response variable, then the data and SLR best-fit line plots are below the 1:1 line.

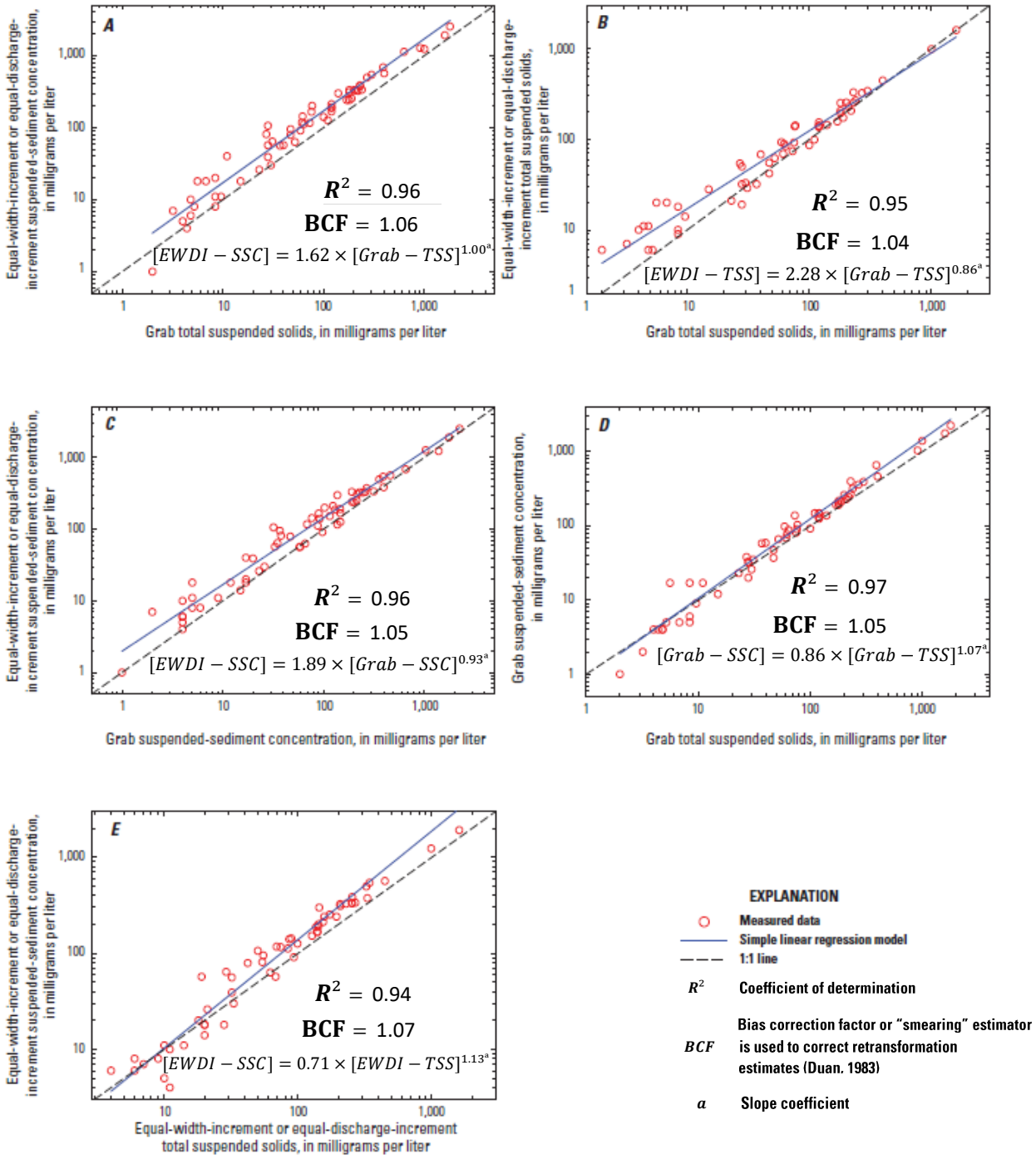

Figure 3. Relations between A, different field sampling and laboratory analysis methods, B and C, field sampling methods, and D and E, laboratory analysis methods in Minnesota, water year 2016.

Patterns among the field sampling and laboratory analysis methods are indicated on Figure 3. All the combinations had strong and significant relations with coefficients of determination (R^2) greater than or equal to 0.94 and p-values less than 0.01. Even though the grouped data have strong and significant relations, a site-specific relation between SSC and TSS should be the primary method to estimate SSC from TSS (Glysson and others, 2000). The SLR analysis indicated when field sampling and laboratory analysis methods were different, the data plotted farthest above the 1:1 line than all the other comparisons (Figure 3A), indicating Grab–TSS consistently under predicts EWDI–SSC.

For field sampling comparisons (Figures 3B, 3C), EWDI samples are assumed to be the most representative of sediment concentration in the river. When SLR best-fit lines are above the 1:1 line, this indicates that concentrations derived from grab samples underrepresent the sediment concentration (negative bias). For sediment concentrations less than 200 mg/L, concentrations derived from grab samples were negatively biased. As sediment concentrations approach 200 mg/L, this negative bias associated with grab samples decreases. This decrease in negative bias likely is the result of higher water velocities mixing suspended sediment homogenously throughout the stream channel. For SSC analyses, concentrations in grab samples were never positively biased throughout the measured range of sediment concentrations (Figure 3C). Conversely, for TSS analyses, concentrations derived from grab samples approached the 1:1 line when sediment concentrations approached 200 mg/L (Figure 3B).

For laboratory comparisons (Figures 3D, 3E), the SSC samples are assumed to be the most representative sediment concentration. SSC analyses indicated a slight positive bias at sediment concentrations less than 40 mg/L (Figures 3D, 3E). At sediment concentrations greater than 40 mg/L, TSS concentrations were negatively biased (Figures 3D, 3E). These comparisons followed observations by Gray and others (2000) and indicated the TSS laboratory analysis methods were most likely biased because the SSC method captures sand-sized particles (greater than or equal to 0.0625 mm) by measuring the entire sediment mass, whereas the TSS method was unable to capture a representative subsample because of sand settling during the extraction procedure.

Effect of Particle Size on Sampling and Laboratory Analysis Methods

The grab field sampling method may not capture sand contributions to SSCs, resulting in artificially greater percentages of fines compared to EWDI–SSC samples (Gray and others, 2000; Ellison and others, 2014). Stream velocity can affect the occurrence and distribution of sand-sized particles near the streambed or in other sections of the stream cross section. A grab sample only incorporates water from a single location near the water surface (less than 1 meter), and most paired sampling were during stream conditions where water depths exceeded 1 meter. Whereas, samples collected using the EWDI method integrates the vertical water column and excludes the lowest 10 centimeters above the streambed; furthermore, samples collected using the EWDI method incorporates water from 5 to 10 locations across the horizontal stream cross section.

Fines and sands were compared for different sampling and laboratory methods (Figure 4A). The EWDI-SSC-Sands were calculated from Table 2 in Groten and Johnson (2018) by taking EWDI-SSC-Fines (mg/L) and subtracting them from EWDI-SSC (mg/l). The EWDI-SSC-Sands were

then split into four categories based on the percentage of sand in the EWDI-SSC. The percentage of sand in the EWDI-SSC was calculated from subtracting EWDI–SSC–Fines (percent less than 0.0625 mm; Table 2 in Groten and Johnson [2018]) from 100 percent. The four categories (based on the percentage of sand in the EWDI-SSC) the EWDI-SSC-Sands were split into were less than 11 percent, greater than or equal to 11 percent and less than 26 percent, greater than or equal to 26 percent and less than 41 percent, and greater than or equal to 41 percent (Figures 4B, 4C).

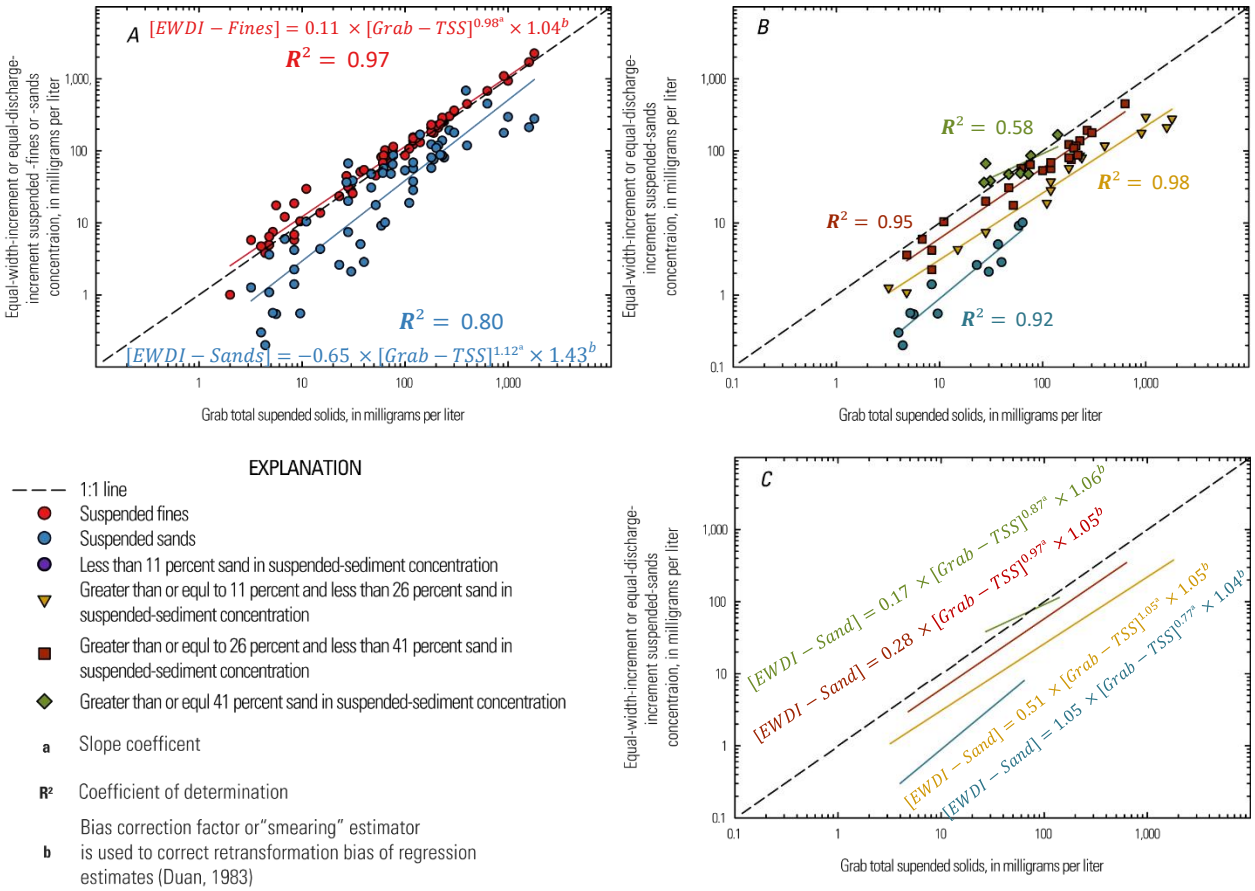

Figure 4. Sand-sized, fine-sized, and different percentages of sand-sized particles and the effect on relations between different field sampling and laboratory analysis methods in Minnesota, water year 2016.

After the dataset was divided into EWDI-SSC-Fines, EWDI-SSC-Sands, and the four categories of EWDI-SSC-Sands based on percentages of sand in the EWDI-SSC, SLR analyses were done on these datasets (Figure 4). All the comparisons had significant relations (p-values were less than 0.03). Five comparisons had strong relations (R^2 values were greater than or equal to 0.80; Figures 4A, 4B) and one did not have as strong of a relation (EWDI-SSC-Sands in the category of greater than or equal to 41 percent; R^2 of 0.58; Figure 4B). The slope coefficients of the SLR models ranged from 0.77 to 1.12 (Figures 4A, 4C).

The fines plotted on the 1:1 line above 10 mg/L in the comparison of EWDI–SSC-Fines to Grab–TSS (Figure 4A). The sands mostly plotted below the 1:1 line in the comparison of EWDI-SSC-Sand to Grab– TSS (Figure 4A) which did not have as strong of a relationship (R^2 of 0.80; Figure 4A) as the fines (R^2 of 0.97; Figure 4A). The EWDI–SSC-Sands to Grab–TSS (Figure 4A)

shows that Grab-TSS underrepresents EWDI-SSC-Sands while the Grab-TSS works well to estimate EWDI-SSC-Fines.

A closer observation of the sands was done by splitting the data into four categories. Three categories plotted below the 1:1 line, and one category plotted near the 1:1 line (Figure 4B). The dataset that plotted near the 1:1 line had the highest percentage of sand in the EWDI-SSC (greater than or equal to 41 percent; Figure 4B). Below the 1:1 line plotted the next highest percentage of sand (greater than or equal to 26 percent and less than 41 percent), and then the next highest percentage of sand (greater than or equal to 11 percent and less than 26 percent) was below. The percentage with the least amount of sand (less than 11 percent) was plotted the farthest below the 1:1 line (Figure 4B). The EWDI-SSC-Sands plotted farther below the 1:1 line (Figure 4B) as the percentage of sand decreased. This indicates that Grab-SSC underrepresents EWDI-SSC-Sands more when the percentages of sand in the EWDI-SSC was less.

Gray and others (2000) stated that the divergence between SSC and TSS expanded when the contribution of sand-size particles was greater than or equal to 25 percent. For this study, the median of all the percentages of the sand in the EWDI–SSC was 26 percent and was selected as a threshold value to produce two groups of data for the dataset. One group consisted of values greater than or equal to 26 percent sands and one group less than 26 percent sands. This value of 26 percent was selected because it was close to the findings of Gray and others (2000) that indicated the differences between SSC and TSS laboratory results were exacerbated when the contribution of sand-size particles was greater than or equal to 25 percent. For the subsequent analysis investigating the effects of percentages of sand-sized particles on field sampling and laboratory analysis methods, EWDI–SSC, Grab–TSS, Grab–SSC, and EWDI–TSS paired values that had greater than 26 percent sand in the EWDI–SSC will hereafter be referred to as “sands,” and values less than or equal to 26 percent sand in the EWDI–SSC will hereafter be referred to as “fines.” It should be noted that even though the data will now be referenced to as “sands” and “fines”, this might not accurately represent the actual fines and sands. Because EWDI-SSC are assumed to be the most representative sediment concentration in the river, it was used to group the rest of the data for the following comparisons.

After the dataset was delineated into sands and fines, SLR analyses were done on the fines and sands datasets. All the comparisons had strong and significant relations (R^2 values were greater than or equal to 0.92 [Figure 5], and p-values were less than 0.01). The slope coefficients of the SLR models ranged from 0.84 to 1.12 (Figure 5). The sands plotted farthest above the 1:1 line in the comparison of EWDI–SSC to Grab– TSS (Figure 5A). Error was cumulative as sand increased because the grab method failed to capture sand in the sample. Additionally, the TSS laboratory analysis method failed to capture sand during the extraction procedure.

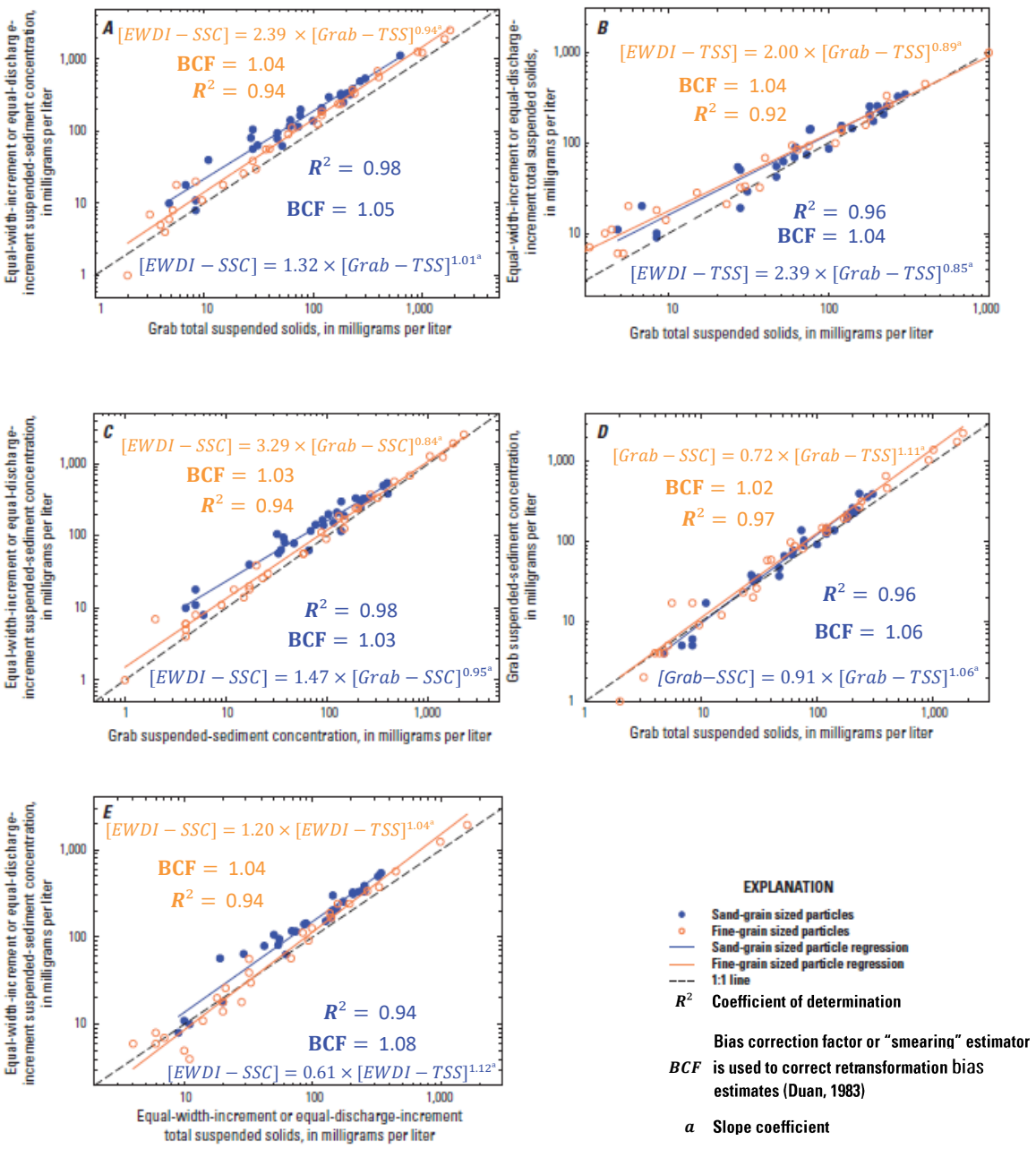

Figure 5. Sand-sized particles effect on relations between A, different field sampling and laboratory analysis methods, B and C, field sampling methods, and D and E, laboratory analysis methods in Minnesota, water year 2016.

When comparing field sampling methods, EWDI samples are assumed to be most representative of the true sediment concentration. For the two different field sampling methods (EWDI compared to grab), samples with greater percentages of sand-size particles provided a marked separation in sands and fines SLR best-fit lines (Figure 5C). The comparisons of EWDI–SSC to Grab–SSC (Figure 5C) provided further evidence that grab samples underrepresent sediment concentrations. The fines best-fit line followed a similar pattern, but the grab samples only slightly underrepresented the sediment concentration (Figure 5C). When comparing EWDI–TSS to Grab–TSS, the small separation between the sands and fines SLR best-fit lines indicated that sand-size particles had less of an effect when the TSS laboratory analysis method was used to

determine concentrations (Figure 5B). A possible explanation for the small separation between sand and fines SLR best-fit lines in Figure 5B was that the TSS laboratory analysis method likely was masking the effect of sand-sized particles.

When comparing laboratory analysis methods, SSC samples are assumed to provide the most representative sediment concentration. Sands had a greater effect on the EWDI–SSC to EWDI–TSS comparison (Figure 5E) than on the Grab–SSC to Grab– TSS comparison (Figure 5D). For EWDI–SSC to EWDI–TSS, the EWDI–TSS sand samples underestimated the most representative sediment concentration throughout the range of samples (Figure 5E). For Grab–SSC to Grab–TSS, the sands followed almost an identical pattern as the fines and had little effect (Figure 5D).

Summary

Suspended-sediment monitoring entails field sampling and laboratory analysis methods to quantify how much sediment is being transported by streams. Quantitative sediment data are useful for addressing sediment impairments in rivers; however, the field sampling and laboratory analysis methods used to collect suspended sediment data can introduce error into the measured results.

This report documents findings based on river suspended sediment data collected by the U.S. Geological Survey and Minnesota Pollution Control Agency. Sediment data were collected at eight sites in Minnesota to determine if differences in concentrations between total suspended solids (TSS) and suspended-sediment concentrations (SSC) can be attributed to field sampling methods, laboratory analysis methods, or both. Grab field sampling and TSS laboratory analysis methods used by Minnesota were compared to standard U.S. Geological Survey field sampling methods and laboratory analysis methods to determine if methods used by agencies in Minnesota underrepresent the amount of suspended sediment in rivers.

Results obtained using grab field sampling and TSS laboratory analysis methods were biased low compared to equal-width-increment or equal-discharge-increment (EWDI), isokinetic, and depth-integrated field sampling and SSC laboratory analysis methods. Differences in both field sampling and laboratory analysis methods caused grab and TSS methods to be significantly biased low, and the difference between laboratory analysis methods was slightly greater than the difference between field sampling methods. The largest difference was observed when the assumed most representative field sampling (EWDI) and laboratory analysis (SSC) methods and assumed least representative field sampling (grab) and laboratory analysis (TSS) methods were compared.

Grab samples analyzed for TSS represented EWDI samples analyzed for concentration of fines well but did not accurately capture EWDI samples being analyzed for concentration of sands in the SSC. This suggests that grab field sampling and TSS laboratory analysis methods are not sufficiently capturing sand-sized particles but are capturing fine-sized particles.

Grab field sampling and TSS laboratory analyses are biased low because these methods do not effectively capture and measure sand moving through the stream channel. Grab field sampling only incorporates water from the top 1 meter of the water column at a single location in the horizontal stream cross section. In contrast, EWDI samples incorporate water throughout the vertical and horizontal water column, except the bottom 10 centimeters. The occurrence of sand is often greater near the streambed, and sand may not be evenly distributed throughout the horizontal stream cross section. The TSS laboratory analysis method also biases the sample low if the sample includes a high proportion of sand. The heavier sand-sized particles tend to fall out of suspension before a representative subsample can be collected for TSS laboratory analysis. Even though differences are present, the presence of relatively strong correlations between SSC and TSS concentrations provides the opportunity to develop site specific relations to address transport processes not captured by grab field sampling and TSS laboratory analysis methods.

References

American Society for Testing and Materials [ASTM], 2000, Standard test methods for determining sediment concentration in water samples: West Conshohocken, Pa., American Society for Testing and Materials International, D3977–97, v. 11.02, Water (II), p. 395–400.

Clesceri, L.S., Greenberg, A.E., and Eaton, A.D., eds., 1998, Standard methods for the examination of water and wastewater (20th ed.): Washington, D.C., American Public Health Association, American Water Works Association, Water Environment Federation, [variously paged].

Davis, B.E., and the Federal Interagency Sedimentation Project, 2005, A guide to the proper selection and use of Federally approved sediment and water-quality samplers: U.S. Geological Survey Open File Report 2005–1087, 20 p. [Also available at https://pubs.er.usgs.gov/publication/ ofr20051087.]

Duan, Naihua, 1983, Smearing estimate—A nonparametric retransformation method: Journal of the American Statistical Association, v. 78, no. 383, p. 605–610. [Also available at https://doi.org/10.2307/2288126.]

Edwards, T.K., and Glysson, G.D., 1999, Field methods for measurement of fluvial sediment: U.S. Geological Survey Techniques of Water-Resources Investigations, book 3, chap. C2, 89 p. [Also available at https://pubs.usgs.gov/ twri/twri3-c2/.]

Ellison, C.A., Savage, B.E., and Johnson, G.D., 2014, Suspended-sediment concentrations, loads, total suspended solids, turbidity, and particle-size fractions for selected rivers in Minnesota, 2007 through 2011: U.S. Geological Survey Scientific Investigations Report 2013–5205, 43 p. [Also available at https://doi.org/10.3133/sir20135205].

Glysson, G.D., Gray, J.R., and Conge, L.M., 2000, Adjustment of total suspended solids data for use in sediment studies—Proceeding of the Joint Conference on Water Resource Engineering and Water Resources Planning and Management, Minneapolis, Minn., July 30–August 2, 2000: American Society of Civil Engineers, 10 p. [Also available at https://doi.org/10.1061/40517(2000)270.]

Gray, J.R., Glysson, G.D., Turcios, L.M, and Schwarz, G.E., 2000, Comparability of suspended-sediment concentration and total suspended solids data: U.S. Geological Survey Water-Resources Investigations Report 00–4191, 14 p. [Also available at https://pubs.usgs.gov/wri/wri004191/.]

Groten, J.T., and Johnson, G.D., 2018, Comparability of river suspended-sediment sampling and laboratory analysis methods: U.S. Geological Survey Scientific Investigations Report 2018–5023, 23 p., https://doi.org/10.3133/sir20185023

Guy, H.P., 1969, Laboratory theory and methods for sediment analysis: U.S. Geological Survey Techniques of WaterResources Investigations, book 5, chap. C1, 58 p. [Also available at https://pubs.usgs.gov/twri/twri5c1/.]

Helsel, D.R., and Hirsch, R.M., 2002, Statistical methods in water resources: U.S. Geological Survey Techniques of Water-Resources Investigations, book 4, chap. A3, 522 p. [Also available at https://pubs.usgs.gov/twri/twri4a3/.]

Minnesota Department of Natural Resources [MNDNR], 2019, MNDNR/MPCA cooperative stream gaging: Minnesota Department of Natural Resources, digital data, accessed March 3, 2017, at http://www.dnr.state.mn.us/ waters/csg/index.html.

Minnesota Pollution Control Agency [MPCA], 2009, Total maximum daily load (TMDL) projects: Minnesota Pollution Control Agency website, accessed May 12, 2017, at http:// www.pca.state.mn.us/water/tmdl/index.html.

Minnesota Pollution Control Agency [MPCA], 2019, Environmental data, accessed May 25, 2017, at https://www.pca. state.mn.us/environmental-data.

Minnesota Pollution Control Agency [MPCA], 2017, Watershed Pollutant Load Monitoring Network: Minnesota Pollution Control Agency website, accessed August 17, 2017 at https://www.pca.state.mn.us/water/watershed-pollutantload-monitoring-network.

U.S. Army Corps of Engineers, 2006, Sedimentation in the upper Mississippi River Basin: St. Louis, Mo., U.S. Army Corps of Engineers, St. Louis District, 142 p., accessed May 25, 2017, at http://mvs-wc.mvs.usace.army.mil/arec/ Documents/Geomorphology/Sedimentation_Upper_Mississippi_River_Basin_2.pdf.

U.S. Geological Survey [USGS], 2019, National Water Information System—USGS water data for the Nation: U.S. Geological Survey database, accessed May 25, 2017, at http://waterdata.usgs.gov/nwis. [Also available at https:// doi.org/10.5066/F7P55KJN.]

U.S. Geological Survey [USGS], 2017, Sediment Laboratory Quality Assurance Project: U.S. Geological Survey website, accessed June 22, 2017, at https://bqs.usgs.gov/slqa/.

Ward, J.R., and Harr, C.A., eds., 1990, Methods for collection and processing of surface-water and bed-material samples for physical and chemical analyses: U.S. Geological Survey Open-File Report 90–140, 71 p. [Also available at https:// pubs.er.usgs.gov/publication/ofr90140.]

Facilities, Data, and Analytical Methods Used to Derive Sand- and Gravel-Trapping Efficiencies for Four Types of Pressure-Difference Bedload Samplers

John R. Gray[1], Gregory E. Schwarz[2], Jonathan A. Czuba[3], Kyle Strom[4], and Panayiotis Diplas[5]

[1]Scientist Emeritus, U.S. Geological Survey, Reston, VA; [2]U.S. Geological Survey, Reston, VA; [3]Department of Biological Systems Engineering, Virginia Tech, Blacksburg; [4]Department of Civil And Environmental Engineering, Virginia Tech, Blacksburg; [5]Department of Civil and Environment Engineering, Lehigh University, Bethlehem, PA

Bedload-trapping efficiencies (coefficients) were derived for four types of pressure-difference bedload samplers at the St. Anthony Falls Laboratory, University of Minnesota, in January-March, 2006 (Marr and others, 2010; Singh and others, 2013). A Helley-Smith (intake-nozzle width and height of 76.2 mm x 76.2 mm), BLH-84 (76.2 mm x 76.2 mm), Elwha (203 mm x 102 mm) and Toutle River-2 (TR-2; 305 mm x 152 mm) were deployed by hand-held rod in the main flume during the first two phases of the StreamLab06 experiments. The trapping-efficiency tests, which were conceived, designed and administered by the U.S. Geological Survey, took place in the sediment-recirculating main flume. Representatives from the St. Anthony Falls Laboratory, National Center for Earth-surface Dynamics, Federal Interagency Sediment Project, Bureau of Reclamation, academia and the private sector joined the U.S. Geological Survey in the implementation of the tests. The 7-phase StreamLab06 experiments were made possible and supported by the National Center for Earth-surface Dynamics, University of Minnesota.

Six combinations of sampler type and bed composition were tested. The BLH-84, Elwha, and Helley-Smith samplers were deployed on a sand bed (D_{50} = 1.0 mm) during five steady flows ranging from 2.0-3.6 m^3/s. The BLH-84, Elwha, and Toutle River-2 samplers were deployed on a gravel bed (D_{50} = 11.2 mm) at four steady flows ranging from 4.0-5.5 m^3/s. Thirty-seven trials – tests of a given bedload sampler for a given steady flow and bed composition – took place.

A total of 2,030 manually collected and weighed bedload samples, and some 3.8-million automated mass measurements produced by five contiguous weigh drums in a slot spanning the width of the flume were used to derive trapping coefficients for the samplers. The bedload samplers were deployed by hand-held rod using an at-a-point sampling scheme in a cross section 8.5 meters upstream from the flume slot. Each weigh drum independently and automatically weighed bedload falling into the slot at approximately 1.1-second intervals. An automated sediment-recirculation system evacuated sediments that were episodically dumped by the weigh drums into the bottom of the slot. An auger at the bottom of the slot evacuated the accumulating sediment to a side-channel pump. The captured sediments were piped upstream and discharged back to the flume.

Bedload-transport rates and ancillary data from the bedload samplers and weigh drums were used to calculate and compare trapping coefficients for the samplers using the following analytical methods, listed from most-to-least computationally intensive and complex:

Modified Thomas-Lewis Model: The original Thomas and Lewis (1993) model was modified to use untransformed transport-rate data in addition to cube root-transformed data, and to use averages of data from three combinations of weigh drums and three drum time "windows" – of relatively short, medium, and long durations – to calculate trapping coefficients for the bedload samplers. The original 3-step model:

1. Regressed cube root-transformed sampler-derived bedload-transport rates on time-window averaged cube transport rates from one or a combination of weigh drums,
2. Squared the regression residuals from the first step on the variance of the cube root of the interval-mean transport rate for the time window, and
3. Inverted the predicted values from the 2nd regression and used them as weights to re-estimate the first regression.

Coefficients computed in cube root space were back-transformationed to real space. Neither this computational procedure nor that using untransformed data required adjustment for bias.

Average of Ratios: This method, based on untransformed data, developed average transport rates from data produced by the weigh drums for each of the 2,030 bedload samples. Transport-rate averages were calculated for the drums in a boxcar-fashion at intervals equal to the duration of a single at-a-point bedload measurement, which ranged from 15-180 seconds. Ratios (trapping coefficients) were calculated by dividing each single-sample trap rate by the respective interval average from one or a combination of weigh drums. Those ratios were averaged to produce a single trapping coefficient for a trial which, in turn, were combined to derive a single coefficient for each combination of bedload sampler and bed type.

Ratios of Averages: This relatively simple and straight-forward method calculated averages of untransformed bedload-transport rates derived for each of the 37 trials for a given bedload sampler and the nine combinations of weigh drums and time windows.

Trapping coefficients thusly were computed for each sampler and bed composition pairing. Hence, the BLH-84 and Elwha samplers each have two provisional trapping coefficients derived from the sand- and gravel-bed tests. The Helley-Smith sampler (sand bed) and TR-2 sampler (gravel bed) each have a single provisional trapping coefficient. When verified, sampler-specific trapping coefficients may be used to adjust contemporary as well as historical bedload-transport rates produced by these samplers for bed types similar to those in which they were tested during the StreamLab06 experiments.

References Cited:

Marr, J.D.G., Gray, J.R., Davis, B.E., Ellis, C., and Johnson, S., 2010, Large-scale laboratory testing of bedload-monitoring technologies—Overview of the StreamLab06 experiments, *a paper submitted as part of* Gray, J.R., Laronne, J.B., and Marr, J.D.G., eds., Bedload-surrogate monitoring technologies: U.S. Geological Survey Scientific Investigations Report 2010–5091, p. 266–282, accessed March 6, 2019, at https://pubs.usgs.gov/sir/2010/5091/papers/Marr.pdf.

Singh, A., Czuba, J.A., Foufoula-Georgiou, E., Marr, J.D.G., Hill, C., Johnson, S., Ellis, C., Mullin, J., Orr, C.H., Wilcock, P.R., Hondzo, M., and Paola, C., 2013, StreamLab Collaboratory—Experiments, data sets, and research synthesis: Water Resources Research, v. 49, no. 3, p. 1746–1752, accessed March 6, 2019, at https://doi.org/10.1002/wrcr.20142.

Thomas, R.B., and Lewis, J., 1993, A new model for bed load sampler calibration to replace the probability-matching method: Water Resources Research, v, 29, no. 3, p. 583–597, accessed March 6, 2019, at https://doi.org/10.1029/92wr02300.

FISP: What's New in Samplers and Sediment Measurement Technologies

Tim Straub, Acting FISP Chief, U.S. Geological Survey, Urbana, IL, tdstraub@usgs.gov

Abstract

The Federal Interagency Sedimentation Project (FISP) is an example of effective interagency cooperation a cross-cutting science issue. The FISP was created in 1939 to research and standardize fluvial sediment science methods and instruments. That mission remains relevant today as research continues on emerging tools and technologies for measurement and analysis of sediment properties.

Introduction

FISP instrumentation and research encompasses suspended sediment, bedload sediment, bed material, bed topography, and water quality. The currently active FISP agencies are the U.S. Bureau of Reclamation, U.S. Army Corps of Engineers, U.S. Department of Agriculture-Agricultural Research Service, U.S. Forest Service, and U.S. Geological Survey (USGS). Sponsoring agencies and the public benefit from the cooperative action that leads to comparable, meaningful sediment information obtained using common instruments, standards, and procedures.

The FISP was created in 1939 to research and standardize fluvial sediment science methods and instruments (Gray and Landers, 2015). The 20th century focus was on designing and building physical samplers with an emphasis on the mechanical and hydraulic aspects. Prior to 1939, samplers for both suspended sediment and bedload were non-isokinetic (velocity of water going into the sampler was not the same as the undisturbed velocity of water at that sample location) which biased the sample concentration and made results non-comparable. The FISP developed

a series of samplers that could be used to collect point and depth integrated suspended sediment, bedload, and bed material (Davis, 2005). The results from samples collected in these samplers are comparable within the conditions referenced in Davis (2005) if equivalent techniques are followed. Starting in 1981, a transition in the development of the samplers ensured that they were capable of sampling for trace constituents without introducing contamination (Davis, 2005).

In 2005 there was a logistical change to the FISP, with sampler supply, testing, and maintenance support duties transferred to the USGS Hydrologic Instrumentation Facility (HIF) (2019) at Stennis Space Center, Mississippi. The HIF now manages all contracts with manufacturers, inventory, orders, testing of equipment prior to shipping, and conducts repairs on equipment that is returned. From 2005 to present, the focus of FISP activities has shifted from the development and support of physical samplers towards research, development, and evaluation of sediment surrogate technologies.

Current or Recent FISP Sponsored Research

Information on the recent and current FISP research can be found on the FISP website (Federal Interagency Sedimentation Project, 2019). Although the primary focus in recent years has been on sediment surrogate technologies, physical samplers have also been researched. These research topics have included suspended sediment sampler efficiency and accuracy, and bedload sampler efficiency while varying mesh size and type.

Numerical modeling analysis was used for both the efficiency and accuracy studies involving suspended sediment samplers while laboratory testing was used to test the hydraulic efficiency of pressure difference samplers while varying mesh size and type. More information on the

setup and results of the testing can be found in the research section of the FISP website (Federal Interagency Sedimentation Project, 2019).

The FISP website highlights more than ten sponsored sediment surrogate technology research projects and topics, including:

- Acoustics for suspended-sediment concentration (SSC) monitoring
- Laser diffraction for particle-size monitoring and concentration
- Close-range remote sensing for SSC monitoring
- Density difference for SSC monitoring
- Passive-acoustic bedload monitoring

Acoustic technology is increasingly used for velocity measurements, and the FISP has and continues to invest in testing and developing methodologies for using this same technology as a surrogate for estimating SSC. The testing includes the use of point and profiling acoustic instruments. The profiling instruments measure the backscatter of sound waves in either the horizontal or vertical directions in a river. A techniques and methods document has been published for estimating SSC using the horizontal methodology, and testing continues on the vertical methodology (Sediment Acoustic Leadership Team, 2019).

Another technology getting increased use is laser diffraction. This instrumentation is being used in both the laboratory and field. The methodology is advancing the ability to more quickly obtain particle-size distribution and volumetric sediment concentration. The FISP is helping support the development of laboratory standards and continues to support field testing of in-situ laser diffraction instruments at multiple sites across the United States (Czuba and others, 2015).

The FISP has also supported the evaluation of spectral imagery from commercially-available cameras as a non-contact surrogate for SSC at a field site where samples and turbidity readings also were collected.

The density difference methodology for SSC monitoring is an option at sites where concentrations above 20,000 mg/L are observed because these concentrations are high enough to be outside the measurement range of most if not all other surrogates. The FISP supported testing at a site where these conditions exist (Brown and others, 2015).

Lastly, passive-acoustic bedload monitoring uses hydrophones to listen to collisions of gravel particles, as a surrogate for bedload. The FISP has supported testing of this methodology in both the lab and the field (Wren and others, 2015; Federal Interagency Sedimentation Project, 2019-Research Tab).

The FISP plans to continue research on emerging tools and technologies for measurement and analysis of sediment properties into the future. The public will continue to benefit from the effective interagency cooperation that leads to comparable and meaningful sediment information.

References

Brown, J.E., Gray, J.R., Hornewer, N.J., 2015, In Situ Densimetric Measurements as a Surrogate for Suspended Sediment Concentrations in the Rio Puerco, New Mexico, Proceedings of the 3rd Joint Federal Interagency Conference (10th Federal Interagency Sedimentation Conference and 5th Federal Interagency Hydrologic Modeling Conference), April 19 – 23, 2015, Reno, Nevada.

Czuba, J.A., Straub, T.D., Curran, C.A., Landers, M.N., and Domanski, M.M.. 2015, Comparison of fluvial suspended-sediment concentration sand particle-size distributions measured with in-stream laser diffraction and in physical samples, Water Resour. Res., 51, 320–340, doi:10.1002/2014WR015697.

Davis, B.E. 2005, A Guide to the Proper Selection and Use of Federally Approved Sediment and Water-Quality Samplers: Vicksburg, MS, U.S. Geological Survey, Open File Report 2005-1087, 20 p.

Federal Interagency Sedimentation Project. 2019, Federal Interagency Sedimentation Project Website, https://water.usgs.gov/fisp/, last accessed February 15, 2019.

Gray, J.R. and Landers, M.N., 2015, History of the Federal Interagency Sedimentation Project, Part V: Proceedings of the 3rd Joint Federal Interagency Conference (10th Federal Interagency Sedimentation Conference and 5th Federal Interagency Hydrologic Modeling Conference), April 19 – 23, 2015, Reno, Nevada, P. 264-275. http://acwi.gov/sos/pubs/3rdJFIC/Contents/2C-Gray.pdf and http://acwi.gov/sos/pubs/3rdJFIC/Proceedings.pdf, last accessed April 18, 2019.

Sediment Acoustic Leadership Team, 2019, Sediment Acoustic Leadership Team website, https://water.usgs.gov/osw/SALT/index.html, last accessed February 15, 2019.

Wren, D.G., Goodwiller, B.T., Rigby, J.R., Carpenter, W.O., Kuhnle, R.A., Chambers, J.P., Sediment-Generated Noise (SGN): Laboratory Determination of Measurement Volume, Proceedings of the 3rd Joint Federal Interagency Conference (10th Federal Interagency Sedimentation Conference and 5th Federal Interagency Hydrologic Modeling Conference), April 19 – 23, 2015, Reno, Nevada.

U.S. Geological Survey, Hydrologic Instrumentation Facility, 2019, Hydrologic Instrumentation Facility Website, https://water.usgs.gov/hif/, last accessed February 15, 2019.

Bedload Flux and Characteristic from Flash Floods in the Arroyo de los Piños, NM – Initial Results

Daniel Cadol, New Mexico Institute of Mining and Technology, Socorro, NM, daniel.cadol@nmt.edu

Kyle Stark, New Mexico Institute of Mining and Technology, Socorro, NM, kyle.stark@student.nmt.edu

Jonathan B. Laronne, Ben Gurion University of the Negev, Beer Sheva, Israel, john@bgu.ac.il

David Varyu, United States Bureau of Reclamation, Denver, CO, dvaryu@usbr.gov

Madeline Richards, New Mexico Institute of Mining and Technology, Socorro, NM madeline.richards@student.nmt.edu

Abstract

Sampling bedload by conventional means is not possible in unwadeable flash floods, typical of large tracts of land in the American Southwest and in deserts worldwide. Instead, automated methods are required to monitor bedload. Reid-type (formerly termed Birkbeck) slot samplers have been demonstrated to be hydraulically efficient at monitoring and sampling bedload, have been deployed in various regions and climates, and have been used to calibrate surrogate techniques. Yet they are expensive and require considerable person-power to deploy. In addition to the Oak Creek vortex tube, automatic slot samplers have been deployed in the US (Wyoming and California) and presently by the ARS in Coon Creek. We report on preliminary results of monitoring bedload in the Arroyo de los Piños.

Three slot samplers, each with ≈ 0.5 m^3 capacity, are deployed across a 10 m wide constricted reach of the Piños, near the confluence with the Rio Grande. The local slope is 1.3%, drainage area is 31 km^2, and sand and gravel yields are presumed to be high. These sediments are transported directly to the Rio Grande during the infrequent summer-season monsoon flash floods. The channel bed is unarmored, with coarser pebble-cobble rich bars and finer-grained thalwegs containing sand-rich gravels. The approach reach has two thalwegs with inter-event switching as to which is the deepest, thereby transporting higher bedload fluxes at shallow depths. The thalwegs are separated by a subdued (ca 10 cm) bar. The channel bed as a whole contains about equal proportions of sand, granules (2-8 mm) and coarser particles. The monitoring station contains a large number of surrogate bedload devices, and as it is located near New Mexico Tech, manual bedload sampling at wadeable depths is undertaken in most flash floods.

Five bedload-transporting events were monitored during 2018. Initial analyses establish that bedload fluxes are very high by global standards, as expected in unarmored, ephemeral channels (6.5 – 16.5 kg s^{-1} m^{-1}). Bedload transport is initiated even by shallow flow events (ca 8 cm depth at the site, similar to the depth in the feeder thalweg. At very shallow depths of flow (5-10 cm) such as in the September 1, 2018 event, bedload flux increased with depth in the range 0.1 – 1 kg s^{-1} m^{-1}, though with considerable scatter.

Introduction

Bedload transport processes in ephemeral channels

Ephemeral streams constitute a large portion of most channel networks. This proportion varies with climate, with drier conditions typically increasing the proportion, but even wet regions have many low-order channels that only flow during precipitation events. Quantifying flow and sediment transport in ephemeral streams is inhibited by several challenges not present in perennial systems. First, the observer must wait for flow. This is analogous to waiting for floods in perennial systems, but whereas a great deal of work can happen during base flow in a perennial stream, limited useful data can be gleaned during no-flow. Second, the cross-sectional geometry of ephemeral streams changes more than most perennial streams during flood. There is widespread bed scour, bank erosion, and bar deposition, causing relationships between stage and discharge to change significantly over the course of a flow event. Finally, because they are not major sources of water, few ephemeral streams are gauged by federal or state agencies. There is a dearth of flow data from ephemeral streams, even in semi-arid regions such as the Southwest United States. In part this is due to challenges related to the typically rapid rising limb of the flood and the often-unpredictable timing (Cohen and Laronne, 2005). Additional challenges related to bedload measurement are the high magnitude and variability of these fluxes (Laronne and Reid, 1993; Reid et al., 1995).

Yet because of their ubiquity and high sediment transport capacity, ephemeral streams can dominate the fluvial system and its response to climate and land use change. Sediment delivered from ephemeral streams controls the geomorphology of many major perennial rivers and dictates the filling rate of reservoirs. Most destructive floods in semi-arid regions, even on perennial rivers, derive most of their water from ephemeral portions of the channel network. And because of their relatively large bed surface area and sequential wetting and drying, biogeochemical reactions on beds of ephemeral streams can be significant or even dominant at the landscape scale. Understanding the runoff generation, sediment transport, and biogeochemical cycling of ephemeral rivers is key to managing the scarce surface water resources of dryland societies.

The relationship between temporal intermittency and total sediment delivery is poorly understood. Ephemeral streams typically have higher sediment loads than perennial streams when they are flowing (Reid et al., 1995), but total sediment transport integrated through time may be smaller given the shorter duration of flow. Bed sediment is typically finer in ephemeral streams, all else being equal, because the time available for winnowing of fines is reduced. Additionally, flow rates typically change rapidly from high to low energy, allowing fines to drop out of transport throughout the channel network at the end of a flood event.

Most early efforts to quantify bedload transport focused on average conditions within perennial channels (e.g., Shields, 1936; White, 1940). But even these early researchers recognized that localized variations within the water column and in the bed structure could change the force balance acting on a grain. For example, grain protrusion reduces the shear stress required for grain entrainment because grains that are exposed above the rest of the bed will experience enhanced drag forces (Fenton & Abbott, 1977; Brayshaw et al., 1983). The protruding grains can also shield smaller grains downstream, altering sorting and grain size distribution within the reach (Brayshaw et al., 1983; Kirchner et al., 1990). Relative grain size plays a large role in grain protrusion and shielding; large grains tend to protrude and small grains tend to be shielded, helping to reduce the difference in transport thresholds across the bed material mixture, even in

armored perennial streams. Grains also tend to protrude into the water column if the bed on which they lie is very uniform. The result is that critical shear stress for a given bed is a probability distribution, not a single value (Kirchner et al., 1990). Grains on one part of the bed may readily erode because they are exposed to greater tractive forces, while grains of the same size in another part of the bed may be entrapped by still larger, more immobile grains. In spite of this, in laboratory flume experiments, grain sorting has been shown to have little effect on critical shear stresses for each grain size fraction (Wilcock, 1988). As shear stress increases, the percentage of coarser particles mobilized increases until some critical shear stress value when all fractions become mobilized.

Practical sediment transport equations are typically based on shear stress or stream power and are calibrated to perennial streams. Sediment supply is typically a limiting factor in perennial streams and plays an important role in the empirical calibration of most transport equations, but it is much less important in ephemeral streams (Reid et al., 1995) resulting in poor performance of equations calibrated in perennial streams and applied to ephemeral streams. Current methods to calculate sediment load typically involve applying sediment transport equations for the particular field conditions of the channel, often with very large incompatibility of equations for given conditions (Cao et al., 2010). In part, this is because nearly all transport equations have been developed based on perennial systems (Gomez & Church, 1989; Shih & Diplas, 2018). Water resource and reservoir managers are faced with multiple orders of magnitude of uncertainty in estimates of sediment delivery to regulated semi-arid rivers. Yet the need for data is essential to best manage the vital rivers in a large area in the American Southwest, where the input of bedload from such tributaries to main stems is a key constraint on predictive understanding. Agencies such as the United States Bureau of Reclamation (USBR) and the United States Army Corps of Engineers (USACE) have had to estimate lateral inputs with no data available to substantiate bedload formulae.

The most relevant formulae to be tested are those originally suggested for streams transporting both gravel and sand (e.g., Wilcock and Kenworthy, 2002). Because of the bed armoring and shielding in perennial streams, more complex bedload discharge models have been developed (Miwa & Parker, 2017; Wilcock & Crowe, 2003; Wilcock & Kenworthy, 2002). Though they are developed for perennial streams, they are one of the limited options for estimating bedload transport in ephemeral streams. This extrapolation may be partly justified due to these models' conceptualization of the bedload into a two-component system: sand and gravel. In both flume experiments and field observations, grain entrainment depends on the sand content. With an increasing sand fraction, the gravel fraction becomes more mobile (Miwa & Parker, 2017) because effects of grain protrusion become more prominent. This effect continues until the sand fraction is 40% of the bed material. At this stage, model results indicate that the critical shear stress required for gravel entrainment increases. This transition has been interpreted to be the transition from a grain-supported bed to a matrix-supported bed (Wilcock & Crowe, 2003). Increasing the sand fraction beyond the 40% threshold continues to decrease the critical shear stress required to mobilize the sand fraction, but the shear necessary to transport the gravel fraction increases (Wilcock & Kenworthy, 2002). In effect, the importance of the protrusion and hiding effects of the gravel fraction fades away. Hence, ephemeral streams, with their broad bed grain size distribution, are excellent candidates to investigate this sand fraction effect.

Previous bedload transport quantification in ephemeral channels

Direct measurement of ephemeral, semi-arid channel bedload has taken place at a limited number of sites worldwide. The three most productive sites have been the Nahal Eshtemoa, the Nahal Yatir, and the experimental watershed at Walnut Gulch (Laronne et al., 1992, 1994;

Nichols et al., 2008). These previous studies demonstrate that rates of bedload transport are very high, primarily due to lack of armoring and readily erodible sediment (Cohen & Laronne, 2005; Laronne & Reid, 1993; Powell et al., 1996).

Transport events at all three sites are driven by high intensity precipitation that generates overland flow. The bedload flux in the Yatir and Eshtemoa channels varies linearly with boundary shear stress (Cohen et al., 2010), in contrast to their perennial counterparts, which are governed by a power function relationship. This linear relationship is dependent on sediment source and flood type. Changes in sediment storage during flooding is minimal in these regions due to the availability of sediment for entrainment (Powell et al., 2007). Total bedload flux is high when compared to global averages, with values reported up to 10 kg s^{-1} m^{-1} (Powell et al., 1996).

Study Site

Our bedload monitoring efforts have focused on the Arroyo de los Piños. Streams like the Piños are common in the Southwest: tributaries to a large, societally important river that has been dammed for water allocation and flood control. These main stem dams impede the transport of sediment downstream, leaving the tributaries as the primary contributors of sediment to the main river, which subsequently suffers from geomorphic instability (Kondolf, 1997; Graf, 2006). Yet there is no cost-effective way to quantify this important tributary flux. The USBR alone spends millions of dollars annually on river maintenance merely in the Middle Rio Grande, and uncertainty regarding sediment flux leads to over-engineering of river infrastructure nationwide. Therefore the USBR, with assistance from the USACE, decided to fund the construction of a state-of-the-art long-term sediment transport observatory at the Arroyo de los Piños.

The Arroyo de los Piños watershed (31.5 km^2) has an average slope of 3.5%, with the channel slope decreasing downstream to 1.3% at the constricted monitoring site near the Rio Grande confluence. The upper two-thirds of the basin consists of extensively faulted Paleozoic limestone, sandstone, and shale, while the lower third of the basin is carved into Quaternary basin fills of the axial Rio Grande Rift. The channels in the upper two thirds of the basin are single thread and constrained by bedrock slopes, whereas in the lower portion an anastomosing pattern prevails, in part due to the abundance of bushes scattered throughout the unconfined valley floor, as is typical of the washes in the region. Creosote is the dominant vegetation, with interspersed grasses and other small shrubs such as saltbush. There is moderate grazing pressure throughout the basin, administered by the Bureau of Land Management. Occasional juniper trees are scattered about the basin, primarily concentrated on localized sand sheets or on limestone hillslopes.

Flow in this basin is almost exclusively generated by intense localized thunderstorms associated with the North American Monsoon. Precipitation averages 250 mm annually, with over 150 mm falling during the monsoon season of July-October. Monsoon season storms tend to be short duration and high intensity, with limited spatial extent, while winter precipitation tends to be widespread and low intensity, rarely generating runoff.

Approximately 200 m upstream of the Piños' confluence with the Rio Grande an agricultural drain ditch crosses under the arroyo. Constructed in the 1950s, it is presently unused and unmaintained, with negligible farming activity on this side of the Rio Grande. However, levees at the crossing prevent the wash from flowing into the drain and constrict the channel to a width of 10 m. The monitoring site is located here, to take advantage of the fixed cross-section. The bed

material of the channel at the monitoring station is unarmored, as is typical of ephemeral desert washes (Laronne et al, 1994), and contains approximately equal amounts of sand, granules (2-8 mm) and coarser gravel. The pebbles and cobbles are somewhat angular. Further upstream in the Paleozoic bedrock the fraction of sand decreases and the median and maximum grain sizes increase to cobbles and occasional boulders. With three depth transducers and two rain gauges already deployed at the monitoring site and in the upper basin, during the 2017 monsoon season we monitored ten flow events with rainfall depths as high as 40 mm/event, flow depth at the site up to 0.5 m, depth averaged water velocity up to 2.6 m/s, and SSC in the range of 1-5% (10,000-50,000 mg/L).

Methods

Direct bedload sampling over extended periods and in deep (greater than 40 cm) flows presents both technical and safety challenges. Handheld samplers (e.g., Helley-Smith) alter near-bed hydraulics, and wading becomes dangerous in many flood stages when bedload transport is often high. Collection reservoirs permit cumulative estimates at event-scale resolution, but cannot describe intra-flood variation. One solution is to install Reid-type slot samplers (aka pit traps) with weighing pressure pillows in the channel bed, but this solution is costly for adequately large traps and requires diligent maintenance. Three such slot samplers were installed on the Arroyo de los Piños, and were active during five flow events in the 2018 monsoon season.

Bedload flux was determined by the rate of increase of mass within the Reid-type slot samplers (Reid, et al. 1980). Bedload falls through a slot in the channel bed into a buried vault containing a steel box. The width of the slot can be adjusted using sliding plates, set at 11 cm in this case. The chamber below was kept flooded, therefore suspended sediment could not settle into the sampler, but bedload could. The box rests on a pillow that records the pressure change associated with the mass of sediment displacing water within the box. Pressure in the pillow is corrected against a co-located vented water column pressure transducer. These pressure gains are then converted into a time series of bedload flux per unit width of channel. The samplers also allowed determination of the temporal variation in the grain size of bedload based on the known time when given layers of sediment mass accumulated in the samplers (Powell et al., 2001), even when a considerable fraction of the bedload was sandy, as during low depths and low imposed shear stresses (Lucía et al., 2013).

The benefits of slot samplers are well established (e.g., Laronne et al., 2003). They do not alter flow hydraulics, due to their placement within the riverbed. They do not sample suspended sediment, because the box is kept filled with water, meaning that even at the beginning of a flood the exchange of water across the pit opening is minimized, and likewise the delivery of suspended sediment. Instead, flow passes over the slot opening. Only those particles that are dragging or saltating along the bed can descend through the opening. The opening is long in the downstream dimension, so that few particles can hop entirely over the slot. Also, slot samplers record continuously in time, as bedload mass accumulates in the weighing box. Finally, by retaining the sediment, they enable subsequent excavation, sampling, and grain size analysis of the bedload that was actually in transport.

Yet slot samplers have key limitations, and their effective use must properly take these into account. They are expensive to install and require a stabilized channel cross section. Most importantly, the volume of the weighing box acts as a limit on their useful life for each event. In areas with high bedload flux, they fill quickly relative to event duration. Narrowing the slot width can extend this sampling duration, but at the cost of excluding particles that are larger

than the slot width. By nature, slot samplers collect data at a single location in the cross section, however in most installations multiple traps crossing the channel are used to provide data on lateral variability of transport, which is typically significant. Finally, the mass resolution of the pressure pillow necessitates an integration time period. The pressure response can be noisy and variable, due to turbulence and the bouncing or shifting of particles in the box. Therefore, captured sediment pressure trends over longer time periods (minutes) are more representative of the mean than typically fast changes over seconds. In short, while slot samplers are one of the only ways to obtain a bedload sample without altering the observation environment in the process of collecting it, there are limitations in terms of temporal duration and resolution.

Results

In all the Reid-type slot sampler data sets, there is a time limit on the usefulness of the sampler data. Measured flux declines as the box approaches its capacity and capture efficiency decreases. Typically a cone of sediment fills nearly to the opening, at which stage settling and rearrangement of material can permit additional mass to enter, but not at a rate representative of bedload flux. This occurs when the box is roughly 85-95% full. Not all figures in this paper cut off the pressure pillow derived flux data at this stage, but it is clear from the rapid drop off in the captured bedload flux independent of declines in stage or discharge. The bedload flux data are presented as a 3-minute moving average to alleviate noise in the signal due to turbulence.

Bedload flux for the five measured events was generally well correlated with stage (Figure 1). The left slot sampler appears to have collected the most stage-sensitive data, possibly due to the presence of the thalweg on river left. However, the figures presented here show the mean bedload flux for all three samplers.

In the July 16, 2018 event, the flood arrived as a bore, and flux immediately reached peak value. It then declined with stage until the sampler was full. The August 9, 2018 event rose more slowly, and to a lower peak stage (20 cm vs. 45 cm), with a commensurately lower peak cross-section average bedload flux (4 kg s^{-1} m^{-1} vs. 6 kg s^{-1} m^{-1}). The slower stage rise is mirrored in a slower flux rise. The left sampler, where the stage is used for this comparison, had a somewhat higher peak bedload flux of 8 kg s^{-1} m^{-1} (Figure 2). In both events, there appears to be a small initial flush effect, with greater transport when the flow first approaches the peak. This may be due to the turbulence of the arriving bore, or alternatively, due to bed material reorganization during the flood.

Peak measured fluxes at the left sampler have a non-linear relationship with the stage at the time of peak flux (Table 1). The August 24 event had a higher peak bedload flux than the July 16 event, in spite of its lower peak stage. It may be that this event, as well as the August 9 event, benefited from the major flood on July 26 disrupting the bed structure and leaving readily mobilized sediment as its stage fell. Based on personal communication with residents in the area of the Piños as well as aerial photographic evidence, we estimate the July 26 event had a 10-25 year recurrence interval.

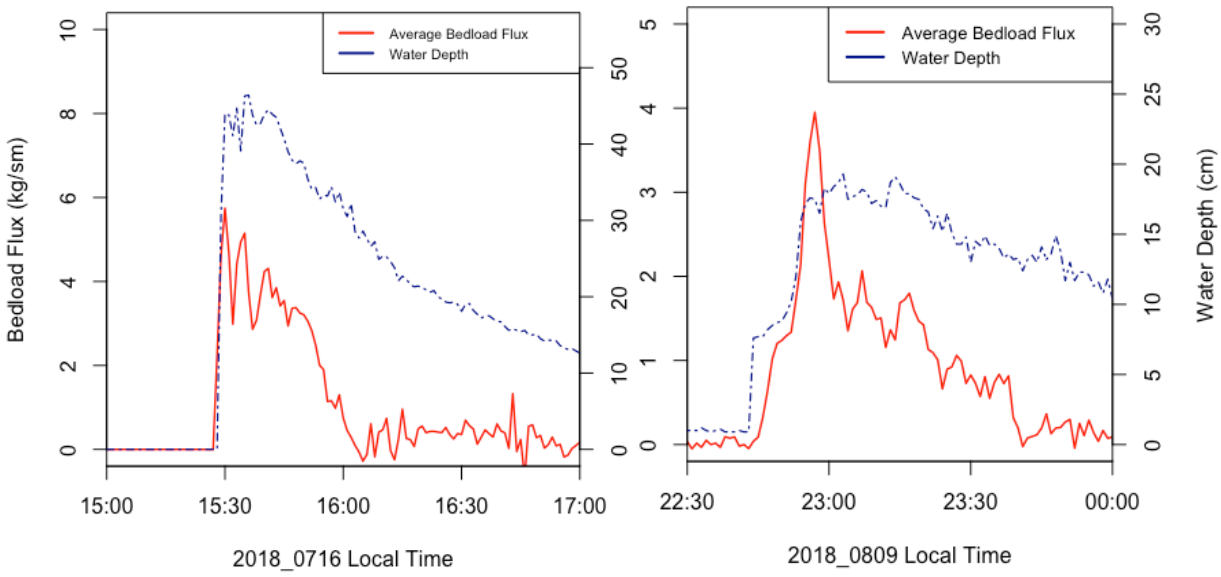

Figure 1: Average bedload flux for the three slot samplers and water depth for the July 16, 2018 event and the August 9, 2018 event.

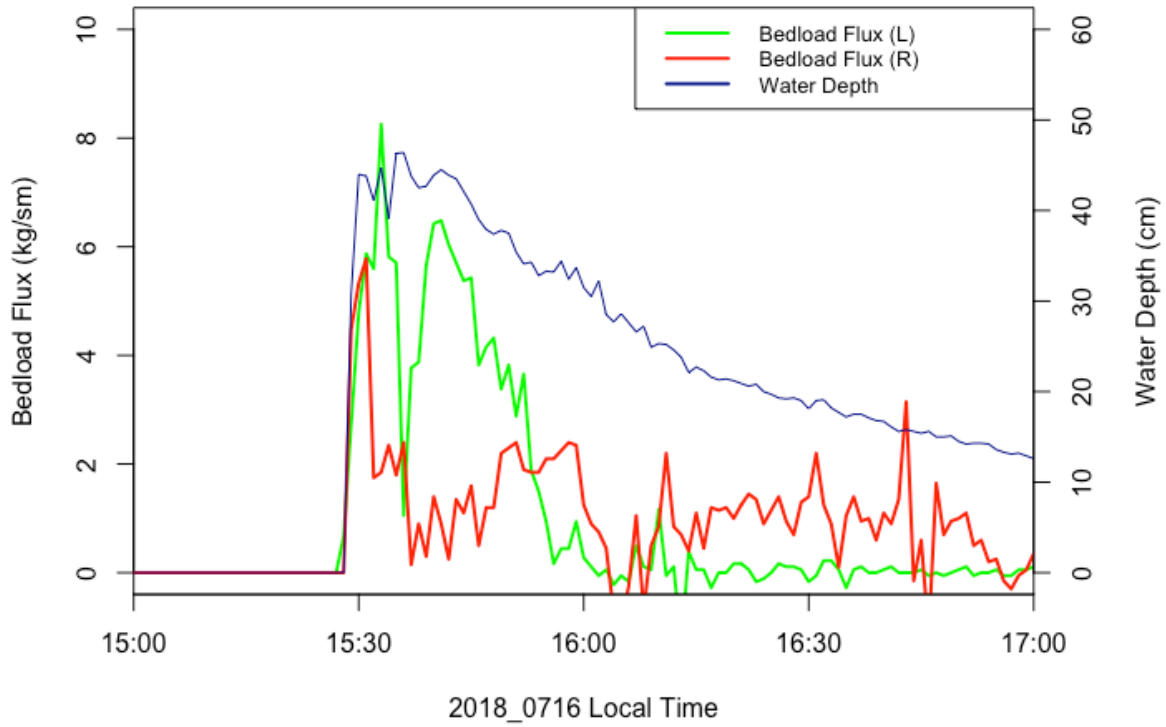

Figure 2: Bedload sediment flux separately monitored at the left and right slot samplers for the July 16, 2018 event.

Table 1: Peak bedload flux and stage at peak flux, sorted by flux

Event Date (2018)	Peak Bedload Flux (kg/sm)	Stage at Peak Flux (cm)	Note
Sept 1	2	15	peak stage
Aug 9	4	20	peak stage
July 16	8	45	peak stage
Aug 24	10	35	peak stage
July 26	16	50	not peak, box filled

In this major flood, the left slot sampler filled within 10 minutes of bedload transport initiation, or 15 minutes following initial flood rise (Figure 3). The peak bedload flux for this sampler, 16 kg s^{-1} m^{-1}, was the highest recorded in our study. At this time, water depth was only 50 cm, well below the eventual peak at 160 cm, suggesting it may have continued to rise. In contrast, the right sampler filled more slowly, and had a peak flux of 5 kg s^{-1} m^{-1}, which was sustained across a wide range of flow depths, from 50 to 120 cm. Yet bedload transport was initiated earlier on the right side of the channel. This lateral variability and apparent migration of the thalweg is characteristic of our observations from the Piños, likely due to the topography of the approach reach.

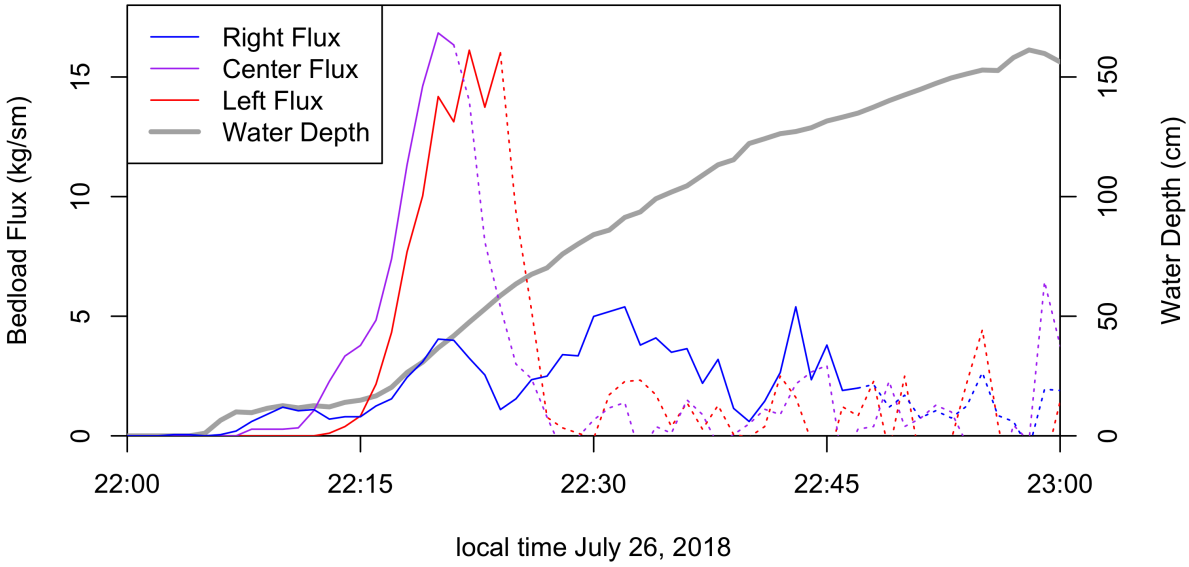

Figure 3: Time series of right, center, and left sampler bedload flux during July 26th event (peak stage: 160 cm). Flux lines are dotted where it is inferred that the sampler was full or nearly so. Left sampler filled within ~ 15 minutes of beginning of flood; right sampler within ~ 30 minutes.

For individual events, there are typically strong relationships between flux and stage, at least within the limits of the trap accuracy and data collection duration. However, the slope of this relationship is not necessarily the same for all three slot samplers. For example, in the August 24 event, the left sampler experienced greater bedload transport for a given stage (Figure 4). This may be due to slight differences in the height of the sill in which the samplers are set. Due to settling during pouring of the concrete, the left sampler is approximately 3 cm lower than the right, yet we use a single stage height, from the left sampler, for this analysis. In this case, the resulting difference in water depth would not be enough to explain the entire difference in the stage-flux relationship, suggesting an additional role for thalweg location. However during the September 1 flow event, a low stage event with multiple flood waves (Figure 5), using the stage

data collected immediately above the different samplers does appear to fully explain the different fluxes and result in a consistent stage-flux relationship (Figure 6).

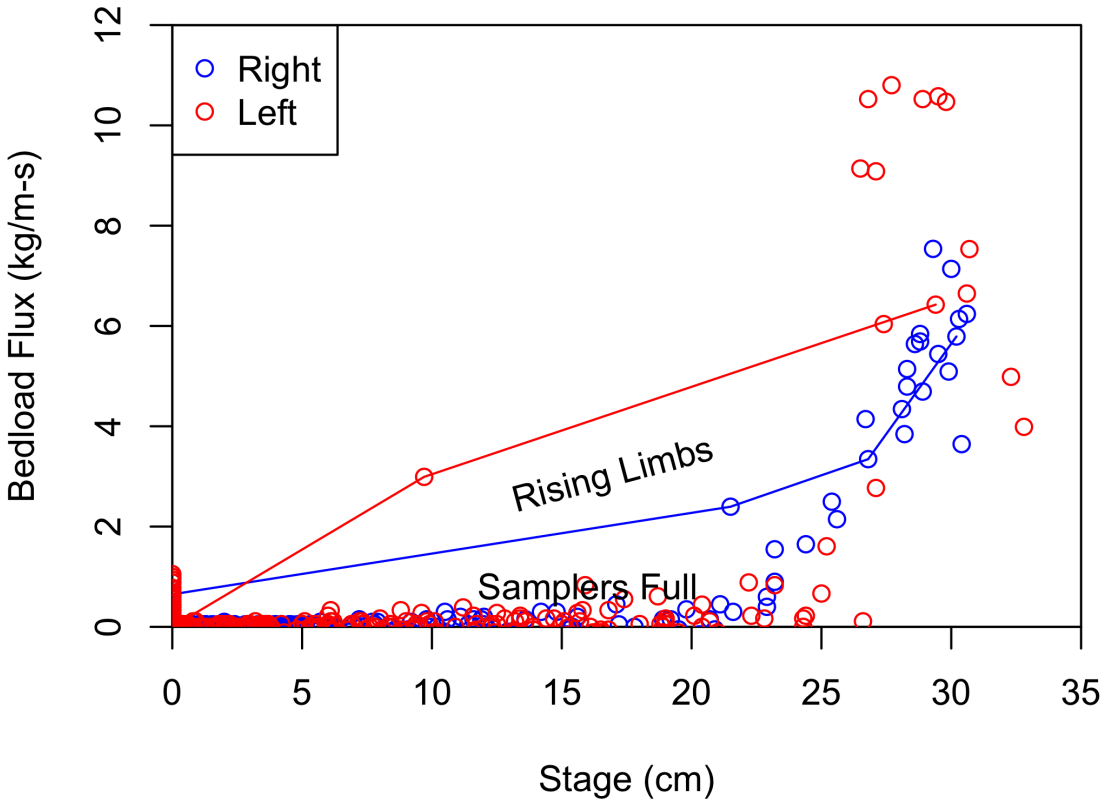

Figure 4: Stage-flux relationship for August 24th event (33 cm max depth).

The stage-flux relationship in Figure 4 superficially appears to show a clockwise hysteresis. Unfortunately, this observation may simply be an artifact driven by trap capacity and capture efficiency. Because the box fills and collects no data during most of the falling limb, such a hysteretic effect would be greatly exaggerated or even falsely created. The flux-stage data for the September 1 event (Figure 6) are noisy, and while a clockwise hysteresis again might be interpreted, the pattern is not clear.

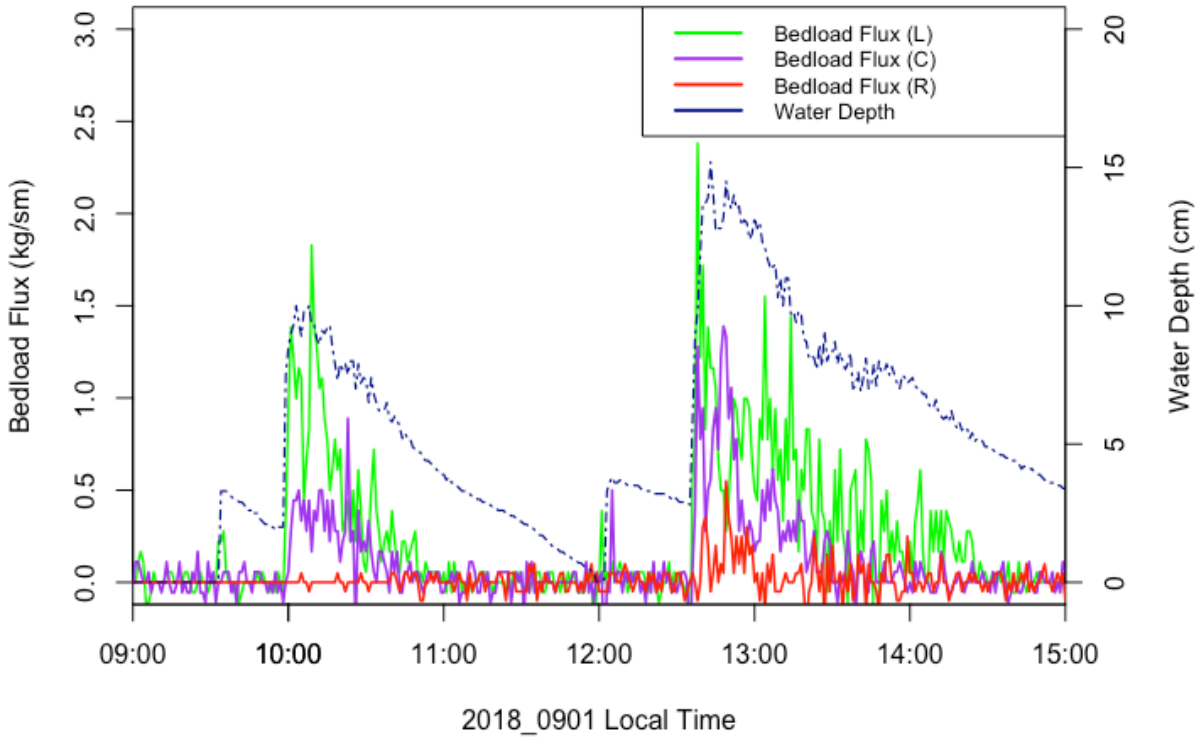

Figure 5: Time series of bedload flux for the three pit samplers (L: left, C: center, R: right) for the September 1 event (two flood waves, peak depth of 15 cm, as measured over left sampler). The lateral variability demonstrated here is present to varying degrees in most events. In this case, the thalweg in the approach reach was located near the left bank.

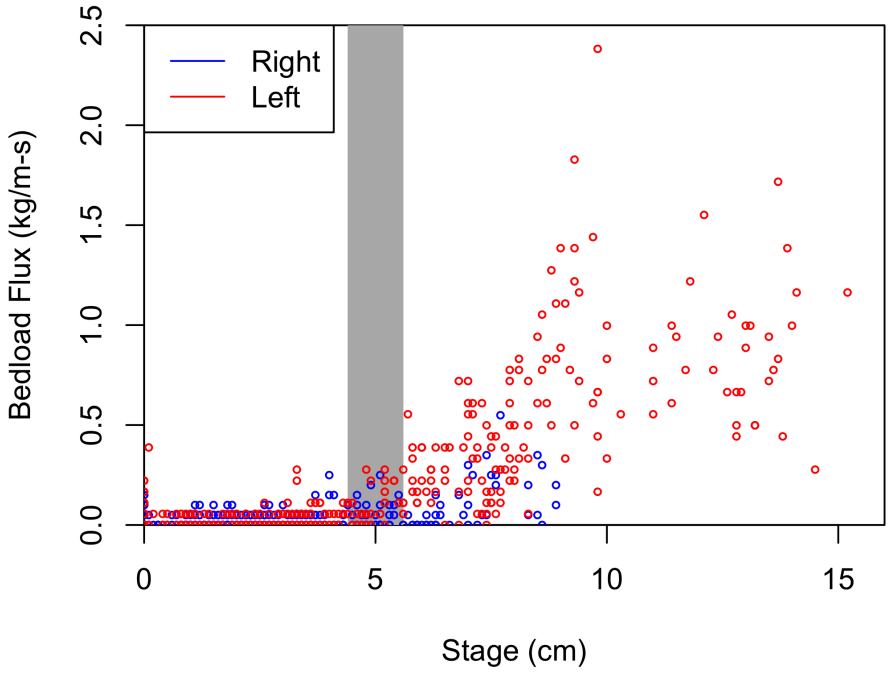

Figure 6: Influence of local water depth on bedload flux during the September 1 event. Gray bar indicates approximate depth at initiation of bedload transport. Shallower water on right bank can explain lower transport rates seen in Figure 5.

The initiation of bedload transport occurs at flow depths of approximately 10 cm within our study reach of the Arroyo de los Piños (Table 2). The July 16 event arrived with such a sudden flood bore, that stage went from 0 to 30 cm in the first minute (data recording interval was one minute), meaning that useful initiation data was not collected for that event. For comparison, the July 26 event rose much more slowly; transport commenced at 14 cm depth of water. The three events following the major flood on July 26 initiated motion at less than 10 cm water depth. As with the peak bedload flux data (Table 1), it is possible that the large July 26 event left the bed material in a more easily transported configuration than prior to the event.

Table 2: Stage at initiation of bedload transport

Event Date (all 2018)	Stage at Initiation of Motion (cm)	Note
July 16	30	First minute depth measurement
July 26	14	eventual peak stage: 160 cm
Aug 9	8	eventual peak stage: 19 cm
Aug 24	9	eventual peak stage: 33 cm
Sept 1	8	eventual peak stage: 15 cm

We documented considerable lateral variability of bedload transport through time (Figures 2, 3, and 5). The thalweg migrated across the channel during some flow events; this was more frequent in the 2017 monsoon season (Stark, 2018). The fixed bed elevation may have contributed to somewhat increased stability in 2018. Nonetheless, a mid-channel bar developed and varied in relative height during the season, though it never exceeded 10 cm above the side thalwegs, at least when exposed between floods. It was particularly well developed following the July 26 flood. Additionally, the temporal variability of bedload flux, with short duration spikes frequently observed (e.g., Figure 5) suggests the passage of sediment waves. Some are more extensive than others and affect multiple slot samplers (for example, at 13:10 in Figure 5).

Sieving of the captured bed material reveals greater variability in grain size distribution between events than within events (Figure 7). Samples were taken in 10 cm lifts from the ~ 80 cm deep boxes, yielding 8 samples for most event-sampler combinations. The first two events (July 16 and 26) had similar size distributions, near the middle of the overall distribution (yellow and green hues in Figure 7). The two smallest events (August 9 and September 1), each with ~15 cm maximum flow depth, collected the finest grain size distributions. Unexpectedly, the moderate sized (33 cm peak stage) late season (August 24) event had the coarsest transported material. Within an event, the coarsest samples were typically the earliest collected. We intend to compare these grain size distributions to bed material samples, but these have not yet been sieved.

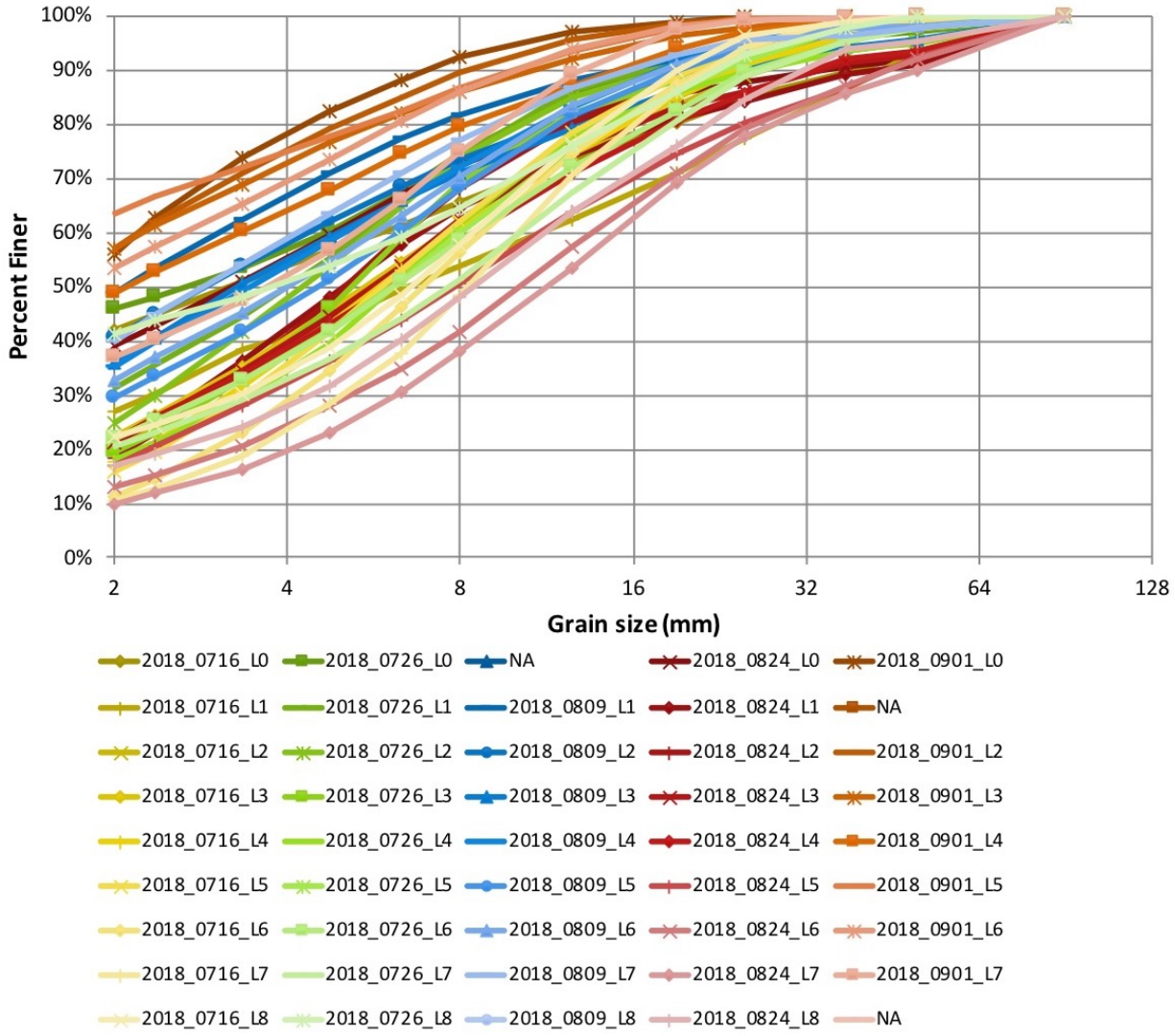

Figure 7: Percent finer grain size distribution for all analyzed transported sediment samples. L0 is the top of the sampler (last collected) and L8 is the bottom (first collected). NA indicates samples that are not yet processed.

Discussion

These bedload data represent the initial results from a new semi-arid site with detailed bedload transport data. The peak measured flux of 16 kg s^{-1} m^{-1} is one of the highest reported from other existing monitored sites. Comparison of measured flux can be made with the other semiarid and arid areas, worldwide: Walnut Gulch (Arizona, USA), Northern Negev Desert (Israel), and the Southern Judean Desert (Israel).

The Walnut Gulch data is not directly comparable, since it records annual changes in stock pond sedimentation. Watershed yields on this annualized basis reach as high as 3 m^3/ha, or 0.3 mm/year of denudation, for a watershed of 44 ha (Nichols, 2006; Nichols et al., 2008). Estimating peak bedload flux from this value that includes all suspended and bedload sediment

from a full year is unreliable. Nevertheless, it helps emphasize the large amounts of sediment moved even though the channel is ephemeral.

Bedload flux rates up to 10 kg s^{-1} m^{-1} are reported from the Nahal Eshtemoa in the Northern Negev Desert of Israel, measured using slot samplers, with flux interacting linearly with shear stress in most cases (Cohen et al., 2010). The nearby Nahal Yatir has a similar maximum value, ~ 7 kg s^{-1} m^{-1} (Reid et al., 1995). The range of bedload flux rates we observed at the Piños generally overlaps with the range from the Eshtemoa and Yatir. Only during the July 26 flood did our observations exceed those at the Eshtemoa. The highest reported bedload flux in the published literature is from the Nahal Rahaf, in the Southern Judean Desert of Israel, where the maximum 1-minute flux was 37 kg s^{-1} m^{-1} (Cohen et al., 2005). The maximum reported value from the nearby Nahal Qanna'im was 15 kg s^{-1} m^{-1}. The Rahaf is slightly steeper than the Piños at 1.7% slope and drains a larger catchment (78 km^2). The Qanna'im is steeper still, at 2.7% slope.

The threshold for motion in the Piños is very low, with a mere 10 cm initiating flow (Table 1). Before the flow depth even reaches 35 cm, the full bed is mobile, as demonstrated by the coarse grain size and abundant clasts exceeding 50 mm diameter transported throughout the August 24 event (Figure 7). This ready mobility may be attributable to the mix of sand and gravel in the bed material, not far from the 40% sand optimum observed by Wilcock & Kenworthy (2002).

Within an event, the coarsest samples were typically the earliest collected (Figure 7). This could be explained by flood bore turbulence enhancing the transport capacity of the flow. Within a flow event, the grain size distribution curve does not otherwise vary systematically. A possible explanation for this variability is the passage of discrete waves of coarser bedload sediment within a more consistent supply of finer bedload. Variation in grain size distribution between events is broader than within an event. The events with lowest peak stage produced the finest sediment distributions.

Though channel geometry is rectangular and simple at the monitoring site, cross sectional variations occur, due to the morpho-texture of the feeder reach. As of next year the inter-event morphology and texture of the feeder reach will be determined using SfM-based DEMS. We identified many gravel deposits and respective high water marks after the July 26, 2018 flood. These demonstrate that bedload fluxes were also very high in anabranches throughout the 250 m wide braided reach located immediately upstream of the monitoring site, so typical of many washes in the SW.

We do not observe any backwater effects from the Rio Grande at the monitoring station. During the large July 26 flood, in fact, the Rio Grande stage (which serves as local base level) was so low that knickpoint incision occurred, lowering the channel bed elevation by ~ 60 cm just downstream of the site. The sill containing the slot samplers acted as a grade control structure during this event, preventing the incision from advancing farther upstream. Despite this major downstream morphology change, the upstream morphology remained qualitatively the same to pre-flood, with no notable change in the grain size distribution of the bars or thalweg. We anticipate slow re-aggradation of the reach between the samplers and the Rio Grande in future events, both due to the lowered slope and the likelihood of higher river stage in future floods.

In conclusion, we observe high bedload fluxes at the Arroyo de los Piños, up to 16 kg s^{-1} m^{-1}. Initiation of transport occurs at very low water depths, less than 10 cm, so bedload transport occurs essentially whenever flow concentrates in the channel, even in very small, shallow flow events. Both observations are consistent with previously reported results from other unarmored ephemeral channels.

References

Brayshaw, A. C., Frostick, L. E., & Reid, I. (1983). The hydrodynamics of particle clusters and sediment entrapment in coarse alluvial channels. *Sedimentology*, *30*(1), 137–143.

Cao, Z., Hu, P., & Pender, G. (2010). Reconciled bedload sediment transport rates in ephemeral and perennial rivers. *Earth Surface Processes and Landforms*, *35*(14), 1655–1665. https://doi.org/10.1002/esp.2005.

Cohen, H., & Laronne, J. B. (2005). High rates of sediment transport by flashfloods in the Southern Judean Desert, Israel. *Hydrological Processes*, *19*(8), 1687–1702.

Cohen, H., Laronne, J. B., & Reid, I. (2010). Simplicity and complexity of bed load response during flash floods in a gravel bed ephemeral river: a 10 year field study. *Water Resources Research*, *46*(11).

Fenton, J. D., & Abbott, J. E. (1977). Initial movement of grains on a stream bed: The effect of relative protrusion. *Proceedings of the Royal Society of London A: Mathematical, Physical and Engineering Sciences*, *352*(1671), 523–537.

Gomez, B., & Church, M. (1989). An assessment of bed load sediment transport formulae for gravel bed rivers. *Water Resources Research*, *25*(6), 1161–1186.

Graf, W. L. (1981). Channel instability in a braided, sand bed river. *Water Resources Research*, *17*(4), 1087–1094. https://doi.org/10.1029/WR017i004p01087

Graf, W. L. (2006). Downstream hydrologic and geomorphic effects of large dams on American rivers. *Geomorphology*, *79*(3-4), 336-360.

Kirchner, J. W., Dietrich, W. E., Iseya, F., & Ikeda, H. (1990). The variability of critical shear stress, friction angle, and grain protrusion in water-worked sediments. *Sedimentology*, *37*(4), 647–672.

Kondolf, G.M. (1997). Hungry water: effects of dams and gravel mining on river channel. *Environmental Management 21*, 5-551.

Laronne, J. B., & Reid, I. (1993). Very high rates of bedload sediment transport by ephemeral desert rivers. *Nature*, *366*(6451), 148–150. https://doi.org/10.1038/366148a0

Laronne, J. B., Reid, I., Yitshak, Y., & Frostick, L. E. (1992). Recording bedload discharge in a semiarid channel, Nahal Yatir, Israel. *Erosion and Sediment Transport Monitoring Programmes in River Basins*, *210*, 79–96.

Laronne, J. B., Reid, I., Yitshak, Y., & Frostick, L. E. (1994). The non-layering of gravel streambeds under ephemeral flood regimes. *Journal of Hydrology*, *159*(1–4), 353–363. https://doi.org/10.1016/0022-1694(94)90266-6

Laronne, J.B., Alexandrov, Y.U., Bergman, N.A., Cohen, H., Garcia, C.E., Habersack, H.E., Powell, D.M., Reid, I. (2003) The continuous monitoring of bed load flux in various fluvial environments. IAHS publication, pp.134-45.

Lucía, A., Recking, A., Martin-Duque, J.F., Storz-Peretz, Y. & Laronne, J.B., 2013. Continuous monitoring of bedload discharge in a small steep sandy channel. *Journal of Hydrology*, *497*, 37-50. doi: 10.1016/j.jhydrol.2013.05.034

Miwa, H., & Parker, G. (2017). Effects of sand content on initial gravel motion in gravel-bed rivers. *Earth Surface Processes and Landforms*, *42*(9), 1355–1364.

Nichols, M. H. (2006). Measured Sediment Yield Rates from Semiarid Rangeland Watersheds. *Rangeland Ecology and Management*, *59*, 55–62.

Nichols, M. H., Stone, J. J., & Nearing, M. A. (2008). Sediment database, Walnut Gulch Experimental Watershed, Arizona, United States. *Walnut Gulch Experimental Watershed Water Resour. Res*, *44*, 5–6. https://doi.org/10.1029/2006WR005682

Powell, D. M., Brazier, R., Parsons, A., Wainwright, J., & Nichols, M. (2007). Sediment transfer and storage in dryland headwater streams. *Geomorphology*, *88*(1), 152–166.

Powell, D.M., Reid, I. and Laronne, J.B. 2001. Evolution of bedload grain-size distribution with increasing flow strength and the effect of flow duration on the calibre of bedload sediment

yield in ephemeral gravel-bed rivers. *Water Resources Research*, *37*(5), 1463-74, doi:10.1029/2000WR900342.

Powell, D. M., Reid, I., Laronne, J. B., & Frostick, L. (1996). Bed load as a component of sediment yield from a semiarid watershed of the northern Negev. *IAHS Publications-Series of Proceedings and Reports-Int'l Assoc. Hydrological Sciences*, *236*, 389–398.

Reid, I., Layman, J. T., & Frostick, L. E. (1980). The continuous measurement of bedload discharge. *Journal of hydraulic research*, *18*(3), 243-249.

Reid, I., Laronne, J. B., & Powell, D. M. (1995). Bed load sediment transport in an ephemeral stream and a comparison with seasonal and perennial counterparts. *Water Resources Research*, *31*(3), 773–781.

Shields, A. (1936). *Application of similarity principles and turbulence research to bed-load movement*. Soil Conservation Service.

Shih, W., & Diplas, P. (2018). A unified approach to bed load transport description over a wide range of flow conditions via the use of conditional data treatment. *Water Resources Research*, *54*(5), 3490–3509. https://doi.org/10.1029/2017WR022373

Stark, K.A. (2018). A two-year study of flash flood characteristics in New Mexican and Israeli ephemeral channels. (Unpublished MS Thesis). New Mexico Institute of Mining and Technology, Socorro, NM.

White, C. M. (1940). The equilibrium of grains on the bed of a stream. *Proceedings of the Royal Society of London. Series A, Mathematical and Physical Sciences*, 322–338.

Wilcock, P. R. (1988). Methods for estimating the critical shear stress of individual fractions in mixed-size sediment. *Water Resources Research*, *24*(7), 1127–1135.

Wilcock, P. R., & Crowe, J. C. (2003). Surface-based transport model for mixed-size sediment. *Journal of Hydraulic Engineering*, *129*(2), 120–128.

Wilcock, P. R., & Kenworthy, S. T. (2002). A two-fraction model for the transport of sand/gravel mixtures. *Water Resources Research*, *38*(10).

Investigation of Suspended-Sediment Concentration in the Mississippi River using LISST and Remote Sensing Surrogate Methods

Amanda Cox, Associate Professor, Saint Louis University, Saint Louis, Missouri, amanda.cox@slu.edu
Megan Martinez, Graduate Student, Saint Louis University, Saint Louis, Missouri, megan.martinez@slu.edu

Abstract

Suspended sediment affects the geomorphological characteristics that maintain ecological health and river navigability. Methods for estimating suspended-sediment concentration (SSC) in fluvial systems have evolved over several decades from in-situ direct measurements to surrogate techniques including acoustic, laser diffraction, and remote sensing methods. Several versions of the Laser In Situ Scattering and Transmissometry (LISST) instrument have been used to measure volume SSC and particle size distribution (PSD) in fluvial environments. Within the past few years, remote sensing has been used as a tool to measure SSC in large rivers such as the Mississippi River and the Amazon River. Remote sensing techniques for estimating SSC use surface reflectance measured from the water surface. The objectives of this study were to compare the LISST and remote sensing surrogate methods of measuring SSC and to investigate distributions of suspended sediment in the Mississippi River to provide insight into remote sensing methods of monitoring. A LISST-200X was used to collect SSC and PSD data at two cross-sections along the Mississippi River. Vertical distributions of SSC were collected using the LISST-200X at multiple points along the cross section. The LISST-200X volume SSC and PSD were converted to mass SSC and PSD by comparing the LISST-200X data to physical water samples concurrently collected by a US D-96 and US P-6 suspended-sediment sampler. Suspended-sediment concentration was estimated using from remote sensing by using Landsat satellite surface reflectance-SSC models created for the Middle Mississippi River. The LISST-200X SSC data were compared to the Landsat satellite surface reflectance-SSC. Further, vertical SSC distribution profiles from the LISST-200X were compared to theoretical distribution profiles from the Rouse equation, which shows increasing SSC from the water surface to the channel bottom.

Introduction

Background

Suspended sediment plays a significant role in river systems. Sediment is constantly being transported and deposited, affecting the geomorphological and chemical characteristics that control river navigability and ecological health. Sediment monitoring has become increasingly important because of the necessity to measure suspended-sediment concentration (SSC) and understand sediment movement and transport. The United States Geological Survey (USGS) has several gaging stations located along the Mississippi River and its tributaries that take discrete, daily samplesof SSC. The number of gaging stations collecting daily measurements has decreased in recent years. Collecting direct daily measurements is labor intensive requiring the use of Federal Interagency Sedimentation Project (FISP) sediment samplers. These samplers collect a water sample which must be processed in a lab to quantify SSC. Surrogate methods of

estimating SSC such as laser diffraction instruments require field data collection, but after initial calibration the processing time is minimal compared to processing of physical water samples. SSC estimated using remote sensing can also be a cost-effective way of measuring SSC if freely-available Landsat data are used. However, Landsat satellite surface reflectance data can be greatly affected by cloud coverage.

LISST-200X: Laser-diffraction based particle size analyzers are currently being used to measure particle sizes and concentrations in fluvial, and marine and coastal environments. Sequoia Scientific, Inc. introduced the world's first submersible commercial instruments for particle sizing based on laser diffraction. Sequoia Scientific's Laser In-Situ Scattering and Transmissometry (LISST) instrument systems are self-contained, compact, and programmable. Several versions of the LISST instrument have been used to measure SSC and particle size distribution (PSD) in fluvial environments (Topping et al., 2006; Agrawal et al., 2012; Baranya et al., 2012; Huan et al., 2015; Czuba et al., 2015; Agrawal et al., 2015). The LISST-200X measures particle size distribution (PSD) and concentration, as well as small-angle optical volume scattering function (VSF). The LISST-200X measures particle size from 1.0 to 500 micrometers and volume concentration at a 0.1 μL/L resolution.

Remote Sensing: The remote sensing method of estimating SSC uses measurements of reflectance from the water surface. Landsat satellites collect data with moderate temporal and spatial resolution and provide that data to the public to facilitate monitoring and research on the world's natural resources. The Landsat program is a joint effort between the USGS and the National Aeronautics and Space Administration (NASA). Landsat satellite data can be accessed for free through Landsat Data Access Portals. Pereira et al. (2017) created reflectance-SSC models for the Middle-Mississippi River (MMR) using surface reflectance measured by freely-available Landsat satellites. A revised version of Pereira et al. (2017) models were created using a power-regression model (Table 1). Remote Sensing detects SSC at the water surface and may not effectively represent the concentration throughout the entire water column.

Table 1. Reflectance-SSC empirical relationship created for the Middle-Mississippi River

Landsat Sensor	Reflectance-SSC Empirical Relationship	R^2
8 OLI/TIRS	$\mathrm{SSC(mgL^{-1})} = 159.9 * \left(\frac{b2}{b5}\right)^{-0.1337} * \left(\frac{b3}{b5}\right)^{-5.182} * \left(\frac{b4}{b5}\right)^{3.663} + 87.67$	0.87
7 ETM+	$\mathrm{SSC(mgL^{-1})} = 111.3 * \left(\frac{b1}{b4}\right)^{-0.2684} * \left(\frac{b2}{b4}\right)^{-6.033} * \left(\frac{b3}{b4}\right)^{5.031} + 63.84$	0.73
4-5 TM	$\mathrm{SSC(mgL^{-1})} = 74.80 * \left(\frac{b1}{b4}\right)^{-1.387} * \left(\frac{b2}{b4}\right)^{-4.639} * \left(\frac{b3}{b4}\right)^{4.227} + 80.68$	0.72

Note: b2, b3, b4 and b5 are Blue, Green, Red, and Near-Infrared band reflectance respectively for Landsat 8; b1, b2, b3, and b4 are Blue, Green, Red and Near-Infrared band reflectance respectively for Landsat 4-5 and Landsat 7 Satellites.

Suspended-Sediment Profiles: Rouse (1937) studied the vertical distribution of SSC in fluvial systems and found that for a given state of flow, the relative vertical distribution of the different particle sizes is based upon their settling velocities (Figure 1). The Rouse (1937) formula for vertical distribution of SSC is defined as the following:

$$\frac{C}{C_a} = \left(\frac{h-z}{z}\frac{a}{h-a}\right)^{P=\frac{\omega}{\kappa u_*}} \quad (1)$$

where C is suspended-sediment concentration at z (mgL^{-1}); z is elevation above the bed (m); C_a represents the reference suspended-sediment concentration at a (mgL^{-1}); a is reference elevation above the bed elevation (m); h is flow depth (m); ω is the settling velocity (ms^{-1}); κ is Von Karman's constant; u_* is shear velocity (ms^{-1}); and P is the Rouse Number. The sediment distribution curves developed from the Rouse equation show increasing SSC from the water surface to the channel bottom (Figure 1).

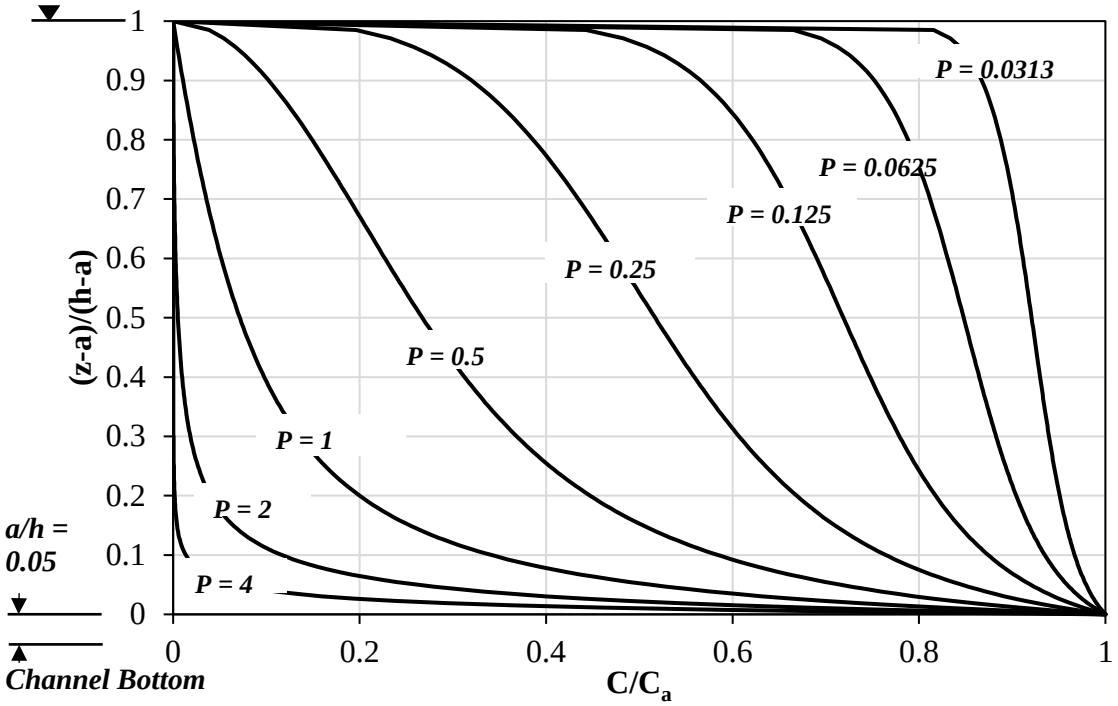

Figure 1. Rouse profile for various Rouse numbers

Methods

Data Collection

Two data collection sites along the Middle Mississippi River (MMR) were used for this study. These collection sites were located at USGS gaging stations at Chester, IL (07010000) and St. Louis, MO (07020500). Field data collection dates coincided with Landsat 8 satellite collection dates, so that LISST-200X SSC data and SSC determined from the physical water samples could be compared to SSC estimated from the reflectance-SSC models. Field data collection dates were also selected to occur during the summer months for there to be a lesser likelihood of cloud coverage since Landsat surface reflectance data are affected by clouds. The two field collection dates were on June 14th, 2018 and August 1st, 2018 for the Chester site and St. Louis site, respectively.

Data were collected at the two Mississippi River cross-sections (Chester and St. Louis gages sites) using the LISST-200X. Physical water samples were taken concurrently with the LISST -

200X using a US D-96 depth integrating suspended-sediment sampler and a US P-6 point integrating suspended-sediment sampler. LISST-200X and US D-96 depth-integrated samples were taken vertically along the Chester, IL cross-section and the St. Louis, MO cross-section. Five depth-integrated samples were collected using a US D-96 sampler at the 10%-, 30%-, 50%-, 70%- and 90%-discharge width points at Chester. The 10%-discharge width point was located at the Illinois side of the Mississippi River and the 90%-discharge width point was on the Missouri side. Ten depth-integrated samples were taken at 5%-, 15%-, 25%-, 35%-, 45%-, 55%-, 65%-, 75%-, 85%-, and 95%-discharge width points at St. Louis. The 5%-discharge width location was on the Illinois side of the Mississippi River and the 95%-discharge width location was on the Missouri side. For the LISST-200X depth-integrated data collection, the instrument was slowly lowered to the approximately 0.5 m above the channel bed and then brought back to the top of the water. The LISST-200X collects measurements at a rate of one Hz.

Point samples were taken using the US P-6 sampler at both Chester and St. Louis. Seven point samples were taken at the Chester 50%-discharge width point at five-foot depth increments from five to thirty feet (5, 10, 15, 20, 25, 30, and 35 ft). Twelve points samples were taken at the St. Louis 25%- and 75%-discharge width locations; six samples at 25%-discharge width and six samples at 75%- discharge width. The St. Louis point samples were taken at five-foot depth increments from five feet to thirty feet (5, 10, 15, 20, 25, and 30 ft) and five feet to thirty-five feet, excluding the twenty-foot point, (5, 10, 15, 25, 30 and 35 ft) at the 25%- and 75%-discharge width points respectively. The LISST-200X ‘point’ samples were taken by lowering and stopping the LISST-200X at five-foot increments. The LISST-200X was kept stationary at five-foot increments for one-minute periods. Since the sampling rate for the LISST-200X collection was set at 1 Hz, at least 60 measurements were made during each one-minute period. The average of the measurements was used to represent the LISST-200X ‘point’ samples.

Data Processing

LISST-200X: LISST-200X volume SSC was converted to mass SSC by correlating the LISST-200X data to data collected by the US P-6 and US D-96 suspended-sediment samplers for each station. Regression analysis was performed for the whole data set and for the two separate stations. The best fit regression equation was a power function. The coefficient of determination for the whole dataset, combing Chester and St. Louis data, was 0.524. When regression analysis was separated into individual stations, coefficients of determination increased from 0.5211 to 0.671 and 0.572 for Chester and St. Louis, respectively (Figure 2 and Figure 3). The LISST-200X data were converted using the individual station regression power equations.

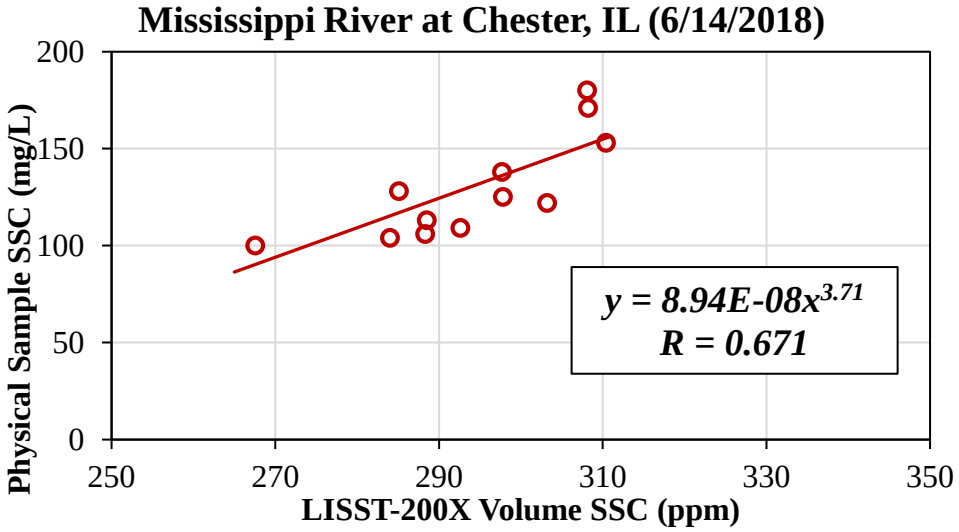

Figure 2. Physical Sample Mass SSC – LISST-200X Volume SSC Regression for Chester, IL Dataset

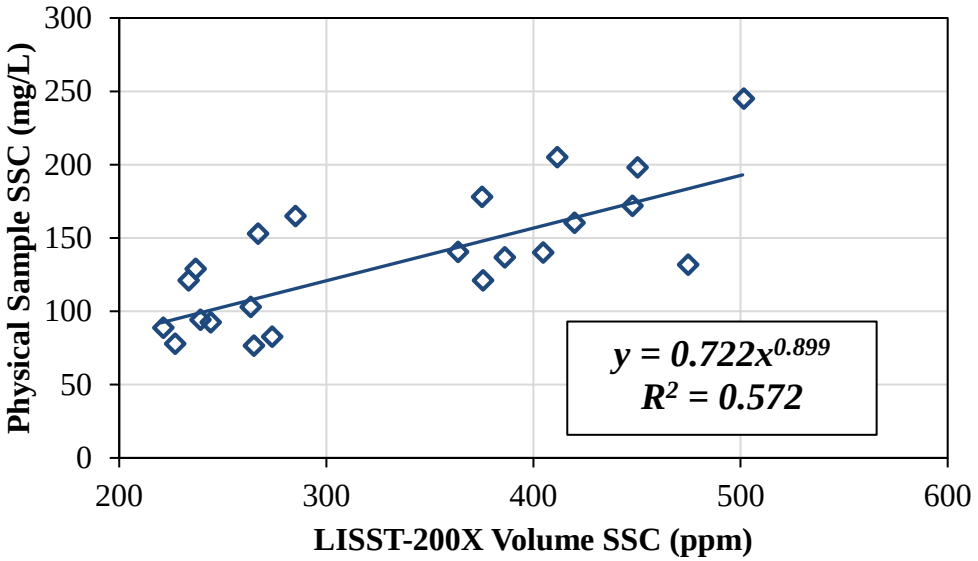

Figure 3. Physical Sample Mass SSC – LISST-200X Volume SSC Regression for St. Louis, MO Dataset

Remote Sensing: The surface reflectance-SSC model (Table 1) for Landsat 8 was used to determine SSC at Chester and St. Louis stations. Cirrus clouds were over the exact data collection location at the Chester site (Figure 4). Surface Reflectance-SSC for the Chester site was therefore taken upstream from the physical data collection points. St. Louis surface reflectance-SSC was calculated for each point that physical samples were taken (Figure 5).

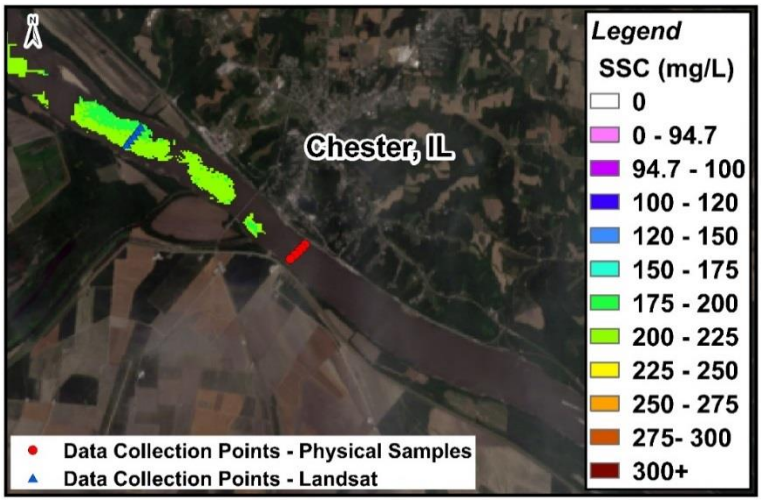

Figure 4. Surface Reflectance-SSC at Chester, IL

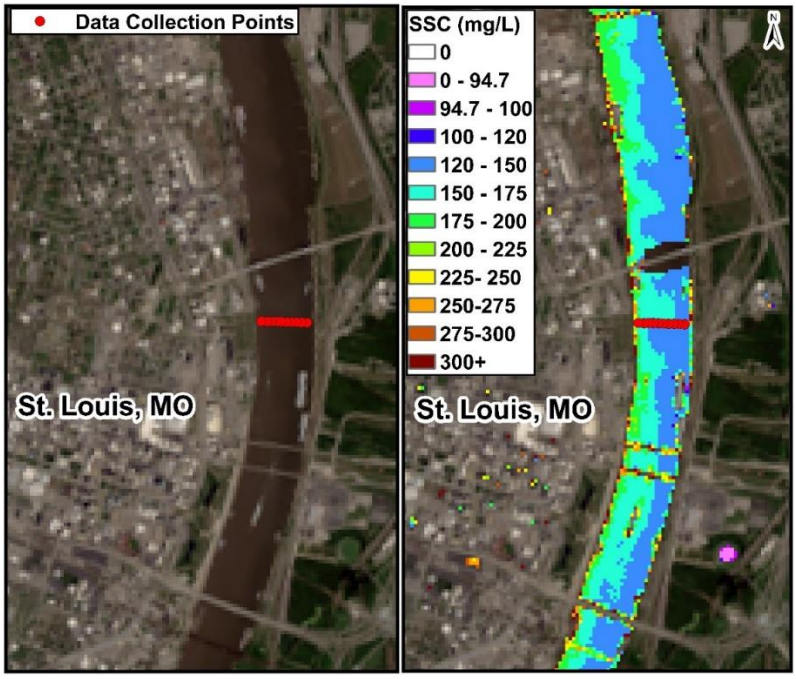

Figure 5. Surface Reflectance-SSC at St. Louis, Missouri

Results

Comparing Surrogate Methods

Depth-integrated SSC from the US D-96 sediment sampler was compared to two surrogate methods of determining SSC: the laser diffraction method using the LISST-200X instrument and surface reflectance-SSC method using Landsat 8 satellite. Ascending and descending depth-integrated SSC was calculated from LISST-200X vertical SSC profiles SSC and the average of the two depth-integrated values were used as the final depth-integrated LISST-200X SSC values.

At the Chester Landsat data collection cross-section, the SSC on the Missouri side was 204 mgL^{-1} and the Illinois side was 200 mgL^{-1}. The Missouri and Illinois sides of the river cross-section were only different by 2%. The Landsat surface-reflectance method overestimated SSC by 1.3 – 1.8 times when compared to the physical sample direct measurements at each point at Chester (Figure 6). Figure 6 shows that SSC was higher on the Missouri side of the Mississippi River for both surrogate methods but the calibrated LISST-200X predicted SSC closer to the physical samples.

The August 1st Landsat 8 SSC image at the St. Louis, MO station showed a higher SSC on the Missouri side of the Mississippi River (Figure 5). The Landsat surface reflectance-SSC at the point closest to the Missouri side was 182 mgL^{-1} and 134 mgL^{-1} at the point nearest to the Illinois side. The physical samples and the LISST-200X samples consistently showed that the Illinois side had the lower concentrations of SSC than the Missouri side of the Mississippi River (Figure 7). Sixty percent of the time, the LISST-200X predicted SSC better than Landsat surface reflectance-SSC. On the Missouri side, the LISST-200X predicted SSC the best, while one the Illinois side, Landsat surface-reflectance predicted SSC the best. Both surrogate methods were able to predict higher SSC on the Missouri side of the Mississippi River as expected. The Missouri River drains 43% of the total area of the Mississippi River basin. The Missouri river only contributes 12% of the total flow but is by far the major contributor of sediment to the Mississippi River (Meade and Moody, 2010).

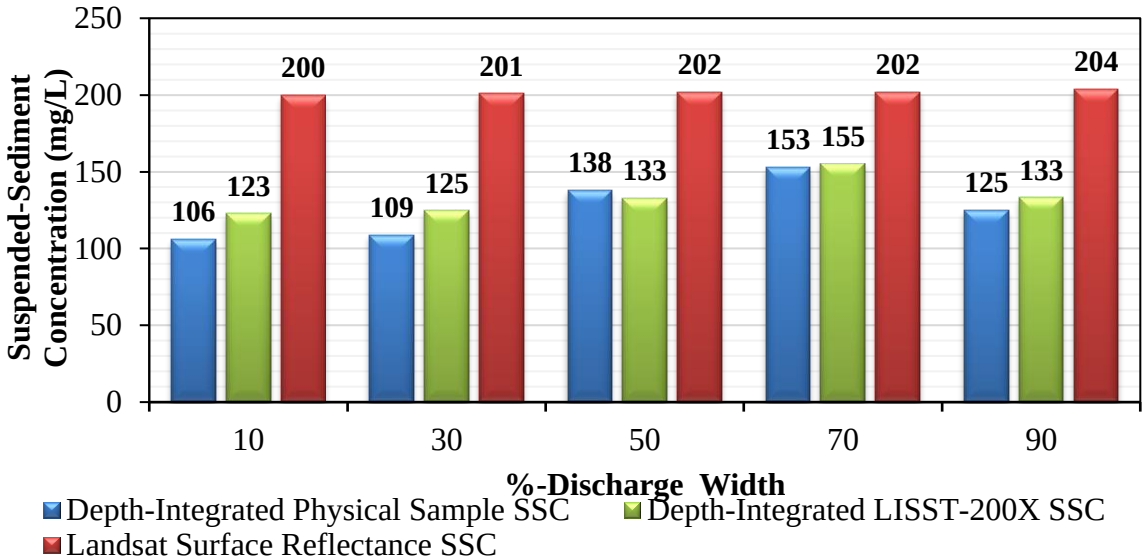

Figure 6: Comparison of SSC determined from Physical samples to surrogate methods of determining SSC (LISST-200X and Landsat Satellite) at Chester, IL on June 14, 2018

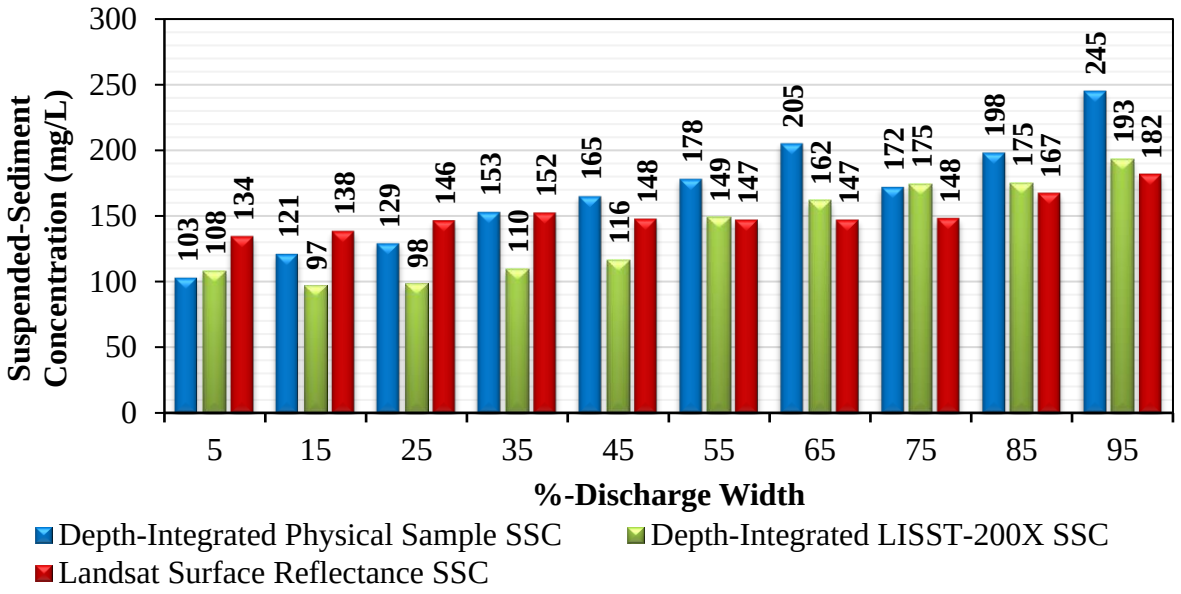

Figure 7. Comparison of SSC determined from Physical samples to surrogate methods of determining SSC (LISST-200X and Landsat Satellite) at St. Louis, MO., on August 1, 2018

SSC Vertical Profiles

Vertical SSC profiles were created using LISST-200X converted SSC data. Suspended-sediment concentration profiles were created using descending and ascending LISST-200X data. Vertical SSC profiles were also created from data when the LISST-200X was descending at five-foot increments for one minute (Figure 8 and Figure 9). The SSC data collected within the one-minute periods had a standard deviation ranging between 15.1 to 60 mg/L for Chester, IL. The averages of the SSC collected are plotted in Figure 8 for each of the one-minute periods which shows an increase of SSC with depth below water surface. Data from the vertical SSC profile created from St. Louis, MO in Figure 9 shows similar high variability within one-minute period measurements with a standard deviation ranging from 3.0 to 12.1 mg/L. The average SSC from the one-minute periods shows increases in SSC with depth for both the 25%-discharge width and 75%-discharge width locations.

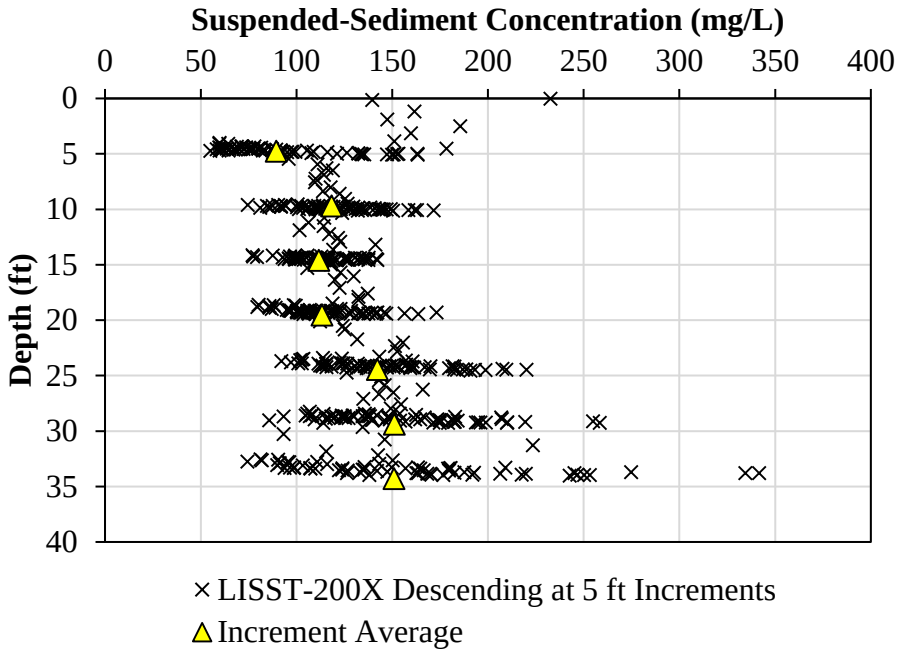

Figure 8. Vertical SSC profile from LISST-200X one-minute period measurements at five-foot increments at Chester, IL

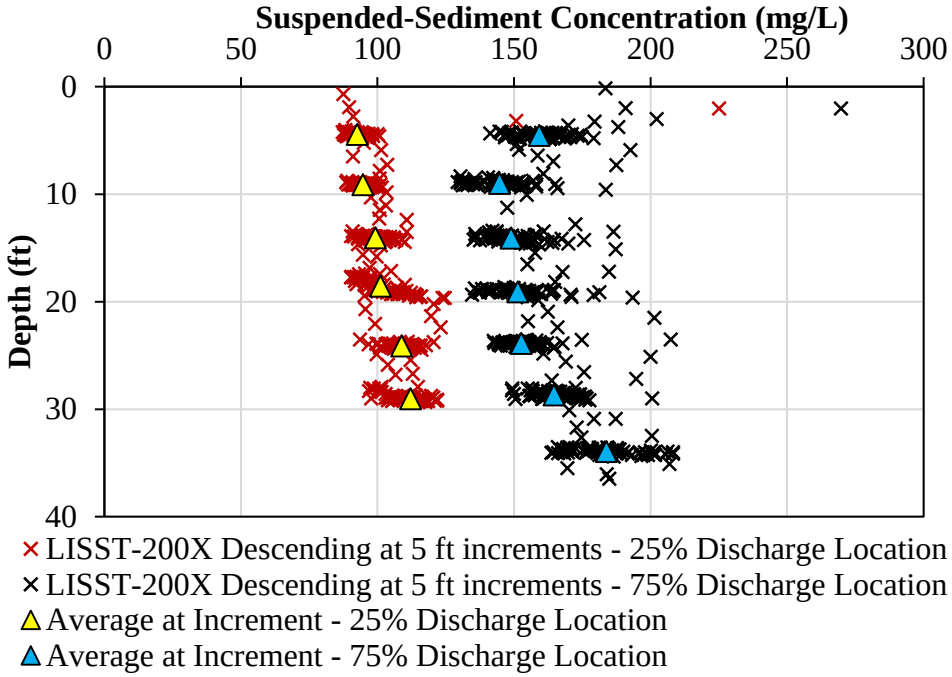

Figure 9. Vertical SSC profile from LISST-200X one-minute period measurements at five-foot increments at St. Louis, MO

The descending-ascending LISST-200X SSC profiles for 90%- and 10%-discharge width locations at Chester (Figure 10) and for 95%- and 5%- discharge width locations at St. Louis (Figure 11) show increasing SSC with depth to some degree. Although some areas of profile the

SSC would vary irregularly, each descending-ascending LISST-200X SSC profile shows a general increase in SSC with depth. The 5%-discharge width channel width location at St. Louis shows the least variability of SSC with depth. Similar trends were also observed in the 45%-, 35%-, 25%-, and 15%-discharge width locations. The profiles on the Missouri side of the Mississippi river (55%-, 65%-, 75%-, 85%-, and 95%-discharge width locations) had areas of fluctuation in their profiles. The shape of the St. Louis profiles could be due to the influx of SSC and discharge from the Missouri River. The delayed mixing of the Missouri River SSC with pre-confluence Mississippi River SSC could be the reason behind the lower SSC on the Illinois side. Therefore, the influx may not be affecting the Illinois side of the river at that location, leading to less variability in the profile and lower SSC on that side of the River.

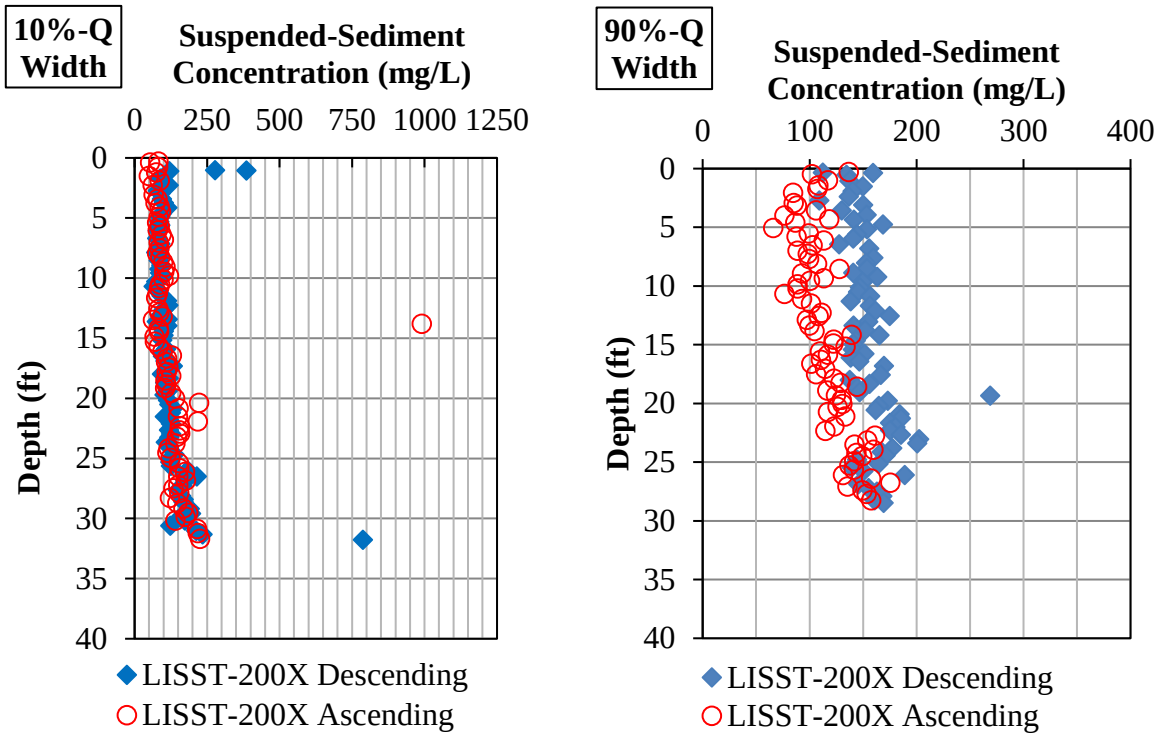

Figure 10. Chester, IL LISST-200X Vertical Profiles

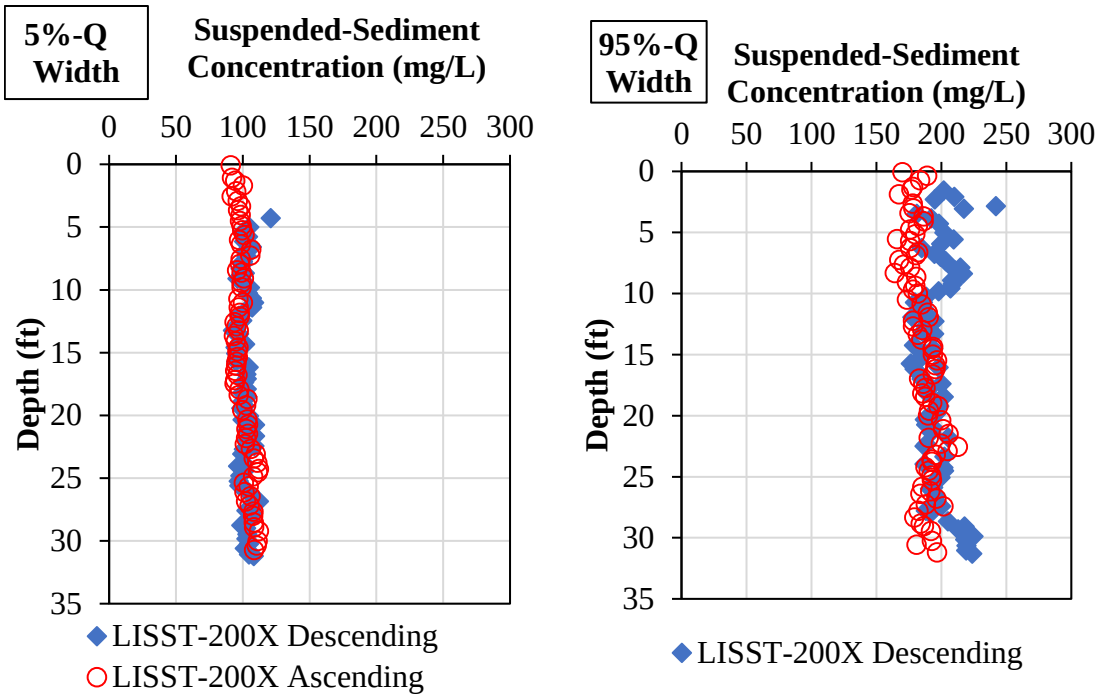

Figure 11. St. Louis, MO LISST-200X SSC Vertical Profiles

The descending-ascending LISST-200X SSC profiles plotted in Figure 11 show that at equivalent depths, SSC was not always identical. The profiles mostly indicate higher concentrations at equivalent depths when the LISST-200X was descending. The averages of the SSC collected in each one-minute increment fit in between the ascending and descending SSC profiles although the SSC collected within one-minute period was highly variable (Figure 8).

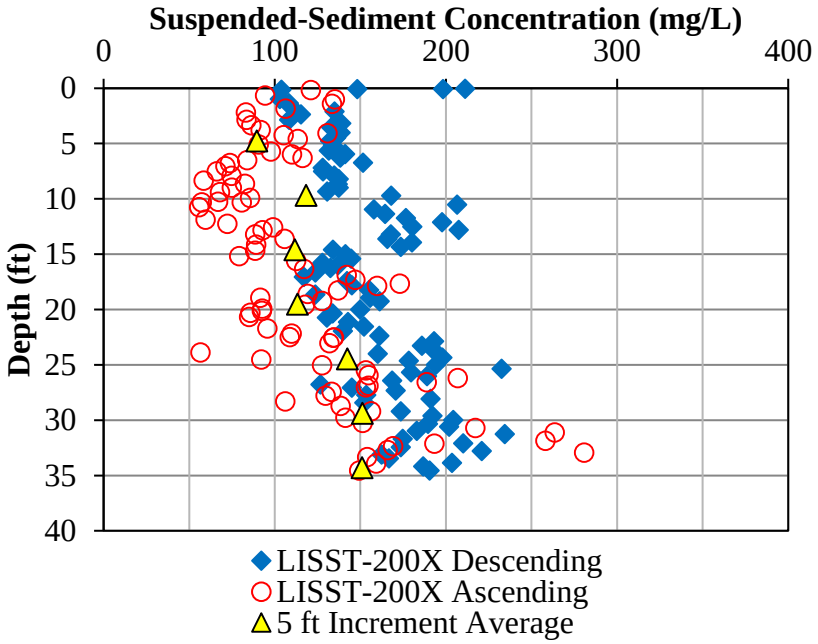

Figure 11: LISST-200X Vertical SSC profile at the 50%-Discharge width location at Chester, IL

The vertical SSC profiles from physical point samples and the LISST-200X averaged SSC from one-minute collection periods are shown in Figure 12. Both profiles exhibit an increase in SSC with depth. Although the physical sample SSC profile was not uniformly increasing at each depth increment, the profile increased from 100 mgL^{-1} at 5 ft to 180 mgL^{-1} at 35 ft. LISST-200X SSC increased from 89.5 mgL^{-1} at 5 ft to 151.1 mgL^{-1} at 35 ft.

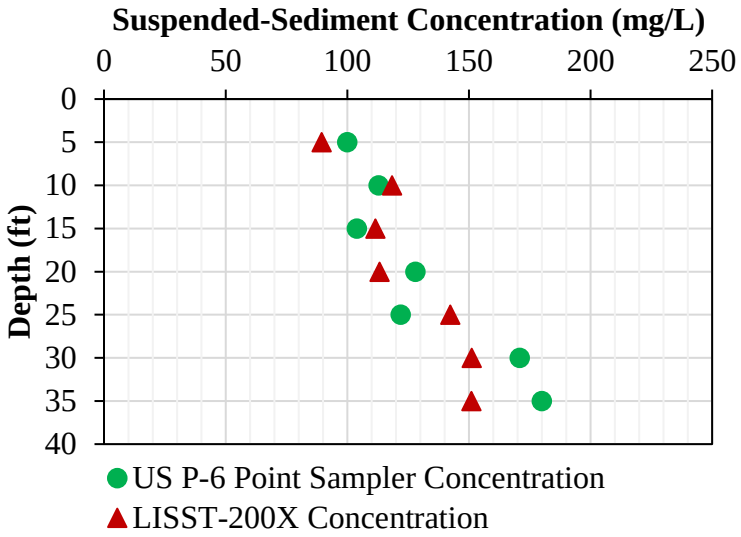

Figure 12: Vertical SSC profile at Chester, IL

Vertical SSC profiles for St. Louis are shown in Figure 13. The SSC profile at the 75%-discharge width location were on average 1.7 times higher than the SSC at the 25%-discharge width location. The profiles reflect the predicted higher SSC coming from the Missouri River. Vertical SSC profiles from the LISST-200X show a clear increasing trend in SSC with depth. The physical sample SSC vertical profiles both fluctuated irregularly and did not uniformly increase with depth. The profile at the 25%-discharge width location decreased, increased, and decreased again so that the SSC at the deepest point was lower than the SSC at the 5 ft point. The 75%-discharge width location had the same decrease, increase, and decrease pattern of SSC at the deepest point lower than at the 5 ft point.

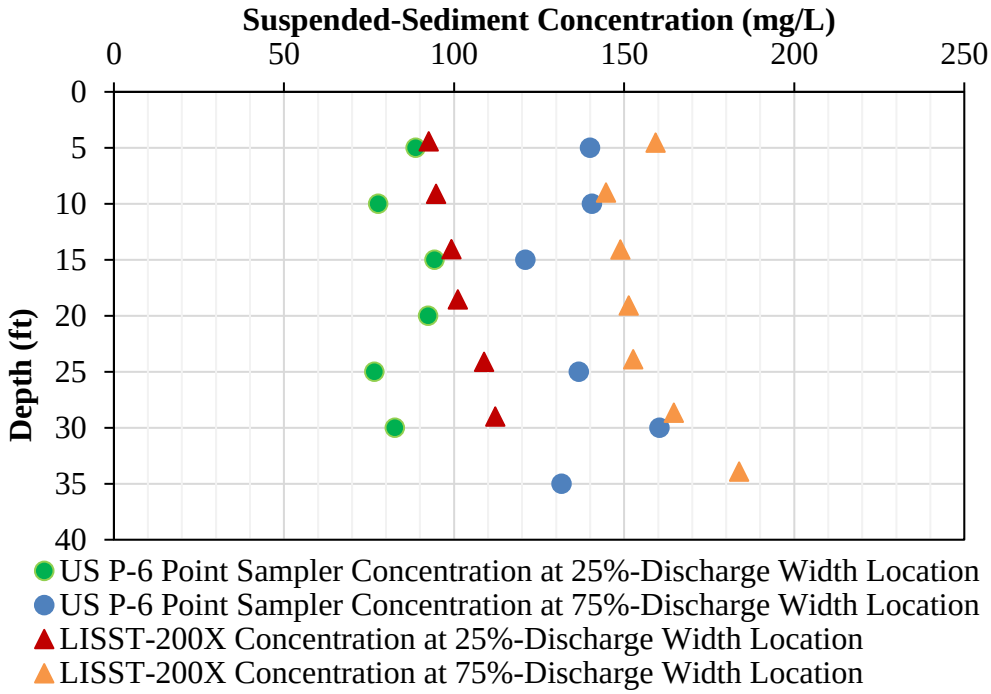

Figure 13: Vertical SSC profile for St. Louis, MO data from US P-6 Sediment Sampler and LISST-200X

Rouse Profile

A Rouse profile was created using equation (1) with data for the Chester, IL collection site. The Rouse number was calculated using Stokes settling velocity in clear water, ω_o, equation (2) and equation for shear velocity, u_*, equation (3) as follows:

$$\omega_0 = \frac{1}{18}\frac{(G-1)g}{\upsilon} {d_s}^2 \tag{2}$$

$$u_* = \sqrt{\frac{\gamma h S_0}{\rho}} \tag{3}$$

where, G is relative density, g is acceleration due to gravity (ms^{-2}); υ is kinematic viscosity of water (m^2s^{-1}); d_s is particle diameter (m); γ is specific weight of water (kgm^{-3}); h is flow depth (m); S_o is bed slope; and ρ is density of water (Nm^{-3}). The flow was assumed to be steady, and uniform, therefore the bedslope, S_o, was assumed to be equal to the water surface slope, S_w, which was calculated as 0.0001 from gaging data. Shear velocity was found to be 0.110 m/s and 0.102 m/s at Chester and St. Louis, respectively. Settling velocities were calculated using the median particle diameter, d_{50} as the particle diameter, d_s. Median particle diameters were found from the LISST-200X particle size distribution curves. The average median particle diameter for Chester, IL samples was found to be 0.034 mm. For St. Louis, the average median particle diameter was found to be 0.030 mm. The settling velocity was calculated to be 0.125 cms^{-1} for the Chester, IL dataset. Using the calculated settling velocity, the corresponding theoretical calculated Rouse number, P_t, for the Chester site was 0.0285. For St. Louis, the settling velocity was calculated to be 0.0818 cms^{-1}, The corresponding theoretical Rouse number, P_t, for St. Louis was 0.0238. The experimental Rouse number, P_e, was found by correlating LISST-200X relative SSC data, C/C_a,

to $\left(\frac{h-z}{z}\frac{a}{h-a}\right)$, z,' to find the best fit power regression use the least-squares regression method. Experimental Rouse numbers were found for all fifteen LISST-200X vertical SSC dataset, five from Chester and ten from St. Louis shown in Table 2 and Table 3, respectively. An example of one of the fifteen best fit power curves is shown in Figure 14.

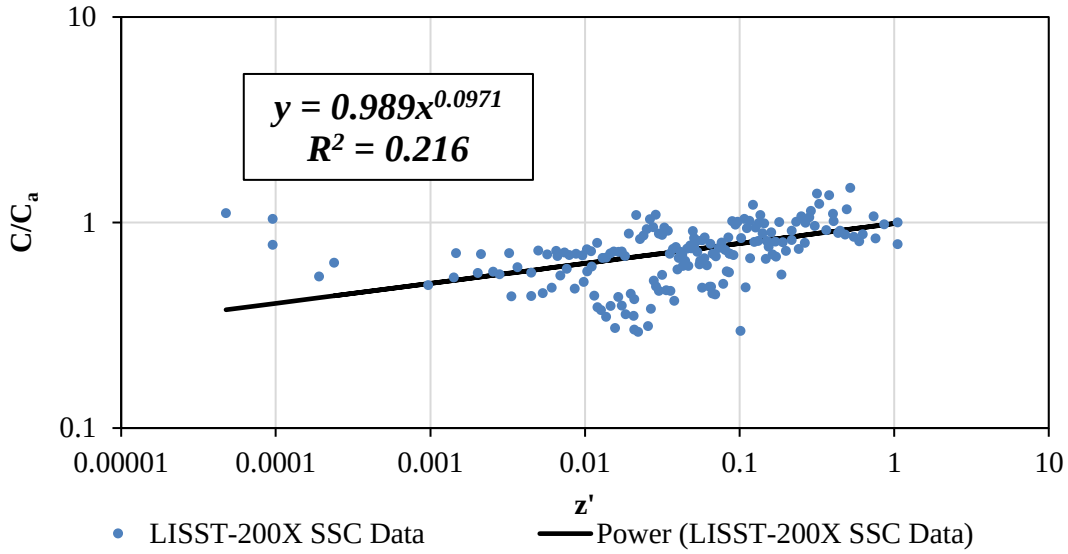

Figure 14: Best fit power regression curve for LISST-200X SSC data from the 50%-Discharge width Location at Chester, IL

An average experimental Rouse number, $P_{e,avg}$, was found for Chester and St. Louis. The experimental Rouse numbers were found to be 0.145 and 0.0253 for Chester and St. Louis respectively separately. The predicted Rouse profiles were plotted using both theoretical, experimental average, and experimental location-specific Rouse numbers (Figure 15, Figure 16, and Figure 17). The Chester predicted Rouse profiles (Figure 15) from the experimental Rouse numbers fit well with the vertical SSC profiles both physical sample and LISST-200X points. However, the St. Louis predicted Rouse profiles were not as successful at fitting the physical and LISST-200X SSC samples. The experimental Rouse profile for St. Louis overestimated SSC in both profiles (Figure 16 and Figure 17). The theoretical Rouse numbers were almost equal for Chester and St. Louis. The predicted Rouse profiles from the theoretical Rouse numbers did not fit the points from physical sample and LISST-200X data as closely as the experimental Rouse numbers.

Table 2. Experimental Rouse numbers, P_e, for Chester, IL.

%-Discharge Width	Rouse Number, P_e
10%	0.214
30%	0.223
50%	0.0971
70%	0.127
90%	0.0629
Average	*0.145*

Table 3. Experimental Rouse Numbers, P_e, for St. Louis, MO.

%-Discharge Width	Rouse Number, P_e
5%	0.0175
15%	0.0174
25%	0.0176
35%	0.0207
45%	0.0240
55%	0.0417
65%	0.0275
75%	0.0345
85%	0.0374
95%	0.0142
Average	*0.0253*

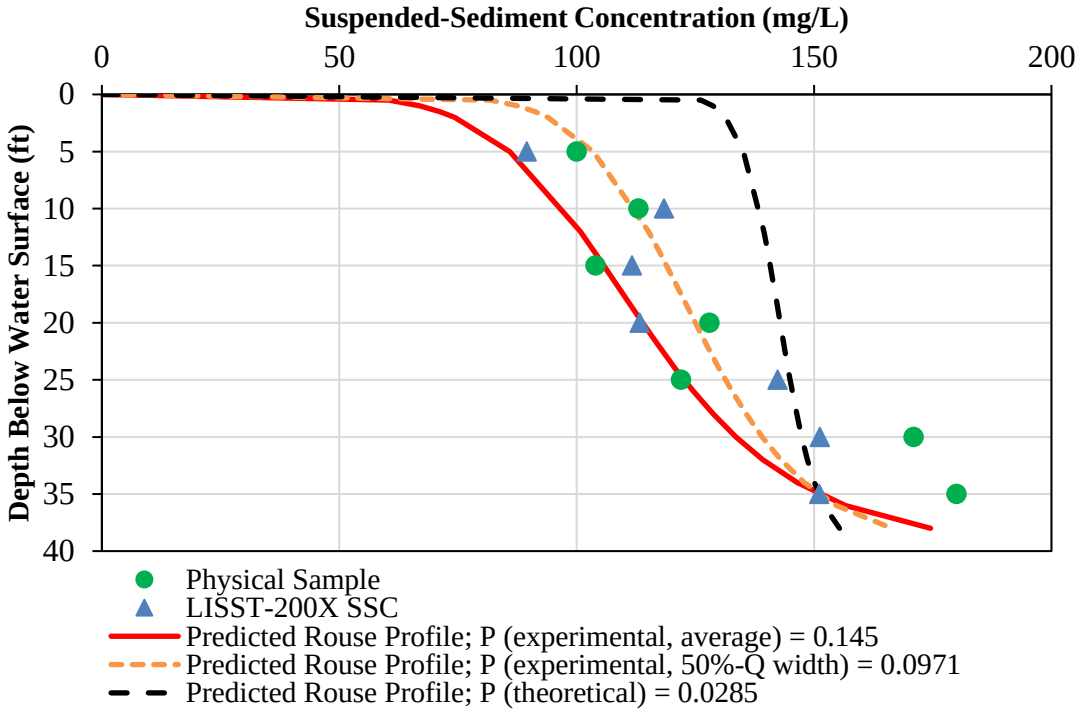

Figure 15: Predicted Rouse Profiles from Experimental and Theoretical Rouse Numbers for 50%-discharge width location at Chester

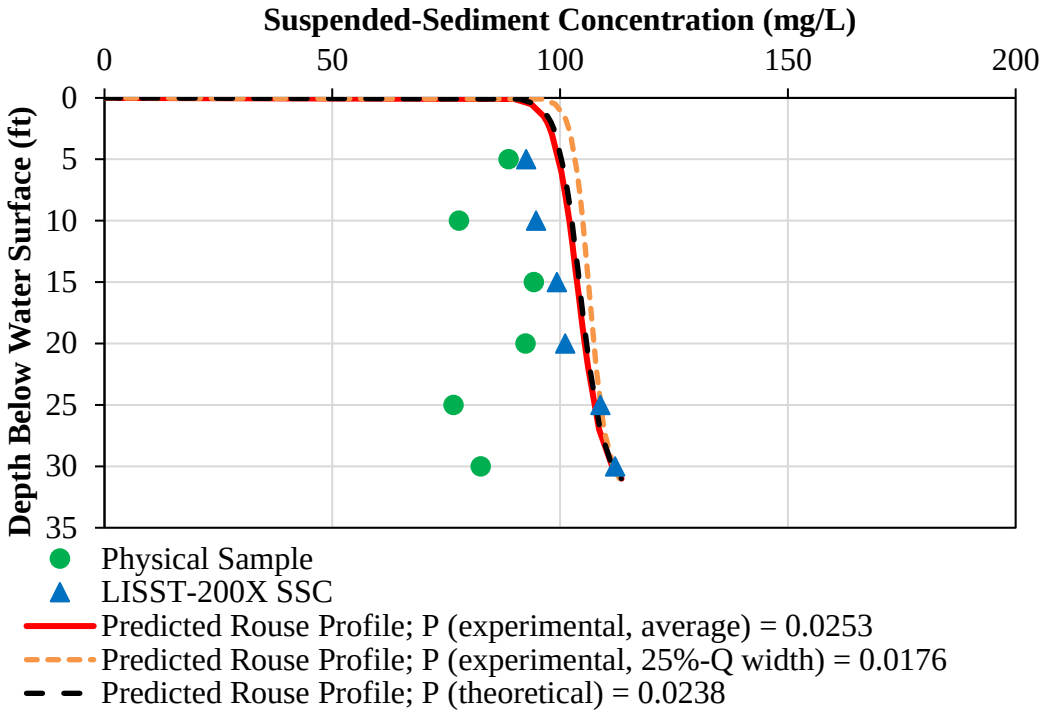

Figure 16: Predicted Rouse Profiles from Experimental and Theoretical Rouse Numbers for the 25%-discharge width location at St. Louis

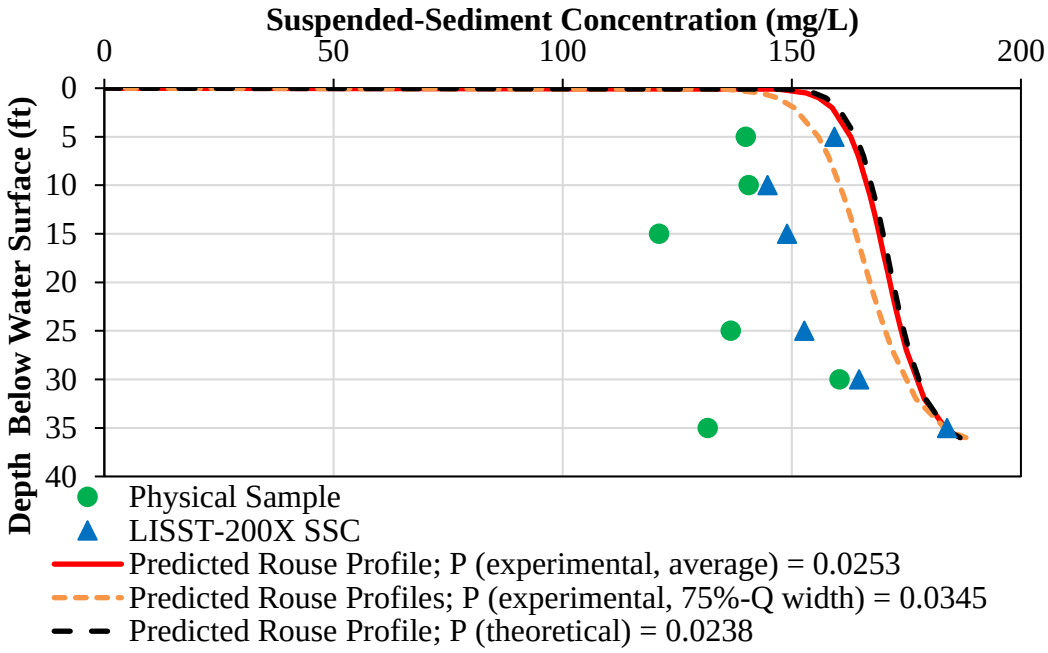

Figure 17: Predicted Rouse Profiles from Experimental and Theoretical Rouse Numbers for the 75%-discharge width location at St. Louis

Conclusions and Future Work

The following main final conclusions were made on this study:

1. laser diffraction was an effective surrogate method for measuring SSC when used in a large river such as the Mississippi River;
2. from the LISST-200X data, temporal variability was observed in SSC at stationary points in a water column (standard deviations ranging from 15.1 to 60.0 and 3.0 to 12.1 for Chester and St. Louis, respectively);
3. the LISST-200X instrument may not have been fully measuring the total SSC due to the instrument's particle measurements range;
4. the remote sensing surrogate method estimated SSC at lower concentrations best (St. Louis dataset), which supports the theory that surface-reflectance-SSC may not be fully capturing SSC in an entire water column;
5. the remote sensing surrogate method using Landsat imagery is not an ideal method for continuous SSC monitoring on the Mississippi River due its limited temporal resolution (16 days between measurements) and dependence on clear weather conditions; however, these limitations could be overcome by utilizing terrestrial-based remote sensing equipment;
6. the LISST-200X SSC (13.1%) had a lower percent error when predicting SSC than the Landsat surface-reflectance SSC (27.3%);
7. when comparing Rouse profiles created from experimentally and theoretically derived Rouse numbers, the theoretical Rouse number (P_t = 0.0285) was smaller than the experimental Rouse Numbers ($P_{e,avg}$ = 0.145 and $P_{e,50\%\text{-}Q\ width}$ = 0.0971) for Chester and the experimental Rouse number profiles matched the SSC profile the best while for St. Louis, theoretical and experimental Rouse numbers differed minimally (P_t =0.0238, $P_{e,avg}$ =0.0253, $P_{25\%\text{-}Q\ width}$ = 0.0176, and $P_{75\%\text{-}Q\ width}$ = 0.0345) but all Rouse number profiles did not match the SSC profile well.

The LISST-200X provides a time-saving surrogate method for collecting SSC with high temporal resolution. The spatial resolution can be determined by the data collector. If several vertical samples are taken to create good spatial resolution, the data could be used to create an entire cross-sectional SSC river profile. These cross-sectional SSC profiles could be helpful in studying sediment transport and aid in creating sediment transport models.

The remote sensing surrogate method provides high spatial-resolution SSC for the Mississippi River. A clear distinction in SSC contribution from the Missouri River was observed with higher SSC values on the Missouri side of the Mississippi river at the St. Louis site. The effect of cloud coverage was shown in the Chester, IL dataset. The loss of data is a disadvantage of the remote sensing surrogate method but it can still provide valuable data for large-scale monitoring of SSC with high spatial resolution.

The Rouse profiles created using the best-fit experimental Rouse number matched the measured vertical SSC profile more closely than the theoretically calculated Rouse numbers. The Rouse profile was created originally for use in streams rather than big rivers such as the Mississippi River. The poor performance of the predicted Rouse profiles could be due to the fact that in larger rivers a wide range of particle sizes are in suspension and determining a representative fall velocity for the range of sizes may not be possible.

Future research may be done to address multiple issues faced when using Landsat satellites. The effect of cloud coverage combined with the temporal resolution of Landsat could cause large gaps in the SSC dataset. To address these problems, a terrestrial multispectral camera could be used to collect images that can then be correlated to SSC, like the Landsat surface reflectance-SSC correlation. Terrestrial multispectral cameras can be either mounted at a USGS gaging station or attached to a drone for data collection. A mounted terrestrial multispectral camera would eliminate the time required for physical data collection because it could be programmed to take periodic images that could remotely accessed. Multispectral cameras as a surrogate method of estimating SSC could also provide a finer spatial resolution than Landsat's 30 m by 30 m resolution.

References

Topping, D. J., Wright, S. A., Melis, T. S., and Rubin, D. M. (2006), High resolution monitoring of suspended-sediment concentration and grain size in the Colorado river using laser-diffraction instruments and a three-frequency acoustic system.

Agrawal Y. C., Mikkelsen, O. A., and Pottsmith, H.C. (2012), Grain size distribution and sediment flux structure in a river profile measure with a LISST-SL instrument, *Sequoia Scientific, Inc.* Report.

Baranya, S., Józsa, K, Török, G.T., and Rüther, N. (2012), A comprehensive field analysis of a river confluence. In *River Flow 2012 – Proceedings of the International Conference of Fluvial Hydraulics* (Vol. 1, pp. 565-571)

Huan, S., Rüther, N., Baranyra, S., and Guerrero, M. (2015), Comparison of real time suspended sediment transport measurements in river environment by LISST instruments in stationary and moving operation mode, *Flow Measurements and Instrumentation, 41,* 10-17. doi:10.1016/j.flowmeasinst.2014.10.009

Czuba, J. A., Straub, T. D., Curran, C. A., Landers, M. N., and M. M. Domanski (2015), Comparison of fluvial suspended-sediment concentrations and particle-size distributions measured with in-stream laser diffraction and in physical samples, *Water Resour. Res., 51,* 320-340, doi:10.1002/2014WR05697

Agrawal, Y. C., and Hanes, D. M. (2015), The implications of laser-diffraction measurements of sediment size distributions in a river to potential use of acoustic backscatter for sediment measurements, *Water Resour. Res., 51,* 8854-8867, doi:10.1002/2015WR017268.

Pereira, L. S. F., Andes, L. C., Cox, A. L., and Ghulam, A. (2017), Measuring Suspended-Sediment Concentration and Turbidity in the Middle Mississippi and Lower Missouri Rivers using Landsat Data. *J. Am. Water Resour. Assoc., 54(3),* doi:10.1111/1752-1688.12616.

Meade, R. H., and Moody, J. A. (2010), Causes for the decline of suspended-sediment discharge in the Mississippi River system, 1950-2007. *Hydrol. Process., 24, 35-49,* doi:10.1002/hyp.7477

Rouse, H. (1937), Modern conceptions of the mechanics of fluid turbulence. *Transaction of the American Society of Civil Engineers*, 102(1), 523-537.

Julien, P.Y. (2010). *Erosion and Sedimentation*. Cambridge, UK: Cambridge University Press.

Sequoia Scientific, Inc., 2014. LISST-200X Next Generation Submersible Particle Size Analyzer. 2p. (accessed online on 1 February 2018)

Mobile Bed Discharge Gaging

Stephen W. Brown, Hydrologic Engineer, USACE, Albuquerque, NM
stephen.w.brown@usace.army.mil

Extended Abstract

Introduction

A cornerstone to calibration of hydrologic, hydraulic, and sediment transport models is accurate flood discharge data. High energy floods and debris flows destroy pressure transducers and associated gaging stations leaving non-contacting instrumentation as the only viable option for capturing events. Current non-contact technologies are ineffective in mobile bed channel systems due to changing channel geomorphology. Channel cross sections need to be surveyed after each flood event. Additionally, flow velocities vary with time due to sediment transport-initiated variations in bed slope and storm intensity.

Low cost, autonomous gaging, collecting data at high temporal frequency, allows previously uncollectable data to be incorporated in hydrologic and hydraulic models. High resolution terrain data before and after storm events may increase engineering understanding of high frequency channel geomorphology. Analysis of bedforms and grain/gravel sizes may inform energy distribution through the hydrograph.

The Mobile Bed Discharge (MoBeD) gage was developed to be a low cost, automated, non-contact multidimensional data collection tool for ephemeral streams. MoBeD provides critical discharge, sediment, and vegetation data in otherwise ungagable systems. The gage is developed with Arduino and Raspberry Pi hardware capable of controlling an array of sensors collecting stereo 4-band orthoimagery, velocity data, and stage. The stereo imagery produces a point cloud of channel topography resulting in a rich dataset of geomorphologic change for all discharge events. MoBeD was designed to capture channel bed geomorphology before and after a flood event. Video collected during the event is used to estimate surface velocity. The stage of the hydrograph can be captured from images of a staff gage in channel or via radar.

Observed hydrologic measurements are critical for refined model calibration and validation for a full range of frequency events. The MoBeD gage is an open source effort to provide comprehensive field data where none is currently available.

Methods

The first phase of MoBeD development is a benchtop prototype. USACE Albuquerque developed the hardware configuration for MoBeD. 3AEGreen developed the software to record and deliver collected data. This project employed a software development method of Agile, as

opposed to Waterfall or Spiral. This was an iterative process of the hardware team at USACE and the software team at 3AEGreen. During this project, there were multiple iterations of instrumentation control, software libraries, and power management. Agile development works well for collaborative groups of cross functional teams that evolve a project through continuous, flexible responses to change.

Critical measurements for the prototype include: channel geometry, water velocity via video analysis, and stage (water level). With these three measurements it is possible to compute estimates of discharge. Video and stage are collected together by pointing the camera at a staff gage in the channel, recording changing stage and the water surface for velocity calculations. Stage may also be collected with a sonar sensor. Collecting the cross-section requires a novel approach.

Two methods of measuring channel geometry are implemented. One incorporates a laser rangefinder on a servo motor to sweep the channel collecting elevations. The second uses Structure from Motion (SfM) to produce a point cloud from a series of photos. Four cameras are installed, two RGB and two NIR, in a stereo configuration. The inclusion of an infrared LED array allows photos to be taken day or night. Each of these solutions have strengths and weaknesses depending upon installation site.

Additional sensors are installed to capture environmental conditions. Temperature and humidity inside and outside of the gage are used for environmental monitoring and activation of heating and cooling of the gage housing. A three-axis accelerometer is included to capture movement of the gage to estimate error during data collection. Standard communication protocols allow dozens of sensors to be added for thorough environmental monitoring.

The gage is designed to mount to a tree, pole, or cliff providing a wide field of view for the camera array. Multiple gages can be installed in a canyon to fully cover the active stream channel (**Figure 1**). Due to the potential difficulty reaching the gage to retrieve data, an infrared receiver was installed for remote activation. Using a remote control, the field tech turns on the gage which in turn starts a Wi-Fi hotspot and webserver. Using a cell phone or tablet to connect to the hotspot allows access to a PHP based data download system via the gage's IP address.

Figure 1. MoBeD Gage sample installation

A key feature of the MoBeD gage is multiple cameras. Initially Arduino was considered for the primary controller but limited camera availability and control was problematic. Raspberry Pi (RPi) was a good solution but they are built with only one camera connector. Further research revealed IVmech's IVport add-on board for RPi that multiplexed the one camera port to four. Using the RPi with the camera multiplexer resulted in flexible photo and video capabilities due to the full Linux operating system running on the device. The trade-off is excessive power usage for a remote, battery operated installation.

Arduino microcontrollers are designed for efficient power management, the RPi is not. Reducing the power footprint of the RPi was essential for extended remote operation. The SleepyPi add-on board by Spell Foundary provided an efficient method of managing the RPi power. The SleepyPi used an Arduino as a lower power controller to manage wake and sleep cycles of the RPi. Additionally, the Arduino is used to collect data from sensors and manage event triggering.

The hardware is driven by software in three key categories; sensor control, camera control, data delivery. The RPi runs Linux which allows for Python camera control libraries and a PHP based web server for data delivery. The sensor control is handled by the Arduino in C.

Postprocessing the camera data requires SfM software. PhotoScan by Agisoft was chosen to convert the raw photos to stitched orthophotos and point clouds. Safe Software's Feature Manipulation Engine was used for additional data preparation and processing.

Results

Primary development focused on hardware and software integration and verification that the equipment is technologically capable of capturing the required measurement. Before any electronic instrumentation can be installed in the field, comprehensive testing must be done in the electronics lab. The gage is currently an advanced benchtop prototype. Initial sensor and camera testing show positive results. Lessons learned from the initial prototypes and programing are rolled into the current generation. Key improvements are ease of access to developmental hardware for updates, modular power management, and modular sensor arrays.

Figure 2 shows the MoBeD data logger stack. The top circuit board is the SleepyPi Arduino power and sensor controller. Four patch cables are connected from the SleepyPi to the ethernet port for data communication with external sensors. Below the SleepyPi is the IVMech camera multiplexer with ribbon cables connecting the two RGB and two NIR cameras. At the bottom of the stack is the Raspberry Pi showing the 64GB USB storage module and USB Wi-Fi module.

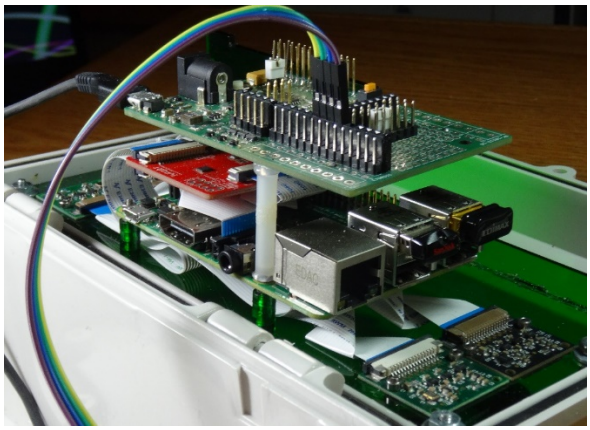

Figure 2. Data logger and stereo camera array

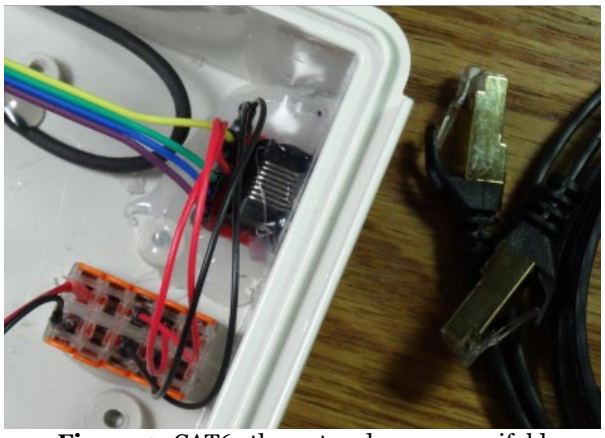

Figure 3. CAT6 ethernet and power manifold

Power to the sensor array is isolated from that of the data logger stack. There are two key benefits from this design. The first is preventing sensor activation current drop from impacting the operation of the RPi. Second, sensor arrays will be powered only when collecting data to reduce battery drain when inactive. Modular sensor arrays allow the data logger to be placed away from the flood plain, protected from damage. The sensors have been configured to get data and power communications via ethernet (**Figure 3**). Using power over ethernet standards, standard CAT6 cable can be used to connect small sensor outriggers.

Data collection to test the stereo photogrammetric capabilities of MoBeD was conducted from a walking bridge on a low relief arroyo. The gage was approximately ten feet from the bed. Given the low relief of the channel bed being photographed, the detail captured by the 5MP cameras was sufficient to produce a high resolution orthoimage, point cloud, and contours (**Figure 4**). Image quality from the test was very good with small leafy debris clearly visible (**Figure 5**).

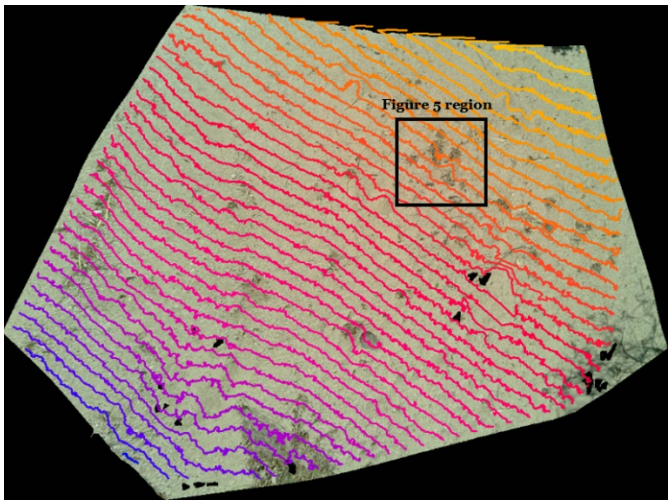

Figure 4. Stereo photogrammetry camera view

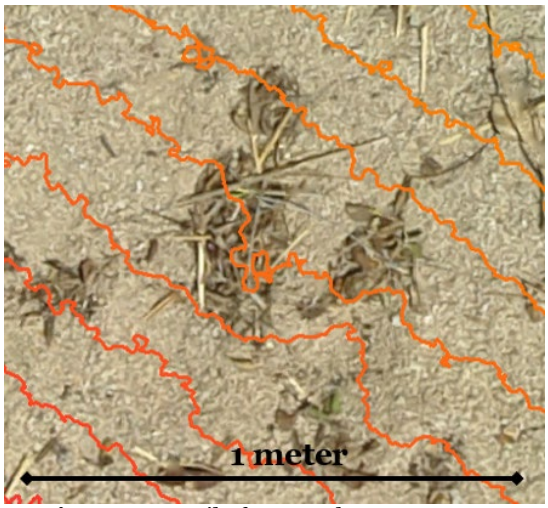

Figure 5. Detail of stereo photogrammetry

Discussion and Conclusions

As a functional benchtop prototype this phase of development is a success. The primary challenge for phase two (field testing) is hardening the gage to survive in the field. The laser range finder and cameras require unobstructed views for optimal data collection. However, having an opening in the box will dramatically reduce the life expectancy of the electronics due to dust, moisture, and animals. Several options have been explored to open and close windows during data collection. Field testing is planned for 2019 given adequate budget and time.

These gages can be built for less than $500. Lowering the cost allows for more installations on remote drainages, building a robust picture of these systems' hydrologic response. A rich set of data, previously unobtainable without high cost or extensive labor, is now within reach.

Acknowledgements

USACE Engineering Research and Development Center (ERDC) has provided hardware and labor funding in addition to technical guidance. The Middle Rio Grande Endangered Species Collaborative Program (MRGESCP) supported software development. The University of New Mexico's GISciences for the Environmental Management (GEM) Lab provided photogrammetric technical guidance related to hardware and post processing. The author would like to thank Quelab members for hardware fabrication and testing assistance.

Scooping-Induced Bias of Physical Bedload Measurements and A Recommended Solution for Pressure-Difference Bedload Samplers

David Pizzi, PE, Sr. Hydraulic Engineer, Tetra Tech, Fort Collins, CO,
David.Pizzi@tetratech.com
Michael Pierce, PE, Sr. Hydraulic Engineer, Tetra Tech, Fort Collins, CO,
Michael.Pierce@tetratech.com

Abstract

The ability of rivers to transport sediment is often a key consideration for ensuring that improvements to both riverine habitat and infrastructure are resilient and sustainable. Pressure-difference bedload samplers are the most widely-used devices for directly measuring physical bedload transport in U.S. streams and rivers. Because of hydraulic forces exerted on such samplers when lowered to, and raised from, the channel bed, these samplers are susceptible to scooping bed material. Scooping can introduce substantial error to the collected sample, leading to inaccurate measurements of both bedload transport and the maximum size of sediment in transport. Current practice relies on the equipment operators to evaluate scooping-induced bias, which is challenging even under ideal conditions with experienced operators.

Bedload measurements frequently establish the prototype against which numerical models of bedload transport and incipient motion are compared, so substantial error in the prototype can confound the calibration and application of a model, compromise the reliability of interpretations of modeled results, and prevent appropriate consideration of risk in decisions based on modeled results.

Available data can be used to demonstrate situations where scooping bias was likely introduced into the bedload measurements. For example, a dataset collected in Alaska in the mid-1980s shows that the coarsest gravels were collected at the lowest discharges, yet these discharges were unlikely capable of mobilizing and transporting these gravels. Another example dataset collected on the San Joaquin River in the mid-2010s includes cobbles when underwater video does not confirm appreciable mobilization of the cobble-dominated bed surface. In both datasets, scooping of the bed surface into the bedload measurement is suspected.

Currently-available and actively-implemented tools to avoid or mitigate the effects of scooping on measurements collected with pressure-difference bedload samplers are not commonly used in the industry. Tetra Tech has formulated a potential solution based on observations made while collecting boat-based bedload measurements during challenging flood conditions. Tetra Tech's proposed solution would prevent the inadvertent collection of dislodged or scooped sediment, and it would be particularly valuable when operating under a limited ability to see or feel the sampler contacting the bed. The proposed solution is an attachment on the nozzle of the bedload sampler that would allow the operator to remotely open a door on the attachment such that water and bedload can enter the sampler nozzle only when the operator is ready; the operator then closes the door to exclude water and sediment from entering the sampler nozzle before raising it from the bed.

A potential drawback to such an attachment is that it could induce differences in the hydraulic and sediment collection efficiency of the sampler, either of which could complicate comparisons to previous samples measured without the attachment. Tetra Tech is pursuing grant funding to further develop and test this attachment, in hopes of improving the industry standard while maintaining consistency in the intended sampler performance. This paper will (1) provide an overview of the potential sources of error associated with bedload sampling, (2) summarize Tetra Tech's proposed solution to this problem, and (3) summarize recommended next steps in further development of the idea.

Introduction

One of the principal concerns in studies of sediment transport is the determination of the total sediment discharge of coarse sediments; because suspended sediment can easily be measured, the main problem is the determination of bedload (the sediment that slides, rolls, or skips along in almost-continuous contact with the stream bed) (Hubbell 1967). The collection of accurate bedload samples has always been a challenge; however, sampling programs using manually-operated portable samplers continue to be the method of choice (Diplas et al. 2008). The U.S. Federal Interagency Sedimentation Project (FISP) requires all bedload sampling be performed with pressure-difference type samplers (Davis 2005), a type of manually-operated portable samplers. In part, because of the FISP's endorsement, pressure-difference bedload samplers are the most widely-used devices for directly measuring physical bedload transport in U.S. streams and rivers.

Background for Scooping-Induced Bias of Physical Bedload Measurements

Despite the FISP's endorsement of pressure-difference bedload samplers, replicate bedload samples collected with such equipment can be highly variable. This variability is influenced by both the inconsistent (in space and over time) nature of bedload transport (Hubbell 1967, Emmett 1980, Carey 1985, Kuhnle et al. 1989, Childers 1999, Dhont and Ancey 2018), and, as noted by Hubbell (1967), the inadvertent collection of bed material. Regarding this second source of variability, which is an error in the sampling as opposed to natural variability in transport, Van Rijn and Gaweesh (1992) identify the *initial effect* (disturbance of the bed when the sampler initially contacts the bed) and the *scooping effect* (when drag on the sampler causes it to act as a grab sampler). Van Rijn and Gaweesh (1992) note that both of these inadvertent collections lead to oversampling, thus biasing the bedload sample high. Childers (1999) redefined these effects as (1) potential for *scooping errors* if the sampler nozzle contacts the bed before other sampler points touch, and (2) *dredging errors* if the sampler is dragged along the streambed. Thus, researchers and practitioners are aware of the potential for scooping-induced bias in bedload samples collected with pressure-difference samplers, yet there are no known solutions to avoid or at least mitigate the biasing effects of scooping.

Physical Bedload Measurements as Prototypes

Bedload measurements are frequently used to establish the prototype for comparing to numerical models of bedload transport or incipient motion. Substantial error in the prototype can confound the calibration and application of a model, compromise the reliability of

interpretations of modeled results, and prevent appropriate consideration of risk in decisions based on modeled results.

Prototype Bedload Transport

Development of a bedload transport function: Barry et al. (2004) proposed a new bedload transport equation developed using 2,104 bedload transport observations in 24 gravel-bed rivers in Idaho. The observations were obtained using a 3-inch Helley-Smith (1971) pressure-difference sampler, and multiple lines of evidence indicated that during the largest flows almost all sizes of bed material were mobilized, including sizes larger than the orifice of the sampler. The observations were typically collected following methods presented in Edwards and Glysson (1999) at 20 equally-spaced positions across the wetted width. Barry et al. reviewed each observation for quality, and they removed 284 out of 2,388 observations; only 41 of these removals were because of concern that significant amounts of measured transport at extremely low discharges indicated scooping.

While the choice of Barry et al. (2004) to exclude potentially biased observations from the prototype dataset upon which they developed their bedload transport function is not ideal, no other options are available to reliably calculate potential scooping bias and remove it. Excluding such measurements not only has a direct financial cost associated with the collection of the measurement but also an indirect cost associated with the lost opportunity (perhaps during relatively infrequent hydrologic conditions) to have collected a robust measurement.

Calibration of a numerical model: Using the U.S. Army Corps of Engineers' HEC-RAS software, Tetra Tech developed a one-dimensional bed evolution model (BEM) of the Susitna River near Anchorage, AK. The purpose of the BEM was to assess potential effects of a proposed hydroelectric project on the dynamic geomorphology of the river downstream of the proposed project. The BEM was calibrated to observations of sediment transport and geomorphic change. A concern arose because of differences between the simulated grain size distribution of transported loads and the USGS's measurements of bedload transport (Knott and Lipscomb 1983, Knott and Lipscomb 1985, Knott et al. 1986, Knott et al. 1987), particularly transport of sediment coarser than 16 mm (Tetra Tech 2015). The USGS used a 3-inch Helley-Smith (1971) pressure-difference sampler deployed from a boat to collect 30 bedload measurements.

Because the USGS reported hydraulic conditions during the bedload measurements, Tetra Tech (2015) was able to calculate total shear stress and estimate dimensionless shear stress (also referred to as the Shields (1936) parameter) for the median grain size of the bed surface (D50) (which was based on Tetra Tech's sampling). Tetra Tech cited various references for critical dimensionless shear stresses (Vanoni 1967, Neill 1968, Andrews 1983, Buffington and Montgomery 1997) as a basis for determining that the estimated values, all being less than 0.027, indicated none of the flow conditions were likely to have mobilized the D50.

Tetra Tech (2015) noted a concern that all the coarsest bedload was collected during the first three of the USGS's measurements in 1982, at relatively low flows; measurements at the greatest measured flows contained none of the coarsest bedload and even relatively little gravel between 2 and 32 mm. The most-likely reasons Tetra Tech offered for this discrepancy were (1) disturbances as the Helley-Smith sampler contacted the bed surface causing dislodged particles to enter the sampler, and (2) scooping the bed with the Helley-Smith sampler. Tetra Tech recognized the difficulty of collecting these bedload measurements using a sampler deployed

from a crane mounted on a boat in high-velocity flows. Tetra Tech estimated the sampled transport rates of the coarsest gravels were probably derived from collecting only a few individual particles, which could reasonably have been collected from disturbance or scooping during the difficult sampling conditions. Thus, dislodgement or scooping of just a few particles can substantially bias the measurement.

After removing the first three of the available 30 measurements and adjusting the gradations of the prototype bedload rating curve, Tetra Tech found that the simulated bedload gradation closely aligned with the prototype. These three measurements, representing 10-percent of the available measurements, were reluctantly excluded because Tetra Tech stated that if the Helley-Smith sampler disturbed or scooped the bed, finer shielded particles likely also entered the sampler, but the degree of bias in the sample was unknown. Lacking a reliable method to adjust the load and gradation of a bedload sample, excluding the samples from further consideration was the only reasonable option.

Prototype Incipient Motion

Evaluation of bed surface mobilization: In 2014 and 2017 Tetra Tech (in preparation) carried out bedload measurements on the San Joaquin River near Fresno, CA to improve the understanding of the relationship between hydrology, hydraulics, and bed surface mobilization. Bedload measurements were collected over riffles following standard USGS methods (Edwards and Glysson 1999) using a Toutle River (TR-2, 6-inch-high by 12-inch-wide nozzle) sampler deployed from a work platform on a 16-foot-long cataraft (Figure 1).

Figure 1. Tetra Tech engineers sampling bedload on the San Joaquin River in January 2017

During the near-bankfull flows in June 2014, Tetra Tech staff could see through the relatively shallow and clear flows to confirm that the bed surface was not mobilized, so cobbles collected in the samples were judged to have been either dislodged or scooped. Because these observations were made in real time, each vertical could be re-sampled if it was judged to be biased. This was

critically important because subsequent calculations of incipient motion would be based on the largest sizes in transport (i.e., collected in the samples).

During the major flooding in January 2017, flow depths were much greater than depths in June 2014, and the elevated suspended sediment load precluded observing the sampler move through the water column and contact the bed surface. Further, the greater flow velocities substantially increased the drag on the sampler as it was lowered into the water, so the operators lost nearly all ability to feel when the sampler contacted the bed. Under these conditions, judgment is too subjective to reliably determine whether a bedload measurement was biased by dislodgement or scooping of the sample.

Unlike the applications where bedload measurements are used to develop prototype rating curves, the coarsest fractions can be excluded from a measurement used to inform the largest size in transport. This is because the sizes, and not the sampled masses, are of interest; when developing rating curves, even if coarse scooped particles are excluded, finer particles entrained with the coarser scooped particles cannot be reliably excluded from the sampled mass. However, the determination of which sizes to exclude and which to retain can still be subjective, which may eliminate, or at least limit, the utility of the adjusted sample gradation for informing the largest grain size in transport.

Proposed Solution

As noted in the examples above, scooping-induced bias in bedload samples can preclude the utility of such samples, coming with both direct and indirect costs. To reduce the potential for dislodged or scooped bed material to bias bedload measurements collected with pressure-difference samplers, Tetra Tech is developing an attachment that will mount to the nozzle of existing samplers (Figure 2 and Figure 3). This attachment will operable so that it can be (1) shut as the sampler is lowered through the water column to the bed, (2) opened once the sampler is positioned on the bed, and (3) closed before the sampler is raised from the bed.

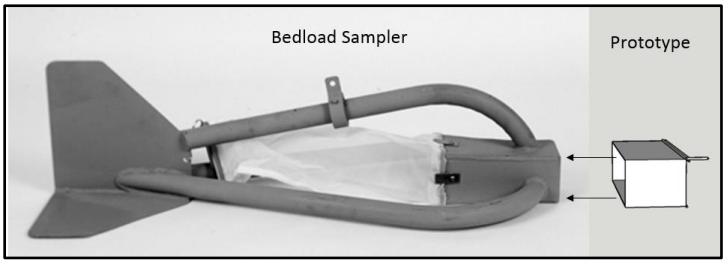

Figure 2. BL-84 bedload sampler and prototype of proposed attachment

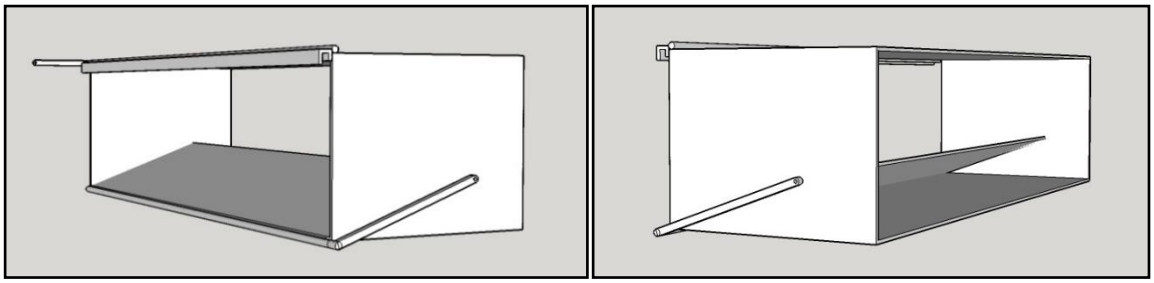

Figure 3. Schematics of proposed attachment – front (left) and back (right)

Tetra Tech has considered alternate configurations of the operable door, such as a bi-fold door hinged along the sides of the attachment to allow water and sediment to be shed through open sides of the attachment. Such a configuration could reduce drag when the sampler is lowered and raised through the water column, but it would be more mechanically complex. Additional considerations include the mechanism to operate the door, including a basic system that opens and closes in response to the sampler contacting the bed (e.g., a spring-loaded plate on the bottom of the attachment and downstream of the nozzle entrance) or an automated mechanism operated by the sampling crew.

A primary objective behind the design of the attachment is to improve bedload measurements without impairing meaningful comparisons to samples collected without the attachment. For example, in fiscal year 2016 the FISP funded testing of the influence of sampler bag mesh size and type on the hydraulic efficiency of pressure-difference bedload samplers (Bunte et al. 2017). The attachment could change the hydraulic efficiency of the samplers, so avoiding such a change, or at least minimizing the change, is desirable. However, Bunte et al. (2017) identified that scooping a few gravel particles into a sampler may well introduce more error than bag mesh size and type. This finding indicates that eliminating scooping-induced bias in a sample could more than offset a small change in hydraulic efficiency. And the attachment may be designed to change the sampling efficiency if eliminating scooping-induced bias brings this efficiency closer to unity.

Future Steps for Developing the Proposed Solution

In early 2017, Tetra Tech contacted the USGS's Hydrological Instrumentation Facility (HIF) to ask whether equipment was available to prevent scooped sediment from biasing a bedload measurement; HIF staff reported that no such equipment was available. By the end of 2017, Tetra Tech completed a patentability search for a bedload sampler attachment, which indicated that such an attachment may be novel and eligible for a patent. Tetra Tech is unaware of alternate embodiments of such an attachment. However, financial considerations prevented Tetra Tech from internally pursuing development and testing of such an attachment. In 2018 Tetra Tech had informal conversations with engineers at Reclamation's Technical Service Center, the Corps of Engineers' Hydrologic Engineering Center, and the USGS's New Mexico Water Science Center that confirmed support for developing and testing an attachment to

pressure-difference bedload samples that would improve the quality of bedload measurements. In late 2018, Tetra Tech submitted a proposal to the FISP requesting funding to develop and test this attachment, but no decision has yet been shared with Tetra Tech.

If FISP funding is not forthcoming, Tetra Tech is interested in a partnership to advance the proposed solution to scooping-induced bias of physical bedload measurements collected with pressure-difference samplers. Tetra Tech has invested sweat-equity in refining this solution from its origin as a sketch on a napkin and hopes that such a solution will benefit all sampling and monitoring programs that rely on bedload transport measured with pressure-difference samplers.

References

Andrews, E.D. 1984. "Bed-material entrainment and hydraulic geometry of gravel-bed rivers in Colorado," Geological Society of America Bulletin, Vol. 94: 1225-1231.

Barry, J.J., Buffington, J.M., and King, J.G. 2004. "A general power equation for predicting bed load transport rates in gravel bed rivers," Water Resources Research, 40(10): W10401, doi:10.1029/2004WR003190.

Buffington, J.M. and Montgomery, D.R. 1997. "A Systematic Analysis of Eight Decades of Incipient Motion Studies, with Special Reference to Gravel-bedded Rivers," Water Resources Research, 33(8): 1993-2029.

Bunte, K., Klema, M., Hogan, T., and Thornton, C. 2017. "Testing the Hydraulic Efficiency of Pressure Difference Samplers While Varying Mesh Size and Type," Submitted to the Technical Committee of the Federal Interagency Sedimentation Project, Colorado State University, Engineering Research Center, Fort Collins, CO, pp 75, plus appendix.

Carey, W.P. 1985. "Variability in measured bedload-transport rates," Journal of the American Water Resources Association, 21(1): 39-48.

Childers, D. 1999. "Field Comparisons of Six Pressure-Difference Bedload Samplers in High-Energy Flow," U.S. Department of the Interior, Geological Survey, Water Resources Investigations Report 92-4068, Vancouver, WA, pp 35, plus appendices.

Davis, B.E. 2005. "A Guide to the Proper Selection and Use of Federally Approved Sediment and Water-Quality Samplers," U.S. Department of the Interior, Geological Survey, Open-File Report 2005-1087, Vicksburg, MS, pp 20.

Dhont, B., and Ancey, C. 2018. "Are Bedload Transport Pulses in Gravel Bed Rivers Created by Bar Migration or Sediment Waves?" Geophysical Research Letters, 45: 5501-5508.

Diplas, P., Kuhnle, R., Gray, J., Glysson, D., and Edwards, T. 2008. "Sediment Transport Measurements," In: Garcia, ed. Sedimentation Engineering, Reston, VA: ASCE, pp 307-353.

Edwards, T.K. and Glysson, G.D. 1999. "Field Methods for Measurement of Fluvial Sediment," In: Techniques of Water-Resources Investigations of the U.S. Geological Survey, Book 3, Applications of Hydraulics, Reston, VA: U.S. Government Printing Office, pp 89.

Emmett, W.E. 1980. "A Field Calibration of the Sediment-Trapping Characteristics of the Helley-Smith Bedload Sampler," U.S. Department of the Interior, Geological Survey, Professional Paper 1139, U.S. Government Printing Office, Washing, D.C., pp 44.

Helley, E.J. and Smith, W. 1971. "Development and Calibration of a Pressure-Difference Bedload Sampler," United States Department of the Interior, Geological Survey, Water Resources Division, Open-File Report, Menlo Park, CA, pp 18.

Hubbell, D.W. 1967. "Apparatus and Techniques for Measuring Bedload," United States Department of the Interior, Geological Survey, Water-Supply Paper 1748, U.S. Government Printing Office, Washington, D.C., pp 74.

Knott, J.M. and Lipscomb, S.W. 1983. "Sediment Discharge Data for Selected Sites in the Susitna River Basin, Alaska, 1981-82," United States Department of the Interior, Geological Survey, Open-file Report 83-870, Prepared in cooperation with the Alaska Power Authority, Anchorage, AK.

Knott, J.M. and Lipscomb, S.W. 1985. "Sediment Discharge Data for Selected Sites in the Susitna River Basin, Alaska, October 1982 to February 1984," United States Department of the Interior, Geological Survey, Open-file Report 85-157, Prepared in cooperation with the Alaska Power Authority, Anchorage, AK.

Knott, J.M., Lipscomb, S.W., and Lewis, T.W. 1986. "Sediment Transport Characteristics of Selected Streams in the Susitna River Basin, Alaska, October 1983 to September 1984," United States Department of the Interior, Geological Survey, Open-file Report 86-424W, Prepared in cooperation with the Alaska Power Authority, Anchorage, AK.

Knott, J.M., Lipscomb, S.W., and Lewis, T.W. 1987. "Sediment Transport Characteristics of Selected Streams in the Susitna River Basin, Alaska: Data for Water Year 1985 and Trends in Bedload Discharge, 1981-85," United States Department of the Interior, Geological Survey, Open-file Report 87-229, Prepared in cooperation with the Alaska Power Authority, Anchorage, AK.

Kuhnle, R.A., Willis, J.C., Bowie, A.J. 1989. "Variations in the transport of bed load sediment in a gravel-bed stream, Goodwin Creek, northern Mississippi, U.S.A.," Proceedings of the Fourth International Symposium on River Sedimentation, Science Press, Beijing, China, pp 539-546.

Neill, C.R. 1968. "A Re-Examination of the Beginning of Movement for Coarse Granular Bed Materials," Int. 68, Wallingford, Ministry of Technology, Hydraulic Research Station. England, pp 37, plus figures and tables.

Shields, I.A. 1936. "Application of Similarity Principles and Turbulence Research to Bed-Load Movement," Translated from: Anwendung der Aehnlichkeitsmechanik und der Turbulenzforschung auf die Geschiebebewegung. Mitteilungen der Preussischen Versuchsanstalt fur Wasserbau und Schiffbau, Berlin, Translated by W.P. Ott and J.C. van Uchelen, U.S. Department of Agriculture, Soil Conservation Service, Hydrodynamics Laboratory, California Institute of Technology, Pasadena, CA, pp 36, plus references and figures.

Tetra Tech. 2015. "Fluvial Geomorphology Modeling below Watana Dam, Study Plan Section 6.6, 2014-2015 Study Implementation Report, Attachment 1: Appendix A, 1-D Bed Evolution Model of the Middle and Lower Susitna River: Model Development and Calibration," Prepared for Alaska Energy Authority, Seattle, WA, pp 79.

Van Rijn, L.C. and Gaweesh, M.T.K. 1992. "New Total Sediment-Load Sampler," Journal of Hydraulic Engineering, 118(12): 1686-1691.

Vanoni, V.A. 1967. "Closure of Sediment Transportation Mechanics: Initiation of Motion," Progress Report of the Task Committee on Preparation of Sedimentation Manual, Committee on Sedimentation, Vito A. Vanoni, Committee Chairman, ASCE Journal of the Hydraulics Division, Vol. 93(5): 297-302.

Strategic Directions of the USGS Water Mission Area's Fluvial Sediment Science Program

Molly S. Wood, National Sediment Specialist, U.S. Geological Survey, Boise, Idaho, mswood@usgs.gov
Tim Straub, Federal Interagency Sedimentation Project Chief, U.S. Geological Survey, Urbana, Illinois, tdstraub@usgs.gov

Abstract

The USGS Water Mission Area's Sediment Science Program provides leadership, training, and methods development in fluvial sediment science for the USGS and its external partners. Overarching objectives of the USGS Sediment Science Program (which includes the Federal Interagency Sedimentation Project) include: 1) developing and promoting innovative sediment monitoring techniques that result in cost effective, accurate, and high resolution fluvial sediment data for the Nation; 2) advancing sediment science through collaboration with external agencies to ensure USGS science and leadership directions are aligned with external agency and public needs; and 3) providing technical support to sediment data collectors and scientists, in an effort to improve quality assurance/quality control practices and efficiencies in field data collection and analysis.

The USGS Sediment Science Program works to develop a unified vision to promote the growth and ensure the quality of USGS sediment science and monitoring. Strategic directions for the Program in the next five years include:

- Developing operational methods for using down-looking acoustic Doppler current profilers to estimate and map suspended-sediment concentrations in river reaches;
- Developing and promoting other surrogate methods for estimating suspended and bedload sediment;
- Strategizing on and developing a tool for predicting erosion and sediment transport in the Nation's rivers, in collaboration with external partners;
- Increasing access to river corridor bathymetric data to support geomorphic assessments and modeling activities; and
- Creating software and scripts and providing training to promote data quality and increase efficiency in field data collection and analysis.

Introduction

Relevance of Sediment Science

Excessive sediment is one of the leading causes of water-quality impairment in water bodies in the United States, according to the U.S. Environmental Protection Agency (U.S. Environmental Protection Agency, 2016). Sediment is unlike many other "pollutants" in that it's naturally occurring and ubiquitous, and some level is needed to support ecosystem functions (Waters, 1995). However, damages from high sediment loads and sediment-related impairments in North America are estimated to be over $20B annually (Osterkamp and others, 2004). Sediment

science and prediction are essential to informed solutions to sediment-related issues, including dam/reservoir sustainability, flood protection, waterway navigation, agricultural productivity, water quality impairments, coastal land preservation, and ecosystem health. The U.S. Geological Survey (USGS) has shown that it is committed to advancing fluvial sediment science through its involvement in inter-agency sediment standardization committees since the 1930s and the creation of the Federal Interagency Sedimentation Project (FISP) in 1939 (Gray and Landers, 2015). As with all agencies, science priorities for the USGS and funding resources change from year to year. However, sediment research and management continue to be an annual need among federal agencies.

Reorganization of the Water Mission Area

The USGS' Water Mission Area implemented a broad reorganization of its functions and programs in October 2017 to better address national science priorities. Five new divisions were formed to conduct national-level science oversight, research, and science support: Observing Systems Division, Laboratory and Analytical Services Division, Earth System Processes Division, Integrated Modeling and Prediction Division, and Integrated Information Dissemination Division. Functions and projects related to sediment data collection and processing that were formerly under the Office of Surface Water were placed under the new Observing Systems Division. Research and modeling of fluvial sediment and geomorphic processes were placed under the Earth System Processes and Integrated Modeling and Prediction Divisions. The USGS National Sediment Specialist and other national USGS sediment experts communicate and coordinate sediment activities across these divisions to advance a broad USGS Fluvial Sediment Science Program.

Strategic Directions

The following strategic directions have been identified as priorities for the reorganized USGS Water Mission Area and Sediment Science Program for 2019 - 2024. Many of these priorities are at the scoping stage, and funding is actively being sought through congressional appropriations or interagency partnerships.

Next Generation Water Observing System (NGWOS)

The USGS is developing a next-generation water observing system (NGWOS) to provide high-fidelity, real-time data on water quantity and quality necessary to support modern water prediction and decision support systems for water emergencies and daily water operations. The technologies advanced through NGWOS will be instrumental in developing and modernizing nationwide monitoring networks and in building modeling applications that support priorities listed elsewhere in this paper. Funding was appropriated from Congress in 2018 to initiate an NGWOS pilot in the Delaware River basin. Though the primary foci of NGWOS efforts in the Delaware River basin are streamflow/water availability, temperature, and specific conductance, it is expected that future NGWOS basins will include sediment transport as a focus.

Sediment Science Program activities under the umbrella of NGWOS include the ongoing development and testing of sediment surrogate technologies. Sediment monitoring is often an essential piece of water resource management and hazard mitigation for infrastructure. Tackling these issues often requires accurate and high temporal/spatial resolution sediment data. The USGS and other researchers are using acoustic Doppler meters, which are routinely used for

discrete and continuous streamflow measurements, to estimate suspended-sediment concentrations in rivers. Most efforts have been focused on the use of fixed-mounted, horizontal acoustic Doppler velocity meters (ADVMs) to continuously estimate suspended-sediment concentration and load (Figure 1; Wood, 2014; Landers and others, 2016). Efforts typically leverage existing uses of the acoustic meter for computation of discharge using index-velocity methods, described in Levesque and Oberg (2012). These in-situ side-looking methods can provide continuous, high temporal resolution data on sediment concentration, load, and size based on a horizontal section of the streamflow. This surrogate technique has shown great potential for helping USGS customers and partners better understand and manage sediment and water resources because side-looking ADVMs integrate a signal across a larger portion of a cross section than traditional point measurements of turbidity, the most widely used sediment surrogate. Additionally, measuring backscatter from different acoustic frequencies can permit differentiation of sediment particle sizes in some fluvial systems.

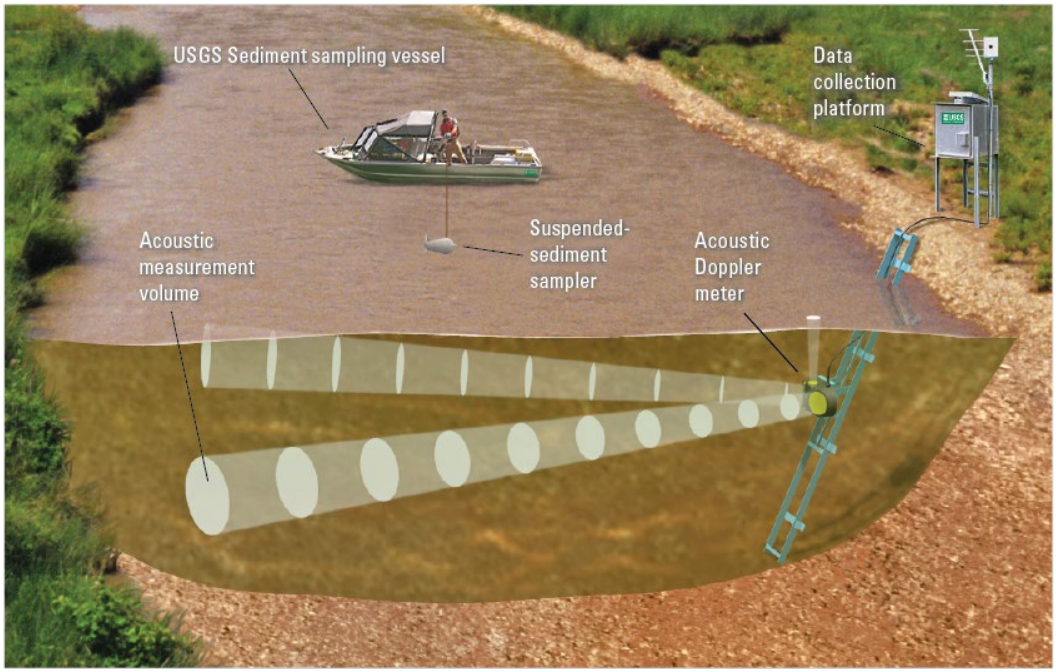

Figure 1. Example of a sediment acoustic index monitoring station with a horizontally-mounted, side-looking acoustic Doppler velocity meter for estimating fluvial suspended sediment (from Wood, 2014, and Landers and others, 2016)

The USGS is actively researching the use of down-looking acoustic Doppler current profilers (ADCPs) for estimating and mapping suspended-sediment concentration and load in a river cross section or reach (Wood and others, 2019), which would provide sediment data at a higher spatial resolution than samples alone or the previously mentioned side-looking surrogate method. Several datasets have been collected in the U.S. and Argentina to evaluate the efficacy and transferability of the method. If an operational method could be developed, the use of ADCPs would revolutionize global sediment science by allowing rapid and accurate measurements of sediment transport and distribution at spatial and temporal scales that are far beyond the capabilities of traditional physical samplers. Such spatial resolution of concurrent sediment, hydraulic, and fluvial geometric data has not been previously possible and can immediately address and improve our understanding, modeling, and prediction of fluvial sediment transport.

Other NGWOS sediment surrogate methods actively promoted and funded by the USGS Sediment Science Program and the FISP include but are not limited to:

- Sediment generated noise (hydrophones) for improved estimates of bedload in gravel bed rivers;
- Laser diffraction for in-situ estimates of concentration and particle size distribution of suspended sediment;
- Point measurements of acoustic backscatter for in-situ estimates of suspended sediment;
- Densimetric technique for suspended sediment estimates in very high concentrations (typically >20,000 mg/L); and
- Multispectral imagery (cameras) as a non-contact, remote sensing application for estimates of fine particles of suspended sediment.

Water Prediction Work Program (2WP)

The USGS has developed in-channel monitoring and surrogate techniques that allow estimation of sediment transport or channel geometry at times when a physical sample or cross section data can't be collected. Unfortunately, these techniques often provide information within a limited time frame and spatial extent, and the resulting estimates typically become obsolete if variations in weather, climate, hydrology, land cover, sediment sources, or sediment delivery mechanisms are ignored. High temporal or spatial resolution modeling of erosion, deposition, and sediment transport has been conducted at multiple locations across the nation to answer specific science questions, but no broad-scale models or decision support tools are available that accurately describe the full sediment transport process from uplands to terminal receiving waters. Such broad-scale, linked tools could be calibrated and validated with monitoring program data and could be used to answer multiple resource management questions. Additionally, such tools could be used to predict sediment response to changes in climate, land cover/use, and hydrology, and to evaluate effectiveness of sediment management practices.

The goal of the USGS Water Mission Area Water Prediction Work Program's (2WP's) Sediment Science Team is to envision and develop an operational tool that predicts erosion, sediment transport, and geomorphic changes at multiple temporal and spatial scales. The tool is hoped to drive new scientific vision and understanding of sediment processes to help benefit environmental and societal needs. The work would build USGS predictive capacity while connecting, expanding, and improving observational (monitoring) networks and our understanding of process science. The observational networks and process science would provide a feedback loop to help verify and improve the predictive tool.

If funded, efforts may start in a pilot watershed and then expand to additional watersheds, with improvements and adjustments made during each new implementation. The inputs to the erosion and sediment prediction tool would likely include available modeling applications and observational network data, the National Water Model's or National Hydrologic Model's streamflow predictions, and other products developed by the 2WP Topo-Bathymetry team, 2WP Constituents team, USGS National Geospatial Program, and other USGS geospatial project teams. Successful implementation of 2WP will heavily rely on collaboration with other agencies.

River Corridor Bathymetric and Geomorphic Data

Access to river corridor geometry and bathymetry and other data needed for geomorphic assessments is frequently identified as a critical need across multiple agencies. Many agencies

and academic institutions collect and store river bathymetry, geometry, slope, and bed roughness data (for example) in various formats and have developed disparate tools for synthesizing and visualizing the data. These data are needed to make water resource management decisions in river rehabilitation, resource protection, infrastructure design and sustainability, and flood risk mitigation. Addressing these needs across broad spatial and temporal scales would be made more efficient if the data were publicly and broadly available in a centralized database or integrated with a national geospatial fabric, such as the National Hydrography Dataset or National Hydrography Infrastructure. The USGS and U.S. Army Corps of Engineers are leading a workgroup to strategize on the development of a searchable, georeferenced Geomorphology Data Exchange Portal. The workgroup held a face-to-face scoping meeting in April 2019 to brainstorm the creation of a prototype portal (currently called the Stream Morphology Information Resource InterFace (SMIRF)) in a river reach or basin with existing channel bathymetry, geomorphic, streamflow, and sediment data. The success of this workgroup depends on collaboration with geospatial data experts and integration with other partner agency efforts.

Technical Support to the Field

The USGS Sediment Science Program provides training and technical support to field staff on sediment data collection and analysis. The goals are to promote consistency and accuracy in sediment sampling and associated data collection across all USGS offices and programs. These goals include the development of software and scripts to improve the efficiency, consistency, and quality of data collection. The following software and scripts have been developed and are actively supported:

- Sediment Field Forms (SedFF), a USGS internal, web-based, field note application used to document sediment sampling activities and ensure consistency in sample metadata;
- SedReview, a USGS internal, R-based web application for reviewing discrete sediment data to detect major problems with samples or inconsistencies with USGS policies;
- Graphical Constituent Loading Analysis System (GCLAS), a constituent load record computation tool;
- Surrogate Analysis Index Developer (SAID), a Python-based software package for developing suspended sediment surrogate ratings and computing continuous estimates of suspended sediment concentrations and loads; and
- Sediment Transect Acoustics (STA) (currently in beta release), a Matlab-based software package for estimating suspended sediment concentrations and loads using down-looking ADCPs.

The USGS Sediment Science Program offers several classroom and web-based training courses, open to employees of USGS and partner agencies. These courses include:

- Sediment Data Collection Techniques (SW1091), week long, in-person class typically offered annually in spring in Castle Rock, WA, based on USGS sediment data collection practices in Edwards and Glysson (1999);
- Geomorphic Analysis of Fluvial Systems (QW1169), week long, in-person class offered annually at various times and places;
- Sediment Acoustic Index Method for Estimating Fluvial Sediment (USGS-H-17-037), week long, in-person class typically offered annually in summer in Minneapolis, MN, based on techniques in Landers and others (2016);

- Sediment Records Computation and Interpretation (SW2096), week long, in-person class offered multiple times per year at various times and places;
- Field Methods for the Collection of Sediment and Water-Quality Samples with Large Samplers from Boats on Large Rivers (ID1837), week long, in-person class typically offered annually in winter or spring in Vicksburg, MS; and
- Sound Sediment Science, an online, publicly-available, on-demand course offering an overview of the sediment acoustic index method for estimating suspended sediment concentrations and loads using ADVMs.

Registration information for all in-person courses can be found on DOI Talent or by contacting the USGS National Training Center.

The Future

The promise of new advances in sediment research, monitoring, and tools for sediment management is exciting. The combination of new investments in technology, methods, and modeling from NGWOS and 2WP; coordinated data sharing through the efforts like SMIRF; and emphasis on training and new tools for field staff; are intended to target identified needs from scientists in USGS and partner agencies. Ongoing coordination within the USGS and partner agencies will help refine these strategic directions and identify new priorities in research as information and needs change.

References

Edwards, T.K. and Glysson, G.D. 1999. "Field methods for measurement of fluvial sediment," U.S. Geological Survey Techniques of Water-Resources Investigations of the U.S. Geological Survey, book 3, chap. C2, 97 p., https://pubs.usgs.gov/twri/twri3-c2/.

Gray, J.R., and Landers, M.N. 2015. "History of the Federal Interagency Sedimentation Project," Proceedings of the 3rd Joint Federal Interagency Conference on Sedimentation and Hydrologic Modeling, April 19-23, 2015, Reno, Nevada, pp 264-275.

Landers, M.N., Straub, T.D., Wood, M.S., and Domanski, M.M. 2016. "Sediment acoustic index method for computing continuous suspended-sediment concentrations," U.S. Geological Survey Techniques and Methods, book 3, chap. C5, 63 p., http://dx.doi.org/10.3133/tm3C5.

Levesque, V.A., and Oberg, K.A. 2012. "Computing discharge using the index velocity method," U.S. Geological Survey Techniques and Methods, book 3, chapter A23, 148 p., http://pubs.usgs.gov/tm/3a23/.

Osterkamp, W.R., Heilman, Phil, and Gray, J.R. 2004. "An invitation to participate in a North American sediment-monitoring network," Eos, Transactions American Geophysical Union, 85 (40): 386–388.

U.S. Environmental Protection Agency. 2016. "National summary of state information, causes of impairment in assessed rivers and streams," accessed March 1, 2019, at http://ofmpub.epa.gov/tmdl_waters10/attains_nation_cy.control#total_assessed_waters.

Waters, T. F. 1995. "Sediment in streams: sources, biological effects, and control," American Fisheries Society Monograph 7, Bethesda, MD, American Fisheries Society.

Wood, M.S. 2014. "Estimating suspended sediment in rivers using acoustic Doppler meters," U.S. Geological Survey Fact Sheet 2014–3038, 4 p., http://dx.doi.org/10.3133/fs20143038.

Wood, M., Szupiany, R., Boldt, J., Straub, T., and Domanski, M. 2019. "Measuring suspended sediment in sand-bedded rivers using down-looking acoustic Doppler current profilers," Proceedings of the 4th Joint Federal Interagency Conference on Sedimentation and Hydrologic Modeling, June 24-28, 2019, Reno, Nevada.

Post Fire Analysis & Restoration

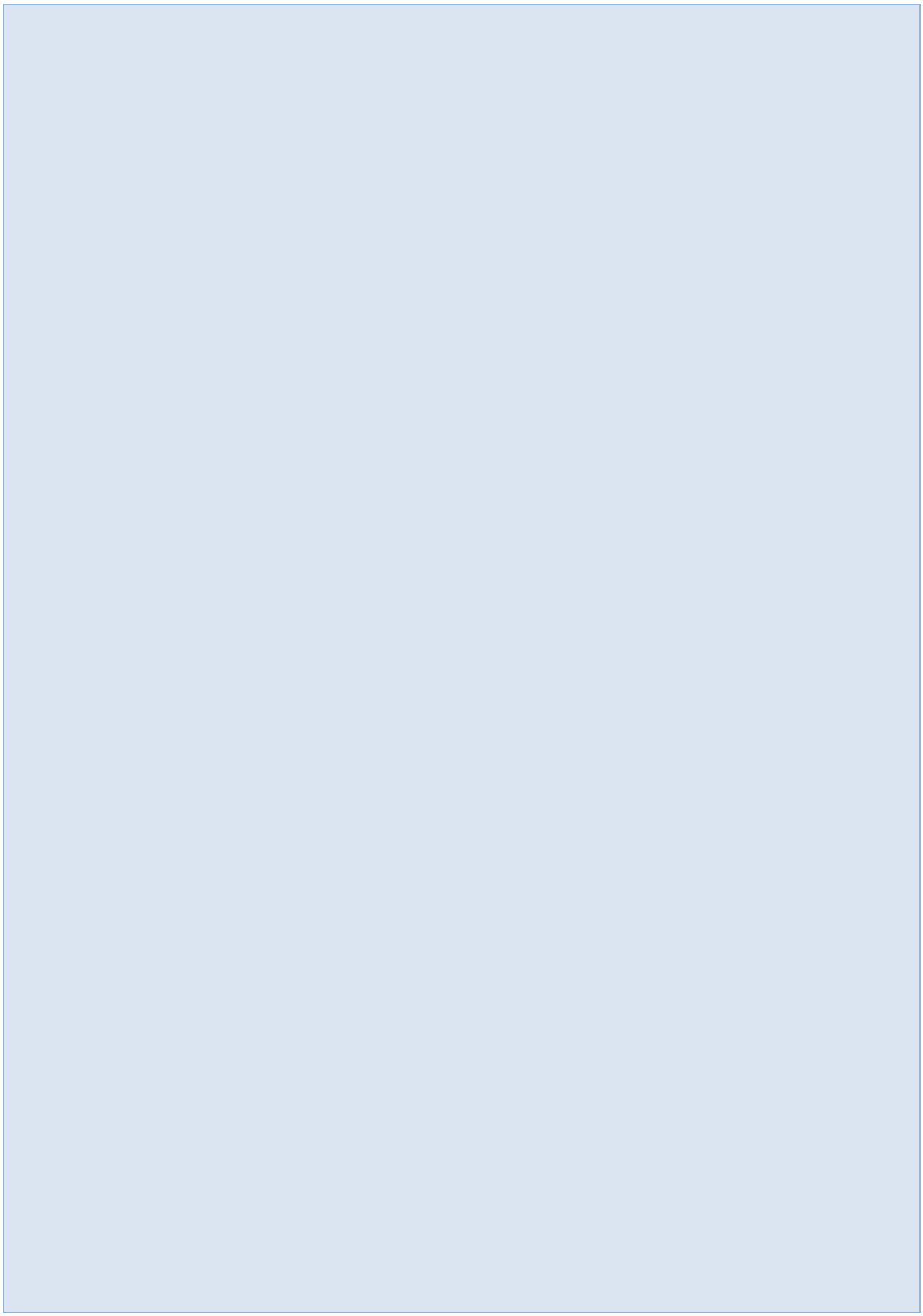

Debris Basin Performance during Post-fire Debris Flow

Julia Grim, P.G., Geologist, United States Department of Agriculture-Natural Resources Conservation Service, Davis, CA, Julia.Grim@usda.gov
Daniel Little, P.E., Civil Engineer, United States Department of Agriculture-Natural Resources Conservation Service, Corpus Christi, TX, Daniel.Little@usda.gov
Greg Norris, P.E., State Conservation Engineer, United States Department of Agriculture-Natural Resources Conservation Service, Davis, CA, Greg.Norris@usda.gov

Abstract

The United States Department of Agriculture (USDA)– Natural Resources Conservation Service (NRCS) provided technical and financial assistance for the construction in 1978 of the Santa Monica Creek Debris Basin (SMDB), to reduce hazards associated with recurring flood and debris flows that historically impacted the City of Carpinteria in Santa Barbara County, California. In this region, high intensity rainfall in the Santa Ynez Mountains periodically trigger debris flows, sending surges of mud and debris onto the coastal plain where Carpinteria, nearby Montecito, and other communities are located. The NRCS planned and designed the SMDB, which was constructed in 1978,as part of the Carpinteria Valley Watershed Project. Santa Barbara County operates and maintains the SMDB.

The SMDB is a 102 foot-high earthen embankment structure with a reservoir capacity of 79 acre-feet at the auxiliary crest elevation, and a 120 acre-foot debris storage capacity. It includes a 48-inch diameter concrete pipe principal spillway (PSW) and a concrete chute auxiliary spillway. The elevations of the three PSW inlet towers in the basin are staggered so that the basin will continue to drain if a lower tower plugs with debris.

In December 2017, the Thomas Fire burned 281,893 acres across the Santa Ynez Mountains, including almost 90 percent of the approximately 2,200-acre Santa Monica Creek drainage above the SMDB. On January 9, 2018, just days before the wildfire was fully contained, spatially variable but locally intense precipitation triggered debris flows, mudflows, and sediment-laden floods in many of the burned canyons, including ones above Montecito and Carpinteria. Above Montecito, debris flows overwhelmed debris basins, sending slurries of boulders, debris, and mud through the community, destroying homes, closing Highway 101, and killing 23 people. Above Carpinteria, the SMDB filled with its first true post-fire debris flow but did not overtop.

The debris flow deposit that filled the SMDB was a fanglomerate consisting primarily of non-bouldery sediment, with lesser amounts of boulders up to 12 feet, woody debris, and other material including the remnants of a failed steel bridge. The deposits were up to 50 feet thick in the SMDB, extended roughly 1,000 feet upstream, and filled the inlet channel up to 40 feet deep.

The debris flow plugged all three PSW inlet towers in the SMDB and filled the PSW pipe, hampering initial cleanout efforts; work crews drilled horizontally through the plug to drain the basin and begin cleanout. The U.S. Army (USA) Corps of Engineers and Santa Barbara County ultimately removed roughly 161,000 cubic yards (approximately 10,000 truckloads) of material from the SMDB, at a cost of about $21 million.

Santa Barbara County is considering measures to expedite future cleanout, including: improving excavator access to the PSW inlet towers; increasing the height of the tower roofs to help locate

them when the basin is full; installing cleanouts along the PSW; retrofitting the trash racks; and improving equipment access to the spillway outlet.

1969 – Flooding and the Carpinteria Valley Watershed Project

In January and February 1969, a series of storms swept across Central- and Southern California, causing widespread flooding that killed 51 and resulted in accumulated damages exceeding a quarter of a billion dollars (Waananen 1969). In Santa Barbara County, the community of Carpinteria was most severely impacted (USA Corps of Engineers 1969), with flooding, scour, and sedimentation damaging agricultural, residential, and commercial areas (California State Department of Conservation 1969). Santa Monica Creek overtopped its banks during the third storm in the series on January 25, causing extensive gullying in citrus and avocado groves above Foothill Road, then commingling with debris-laden floodwaters from the Franklin Creek watershed to the east and impacting the urban areas in town.

Just two days before the January 25, 1969 flood, the USDA- Soil Conservation Service (subsequently renamed the NRCS) sent a draft Work Plan for the Carpinteria Valley Watershed Project to Washington for final approval. The Carpinteria Valley Watershed Project was conceived and approved as a PL-566 project in 1964, citing a major flood/debris event in 1914, minor flooding that occurred along Franklin Creek in 1962, and renewed flooding again in November 1965 (California State Department of Conservation 1969). PL-566 refers to the original legislation that authorizes the NRCS to provide technical and financial assistance to local sponsors, to plan, design, and install structural and land treatment measures for flood control and other resource-based issues in small watersheds.

Structural components of the Carpinteria Valley Watershed Project listed in the 1968 Work Plan included 6.7 miles of channel improvements throughout Carpinteria, and a debris dam across Santa Monica Creek about one-half mile upstream of Foothill Road (Santa Barbara Soil Conservation District et al. 1968). Following the Romero Fire in 1971, which burned across most of the Santa Monica Creek drainage above the dam site, the storage capacity of the debris basin was increased from 65- to 120 acre-feet (USDA-NRCS in prep.). In 1974, the location of the debris dam was moved approximately 3,500 feet upstream of the Work Plan site, based on results of supplemental geologic investigations and engineering analyses by the Soil Conservation Service. Finally, the 1976 Design Report for the SMDB, prepared by Los Angeles-based Koebig Inc., set the crest of the dam at or near 407 feet elevation to provide for at least 120 acre-feet of debris storage (USDA-NRCS in prep.).

1977-78 - Santa Monica Debris Basin Construction and Post-Construction Maintenance

Construction of the SMDB began in February 1977 and continued through April 1978, when Keobig Inc. submitted As-Built drawings. The Carpinteria Valley Watershed Project was completed in September 1981.

As constructed, the SMDB is a high hazard, earthen embankment structure that is approximately 467 feet long, with a maximum height of 102 feet. The basin has a 79 acre-foot (128,000 cubic yard) reservoir capacity at the auxiliary spillway crest elevation, and a debris capacity of 120 acre-feet (194,000 cubic yards; USDA-NRCS in prep.). The debris capacity was sized to accommodate the 1 percent event (100 acre-feet, estimated in 1971), with additional capacity for up to two annual events estimated to yield 10 acre-feet each. The SMDB is the

largest of Santa Barbara County's 11 debris basins along the coastal side of the Santa Ynez Mountains.

The principal spillway consists of a series of three PSW inlet towers with staggered elevations; the lowest tower feeds directly into a 48-inch, concrete outlet conduit, while the middle- and upper towers connect to the 48-inch conduit via steep 42-inch concrete sections (USDA-NRCS in prep.). All three PSW tower intakes are four feet wide by five feet high.

The SMDB is a jurisdictional structure (CA01134). The Santa Barbara County Flood Control and Water Conservation District (SBCFCD) operates and maintains the SMDB, conducts annual inspections of the facility with NRCS, and maintains an updated Emergency Action Plan. The SBCFCD removed sediment and debris from the basin in 1995, 1998, and again in January 2005 when they removed approximately 100,000 cubic yards to maintain capacity during a series of large events in December and January (Santa Barbara County Department of Public Works 2005). In each instance, sediment buried the lower two PSW inlet towers, which were damaged during clean out. The inspection team in November 2017 observed the SMDB was in working order, and the sediment level was at the lowest PSW inlet tower spill elevation.

2017-18 – The Thomas Fire and January Debris Flows

In December 2017, the Thomas Fire burned 281,893 acres across the Santa Ynez Mountains, including almost 90 percent of the approximately 2,200-acre Santa Monica Creek drainage above the SMDB, which burned predominantly at a moderate soil burn severity. As part of their preliminary debris flow hazard assessment of small watersheds burned by the Thomas Fire, the United States Geological Survey (USGS) concluded there was a 60- to 80 percent likelihood that a 15-minute peak rainfall intensity of 24 mm per hour would trigger debris flows in the two largest burned subbasins above the SMDB. Assuming the same rainfall intensity threshold, results of their empirically-based modelling suggested a total debris yield to the SMDB somewhere between 10,000- to 100,000 cubic meters (~13,000-131,000 cubic yards; Keane and Staley 2018).

On January 9, 2018, before the Thomas Fire was fully contained, a storm described as a Narrow Cold Frontal Rainband swept across the western margin of the burn area, dropping variable but generally intense rainfall that triggered debris flows in many of the burned canyons above Santa Barbara's coastal plain, including those above Montecito, and Santa Monica Creek above the SMDB (Lindsay et al. 2018). The rainfall gage at Carpinteria recorded a 15-minute peak rainfall intensity of 87.4 mm/hr, which corresponds to a 50-year exceedance, more than three times the 24 mm/hr hazard threshold assumed by USGS (Lancaster et al. 2018).

Above Montecito, debris flows triggered by the rainfall on January 9 overwhelmed debris basins, sending a slurry of boulders, debris, and mud through the community, destroying homes, closing Highway 101, and killing 23 people.

Above Carpinteria, the SMDB filled with an estimated 162,000 cubic yards of debris from the debris flow (Table 1). The debris flow deposits that filled the SMDB generally consisted of a fanglomerate with roughly 70 percent finer-grained sediment, 15- to 20 percent boulders to 12-feet diameter, 10-15 percent woody debris, and remnants from failed infrastructure including a steel bridge from upstream. The January 9 event was the first post-fire debris flow to fill the SMDB.

Table 1. Estimated volumes of material associated with the debris flow on January 9, 2018, that were deposited in and near the Santa Monica Creek Debris Basin (SMDB), and in the estuary at the mouth of Santa Monica Creek (SBFCD *in* USDA-NRCS in prep.)

	Volume of Material Deposited (cubic yards)			
Location	Sediment	Rock	Woody Debris	All
Inlet Channel	10,000	22,000	0	32,000
SMDB	114,000	27,000	21,000	162,000
Plunge Pool	20,000	0	0	20,000
Estuary	22,000	0	0	22,000
Totals	166,000	49,000	21,000	236,000

2018 - Debris Basin Performance and Repairs

The SMDB intercepted and stored most or all boulders and other large debris transported down Santa Monica Creek as part of the January 9 debris flow without overtopping, protecting downstream properties from potential debris damage and averting possible fatalities. The SMDB also trapped a large portion of the finer-grained sediment within the flow and reduced peak streamflows downstream, reducing the potential flood hazard along Santa Monica Creek through Carpinteria; an estimated 42,000 cubic yards of sediment passed through the basin's PSW and auxiliary spillway without causing Santa Monica Creek to flow out of its banks (USDA-NRCS in prep.; Table 1).

The success of the SMDB to reduce downstream damages notwithstanding, the January 9 debris flow damaged (or otherwise impacted) the structure, hampering efforts to restore basin capacity and function before the next anticipated flood/debris event(s): (USDA-NRCS in prep.):

- Sediment completely buried all three PSW inlet towers, making them difficult to locate;
- The lowest PSW inlet tower and its steel trash rack were damaged during cleanout; and
- Fine-grained (2-inch minus) debris and ash plugged the PSW outlet conduit, hampering efforts to drain the basin and initiate cleanout.

To restore drainage out of the basin, the County pumped the liquid slurry over the top of the embankment, and then in March 2018 hired a contractor to clear out the 48-inch PSW outlet conduit by drilling through the plug 1,130 feet horizontally, from the pipe outlet conduit to the lowest PSW inlet tower (USDA-NRCS in prep.). Basin cleanout was 90 percent complete by mid-April, after three months of working 24 hours a day, seven days a week, and approximately 10,000 truckloads. Boulders too large for trucking were blasted in place and hauled out in pieces. The remaining 10 percent of the basin was cleaned out in September 2018.

2019 - Investigation Findings and Proposed Modifications

Santa Barbara County is considering measures to expedite future cleanout, including:

- Improving excavator access to the three PSW inlet towers;
- Increasing the height of the tower roofs for faster tower location when the basin is full;
- Installing cleanouts along the PSW pipe conduit;
- Retrofitting the trash racks to prevent larger debris from entering the PSW; and
- Improving equipment access to the PSW outlets.

References

California State Department of Conservation, August 1968, Engineering Design Appendix, Carpinteria Valley Watershed, Santa Barbara County, California: Report by the Division of Soil Conservation, 32 p. plus tables and plates.

California State Department of Conservation, April 1969, Economic Analysis of the January – February 1969 Floods in the Carpinteria Valley Watershed: Report by the Division of Soil Conservation, 52 p. plus plates.

Kean, J. and Staley, D., 2018, Emergency Assessment of Post-Fire Debris-Flow Hazards- Thomas Fire: https://landslides.usgs.gov/hazards/postfire_debrisflow/detail.php?objectid=178 (Accessed 1/15/19).

Lancaster, J., Swanson, B., Oakley, N., Lindsay, D., and Short, W., 2018, The Santa Barbara and Carpenteria Debris Flows of January 9, 2018: Post-Fire Debris Flow Initiation Areas and Triggering Precipitation: Program with Abstracts, AEG 61st Meeting/IAEG XIII Congress, San Francisco, CA, September 2018.

Lindsay, D., Lancaster, J., Hernandez, J., and Short, W. 2018, Emergency Assessment of Post-Fire Debris Flows that Impacted the Communities of Montecito and Carpinteria, Santa Barbara County, California, on January 9, 2018: Program with Abstracts, AEG 61st Meeting/IAEG XIII Congress, San Francisco, CA, September 2018.

Santa Barbara County Flood Control and Water Conservation District, 1995, 1995 Floods: 114 p. https://www.countyofsb.org/uploadedFiles/pwd/Content/Water/1995FloodsRpt.pdf (Accessed 1/15/2019).

Santa Barbara County Public Works Department, 2005, 2004-05 Winter Report: Prepared by Matt Naftaly and Jerrett McFarland (Hydrology Section), 13 p. plus appendices. https://www.countyofsb.org/uploadedFiles/pwd/Content/Water/2005WinterRpt.pdf (Accessed 1/15/19).

Santa Barbara Soil Conservation District, Santa Barbara Flood Control and Water Conservation District, and the City of Carpinteria, November 1968, Watershed Work Plan, Carpinteria Valley Watershed, Santa Barbara County, California: Prepared with assistance by California Department of Conservation Division of Soil Conservation, USDA- Soil Conservation Service, and USDA- Forest Service, 63 p.

United States Army (USA) Corps of Engineers 1969, Report on Floods of January and February 1969 in Southern California: Los Angeles District report, 51 p. plus plates and Appendices.

United States Department of Agriculture (USDA)- Soil Conservation Service, 1976, Carpinteria Valley Watershed Project, Santa Barbara County California- Santa Monica Creek Debris Basin: As-Built Plans prepared by Koebig Inc., 52 sheets.

United States Department of Agriculture (USDA)-Natural Resources Conservation Service (NRCS), in preparation, Draft Engineering Report, Santa Monica Debris Basin Investigation: Unpublished Report prepared for the California NRCS State Office, 20 p (1/15/19 draft).

Waananen, A.O., May 1969, Floods of January and February 1969 in Central and Southern California: United States Geological Survey (USGS) Open-File Report, 233 p.

Post-Wildfire Geomorphic Stream Response Since 1996 in Twelve New Mexico Watersheds

Aljaz Praznik, 3208 Loma Vista, 87106 Albuquerque, New Mexico

Kyle Shour, Virginia dr., Albuquerque, New Mexico

Abstract

The severity, size, and frequency of wildfires has increased dramatically in New Mexico and across the American West over the past several decades. The severe nature of these fires has resulted in catastrophic consequences for downstream communities and ecosystems. Therefore, it is important to understand the geomorphic response of stream's burned watersheds decadal timescale to allow for design of resilient infrastructure and sustainable stream and riparian ecological restoration.

Introduction

In this research, we examined the geomorphic response of several streams in New Mexico after a wildfire, by analyzing changes in morphometric parameters using historical aerial photography sequences and by field reconnaissance on first through fourth order streams.

We visited four sites in New Mexico that were burned by a wildfire between 1996 and 2013 and performed a reconnaissance on each location. The drainage area varied from 1.2 to 13.4 square miles. Stream channels at these sites were largely ephemeral, but a few were perennial. We observed signs of post-fire erosion and sedimentation, bed sorting, vegetation establishment and other indicators of watershed recovery focusing on identifying recent and on-going geomorphic activity in low and higher-order channels.

We conducted GIS analysis using available historical aerial photography sequences at 12 sites to digitalize active channel area and channel centerline from second order headwater streams to fourth order channels near canyon mouths. Streams were divided into reaches by confluence locations. Changes in reach-averaged active channel area and sinuosity were evaluated.

We will present the results of the changes in morphometric parameters through time as well conceptual models that have been developed by combining the morphometric parameter analysis with field observations.

Other major headings

Field Visits

Geomorphic field reconnaissance was performed at three burned watersheds over the course of four days with the goals of evaluating:

- Post-wildfire depositional and erosional processes, emphasizing the most recently active processes to begin to understand which processes occur at which durations post-wildfire. This includes aggradation, degradation, lateral erosion, widening, gully evolution, and fan building.
- Post-wildfire bed material sorting. This includes determining when gradations at the surface and sub-surface start to differ and inception of riffles, steps, and pools.
- When riparian and upland vegetation re-establishes and how vegetation species differ from pre- to post-wildfire.
- The suitability of a site for additional detailed data collection to support future studies.
- Active channel width at a few locations to help quantify uncertainty in the associated morphometric parameter analysis results.

Silver

The Silver Fire burned the west slope of the Black Mountains in the Gila National Forest in 2013. Two streams were visited on July 28, 2018. For much of the visited watershed, the effects of the burn did not seem severe. Limited gullying and debris flow scars were observed. Oak and pines species both had several trees that survived the fire and stands of even age pioneer species (e.g., aspen and locust) were few.

The lessons learned from this field visit are:

- Burn severity and slope play an important role in the magnitude of geomorphic response. This may be important 5-years after the wildfire.
- Geologic controls play affect the type, magnitude, and location of the geomorphic response on both lower and higher order channels.

Pinatosa

The Pinatosa burn scar is located in the Gallinas Mountains southwest of Cordova, New Mexico in the Cibola National Forest. The burn occurred in 1996. The site was visited on July 28, 2018 (Figure 1). Based on the surrounding, unburned watershed, the canopy cover was ponderosa and mixed pinyon-juniper. Much of the canopy was destroyed by the fire. While the predominate vegetation cover was grass and forbs, trees have grown to as much as 10 feet tall. Trees are primarily New Mexico Locust and juniper.

The primary lessons learned from this site were:

- The material deposited by the fire is largely stable. Perhaps only being mobilized in an infrequent, large magnitude flood.
- Watershed vegetation re-establishment is on-going after 22 years; riparian vegetation is not expected to establish because of the ephemeral nature of the flow.
- Bed material sorting did not occur because of the ephemeral nature of the flow. This may prolong the fluvial geomorphic response relative to a perennial or intermittent flow stream.

Las Conchas - Cochiti Canyon

The Las Conchas Fire burned the Cochiti Canyon watershed on the east slope of the Jemez Mountains in 2011. This site was visited on August 6 and 16, 2018. The first visit was used to gain an overview of watershed and select tributaries along the north side of the main canyon. The second visit was used to observe the main channel and tributary confluences.

Throughout the reach observed, the active channel width increased post-wildfire and channel aggraded, even above the pre-wildfire floodplain (Figure 2). Imbricated bars formed. As bed material supply decreased, a low flow channel incised into the post-wildfire deposits. In erosional reaches as the bed continued to adjust, meander development occurred, and pool, riffle, and step formation initiated. This has led to formation of a new floodplain surface, which is now well vegetated with locust, elder, oak, willow, roses, sedges, grasses, and forbs. The banks to the new floodplains are low. In depositional reaches, the active channel narrowing is less pronounced, and several bar surfaces exist. Some step and riffle formation were observed.

Computer Analyses

We conducted GIS analysis using available historical aerial photography sequences at 12 sites to digitalize active channel area and channel centerline from second order headwater streams to fourth order channels near canyon mouths. Streams were divided into reaches by confluence locations. Changes in reach-averaged active channel area and sinuosity were evaluated.

We compared pre and post fire active channel lengths within different stream orders.

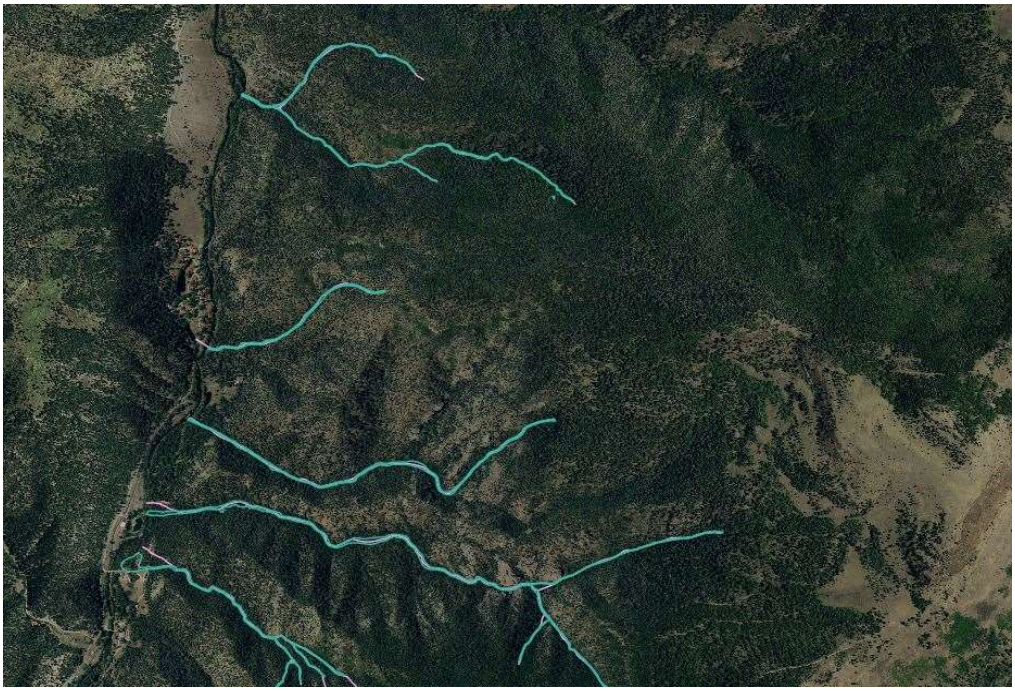

Figure 1. Aerial photo of the area before the Tres Lagunas fire, the blue lines show river streams

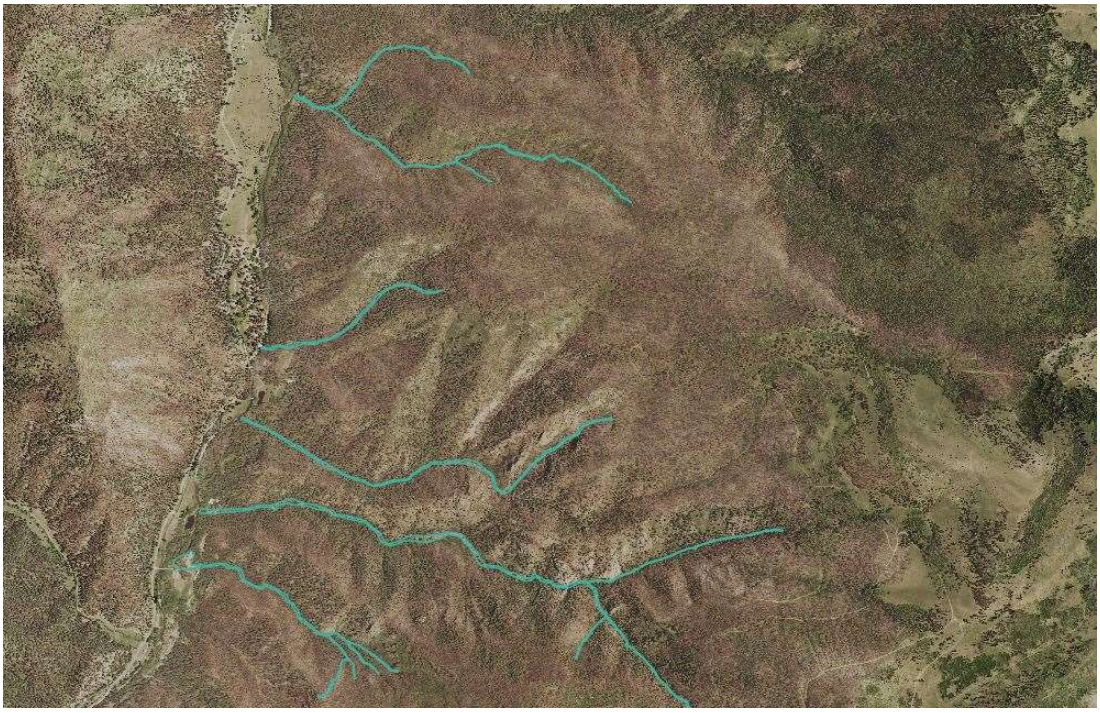

Figure 2. Burning scar after the Tres Lagunas fire, the blue lines show different stream orders

Improving Resiliency and Sustainability of Watershed Resources and Infrastructure

- Climate Variability and Sediment
- Dam Removal or Rehabilitation
- Fluvial Geomorphology
- Gully Erosion
- Hydraulic and Sediment Transport Modeling
- Infrastructure in the Stream Environment
- Physical Sediment Load Measurements
- Regional Sediment Management
- Remote Sensing and Monitoring
- Reservoir Sedimentation and Sustainability
- Sediment Impacts on Wildlife and Habitat
- Sediment Properties
- Sediment Surrogate Measurements
- Sediment Yield and Fingerprinting
- Stream Restoration

Scaling Post-Fire Effects from Hillslopes to Watersheds: Processes, Problems, and Implications

Lee H. MacDonald, Senior Research Scientist, NREL, and Professsor Emeritus, Department of Ecosystem Science and Sustainability, Colorado State University, Fort Collins, Colorado, USA; lee.macdonald@colostate.edu
Dan J. Brogan, Department of Civil and Environmental Engineering, Colorado State University, Colorado State University, Fort Collins, Colorado, USA; buckhtr@gmail.com
Peter A. Nelson, Associate Professor, Department of Civil and Environmental Engineering, Colorado State University, Colorado State University, Fort Collins, Colorado, USA;
Stephanie Kampf, Associate Professor, Department of Ecosystem Science and Sustainability, Colorado State University, Fort Collins, Colorado, USA; Stephanie.kampf@colostate.edu
Joe W. Wagenbrenner, Research Hydrologist, USDA Forest Service, Pacific Southwest Research Station, Arcata, California USA; jwagenbrenner@fs.fed.us

Introduction

Over the last two decades we have made considerable progress on understanding and predicting the effects of wildfires on runoff and erosion at the hillslope scale. One cannot, however, sum up the hillslope-scale effects to predict what happens downstream because of the scale-dependent changes in the driving variables and controlling processes; yet resource managers need an understanding and predictive capability to assess post-fire risks at watershed scales, and to prioritize post-fire treatments among watersheds and fires. Our objectives are to: 1) show how post-fire sedimentation effects vary over spatial scales and over time; 2) summarize the results of our four-year study on post-fire erosion and deposition at different spatial scales in two approximately 15 km^2 watersheds after the High Park Fire in northcentral Colorado (Figure 1); and 3) discuss the implications of this and other studies for predicting post-fire sediment deposition and delivery at the watershed scale.

Post-Fire Sediment Production and Delivery

Extensive research has shown that the two most important controls on post-fire runoff and erosion in mountainous areas are percent bare soil—which can be inferred from soil burn severity—and rainfall intensity (Benavides-Solorio and MacDonald, 2005). Infiltration rates drop to less than 10 mm hr^{-1} after high and moderate severity fires, so even moderate-intensity rainstorms generate infiltration-excess overland flow. The very low surface cover usually leads to orders of magnitude increases in surface erosion by rainsplash and sheetwash, and the increased runoff causes rilling and a tremendous headward expansion of the channel network (Wohl, 2013). The greater channel density and reduced surface roughness greatly increases hillslope-stream connectivity, resulting in nearly all of the post-fire hillslope runoff and erosion to be delivered to the channel network and transmitted downstream to the lower-gradient channels. In some geomorphic process domains, such as southern California, higher-intensity rainfalls also can lead to devastating debris flows in addition to the more commonly observed increases in hillslope surface erosion (Kean et al., 2011).

In unburned areas sediment delivery ratios almost always indicate that the vast majority of eroded sediment is stored regardless of the size of the area being assessed (Walling, 1983). In contrast, there may be little or no decline in sediment production and delivery rates in the first one to two years after high and moderate severity forest fires for areas up to a few hectares

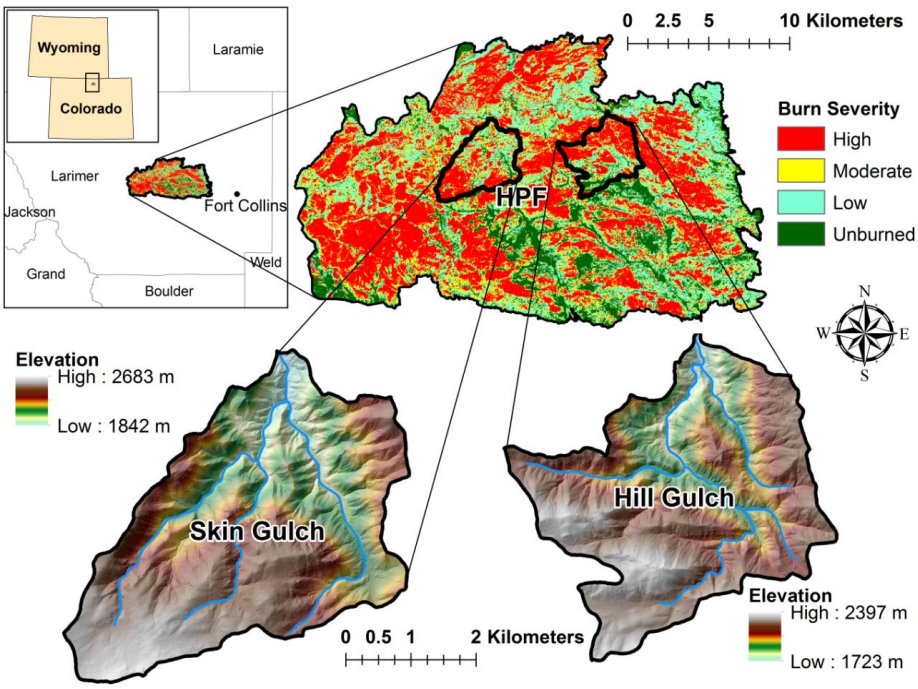

Figure 1. Location and burn severity of the 2012 High Park Fire in northern Colorado just west of Fort Collins, and maps of our two study watersheds where we intensively monitored channel changes using both field methods (cross sections and longitudinal profiles) and post-fire erosion and deposition in the valley bottoms by differencing five sequential lidar datasets.

(Figure 2). Our intensive field surveys and lidar differencing in two 15 km² watersheds after the 2012 High Park Fire found that beyond about 1 km² the tendency for decreasing channel gradients and confinement caused much of the coarser post-fire sediment to be deposited and stored in the channels and valley bottoms (Figure 3) (Brogan et al., 2019a, b). This predominance of deposition has been documented for a wide variety of post-fire erosion processes (e.g., McPhee, 1989; Benda, 2003). In the Rocky Mountains we've observed that post-fire snowmelt, lower-intensity rainstorms, and higher baseflows do not cause much hillslope erosion, but further downstream the accumulated runoff can erode and transport substantial amounts of the finer and lower-lying post-fire sediment deposits (Figure 3).

After fires the predominant pattern is for the coarse sediments to be readily deposited once stream gradients decline, and this is true for both the debris flows regimes in southern California as well as the much more common fluvially-dominated regimes in most of the western U.S. In contrast, the ash, silts, and clays are readily conveyed to the watershed outlets, resulting in a much higher sediment delivery ratio for these constituents (Figure 4). These finer constituents are often of greatest concern for domestic water providers as they are much more difficult to treat and remove than the coarser particles that can be easily captured in settling basins. A second key observation is that post-fire sediment inputs have a much smaller geomorphic effect in larger streams and rivers because so much sediment is stored in the middle portions of a watershed. The larger streams and rivers downstream of a fire also can readily transport most of the sediment delivered to them, particularly when this is finer-textured. However, post-fire sediment can be a major concern when there are either downstream reservoirs or debris basins with limited sediment storage capacities. For example, post-fire sediment from a succession of fires reduced the storage capacity of Strontia Springs reservoir

southwest of Denver by approximately 750,000 m^3, and Denver Water spent $30 million in a largely unsuccessful effort to dredge the accumulated sediment.

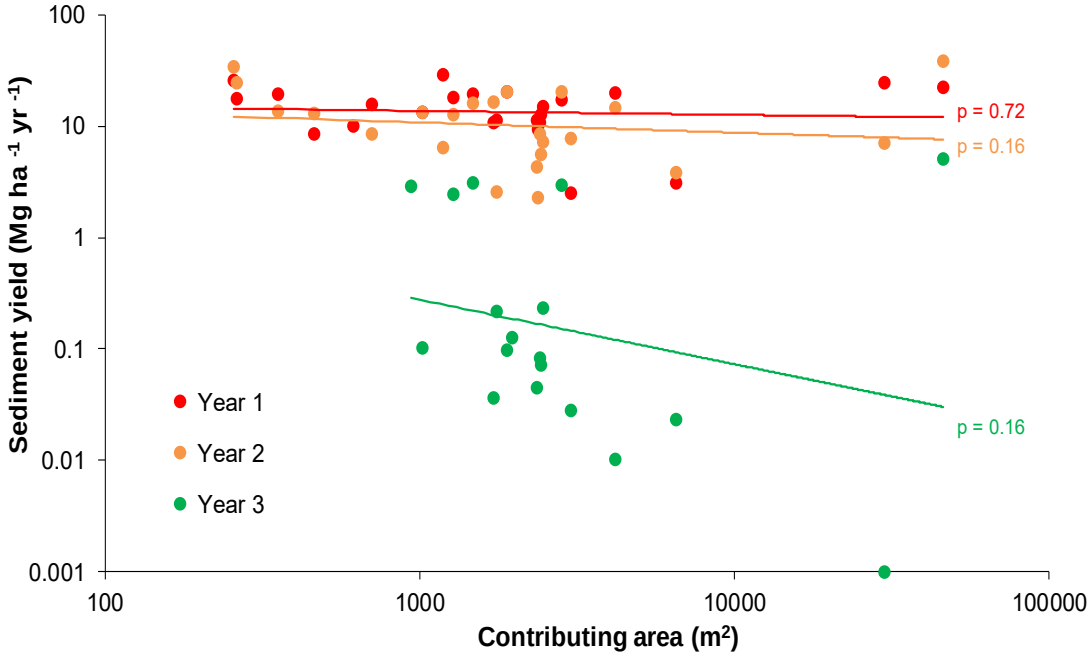

Figure 2. Annual sediment production per unit area for different-sized hillslopes and small watersheds for the second, third and fourth summers after burning following the June 2002 Hayman fire in Colorado. These are labeled as Years 1-3, respectively, as the first summer is immediately after burning, and in this area virtually all of the annual sediment yield is caused by summer thunderstorms. The Year 3 point in the upper right was due to a large storm on one of the two watersheds we were monitoring, while the other small watershed generated no sediment. The former point greatly affects the slope and significance of the Year 3 regression line. For reference one Megagram (Mg) is 1.1 English tons, and 10,000 m^2 is one hectare or 2.47 acres.

Figure 3. The large amounts of sediment deposited in Skin Gulch after the High Park fire resulted in a very flat valley bottom profile as shown in the picture in the hands of Dr. Peter Nelson. Subsequent snowmelt and lower-intensity rainstorms incised a channel into these deposits and removed some of the finer, lower-lying surface material. Picture was taken in spring 2013, about 11 months after burning.

Post-fire deposition is expected to be particularly high when post-fire runoff and erosion is primarily due to summer convective storms, as the intense rainfall generally falls over a limited portion of a watershed (Kampf et al., 2016) and unit area runoff rates rapidly decline with increasing watershed area. By one to three years after a fire vegetative regrowth sharply decreases overland flow, hillslope erosion, hillslope-stream connectivity, and downslope sediment transport (Benavides-Solorio and MacDonald, 2005; Wohl and Scott, 2017) (Figure 5). These changes cause a corresponding reduction in downstream sediment deposition as well as the high flows needed to erode the initial post-fire sediment deposits.

Figure 4. High flows generated by a summer thunderstorm with high concentrations of suspended sediment and ash at the outlet of the 14 km² Hill Gulch watershed in summer 2012, two months after the High Park Fire.

Figure 5. A rill (light blue dashed line) that had formed almost immediately after burning on a bare convergent hillslope in lower Hill Gulch was largely obscured by regrowth just 14 months later, and did not appear to be actively eroding. The vegetative regrowth would tend to capture sediment and reduce sediment delivery from the hillslope to the stream network.

In the High Park Fire the usual trend of post-fire deposition in downstream areas was completely reversed by a highly unusual, long-duration flood 15 months after burning (Brogan et al., 2019a,b). The sustained high flows had sufficient stream power to scour out nearly all of the post-fire sediment deposits along with much of the pre-existing sediment deposits in the valley bottoms, leaving significantly coarser channels and floodplains (Brogan et al., 2019a,b). We found that the changes in sediment volumes for 50-m long segments of the valley bottom were significantly but usually only weakly correlated with contributing area and valley width, percent area burned at high or moderate burn severity, channel slope, maximum rainfall intensity, and total rainfall (Brogan et al., 2019b).

Current Capabilities and Larger-scale Predictions

Taken together, our results show that accurately predicting post-fire sediment deposition and delivery with increasing watershed area is still beyond our capabilities. On the plus side a process-based understanding—when combined with burn severity, a specified rainstorm, and morphometric data (e.g., channel slope and valley width or confinement)—can help assess relative risks of post-fire flooding, erosion, and deposition in different locations at scales of up to perhaps 20-50 km^2. These assessments can then help decide which sub-watersheds are most likely to either store or transmit post-fire runoff and sediment, and hence which sub-watersheds pose the highest risk for downstream delivery and should have priority for post-fire treatments to reduce hillslope erosion.

As watershed size continues to increase the risks of downstream post-fire flooding and deposition should rapidly diminish for several reasons. First, fires are a mosaic of burn severities and rarely burn all of a large watershed. Hence the large increases in runoff and erosion from areas burned at high and moderate severity are diluted by the much lower runoff and erosion from low severity and unburned areas. Second, high-intensity storms that drive much of the post-fire runoff and erosion are often limited in spatial scale, which leads to rapid declines in unit area peak flows with increasing watershed area. Third, the usual trends for stream gradients to decrease and valley bottom widths to increase with increasing watershed area generally forces relatively rapid deposition of post-fire sediment in the downstream direction. These overall trends do not obviate the tremendous local threats to communities located at the base of a steep mountain front as so tragically observed after fires in southern California. A more explicit identification of the key physical processes and how these change across different spatial scales is essential to better evaluate post-fire risks to life, property, and water quality as well as guide post-fire mitigation treatments.

References

Benavides-Solorio, J. and MacDonald, L.H. 2005. “Measurement and prediction of post-fire erosion at the hillslope scale, Colorado Front Range,” International Journal of Wildland Fire 14:1-18.

Benda, L., Miller, D., Bigelow, P., and Andras, K. 2003. “Effects of post-wildfire erosion on channel environments, Boise River, Idaho,” Forest Ecology and Management 178(1-2): 105-119.

Benavides-Solorio, J. and MacDonald, L.H. 2005. “Measurement and prediction of post-fire erosion at the hillslope scale, Colorado Front Range,” International Journal of Wildland Fire 14:1-18.

Brogan, D.J., MacDonald, L.H., Nelson, P.A., and Morgan, J.A. 2019a. “Channel geomorphic complexity and sensitivity to fires and floods in mountain catchments,” Geomorphology 337: 53-68.

Brogan, D.J., Nelson, P.A., and MacDonald, L.H., in press. “Spatial and temporal patterns of sediment storage and erosion following a wildfire and extreme flood,” Earth Surface Dynamics.

Kampf, S.K., Brogan, D.J., Schmeer, S., MacDonald, L.H., and Nelson, P.A. 2016. “How do geomorphic effects of rainfall vary with storm type and spatial scale in a post-fire landscape?” Geomorphology 273: 39-51.

Kean, J.W., Staley, D.M. and Cannon, S.H., 2011. "In situ measurements of post-fire debris flows in southern California: Comparisons of the timing and magnitude of 24 debris-flow events

with rainfall and soil moisture conditions." Journal of Geophysical Research: Earth Surface 116, no. F4.
MacDonald, L.H., 2018. “Post-fire debris flow problems aren’t new and likely to get worse,” Conversations, 16 January 2018, 5 pp.
McPhee, J.A., 1989. The control of nature. Farrar, Straus, and Giroux, New York.
Schmeer, S., Kampf, S.K., MacDonald, L.H., Hewitt, J., and Wilson, C. 2018. “Empirical models of annual post-fire erosion on mulched and unmulched hillslopes,” Catena 163:276-287.
Walling, D.E., 1983. "The sediment delivery problem", Journal of Hydrology 65(1-3): 209-237.
Wohl, E. 2017. “Migration of channel heads following wildfire,” Earth Surface Processes and Landforms 22(9): 1049-1053.
Wohl, E., and Scott, D.N. 2017. “Transience of channel head locations following disturbance,” Earth Surface Processes and Landforms 42(7): 1132-1139.

Professional Development & Engineering Ethics: Advancing Your Career through Board Certification

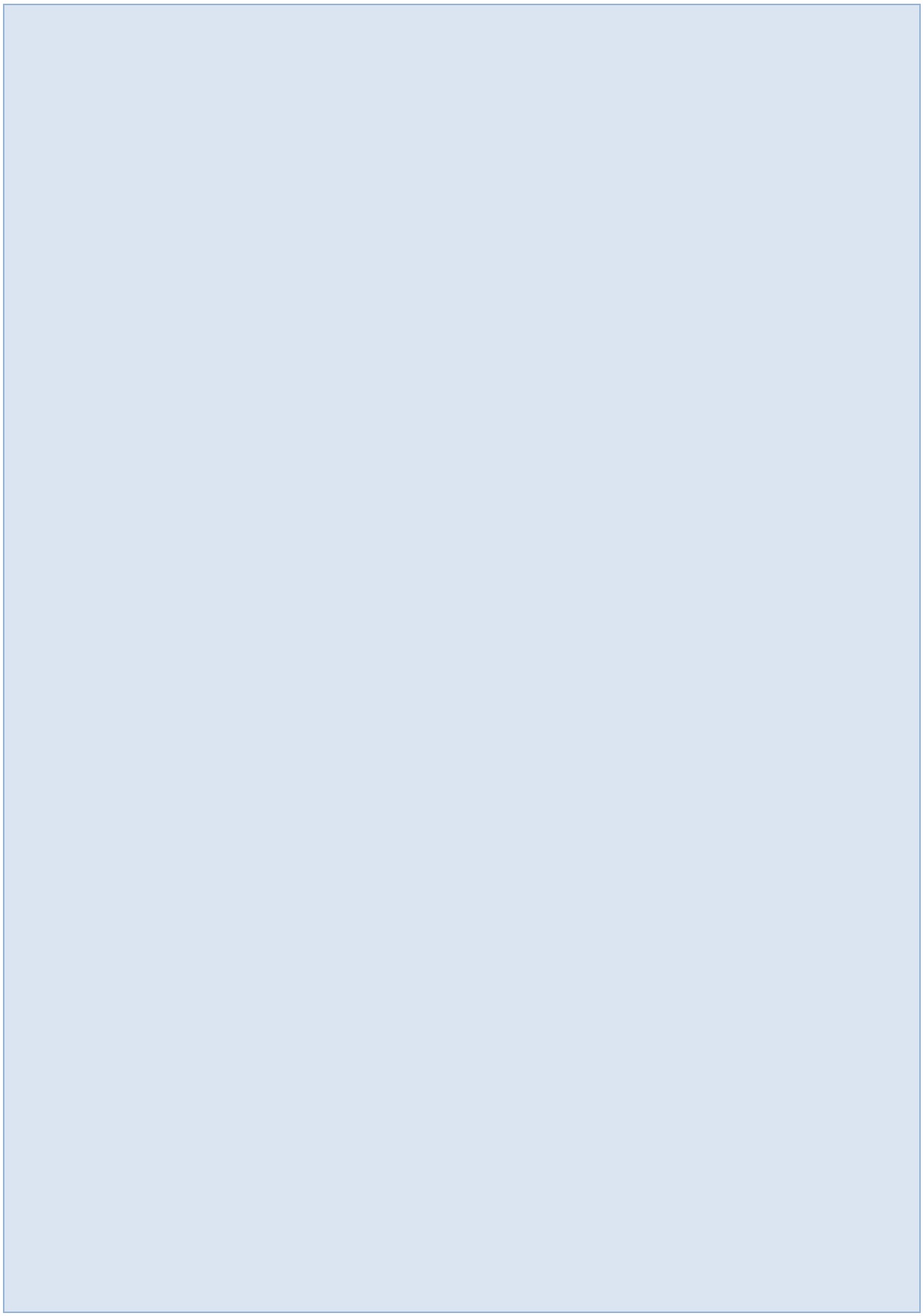

Hydrologists, Get Certified! Informational Presentation on Professional Hydrologist (PH) Certification and Hydrologic Technician (HT) Certification

Jamil Ibrahim, PH[1,2], jamil.ibrahim@stantec.com
David T. Williams, PH[3,4] , david@dtwassoc.com
Julé Rizzardo, PH[5,6], jule.rizzardo@waterboards.ca.gov

Abstract

The American Institute of Hydrology (AIH) is dedicated to the certification and registration of professionals in all fields of hydrology. The purpose of AIH is to enhance and strengthen the standing of hydrology as a science and profession. Currently, there are approximately 500 professional members of AIH across the U.S. and abroad. Our members include scientists, engineers, and planners from academic and research institutions, public agencies, private industries, and professional consulting companies. We offer a variety of types of certification at different levels, ranging from student memberships and Hydrologic Technicians to Professional Hydrologists. Join us for an engaging presentation on the benefits of certification and learn about the exciting new initiatives AIH is launching in 2019 and beyond.

Introduction

Hydrologists are experts in interdisciplinary sciences related to water and are working to address water issues. Their work, and the science of hydrology, encompasses the occurrence, distribution, movement and properties of waters of the earth and their relationship with the environment within each phase of the hydrologic cycle. Roles and responsibilities of hydrologists are as varied as the uses of water and may range from planning large-scale water resources projects to monitoring water quality and flow conditions in local streams. While many hydrologists are certified in technical disciplines that may include or relate to hydrology (e.g. Professional Engineer, Professional Geologist, Certified Floodplain Manager, etc.), hydrologists who obtain certification as a Professional Hydrologist (PH) or Hydrologic Technician (HT) can demonstrate their technical expertise in hydrology among a nationwide network of recognized experts.

AIH was founded in 1981 as a non-profit scientific and educational organization dedicated to the certification and registration of professionals in all fields of hydrology. AIH is the only nationwide organization that offers certification to qualified professionals in all fields of hydrologic science.

Certification and Membership Types Offered

AIH offers certification and membership types based on an applicant's demonstrated qualifications. In addition to the certified membership types, individuals or organizations may obtain membership with AIH as affiliates but would not be certified for professional competence

in the field of hydrology. Affiliate membership types include Student Member, Individual Affiliate Member, and Organizational Affiliate Member.

Below sections describe member certification types offered by AIH for applicants to demonstrate their technical expertise in hydrology among a nationwide network of recognized experts.

Professional Hydrologist

Professional Hydrologist, or PH, certification is conferred by AIH on professionals who demonstrate competence in the field of hydrology through meeting specified education and professional experience requirements, maintaining personal integrity, and successfully passing the Fundamentals Examination (or Part I examination) and the Principles and Practice Examination (or Part II examination). Applicants for PH certification specify their area of specialization (surface water, groundwater, or water quality) and take a Principles and Practice Examination (or Part II examination) for their specialty area. The Part II examination may be waived for PH applicants who demonstrate fulfillment of specified education and professional experience requirements, and based on approval by the AIH Board of Registration. Once certified by AIH as a Professional Hydrologist (or PH), such members can represent themselves as certified Professional Hydrologists in their specialty areas of either surface water, groundwater, or water quality.

Hydrologists in Training

The Hydrologist-In-Training (HIT) membership is for new college graduates and/or early career professionals who have passed the Part I examination but either have not taken or passed the Part II examination (see above), or do not have enough experience to qualify for PH certification. The Part I examination may be waived for HIT applicants who demonstrate fulfillment of specified education and professional experience requirements, and based on approval by the AIH Board of Registration. An HIT member has all the same benefits as the other member categories with AIH; however, an HIT cannot represent themselves as a certified Hydrologist until they have met the professional experience requirements and have successfully passed the Part II examination.

Hydrologic Technicians

The Hydrologic Technician (HT) certification type is offered for applicants to emphasize hands-on knowledge and hydrology field experience. Their contribution to the hydrology profession is demonstrated through collection of hydrologic data in all weather conditions and environments while applying representative quality management procedures for data collection and hydrologic measurements. Levels of HT certification are conferred by AIH on professionals who demonstrate, through an application, that they meet the minimum education, personal integrity, and experience requirements and have passed the appropriate examination(s) administered by AIH. Hydrologic Technicians can be certified in surface water, groundwater, or water quality at the general, intermediate, or advanced level.

Benefits of Membership

Certification by AIH provides a means by which the public, employers, and clients can recognize those hydrologic professionals who are judged by their peers to possess the proper and

necessary qualifications to practice their profession with integrity. Benefits of being certified by AIH include:

- Peer and employer recognition of professional competence in hydrology for career advancement;
- Certification to perform certain duties/functions, as specified by certain agencies;
- Association to a nationwide network of hydrologists;
- Access to and opportunities for contributing to AIH Bulletin;
- Access to career development and continuing education resources; and
- Eligibility for annual awards nominations to hydrologists demonstrating outstanding accomplishments in the fields of groundwater, surface water, water quality, and institute development.

Join us for an engaging presentation on the benefits of certification as a PH and the importance of seeking out certified PHs for water resources projects and tasks. Come learn how the move of our headquarters to Denver under professional management and our transition to online testing is helping our organization grow. Elevate your career and get involved with the exciting initiatives AIH is planning to roll out in 2019 and beyond.

American Institute of Hydrology | Phone: 303-339-0523 | admin@hydrology.org

References

[1] President Elect, American Institute of Hydrology, PO Box 3948, Parker, Colorado 80134

[2] Principal Hydrologist, Stantec, 3301 C Street, Suite 1900, Sacramento, California 95816

[3] Board of Registration Chair, American Institute of Hydrology, PO Box 3948, Parker, Colorado 80134

[4] President, DTW and Associates, Engineers, LLC, 12611 E. 104th Avenue, Suite 800, PMP 100, Commerce City, Colorado 80022

[5] Vice President for Institute Development, American Institute of Hydrology, PO Box 3948, Parker, Colorado 80134

[6] Assistant Deputy Director, Water Rights, California State Water Resources Control Board, 1001 I Street, Sacramento, CA 95814

Regional Sediment Management

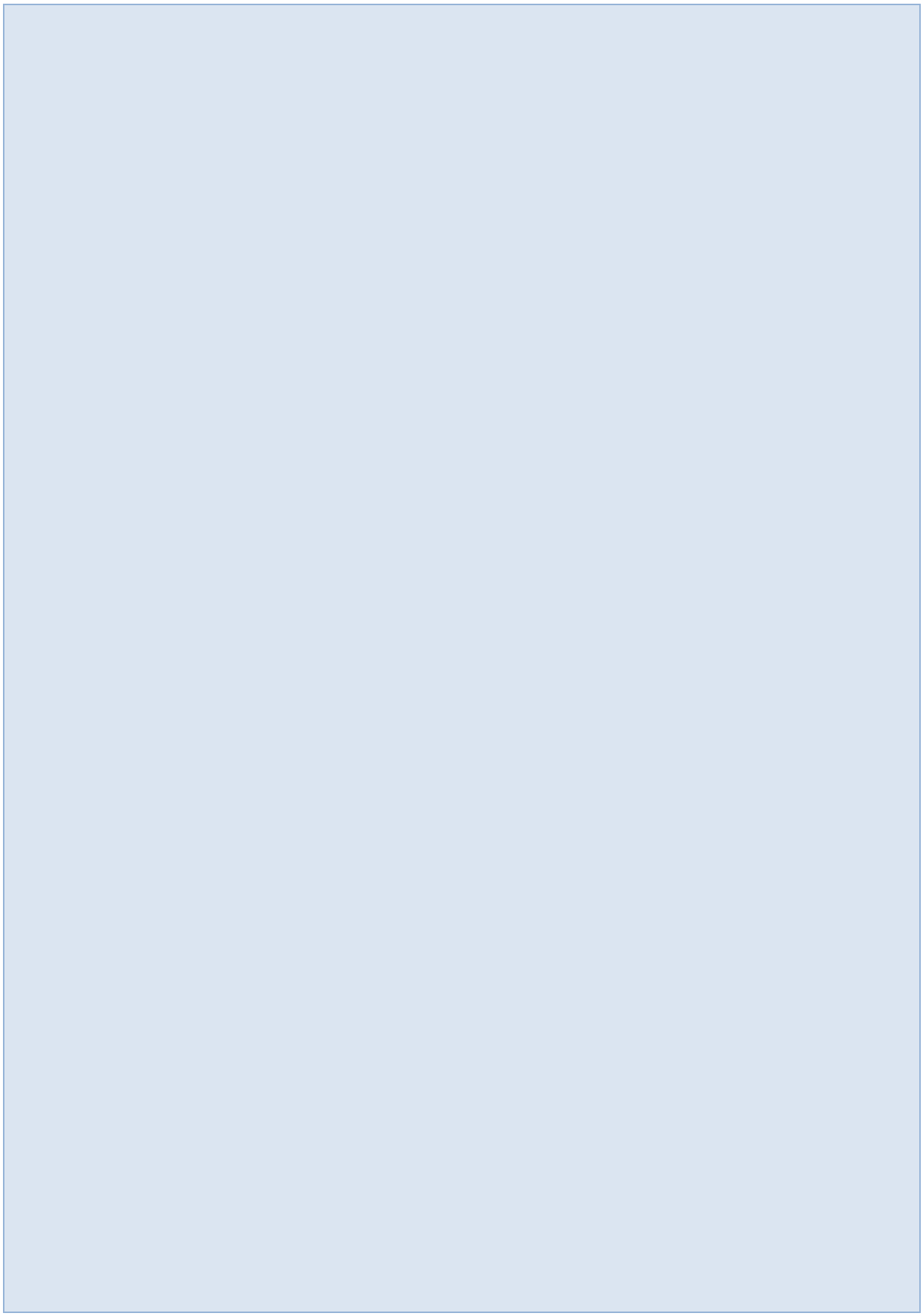

Early Results - Salt Marsh Response to Changing Fine-Sediment Supply Conditions, Humboldt Bay, CA

Jennifer A. Curtis, Geologist, U.S. Geological Survey, Eureka, CA, jacurtis@usgs.gov
Chase Freeman, Biologist, U.S. Geological Survey, Davis, CA, cfreeman@usgs.gov
Karen Thorne, Research Ecologist, U.S. Geological Survey, Davis, CA, kthorne@usgs.gov

1.0 Introduction

The resiliency and vulnerability of natural and restored salt marshes is highly dependent upon the mineral sediment supply (Weston, 2014; Ganju et al.,2015) carried by the water that inundates the marsh surface. Marsh surface elevations are maintained through complex morpho-dynamics and marsh evolution models assume that sediment deposition, vertical accretion and elevation gain are directly proportional to suspended-sediment concentrations (Kirwan and Murray, 2007; Fagherazzi et al., 2012). In this study we use direct measurements of vertical accretion, marsh elevation change, and suspended-sediment concentrations (SSC) to investigate salt marsh response to changing fine-sediment (<63 μm) supply conditions in Humboldt Bay, CA.

Both mineral- and organic-sediment supply maintain marsh surface elevations (D'Alpaos et al., 2011; Thorne et al., 2016), which must keep pace with relative sea-level rise (RSLR) to avoid submergence and conversion to subtidal habitat if marsh transgression is not possible (Kirwan et al., 2010; Thorne et al., 2018). Modeling and field-based studies agree that sediment-rich marshes are less vulnerable to RSLR and sediment-limited marshes are more vulnerable to RSLR (Patrick and DeLaune, 1990; Thom, 1992; Stralberg et al., 2011; Thorne et al., 2016).

There is a dynamic balance that exists between the rates of RSLR, local morphology, sediment supply, hydrodynamics, plant productivity, and the ability of marsh vegetation to trap and stabilize available sediment (Thom, 1992; Callaway et al, 1996; Cahoon, 1997; Morris et al., 2002). To manage and restore salt marshes effectively and sustainably, we need to understand resiliency and how they respond to changing sediment supply conditions. In Humboldt Bay, where long-term RSLR ranges from 3.11 to 5.56 mm/yr (Anderson, 2015), which is greater than most west coast regions due to tectonic subsidence (Russell, 2012; Montillet et al., 2018), an adequate sediment supply is critical if existing and restored salt marshes are to persist into the future. This study was designed to inform management actions that may affect the trajectory of vertical marsh accretion and vulnerability to sea-level rise (SLR) such as regional sediment management, dredging, and tidal restoration to subsided former baylands.

2.0 Regional Setting

Humboldt Bay is located on the north coast of California (Figure 1). The bay is protected by coastal barriers and sand spits but is subject to energetic conditions driven by storms, waves, and wind events. Costa (1982) described the bay as a tide-driven coastal lagoon with limited freshwater contributions that occur primarily during large winter storms. There are three subembayments referred to as the Entrance Bay, North Bay and South Bay. The subembayments are connected by the entrance channel and a network of navigation channels that require periodic maintenance dredging (HBHRCD, 2007). Dredging began in 1881 and currently the average annual volume of dredged fine-sediment (<63 μm) is approximately 60,500 m3 (CCSMW, 2017), which equates to 0.10 Mt/yr using a conversion factor of 1.7 Mt/m3. The sheltering effect of the barrier spits protects the interior of the bay from wave exposure and allowed expansive areas of salt marsh to form historically in low energy

environments along the bay margins. In 1870 salt marshes occupied approximately 36 km2 (Figure 1) but the present distribution represents less than 10% of the former extent (Pickart, 2001). Currently, salt marshes exist as fragments along the bay's margins, at the mouths of local tributaries, or recessed upstream within tidal slough channels. Approximately 70, 25, and 5% of the remaining salt marshes (<3.6 km2) are found in the North Bay, Entrance Bay and South Bay, respectively (Schlosser and Eicher, 2012). These tidal marshes are important habitat for migratory and resident birds and juvenile coho salmon (Oncorhynchus kisutch).

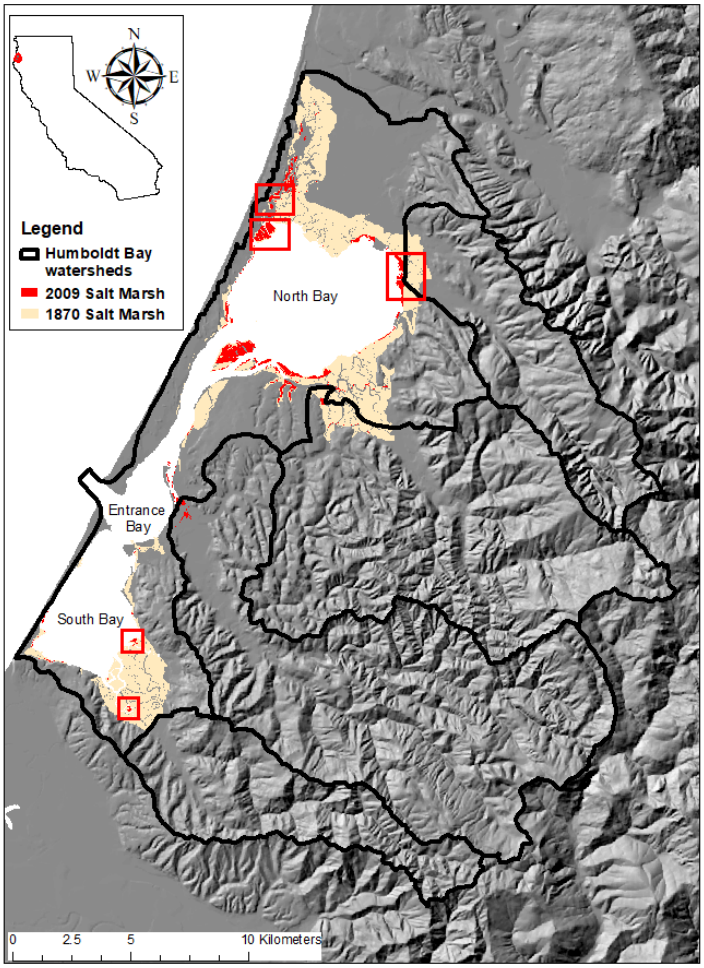

Figure 1. Humboldt Bay study area showing spatial extent of tidal salt marshes in 1870 (Laird, 2007) and 2009 (Schlosser and Eicher, 2012). Red bounding boxes delineate five salt marsh study sites (see Figure 2 for detailed study marsh maps).

2.1 Hydrodynamics

Humboldt Bay is relatively shallow with 39 km2 of mudflats exposed at mean lower low water (MLLW) and the mean daily tidal exchange volume is approximately 114 million m3/day (Anderson, 2015). The exchange volume, or tidal prism, is quite large in comparison to the freshwater discharge from the local watersheds. The mean annual freshwater discharge is

approximately 0.6 million m3/yr (Curtis et al., in review). The relatively small freshwater inflow from the bay watersheds results in tidally-dominated circulation, with estuarine conditions existing only during the winter-runoff season at the tributary-bay interface.

The bay experiences mixed-semidiurnal tides with a mean diurnal range of 2.1 meters (estimated as the difference between MLLW and MHHW) and mean tide of 1.49 meters (National Oceanic and Atmospheric Agency Station, North Spit, 9418767; https://tidesandcurrents.noaa.gov/). The North Bay is deeper relative to South Bay and the contributions to the tidal prism are ~50% and ~25% respectively (Anderson, 2015).

Notably, the flushing rates of North Bay are lower than South Bay due to the bay's morphology (Costa, 1982) and this influences the amount of marine-derived sediment that can enter and the amount of freshwater-derived sediment that can exit. Because the volume of the three subembayments is large in comparison to the tidal channels, water that flows into the bay on a high tide cannot be completely replaced during a single tidal exchange. Approximately 41% of the water is replaced during each tide cycle and full tidal exchange can take 4 to 21 days (Schlosser and Eicher, 2012).

2.2 Climate, hydrology, and fine-sediment supply

Humboldt Bay is located at the transition between the Pacific Northwest and California climate regions, within the Coast Range geologic province, and has a Mediterranean climate with distinct cool-dry summers and mild-wet winters. The average annual precipitation is 1,585 mm/yr, of which only 3% falls between June and September (Curtis et al., in review). The orographic effect of the Coast Range creates a strong precipitation gradient and the hydrology is characterized by extremes. Winter discharge peaks are typically rainfall-driven, and snowmelt plays a less significant role. However heavy rain events, referred to as atmospheric rivers (Dettinger et al., 2011), can produce dramatic floods (Brown and Ritter, 1971; Waananen, 1971).

Watersheds that deliver sediment to the north coast of California are characterized by steep-forested uplands and low-lying areas near the mouth composed of floodplains, pastures and wetlands. These coastal watersheds have high rates of fine-sediment yield related to regional tectonics, erodible lithology, climate and land use history (Brown and Ritter, 1971; Kelsey, 1980; Milliman and Farnsworth. 2001; Warrick et al., 2013).

Humboldt Bay receives direct inputs of fine-sediment and freshwater from several small tributary watersheds with a combined contributing area of 442 km2 (Figure 1). Historically, the upland forests were extensively logged (Leithold et al., 2005; Klein et al., 2012) and low-lying areas have been diked and leveed (Schlosser and Eicher, 2012).

The coastal sediment budget is dominated by sediment discharged from the Eel River (9,415 km2) during winter runoff events (Wheatcroft et al., 1997; Wheatcroft and Borgeld, 2000; Farnsworth and Warrick, 2007, Warrick, 2014). Sediment discharge from the coastal rivers of northern California peaked in water year 1965 and have since declined (Warrick et al., 2013). The peak in sediment discharge was related to intense logging and a devastating flood in 1964 (Brown and Ritter, 1971; Waananen, 1971). Because the daily tidal exchange within Humboldt Bay is much larger than the annual freshwater input, the bay may be a sink for fine-sediment derived from oceanic sources but there are no direct measurements available to support this assertion.

3.0 Salt Marsh Descriptions

We selected five study marshes (Table 1) distributed throughout Humboldt Bay (Figure 2) for monitoring salt marsh accretion and elevation change. Two of the sites (Mad River and Manila) were established in 2013. Baseline measurements for this study began in November of 2015. Mad River marsh and Manila marsh are in the western region of North Bay. Mad River

marsh is a high elevation island marsh located upstream within Mad River Slough; while Manila marsh is a low elevation fringe marsh located at the bay margin. Sediment is supplied from the tidal channels; however, there is freshwater drainage from the dunes to the west and a perennial stream that emerges at the base of the moving dunes that discharges to Mad River Slough. Jacoby marsh, located on the eastern edge of North Bay at the mouth of Jacoby Creek, is a high elevation deltaic marsh with direct inputs of freshwater and sediment. White marsh and Hookton marsh are in the eastern region of South Bay. White marsh is a low elevation island marsh located at the bay margin; while Hookton marsh is a low elevation island marsh located upstream within Hookton Slough. Salmon Creek flows into Hookton Slough downstream from Hookton marsh and supplies direct inputs of freshwater and sediment.

Four of the study marshes (Mad River, Manila, White and Hookton) are within the USFWS Humboldt Bay National Wildlife Refuge and are part of a regional Spartina densiflora eradication program. *S.densiflora* is an invasive cordgrass that has infested approximately 90% of the salt marshes within Humboldt Bay (Pickart, 2001). Manila marsh, managed by the California Department of Fish and Wildlife, is not part of the eradication program. In 2006, pilot studies for mechanical treatments to remove *S.densiflora* began in Mad River Slough and in 2010 a regional eradication effort began (Pickart, 2012). During mechanical treatments low elevation zones and microtopography are created that could contribute to incremental lowering of marsh surface elevations. Pickart (2013) conducted repeat laser level surveys at Jacoby marsh to measure changes in mean marsh elevations related to various *S.densiflora* treatments. After 1.5 years marsh elevations had recovered and were within +/-1.3 cm of the baseline elevations; but this may have been accelerated due to the site being located at the mouth of Jacoby Creek, which is one of the primary tributaries that contributes sediment to the bay (Curtis et al., in review).

Table 1. Descriptions and attribute information for five salt marshes located in Humboldt Bay, CA. Relative sea-level rise (RSLR) estimates are from Anderson, 2015.

Site Name	Geomorphic Setting	Area (km²)	RTK-GPS (Number of points)	Elevation (NAVD88)		Spartina Treatment	Base Line Date	RSLR (mm/yr)
				Mean (m)	Range (m)			
North Bay Marshes								
Mad River	Island	0.06	852	2.05	1.20-2.29	2006, 2008, 2013 + maintenance	11/19/15	3.11
Manila	Fringe	0.13	732	1.72	0.79-2.53	none	11/19/15	3.11
Jacoby	Deltaic	0.12	558	2.02	1.03-2.43	2010, 2011 + maintenance	11/20/15	3.11
South Bay Marshes								
White	Island	0.03	109	1.79	1.00-1.99	2010, 2011+ maintenance	11/22/15	5.56
Hookton	Island	0.02	83	1.83	1.12-2.17	2010, 2011+ maintenance	11/22/15	5.56

4.0 Methods

4.1 Marsh Elevation and Vertical Accretion Monitoring

We installed deep rod Surface Elevation Table (SET) and feldspar marker horizon (MH) plots (Figure 3) to quantify the relative contributions of surface and subsurface processes to vertical accretion and elevation change in each of the five study marshes. The SET-MHs were installed in Mad River and Manila marshes in 2013. The SET-MHs were installed in Jacoby, White and Hookton marshes in 2015. A summary of the SET-MH protocol was published by Lynch et al. (2015).

Vertical changes in the marsh surface are the result of accretion, erosion, decomposition, compaction, shrink-swell caused by groundwater flux, swell caused by root growth, and deeper processes such as regional subsidence or uplift. The SET measurements quantify surface elevation change and the MH measurements quantify vertical accretion above a feldspar layer applied on the marsh surface. Vertical accretion is defined as the buildup of mineral and organic sediment on the marsh surface, and elevation change is defined as a change in the height of the wetland surface relative to a local benchmark.

At each study marsh two representative sites were selected after considering surface elevations, vegetation composition and distance from tidal sources (Figure 2). One SET and three MHs were deployed at each site (a total of two SETs and six MHs per marsh) following standardized methods (Cahoon et al., 2002; Webb at al., 2013). SET-MHs were measured during quarterly site visits. Measurement of the MH entails removing a small plug of soil using a soil knife, measuring the depth of surface accretion above the feldspar layer, and replacing the plug. Elevation change is measured by attaching the SET instrument to a collar installed at the top of the local benchmark, in this case the top of the deep rod. The SET instrument provides a constant reference plane in space from which the distance to the marsh surface can be measured. Nine pins are lowered to the surface in four ninety-degree cardinal directions yielding 36 observations. Repeat measurements can resolve millimeter-scale change (Cahoon et al, 2002) because the orientation of the table in space remains fixed in time.

4.2 Bias-Corrected Digital Elevation Model Generation

Baseline elevation RTK-GPS surveys, completed in 2012 and 2013 at the five study marshes (Takekawa et al., 2013), were used to correct the vegetation bias in an available bare-earth high resolution (1 meter) digital elevation model (DEM; CA-SCC, 2012). The bias-corrected DEM was used to estimate the marsh elevations presented in Table 1. Elevations were surveyed using a Leica survey-grade GNSS rover (Viva GS15 and RX1250X models). GPS real-time kinematic (RTK) corrections were streamed to the rover from a Leica base station (Leica GNSS Receiver GS10 with Leica AS10 antenna) during the surveys. The mean vertical error was ±2 cm (Thorne et al. 2015, Thorne et al., 2016) and the ellipsoid heights of the marsh surface were post-processed to determine orthometric heights referenced to NAVD88 and the geoid 12A model.

The RTK-GPS elevations and a Normalized Difference Vegetation Index (NDVI) were used to correct a positive bias in the marsh DEMs related vegetation cover using the LEAN method (Buffington et al., 2016). We obtained LiDAR-derived DEMs from the Digital Coastal Data Access Viewer (https://coast.noaa.gov/dataviewer/) and 2016 multispectral airborne imagery data from the National Agriculture Imagery Program (NAIP; https://catalog.data.gov/dataset/naip-public-image-services). From the NAIP imagery we calculated an NDVI:

$$NDVI = ([NIR-Red]/[NIR+Red])$$

where "Red" included wavelengths of 608-662 nm and "NIR" included wavelengths of 833-887 nm. Using the LEAN method, the positive bias in the LiDAR -DEM was calculated by determining elevations difference between the LiDAR -DEM and the RTK-GPS elevations. We then used a multivariate linear regression model to define a statistical relationship between LiDAR error, NDVI, and LiDAR elevation. The regression model was used to develop bias-corrected mean elevations estimates for each study marsh (Table 1).

4.3 Water Quality and Suspended-Sediment Monitoring

Water quality stations (Table 2) were established in Mad River Slough (USGS 405219124085601 MAD R SLOUGH NR ARCATA CA) and Hookton Slough (USGS 404038124131801 HOOKTON SLOUGH NR LOLETA C) in the primary tide tidal channels that supply sediment to the adjacent study marshes (Figure 2). Water quality sondes (YSI-EXO2), equipped with a turbidity sensor and a combined temperature and specific conductance sensor, were deployed in March of 2016 at a fixed water depth of 1.0 meter. The sondes and sensors were cleaned monthly and calibrations checked during quarterly site visits. Specific conductance was converted to salinity using a temperature (25° C) compensated method (*Wagner et al., 2006*). Continuous 15-minute records of turbidity, temperature, specific conductance, and salinity are available for each station at https://waterdata.usgs.gov/nwis/qw .

Water samples were collected, and water depths measured, during quarterly site visits. A Van-Dorn sampler was used to collect 1-liter water samples throughout a rising and falling tide at 1.5-hour intervals. During each visit one replicate sample was collected to address variability and field blanks were collected periodically to verify adequate cleaning procedures. Water samples were stored in brown HDPE bottles, kept cool and shipped to the USGS Cascade Volcanic Observatory sediment laboratory (Vancouver, WA) for analysis. Suspended-sediment concentrations (SSC) were determined by filtration methods for all the samples. Due to funding limitations percent organic material was determined by loss on ignition (LOI) for a subset of samples, typically two samples per site per visit. The water sample data are also available for each station at https://waterdata.usgs.gov/nwis/qw.

Turbidity can be used as a surrogate for SSC (*Rasmussen et al., 2009*) and we used ordinary least-squares regression to convert the turbidity time series to SSC. The time and date stamp for each of the water samples was synced with the turbidity time series to determine associated turbidity values. A least-squares linear regression equation was determined using the lab-derived SSC and associated turbidity values. The regression model was used to convert turbidity values to SSC and derive a continuous 15-minute SSC time series. The converted SSC time series was used to assess variations in SSC and to investigate correlations with marsh accretion measurements.

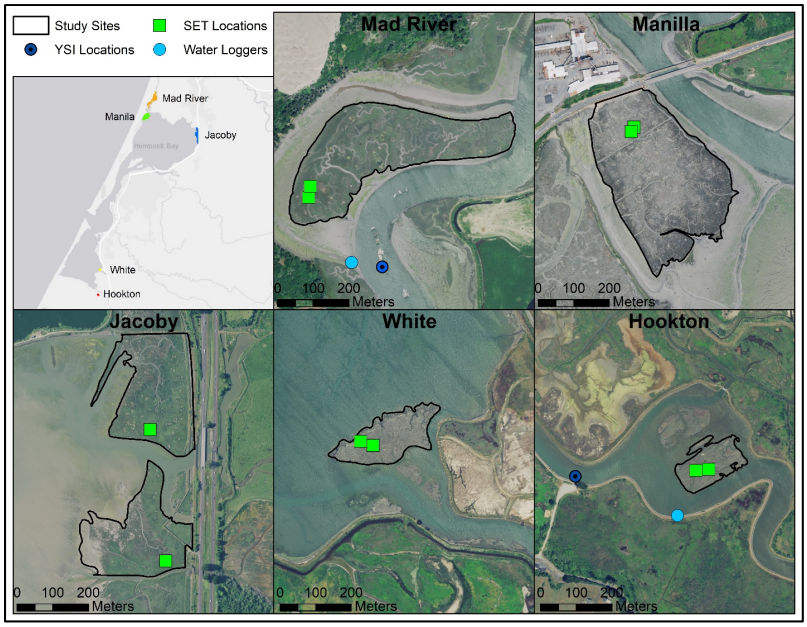

Figure 2. Five study marsh monitoring sites in Humboldt Bay, CA. Map shows the location of study marshes, Sediment Elevation Tables (SET), Marker Horizons (MH), water quality sondes (YSI), and water level loggers.

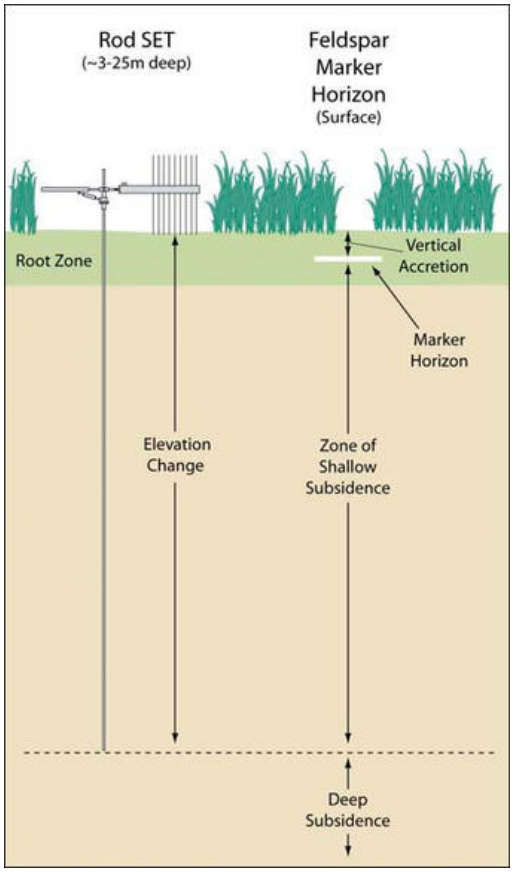

Figure 3. Conceptual diagram showing how the soil profile is measured to assess marsh surface and subsurface processes by Surface Elevation Table (SET) and Marker Horizon (MH) techniques (Cahoon et al, 2002).

Table 2. Descriptions of two water quality monitoring stations located in Humboldt Bay, CA.

Water Quality Station	Instruments	Parameters	Easting	Northing	Deployment Date
USGS 405219124085601 MAD R SLOUGH NR ARCATA CA	YSI-EXO2	Turbidity (FNU) Specific conductance (µs/cm @25°C) Temperature (°C)	403198	4525162	3/5/2016 - present
	Hobo U20	Water level (m)	403133	4525173	3/17/2016 – 12/8/16
	LT Edge (2…)	Water level (m)	403133	4525173	12/8/16 - present
USGS 404038124131801 HOOKTON SLOUGH NR LOLETA C	YSI-EXO2	Turbidity (FNU) Specific conductance (µs/cm @25°C) Temperature (°C)	396746	4503666	3/5/2016 - present
	Hobo U20	Water level (m)	397033	4503557	3/17/2016 – 12/8/16
	LT Edge (2…)	Water level (m)	397033	4503557	12/8/16 - present

5.0 Results

5.1 Marsh Elevation and Accretion Measurements

There were nine SET-MH measurements collected during the 2-year study period between November 22nd, 2015 and December 3rd, 2017. Again, SET measurements quantify elevation change and feldspar MH measurements quantify vertical accretion (Cahoon et al., 2002; Lynch et al., 2015). If vertical accretion is greater than elevation change, shallow subsidence (accretion minus elevation change) related to decomposition or compaction may be occurring. If accretion is equal to elevation change we can infer that surface accretion is driving elevation change and subsurface processes are negligible. If accretion is less than elevation change we can infer that shallow expansion related to swelling of soils by water storage or an increase in root volume may be occurring.

Over the 2-year study period elevation changes and accretion was spatially and temporally variable (Table 3). At the South Bay sites (Hookton and White) accretion rates were about 1.5 times greater than elevation changes; but changes in elevation and accretion were about equal at the North Bay sites (Mad River, Manila, and Jacoby). Across all the sites elevation change and accretion were lower during 2016 (-0.26mm ±0.64; 1.56mm ±1.66) and higher in 2017 (3.15mm ±0.30; 2.82mm ±1.04).

We also compared the annual rates of elevation change and accretion to estimates of long-term trends in RLSR (Figure 4) estimated for the Humboldt Bay region (Anderson, 2015). RSLR estimates for North Bay and South Bay are 3.11 mm/yr and 5.56 mm/yr respectively (Table 1). During the 2-year study period the rates of annual elevation gain did not outpace long-term trends in RSLR; however, these short-term results represent initial baseline measurements and should be interpreted with caution within the framework of the longer-term trends in RSLR. Continued monitoring, over decadal or longer periods, is required to detect trends in elevation gain and vertical accretion.

Table 3. Summary of elevation change and accretion measurements and the associated standard errors over a 2-year period for five study marshes located in Humboldt Bay, CA.

	2016		2017		Cumulative		Average Annual	
Site	Elevation change (mm)	Accretion (mm)	Elevation change (mm)	Accretion (mm)	Elevation change (mm)	Accretion (mm)	Elevation change (mm/yr)	Accretion (mm/yr)
North Bay Marshes								
Mad River	-0.89 ± 0.37	-4.29 ± 0.21	0.52 ± 0.18	5.33 ± 0.46	-0.38 ± 0.55	1.04 ± 0.67	-0.19 ± 0.28	0.52 ± 0.34
Manila	-3.04 ± 1.54	-0.3 ± 4.67	5.54 ± 0.44	0.67 ± 2.08	2.50 ± 1.98	0.36 ± 6.75	1.25 ± 0.99	0.19 ± 3.38
Jacoby	0.71 ± 0.40	2.13 ± 0.88	2.49 ± 0.18	0.75 ± 0.04	3.19 ± 0.58	2.88 ± 0.92	1.60 ± 0.29	1.44 ± 0.46
South Bay Marshes								
Hookton	1.09 ± 0.52	7.90 ± 2.23	3.25 ± 0.60	1.60 ± 2.08	4.34 ± 1.12	9.50 ±4.31	2.17 ± 0.56	4.75 ± 2.16
White	0.81 ± 0.37	2.38 ± 0.38	3.95 ± 0.11	5.75 ± 0.54	4.76 ± 0.48	8.13 ± 0.92	2.38 ± 0.24	4.07 ± 0.46
North Bay	-1.07 ± 0.77	-0.82 ± 1.89	2.85 ± 0.27	2.25 ± 0.86	1.77 ± 1.04	1.43 ± 2.78	0.89 ± 0.52	0.71 ± 1.39
South Bay	0.95 ± 0.45	5.14 ± 1.31	3.60 ± 0.36	3.68 ± 1.31	4.55 ± 0.80	8.82 ± 2.62	2.28 ± 0.40	4.41 ± 1.31
All sites	-0.26 ± 0.64	1.56 ± 1.66	3.15 ± 0.30	2.82 ± 1.04	2.88 ± 0.94	4.38 ± 2.71	1.44 ± 0.47	2.19 ± 1.36

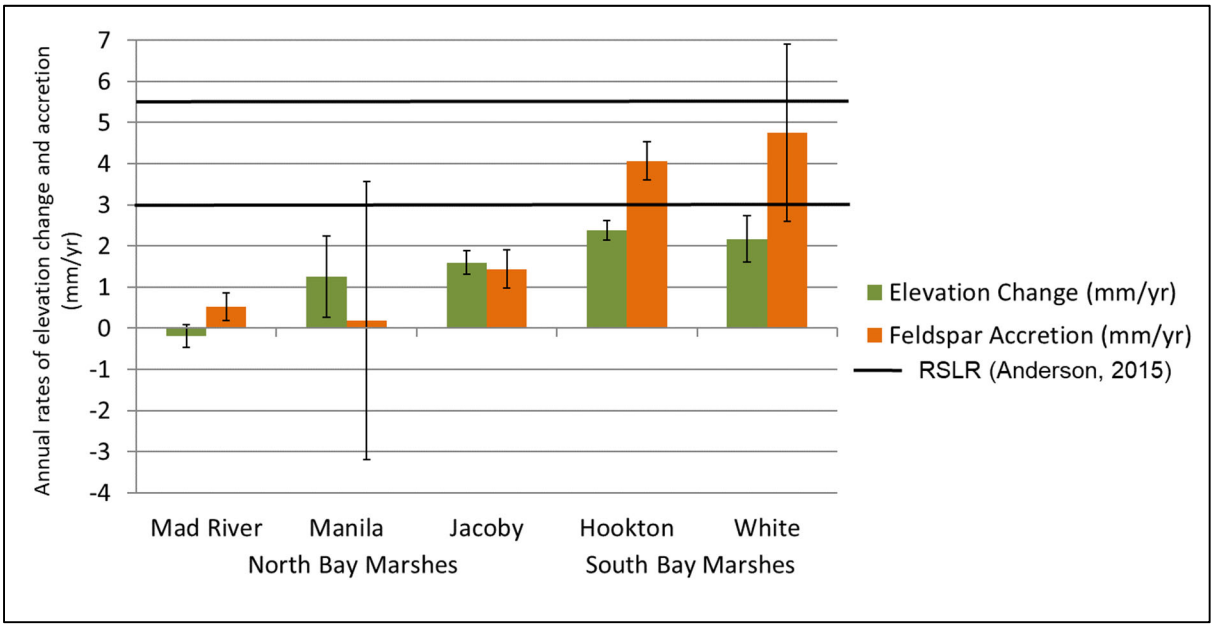

Figure 4. Summary of mean annual rates of elevation change and accretion for five study marshes located in Humboldt Bay, CA. When accretion is greater than elevation change this indicates shallow subsidence that can be caused by decomposition and compaction. When elevation change is greater than accretion this indicates accumulation of below-ground biomass or swelling of soils by water storage. The range of relative sea level rise (RSLR; Anderson, 2015) for Humboldt Bay (3.11 to 5.56 mm/yr) is shown with horizontal black lines. Uncertainty in the elevation change and accretion measurements is captured by the standard error shown as vertical error bars.

5.2 Water Quality and Suspended-Sediment Supply

We converted the turbidity records into a SSC time series using eq.1 and eq.2 and computed summary statistics for each monitoring station (Table 4). The mean SSC measured at Hookton slough (41.1 mg/L) was 2.5 times greater than the mean SSC measured at Mad River slough (16.8 mg/L). The median SSC values for the two sites were similar indicating that the bay

is well-mixed and tidally-dominated for most of the year. The standard deviation (SD), coefficient of variation (CV) and range in SSC values are measures of statistical variance, which were much greater at Hookton indicating more variability in the sediment supply due to large episodic freshwater inputs.

Hookton SSC = 1.274+ 1.95 * Turbidity r^2= 0.928 $p < 0.0001$, N=46 eq.1
Mad River SSC = 4.14+ 1.26 * Turbidity r^2= 0.396 $p < 0.0001$, N=45 eq.2

The lack of variance in SSC measurements at Mad River Slough heavily influenced the regression model used to convert the turbidity signal to SSC values. Although the p-values indicate the Mad River and Hookton regression models are statistically significant, the lack of variance in the SSC values for the Mad River model resulted in a much lower slope and r^2 value.

Table 4. Statistical metrics for suspended-sediment concentrations (SSC) derived from continuous turbidity records collected over a 2-year study period at two water quality monitoring stations in Humboldt Bay, CA. Note: SD is the standard deviation and CV is the percent coefficient of variation.

Monitoring Station Location	USGS Water Quality Station Number	Mean SSC (mg/L)	SD SSC (mg/L)	CV SSC (%)	Min SSC (mg/L)	Max SSC (mg/L)	Median SSC (mg/L)
Mad River Slough	405219124085601	16.8	7.1	42	4.9	414.0	15.7
Hookton Slough	404038124131801	41.1	81.5	198	8.0	1598.0	19.7

6.0 Discussion

6.1 Geomorphic stability and vulnerability to SLR

Sediment supply is a primary variable for determining geomorphic stability and salt marsh vulnerability to RSLR (*Callaway, 1996; Pethick and Crooks 2000; Weston, 2014; Ganju et al., 2015 Thorne al., 2016*). Sufficient sediment supply must be available for salt marshes to gain elevation and persist in place. This study focused on direct measurements of three variables that control salt marsh resiliency and vulnerability to SLR in Humboldt Bay: fine-sediment supply, marsh elevation, and marsh accretion.

Salt marshes respond dynamically to accommodate change and have been referred to as "ephemeral landforms" (*Orr et al., 2003*). In general, wave and tidal energy is attenuated through the transfer of sediment from high-energy source areas, where transport and erosion occur, to low-energy sinks where sediment deposition and accumulation occurs. This transfer of sediment and the associated energy attenuation creates a strong morpho-dynamic response with wave and tidal energy creating morphologic change, which creates feedback that alters the local energy environment (*Pethick 1996; D'Alpaos et al., 2011; Fagherazzi et al., 2012*). The form and function of salt marshes therefore depends upon a dynamic balance between the energy regime and the transport and deposition of fine-sediment.

During periods of increased coastal energy, the natural marsh response is landward transgression to lower energy environments while the seaward edge of the marsh experiences erosion and is replaced by mudflat and subtidal habitat. Approximately 75% of the bay's shoreline is composed of artificial hard structures, including Highway 101 and a former railroad grade (*Laird, 2013*). Under current conditions much of the space to accommodate dynamic marsh transgression has been lost.

Recent studies indicate that sediment transport-based metrics are good indicators of vulnerability and wetland stability (*Ganju et al., 2013; Ganju et al., 2015*). In this study, we

assumed that SSC is representative of the fine-sediment supply available for accretion. The SSC-metrics in Table 4 indicate Hookton slough (South Bay) is sediment-rich. In comparison, Mad River slough (North Bay) is sediment-limited with less fine-sediment available for accretion.

We further investigated our results to assess the correlation between accretion and SSC in Hookton and Mad River marsh using quarterly measurements of accretion and the average SSC estimated during eight quarterly intervals over the 2-year study period. There was a positive correlation between accretion and SSC for Hookton marsh where sediment-rich conditions exist, but the correlation was not statistically significant (r^2=0.16, p=0.3270). There was no correlation for Mad River marsh, where sediment-limited conditions exist ($r^2$0.00, p=0.9025) (Figure 5). Additional data collected in 2018 and 2019 may improve the correlations

In summary, the North Bay is sediment-limited and is experiencing lower long-term rates of RSLR (3.11 mm/yr). Our early results show that the North Bay marshes (Mad River, Manila, and Jacoby) are experiencing lower rates of vertical accretion (0.71±1.39 mm/yr) and elevation change (0.89±0.52 mm/yr) but there is high uncertainty associated with these measurements. In comparison, South Bay is sediment-rich and is experiencing higher long-term rates of RSLR (5.56 mm/yr) due to tectonic subsidence, which is mitigated somewhat by higher rates of accretion (4.41±1.31mm/yr) and elevation change (2.28±0.40 mm/yr). The South Bay accretion rates were greater than elevation changes, which may indicate that shallow subsidence, related to decomposition or compaction, could be a limiting factor influencing elevation gains.

The sediment-limited conditions in North Bay make Mad River and Manila marshes more vulnerable to accelerated RSLR, however, Jacoby marsh is a deltaic marsh located in the eastern region of North Bay with higher fetch and wind-wave exposure. Generally, deltaic marshes tend to have higher accretion rates (*Cahoon et al., 2006*) and the direct input of fine-sediment at Jacoby marsh may mitigate vulnerability, in this higher energy but more sediment-rich region of North Bay. South Bay marshes are more vulnerable than North Bay marshes to submergence due to higher rates of RLSR, but this is mitigated somewhat by greater sediment supply.

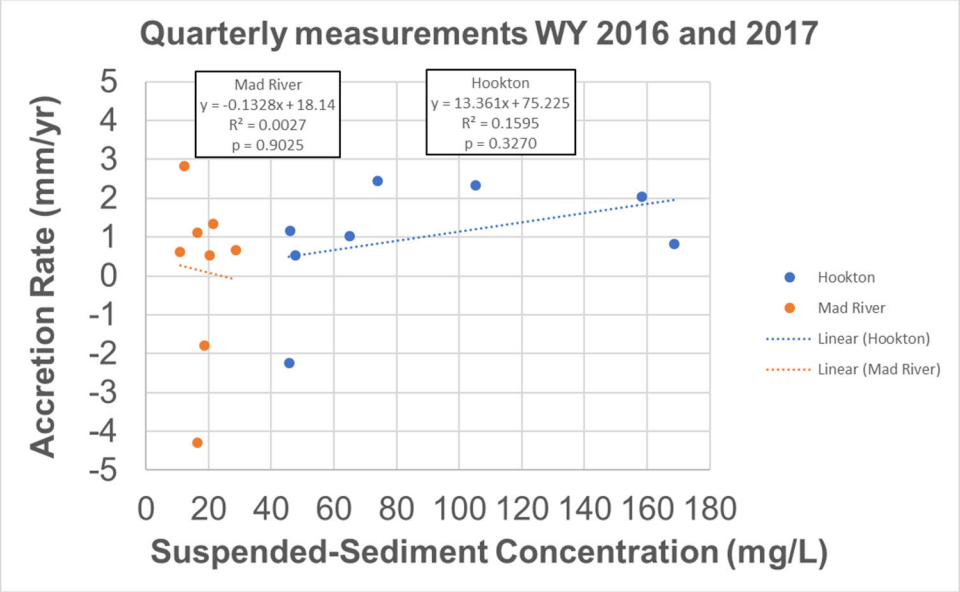

Figure 5. Correlation graph showing the relation between suspended-sediment concentration (SSC) and vertical accretion rates for two study marshes in Humboldt Bay, CA.

6.2 Fine-Sediment Budget and Management Implications

There are ongoing management and restoration activities that impact the fine-sediment budget of Humboldt Bay, which may alter the availability of sediment for marsh accretion and elevation gain. We assessed the potential impacts on the fine-sediment budget related to the regional *S.densiflora* eradication program, maintenance dredging of harbors and channels, and tidal restoration in subsided former baylands. All of these management activities alter local topography and create low elevation zones in the tidal prism. These low elevation zones impact the fine-sediment budget by increasing "sediment demand", which may reduce the "sediment supply" available for marsh accretion and elevation gain.

The regional *S.densiflora* eradication program in Humboldt Bay uses mechanical treatments that create low-elevation microtopography. The impact of the *S.densiflora* treatments on marsh elevations was assessed at the Jacoby marsh (*Pickart, 2013*). Repeat laser level measurements indicated that after 1.5 years the surface elevations were within ± 1.3 cm of the original elevation. However, Jacoby marsh is a deltaic marsh with direct inputs of sediment and relatively high rates of accretion and elevation change and may not be representative of other North Bay marshes located in sediment-limited regions.

In a companion study Curtis et al. *(in review*) estimated the fine-sediment supply to Humboldt Bay from local watersheds (0.05 Mt/yr) and defined an imbalance created by maintenance dredging (0.10 Mt/yr). This fine-sediment deficit may be filled by natural deposition of sediment supplied from terrestrial or marine sources or by local recruitment of sediment within the bay through erosion of existing mudflats and marshes

Tidal restoration to subsided former baylands also impacts the fine-sediment budget by creating large "sediment sinks" and increasing "sediment demand". There are several completed and planned tidal restoration projects within Humboldt Bay that involve strategically breaching dikes and levees to allow natural deposition and filling of subsided lands. A recently completed beneficial reuse study (*HBHRCD, 2015*) estimated the "sediment demand" associated with two projects in South Bay equates to 0.31 Mt, which is three times the annual maintenance dredging and 6 times the annual supply from the local watersheds.

Incorporating fine-sediment augmentation by direct placement into tidal restoration projects could ameliorate "sediment demand" and accelerate the rate of recovery to achieve adequate elevations to support salt marsh vegetation. A recent modeling study concluded that although RSLR is the primary controlling factor for marsh accretion and elevation gain, the starting surface elevation had the second greatest impact on elevation gain followed by the mineral-sediment supply (*Thorne et al., 2016*). Thus, initial elevation and sediment accretion rates, which are dependent on sediment supply, determine the effectiveness and success of salt marsh restoration.

Tidal restoration in subsided former baylands in sediment-rich areas of the bay may quickly fill and achieve the necessary elevations for the colonization of marsh vegetation. Conversely, projects located in sediment-limited areas may require augmentation to achieve desired increases in elevations to support marsh vegetation. Although sediment augmentation can add significantly to restoration project costs, and it may be a limiting factor, the beneficial reuse of dredged fine-sediment is one promising approach for salt marsh restoration that mitigates "sediment demand" and avoids recruitment of sediment from existing subtidal and intertidal habitats.

7.0 Conclusions and Future Work

This study improved our understanding of how salt marshes respond to changing sediment supply conditions in Humboldt Bay, CA. South Bay is shallower and rates of RSLR are

higher due to tectonic subsidence, but this is balanced by a larger sediment supply and higher rates of marsh accretion and elevation change. North Bay is deeper, much larger volumetrically with lower rates of RSLR, sediment supply, accretion, and elevation change. Salt marshes are highly dynamic systems that keep pace with SLR by vertical accretion and horizontal retreat when space for retreat is available. Without an adequate sediment supply, the salt marshes in Humboldt Bay are more vulnerable to submergence due to accelerated SLR. Early results indicate short-term rates of elevation gain were lower than the long-term estimates of RSLR for all five of the study marshes.

Continued monitoring of the fine-sediment budget, marsh accretion and elevation change is essential to understand the trajectory of marsh formation within the framework of accelerated SLR and to determine whether future management actions will be needed to mitigate additional marsh loss. With informed regional sediment management and environmental planning, it may be possible to mitigate the sediment demand created by management activities and associated impacts. Marsh augmentation, using excess fine-sediment derived from maintenance dredging, is a potential approach for alleviating imbalances in the fine-sediment budget that impact the sediment supply available for marsh accretion and elevation gain.

8.0 References

Anderson, J.K., 2015. Humboldt Bay: Sea Level Rise, Hydrodynamic Modeling and Vulnerability Mapping. Prepared for the State Coastal Conservancy and Coastal Ecosystems Institute of Northern California. McKinleyville, CA: Northern Hydrology & Engineering.

Brown III, W. M., and Ritter, J. R. 1971. Sediment transport and turbidity in the Eel River Basin, California. U.S. Geol. Survey. Water Supply Paper 1986.

Buffington, K.J., Dugger, B.D., Thorne, K.M. and Takekawa, J.Y., 2016. Statistical correction of lidar-derived digital elevation models with multispectral airborne imagery in tidal marshes. *Remote Sensing of Environment*, *186*, pp.616-625.

Cahoon, D. 1997. Global warming, sea-level rise, and coastal marsh survival. USGS National Wetlands Research Center. USGS FS-09 1-97.

Cahoon, D.R., Lynch, J.C., Hensel, P., Boumans, R., Perez, B.C., Segura, B., and Day, J.W., 2002, High precision measurements of wetland sediment elevation—I, recent improvements to the sedimentation-erosion table: Journal of Sedimentary Research, v. 72, p. 730–733.

Cahoon, D.R., Hensel, P.F., Spencer, T., Reed, D.J., Mckee, K.L., and Saintilan, N., 2006. Coastal wetland vulnerability to relative sea-level rise: wetland elevation trends and process controls. Ecological Studies 190:271–292.

California Coastal Sediment Management Workgroup (CCSMW), 2017. Eureka Littoral Cell-Coastal Regional Sediment Management Plan, p. 176.

California State Coastal Conservancy (CA-SCC) 2012. California Coastal Conservancy Coastal Lidar Project Bare Earth Lidar Digital Elevation Data.

Callaway, J. C., J. A. Nyman, and R. D. DeLaune. 1996. Sediment accretion in coastal wetlands: A review and a simulation model of processes. Current Topics in Wetland Biogeochemistry 2:2-23.

Costa, S. L. 1982. The physical oceanography of Humboldt Bay. Proceedings Humboldt Bay Symposium. C. Toole and C. Diebel (ed.), HSU Center for Community Development, Arcata, CA.

Curtis, J, A., Flint, L.E., Stern, M.A., Lewis, J., and Klein, R.D. in review. Fine-sediment supply under current and future climates for Humboldt Bay, CA, submitted to Estuaries and Coasts

D'Alpaos A., Mudd, S.M., and L. Carniello, 2011. Dynamic response of marshes to perturbations in suspended sediment concentrations and rates of relative sea level rise: Earth Surface, v. 116, no. F4,

Dettinger, M.D., Ralph, F.M., Das, T., Neiman, P.J. and Cayan, D.R., 2011. Atmospheric rivers, floods and the water resources of California. *Water*, *3*(2), pp.445-478.

Fagherazzi, S., Kirwan, M.L., Mudd, S.M., Guntenspergen, G.R., Temmerman, S., D'Alpaos, A., van de Koppel, J., Rybczyk, J.M., Reyes, E., Craft, C. and Clough, J., 2012. Numerical models of salt marsh evolution: Ecological, geomorphic, and climatic factors. *Reviews of Geophysics*, *50*(1).

Farnsworth, K.L., Warrick, J.A., 2007, Sources, Dispersal, and Fate of Fine Sediment Supplied to Coastal California: U.S. Geological Survey Scientific Investigations Report 2007–5254, 77 p.

Ganju, N. K., N. J. Nidzieko, and M. L. Kirwan, 2013. Inferring tidal wetland stability from channel sediment fluxes: Observations and a conceptual model, J. Geophys. Res. Earth Surf., 118, 2045.

Ganju, N. K., M. L. Kirwan, P. J. Dickhudt, G. R. Guntenspergen, D. R. Cahoon, and K. D. Kroeger, 2015. Sediment transport-based metrics of wetland stability, Geophys. Res. Lett., 42, 7992–8000.

Humboldt Bay Harbor Recreation and Conservation District (HBHRCD), 2015. Beneficial Reuse of Dredged Materials for Tidal Marsh Restoration and Sea Level Rise Adaptation in Humboldt Bay, California, Eureka, CA.

Kelsey, H.M., 1980. A sediment budget and an analysis of geomorphic process in the Van Duzen River basin, north coastal California, 1941–1975: summary. Geological Society of America Bulletin, Part I 91, 190–195.

Klein, R.D., Lewis, J. and Buffleben, M.S., 2012. Logging and turbidity in the coastal watersheds of northern California. *Geomorphology*, *139*, pp.136-144.

Kirwan, M. L., G. R. Guntenspergen, A. D'Alpaos, J. T. Morris, S. M. Mudd, and S. Temmerman (2010), Limits on the adaptability of coastal marshes to rising sea level, Geophys. Res. Lett., 37, L23401, doi:10.1029/2010GL045489.

Laird, A., B. Powell, J. Robinson and K. Shubert. 2007. Historical atlas of Humboldt Bay and the Eel River delta. Humboldt Bay Harbor, Recreation and Conservation District, Eureka, CA. Electronic document: DVD.

Laird, A. 2013. Humboldt Bay Shoreline Inventory, Mapping and Sea Level Rise Vulnerability Assessment. Prepared for State Coastal Conservancy. Trinity Associates, Arcata, CA.

Leithold, E.L., Perkey, D.W., Blair, N.E., Creamer, T.N., 2005. Sedimentation and carbon burial on the northern California continental shelf: the signatures of land-use change. Continental Shelf Research 25 (3), 349–371.

Lynch, J. C., P. Hensel, and D. R. Cahoon. 2015. The surface elevation table and marker horizon technique: A protocol for monitoring wetland elevation dynamics. Natural Resource Report NPS/NCBN/NRR—2015/1078. National Park Service, Fort Collins, Colorado.

Milliman, J.D., Farnsworth, K.L., 2011. River Discharge to the Coastal Ocean – A Global Synthesis. Cambridge University Press, Cambridge, UK, 384pp.

Montillet JP, Melbourne TI, Szeliga, WM (2018) GPS vertical land motion corrections to sea-level rise estimates in the Pacific Northwest. Journal of Geophysical Research: Oceans 123:1196–1212.

Morehead, M.D. and Syvitski, J.P. (1999) River-plume sedimentation modeling for sequence stratigraphy: application to the Eel margin, northern California. *Mar. Geol.*, **154**, 29–41.

Morris, J.T., P.V. Sundareshwar, C.T. Nietch, B. Kjerfve, and D.R. Cahoon. 2002. Responses of coastal wetlands to rising sea level. Ecology 83:2869-2877.

Orr, M., Crooks, S. and Williams, P.B., 2003. Will restored tidal marshes be sustainable? *San Francisco Estuary and Watershed Science*, *1*(1).

Patrick, W., & DeLaune, R., 1990. Subsidence, Accretion, and Sea Level Rise in South San Francisco Bay Marshes. *Limnology and Oceanography, 35*(6), 1389-1395.

Pethick JS. 1996. The geomorphology of mudflats. In: Nordstrom KF, Roman CT, editors. Estuarine shores: evolution, environment and human health. Chichester, UK: John Wiley. p 185-211.

Pethick JS, Crooks S. 2000. Development of a coastal vulnerability index: a geomorphological perspective. Environmental Conservation 27:359-367.

Pickart, A. 2001.The distribution of *Spartina densiflora* and two rare salt marsh plants in Humboldt Bay 1998-1999. Unpublished report, U.S. Fish and Wildlife Service, Humboldt Bay National Wildlife Refuge, Arcata, California.

Pickart, A. 2012. *Spartina densiflora* invasion ecology and the restoration of native salt marshes, Humboldt Bay, California. unpublished report, U.S. Fish & Wildlife Service, Arcata, California

Pickart, A, 2013, A Comparison of Mechanical Treatments for the Control of *Spartina densiflora* at Jacoby Creek Unit, Humboldt Bay National Wildlife Refuge**,** unpublished report, U.S. Fish & Wildlife Service, Arcata, California.

Rasmussen, P.P., Gray, J.R., Glysson, G.D., and Ziegler, A.C., 2009, Guidelines and procedures for computing time-series suspended-sediment concentrations and loads from in-stream turbidity-sensor and streamflow data: U.S. Geological Survey Techniques and Methods, book 3, chap. C4, 52 p.

Russell, N.; Griggs, G., 2012. Adapting to Sea Level Rise: A Guide for California's Coastal Communities. Prepared for the California Energy Commission Public Interest Environmental Research Program, University of California Santa Cruz. 50 pp.

Schlosser, S., and A. Eicher. 2012. The Humboldt Bay and Eel River Estuary Benthic Habitat Project. California Sea Grant Publication T-075, 246 p.

Stralberg, D., Brennan, M., Callaway, J.C., Wood, J., Schile, L., Jongsomjit, D., Kelly, M., Parker, V.T., and Crooks, S. (2011). Evaluating tidal marsh sustainability in the face of sea-level rise: a hybrid modeling approach applied to San Francisco Bay. PLOS ONE, 6.11: e27388.

Takekawa, J.Y., Thorne, K.M., Buffington, K.J., Freeman, C.M., Powelson, K.W., and Block G. 2013. Assessing marsh response from sea-level rise applying local site conditions: Humboldt Bay National Wildlife Refuge. Unpubl. Data Summary Report. USGS Western Ecological Research Center, Vallejo, CA. 44pp + Appendices.

Thom, R. M. 1992. Accretion rates of low intertidal salt marshes in the Pacific Northwest. Wetlands

Thorne, K.M., MacDonald, G.M., Ambrose, R.F., Buffington, K.J., Freeman, C.M., Janousek, C.N., Brown, L.N., Holmquist, J.R., Gutenspergen, G.R., Powelson, K.W., Barnard, P.L., and Takekawa, J.Y., 2016, Effects of climate change on tidal marshes along a latitudinal gradient in California: U.S. Geological Survey Open-File Report 2016-1125, 75 p.

Thorne, K.M., G. MacDonald, G. Guntenspergen, R. Ambrose, K. Buffington, B. Dugger, C. Freeman, C. Janousek, L. Brown, J. Rosencranz, J. Holmquist, J. Smol, K. Hargan, and J. Takekawa. 2018. U.S. Pacific coastal wetland resilience and vulnerability to sea-level rise: Science Advances, v. 4, no. 2.

van Proosdij, D., Lundholmb, J., Neatt, N., Bowron, T., Graham, J., 2010. Ecological reengineering of a freshwater impoundment for salt marsh restoration in a hypertidal system. Ecological Engineering 36, 1314e1332.

Waananen, A.O., Harris, D.D. and Williams, R.C., 1971. *Floods of December 1964 and January 1965 in the Far Western States; Part 1 Description* (No. 1866-A). US Govt. Print. Office. 276p.

Wagner, R.J., Boulger, R.W., Jr., Oblinger, C.J., and Smith, B.A., 2006, Guidelines and standard procedures for continuous water-quality monitors—Station operation, record computation, and data reporting: U.S. Geological Survey Techniques and Methods 1–D3, 51 p.

Warrick, J.A., Madej, M.A., Goñi, M.A., Wheatcroft, R.A., 2013. Trends in the suspended sediment yields of coastal rivers of northern California, 1955–2010. Journal of Hydrology 489, 108–123.

Warrick, J.A., 2014. Eel River margin source-to-sink sediment budgets: Revisited. *Marine Geology*, *351*, pp.25-37.

Webb, E.L., Friess, D.A., Krauss, K.W., Cahoon, D.R., Guntenspergen, G.R., and Phelps, J., 2013, A global standard for monitoring coastal wetland vulnerability to accelerated sea-level rise: Nature Climate Change, v. 3, p. 458–465.

Wheatcroft, R.A., Sommerfield, C.K., Drake, D.E., Borgeld, J.C., Nittrouer, C.A., 1997. Rapid and widespread dispersal of flood sediment on the northern California margin. Geology 25, 163–166.

Wheatcroft, R.A., Borgeld, J.C., 2000. Oceanic flood deposits on the northern California shelf: large-scale distribution and small-scale physical properties. Continental Shelf Research 20, 2163–2190.

Erosion and Sedimentation Issues in the Central and Southern Florida (C&SF) Water Management System

Seyed Hajimirzaie, Senior Engineer, South Florida Water Management District (SFWMD), West Palm Beach, Florida, shajimir@sfwmd.gov
Matahel Ansar, Section Administrator, Applied Hydraulics Section, South Florida Water Management District (SFWMD), West Palm Beach, Florida, mansar@sfwmd.gov
Jie Zeng, Principal Engineer, South Florida Water Management District (SFWMD), West Palm Beach, Florida, jzeng@sfwmd.gov

Abstract

The South Florida Water Management District (SFWMD) manages, operates, and maintains one of the most complex, water management systems in the world, the Central and Southern Florida (C&SF) project, which was authorized by Congress in 1948. This system includes over 4,300 miles of canals and levees, over 850 major water control structures (spillways, pumps, culverts, weirs), and over 700 smaller project culverts. The system serves over seventy secondary drainage Districts (298 Districts), over 8 Million people in 16 counties (18,000 Mi^2), and provide sources of water to vast natural areas such as the world-renowned Everglades, Biscayne National Park, and Big Cypress National Preserve.
Erosion and sedimentation issues are ubiquitous in the C&SF water management system. Historically, the C&SF project had considered erosion and sedimentation control in the design. However, several areas of the C&SF system experience sedimentation and erosion issues including (i) canal degradation through bank sloughing and bed erosion, (ii) canal aggradation and loss of conveyance capacity through shoaling from the settling of sediments transported from upstream canal reaches and drainage areas (iii) the transport of suspended sediments in canal discharges to ecologically sensitive water bodies, (iv) considerable land uses change over 70 years since the design of C&SF project resulted in peak flows increases (especially in highly urbanized areas) and the corresponding changes in the peak velocities, and (v) unique C&SF challenges due to wave induced erosion caused by boat navigation or by hurricane-induced lake storm surges. In this paper, we describe sedimentation and erosion issues in the C&SF water management system, the potential causes, and provide potential solutions to address these immense challenges.

Introduction

In south Florida, waterways move significant amounts of sediment annually in this never-ending process of erosion, transportation, and deposition. An understanding of the dynamic equilibrium between upstream sediment supply and a river's sediment transport capability is important for the success of river engineering design, operation, and maintenance.
Sediment transport is a common element considered in the formulation and design of water control facilities across the globe. The Central and Southern Florida (C&SF) project is no exception. The C&SF Project, first authorized by Congress in 1948 as part of the Flood Control Act, is a multi-purpose project that provides flood control, water supply for municipal, industrial, and agricultural uses, prevention of saltwater intrusion, water supply for Everglades National Park (ENP), and protection of fish and wildlife resources (Figure 1). The primary

system includes about 2,115 mi of levees, 2,164 mi of canals, 75 pump stations, over 800 water control structures, and regional telemetry and real time hydrometeorological monitoring systems. The C&SF was constructed by the United States Army Corps of Engineers (USACE) with the South Florida Water Management District (SFWMD) as a local sponsor.

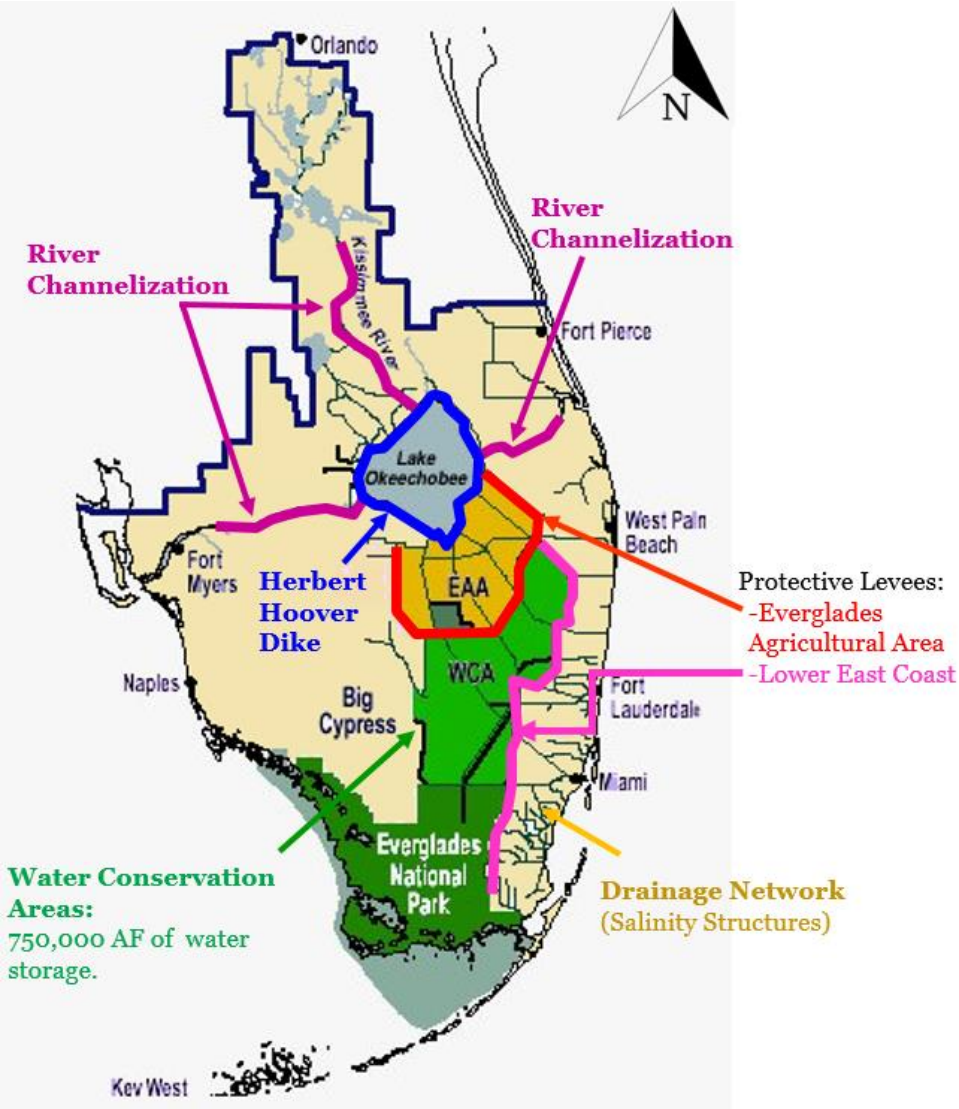

Figure 1. Major components of the Central and Southern Florida (C&SF) project

Today, the SFWMD is operating 62,000 acres of treatment wetlands known as Stormwater Treatment Areas (STAs) and 105,000 ac-ft of Flow Equalization Basins (FEBs) to improve Everglades water quality (Figure 2).

In this paper, considerations for sedimentation in the design of the C&SF project, focusing on the St. Lucie Estuary, are discussed. The paper also narrates challenges in assessing sedimentation issues, some potential solutions, and recommendations for future work.

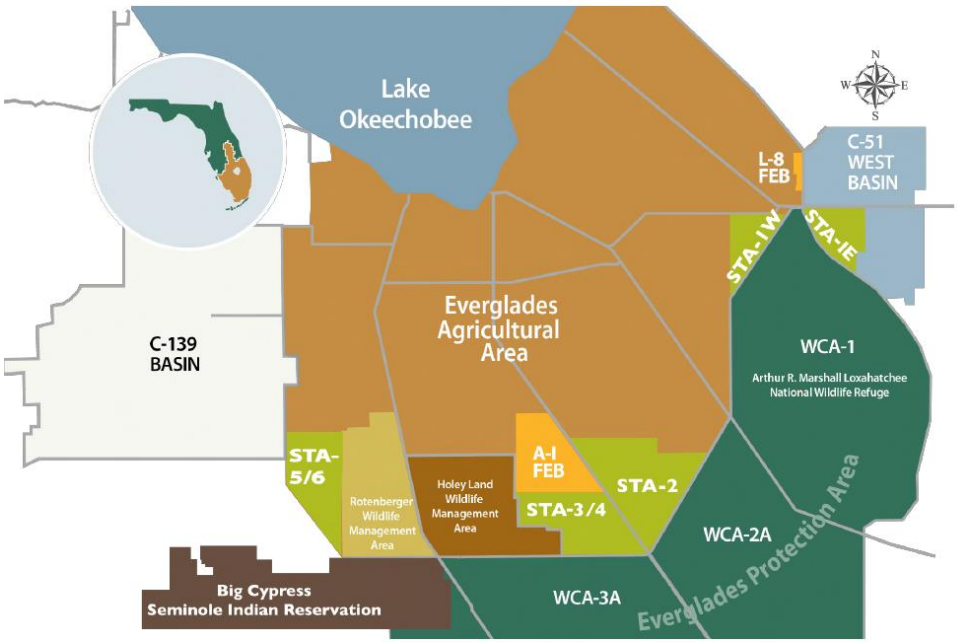

Figure 2. Everglades Water Quality Improvement through Stormwater Treatment Areas (STAs) and Flow Equalization Basins (FEBs)

Sedimentation Considerations in the Design of the Central and Southern Florida (C&SF) Project

General Sedimentation Control Considerations

Historically, C&SF canal systems were designed with bottom slopes and cross sections that would maintain flow velocities at relatively slow rates (typically less than 2.5 ft/s) to minimize the scouring of sediments within the channel section. The design velocities were based on the goal of minimizing the erosion of sand, the most common component of soils in the region. They were not intended to maintain the water velocities necessary to minimize the movement of fine organics.

As an example, in the "C&SF General Design Memorandum, Part IV, Supplement 6, Caloosahatchee River and Control Structures" (USACE 1957), a design velocity of 2.5 ft/s was used for the design of the C-43 canal. Another example is in the "C&SF General Design Memorandum Part II, Supplement 5, Kissimmee River Basin" (USACE 1956), canals were also designed with a maximum permissible velocity of 2.5 ft/sec. Design velocities larger or smaller than this value, however, may have been used in other projects depending on the site conditions encountered.

Similarly, channel side-slopes were designed to maintain a structurally stable bank and to reduce the opportunity for shoaling. This design feature also helped to minimize the natural tendency of the canal to meander and potentially increase the sediment load from the watershed.

Another sedimentation control consideration in the C&SF project is in the design of project culverts that convey flow from the secondary systems to the primary system. Project culverts were typically designed with flashboard risers to maintain upstream water levels and control both sedimentation and the discharge of floating vegetation from the contributing basins. Additionally, nonpoint discharges into canals were often controlled through inflow control mounds constructed along the banks. This design feature prevented sediment and sheet flow from adjacent lands from flowing directly into the canal.

Current C&SF System Erosion and Sedimentation Issues

Currently, the three predominant sources of sediments within the C&SF project are:

- Channel bed and bank erosion within project canals
- Suspended sediments in discharges from Lake Okeechobee
- Land surface erosion (sheet and rill erosion) from agricultural land tracts

Consequently, the primary C&SF sedimentation issues are (i) canal degradation through bank sloughing and bed erosion, (ii) canal aggradation and loss of capacity through shoaling from the settling of sediments transported from upstream canal reaches and drainage areas, (iii) the transport of suspended sediments in canal discharges to ecologically sensitive water bodies, (iv) erosion and deposition immediately downstream of water control structures, leading to structure stability concerns, and (v) sediment deposition and (re)-suspension in large water bodies (Lakes, FEBs, and reservoirs). Despite the design considerations discussed above, several areas of the C&SF project have nonetheless experienced these sedimentation issues. In particular, they are due to the following factors:

- The predominant soil types (sand-sandy clay) are easily erodible (USACE 2008).
- Significant yearly rainfall and runoff that produce frequent flows with erosive velocities (USACE 1994).
- Extreme hydrological conditions associated with tropical events produce high flows and rapid changes in the water surface elevation.
- The project encompasses large agricultural areas that produce sediment-laden runoff (USACE 2008).
- Primary C&SF project objectives such as water supply and flood control sometimes conflict with the need for effective sediment control, especially during extreme storm events.
- A secondary purpose of the project is to provide navigation, which is known to promote bank erosion through boat wakes (USACE 1994).
- Last, but not least, land uses have changed considerably in the 50+ years since the C&SF project was constructed. Land uses are significantly more intensive than originally anticipated and conceived by the designers of the project. The resulting increases in peak flows (especially in highly urbanized areas) and the corresponding changes in the peak velocities can also be a contributing factor (USACE 2008).

It should be pointed out that one of the concepts pertaining to the larger reservoirs proposed in the Comprehensive Everglades Restoration Plan was that they would capture and ‘trap’ sediments of most gradations as flows were directed away from sensitive downstream water bodies into the constructed storage reservoirs. Additionally, similar to the role of the STAs for the Everglades, both FEBs (Figure 2) are expected to serve as large regional sediment traps.

Sedimentation in St. Lucie Estuary: An example of C&SF Sedimentation Issues

The picture shown in Figure 3 below depicts the St. Lucie Estuary and its tributary basins, including major structures and canals. The St. Lucie River is a 7-mile-long (11 km) estuary linked to a coastal river system in St. Lucie and Martin counties in southeast Florida.

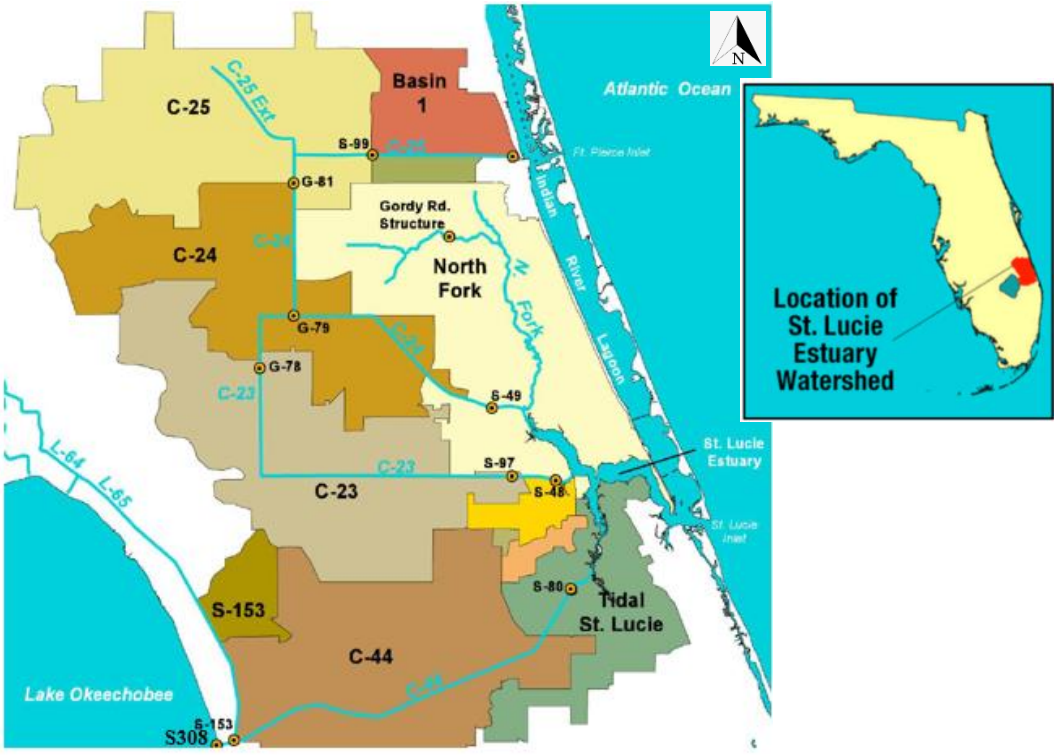

Figure 3. Greater St. Lucie Basin map (after Sun & Wan, 2014)

C-23/C-24 Canals: According to the design memorandums (USACE 1957), the US Army Corps of Engineers designed canals and structures in C-23 and C-24 canals to "hold sedimentation to a minimum. This does not apply to organic material". Furthermore, in 1969, the United States Geological Survey (USGS) characterized the suspended sediments carried by the C-23 and C-24 Canals. In this study it was estimated that C-23 and C-24 canals, respectively, discharged 4,500 and 9,000 tons of sediment to the St. Lucie Estuary (VanArman et al. 2002). The sediments were also characterized by Pitt (1972) as very fine organic sediments.

During major storms, C-23 and C-24 have historically experienced significant bank sloughing, resulting in the need for major bank stabilization projects. The bank sloughing occurred during large flood control discharges that resulted in high velocities through the canal along with occasional rapid changes in water levels (VanArman et al. 2002).

In recent years, the SFWMD has embarked on significant bank stabilization projects in the C-23 and C-24 canals, costing up to several million dollars per project. The projects are intended to remediate bank erosion issues similar to those shown in Figures 4 through 5 below (Guardiario 2014).

Figure 4. C-23 Canal bank erosion issues and repairs

Figure 5. C-24 Canal bank erosion issues and repairs

C-44 Canal: The C-44 canal (Figure 3) has historically experienced chronic and significant sedimentation problems in relation to its discharges. These first became apparent in the 1950s (Gunter and Hall 1963). The C-44 canal, also known as St. Lucie Canal, discharges have historically transported both sand and very fine, organic-rich suspended material to the St. Lucie estuary.

The quantity of suspended solid material passing through the S-80 structure (Figure 3) reached a peak rate of 8,000 tons a day when daily discharges neared 7,000 cfs in 1983 (VanArman et al. 2002). This is primarily due to the fact that the C-44 canal was originally excavated through mostly sandy soils throughout its entire length, between S-308 and S-80, resulting in excessive bank sloughing. This is evident in canal banks that are nearly vertical (USACE, 2008). Periodically, high canal discharges are one cause of this bank erosion. In addition, historic survey data indicate that the top width of the C-44 canal is increasing at an average rate of 1.7 feet per year; even in years with reduced regulatory discharges. From this observation the USACE concluded that bank erosion is also caused by wakes generated through boat traffic (USACE 1994).

Attempts to control bank sloughing through stabilization techniques have been considered. The types of structural measures, however, that would be required to achieve bank stabilization have

historically been deemed cost prohibitive. For example, the USACE report (USACE 1994) identified four sites along the canal where bank erosion is critical. The report recommended land acquisition at three of the sites where bank erosion has already consumed the right of way. Only at one of the sites did the U.S. Army Corps of Engineers recommend bank stabilization measures since bank erosion at this location was occurring next to critical infrastructure.

Lateral Inflows: Drainage from agricultural lands also contains a sediment load. However, sediment loads in runoff from adjacent agricultural tracts were estimated by the USACE (1954) to be a relatively small portion of the total sediment load. Additionally, some of the major lateral inflow ditches to the C-44 have relatively large concrete weir structures at their confluences. These structures are expected to hold back a significant quantity of heavier sediments (e.g., sand), but are probably ineffective in controlling fine sediments (silt and clay). The pictures in Figures 6 and 7 below portray one of these lateral inflow sediment control structures.

Figure 6. Lateral inflow structure discharging into the C-44 canal, near the C-44 reservoir

Figure 7. Sediment accumulation upstream of the lateral inflow weir shown in Figure 6

Sediment Loads to the Downstream Estuary: In 1984, the SFWMD provided funding to the University of South Florida to study sedimentation within the St. Lucie Estuary (Van Arman et al. 2002). In this study, sedimentation rates were estimated to be as high as 0.5 to 1.0 centimeters per year over the past 100 years based upon historical bathymetry. An estimate of 1.0 to 2.6 centimeters per year was also obtained using a radioactive dating technique (Davis and Schrader 1984; Schrader 1984). Furthermore, deposited sediments were characterized as a black, organic-rich muck covered by a flocculent layer. The flocculent layer varied in thickness, with an average depth of 1.6 feet (Schrader 1984).

While some of the estuary's sediment load is transported directly from the ocean, erosion within the C-44 canal and suspended sediments from Lake Okeechobee are the primary sources of the sediment transported to the estuary, as discussed previously. Because of this, the use of the S-80 lock for flood control purposes can abruptly increase sediment transport to the estuary. This conclusion is consistent with observations of a sediment basin (trap) constructed in 1969, just upstream of S-80. Originally, 87,000 cubic yards were excavated in constructing the trap. Only nine months later, 70% of the trap was filled with sediment that transported during flood control operations (USACE 1994). As a result, the U.S. Army Corps of Engineers highlighted the effectiveness of the trap, but also expressed concern about the associated maintenance costs. In contrast to the sediment loads comprised of sand particles, the organic fine suspended solids that are transported to the estuary through C-44 originate mostly from Lake Okeechobee as opposed to the C-44 canal itself (USACE 1994). As mentioned above, organic suspended solids can, under certain conditions, flocculate in the estuary, settle to the bottom, and create undesirable bottom deposits. This has proven to be harmful to the marine organisms that live on the estuary floor (see example cases in VanArman et al. 2002).

Potential Solutions for Sedimentation Control

The following are some common sediment control measures. Since the implementation of each measure poses unique challenges, a good understanding of the transport dynamics and specific characteristics of the sediments in a particular canal is necessary before selecting a cost-effective solution:

- Bank Stabilization - The U.S. Bureau of Reclamation (USBR, 2006) generally recommends the use of softer types of bank protection. This allows the banks to move laterally and adapt to different flow regimes and patterns. Softer bank protection can incorporate re-vegetation, root wads, geotextiles, and a number of other combinations that create a deformable rough surface and dissipate energy. In particular, some of the new geotextiles on the market may prove to be cost effective in resolving bank stability problems. In any case, the high costs of bank stabilization should be weighed against potential benefits. For example, previous studies (USACE 1994) of structural measures suggest that this may be a cost prohibitive solution.
- Weirs - The effectiveness of weir structures as sediment control barriers needs to be carefully assessed since this type of structure will reduce canal conveyance capacity, impede navigation, compromise flood protection and may be subject to numerous and stringent regulatory requirements. Additionally, while weir structures can effectively trap larger sediment particles, their ability to control organic suspended sediments or finer material is limited. Furthermore, flood control operations typically require a lowering of the weir crest elevation which tends to flush any sediment that was previously accumulated upstream.

One cannot also stress enough the potential complications associated with this approach that go largely unaddressed when these solutions are first proposed. As pointed out earlier, simply installing a different type of gate or weir does not necessarily preclude the subsequent release of lighter sediments during relative high flow events. It requires either a very large sedimentation basin/trap to achieve very low velocities or there has to be a very aggressive maintenance effort that quickly removes and disposes of the sediments between discharge events. The disposal process also comes with its complications. These sediments frequently contain some level of contaminants that could require environmental remediation (VanArman et al. 2002).

- Best Management Practices (BMPs) at the source - BMPs can be investigated for managing agricultural runoff from the contributing basins. Frequent BMPs include water table management and watershed agricultural cropping systems (VanArman et al. 2002). The impact of installing these BMPs in local basins will likely be minimal in the C-44 basin (Figure 3) considering that most sediment pollution appears to come from canal bank erosion (sand) and fine organic sediments accumulated in Lake Okeechobee (VanArman et al. 2002). BMPs implemented in the Kissimmee River Basin (south of Orlando, Florida), however, are expected to result in long-term reductions in lake sediments since they would lead to reduced sediment inflows to the Lake Okeechobee (VanArman et al. 2002) (Figure 1). Short term benefits, on the other hand, may not be evident since the Lake currently contains a large amount of accumulated sediment that becomes suspended as a result of wind and wave action and subsequently is discharged into canals (VanArman et al. 2002).
- Flashboard risers. The installation of flashboard risers at Project Culverts that currently have no flashboards, will reduce sediment discharges from secondary canals. In order for this solution to be effective, periodic removal of accumulated sediments will be necessary.
- Sediment Traps and Dredging. This may result in cost prohibitive Operation and Maintenance costs.

Potential capital and, especially, maintenance costs are key issues to consider in contemplating potential solutions. For example, in the case of a sediment trap or settling basin, its size is directly linked to the settling rate of the material to be trapped. The finer the material, the lower the velocity has to be in order to 'trap' the sediment. This, in turn, increases the size (volume) of the trap. A larger size trap results in higher capital and maintenance costs.
The sediment characteristics (e.g. specific weight and gradation) play a crucial role in the transport capacity of the flow. So, the concept of 'Sediment Control' and the effectiveness of a proposed control solution are highly dependent upon the type/grade of material that is expected to be managed.

Conclusions and Summary

A great deal of sedimentation and erosion control measures were taken into account in the original C&SF Project design including non-erosive design velocities in canals (sandy canals), sediment-controlling flashboard at project culverts, sediment control mounds along canals, and appropriate bank slopes design. Despite these design features, C&SF project which has now evolved into a C&SF Water Management System, continue to experience sedimentation and erosion issues, including canal aggradation and degradation, sediment erosion and deposition downstream of water control structures, sediment deposition and suspension in large water bodies, and undesirable sediment discharges in ecologically sensitive water bodies.

Sediment control is very challenging in a multi-objective project such as the C&SF system. The primary objectives of the C&SF project are flood control and water supply while a secondary objective is navigation. At times, these conflict with the need for effective sediment control. For example, large regulatory discharges from Lake Okeechobee, combined with large local basins runoff, are critical for flood control during major storms. These are known to carry significant sediment loads to the estuaries. Another example is that navigation is known to cause bank erosion through boat wakes. Additionally, operations of the boat locks for flood control promote sediment transport to the estuaries.

Solutions to this complex problem are case specific and a better understanding of the types of sediments along with the sources and magnitudes of sediment discharges in the selected basin are needed in order to devise effective sediment control measures. Most sediment control measures for canals are structural in nature and are therefore expensive.

Future C&SF project challenges include sedimentation and erosion issues at newly constructed FEBs and reservoirs. In particular, a better understanding of sediment budget at our reservoirs and FEBs would help better elucidate the life expectancies of these critical infrastructure.

References

Central and Southern Florida Flood Control Project Report, Eight Years of Progress, 1948-57. 1957. Published by the Central and Southern Florida Flood Control District.

Davis, R.A., and D. Schrader. 1984. “Sedimentation in the St. Lucie Estuary, Martin and St. Lucie Counties, Florida,” Department of Geology, University of South Florida, Tampa, FL.

Guardiario, J. 2014. Personal Communication, Engineering and Construction Bureau, SFWMD.

Gunter, G., and G.E. Hall. 1963. “Biological investigations of the St. Lucie Estuary (Florida) in connection with Lake Okeechobee discharges through the St. Lucie Canal,” Gulf Research Reports 1(5), Ocean Springs, MS.

Pitt, W.A., Jr. 1972. “Sediment Loads in Canals C-18, C-23 and C-24 in Southeastern Florida,” Open File Report 72013, United States Geological Survey (USGS), Tallahassee, FL.

Simons, D., and Sentürk, F. 1992. Sediment Transport Technology: Water and Sediment Dynamics. Water Resources Publications, Colorado.

Sun, D., and Wan, Y. 2014. “Estuarine Hydrodynamic and Water Quality Modeling,” SFWMD UNESCO-IHE Modeling Series Lectures.

VanArman, J., Haunert, D., Konyha, K., and Doering, P. 2002. “Technical Documentation to Support Development of Minimum Flows for the St. Lucie River and Estuary,” Water Supply Department, SFWMD, May.

U.S. Army Corps of Engineers. 1954. “Central and Southern Florida Project for Flood Control and other Purposes,” Part IV – Lake Okeechobee Outlets. Supplement 4 – Design Memorandum, Effects of Fresh-Water Discharges through St. Lucie Canal. U.S. Army Engineer District, Jacksonville Corps of Engineers, Jacksonville, FL.

U.S. Army Corps of Engineers. 1956. “Central and Southern Florida Project for Flood Control and other Purposes,” Part II – Kissimmee River Basin and Related Areas. Supplement 5 – General Design Memorandum, Kissimmee River Basin. U.S. Army Engineer District, Jacksonville Corps of Engineers, Jacksonville, FL.

U.S. Army Corps of Engineers. 1957. “Central and Southern Florida Project for Flood Control and other Purposes,” Part III – Upper St. Johns River Basin and Related Areas. Supplement 1 – General Design Memorandum, St. Lucie County Canals and Control Structures (Canals 23,

23A, 24, and 25, and Control Structures 48, 49, 50, 97, 98, and 99). U.S. Army Engineer District, Jacksonville Corps of Engineers, Jacksonville, FL.

U.S. Army Corps of Engineers. 1957. Central and Southern Florida Project for Flood Control and other Purposes," Part IV – Lake Okeechobee and Outlets. Supplement 6 – General Design Memorandum, Caloosahatchee River and Control Structures (Canal 43, and Lock Spillway Structures 77, 78, and 79). U.S. Army Engineer District, Jacksonville Corps of Engineers, Jacksonville, FL.

U.S. Army Corps of Engineers. 1959. "Central and Southern Florida Project for Flood Control and other Purposes," Part IV – Lake Okeechobee Outlets. Supplement 10 – General Design Memorandum, Biological Investigations of St. Lucie Estuary in Connection with Lake Okeechobee Discharges through St. Lucie Canal. U.S. Army Engineer District, Jacksonville Corps of Engineers, Jacksonville, FL.

U.S. Army Corps of Engineers. 1994. "St. Lucie Canal Bank Stabilization and Restoration of Rights-of-Way Letter Report," U.S. Army Engineer District, Jacksonville Corps of Engineers Jacksonville, FL.

U.S. Army Corps of Engineers. 2008. "Central and Southern Florida Project – Water Control Plan for Lake Okeechobee and Everglades Agricultural Area," U.S. Army Engineer District, Jacksonville Corps of Engineers, Jacksonville, FL.

U.S. Bureau of Reclamation. 2006. "Erosion and Sedimentation Manual," Technical Service Center, Sedimentation and River Hydraulics Group, Denver, Colorado.

Shrader, D.C. 1984. "Holocene Sedimentation in a Low Energy Microtidal Estuary, St. Lucie River, Florida," M.Sc. thesis, University of South Florida, USA.

Monitoring Hydroacoustic Flow and Tracers of Offshore Dredge Material near South Padre Island, Texas

Douglas J Schnoebelen, Hydrologist, U.S. Geological Survey, San Antonio, TX, dschnoebelen@usgs.gov
Frank L. Engel, Geographer, U.S. Geological Survey, San Antonio, TX, fengel@usgs.gov
Brian Petri, Hydrologic Technician, U.S. Geological Survey, San Antonio, TX,
Charles Hartman, Hydrologic Technician, U.S. Geological Survey, San Antonio, TX,
Patrick Bryan, Hydrologic Technician, U.S. Geological Survey, San Antonio, TX pbryan@usgs.gov
Michael Lee, Hydrologist, U.S. Geological Survey, Houston, TX, mtlee@usgs.gov
Dwight Sparks, Hydrologic Technician, U.S. Geological Survey, Austin, TX, dsparks@usgs.gov

Abstract

Beaches and water recreation are important to the South Padre Island, Texas area and across the United States. The movement of sediment in channels along beaches and the nearshore environment is important for coastal stakeholders and resource managers. Sediment removed by maintenance dredging is often placed back into the littoral system for potential beach replenishment. The movement of sediment from offshore berms to onshore beaches is not well known. Sediment transport is highly dependent on local current conditions and seasonal conditions. This study combines the use of tracer sand, sediment sampling, and continuous hydroacoustic data to provide valuable monitoring data for understanding the water/sediment resource and how the sediment delivery system operates. These data are vital for regional sediment management to assess 1) the best locations for placing dredged sediment offshore, 2) if sediment material places in offshore berms can replenish beach areas, and 3) providing data to other coastal areas across the Nation.

Introduction

The movement of sediment in channels along beaches and the nearshore environment is important for coastal stakeholders and resource managers. Sediment can deposit over time in entrances to harbor channel areas impeding boat traffic and requiring dredging. Beaches can erode with time losing valuable shoreline areas. In addition, beaches often are often not self-sustaining and require the replenishment of sand to maintain recreational areas. One tool to help maintain beaches is the placement of the sediment dredge material in offshore berms that may have the potential to replenish beaches as this sediment migrates alongshore (Poleykett and others, 2018).

Understanding the sediment and water interaction and how the sediment delivery system operates is needed for beach management. However, the movement of sediment from offshore berms to onshore beaches needs to be better quantified. In addition, sediment transport is highly dependent on local current conditions. Monitoring data (temporal and spatial) for the near shore and offshore environment (velocities, sediment sampling, and currents to name a few) are needed to better evaluate the success of offshore beach replenishment projects

(Peterson and Bishop, 2005). Monitoring data are vital for resource managers in making informed decisions for future prioritization of project and funds. These monitoring data also are important for the calibration and validation of sediment transport models that can help predict "what if" scenarios and future planning.

Study Design and Methods

An channel area near South Padre Island, Texas was dredged in July of 2018 by the US Army Corps of Engineers (USACE). The dredge material, dominated by fine sands (similar in size to existing beach material), was placed in an offshore berm from South Padre Island beaches. The City of South Padre Island contracted with Partrac GeoMarine, Inc. (Partrac) to place sediment tracer material on the offshore berm to be used in the future tracking of sediment movement. The U.S. Geological Survey (USGS) also was contracted to do the sediment sampling and hydroacoustic data collection for the study. The movement of tracer or "tagged" sediment particles in context of hydrodynamic (currents, waves, and velocities) data can help in the understanding sediment migration from the berm to the beach over time. The tracer material is a fine quartz sand (125–250-micron size range) with a fluorescent pigment and magnetic coating applied (fig. 1). The material is nontoxic and inert. The goal of the study is to better understand sediment movement for beach replenishment. The final offshore berm (600 m by 1,500 m in size) was constructed 1.2 km to 1.5 km off shore of South Padre Island Beaches. Approximately 2000 kg of tracer sand material was added to the berm after completion.

In August of 2018 the sediment sampling collection surveys (campaigns) and hydroacoustic date collection began. Campaigns consisted of both an off-shore and on-shore sampling events. Following tracer placement, approximately eight (8) sediment sampling campaigns were conducted from August 2018 to May 2019. There were 60 sediment offshore grab samples and 60 onshore grab samples collected per campaign. The off-shore sample grid locations were approximately centered over the berm—with grid squares about 300 m in size. The offshore sediment samples were collected using a Van Veen or Ponar type sampler from a stationary vertical from the boat (fig. 1), according to USGS protocols (Edwards and Glysson, 1999). Onshore samples are collected at the land/water line during low tide at approximately 600 ft intervals along the beach. The onshore samples were collected using a 10 cm by 10 cm square box core. For each of the campaigns, samples are collected from the same fixed site locations to allow for comparability between campaigns. The approximate amount of sediment material in the sampler (full, ½ full, ¼ full etc.) was noted. Texas A&M University laboratory is measuring the amount of tracer material in each sample. In addition to scheduled sampling periods, a post storm campaign (if needed) may be performed if a tropical storm hits the area.

Hydroacoustic data (current, velocity, and bed movement) at each sampling campaign was collected by the USGS from a boat mounted ADCP (Acoustic Doppler Current Profiler) at The USGS followed standard USGS protocols for collection, processing, and storing of the hydroacoustic data (Montgomery and others, 2016). These data provide a synoptic "snapshot" of currents, velocities, and bed movement at the time of sample collection. In addition, the USGS deployed a continuous ADCP instrument for gathering wave and current data between the berm and nearshore from the beginning of the sampling to run until the end of the study. The ADCP is fixed to a sea mount "barnacle" that sits on the sea floor in about 30 to 50 feet of water depth (fig. 2). Data from the ADCP are downloaded approximately every month. Together, the boat mounted and barnacle mounted ADCP data will provide more continuous data and a better understanding of local current conditions affecting sediment transport through the life of the project. These data are critical calibration datasets for developing computer simulation models of sediment transport. When coupled with the sediment concentration data as verification

datasets (that is, how much sand moved and where did it actually transport to), model simulations are anticipated to be significantly enhanced and give decision makers unique sophisticated tools to represent real world conditions.

Figure 1. Tracer sand and sediment sampler used in the sediment tracking study.

Figure 2. USGS barnacle before deployment and immediately after recovery with hydroacoustic instrumentation used for the study.

References

Edwards and Glysson, 1999, A revision of "Field Methods for Measurement of Fluvial Sediment, by Harold P. Guy and Vernon W. Norman", U.S. Geological Survey Techniques of Water-Resources Investigations, Book 3, Chapter C2, published in 1970.

Montgomery, E.T., Martini, M.A., Lightsom, F.L. and Butman, Bradford, 2016, Documentation of the U.S. Geological Survey Oceanographic Time-Series Measurement Database (ver 2.0, April 2016): U.S. Geological Survey Open-File Report 2007, 1194, http://dx.doi.org/10.3133/ofr20071194.

Peterson, C.H. and Bishop, M.J., 2005, Assessing the Environmental Impacts of Beach Nourishment, BioScience, vol. 55, issue 10, p. 887–896, https://doi.org/10.1641/0006-3568(2005)055[0887:ATEIOB]2.0.CO;2

Poleykett, J., K. Black, M. Wright, and P. Friend, 2018, The application of an active sediment tracing technique to assess the efficacy of nearshore placement of dredged material for beach nourishment purposes. Conference: WEDA 2018 Dredging Summit "Navigating the Future in dredging", At Norfolk, Virginia

Sediment Yield Analysis of the Baro-Akobo-Sobat Subbasin in Ethiopia

K Kiringu, PhD student, Department of Civil Engineering, Stellenbosch University, Stellenbosch, South Africa
GR Basson, Head: Water Division, Department of Civil Engineering, Stellenbosch University, Stellenbosch, South Africa, grbasson@sun.ac.za

Abstract

In order to develop an integrated water resources development plan, accurate prediction of sediment yields in a basin is important. The study area is one of the four major sub-basins in the Eastern Nile Portion of the Nile basin. It is located in the southernmost portion of the Eastern Nile Basin contributing about 26 billion m^3 of water every year to the Nile system at Khartoum. The physically based and distributed hydrological model SHETRAN was applied to the Baro-Akobo-Sobat (BAS) sub-basin in Ethiopia (468,216 km^2) to develop a catchment sediment yield map. Due to the large catchment size and limitations of the model, smaller sub-catchments were delineated, and the model was calibrated against observed field data where available.

Long-term daily sediment loads were simulated for a 40-year period. The maximum sediment yield in the BAS highlands was simulated as 872 t/km^2.annum and a relatively low sediment yield (< 30 t/km^2.annum) was found in the lowlands. The proposed future water resources developments (dams) are mainly planned in the highlands where the sediment yields are higher.

Introduction

To successfully develop an Integrated Water Resources Development and Management Plan (IWRDMP) for the Baro-Akobo-Sobat catchment sediment yields are required. This paper discusses the simulation of sediment yields by using the SHETRAN model.

The Baro-Akobo-Sobat-White Nile sub-basin is one of the four major sub-basins in the Eastern Nile Portion of the Nile basin. It is located between 3° 25' 52"-15° 47' 40" N and 29° 24' 43"-3° 25' 52" E, covering a total area of 468,216 km^2 contributing to about 26 billion m^3 of water every year to the Nile system at Khartoum (ENTRO, 2007). The study area location is indicated in Figure 1. The general flow direction is from the East to West originating from the highlands and dropping to the Gambela and Marchar marshland, before joining the White Nile at Malakal (TAMS_1B, 1997).

SHETRAN is a physically based, spatially distributed model with integrated surface/ subsurface modelling system for water flow, sediment transport and contaminant migration in river basins. Runoff is derived from the model's ability to accurately describe the hydrological cycle. The sediment loads are generated by considering rainfall-runoff-erosion processes, bank erosion and routing the sediment considering sediment transport capacity in overland and channel flow (Wick & Bathurst, 1995) and (Lukey, et al., 1995).

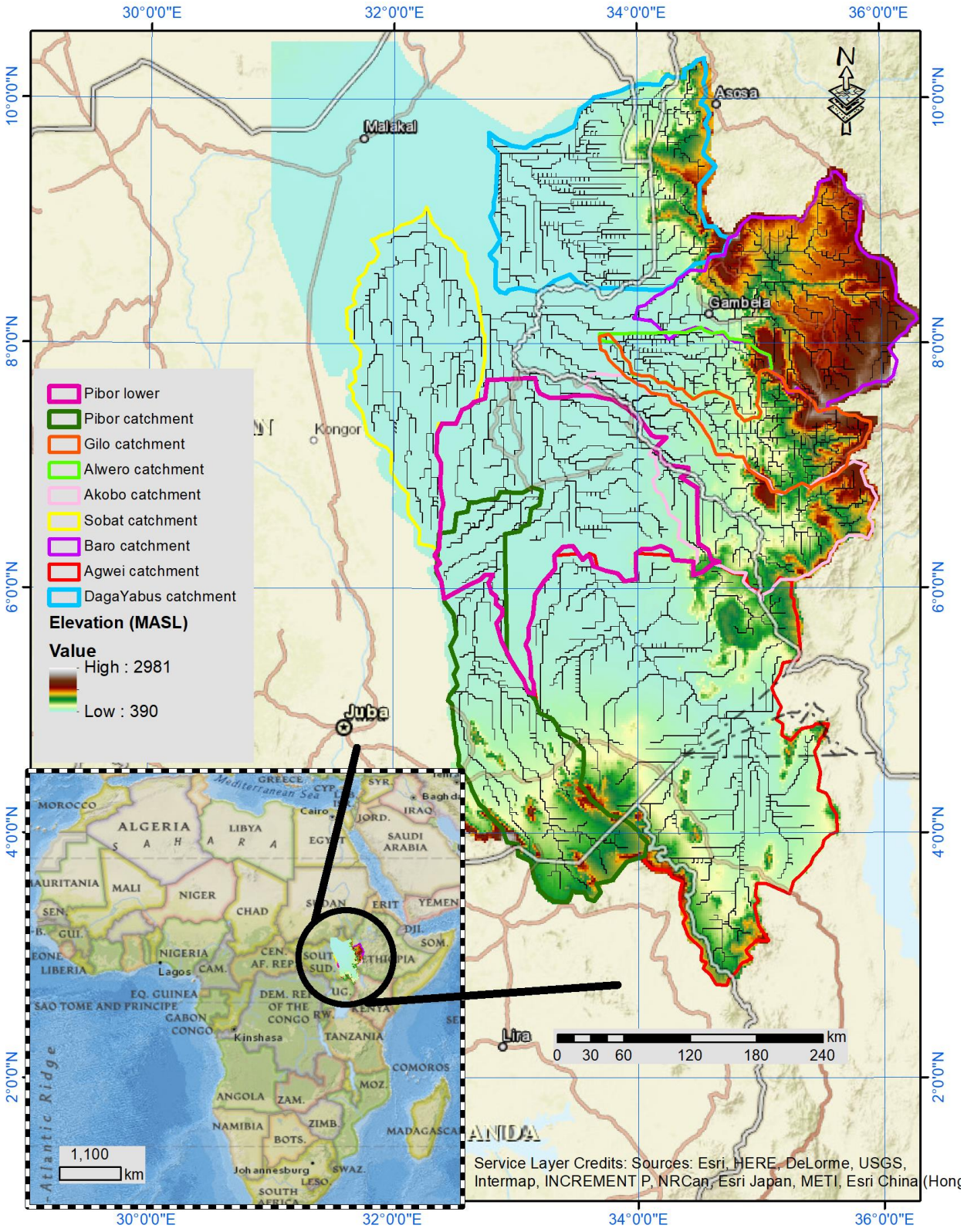

Figure 1. Location of the study area in Africa

An orthogonal grid and vertical columns in horizontal layers describes the spatial distribution of catchment properties as illustrated in Figure 2 . Hydrologic process parameters utilized by the model, such as rainfall (max daily), evaporation (max monthly), land cover distribution, soil distributions, properties, grading, depth and daily flow record and sediment load calibration data can be obtained from field measurement data. However, sediment parameters such as erodibility coefficients, plant parameters such as root density, leaf area index and canopy storage capacity are not commonly measured in the field, and thus require calibrating in the model.

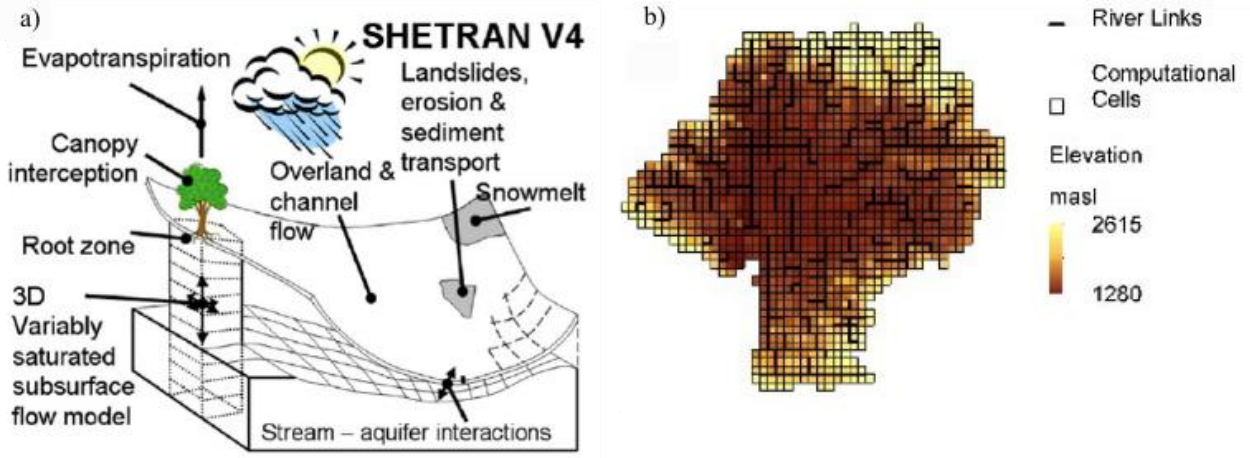

Figure 2. (a) Shematic diagram of the SHETRAN model; (b) SHETRAN model computationals cells, generated river links over elevation DEM adapted from (Bathurst, Bovoloa, & Cisnerosb, 2009)

SHETRAN Model Setup

The model has catchment size limitations but can accurately describe the physical processes in catchments of less than 2,000 km^2. However, it has successfully been implemented in large basins of approximately 1,808,500 km^2 but it is recommended for basins of about 10,000 km^2 (SHETRAN, 2013); (Birkinshaw, et al., 2017). SHETRAN (V4.4.2v2) is used in this study.

SHETRAN requires the hydrological model to be well calibrated and validated before the sediment module is activated. Data required for the adequate description of hydrological processes in the catchment is discussed below.

Catchment delineation

Based on the SHETRAN model's 200 x 200 grid limitation and 1500 river channel links, a 30 arc Digital Elevation Model (DEM) was used to delineate various watersheds of 1.9 x 1.9 km spatial resolution shown in Figure 3. The topographic elevation ranges from 2981 to 390 masl. Model river links were derived from the topographical maps. Due to complex flow patterns in the Gambela Floodplain and Machar Marshes, no river links were derived in these areas.

Land use and soil distribution

Two main soil types were identified: vertisols described as silty clay in the lowlands and nitisols described as clay loam to sandy loam in the highlands (ENTRO, 2007). Default soil parameters such as saturated water content, residual water content and vanGenuchten values were used as given in SHETRAN, (2013) data parameters with the saturated conductivity of the top 1m layer

varying between 5 to 15 m/day and the lower 14m layer between 0.1 to 1 m/day depending on the sub-basin. This approximation of soil properties was a source of uncertainty in the model.

Limited to the SHETRAN library, five predominant land uses were identified; shrub, grass, forest, arable and urban from the ENTRO (2007) report and the distribution in the catchment is shown in Figure 4. Default SHETRAN vegetation parameters such as canopy storage capacity, leaf area index, maximum rooting depth and Actual Evaporation and Potential Evaporation (AE/PE) at field capacity were used as a starting point for calibration.

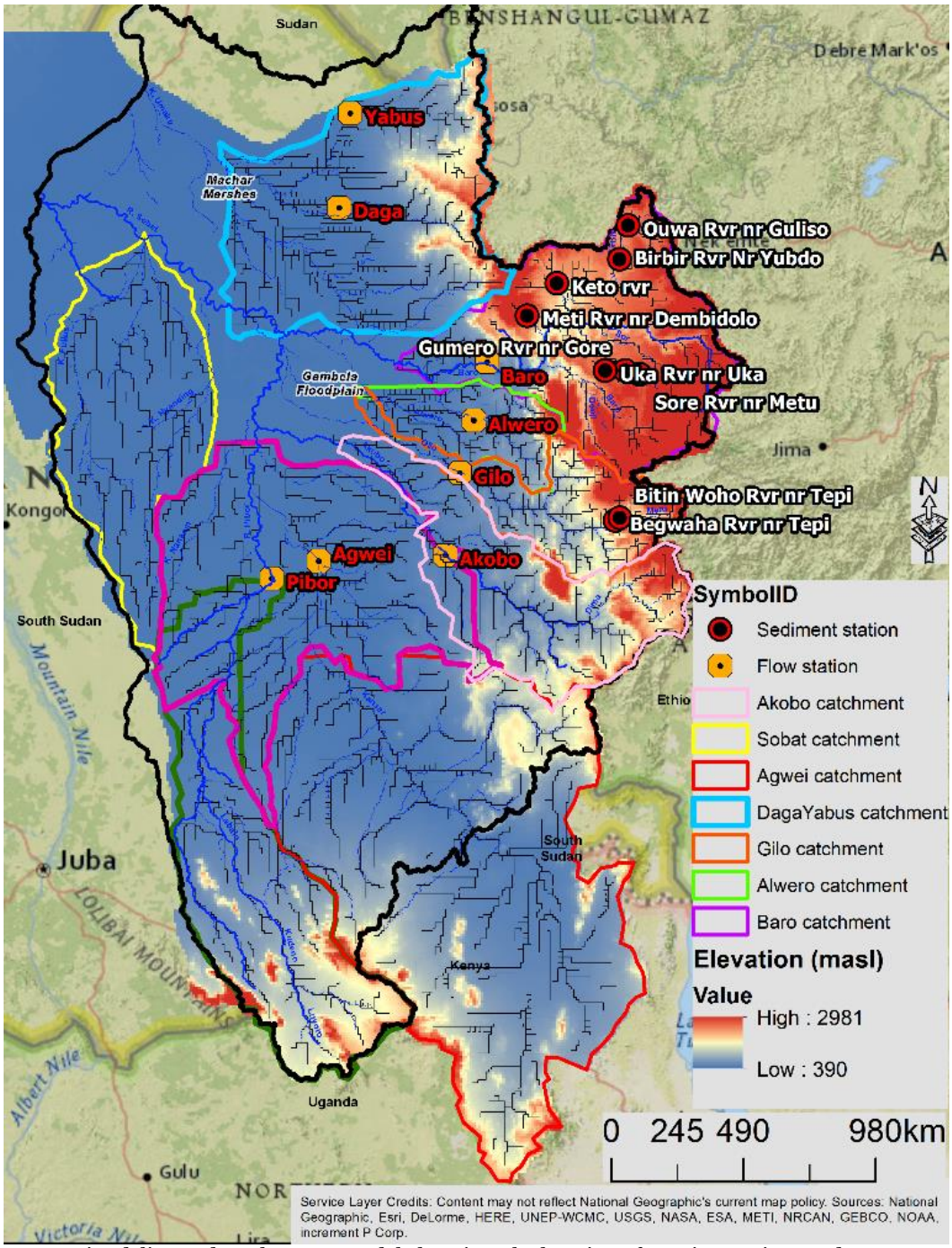

Figure 3. Major delineated catchments, model elevation, the location of gauging stations and SHETRAN river links (black) as used in the SHETRAN model

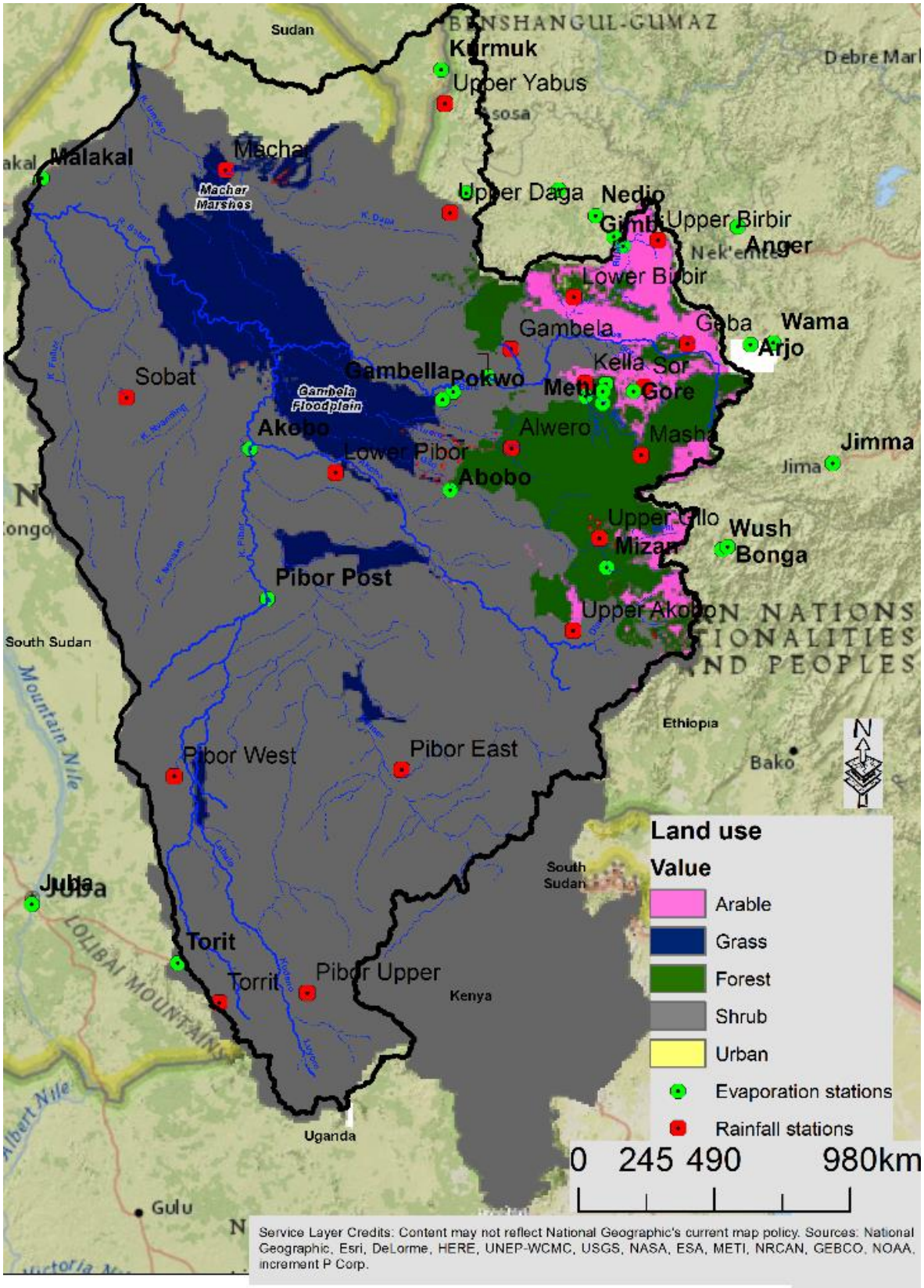

Figure 4. Baro-Akobo-Sobat land use distribution, rainfall stations and evaporation stations as used in the SHETRAN model

Rainfall, potential evaporation, flow and sediment records

For the period 1952 to 1992 daily rainfall, monthly discharge and monthly evaporation data were available from stations maintained by the Ethiopian government. Nineteen rainfall stations were available for the whole catchment with their distribution in the catchment shown in Figure 4. The Thiessen polygon method was used to determine the area of influence of each station. Thiessen polygon method is a widely accepted objective methodology for distribution of areal point rainfall (Thiessen, 1911). Twenty-five monthly evaporation stations were available with their distribution shown in Figure 4 with the area of influence determined by the Thiessen polygon.

Monthly river discharge data was available at eight gauging stations as shown in Figure 3. Based on rainfall patterns in the catchment area, 1 April to 31 March was taken as the hydrological year. Limited sediment load sampling field data was available at ten stations shown in Figure 3.

SHETRAN Calibration and Simulations

Hydrological and sediment model

The SHETRAN model is a physically based model and should ideally not be calibrated as it represents measured values in the field, but due to approximations of soil, plant parameters and errors introduced due to the course grid, calibration is necessary. Setting up and calibration of the model is a time-consuming process necessitating sensitivity analysis. From the BAS sensitivity analysis, the AE/PE at field capacity and Strickler overland flow coefficient influenced the flood peaks while the saturated conductivity and soil depth influenced the baseflows. Only these parameters were adjusted in the physically acceptable range. All the other parameters were kept as default model values.

Each delineated sub-basin was calibrated for the period the 1960 to 1992. Calibrated and validated model parameters are summarized in Table 1.

Table 1: Various calibration parameters used in SHETRAN

Parameter /catchment	Baro	Alwero	Gilo	Akobo	Pibor	Agwei	Yabus	Default
AE/PE								
Arable	0.7	0.7	1.2	1.4	-	-	0.7	0.6
Forest	1.0	1.0	1.5	1.7	-	-	1.0	1.0
Shrub	0.7	0.7	1.2	1.4	0.4	0.6	0.7	0.4
Grass	-	-	-	-	0.6	0.6	0.7	0.4
Urban	-	-	0.4	0.4		-	-	0.4
Strickler overland flow coefficient (M)								
Arable	1.5	1.5	1.5	1.5	-	-	1.5	1.5
Forest	0.5	0.5	0.5	0.5	-	-	0.5	0.5
Shrub	1.0	1.0	1.0	1.0	-	-	1.0	1.0
Grass	-	-	-	-	1.0	1.0	1.0	1.0
Urban	-	-	5.0	5.0	-	-	-	5.0
Main channel	20.0	30.0	20.0	32.0	25.0	25.0	25.0	20
Soil depth (m)								
Upper layer	1	1	1	1	1	3	1	NA
Lower layer	14	14	14	14	12	12	14	NA
Saturated conductivity (m/day)								
Upper layer	20	20	15	15	15	15	15	NA
Lower layer	5	5	5	5	5	5	5	NA

The calibrated and validated hydrological model was simulated for the whole period 1952-1992 and the resulting monthly flows at various gauging station in the catchment are shown in Figure 5. Good hydrological fit between the observed and simulated flows was generally achieved and the correlation is summarized in Table 2. For sediment yield modeling, flood peaks play a crucial role and the simulated peaks should not underpredicted to ensure sufficient sediment transport capacity.

Table 2: SHETRAN model calibration correlation

River	Baro	Alwero	Gilo	Akobo	Pibor	Agwei	Daga	Yabus
Correlation	0.87	0.63	0.63	0.45	0.66	0.56	0.72	0.65

At eight sampling stations, only 101 sediment load measurements in the catchment were available for the period 1983 to 1990. The observed sediment load data were unfortunately generally obtained during small flood flows and not during larger floods. Due to the limited calibration data, the SHETRAN model was conservatively calibrated comparing the sediment loads to previous studies done in the catchment and various publications (Norplan, 2006), (Walling & Webb, 1996) and (TAMS_1F, 1997). The parameters calibrated are summarized in Table 3. Sediment rating curves were plotted for the period where corresponding measured data was available, and the resulting graphs are shown in Figure 5. The sediment load calibrations are not perfect. Some of the simulated sediment load ratings overestimate the observed data, while others underestimate the data, but in general the simulations are in the same order as the

observed data. Due to the limited field data available at all the gauging stations, the model parameters were kept as close as possible to realistic and default values without forcing the model output.

Table 3: SHETRAN sediment calibration parameters

Parameters/ Catchment:	**Baro**	**Alwero**	**Gilo**	**Akobo**	**Pibor**	**Agwei**	**Yabus**
Raindrop and drip erodibility coefficient (J)	18.0	18.00	18.0	18.0	18.0	18.0	18.0
Overland flow soil erodibility ($kg/m^2/s$)	$1.0x10^{-5}$	$1.0x10^{-5}$	$1.0x10^{-5}$	$1.0x10^{-5}$	$1.0x10^{-5}$	$1.0x10^{-5}$	$1.0x10^{-5}$
Bulk soil density (kg/m^3)	1537.00	1537.00	1537.00	1537.00	1537.00	1537.00	1537.0
Fractional clay content of soil	0.26	0.26	0.26	0.26	0.26	0.26	0.26
Channel bank erodibility coefficient (J)	$5.5x10^{-6}$	$4.0x10^{-6}$	$4.5x10^{-6}$	$4.5x10^{-6}$	$5.5x10^{-6}$	$5.0x10^{-6}$	$5.5x10^{-6}$

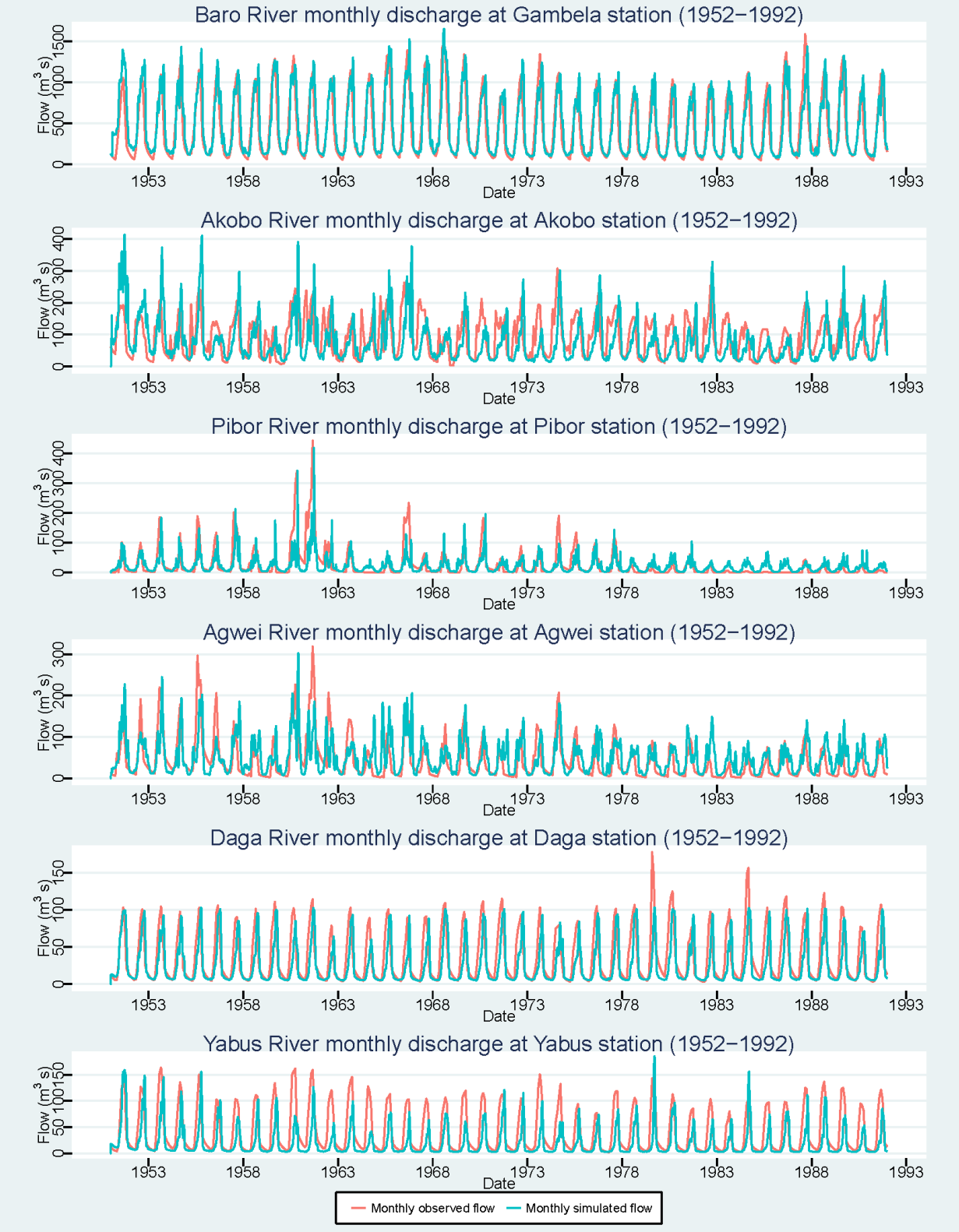

Figure 4. Comparison of simulated and observed monthly flow at various gauging station in the BAS catchment for periods 1952-1992

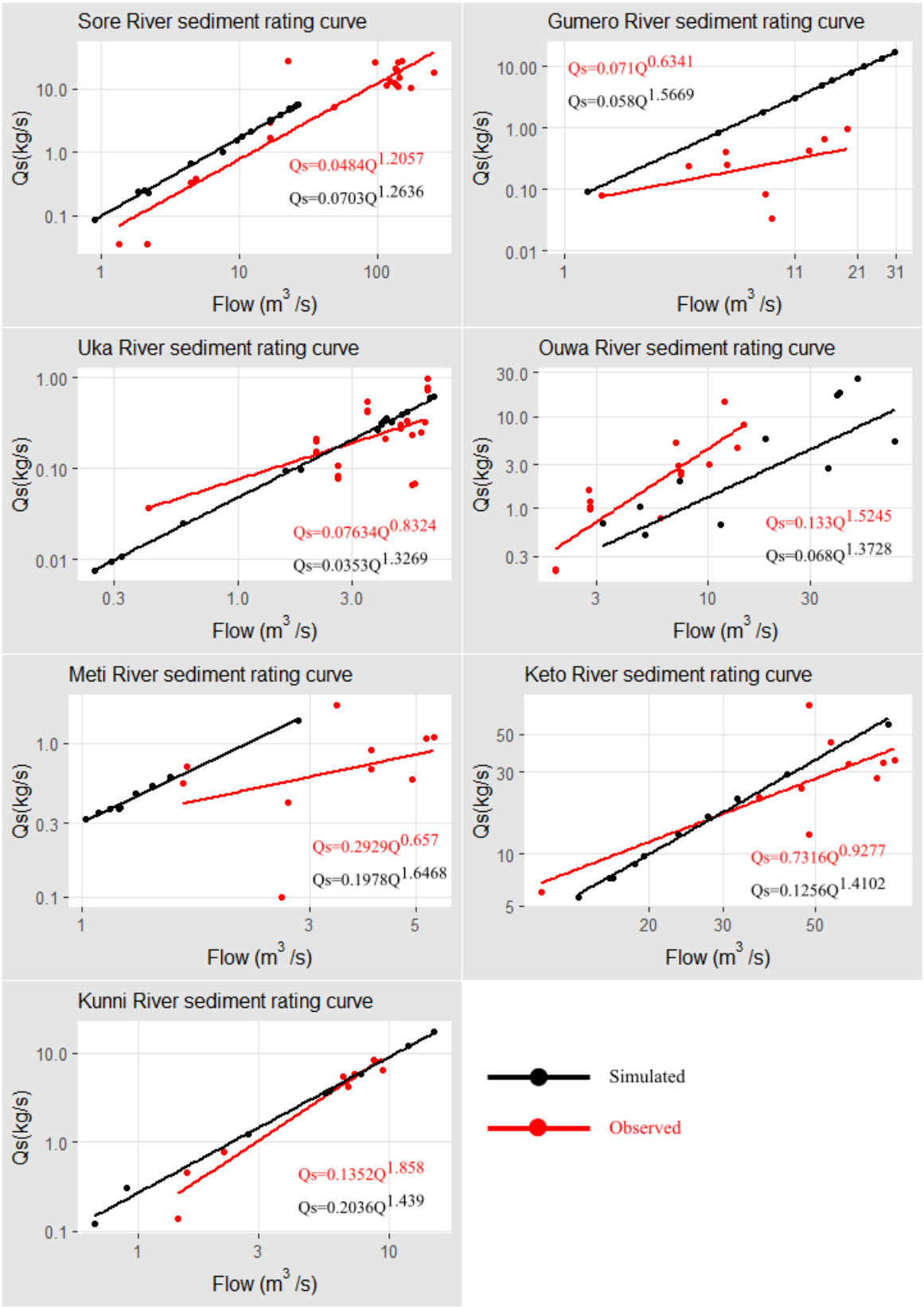

Figure 5. Sediment rating curve of simulated and measured sediment loads at various sampling stations in the BAS catchment

Sediment yield map

From the SHETRAN long-term simulations (40 years), smaller sub-catchments were delineated, and data extracted on the river channels at the locations of interest for the whole simulated period (1952-1992) and sediment yields were calculated. Where sediment yields were less than 10 t/km².annum they were adjusted to a conservative minimum yield 10t/km².annum considering the accuracy of predictions. In the un-simulated marshlands of Gambela and Machar, no sediment yields were predicted but they are expected to be small. The marshland sediment yields have to be simulated by two dimensional hydrodynamic modelling to route the upstream sediment loads through the marshes to evaluate their sediment trap efficiency.

Figure 6 shows the resulting sediment yield map of the BAS catchment with values indicated showing yields of the total catchment draining to a specific location for the current development scenario, based on historical data.

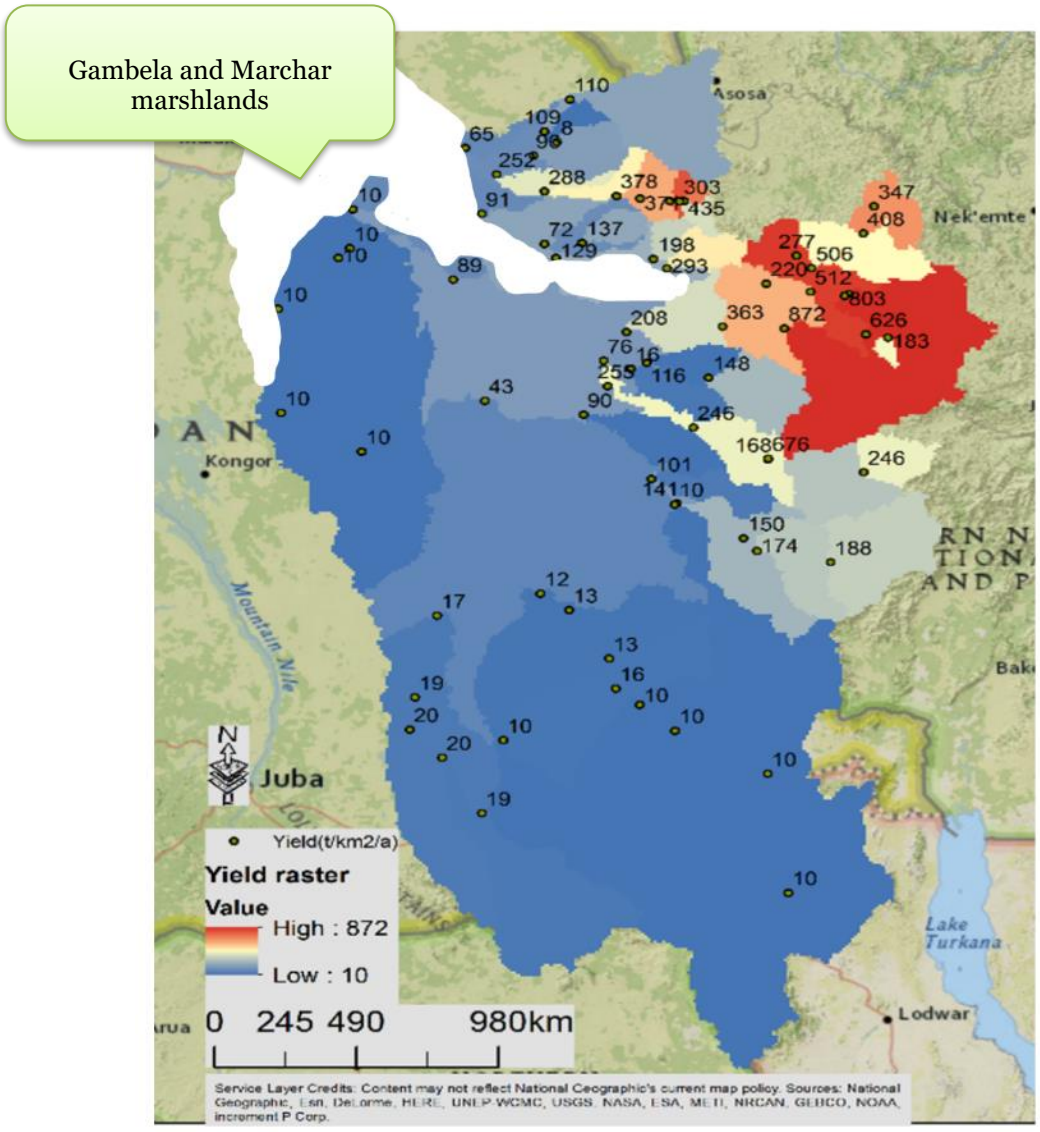

Figure 6. Baro-Akobo-Sobat sediment yield map for the current development scenario (values on map indicate sediment yields of the total catchment draining to that location)

Conclusions

A detailed methodology was followed utilizing the SHETRAN hydrological model to produce a sediment yield map for the BAS catchment. The physically based rainfall-runoff-sediment transport model was set up on a 30 arc Dem, and sub-catchment flows were calibrated where observed flow records are available. Simulated daily sediment loads were also calibrated against observed sediment loads in the rivers where records were available. A 40-year daily flow record and sediment loads were then simulated to obtain the mean long-term sediment loads and yields in the study area. Due to the complex flow network and SHETRAN limitations, the marshlands in the north-west of the study area were not simulated. The marshland sediment yields have to be simulated in future by two dimensional hydrodynamic modelling to route the upstream sediment loads through the marshes to evaluate their sediment trap efficiency.

The highest sediment yields were simulated in the east of the study area in the highlands, with a maximum of 872 t/km^2.annum, while in the south and west of the study area the yields are relatively small, in the order of 10 to 20 t/km^2.annum. The proposed future water resources developments (dams) are mainly planned in the highlands where there are better dam sites, but where the sediment yields are higher. For future water resources planning, future land use change in the catchment as the populations grows as well as climate change impacts have to be considered. The proposed dams have to be planned for future sedimentation for a period of 100 years.

References

Bathurst, J. C., Bovoloa, C. I., & Cisnerosb, F. (2009). Modelling the effect of forest cover on shallow landslides at the river basin scale. *Ecological Engineering*, 317-327.

Birkinshaw, S. J., Guerreiro, S. B., Nicholson, A., Liang, Q., Quinn, P., Zhang, L., . . . Fowler, H. J. (2017). Climate change impacts on Yangtze River discharge at the Three Gorges Dam. *Hydrology and Earth System Sciences*, 1911-1927.

Case Study 5 - Climate Change in the Yangtze Basin. (n.d.). Retrieved March 23, 2016, from http://research.ncl.ac.uk/shetran/CaseStudy5.htm

ENTRO. (2007). *Water Atlas of THE BARO-AKOBO-SOBAT AND WHITE NILE SUB-BASIN*.

Lukey, B., Sheffield, J., Bathurst, J., Lavabre, J., Mathys, N., & Martin, C. (1995). Simulating the Effect of Vegetation Cover on the Sediment Yield of Mediterranean Catchments Using SHETRAN. *Phys. Chem. Earth, 20*, 427-432.

Norplan, N. a. (2006). *BARO 1 & 2 MULTIPURPOSE PROJECTS Including Genji Diversion Scheme FEASIBILITY STUDY Draft Final Report*.

SHETRAN. (2013). *SHETRAN version 4 Data requirements, data processing and parameter values*. Retrieved from http://research.ncl.ac.uk/shetran/Documentation.htm

TAMS_1B. (1997). *Baro Akobo River Basin Integrated Development Master Plan Study-Annex1B-Water resources*.

TAMS_1F. (1997). *Baro Akobo River Basin Integrated Development Master Plan Study-Annex1F-Sediment studies*.

Thiessen, A. (1911). Precipitation Averages for Large Areas. *Monthly Weather Review*, 1082-1089.

Walling, D. E., & Webb, B. W. (1996). Erosion and sediment yield: a global overview. *Exeter Symposium*. IAHS.

Wick, J. M., & Bathurst, J. C. (1995). SHESED: a physically-based, distributed erosion and sediment yield component for the SHE hydrological modelling system. *Journal of Hydrology* , 213-238.

The Presence and Transport Processes of Bed Aggregates within the James River Estuary, Virginia

David Perkey, Research Physical Scientist, U.S. Army Corps of Engineers-Engineer Research and Development Center, Vicksburg, Mississippi, David.Perkey@usace.army.mil
Jarrell Smith, Civil Engineer, U.S. Army Corps of Engineers-Engineer Research and Development Center, Vicksburg, Mississippi, Jarrell.Smith@usace.army.mil
Kelsey Fall, Research Physical Scientist, U.S. Army Corps of Engineers-Engineer Research and Development Center, Vicksburg, Mississippi, Kelsey.A.Fall@usace.army.mil

Abstract

Aggregation can significantly impact the size and density of sediment particles, and thus alter the transport characteristics of sediments. Past scientific literature has shown that mud aggregates have frequently been observed in both the geologic record and modern depositional environments. For example, terms such as rip-up clasts (e.g. Knight 1999, Fujiwara et al., 2000; Benito et al., 2003; Bondevik et al., 2003; Donnelly, 2005; Goto et al., 2011), mud balls (e.g. Little 1982; Bachmann, 2014); and mud pebbles (e.g. Karcz, 1972; Durian et al., 2007) are commonly used to describe mud aggregates associated with high energy events such as floods, storms, and tsunamis. However, mud aggregates have also been observed and described in less energetic environments (e.g. Rust and Nanson 1989; Wright and Marriott 2007; Plint et al. 2012; Gastaldo 2013). Additionally, anthropogenic activities such as dredging have also been noted to produce aggregated clasts from the consolidated bed (e.g. Fettweis et al., 2009; Smith and Friedrichs, 2011). The above cited research has shown that these mud aggregates can be transported in both suspension and in bedload, and that transport of eroded bed aggregates over distances of kilometers might be possible in some conditions. Currently, relatively dense mud aggregates associated with cohesive sediment erosion are largely absent from numerical models used to predict sediment transport. Instead, transport models frequently rely on sediment properties obtained from the analysis of disaggregated bed samples. The results of these analyses may not best represent the physical state of material mobilized from cohesive beds. The USACE has recently developed the Flume Imaging Camera System (FICS) to be paired with the Sedflume erosion flume (McNeil et al. 1996) to allow for the imaging and size analysis of material immediately following mobilization from the sediment bed. The goal of this work is to present sediment data that documents the presence and erosion of mud aggregates in an environment where frequent dredging and efficient sediment management practices are a concern for the USACE, the James River Estuary.

The James River Estuary is located in southeastern Virginia and spans approximately 90 miles from Richmond, VA downstream to the mouth of the James River at the entrance to the Chesapeake Bay (Figure 1). Federally maintained navigation channels span this region, and it is estimated that 45-92% of the river sediments being brought down the James River are deposited within the estuary (Nichols, 1990). To maintain the federal channel, the USACE performs routine maintenance dredging. From 2015-2018 dredging projects have removed an average annual volume of $7.7x10^5$ yd^3 of sediment from the channel at an average cost of approximately $5 million per year. In many locations throughout the estuary, these dredging projects place material in disposal areas adjacent to the navigation channel.

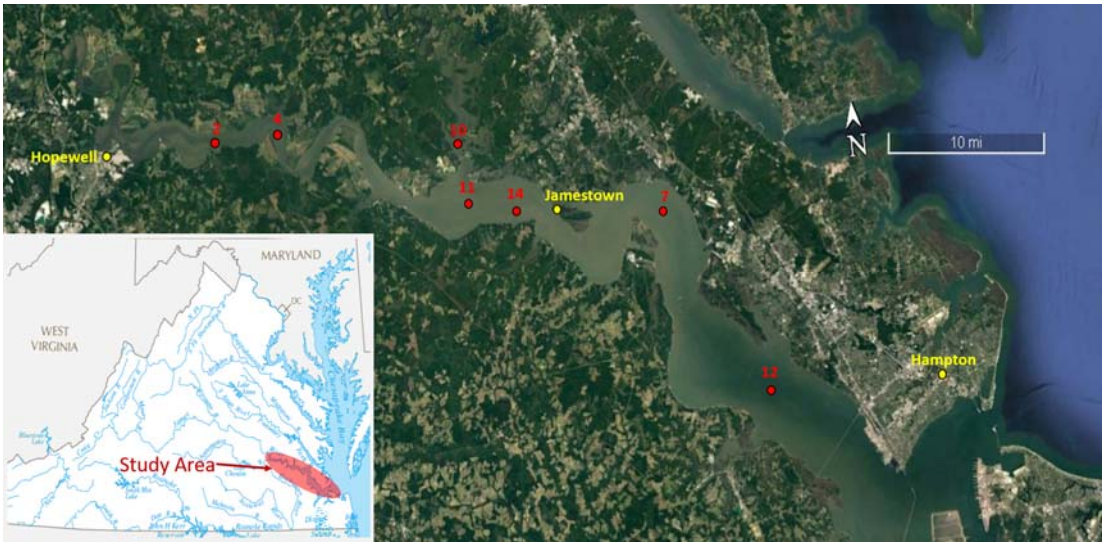

Figure 1. James River Estuary Study Site. Core locations indicated by red circles.

In November of 2017, erosion testing of sediment cores from the James River Estuary were performed as part of an ongoing Regional Sediment Management (RSM) study to evaluate the transport of placed dredged material within the estuary and improve the understanding of sediment transport patterns within the system (Figure 1). Of particular concern was the infilling of the navigation channel and if channel adjacent placement practices were impacting infill rates. The coupled FICS and Sedflume devices were utilized to evaluate the physical properties of eroded James River Estuary sediment cores. Laser Diffraction Particle Size Analysis (LDPSA) of disaggregated bed material samples collected from the upper 2 cm of the cores showed the estuary floor to be dominated by muddy sediment with median grain sizes that ranged from 13-172 μm (Figure 2). However, physical samples of eroded sediments collected from the flume outflow, along with corresponding FICS videos, indicated that the majority of the eroded sediment was in the form of larger aggregated particles (Figure 3). Analysis of FICS videos showed that median size based on particle count ranged from 200-270 μm, or roughly an order of magnitude greater than LDPSA median sizes of the disaggregated bed. FICS size distributions based on eroded volume produced median values that were frequently ~1 mm, or nearly two orders of magnitude greater than LDPSA medians of the disaggregated bed. Only the core surfaces with sand content >50% (Cores 2 & 10) produced median values that agreed within 1 order of magnitude, suggesting that larger bed aggregates are not commonly produced in sand dominant beds (Figure 2). Variation of median grain size values on this scale could significantly impact sediment transport processes and predictive model results.

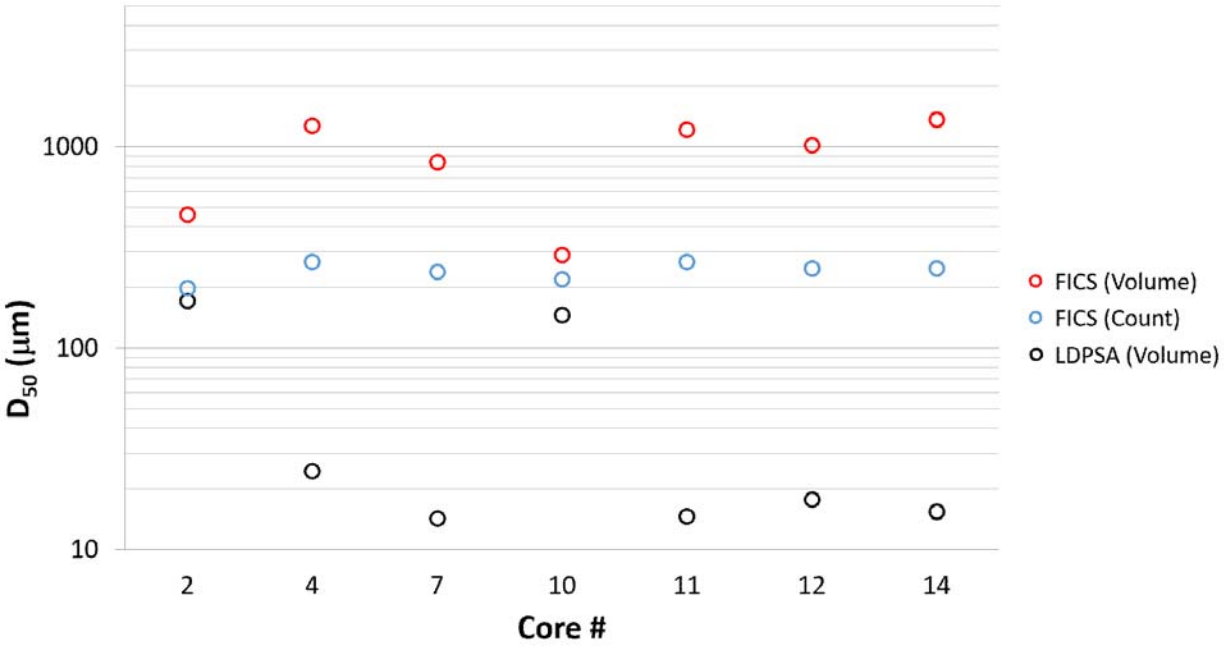

Figure 2. Plot of median grain sizes for sediments within the upper 2 cm of each core.

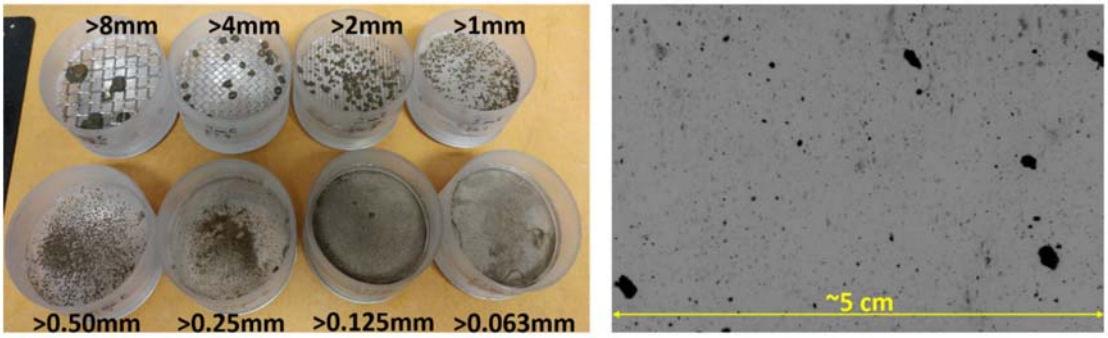

Figure 3. Sediment eroded from 0.7 cm depth of Core 14, retained on sieves (left) and imaged by FICS (right).

To illustrate potential impacts of aggregation on fine sediment transport within the James River Estuary, depth averaged velocity data obtained from the Coastal Hydrodynamics three-dimensional (CH3D) model were utilized to estimate theoretical transport thresholds and modes of sediment transport. The CH3D model has been utilized previously in numerous studies to simulate the hydrodynamics of the Chesapeake Bay system, including the James River (e.g. Johnson et al., 1993; Wang and Johnson, 2000; Cerco et al., 2002; Park et al., 2008; Cerco et al., 2013). In this simulation velocity data from the time period April 1-9, 2000 were utilized to simulate typical tidal flow conditions with maximum current speeds of ~50 cm/s.

Assuming that initial mobilization of the aggregated particles has already occurred, continued transport of these discrete clasts was then estimated by well-established relationships for transport and settling of sediment particles (Schiller and Naumann 1933; Shields 1936; VanRijn 1984). Figure 4 presents results of these simulations and shows that disaggregated mud

particles with an assumed density of 2.65 g/cm^3 were almost entirely maintained in suspension following initial mobilization. Conversely, larger aggregated mud particles with a density similar to a consolidated bed (1.5 g/cm^3) were frequently transported in bedload or remained immobile on the bed following initial erosion. Further, durability testing of James River Estuary mud clasts revealed that following 20 minutes of tumbling within a modified Slake Durability device, 30-50% of the bed aggregate mass remained >250 μm. This suggests that mobilized bed aggregates are robust enough to survive bedload transport over distances of 100's of meters within the James River Estuary. Current dredge material management practices within the estuary frequently calls for the placement of dredged sediments in areas <1 km from the navigation channel. In environments such as these, the presence of bed aggregates could significantly impact management issues such as channel infilling rates and sustainable use of placement areas.

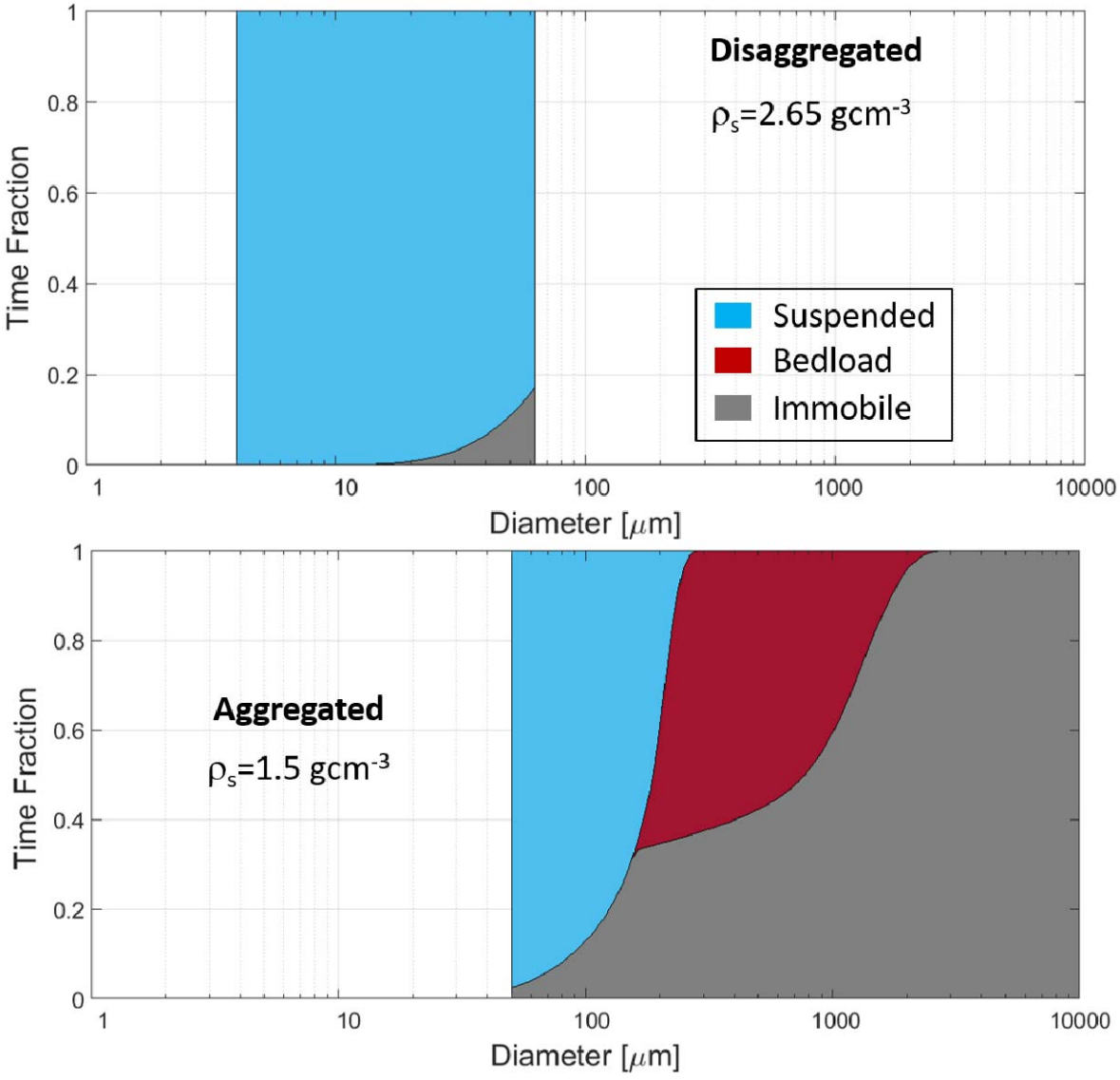

Figure 4. Estimated transport mode for mud sized primary mineral sediment (A) and aggregated mud (B) particles.

These resulting data showcase the potential importance of including aggregated bed clasts in the modeling of sediment transport in environments with cohesive sediment. Ongoing work is being conducted to incorporate the bed aggregate properties measured in this study into the USACE Long-term Fate of Dredge Material (LTFATE) sediment transport model. Model sensitivity testing is planned to evaluate the impact of aggregation state on the life cycle of dredge material mounds and disposal areas within the James River Estuary.

References

Bachmann, G.H. and Wang, Y. 2014. "Armoured mud balls as a result of ephemeral fluvial flood in a humid climate: Modern example from Guizhou Province, South China," Journal of Palaeogeography, 3(4):410-418.

Benito, G., Sánchez-Moya, Y. and Sopeña, A. 2003. "Sedimentology of high-stage flood deposits of the Tagus River, Central Spain," Sedimentary Geology, 157(1-2):107-132.

Bondevik, S., Mangerud, J., Dawson, S., Dawson, A. and Lohne, Ø. 2003. "Record-breaking height for 8000-year-old tsunami in the North Atlantic," Eos, Transactions American Geophysical Union, 84(31):289-293.

Cerco, C.F., Linker, L., Sweeney, J., Shenk, G. and Butt, A.J. 2002. "Nutrient and solids controls in Virginia's Chesapeake Bay tributaries," Journal of Water Resources Planning and Management, 128(3):179-189.

Cerco, C.F., Kim, S.C. and Noel, M.R. 2013. "Management modeling of suspended solids in the Chesapeake Bay, USA," Estuarine, Coastal and Shelf Science, 116:87-98.

Donnelly, J.P. 2005. "Evidence of past intense tropical cyclones from backbarrier salt pond sediments: a case study from Isla de Culebrita, Puerto Rico, USA," Journal of Coastal Research, 42:201-210.

Durian, D.J., Bideaud, H., Duringer, P., Schröder, A.P. and Marques, C.M. 2007. "Shape and erosion of pebbles," Physical Review E, 75(2):1-9.

Fettweis, M., Houziaux, J.S., Du Four, I., Van Lancker, V., Baeteman, C., Mathys, M., Van den Eynde, D., Francken, F. and Wartel, S. 2009. "Long-term influence of maritime access works on the distribution of cohesive sediments: analysis of historical and recent data from the Belgian nearshore area (southern North Sea)," Geo-Marine Letters, 29(5):321-330.

Fujiwara, O., Masuda, F., Sakai, T., Irizuki, T. and Fuse, K. 2000. "Tsunami deposits in Holocene bay mud in southern Kanto region, Pacific coast of central Japan," Sedimentary Geology, 135(1-4):219-230.

Gastaldo, R.A., Pludow, B.A. and Neveling, J. 2013. "Mud aggregates from the Katberg Formation, South Africa: additional evidence for Early Triassic degradational landscapes," Journal of Sedimentary Research, 83(7), pp.531-540.

Goto, K., Chagué-Goff, C., Fujino, S., Goff, J., Jaffe, B., Nishimura, Y., Richmond, B., Sugawara, D., Szczuciński, W., Tappin, D.R. and Witter, R.C. 2011. "New insights of tsunami hazard from the 2011 Tohoku-oki event," Marine Geology, 290(1-4):46-50.

Johnson, B.H., Kim, K.W., Heath, R.E., Hsieh, B.B. and Butler, H.L. 1993. "Validation of three-dimensional hydrodynamic model of Chesapeake Bay," Journal of Hydraulic Engineering, 119(1):2-20.

Karcz, I. 1972. "Sedimentary structures formed by flash floods in southern Israel," Sedimentary Geology, 7:161-182.

Knight, J. 1999. "Morphology and palaeoenvironmental interpretation of deformed soft-sediment clasts: examples from within Late Pleistocene glacial outwash, Tempo Valley, Northern Ireland," Sedimentary geology, 128(3-4):293-306.

Little, R. D. 1982. "Lithified armored mud balls of the Lower Jurassic Turners Falls sandstone, north-central Massachusetts," The Journal of Geology, 90(2):203-207.

McNeil, J., Taylor, C., & Lick, W. 1996. "Measurements of erosion of undisturbed bottom sediments with depth," Journal of Hydraulic Engineering, ASCE, 122(6):316-324.

Nichols, M.M. 1990. "Sedimentologic fate and cycling of Kepone in an estuarine system: example from the James River estuary," Science of the Total Environment, 97:407-440.

Park, K., Wang, H.V., Kim, S.C. and Oh, J.H. 2008. "A model study of the estuarine turbidity maximum along the main channel of the upper Chesapeake Bay," Estuaries and Coasts, 31(1):115-133.

Plint, A.G., Macquaker, J.H.S., Varban, B.L. 2012. "Bedload transport of mud across a wide, storm-influenced ramp: Cenomanian– Turonian Kaskapau formation, Western Canada foreland basin. J. Sediment. Res. 82:801–822.

Rust, B.R. and Nanson, G.C. 1989. "Bedload transport of mud as pedogenic aggregates in modern and ancient rivers," Sedimentology, 36(2):291-306.

Schiller, L. and A. Naumann. 1933. "Über die grundlegenden berechnungen bei der schwerkraftaufbereitung," VDIZeitschr 77(12S):318–320.

Shields, A., 1936. "Anwendung der Aehnlichkeitsmechanik und der Turbulenzforschung auf die Geschiebebewegung," PhD Thesis Technical University Berlin.

Smith, S.J., Friedrichs, C.T., 2011. "Size and settling velocities of cohesive flocs and suspended sediment aggregates in a trailing suction hopper dredge plume," Continental Shelf Research, 31:S50-S63.

Van Rijn, L.C. 1984. "Sediment transport, part II: suspended load transport," Journal of Hydraulic Engineering, ASCE, 110(11):1613-1641.

Wang, H.V. and Johnson, B.H. 2000. "Validation and application of the second generation three dimensional hydrodynamic model of Chesapeake Bay," Water Quality and Ecosystems Modeling, 1(1-4):51-90.

Wright, V.P., Marriott, S.B. 2007. "The dangers of taking mud for granted: Lessons from Lower Old Red Sandstone dryland river systems of South Wales," Sedimentary Geology, 195:91-100.

Post-Wildfire Watershed Modeling Using the Distributed Curve Number Method

Joe Lange, State Design Engineer, USDA – Natural Resources Conservation Service, Wenatchee, WA, joe.lange@wa.usda.gov

Abstract

Wildfires can cause dramatic short-term impairments to watersheds creating threats from flooding and debris flows. During such emergencies, a rapid response is needed to assess the potential threats to life and/or property. Post-wildfire watershed modeling is a key component in completing an emergency assessment. In Washington State, both the USDA Forest Service and USDA Natural Resources Conservation Service, use WILDCAT5 for Windows (WILDCAT5).

WILDCAT5 for Windows (Hawkins and Barreto-Munoz, 2016) is an interactive Windows™ Excel software package designed to assist watershed specialists in analyzing rainfall runoff events to predict peak flow and runoff volumes generated by single event rainstorms for a variety of watershed soil and vegetation conditions. WILDCAT5 is a direct runoff model that uses the Distributed Curve Number (CN) method. The Distributed CN method calculates direct runoff, using the NRCS runoff CN method, by summing the runoff for each individual hydrologic soil-cover complex (source areas). It does not use the Average (Weighted) CN method. The example below illustrates the difference between these two methods.

Example

Problem: Determine the difference between post-fire hydrologic modeling by distributed CN and average CN methods.

Given: A 1,000-acre watershed recently burned from a wildfire. The watershed has 230 acres (23%) high soil burn severity, 320 acres (32%) moderate soil burn severity, and 450 acres (45%) low soil burn severity. The design storm has 1.0 inches of rainfall, the Antecedent Runoff Condition (ARC) is II, and Ia/S is 0.20. The pre-wildfire CN is 60. The post-wildfire CNs are as follows: High soil burn severity, CN = 95; Moderate soil burn severity, CN = 85; Low soil burn severity, CN = pre-wildfire CN + 5 = 65 (USDA-FS, BAER Tools).

Determine: Estimate the direct runoff by both the Distributed CN and the Average CN methods.

Solution: Distributed CN Method

Step 1. Determine the runoff, proportioning by hydrologic soil-cover complex.

$$S_{05} = (1000 / CN_{20}) - 10 \quad (1)$$

$$Q = (P - 0.2 \times S_{20})^2 / (P + 0.8 \times S_{20}) \quad (2)$$

Where (CN) is the curve number, (S) is the storage index (inches), (A) is the drainage area (acres), (P) is rainfall (inches), and (Q) is runoff (inches).

Cover	CN	S	A	Q	Q×A
Low SBS	65	5.4	450	0.00	0
Moderate SBS	85	1.8	320	0.17	54
High SBS	95	0.5	230	0.56	129
Totals			1,000		183

Step 2. Determine the Distributed CN weighted runoff.

$$\text{The Distributed CN runoff (Q)} = \frac{\Sigma Q \times A}{\Sigma A} = \frac{183 \text{ acre-in}}{1{,}000 \text{ acres}} = 0.18 \text{ inch} \quad (3)$$

Solution: Average CN Method

Step 1. Determine the Average CN, proportioning by hydrologic soil-cover complex.

Cover	CN	A	CN×A
Low SBS	65	450	29,250
Moderate SBS	85	320	27,200
High SBS	95	230	21,850
Totals		1,000	78,300

$$\text{The Average CN} = \frac{\Sigma CN \times A}{\Sigma A} = \frac{78{,}300 \text{ acres}}{1{,}000 \text{ acres}} = 78.3 \text{ . Use } 78. \quad (4)$$

Step 2. Determine the Average CN runoff.

$S_{20} = (1000 / 78) - 10 = 2.8$

$$\text{The Average CN runoff (Q)} = (1 - 0.2 \times 2.8)^2 / (1 + 0.8 \times 2.8) = 0.06 \text{ inch} \quad (5)$$

The runoff estimate using the Distributed CN method is 3 times greater than the runoff estimate using the Average CN method.

The example illustrates the limitations of the Average CN method and the importance of using the Distributed CN method for post-fire analysis. By using the Distributed CN method in this example, it shows how 77% of the total runoff occurs from only 23% of the area (high soil burn severity). Where differences in CN for a watershed are large, the Average CN method either under- or over-estimates Q, depending on the size of the storm (USDA-NRCS, 2004). For burned watersheds, the Average CN method under-estimates the amount of runoff, as shown in this example. The method of weighted Q (Distributed CN) always gives a more precise result (in terms of the given data) but it requires more work than the weighted-CN (Average CN) method especially when a watershed has many complexes (USDA-NRCS, 2004). WILDCAT5 is the only hydrologic model that uses the Distributed CN method.

Runoff hydrographs are then developed by applying the runoff volume, estimated by the Distributed CN method, and a time of concentration to a dimensionless unit hydrograph.

Acknowledgements

A cost-share agreement between the University of Arizona and the USDA Forest Service, Stream Systems Technology Center provided support for software development of WILDCAT5.

Appreciation is expressed to Dr. Richard H. Hawkins and Armando Barreto-Munoz (University of Arizona) for their work in developing WILDCAT5; to the USFS Remote Sensing Applications Center (RSAC) for providing BARC data; to the First Creek fire BAER team for their field data verifications and development of the soil burn severity map; to Claudia Hoeft (NRCS National Hydraulic Engineer, Conservation Engineering Division), Dan Moore (NRCS Hydraulic Engineer, West National Technology Support Center), Marty Walther (Hydrology/Hydraulics Engineer, Washington State Department Ecology – Dam Safety Office), and Molly Hanson (USFS Region 6 Forest Hydrologist, Okanogan-Wenatchee National Forest) for their peer review. I would also like to acknowledge Greg Kuyumjian, (USFS, retired) for contributing his extensive knowledge and expertise in post-wildfire hydrologic modeling and BAER team leadership.

References

Hawkins, R.H.; Barreto-Munoz, A. April 2016. WILDCAT5 for Windows. University of Arizona, Tucson AZ. USFS contact: Rocky Mountain Research Station, Stream Systems Technology Center, 2150 Centre Ave., Bldg. A, Suite 368, Fort Collins, CO. Available at: https://www.fs.fed.us/biology/nsaec/products-tools.html

USDA-FS (U.S. Department of Agriculture-Forest Service), Burned Area Emergency Response BAER) Tools, Curve Number Methods. Available at: https://forest.moscowfsl.wsu.edu/BAERTOOLS/ROADTRT/Peakflow/CN/supplement.html#CNKuyumjian

USDA-NRCS (U.S. Department of Agriculture-Natural Resources Conservation Service), 2004. NRCS National Engineering Handbook, Part 630 Hydrology, Chapter 10, Estimation of Direct Runoff from Storm Rainfall. Available at: https://directives.sc.egov.usda.gov/OpenNonWebContent.aspx?content=17752.wba

Regional Sediment Management Informed by Geochemical Fingerprinting: Calcasieu Ship Channel, USA

Brandon Boyd, Research Scientist, US Army Corps of Engineers
Vicksburg, MS, brandon.m.boyd@usace.army.mil
David Perkey, Research Scientist, US Army Corps of Engineers
Vicksburg, MS, david.perkey@usace.army.mil
Jeffery Corbino, Environmental Specialist, US Army Corps of Engineers
New Orleans, LA, jeffery.m.corbino@usace.army.mil

Abstract

One principle of Regional Sediment Management (RSM) is focused on using system- or regional-scale approaches to maximize benefits and minimize negative consequences of project-scale sediment management (Figure 1).

Figure 1. The Regional Sediment Management (RSM) Process (National Regional Sediment Management Program).

Often multiple sources of sediment could potentially be responsible for increasing maintenance dredging of a given project. Identification of the afflicting source or sources may allow for targeted remediation or prevention strategies such as sediment retention or flow modification structures at a lesser cost or greater benefit than traditional dredged material management.

One such case is the Calcasieu Ship Channel (CSC), a Federal deep-draft navigation channel servicing the Port of Lake Charles in Southwest Louisiana, USA (Figure 2).

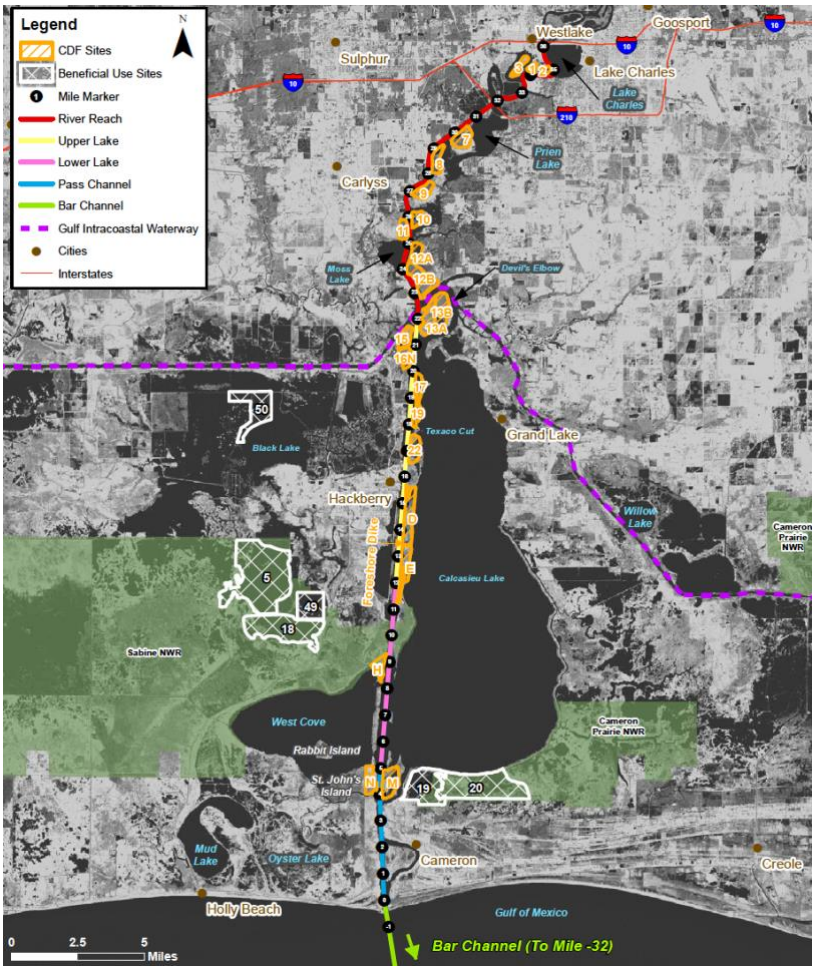

Figure 2. Map of the Calcasieu Ship Channel and surrounding area (USACE, 2010).

High rates of shoaling in the inland portion of this waterway impacts navigation to this strategic port, requiring 3 million m^3 (4 million yd^3) of maintenance dredging annually at a cost of about $20M per year. Multiple sources could be contributing sediments to the CSC: Flanking wetlands, riverine, offshore, and adjacent banks. Previous sediment transport simulations by Brown (in preparation) estimated the contribution of these sources but have not been verified. Based on modeled sediment transport, this study was derived using a combination of field- and laboratory-based approaches to verify the shoaling due to these sediment sources. A reconnaissance-type sampling approach will first utilize a suite of geochemical assays to identify robust and cost-effective tracers, followed by more intensive analysis of channel shoal material for the presence of these tracers. The characteristics of sediment sources and channel shoals will be evaluated with principle component analysis (PCA) to examine the distribution of unique tracers and identify shoaling patterns. A mixing model will then be used to determine the relative contributions of the source materials. The results of this study may highlight an alternate approach to management of sediment at the source or at least before deposition in the CSC. This geochemically informed mitigation approach could then be applied to other projects in the Gulf of Mexico region and, additionally, the framework of that approach used in other systems where the contributions of multiple sediment sources to maintenance dredging are

unknown. We present the project motivation, the methodological approach to geochemical fingerprinting used in this work, preliminary results, and hypothetical conclusions.

References

Brown, Gary (in preparation). Investigation of Sources of Sediment Associated with Deposition in the Calcasieu Ship Channel. FY18 RSM project report prepared for US Army Engineer District, New Orleans.

US Army Corps of Engineers New Orleans District (USACE). 2010. Calcasieu River and Pass, Louisiana Dredged Material Management Plan and Supplemental Environmental Impact Statement.

Remote Sensing & Monitoring

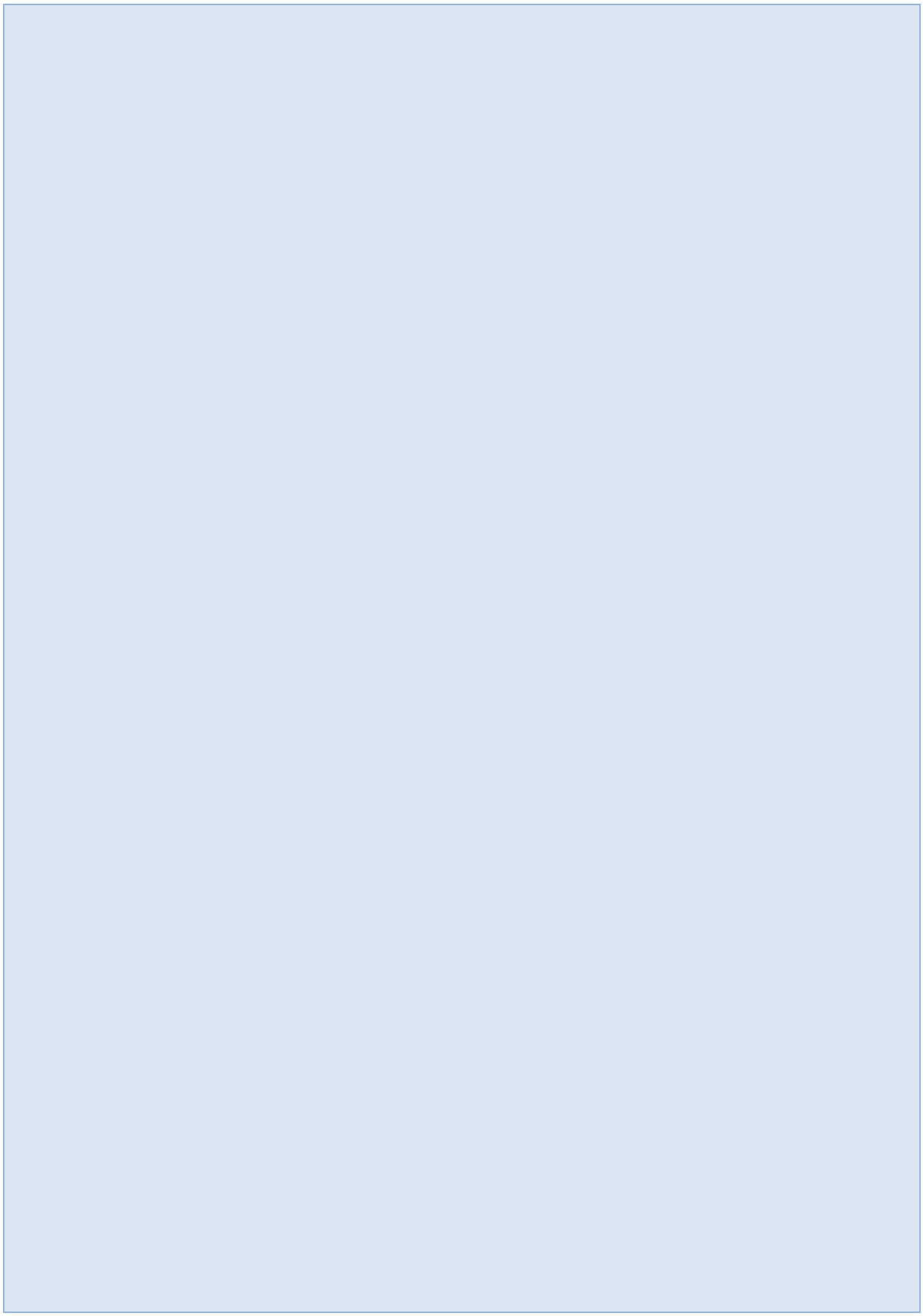

Comparison of Reservoir Evaporation Rates from the Collison Floating Evaporation Pan to Atmospheric Evaporation Techniques and the Importance of Wind Speed and Direction

Jake Collison, University of New Mexico, Albuquerque, NM, jakec@unm.edu
Mark Stone, Associate Professor, University of New Mexico, Albuquerque, NM, stone@unm.edu
Dagmar Llewellyn, Hydrologist/Civil Engineer, US Bureau of Reclamation, Albuquerque, NM, dllewellyn@usbr.gov
Kenneth Richard, Project Manager/Hydrologist, US Bureau of Reclamation, Albuquerque, NM, karichard@usbr.gov

Extended Abstract

Accurate tracking of open-water evaporative losses, one of the largest consumptive uses of water in the Southwestern United States, will become increasingly important in the future with anticipated climate shifts toward warmer temperatures and longer, more severe droughts. The current methods for estimating reservoir evaporation have uncertainties ranging from ±20 to 70 percent. Reduction of these uncertainties through improved evaporation monitoring tools could provide water-resource managers with a better understanding of current and future water supplies, and allow for improved real-time water management.

With funding from the US Bureau of Reclamation and the US Army Corps of Engineers, the University of New Mexico is testing a new tool for improved real-time monitoring of reservoir evaporation rates, the Collison Floating Evaporation Pan (CFEP, Figure 1, U.S. Patent 10,082,415, Collison [2018]). In 2017, testing of this device was initiated on a 50,000-acre-foot flood-control reservoir, Cochiti Lake, located in central New Mexico. Since then, additional CFEPs have been planned or installed on Lake Powell in Utah, and Elephant Butte Reservoir in southern New Mexico. Through innovative design and extensive field measurements, this study aims to develop a more accurate, robust, automated, and real-time technique for measuring near-actual reservoir evaporation rates, leading to effective long-term monitoring and management of the nation's water resources.

The CFEP is semi-submerged to minimize the difference in water temperature between the CFEP and the reservoir. Additionally, the CFEP's design has minimal influence on the atmospheric boundary layer (imagine a dome of cooler, wetter air overlying the body of water) overlying the pan relative to the reservoir. The CFEP's accuracy was verified through the use of a hemispherical evaporation chamber designed to measure near-actual evaporation rates adjacent to the CFEP. In addition to measuring evaporation, the CFEP has a full micrometeorological weather station attached to it, allowing for other evaporation models to be calculated and compared to the CFEP. Results from the Cochiti Lake CFEP were compared to other evaporation models, including Hamon (Hamon, 1961), Hargreaves's (Hargreaves, 1975), and U.S. Weather Bureau equation (Kohler and others, 1955) and to the on-site Class A Evaporation Pan managed by the U.S. Army Corps of Engineers, see Figure 2 below.

Figure 1. Collison Floating Evaporation Pan (CFEP) on Cochiti Lake, New Mexico (8-foot diameter evaporation pan and 16-foot diameter outer wave guard).

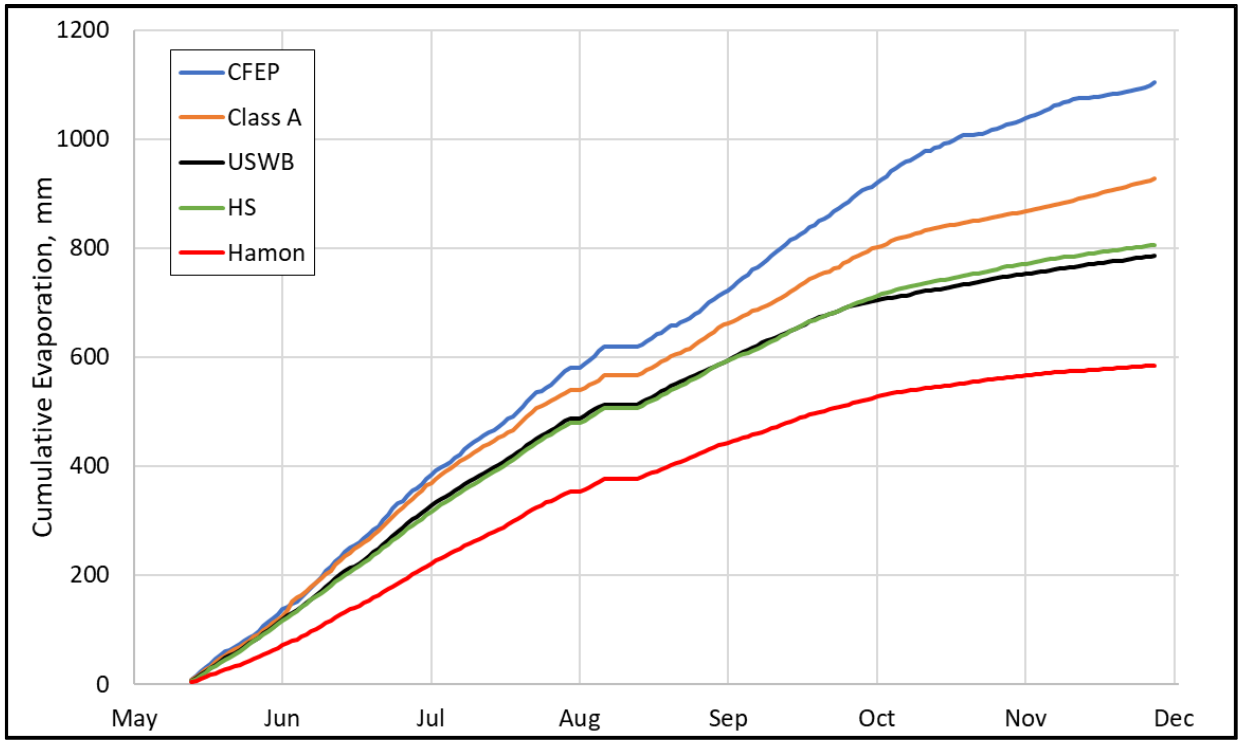

Figure 2. Cumulative evaporation for the CFEP (Collison Floating Evaporation Pan), Class A Pan, USWB equation (U.S. Weather Bureau), HS equation (Hargreaves-Samani), and Hamon equation.

The agreement between the CFEP and Class A Pan was the closest of all evaporation estimation techniques calculated, especially in May and June, but this agreement begins to decrease in late

summer through fall. The difference in evaporation estimated by the CFEP and the other four techniques is most apparent in the fall, due to the energy stored in the reservoir during the spring and summer being released through increased evaporation rates in the fall. This increase in evaporation in the fall is captured by the CFEP due to its being placed within the atmospheric boundary conditions of the reservoir whereas the other four techniques do not account for this.

Figure 3 below represents one week of evaporation (blue line), vapor pressure deficit (red line), and wind speed (green line) data collected by the Cochiti Lake CFEP, where vapor pressure deficit (VPD) is determined as the difference between the maximum potential vapor pressure in the air at the current air temperature (function of air temperature) and the current ambient vapor pressure. The high correlation between evaporation rate and wind speed is clearly evident, but so is the correlation between evaporation rate and high VPD values. Wind at this location predominately came from the south during the course of the study, except between 5 a.m. and 8 a.m., when it came from the north. The Cochiti Lake CFEP has roughly 110 meters of open water to the south and 2,000+ meters of open water to the north. Thus, when wind comes from the south, it is traveling off the hot and dry desert. This hot and dry air has a high VPD, and, when coupled with an increase in wind speed, causes a spike in evaporation rates at the CFEP location. Increases in wind speed during the mornings of July 10th and 14th are not associated with a large spike in evaporation because these winds are coming from the north and have traveled across 2,000+ meters of open water. This effect of windward (shore-to-lake) and leeward (lake-to-shore) winds on evaporation rates is apparent in Figure 3, where higher evaporation rates are associated with windward, southerly, wind directions.

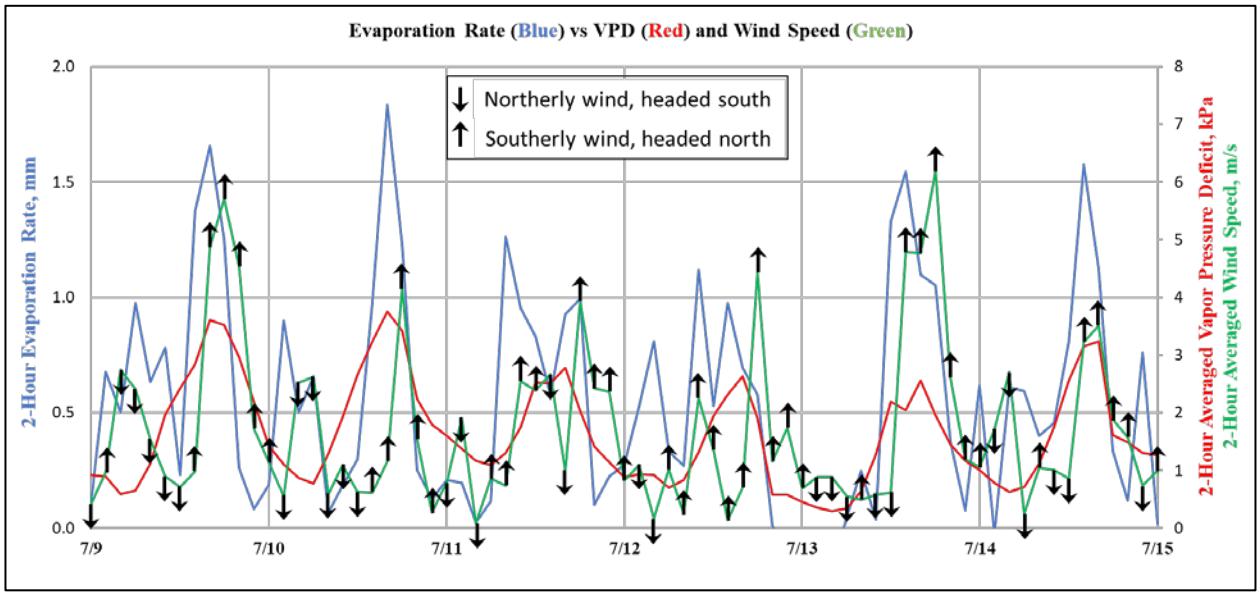

Figure 3. Evaporation Rate measured by the Collison Floating Evaporation Pan vs Vapor Pressure Deficit (VPD) and Wind Speed and Associated Wind Direction.

The large spikes in evaporation during southerly wind events and smaller spikes in evaporation during northerly wind events occur year-round at this site. It is reasonable to assume that similar evaporation spikes occur at other reservoirs and lakes in arid and semi-arid environments, and occur more strongly when winds arrive at a given location from dry land without flowing over a significant area of open water. These spikes represent a considerable amount of the daily evaporative losses at the CFEP measurement location on Cochiti Lake,

where evaporation during southerly winds accounted for 62% of the evaporation during this study. These southerly, hot, dry winds, especially during high wind events, destabilize the normally wet, cool atmospheric boundary conditions over Cochiti Lake, increasing the evaporation rate significantly and illustrating the destabilization of atmospheric boundary conditions present over large bodies of water. Atmospheric boundary conditions over reservoirs impede evaporation, as seen by the magnitude of evaporation and VPD values based solely on wind direction at Cochiti Lake.

The analyses presented here demonstrate that techniques describing evaporation rates from large water bodies must include stored energy, wind speed, and wind direction in order to accurately estimate evaporation losses. Additionally, this study was able to quantify the importance of wind direction on evaporation rates, specifically shore-to-water and water-to-shore, where shore-to-water winds accounted for 62% of the evaporation estimated. In the Western and Southwestern U.S., reservoirs are often built within canyons that are long and narrow; based on this study, winds which travel along the minor axis of these reservoirs will have a considerably larger evaporation rate than winds traveling along the major axis. Understanding and accounting for spatially varying evaporation rates will greatly enhance the accuracy of evaporation estimates instead of just applying a single evaporation rate to the whole body of water.

At the Cochiti Lake CFEP study site, data from the CFEP have demonstrated that wind conditions are the major driving force for reservoir evaporation. Furthermore, the CFEP data have demonstrated the importance of wind direction, as an indicator of the amount of open water over which air has passed before reaching the measurement location, in the measured evaporation rate. Additional monitoring and research are needed to determine the impacts of these differences in wind direction and local evaporation rates on the overall evaporative losses from the reservoir.

References

Collison, J.W., 2018, “Floating evaporation pan with adjustable freeboard and surrounding wave-guard,” U.S. 10,082,415 September 25, 2018.

Hamon, W.R, 1961, “Estimating potential evapotranspiration,” Journal of the Hydraulics Division, ASCE. 87(HY3):107-120.

Hargreaves, G.H., 1975, “Moisture availability and crop production,” Trans. Am. Soc. Agric. Eng. 18(5):980-984.

Kohler, M.A., Nordenson, T.J., and Fox, W.E., 1955, “Evaporation from pans and lakes,” U.S. Weather Bureau Research Paper 38, 82 p.

Near-Field Remote Sensing of Alaskan Rivers

Paul Kinzel, Hydrologist, U.S. Geological Survey, Golden, CO, pjkinzel@usgs.gov
Carl Legleiter, Hydrologist, U.S. Geological Survey, Golden, CO, cjl@usgs.gov
Jonathan Nelson, Hydrologist, U.S. Geological Survey, Golden, CO, jmn@usgs.gov
Jeff Conaway, Hydrologist, U.S. Geological Survey, Anchorage, AK, jconaway@usgs.gov
Adam LeWinter, Physical Scientist, U.S. Army Corps of Engineers, Hanover, NH, Adam.L.Lewinter@erdc.dren.mil
Peter Gadomski, Physical Scientist, U.S. Army Corps of Engineers, Hanover, NH, Peter.J.Gadomski@erdc.dren.mil
Dominic Filiano, Physical Scientist, U.S. Army Corps of Engineers, Hanover, NH, Dominic.L.Filiano@erdc.dren.mil

Abstract

The U.S. Geological Survey (USGS) Geomorphology and Sediment Transport Laboratory (GSTL), in collaboration with the U.S. Army Corps of Engineers Cold Regions Research and Engineering Laboratory (CRREL), acquired remotely sensed data from several Alaskan rivers in 2017 and 2018 with the goal of developing a methodology for measuring streamflow from a helicopter. CRREL operates a custom airborne light detecting and ranging (lidar) system that can be deployed in a helicopter-based pod (HeliPod). Data were collected with the HeliPod near existing USGS streamflow information stations on the Knik, Matanuska, Chena, and Salcha Rivers in both 2017 and 2018. Sites on the Tanana and Snow Rivers were added in 2018. In 2018, the HeliPod was modified to accommodate both a thermal infrared and a visible camera. The cameras were integrated with the flight management software to simultaneously acquire imagery with lidar. The Global Navigation Satellite System (GNSS) and inertial measurement unit (IMU) in the HeliPod were used to compute trajectories with precise position and orientation information needed for image orthorectification. The HeliPod sensors provide data for measuring river channel characteristics. Lidar can map the elevation of the water surface and thus be used to measure water-surface slopes and return intensity can be used to delineate the extent of the wetted river channel. Various approaches are currently being evaluated to estimate surface flow velocity from visible and thermal image time series. In this paper, we examine and compare water-surface elevation returns and slopes derived from the HeliPod lidar and report good agreement with measurements made using conventional field-based techniques.

Introduction

The USGS Alaska Science Center (ASC) presently operates 108 streamflow information stations distributed throughout Alaska (https://waterdata.usgs.gov/ak/nwis/current/?type=flow). As many of these stations are remote, considerable effort is needed to collect periodic measurements and maintain gages. Thus, developing remote sensing methods for measuring streamflow in this vast, largely inaccessible State is important for many reasons. Such a capacity could potentially augment and economize the current USGS hydrologic network in Alaska, reduce or eliminate risk to personnel during extreme events, and provide a better understanding of water fluxes in ungauged watersheds.

Motivated by these objectives, GSTL is pursuing innovative methods of inferring flow velocity and channel geometry from various types of remotely sensed data. Specifically, we are testing Particle Image Velocimetry (PIV)-based approaches for retrieving surface velocity vectors from time series of passive optical and thermal image data (Kinzel et al. 2017; Legleiter et al. 2017). To characterize river bathymetry, we are evaluating both established spectrally based depth retrieval algorithms applicable to clear-flowing streams (Legleiter et al. 2009), as well as a new inversion technique that involves using the governing equations of fluid flow to infer depth based on observations of water-surface elevation and velocity (Nelson et al. 2016). As we work toward these goals, we are collaborating with CRREL to perform sensor integration and acquire remotely sensed data and with the ASC to collect field-based measurements of velocity, depth, and discharge for verification.

The objective of this paper is to summarize our 2017 and 2018 field campaigns with a specific focus on our on-going efforts remotely sensing Alaskan rivers in the near-field. The 'near-field' designation is intended to distinguish this approach from parallel and complementary efforts of estimating river characteristics using satellite platforms (Bjerklie et al. 2018; Dai et al. 2018). In addition, this paper describes an approach to deriving river slope from lidar data acquired via a helicopter platform and compares these slope estimates to both stage data measured at a gaging station and to submersible pressure transducers distributed along one of the surveyed rivers.

Methods

HeliPod Data Collection and Processing

CRREL operates a lidar system that can be mounted on both fixed-wing and helicopter platforms. For helicopter-based surveys, the system is installed in a light-weight, easily mounted, external HeliPod that is Federal Aviation Administration (FAA) certified for operation on a Robinson R44 Raven II helicopter (Figure 1). The HeliPod provides both vibration stabilization and a weatherproof enclosure for the aerial survey instrumentation. In 2017, the payload included a Riegl VQ-580 lidar (1064-nanometers), an iXBlue ATLANS-C IMU and a FLIR 8343 Mid-wave infrared (MWIR) camera. In 2018, a Riegl VQ-480 (1550-nanometers) lidar was used and a Hasselblad A6D 100-megapixel optical camera was installed alongside the FLIR (Figure 1). Enhancements were made for the 2018 flights to allow direct georeferencing of both thermal and visible imagery. The NexTrack2 flight management system (FMS) used to navigate flight lines and trigger lidar acquisition was modified to provide precise event markers from the GNSS-IMU for geolocation and orientation of imagery. At present, image processing from the 2018 field campaign is on-going.

Figure 1. HeliPod mounted on R44 Raven II Helicopter and top view of 2018 HeliPod instrumentation payload

The aerial surveys conducted in 2017 and 2018 included study sites on the Knik, Matanuska, Chena and Salcha Rivers; additional sites on the Tanana and Snow Rivers were added in 2018 (Figure 2). The target flying height for the surveys was site specific, but a nominal flying height of 300 meters provided a laser swath width of 346 meters. Flight lines were spaced to ensure at least 50 percent overlap and were flown at a nominal airspeed of 26 meters/second. A field crew operated a GNSS base station at each site to assist in computing flight trajectories and to post-process ground control check points collected to assess the accuracy of the lidar survey.

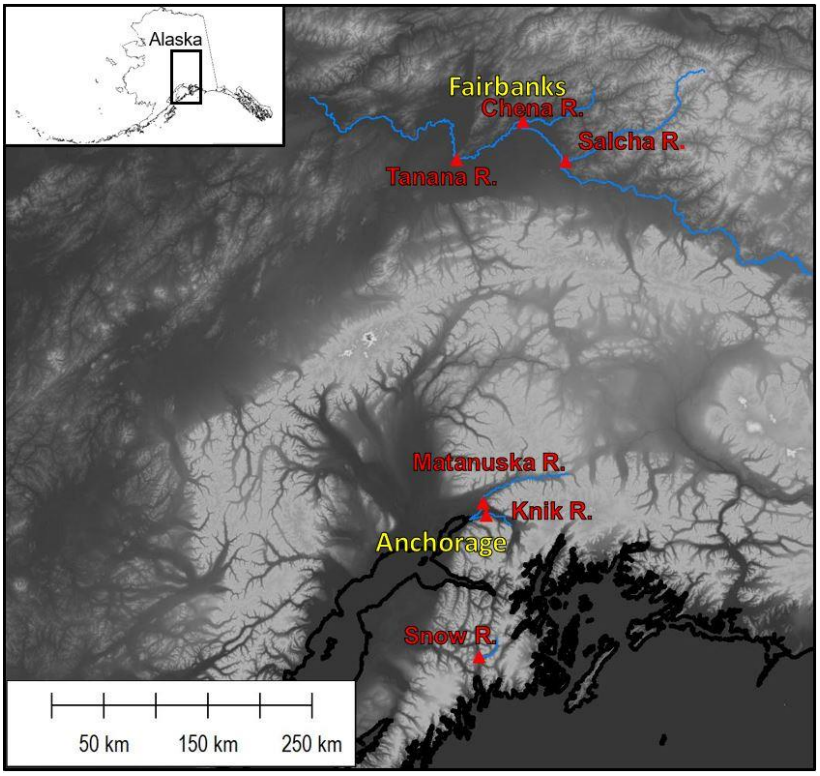

Figure 2. Location of the study sites

Lidar data were processed using iXBlue APPS software (trajectory solution), Riegl RiPROCESS (point cloud processing), Trimble Business Center (ground control), LP360 (quality assurance/quality control and accuracy assessment), and the Point Data Abstraction Library PDAL (bare earth extraction via a Simple Morphological Filter (Pingel et al. 2013), DEM and DSM creation). Final products included point clouds (LAZ v.1.2), a bare earth digital elevation model (GeoTIFF from PDAL-processed ground points), and an intensity digital surface model (GeoTIFF from PDAL-processed intensity values or reflectance). All products are referenced to NAD83(2011) EPOCH:2010/ NAVD88 GEOID12B and projected in UTM Zone 6N (meters) and are available via USGS ScienceBase data releases (Kinzel et al. 2019a; Kinzel et al. 2019b).

USGS streamflow information stations operated within the study reaches provided a continuous record of river stage or gage height at 15-minute intervals. The mean gage height and rated discharge at each of these stations during the date and time of lidar acquisition are given in Tables 1 and 2. Discharge and velocity measurements were collected with acoustic Doppler current profilers (ADCPs) and in most, but not all, sites closely coincided with the overflights.

For completeness and to provide a time average over the entire flight duration for all sites, Tables 1 and 2 contain the average values recorded at the gaging stations.

Seven submersible pressure transducers were positioned on the river bottom of the Tanana and Salcha sites in July 2018. At each site, an additional transducer was placed on the bank above water to correct for barometric pressure fluctuations. At the time of deployment, the bank position near each transducer and the water-surface elevation were measured with real-time kinematic GNSS equipment in the same horizontal and vertical datums as the lidar. The transducers collected a depth measurement every 15 minutes until they were recovered in October 2018. The water-surface elevation at 15-minute intervals was computed by adjusting the water elevation measured at deployment by the difference between the depth measured at the time the sensor was deployed and each of the subsequent depth measurements recorded by the transducer.

Table 1. List of study sites and mean discharge and gage height in local gage datum during the 2017 aerial surveys

Study Site	Date and Time of Aerial Survey (Alaska Daylight Time)	Mean Discharge (m^3/s)	Mean Gage Height (m)
Knik	8/8/17 (10:09AM– 11:47AM)	780	3.45
Matanuska	8/8/17 (1:36 PM – 2:34 PM)	278	2.76
Chena	8/9/17 (4:37 PM – 5:08 PM)	38	0.27
Salcha	8/9/17 (8:25 PM – 9:27 PM)	53	2.12

Table 2. List of study reaches and mean discharge and gage height in local gage datum during the 2018 aerial surveys.

Study Site	Date and Time of Aerial Survey (Alaska Daylight Time)	Mean Discharge (m^3/s)	Mean Gage Height (m)
Knik	8/27/18 (1:25PM – 2:25 PM)	647	3.31
Matanuska	8/27/18 (5:09 PM – 6:27 PM)	379	2.73
Tanana	8/29/18 (11:11AM – 2:13 PM)	1843	3.04
Chena	8/29/18 (5:23 PM – 5:55 PM)	129	1.42
Salcha	8/31/18 (9:47AM – 10:57 AM)	228	3.20
Snow	9/1/18 (11:42 – 1:35 PM)	31	2.18

Deriving Lidar Water-surface Elevation Maps

Water-surface elevation maps and profiles were extracted from the lidar using the following workflow. The lidar intensity values were used to identify the extent of the wetted channel and guide manual digitization of a bounding polygon. The lidar points that fell within the polygon and were within a range of upstream and downstream water-surface elevations manually identified in the point cloud were selected from all the LAZ files. The resulting lidar point cloud was filtered to remove any non-water returns (i.e. islands, sandbars) and a spatial grid was generated with a binning algorithm in the add-on lidar module for Global Mapper v. 19.0.2

(Blue Marble Geographics 2017). The binning algorithm places a defined grid over the point cloud and the average of the point elevations in each bin or grid cell is computed. We allowed the software to automatically select the optimal grid spacing. Gaps in the grid cells are filled using an inverse weighted distance algorithm. The result is an interpolated water-elevation surface raster within the digitized channel area (Figure 3). The Global Mapper software was used to digitize a centerline along the raster and extract a water-surface elevation profile in the streamwise direction (Figure 3). The lidar-derived profiles and slopes can be compared amongst rivers (Figure 4).

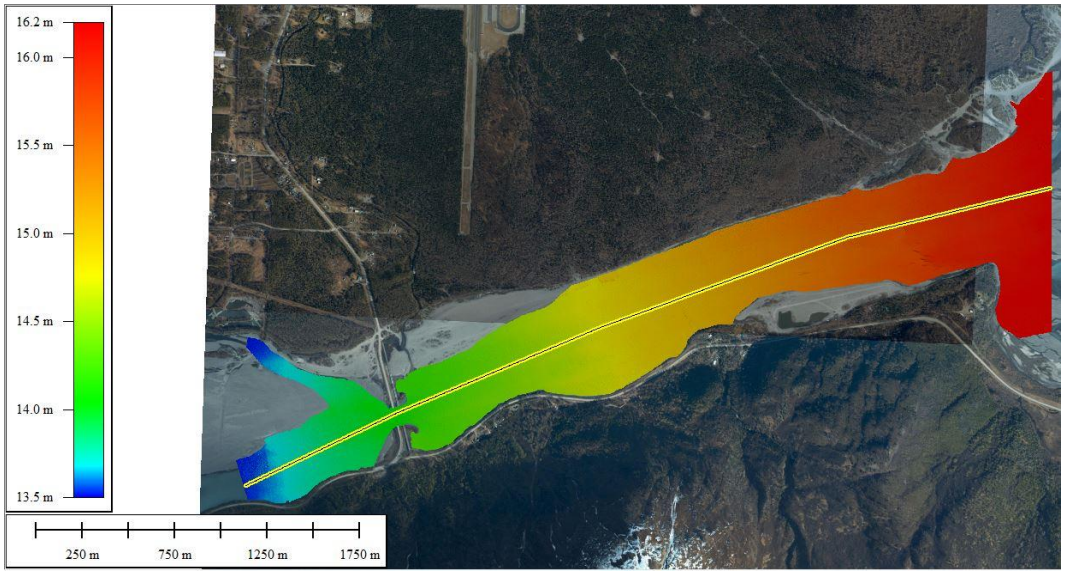

Figure 3a. Map of interpolated lidar water-surface elevation and profile (yellow) for the Knik River in 2017

Figure 3b. Map of interpolated lidar water-surface elevation and profile (yellow) for the Chena River in 2017

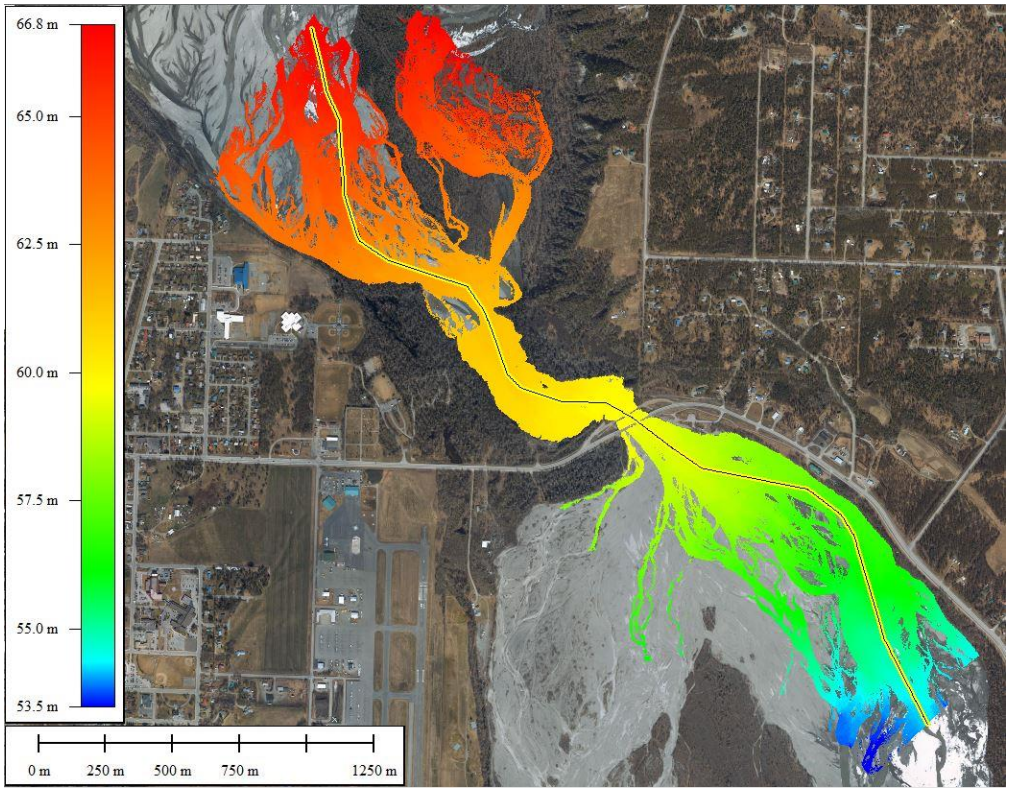

Figure 3c. Map of interpolated lidar water-surface elevation and profile (yellow) for the Matanuska River in 2017

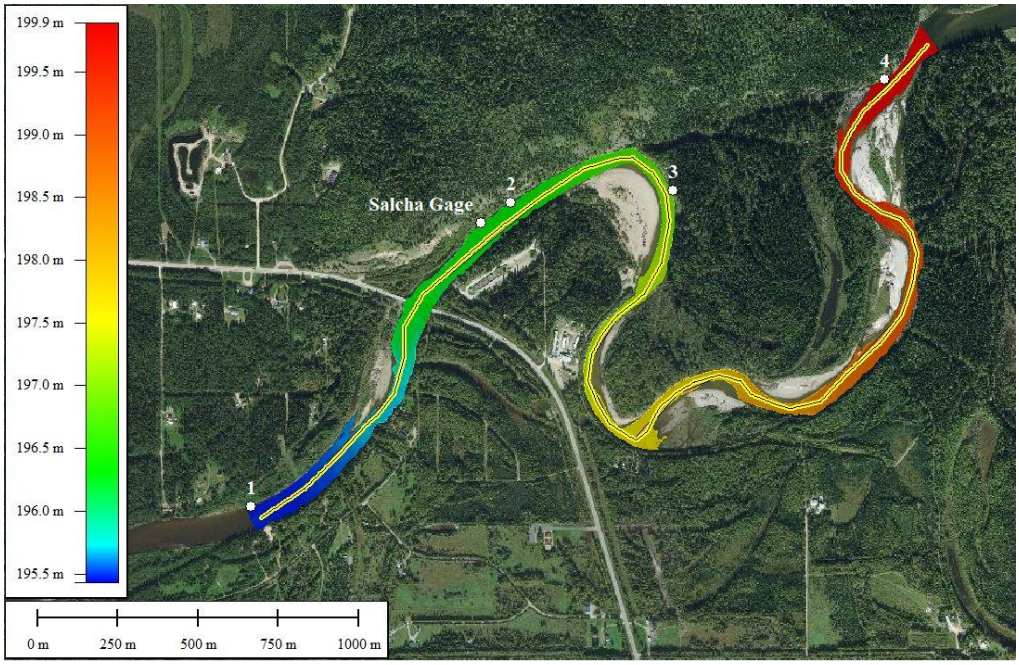

Figure 3d. Map of interpolated lidar water-surface elevation and profile (yellow) for the Salcha River in 2017. The location of the streamflow information station and pressure transducers (1-4) installed in 2018 are also shown.

Results

Lidar Water-surface Elevation Maps

Near-infrared wavelength lidar returns from water are typically characterized by a high number of dropouts (no data returned to the detector) and by low backscatter energy. This is due to the strong attenuation of near-infrared light by water, which results in minimal penetration of the laser pulses into the water such that most of the laser energy is returned from the water surface (Höfle et al. 2009). Additional factors that can influence the number of returns include: laser power, flying height, and incident angle. To compute the spatial density of lidar returns for each river reach surveyed, we divided the total number of lidar returns collected in the channel by the digitized area of the river reach. For the Knik and Matanuska lidar surveys collected in 2017, the quantity and spatial density of water returns were high, approximately 7 and 27 points, respectively, per square meter of channel area. These large, glacially fed rivers carried a large amount of suspended material that reflected laser pulses back to the lidar detector. Schmugge et al. (2002) reported a small increase in the reflection of infrared light with turbidity. The water surface of the Matanuska was also relatively rough, which also might contribute to the high spatial density of returns. The smaller Chena and Salcha Rivers were, by comparison, much clearer and laser energy was more commonly absorbed, which resulted in both having a relatively sparser spatial distribution of water returns in the river channel: 0.3 and 0.6 point per square meter of channel area, respectively.

Comparison of Lidar Water-surface Elevations (2017 and 2018)

The 2017 lidar water-surface elevations extracted from the profiles in Figure 3 were normalized and plotted in Figure 4. The steepest river was the braided Matanuska (0.003) and the most gradual slope, the meandering Chena (0.0003). We used the same methodology described above to post-process the lidar returns collected in 2018. For brevity, we present an example of a multi-year comparison of lidar water-surface elevations along the Salcha River. As indicated in Tables 1 and 2, the mean discharge and gage height of the Salcha were considerably different between the two lidar surveys. The gage height recorded at the streamflow station (Figure 3d) was 1.08 meters greater in 2018 than 2017 (Table 1 and 2). The elevation of the lidar points returned from the water surface near the gage in 2018 was 1.06 meters greater than in 2017.

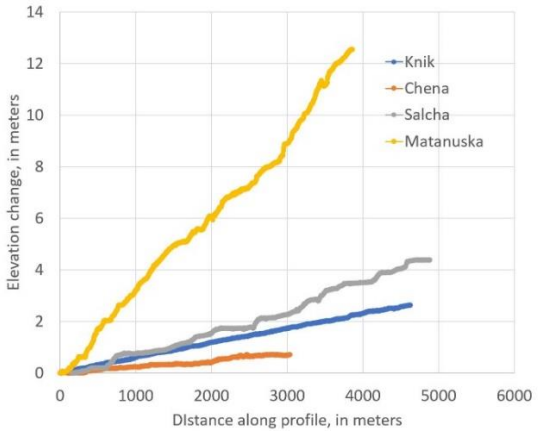

Figure 4. Lidar derived water surface slopes measured in 2017

Comparison of Lidar Water-surface Elevations with Submersible Pressure Transducer Elevations (2018)

Seven submersible pressure transducers were deployed along the Salcha River in July 2018, but only five were recovered in October. Of the five that were recovered, one yielded suspect data that did not correlate with the trends observed in the other transducers. Thus, we used four transducers installed in July for comparison to the lidar elevations (Figure 3d). The coincident elevations determined from the lidar and the transducers are shown in Table 3. The transducer data are available via USGS ScienceBase data release (Kinzel et al. 2019c). The lidar-measured water-surface elevation was consistently less than that computed from the transducers. However, it is important to emphasize that lidar makes a direct measurement of the range to the water while the transducer elevations were computed from two distinct measurements. One measurement is the water-surface elevation at the time the transducer was deployed. The second measurement is the hydrostatic pressure on the submerged transducer, which was then corrected for barometric pressure changes and converted to a corresponding water depth. The vertical precision of the GNSS water-surface surveys was approximately 0.04 meter, and the precision of the depth measured by the transducers is reported by the manufacturer to be +/- 0.01 meter. The installed transducers were also positioned directly on the river bottom, so sedimentation or erosion could have influenced the measurements. When the transducers were recovered in October 2018, the water-surface elevation was surveyed again. Check points indicated that the vertical precision of the lidar is consistent with the precision of the GNSS ground surveys. However, errors could have been introduced by water-surface irregularities or the lidar interpolation process. Taken together, while we observed relatively small differences in the elevations collected by the lidar and pressure transducers, some differences are to be expected given the precision of the techniques. In addition, errors of this magnitude had a negligible influence on the calculation of reach slopes.

Table 3. Lidar and submersible pressure transducer water-surface elevation measured at the Salcha River at the time of the 2018 lidar survey

Transducer Number	Transducer Water-surface Elevation (m)	Lidar Water-surface Elevation (m)	Transducer – Lidar Elevation (m)
1	196.39	196.36	0.03
2	197.46	197.4	0.06
3	198.11	198.10	0.01
4	200.79	200.78	0.01

Conclusions

In this paper, we provided technical details of the instrumentation and results from ‘near-field’ remote sensing campaigns conducted in 2017 and 2018 along several rivers in Alaska using the CRREL HeliPod system. Specifically, we focus on evaluating the lidar data obtained from the water surface as a first step toward collecting the hydraulic variables necessary for remotely sensing river discharge. The quantity and spatial density of lidar returns varied among the rivers surveyed with a maximum of 27 points per square meter of channel area in the Matanuska River

and a minimum of 0.3 point per square meter on the Chena River in 2017. Continuous water-surface elevation maps were interpolated from the lidar returns located in the channels. Water-surface profiles were extracted from the maps and the slopes for the various rivers were compared. The slopes varied over an order of magnitude and ranged between 0.003 for the Matanuska River to 0.0003 for the Chena River. Comparison of lidar returns collected in 2017 and 2018 along the Salcha River showed the ability of the serial lidar surveys to detect the over 1-meter increase in water-surface elevation measured from 2017 to 2018 at the streamflow gaging station. A series of pressure transducers installed along the Salcha River in 2018 recorded a longitudinal profile of water-surface elevations that was coincident with the 2018 lidar survey. The elevations were in good agreement with those measured by lidar. In summary, the 'near-field' remote sensing approach to determining water-surface elevation produced results that are comparable both in terms of detecting differences in gage height or stage between aerial lidar surveys and measuring water-surface profiles and slopes that are consistent with submersible pressure transducers.

Acknowledgements

The authors would like to thank Heather Best, Karenth Dworsky, and Johnse Ostman (USGS-AK) for assistance in collecting streamflow measurements. John Fulton and Mike Kohn (USGS-CO) installed, surveyed, and processed the pressure transducer data. Any use of trade, firm, or product names is for descriptive purposes only and does not imply endorsement by the U.S. Government.

References

Bjerklie, D.M., Birkett C.M., Jones J.W., Carabajal C., Rover J.A., Fulton J.W., and Garambois P.A. 2018. "Satellite Remote Sensing Estimation of River Discharge: Application to the Yukon River Alaska," Journal of Hydrology, 561: 1000-1018.

Blue Marble Geographics, 2017. Global Mapper, v 19.0.2 with LiDAR Module, http://www.bluemarblegeo.com/products/global-mapper.php

Dai, C., Durand, M., Howat, I.M., Altenau, E.H., and Pavelsky, T.M. 2018. "Estimating river surface elevation from ArcticDEM," Geophysical Research Letters, 561: 3107-3114.

Höfle, B., Vetter, M., Pfeifer, N., Mandlburger, G., and Stötter, J. 2009. "Water surface mapping from airborne laser scanning using signal intensity and elevation data," Earth Surface Processes and Landforms, 34: 1635–1649.

Kinzel, P.J., Legleiter, C.J., Nelson, J.M. and Conaway, J., 2017. "Remote measurement of surface-water velocity using infrared videography and PIV: a proof-of-concept for Alaskan rivers," E-proceedings of the 37th IAHR World Congress August 13 – 18, 2017, Kuala Lumpur, Malaysia, 9 p.

Kinzel, P.J., Legleiter, C.J., LeWinter, A.L., and Gadomski, P.J., 2019a, Topographic LiDAR surveys of rivers in Alaska, August 8-9, 2017, U.S. Geological Survey data release. https://doi.org/10.5066/P9IQCVJU

Kinzel, P.J., Legleiter, C.J., LeWinter, A.L., Gadomski, P.J., and Filiano, D.L., 2019b, Topographic LiDAR surveys of rivers in Alaska, August 27 - September 1, 2018, U.S. Geological Survey data release. https://doi.org/10.5066/P9A4YP05

Kinzel, P.J., Fulton, J., and Kohn, M. 2019c. Water-surface elevations derived from submersible pressure transducers deployed along the Salcha River, AK, July – October 2018, U.S. Geological Survey data release. https://doi.org/10.5066/P95L1YXY

Legleiter, C.J., Roberts, D.A. and Lawrence, R.L., 2009. “Spectrally based remote sensing of river bathymetry,” Earth Surface Processes and Landforms, 34: 1039-1059.

Legleiter, C.J., Kinzel, P.J., and Nelson, J.M. 2017.“Remote measurement of river discharge using thermal particle image velocimetry (PIV) and various sources of bathymetric information,” Journal of Hydrology, 554: 490-506.

Nelson, J.M., Kinzel, P.J., McDonald, R.R. and Schmeeckle, M.W. 2016. “Noncontact methods for measuring water-surface elevations and velocities in rivers: Implications for depth and discharge extraction,” in RiverFlow 2016, Constantinescu, Garcia, and Hanes, eds., Taylor and Francis, London, p. 637-645.

Pingel, T.J., Clarke, K.C., and McBride, W.A. 2013. “An improved simple morphological filter for the terrain classification of airborne LIDAR data,” ISPRS Journal of Photogrammetry and Remote Sensing, 77: 21-30.

Schmugge T.J., Kustas W.P., Ritchie J.C., Jackson T.J., and Rango A. 2002. “Remote sensing in hydrology,” Advances in Water Resources, 25(8–12): 1367–1385.

Operationalizing Small Unoccupied Aircraft Systems for Rapid Flood Inundation Mapping and Event Response

Frank L. Engel, Geographer, U.S. Geological Survey, San Antonio, Texas, fengel@usgs.gov
Rogelio Hernandez, Hydrologic Technician, U.S. Geological Survey, San Antonio, Texas, rhernandez@usgs.gov

Abstract

Small Unoccupied Aircraft Systems (sUAS) offer the capability to collect rapid and accurate aerial survey data during flood response. The rapid collection of aerial flood data can potentially enable scientists to produce detailed geospatial products and related datasets in time for decisional support. A workflow for sUAS event response before, during, and after flood events is discussed.

Introduction

Flood impacts across the United States from 1988 to 2018 have led to 441 fatalities and nearly $114 billion in losses over that same period (National Oceanic and Atmospheric Administration 2019a). In 2011 alone, flooding caused a reported $5.7 billion in direct damages and 12 reported fatalities in the United States (National Oceanic and Atmospheric Administration, 2019b). Although the effects of floods on people are impossible to completely mitigate, and there is no way to guarantee protection of property, the U.S. Geological Survey (USGS) and other federal, state, and local agencies have demonstrated that the economic impacts and loss of life associated with flooding can be greatly reduced with more informed flood warning systems (EASPE 2002). Often, these flood warning systems employ flood inundation mapping and modeling efforts to gain insight for flood mitigation and event response. Small Unoccupied Aircraft Systems (sUAS) offer the capability to collect rapid and accurate aerial survey data that can be used in these flood inundation models. Rapid collections of aerial flood data (hereinafter as “data collects”) can potentially enable scientists to produce detailed flood inundation maps and related datasets in time for decisional support by local emergency responders, flood managers, and others.

The use of sUAS for hydrologic-data collection provides a cost-effective means to improve the quality and timeliness of flood mapping and modeling efforts through collection of high resolution (typically < 10 cm) imagery over areas tens of acres in size. Survey teams of as few as 1–2 people equipped with sUAS can be deployed during flood events to collect high resolution aerial imagery data for use in flood models (Wang 2015). The ability to put “eyes in the skies” at precise locations during flood events can be beneficial for emergency managers who need vital situational awareness information to aid in protection of life and property (Restas 2015). In addition to situational awareness and near real-time mapping of flooding extents, sUAS can produce a range of invaluable data such as images, video, multispectral, and thermal video. These data are being collected for validation of hydraulic models and science support among other things. Small UAS are also being used to map streamflow and velocities directly with computer vision techniques (Lewis et al. 2018; Tauro et al. 2016).

This paper presents a workflow for operationalizing sUAS data collection prior to, during, and after flooding events. Recommendations for how best to mobilize and perform required data collects as a part of flood event response are given. Specifically, perspectives on Federal Aviation Administration (FAA) and flight plan requirements, safety concerns, and data management of longer term projects are shared. Also, examples of the benefits of rapid event response and situational awareness are presented. Lastly, some perspectives on the establishment of long-term project management infrastructure, as well as lessons learned from our experiences with sUAS for event response are discussed.

Mission Planning and Operations

In the United States, national airspace authority and control is maintained by the Federal Aviation Administration (FAA). Prior to any sUAS flight, the authority to fly must be established. Currently, FAA-certified remote pilots can fly in Class G airspace below 400 feet above ground level (ft AGL) so long as the sUAS is operated more than the required distance away from the nearest airports (5 statute miles in most cases), visibility is greater than 3 statute miles (SM), and sUAS operations maintain at least a 500 ft vertical and 2,000 ft horizontal separation between the sUAS and clouds based on Title 14 of the Code of Federal Regulations, Part 107 (Electronic Code of Federal Regulations 2019; “Part 107 Rules” hereinafter). Additionally, remote pilots must maintain visual line of sight (VLOS) with the sUAS at all times. There are instances where flight authority in other controlled airspace can be obtained (such as during an emergency response), but this requires an application process for a waiver of specific requirements of the Part 107 Rules. Within the Department of Interior, there are means for gaining standing FAA approval for flight operations outside of Part 107 rules, including emergency response flights in temporary flight restriction (TFR) areas, night operations, and flights above the 400 ft AGL Part 107 Rules ceiling. For example, in the case of sUAS flights in support of the 2018 Kilauea volcanic eruption, waivers were approved for sUAS flights exceeding both the VLOS and the 400 ft AGL ceiling within the TFR area.

In river reaches where flooding is expected, or where there is an existing project is in place, pre-planning allows for quick response flights when the event occurs. A common approach is to pre-plan flight areas where authority exists automatically as indicated in Part 107 rules, for example in Class G airspace below 400 ft AGL. For agencies in the Department of Interior (including USGS), this preplanning is required and is documented in a Project Aviation Safety Plan (PASP) which states most details of planned flights for a particular area (U.S. Department of the Interior 2019). A PASP can be designed for single flight missions, or as a standing document for multiple flights over a specific area. Regardless of requirements, generating PASP is a valuable exercise, and can also aid in fast-tracking the FAA Part 107 Rules Waiver process if needed for a mission. This preplanning approach was recently used to safely collect aerial streamflow data during a flood using the Large-Scale Particle Image Velocimetry method (Lewis et al. 2018) during severe flooding in October 2018 on the Llano River in central Texas. The mission PASP was put in place prior to the event, allowing the sUAS crew to deploy within hours and capture the extreme flooding conditions (Figure 1).

During sUAS flight missions, the highest priority is safety. Flights must be done in a manner that protects people, property, and the aircraft and its payload. Once on site, preflight examination of the immediate airspace for ground and aerial hazards can prevent most accidents before they occur. Suitable takeoff and landing space may be difficult to find when attempting to fly during large flood events. By using a visual observer(s) (VO)—a crew member

who provides an extra set of eyes on the flight area to watch for ground and aerial hazards—sUAS pilots can promote safe flight by mitigating risks associated with flying in more confined or dynamic environments.

Typical sUAS science missions will produce hundreds of individual images encompassing the flight area. It is important to consider how data will be managed from initial collection to when the data are publicly released as required by the USGS Public Access Plan (U.S. Geological Survey 2016). Processing steps, like Structure from Motion (SfM) photogrammetry (Fonstad et al. 2013), can produce multiple gigabytes of digital data for even small flight area missions. In the field, we implement a "rolling backup" approach where numbered data cards are immediately removed from the sUAS after landing during a mission.

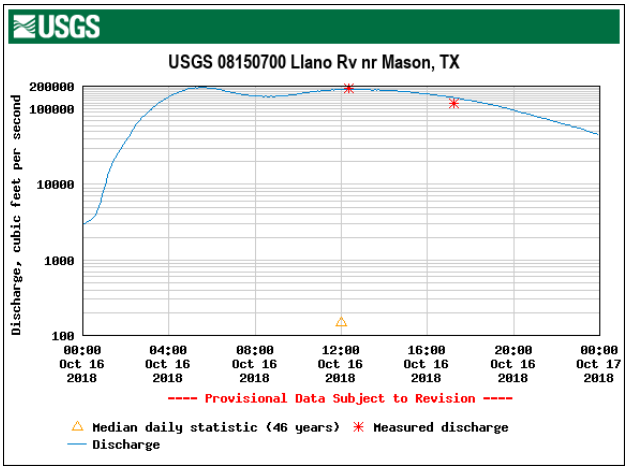

Figure 1. Flood hydrograph of the Llano River near Mason, Tex. for event October 16, 2018, where sUAS was used to measure streamflow (U.S. Geological Survey 2019). Red asterisks indicate field measurements. The second measurement at 17:13 was acquired with sUAS.

In the field, the contents of data cards are first copied to a laptop computer and then to a solid-state hard drive. Once the contents of the data card have been successful copied and the contents have been verified, the next numbered data card in sequence is used in the subsequent sUAS flight. During most missions, we travel with at least eight data cards, enabling sUAS crew to fly eight missions without fear of overwriting any one data card. Upon returning to the office, the collected data are copied to a network drive that is regularly backed up. This rolling backup procedure becomes invaluable when flight conditions are dynamic, or the mission requires multiple or continuous flights. In missions that require rapid data handling and processing, assignment of one crew member as "data handler" can enable quick turnaround on provisional products. The data handler's role on a sUAS crew is to operate a field laptop, facilitate the rolling backup process, and process initial data into the maps needed for emergency responders. Often, initial processing is done at a lower precision to enable quick turnaround of data products for decisional support, many times within hours of the sUAS flight; full quality processing of the datasets are generated later for analysis and publication. For example, in 2018 Kilauea volcanic eruption, orthomosaic aerial maps and terrain models of the lava flow field were immediately processed in the field by the data handler, and provisional maps delivered to the Forward Operating Base (FOB) for evaluation within 2 to 5 hours from when the sUAS began flying. In at least one case this level of turnaround was fast enough that subsequent requests for specific flights were made from the FOB in the same day as the previous data collects.

In some cases, sUAS flights during events can be used to provide valuable situational awareness (SA) to emergency responders. The primary objective of emergency responders is the protection of life and property during events. Small UAS can provide real-time “eyes in the skies” to view ground conditions in areas that are either difficult, unsafe, or impossible to reach over ground. If flights are planned as a part of providing SA, extra steps should be taken to ensure safe flight. Planning should include providing room and space around the remote pilot so that they can focus on flight. One approach is to use either a separate monitor or live feed system to clone the view of the ground control system (GCS) display during flight. The power of a such a system is hard to overestimate. During the response to the 2018 Kilauea volcanic eruption, the USGS was tasked to provide advanced SA of the developing lava flow field in a 24/7 rotation for several weeks. To ensure safe flight conditions, a live streaming setup was used to broadcast the Ground Control Station view during flight to a FOB on site. Emergency responders were in radio communication with the sUAS crew and could make requests for where to deploy sUAS assets. During flight, responders remotely viewing the live stream often made SA requests over the radio or cellular phone even while the sUAS was airborne.

Conclusion

This paper presents a workflow for planning operationalization of sUAS for flood mapping work prior to, during, and after flooding events. Small UAS provide a low-cost and effective means to rapidly acquire hydrologic data to improve the quality and timeliness of flood mapping, as well as provide real-time situational awareness in flooding emergencies. Through careful preplanning, it is possible to respond quickly to events, potentially providing datasets in time for decisional support.

References

EASPE, Inc. 2002. "Use and benefits of the National Weather Service river and flood Forecasts," accessed March 14, 2019, at http://www.nws.noaa.gov/oh/ahps/AHPS Benefits.pdf.

Electronic Code of Federal Regulations. 2019. "Small unmanned aircraft systems, Code of Federal Regulations Title 14 C.F.R Part 107," accessed February 8, 2019 at: https://ecfr.io/Title-14/pt14.2.107.

Federal Aviation Administation. 2017. "Aeronautical information Manual—Official guide to basic flight information and ATC Procedures," U.S. Department of Transportation, accessed February 8, 2019, at https://www.faa.gov/air_traffic/publications/media/AIM.pdf.

Fonstad, M.A., Dietrich, J.T., Courville, B.C., Jensen, J.L., and Carbonneau, P.E. 2013. "Topographic structure from motion: a new development in photogrammetric measurement," Earth Surface Processes and Landforms, 38(4), 421–430. doi: 10.1002/esp.3366

Lewis, Q.W., Lindroth, E.M., and Rhoads, B.L. 2018. "Integrating unmanned aerial systems and LSPIV for rapid, cost-effective stream gauging," Journal of Hydrology, 560, 230–246. doi: 10.1016/j.jhydrol.2018.03.008.

National Oceanic and Atmospheric Administration, 2019a, National Centers for Environmental Information (NCEI)— U.S. Billion-Dollar Weather and Climate Disasters [Billion-dollar events to affect the U.S. from 1988 to 2018 (CPI-Adjusted)]: NCEI database, accessed March 15, 2019, at https://www.ncdc.noaa.gov/billions/summary-stats.

National Oceanic and Atmospheric Administration, 2019b, National Centers for Environmental Information (NCEI)— U.S. Billion-Dollar Weather and Climate Disasters [Billion-dollar events to affect the U.S. in 2011 (CPI-Adjusted)]: NCEI database, accessed March 15, 2019, at https://www.ncdc.noaa.gov/billions/summary-stats.

Restas, A. 2015. "Drone applications for supporting disaster management," World Journal of Engineering and Technology, 03(03), 316–321. doi: 10.4236/wjet.2015.33C047.

Tauro, F., Petroselli, A., and Arcangeletti, E. 2016. "Assessment of drone-based surface flow observations," Hydrological Processes, 30(7). doi: 10.1002/hyp.10698.

U.S. Department of the Interior. 2019. "OPM-11 DOI Use of unmanned aircraft systems (UAS) (updated)," accessed February 5, 2019, at: https://www.doi.gov/aviation/pressreleases/updated-opm-11-doi-use-unmanned-aircraft-systems-uas.

U.S. Geological Survey. 2016. "Public access to results of Federally funded research at the U.S. Geological Survey—Scholarly publications and digital data," accessed February 13, 2019, at https://www2.usgs.gov/quality_integrity/open_access/downloads/USGS-PublicAccessPlan-APPROVED-v1.03.pdf.

U.S. Geological Survey, 2019, "USGS 08150700 Llano River NR Mason TX, in USGS water data for the Nation: U.S. Geological Survey National Water Information System database, accessed February 8, 2019, at http://dx.doi.org/10.5066/F7P55KJN." [Site information directly accessible at https://waterdata.usgs.gov/nwis/uv?site_no=08150700.]

Wang, Y. 2015. "Advances in remote sensing of flooding," Water, 7(11), 6404–6410. doi: 10.3390/w7116404.

Reservoir Sedimentation & Sustainability

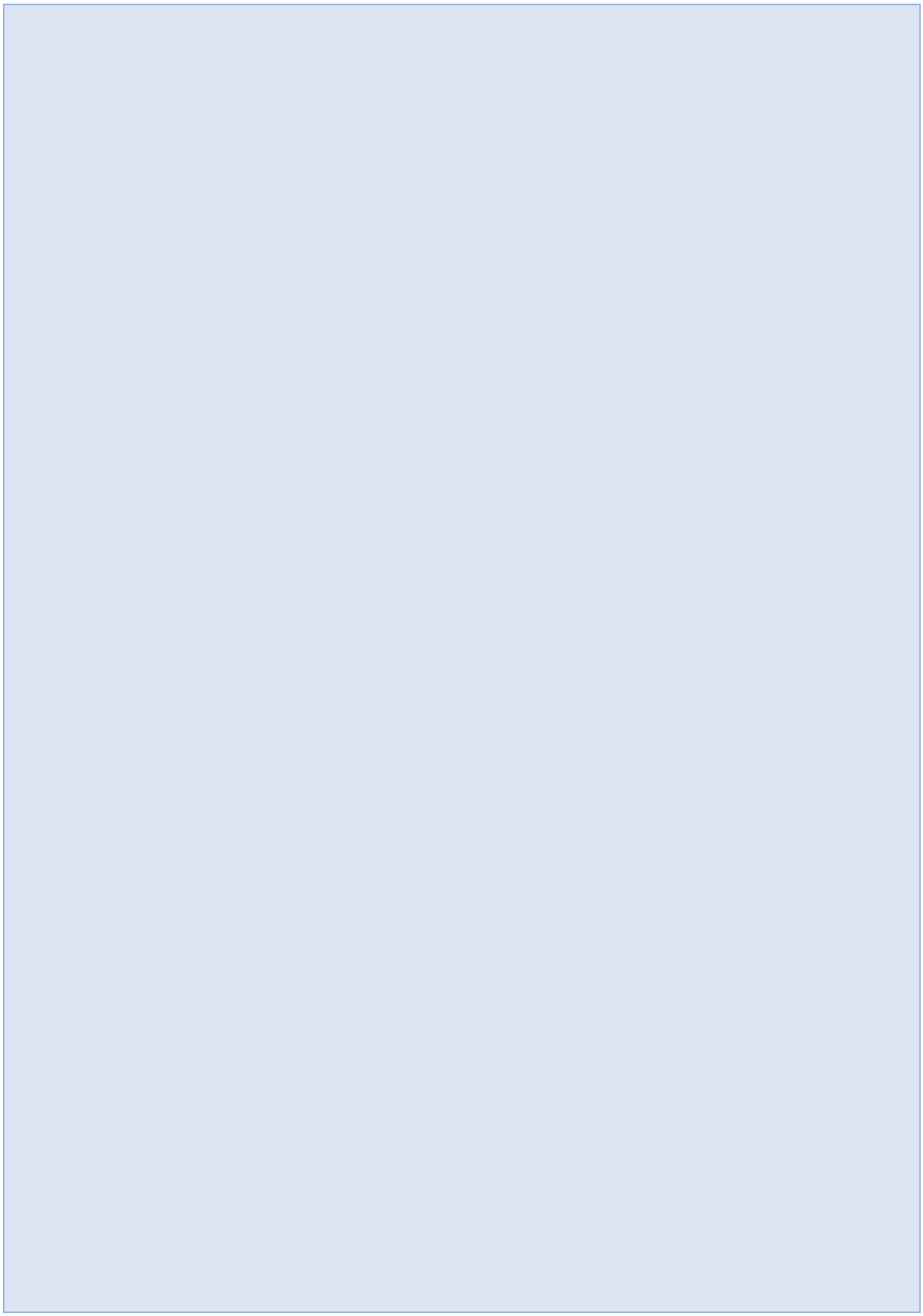

Balanced Sediment Throughput Reservoir Dredging

Douglas M. Raitt, PE, PMP, Engineering Manager – Construction, Denver Water, Denver, Colorado, douglas.raitt@denverwater.org

Abstract

Historically, a design life of 50, 100 or even several hundred years was an acceptable timeline for a reservoir's economic life. Little thought was given to the disposition of the facility at the end of that lifespan, either in the scope of removal from service or, the challenges to securing an alternate replacement. Consequently, many reservoirs have reached the end of their useful life, or will in the foreseeable future, and the realized cost of their retirement is now before us. What is becoming evident is that the replacement of existing reservoir facilities is far costlier and more environmentally detrimental than was ever envisioned. It is now the responsibility of today's facility operators and water resource professionals to reassess the current approach to reservoir preservation and create a new environmentally responsible and sustainable practice to ensure the conservation of existing reservoir facilities. One of the biggest threats to reservoir sustainability is the accumulation of sediment in the reservoir pool that ultimately reduces capacity and impairs the operation of the facility to the point that retirement must be considered.

This paper provides a sustainable approach to reservoir sediment management that stabilizes the volume of existing sediment deposits and minimizes the reduction in capacity that would normally occur without active intervention. Specifically, the process provided in this approach utilizes a hydraulic dredge to equalize the mass of sediment entering the reservoir with the mass of sediment in downstream outflows by synchronizing the sediment slurry discharge from an operating hydraulic dredge with the unregulated suspended sediment release from the reservoir outlet system. The system utilizes remote instrument stations located on inflow streams to the reservoir and remote downstream instrument stations that collect data used by the dredge control system to adjust the dredge mass flow output to match the combined downstream sediment mass outflow with reservoir sediment mass inflows.

The fundamental change to reservoir management that this system requires is the equalization of sediment inflows and outflows over an appropriate timeframe, as if the reservoir is effectively indiscernible in the downstream water course. Current regulations and environmental policies discourage the direct discharge of reservoir sediment into "Waters of the US". Regulations indirectly encourage the reduction in downstream turbidity that occurs with any reservoir that impounds sediment. Any new active reservoir operational activity that might increase the sediment content of the release and might affect adapted downstream vertebrate and invertebrate species is restricted. What is often not considered is the long-term consequence of accepting reductions in sediment throughput for stream and river courses throughout watershed systems and, ultimately, the relatively uncontrolled release of sediment deposits that will occur when the forced retirement of reservoirs is required. Use of the Balanced Sediment Throughput Reservoir Dredging system provides an alternative for sediment management that allows existing reservoirs to remain in service for a significantly increased period, will restore

downstream ecosystems, and will prevent costly and unnecessary replacement of facilities that could otherwise be preserved.

Specific Solution Topic

The principal benefit of the process is that it would allow the direct discharge of excavated sediment to the downstream channel immediately below the reservoir with minimal ecosystem impact since the original upstream conditions are replicated. The upstream and downstream instrument systems provide real time data collection to ensure target sediment concentrations are maintained. By matching the sediment content of reservoir inflows and outflows over the selected operational interval, the effect of the reservoir on water quality is minimized while the benefits of storage are preserved.

The process is scalable and can be tailored to a variety of reservoir configurations. The process can be utilized to remove a large fraction of sediment inflows that enter the reservoir pool and extend the service life of the reservoir. The use of a hydraulic dredge allows for the efficient removal of submerged sediment deposits from shallow deposits as well as those over 100 feet in depth. Excavated sediment can be transported over many miles by pipeline with properly sized and spaced booster pumps. Dredging can also be suspended during critical periods, such as spawning windows for aquatic vertebrate species. It can also be increased during high river-flow periods if the total sediment throughput is balanced for the target period of operation (Specific Solution Requirements No. 7).

Technical Description of Method

The proposed utilizes a system of upstream and downstream remote instruments that provide inputs to a control system that allows equalization of reservoir sediment inflows and outflows by supplementing the normal outlet works sediment discharge with slurry discharged from a hydraulic dredge operating on the reservoir.

The rate of flow of runoff for each stream flow entering the reservoir can be measured by a stage recorder or similar stream flow measuring instrument. That data can be transmitted via a powered transmitter to a central data receiving instrument. A measurement of the amount of particulate sediment in each stream flow entering the reservoir inflow can be indirectly measured using an instrument that measures the suspended solids or turbidity of the water column. This instrument can be a turbidity meter, optical backscatter sensor, acoustic Doppler current profiler (ADCP)[i], or a similar instrument that indirectly measures the solids content of water in which it is immersed. The output of this instrument can be calibrated to the corresponding suspended solids carried by the downstream flow with a sampling program that provides direct measurements of sediment loads for the corresponding stream flow rate and instrument reading[ii]. Sediment bed loads that correspond to various river stages can be estimated through a sampling program and incorporated in total sediment inflow rating curves for measured tributary flows.

The instrument used to indirectly measure the suspended sediment load in the selected upstream flow path entering the reservoir can be suspended from an anchored floating pontoon or barge. A photovoltaic power supply can be used to provide power to the floating instruments. A transmitter sends the data to a central data receiving instrument.

The flow released from the reservoir is generally equal to the release rate through the outlet works of the reservoir plus the flow released over the spillway of the dam, less any diversions. The combined flow rate released from the dam can computed using a stage recorder located downstream of the dam and converting the output to a flow rate based on rating curves developed from measured flow data. That flow rate data can be transmitted via a powered transmitter to a central receiving instrument.

The amount of sediment in the downstream flow can also be indirectly measured using a similar approach to that used for upstream inflows. The instrument used to indirectly measure the sediment load in the downstream flow path can be shore mounted or suspended from an anchored floating pontoon or barge. A photovoltaic power supply can be used to provide power to the downstream instruments. A transmitter can send the collected data to a central data receiving instrument.

The dredge can be initially positioned in the reservoir at the leading edge of the accumulated sediment deposit. The main dredge pump is started, and reservoir water is drawn into the discharge pipeline to prime the system. The rotating cutterhead is lowered into position and the sediment and water mixed slurry is introduced into the pipeline. The slurry is then transported under pressure to the point of discharge downstream of the dam (See Figure 1).

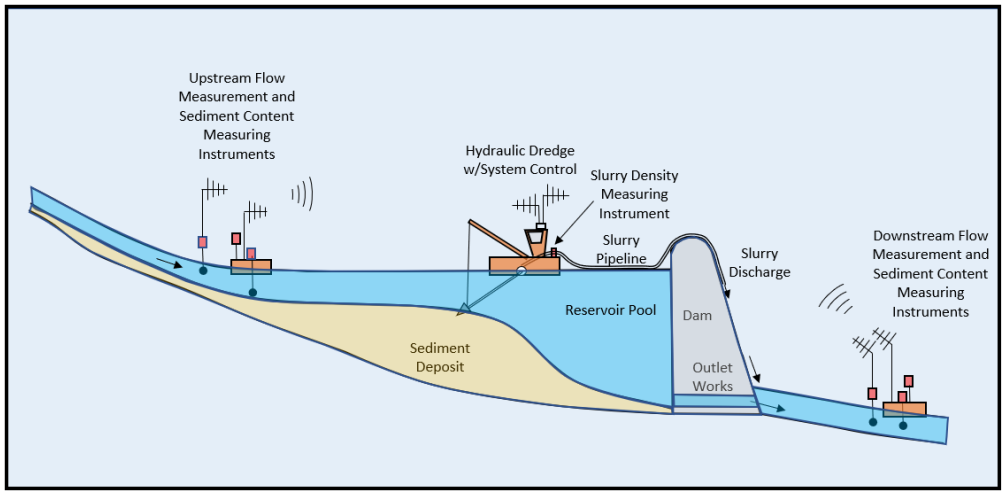

Figure 1. Balanced Sediment Throughput Reservoir Dredging System

The concentration of the sediment in the slurry can be measured with a radiometric non-contact density measurement instrument. The flow rate of the slurry through the dredge pipeline is determined by the operating speed control of the dredge pump and can be measured with a flowmeter. The density or concentration of solids in the slurry can be modulated by adjusting the operating speed of the dredge pump and adjusting added reservoir water to the dredge intake using the dredge operating control system.

An optimum slurry concentration is typically targeted based on the pipeline transport capacity and is generally dependent on the particle size distribution of the sediment deposit being excavated. Guidelines such as those found in the ANSI/HI Rotodynamic Centrifugal Slurry Pumps design and application standards[iii] can be used to determine the appropriate concentration of the dredge slurry after system requirements are considered (See Figure 2). Since the classification of different layers of sediment can vary significantly, it is important that

the average particle size of the layers in the deposits be used to size the dredge pumps so that sediment removal rates and pipeline head losses are accurately anticipated.

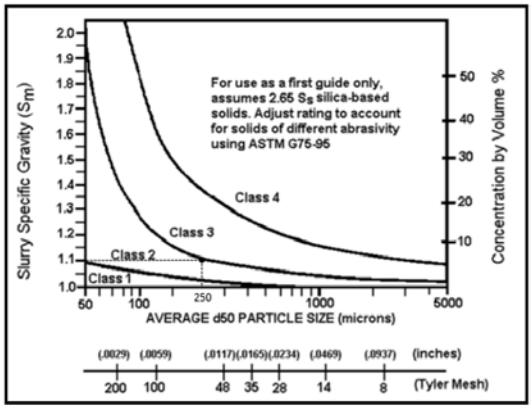

Figure 2. ANSI HI 12.1-12.6-2016

Sample Calculation of Balanced Throughput

The process to determine the target dredging discharge requirements is as follows:

1. Determine reservoir sediment volume increase for study period. Periodic bathymetric surveys are a useful technique to determine the rate of sediment accumulation and the distribution of sediment throughout the reservoir.
2. Determine the average density of deposit through a sampling program to establish dredge equipment selection parameters.
3. Estimate the rate of reservoir sediment inflow and measure the rate of reservoir suspended and bed load sediment inflow for various stream flow rates.
4. Measure the rate of reservoir sediment outflow for various stream flow rates.
5. Calculate the rate of sediment solids discharge required to match sediment solids inflows to outflows over the selected time period.
6. Determine the concentration of solids in the dredge slurry and the required discharge flow rate range after considering the properties of the sediment deposit (particle size distribution and abrasivity).
7. Select equipment and pipeline material based on sediment properties, sediment deposit location, and spillway configuration.

Example calculation for a small reservoir:

1. Determine reservoir sediment volume increase for study period, determine in situ bulk density. The amount of suspended sediment entering the reservoir and deposited can be determined by a bathymetric survey that compares the previous period end surface profile of the reservoir with the current reservoir surface profile. Any removals during the period should be accounted for. Take physical samples of sediment to determine the unit weight of the sediment deposit.
    a. SEDper (Period Sediment Accumulation Volume) = CAPnow (Current Bathymetric Survey Reservoir Capacity) – CAPprev (Previous Reservoir Capacity)

Use 40,000 cubic yards (CY) for measured sediment inflow between surveys

b. P (Duration of Period Between Bathymetric Surveys)

Use 1 year between surveys

c. SEDRATEper (Rate of Reservoir Sediment Accumulation for Period) = SEDper/P

= 40,000 CY/year

d. SEDDENSITY (Bulk Density of Reservoir Sediment Deposit)

Use 95 lb./cubic foot

Verify with a sediment sampling program.

2. Determine the reservoir capture efficiency. Reservoir sediment deposits are generally correlated to sediment inflows by the size, shape, and ratio of capacity to annual inflow. Various studies have established widely accepted formulaic relationships between reservoir shapes and rates of stream inflow. A specific example is the family of curves that provide expected sediment capture efficiency as published by Brune[iv] (Figure 3). These correlations can be used to estimate long term sediment deposition rates.

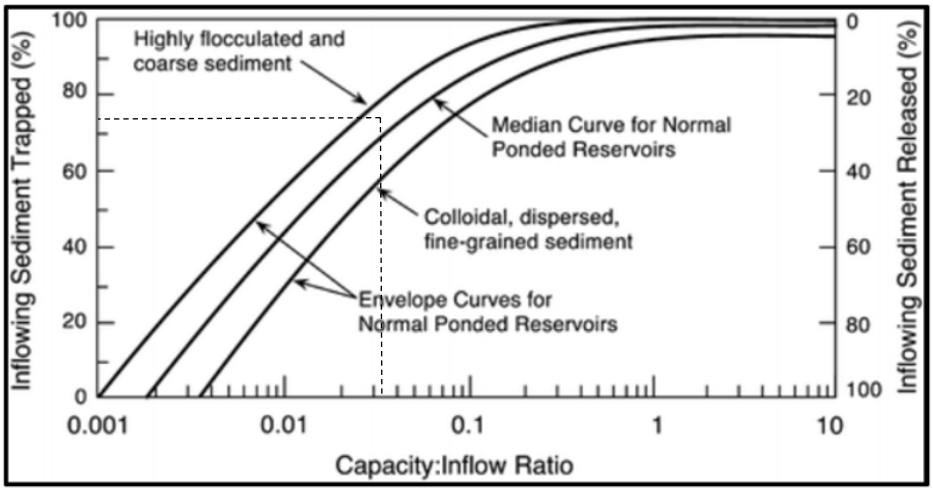

Figure 3. Reservoir Sediment Capture Efficiency

a. Average Reservoir Capacity for Period (CAPper)
Use 7,700 Acre-ft

b. Average Reservoir Runoff Inflow for Period (INFLOWper)

Use 250,000 Acre-ft/Year

= 250,000 Acre-ft/Year * 43,560 cubic feet/Acre-foot / 365 days/ year / 24 hours/day / 60 min/hour/ 60 sec/min = 345.3 cubic feet/sec

c. Capacity Inflow Ratio = CAPper / INFLOWper

= 7,700 Acre-ft / 250,000 Acre-ft/ Year = 0.0308

d. Period Trap Efficiency (EFFper)

From Brune Chart (Figure 3) use 74% trap efficiency

3. Make a first pass at an estimate for the reservoir outflow sediment concentration. First estimate the rate of reservoir sediment inflow and measure the rate of reservoir sediment inflow for various flow rates using an instrument system

   a. Sediment Inflow Rate to Reservoir (INRATEper) = SEDRATEper (Rate of Sediment Accumulation for Period) / EFFper

      = 40,000 CY/Year / .74 = 54,054 CY/Year

      = 54,054 CY/Year * 27 cubic feet/CY / 365 days/Year / 24 hrs./day / 60 min/hr. = 2.78 cubic feet /minute

      Also perform physical sediment surveys to determine sediment inflow rates for various stream flow rates

4. Determine estimated rate of reservoir sediment outflow and measure the rate of reservoir sediment outflow for various flow rates using an instrument system

   a. Period Sediment Outflow Rate (OUTRATEper) = Sediment Inflow Rate to Reservoir (INRATEper) - SEDRATEper (Rate of Reservoir Sediment Accumulation for Period)

      = 54,054 cy/year - 40,000 cy/year = 14,054 cy/year

      = 14,054 cy/year * 27 cubic feet/cy / 365 days/yr. / 24 hrs./day / 60 min/hr. = 0.72 cf/min

      Also perform physical sediment surveys to determine sediment outflow rates for various stream flow rates

5. Calculate the rate of sediment solids discharge required to match sediment solids inflows to outflows

   a. Period Average Required Sediment Volumetric Dredge Discharge (DREDGERATEavg) = Sediment Inflow Rate to Reservoir (INRATEper) - Period Sediment Outflow Rate (OUTRATEper)

      = 54,054 cy/year - 14,054 cy/year = 40,000 cy/year = 2.05 cf/min

   b. Period Average Required Sediment Weight Dredge Discharge (DREDGEWTRATEavg) = Period Average Sediment Dredge Discharge (DREDGERATEavg) * SEDDENSITY (Bulk Density of Reservoir Sediment Deposit)

      = 2.05 cf/min * 95 lb/cf = 194.8 lb/min

6. Determine the concentration of solids in the dredge slurry discharge after considering the characteristics of the sediment deposit (particle size and shape)

   a. Target Slurry Solids Volumetric Concentration = - (Target Slurry Specific Gravity – 1) / (1- Solids Specific Gravity)

      Figure 2 provides a chart from ANSI HI 12.1-12.6-2016, American National Standard for Rotodynamic Centrifugal Slurry Pumps, which can be used to determine the appropriate concentration of the dredge slurry based on the properties of the deposit.

Use an average particle size D_{50} of 0.25 mm (250 microns), solids specific gravity of 2.65 and Class 2 (borderline Class 3) slurry pump service class with an average particle abrasivity. Allow for a normal amount of machinery maintenance.

Use Target Slurry Specific Gravity = 1.1

Figure 4 provides an illustration showing the volumetric fraction of sediment and the volumetric fraction of liquid in the stream flow compared to the mass fraction of solids and the mass fraction of liquid resulting from the different respective specific gravities of the solid and liquid.

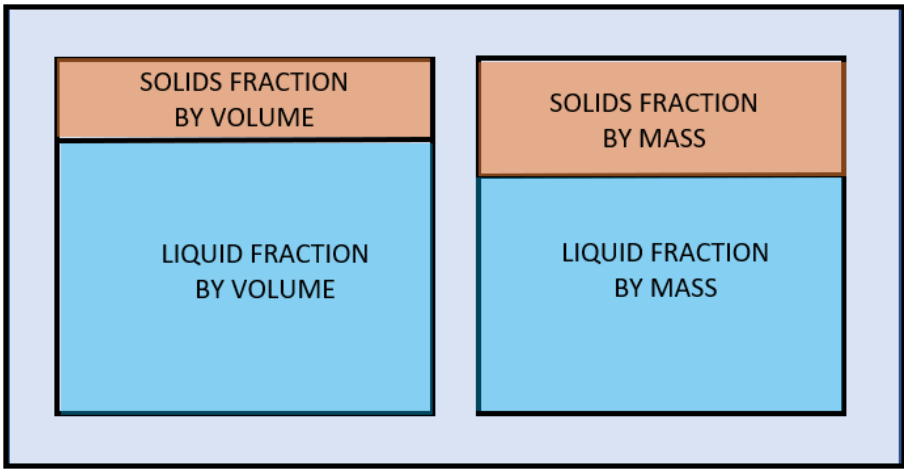

Figure 4. Dredge Slurry Solids by Mass vs. Volume

Target Slurry Solids Volumetric Concentration = - (1.1-1) / (1 - 2.65) = 0.061 = 6.1% Solids concentration by volume.

7. Determine the dredge discharge rate at the Target Slurry Solids Volumetric Concentration for continuous operation for equalization of sediment inflows and outflows inputs from the upstream and downstream sediment monitoring instruments.

   a. For continuous dredge operation DREDGERATEper (Period Slurry Pumping Rate) = Period Average Sediment Weight Dredge Discharge (DREDGEWTRATEavg) / (Target Slurry Solids Volumetric Concentration % * Solids Specific Gravity * Unit Weight of Water)

      = 194.8 lb/min / (0.061 * 2.65 * 62.4 lb/cf) = 19.3 cf/min (144 gpm)

Selecting Sediment Throughput Equalization Period

Determine the target dredge discharge rate after finalizing the period for equalization of sediment flows (hourly, weekly, annually, etc....) and operate the dredge using a slurry concentration control system with inputs from the upstream and downstream sediment monitoring instruments. Dredging equipment can be selected and operated using the control system to allow the combined dredged sediment discharge flowrate and reservoir sediment outflow rate to match the reservoir inflow rate and achieve a balanced period throughput.

Use average annual reservoir inflow as the basis of determining balanced throughput (Table 1):

Table 1, Dredge Discharge Rates for Various Operating Approaches

Operations Schedule	Dredge Operating Parameters	Example Dredge Discharge Rates (7.48 gpm/cfm)
Continuous	12 Months/Year, 7 Days per Week, 24 Hours/Day	19.3 cf/min (144 gpm)
Partial Week, Multiple Shifts	12 Months/Year, 6 Days per Week, 2 ea. 10 Hour Shifts/Day	27.0 cf/min (202 gpm)
Seasonal, Partial Week, Multiple Shifts	8 Months/Year, 6 Days per Week, 2 ea. 10 Hour Shifts/Day	40.5 cf/min (303 gpm)
Seasonal, Partial Week, Single Shift	8 Months/Year, 6 Days per Week, 1 ea. 12 Hour Shift/Day	67.6 cf/min (505 gpm)

With reference to Figures 5 and 6, an illustration of a typical annual flow regime is provided for inflows to a reservoir with seasonal variations due to snowmelt and precipitation runoff events. Conveyed sediment in the form of a clastic or suspended load is transported in varying amounts correlated to the flow rate of the stream inflows. Sediment removal can be planned for periods when surface ice is not present for northern reservoirs. Spawning windows can be avoided if habitat considerations need to be accounted for with dredging operations.

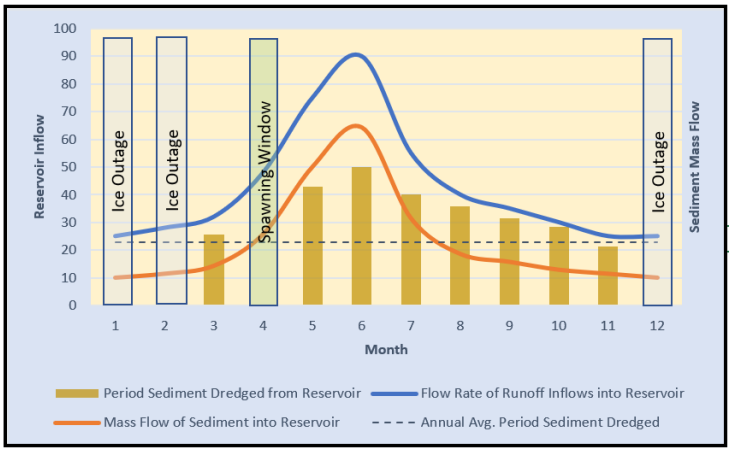

Figure 5. Typical Reservoir Inflows and Balanced Sediment Removal

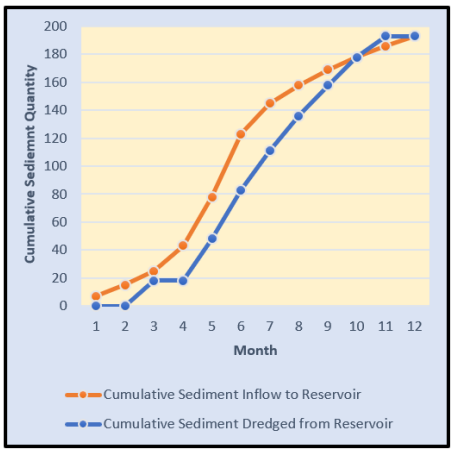

Figure 6. Cumulative Sediment Inflows and Removals

To more closely match sediment removal to seasonal inflow rates, the dredging discharge rate can be varied (See Table 2).

Table 2, Dredge Discharge Rates for Various Seasonal Operating Approaches

Operations Schedule	Dredge Operating Parameters	Reservoir Inflow Rate	Example Dredge Discharge Rates (7.48 gpm/cfm)
Seasonal, Partial Week, Multiple Shifts	8 Months/Year, 6 Days per Week, 2 ea. 10 Hour Shifts/Day	Low flow, - 25% of annual average	10.1 cf/min (75 gpm)
Seasonal, Partial Week, Multiple Shifts	8 Months/Year, 6 Days per Week, 2 ea. 10 Hour Shifts/Day	Higher flow, - 200% of annual average	81.1 cf/min (607 gpm)

This example consumes less than 250 acre-feet of water in order to convey the targeted volume of sediment. The reservoir used to model this approach passes on average 250,000 acre-feet of flow per year. The amount of water to be used for process water is approximately 0.1% of the annual flow. This volume should be accounted for if water rights are affected. A slight reduction in power production may also be a consideration when evaluating this process.

Exhibit 1 provides a sample daily report for the operation of the dredging system on a larger reservoir with a single shift and daily sediment mass balance approach. If a significant fraction of inflow is diverted for irrigation or raw water supply purposes away from the outlet watercourse then a corresponding fractional mass reduction in targeted sediment removal may be required.

This approach produces as a result an equalization of the concentration of reservoir sediment inflows with outflows. It is possible that limitations may be imposed on the concentration or absolute volume of sediment discharged downstream due to physical or other constraints. These constraints limit the long-term effectiveness of this process but may be unavoidable until the constraints can be removed or mitigated.

Dredging Equipment Selection

Excavation of submerged sediment can be accomplished with either mechanical or hydraulic dredging. Hydraulic dredging allows for the efficient excavation and transport of submerged sediment and makes direct discharge to the downstream channel efficient. Floating booster pumps can be utilized to convey sediment slurries long distances allowing large areas of reservoir sediment to be included in sediment removal programs. A wide variety of hydraulic dredges are available to meet the various demands of different facilities (See Figure 7a and 7b). Some factors that should be considered in the selection of a hydraulic dredge include:

- Determine the maximum size of equipment that can be mobilized to the site. Transportable dredges can be disassembled into major components that can be reassembled on the water.
- The desired maximum depth of cut and the maximum rate of sediment removal dictate the overall size and capacity of the dredge equipment.

- The average particle size of the sediment deposit, particle size distribution, presence of submerged woody debris and duration of the dredging operation all affect the selection of dredging equipment.
- If the depth of desired sediment removal is below the limit of surface mounted dredge pumps, then a ladder mounted submerged pump may be necessary. Sediment removal depths of up to 200 feet can be achieved with equipment configured for this application (See Figure 7a and 7b).
- The cutterhead of the dredge should employ a screen to prevent oversized material from being introduced onto the slurry pipeline.
- An upstream log boom can be employed to minimize the amount of submerged woody debris that enters the area planned for dredging operations. Ground penetrating radar (GPR) is an imaging technology that allows detection of subsurface obstructions like logs or other debris that might foul the cutterhead of the dredge. A program of investigation for submerged obstructions should be performed as part of the initial geotechnical investigation of the sediment deposit. Removal of large submerged woody debris by a grapple may be required prior to hydraulic dredging.
- If an electrical power source is available nearby, submarine rated power supply cabling can be employed allowing electrically powered dredge pumps to be utilized.

Figure 7a. Ellicott 670, Max Depth 42 ft. (Ellicott® Dredges, LLC)[v]

Figure 7b. Marlin Class Dredge Max Depth 96 ft. (std.), 200 ft. (custom) (DSC Dredge, LLC)[vi]

Slurry Transport Considerations

The pumps on the hydraulic dredge are designed to convey sediment slurry under pressure at a target specific gravity for a predetermined distance before discharge or, to the intake of a downstream booster pump. If the sediment deposit is close enough to the dam and outlet works then booster pumps may not be necessary. Also, if the sediment discharge is conveyed over the dam crest then the added pressure head that needs to be overcome to push the slurry over that elevation needs to be considered in the pump, pipeline selection, and booster pump spacing.

Transport systems should consider the following factors:

- The coarsest sediment deposits will have the highest transport head loss and the highest minimum transport velocity (critical velocity) for the same concentration of the slurry being conveyed. Head loss calculations need to anticipate the most severe condition that the system will experience to avoid blockages due to particle settling in the pipeline.

Sediment deposits selected for removal need to be sampled and characterized so that the appropriate slurry pump configuration and pipeline size are selected.

- Low coefficient of friction pipeline materials such as high-density polyethylene (HDPE) can reduce the necessary pipeline size and allow wider spacing of booster pump equipment. Proper fusing techniques and reaming of interior welds need to be performed to prevent localized wear. The pipeline wall thickness should be selected based on the maximum operating pressure. The pipeline wall thickness should also be periodically checked using non-destructive techniques to monitor for thin areas that could fail under pumping loads.
- The use of steel transport pipelines may be more economic for extended service or for coarse or high abrasivity slurry applications.
- The abrasivity of the sediment can cause accelerated wear of the pipeline if an inappropriate material is selected. Abrasivity testing of the deposits selected for removal should be performed so that the appropriate pipe material is selected.
- Booster pumps should be spaced such that the minimum pump inlet pressure is maintained and the maximum pipeline pressure stays below the recommended operating pressure of the pipeline material. Horizontal pipe restraints and long radius elbows should be used where the pipeline changes direction.
- Booster pumps require a supply of clean water for seal water systems. Filtered reservoir water may be suitable for a separate water supply source for each booster pump to extend the life of pump shaft seal and packing components.
- The dredge and booster pumps need to be linked via wireless telemetry to a central control system that allows synchronized operation.
- A vacuum release valve system may be required at the high point of the slurry pipeline above the point of discharge to atmosphere on the downstream side of the dam. The use of an extended discharge pipeline on the downstream side of the dam needs to consider the potential for open channel flow in the pipeline. Significant wear in the discharge pipeline could be experienced if the slurry is abrasive in nature and velocities become high. A separate source of reservoir water can be introduced into the discharge flow on the downstream side of the dam to reduce the concentration of solids in the discharge flow and thus reduce wear of the discharge system.
- Enough pipeline floats should be provided to eliminate sags that can lead to settlement of large sediment particles which, in turn, can lead to pipeline blockages. The buoyancy of the pipeline changes as the slurry is introduced causing it to submerge deeper between floats if not properly supported. Steel pipelines require more support than HDPE pipelines.
- If the slurry discharge pipeline passes over a gated spillway then a casing should be considered through the crest to allow uninterrupted operation of the gate and replacement of worn pipe sections.
- Corrosion protection should be considered for steel slurry pipelines. Isolation joints and sacrificial anodes may prove beneficial to preventing premature deterioration of the pipe material. Periodic inspections of the interior and exterior of the pipeline should be performed. Slurries cause higher wear on the invert of pipelines when more abrasive sediment particles are transported. Radial marking of the pipeline to allow periodic rotation can extend the life of the pipe.
- If an electrical power source is available nearby, submarine rated power supply cabling can be employed allowing electrically powered booster pumps to be utilized.

Strategy for Addressing Environmental Effects of Solution

Many reservoirs have sediment deposits that contain concentrations of dissolved and suspended substances that may be classified as hazardous to aquatic life and water supply consumers. Heavy metals, including iron and manganese, among many others, can concentrate in the pore water of sediment deposits over time. The hydraulic dredging process brings sediment pore water into the slurry pipeline along with reservoir water as the desired slurry solids concentration is achieved.

The potential for treatment of the discharged slurry should be assessed when the sediment deposit test results are available prior to the start of dredging. Factors to consider when evaluating the need for treatment of the sediment slurry directly discharged downstream should consider the following:

- Is there a potential for hazardous concentrations of substances to be present in the slurry discharged downstream of the reservoir?
- If so, can a mixing zone in the channel downstream of the point of slurry discharge be utilized to reduce the concentration of regulated substances to an acceptable level of dilution at the sampling points for regulatory reporting?
- Can areas of concentrated contaminates be avoided by mapping deposits and developing a dredge management plan that acceptably minimizes contaminants discharge?
- If treatment of the discharge water is required, a process should be developed that maintains the discharge rate of sediment solids to the downstream channel while process water is separated and treated for removal of contaminants (See Figure 8).
- Consider the use of a parallel supply of reservoir water to convey separated sediment solids to the downstream channel while slurry process water is treated for removal of undesirable contaminants.
- The effect of an increased sediment load on downstream navigation channels and raw water diversions also needs consideration and further mitigation if impacts are sufficiently adverse.

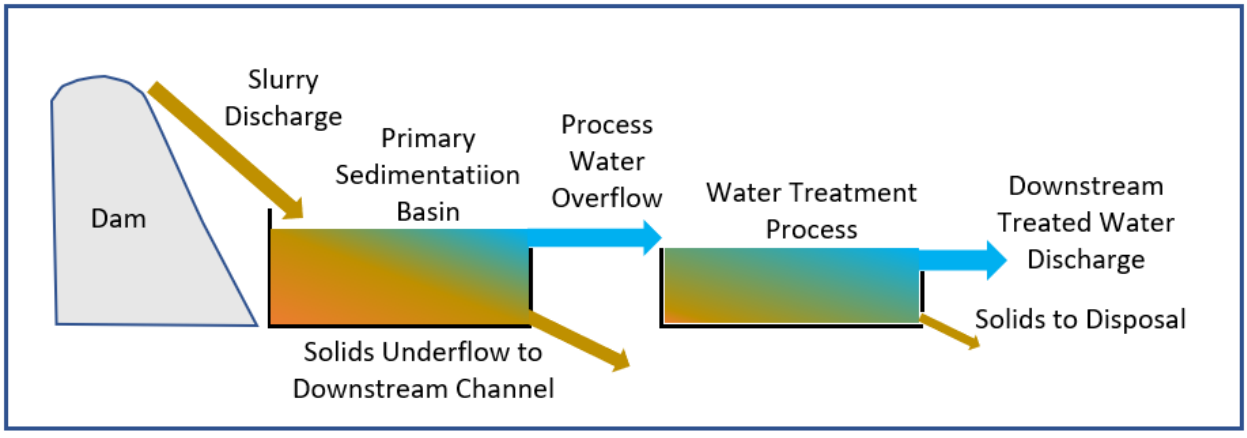

Figure 8. Treatment of Slurry for Contaminates

Dredge and pump equipment can also be configured to minimize the environmental impact. If diesel equipment is utilized, then Tier 4 Marine emissions engines should be specified. Electrically powered pump motors can reduce emissions if a local power supply is available. A

central power plant may also provide lower overall emissions than individual diesel power units on the dredge and each booster pump. Also, consider the use of “hospital grade” mufflers on diesel power units to reduce noise impacts. Downcast lighting should be considered for area lighting applications to minimize light pollution.

Regulatory Considerations

The direct discharge of sediment slurry directly into waters of the United States will make the activity subject to regulations under section 404 of the Clean Water Act[vii]. An individual permit may be required if the impacts of the dredging action are significant enough to warrant a more thorough evaluation of the effects of the operation on the local and regional ecosystem.

Stakeholders that may be involved in the evaluation of impacts resulting from the dredging program include:

- US Army Corps of Engineers
- The Environmental Protection Agency
- State environmental regulatory agencies
- State and Federal wildlife protection agencies
- Local and regional treated or raw water supply system owners and operators
- Downstream reservoir owners and operators
- Regional flood control agencies
- Commercial navigation interests
- Local and regional recreation interests
- Public and private property owners in the area of influence

The process to discern the impacts on stakeholders will likely be time consuming and involve significant expense. Enough resources should be budgeted to allow the process to be carried through until a consensus is achieved for operating parameters among interested parties and regulators can establish the constraints for operation of the system.

Other alternatives that should be considered before implementing a continuous and perpetual process as described in this paper may include periodic removal of deposits that are impairing the outlet works or diversion intake structures. The use of Confined Disposal Facilities (CDF) in or adjacent to the reservoir offer alternatives that may prove economic in the short run. Excavation with a lower pool, flushing, sluicing, bypassing, and upstream sediment stabilization, are also techniques that can be utilized to manage sediments but, most do not entirely mitigate the long-term degradation of overall capacity. Taking the long view leads one to the Balanced Sediment Throughput Reservoir Dredging process as one of the few truly sustainable approaches available to preserve most reservoir facilities.

The “no action” alternative to sustainable dredging is a choice to allow degradation of the reservoir that inevitably leads to retirement. Dam removal and replacement will likely have a substantially greater impact than the approach to ongoing maintenance that Balanced Sediment Throughput Reservoir Dredging presents.

An Approach to Implementation

Approval of the process will require a partnership of reservoir operators, regulatory agencies, consulting engineers, a contracting team, and equipment suppliers to implement.

Owner/Operator of Facility

- A sponsorship level team of leaders from the executive, operations, regulatory compliance and legal departments of the organization should be identified. They will ensure enough resources are allocated to support the program.
- A dedicated team should be assigned to execute the support of early permitting and environmental studies necessary to obtain regulatory approval. This team will also supervise any 3rd party consultants or contractors employed throughout the execution of the program.

Consulting Engineers:

- An Owner's Representative with expertise in managing a complex procurement process under significant regulatory oversight should be considered.
- Geotechnical investigations of the reservoir sediment deposit and geomorphologic studies of the stream conditions can be managed by an owner's consulting engineer.
- Hydrologic modeling of streamflow and sediment deposition for environmental studies.
- Specific discipline consulting engineers can be employed to evaluate aquatic species impacts, address regulatory interests in water quality and provide guidance for development of dredging procurement requirements.

Dredging Contractors and Equipment Manufacturers:

- Early contractor involvement should be considered as regulatory requirements are being developed to ensure that economic solutions are incorporated in the final regulations for the permitted dredging solutions.
- The Construction Manager/General Contractor (CMGC) approach allows for the competitive selection of qualified contractors to assist the team with process design development and budgetary input for the selection of optimum system configurations. Dredge equipment suppliers will play an integral part in the configuration of a system that meets regulatory requirements.

Funding Considerations

"No bucks, no Buck Rogers"[viii] is a quote that describes the dilemma facing sponsors of the implementation of a comprehensive sediment management program for reservoirs. With increasing pressure on budgets due to aging infrastructure, most utilities and agencies are hard pressed to find funding for new categories of expenditures with limited visible and immediate benefits. Only with high level sponsorship will long term budgets be properly allocated so that higher operating budgets are provided that include enough sediment management funding. Steps to achieve this goal should consider:

1. Identification of highest risk facilities for early sedimentation impairment. Funding of bathymetric surveys and studies should be provided to determine the expected service life of high-risk reservoirs.
2. Development and disclosure of estimated retirement costs for high risk facilities should be made, including facility full replacement costs. Net Present Value calculations need to consider the historical annual cost escalation of over 3.5% experienced for similar installations since 1977[ix].
3. Cui Bono? Who benefits from the uninterrupted operation of a reservoir is an important consideration in the funding process. Potential sources of funds outside traditional operating budgets include:
    a. A flood insurance premium surcharge could be considered for funding the extension of the facility service life. Also, a supplemental fee could be assessed on new development within the protected floodplain so that existing insurance payers are not burdened.
    b. Increased raw water supply assessments in return for an extended facility service life.
    c. Increased power prices for protected hydroelectric facilities.
    d. Increased recreation fees.
    e. Privatization of facility operations through public private partnerships to allow monetization of existing budget streams in return for added sedimentation management operations. Ownership would remain with the agency, but operating revenue streams would finance active sediment management operations.

Benefits of the solution

Cost

The benefits of the proposed process can be characterized from both a direct and indirect viewpoint. First, the direct cost of implementing this approach can be optimized so that resources, including labor, equipment, and finances can be applied in the most efficient manner to affect the transport of sediment through the reservoir for the maximum extension of the facility service life. Direct benefits of the method include the following:

1. An initial direct benefit is the elimination of the need to secure, permit, construct and maintain a confined disposal area in or adjacent to the reservoir.
2. The use of hydraulic dredging allows for an efficient transport method for sediment directly from the reservoir deposit to the downstream water course, eliminating the multiple handling steps required for mechanical dredging.
3. Higher solids concentrations in slurry content and the resultant smaller system equipment needs can be targeted if hardened pump wear parts and pipeline materials can be utilized such as are used for concrete pumping equipment.
4. An optimum capacity range can be selected that achieves the desired system throughput while accommodating seasonal variations in source water inflows.

An indirect cost reduction for the facility is realized when the life cycle is extended, upstream and downstream impacts are minimized, and retirement and/or replacement is deferred or potentially eliminated. Specific benefits include:

1. Reduced outlet works maintenance expenditures are realized as sediment is prevented from reaching the outlet of the reservoir.
2. Reduced hydroelectric machinery maintenance expenditures are realized as sediment is prevented from reaching the outlet of the reservoir.
3. Downstream channel degradation is reduced thereby minimizing necessary bank and channel stabilization demands.
4. Upstream channel aggradation is prevented which also minimizes bank and channel protection or relocation of infrastructure due to increasing flood risk.
5. Retirement of the current facility can be significantly deferred or eliminated.
6. Permitting, site procurement, design and construction of a replacement facility can be significantly deferred or eliminated.
7. The loss of flood control capacity that would otherwise result in higher downstream flood risk and the potential for property losses is reduced.
8. Ultimately, if a significant number of facilities employ this process, sediment flows to the ocean can be increased and coastal erosion processes mitigated.

Cost-Benefit Considerations

Alternative solutions must be studied when a reservoir dredging operation is considered. One study that is always evaluated is the “no action” alternative. This essentially involves continuing the practice of allowing sediment to accumulate in the reservoir pool without any meaningful removal of material. This practice virtually guarantees that the service life of the facility will be reached in a reasonably predictable amount of time.

The consequence of reaching the end of the service life of a reservoir is that retirement of the facility is then required. An example that highlighted the complexity of the removal of dam facilities with significant sediment accumulation involved the retirement of two hydroelectric dams on the Elwha River. The 105-foot-tall Elwha Dam was constructed in 1913 and upstream 210-foot-tall Glines Canyon Dam was completed in 1927. Approximately 24 million cubic yards of sediment accumulated throughout their operational life and ultimately, removal was required to restore a path for endangered anadromous (sea-run) fish to reach historic spawning areas. A contract for removal of the two dams was awarded in 2011 for $27 million[x] allowing as part of the original estimated total cost of Elwha River Restoration at $325 million[xi].

This effort highlights the extensive scope involved in a dam decommissioning action that requires expenditures in addition to the direct cost of dam removal. The Elwha removal action required significant mitigation work over many years to water supply facilities downstream of the removed dams as a result of the sediment release. The proper approach to evaluation of a “no action” alternative needs to include a comprehensive cost estimate of all effects related to retirement of the dam. For flood control facilities, retirement should also consider the increased flood damage risk that results from the loss of the facility.

It is also important to acknowledge that escalation of construction costs can take many forms. Recent annual escalation rates of 5%+ for construction costs in major markets can equal or exceed long term discount rates used in past cost-benefit calculations[xii]. A higher escalation rate can result in an ever-increasing present valuation the longer decommissioning is postponed in the “no action” alternative.

Improved Efficiency

Efficiency of reservoir operations and efficiency of sediment removal are both maximized with the use of proposed process. First, the existing volume of the reservoir pool can be maintained longer, possibly indefinitely, allowing the current storage capacity of the reservoir to be preserved. The operating range of the reservoir pool can also be maintained thereby allowing continuing and unaltered operation of the reservoir for flood control, water supply and recreation.

Secondly, the use of hydraulic dredging eliminates the requirement for procurement of periodic capital projects required for the clearance and repair of outlet works or sediment disposal on adjacent properties. Overall expenditures can be reduced, and staffing demands arranged with less variability.

Conclusion

Balanced Sediment Throughput Reservoir Dredging offers a potential economic solution to the growing risk that reservoir sedimentation presents throughout the nation's system of reservoirs. If implemented, this alternative allows for a significant extension in the service life of existing reservoirs and defers the disruptive replacement of facilities that society has become reliant upon. Existing technology utilized in this system offers an approach to enhancing the condition of existing infrastructure while improving ecosystems above and below reservoirs while fulfilling the requirements of regulations that protect the environment.

Exhibit 1

Balanced Sediment Throughput Reservoir Dredging
Daily Operating and Discharge Report

Date: 1/4/2019
River Mile: 112.5
Dredge Management Unit(s) Worked: 108, 110

Target Slurry Specific Gravity: 1.10
Target Slurry % Solids: 14.8%

Hour	Inflow #1 Streamflow - cfs	Inflow #1 Turbidity - NTU	Inflow #1 Calculated Sediment Concentration - mg/l	Inflow #1 Calculated Sediment Inflow - lb/s	Inflow #1 Calculated Sediment Inflow - lb/hr	Inflow #1 Cumulative Daily Sediment Inflow - lb	Dredge Discharge Rate - gpm	Measured Dredge Slurry Specific Gravity	Hourly Slurry Discharge - lbs	Daily Cumulative Slurry Discharge - lbs	Reservoir Outlet Flow - cfs	Reservoir Outlet Turbidity - NTU	Period Outlet Discharge - lbs	Outlet Cumulative Daily Sediment Outflow - lb	Hourly Sediment Inflow Less Outflow Change - lb	Net Cumulative Daily Sediment Change - lb	Combined Slurry an Outlet Flow - cfs	Measure Combined Flow - Turbidity - NTU	Outflow Cumulativ e Daily Sediment Inflow - lb
12:00 AM	2000	15	513	6.41	23,069	23,069			0	0	2500	6	11,535	11,535	11,535	11,535	2,500	6	11,535
1:00 AM	2000	15	513	6.41	23,069	46,138			0	0	2500	6	11,535	23,069	11,535	23,069	2,500	6	23,069
2:00 AM	2000	15	513	6.41	23,069	69,207			0	0	2500	6	11,535	34,604	11,535	34,604	2,500	6	34,604
3:00 AM	2000	15	513	6.41	23,069	92,276			0	0	2500	6	11,535	46,138	11,535	46,138	2,500	6	46,138
4:00 AM	2000	15	513	6.41	23,069	115,346			0	0	2500	6	11,535	57,673	11,535	57,673	2,500	6	57,673
5:00 AM	2000	15	513	6.41	23,069	138,415			0	0	2500	6	11,535	69,207	11,535	69,207	2,500	6	69,207
6:00 AM	2000	15	513	6.41	23,069	161,484			0	0	2500	6	11,535	80,742	11,535	80,742	2,500	6	80,742
7:00 AM	2250	20	68.4	9.61	34,604	196,087			0	0	2500	6	11,535	92,276	23,069	103,811	2,500	6	92,276
8:00 AM	2500	25	85.5	13.35	48,061	244,148	1250	1.10	100,479	100,479	2500	6	11,535	103,811	-63,953	39,858	2,503	25	140,391
9:00 AM	2750	25	85.5	14.69	52,867	297,015	1250	1.10	100,479	200,959	2500	6	11,535	115,346	-59,147	-19,290	2,503	40	217,373
10:00 AM	3000	30	102.6	18.22	69,207	366,222	1250	1.10	100,479	301,438	2500	6	11,535	126,880	-42,807	-62,096	2,503	50	313,602
11:00 AM	3250	30	102.6	20.83	74,975	441,197	1250	1.10	100,479	401,918	2500	6	11,535	138,415	-37,039	-99,136	2,503	55	419,453
12:00 PM	3500	35	119.8	26.17	94,199	535,396	1250	1.10	100,479	502,397	2500	6	11,535	149,949	-17,815	-116,951	2,503	60	534,927
1:00 PM	3500	35	119.8	26.17	94,199	629,595	1250	1.10	100,479	602,877	2500	6	11,535	161,484	-17,815	-134,766	2,503	60	650,401
2:00 PM	3400	35	119.8	25.42	91,507	721,102	1250	1.10	100,479	703,356	2500	6	11,535	173,018	-20,507	-155,272	2,503	60	765,875
3:00 PM	3300	30	102.6	21.15	76,128	797,230	1250	1.10	100,479	803,835	2500	6	11,535	184,553	-35,886	-191,158	2,503	60	881,349
4:00 PM	3200	30	102.6	20.51	73,821	871,051	1250	1.10	100,479	904,315	2500	6	11,535	196,087	-38,193	-229,351	2,503	60	996,823
5:00 PM	3000	30	102.6	19.22	69,207	940,259			0	904,315	2500	6	11,535	207,622	57,673	-171,678	2,500	30	1,054,496
6:00 PM	2800	25	85.5	14.95	53,828	994,087			0	904,315	2500	6	11,535	219,157	42,293	-129,385	2,500	22	1,096,789
7:00 PM	2500	25	85.5	13.35	48,061	1,042,147			0	904,315	2500	6	11,535	230,691	36,526	-92,859	2,500	15	1,125,626
8:00 PM	2400	20	68.4	10.25	36,911	1,079,058			0	904,315	2500	6	11,535	242,226	25,376	-67,483	2,500	12	1,148,695
9:00 PM	2200	20	68.4	9.40	33,835	1,112,892			0	904,315	2500	6	11,535	253,760	22,300	-45,183	2,500	10	1,167,919
10:00 PM	2100	20	68.4	8.97	32,297	1,145,189			0	904,315	2500	6	11,535	265,295	20,762	-24,420	2,500	8	1,183,299
11:00 PM	2000	20	68.4	8.54	30,759	1,175,948			0	904,315	2500	6	11,535	276,829	19,224	-5,196	2,500	6	1,194,833
12:00 AM	2000	20	68.4	8.54	30,759	1,206,707			0	904,315	2500	6	11,535	288,364	19,224	14,028	2,500	6	1,206,368

For this example use # mg/l = 3.4215 NTU[1]

References

[i] Gotvald, Anthony J., Oberg, Kevin A , Acoustic Doppler Current Profiler Applications Used in Rivers and Estuaries by the U.S. Geological Survey,. U.S. Department of the Interior, U.S. Geological Survey, Fact Sheet 2008–3096 February 2009

[ii] Topping, D.J., Wright, S.A., Melis, T.S., and Rubin, D.M., 2007, High resolution measurements of suspended-sediment concentration and grain size in the Colorado River in Grand Canyon using a multi-frequency acoustic system: Proceedings of the Tenth International Symposium on River Sedimentation, August 1–4, 2007, Moscow, Russia, v. 3, p. 330–339.

[iii] American National Standard for Rotodynamic Centrifugal Slurry Pumps for Nomenclature, Definitions, Applications, and Operation. ANSI/HI HI 12.1-12.6-2016. Hydraulic Institute, 2016.

[iv] Brune, G. M. (1953), Trap efficiency of reservoirs, Trans. Am. Geophysical. Union, 34, 407–418

[v] Ellicott Dredges, Dragon Series 670 Dredge. (2018, November). Retrieved from, http://www.dredge.com/dredge-equipment-models/670-dragon-cutterhead-dredge/670.pdf

[vi]DSC Dredge, LLC, Marlin Dredge. (2018, November). Retrieved from, http://www.dscdredge.com/products/marlin-class-dredge

[vii] U.S. Army Corps of Engineers' (USACE) Regulatory Program and Permits, (2018, November), Retrieved from,https://www.usace.army.mil/Missions/Civil-Works/Regulatory-Program-and-Permits/Obtain-a-Permit/

[viii]Winkler, I., Chartoff, P. (Producers), Kaufman, P. (Director). (1983). Kaufman, P: The Right Stuff [Motion picture]. United States: Warner Bros. (1983), written and directed by Philip Kaufman.

[ix] U.S. Department of the Interior, Bureau of Reclamation, Construction Cost Trends (2018, November). Retrieved from, https://www.usbr.gov/tsc/techreferences/mands/cct.html

[x] Thomas E. Hepler, P.E. U.S. Department of the Interior, Bureau of Reclamation, Technical Service Center, Retrieved from, https://cdn.ymaws.com/www.aegweb.org/resource/resmgr/Dams/ds11_elwha-river-restoration.pdf

[xi] National Park Service, Elwha River Restoration Frequently Asked Questions, (2018, November), Retrieved from, https://www.nps.gov/olym/learn/nature/elwha-faq.htm

[xii] Turner's Third Quarter Building Cost Index, (2018, November), Retrieved from, http://www.turnerconstruction.com/cost-index

Cherry Creek Pressure Flushing Analysis

Kent Collins, P.E., Hydraulic Engineer, US Bureau of Reclamation, Denver, CO, kcollins@usbr.gov
Paul Boyd, Ph. D., P.E., Hydraulic Engineer, US Army Corps of Engineers, Omaha, NE, paul.m.boyd@usace.army.mil
John Shelly, Ph. D., P.E., Hydraulic Engineer, US Army Corps of Engineers, Kansas City, MO, john.shelley@usace.army.mil
Daniel Dombroski, Ph. D., P.E., Hydraulic Engineer, US Bureau of Reclamation, Denver, CO, ddombroski@usbr.gov
Blair Greimann, Ph. D., P.E., Hydraulic Engineer, US Bureau of Reclamation, Denver, CO, bgreimann@usbr.gov

Abstract

The US Army Corps of Engineers (USACE), US Geological Survey (USGS), and US Bureau of Reclamation (Reclamation) are collaborating on the study of reservoir outlet maintenance activities on Cherry Creek Dam and Reservoir in Denver, CO. Repeat land and bathymetric surveys, sediment sampling, suspended sediment concentration measurement, and three-dimensional numerical modeling are being used to evaluate the effectiveness of current pressure flushing operations. Evaluation of collected data indicates that improvements to gate operations could be made to increase the efficiency of sediment removal from the reservoir during pressure flushing events. Results also suggest that acoustic backscatter measurements collected are a viable surrogate to direct measurements at this site and under the flushing conditions studied. Correct calibration and application may allow the acoustic backscatter instrument to be used at additional sites over a wide range of conditions. This study further validated the utility of engaging complementary approaches in the investigation of reservoir sedimentation issues. Further studies at multiple sites have been proposed and are ongoing.

Introduction

Cherry Creek Dam and Reservoir are located on Cherry Creek in south Denver, CO (Figure 1). Completed in 1950, the dam and reservoir are operated by the US Army Corps of Engineers (USACE) to provide flood risk reduction and recreation to the Denver Region from the South Platte River watershed. The mean annual sedimentation rate at Cherry Creek Reservoir is 69.1 acre-feet (111,546 cubic yards) per year according to USACE repeat surveys in 1950 and 2007 (https://corpsmapz.usace.army.mil/apex/f?p=303:1). Each spring, as part of their annual maintenance activities, USACE operators open the radial gates to clear sediment and debris deposited on the upstream face of the gates, allowing the gates to operate freely if and when needed. During the annual flow release, sediment is flushed through the outlet works and transported downstream. In late-May 2017 and 2018, USACE, US Geological Survey (USGS), and US Bureau of Reclamation (Reclamation) crews collected hydraulic, sediment, and bathymetric data necessary to verify gate discharge curves, develop sediment discharge relationships, and measure the volume of sediment removed from the reservoir during the annual flush. Numerical modeling efforts are underway to replicate measured changes in the reservoir bottom sediment resulting from the annual flow releases. In the future, the numerical model could potentially be used to estimate the volume of sediment removed from the reservoir for various release hydrographs. Physical measurements of sediment loads and deposits,

empirical relationships between water and sediment discharge, and numerical modeling can be combined to support efforts to improve flushing efficiency. The USACE expects to use the results to evaluate the efficiency of the flush and examine any management changes that may increase flush efficiency and/or reduce water consumption as part of the flush.

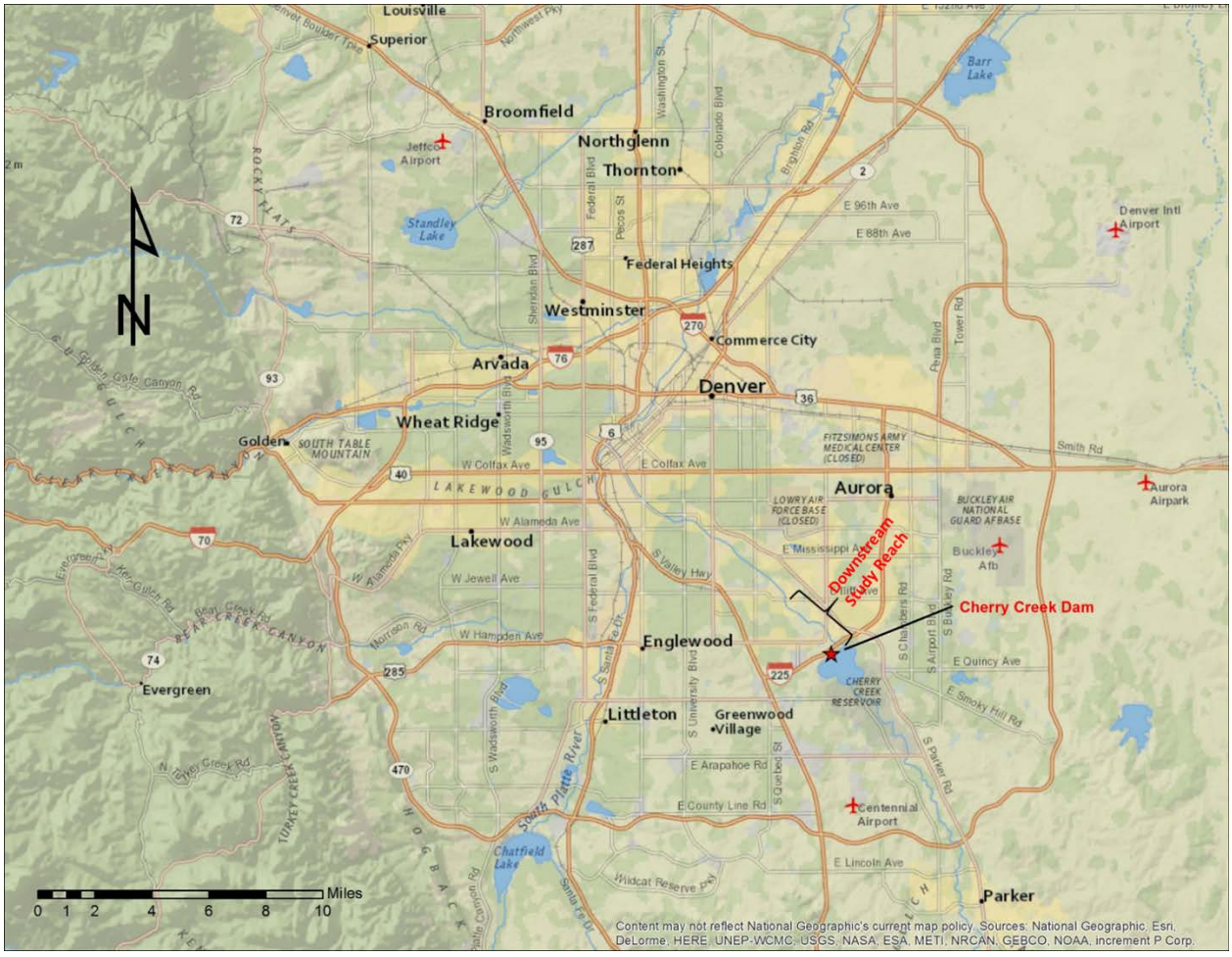

Figure 1. Location map showing Cherry Creek pressure flushing study area

2017 and 2018 Flushing – Dam Operation Regime

Flow through the Cherry Creek Dam outlet works is controlled by a series of five independently operated radial gates. Reservoir water enters the intake, passes through the dam, then is discharged into one of three rectangular concrete outlet chutes and a stilling basin before entering Cherry Creek downstream. Figure 2 is a photograph of the intake for the outlet works in 1952, shortly after closure Cherry Creek Dam.

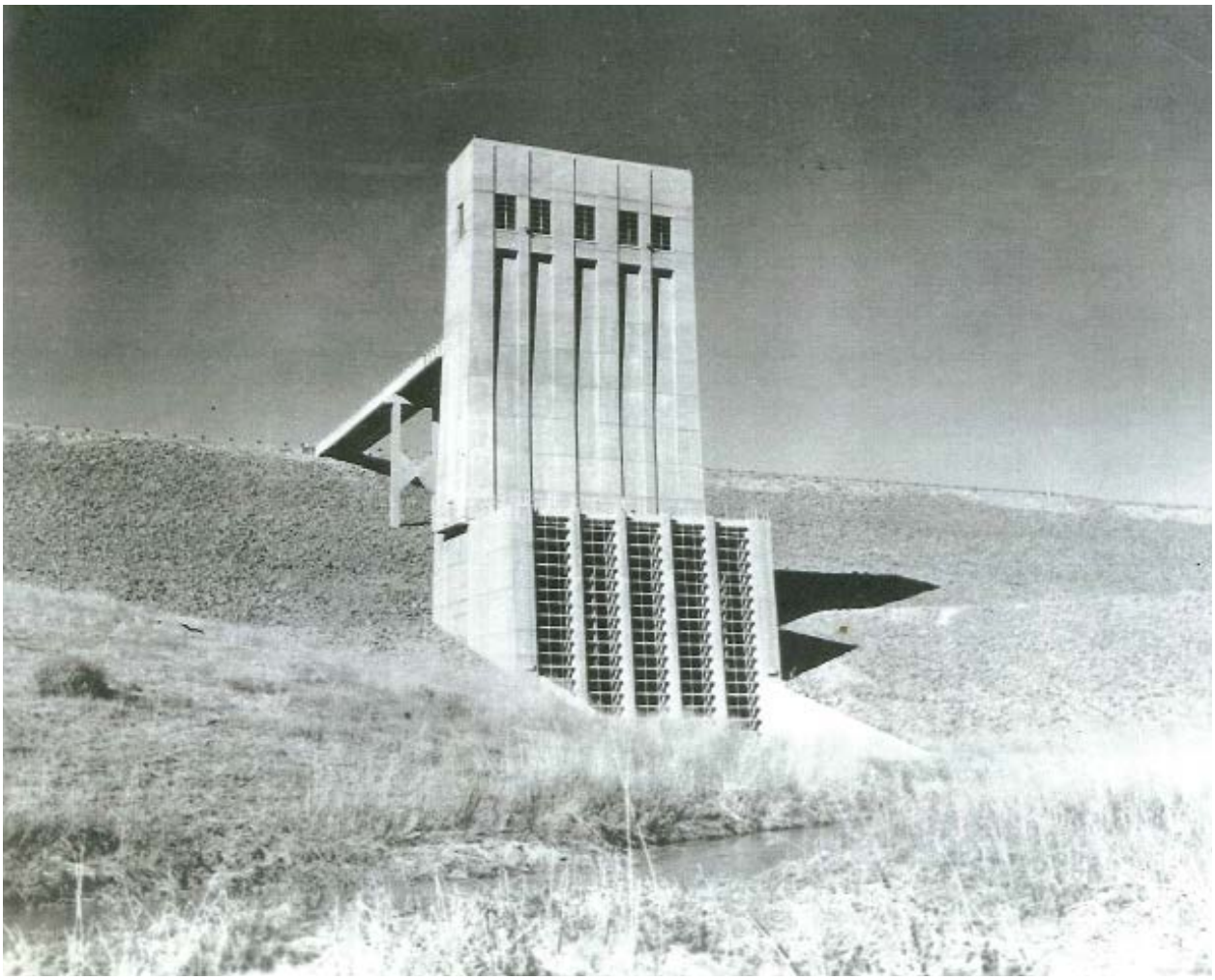

Figure 2. Intake for Cherry Creek Dam outlet works in 1952 (photo courtesy of USACE)

One of the USACE annual maintenance activities is to open the intake gates to flush sediment and debris deposited immediately upstream, ensuring free and clear operation when needed. Each year, all five radial gates are opened and closed individually, in varying order, for a set amount of time. Releases during this maintenance exercise typically alternate between high flows and low flows on a yearly basis. On May 24, 2017, the flushing operation schedule included releases of 250 cubic feet per second from each gate for at least 15 minutes, constituting a low flow flush. On May 23, 2018, releases of 1,300 cubic feet per second for a minimum of 10 minutes were scheduled for each gate, constituting a high flow flush. Various data were collected in the reservoir and in Cherry Creek downstream of the dam prior to, during, and following flushing operations in 2017 and 2018 to provide a basis for comparison between low and high flow flushing regimes.

2016 and 2017 Reservoir Sediment Samples

The USACE and Reclamation collected bottom sediment samples in Cherry Creek Reservoir near the intake to determine characteristics of deposited sediments, provide input for numerical modeling, and track changes in sediment properties in the reservoir and in Cherry Creek

downstream. Both sampling efforts produced similar sediment characteristics near the dam with both comprised primarily of silt and clay sized particles.

2016 USACE Reservoir Sediment Samples

In summer 2016, the USACE collected sediment core samples at 13 locations throughout Cherry Creek Reservoir to define sediment characteristics and variation in deposited material at different locations throughout the reservoir. As would be expected, sediment sizes generally became progressively finer the further downstream they were collected. The two samples collected nearest the intake were both comprised primarily of silt-sized sediment with median diameters between 0.004 and 0.062 millimeters.

2017 Reclamation Reservoir Sediment Samples

On May 16, 2017, a Reclamation crew collected three vibrating core samples across the gates within 200 feet of the intake. Sediment sample lengths (sample thicknesses) ranged from 4.3 to 6.3 feet with the longest sample reaching native soil beneath the deposits. Samples were analyzed for physical properties of dry unit weight, moisture content, gradation, plasticity, and specific gravity through a series of standard tests. The erodibility of the samples was also tested using water jet testing on various layers of the samples. Dry unit weights generally increased and water content decreased with depth, indicating consolidation of in-situ sediments over time. All but one sample were classified as “erodible” to “very erodible” with critical shear stresses varying between 0.013 and 0.295 pounds per square foot (Armstrong, 2017). Critical shear stresses were generally higher at greater sample depths, again indicating consolidation of older sediment deposits.

Reservoir Multibeam Bathymetric Surveys

A series of bathymetric surveys were conducted by the USACE and Reclamation to establish baseline and pre-flush conditions and to track changes in bottom elevation that occurred near the intake during pressure flushing.

2016 USACE Multibeam Survey

During the summer of 2016, USACE surveyors mapped the underwater portions of Cherry Creek Reservoir using a multibeam sonar and global positioning system (GPS) mounted to a survey vessel. The entire reservoir accessible by boat was surveyed to provide updated bottom topography upstream of the dam. The 2016 USACE survey was used by Reclamation survey crews to identify bottom features, locate sediment core sample sites, and define the extent of bathymetry survey necessary to map areas of interest for the flushing activities.

2017 Reclamation Pre- and Post-Flush Multibeam Surveys

On May 22, 2017, two days prior to 2017 pressure flushing, a Reclamation survey crew conducted a multibeam bathymetric survey of the reservoir area surrounding the intake for the outlet works using an real-time kinematic (RTK) GPS integrated with a multibeam sonar transducer. The objective of the survey was to measure pre-flush bottom topography, establishing a baseline for post-flush comparison. For comparison to previous and future surveys, all reservoir bottom elevations measured during 2017 bathymetric survey were

referenced to the water surface elevation gage at the dam. The resulting three-dimensional surface generated from the 2017 bathymetry is shown in Figure 3.

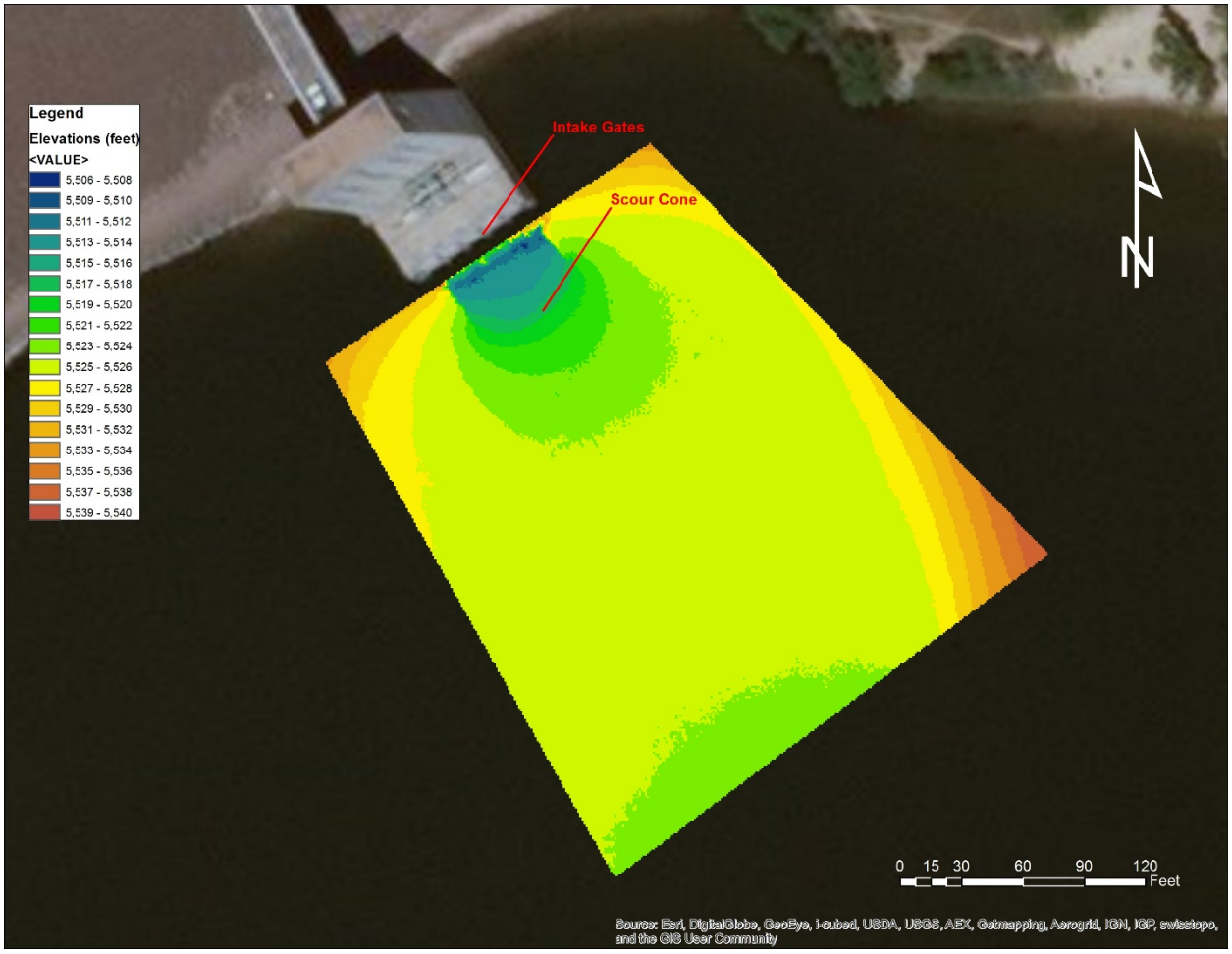

Figure 3. 2017 pre-flush topography near the intake tower showing scour cone and area used for comparison to post-flush geometry (background photo courtesy DigitalGlobe)

The measured depth of the scour cone upstream of the intakes was between 15 and 20 feet and the diameter of the cone at the top was 100 to 160 feet. The estimated volume of the scour cone was between 1,500 and 5,000 cubic yards prior to the 2017 flushing.

The same bathymetric survey in the same area was repeated by a Reclamation survey crew on May 25, 2017, one day after the 2017 low flow pressure flushing. The 2017 post-flush survey measured a minimal volume change, less than 1 percent of the mean annual sedimentation volume, over the area of comparison showed in Figure 3.

2018 Reclamation Pre- and Post-Flush Multibeam Surveys

The same survey equipment and control was used to map the underwater area near the intake two days prior to the 2018 pressure flush on May 21, 2018 and immediately following the flush on May 23, 2018. Survey results again measured minimal change in bottom elevation or sediment volume, again less than 1 percent of the mean annual sedimentation volume, near the intakes due to the high flow flushing operations. It is unknown if the negligible volume change

measured during the multibeam surveys in 2018 partially resulted from beginning the post-flush bathymetric survey within an hour of concluding the pressure flush. Not allowing fine sediments mobilized during the flush to settle back to the reservoir bottom before collecting post-flush bathymetry may have affected depths measured by the multibeam transducer. The high frequency sonar signal may have reflected off the fine sediment remaining in suspension just above the bed rather than penetrating to the actual reservoir bottom.

Downstream Suspended Sediment Measurements

During the 2017 and 2018 pressure flushes, USGS and Reclamation crews collected measurements to determine the variation in suspended sediment concentration throughout the flow releases. A golf cart bridge spanning Cherry Creek approximately 0.6 miles downstream of the dam outlet was used for the 2017 measurements. Another creek-spanning golf cart bridge about 0.3 miles downstream of the dam outlet was used for the 2018 measurements as the downstream bridge used in 2017 was inundated during the high flow flush. The USGS and Reclamation collected suspended sediment measurements from the same bridge during each low flow and high flow flushes with the USGS working off of the upstream side of the bridge and Reclamation working off of the downstream side concurrently. Direct measurements collected by the USGS were compared to surrogate measurements collected by Reclamation to validate suspended sediment surrogate results.

USGS

The USGS was contracted by the USACE to collect direct physical measurements of suspended sediment in Cherry Creek downstream of the dam during the 2017 and 2018 pressure flushes. USGS crews measured suspended sediment from the upstream side of bridges spanning Cherry Creek downstream of the dam prior to, during, and following flushing operations using a Federal Interagency Sedimentation Project (FISP) approved DH-95 sampler suspended from a crane. The DH-95 is a standardized depth-integrated sampler for direct measurement of suspended sediment.

Reclamation

Coincident with the USGS suspended sediment sampling, Reclamation crews collected suspended sediment surrogate measurements from the downstream side of the same bridge for the 2017 and 2018 pressure flushes. Suspended sediment concentrations were estimated using an acoustic backscatter instrument from Sequoia Scientific, Inc (www.sequoiasci.com/product/lisst-abs/), also suspended from a crane. Once calibrated to direct measurements at a specific site, the signal measured by the acoustic backscatter instrument can be used as a surrogate for suspended sediment concentration.

Results of Direct and Surrogate Suspended Sediment Measurements

Data from the DH95 direct measurements and acoustic backscatter surrogate measurements were compiled and analyzed to estimate suspended sediment in Cherry Creek as a function of gate operations and release flows. Comparison of resulting suspended sediment concentrations measured during the 2017 and 2018 pressure flushing exercises showed strong correlation between the two methods. Figures 4 and 5 are plots of continuous acoustic backscatter

measurements compared to DH-95 measurements from the 2017 and 2018 pressure flushes respectively. The flow release schedules are plotted above the concentrations for reference.

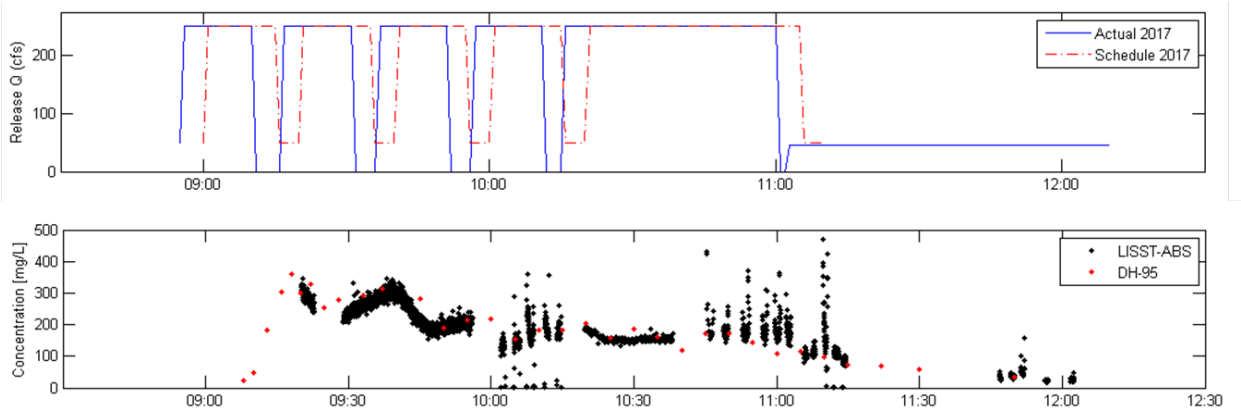

Figure 4. Continuous record of suspended sediment concentrations from acoustic backscatter surrogate measurements compared to DH-95 direct measurements for the 2017 pressure flushing (Dombroski, 2018)

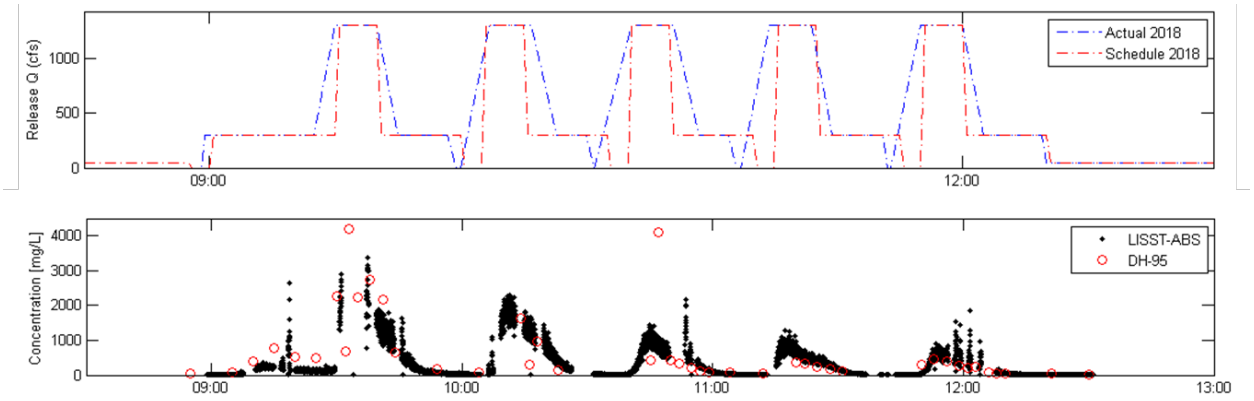

Figure 5. Continuous record of suspended sediment concentrations from acoustic backscatter surrogate measurements compared to DH-95 direct measurements for the 2018 pressure flushing (Dombroski, 2018)

As expected, larger peak discharges during the 2018 high flow flush suspended significantly more sediment in the water column than the smaller peaks during the 2017 low flow flush. The effect of gate openings is far more apparent in the 2018 suspended sediment concentrations than in the 2017 measurements. Lower peak discharges and a sampling site further downstream of the dam in 2017 likely attenuated the wave signal produced by the gate openings (Dombroski, 2018).

Suspended sediment measurements from the 2017 and 2018 flushing events both reveal decreases in concentration with time. Not only do the magnitudes of the peak concentration and total volume of sediment diminish over the course of the low and high flow flushes, but the measured sediment concentration peaks quickly then declines rapidly within each gate opening event. The decrease in peak magnitude and volume over the course of the entire flush indicates a reduction in effectiveness over time while the rapid attenuation of the peak concentration within each gate opening event indicates that dam operators may be able to flush nearly the same volume of sediment with gate openings of shorter duration. Reducing the duration of gate

openings decreases the volume of water used and increases the efficiency of the flushing operation.

Figure 4 and Figure 5 show that several of the suspended sediment concentrations measured by the DH-95 at peak flows were not duplicated by the acoustic backscatter instrument measurements, particularly during the 2018 high flow flush. Greater spatial and temporal variability of sediment concentrations at higher flows, a wider range of sediment grain sizes in suspension during peak flows, and systematic instrument bias are all possible explanations for the discrepancy between acoustic backscatter and DH-95 measurements.

In general, acoustic backscatter suspended sediment concentration measurements matched DH-95 measurements well, especially at lower and intermediate discharges. The close correlation of acoustic backscatter and DH-95 measurements validates the use of the acoustic backscatter instrument as a suspended sediment surrogate at this Cherry Creek site in these conditions.

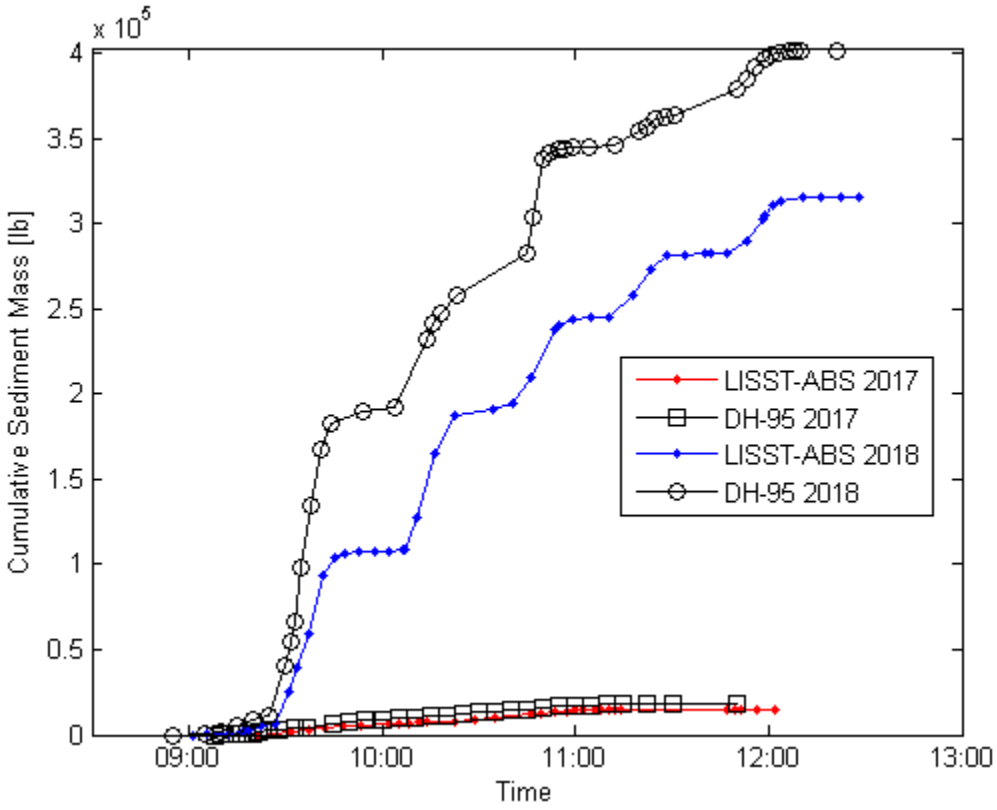

Figure 6. Total sediment mass transported during the 2018 high flow flush, estimated by integrating the sediment transport rate over the duration of the record and converting volume to mass (Dombroski, 2018)

Suspended sediment measurements estimated approximately 300,000 pounds or 380 cubic yards of sediment passed the monitoring station during the 2018 high flow flush (Figure 6, Dombroski, 2018). Compared to the mean annual sedimentation rate at Cherry Creek Reservoir of 111,546 cubic yards, less than 1 percent of the annual inflow was flushed downstream during the 2018 high flow exercise. The negligible volume of sediment removed during flushing indicates that current operations are effective at maintaining free and clear operation of outlet gates regardless of the amount of sediment mobilized.

USACE Downstream Cross Section Surveys and Sediment Samples

Before and after the 2017 and 2018 flushes, USACE field crews surveyed a series of river channel cross sections from Cherry Creek Dam 3 miles downstream. Comparison of cross section plots showed changes in average bottom elevation of 1 foot or less at all locations resurveyed with most repeat cross sections showing changes less than 0.5 feet. Sediment samples were also collected from the bed and banks at several downstream cross sections pre- and post-flush in both 2017 and 2018, but showed minimal change in size gradation. Slightly more fine material deposited on cross sections, but no deposition of coarse sediment was detected. Even high flow flush releases did not mobilize measurable amounts of coarse sediment from the reservoir or Cherry Creek downstream.

USGS Downstream Gage and Discharge Measurements

During the 2017 and 2018 pressure flushing events, USGS crews measured discharge at various locations in Cherry Creek in the 3-mile study reach downstream of the dam using Acoustic Doppler Current Profilers to verify gate discharge curves. Readings at 5-minute intervals from USGS Stream Gage 06713000 Cherry Creek below Cherry Creek Lake, CO further validated the gate discharge curves used for dam and reservoir operations. Discharge measurements and published gage records matched well with rating curve values for the Cherry Creek Dam outlet gates (Boyd, 2018).

Conclusions

Data collection and analysis before, during, and after the 2017 and 2018 pressure flushing events indicate that current operations are successful in removing sediment deposits from the upstream face of the intake gates at Cherry Creek Dam. Flushing is an effective method of maintaining normal gate operations and open outlet works, despite the fact that less than 1 percent of the mean annual inflowing sediment was mobilized and transported downstream. The sequence, magnitude, and duration of gate openings required to remove sediment and transport it downstream through Cherry Creek during flushing operations is uncertain. Measurements taken during low and high flow flushing events suggest that improvements in flushing efficiency are possible.

Favorable comparison of suspended sediment concentrations collected through direct (DH-95) and surrogate acoustic backscatter measurement methods imply that the acoustic backscatter instrument used here is a reasonable surrogate for measurement of suspended sediment concentration at Cherry Creek for the conditions created by the 2017 and 2018 pressure flushing activities. The inability of the acoustic backscatter instrument to match DH-95 measurements at some peak discharges is likely due to large variability in suspended sediment concentration profiles and grain size distributions at higher flows. Additional measurements and calibration at other sites over a wide range of conditions are necessary to confirm the general usefulness of the acoustic backscatter instrument for suspended sediment concentration monitoring.

The multiple complimentary methods of data collection and analysis utilized in this study allowed resolution of the effects of low flow and high flow flushing operations at Cherry Creek Reservoir. Although repeat multibeam bathymetry in the reservoir and cross section surveys in the creek downstream were unable to track the movement of sediment through the system

during the flush, suspended sediment measurements downstream provided valuable insight to the impacts of gate operations for high and low flow flushing events. In many cases such as this, multiple simultaneous data collection approaches provide redundancy, validation, and greater resolution of sediment related patterns and processes.

Acoustic Doppler Current Profiler (ADCP) measurement of velocity profiles within the reservoir before and during flushing could help determine the increase in flow velocities at the intake resulting from gate opening. ADCPs measure flow velocities over a range of depths using the hydroacoustic return signal from particles within the water column. Significant progress has been made in using down-looking ADCP backscatter signals to measure suspended sediment concentrations. Calibration is difficult and involves point measurement of suspended sediment concurrent to ADCP measurements, but the technology could be used to estimate suspended sediment transport at the intakes during flushing events. These data may be used to determine the most effective magnitude and timing of gate operations for pressure flushing of sediments and would provide calibration data for ongoing numerical modeling efforts.

Ongoing Study

Three-dimensional numerical sediment transport modeling is underway at Reclamation to replicate changes in suspended sediment concentration downstream of Cherry Creek Dam measured during flushing operations. Successful calibration of the 3-D model will provide a tool for the prediction and evaluation of multiple pressure flushing scenarios to help determine the most efficient operations. The 3-D numerical modeling tool could be used to evaluate flushing operations at reservoirs world-wide.

References

Armstrong, B. 2017. *Cherry Creek Reservoir Sediment Erosion Testing Results*. Technical Memorandum No. 8530-2017-22, US Bureau of Reclamation, Denver, CO.

Boyd, P. 2018. “2018 Range and Sed DataWORKING.xlsx,” Microsoft Excel File. US Army Corps of Engineers, Omaha District, Omaha, NB.

Boyd, P. 2018. “Cherry Creek Flushing Operation Schedule Wed May 24, 2017,” Adobe Acrobat pdf. US Army Corps of Engineers, Omaha District, Omaha, NB.

Dombroski, D. 2018. *Suspended Sediment Monitoring Techniques: An Investigation Coincident with the Cherry Creek Reservoir Flush*. Report No. ST-2018-1893-01, US Bureau of Reclamation, Denver, CO.

https://corpsmapz.usace.army.mil/apex/f?p=303:1. May 3, 2019. US Army Corps of Engineers Reservoir Sedimentation Information website.

www.sequoiasci.com/product/lisst-abs/. January 3, 2019. Sequoia Scientific, Inc. LISST-ABS.

Comparing Reservoir Sediment Yield, Depletion, and Sustainability within the Missouri River Basin

Daniel Pridal, PE, Omaha District, US Army Corps of Engineers, Omaha, NE
Daniel.B.Pridal@usace.army.mil
Paul M Boyd, PhD, PE, Omaha District, US Army Corps of Engineers, Omaha, NE
Paul.M.Boyd@usace.army.mil
Larry J Morong, Omaha District, US Army Corps of Engineers, Omaha, NE
Larry.J.Morong@usace.army.mil

Abstract

Repetitive reservoir storage capacity surveys are often thought to provide one of the most accurate methods to assess basin sediment yield. The Omaha District conducts a large scale sediment data collection and analysis program for six Missouri River mainstem and twenty-two tributary reservoirs. An analysis was conducted to compare the sediment yield, reservoir capacity, depletion trends, and comparison between projects for effects on project sustainability. Trend analysis is complicated by temporal variation in conservation practices that affect sediment yield, new reservoir survey techniques, and revised capacity computation methods. Results provide insight on the variation in basin sediment yield, reservoir depletion rates, variation due to a change in survey method, and impacts on long term reservoir sustainability.

Introduction

The U.S. Army Corps of Engineers (USACE), Omaha District conducts sediment monitoring and computational analyses within the upper Missouri River basin. The Missouri River basin has an area of 529,350 square miles covering parts of seven states which is over one-sixth of the United States drainage area. The Omaha District River and Reservoir Engineering Section conducts monitoring and analysis activities for federally constructed reservoirs on both the six Missouri River mainstem and twenty-two tributary streams.

The Missouri River mainstem reservoirs are comprised of six reservoirs that contain a total of about 73.4 million acre-feet of storage capacity, nearly three times the average annual flow of the Missouri River at Sioux City, Iowa. Authorized operating purposes for the system includes flood control, navigation, hydroelectric power, irrigation, water supply, water quality control, recreation, and fish and wildlife (USACE 2006). The mainstem dams are composed of six large earthen embankments which impound a series of reservoirs that extend upstream for 1,257 river miles from Gavin's Point Dam near Yankton, South Dakota to the head waters of Fort Peck Lake north of Lewiston, Montana. Fort Peck Dam, the oldest of the six dams, was closed and began storing water in 1937. Fort Randall Dam was closed in 1952, followed by Garrison Dam in 1953, Gavin's Point Dam in 1955, Oahe Dam in 1958, and Big Bend Dam in 1963.

The Missouri River dams intercept the sediment from one of the largest and highest sediment yielding regions in the continental United States. In its pre-dam state, the Missouri River transported an estimated total sediment load averaging 25 million tons per year in the vicinity of Fort Peck, Montana, 150 million tons per year at Yankton, South Dakota, 175 million tons per

year at Omaha, Nebraska, and approximately 250 million tons per year at Hermann, Missouri near its confluence with the Mississippi River (USACE, 2006).

The twenty-two Missouri River tributary reservoirs were constructed primarily as local flood control projects with other authorized purposes including recreation and fish and wildlife. Fourteen reservoirs are located in Nebraska; three in South Dakota; three in Colorado; and two in North Dakota. Tributary reservoir projects were constructed primarily in the 1960's thru the early 1980's. The location of the mainstem and tributary reservoir projects within the Omaha District sediment monitoring program are shown in Figure 1. For purposes of figure clarity, the eight projects in the Lincoln, Nebraska vicinity are labeled as Salt Creek and the four projects in the Omaha, Nebraska vicinity are labeled as Papillion Creek.

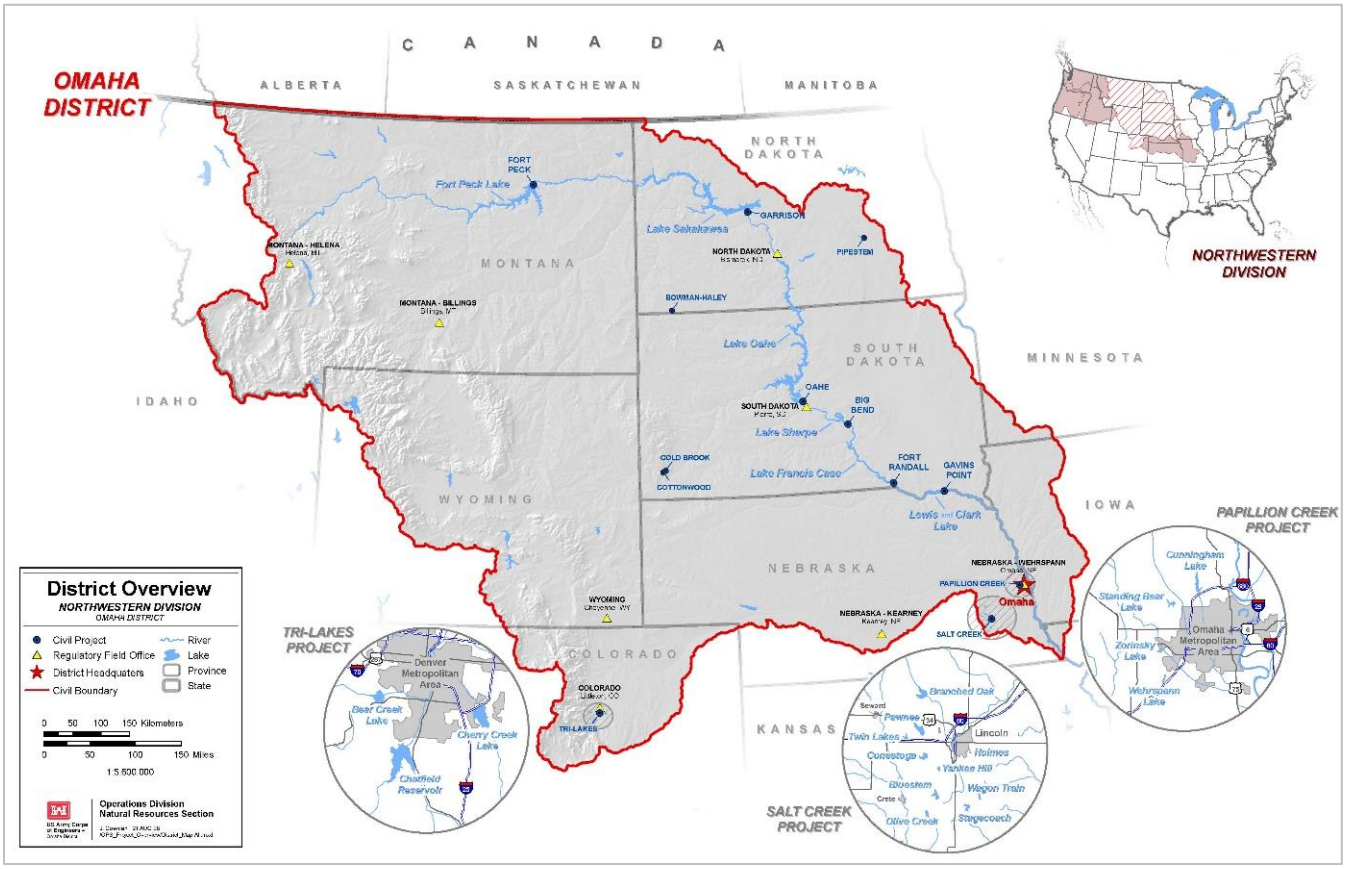

Figure 1. Omaha District - Reservoir Project Location Map

Reservoir Sedimentation

Processes

Reservoir sediment trapping has consequences that extend from the river channel above the reservoir pool, through the storage pool, and to the river reach below the dam. Missouri River sediment deposition has resulted in reservoir capacity depletion throughout the Omaha District. Sediment deposition observed from periodic surveys in the reservoir headwaters may increase

river stages over time, block municipal water intakes, and restrict recreational use of the reservoir.

Trap Efficiency

Due to the large reservoir storage volumes on the Missouri, reservoir trap efficiency for the mainstem reservoirs is nearly 100% and water released from each dam contains virtually no sediment. The twenty-two tributary reservoirs also have trap efficiencies that are nearly 100%. Comparison between reservoir capacity depletion rates assumes that variation in trap efficiency between projects is insignificant.

Reservoir Storage Zones

Capacity at USACE reservoirs includes the total storage along with capacity within pool zones provided for various designated purposes. Terms used for the USACE pool zones vary by project and location. For the purposes of this analysis, storage depletion was evaluated for total storage (top of the exclusive \ flood control pool) and the sediment pool (top of the conservation, sediment, or inactive pool).

Omaha District Data Collection

Reservoir survey methods employed today have evolved significantly since the principal dam construction era from 1950 through 1980 within Omaha District. Survey technological advancements have generally increased data accuracy, precision, and data density and have provided variable cost savings dependent on many site-specific factors. Remote sensing capabilities continue to evolve with new techniques that may become standard in the future.

Early Methods

Each reservoir had a series of cross sections called sediment ranges that were monumented and surveyed using transit and plane table instruments to produce an original data set. Resurveys of these sediment ranges using these early methods continued within USACE into the 1980s followed by a transition to optical total station methods and then GPS technology in the 1990's. For most of the past century, aerial photogrammetry has been relied on for stereo-compilation of 2D planimetric maps and 3D topographic maps including contours (USACE 2007). For project bathymetry, USACE started to employ acoustic depth measurements (echo sounding) in the 1950s (USACE 2013). Omaha District collection methods followed the USACE national methods.

Current Methods

Surveys of the six mainstem reservoirs still rely on sediment range surveys using GPS survey methodology. These reservoirs are too large and remote to allow for economical high density topographic/bathymetric surveys. However, the twenty-two tributary reservoirs now use a combination of aerial LiDAR and either high-density single-beam or multibeam bathymetry. Sediment ranges are also frequently resurveyed as a check to verify the accuracy of LiDAR.

Omaha District Program

The Omaha District has conducted post-construction surveys since closure of each project at 10- to 20- year intervals as part of the data collection and analysis monitoring program. Analyses of the survey data have provided information on both the rate at which reservoir storage volume is being lost due to sedimentation and the location of these deposits both longitudinally and vertically within the reservoir pools.

Computation Methods

Original Storage Estimates

Original storage estimates for each Omaha District reservoir project were based on the best available information at the time of project construction. At most projects, this consisted of a pre-construction survey to the top of reservoir pool elevation. Contour maps were typically created from bathymetric surveys combined with field surveys or aerial photogrammetry. Storage volumes were derived from planimetered area on contour maps that were usually either a 5- or 10-foot intervals. Omaha District employed a modified average end area (MAEA) with ratio tables to replicate the contour area volume. This technique was used to allow for future repetitive surveys along the sediment ranges to compute reservoir capacity with increased accuracy compared to the simple average end area method (USACE 1984).

Current Computational Methods

This original MAEA technique is still used to compute storage capacity changes at the six Missouri River mainstem reservoirs because of survey limitations. The 22 tributary reservoir volume computations now use geographic information system (GIS) computation capabilities with digital elevation models (DEM) developed from the combined high-density data sources (LiDAR and dense hydrographic data). When sediment range surveys are available, capacity computations are also performed with the sediment range MAEA method to compare sediment depletion rates and inform on capacity variation due to the change in methodology.

Sediment Depletion

The reservoir storage capacity depletion rate is a useful metric that can be computed from capacity changes and indicates how quickly reservoir capacity is lost. Future reservoir operations and storage capacity rely on accurate estimates of the storage depletion rate. Variations in computed long-term reservoir depletion rates occur due to several factors.

a) Land Use and Natural Variability. Reservoir storage depletion will vary between survey periods due to man-made land use changes (site grading, environmental restoration projects, road construction, etc.) that affect sediment yield and natural factors (variability in annual runoff volume, precipitation intensity, etc.). Storage depletion rates are highly event driven and respond to extreme hydrologic events.
b) Future Variability. Future storage depletion rates may vary significantly from historical rates due to multiple factors that affect sediment yield such as land use, climate change, fire, and stream degradation.

c) Source Data Accuracy and Density. Data collection methods have evolved over time that has affected data accuracy due to changes in vertical point accuracy and point density. Collecting high density data is generally regarded as the best method to capture topography variation.

d) Methodology. When switching data collection and analysis methodologies, differences can occur due to the change in methodology (e.g. MAEA vs. GIS) rather than an actual variation in the storage depletion rate. Therefore, it is recommended to compute reservoir storage capacity with both methods when a methodology change is made to allow examination of any shift in capacity that may be associated with the change in methodology.

e) Sediment Range Localized Changes. The MAEA method assumes that elevation change on the bounding sediment ranges are representative of elevation change for the entire segment. Depletion for each segment occurs when the bounding sediment range average end area changes. Therefore, minor localized sediment range elevation changes have magnified impacts on capacity.

Capacity Comparison

Reservoir storage capacity at each reservoir was compiled from most recent reservoir surveys and capacity computation method as previously described. Figure *2* illustrates the storage capacity depletion that has been measured at all Omaha District reservoirs since project construction.

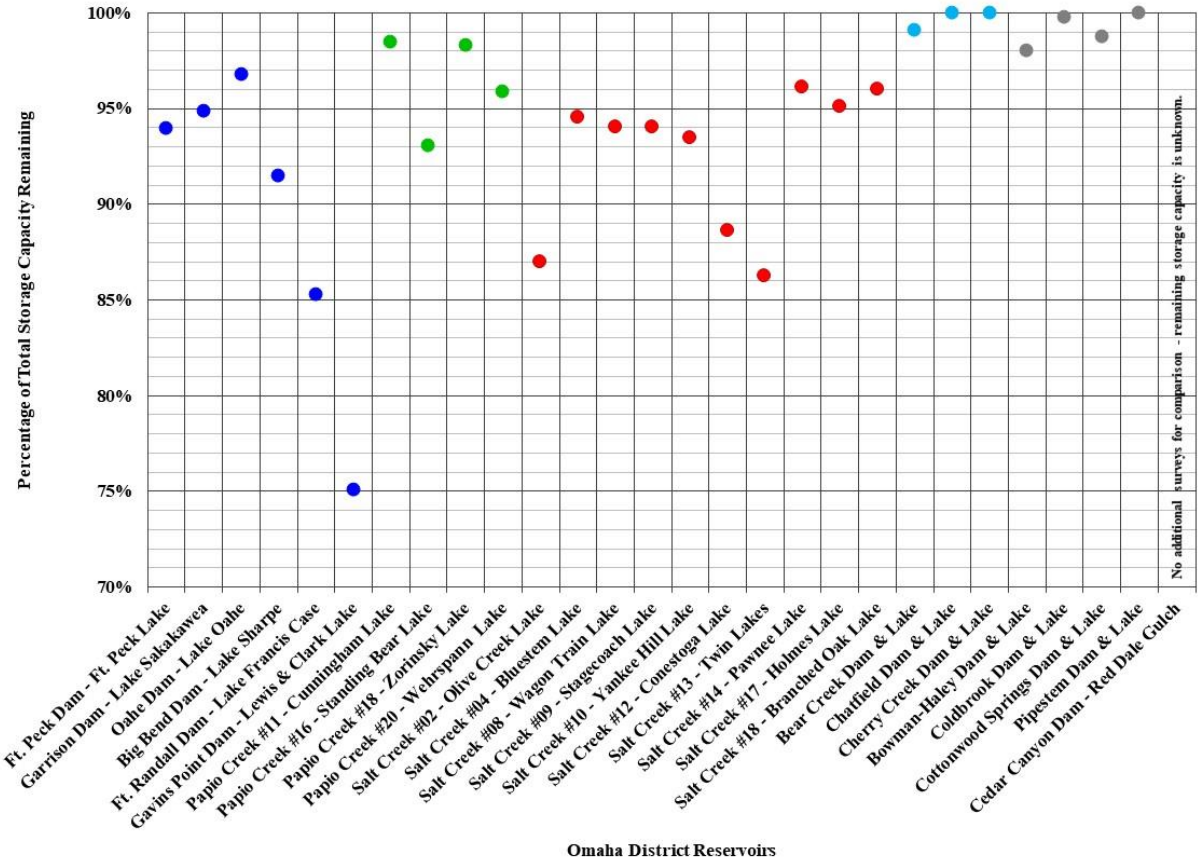

Figure 2. Omaha District Reservoirs – Percentage of Remaining Storage Capacity (Total Storage)

Reservoir storage capacity was normalized using the reservoir drainage area to allow comparison between projects as shown in Figure 3. A wide variation between depletion rates within the Omaha District is shown. The wide variation is not surprising given the large geographic area covered by the reservoirs (Figure 1) along with wide variability in watershed size, soil erodibility, precipitation, and similar factors that affect watershed sediment yield.

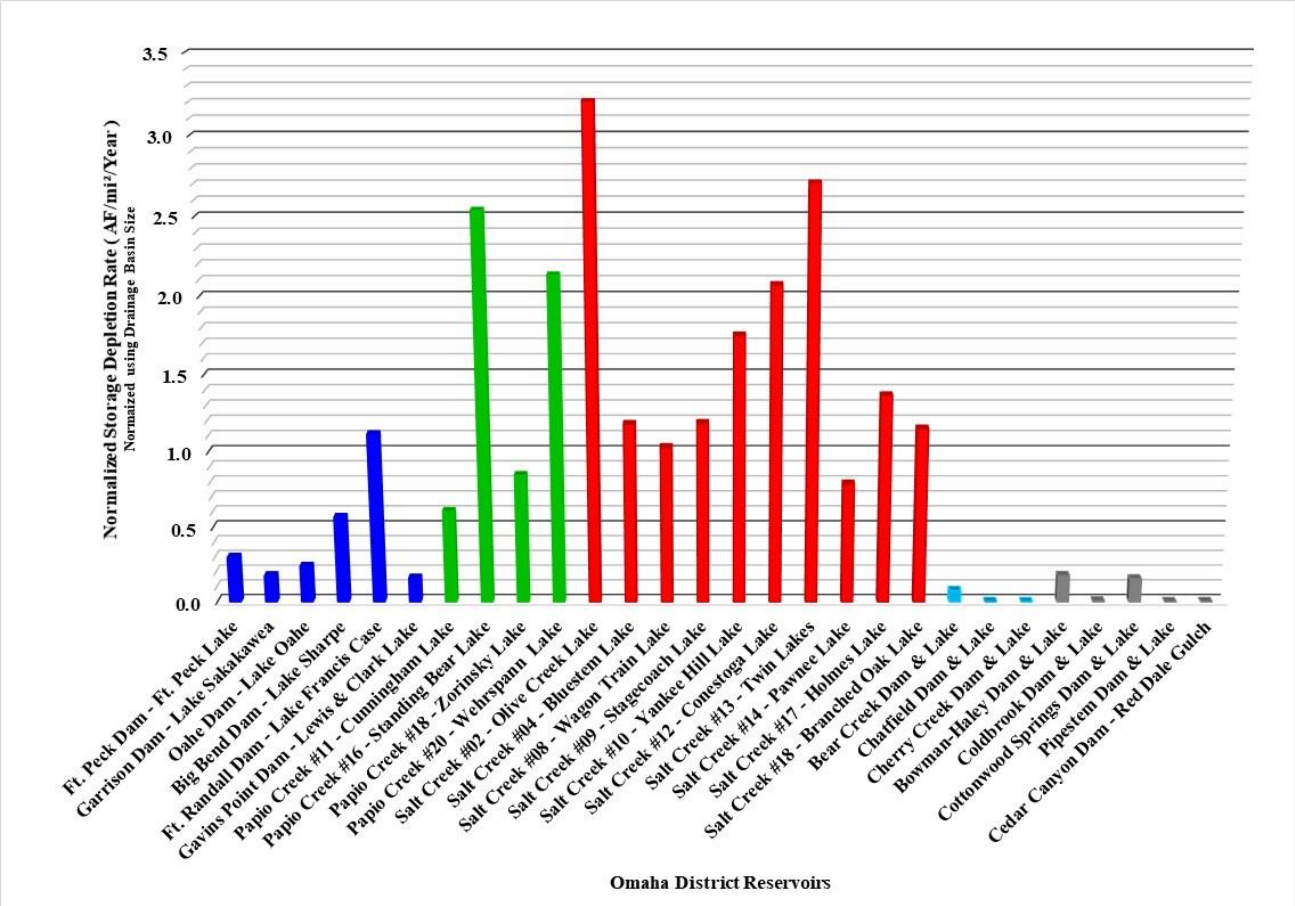

Figure 3. Omaha District Reservoirs – Normalized Storage Capacity Depletion (AF/mi²/Year)

Additional analysis was performed to compare reservoir depletion on similar size projects. Comparison of the Missouri River mainstem reservoirs is shown in Figure *4*. A comparison was performed between total reservoir storage and the sediment/inactive storage zone. A large variation between the two pool levels was not observed. Correlation of mainstem reservoir depletion between reservoir projects was poor.

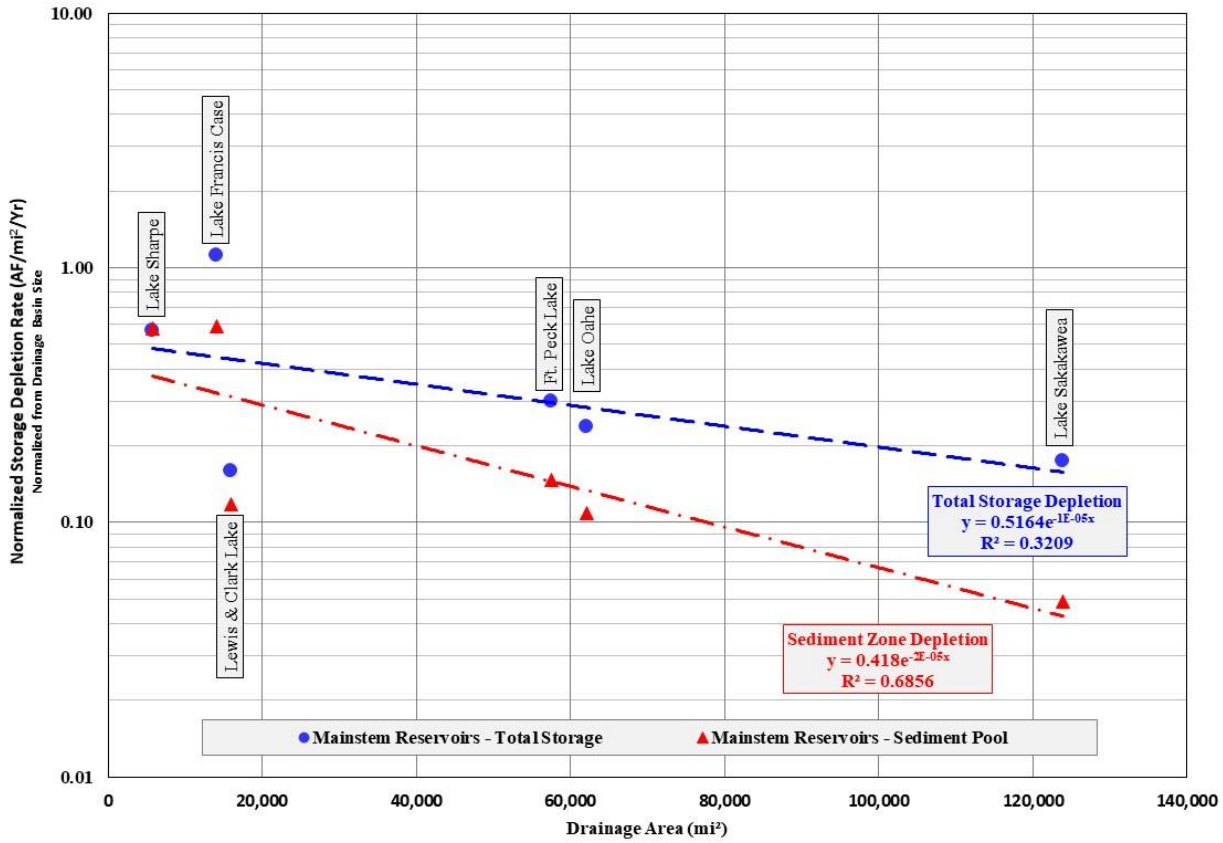

Figure 4. Missouri River Mainstem Reservoirs – Normalized Storage Capacity Depletion (AF/mi²/Year)

A comparison of the depletion at tributary reservoirs is shown in Figure 5. Comparison was performed for both the total storage and the sediment/inactive storage zone. Similar to the mainstem reservoirs, a large variation between the two pool levels was not observed. Tributary reservoirs were grouped by the two main areas, Salt Creek dam sites in the Lincoln, Nebraska vicinity, and the Papillion Creek reservoirs near Omaha, Nebraska. Correlation of depletion rates between the reservoir projects was significantly improved due to similar basin size, soil types, and land use compared to the mainstem dams.

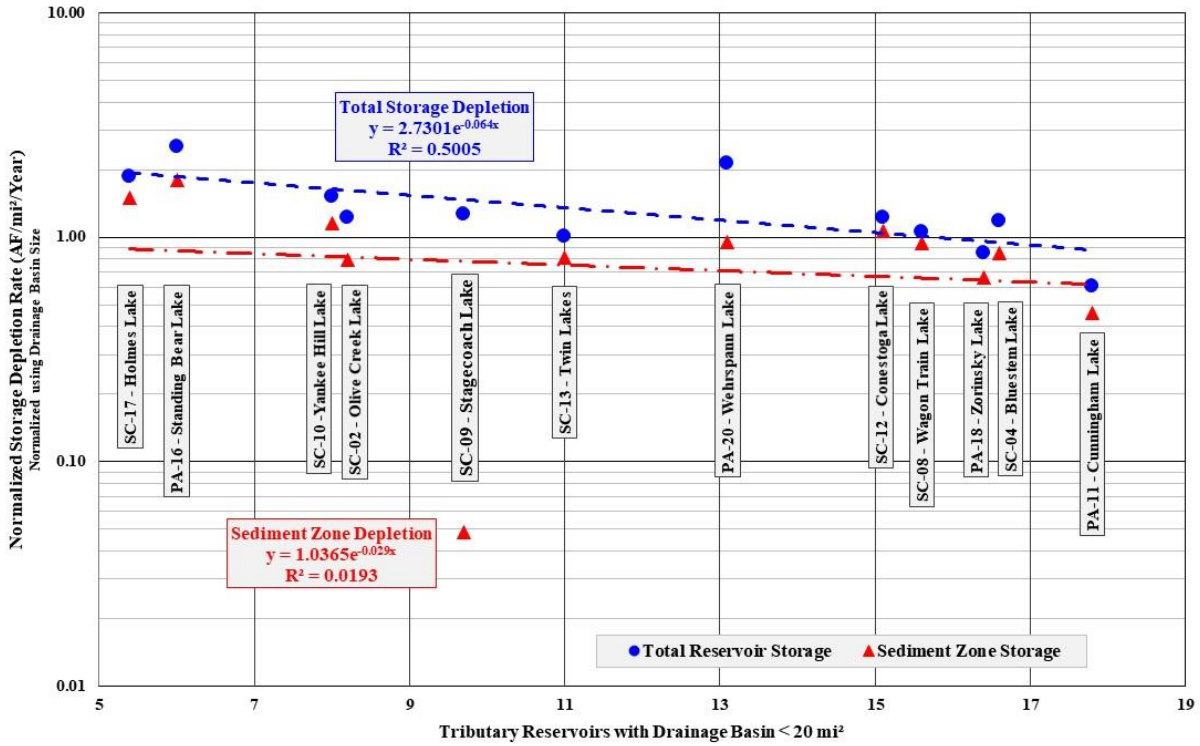

Figure 5. Tributary Reservoirs – Normalized Storage Capacity Depletion (AF/mi²/Year)

Comparison of depletion rates is recommended when conducting studies that require long term estimates of basin sediment yield. The variation and limited correlation can be due to a wide range of factors as previously discussed. However, using a single reservoir depletion rate based on historical surveys may not provide any indication of future rates. Development of an upper bound curve such as shown in Figure 5 based on multiple area reservoirs can improve estimates. This could be further enhanced with results from a basin sediment yield model.

Reservoir Sustainability

Sustainable reservoir sediment management seeks to achieve sediment transport equilibrium through the reservoir while still maintaining the storage capacity and beneficial uses. Limited sediment management may include slowing the deposition rate or may focus on minimizing impact to specific project benefits, such as removing sediment near water intakes, rather than overall sediment sustainability. USACE reservoirs within Omaha District were typically designed to trap and store incoming sediment in an area designated within the reservoir for sediment storage. The adequacy of this zone was usually evaluated based on an economic project life of 50 years. As reservoirs age, additional sediment accumulation displaces storage relied on for all project benefits. In addition, continued sediment trapping in reservoirs can cause upstream and downstream economic and environmental effects, including flooding, in-reservoir water quality impairment, recreational impacts, and downstream degradation and displacement of turbidity-dependent native species (USACE 2019).

For each reservoir, sustainability will have a different definition. That definition will be driven by the current and future operational goals of that reservoir. What should be common with all USACE reservoirs is a reservoir sustainability plan to assess the current and future sediment

and water supply conditions at each reservoir (USACE 2019). Reservoir sustainability plans should consider future climate change (Pinson et al. 2016) and project resilience to those changes. Global changes facing USACE reservoirs include increasing water demand and the potential for increased sedimentation rates, both of which impact key reservoir functions including flood risk management, water supply, and recreation, among others.

Omaha District - Reservoir Life and Design Function Impacts

USACE reservoirs included sediment yield in project design and normally allowed a certain volume for sediment deposition over the project life. Morris and Fan (2008) point out that sediment deposition will seriously interfere with design function long before the entire storage volume is depleted and propose that a half-life metric is a more useful indicator of the period of effective reservoir operational life. This metric is defined as the period required to fill one-half of the original capacity using the estimated sediment load.

Reservoir life and design function impacts were qualitatively evaluated within Omaha District mainstem reservoirs. At Garrison Reservoir, Figure 2 illustrates that the remaining capacity is still about 95%. Sediment depletion at the historic rate since closure will result in the reservoir reaching 50% capacity in about 570 years from closure. However, significant sediment impacts have occurred in the reservoir delta zone. Over a 40 to 60 mile long river reach, observed river levels have increased by over 10 feet. In response, the Omaha District has purchased flowage easements, altered water intakes, encountered increased seepage rates and raised groundwater levels, and addressed.

At Gavin's Point Dam, Figure 2 illustrates that the remaining capacity is less than 75% of original. This reservoir has encountered many of the same issues that have occurred at Garrison Dam. USACE property purchases have been extensive. The large difference in capacity depletion between the two reservoirs has not resulted in a correlated difference in impacts. Therefore, caution should be applied when assuming that reservoirs with small capacity losses will have lower resource impacts than those with large capacity losses.

Sustainability Case Study – Climate Change

USACE has recognized the necessity of using the best current, actionable science on climate change impacts to water resources in evaluating reservoir sedimentation impacts, conducted numerous studies, and developed guidance (Pinson et al 2016).

Within the Omaha District, the Garrison Reservoir Climate Change Associated Sediment Yield Impact Study (USACE 2012) was undertaken to evaluate how climate change will affect the future basin runoff, sedimentation rates, and operations of Garrison Dam. This study was part of a larger inter-agency effort that included members of USACE, Reclamation, USGS, and NOAA. The study included both hydrologic and sediment aspects of climate change within the basin.

Two separate method were used to evaluate how hydrologic and sediment factors could affect sediment yield to Garrison Reservoir. First, Yellowstone River suspended sediment measurements were used to examine how altered seasonal runoff patterns could affect sedimentation rates. This analysis was performed to assess how a basin wide change in runoff could affect sediment yield. This analysis determined minor adjustment in future sedimentation rates due to seasonal affects but fairly large changes due to hydrologic effects.

Second, a SWAT model was used to evaluate hydrologic and seasonal changes on sediment yield for the Little Missouri River watershed. This small watershed (9,513 mi^2) analysis within the very

large Garrison watershed (181,400 mi²) was performed to assess the impacts of climate change on sediment yield when the precipitation is not evenly distributed, and variables including soil type, land use, slope, and vegetation are considered. This analysis determined measurable impacts. Results from both methods were extrapolated to the entire Garrison Reservoir drainage basin. Results were applied with different climate project scenarios to determine impact on sedimentation rates as shown in Figure 6. Results show that even climate scenarios with less discharge can result in increased reservoir sedimentation inflows due to changes in timing. This finding was evident in the stream gage based analysis as well as in the results of the ArcSWAT model. Findings indicate that, when performing studies in which reservoir depletion rates are critical, assuming that future rates are the same as historic rates is likely non-conservative. Methods to assess climate change effect on sediment depletion may be warranted.

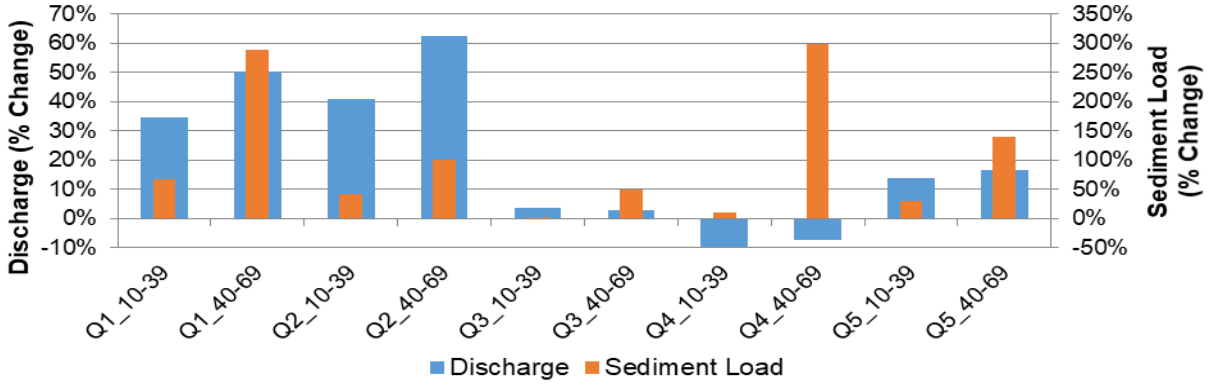

Figure 6. Climate Change Evaluation Comparing Discharge and Sediment Load Change at Garrison Reservoir

Summary and Recommendations

The Omaha District conducts a large-scale sediment data collection and analysis program for six Missouri River mainstem and twenty-two tributary reservoirs. Topographic and bathymetric data collection and computation methods have evolved since reservoir construction. Reservoir storage capacity depletion trends were compared between projects. Trend analysis is complicated by temporal variation in conservation practices that affect sediment yield, new reservoir survey techniques, and revised capacity computation methods. Reservoir sustainability was also evaluated for two specific instances.

Results provide insight on the variation in basin sediment yield, reservoir depletion rates, variation due to a change in survey method, and impacts on long term reservoir sustainability. Comparison of reservoir sediment depletion rates within similar watersheds indicated that developing an upper bound estimate from historic surveys is feasible. A climate change case study indicated that investigating how future sediment depletion rates may vary from historic is recommended. Combining results from the different methods, including an assessment of variation due to changes in data collection and computation methods, is recommended when developing long term estimates of future sediment depletion. These estimates, combined with observations regarding current reservoir capacity levels and impacts, are a critical factor in assessing long term sustainability at reservoirs within the Omaha District.

References

Morris, G.L., and J. Fan. 1998. "Reservoir Sedimentation Handbook: Design and Management of Dams, Reservoirs and Watersheds for Sustainable Use," McGraw-Hill Book Co., New York.

Pinson, A., Baker, B., Boyd, P., Grandpre, R., White, K.D., Jonas, M. 2016 "U.S. Army Corps of Engineers Reservoir Sedimentation in the Context of Climate Change. Civil Works Technical Report, CWTS 2016-05, U.S. Army Corps of Engineers: Washington DC.

US Army Corps of Engineers. 2019. "Sedimentation Investigation of Rivers and Reservoirs, DRAFT, Engineer Manual 1110-2-4000," U.S. Army Corps of Engineers, Washington, D.C.

US Army Corps of Engineers. 2013. "Hydrographic Surveying, Engineer Manual 1110-2-1003," U.S. Army Corps of Engineers, Washington, D.C.

US Army Corps of Engineers. 2012. "Climate Change Associated Sediment Yield Impact Study: Garrison Dam Specific Sediment and Operation Evaluations – Sedimentation Focus," U.S. Army Corps of Engineers, Omaha District, Omaha, NE.

US Army Corps of Engineers. 2007. "Control and Topographic Surveying, Engineer Manual 1110-1-1005," U.S. Army Corps of Engineers, Washington, D.C.

US Army Corps of Engineers. 2006. "Missouri River Mainstem Reservoir System, Master Water Control Manual, Missouri River Basin," U.S. Army Corps of Engineers, Northwestern Division – Missouri River Basin, Reservoir Control Center, Omaha, NE.

US Army Corps of Engineers. 1984. "Missouri River Division Sediment Series #34, Aggradation and Degradation of the Missouri River Main Stem Dams," Omaha District Corps of Engineers.

Effects of Bank Stabilization on Regional Sediment Management (RSM)

Aaron Williams P.E., Hydraulic Engineer, U.S. Army Corps of Engineers
Kansas City District, Kansas City, MO, Aaron.R.Williams@usace.army.mil

John Shelley Ph.D. P.E., Hydraulic Engineer, U.S. Army Corps of Engineers
Kansas City District, Kansas City, MO, John.Shelley@usace.army.mil

Abstract

Accumulation of sediment has and continues to be a major problem facing reservoir managers and stakeholders. Sediment accumulation can be reduced by either preventing sediment from entering the reservoir or by removing it once it has been deposited, typically by dredging and upland disposal. Sediment transported into reservoirs is generated from overland run-off and erosion of river beds and banks from upstream watersheds. This paper presents an analysis of bank stabilization as a means of regional sediment management within the U.S. Army Corps of Engineers (USACE) Kansas City District (NWK).

Introduction

USACE has a long history of streambank stabilization. Section 14 of the 1946 Flood Control Act, as amended, provides authority for USACE to plan and construct emergency streambank and shoreline protection projects to protect endangered highways, highway bridge approaches, and other nonprofit public facilities. These and similar projects have not historically counted the reduction in sediment loading to the river as a benefit during alternatives analysis. However, in many cases downstream projects including reservoirs, actively maintained navigation channels, and sensitive floodplain habitats can substantially benefit from the sediment reduction. This study includes analysis of two categories of streambank stabilization projects that differ in their level of robustness in the Kansas River Basin and Grand River Basin.

Kansas River Basin

The first category includes streambank stabilization projects built by the State of Kansas agencies upstream of Corps reservoirs in the Kansas River Basin. Many watersheds within the Kansas River Basin derive the predominant portion of their sediment load from erosion of beds and banks rather than from overland run-off (Juracek and Ziegler 2009). A disproportionate amount of the total bank-derived sediment comes from a limited number of tall banks with high erosion rates (USACE 2011). The Kansas Water Office (KWO) estimated that sediment load reduction through stabilization of these bank erosion "hot spots" could be as much as 21 times more cost effective than traditional reservoir dredging (Gnau 2013). Approximately 13 million cubic yards per year (M yd3/year) of sediment are deposited in Tuttle Creek, Milford, Kanopolis, Wilson, Harlan County, and Wakunda Lakes (Shelley et al. 2016). The State of Kansas has constructed miles of streambank stabilization in an effort to reduce the sediment loading to the reservoirs. These projects were built specifically for erosion reduction, not infrastructure

protection, and are less robust (minimal or absent toe protection, fewer or absent keys.) Ten projects were analyzed in the study and reported in this paper.

Grand River Basin

The second category includes eight Section 14 streambank stabilization projects constructed by the Kansas City District Army Corps of Engineers upstream of ecologically sensitive floodplain habitats in the Grand River Basin. The purpose of these projects was to protect critical infrastructure, typically bridges and roads. The targeted banks were not as erosive, and significantly more rock was used in the projects when compared to the State of Kansas projects. Figure 1 shows a general location map of the bank stabilization projects. Figures 2 and 3 provide maps of the Kansas River and Grand River Basins, respectively.

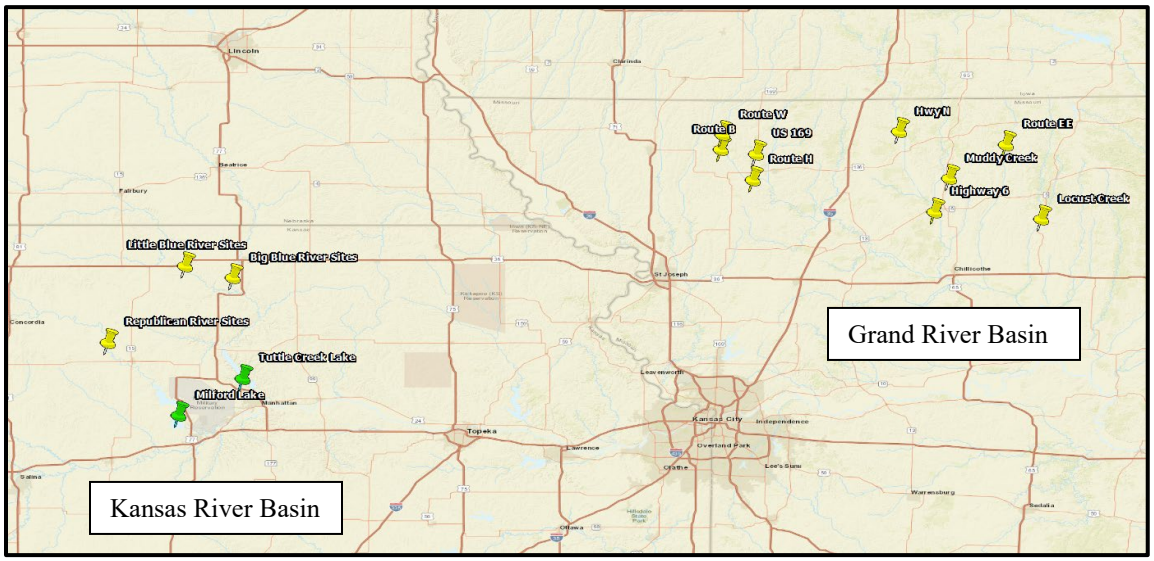

Figure 1. General location map of streambank stabilization projects (Green Pins = Reservoirs, Yellow pins = Project Sites).

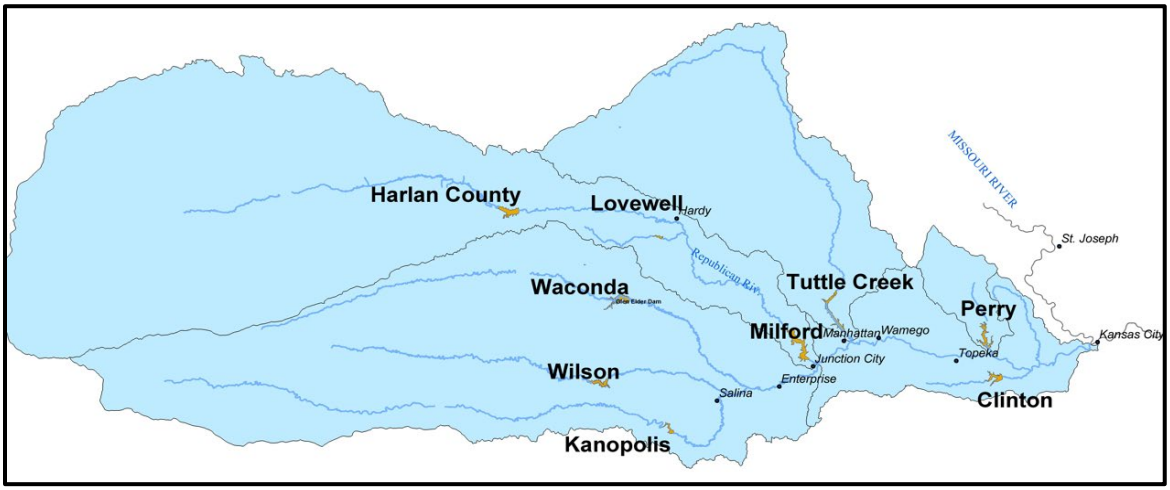

Figure 2. Kansas River Basin map.

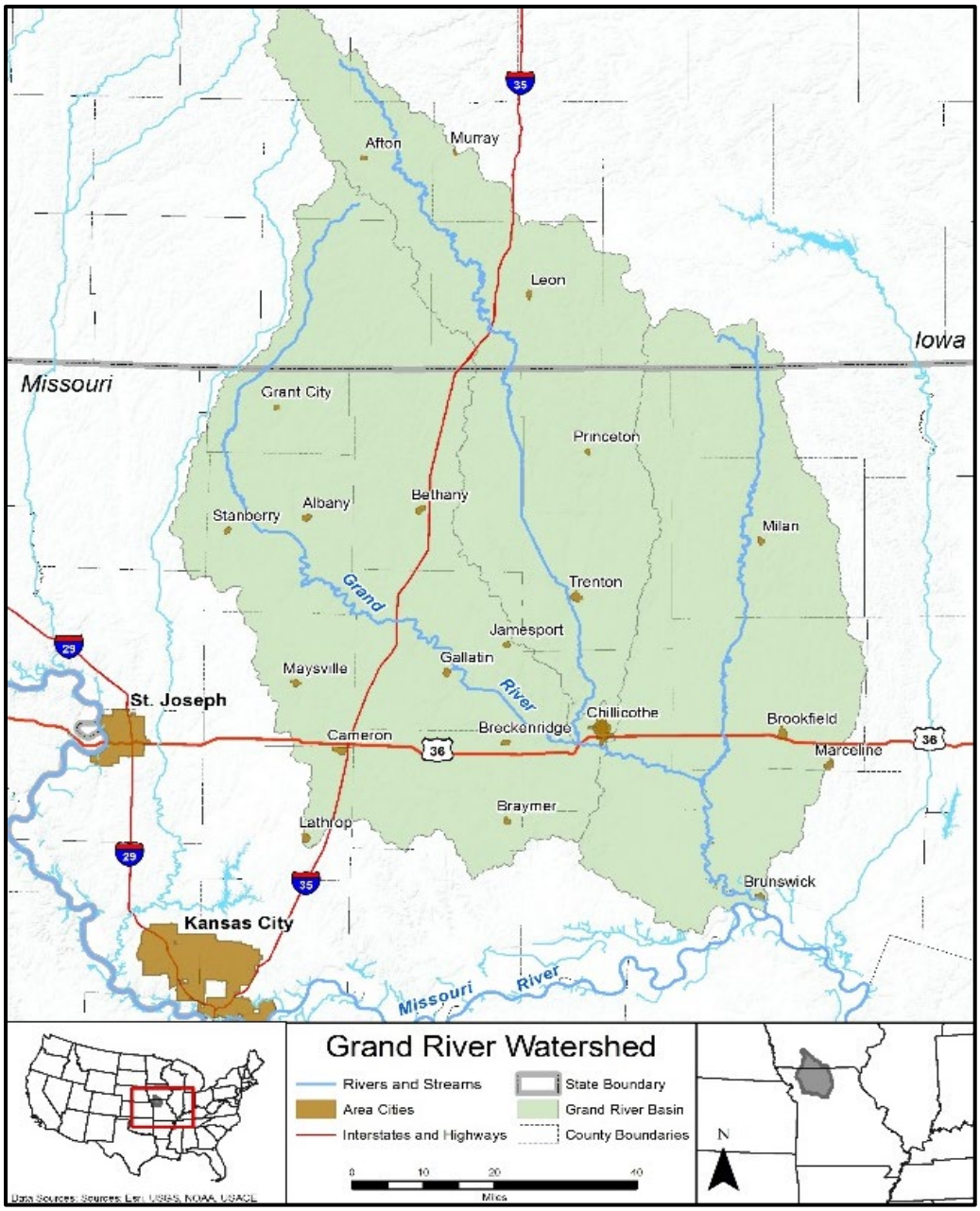

Figure 3. Grand River Basin map.

Study Analysis and Assumptions

Comparison to Dredging Costs

A first approximation for the economic value of the streambank stabilization from an RSM perspective can be estimate by the cost to dredge an equivalent volume of sediment from a downstream reservoir. A 2016 hydraulic dredging project at John Redmond Reservoir removed 3 M yd^3 at a cost of \$20 M, or \$6.67/yd^3 (KWO 2016). Promising and potentially less expensive

dredging techniques such as hydrosuction (Shelley 2017) and water-injection dredging are currently being analyzed for effectiveness on reservoirs within the Kansas River Basin. However, due to unknowns, limitations, and current regulatory hurdles associated with these methods, this study used a sediment removal cost of $6.67/yd^3 to assess the monetary value of reducing sediment loads via streambank stabilization. The additional benefits of stream bank stabilization that accrue to local landowners are not included.

Sediment Reduction Computations

The reduction in sediment loading due to the construction of bank stabilization projects was computed in three steps. (1) Aerial photography from 1991 to 2008, along with the construction dates, provided an annual area erosion rate. (2) The annual area erosion rate was transformed into an annual volume using field measurements for bank heights. And (3) sediment size gradation samples were used to compute the volumetric erosion rate of only the wash load portion of bank sediments. Wash load that enters streams from eroding banks quickly transports downstream at approximately the same velocity as the water (Biedenharn 2006) and deposits in the reservoirs. Reducing the wash load results in a comparable near-term reduction in sediment loading to the reservoir. Conversely, a reduction in the coarse fraction of the bank material could take decades to translate into reduced sediment loading to the reservoirs. For this study, only wash load material is used for the volume estimates.

For the purpose of this study, wash load was defined as the grain size for which 10% of bed mixture is finer (Einstein 1950). Sediment samples were collected during field assessments and analyzed for particle size. One requirement in the wash load definition is that bed samples are not collected at low flows (Einstein 1950). Due to low flow conditions during sampling for this study, the particle size and percentage of bank material constituting wash load is likely conservatively low, which will lead to an underestimate of the sediment reduction from the bank stabilization. Figure 4 presents the results of the size gradation analysis of the bed and banks.

Rock Quantities

Design documents listing the quantity of rock used during construction were available for seven of the of the 10 State of Kansas projects. Rock quantities for the remaining three projects without design documents were estimated using a relationship between project length and rock quantity developed from the seven projects with known rock quantities. Only one of the 10 State of Kansas projects had information available for the volume of earthwork required during construction, so a relationship was developed between the quantity of rock used and volume of earthwork required from the Section 14 projects. Due to the varying level of design of the eight Section 14 projects constructed in the Grand River Basin, only the four projects with known rock and earthwork quantities were used in the sediment reduction analyses. Estimated project costs are calculated by summing the cost to purchase and place rock, assumed to be $50/ton, and the cost to perform earthwork, assumed to be $6.40/yd^3. These prices are based on recent cost estimates developed within the Kansas City District for similar projects in the same vicinity. While the estimated project costs in this study (on average $65 per linear foot) are a simplified presentation of actual costs, they fall within the anticipated costs to implement stream bank stabilization (USACE 2011). For each project, the annual erosion volume rate was multiplied by the percent of the bank material computed to be wash load to estimate the reduction in wash load. This quantity was then multiplied by $6.67/yd3 (KWO 2016) to estimate the annual cost to dredge an equivalent quantity of sediment.

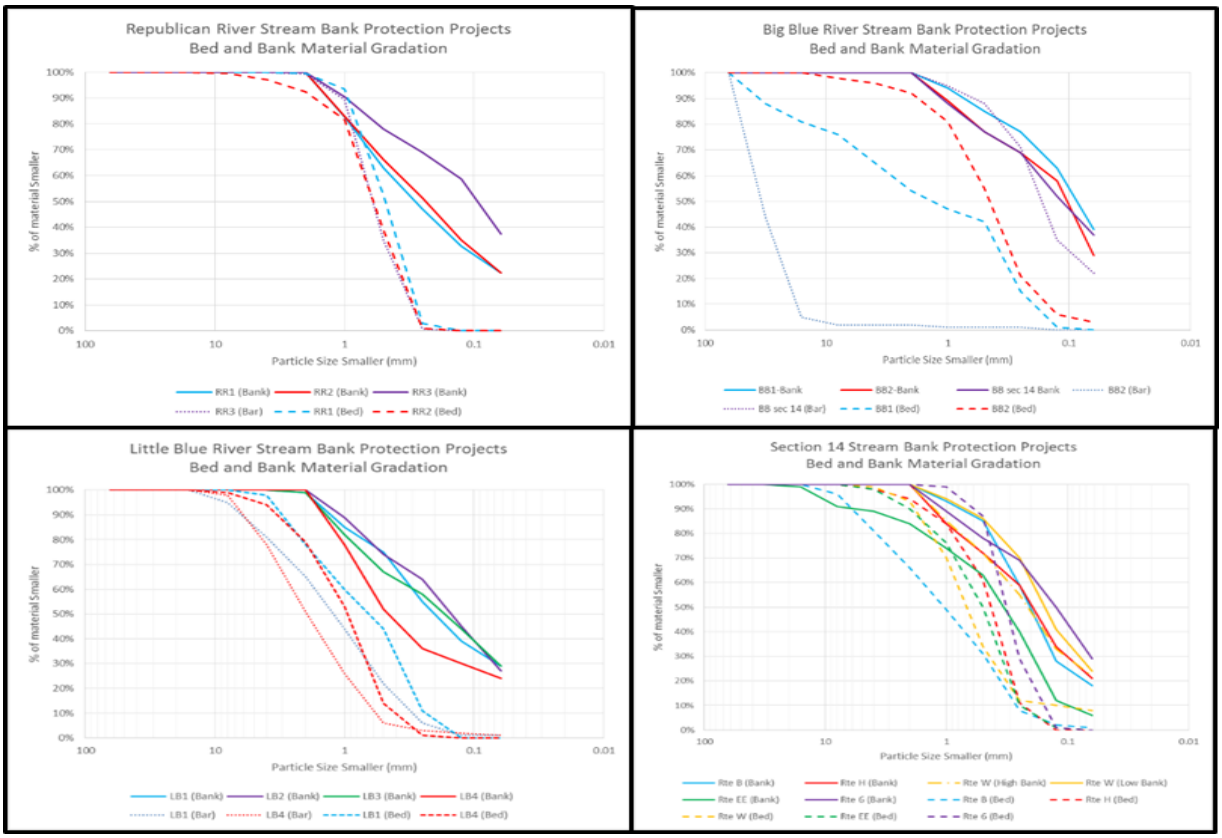

Figure 4. Bed/bank sample gradations

Study Results

Tables 1-4 provide results of the sediment reduction and project cost analyses and Figures 5-8 show the location of the projects sites. As seen, the 10 State of Kansas bank stabilization projects upstream of Corps reservoirs are estimated to be on average 14 times more cost effective than reservoir dredging, assuming a 20-year design life. For the four Section 14 projects in the Grand River Basin designed to protect infrastructure, bank stabilization is estimated to be approximately equal to the cost of reservoir dredging over a 20-year period. In fact, the actual sediment reduction benefits from these Section 14 projects result from decreasing negative impacts to ecologically sensitive floodplain habitats downstream. Sediment removal from these habitats would be much more expensive than the $6.67/yd3, and also comes at the expense of having to damage the habitat to remove the sediment. Project costs are much higher for the Section 14 projects than the State of Kansas projects due to failure risks. Section 14 projects are an emergency action to protect critical infrastructure and require much more robust design than the State of Kansas projects, whose failure would not jeopardize critical infrastructure.

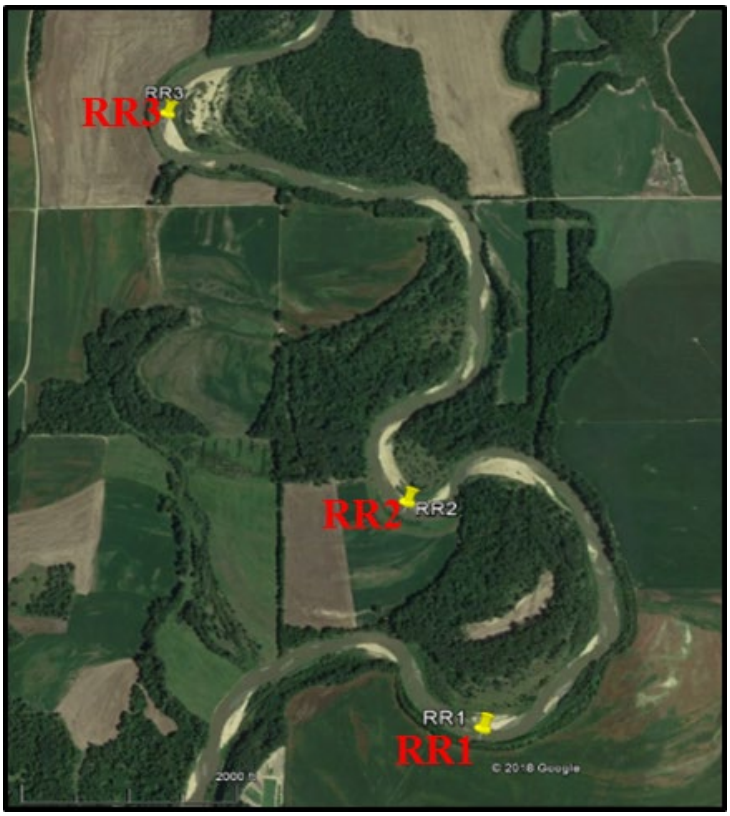

Figure 5. Republican River Project Location Map

Table 1. Republican River Sediment Reduction and Project Costs

Republican River			
Site Identifier	RR1	RR2	RR3
Year Constructed	2004	2006	2004
Erosion Area (ac)	7.5	5.5	10.6
Bank Height (ft)	13.8	13.8	13.8
Erosion Rate (yd^3/yr)	12,700	8,200	18,100
% Bank Wash Load	71%	55%	49%
20-year Wash Load Reduction (yd^3)	180,340	90,200	62,100
Quantity of Rock (ton)	1,844	1,685	1,727
Volume of Earthwork (yd^3)	706	645	661
Estimated Project Cost	$97,000	$88,000	$91,000
20-Year Wash Load Dredging Cost	$1,200,000	$600,000	$410,000

Figure 6. Big Blue River Project Location Map

Table 2. Big Blue River Sediment Reduction and Project Costs

Big Blue River			
Site Identifier	BB1	BB2	BB3
Year Constructed	2003	2010	2010
Erosion Area (ac)	6.2	3.8	2.3
Bank Height (ft)	20.3	19.4	22.3
Erosion Rate (yd^3/yr)	16,900	7,000	4,800
% Bank Wash Load	72%	61%	60%
20-year Wash Load Reduction (yd^3)	243,360	85,400	57,600
Quantity of Rock (ton)	993	*1,164**	*744**
Volume of Earthwork (yd^3)	380	446	285
Estimated Project Cost	$53,000	$61,000	$39,000
20-Year Wash Load Dredging Cost	$1,620,000	$570,000	$380,000

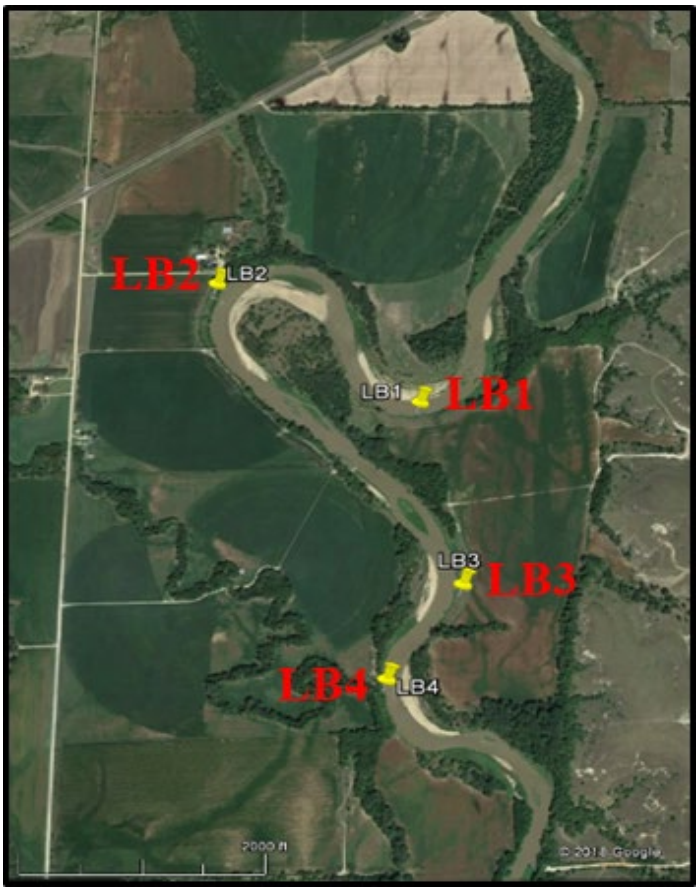

Figure 7. Little Blue River Project Location Map

Table 3. Little Blue River Sediment Reduction and Project Costs

Little Blue River				
Site Identifier	LB1	LB2	LB3	LB4
Year Constructed	2002	2004	2002	2011
Erosion Area (ac)	7.2	7.1	1.5	2.0
Bank Height (ft)	21.0	21.0	17.9	21.0
Erosion Rate (yd^3/yr)	22,000	18,500	3,900	3,900
% Bank Wash Load	54%	62%	57%	52%
20-year Wash Load Reduction (yd^3)	237,600	229,400	44,460	40,560
Quantity of Rock (ton)	1,017	*1,080**	2,016	1,121
Volume of Earthwork (yd^3)	390	414	772	429
Estimated Rock Cost	$53,000	$57,000	$106,000	$59,000
20-Year Wash Load Dredging Cost	$1,580,000	$1,530,000	$300,000	$270,000

Figure 8. Section 14 Project Location Maps

Table 4. Republican River Sediment Reduction and Project Cost

Section 14 (Grand River Basin)				
Site Identifier	Highway 6	Route B	Route EE	Route N
Year Constructed	2005	2012	2011	2013
Erosion Area (ac)	2.4	0.2	1.2	1.2
Bank Height (ft)	25.0	16.0	24.0	26.0
Erosion Rate (yd^3/yr)	10,756	323	3,098	2,961
% Bank Wash Load	54%	55%	55%	56%
20-year Wash Load Reduction (yd^3)	116,200	3,500	34,100	33,200
Quantity of Rock (ton)	10,900	5,140	5,230	4,362
Volume of Earthwork (yd^3)	2,658	1,365	3,520	1,527
Estimated Project Cost	$562,000	$257,000	$261,500	$218,100
20-Year Wash Load Dredging Cost	$780,000	$20,000	$230,000	$220,000

Conclusion

This study included analysis of bank stabilization as a means of regional sediment management using assessments of 18 projects within the Kansas River and Grand River Basins. This study also distilled lessons learned from project successes and failures, which will be available in an upcoming technical note. Based on this analysis, the cost of constructing bank stabilization projects similar in design to the State of Kansas projects will offset the cost of dredging an equivalent volume of material within 1-2 years, with most projects functioning for decades. Of the State of Kansas projects analyzed in this study, stabilization of erosion hot spots is, on average, 14 times more cost effective than traditional dredging over a 20-year assumed life. For the Section 14 projects, the dredging cost approximately equals the project cost; however, these projects will likely last beyond the assumed 20 year life. The Section 14 projects were economically justified based on benefits to critical infrastructre alone.

References

Biedenharn, S., C. Thorne, and C. Watson. 2006. Wash load/bed material load concept in region sediment management. Proceedings of the Eighth Federal Interagency Sedimentation Conference (8thFISC). Reno, NV. https://pubs.usgs.gov/misc/FISC_1947-2006/pdf/1st-7thFISCs-CD/

Einstein, H. A. 1950. The bed-load function for sediment transportation in open-channel flows. U.S. Department of Agriculture, Soil Conservation Service, Technical Bulletin No. 1026. Washington, DC. https://naldc.nal.usda.gov/download/CAT86201017/PDF

Gnau, C. 2013. Streambank stabilization effectiveness on Little and Big Blue Rivers. Presentation at the Governor's Conference on the Future of Water in Kansas. October 25, 2013.

Juracek, K. E. and A. C. Ziegler. 2009. Estimation of sediment sources using selected chemical tracers in the Perry Lake Basin, Kansas, USA: International Journal of Sediment Research. v. 24, pp. 108-125. https://doi.org/10.1016/S1001-6279(09)60020-2

KWO. 2016. John Redmond Reservoir dredging fact sheet. Kansas Water Office. http://www.kwo.org/Projects/JRDredging/JRRD%20Fact%20Sheet.pdf

Shelley, J., M. Boyer, J. Granet, and A. Williams. 2016. Environmental benefits of restoring sediment continuity to the Kansas River. ERDC/CHL CHETN-XIV-50. Vicksburg, MS: U.S. Army Engineer Research and Development Center. http://hdl.handle.net/11681/20279

Shelley, J. 2017. Tuttle Creek Lake Hydrosuction Assessment. CENWK-EDH-R Memorandum for Record, 21 September, 2017. U.S. Army Corps of Engineers, Kansas City District.

USACE. 2011. Kansas River basin regional sediment management Section 204 stream and river channel assessment. Prepared by Gulf South Research Corporation and The Watershed Institute for the U.S. Army Corps of Engineers, Kansas City District. http://cdm16884.contentdm.oclc.org/cdm/ref/collection/p16884coll78/id/144

Erodibility Characteristics of Cohesive Sediment Deposits in a Large Midwestern Reservoir

John E. Shelley, Civil Engineer, U.S. Army Corps of Engineers, Kansas City District, 601 E 12th St., Kansas City, MO, john.shelley@usace.army.mil

Robert R. Wells, Research Civil Engineer, USDA-ARS National Sedimentation Laboratory, Oxford, MS, robert.wells@ars.usda.gov

Abstract

In September 2015, researchers from the U.S. Department of Agriculture's Agricultural Research Service (USDA-ARS) and the U.S. Army Corps of Engineers Kansas City District collected eight six-inch diameter sediment cores from Tuttle Creek Lake, the largest reservoir on tributaries to the Kansas River. At varying depths, these cores were analyzed to determine the critical shear stress, erodibility, Atterberg limits, and bulk density of the reservoir sediment deposits. This paper documents the findings and correlations between sediment parameters and discusses implications for reservoir sediment management. Critical shear stress, erodibility, bulk density, and liquid and plastic limits of the reservoir sediment vary with distance from the dam and with depth below the reservoir bed. There is high erodibility and low critical shear stress closer to the dam. Erodibility of the sediment increases with depth into the deposit. This implies the removal of recently deposited sediments and sediments deposited closer to the dam would require less energy and be less expensive than removing older deposits and deposit farther from the dam.

Introduction

Sediment accumulation in reservoirs is a widespread problem with tremendous societal implications (Annandale 2013). Sediment accumulation replaces water storage needed for many purposes, including water supply, drought mitigation, navigation support, and environmental releases. Sediment accumulation is especially problematic in the Kansas River Basin in the Midwestern United States. Due to sediment accumulation and rising demand, large federal reservoirs will no longer be able to supply water against the design drought by 2057 (KWO 2018). At the same time, the downstream Kansas River is suffering from a lack of turbidity (Shelley et al. 2016).

Tuttle Creek Lake (Figure 1) is the largest reservoir in the Kansas River basin, with an original multi-purpose pool volume of 425,312 ac-ft. From 1963 to 2009, Tuttle Creek Lake lost 168,298 ac-ft of storage volume in the multi-purpose pool, which equates to a 41% loss. The average annual rate of sediment accumulation over this time period was 3,594 ac-ft/yr, which is close to the original design estimate of 4,151 ac-ft/yr. The flood control pool is also experiencing sediment accumulation, but at a much slower rate compared to the total flood control storage volume. The sediment deposits in the multi-purpose pool are 86 to 90% clay, 6 to 10% silt, and 4 to 6% sand with no observable change or gradient with depth (KBS 2013). The trapping

efficiency of the reservoir is 98% (Juracek, 2011). Loss of benefits and costly impacts accrue as sediment deposition continues.

Figure 1. Location of Tuttle Creek Lake (Left). Tuttle Creek Lake (Right).

Sediment Parameters for Reservoir Sediment Management

Long-term reservoir sustainability requires the annual removal of sediment at the rate it enters the reservoir. Two methods for removing the sediment are drawdown flushing (more common outside the United States) and hydraulic dredging (more common in the United States). The efficiency of both these methods depends on the sediment properties.

Drawdown flushing includes lowering the reservoir pool completely to allow hydraulic forces to erode and flush out the sediment. The efficacy of this action depends on the erodibility of the sediment deposits. In cohesive sediments, site-specific measurements are needed to estimate the erodibility. The rate of erosion is often approximated by the following equation (Hanson and Cook 1997):

$$E = k(\tau - \tau_c)^a$$

where E = the rate of erosion [units of volume per time]

τ = the applied shear stress [units of force per area]

τ_c = the critical shear stress, or the shear stress required to initiate motion [units of force per area]

k = an erodibility coefficient, also termed the erodibility, which relates excess shear stress to rate of erosion [units of volume per force per time]

a = exponent, often taken to be 1 [dimensionless]

Hydraulic dredging also depends on soil properties. The ease with which material can be removed, transported, and deposited via hydraulic dredging methods is known as "dredgeability." Spigolon (1993) indicates that the dredgeability of a material is related to sediment properties such as bulk density and Atterberg limits (i.e. limits of soil consistency or basic measure of a material's critical water contents: shrinkage limit, plastic limit, liquid limit). These same erodibility and "dredgeability" properties are also important for other sediment removal methodologies such as hydrosuction and water injection dredging.

Sampling and Testing

In September 2015, researchers from the U.S. Department of Agriculture's Agricultural Research Service (USDA-ARS) and the U.S. Army Corps of Engineers Kansas City District collected eight six-inch diameter sediment cores from Tuttle Creek Lake for purposes of determining the critical shear stress, erodibility, Atterberg limits, and bulk density of the reservoir sediment deposits. Sampling was accomplished by vibracoring a 10-ft long, 6-in diameter steel tube into the reservoir bottom. As the sample could slide from the pipe while the pipe was being extracted from the reservoir bottom, actual core thickness ranged from 62 to 110 inches. Figure 2 maps the sampling locations.

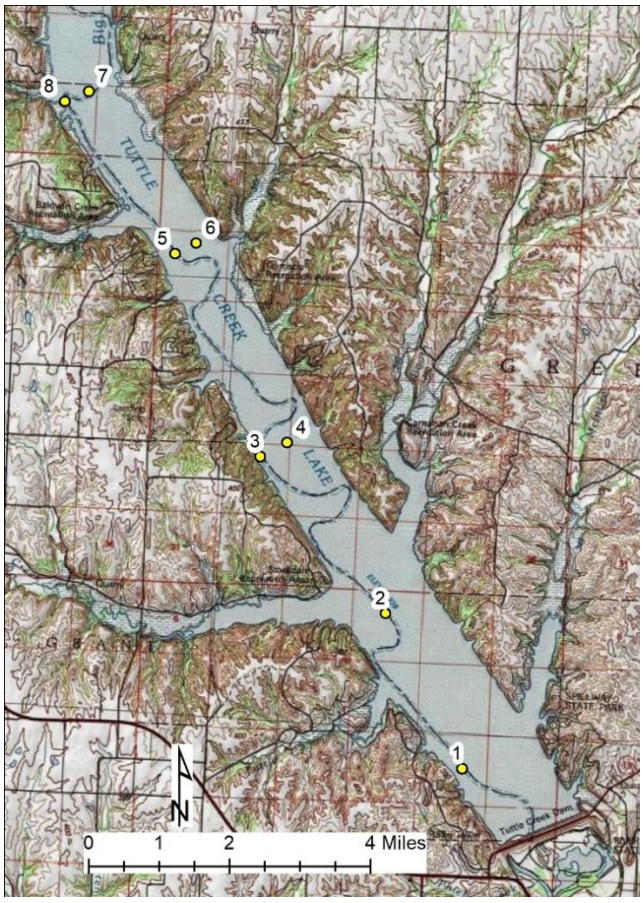

Figure 2. Sampling Locations

Following sample collection, USDA-ARS segmented the cores into 23, 6-in samples for jet erosion testing, 11, 3-in samples for Atterberg Limits, and 40, 2-in samples for bulk density testing. The protocol allows the assessment of both longitudinal and vertical variations in sediment parameters. The jet erosion testing was accomplished with a laboratory jet erosion tester (Hanson and Cook, 2004; see Figure 3). The test continued with a constant head until sufficient points were generated to define the curve, which due to differences in erodibility ranged from 2 to 129 minutes. In all cases, the final scour was similar (around 0.23 to 0.34 ft). The Blaisdell solution method was used to compute erodibility parameters (Blaisdell et al., 1981).

Figure 3. Laboratory Jet Erosion Tester (Left). Core 8 after testing (Right).

Results and Relationships

The results of erodibility and critical shear stress for the eight cores are presented in Table 1. The erodibility data showed a general trend with depth and with distance from the dam. Deeper (older) deposits are markedly less erodible than the highest (newest) deposits. Fresh deposits have not had time to consolidate. Likewise, deposits further upstream are markedly less erodible than the deposits further downstream. This may be a function of grain size differences; finer grains transport further into a reservoir than coarser grains. However, Cores 7 and 8 did not sample the coarse-grained delta, the sample texture still suggested predominantly clay and silt, though no grain size analysis was conducted.

The critical shear stress results also indicated a trend with depth, with deeper deposits generally having higher critical shear. This effect is not nearly as pronounced as the change in erodibility. Unlike the erodibility, the critical shear stress does not vary with distance from the dam. Moreover, the cores sampled from the historic channel have higher erodibility and lower critical shear stress compared to adjacent cores in the historic floodplain.

The deepest two samples in Core 2 do not follow the overall trends with depth—they have greater erodibility and lower critical shear stress than several of the overlying samples. The data are insufficient to conclude whether this was a different type of sediment at this depth or error in sampling/testing.

Table 1. Erodibility (left) and critical shear stress (right) of reservoir sediment deposits with depth. Red = most erodible/lowest critical shear. Green = least erodible/highest critical shear.

Erodibility (cm^3/N-s)								
Depth (in)	Core#							
	1	2	3	4	5	6	7	8
3	316	143	311	116	45	32	42	18
							40	
22	105	63	24	13	42	6		16
					17	9		9
		19	30					
44	24	15						
	1							
						6		4
67		10	5					
						6		
		44						
90		26						

Critical Shear Stress (Pa)								
Depth (in)	Core#							
	1	2	3	4	5	6	7	8
3	0.4	0.2	0.1	0.2	0.3	0.3	0.3	0.4
							1.0	
22	0.5	0.6	0.4	0.9	0.3	1.6		0.5
					0.3	0.6		0.7
		0.7	0.7					
44	0.4	1.4						
	0.7							
						1.5		1.1
67		0.7	1.6					
						1.5		
		0.2						
90		0.3						

The results of dry bulk density of the samples are presented in Table 2. The bulk density increases slightly with depth, but much more significantly with distance from the dam. This is likely due to coarser sediments depositing further upstream in the reservoir.

Table 2. Dry bulk density of reservoir sediment deposits with depth. Red = lowest bulk density. Green = highest bulk density.

Dry Bulk Density (g/cm^3)								
Depth (in)	Core#							
	1	2	3	4	5	6	7	8
9	0.34	0.37	0.50	0.38	0.41	0.44	0.87	1.04
23	0.36	0.36	0.50	0.40	0.46	0.48	1.06	0.74
37	0.39	0.39	0.46	0.48	0.53	0.47	1.23	1.14
53	0.47	0.49	0.54	0.47	0.52	0.49	1.21	1.16
67	0.45	0.45		0.51		0.49	1.02	1.18
81	0.48							
91		0.47						

The results of Atterberg Limits (Liquid Limit and Plastic Limit) are presented in Table 3. The Atterberg Limits were only determined for Cores 1, 2, 3, 6, and 8. There appears to be a decrease in both the Liquid Limit and Plastic Limit with distance from the dam. Changes with depth are harder to generalize.

Table 3. Atterberg Limits. Liquid Limit (Left) and Plastic Limit (Right). Red = highest limit. Green = lowest limit.

Liquid Limit (%)						Plastic Limit (%)					
Depth	Core#					Depth	Core#				
(in)	1	2	3	6	8	(in)	1	2	3	6	8
0	88	83	69	81	66	0	59	47	54	60	36
					40						24
			84	79					38	46	
27	97					27	51				
61			94			61			38		
					56						31
96					49	96					

Figure 4 illustrates the relationship between critical shear stress and erodibility. As expected, increasing critical shear correlates with decreased erodibility. Bulk density vs. erodibility for segments containing both tests is plotted in Figure 5. For Cores 1 – 6, which consist mostly of clays and silts, the erodibility drops over a very small range in bulk density. The results of bulk density versus erodibility for Cores 7 – 8 suggest that more sand may have been present, even though visual inspection of the samples indicated they were still predominantly fines.

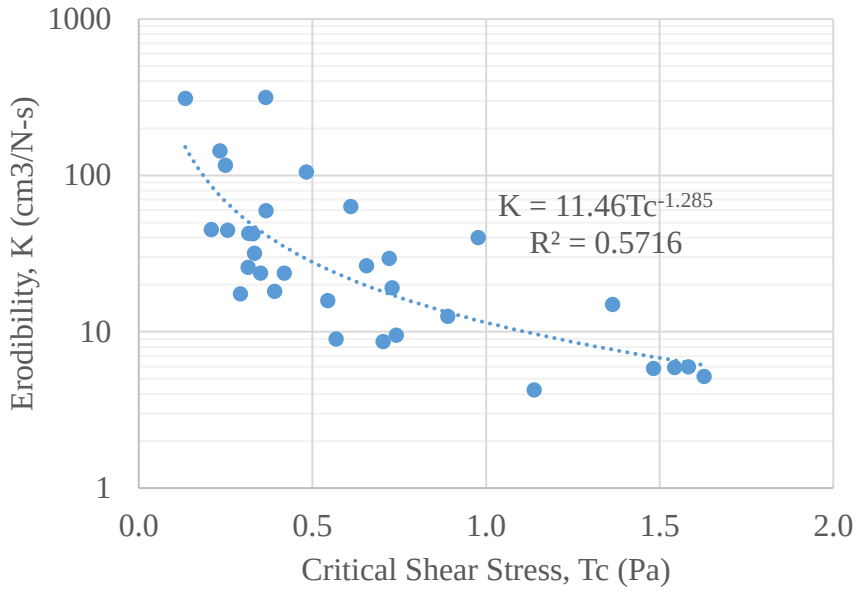

Figure 4. Relationship between Critical Shear Stress and Erodibility

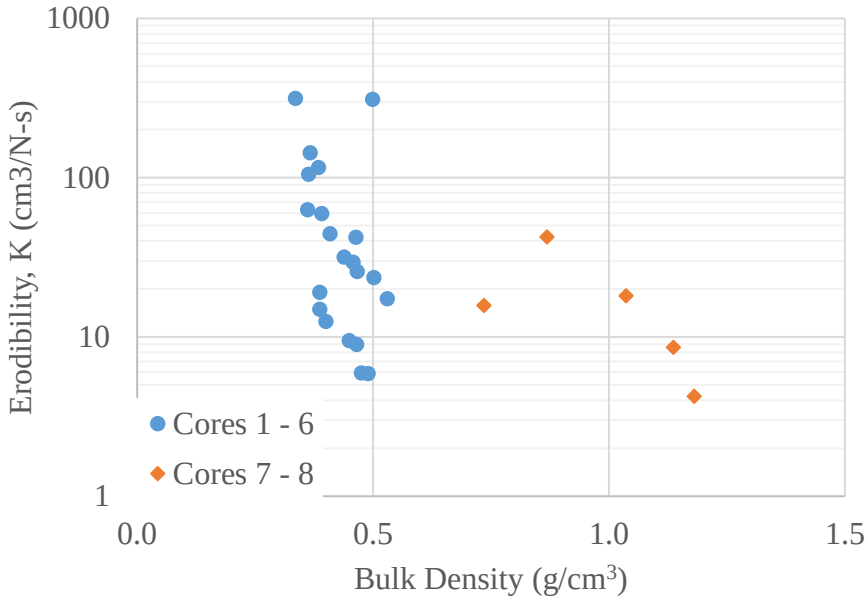

Figure 5. Relationship between Bulk Density and Erodibility

Figure 6 illustrates that the erodibility significantly decreases further upstream compared to closer to the dam. This effect is especially pronounced for the top-most sample in each core (indicated by red dots in Figure 6). Figure 7 displays erodibility as a function of depth. As seen,

the erodibility decreases significantly in the deeper deposits. The two deepest samples, both from Core #2, have relatively high erodibility. As mentioned before, they also have surprisingly low critical shear.

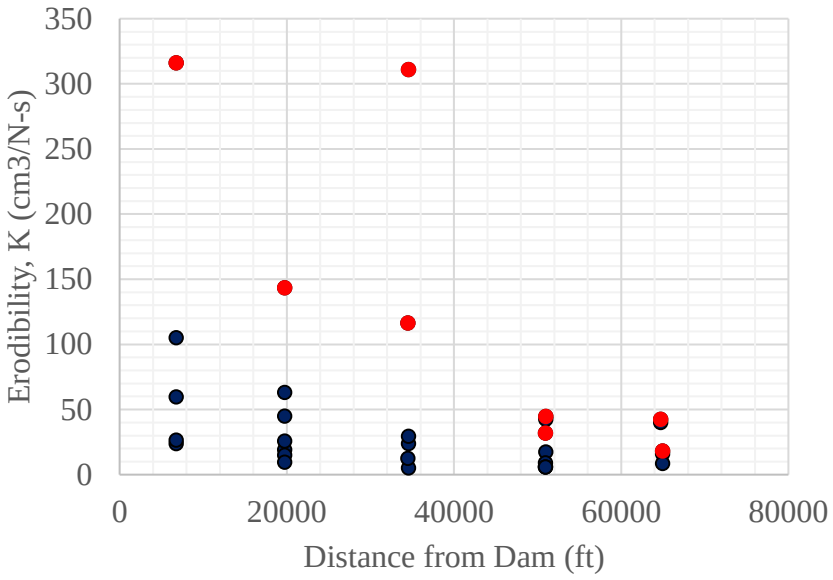

Figure 6. Relationship between Distance from Dam and Erodibility. Red = the top-most sample in each core.

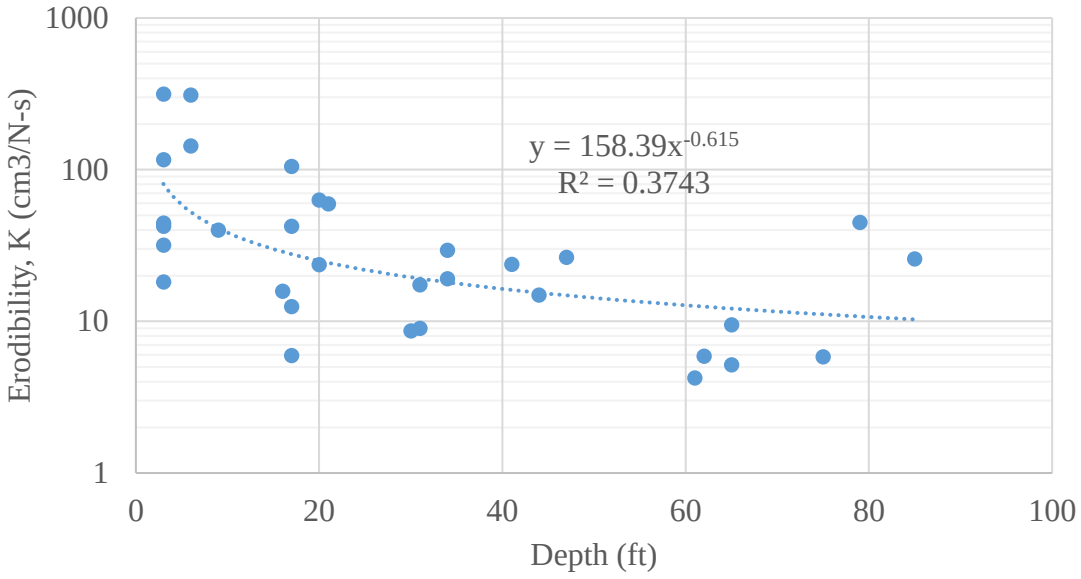

Figure 7. Relationship between Depth and Erodibility

Conclusion and Implications for Management

The results of jet erosion testing of 32 samples from 8 sediment cores in Tuttle Creek Lake indicated that the erodibility ranged from 1 to 316 (cm^3/N-s). The two major factors influencing the critical shear stress, erodibility, bulk density, and liquid and plastic limits of the material are distance from the dam and depth below the reservoir bed. These findings carry important implications for sediment management at Tuttle Creek Lake.

First, sediment characteristics are highly favorable for erosion (high erodibility and low critical shear stress) close to the dam. This is encouraging, as lower-cost sediment management options target sediments close to the dam for movement through or over the dam.

Second, the erodibility of the material increases with depth into the sediment deposit. This implies that significantly more energy would be required to remove sediment if left to consolidate, versus removal soon after it deposits. The longer it sits, the harder it is to remove.

The variability and trends in this reservoir underscore the need for sufficient sampling and testing of reservoir sediment deposits at other reservoirs where sediment management actions are being considered.

References

Annandale, G., 2013. Quenching the Thirst: Sustainable Water Supply and Climate Change. CreateSpace Independence Publishing Platform, North Chareleston, SC.

Blaisdell, G., Hebaus, G., and Anderson, C., 1981. Ultimate Dimensions of Local Scour. Journal of the Hydraulics Division, Vol. 107 (3), 327 – 337.

Hanson, G.J. and Cook, K.R. 2004. Apparatus, testing procedures, and analytical methods to measure soil erodibility *in situ*. ASABE Applied Engineering in Agriculture. 20(4), 455-462.

Juracek, K., 2011. Suspended-sediment loads, reservoir sediment trap efficiency, and upstream and downstream channel stability for Kanopolis and Tuttle Creek Lakes, Kansas, 2008–10: U.S. Geological Survey Scientific Investigations Report 2011–5187, 35 p.

KBS, 2013. Data Report: Tuttle KBS Reservoir Sediments Box #601. 6-13-13. Kansas Biological Survey.

KWO, 2018. State of the Resource and Regional Goal Action Plan Implementation Report: Kansas Regional Planning Area. Kansas Water Office, August 2018. https://www.kwo.ks.gov/docs/default-source/State-of-the-Resource/stateoftheresource_kansas_final.pdf?sfvrsn=779c8414_0

Shelley, J., Boywer, M., Granet, J., and Williams, A., 2016. Environmental Benefits of Restoring Sediment Continuity to the Kansas River. ERDC/CHL CHETN-XIV-50.

Evaluating Post-Wildfire Impacts to Cochiti Lake Flood-Risk Management: Las Conchas Wildfire, New Mexico

Marielys Ramos-Villanueva, Research Civil Engineer, Marielys.Ramos-Villanueva@usace.army.mil
Ian E. Floyd, Research Physical Scientist, Ian.E.Floyd@usace.army.mil
Ronald E. Heath, Research Civil Engineer Ronald.E.Heath@erdc.dren.mil
US Army Corps of Engineers, Engineer Research and Development Center, Coastal and Hydraulics Laboratory, Vicksburg, Mississippi
Stephen W. Brown, Hydrologist, Stephen.W.Brown@usace.army.mil
Stephen K. Scissons, Flood Risk Manager, Stephen.K.Scissons@usace.army.mil
John Peterson, Geospatial Unit Leader, John.L.Peterson@usace.army.mil
US Army Corps of Engineers, Albuquerque District, Albuquerque, New Mexico

Abstract

The 2011 Las Conchas Wildfire burned over 600 km^2 of forested land in the Jemez Mountains in New Mexico. The burn severity was greatest in the headwaters of 15 streams that drain directly into Rio Grande and into U.S. Army Corps of Engineers (USACE) Cochiti Reservoir, a multipurpose reservoir upstream of Albuquerque, New Mexico. The affected basins have shed sediment at rates far above their historic quantities. Recovery of these watersheds is decades away, creating an ongoing sediment management problem at Cochiti Reservoir, which will result in a reduction of reservoir storage available for project uses. Observational and limited modeling data indicate dramatic changes in watershed hydrology, geomorphology, and ecology have occurred within the burn area. Watershed hydrologic studies at Santa Clara Creek found that post-fire peak flow conditions increased by 400% (e.g., 1% chance event increased from 140 to 560 m^3/s). Frijoles Canyon in Bandelier National Monument and other tributaries where data have been collected, show similar ongoing changes in flood hydrology. These changes could result in significant life-safety and infrastructure hazards, uncertainty in debris-flow frequency-magnitude relationships, and significant environmental impacts. In this effort, we evaluate post-fire geomorphic effects of the Las Conchas Wildfire to quantify the empirical impacts on flood-risk management operations on the Middle Rio Grande River and Cochiti Reservoir.

Introduction

In the arid and semi-arid regions of the southwestern US, wildfires are a natural and human induced impact that may significantly contribute to flood risks (DeBano et al., 1998; Neary et al., 2005; Moody et al., 2013). The frequency, duration and spatial extent of these wildfires have significantly increased in the last decades (Westerling et al., 2006; Williams et al., 2012). Longer wildfire seasons due to earlier snowmelt, severe drought, and higher temperatures are directly related to these increments (Westerling et al., 2006). According to Williams et al. (2012), the total forested area burned from 1987 to 2003 is 6.7 times the size of the areas burned from 1970 to 1986. They also predict that the accelerated warming and drying of the western area of United States will result in continuous growth of higher wildfire activity. Wildfires threaten life and property not only by direct impact but also through secondary effects such as floods and debris flows triggered by storm events after a fire.

In the years following a wildfire, ecotone shifts, gully formation, and channel incision alter the hydrologic system response, resulting in dramatic changes in hydraulic and sediment impacts down-system. In most of the western arid and semi-arid mountainous United States, post-wildfire recovery can take decades, posing potential long-term operation and management concerns for USACE and other federal, state, and local agencies. Since burned regions lack vegetation to intercept and slow surface runoff produced by rainfall events, post-fire peak flows in those areas usually reach all-time highs, with documented hyper-concentrated flows (Tillery et al. 2011; Rio Grande Water Fund, 2015). These flows often carry large boulders, trees, and even vehicles because of the high density and tremendous momentum of the sediment-laden flows. Several post-wildfire debris flows in western United States have been documented, and are usually caused by short-duration, high-intensity storms (Cannon et al., 2007; Cannon et al., 2008; Cannon et al., 2009).

Las Conchas Wildfire

Study Area: The study area is located upstream of the Cochiti Lake, in the forested land of the Jemez Mountains, north-central New Mexico. Burn severity was the highest at the headwaters of 15 watersheds west of the Rio Grande, which drain into the river and reservoir (Figure 1). The Santa Clara Canyon is at the northern end of the burned extent, and Peralta, Cochiti, and Bland Canyons at the southern end. It also affected areas of the City of Los Alamos, Los Alamos National Laboratory, archeological sites of Bandelier National Monument and Tribal Lands.

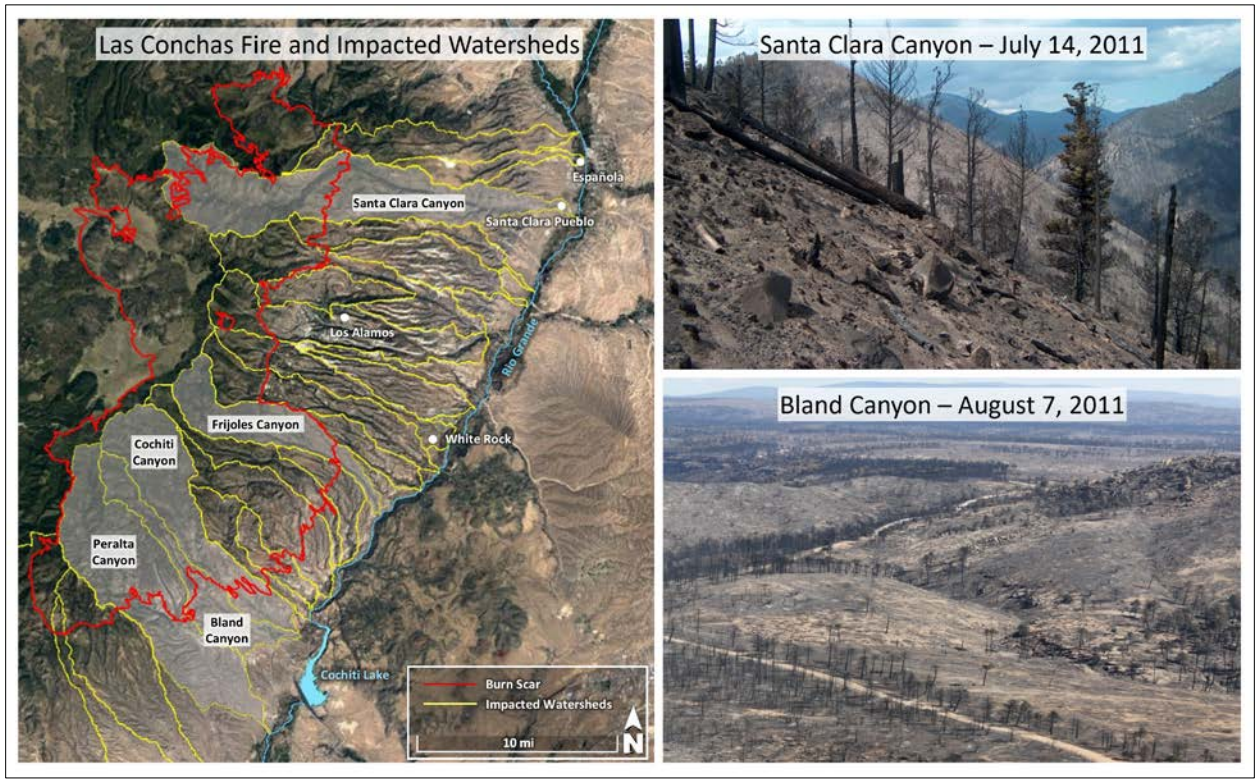

Figure 1. Las Conchas Wildfire burn scar and impacted watersheds, with post-fire photographs of Santa Clara and Bland watersheds.

The southwestern area of the United States is dominated by arid and semi-arid climates. These climates are classified in sub-categories depending on mean annual temperatures and precipitation that the region receives. The area burned by Las Conchas Fire is identified as *Cold Semi-Arid (Steppe)* climate, or *BSk* classification, following the Köppen-Geiger method (Köppen-Geiger, 1954; Kottek et al., 2006). Semi-arid climates tend to receive low annual precipitation compared to the potential evapotranspiration, but the precipitation deficiency is not so severe as to be classified as desert or arid climate. Cold semi-arid climates usually have warm to hot summers and cold winters, with mean annual temperatures lower than 64.5 F (18°C).

The topography of north-central New Mexico burned by the Las Conchas Fire is varied, including some flat valleys from Valle Grande, as well as some of the steepest, rugged mountains of the state at the Sierra de los Valles. New Mexico is divided into six physiographic provinces highlighting distinctive landforms and geologic backgrounds. The land where Las Conchas Fire occurred coincides with the Southern Rocky Mountains and Rio Grande Rift provinces. The Southern Rocky Mountains province is characterized by its rugged mountainous terrain, and its southern end is considered to be at the Jemez Mountains where Las Conchas Fire occurred. The part of the burned area that occurred in the Rio Grande Rift province is located at the Española basin. This area of the province is fairly narrow with rugged finger-mesa and canyon topography.

Soils and sediment are part of the natural resources of any region, and the type of soil present in the area and its properties affects various hydraulic and hydrologic processes. Post-fire soil changes could be harmful to the soil and ecosystem stability depending on the severity of the fire. Many studies have found that the soil pH increases immediately after a fire (Velizarova et al. 2001, Verma & Jayakuma, 2012; Boerner et al. 2009, Tüfekçioğlu et al. 2010, Aref et al. 2011), becoming significant with higher fire severity. Breakdown of coarse sediment creates an increment on fine sediment and soil bulk-density. Clogged voids due to this increment of fine sediment and ashes, combined with burned organic matter residues (Letey, 2001; Doerr et al., 2009), result in a decrease in the soil porosity and permeability (Certini, 2005; Bogdanov 2014; Jhariya, 2014) becoming hydrophobic in the areas where the fire was severe. The Harmonized World Soil Database (HWSD) v1.2 displays 28 main soil types around the world, using data compiled by a group of institutes and organizations from different countries (FAO/IIASA/ISRIC/ISSCAS/JRC, 2012). According to the HWSDv1.2 map, the area burned by Las Conchas Fire contains a combination of Regosol (RG) and Luvisol (LV) soils. Regosols are unconsolidated medium-to-fine mineral soils. A study performed by Badía et al. (2011) shows that Regosol soils develop significantly higher runoff and erosion levels compared to other soils after being exposed to wildfires in semi-arid climates. Luvisols are soils with high accumulation of clays and iron in the subsurface zone, under a surface accumulation of non-living fine organic matter. Bogdanov (2014) conducted experiments exposing Luvisol soils to different severities of fire, which caused breakdown of coarser grains reducing soil porosity and permeability.

Wildfire History: Three previous wildfires affecting the northern region of New Mexico coincide with some of the areas burned by Las Conchas Fire: 1977 La Mesa Fire (62.5 km^2) in Los Alamos County including part of Bandelier National Monument and part of the Los Alamos National Laboratory (LANL), 1996 Dome Fire (66.8 km^2) burned part of the Santa Fe National Forest and Bandelier National Monument, and 2000 Cerro Grande Fire (190 km^2) affected Los Alamos and 112 structures at LANL (Tillery et al., 2011). Studies preceding 2011 Las Conchas Fire show post-wildfire hydrologic impacts including increased peak-flows (Vieira et al., 2004; Veenhuis, 2002).

The Las Conchas Wildfire began on 26 June 2011 at 1:00 PM when a tree fell over a power line near the Bandelier National Monument Park. Strong winds and extreme drought allowed the fire to grow and spread at a rate of an acre per second during the first 13 hours. After continuous

efforts, Las Conchas Wildfire was 100% contained on August 3. It burned 634 km^2 (nearly 150,000 acres) of the forested land in the Jemez Mountains, becoming the largest wildfire to be recorded for the state of New Mexico. Soon after the fire, a broad coalition of federal and non-federal partners including the U.S. Federal Emergency Management Agency, the U.S. Bureau of Reclamation, and the U.S. Bureau of Indian Affairs have invested in aiding the recovery of communities from post-fire flooding in this region. The increased sediment loading has negatively impacted natural resources through significant sediment-laden flood events, destruction of infrastructure (i.e., bridges, culverts, and community water intake structures), and complex reach-specific flood responses on agency lands along the Rio Grande River and at the delta of Cochiti Lake. The USACE owns, operates and manages Cochiti Lake, and has a direct need to understand sediment movement downstream of any burn scar that could affect the lake, including 15 streams affected by the Las Conchas Fire.

Cochiti Lake: For decades, the Middle Rio Grande has had the conflicting objectives of water supply for agriculture, industrial and municipal uses while maintaining safe ecological environments for native fish and bird species (Richard, 2001). The Cochiti Dam was completed on 1973 and the pool was filled by 1975 on the Cochiti Reach, which lays within the Middle Rio Grande, primarily for flood and sediment control and to provide a 1,200-surface-acre pool for fish and recreation.

Most of the watersheds burned by the Las Conchas Fire drain into the Rio Grande upstream of Cochiti Lake. As the movement of sediment progresses downstream and reaches Cochiti Lake, it is trapped inside the reservoir. Wolf Engineering (2017) conducted a survey along the Cochiti Range Lines to determine sediment deposition in the reach that could reduce the storage capacity of the reservoir. Historical Range Line and Bathymetric data collected around the sediment delta was compared to the 2017 survey. The unprecedented delta progradation that has been observed after 2011 is shown in Figure 2. This rapid sediment deposition at the delta continues as a result of increased sediment and debris load to the Rio Grande from rainfall events taking place on the Las Conchas Fire burn scar. Debris flows are enabling coarser sediment, ashes and organic material to reach and enter the impoundment resulting in reservoir storage capacity loss and water quality degradation (Dahm et al., 2015). Figure 3 presents historical cross sectional survey data near station 155+00 of Range Line 7 where the delta topset has reached already due to the increased sediment deposition rates. Range line data is frequently used to calculate storage capacity changes between surveys. Comparing data from before and after Las Conchas Fire, demonstrates a significantly higher storage capacity loss rate during the three years following the fire (Figure 4). From 2014 to 2017 the capacity loss rate seems to decrease, and it could be the result of a combination of factors including compaction of the previously deposited sediment.

Even though sediment deposition at the reservoir is significantly higher after the fire, sediment management practices for the Cochiti Reservoir have not changed. Sediment removal such as flushing or dredging have had limited consideration due to a general concern of possible chemicals or contaminants buried within earlier sediment deposition coming from upstream LANL waste, previous fires, agricultural runoff, mining, wastewater, storm water, atmospheric deposition, and/or naturally present in watershed soils. The Cochiti Baseline Study (USACE-SPA, 2013) compiles a series of studies that present historical and existing environmental conditions in the Cochiti Reach area. Sediment baseline studies found elevated metals concentrations in Cochiti Lake surficial and core samples, that could be a result of the high clay and organic material content. Metals concentration levels found in the lake present a low risk potential for human health recreational and residential activities, but some were higher than the Regional Statistical Reference Levels. The Cochiti Baseline Study also included a HEC-RAS numerical sediment transport model of the Rio Grande upstream and downstream of the Cochiti Lake to provide better understanding of the sediment processes in the reservoir and

study reach, and to evaluate potential future changes in dam operations pursuing sustainability and the sedimentation effects. The study determined that the dam infrastructure, including minimum pool elevation create operational constrains that would make it difficult to *pass-through* a significant sediment load if performing flushing or drawdown sediment management techniques. They concluded that, regardless of reservoir sedimentation, the Cochiti Dam will be likely able to meet its original main objectives and other modified purposes for at least another 50 years (Davis et al., 2015).

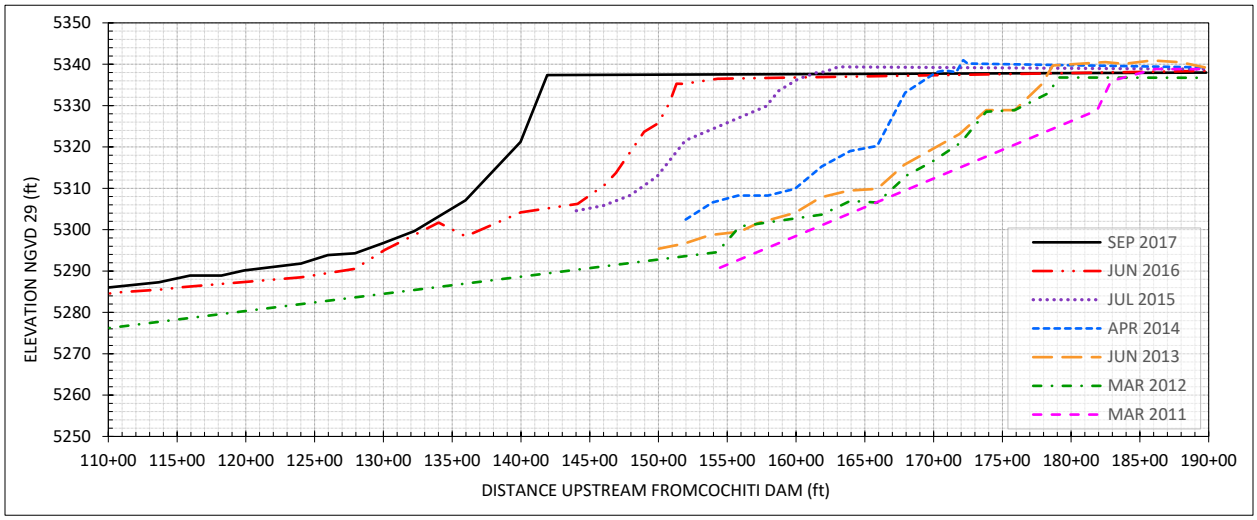

Figure 2. Rio Grande Longitudinal profile at Range Line 7 along the Cochiti Reservoir sediment delta, highlighting post-fire sediment deposition and aggradation from 2011 to 2016 (Wolf Engineering, 2017).

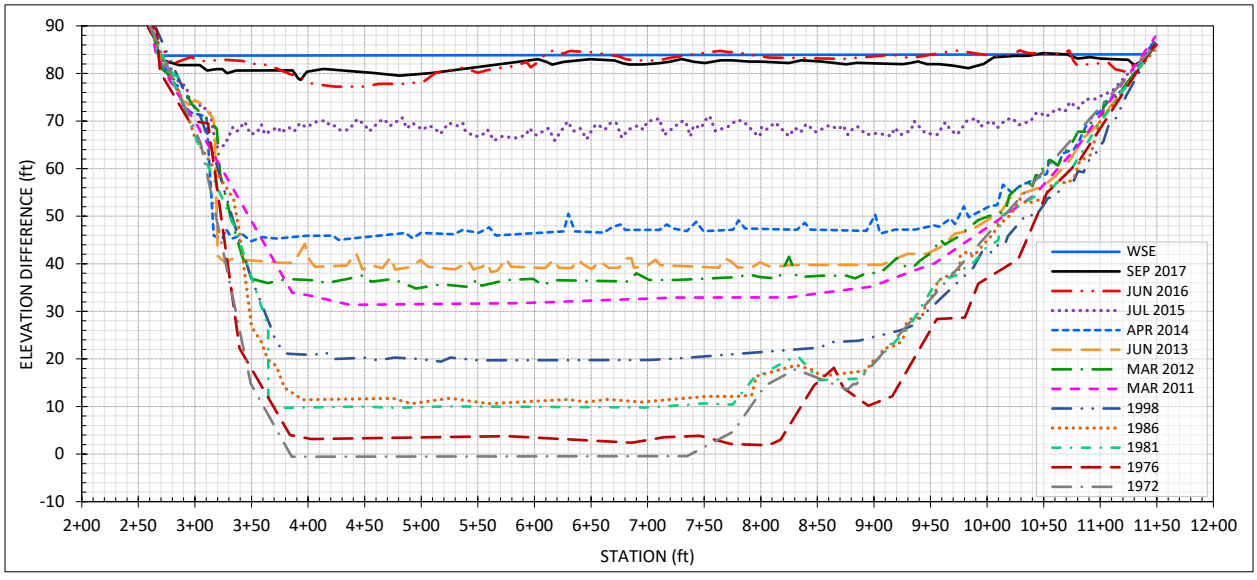

Figure 3. Rio Grande Cross Sectional profile near Station 155+00 (from Figure 2) at the Cochiti Reservoir sediment delta, comparing progression of sediment deposition and aggradation before and after Las Conchas Wildfire during Summer 2011.

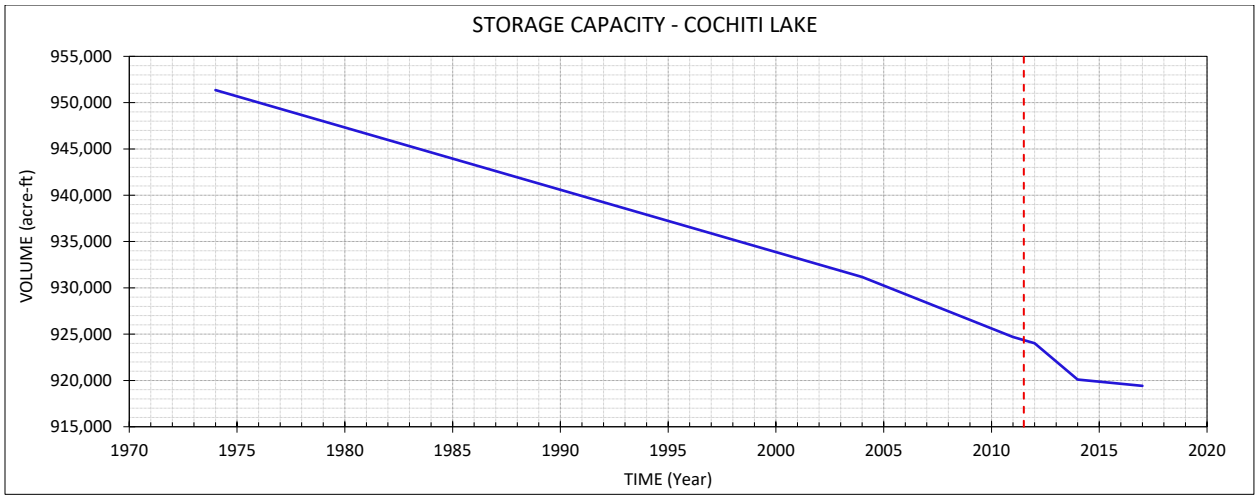

Figure 4. Storage capacity of Cochiti Lake from 1974 to 2017. The red line marks the Las Conchas Fire date and change in storage capacity average loss rate (slope).

Hydrology & Hydraulics

Wildfires bring drastic alterations to the natural state effecting the geomorphology, hydrology and sedimentation processes in any region affected. Arid and semi-arid regions are especially sensitive to the post-fire effects due to the slow recovery process. Destruction of groundcover, exposure of fine sediment, and the addition of ashes alter the surface permeability and runoff retention. When vegetation (canopy) and the organic matter covering the ground are reduced to debris and ashes, runoff retention decreases drastically. Ashes block pore space and, in a mixture with exposed fine sediment, work as sealers limiting the depth and amount of infiltration turning the soils hydrophobic. Following a wildfire, soil fragmentation (i.e. gully formation, landslides, channel incision) usually follow due accelerated erosion rates. The result of all these is a dramatic change in hydraulic and sediment impacts down system: increased surface runoff, water and sediment discharge, debris, mud and hyperconcentrated flows (Certini, 2005; Moody and Martin, 2001; Moody et al., 2009; Ebel et al., 2012).

Hydrology: Post-wildfire effects on the hydrology regime involve changes to evapotranspiration, surface and substrate moisture storage, and surface and substrate flows, decreased watershed lag time, higher peak flows, reduced interception, and reduce infiltration capacity (Neary et al., 2003; WEST, 2011). Data from Veenhius (2002) indicates that the hydrologic effects of post-wildfire after the 1977 La Mesa and 1996 Dome Wildfires were more pronounced during the first three years following the fire. As recovery starts, the slow reestablishment of vegetation and washing the ashes from burned areas helps progressing towards normalization of magnitude and frequency of annual peak flows.

The Las Conchas Fire burned about 15 watersheds that drain into the Rio Grande. Soon after the fire, post-fire hydrological analyses were conducted for watersheds draining directly into the Middle Rio Grande and upstream of Cochiti Lake to generate new runoff hydrographs based on post-fire hydrological conditions (USACE-SPA, 2011a, 2011b, and 2011c). Numerical models were conducted using the USACE Hydrologic Engineering Center's Hydrologic Modeling System (HEC-HMS) using available precipitation data. Infiltration parameters for watersheds in the Española area were estimated prior to the fire based on historic flow data from the Santa Clara Creek, and were updated after the fire. 'Calibrated' hydrologic studies at Santa Clara Creek found that post-fire peak flow conditions increased by 400% (e.g., 1% chance event increased from 140 to 560 m^3/s). Affected channels initially incised but now have aggraded 2 - 5 meters, in

several watersheds and reaches, analogous to super slug theory from Moody (2017). The flood hydrology of the other tributaries present similar magnitudes of change. The infiltration values for each watershed were reduced considering the percentage of the area that was burned and the severity of the burn. The amount of future aggradation is unknown.

Frequency and Magnitude: Post-fire flooding impacts are commonly defined by the given event probability, magnitude, and intensity. Probability is the likelihood of an event to occur in the future, while frequency represents how often a given event occurs (inverse of the return period). The probability (*P*) or likelihood of a debris flow occurring can be estimated using Cannon et al. (2010), defined as,

$$P = \frac{e^x}{(1-e^x)} \tag{1}$$

$$x = -0.7 + 0.03(SG) - 1.6(R) + 0.06(AB) + 0.07(I) + 0.2(C) - 0.4(LL) \tag{2}$$

where,

SG = the percent of the drainage basin area with slope greater than or equal to 30 %
R = the watershed ruggedness, or the change in drainage basin elevation dived by the square root of the drainage basin area (m/m^2)
AB = the percentage of drainage basin area burned at moderate and high severity (%)
I = the average storm intensity (mm/hr)
C = the percent clay content of the soil (%)
LL = the liquid limit of the soil (%)

The magnitude of post-fire flood events is typically expressed as total flow volume, peak discharge, or area inundated. Some common and practical flood event intensity parameters are velocity, depth, runout potential, and impact forces on in-channel infrastructure. The initiation of post-fire debris flood events is commonly attributed to two main processes: runoff driven erosion by surface flows, and infiltration triggered failures and movement of distinctive landslide mass (Cannon and Gartner, 2005). Flood events generated through runoff-based processes are commonly the result of a high-intensity, short duration storms (Cannon and Gartner, 2005). As such, there exist a precipitation threshold condition describing the onset of debris flow generation. Cannon et al. (2001a) defined the threshold rainfall intensity-duration by

$$I = 7.0D^{-0.6} \tag{3}$$

where,

D = the duration of rainfall intensity (hr)
I = the rainfall intensity (mm/hr)

This threshold is a useful metric for issuing warnings and emergency response in the western United States and is appropriate in steep, recently burned watersheds underlain by easily erodible soils and sediments with thin deposits of colluvium and alluvium. Cannon et al. (2010) highlights an empirical debris-flow volume model used to estimate the mean volume of material deposited by a debris flow at the outlet of a recently burned basin in the U.S. intermountain west, defined as

$$\ln V = 7.2 + 0.6(\ln SG) + 0.7(A_B)^{\frac{1}{2}} + 0.2(\mathrm{T})^{\frac{1}{2}} + 0.3 \tag{4}$$

where,

V = the deposited volume (m^3)
T = the total storm rainfall (mm)
A_B = burned area (m^2)

Additional relationships to estimate debris flow volume and peak discharge have been documented in the literature (Cannon et al., 2001b; Cannon and Gartner, 2005; Cannon et al., 2010), with site-specific coefficients and range of application. An emergency assessment example is provided to demonstrate computation of debris flow frequency and volume for a given rainfall event. The example focuses on five watersheds immediately upstream of Cochiti Reservoir (Figure 5).

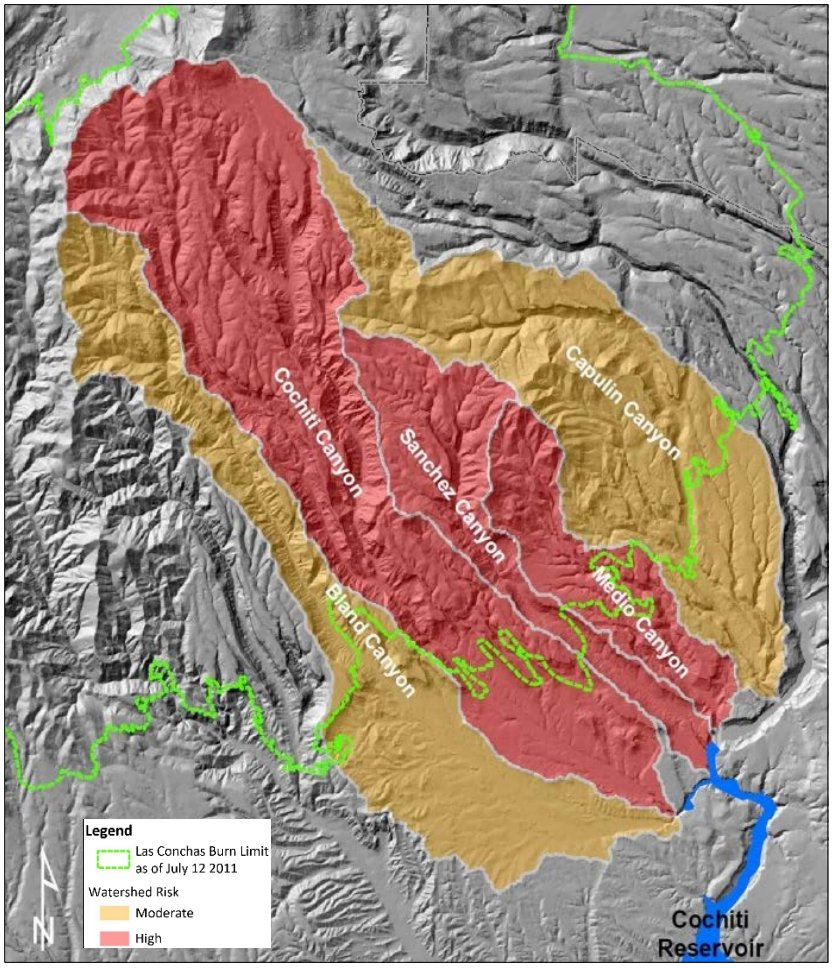

Figure 5. Post-fire emergency assessment and burn severity for five impacted watersheds upstream of Cochiti Reservoir**.**

The probability of debris-flow and volume were computed using the approach developed by Cannon et al. (2010) provided above in Eq. (1), (2), and (4) for a 5-year return period rainfall event. The computed probability of a debris flow occurring and the volume of the debris flow for the five watersheds is provided in Table 1.

Table 1. Computed debris flow probability and volume of a 5-year rainfall event for five impacted watersheds.

Computed Probability and Volume for a 5-Year Rainfall Event		
Watershed Name	**Computed Probability (%)**	**Computed Volume (m^3)**
Bland Canyon	47	$8x10^6$
Cochiti Canyon	94	$54x10^6$
Sanchez Canyon	91	$42x10^6$
Medio Canyon	76	$18x10^6$
Capulín Canyon	75	$20x10^6$

Cannon et al. (2004) successfully defined a relationship between peak discharge, burned area, average watershed gradient, and precipitation intensity, estimated by

$$Q_p = 171 + 0.552\theta + 2.84 \log A_b + 3.6I$$

where,

Q_p = the debris-flow peak discharge (m^3/s)
θ = the average basin gradient (%)
A_b = the area of the basin burned at all severities (m^2)
I = the average storm rainfall intensity (mm/hr)

Most empirical-based models are restricted to use in watersheds with similar physical and ecological characteristics to empirical model of interest. In addition to empirical-based approaches analytical models can be useful when coupled with a hydrologic numerical model like Hydrologic Engineering Center Hydrological Modeling System (HEC-HMS). This is accomplished to increase the water discharge to account for high concentrations of sediment in the flow, due to sediment entrainment. A bulking factor (BF) is commonly applied to the peak water discharge to estimate the total (bulked) peak discharge, and serves as a safety factor in water resource design (Hamilton and Fan, 1996). In undeveloped watershed with sufficient sediment storage, the bulked peak discharge is defined as

$$Q_B = Q_w + Q_s$$

where,

Q_B = the bulked peak discharge (m^3/s)
Q_w = the clear-water discharge (m^3/s)
Q_s =the volumetric sediment discharge (m^3/s)

The BF is the ratio of the bulked discharge to the clear-water discharge

$$BF = \frac{(Q_w + Q_s)}{Q_w}$$

Using this definition, the bulked peak discharge may be defined as

$$Q_B = BF * Q_w$$

The BF may also be computed based on the concentration of sediment in the flow

$$BF = \frac{1}{1 - \frac{C_v}{100}}$$

Hydraulics: Post-wildfire recovery in arid and semi-arid climates can take decades, posing potential long-term flood operations and management concerns for federal, state and local agencies. Lack of vegetation and hydrophobic soils present lower to non-existent watershed ability to retain and absorb runoff produced by rain events, which results on post-wildfires all-time high peak-flows causing dramatic changes in hydraulic and sediment impacts down system as well. More and coarser sediment is entrained because of higher runoff volume and velocities, producing hyperconentrated flows (Figure 6). These flows often carry large boulders, trees and even cars.

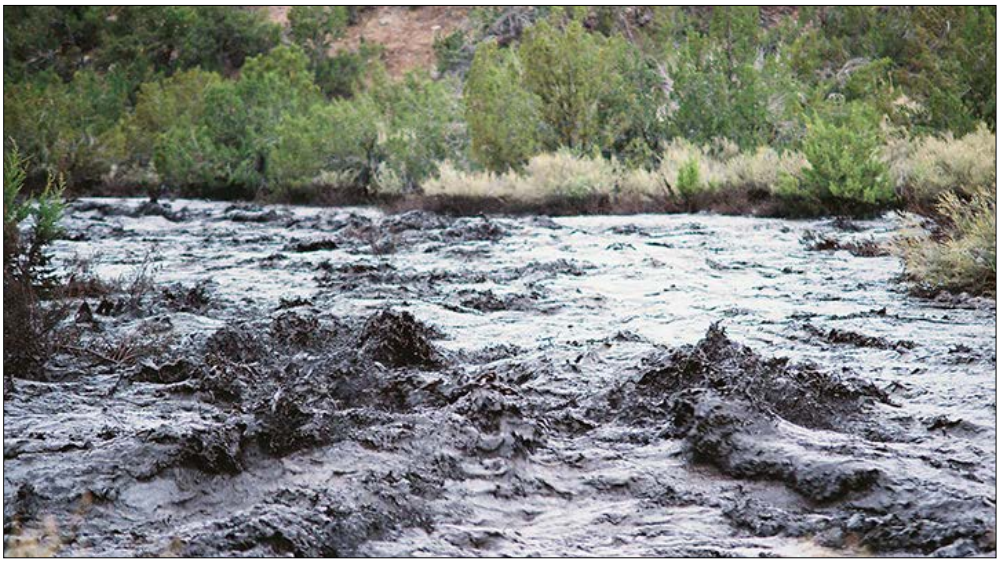

Figure 6. Hyper-concentrated flow in the Rio Grande (Rio Grande Water Fund, 2015).

Common hydraulic intensity parameters useful in predicting post-fire flood events include; flow depth and velocity, run-out distance, and impact forces on in-channel structures. Julien and Paris (2010) provides relationships describing mean velocity of mudflows, hyperconcentrated flows, and debris flows developed from 350 field and laboratory datasets. The authors derive three approaches to estimate velocity, parameterized from field and laboratory data using Darcy-Weisbach and Manning-Strickler flow resistance relationships (Table 2).

Table 2. Resistance to flow mean velocity approximation for hyperconcentrated flows.

Resistance Approach	Mean Velocity Relationship
Dispersive	$V = 0.4\left(\frac{h}{d_{50}}\right)^{1/6}(ghS)^{\frac{1}{2}}$
Manning	$V = 5.0\left(\frac{h}{d_{50}}\right)^{1/6}(ghS)^{\frac{1}{2}}$
Turbulent	$V = 5.75\log\left(\frac{h}{d_{50}}\right)(ghS)^{\frac{1}{2}}$
Bingham	$V \cong \frac{h(\tau - \tau_y)}{2\mu_m}$

where,

V = mean velocity (m/s)
h = flow depth (m)
d_{50} = the median grain diameter (m)
g = acceleration due to gravity (m/s^2)
S = the friction slope
τ = the shear stress (= $\rho_m$ghS)
τ_y = the non-Newtonian slurry dynamic yield strength (Pa).

Newtonian and Non-Newtonian Mechanics: Sediment-laden flows reach non-Newtonian behavior by increasing the concentration of sediment in relation to water. Mixtures containing 5 to 10 % of cohesive sediment by volume deform and/or flow with minimal shear stress applied as non-Newtonian fluids According to Bagnold (1954), sediment-water mixtures become non-Newtonian fluids when sediment concentrations reach a volume fraction from 0.05 to around 0.615 (C_{max}) for ideal homogeneous spheres. C_{max} is commonly referred to as the maximum packing fraction termed by Bagnold (1954).

Post-fire flood events exhibit other unique non-Newtonian properties that deserve discussion and defining, including settling velocity (deposition) and boundary shear stress (erosion). Impacts on particle settling could best be described by visualizing the differences in fall velocity of equal size steel spheres dropped into suspensions of clear water versus honey. The spheres dropped in honey will settle a significantly slower velocities compared to water. In non-Newtonian mechanics this phenomena is referred to as hindered settling. In sediment slurries, when concentrations increase to around 0.05 volumetric concentration, the sediment particles begin to hinder each other and imped settling. Most hindered settling expressions for non-cohesive sediment are based on the formulation by Richardson and Zaki (1954) where return flow, wake formation, and buoyancy are accounted for empirically – defined as,

$$w_s = w(1 - C_v)^m$$

where,

w_s = settling velocity (m/s)
w = settling velocity of single particle in still water (m/s)
C_v = volumetric concentration of primary particles within a sediment mixture (-)
m = an empirical coefficient (-)

The effects of hindered settling are commonly observed in post-fire floods via very large boulders being transported considerable distances from the source location. Boundary (or bed) shear stress is another key parameter when estimating erosion and deposition potential. The boundary shear stress is defined as a function of gravity, flow depth, sediment slurry density, and channel slope defined as

$$\tau_0 = \rho_m g h S_f$$

where,

τ_0 = boundary shear stress (Pa)
ρ_m = slurry mass density (kg/m^3)
g = acceleration due to gravity (m/s^2)
h = flow depth (m)
S_f = friction slope (m/m)

Slurry mass densities in natural non-Newtonian flows can be considerably larger than in Newtonian *clear water* open channel flows; thereby, significantly increasing the bed shear stress

and potential for sediment entrainment. A practical application is sizing rip rap for post-wildfire mitigation and management infrastructure. For *clear water* flows, the boundary shear stress is estimated using the density of the fluid, which is approximately 1000 kg/m^3. In most post-fire floods the mass density is approximately 1500 kg/m^3 resulting in a 40 % increase in boundary shear stress.

Summary & Conclusions

During the summer of 2011, the Las Conchas Fire burned approximately 634 km^2 in the Jemez Mountains of north-central New Mexico. Areas inside the Las Conchas burned scar were previously affected by 1977 La Mesa Fire, 1996 Dome Fire, and 2000 Cerro Grande Fire. This area has a cold semi-arid climate, and steep rugged mountains forming canyons that drain into the Rio Grande. Vegetation was removed and finer sediment was exposed, reducing permeability of soils resulting in increased discharge, sediment transport, and debris flows. Watersheds inside the Las Conchas Fire limits area are now at significant risk of damage from post-wildfire sedimentation hazards such as those associated with debris flows, mudflows and debris floods. Surface runoff and debris flow processes in burned watershed are complex often non-linear processes. Most of these watersheds drain into the Rio Grande upstream of Cochiti Lake. As the movement of sediment progresses downstream, it is being trapped at the reservoir. Unprecedented delta progradation has been observed after the fire occurred, resulting on reservoir storage capacity loss. Post-fire hydrology and debris flow models can be useful tools for assessing wildfire impacts by estimating post-fire flow and debris flow.

Post-fire hydrology and debris flow models can be useful tools for assessing wildfire impacts by estimating post-fire flow and debris flow. In this effort, we evaluate post-fire geomorphic effects of the Las Conchas Wildfire to quantify the empirical impacts on flood-risk management operations on the Middle Rio Grande River and Cochiti Reservoir. Debris flow probability and volume of a 5-year rainfall event for five impacted watersheds were calculated using empirical methods developed by Cannon et al. (2010). Most empirical-based models are restricted to use in watersheds with similar physical and ecological characteristics to empirical model of interest. The Las Conchas Fire is not a unique event. Results from this project will be applied to several other areas affected by other western wildfires (e.g., Waldo Canyon, Colorado; Tres Lagunas, New Mexico; Hayden Pass, Colorado; Carpenter 1, Nevada; and Eagle Creek, Oregon).

References

Aref, I.M., El Atta, H.A., Al Ghamde, ARM. (2011). “Effect of forest fires on tree diversity and some soil properties.” International Journal of Agriculture & Biology, 13(5), 659-664.

Badía, D., Martí, C. and Charte, R. (2011). “Soil erosion and conservation measures in semiarid ecosystems affected by wildfires.” In Soil erosion studies. InTech.

Bagnold, R.A. (1954). “Experiments on gravity-free dispersion of a large solid sphere in a Newtonian fluid under shear.” Proceedings of the Royal Society of London, Series A. 224, p. 49-63.

Boerner, R.E., Huang, J. and Hart, S.C. (2009). “Impacts of Fire and Fire Surrogate treatments on forest soil properties: a meta-analytical approach.” Ecological Applications, 19(2), pp.338-358.

Bogdanov, S. (2014). “Soil texture changes in gray forest soils (Gray Luvisols) influenced by forest fires in deciduous forests.” Forestry Ideas, 2014, 20 no.2 (48), pp. 135–140.

Cannon, S. H., Bigio, E. R. and Mine, E. (2001a). “A process for fire-related debris-flow initiation, Cerro Grande Fire, New Mexico.” Hydrological Processes, 15, pp. 3011-3012.

Cannon, S.H., Kirkham, R.M. and Parise, M. (2001b). “Wildfire-related debris-flow initiation processes, Storm King Mountain, Colorado.” Geomorphology, 39(3-4), pp. 171-188.

Cannon, S. H. and Gartner, J. E. (2005). “Wildfire-related debris flow from a hazards perspective.” In: M. Jakob and O. Hungr (Editors). Debris-flow hazards and related phenomena. Chapter 16. Springer-Praxis Books in Geophysical Sciences, pp. 363-385.

Cannon, S.H., Gartner, J.E. and Michael, J.A. (2007). “Methods for the emergency assessment of debris-flow hazards from basins burned by the fires of 2007, Southern California.” US Geological Survey.

Cannon, S.H., Gartner, J.E., Wilson, R.C., Bowers, J.C. and Laber, J.L. (2008). “Storm rainfall conditions for floods and debris flows from recently burned areas in southwestern Colorado and southern California.” Geomorphology, 96(3-4), pp.250-269.

Cannon, S.H., Gartner, J.E., Rupert, M.G., Michael, J.A., Staley, D.M. and Worstell, B.B. (2009). “Emergency assessment of post-fire debris-flow hazards for the 2009 Station fire, San Gabriel Mountains, Southern California (No. 2009-1227).” US Geological Survey.

Cannon, S. H., Gartner, J. E., Rupert, M. G., Michael, J. A., Rea, A. H. and Parrett, C. (2010). “Predicting the probability and volume of post-wildfire debris flows in the intermountain western United States.” Geological Society of America. Bulletin 122 (1/2), pp. 127-144.

Certini, G. (2005). “Effects of fire on properties of forest soils: A review.” Oecologia, 143, pp. 1-10.

Dahm, C.N., Candelaria-Ley, R.I., Reale, C.S., Reale, J.K. and Van Horn, D.J. (2015). “Extreme water quality degradation following a catastrophic forest fire.” Freshwater biology, 60(12), pp.2584-2599.

Davis, C.M., Bahner, C., Eidson, D., Gibson, S. (2015). “Rio Grande and Cochiti Reservoir Sedimentation Issues: Are There Sustainable Solutions?” presented at Sedimentation and Hydrologic Modeling (SEDHYD) Conference, Reno, NV, 2015.

DeBano, L.F., Neary, D.G. and Ffolliott, P.F. (1998). “Fire effects on ecosystems.” John Wiley & Sons.

Doerr, S.H., Shakesby, R.A. and MacDonald, L.H. (2009). “Soil water repellency: a key factor in post-fire erosion.” Fire effects on soils and restoration strategies, 5.

Ebel, B. A., Moody, J. A. and Martin, D. A. (2012). “Hydrologic conditions controlling runoff generation immediately after wildfire.” Water Resources Research, 48(3), pp. 1-13.

FAO/IIASA/ISRIC/ISSCAS/JRC (2012). “Harmonized World Soil Database (version 1.2).” FAO, Rome, Italy and IIASA, Laxenburg, Austria.

Hamilton, D.L. and Fan, S.S. (1996). “Reliability of sediment transport modeling for shallow flow on initially dry areas.” Proceeding of the Sixth Federal Interagency Sedimentation Conference, March 10-14, 1996, Las Vegas, Nevada.

Julien, P. Y. and Paris, A. (2010). “Mean velocity of mudflows and debris flows.” Journal of Hydraulic Engineering, 136(9), pp. 676-679.

Köppen, W. and Geiger, R. (1954). “Klima der Erde (map).” Justus Perthes, Darmstadt, Germany.

Kottek, M., Grieser, J., Beck, C., Rudolf, B. and Rubel, F. (2006). “World map of the Köppen-Geiger climate classification updated.” Meteorologische Zeitschrift, 15(3), pp.259-263.

Letey, J. (2001). “Causes and Consequences of Fire-Induced Soil Water Repellency.” Hydrological Processes, 15(15), pp.2867-2875.

Moody, J. A., Kinner, D. A. and Ubeda, X. (2009). “Linking hydraulic properties of fire affected soils to infiltration and water repellency.” Journal of Hydrology, 379, pp. 291-303.

Moody, J.A. and Martin, D.A., 2001. "Post-fire, rainfall intensity–peak discharge relations for three mountainous watersheds in the western USA." Hydrological processes, 15(15), pp.2981-2993.

Moody, J.A., Shakesby, R.A., Robichaud, P.R., Cannon, S.H. and Martin, D.A. (2013). "Current research issues related to post-wildfire runoff and erosion processes." Earth-Science Reviews, 122, pp.10-37.

Moody, J.A. (2017). "Residence times and alluvial architecture of a sediment superslug in response to different flow regimes." Geomorphology, 294, pp.40-57.

Neary, D. G., Gottfried, G. J. and Folliott, P. F. (2003). "Post-wildfire watershed flood responses." 22nd International Wildland Fire Ecology and Fire Management Congress.

Neary, D.G., Ryan, K.C. and DeBano, L.F. (2005). "Wildland fire in ecosystems: effects of fire on soils and water." Gen. Tech. Rep. RMRS-GTR-42-vol. 4. Ogden, UT: US Department of Agriculture, Forest Service, Rocky Mountain Research Station. 250 p., 42.

Richardson, J.F. and Zaki, W.N. (1954). "The sedimentation of a suspension of uniform spheres under conditions of viscous flow." Chemical Engineering Science, 3(2), pp. 65-73.

Richard, G.A. (2001). "Quantification and prediction of lateral channel adjustments downstream from Cochiti Dam, Rio Grande, NM." Doctoral Dissertation, Colorado State University.

Rio Grande Water Fund. "The Nature Conservancy in New Mexico. The Nature Conservancy. (2015). Web, 6 July 2015."

Tillery, A.C., Darr, M.J., Cannon, S.H. and Michael, J.A. (2011). "Post-wildfire preliminary debris flow hazard assessment for the area burned by the 2011 Las Conchas Fire in North-Central New Mexico." DOI US Geological Survey Open-File Report, 1308.

Tüfekçioğlu, A., Küçük, M., Sağlam, B., Bilgili, E. and Altun, L. (2009). "Soil properties and root biomass responses to prescribed burning in young corsican pine (Pinus nigra Arn.) stands." Journal of Environmental Biology, 31, pp. 369-373.

USACE-SPA (2011a). "2011 Las Conchas Fire: Post Fire Hydrological Modeling Results for Cochiti Canyon."

USACE-SPA (2011b). "2011 Las Conchas Fire: Post Fire Hydrological Modeling Results for Frijoles Canyon."

USACE-SPA (2011c). "2011 Las Conchas Fire: Post Fire Hydrological Modeling Results for Bland Canyon."

USACE-SPA (2013). "Cochiti Baseline Study: A Data Compendium."

Veenhuis, J.E. (2002). "Effects of wildfire on the hydrology of Capulin and Rito de los Frijoles Canyons, Bandelier National Monument, New Mexico (Vol. 2, No. 4152)." US Department of the Interior, US Geological Survey.

Velizarova, E., Yorova, K. and Tashev, A. (2001). "Investigations of some characteristics of forest soils influenced by fire in plantation of Black Pine (Pinus nigra Arn.)." Nauka za gorata 1–2: 29–34 (in Bulgarian).

Verma, S. and Jayakuma, S. 2012. "Impact of forest fire on physical, chemical and biological properties of soil: a review." Proceedings of the International Academy of Ecology and Environmental Sciences, 2(3):168-176.

Vieira, N.K., Clements, W.H., Guevara, L.S. and Jacobs, B.F. (2004). "Resistance and resilience of stream insect communities to repeated hydrologic disturbances after a wildfire." Freshwater Biology, 49(10), pp.1243-1259.

WEST Consultants, Inc. 2011. “Sediment/debris bulking factors and post-fire hydrology for Ventura County: Final Report.” Prepared for Ventura County Watershed Protection District, Ventura, CA.

Westerling, A.L., Hidalgo, H.G., Cayan, D.R. and Swetnam, T.W. (2006). “Warming and earlier spring increase western US forest wildfire activity.” Science, 313(5789), pp.940-943.

Williams, A.P., Allen, C.D., Macalady, A.K., Griffin, D., Woodhouse, C.A., Meko, D.M., Swetnam, T.W., Rauscher, S.A., Seager, R., Grissino-Meyer, H.D., Dean, J.S., Cook, E.R., Gangodagamage, C., Cai, M., and McDowell, N.G. (2012). “Temperature as a potent driver of regional forest drought stress and tree mortality.” Nature Climate Change, 3(3), p.292.

Wolf Engineering (2017) Hydrographic Data Collection Report. “Field Survey Cross Sections and Sediment Delta Cochiti Lake Range Lines, Summer 2017.” US Army Corps of Engineers, 2011que District.

Factors Controlling Reservoir Sedimentation Rates in the Little Washita River Experimental Watershed, Oklahoma

Daniel Moriasi, Research Hydrologist, USDA Agricultural Research Service, El Reno, OK, daniel.moriasi@ars.usda.gov

Jean Steiner, Laboratory Director and Research Leader (Retired), USDA Agricultural Research Service, El Reno, OK, jean.steiner@hughes.net

Sara Duke, Statistician, USDA Agricultural Research Service, College Station, TX, sara.duke@ars.usda.gov

Patrick Starks, Acting Research Leader and Soil Scientist, USDA Agricultural Research Service, El Reno, OK, patrick.starks@ars.usda.gov

Alan Verser, Hydrologist Technician, USDA Agricultural Research Service, El Reno, OK, alan.verser@ars.usda.gov

Abstract

In the 1930s, severe drought and lack of proper farming methods resulted in lack of vegetation, which combined with subsequent periods of intense rainfall caused increased erosion and flooding. Following passage of the Watershed Protection and Flood Prevention Act 1954, USDA installed 45 flood-retarding structures (here after referred to as reservoirs) between 1969 and 1982 in the Little Washita River Experimental Watershed (LWREW), located in central Oklahoma. Over time, these reservoirs lose sediment and flood storage capacity due to sedimentation, at rates dependent on upstream land use and climate variability. In this study, sedimentation rates for 12 reservoirs representing three major land use categories within LWREW were measured based on bathymetric surveys from an acoustic profiling system. Physiographic and climate attributes of drainage area of surveyed reservoirs were extracted from publicly available data sources including topographic maps, digital elevation models, USDA Natural Resource Conservation Service (NRCS) soils, and weather stations databases. The variables were correlated with normalized reservoir sedimentation rates (ReSRa) to determine the major variables controlling sedimentation within the LWREW. Percent of drainage area with extreme slopes, saturated hydraulic conductivity, and maximum daily rainfall event recorded in spring explained most of the variability in ReSRa. Results of current reservoir sediment and flood capacities, reservoir sedimentation rates, projected lifespans, and all analyzed variables are presented. The implications of the results are discussed. Evaluation of these reservoirs fits into the goal of the Conservation Effects Assessment Project (CEAP) to quantify the environmental benefits of conservation practices.

Brief Introduction and Methods

This extended abstract presents a brief description of the methods and results of the study carried out by Moriasi et al. (2018). The study was conducted in the LWREW, located in central Oklahoma,

which covers an area of 610 km² (Figure 1) containing the selected 12 of the 45 reservoirs impounded between 1969 and 1982 (Allen and Naney, 1991). The average land use in the LWREW for the period 1974 to 1994 were 72% grass, 15% cropland, and 12% trees while for the period 1994 - 2008, it was 65% grass, 16% cropland and 13% trees (Starks et al., 2014). The climate is sub-humid with most of the annual rainfall and flooding occurring during the spring and fall seasons (Steiner et al., 2014). The characteristics of the 12 selected reservoirs are presented in Table 1.

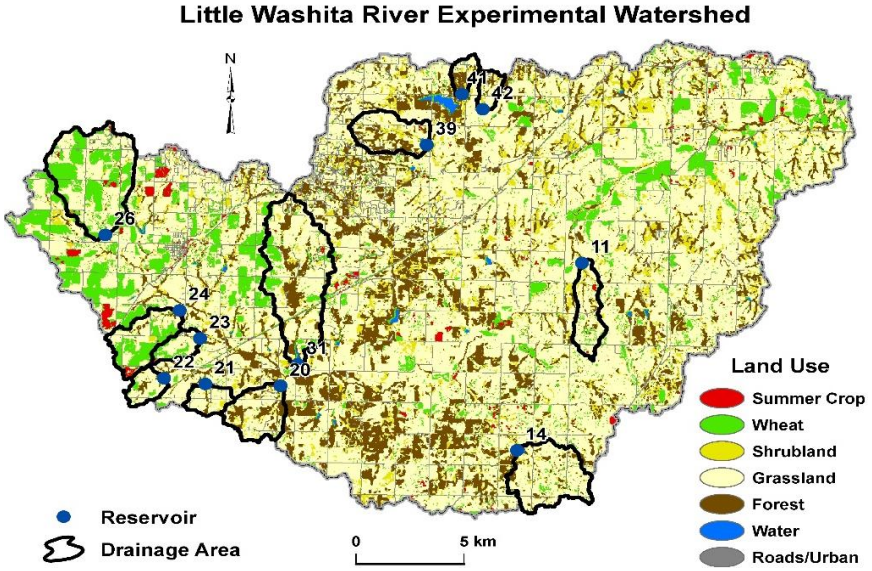

Figure 1. Selected reservoirs in the Little Washita River Experimental Watershed

Table 1. Information of reservoirs surveyed in the LWREW (Allen and Naney, 1991; Moriasi et al., 2018)

Reservoir ID	Date Construction Completed	Drainage Area (km²)	Storage Capacity † (m³)	Surface Area (m²)	% Drainage Area Under LU‡			% Drainage Area Under Texture		
					Crop	Grass	Forest	Sandy Loam	Silt Loam	Loam
11	6/11/1973	4.9	104809	44515	10	73	15	53	23	9
14	4/14/1978	10.8	242910	97125	5	75	16	98	0	0
20	10/27/1982	6.7	215783	76890	2	60	33	68	0	29
21	5/-/70	2.8	73983	24281	3	80	11	66	2	26
22	4/8/1977	2.9	115906	28328	15	69	13	17	9	75
23	7/27/1971	2.5	75216	36422	34	59	2	17	18	65
24	11/8/1976	7.0	166461	48562	43	46	6	21	43	36
26	12/-/71	18.0	514180	109265	42	50	2	1	84	15
31	9/14/1978	19.2	525277	169968	14	60	21	31	57	12
39	6/26/1978	6.3	141800	80937	1	56	35	97	0	0
41	10/-/69	2.0	51788	20234	2	44	44	100	0	0
42	10/-/69	1.9	56720	28328	4	66	24	94	2	4

†Total storage at the principal spillway elevation. ‡LU = Land use category

Water and sediment volumes were determined based on a bathymetric survey carried out in May 2012 in the LWREW using a multi-frequency acoustic profiling system (APS, Figure 2). Dunbar et al. (1999) describe the APS in detail while Moriasi et al. (2018) describe how APS was utilized in this study. In this study, volumetric sedimentation rates (ReSR) were computed by dividing the difference between current storage capacity determined during bathymetric surveys and the "as-built" total storage capacities (OSC) (Table 1) by the number of years since impoundment. The projected lifespans (PLS) were then estimated by dividing OSC by ReSR. The ReSR values were

divided by reservoir drainage areas to obtain normalized volumetric sedimentation rates (ReSRa), which were correlated with selected variables.

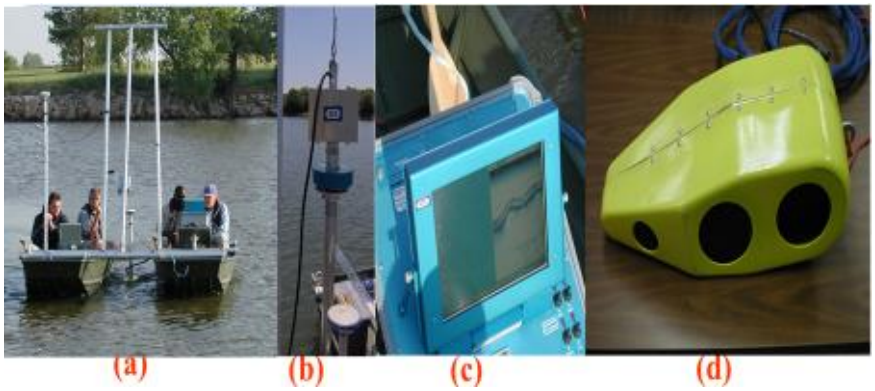

Figure 2. The acoustic profiling system and vibracoring device (a) on a pair of linked Jon boats, (b) vibracoring device, (c) control module, and (d) acoustic profiler transducer array (240 kHz, 50 kHz, and 24 kHz)

Initially, several topographic, land cover type proportions, climate, and soils variables were created and correlated with ReSRa. Variables with correlation values≥ 0.25 [absolute] were considered to have some predictive power on ReSRa and therefore included for further investigation (Table 2). Parametric and non-parametric Spearman rank correlations, principal component analysis, and stepwise regression statistical analyses were carried out using JMP version 13 (SAS Institute Inc., 2016) to identify variables that were most predictive of ReSRa.

Table 2. Contributing variables selected. AS = average slope of the drainage area (%), PES = percent of drainage area with extreme slopes (>20%), LS = slope length (m), PAF = pond area factor defined as total pond area divided by total drainage area, CLL = weighted average overland % clay content from reservoir drainage area, OC = weighted average overland % organic carbon from reservoir drainage area, Ksat = weighted average saturated hydraulic conductivity (mm hr^{-1}) within reservoir drainage area, MR2Q= maximum daily rainfall event recorded within reservoir drainage area during the second quarter since construction (mm), DR2Q = number of days per year with precipitation between 51 and 65 mm in the second quarter (April - June), PRRSA =percent reduction in reservoir surface area (%) (Moriasi et al., 2018)

	Physically-based Variables									Derived Variable
Reservoir ID	AS (%)	PES (%)	LS (m)	PAF	CLL (%)	OC (%)	Ksat ($mmhr^{-1}$)	MR2Q (mm)	DR2Q	PRRSA (%)
11	7.7	4	39	0.76	15	1.1	32	19	14	0
14	7.5	3	43	0.10	14	0.8	29	20	15	25
20	7.1	4	43	0.44	16	1.1	24	24	17	26
21	5.6	2	48	0.29	15	1.1	27	24	18	0
22	8.7	10	33	0.36	20	1.8	12	24	18	51
23	6.6	5	44	0.35	20	1.8	12	24	18	7
24	5.5	4	69	0.66	20	1.7	13	24	18	10
26	5.1	3	49	0.35	21	2.0	9	30	17	48
31	7.6	1	70	0.54	19	1.6	15	32	15	27
39	7.4	2	75	0.22	14	0.8	30	19	16	8
41	7.4	2	18	0.04	14	0.8	28	22	15	0
42	7.4	3	40	0.72	14	0.8	27	22	15	10

Summary of Major Findings and Recommendations

Reservoir sediment and flood storage capacity loss varied from 0.84%/yr to 2.20%/yr. Sedimentation rates ranged from 181 $m^3/km^2/yr$ to 873 $m^3/km^2/yr$ with lifespans ranging from 45

to 118 years. It is possible to estimate sediment and flood storage capacity and projected lifespan for various reservoirs using climate, soils, and topographic variables. Physically based percent of drainage area with extreme slopes (>20%), saturated hydraulic conductivity, and maximum daily rainfall event recorded in spring variables explained most of the variability in ReSRa. Percent reduction in reservoir surface area, a derived variable from readily available data, explained more variability in ReSRa than the combined three most predictive physically based variables. This provides a reasonable cost-effective approach that can be tested in other areas with reservoir sedimentation challenges. Reservoir sediment and flood storage capacity and projected lifespan information obtained from bathymetric survey or estimated using physically based variables can help water resource managers in prioritizing dams for rehabilitation and/or decommissioning. Reservoir water storage capacity information could also impact the development of Emergency Action Plans as part of the Federal Guidelines for Dam Safety.

Table 3. Reservoir sedimentation rates (ReSR), projected lifespan (PLS), normalized reservoir sedimentation rates (ReSRa), and reservoir volume on survey date (RVSD)

Reservoir ID	Years of Operation on Survey Date	Capacity Loss Rate (%) per year	PLS (years)	ReSRa ($m^3/km^2/year$)	RVSD (m^3)
11	42	0.84	118	181	67818
14	37	1.63	61	368	96054
20	33	1.63	61	526	99877
21	45	1.13	88	294	36498
22	38	2.20	45	873	18989
23	44	1.03	96	305	41060
24	39	1.11	89	265	94205
26	44	1.94	51	557	74599
31	38	1.54	64	423	217263
39	38	1.28	77	288	72626
41	46	1.55	64	410	14920
42	46	1.07	93	320	28853

References

Allen, P.B. and Naney, J.W. 1991. "Hydrology of the Little Washita River watershed, Oklahoma", United States Department of Agriculture, Agricultural Research Service, ARS-90 p.74. (Available in digital form at ftp://164.58.150.49/pub/little_washita/ars-90.pdf; accessed 27 November, 2012).

Dunbar, J.A., Allen, P.M., and Higley, P.D. 1999. "Multifrequency acoustic profiling for water reservoir sedimentation studies", Journal of Sedimentation Research, 69(2):518-527, https://doi.org/10.2110/jsr.69.518.

Moriasi, D.N, Steiner, J.L., Duke, S.E., Starks, P.J. and Verser, A.J. 2018. Reservoir sedimentation rates in the Little Washita River Experimental watershed, Oklahoma: measurement and controlling factors", Journal of the American Water Resources Association, 54 (5):1011–1023. https://doi.org/10.1111/1752-1688.12658.

SAS Institute Inc. 2016. JMP 13. Cary, NC: SAS Institute Inc.

Starks, P.J., Steiner, J.L., and Stern, A.J. 2014. "Upper Washita River experimental watersheds: land cover data sets (1974-2007) for two southwestern Oklahoma agricultural watersheds", Journal of Environmental Quality, 43:1310-1318, doi:10.2134/jeq2013.07.0292.

Steiner, J.L., Starks, P.J., Garbrecht, J.D., Moriasi, D.N., Zhang, J.X., Schneider, J.M., Guzman, J.A., and Osei, E. 2014. "Long-term environmental research: the Upper Washita River Experimental watersheds, Oklahoma, USA", Journal of Environmental Quality, 43(4): 1227-38, doi:10.2134/jeq2014.05.0229.

Improving Sediment Management in the Cowlitz Falls Hydropower Facility

Achilleas Tsakiris, Hydraulic Specialist, Northwest Hydraulic Consultants, Olympia, WA, atsakiris@nhcweb.com
Casey Kramer, Principal Hydraulic Engineer, Northwest Hydraulic Consultants, Olympia, WA, ckramer@nhcweb.com
Brad Hall, Principal Hydraulic Engineer, Northwest Hydraulic Consultants, Sacramento, CA, bhall@nhcweb.com
Jose Vasquez, Principal Hydraulic Engineer, Northwest Hydraulic Consultants, North Vancouver, BC, Canada, jvasquez@nhcweb.com
Joe First, Project Manager, Cowlitz Falls Hydroelectric Project, Lewis County Public Utility District, Morton, WA, joef@lcpud.com

Introduction

The Cowlitz Falls Project is a run-of-the-river hydropower facility located on the Cowlitz River, WA, approximately 1.5 miles downstream of its confluence with the Cispus River (Figure 1). It is the first of three hydropower facilities on Cowlitz River, with the Mossyrock and Mayfield Dams located approximately 17 and 27 miles further downstream.

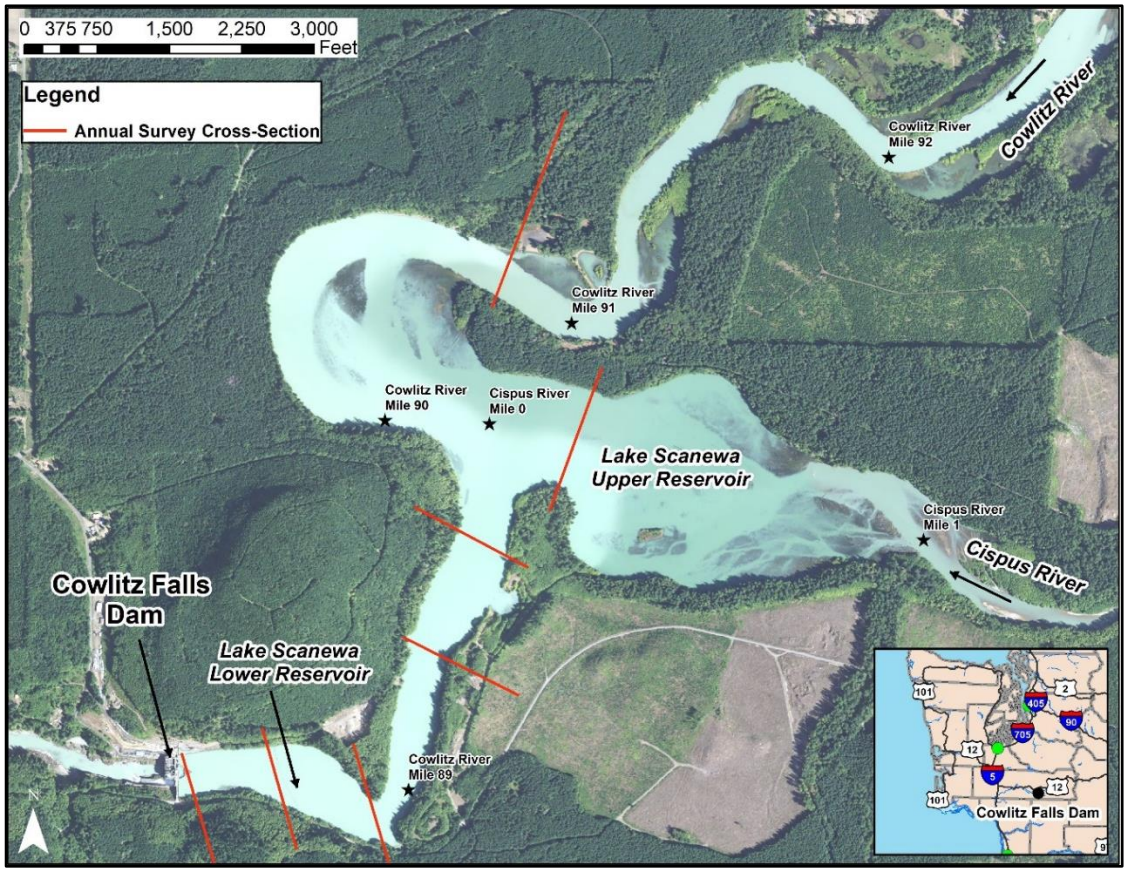

Figure 1. Vicinity map of the Cowlitz Falls Dam

The Cowlitz Falls Dam impounds the Lake Scanewa reservoir, which has a capacity of 11,000 acre-feet and is delineated into the Lower and Upper Reservoir downstream and upstream of the confluence between the Cowlitz and Cispus Rivers, respectively (Figure 1). The Cowlitz and Cispus Rivers originate from the Cascade Mountains and are characterized by rainfall-driven flood events in the fall winter and snowmelt-driven early spring floods, followed by low-flow periods during the summer. Flows are also affected by periods of glacial melt from Mt. Rainier during the late summer and fall. During these floods, an estimated 500,000 cubic yards of predominantly sand and silt, with some traces of gravel is conveyed annually to the reservoir. Sediment deposited in the reservoir is flushed during reservoir drawdowns during the low-flow periods, as well as during drawdowns for flood operations (CFHP-SOP, 2017).

The primary goal of this project is to assess the performance of these drawdowns in evacuating the deposited sediment from the reservoir and to evaluate alternatives for reducing the amount of sediment accumulation in the reservoir, given that lowered reservoir conditions result to losses of hydropower production. The objective of the study presented herein is to present the development and calibration of a 1D, mobile bed model, for simulating sediment transport processes in the vicinity of the Cowlitz Falls dam.

The Cowlitz and Cispus Rivers watersheds are 588.7 and 434.2 square miles upstream of the project site. Their drainage basins receive on average, 74.6 and 78.0 inches of precipitation annually (PRISM Climate Group, 2015). Flow data on the Cowlitz River was acquired from gaging station No. 14231000, which is approximately 11 miles upstream of the project site. Flow on the Cispus River was retrieved from gaging station No. 14232500 located approximately 15 miles upstream of the project site. The flows from these gaging stations were extrapolated to the project site, using the procedure of Mastin et al. (2016). The water surface elevation upstream of the Cowlitz Falls Dam was acquired from gaging station No. 14233490. Grain size distributions of the Cowlitz and Cispus River bed material were derived from grab samples taken at six representative locations within the project site, which revealed that the bed of these rivers is comprised predominantly of sand and silt, with some traces of gravel. The bathymetry at the project site was mapped on September 8th, 2017, while the annual cross sectional survey of the reservoir and along Cowlitz River (Figure 1) was conducted on January 31st, 2018.

Methods

The hydraulic analysis was performed using the HEC-RAS 1D hydrodynamic software (USACE, 2018). The downstream end of the modeling domain was at the Cowlitz Falls Dam and extended approximately 5 miles upstream along the Cowlitz River and 1 mile along the Cispus River upstream of its confluence with the Cowlitz River. Cross-sections for specifying the HEC-RAS model geometry were extracted with a 400-foot average spacing from a bathymetric survey conducted on September 8th, 2017. The Manning's n roughness coefficient for the main channel and floodplain areas of the model was specified to be 0.035 and 0.08, based on site observations. A quasi-unsteady, mobile-bed flow simulation of the period between September 8th, 2017 and January 31st, 2018 was performed, as it included the annual sediment flushing drawdown and three typical drawdowns for flood regulation (Figure 2). The downstream boundary condition for the simulation was the Lake Scanewa water surface elevation time series during this period (Figure 2) and the corresponding model inflow was the discharge times series on the Cowlitz and Cispus Rivers (Figure 2). Due to lack of sediment transport rate measurements, a sensitivity analysis was performed, and determined that the combination of an input sediment load equal to half the equilibrium transport rate and the Ackers and White

transport function produced the best agreement between the computed geometry at the end of the simulations and the measured deposition at surveyed cross-sections. Utilizing half the equilibrium transport rate indirectly captures the effects that armoring of the gravel found atop the bed surface has on the transport rate of the finer sand and silt sediment fractions.

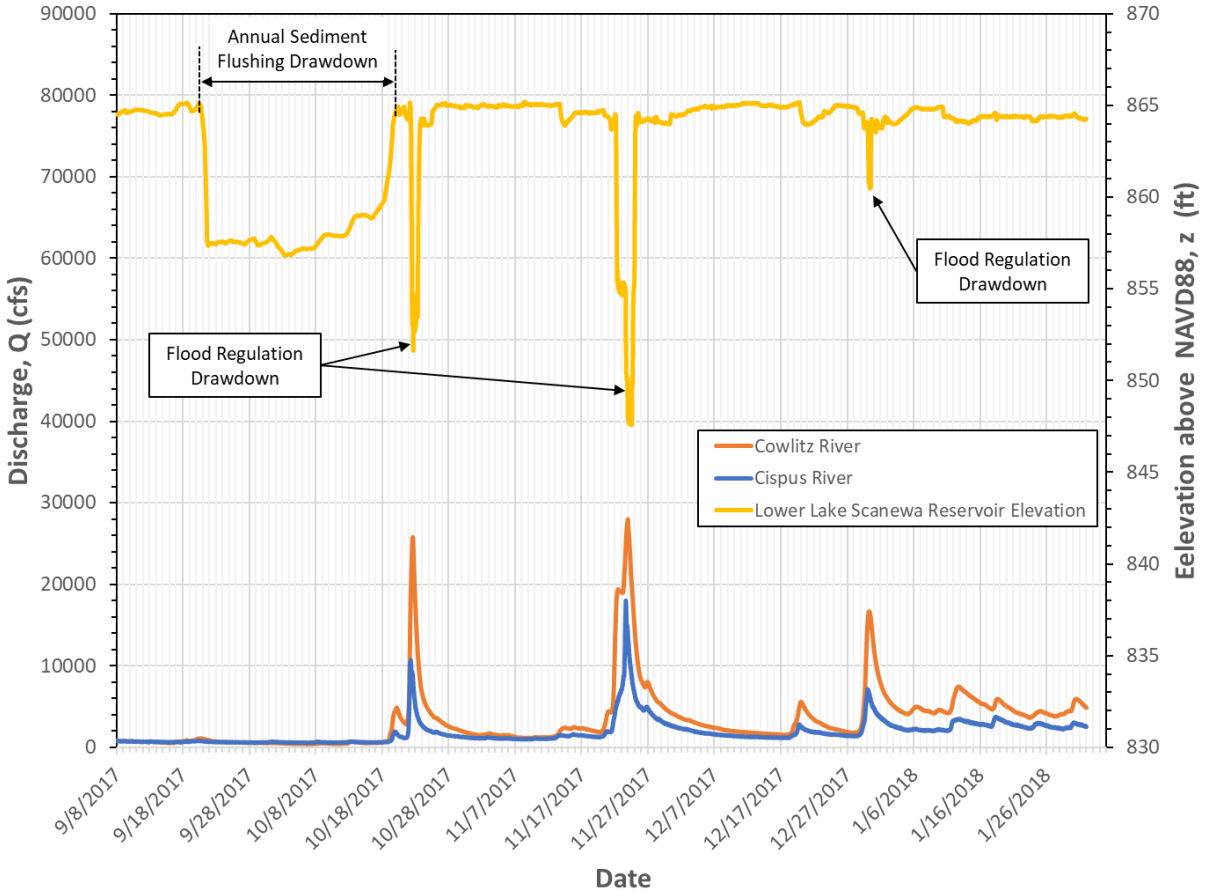

Figure 2. Cowlitz and Cispus River hydrograph and Lake Scanewa water surface elevation between September 8th, 2017 and January 31st, 2018

Results

The model predicted an overall tendency of the Cowlitz River bed to erode upstream of station 8,000 feet (Figure 3). The simulation also revealed deposition to occur in a 6,000-foot long reach extending between stations 2,000 and 8,000 (Figure 3), which corresponds to the upper reservoir. This trend was consistent with the comparison of the cross-sectional surveys conducted January, 31st, 2018 to the original bed topography on September 8th, 2017. The deposition of the incoming sediment between stations 2,000 and 8,000 feet in Figure 3, potentially reduces the sediment supply in the lower reservoir within the first 2,000 feet from the Cowlitz Falls Dam, likely causing the absence of notable deposition nearest the dam at this most downstream segment of the reservoir.

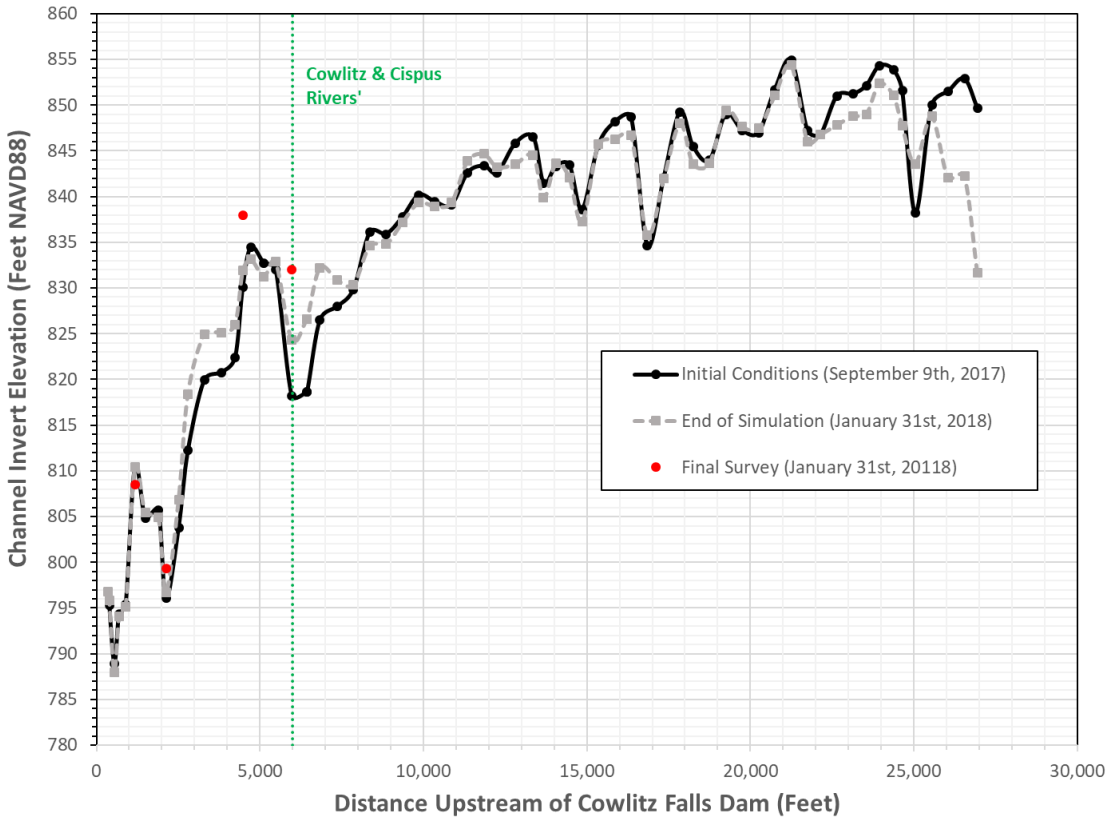

Figure 3. Comparison of the initial longitudinal profile to the final simulated profile and surveyed topography

Conclusions and Future Directions

Future simulations with the developed and calibrated 1D mobile-bed model will aim to determine the optimal magnitude, timing, and duration of future sediment flushing drawdowns that maximize the amount of flushed sediment with minimal hydropower losses. Additional simulations will identify the magnitude and temporal characteristics of drawdowns during flood conditions that minimize sediment deposition near the dam. These simulations will be verified with on-site, real-time flow, sediment transport and bed topography data and will be utilized for developing a detailed 3D CFD mobile bed model of the dam vicinity. This combined modeling and field monitoring effort will ultimately provide the dam managers with an improved operational protocol for better sediment management and more efficient facility operation.

References

CFHP-SOP. 2017. "Cowlitz Falls Hydroelectric Project Standard Operating Procedures", Revision No. 4, Lewis County Public Utility District, Morton, WA.

Mastin, M.C., Konrad, C.P., Veilleux, A G. and A.E. Tecca. 2016. "Magnitude, frequency, and trends of floods at gaged and ungaged sites in Washington, based on data through water year 2014,"*: Scientific Investigations Report 2016-5118*. U.S. Geological Survey. Reston, VA.

PRISM Climate Group. 2015. "30-Year normal precipitation: annual", Oregon State University. http://www.prism.oregonstate.edu/normals/ (accessed November 2017).

United States Army Corps of Engineers. 2018. "HEC-RAS River Analysis System" V.5.0.5.

It can be a dirty job! ~ How the NRCS Deals with Sedimentation

Jon Fripp, PE, Hydraulic Engineer, United States Department of Agriculture – Natural Resources Conservation Service, National Design Construction and Soil Mechanics Center, Fort Worth, Texas, jon.fripp@usda.gov
Karl Visser, PE, Hydraulic Engineer, United States Department of Agriculture – Natural Resources Conservation Service, National Design Construction and Soil Mechanics Center, Fort Worth, Texas, karl.visser@usda.gov
Claudia C. Hoeft, PE, National Hydraulic Engineer, United States Department of Agriculture – Natural Resources Conservation Service, Conservation Engineering Division, Washington, D.C., claudia.hoeft@usda.gov

Introduction

Sedimentation is a critical consideration for stream, river, and reservoir projects. Sedimentation analysis is a key aspect of design since many projects fail due to excessive erosion or deposition. This presentation includes an overview of the variety of analysis and design techniques employed by the Natural Resource Conservation Service (NRCS) in the planning, design and maintenance of watershed or river/stream projects. This presentation discusses the scope of the problem and provides an overview of the methods used to model and predict sedimentation.

NRCS and Work that is Impacted by Sedimentation

For more than 80 years, NRCS and its predecessor agencies worked and continue to work in close partnerships with farmers and ranchers, local and state governments, and other federal agencies to maintain healthy and productive working landscapes. NRCS provides America's farmers and ranchers with financial and technical assistance to voluntarily put conservation on the ground. The work includes the planning and design of a variety of water infrastructure projects including dams, waterways, and stream restoration.

All of these infrastructure projects provide important economic benefits. For example: across the nation, watershed dam projects provide an estimated annual benefit of $2.2 billion in reduced flooding and erosion damages, and improved wildlife habitat, recreation, and water supply for an estimated 47 million people. These projects provide additional benefits, such as improved water quality through sediment and erosion control. Watershed rehabilitation projects also can create rural economic growth and job opportunities. As of 2016, the United States National Inventory of Dams (NID) contained the records of 90,580 dams, of which NRCS aided with approximately 1/3 of this number.

All of these infrastructure projects require consideration of the potential effects of sedimentation. For example, when rivers and streams enter a reservoir, the reservoir traps most of the sediment carried by the stream rather than continuing downstream. Over a period of years these sediment deposits gradually displace the volume originally designated for water storage. Once the planned sediment storage is lost, the water storage volume designed as part of the beneficial purpose of the reservoir is impacted. As this water storage volume is lost, the beneficial uses that depend on storage – such as water supply and flood control – will decline and eventually be lost.

Watershed Projects and Sedimentation

Sedimentation adversely impacts reservoirs. On a world-wide average, the rate of reservoir storage lost to sedimentation is greater than the rate of storage added by construction. World-wide reservoir storage per capita peaked in the 1980s and is now back to 1965 levels due to sedimentation (Annandale 2013). Garcia estimated that the average annual reservoir storage capacity loss rate due to sedimentation is 0.2 percent in the United States (Garcia 2008). This is a serious infrastructure concern.

NRCS traditionally deals with the impacts of sedimentation in reservoirs in the planning phase. Dam planning and construction regulations require that significant implementation of soil conservation measures in the contributing watershed. NRCS implements a variety of techniques and practices to slow runoff, promote infiltration, stabilize gullies, and slow erosion under a variety of NRCS programs. These measure not only improve agricultural productivity but significantly reduce sedimentation into the reservoirs.

While the NRCS and its predecessor agencies long implemented soil conservation, even the best measures will not eliminate sediment flowing into and becoming trapped in reservoirs. Sedimentation prediction uses the following:

- Regional relationships
- Local measurements and observations
- Calculations (typically using modifications of RUSLE)

Specifics for these approaches are available in Soil Conservation Service (SCS) National Engineering Handbook Section 3 (NEH Section 3). Using these techniques, it is possible to estimate an adequate sediment storage for the project design life. The sediment pool is part of the planned reservoir volume.

NRCS planned most dams with a 50-year life and constructed many of these dams in the 1960s and 1970s. Of the 11,000 NRCS project dams, 4,300 have reached the end of their project life. In reviewing these projects, NRCS found that soil conservation practices in the watershed generally resulted in less sedimentation than originally planned but this is not the situation for all NRCS dams. Even when there is less sediment impacts, the loss of reservoir storage can still be a factor in rehabilitation efforts. This is particularly the case if the planned sediment storage capacity has been exceeded or current operation of the outlet works, or other withdrawal infrastructure have been impacted. When sedimentation must be addressed as part of NRCS rehabilitation efforts, the approach is to either dredge the dam or raise the embankment.

Stream Projects and Sedimentation

The success of any constructed channel reach is based on its ability to transport the inflowing water and sediment load without excessive sediment deposition or scouring on the channel bed. Excess scour can cause banks to fail while excess deposition can reduce flood carry capacity and cause flooding. Even a bank protection project is generally ineffective if the bed is unstable. Therefore, a critical step of any channel design project is a sediment impact assessment. Sediment impact assessments can widely range in effort and output. These assessments use visual or qualitative techniques for relatively simple projects or numerical models that incorporates solution of the sediment continuity equation for more complex projects. A final

sediment impact assessment should be viewed as a closure loop at the end of the design process to:

- Validate the efficacy of the design channel geometry and guide designers to needed changes in the design or approach
- Identify flows which may cause aggradation or degradation over the short term (these changes are inevitable and acceptable in a dynamic channel)
- Recommend minor adjustments to the channel design to ensure dynamic stability over the medium- to long-term.

The type of sediment impact assessment employed affects the certainty of the result as well as the precision of an assessment as to whether the channel will aggrade, degrade, or remain stable. The choice of the appropriate technique to assess the sediment impact of a proposed project includes an assessment of not only the project goals and watershed condition but also an assessment of the impact of project failure. Visual and qualitative assessments are typically only appropriate for sites where there is low risk and minimal change to an otherwise stable system. These can be accomplished with the aid of primarily judgment-based tools. As a project complexity increases and where there is a higher risk to life and property, more analytical approaches are usually employed. While there is a wide selection of different analytical techniques, they all typically require the calculation of hydraulic parameters such as velocity and shear stress for the range of natural discharges. They all require data determined from field observations and measurements as well as calculations. Such assessments may require a non-trivial investment of time, but that time may be well spent when compared to the impacts of a project not performing as intended. Table 1 below illustrates some typical sediment impact analysis for different project types and watershed conditions.

Table 1: Selection guidance for sediment impact assessment technique

Project Type	Site / Watershed Assessment	Risk to life, property, or project investment	Suitable Sediment Impact Assessment
Bank stabilization. No significant change to cross section, slope, or planform.	Relatively stable watershed and site.	Low	Confirm that there is no significant change in the local hydraulic conditions from pre to post project and note watershed stability.
Bank stabilization. No significant change to cross section, slope, or planform.	Moderately active watershed and site.	Moderate	Assess stable channel grade at design flows. Field check indications of future channel evolutionary change
Bank stabilization. No significant change to cross section, slope, or planform.	Moderately active watershed and site.	High	Rating Curve comparison of above and through site
Channel modification. Small change to cross section, slope, or planform.	Moderately active watershed and site.	Low	Rating Curve comparison of above and through site as well as pre and post project
Channel Modification. Significant change to cross section, slope, or planform.	Moderately active watershed and site.	Moderate	Sediment Budget analysis with SAM or spreadsheet-based type analysis
Channel Modification. Significant change to cross section, slope, or planform.	Active watershed and site.	High	Long term numerical modeling with HEC-RAS type analysis

The selection of the appropriate methodology requires a firm understanding of the assumptions, accuracy, data requirements, and limitations of the approach. NRCS guidance in NEH-654 provides more details and guidance in the specific techniques.

Conclusion

Sedimentation is a critical component in the planning, design and operation of any watershed or stream/river project. A variety of analysis techniques are used. While no model or assessment eliminates all possibility of a project not performing as intended, the use of the appropriate tool as discussed in NEH-654 and NEH Section 3 reduces the possibility of poor project performance.

References

Annandale, G. (2013). *Quenching the Thirst, Sustainable Water Supply and Climate Change,* Create Space Independent Publishing Platform, North Charleston, SC, 231 pages.

Garcia, M. H. (2008). *Sedimentation engineering: processes, measurements, modeling and practice,* American Society of Civil Engineers.

U.S. Department of Agriculture – Soil Conservation Service, National Engineering Handbook, Section 3, Sedimentation (NEH Section 3).

U.S. Department of Agriculture – Natural Resources Conservation Service, National Engineering Handbook, Part 654, Stream Restoration Design Handbook (NEH-210-VI-654 or NEH-654).

Lahar Flood Risk Management for Mud Mountain Dam on the White River Below Mt. Rainier, Washington State

Karl Eriksen, P.E. Seattle District (retired), USACE, grandpa@eriksens.org
Zachary P. Corum, P.E. Seattle District, USACE, Zachary.P.Corum@usace.army.milKenneth E. Brettmann, P.E. Seattle District, USACE, Kenneth.E.Brettmann@usace.army.mil Brendan C. Comport, P.E. Seattle District, USACE, Brendan.C.Comport@usace.army.mil

Introduction

Lahars from the Mt Rainier volcano present an unusual risk to Mud Mountain Dam (MMD) located downstream on the White River in western Washington State. The current lahar potential at MMD can be described as a low probability, high impact event, with lahars potentially ranging from 10 million cubic yards (mcy) up to extremely large and rare lahars of billions of cubic yards caused by the melting of snow and ice by an eruption of Mt Rainier. The focus of this paper will be the Flood Risk Management Plan (FRMP) actions to reduce the impacts to MMD caused by what has been termed the operational lahar. The operational lahar is defined as largest lahar for which the FRM actions can mitigate impacts to MMD. This event is estimated to have a volume of 40 mcy of sediment and water, with a risk loosely defined as <1% annual exceedance probability (AEP). MMD is a single purpose flood regulation project and the reservoir is normally empty. Without implementing any FRMP actions, lahars in the 5-40 mcy range have the potential to deposit approximately 120-210 feet of mud, rocks, and trees around the MMD outlet structure. Such deposits could severally restrict gate operations and even threaten the stability of the trash rack and sustainability of the dam and reservoir.

A critical factor in developing this FRMP was identifying an “operational lahar”. This is the maximum size lahar which FRMP measures would be formulated. There is no existing U.S. Army Corps of Engineers (USACE), or other guidance, for identifying an operational lahar. In this paper, the operational lahar is defined as the largest lahar for which FRMP actions can limit impacts to MMD. After an operational lahar the project would be able to return to operation after a short recovery period of days to weeks. Prior analysis (USACE, 2018) has estimated that a lahar in the 40-mcy range meets those criteria. Lahars in this range have the potential to cause significant damage if they reach the outlet structure at MMD unimpeded. Lahars over 100 mcy do not fit the operational lahar criteria because FRMP actions are unlikely to reduce the potential for those lahars to entirely bury the trash rack at MMD and fill most of the reservoir with sediment. This would cause extensive damage and leave the project inoperable for an extended period. The benefits, if any, of FRMP actions for lahars between 40 mcy and 100 mcy are too indeterminate to be identified at this time.

Lahar Characteristics: Lahars are slurries of water, soil, and rock that originate in volcanic areas and may reach solids concentrations of up to 60-80% by volume. Lahars can travel very fast. In the steep, narrow canyons of the White River, may reach flow velocities of over 50 ft/sec. Lahar hydrographs tend to raise very quickly and have durations of only a few hours. A common analogy for the nature and movement of a lahar is a wet-concrete slurry. Numerous lahars, some of them of catastrophic proportions, have occurred at Mt Rainier in the past 10,000 years. The largest ancient lahar identified at Mt Rainier, the Osceola mudflow, traveled through the White River basin to Puget Sound near Seattle around 5,700 years ago. That lahar had a volume estimated at one-half cubic mile (Crandell, 1971) and the deposits, averaging approximately 20 ft. deep, cover over 200 square miles.

Flood Risk Management Plan

This FRMP focuses on actions that can be taken to prepare for and respond to lahars in the range of 5-40 mcy that could be generated by an eruption of Mt Rainier. This size of lahar could be triggered by a small

eruption or as a secondary product of a large eruption directed to the south or west of the mountain. An eruption at Mt Rainier is likely to be proceeded by seismic warning signs and an eruption alert implemented by State and Federal emergency management agencies. An eruption alert could last for weeks to months and can have increasing threat levels. This FRMP describes emergency actions to be taken before, during, and after an eruptive period to reduce the lahar risks. The four phases of emergency management: mitigation, preparedness, response, and recovery are addressed below.

Mitigation: The FRMP goal is to establish a general pool management plan that reduces the risk to MMD during an operational lahar (up to 40 mcy). The MMD pool is normally empty and lahars would travel unimpeded through the empty reservoir and directly impact the dam. Without any FRMP actions, lahars in the 5-40 mcy range have the potential to create a deposit approximately 120-210 feet deep of mud, rocks, and trees at the MMD outlet structure. Such deposits could severely restrict gate operations and even threaten the stability of the trash rack. Lahars over 30 mcy could completely bury the trash rack. One approach to mitigating the potential impacts to the MMD outlet structure from an operational lahar is to have a long pool in the reservoir to encourage lahar deposition upstream of the dam. A long pool would be established following the issuance of an eruption alert, and then maintained throughout the alert period; as the 1-2 hour lahar travel time from Mt Rainier would not be sufficient time to raise the pool once a lahar has begun. At elevation 1180 ft, the pool has a volume of 70,341 ac-ft and will take some time to fill under normal White River flows. During the low flow season (August, September, and October) average monthly streamflows are in the 600-850 cfs range and it could take three months to fill the reservoir to 1180 ft. depending on the minimum allowable outflow. During the November through July period when average monthly streamflows are around 1400-2100 cfs, it may require 25-35 days to fill to 1180 ft, assuming a minimum outflow of 500 cfs. Well before implementation of this FRMP there should be a careful examination of downstream flood risk management and dam safety issues.

The key to establishing a sustainable pool elevation is to balance the lahar risks and riverine flood risks. During the 1980 eruption of Mount St Helens, lahars formed in Pine Creek and Muddy River, and flowed into PacifiCorp's Swift No 1 reservoir. The volume and discharge rates of the lahars were examined by the U.S. Geological Survey- Cascade Volcanic Observatory (USGS-CVO), but there had been no prior analysis of the longitudinal distribution of the lahar deposits within the reservoir. USACE (2018) found that the 18-mcy lahar traveled 3.8 miles through Swift No. 1 reservoir during the Mount St. Helens eruption, demonstrating the ability of lahars to travel long distances underwater on valley slopes similar to those at MMD. The characteristics of the lahar that impacted the Swift No 1 reservoir are analogous to what may happen at MMD. Table 1 shows the MMD pool lengths and volumes at selected pool elevations between 1150-1200 ft. A sustainable pool elevation should provide as much distance as possible for lahar deposition, but still allow the reservoir to contain the lahar volume without uncontrolled outflow and provide some degree of riverine flood regulation. A 5.7 mi long full pool would provide the maximum lahar risk reduction, but would maximize downstream flood risks, as the project would have no storage capacity remaining to regulate outflows. Conversely, a 3.8 mi long pool would provide 75% of the original flood storage, but lahars over 20 mcy would likely reach the dam.

Table 1. Mud Mountain Dam Pool Lengths and Volumes

Elevation in Feet	Length in Miles	Storage Volume in Ac-FT	Storage Volume in MCY
1150	4.4	48,210	78
1160	4.6	55,000	89
1170	4.8	62,438	101
1180	5	70,341	113
1190	5.2	78,701	127
1200	5.4	87,624	141
1215	5.7	102,041	165

Additional analysis and coordination with a range of disciplines is required before any particular pool elevation can be identified as optimally balancing risk. Another factor to consider is the risk of a Tsunami being generated by a lahar as it enters the pool. A pool elevation of 1180 feet is the minimum pool elevation that is likely to absorb the operational lahar. Lower pool elevations would result in higher lahar risk but would provide greater flood storage. This elevation provides a 5.0 mi long pool and 32,000 ac-ft (52 mcy) of remaining storage available for flood regulation or to absorb an inflowing operational lahar before producing uncontrolled outflow. This is 1.2 mi longer than the 1980 deposit in Swift No. 1 reservoir, but those lahars only totaled 18 mcy, just 45% of the maximum 40-mcy lahar considered in this FRMP. From strictly the lahar risk perspective, it would be desirable to provide this longer travel distance given the potential for larger lahars at MMD.

The lahar deposition in the Swift No 1 reservoir can be used in a couple of ways to estimate the deposition potential of a 5 mi long pool at MMD. The simplest way is to scale up the deposition based on the total lengths and volumes of deposition: 5 mi at MMD divided by 3.8 mi at Swift times 18 mcy at Swift equals roughly 25 mcy at MMD. Another way is to look only at the main deposition zone at Swift and scale that up to MMD. This approach requires an estimate of the Swift's main deposit volume and an assumption as to the length of the deposition in the MMD reservoir. The main Swift reservoir deposit had a length of 1.8 mi and an estimated volume of around 15 mcy. Assuming significant deposition does not start until the lahar becomes submerged in the MMD pool, about ½ mi downstream of the upstream pool boundary, and that only a limited volume of deposition in the narrow channel in the first 1/3 mile upstream of the dam, the length of deposition at MMD is estimated to be 4.2 mi. Given these conditions, somewhere around of 25-35 mcy (5/3.8 x 18 and 4.2/1.8 x 15) of lahar could be deposited in the MMD pool. There are topographic differences between the two reservoirs that are likely to produce different depositional patterns that cannot be accounted for in this simplified analysis. The major difference is that overall the MMD reservoir is narrower than the Swift reservoir and will not let the lahar spread as far laterally, potentially reducing deposition through the upstream end of the MMD reservoir, but with increased longitudinal distance.

While significant lahar deposition can be expected to occur in a 5 mi long pool, it is likely that some portion of any lahar would reach the MMD outlet structure. The volume and/or composition of any lahar reaching the dam cannot be reliably determined from the available information, but both are expected to be considerably smaller than without the long pool. A lahar may remain a high concentration slurry of rocks, boulders, and other debris as it travels through the reservoir, or it could be transformed at some point into a lower concentration hyper-concentrated flow. If the lahar degrades to hyper-concentrated flow, it is likely to be transporting mostly sand and smaller material, with some gravel and few boulders. Most of a hyper-concentrated flow reaching the dam would probably pass through the outlets. However, if it is still a lahar when it reaches the dam, with large amounts of rock and debris, it is likely to block at least portions of the outlets. A study is needed to determine the effects of holding a lahar mitigation pool on Water Management ability to adequately reduce flood peaks, and what reservoir management strategies might be effective in advance of a storm prediction.

Preparedness: In this FRMP, preparations for a lahar focus on actions that can be taken to reduce the risk to MMD, but the final FRMP must also incorporate the potential impacts and responses around the region during and after a Mt. Rainier eruption. The MMD lahar FRMP should be coordinated with other eruption response plans including the Pierce County Mount Rainier Volcanic Hazards Plan and any plans developed by King County or the State of Washington.

Part of being prepared for a lahar is to have a warning system in operation so FRMP can be implemented in time. A lahar warning system is in place on the west side of Mt Rainier, operated by Peirce County, State of Washington, University of Washington, and the USGS-CVO. Those agencies have plans to expand the lahar monitoring system to the White and West Fork White rivers in the next few years.

The USGS-CVO plans to install new Lahar Detection stations on the White and West Fork White rivers at sites that border the northeast side of Mt Rainier National Park (USGS-CVO, 2018). The sites under consideration are approximately 30 miles upstream of MMD and are shown on the USGS map in Figure

1. The sites would be on U.S. Forest Service (USFS) land. USGS-CVO plans to begin the permitting process in 2019 and construction in 2020 or 2021. They plan 2 digital stations with broadband seismic sensors, trip wires, GPS receiver, and a radio transmitter on each river. The seismic sensors will be able to detect seismic activity on Mt Rainier and lahar flows in the river. The trip wires would provide an indication of the size of a lahar. It is estimated that these monitoring stations could provide MMD with a one-hour warning of an approaching lahar.

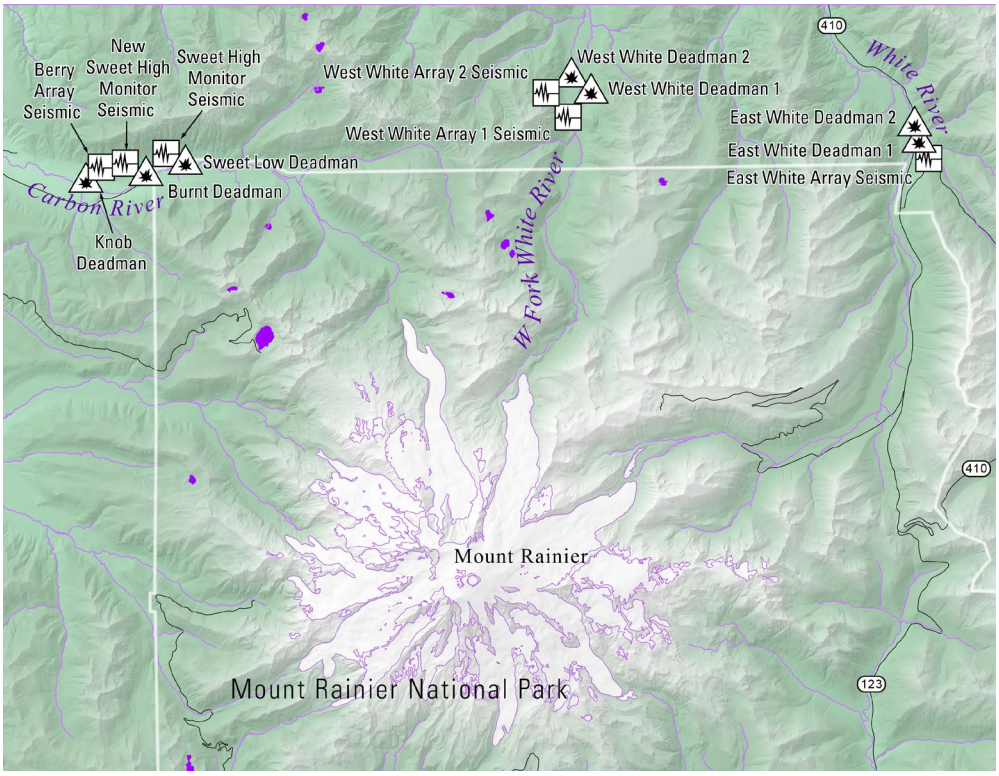

Figure 1. Map showing potential USGS-CVO lahar monitoring sites on the White and West Fork White rivers. (USGS-CVO, 2018)

Response: During a lahar, the lahar warning system discussed above could provide MMD with roughly a one-hour warning before the lahar arrives at the dam. An evacuation of the entire facility (staff, visitors, etc.) should begin immediately upon receipt of the warning. Prior to leaving, MMD staff could raise the one open gate (R1 or R2) to 80 or 100% and leave the other gates closed. This minimizes the risk of all the gates being blocked by rocks in the lahar and would not cause a significant downstream flood risk. The open gate would provide a 9.2-11.5 ft. high by 27 ft. wide opening that should allow rocks and boulders that pass through the trash rack's 1.67 ft. openings to pass out through the gate and into the 23-ft. tunnel. Water outflows at 80% gate opening would be about 6,400 cfs, exceeding the 6,000 cfs discharge target creating a minor downstream flood threat around Pacific and Sumner. At 100% gate opening the water outflow would be 10,000 cfs, enough to create a significant downstream flood threat. Opening the gate to 80-100% could also allow more of the lahar to pass downstream of MMD and perhaps reduce deposition near the outlet structure. It is likely that the lahar sediment passing through the trash rack will be mainly sand and finer material, and that it will mix with reservoir water to become hyper-concentrated flow. However, those lahar sediments are likely to deposit in the downstream channel, increasing flood risks and possibly aggravating any other eruption caused river problems. The tradeoffs between lahar risks and flood risks are beyond the scope of this paper and need to be evaluated before a final FRMP is adopted. Also beyond the scope of this paper are any predictions about blockages or restriction to flow caused by lahar material interacting with the trash rack, mixing chamber, gates, or tunnels. There is likely to be much confusion and uncertainty about the ongoing eruption and lahar activities, so to be safe, a total evacuation of the project may need to be completed. If reliable information becomes available indicating that the lahar the does not pose a threat to MMD, staff may return to the project to observe events and begin recovery.

Prior to a lahar, Seattle District Water Management would be actively managing MMD discharges to maintain the pool and regulate discharges. During a lahar Water Management would monitor pool elevations and advise other agencies as to the discharges that might be expected from MMD, similar to normal flood operations. Monitoring is remote from the Seattle District office (provided the pool sensors at the project remain working). If the gate is opened to 80-100% during a lahar, Water Management should immediately notify the appropriate emergency management agencies. This response is only related to the lahar risk and does not account for all eruption risks. When an eruption alert is issued, MMD activities should be coordinated with the Washington State Emergency Operations Center, Pierce County, USGS-CVO, and other emergency management agencies. MMD is 21 mi from Mt Rainier and could possibly fall within an eruption exclusion zone, requiring complete evacuation of the project for extended periods during an eruption alert.

Recovery: The immediate post-lahar situation at MMD will be highly uncertain. The magnitude of the impacts to MMD will depend on the size and nature of the lahar, the performance of the outlet structure, and to a large extent, chance. This recovery plan will focus on the aftermath of the 40-mcy operational lahar. Larger, more destructive lahars are possible, but are outside the scope of this FRMP.

At a pool elevation of 1180 ft, MMD reservoir will capture nearly all of the 40-mcy lahar. Lahar deposition will occur throughout the 5 mi long pool, with most of the deposit likely to settle within the 4.5 mi upstream of the dam. The depth of the deposits could range from less than 10 ft. at the upstream end, to conceivably over 150 ft. about a mile upstream of the dam. There could possibly be upwards of 1 mcy deposited up to 200 ft. deep in the 0.3 mile immediately upstream of the dam. Because of the upstream deposition, it is likely that as the lahar approaches the dam it will be a hyper-concentrated flow composed mostly of sand and finer materials, rather than a full lahar with lots of gravel and up to 10-20% boulders. The hyper-concentrated flow is likely to pass through the outlet works without causing any blockages. A large amount of floating woody debris may reach the dam, but most rocks and boulders are expected to deposit upstream. The lahar of 40 mcy could raise the pool level to around elevation 1208 ft, the water would be very turbid, and there would be a large amount of floating debris throughout the reservoir. There is some possibility of at least a partially blocked trash rack by debris, and possibly some coarse lahar deposits near the outlet structure. Damage to and the safety of the trash rack and elevator/stair tower would be unknown, limiting immediate access to the gate structure. For this FRMP, it will be assumed that one gate is open 80% and discharging 6,400 cfs. The open gate might be operable.

The primary recovery action at MMD should be to restore and/or maintain the capacity to regulate discharges. A 40-mcy lahar flowing into a pool already at elevation 1180 ft, would quickly reduce the storage available below the spillway crest to only about 7,000 ac-ft. The first step should be to check how much flow is being discharged from the outlet of the 23-ft. tunnel. This will give an indication of how efficiently the sediment-laden flow is moving through the outlet works. The next step is to determine if the open gate is operable. If this gate is operable, there will be some immediate capacity to regulate MMD water and sediment releases. If the lahar is a hyper-concentrated flow at the dam there is a good chance that it will have caused minimal structural damage to the trash rack. The high concentrations of sand and gravel in a hyper-concentrated flow can be very abrasive, but they are not likely to block the trash rack or discharge tunnels. If there is access to the gate control structure, the radial and emergency gates should be tested to determine if they could be opened.

The lahar deposit will eventually have to be removed if MMD is to be returned to full flood regulation capacity. One option would be to excavate the sediment and possibly dispose of it on the bluff above the reservoir. Another option would be to allow the sediment to erode and move downstream. This could probably remove most of the gravel and finer materials from the deposit, but 10-20% of the material could be boulders that would remain in the reservoir. Allowing the deposit to erode would produce much higher than normal sediment loads, and very likely cause serious channel deposition and flooding problems downstream of the dam, especially in the White River near Pacific and Sumner, in the Puyallup River in Tacoma.

Summary

Lahars from Mt Rainier pose a serious, but low probability risk to MMD. Having a FRMP in place before a lahar occurs is critical to safety at MMD and downstream populations. A preliminary lahar FRMP has been proposed that involves installation of a lahar warning system, providing a 5 mi long pool to encourage lahar deposition, adopting an evacuation plan with final gate settings, and identifying some initial recovery steps. A plan needs to be developed for managing the reservoir in the immediate post-lahar period. This plan only offers a starting point for the development of a comprehensive lahar FRMP. Much more study and evaluation of lahar risks, flood risk management, and dam safety issues are necessary before a FRMP can be finalized. There are many issues that remain to be resolved before this FRMP can be implemented. Some of the more significant issues are: lahar flow/deposition within the reservoir, lahar versus flood risks, hydraulic and geotechnical dam safety concerns with a prolonged high pool level, and potential downstream impacts.

References

Crandell, D.R., 1971. Postglacial Lahars from Mt. Rainier Volcano, Washington, USGS Professional Paper 677.

USACE, 2018. Mud Mountain Dam Lahar Risk Management Plan. Seattle District. September 2018.

USGS-CVO, 2018. Personal communication with Benjamin Pauk on the development of Lahar warning stations on the White River, WA.

Linking Sedimentation and Erosion Patterns with Reservoir Morphology and Dam Operations during Streambed Drawdowns in a Flood-control Reservoir in the Oregon Cascades

Mackenzie K. Keith, Hydrologist, U.S. Geological Survey, Portland, Oregon, mkeith@usgs.gov
Laurel E. Stratton, Hydrologist, U.S. Geological Survey, Portland, Oregon, lstratton@usgs.gov

Abstract

Since water-year (WY) 2011, pool levels at Fall Creek Lake, Oregon, are temporarily lowered to an elevation near historical streambed each fall, creating free-flowing channel conditions that facilitate downstream passage of juvenile spring Chinook salmon. These drawdown operations have also mobilized substantial quantities of predominantly fine (<2 mm) reservoir sediment as well as some coarser gravels. To assess the potential impact of reservoir sediment erosion and transport on downstream reach morphology and habitats, linkages between reservoir sedimentation in Fall Creek Lake and drawdown-related reservoir erosion are inferred from geomorphic mapping and volumetric change analyses developed from high resolution aerial photographs and digital elevation models of the empty reservoir. Recent and historical drawdown operations have helped maintain a thalweg in much of Fall Creek Lake, constraining most coarse-grained sediment transport and re-deposition, whereas fine-grained deposition has mainly occurred on the former floodplain and lowermost reservoir reaches. Fine-grained sediment deposits are thickest and bury pre-dam morphology immediately upstream of the dam where they are accessible to fluvial erosion during streambed drawdown operations. Farther from the dam, where pre-dam morphology has not been buried, erosion is limited to sediment accumulation in the reservoir thalweg and minor tributary and 'drawdown' channels. In former floodplain regions of the reservoir not adjacent to the thalweg, thicker sediment deposits are inaccessible to fluvial erosion at full streambed drawdown. Altogether, these findings highlight controls on patterns and processes of reservoir erosion during drawdowns. This understanding of long-term sedimentation and streambed-drawdown erosion at Fall Creek Lake allows better evaluation and anticipation of the timing, magnitude, and sediment characteristics delivered to downstream reaches.

Introduction

At Fall Creek Dam in northwestern Oregon (Figure 1), flow managers with the U.S. Army Corps of Engineers (USACE) lower lake levels to streambed each fall to facilitate the downstream passage of juvenile spring Chinook salmon through the 55-m tall dam, creating temporary free-flowing channel conditions in Fall Creek Lake. Since water-year (WY) 2011, these streambed drawdown events have mobilized substantial quantities of predominantly fine (<2 mm) sediment, as well as some coarser gravels, which have the potential to impact morphology and habitats of downstream gravel-bed reaches. Understanding short and long-term geomorphic impacts to downstream reaches requires an evaluation of the processes and patterns of reservoir erosion and likely responses to future changes in inflows or dam operations. Process-based geomorphic mapping of landforms and reservoir substrate from high-resolution datasets acquired in WY 2016 provide a basis for linking sedimentation and erosion processes to dam

operations, while analyses of historical and recent datasets are used to characterize the magnitude of changes inferred from geomorphic mapping. The findings presented here are part of a larger study that investigates the upstream-downstream coupled geomorphic responses to drawdown operations. In this paper, we focus on (1) understanding the patterns and processes of sedimentation and erosion in Fall Creek Lake and (2) identifying key factors that control erosion and sediment export from the reservoir during streambed drawdown operations.

Background and Study Area

Fall Creek Dam captures flow and sediment from a 477 km^2 area of western Oregon. Volcanic and volcaniclastic rocks of Eocene to Miocene age dominate the Western Cascades geology underlying the Fall Creek basin (Smith and Roe, 2015). The basin is characterized by a Mediterranean climate with warm dry summers and cool wet winters, with most winter precipitation falling as rain and a mean annual precipitation of 170 cm/year. Fall Creek Dam was completed in 1966 as part of the Willamette Valley Project, a system of 13 dams on tributaries of the Willamette River, which were constructed for the primary purpose of flood risk management (USACE 2019b). The dam is a rock fill structure with concrete spillway and three sets of nested fish horns at different elevations that pass water and fish downstream, although the horns are inadequate for downstream fish passage (USACE, written commun.). Unique to this infrastructure among Willamette Valley Project dams are two regulating outlets at the base of the dam. The 55-m-high, 1,554-m-long dam is operated primarily for flood risk management, as well as water quality, irrigation, recreation, and habitat, and has a storage capacity of 115,000 acre-feet (USACE, 2019a) and sediment trapping efficiency of about 74 % (Schenk and Bragg, 2014).

During the flood season from November to March, pool levels are restricted to 252 m (NAVD 88; 44 m above full drawdown) with minimum pool at 222 m (14 m above full drawdown) (Figure 1). Conservation season from April to November is not restricted to a maximum pool elevation (USACE, 2019a). The 2008 Biological Opinion for USACE's Willamette Valley Project (referred to as the 'BiOp') identified actions for Fall Creek Dam to improve downstream passage and survival of juvenile spring Chinook salmon that included lowering lake levels below elevation 219 m (11 m above full drawdown; NMFS, 2008; Figure 1). In WY2012, annual experimental streambed drawdowns to 208 m (Figure 1) at Fall Creek Dam lowered pool levels to free-flowing conditions. This magnitude of drawdown is now part of the standard operations. Historical lake level records and anecdotal reports (USGS gage 14150900, Fall Creek Lake near Lowell, Oregon; USACE, 2017) indicate streambed drawdowns also occurred in multiple years prior to WY 2012 (WYs 1969–75, 1977, 1982), and pool levels have been drawn below minimum conservation pool, but not as far as streambed in many other years.

Approaches

Geomorphic Mapping to Characterize Fall Creek Lake Processes

A processed-based framework through geomorphic mapping is used to interpret the evolution of reservoir sedimentation and erosion. Digital maps documenting surface landforms in Fall Creek Lake were developed from Digital Elevation Models (DEMS) and aerial photographs (acquired WY 2012 and 2016). Landform mapping units were developed to better understand potential sediment mobilization and delivery to reaches downstream of the dam. Here, we focus on five key mapping units (Table 1); the completed mapping hierarchy includes 17 geomorphically distinct landform mapping units and is more fully described in Keith and Stratton (in progress).

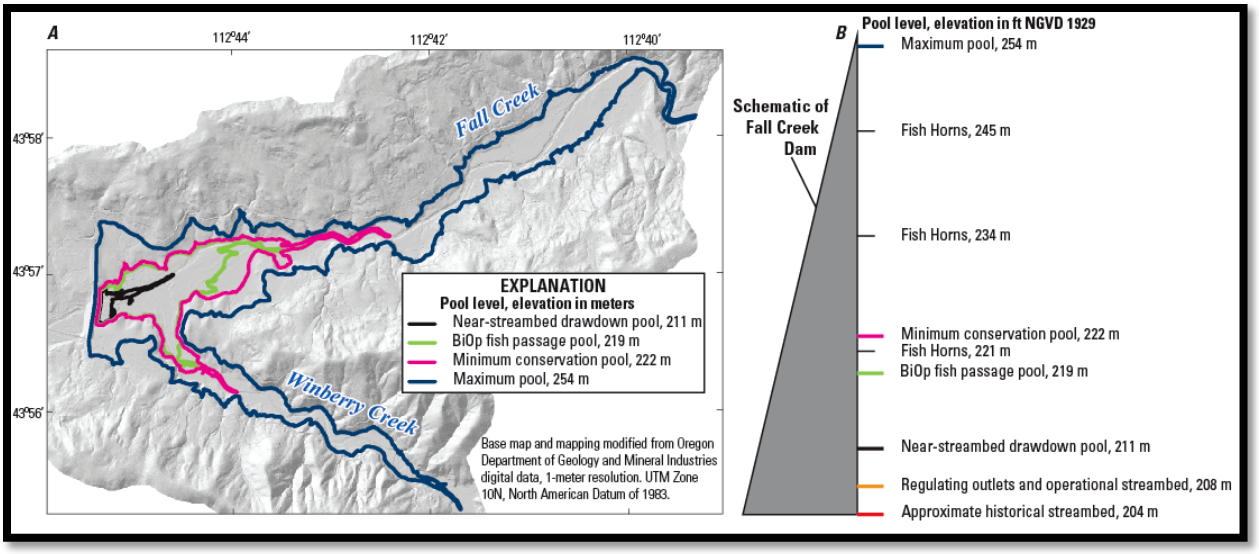

Figure 1. (A) Fall Creek Lake, Oregon, study area including key pool elevation contours and (B) schematic of Fall Creek Dam scaled to dam height (horizontal exaggeration) with key elevations related to operational pool levels and infrastructure.

Table 1. Key landform mapping units related to sedimentation regime.

[See Keith and Stratton (in progress) for additional landform mapping units and more detailed descriptions of mapping domains, landforms, and substrate.]

Landform mapping unit	Description	Sediment Regime Between Minimum and Maximum Pool Level	Sediment Regime: During Streambed Drawdown Conditions
Drawdown distributary zone	Broad areas of the reservoir floor that are morphologically similar to drawdown surfaces but form a series of splays and small deltaic lobes cross-cut by erosional features.	Lacustrine deposition	Deposition of newly eroded sediments and scour of channels
Drawdown surface	Typically planar surfaces created from incision and abandonment or dissection from reservoir floor by channel erosion around the feature.	Lacustrine deposition	Fluvial erosion of reservoir floor
Drawdown channel	Channels that typically originate on the reservoir floor or reservoir hillslope. Water draining from the low gradient floor may concentrate, increasing local capacity to mobilize and transport fine sediment. Over time, can evolve through knickpoint migration or increases in local slope.	Lacustrine deposition	Fluvial erosion of reservoir floor
Littoral reservoir floor	Localized, relatively flat areas along the reservoir margins adjacent to the mapping boundary at maximum conservation pool elevation.	Neutral with minor lacustrine deposition	Neutral
Pelagic reservoir floor	Low-gradient reservoir floor between reservoir hillslope and main reservoir channels. At maximum conservation pool (254 m), would be deeply inundated by water.	Main area of lacustrine deposition	Neutral with near-channel areas likely to experience fluvial erosion
Reservoir hillslope	Steep, formerly forested valley walls, that often extend from the reservoir floor to the reservoir margins at elevation 254 m.	Wave erosion with re-distribution of sediment downslope	Typically neutral; erosional during rain events or with mass failures

Quantification of Drawdown-Related Erosion

Lidar (light detecting and ranging) data acquired in early WY 2012 during full streambed drawdown and structure-from-motion (SfM) topography acquired on November 10, 2016 (Keith and Mangano, in progress), were used to estimate volumetric changes in sediment erosion and deposition in the lower Fall Creek reservoir, as well as assess spatial patterns of change for that period. Comparisons between datasets were made with Geomorphic Change Detection (GCD) Software (Riverscapes Consortium, 2018) within ArcGIS to quantify net volumetric change. The analyses focused on the reservoir floor and main channel in the lower approximately 2.5 km of the reservoir.

Results and Discussion

Pre-dam Morphology of Fall Creek Lake

Fall Creek Lake occupies a relatively narrow valley defined by the Fall and Winberry Creeks (Figure 2). Pre-dam morphology at Fall Creek Lake reviewed for this study is limited to interpretation of 1936 pre-dam aerial photographs and 2012 lidar displaying buried reservoir topography. Steep, bare reservoir hillslopes were heavily forested prior to dam construction, and much of the reservoir floor appears to have been used for agricultural purposes prior to dam construction, with fields typically extending to a single, discontinuous row of trees along the Fall and Winberry Creek channels. Both creeks appear to have been relatively straight, single-thread channels through the middle of the valley floor with intermittent bedrock outcrops. Where present, gravel bars were as large as 2,700 m^2 and were primarily bare of vegetation. Side channels and alcoves were limited to co-location with gravel bars.

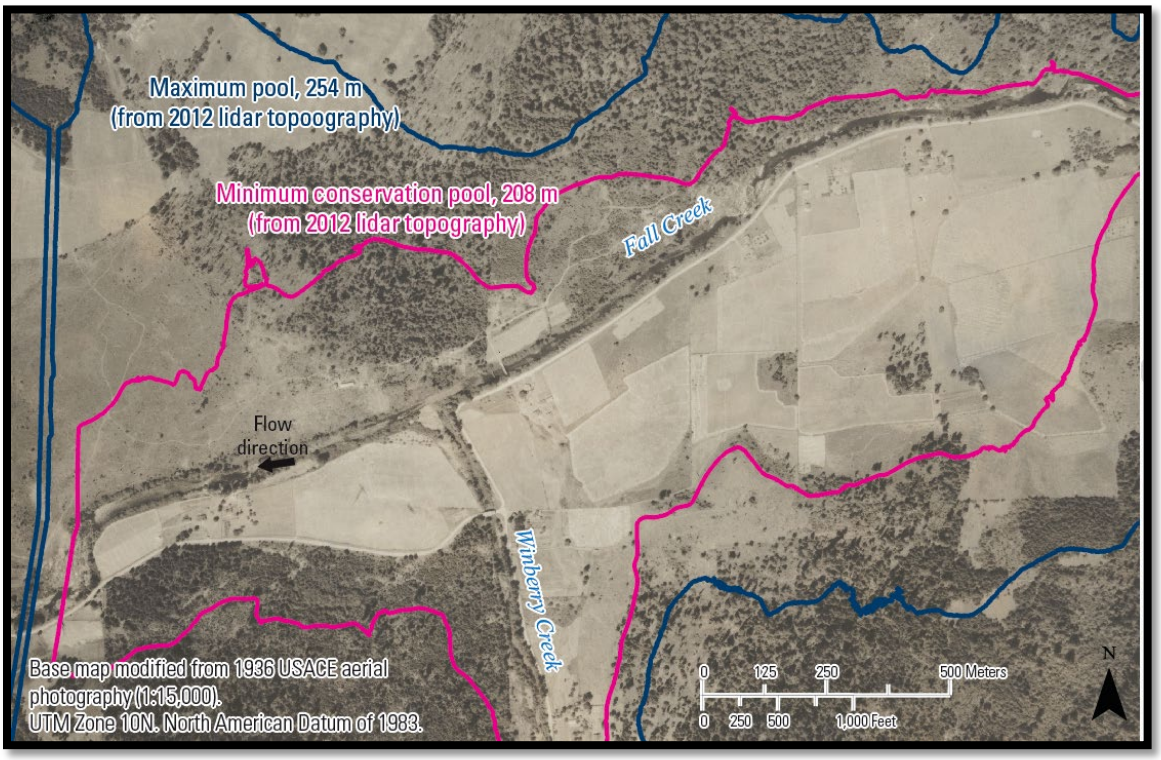

Figure 2. Pre-dam aerial photograph (1936) of the Fall Creek valley in the vicinity of the present-day lower Fall Creek Lake Oregon.

Distribution and Interpretation of Mapped Landforms and Sediment

The exact volume of sediment in Fall Creek Lake was not measured as part of this study; however, storage curves from 1988 and 2012 and a partial storage curve from 1965 (above about 217.5 m elevation) indicate that overall loss in storage for the full reservoir (254 m) is less than 1 %. Sediment accumulation since 1966 is concentrated in the lower portions of the reservoir near the dam, where it is susceptible to erosion during streambed drawdowns.

The relative areal coverage of geomorphic features varies systematically with pool elevation. Mapping (Figure 3) shows that the former Fall Creek valley and its forested hillslopes are now dominated by pelagic reservoir floor (42 % of reservoir area; Figure 3) and reservoir hillslope (35 % of reservoir area). The dominant substrate type overall is sand/mud (43 %). A nearly equal area is mapped as hillslope/pre-dam soil (42 %). Drawdown-associated landforms, including drawdown channels, distributary zones, and drawdown surfaces, account for about 5 % of the total mapped area; however, the total proportion increases substantially at lower pool levels, and 86 % of those drawdown landforms are found below minimum conservation pool. The presence of drawdown landforms above minimum conservation pool suggests formation during regular seasonal operations for flood mitigation rather than drawdowns for fish passage. During full streambed drawdowns, these features likely function as conduits for sediment and water, similar to pre-dam tributaries draining valley hillslopes to Fall and Winberry Creeks.

Below minimum conservation pool (222 m; Figure 1), pelagic floor and drawdown-associated landforms are prominent, occupying 59 % and 18 % reservoir area, respectively. There is a marked decrease in hillslope/pre-impoundment soils (7 %), and a greater proportion of the area is mapped as sand/mud (84 %).

The pool below 211 m is dominated by pelagic floor (47 %), drawdown surfaces (19 %), and wetted channel (18 %). Drawdown-associated landforms (including drawdowns channels, surfaces, and distributary zones) comprise 22 % of the mapped area in this small pool (1.5 % of total mapped area). Substrate at elevations below 211 m is almost entirely sand/mud (94 %). When pool levels are at or below this elevation, the majority of the drawdown landforms within the reservoir area are no longer directly interacting with the water surface, but they can continue to evolve through erosion and re-deposition in response to dewatering of the reservoir floor or precipitation events that generate runoff into the reservoir.

The main channel area cross-cuts all pool levels and acts as the primary active zone for water and sediment transport during full streambed drawdowns; landforms within this domain likely play a crucial role in exporting sediment to reaches downstream of the dam. Within this domain the wetted channel feature class makes up 49 % of the area. Channel banks and slumping banks account for an added 26 % of the mapped area. Aside from bars (10 %), bedrock (5 %), and drawdown surfaces (10 %), other mapped landforms are distinct to other domains such as reservoir floor or hillslope and account for less than 1 % of the area. Bar landforms are dominantly gravel (93 % by area), and the wetted channel area is 35 % gravel and 32 % bedrock. Although small in total area, the presence of bedrock channels within the reservoir suggests there is a relatively high transport capacity during regular seasonal drawdowns (most of this area coincides with a 2.5-km segment of the channel spanning the transition to minimum conservation pool). Bedrock outcrops also indicate erosion-resistant features that likely stabilize local channel position, hindering lateral migration of the wetted channel through reservoir floor deposits.

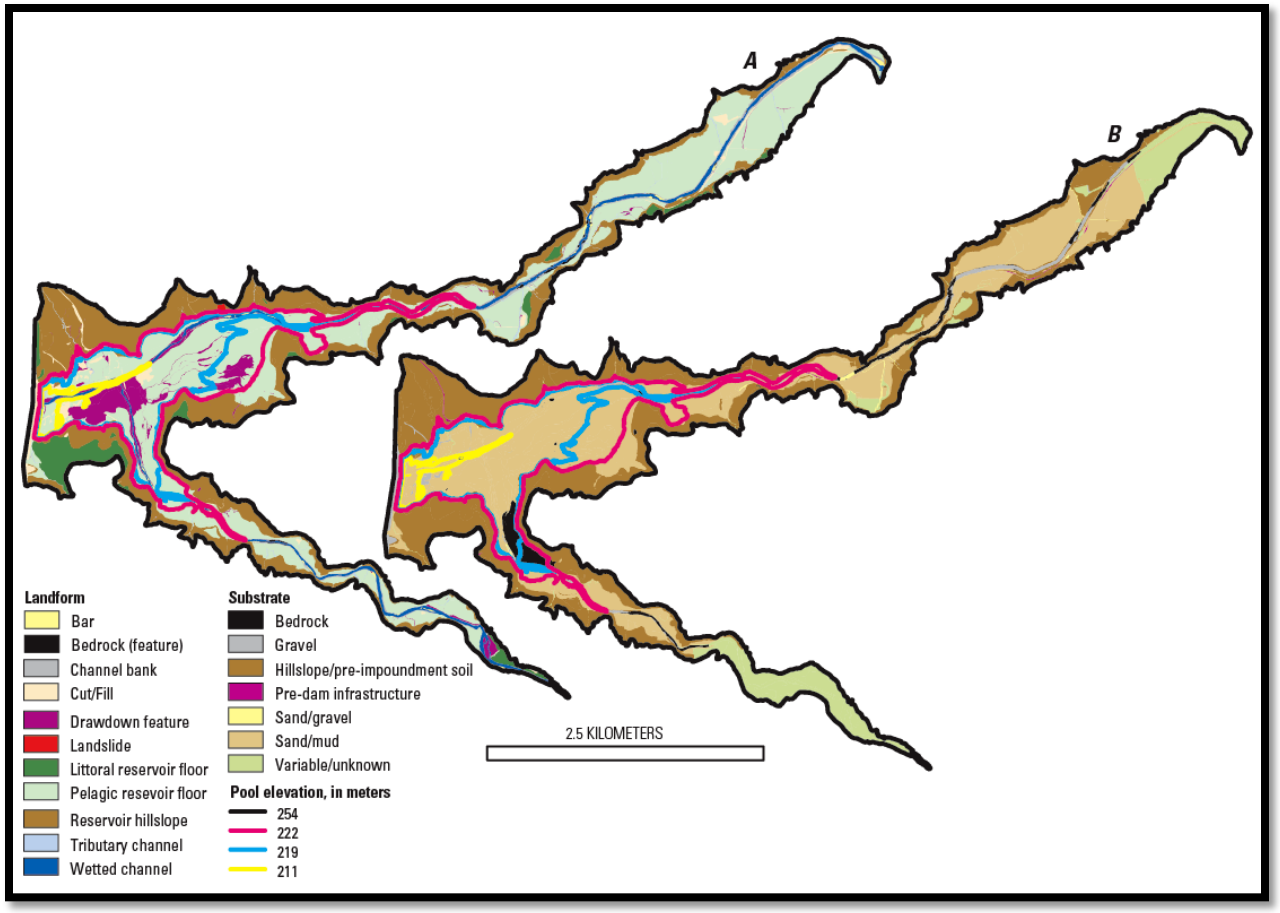

Figure 3. Landforms (A) and substrate (B) mapped within the Fall Creek reservoir, Oregon.

In the upper reservoir, a higher density of channel banks formed in pre-dam soils/hillslope material may indicate features that also functioned as channel banks prior to dam construction based on the presumed pre-dam location of the Fall Creek channel.

Drawdown surface landforms are 99 % sand/mud; though less extensive by area, other drawdown landforms (channels and distributary zones) are also dominantly sand/mud. The topographic signature and substrate type together suggest drawdown landforms primarily form in the finer reservoir-deposit sediment.

Overall, the mapping reveals a dynamic reservoir environment influenced by a blend of depositional processes that are active during lacustrine conditions at high lake levels and erosive processes that are active at lower lake levels when fluvial processes dominate. While the pelagic reservoir floor is mapped as a depositional environment, dominated by gradual deposition of suspended sediment, pre-dam topography is clearly visible in many areas despite more than 60 years of impounded conditions, suggesting relatively low rates of sedimentation and burial. Regular lake-level lowering during winter months for flood control, combined with full streambed drawdowns in the fall, creates erosive conditions that can cut drawdown channels and drawdown surfaces in reservoir deposits and re-distribute sediment within the reservoir. Drawing down lake levels also initiates fluvial processes within the main channel, whereby fine sediment deposits downstream of minimum pool are reworked and coarse sediment along the channel bed can mobilize to form gravel bars, and in some locations expose bedrock. In contrast,

the reservoir hillslope is predominantly an erosional or sediment-neutral environment, as indicated by the presence of exposed, pre-dam hillslope, wave-cut terraces, and exposed root structures of relict stumps.

Magnitude of Erosion Related to Drawdowns

Within the area of interest for Fall Creek reservoir, 224,200 m^3 of erosion and 28,800 m^3 of deposition was calculated with GCD software for net erosion of 195,400 m^3 between January 2012 and November 2016 (Figure 4). This would suggest an annual average net erosion rate over 5 streambed-drawdown years of about 39,000 m^3/year. However, based on observations downstream in Fall Creek (Schenk and Bragg, 2014, 2015; G. Taylor, USACE, oral communication, 2017; Schenk, 2018), and downstream of other reservoirs during dam removals, which are a proxy for streambed drawdown responses (for example, Major and others, 2012 or Collins and others, 2017), it is more likely that larger amounts of sediment were eroded during earlier streambed drawdown periods (WYs 2012–13) than later drawdowns.

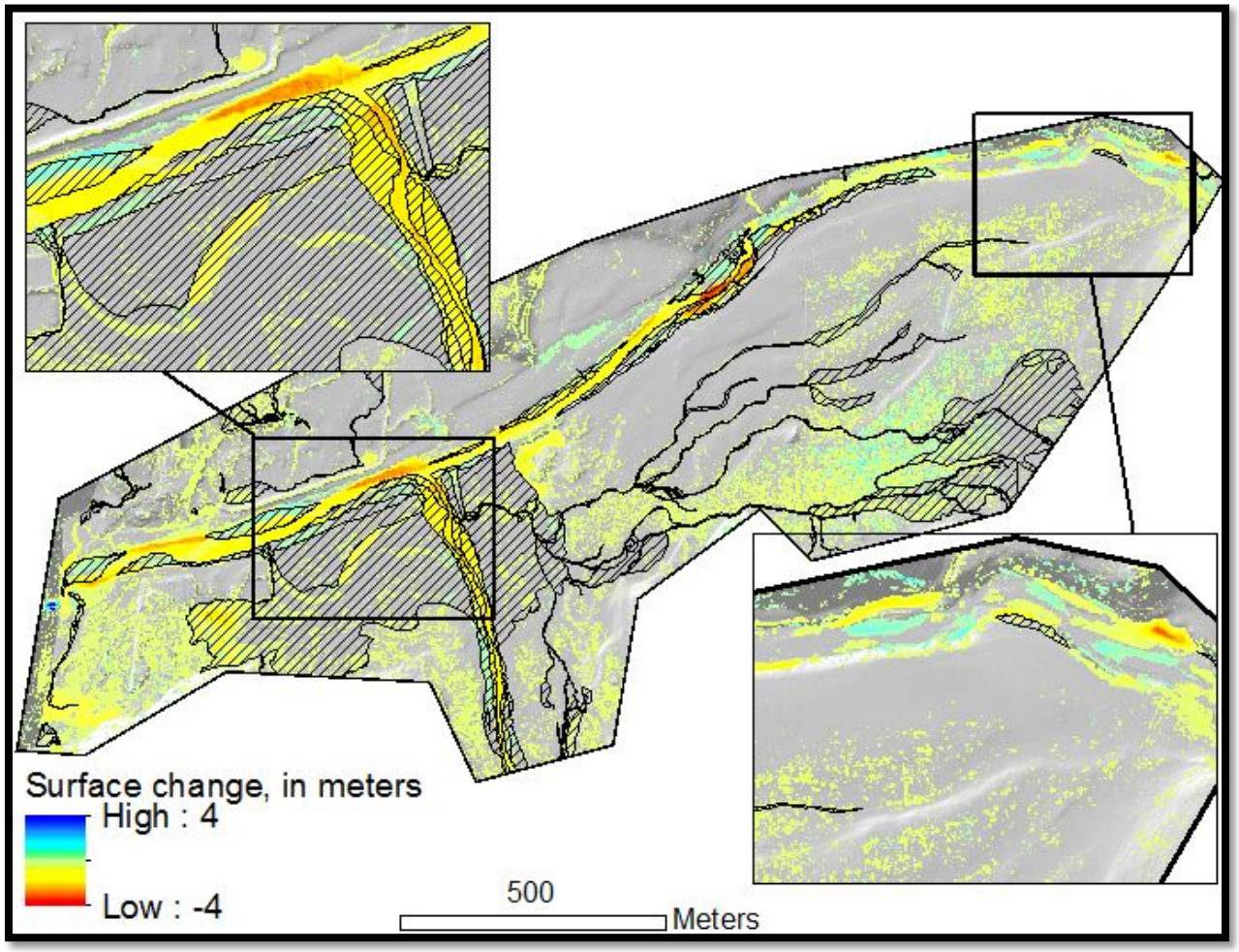

Figure 4. Raster map of change analyses between 2016 structure-from-motion and 2012 lidar within lower Fall Creek Lake Hatched areas indicate drawdown channels, surfaces, and distributary zones from geomorphic mapping.

The distribution of calculated erosion (Figure 4) was similar to that of mapped erosion features, such as drawdown channels and the main Fall and Winberry Creek channels through the reservoir. The largest amount of erosion (up to 3.8 m thick) was located in the main channel corridor. Some deposition (up to about 0.9 m) is likely the product of bars being reworked, slumping bank toes, or drawdown surfaces that have accumulated sediment. Localized areas with little variability of erosion or deposition can also be seen along the channel margins and often coincide with mapped drawdown surfaces. Within the reservoir floor, there are also prominent areas of erosion associated with drawdown surfaces, channels, and distributary zones. The large distributary zone near the confluence of Winberry Creek showed changes in elevation ranging from +0.32 m to -0.9 m, though the feature was dominantly erosional with large areas of no detectable change. Some of the drawdown channels showed incision of as much as 1.8 m near the confluences of the main Fall Creek and Winberry channels.

Controls on Drawdown-Related Erosion and Implications for Future Erosion

Multiple competing controls influence sedimentation and erosion at Fall Creek Lake as pool levels fluctuate seasonally for flood control and rapidly when temporarily drawn down to streambed. These can be generally categorized as direct or indirect controls that are closely tied to inherent physical or operational influences that affect timing, magnitude, and distribution of sedimentation and erosion. This framework for considering the relative roles of controls supports interpretation of future reservoir evolution under similar streambed drawdown management at Fall Creek Dam.

Annual streambed drawdown events since 2011, in combination with earlier intermittent streambed drawdowns, likely create the conditions necessary to maintain a well-defined and actively evolving channel in much of Fall Creek Lake. This channel constrains most coarse-grained sediment transport and re-deposition, whereas fine-grained deposition during lacustrine conditions has mainly occurred on the former pre-dam floodplain and terrace surfaces (presently, the reservoir floor) and areas of the reservoir closest to the dam. Drawdown-influenced erosion through the reservoir floor deposits is mainly limited to areas adjacent to the main reservoir channel, as most of the reservoir floor is topographically higher than or farther from the main reservoir channel and inaccessible to major erosion and reworking. In contrast, areas immediately upstream of the dam, where reservoir sedimentation has buried the pre-dam channel, are subject to more substantial downcutting and lateral migration of fine-grained material.

These observations suggest that a geomorphic framework for evaluating controls on reservoir sedimentation and erosion should consider different zones of the reservoir, their proximity to the main reservoir channel, and the different depositional and erosional processes activate by various dam management and streamflow scenarios. For example, in areas immediately upstream of the dam where fine-grained sediment accumulation is thick and readily accessible to fluvial erosion and transport, the direct controls on erosion are dam operations (predominantly lake level) and streamflow (a function of unregulated flow entering the reservoir). Sediment eroded from the area proximal to the dam and main streambed drawdown channel is more likely to be transported downstream of Fall Creek Dam during streambed drawdowns than sediment mobilized from reservoir margins. Upper elevations of the reservoir floor margins reflect pre-dam floodplain and terraces that indirectly influence streambed drawdown erosion; that sediment must be routed farther through the reservoir prior to export.

Patterns of sediment erosion and evacuation from Fall Creek Lake since WY2012 suggest that fine sediment erosion during streambed drawdowns will decrease in the future and tend to approach the rate of upstream sediment supply to the lower reservoir, because the streambed drawdown channel continues to reoccupy the main reservoir channel without widespread lateral erosion across floodplain deposits. Patterns of reduced sediment transport downstream of the dam are consistent with local suspended sediment loads calculated for WYs 2013–2017 (Schenk, 2018). Also, the majority of sediment deposited in Fall Creek Lake is fine-grained sediment stored in the main reservoir floor and is largely inaccessible to erosion during drawdown operations. This suggests 1) that the likelihood of fine-grained sediment on those surfaces entrained during streambed drawdown operations and subsequent transportation downstream of the dam is low, and 2) if that sediment is transported downstream of the dam, it would primarily travel as suspended load with limited impacts to habitat-related morphology.

Conclusions

Interpreting processes of sedimentation and erosion from reservoir landforms provides a basis for evaluating the evolution of Fall Creek Lake, Oregon, during typical lake conditions and streambed drawdowns. Geomorphic features and the distribution of sediment in the Fall Creek reservoir reflect a complex history of alternating depositional, transport, and erosional processes influenced both by reservoir operations and the morphology of the pre-dam valley and hillslopes. At Fall Creek Lake, pre-dam valley morphology acts as an indirect control influencing the distributions, processes, and magnitudes of reservoir sedimentation and streambed drawdown-related erosion, while dam operations directly control lake levels influencing the overall depositional or erosional regime. Unregulated streamflow entering the reservoir during streambed-drawdown period also directly influences the magnitude of erosion and sediment transfer within the reservoir. Overprinting of multiple processes creates a diverse array of landforms indicative of erosional and depositional processes. The erosion potential of sediment in Fall Creek reservoir is dependent on sediment grain size, reservoir morphology, and its exposure to removal processes. Combining lake level and reservoir morphology establishes the template for understanding processes active under particular operational conditions.

The overall study supports management operations at Fall Creek Lake for downstream fish passage and downstream sediment management. The sedimentation and erosion patterns and their underlying controls are specific to operations at Fall Creek Lake, but the approaches and findings from this study can support a broader understanding of reservoir drawdowns for other purposes, such as sediment management or construction. Furthermore, our findings help us understand the current conditions and predict the longer-term geomorphic responses downstream of Fall Creek Dam. While the underlying purpose for drawdown operations and the drivers of erosion at Fall Creek may differ from other reservoirs, the approaches described here that link process-based mapping and interpretation of erosional landforms to volumetric analyses could be modified to inform drawdown operations at other reservoirs to support sediment management for reservoir sustainability.

Acknowledgments

Funding for this study was provided by the U.S. Army Corps of Engineers. We would like to thank the following for technical and field assistance in support of this study.
USGS: Rose Wallick, Gabe Gordon, Joseph Mangano, James White, Liam Schenk, Heather Bragg, Jon Major, Scott Anderson, Tess Harden, Erin Poor, Alex Costello, Heather Bervid, Brandon Overstreet, Lisa Faust, Jeff Sloan, Todd Burton, Jim O'Connor, Charlie Cannon

USACE: Greg Taylor, Chad Helms, Dough Garletts, Jacob MacDonald, Chris Edwards, Doug Swanson, Mary Karen Scullion, Norman Buccola
Frontier Precision: Chase Fly
Brown-Western Aviation: Gary Brown, Mary Brown
El Museo Nacional de Ciencias Naturales: Mikel Calle Navarro
Oregon State University: Christina Murphy, Sherri Johnson

References

Collins, M. J., Snyder, N. P., Boardman, G., Banks, W. S. L., Andrews, M., Baker, M. E., Conlon, M., Gellis, A., McClain, S., Miller, A., and Wilcock, P. 2017. "Channel response to sediment release: insights from a paired analysis of dam removal," Earth Surf. Process. Landforms, 42: 1636–1651. doi: 10.1002/esp.4108.

Major, J.J., O'Connor, J.E., Podolak, C.J., Keith, M.K., Grant, G.E., Spicer, K.R., Pittman, S., Bragg, H.M., Wallick, J.R., Tanner, D.Q., Rhode, A., and Wilcock, P.R. 2012. "Geomorphic response of the Sandy River, Oregon, to removal of Marmot Dam," U.S. Geological Survey Professional Paper 1792, 64 p.

Morris, G.L., and Fan, Jiahua. 1998. "Reservoir Sedimentation Handbook," McGraw-Hill Book Co. New York, New York, Electronic Version 1.01 with minor updates September 2009.

National Marine Fisheries Service (NMFS). 2008. "Endangered Species Act section 7(a)(2) consultation biological opinion and Magnuson-Stevens Fishery Conservation and Management Act essential fish habitat consultation on the Willamette River Basin Flood Control Project," National Marine Fisheries Service, Northwest Region, Seattle, Washington, National Oceanic and Atmospheric Administration Fisheries Log Number: FINWRl2000/02117 [variously paged], accessed March 2018, http://www.nwr.noaa.gov/hydropower/willamette_opinion/index.html.

O'Connor, J.E., Mangano, J.F., Anderson, S.W., Wallick, J.R., Jones, K.L., and Keith, M.K. 2014. "Geologic and physiographic controls on bed-material yield, transport, and channel morphology for alluvial and bedrock rivers, western Oregon," Geological Society of America Bulletin, 126(3–4): 377–397.

Schenk, L.N. 2018. "Six years of sediment and dissolved oxygen monitoring for the Fall Creek drawdown: Observations, insights, and future directions," Willamette Fisheries Science Review presentation to the U.S. Army Corps of Engineers, February 2018, Corvallis, Oregon, available at http://pweb.crohms.org/tmt/documents/FPOM/2010/Willamette_Coordination/WFSR/.

Schenk, L.N., and Bragg, H.M. 2014. "Assessment of suspended-sediment transport, bedload, and dissolved oxygen during a short-term drawdown of Fall Creek Lake, Oregon, winter 2012–13," U.S. Geological Survey Open-File Report 2014–1114, 80 p.

Schenk, L.N., and Bragg, H.M. 2015. "Suspended-sediment concentrations and loads during an operational drawdown of Fall Creek Lake, Oregon," U.S. Geological Survey Data Release, 15 p., available at https://or.water.usgs.gov/proj/Fall_Creek/Fall_Crk_data_release_2014.pdf.

Smith, R.L., and Roe, W.P. 2015. "OGDC-6, Oregon Geologic Data Compilation, release 6," Oregon Department of Geology and Mineral Industries, digital geodatabase available at http://www.oregongeology.org/pubs/dds/p-OGDC-6.htm.

USACE. 2019a. "Fall Creek Dam and Reservoir website," U.S. Army Corps of Engineers, Portland District, accessed January 2019 at https://www.nwp.usace.army.mil/Locations/Willamette-Valley/Fall-Creek/.

USACE. 2019b. "Willamette Valley Project website," U.S. Army Corps of Engineers, Portland District, accessed January 2019 at https://www.nwp.usace.army.mil/Locations/Willamette-Valley/.

Watershed Sciences, Inc. (WSI). 2012. "Lidar remote sensing data collection Fall Creek," prepared by Watershed Sciences, Inc. WSI, Portland, Oregon, for David Smith and Associates, Portland, Oregon, digital data and report, 27 p., available from Oregon Department of Geology and Mineral Resources at http://www.oregongeology.org/lidar/.

Management of Global Reservoir Sedimentation: An Evaluation of RESCON 2 Beta

Christopher Garcia, Graduate Research Assistant, Brigham Young University, Provo, Utah, christophergarcia216@gmail.com
Rollin H. Hotchkiss, Ph.D., P.E., D.WRE, F.ASCE, Brigham Young University, Provo, Utah, rhh@byu.edu

Abstract

Several methods for managing reservoir sedimentation have been developed to help extend project life. In 2017, the World Bank sponsored REServoir CONservation (RESCON) 2, a pre-feasibility, Excel-based program aimed to help users select sediment management practices to consider for more detailed studies. Perhaps RESCON's greatest contribution to its users is its comparative analysis of different sediment management strategies, wherein net present values are calculated for each alternative, whether or not it is sustainable, and the long-term storage capacity and lifetime of the reservoir.

While this is certainly useful, the objective of this paper is to gain insight into RESCON's efficacy for evaluating and suggesting sediment management options by comparing its results against the Sediment Management Options Diagram (SMOD) and the actual practice in use at the reservoir. Brief descriptions of the SMOD and RESCON 2 will be provided. RESCON-required inputs will be summarized, and some key entries will also be presented.

Twenty reservoirs from around the world were modeled in RESCON 2, with storage capacities ranging between 0.187 million cubic meters and 39.3 billion cubic meters. All sediment management alternatives whose net present values lied within 30% of the highest alternative were deemed practicable for the reservoir. Of the twenty models, ten did not practice sediment management (i.e., no action is being taken to manage sediments at the site). Analyzing only those reservoirs where sediment management is being employed, RESCON predicted the actual practice eight out of ten times.

Introduction

Several methods for managing reservoir sedimentation have been developed to help extend project life (Morris and Fan 1998). In 2017, the World Bank sponsored REServoir CONservation (RESCON) 2, an Excel-based program currently in its beta development stages but expected to be finished over the next two years (Efthymiou 2019). This program can analyze up to nine alternatives and attempts to help users and analysts select practices to consider for more detailed studies. Users input required information and the program returns a pre-feasibility analysis comparing the nine alternatives side-by-side. The analysis identifies practicable solutions for the reservoir, whether or not each method is sustainable, its net present value, and the long-term reservoir storage capacity and reservoir lifetime. The objective of this paper is to gain insight into RESCON's efficacy for evaluating and suggesting sediment management options.

RESCON Background

Originally published in 2003, RESCON was created with the purpose of providing users with a rapid assessment and pre-feasibility analysis of sediment management alternatives (Palmieri et

al. 2003). Similarly, Annandale et al. (2017) commented on what RESCON 2 was and was not designed to do:

> "It is noted that the objective of the RESCON 2 model, as was the objective of the RESCON model, is to assess the technical viability and economic optimality of reservoir sedimentation management alternatives at policy and pre-feasibility level. It is not intended for feasibility and design phases of projects. The intent of RESCON 2 is to identify sediment management strategies that may be considered and analyzed using more detailed analysis approaches during the feasibility and final design stages of projects."

Thus, the main idea behind RESCON 2 is rapidly assessing sediment management alternatives with data that are, generally speaking, readily available. With sound engineering judgment, alternatives may then be selected to study and inspect more closely.

Several improvements have been made to the program since it first launched. The original RESCON only included assessments of sediment removal techniques: flushing, hydrosuction-sediment removal systems (HSRS), dredging, and trucking. Since then, sediment routing and inflow reduction practices have been added (Table 1). In addition to new sediment management strategies, RESCON 2 improved on its economic analysis and added an additional feature assessing climate change effects on reservoir sustainability (Annandale et al. 2017). The economic analysis can consider various implementation schedules for sediment management strategies and optimizes timing or recurrence to produce the highest net present value (NPV). The climate change assessment is comprised of multiple steps which are documented in the RESCON 2 user manual. To summarize, RESCON analyzes possible future climate scenarios and selects a set that "spans the full range of climate futures," and evaluates the different sediment management strategies under these potential conditions (Efthymiou et al. 2017).

Table 1. RESCON 1 and RESCON 2 Sediment Management Alternatives

Included in RESCON 1	Included in RESCON 2
Flushing	Flushing
HSRS	HSRS
Dredging	Dredging
Trucking	Trucking
-	Sluicing
-	Bypass tunnel
-	Catchment management
-	Density-current venting
-	No action

Sediment Management Options Diagram

Aside from RESCON, another practical approach for analyzing sediment management alternatives is the Sediment Management Options Diagram (SMOD). In the past, the SMOD has been referred to as the Basson Diagram (Palmieri et al. 1998; Aras 2009); however, Dr. Basson stated he used work previously done by Chinese researchers to develop this graph, and agreed the name "Sediment Management Options Diagram" would be an appropriate title for the chart (Basson 2018; see also Basson 1996).

The SMOD relates water and sediment inflows to storage capacity, and considers only these physical characteristics of the reservoir when analyzing alternatives (see Figure 1). The x-axis represents the reservoir storage capacity divided by the mean annual inflow. This ratio is

indicative of the hydraulic retention time (HRT), or the amount of time water remains in the reservoir before passing downstream. A low HRT value means water can fill the reservoir regularly, whereas a large HRT value suggests water is slower to enter and leave the reservoir, either because the volume of water entering the reservoir is relatively small or the reservoir capacity is large, or some combination of the two.

The y-axis is representative of the storage capacity divided by the mean annual sediment inflow, and can be interpreted as the reservoir's life expectancy (Auel et al. 2016). This latter ratio does not perfectly represent the lifetime of the reservoir, as reservoirs tend to fill more slowly over time as storage capacity is lost (Morris and Fan 1998). RESCON 2 attempts to account for the decrease in sedimentation rates through various trapping efficiency methods. The SMOD is a somewhat simplistic approach to consider sediment management strategies, but, like RESCON, it is meant to be used at the pre-feasibility stage and can provide practical feedback for selecting alternatives to review under more detailed analyses.

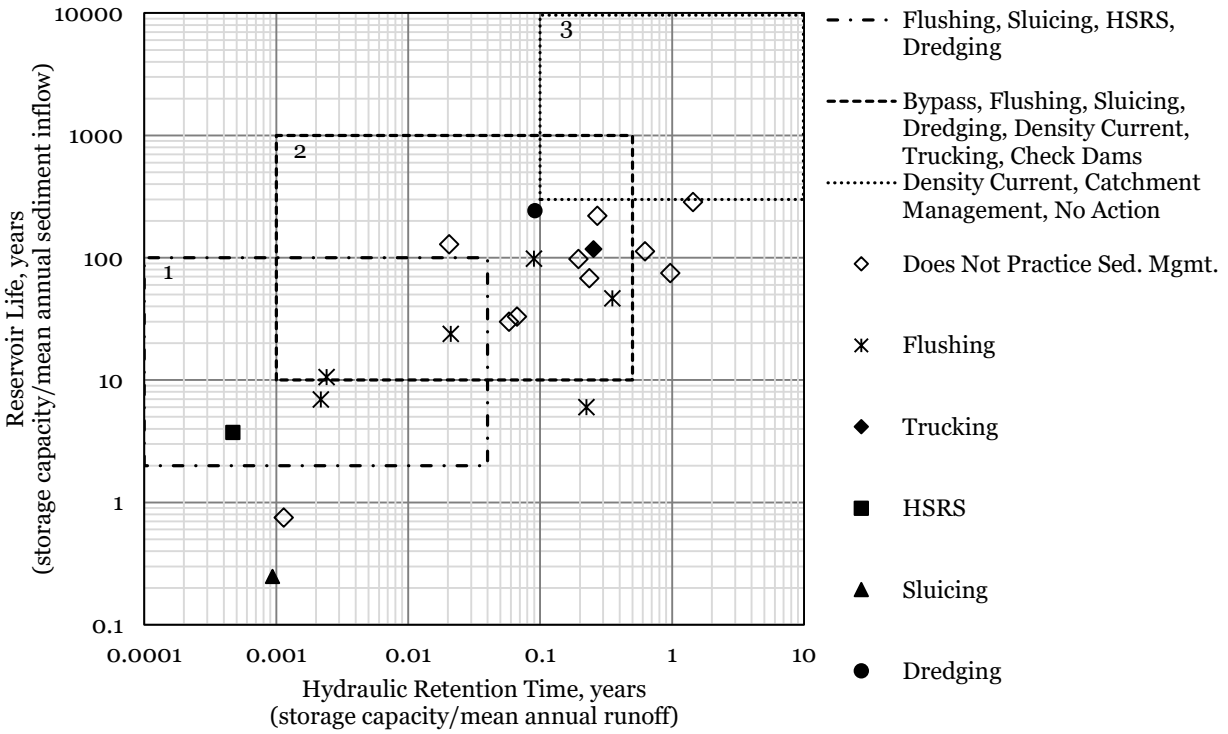

Figure 1. SMOD with RESCON-analyzed reservoirs (source, Annandale 2013; Basson 1996)

Figure 1 contains each RESCON-analyzed reservoir for this study, distinguishing between those reservoirs that do and do not practice sediment management. Reservoirs practicing sediment management are indicated by the various marker types. The three boxes contained within the diagram represent ranges where certain practices are considered more feasible than others (Annandale 2013). Reservoirs lying within or near box 1 were assumed to use either flushing, sluicing, HSRS, or dredging; box 2 to use sediment bypass tunnels, flushing, sluicing, dredging, density currents, trucking, or check dams; and box 3 to use density currents, catchment management or no action. Data for the SMOD can be found in Table 2.

Table 2. SMOD Data for Modeled Reservoirs

Reservoir	**CAP** (million m³)	**CAP/MAR** (years)	**CAP/MAS** (years)	**Source**
Abdel Karim	11.3	0.24	68	Annandale, G.W. (2017)
Baira	2.4	0.0024	11	Annandale, G.W. (2019)
Banja	403	0.27	221	Adhikari, S. (2017)
Bin El Quidine	1,508	1.4	285	Annandale, G.W. (2017)
Çubuk	7.1	0.25	118	Aras, T. (2009)
El Canadá	0.187	0.00047	3.7	Zamora, J. (2018a)
Gavins Point	580	0.020	129	Boyd, P. (2019)
Gebidem	9	0.021	24	Annandale, G.W. (2019)
Ichari	11.6	0.0022	7	Annandale, G.W. (2019)
Iron Gate	100	0.067	33	Annandale, G.W. (2017)
Kali Gandaki	7.7	0.00094	0.25	Annandale, G.W. (2017)
Kulekhani	85.3	0.62	113	Shrestha, H.S. (2012)
Millsite	22.2	0.091	243	Hotchkiss, R.H. (2018)
Mohammed V	726	0.97	75	Annandale, G.W. (2017)
Sanmenxia	9,640	0.22	6	Annandale, G.W. (2019); Wu, B. (2018)
Sefid-Rud	1,760	0.35	47	Annandale, G.W. (2019)
Sidi Driss	7.2	0.058	30	Annandale et al. (2017)
Tarbela	14,350	0.19	98	Annandale, G.W. (2017)
Three Gorges	39,300	0.090	98	Annandale, G.W. (2019)
Upper Karnali	17.9	0.0011	0.8	Annandale, G.W. (2017)

Inputs Needed in RESCON

RESCON 2 attempts to progress pre-feasibility analyses from field observations to empirical approximations, and the number of input parameters dramatically increases. Table 3 illustrates the six input worksheets within RESCON 2, the number of inputs on each page, and some key entries found therein. In total, there are 233 input parameters in RESCON 2. However, note that the sediment management page does not require all 80 inputs to run, as not all sediment management options need to be analyzed. Also, some values can be empirically estimated using functions built into the program, such as the mean annual sediment inflow and the unit cost of dredging. Though the total number of inputs can be somewhat daunting at first glance, RESCON 2 is designed for rapid assessment, and many of the input parameters should be easily accessible to the user.

Table 3. RESCON Required Inputs

Page Name	**Number of Inputs**	**Key Entries**
Project Definition	9	Required reliability of water supply
Environmental Safeguard	97	Allowable environmental and social damage
Reservoir Geometry	12	Storage capacity (live and dead), pool and bed elevations
Hydrology and Sediment	26	Mean annual runoff and sediment inflows
Economic Parameters	9	Unit cost of construction, discount rate, unit value of reservoir yield, maximum duration of financial analysis
Sediment Management	80*	Allowable loss, year of implementation, frequency of events
Total:	233	

* - Optional, does not need all 80 inputs to run

Results

RESCON 2 provides a comparison of sediment management alternatives and summarizes results with three recommendations:

1) A sustainable solution yielding the highest net present value (NPV);
2) A non-sustainable solution yielding the highest NPV that will eventually require decommissioning; and
3) A non-sustainable solution yielding the highest NPV that will eventually become a run-of-river dam.

Additionally, each sediment management technique considered is evaluated and given a sustainable or non-sustainable estimated net present value, long-term storage capacity, and life expectancy under such a regime. This is depicted below in Table 4, an example of RESCON's comparison taken from the Tarbela Reservoir. All alternatives within 30% of the highest NPV were considered practical for the reservoir and are labeled as "RESCON Predicted" solutions in Table 5.

Table 4. RESCON 2 Comparison of Results for Tarbela Reservoir

Sediment Management Strategy			Aggregate Net Present Value	Long Term Reservoir Gross Storage Capacity	Reservoir Lifetime
Technique	Sustainability	Action in case of storage elimination	[US$]	[m³]	[Years]
No Action	Sustainable		N/A	0	224
	Non Sustainable	Decommissioning	187,243,555,417		
		Run-Of-River	187,332,960,214		
Catchment Management	Sustainable		N/A	0	236
	Non Sustainable	Decommissioning	191,248,494,906		
		Run-Of-River	191,317,423,516		
Sluicing	Sustainable		N/A	192,307,615	> 217
	Non Sustainable	Decommissioning	N/A		
		Run-Of-River	249,393,287,482		
By-Pass	Sustainable		N/A	0	284
	Non Sustainable	Decommissioning	176,227,609,498		
		Run-Of-River	176,239,951,715		
Density Current Venting	Sustainable		N/A	0	196
	Non Sustainable	Decommissioning	75,395,440,831		
		Run-Of-River	75,400,274,878		
Flushing	Sustainable		267,331,032,335	1,471,780,945	> 300
	Non Sustainable	Decommissioning	N/A		
		Run-Of-River	N/A		
HSRS	Sustainable		N/A	N/A	N/A
	Non Sustainable	Decommissioning	N/A		
		Run-Of-River	N/A		
Dredging	Sustainable		297,621,522,010	9,855,539,822	> 300
	Non Sustainable	Decommissioning	N/A		
		Run-Of-River	N/A		
Trucking	Sustainable		247,866,217,286	7,409,392,165	> 300
	Non Sustainable	Decommissioning	N/A		
		Run-Of-River	N/A		

Figure 2, Figure 3, and Table 5 display the comparative results between RESCON 2, the SMOD, and the currently employed practice at the reservoir. Figure 2 and Table 5 display the results from all twenty models used in this study. Figure 3 displays only the results from reservoirs practicing some form of sediment management (i.e., anything but "no action"). In Figure 2 and

Figure 3, the term “agree” refers to the sediment management practice in use at the reservoir. Looking at all twenty cases, RESCON and the actual practice agreed thirteen times, while the SMOD agreed with the actual practice twelve times. In four instances were neither model able to correctly predict the currently employed alternative. Considering only those reservoirs that practice sediment management, ten of the twenty models were applicable, and RESCON and the actual practice agreed eight out of ten times, while the SMOD and actual practice agreed in all ten cases.

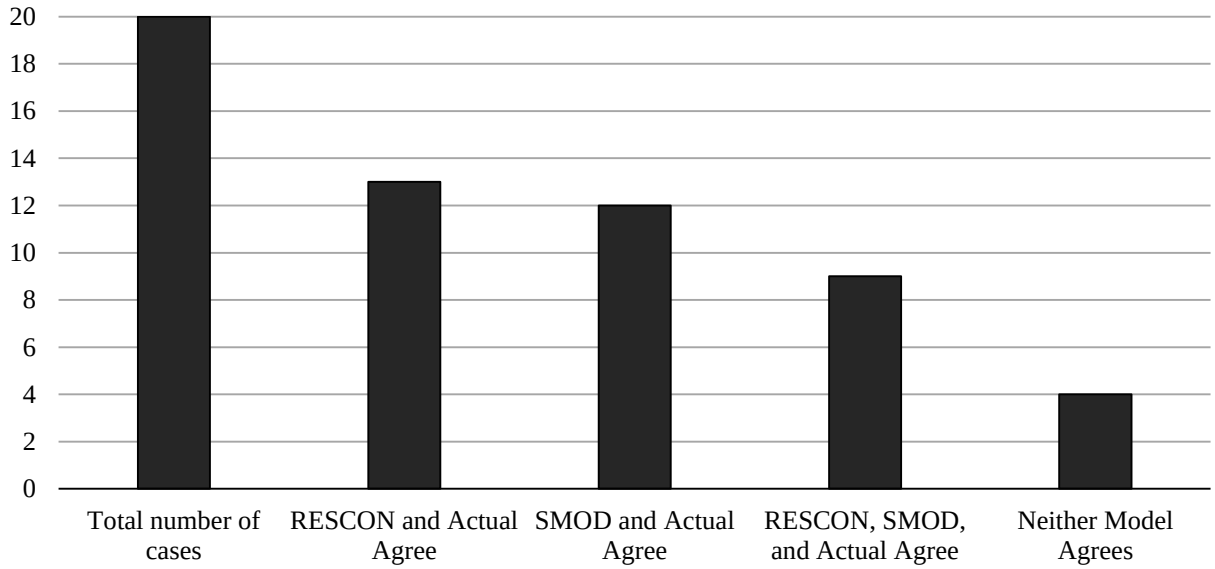

Figure 2. Comparison of predicted alternatives, all cases

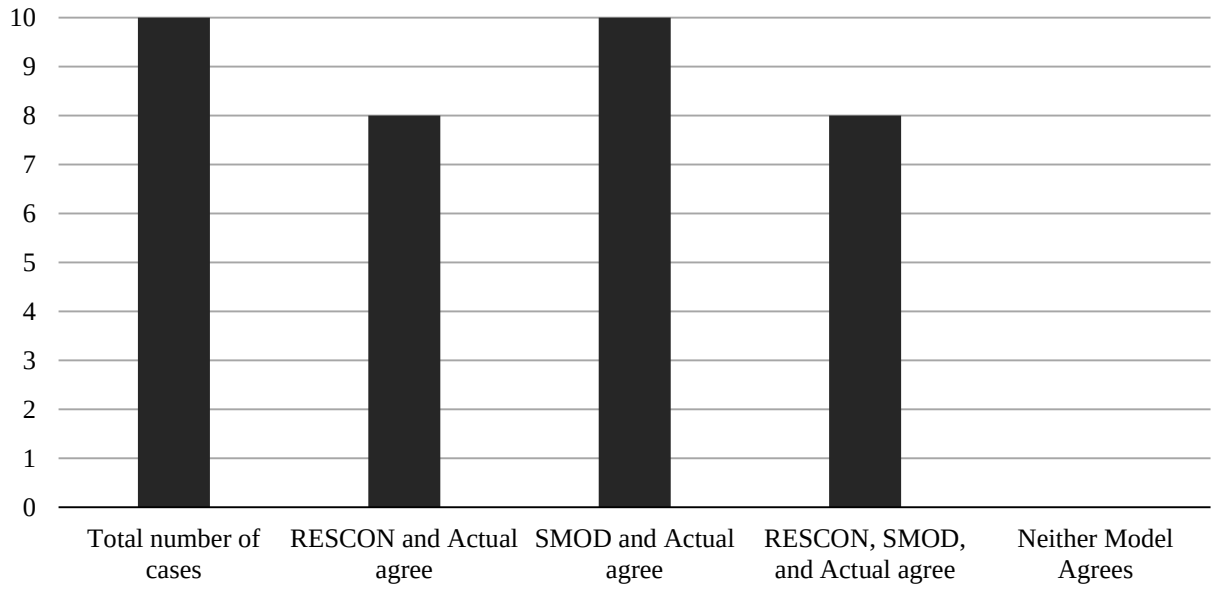

Figure 3. Comparison of predicted alternatives, only reservoirs practicing sediment management considered

Table 5. Comparison of RESCON's Predicted Sediment Management Alternative

Reservoir	RESCON Predicted	SMOD Predicted	Actual Practice
Abdel Karim	No Action, Catchment Management, Sluicing, Flushing, Dredging	Bypass Tunnel, Flushing, Sluicing, Dredging, Density Current, Trucking, Check Dams	No Action
Baira	No Action, Flushing, HSRS	Flushing, Sluicing, HSRS, Dredging, SBT, Density Current, Trucking, Check Dams	Flushing
Banja	Dredging	Bypass Tunnel, Flushing, Sluicing, Dredging, Density Current, Trucking, Check Dams, Catchment Management, No Action	No Action
Bin El Quidine	No Action, Catchment Management, Sluicing, Bypass Tunnel, Density Current, Dredging	Density Current, Catchment Management, No Action	No Action
Çubuk	No Action, Flushing, HSRS, Dredging, Trucking	Bypass Tunnel, Flushing, Sluicing, Dredging, Density Current, Trucking, Check Dams	Trucking
El Canadá	Dredging, No Action	Flushing, Sluicing, HSRS, Dredging	HSRS
Gavins Point	No Action, Flushing, HSRS, Dredging, Trucking	Bypass Tunnel, Flushing, Sluicing, Dredging, Density Current, Trucking, Check Dams	No Action
Gebidem	No Action, Flushing, HSRS	Flushing, Sluicing, HSRS, Dredging, SBT, Density Current, Trucking, Check Dams	Flushing
Ichari	Flushing	Flushing, Sluicing, HSRS, Dredging	Flushing
Iron Gate	No Action, HSRS, Trucking	Bypass Tunnel, Flushing, Sluicing, Dredging, Density Current, Trucking, Check Dams	No Action
Kali Gandaki	Sluicing	Flushing, Sluicing, HSRS, Dredging	Sluicing
Kulekhani*	HSRS	Bypass Tunnel, Flushing, Sluicing, Dredging, Density Current, Trucking, Check Dams	No Action
Millsite	No Action, Bypass Tunnel, HSRS	Bypass Tunnel, Flushing, Sluicing, Dredging, Density Current, Trucking, Check Dams, Catchment Management, No Action	Dredging
Mohammed V	No Action, Catchment Management, Sluicing	Bypass Tunnel, Flushing, Sluicing, Dredging, Density Current, Trucking, Check Dams	No Action
Sanmenxia	Flushing	Flushing, Sluicing, HSRS, Dredging, SBT, Density Current, Trucking, Check Dams	Flushing
Sefid-Rud	Flushing, Dredging	Bypass Tunnel, Flushing, Sluicing, Dredging, Density Current, Trucking, Check Dams	Flushing
Sidi Driss*	Sluicing	Bypass Tunnel, Flushing, Sluicing, Dredging, Density Current, Trucking, Check Dams	No Action
Tarbela	Sluicing, Flushing, Dredging, Trucking	Bypass Tunnel, Flushing, Sluicing, Dredging, Density Current, Trucking, Check Dams	No Action
Three Gorges	No Action, Flushing, HSRS, Dredging	Bypass Tunnel, Flushing, Sluicing, Dredging, Density Current, Trucking, Check Dams	Flushing
Upper Karnali	Bypass Tunnel, Flushing	Flushing, Sluicing, HSRS, Dredging	No Action

* Models not had in possession but results were obtained via sources outlined in Table 2. Thus, other results may be considered practical under "RESCON Predicted."

Discussion

RESCON 2 Beta did not predict the correct alternative for the Millsite and El Canadá Reservoirs. Zamora (2018a) provided some commentary on why RESCON 2 may not apply to El Canadá.

1. It is a small regulation pond (0.187 million m^3), and the reservoir volume is small in comparison with the inflow.
2. It is an off-stream reservoir.
3. There is polyethylene lining in the reservoir.
4. The HSRS analysis included in RESCON seems to have a different approach than the one used at El Canadá.

For Millsite Reservoir, the NPV of the actually used practice (dredging) was approximately 36% lower than the highest NPV alternative (no action). As indicated in Table 2, Millsite has an unmanaged life expectancy of about 243 years, a reasonably long life for a reservoir, which may be why RESCON suggests no action as the ideal alternative. However, looking at life expectancy alone can be misleading, as a dam's functionality and purpose can be compromised well before the life of the reservoir has been fully exhausted (Morris and Fan 1998; Reclamation 2018). This would likely be shown in a detailed study, but the disparity between RESCON's results and the actual practice suggest something is amiss.

RESCON predicted the optimal alternatives for the Gebidem Reservoir would be no action, flushing, and HSRS. At Gebidem, flushing is used quite successfully, and a sediment balance has nearly been achieved—that is, outgoing sediments are equal to incoming sediments (Chamoun et al. 2016; Meile et al. 2014; Emamgholizadeh et al. 2006). Thus, the reservoir life is perpetuated almost indefinitely. However, RESCON suggests the lifetime of Gebidem under a flushing regime would last about 90 years.

Even though RESCON may not yield information revealed in detailed analyses, the rapid assessment and feedback provided by the program is valuable and informative at the conceptual stage of projects. All of the major sediment management techniques thus far developed can be evaluated from both an economic and sustainable development perspective. The SMOD-predicted strategies contained the actually used practice in all ten cases but, unlike RESCON, it provides no economic analysis, is not able to adjust for climate change, does not consider the presence or absence of low-level outlets, nor does it attempt to organize the various alternatives. RESCON 2 can help bridge the gap between potential alternatives and knowing with which practices to begin investigating.

Recommendations

As RESCON 2 progresses from a beta to fully developed program, a few concerns, if addressed, will increase the efficacy of the program and clarity of parameters.

HSRS Operation and Maintenance: Under the "Sediment Management" worksheet, there is no input for HSRS operation and maintenance (O&M) costs. RESCON assumes negligible costs are associated with HSRS O&M (Efthymious 2019), and while they are typically lower than conventional dredging, they aren't necessarily insignificant. In one case, Zamora (2018b) outlined and compared O&M costs for HSRS against conventional dredging at the El Canadá hydropower plant, and found HSRS to cost 75% more over a nine-year period. Thus, it is recommended that an HSRS O&M parameter be added to the program. However, if no such improvement is made, there are at least two possibilities to account for HSRS O&M costs.

First, users could determine the lifetime of the reservoir using HSRS, estimate the annual O&M costs, multiply annual O&M costs by the expected lifetime, and add this number to the initial investment required to install HSRS. The second option is to add HSRS O&M costs to the total O&M costs of the reservoir under the "Input (Economic Parameters)" worksheet of the program. This latter alternative is discouraged because adjusting total reservoir O&M costs would affect all sediment management alternatives, not just HSRS. Thus, at least two separate runs would be needed: one to analyze every other sediment management option, and a second for HSRS.

Unit Benefit of Reservoir Yield: The parameter in RESCON 2 called "unit benefit of reservoir yield" attempts to account for all revenues associated with multiple reservoir purposes, including drinking water and irrigation supply, flood control, and hydropower generation (Efthymiou et al. 2017). This single value plays a significant role in calculating NPVs for all sediment management alternatives. As a pre-feasibility analysis, users are not required to perform a detailed study to gain accurate measurements of each of the revenue sources to depict this parameter. Instead, the RESCON 2 user manual provides references for estimating this value, yet none of these references are currently listed or found in the manual. Additionally, the manual refers to this parameter as "unit benefit of water yield." Using the same term in both the program and manual would likely decrease confusion about this variable, as the program currently only gives this help text: "Where possible use specific data for the project. If no data is available refer to User Manual for guidance."

It may also be beneficial to expand this parameter into multiple variables for which this parameter is meant to consider. For instance, Table 6 gives specific revenue sources that may more clearly indicate which factors apply and potential units for each respective field.

Table 6. Potential Expansion of Unit Benefit of Reservoir Yield

Current Parameter	Recommended Parameters	Unit
Unit benefit of reservoir yield	Hydroelectric generation	$/kWh
	Agricultural use	$/m^3
	Municipality use	$/m^3
	Industrial use	$/m^3
	Flood control	$/year
	Recreational benefits	$/year

Flushing Operation and Maintenance and Annual Sedimentation Capacity: Sensitivity tests indicated that the flushing O&M parameter is not factored into the NPV calculation. For instance, the Tarbela reservoir was run with two very different O&M costs: $0 and $1,000,000,000. The aggregate NPV remained the same for both cases. This phenomenon was confirmed in other models as well. Additionally, there seems to be a cap on how much sediment RESCON 2 can handle. For example, the Sanmenxia Reservoir, which is known for having extremely high sedimentation rates (Wang et al. 2005), could not be simulated without reducing the mean annual sediment inflow by nearly 40%. It was confirmed and assurance was given that these were, in fact, bugs in the program and would be treated in later versions of RESCON 2 (Efthymiou 2019). In lieu of this, it may be helpful to include a list of all RESCON 2 versions with build numbers and bug treatments. This would help users know if they have the most up-to-date version of the program and if their problem has been resolved with new builds. Similarly, having a system for users to report bugs or suggest recommendations could be helpful to further enhance RESCON's efficacy.

Conclusions

RESCON 2 has been developed as a pre-feasibility tool to guide users and analysts in the early project development stages to select practices to consider under detailed studies. The information provided by RESCON 2 is resourceful and valuable, and findings in this report suggest RESCON very often predicts the optimal solution. Furthermore, RESCON allows users and analysts to compare all modern sediment management techniques from both an economic and sustainable perspective. Using additional pre-feasibility models, such as the SMOD, may serve as a check on what accumulated experiences elsewhere have shown.

As a beta program, RESCON 2 can improve by:

1. Including an HSRS O&M parameter;
2. Using identical terms for the unit benefit of reservoir yield parameter in both the model and user manual, and expand this parameter to more explicitly state what this value is meant to consider;
3. Including the sources for estimating unit the benefit of reservoir yield in the user manual's reference list;
4. Incorporating flushing O&M costs to factor into the NPV calculation;
5. Increasing the annual sediment inflow capacity to allow for higher sedimentation rates; and
6. Provide a list of RESCON model builds/versions to clearly indicate which bugs have been treated.

References

Adhikari, S. 2017. "Evaluating sediment handling strategies for Banja Reservoir using the RESCON2 model—A comprehensive study of the rapid assessment tool and sustainable sediment management." Master's thesis, NTNU.

Annandale, G.W. 2019. Personal communication.

Annandale, G.W. 2017. Personal communication.

Annandale, G.W. 2013. "Quenching the Thirst: Sustainable Water Supply and Climate Change." North Charleston, SC. CreateSpace Independent Publishing Platform.

Annandale, G.W., Efthymiou, N., Palt, S., and Karki, P. 2017. "RESCON 2: Rapid identification of optimal strategies to mitigate reservoir sedimentation and climate change impacts on water supply reliability," The International Journal on Hydropower and Dams, Africa 2017.

Aras, T. 2009. "Cost Analysis of Sediment Removal Techniques from Reservoir." Master's thesis, Middle East Technical University.

Auel, C., Kantoush, S.A., and Sumi, T. 2016. "Positive Effects of Reservoir Sedimentation Management on Reservoir Life–Examples from Japan." In 84th Annual Meeting of ICOLD.

Basson, G.R. 2018. Personal communication.

Basson, G.R. 1996. "Hydraulics of Reservoir Sedimentation." Doctoral dissertation, Stellenbosch: Stellenbosch University.

Boyd, P. 2019. Personal communication.

Bureau of Reclamation (Reclamation). 2018. “Sedimentation at Paonia Reservoir.” Upper Colorado Region – Western Colorado Area Office, www.usbr.gov/uc/wcao/progact/paonia/index.html.

Chamoun, S., De Cesare, G., and Schleiss, A.J. 2016. “Managing Reservoir Sedimentation by Venting Turbidity Currents: A Review.” The International Journal of Sediment Research, 31(3):195-204.

Efthymiou, N.P. 2019. Personal Communication

Efthymiou, N.P., Palt, S., Annandale, G.W., and Karki, P. 2017. “Reservoir Conservation Model Rescon 2 Beta. Economic and Engineering Evaluation of Alternative Sediment Management Strategies. User Manual.” Washington, DC: World Bank. License: Creative Commons Attribution CC BY 3.0 IGO.

Emamgholizadeh, S., Bina, M., Fathi-Moghadam, M., and Ghomeyshi, M. 2006. “Investigation and Evaluation of the Pressure Flushing Through Storage Reservoir.” ARPN Journal of Engineering and Applied Sciences, 1(4):7-16

Hotchkiss, R.H. (2018). Personal communication.

Kondolf, G.M. 1997. “PROFILE: Hungry Water: Effects of Dams and Gravel Mining on River Channels.” Environmental Management, 21(4):553-551.

Meile, T., Bretz, N.V., Imboden, B., and Boillat, J.L. 2014. “Reservoir Sedimentation Management at Gebidem Dam (Switzerland).” Reservoir Sedimentation; Schleiss, A., De Cesare, G., Franca, M.J., Pfister, M., Eds, 245-255.

Morris, G.L. and Fan, J. 1998. “Reservoir Sedimentation Handbook: Design and Management of Dams, Reservoirs, and Watersheds for Sustainable Use.” McGraw Hill Professional.

Palmieri, A., Shah, F., Annandale, G., and Dinar, A. 2003. “Reservoir Conservation Volume I: The RESCON Approach.” Washington, DC: World Bank.

Palmieri, A., Shah, F., and Dinar, A. 1998. “Reservoir Sedimentation and the Sustainable Management of Dams.”

Salloum, M. and Gharagozloo, P.E. 2014. “Empirical and Physics-Based Mathematical Models of Uranium Hydride Decomposition Kinetics with Quantified Uncertainty.” Chemical and Engineering Science, 116:452-464.

Shrestha, H.S. 2012. “Sedimentation and sediment handling in Himalayan reservoirs.” Doctoral dissertation, NTNU.

Wang, G., Wu, B., and Wang, Z. 2005. “Sedimentation problems and management strategies of Sanmenxia Reservoir, Yellow River, China,” Water resources research, 41(9).

Wu, B. 2018. Personal communication.

Zamora, J. 2018a. Personal communication.

Zamora, J. 2018b. “Assessment of sediment handling strategies in the regulation pond of El Canadá hydropower plant, Guatemala—Processing and analyzing sediment information collected in situ.” Master’s thesis, NTNU.

National Drought Resilience Partnership Data Collection

Bryan Baker, Remote Sensing-GIS Center of Expertise, Cold Regions Research and Engineering Lab, U.S. Army Corps of Engineers, Hanover, NH, bryan.e.baker@usace.army.mil

Ariane Pinson, Albuquerque District, U.S. Army Corps of Engineers, Albuquerque, NM, mailto:ariane.pinson@usace.army.mil

Sean Kimbrel, U.S. Bureau of Reclamation, Denver, CO, mailto:skimbrel@usbr.gov

Dr. Kate White, Headquarters, U.S. Army Corps of Engineers, Washington, DC, mailto:Kathleen.D.White@usace.army.mil

Ariane Pinson, Los Angeles District, U.S. Army Corps of Engineers, Los Angeles, CA, mailto:Amanda.R.WallerWalsh@usace.army.mil

Extended Abstract

Introduction

Drought in the U.S. has caused over $220B in estimated damages since 1980 (NOAA, 2016), and has led naturally to calls for increasing water storage in the nation's reservoirs. In the future, the duration, intensity, and frequency of drought is expected to increase in many parts of the US (USGCRP). At the same time, increased duration, intensity, and frequency of intense precipitation with the potential for large-scale flooding may also occur during droughts, driving the need to maintain or increase flood storage volumes in these same reservoirs. Record flooding during drought has already been observed in several parts of the U.S., including the Memorial Day floods in central Texas in 2015 [Di Liberto 2015] and September 2013 flood in central Colorado [Howard 2013]. To balance these conflicting needs, accurate and current understanding of capacity of each pool is essential for assessing potential deviations in the operation of a reservoir to provide during drought periods.

While fixed water volumes or pool elevations may be defined for purposes of water operations, the actual capacity of each pool changes over time due to sediment influx to, movement through, and deposition with each reservoir. Sediment deposition is not confined to deadpool, but may occur anywhere in a reservoir. In addition, changing climate and land use cause the rate of sediment influx to vary from the design influx rate. Therefore, accurate information on current reservoir capacities is essential for routine reservoir operation as well as for planning and implementation deviations from existing water control operational plans to alleviate critical drought impacts consistent with authorized dam purposes. Repeated topographic (above water) and bathymetric (below water) surveys are necessary to estimate how the water storage capacity of reservoirs changes as sediment enters from upstream and accumulates, how fast this sedimentation is occurring, and whether the sedimentation rate is changing or remaining constant.

Such surveys can be costly to implement, and in practice are deferred under today's constrained budget environment where operation and maintenance of aging dam infrastructure have a

higher funding priority. Consequently, there is a need for a fast, systematic, accurate and cost-effective means to conduct periodic reservoir sediment surveys.

The National Drought Resilience Partnership (NDRP) was established in 2016 to coordinate Federal drought efforts. The objective of the NDRP was to reduce the vulnerability of communities to current and future drought through better coordination of Federal support for drought-related efforts. Under the NDRP, Federal agencies were charged with implementing policies and actions to achieve six key drought resilience goals, and the implementation plan for the NDRP, "Long-Term Drought Resilience: Federal Action Plan of the National Drought Resilience Partnership" (March 2016) charged U.S. Army Corps of Engineers (USACE) , in conjunction with the Bureau of Reclamation (Reclamation) with investigating new ways of conducting reservoir surveys at drought-induced low reservoir levels that would reduce the cost of reservoir surveys and produce data that could be readily shared with partners and stakeholders.

In response, U.S. Army Corps of Engineers (USACE) staff in conjunction with the U.S. Department of the Interior's Bureau of Reclamation (Reclamation) had begun to experiment with using airborne LiDAR to conduct surveys of reservoirs where drought and lowered reservoir levels exposing substantial portions of the reservoir bottom. Under NDRP, USACE and Reclamation saw an opportunity to test this approach of collecting terrestrial data normally underwater under none severe drought conditions at reservoirs in California, Arizona and Nevada.

This NDRP pilot study seeks to establish a set of standards for deployment of airborne LiDAR to collect topographic data at USACE and Reclamation reservoirs with the goal of creating detailed, geospatially-accurate estimates of current reservoir capacities and changes in these capacities over time. The resulting information is essential for water supply, flood risk management, navigation, recreation, and other planning activities at the Nation's reservoirs.

Methods and Results

Time-efficiencies and the resulting dense, georeferenced data already make airborne LiDAR a cost-effective method for obtaining topographic data for terrestrial areas. However, because LiDAR's difficulty penetrating water, LiDAR has not been widely used to estimate reservoir capacities. Deployment of airborne LiDAR during regional droughts provides an opportunity to collect areas in the reservoir more efficiently leaving a reduced area to be collected with bathometric type surveys.

The areas selected for the pilot effort are in the U.S. Southwest (Figure 1) where drought is ongoing in 2016. The study areas span two USACE Districts, Los Angeles and Sacramento, and two Reclamation Areas, Mid-Pacific and Lower Colorado. Multiple reservoirs were surveyed in each of the areas, including both USACE and Reclamation reservoirs, in order to take advantage of the spatial clustering of reservoirs with low water levels due to drought. The three areas where data collection were planned include: Oxnard (14 reservoirs) and Fresno (12 reservoirs), California, and Phoenix, Arizona (7 reservoirs) and are listed in Table 1.

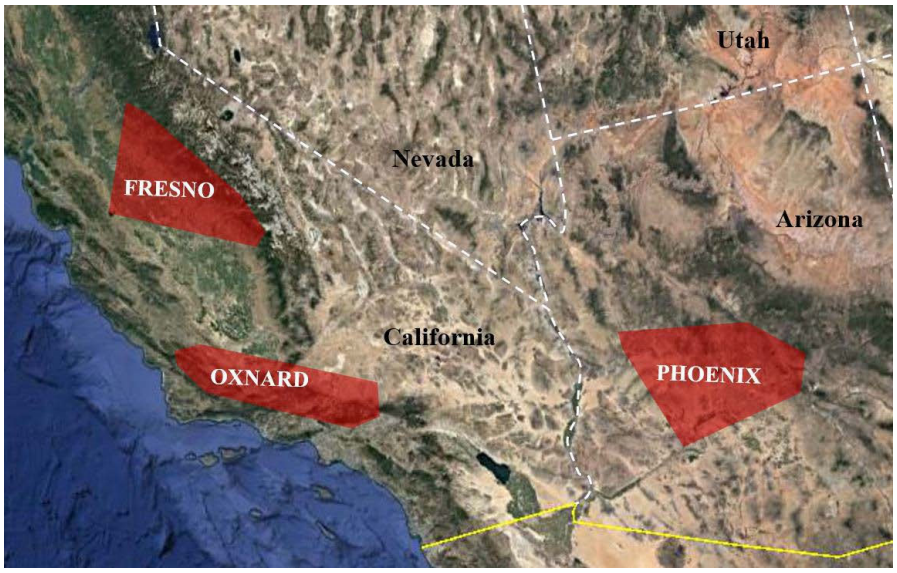

Figure 1 Location of flight areas, highlighted in red. Top left: Fresno CA based sites. Bottom left: Oxnard CA based sites. Bottom right: Phoenix AZ base sites.

Within these three drought-impacted areas, USACE reservoirs were prioritized for data collection based on three criteria:

- Extremely low reservoir water levels occurred due to drought, maximizing the area within each reservoir over which LiDAR data can be successfully collected.

- Regionally, dry conditions have contributed to wildfires in the region. In 2016, the Erskine fire in Kern County, California, burned 48,019 acres on the southeast side of Lake Isabella, and the San Gabriel Complex Fire burned approximately 5,400 acres within the watershed of Santa Fe Reservoir below Morris Dam [Inciweb, 2016]. Because precipitation on recent burn scars can result in extensive erosion and downstream transport, and because USACE reservoirs are positioned to receive this sediment when it rains, collection of LiDAR data at these reservoirs was a priority.

- Age since last survey was the third criteria. Because sedimentation rates are not constant over time, and sediment may move within a reservoir in response to changes in flow, past estimates of sedimentation rates may no longer reflect current conditions. Further, the lack of precision of older methods of determining remaining reservoir capacity for a given pool elevation mean that existing information on sedimentation rates may even be inaccurate for the period over which it was gathered.

The selection of BOR reservoirs for aerial LiDAR surveys was based on one main factor, which is whether the reservoir was at low water levels or less than 40% of total capacity. Several reservoirs have had at least one reservoir survey since dam closure and first filling of the reservoir, however most Reclamation reservoirs have not had a reservoir survey since dam closure.

The priority reservoirs selected for survey are listed in Table 1. The reservoirs share nearly uniform low water levels, with many reservoirs completely dry. Most areas where the reservoirs

are located are in Moderate to Extreme Drought (D2-D4 on the US Drought Monitor Scale established by the Drought Monitor (Source: U.S. Drought Monitor (http://droughtmonitor.unl.edu/). Most of the reservoirs had either never been surveyed, or have never been accurately surveyed using modern methods, such as LiDAR or SONAR.

Table 1 Status of USACE and Reclamation Reservoirs considered for inclusion in the pilot study.

Flight Area	**Reservoir Name**	**Agency***	**Initial Survey Year**	**Last Survey Year**	**Last Survey Method**	**Wildfire within last 5 years basin**	**Reservoir % Full (Oct 1, 2016)**
Phoenix	Painted Rock	U	1953	1993	Satellite Imagery		0
Phoenix	Alamo	U	1968,63	1985	Bathymetric		4
Phoenix	Whitlow Ranch	U	1957, 39, 56	1984	Contour Map	Yes	0
Oxnard	Whitter Narrows	U	1948	2011	Contour Map	Yes	0
Oxnard	Carbon Canyon	U	1961, 37, 41, 49	2009	Contour Map	Yes	0
Oxnard	Brea	U	1939	1994	Contour Map		0
Oxnard	Fullerton	U	1941	1970	Contour Map		0
Oxnard	Santa Fe	U	1943	2010	Contour Map		0
Oxnard	Hansen	U	1940	2004	Contour Map		0
Oxnard	Lopez	U	1954	2010	Contour Map		0
Oxnard	San Antonio	U	1941	2010	Contour Map		0
Oxnard	Mojave River	U	1965, 62	Same	Contour Map	Yes	0
Oxnard	Isabella	U	1953	1977	Other/Unspecified	Yes	17
Fresno	Pine Flat	U	1973	1973	Range Line	Yes	16
Fresno	New Hogan	U	1959	1978	Other/Unspecified	Yes	25
Fresno	Eastman	U	1967	1975	Other/Unspecified	Yes	8
Fresno	Hensley	U	1967	1975	Other/Unspecified	Yes	19
Fresno	Kaweah	U	1961	1987	Other/Unspecified	No	17

Flight Area	Reservoir Name	Agency*	Initial Survey Year	Last Survey Year	Last Survey Method	Wildfire within last 5 years basin	Reservoir % Full (Oct 1, 2016)
Fresno	Bear	U	1968	1975	Other/Unspecified	No	0
Fresno	Burns	U	1968	1975	Other/Unspecified	No	0
Fresno	Mariposa	U	1968	1975	Other/Unspecified	No	0
Fresno	Owens	U	1968	1975	Other/Unspecified	No	0
Oxnard	Twitchell Reservoir	R	1958	--	Never Surveyed	Yes	0
Oxnard	Lake Cachuma	R	1953	1989	Contour Map	Yes	7
Fresno	San Luis	R	1967	--	Never Surveyed	No	25
Fresno	New Melones	R	1979	--	Never Surveyed	Yes	11
Phoenix	Horseshoe Reservoir	R	1949	--	Never Surveyed	Unknown	1
Phoenix	Theodore Roosevelt	R	1909	2013	Contour Map	Yes	36

** U= USACE, R=Reclamation*

ǂ = The sediment allowance was revised upward since the original project design. The rate of sedimentation exceeds the original design but not the revised sediment allowance.

An important opportunity exists to increase the fidelity of sedimentation of a reservoir with LiDAR data collected at reservoirs, in a way that drives down unit costs and maximizes data collection efficiency. In times of drought, a reservoir may be completely or largely drawn down, dewatering an exceptionally large portion of the reservoir bottom. Drought, being a regional phenomenon, likely causes many reservoirs in a local area to experiencing conditions of low water elevations at the same time. This scenario makes it exceptionally cost-effective to fly LiDAR for all the drawn-down reservoirs in a region by reducing the number of unique flights and reducing many of the fixed costs associated with obtaining LiDAR data (primarily mobilization costs). Bathymetry collection via boat has mobilizations costs as well. This also minimizes the amount of sonar data need to be collected to complement the LiDAR data because the extent of the water surface is minimized. A region with a series of dry dams (typically single-purpose flood damage reduction structures) could also achieve similar economies of scale while obtaining LiDAR data.

Post-collection data processing and archiving consists of five basic steps: data processing steps identify and correct errors present in the dataset and provides an estimate of the precision and

accuracy of the data set; the processed data are then uploaded to a geospatial repository for dissemination; reservoir capacities are calculated for different levels of inundation and area-capacity curves; and finally, the area-capacity data and associated curves are loaded into the USACE sedimentation database.

Discussion

This study occurred within a larger NDRP framework in which LiDAR is increasingly used for topographic data collection in support of the many USACE and Reclamation missions. The collection of high resolution LiDAR data are ideal for topographic mapping of the exposed reservoir shoreline and the upstream delta areas, which are difficult and expensive to survey by boat or by wadding or walking. Deltas can often extend well upstream from the full pool of the reservoir, causing problems for upstream lands, and these areas are often ignored during bathymetric reservoir surveys. LiDAR data are also useful for other purposes, including reservoir storage reallocation studies, project planning, and cultural resources.

The data collection effort by the RS/GIS CX consists of a fix cost contract aircraft charter which translates into a number of hours of flight time. Flight conditions and weather may play a key role in the final projects surveyed. The data in the table represent the costs for the data collected based on priorities established to ensure the critical projects from both agencies get collected.

LiDAR data collection produces a significant cost reduction for data collection when compared to previous contracts and data collection efforts with transects and or SONAR technologies. Processing costs for LiDAR are generally constant and therefore a small reservoir would have a high cost per acre. One a whole, 28 reservoirs were collected totaling 203,156 acres using LiDAR technologies at a cost around $1.00 per acre in 2016 and is detailed in Table 2

Table 2 Cost details of USACE and Reclamation surveyed.

Flight Area	Reservoir Name	Agency*	Acres	Estimated Flight Time (min)	Estimated Total Cost	Estimated Cost Per Acre
Phoenix	Painted Rock	U	74,892	488	$13,181	$0.18
Phoenix	Alamo	U	14,525	325	$10,508	$0.72
Phoenix	Whitlow Ranch	U	1,322	75	$6407	$4.85
Oxnard	Whitter Narrows	U	4,325	80	$6,489	$1.50
Oxnard	Carbon Canyon	U	358	16	$5,439	$15.19
Oxnard	Brea	U	294	80	$6,489	$22.07
Oxnard	Fullerton	U	5,616	45	$5,915	$1.05
Oxnard	Santa Fe	U	1,810	76	$6,424	$3.55
Oxnard	Hansen	U	1,297	59	$6,145	$4.74
Oxnard	Lopez	U	82	22	$5,538	$67.53

Flight Area	Reservoir Name	Agency*	Acres	Estimated Flight Time (min)	Estimated Total Cost	Estimated Cost Per Acre
Oxnard	San Antonio	U	229	114	$7,047	$30.77
Oxnard	Mojave River	U	3,596	92	$6,686	$1.86
Oxnard	Isabella	U	7,738	215	$8,703	$1.12
Fresno	Pine Flat	U	5,866	140	$7,473	$1.27
Fresno	New Hogan	U	4,299	82	$6,522	$1.52
Fresno	Eastman	U	1,825	30	$6,161	$3.11
Fresno	Hensley	U	1,587	42	$5,866	$3.70
Fresno	Kaweah	U	1,864	75	$6,407	$3.44
Fresno	Bear	U	295	34	$5,735	$19.44
Fresno	Burns	U	709	60	$6,161	$8.69
Fresno	Mariposa	U	594	34	$5,735	$9.64
Fresno	Owens	U	198	22	$5,538	$27.97
Oxnard	Twitchell Reservoir	R	1,759	203	$8,507	$4.84
Oxnard	Lake Cachuma	R	4,693	101	$6,834	$1.46
Fresno	San Luis	R	20,403	241	$9,130	$0.45
Fresno	New Melones	R	11,757	228	$8,917	$0.76
Phoenix	Horseshoe Reservoir	R	3,334	102	$6,850	$2.05
Phoenix	Theodore Roosevelt	R	27,878	265	$9,524	$0.34

One key difference that must be highlighted is that some water remains in the reservoirs and the surface below the water cannot be collected with LiDAR. One possible solution would be to survey the remaining location underwater with the multi-beam SONAR dataset and merge it with the LiDAR data collected. This would have the benefit of getting a complete surface of the entire reservoir. Because much can change in a short time, it would be advisable to collect the data with the two technologies as close in time as possible.

The reservoir LiDAR survey methodology used in this NDRP reservoir survey project has multiple benefits compared to either a piecemeal LiDAR approach or uses of other technologies alone:

- The higher data density of LiDAR results in a more accurate snapshot of what the real volume of the reservoir is and the location of deposition relative to critical assets like dam outlets, water intakes, and boat marinas, when compared to traditional transect survey and single-beam SONAR methods.

- To a get a complete bathymetric surface, the post-field data processing of LiDAR point clouds are significantly less than with single-beam SONAR for both LiDAR and multi-beam SONAR. There is a little additional preparation on the front end for calibration but once the survey is complete, quality control and getting it the data into the target mapping format remain.

- The LiDAR (as well as multi-beam SONAR) data products are very accurately georeferenced datasets. LiDAR resolution can be improved with added control points even after the data is collected to meet other agency needs, such as design. Thus, if the initial vertical accuracy of the LiDAR data is sufficient for area-capacity estimates, but not for a subsequent engineering task (e.g., a dam safety study), additional control points can be surveyed and that data used to improve the vertical control of the original LiDAR data set. New LiDAR would not necessarily have to be reflown.

- Transect or range line cross section can be produced from the LiDAR and multi-beam SONAR datasets. These can then be used to compare to data from traditional or single beam range line surveys (i.e., the new data is backwardly compatible). The reverse is not true: you cannot build a complete reservoir bathymetry dataset from range line data.

The lessons learned to date are focused on maximizing cost efficiency, facilitating regional deployment, and strategies to reduce data co-registration between the LiDAR and multi-beam SONAR data collection during low pools:

- Because mobilization costs are significant, data collection for the NDRP reservoir survey project capitalized on economies of scale by collecting numerous sites in a geographical region. Instead of standing up the aircraft, LiDAR equipment, and technical teams separately for individual reservoirs, the cost and effort of standing up the LiDAR is amortized across multiple reservoirs. This results in a significant decrease in per-acre survey costs.

- Because drought affects Federal, state, and local reservoirs equally, collaboration among agencies could be used to further reduce costs depending on authorities. By partnering with Reclamation on this effort, total costs of LiDAR data collection are reduced because only one LiDAR effort needs to be mobilized in the area. This is important because reservoirs within a watershed are typically operated as a system in response to a drought (or flood), rather than individually. Accurate data on surface area and capacity across the system, not just at selected reservoirs, provides a stronger foundation for better decision-making. Lower costs ease the burden for smaller municipalities and agencies funding LiDAR data collection at their reservoirs as part of this collective effort, which benefits all.

- Because of the very low per acre costs achieved by the NDRP reservoir survey project, the most cost-effective strategy is to maximize the amount of LiDAR data that can be collected and minimizing the remaining multi-beam SONAR data collection effort. Working with reservoirs experiencing drought or other draw-down minimizes costs while maximizing data quality.

- Additional studies are needed to better understand how changes in method, LiDAR vs. transects, vs. sonar, affect capacity estimates so that long-term sedimentation rates at

the nation's reservoirs can be better estimated, and the factors that affect these rates be identified.

Conclusion

The NDRP lays out a framework under which federal agencies can collaborate to improve community resilience to current drought, whether or not future droughts last longer or occur more frequently. Droughts and floods accelerate and exacerbate the sedimentation problem while simultaneously increasing water demand and the nation's reliance on its reservoirs. Understanding how much sediment is accumulating in our reservoirs, and monitoring the rate of this accumulation, is essential for understanding the magnitude and geographic extent of this problem relative to the nation's water needs. The proposed approach to survey sediment deposition in drought-lowered reservoirs using a combination of LiDAR bathometric type surveys was found to be cost-effective for the 28 locations evaluated.

References

Di Liberto, T. (2015), Flood disaster in Texas and Oklahoma, NOAA Event Tracker, online at https://www.climate.gov/news-features/event-tracker/flood-disaster-texas-and-oklahoma.

Executive Office of the President (2016), Presidential memorandum on building national capabilities for long-term drought resilience (March 2016)

Gruen, A., and D. Akca (2005), Least squares 3D surface and curve mapping, ISPRS Journal of Photogrammentry and Remote Sensing, 59(3), 151-174.

Howard, B. C. (2013), Amid drought, explaining Colorado's extreme floods, National Geographic news, September 13, 2013, online at http://news.nationalgeographic.com/news/2013/09/130913-colorado-flood-boulder-climate-change-drought-fires/.

InciWeb (2016), Current Incidents, online at http://inciweb.nwcg.gov/, accessed 7 November 2016.

Juracek, K.E. (2015), The aging of America's reservoirs: in-reservoir and downstream physical changes and habitat implications, Journal of the American Water Resources Association, 51(1), 168-184.

Maas, H.-G. (2002), Methods for measuring height and planimetry discrepancies in airborne laser-scanner data, Photogrammetric Engineering and Remote Sensing, 68(9), 933-940.

NOAA (2016), Weather and Climate Disasters, Online at https://www.ncdc.noaa.gov/billions/events

Okatani, T., and K. Deguchi (2002), Robust estimation of carmera translation between two images using a camera with a 3d orientation sensor, Proceedings of the 16th International Conference on Pattern Recognition, 2002, IEEE, 1, 275-278.

U.S. Drought Monitor. University of Nebraska, http://droughtmonitor.unl.edu/), Accessed 30 Oct 2016

USGCRP, 2017: Climate Science Special Report: Fourth National Climate Assessment, Volume I [Wuebbles, D.J., D.W. Fahey, K.A. Hibbard, D.J. Dokken, B.C. Stewart, and T.K. Maycock (eds.)]. U.S. Global Change Research Program, Washington, DC, USA, 470 pp., doi: 10.7930/J0J964J6.

Offsetting Patillas Reservoir Storage Decline by Conjunctive Use of a Coastal Aquifer, Salinas, Puerto Rico

Gregory Morris, Principal, GLM Engineering, San Juan, PR, gmorris@glmengineers.com
Juan Portalatín, Principal, GLM Engineering, San Juan, PR, jportalatin@glmengineers.com

Abstract

As reservoirs age they lose storage capacity and firm yield declines. Hydrologic conditions can also be modified as human activities change. At Salinas, Puerto Rico, recharge to the coastal aquifer has historically benefited from copious supplies of high quality irrigation water from the Patillas and Carite reservoirs, delivered in unlined canal and applied by furrow irrigation. As a result, deep percolation of irrigation water historically constituted about half the aquifer recharge.

Today the Patillas reservoir has only 41% of its original year 1914 capacity due to the combined effects of sedimentation and lowered operating level due to dam safety concerns. As a consequence of depleted reservoir capacity, water reallocation to municipal uses, reduced irrigation deliveries and implementation of high-efficiency irrigation techniques, the coastal alluvial aquifer has lost a major source of recharge, resulting in saline intrusion, salinization of municipal water supply wells, and water rationing affecting the municipal water supply. This situation is not unique to Puerto Rico's south coast, but also occurs in other much larger systems, such as Pakistan's Indus River Irrigation System command area.

Lacking other sources of supply and facing extremely high costs to restore reservoir capacity by either dredging or raising the dam, a highly cost-effective alternative is described in this paper which conjunctively utilizes the region's surface and ground water resources, mitigating the loss of reservoir capacity with aquifer storage. This is achieved by restoring aquifer recharge using water from the Patillas reservoir which would otherwise be discharged to the Caribbean Sea.

The strategies developed for Salinas, centering on the conjunctive utilization of both surface and ground water storage and optimization of the existing infrastructure, can be instructive for addressing similar problems in other jurisdictions.

Introduction

Overview: The water management problems faced by the coastal Municipality of Salinas on Puerto Rico's semi-south coast, mimic, on a small scale, the problems faced by many other systems in different parts of the world, including the world's largest and most complex irrigation

system, Pakistan's Indus River System. These systems are characterized by: a regulated surface water supply from a reservoir with diminishing capacity due to sedimentation; a downstream irrigation command area underlain by a fresh water alluvial aquifer in contact with saline water; and a history of "inefficient" furrow irrigation supplied by unlined canals which recharged the aquifer thereby making copious quantities of fresh water available to both irrigation and municipal wells. This type of system is conceptually shown in Figure 1.

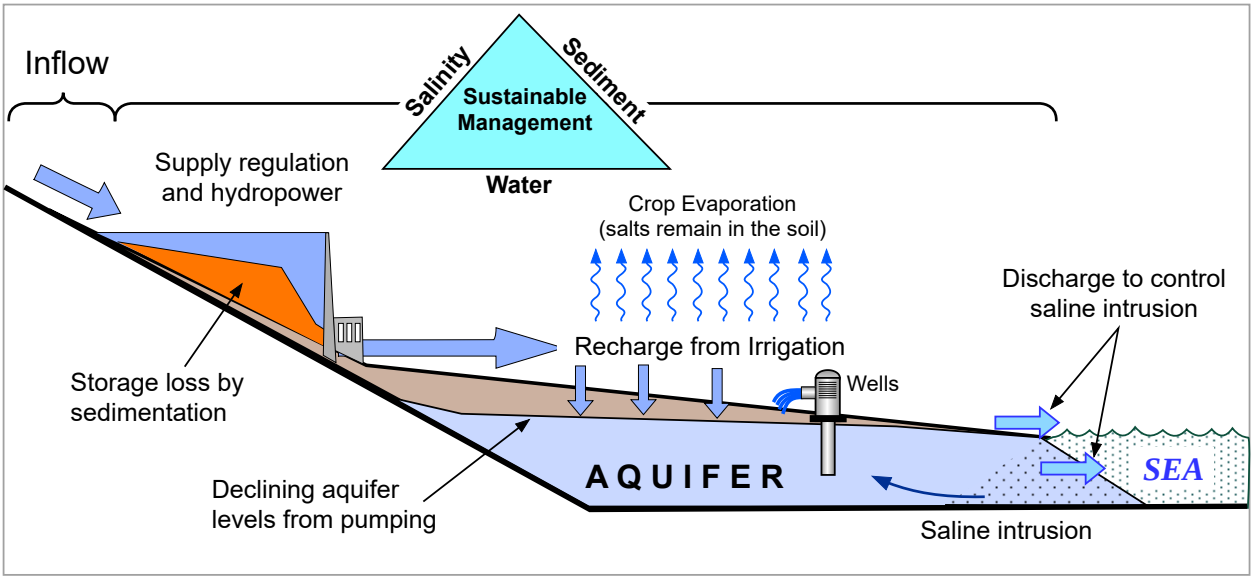

Figure 1: Conceptual model of coastal aquifer under the influence of regulated surface water recharge from irrigation deep percolation.

However, the hydrologic sustainability of these systems is challenged as ground water withdrawals increase for municipal and industrial (M&I) use, reservoir yield declines due to storage loss, and aquifer recharge declines in response to a shift toward "more efficient" technologies including canal lining and sprinkler and drip irrigation. In Salinas there has also been a decline in total acreage under irrigation. These factors adversely modify the historical hydrologic balance, resulting in saline intrusion within the aquifer and a net decline in fresh water availability.

In the Indus River System large scale increases in irrigation efficiency are as yet in the planning stage, and the effects of reservoir sedimentation on water supply availability are only starting to be felt. However, at Salinas the widespread increases in irrigation efficiency have already been implemented, and reservoir firm yield withdrawals have been diminished, resulting in the salinization of municipal ground water supplies and periods of municipal water rationing.

Study Area Description: The Town of Salinas (pop. 31,000), on the semi-arid south coast of Puerto Rico, overlies a coastal alluvial aquifer. About 4 mgd of municipal water is supplied from wells operated by the P.R. Aqueduct & Sewer Authority (PRASA). Industrial and military users also depend on wells, while irrigation supplies come from the combination of

unlined irrigation canals supplied by the Patillas and Carite reservoirs plus wells. These elements are shown in the location map in Figure 2.

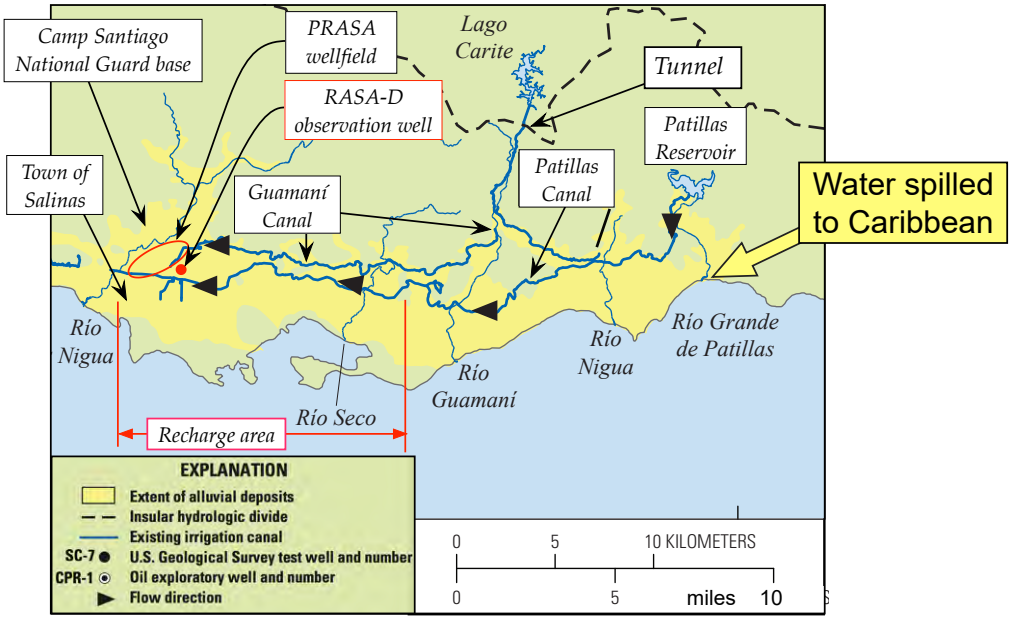

Figure 2: Location map for major hydrologic features of the Salinas area on Puerto Rico's southeastern coast. (adapted from Gómez-Gómez et al. 2014)

The deep percolation of irrigation water from canals and furrow irrigated fields has historically supplied about half the aquifer recharge. As illustrated by the water balance in Figure 3, in the 1960s approximately 30% of irrigation withdrawals percolated back into the aquifer. However, the 1970s saw sugarcane beginning to be replaced with year-around irrigation by crops requiring shorter irrigation seasons, shrinking irrigation acreage, declining canal deliveries, and replacement of furrow irrigation by higher-efficiency sprinkler and drip irrigation (Morris 1979). Data from the irrigation operator, the P.R. Electrical Power Authority (PREPA), show that over the past decade Patillas canal deliveries have averaged ~0.5 m^3s^{-1}, about one-third of delivery rate in the early 1960s. Municipal water also no longer returns to the soil via septic systems. Sewerage systems have been extended to most rural residential communities, and wastewater is now discharged to the sea or used for evaporative cooling following secondary treatment. These factors dramatically reduced the volume of deep percolation back into the aquifer (Rodríguez and Gómez-Gómez 2009).

The resulting unfavorable water balance in this narrow coastal aquifer has resulted in saline intrusion (Rodríguez and Gómez-Gómez 2008, 2009; Torres-González and Rodríguez 2015). The total solids concentration in water supply wells has been gradually increasing for at least 5 years and by 2018 exceeded the recommended secondary drinking water standard of 500 $mg \cdot l^{-1}$.

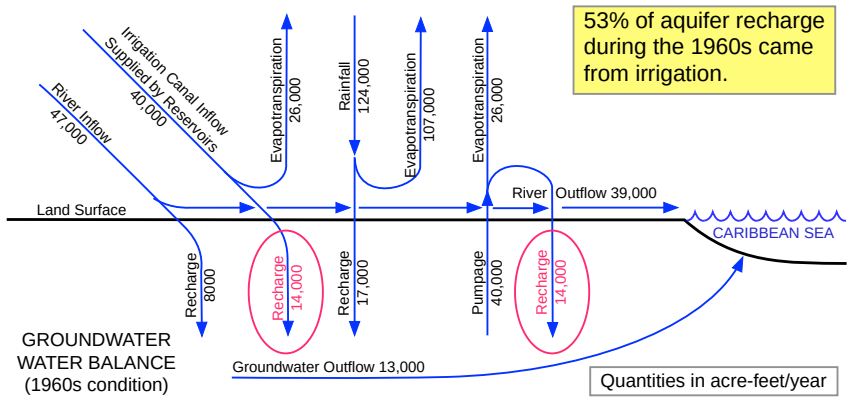

Figure 3: Historical water balance for alluvial aquifer in Salinas area (McClymonds and Díaz 1972).

Tropical reservoirs in semi-arid environments depend on large but infrequent rainfall events for recharge ((Jasechko and Taylor 2015). This has been the experience at Salinas, as seen from the water level data from USGS piezometer RASA-D (Figure 4). Yet surprisingly, the recharge provided by approximately 250 mm of rainfall delivered by hurricane María (Pasch et al. 2018) in September 2017, did not reverse the upward trend in TDS despite a rise of nearly 7 m in the water table. Rodríguez (2006) also documented high nitrate levels in the aquifer which has already caused well closures. Following sewerage connections, the main sources of nitrates are now agricultural fertilizers and manure spreading.

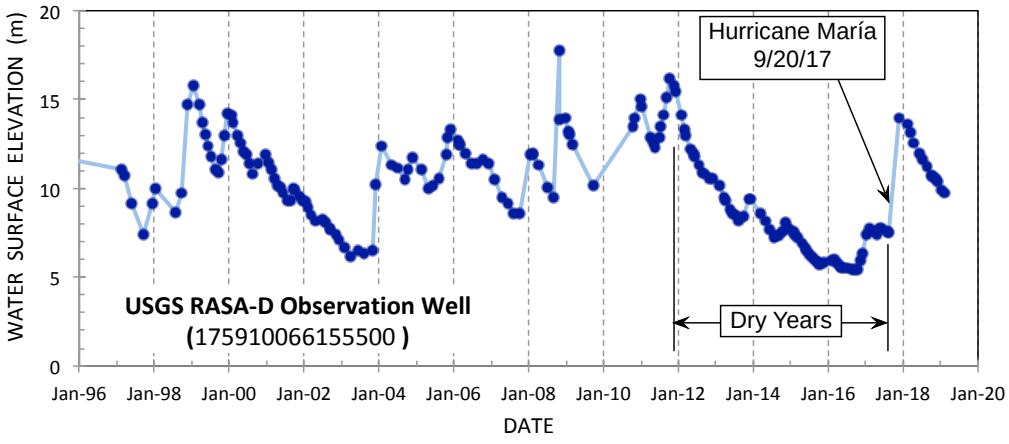

Figure 4: Water level data from RASA-D piezometer in Salinas showing rapid water level increase following large storms and multi-year periods of declining levels. See location in Figure 2 (USGS piezometer 175910066155500).

Responding to the long-term decline in water levels, on October 15, 2014, the P.R. Dept. of Natural and Environmental Resources (DNER) issued the "Technical Report for Critical Area Designation for the South Coastal Aquifer," which established a moratorium on new well construction. However, as 2015 developed into a drought year, increasingly strict measures were

implemented, and in Salinas from July 2015 to February 2016, PRASA was ordered to reduce groundwater withdrawal by 1/3 to protect against saline intrusion. Having no alternative water supply, this reduction was achieved by turning off wells and depressurizing the distribution system on a daily basis. Military, industrial and agricultural wells were unaffected by this order.

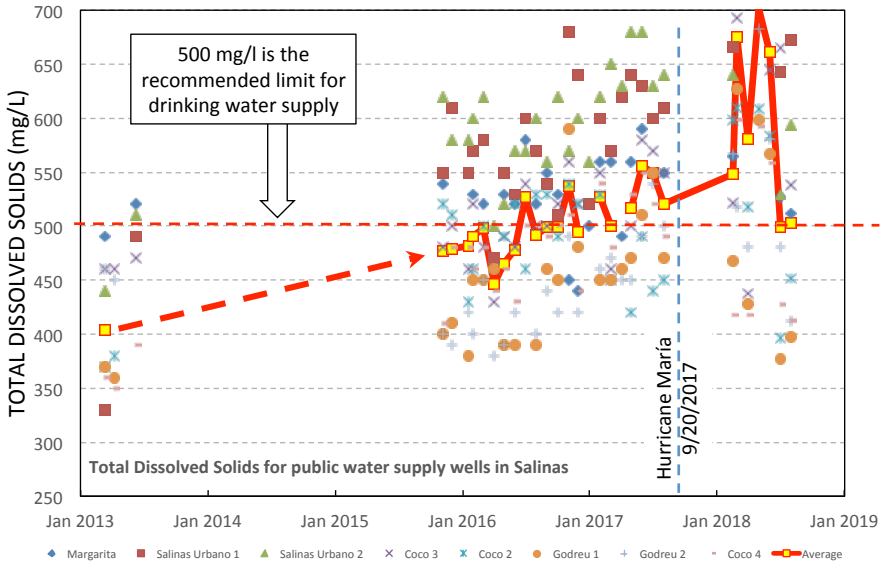

Figure 5: Trend of increasing dissolved solids content in wells for municipal supply in Salinas (data from PRASA)

Water Supply Options

Water supply alternatives for Salinas were evaluated when developing the Water Resources Plan for Puerto Rico (PR DNER 2016). Alternatives considered are briefly described below:

Water Reuse: The reuse of wastewater derived from the local groundwater was not considered feasible due to the high level of dissolved solids. Because Salinas wastewater originates from wells, to return this water to the aquifer after use would only increase the dissolved solids concentration.

Desalination: Seawater desalination was not considered a viable alternative due to high cost plus the availability of other less costly alternatives.

New Surface Water Development: The only streams in the area are ephemeral, Río Nigua in Salinas and Río Coamo about 10 km to the west in Santa Isabel. The Río Coamo irrigation reservoir was abandoned prior to 1970 due to sedimentation. New dam construction was also considered infeasible as no sites were identified in prior surveys of potential water

supply reservoirs. Thus, new surface water development was discarded as a potential alternative.

Enhance Utilization of Existing Reservoirs and Canals: Irrigators in Salinas have historically received water from the Patillas reservoir about 28 km easta of Salinas via the Patillas canal, and from the Carite reservoir via the Río Guamaní and Guamaní canal.

The Carite reservoir was constructed in 1914 in the headwaters of the north-flowing Río La Plata, and diverts water via tunnel into the upper section of the south-flowing Río Guamaní. The diverted water is captured by the Guamaní canal headworks at a lower elevation. The Carite reservoir is fully allocated and its spills flow downstream to the La Plata further downstream, one of the reservoirs supplying the San Juan metropolitan area, which is over-allocated.

However, on many days the Guamaní canal is essentially dry, and streamflow originating in the unregulated south-draining watershed above the Guamaní canal intake can be delivered to Salinas via the canal by simply opening the head gate at the river intake. This stream is ungaged, but based on other gaged streams in the area it is expected to be ephemeral. The flow volume is limited and unregulated and, by itself, cannot restore the aquifer balance.

The Patillas dam was built in 1914 as a hydraulic fill structure. In 2016, prior to hurricane María, gross reservoir capacity at the full supply level (FSL) of 67.7 m was surveyed at 12.7 Mm^3 (GLM Engineering 2016). This represents only 58% of its estimated original 21.9 Mm^3 capacity, which was computed by working backwards from a bathymetric survey in 1961 since data on the original volume data are lost. However, in 2016 it became necessary to permanently lower the normal pool to 64.0 m to mitigate liquefaction hazard during earthquake shaking (the Town of Patillas lies immediately downstream of the dam). This reduced 2016 gross storage to 8.93 Mm^3, leaving the reservoir with only 41% of its original capacity, without counting the additional volume loss by sedimentation from with hurricane María in 2017.

The reservoir's firm yield is already fully allocated by existing users who withdraw on average 0.82 m^3/s, as summarized in Table 1. With a capacity:inflow ratio of only 0.10, on average 62% of the 86 Mm^3 of average annual inflow is spilled and flows to the sea.

Table 1: Existing rates of withdrawal from Patillas Reservoir.

Water Use	m^3/s	Mgd
PRASA Patillas filter plant (floating intake in reservoir)	0.198	4.5
Patillas canal (includes 4.6 Mgd delivery to Guayama filter plant)	0.595	13.5
Evaporation losses from reservoir (calibration parameter)	0.014	0.3
Total	0.807	18.4

Mgd = million gallons per day

Options for Storage Loss

Options for addressing problems of storage loss in reservoirs are summarized graphically in Figure 6. The feasible options at Patillas reservoir fall into two categories: sediment removal and adaptive measures. Sediment removal includes both dredging and flushing, the latter not considered feasible at Patillas based on multiple considerations (lack of low level outlets, environmental impact, and incompatibility with current water supply commitments which requires essentially 100% availability).

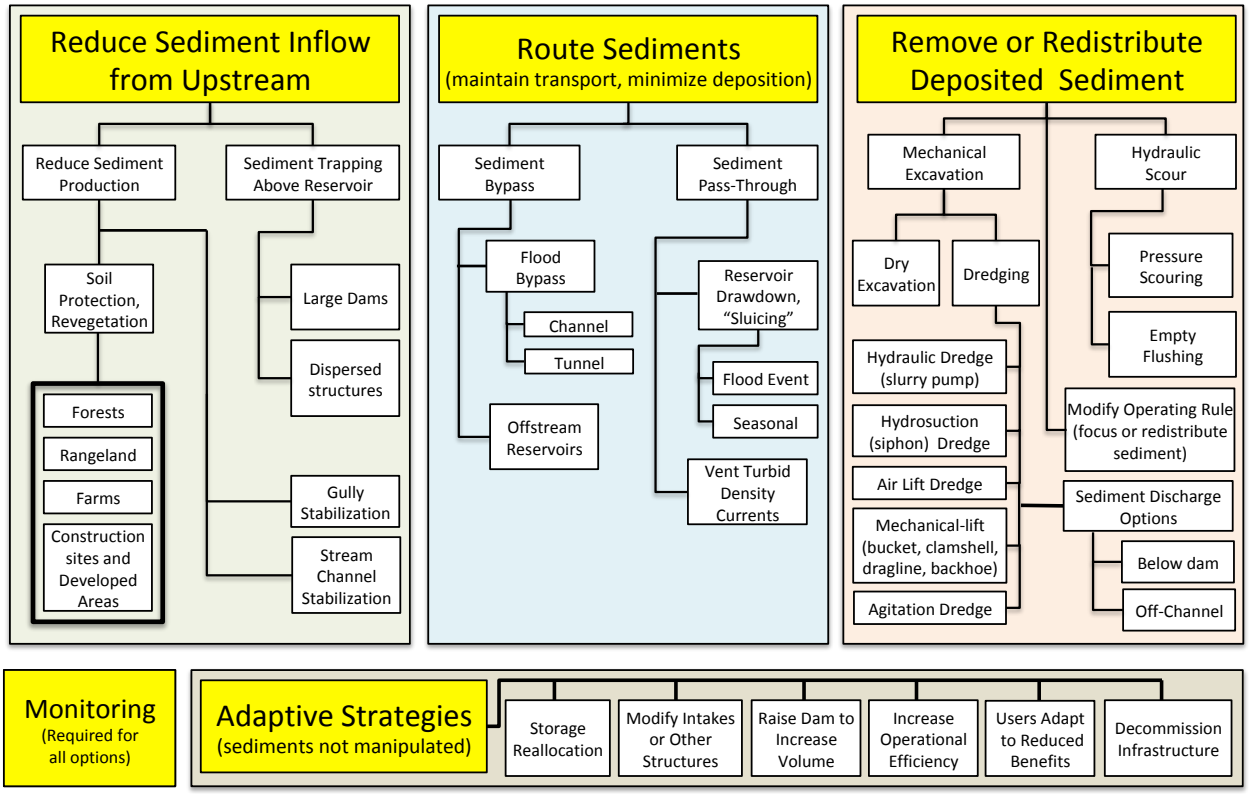

Figure 6: Methods for managing reservoir sedimentation (after Morris 2015).

Dredging and Dam Reconstruction: Two options for recovering reservoir storage capacity at Patillas are dredging and reconstruction of the dam to allow the FSL level to be raised back to 67.7 m. The all-in cost of dredging 6 Mm^3 of sediment from Loíza reservoir in Puerto Rico in 1996-1997 was ~\$10/m^3 (Morris and Fan 1998). To make a ballpark cost estimate this same unit dredging cost was applied to Patillas reservoir. The cost of reconstructing the hydraulic fill dam was roughly estimated to exceed \$50M. Table 2 compares these costs to the corresponding increase in firm yield determined by the reservoir simulation

model described below. Storage recovery by either dredging or dam reconstruction was considered too costly in relation to the water supply benefit to be considered feasible.

Table 2: Cost and Yield Benefit of Reservoir Storage Recovery Options.

Scenario and Description	Storage, Mm^3	Dredge Vol., Mm^3	Cost, $M	Yield m^3s^{-1}	Yield Mgd	Yield Increase m^3s^{-1}	Yield Increase Mgd
1) FSL 64 m, 2016 volume	8.93	0	0	0.82	18.6	0.0	0.0
2) FSL 67.7 m (reconstruct dam)	12.69	0	>50	0.89	20.3	0.1	1.7
3) FSL 64 m, dredge all sediment	18.14	12.97	130	1.00	22.8	0.2	4.2
4) FSL 67.7m, dredge all sediment	21.90	12.97	>180	1.06	24.2	0.2	5.6

Adaptive Strategy to Enhance Yield

Conjunctive Use: Given the substantial volume of water released over the spillway to the Caribbean Sea, and the need to restore aquifer recharge in Salinas, the option of conjunctive use of Patillas reservoir and ground water was evaluated. The strategy would restore higher flow rates along Patillas canal, diverting additional flow into the canal for recharge on an as-available basis, when the reservoir close to or at the point of spilling. The additional volume earmarked for recharge would be released into seasonally dry ephemeral streambeds and spreading basins. The spreading basins would be located in areas of high soil permeability and could be used for crops tolerant to intermittent flooding, such as some grasses for hay production. The main project components are conceptually illustrated in Figure 7.

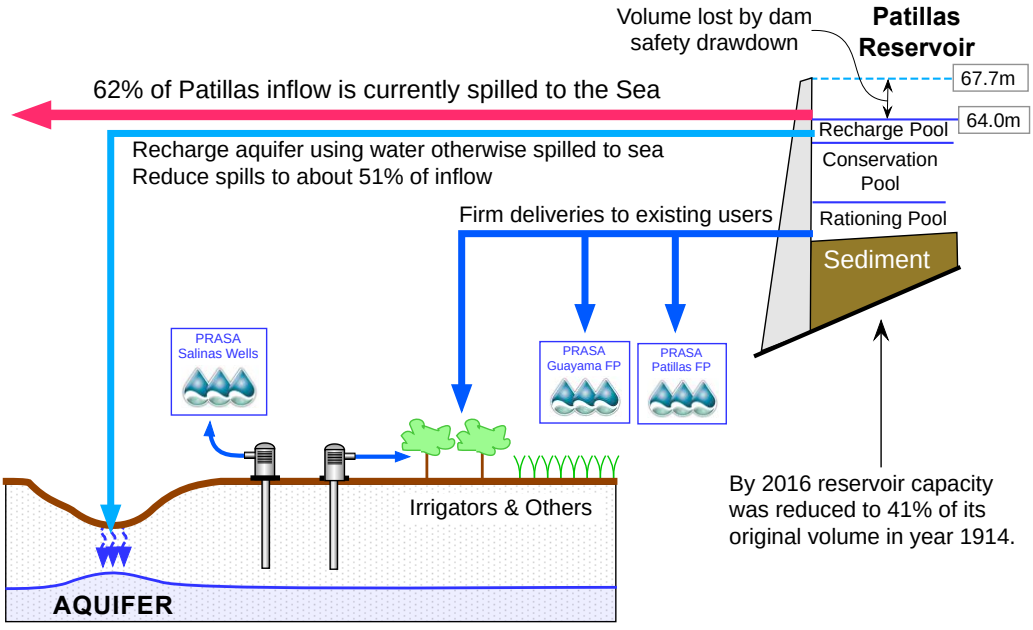

Figure 7: Project conceptualization schematic.

RESERVOIR SIMULATION

A reservoir simulation model was constructed to develop a storage-yield relationship for Patillas reservoir and to also compute the operating rule that could maximize diversions to aquifer recharge without affecting either the volume or reliability of deliveries to existing users.

Reservoir Operations: The reservoir was configured to have three operational pools as previously shown in Figure 7: recharge, conservation and rationing. The operational concept is described below.

1. Water supply deliveries to existing customers are made on a continuous basis, being reduced only when the water level falls into the rationing pool. When the reservoir levels falls within the rationing pool deliveries are reduced to 66% of normal firm yield.
2. Additional water is delivered into the Patillas canal for recharge when the reservoir level enters the recharge pool. The small recharge pool captures as much runoff as possible from small runoff events, and releasing at the highest rate possible to recharge areas subject to hydraulic limitations in the conveyance canal and recharge areas. These additional deliveries are halted as soon as the level drops into the conservation pool.

Reservoir firm yield for any storage capacity is defined by the yield which produces rationing on 1% of the days during the simulation period, and the reservoir is never allowed to empty.

The impact of the recharge pool on firm yield is extremely small because of its small volume. As illustrated in Figure 7, many agricultural users have the option of using either well water or canal water, and the recharge impact on firm yield can be reduced to zero by simply requiring one or two agricultural users to marginally increase their use of well water (which benefits from recharge), instead of using canal water, during periods of drawdown.

Reservoir Simulation Model: A reservoir water balance behavior simulation model (McMahon and Mein 1986) was constructed with a 1-day time step. The operating rules were incorporated into the model. The inflow time series consisted of the historical discharge data reported from 1961 to 2016 at the USGS gage station on Río Patillas (50092000). Rainfall records indicate this data period includes the most severe drought since year 1900, which occurred in 1967-68, as well as the 2015 drought which triggered water rationing in Salinas.

A constant reservoir draft rate was used to compute the firm yield. With little seasonal variation in temperature, water demands in Puerto Rico do not exhibit significant seasonal variations making this a realistic assumption. The model was calibrated against the recent USGS record of reservoir levels (gage 50093045). The gage adjustment factor to account for the 11% ungaged area and reservoir evaporation rate were the two calibration parameters, and both values fell within the expected ranges in the calibrated model. Calibration to historical reservoir levels during the most recent period of significant drawdown is shown in Figure 8 indicating a good fit.

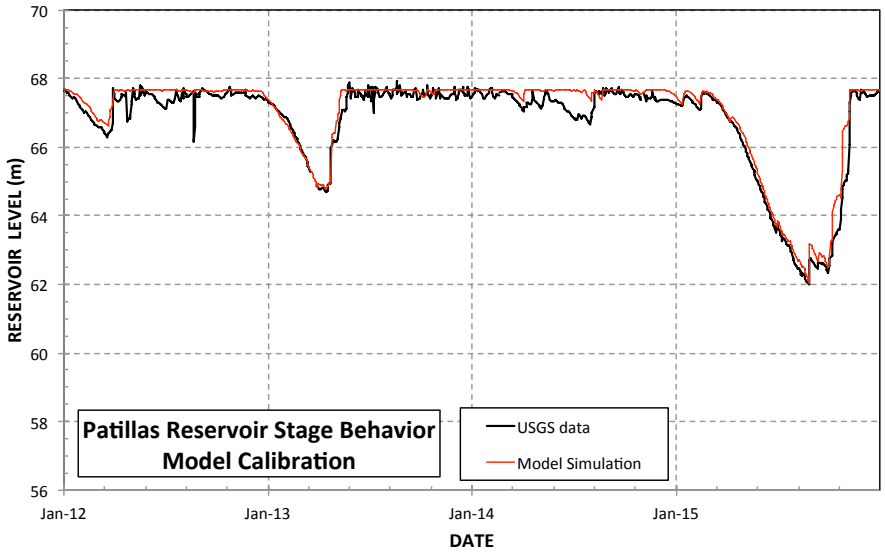

Figure 8: Results of reservoir behavior model calibration to historical water levels.

Simulation Results: The calibrated reservoir model was first exercised to determine the storage-yield relationship used to evaluate the benefits of storage recovery previously described in Table 2. The reservoir has historically not had specific pools assignments, so subsequent modeling focused on establishing pool limits and the draft rate for releases to recharge. Several rates of recharge delivery were evaluated and a maximum rate of 0.42 m^3/s (15 cfs) was selected based on the capacity of the irrigation canal (which has not been used to its design capacity for decades) and the anticipated limit of recharge capacity.

Simulation scenario names are listed below and consist of the pool elevation and the aquifer recharge flow rate: *"Max. Pool El. (ft) – Recharge Flow Rate (cfs)"*.

1. **222-0 (baseline condition)**. This corresponds to the water withdrawals given in Table 1 and the reservoir operated at a FSL of 67.7 m (222 ft). This baseline condition is provided for the purpose of comparison. There is no aquifer recharge under this scenario (there is no recharge pool).
2. **210-0**. Reservoir FSL 64 m (210 ft). This simulation corresponds to the 2016 condition with the reservoir level drawn down to a FSL of 64 m. There is no aquifer recharge under this scenario (there is no recharge pool).
3. **210-5**. Reservoir FSL is 64 m (210 ft). Aquifer recharge rate = 0.14 m^3s^{-1} (5 cfs or 3.2 Mgd).
4. **210-10.** Reservoir FSL is 64 m (210 ft). Aquifer recharge rate = 0.28 m^3s^{-1} (10 cfs or 6.5 Mgd).
5. **210-15**. Reservoir FSL is 64 m (210 ft). Aquifer recharge rate = 0.42 m^3s^{-1} (15 cfs or 10 Mgd).

Simulation results are summarized in Table 3. In all simulations the delivery rate to existing users remains unaltered, and the impact of the different rates of rationing delivery is reflected in the changing number of days of rationing per year. The average realized recharge rate represents total recharge divided by the number of days in the simulation. Note that the total beneficial water use, consisting of delivery to existing users plus the recharge volume, increases significantly. This is important because agricultural users depend on both canal water and ground water, and recharge which helps the aquifer is also helpful to the irrigation sector as well as the municipal and industrial users. Under the recommended alternative, 210-15, the average annual volume diverted to recharge (7.5 Mm^3) is greater than the average annual municipal water supply withdrawal for Salinas of 5.5 Mm^3yr^{-1} (4.0 Mgd).

Table 3: Summary simulation results.

	Yr 2015	Opn. Rule Scenarios for Reduced Storage				
Parameter	222-0	210-0	210-5	210-10	210-15	210-20
Input Parameters:						
Full Supply Level (FSL), m	67.7	64.0	64.0	64.0	64.0	64.0
Constant Delivery to Existing Users , m^3s^{-1}	0.79	0.79	0.79	0.79	0.79	0.79
Max Diversion Flow to Recharge, m^3s^{-1}	0	0	0.14	0.28	0.42	0.57
Simulation Results:						
Days Rationing, % of days	0.7%	1.1%	1.3%	1.4%	1.4%	1.4%
Days Reservoir Empty in Simulation Period	0	0	0	0	0	0
Avg. Days per Year Recharge is Possible	-	-	250	225	205	189
Avg. Realized Recharge Rate, m^3s^{-1}	-	-	0.10	0.18	0.24	0.29
Avg. Annual Recharge Volume, Mm^3		-	3.1	5.5	7.5	9.3
Total Beneficial Water Use, Mm^3yr^{-1}	25.4	25.3	28.4	30.8	32.8	34.6
Spillage to Sea, % of total inflow	62%	62%	58%	54%	51%	48%

Costs: A detailed cost estimate for the recharge system has not yet been worked out. However, inasmuch as this strategy focuses on optimizing the operation of existing canals and other infrastructure, the cost items are expected to consist of minor structures (e.g. recharge turnouts), automation of the Patillas head gate, and miscellaneous improvements, in all totaling less than $0.3M. Another $0.25M, approximately, may be anticipated for monitoring infrastructure including additional observation wells to monitor both level and quality within the aquifer. The most significant cost, if required, will be land acquisition for recharge spreading areas.

Conclusions

Sustaining water supply yield by restoring reservoir capacity can be extremely costly, to the point of being infeasible. However, adaptive water management strategies may exist for sustaining or enhancing water yield which are far less costly than the restoration of reservoir capacity.

This paper described a conjunctive use strategy for a reservoir-coastal aquifer system in which the reservoir operating rule has been optimized to maximize the diversion to aquifer recharge of water that would otherwise be spilled to the sea. Although surface and ground water resources have traditionally managed separately, in Salinas and other systems having similar characteristics, such as the Indus River Irrigation System, surface water deliveries from reservoirs and alluvial aquifers are intimately interconnected. When reservoir capacity is lost to sedimentation in these systems, there is the opportunity to manage both the reservoir and the ground water system to sustain or increase total water yield at low cost compared to other alternatives.

Acknowledgements

This project is being undertaken under contract with the P.R. Department of Natural and Environmental Resources, using FEMA funds for Hazard Mitigation (drought). The Municipality of Salinas, P.R. Electrical Energy Authority and P.R. Aqueduct and Sewer Authority are cooperating agencies.

References

GLM Engineering. (2016). *Sedimentation Survey of Lago Patillas, Puerto Rico*. P.R. Electrical Energy Authority, San Juan, Puerto Rico.

Gómez-Gómez, F., Rodríguez-Martinez, J., and Santiago, M. (2014). *Hydrogeology of Puerto Rico and the Outlying Islands of Vieques, Culebra, and Mona*. USGS Scientific Investigations Map 3296, Reston, Virginia, 40.

Jasechko, S., and Taylor, R. G. (2015). "Intensive rainfall recharges tropical groundwaters." *Environmental Research Letters*, 10(12), 124015.

McClymonds, N. E., and Díaz, J. R. (1972). *Water Resources of the Jobos Area, Puerto Rico: A Preliminary Appraisal 1962*. San Juan.

McMahon, T. A., and Mein, R. G. (1986). *River and Reservoir Yield*. Water Resources Publications, Littleton, Colorado.

Morris, G. L. (1979). "Regional Development and Water Resource Management: Implications of a Changing Agricultural Sector on Puerto Rico's South Coast." PhD Dissertation, Gainesville, FL.

Morris, G. L. (2015). "Management Alternatives to Combat Reservoir Sedimentation." *Proc. Intl. Workshop on Sediment Bypass Tunnels*, Zurich.

Morris, G. L., and Fan, J. (1998). *Reservoir Sedimentation Handbook*. McGraw-Hill Book Co., New York.

Pasch, R. J., Penny, A. B., and Berg, R. (2018). *Hurricane María*. National Hurricane Center Tropical Cyclone Report, NOAA, National Weather Service.

PR DNER. (2016). *Plan Integral de Recursos de Agua*. P.R. Dept. Natural & Environmental Resources, San Juan, Puerto Rico.

Rodríguez, J. M. (2006). *Evaluation of Hydrologic Conditions and Nitrate Concentrations in the Río Nigua de Salinas Alluvial Fan Aquifer, Salinas, Puerto Rico, 2002--03*. Reston, Virginia, 38.

Rodríguez, J. M., and Gómez-Gómez, F. (2008). *Historical ground-water development in the Salinas alluvial fan area,Salinas, Puerto Rico, 1900-2005*. Reston, Virginia.

Rodríguez, J. M., and Gómez-Gómez, F. (2009). *Historical ground-water development in the Salinas alluvial fan area, Salinas, Puerto Rico, 1900-2005*. U.S. Geological Survey.

Torres-González, S., and Rodríguez, J. M. (2015). *Hydrologic Conditions in the South Coast Aquifer, Puerto Rico, 2010–15*. San Juan.

Optimizing Hydropower Facility Operations Via Acoustic Sediment Monitoring

Achilleas Tsakiris, Hydraulic Specialist, Northwest Hydraulic Consultants, Olympia, WA, atsakiris@nhcweb.com
Andre Zimmermann, Principal Geomorphologist, Northwest Hydraulic Consultants, Vancouver, BC, AZimmermann@nhcweb.com
Dawson Meier, Technologist, Northwest Hydraulic Consultants, Vancouver, BC, DMeier@nhcweb.com
Anthony Reynolds, Engineering Technologist, Northwest Hydraulic Consultants, Vancouver, BC, treynolds@nhcweb.com

Extended Abstract

Hydroacoustic monitoring of sediment movement in rivers with hydrophones and geophones has become increasingly popular among agencies and research institutions in recent years, as it provides continuous and unattended observations of sediment movement in a river (e.g., Gray et al., 2010; Hilldale et al., 2014; Rickenmann, 2017). This paper presents the application of a hydroacoustic sediment monitoring system for continuously tracking the relative amount and timing of sediment conveyed through hydropower facilities that builds on testing conducted at pipeline crossing and river systems. The developed hydroacoustic sediment monitoring system allows evaluating when sediment is mobile at the intakes of hydropower facilities and provides their operators with valuable, real-time information on sediment movement. This information can be used to optimize hydropower generation, especially the timing and duration of drawdowns for sediment flushing and flood regulation. The paper first presents the main components that comprise the hydroacoustic sediment monitoring system and then results, which were collected during its deployment at a hydropower facility and demonstrate its capability to monitor sediment movement at the facility intake.

The basis of the developed hydroacoustic sediment monitoring system is a hydrophone sensor that measures the sound generated by the sediment moving at the intake (Figure 1a and b). The hydrophone sensor is mounted on the end of a steel pipe (Figure 1b), which is placed vertically at the intake of a hydropower facility, such that the hydrophone remains submerged during the expected flows at the intake. The hydrophone captures the sound signals that are produced by interaction of moving sediment particles with the bed during a 1-minute interval every 5 minutes. These signals are amplified (Figure 1c) and then recorded on a computer (Figure 1d) as sound files, which are then processed using software developed as part of this project. The processing involves a series of filters to remove noise introduced into the acoustic signal by ambient sources and the electronics. The filtered data are then used to derive the number of sediment particle impacts that have occurred per minute, as well as other descriptive statistics that index how much sediment is moving. This information is conveyed to the facility Program Logic Controller (PLC) using the MODBUS protocol enabling operators to monitor sediment mobility in real-time. The data are also stored remotely in the Aquarius Time-Series database of Northwest Hydraulic Consultants (NHC) and published using the Aquarius Web-portal to provide plant managers and NHC scientists the opportunity to conduct more detailed analysis including the identification of long-term trends in sediment movement patterns.

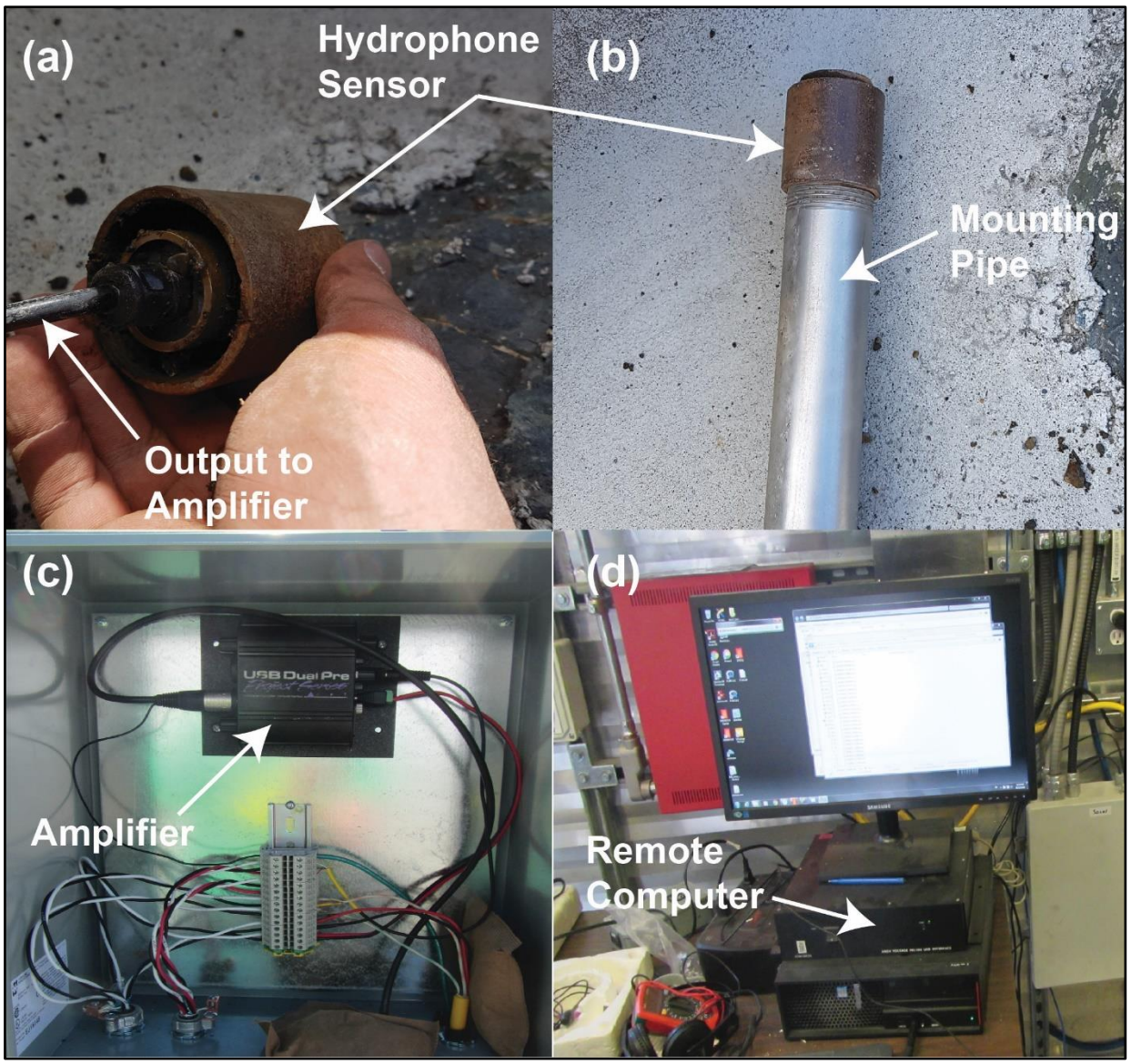

Figure 1. (a) Hydrophone sensor; (b) hydrophone sensor mounted on metal pipe; (c) remote computer for logging; (d) hydrophone signal amplifier

The performance of the sediment acoustic monitoring system was assessed at the Forrest Kerr and the Upper Lillooet hydroelectric facilities, which are located on the Iskut and Lillooet Rivers, respectively. The sediment acoustic monitoring system deployed at the Forrest Kerr facility is considered in this paper for demonstrating the capability of this system. The Forrest Kerr hydropower facility is located in Northwest British Columbia at the confluence of the Iskut River and the Forrest Kerr creek. The facility operates as a run-of-the-river plant and is capable of 195 MW of power generation diverting approximately 8,300 cubic feet per second (250 cubic meters per second). The facility features a sluiceway, which is used to convey incoming bedload to the reach downstream of the facility, thus preventing it from entering the turbine intakes (Figure 2). The hydrophone was deployed along the left bank, near the entrance of the sluiceway for detecting sediment moving in the sluiceway (Figure 2).

Figure 2. Aerial view of the Forrest Kerr hydropower facility and location of the hydrophone sensor (image from Bethany Duarte, HydroReview)

A hydrophone recording from the Forrest Kerr facility between August 27, 2018 and September 17, 2018 is shown in Figure 3 along with the water discharge measured at the plant intake over the same period. The results in Figure 3 show that the hydrophone is capable of detecting the commencement and cessation of sediment motion, which are characterized by a sudden increase and decrease in the detected number of particle impacts. Knowledge of the incipient and cessation of sediment motion further allows estimating the duration of sediment motion.

At the same time, the results in Figure 3 show that the deployed acoustic monitoring system may provide an estimate of the relative magnitude of the amount of sediment that is being transported. During the period between August 30th, 2018 and August 31st, 2018 more than 1.5 million particle impacts were recorded with up to 19,300 particle impacts recorded during a 1-minute recording interval. In the subsequent, smaller flood occurring between September 9th and 12th 2018, only up to 2,200 particle impact detections in a 1-minute interval were detected thus indicating lower mobilization of particles in comparison to the August 30th-31st event.

Synchronous monitoring of the flow discharge along with particle impact number, as in Figure 3, helps to identify the effects that facility operations have on the magnitude and timing of the sediment movement. An increase in the sluiceway discharge for sluicing sediment on August

27th, 2018 resulted in significant sediment mobilization captured by the hydrograph. The hydrophone results show that sediment during this event was predominantly mobilized as the sluiceway discharge was increased, suggesting that an ample supply of sediment had accumulated at the headpond prior to this sluicing event (e.g., Mao et al., 2014). The sluicing of sediment in this first sluicing event depleted its availability in the headpond, leading to smaller sediment mobilization during the larger flows between August 28th and 30th, where fewer particle impacts were detected by the hydrophone. Once the flow in the sluiceway was reduced between August 30th and 31st, 2018, a large sediment transporting event was detected by the hydrophone. This second sediment transporting event occurred during the falling limb of the hydrograph (Figure 3) and is indicative of counterclockwise bedload transport hysteresis due to the limited mobile sediment availability (e.g., Mao et al., 2014).

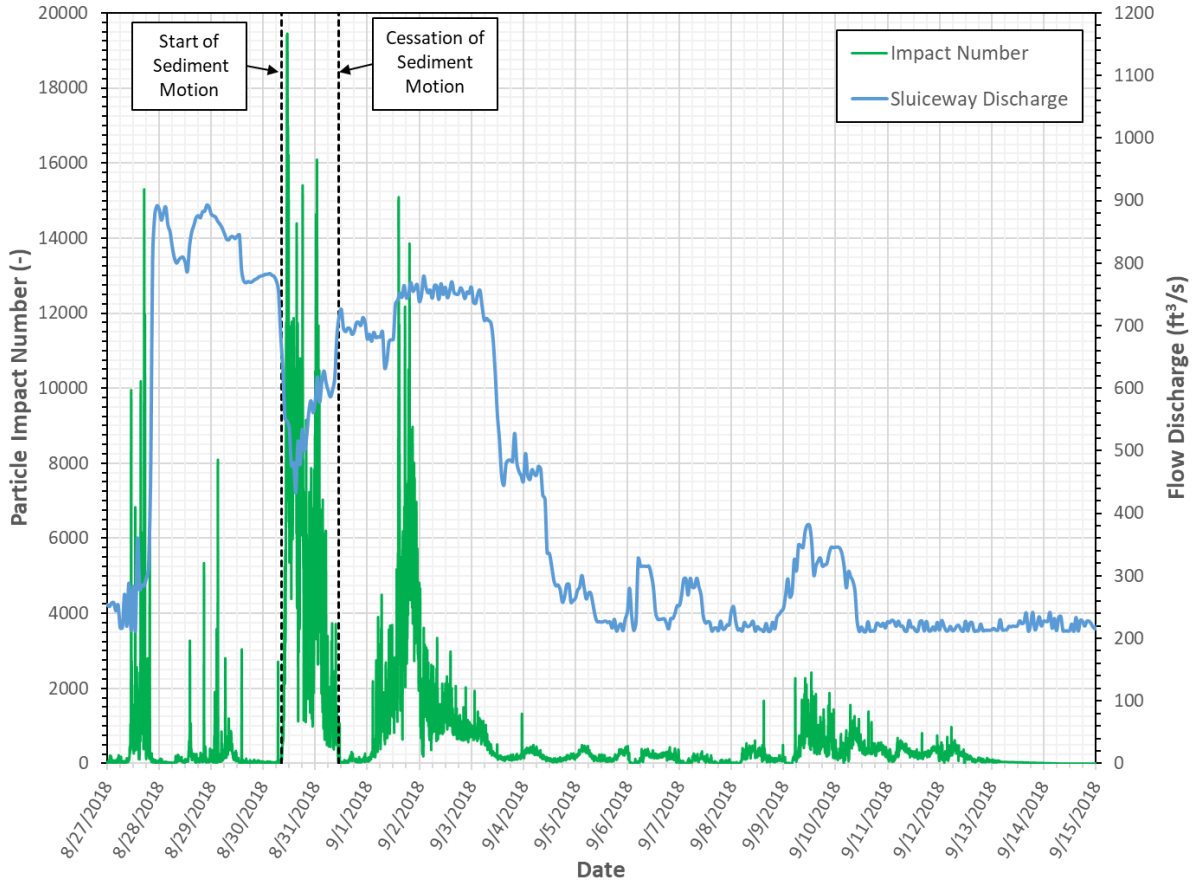

Figure 3. Number of particle impacts recorded by the hydrophone and corresponding discharge measured at the Forrest Kerr facility intake between 8/27/2018 and 9/15/2017

The data obtained with the acoustic sediment monitoring system since its deployment shows that the system is capable of monitoring the timing and relative magnitude of sediment movement at hydropower facilities on a continuous basis. The system can thus provide managers and operators of hydroelectric facilities with a reliable tool for optimizing their operation (see also Zimmermann et al., 2019 in these proceedings). The acoustic sediment monitoring system could also be deployed at other locations along a river and be used to assess when coarse sediment particles (e.g., gravel and cobbles) start to move and the relative intensity of their movement. Such information can help operators and scientists understand the

conditions that lead to the incipient motion of sediment particles and provide useful information for studying the hysteresis in their movement. Along these lines, future work will aim to distinguish the different mobile sediment size fractions based on the acoustic frequency signatures of each fraction (Tsakiris et al., 2014).

References

Gray, J.R., Laronne, J.B., Marr, J.D.G. (2010) Bedload-surrogate monitoring technologies: U.S. Geological Survey Scientific Investigations Report 2010–5091, 37 p. Available at http://pubs.usgs.gov/sir/2010/5091.

Hilldale, R. C., Goodwiller, B., Carpenter, W. O., and Chambers, J. P. (2014). Measuring coarse bed load using hydrophones. Closeout Report SRH-2014-37, United States Bureau of Reclamation Research and Development Office, Science and Technology Program, 24 pp. Available at: https://www.usbr.gov/research/projects/detail.cfm?id=4864.

Mao, L., Dell'Agnese, A., Huincache, C., Penna, D., Engel, M., Niedrist, G. and Comiti, F. (2014) Bedload hysteresis in a glacier-fed mountain river. *Earth Surface Processes and Landforms*, *39*(7), 964-976.

Rickenmann, D. (2017). Bed-load transport measurements with geophones and other passive acoustic methods. *Journal of Hydraulic Engineering*, 143(6), 03117004. DOI: 10.1061/(ASCE)HY.1943-7900.0001300.

Tsakiris, A.G., Papanicolaou, A.T.N. and Lauth, T.J. (2014). Signature of bedload particle transport mode in the acoustic signal of a geophone. *Journal of Hydraulic Research*, 52(2), 185-204.

Zimmermann, A.E., Vasquez, J., Haught, D., Tsakiris, A., and Dudil, A. (2019). Revising the basis of sediment management in rivers: Incorporating real-time sonar, hydroacoustic and hydrodynamic field data. Federal Interagency Sedimentation and Hydrologic Modeling Conference, Reno, NV. June, 2019.

Projected Changes in Sedimentation at Seven USACE Reservoirs on the Southern Plains

Ariane O. Pinson, Climate Science Specialist, U.S. Army Corps of Engineers, Albuquerque District, Albuquerque, NM, Ariane.Pinson@usace.army.mil
Pierre Y. Julien, Professor, Department of Civil and Environmental Engineering, Colorado State University, Fort Collins, CO 80523, pierre@engr.colostate.edu
Bryan E. Baker, Hydraulic Engineer, Remote Sensing-GIS Center of Expertise, Cold Regions Research and Engineering Lab, U.S. Army Corps of Engineers, Hanover, NH, Bryan.E.Baker@usace.army.mil
Kathleen D. White, Climate Preparedness and Resilience Community of Practice Lead, CW Guidance Program, US Army Corps of Engineers Headquarters, Washington, DC, Kathleen.D.White@usace.army.mil

Abstract

Reservoir sedimentation rates are sensitive to both climate and land use activities within the contributing watershed. Current conditions have been successfully modeled using the Revised Universal Soil Loss Equation (RUSLE) to estimate annual soil loss coupled with an estimate of the sediment delivery ratio, the amount of this sediment that arrives annually at a reservoir. To assist with USACE strategic planning efforts, the Climate Preparedness and Resilience Community of Practice has used these same techniques to model future reservoir sedimentation rates using CMIP5 modeled precipitation and runoff data (Bureau of Reclamation 2013), projections of future land use and land cover data from the USGS Land Carbon study (Sleeter et al. 2012), and data from the USACE Reservoir Sedimentation Information Data Portal. The results provide a framework for a screening-level assessment of medium and long-term changes in sedimentation monitoring and mitigation needs within the USACE reservoir portfolio.

Introduction

The US Army Corps of Engineers (USACE) is the largest operator of infrastructure in the United States for the purposes of navigation, flood risk reduction, hydropower generation, recreation, and water supply. Many of these structures have operated for more than 50 years and all are likely to continue to serve their authorized purposes for many future generations (Pinson et al. 2016). Consequently, current infrastructure and planned infrastructure must not only perform under current conditions, but also under future hydrologic conditions that may be significantly different from present (Darcy 2014).

The USACE infrastructure portfolio includes approximately 700 dams and other structures that impound reservoirs. Sedimentation at all reservoirs is an inevitable problem leading to reductions in a reservoir's storage capacity over time (Morris and Fan 1998, Brekke et al. 2009, Graf et al. 2010, Kondolf et al. 2014). This volume reduction due to sedimentation over the life cycle is considered in reservoir design through designating an inactive or dead pool storage zone (USACE 1995, 1997).

Sedimentation rates are not fixed, but vary due to changes in precipitation amount and form, runoff discharge and timing, wildfire, soil conditions, land use and land cover in the contributing watershed, and once in a reservoir, sedimentation may occur outside the inactive pool, thereby affecting reservoir (Morris and Fan 1998). Changing climate, land use and other

conditions in a reservoir's contributing a watershed may cause sedimentation rates to differ significantly from the historical rates used in the reservoir design.

Across the United States, the number of potential new dam sites is limited and reservoirs that fill with sediment cannot easily be replaced (Morris and Fan 1998). In addition, the cost of sediment removal is prohibitive for most reservoirs. Consequently, it is important to manage sedimentation to ensure the long-term sustainability of the reservoir and the authorized functions it provides. For agencies such as USACE that manage large reservoir portfolios (Pinson et al. 2016), identifying reservoirs with current sedimentation problems and those that may become problematic under changing future conditions enables prioritization of sediment monitoring and mitigation activities.

This pilot study investigates long term changes in sedimentation at seven USACE reservoirs in the South Platte, Arkansas, and Canadian River basins under historical and future climate and land use conditions (Figure 1).

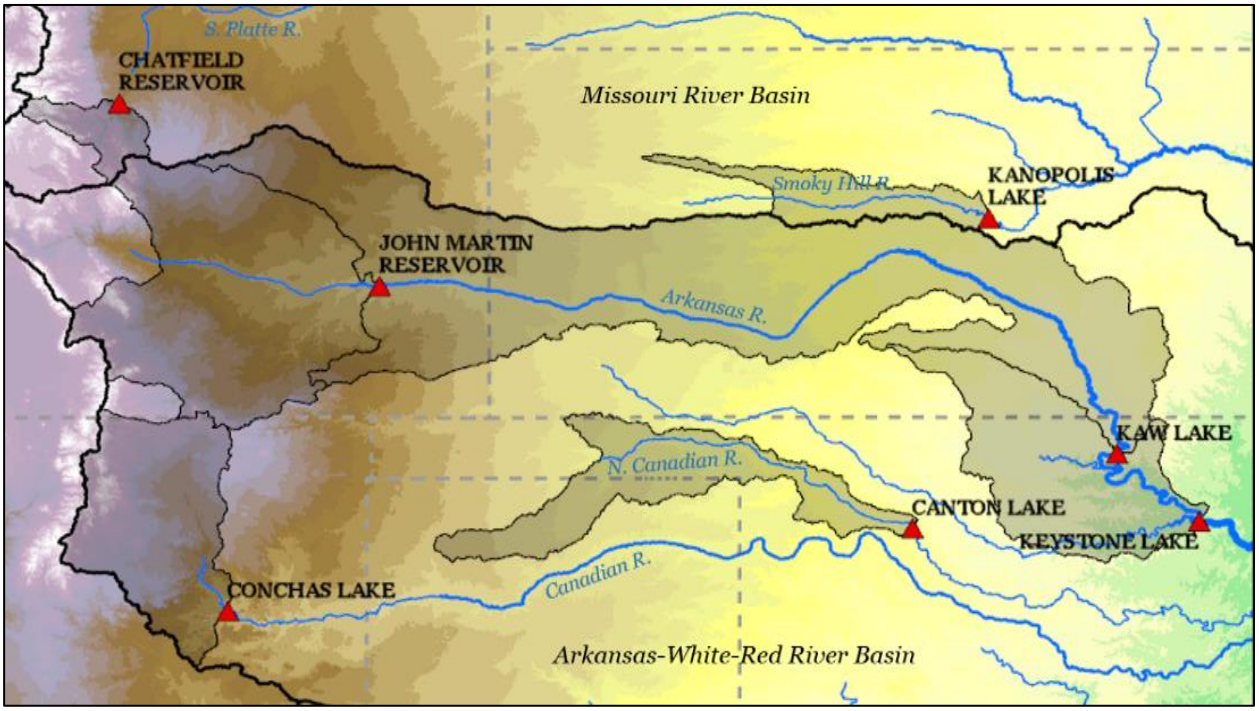

Figure 1. Map showing the contributing watersheds for the seven southern Plains reservoirs in this study (partial watershed boundaries indicate the presence of upstream dams where sediment capture is assumed to be 100%).

Data and Methods

Reservoir Selection

Seven reservoirs (Figure 1, Table 1) were selected from the USACE Reservoir Sedimentation Information Data Portal (https://maps.crrel.usace.army.mil/projects/rcc/portal.html, RSI Portal) with capacity loss data obtained at two points in time separated by a period greater than 20 years and where the methodology used to estimate capacity loss was the same for both end

points. This controlled both for short-term fluctuations in sedimentation rates and changes in capacity loss due to changes in data acquisition method.

Historical Sedimentation

For each reservoir, data from the RSI Portal was used to determine historical sediment yield (SY) at the reservoir as the average annual capacity loss across all pools. For each reservoir's contributing watershed, annual gross soil loss (A) for the period of each reservoir's sedimentation data (POR) was calculated using the Revised Universal Soil Loss Equation (RUSLE) (Wischmeier and Smith 1978, Renard et al. 1997):

$$A = R*K*LS*C*P ,$$

where A is the average annual soil loss (t ha^{-1} y^{-1}), R is the rainfall/runoff erosivity (MJ mm ha^{-1} h^{-1} $year^{-1}$), K is the USDA soil erodibility factor (t ha h ha^{-1} MJ^{-1} mm^{-1}), LS is the slope length and steepness factor (unitless), C is the cover management factor (vegetation cover, unitless), and P is the erosion control practice (unitless, set equal to 1 for landscape studies). Erosivity was calculated using historical precipitation data (Livneh et al. 2013) and the cover management factor was based on historical land cover data for the United States (Sohl et al. 2016). A discussion of the data and calculation of the factors contributing to soil loss is detailed in the appendix. Because the POR for each reservoir's sedimentation data is different, for each reservoir the calculation of historical soil loss used the mean monthly precipitation for the reservoir's POR as well as the land cover (C) for the midpoint year of the POR.

Historic gross soil loss and reservoir capacity loss were used to calculate the sediment delivery ratio (SDR= SY/A) for each reservoir (Julien 2018). The SDR reflects the unique relationship between watershed conditions and SY, implicitly encompassing factors such as streambank and gully erosion, or floodplain storage (Kane and Julien 2007). Streambank and gully erosion are poorly characterized at large spatial scales even though they can contribute as much as 85-90% of the total yield in some watersheds (Fox et al. 2016). Because of floodplain storage and loss, sediment yield may differ significantly from the denudation rate in the source regions (Allen 2017). This study makes the simplifying assumption that the SDR reflects the long term rate at which channel and floodplain erosion and deposition processes move sediment from the watershed to the reservoir, and that, absent other data, this rate will remain constant in the future.

Table 1. Historic sediment delivery ratio (SDR) for seven USACE reservoirs.

NIDID	Reservoir	Method*	Watershed Area (km^2)	Start and End Survey Years	Reservoir Capacity Loss SY (m^3 yr^{-1})	Watershed Soil Loss A (m^3 y^{-1})	SDR (SY/A)
OK10316	Canton	RC1	14,796	1950-1977	1,047,363	4,652,215	0.22513
CO01281	Chatfield	RC1	3,273	1977-2010	71,908	4,870,874	0.01476
NM00006	Conchas	RC1	18,915	1942-1986	2,444,789	37,473,919	0.06524
CO01283	John Martin	RC1	33,957	1957-1999	1,243,834	27,524,751	0.04519
KS00005	Kanopolis	RC10	6,322	1960-1993	547,928	3,867,124	0.14169
OK20509	Kaw	RC1	72,929	1975-1995	3,135,388	20,723,192	0.15130
OK10309	Keystone	RC1	20,347	1965-1988	9,481,829	12,618,622	0.75142

**Survey Method: RC1 = Range Line / Cross Section, 1 ft; RC10 = Range Line/Cross Section, 10 ft*

Future Sedimentation

Change in reservoir SY under changing future climates is modeled as the product of the historic SDR and future annual average gross watershed erosion (A). A is calculated using the RUSLE model, in which the erosivity factor is calculated using the full ensemble of CMIP5 Bias-Corrected Spatially Disaggregated model precipitation runs (see appendix) for the historic (1950-1999) and two future periods: 2050 (2035-2064) and 2085 (2070-2099) for the high CO_2 concentration (RCP 8.5) and low CO_2 concentration (RCP4.5) scenarios (Bureau of Reclamation 2013).

In addition, soil loss was calculated in two ways to better understand the potential roles of both climate and land use change in future rates of reservoir sedimentation: (1) land cover values were kept constant at their 1992 values; and (2) future land cover values were obtained from the USGS Land Carbon dataset (Sohl et al. 2014) for both the low future emissions (B1) and high future emissions (A2) scenarios for the years 2050 and 2085 (see the appendix for a discussion of the relationship between the precipitation and land cover scenarios).

Results

Changes in sediment yield are projected for all seven reservoirs as a result of both changes in precipitation and changes in land use patterns (Figure 2, bottom axis). Holding land cover constant at 1992 values (Figure 2, top row), the impact of changes in precipitation is small (<5%) and variable in sign across the study area under both future precipitation scenarios (RCP 4.5 and 8.5). The exceptions are the larger declines in sediment yield at John Martin and Conchas in the southwestern part of the study area under the higher emissions (RCP 8.5) scenario.

When projected changes in land cover are included in the model (Figure 2, bottom), reservoir sediment yield increases by 5% or more at Kanopolis, Kaw, Canton and Chatfield by 2085 under both scenarios. Except for Chatfield Reservoir, these changes are driven by the projected conversion of natural grasslands to cropland (Figure 3). Changes in sediment yield of less than 5% by 2085 are projected to occur at Conchas, Keystone and John Martin. Conchas and John Martin both see reductions under the higher-emissions scenario, with sediment yield at John Martin decreasing by more than 5%.

Large changes in sediment yield, however, do not directly translate into large changes in the rate of reservoir capacity loss (Figure 2, left axis): if a reservoir is large compared to its current annual sediment yield, it may be resilient to increases in yield. For example, the contributing watershed for Chatfield is steep and forested with low current rates of capacity loss (0.017% yr^{-1}). Small changes in future land use and erosivity have proportionately large effect on yields (increases as high as 14.58%) but comparatively small effect on the average annual rate of capacity loss (<=-0.001359% yr^{-1}). In contrast, Canton has a higher current rate of capacity loss (0.356% yr^{-1}), and a lower change in future sediment yield (increases as high as 8.05%), with a comparatively larger consequence of the average annual rate of capacity loss (a gain of as 0.031% yr^{-1}).

But do these changes translate into significant changes in sedimentation vulnerability? Comparison of observed average annual capacity loss rates with projected future capacity loss rates (Figure 4) shows that the projected capacity loss rates are small compared to current rates: most of the data points fall along the red line, indicating that observed and project loss rates are almost the same. Under a high emissions scenario (RCP 8.5), Conchas, Canton and John Martin

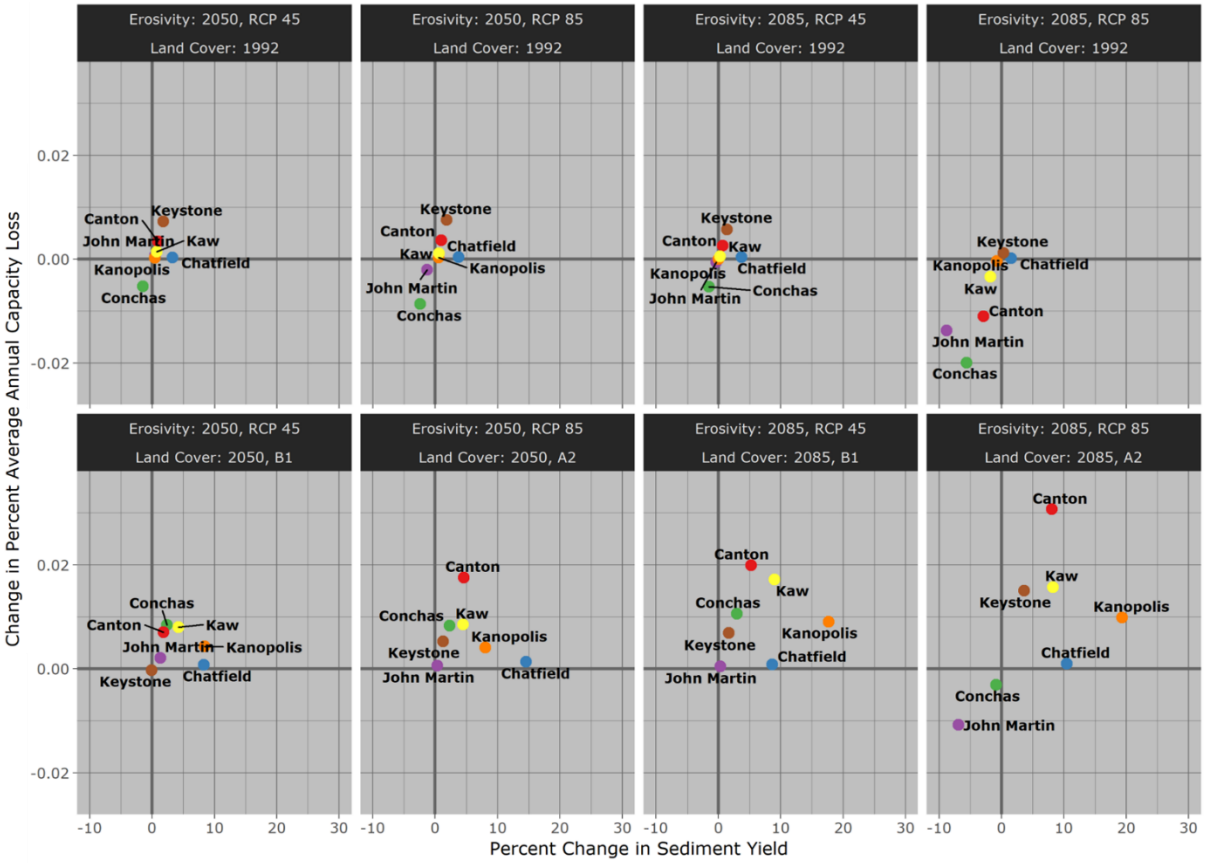

Figure 2. Change in sediment yield at seven USACE reservoirs by climate and land cover scenario.

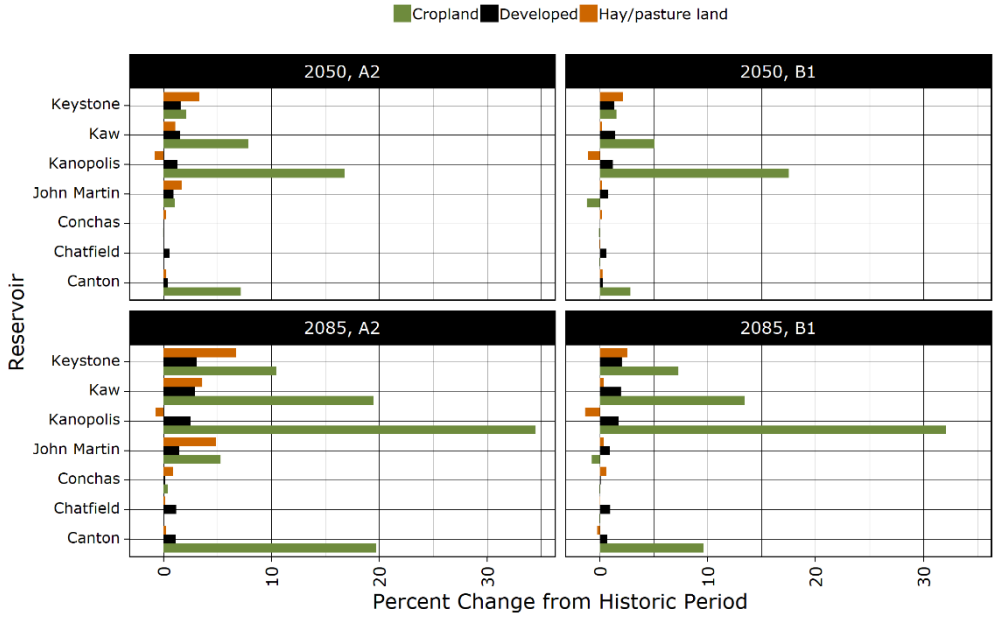

Figure 3. Percent change of watershed in each land cover type by land cover scenario relative to the historic period.

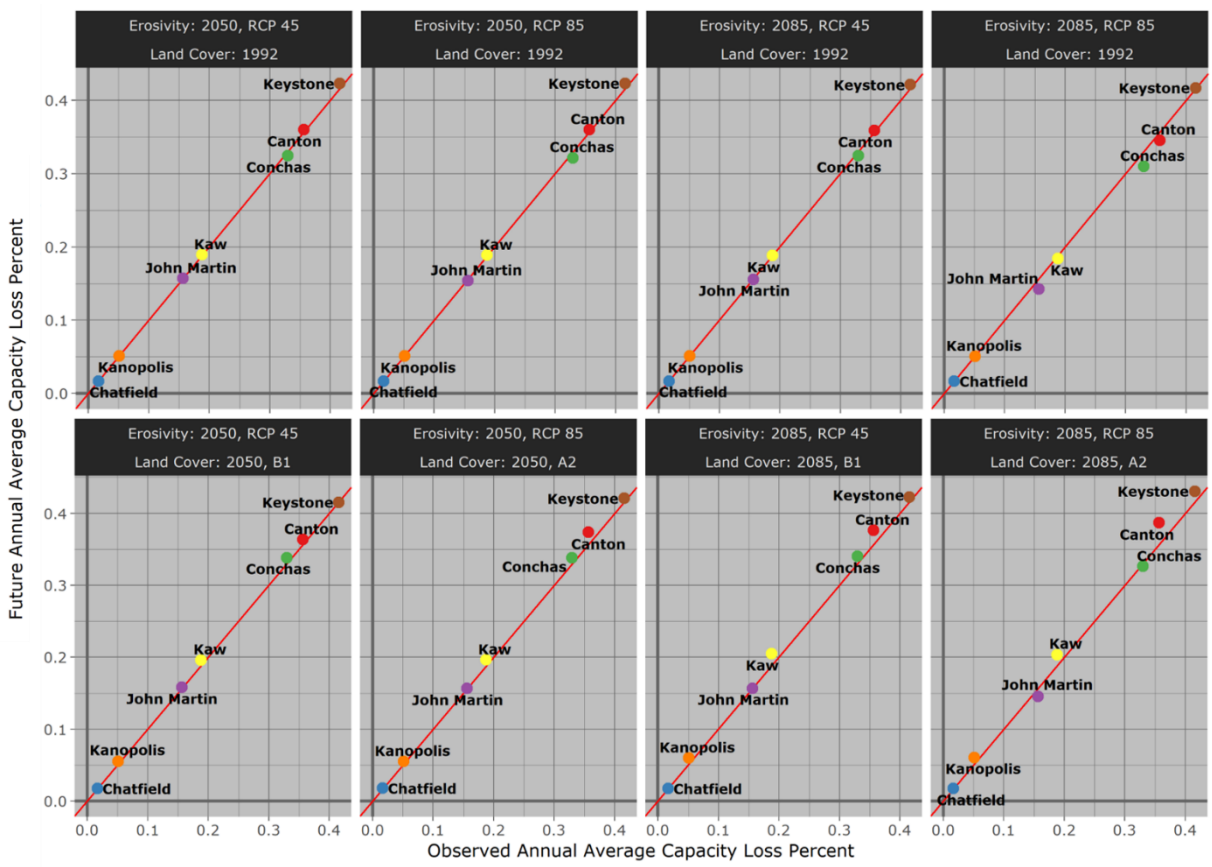

Figure 4. Historical and projected average annual capacity loss by reservoir.

experience slight declines in the annual percent of capacity loss; if land use change is considered along with precipitation change, Canton, Keystone, Kaw and Kanopolis (and Conchas in the lower emissions scenario) fall above the line at 2085, indicating small increases in the annual percent of capacity loss.

Discussion and Conclusion

Changes in soil loss due to climate change have been projected by a number of researchers at the watershed scale (e.g., Nearing et al. 2004, Goode et al. 2012, Segura et al. 2014, Biasutti and Seager 2015). However, changing precipitation seasonality and intensity are only some of the contributing variables; land use and land cover changes are also recognized as exerting significant effects on soil erosion and reservoir sedimentation (Morris and Fan 1998, Julien 2010, Nunes and Nearing 2011, Allen 2017). Recent development of land use and land cover forecasts for the 21st Century have begun to enable researchers to explore the combined effects of climate and land cover change on watershed erosion and sediment transport (e.g., Asselman et al. 2003, Serpa et al. 2015, Li and Fang 2016).

For four of the seven southern Plains reservoirs investigated in the current study, both projected climate and land cover changes are expected to impact sediment yield in the contributing watershed, and result in small increases in the rate of capacity loss at these reservoirs. For reservoirs in the southwestern part of the study area (Conchas Lake and John Martin Reservoir), climate change effects are expected to be the stronger influence on conditions in

these already semi-arid watersheds, especially under the higher emissions scenario (RCP 8.5/A2). Increasingly arid conditions are both likely to reduce runoff and unlikely to result in an expansion of croplands. Consequently, the rate of storage loss to sedimentation is likely to remain similar to the present or decline under all future scenarios, consistent with studies at Cochiti Lake (Pinson et al. 2012) and Elephant Butte Reservoir (Huang and Makar 2013) (both in New Mexico).

In contrast, conversion of grasslands to cropland appears to be the primary driver of increases in sedimentation rates for the four reservoirs in Oklahoma and Kansas (Canton, Kanopolis, Kaw, and Keystone Lakes). The impacts of precipitation change alone on sedimentation are variable and small, and tend towards small reductions in sedimentation under the RCP 8.5 scenario by the end of the century. In contrast, including land cover change in the model results in a small projected increase in sedimentation at all four reservoirs, with the changes being largest at Kanopolis. From a reservoir operations perspective, the increases in capacity loss rates at Canton and Kaw by 2085 may be of concern. However, the reservoirs are large relative to the rate of sediment influx, and the projected changes are unlikely to significantly impact reservoir operations in the coming decades.

In a recent study of USACE reservoir sedimentation vulnerability conducted by the first author (unpublished material), John Martin Reservoir, and Conchas, Canton and Keystone Lakes were flagged as reservoirs where sedimentation is currently a high priority problem based on current rates of capacity loss and the percent of capacity already lost. Kaw and Kanopolis lakes did not rank high on this list. Although the changes projected by this study are unlikely to dramatically alter priority rankings, this may not be true in other areas of the U.S. This study developed a framework for assessing whether future climate and land use changes have the potential to reshape the geographic distribution of USACE's reservoir sedimentation problem and whether changes are necessary in the reservoirs USACE targets for reservoir sediment monitoring and mitigation efforts. Efforts to apply this framework to a broader set of reservoirs is ongoing.

Acknowledgements

For the CMIP5 precipitation datasets, we acknowledge the modeling groups, the Program for Climate Model Diagnosis and Intercomparison (PCMDI) and the WCRP's Working Group on Coupled Modelling (WGCM) for their roles in making available the WCRP CMIP5 multi-model dataset (https://gdo-dcp.ucllnl.org/). Support of this dataset is provided by the Office of Science, U.S. Department of Energy. The Livneh data is provided by the NOAA/OAR/ESRL Physical Sciences Division, Boulder, Colorado, USA, and downloaded from their Web site at https://www.esrl.noaa.gov/psd/.

Slope and slope length data were derived from the 90m Shuttle Radar Topography Mission (SRTM) 90 m dataset (Farr et al. 2007) downloaded from the OpenTopography website http://www2.jpl.nasa.gov/srtm/srtmBibliography.html

The USGS Conterminous United States Projected Land-Use/Land-Cover Mosaics 1938-1992 and the LandCarbon Conterminous United States Land-Use/Land-Cover Mosaics 1992-2100 datasets were developed by the USGS Earth Resources Observation and Science (EROS) Center using the FORE-SCE modeling framework, and were downloaded from https://landcover-modeling.cr.usgs.gov/projects.php.

Thanks to Michaela Biasutti and Richard Seager (Lamont Doherty Earth Observatory, Columbia University) for permission to use their erosivity coefficients dataset for calculating soil erosion

for this project; Tessa Hill (USACE Remote Sensing/GIS Center of Expertise) for assistance in producing the final data layers; and Rachel Marzion (USACE San Francisco District) for help in the early stages of this project.

This work was by the U.S. Army Corps of Engineers Climate Preparedness and Resilience Community of Practice. The views expressed are those of the author(s) and do not necessarily represent those of the US Army Corps of Engineers.

References

Allen, P. A. 2017. Sediment Routing Systems. Cambridge University Press, New York, NY.

Arnoldus, H. M. J. 1980. An approximation of the rainfall factor in the Universal Soil Loss Equation. Pages 127-132 *in* M. De Boodt and D. Gabriels, editors. Assessment of Erosion. John Wiley & Sons Incorporated, Chichester, New York.

Asselman, N., H. Middelkoop, and P. van dijk. 2003. The impact of changes in climate and land use on soil erosion, transport and deposition of suspended sediment in the River Rhine.

Biasutti, M., and R. Seager. 2015. Projected changes in US rainfall erosivity. Hydrology and Earth System Sciences **19**:2945-2961.

Brekke, L. D., J. E. Kiang, J. R. Olsen, R. S. Pulwarty, D. A. Raff, D. P. Turnipseed, R. S. Webb, and K. D. White. 2009. Climate Change and Water Resources Management - A Federal Perspective. U.S. Geological Survey Circular 1331.

Bureau of Reclamation. 2013. Downscaled CMIP3 and CMIP5 Climate and Hydrology Projections: Release of Downscaled CMIP5 Climate Projections, Comparison with preceding Information, and Summary of User Needs. U.S. Department of the Interior, Bureau of Reclamation, Technical Services Center, Denver, Colorado.

Collins, M., R. Knutti, J. Arblaster, J.-L. Dufresne, T. Fichefet, P. Friedlingstein, X. Gao, W. J. Gutowski, T. Johns, G. Krinner, M. Shongwe, C. Tebaldi, A. J. Weaver, and M. Wehner. 2013. Long-term Climate Change: Projections, Commitments and Irreversibility.*in* T. F. Stocker, D. Qin, G.-K. Plattner, M. Tignor, S. K. Allen, J. Boschung, A. Nauels, Y. Xia, V. Bex, and P. M. Midgley, editors. Climate Change 2013: The Physical Science Basis. Contribution of Working Group I to the Fifth Assessment Report of the Intergovernmental Panel on Climate Change. Cambridge University Press, Cambridge, United Kingdom and New York, NY, USA.

Darcy, J. 2014. USACE Climate Preparedness and Resilience Policy Statement. U.S. Army Corps of Engineers, Office of the Assistant Secretary of the Army (Civil Works), June 2014.

de Vente, J., and J. Poesen. 2005. Predicting soil erosion and sediment yield at the basin scale: Scale issues and semi-quantitative models. Earth-Science Reviews **71**:95-125.

Farr, T. G., P. A. Rosen, E. Caro, R. Crippen, R. Duren, S. Hensley, M. Kobrick, M. Paller, E. Rodriguez, L. Roth, D. Seal, S. Shaffer, J. Shimada, J. Umland, M. Werner, M. Oskin, D. Burbank, and D. Alsdorf. 2007. The Shuttle Radar Topography Mission. Reviews of Geophysics 45: 2005RG000183.

Fernandez, C., J. Wu, D. McCool, and C. Stöckle. 2003. Estimating water erosion and sediment yield with GIS, RUSLE, and SEDD. Journal of Soil and Water Conservation **58**:128-136.

Foster, G. R., D. K. McCool, K. G. Renard, and W. C. Moldenhauer. 1981. Conversion of the universal soil loss equation to SI metric units. Journal of Soil and Water Conservation **36**:355-359.

Fournier, F. 1960. Climat et Erosion. Presses Universitaires de France, Paris.

Fox, G. A., A. Sheshukov, R. Cruse, R. L. Kolar, L. Guertault, K. R. Gesch, and R. C. Dutnell. 2016. Reservoir Sedimentation and Upstream Sediment Sources: Perspectives and Future Research Needs on Streambank and Gully Erosion. Environmental Management **57**:945-955.

Goode, J. R., C. H. Luce, and J. M. Buffington. 2012. Enhanced sediment delivery in a changing climate in semi-arid mountain basins: Implications for water resource management and aquatic habitat in the northern Rocky Mountains. Geomorphology **139-140**:1-15.

Graf, W. L., E. Wohl, T. Sinha, and J. L. Sabo. 2010. Sedimentation and sustainability of western American reservoirs. Water Resources Research **46**:n/a-n/a.

Huang, J., and P. Makar. 2013. Reclamation's research on climate change impact on reservoir capacity. World Environmental and Water Resources Congress **2013**:1202-1212.

Julien, P. Y. 2010. Erosion and Sedimentation. Second edition edition. Cambridge University Press, Cambridge, UK.

Julien, P. Y. 2018. River Mechanics, 2nd edition. Cambridge University Press, Cambridge, UK.

Kane, B., and P. Y. Julien. 2007. Specific degradation of watersheds. International Journal of Sediment Research **22**:114-119.

Kondolf, G. M., Y. Gao, G. W. Annandale, G. L. Morris, E. Jiang, J. Zhang, Y. Cao, P. Carling, K. Fu, Q. Guo, R. Hotchkiss, C. Peteuil, T. Sumi, H.-W. Wang, Z. Wang, Z. Wei, B. Wu, C. Wu, and C. T. Yang. 2014. Sustainable sediment management in reservoirs and regulated rivers: Experiences from five continents. Earth's Future **2**:256-280.

Li, Z., and H. Fang. 2016. Impacts of climate change on water erosion: A review. Earth-Science Reviews **163**:94-117.

Linard, J. I., A. M. Matherne, K. J. Leib, N. B. Carr, J. E. Diffendorfer, S. J. Hawkins, N. Latysh, D. A. Ignizio, and N. C. Babel. 2014. Two Decision-Support Tools for Assessing the Potential Effects of Energy Development on Hydrologic Resources as Part of the Energy and Environment in the Rocky Mountain Area Interactive Energy Atlas. USGS Open File Report OFR 2014-1158.

Livneh, B., E. A. Rosenberg, C. Lin, B. Nijssen, V. Mishra, K. M. Andreadis, E. P. Maurer, and D. P. Lettenmaier. 2013. A Long-Term Hydrologically Based Dataset of Land Surface Fluxes and States for the Conterminous United States: Update and Extensions. Journal of Climate **26**: 9384–9392.

Mitasova, H., W. M. Brown, D. Johnston, and L. Mitas. 1996a. GIS tools for erosion/deposition modeling and multidimensional visualization. Part II: unit stream power-based erosion/deposition modeling and enhanced dynamic visualization. Report for USA CERL, University of Illinois, Urbana-Champaign, IL.

Mitasova, H., J. Hofierka, M. Zlocha, and L. R. Iverson. 1996b. Modelling topographic potential for erosion and deposition using GIS. International Journal of Geographical Information Systems **10**:629-641.

Morris, G. L., and J. Fan. 1998. Reservoir Sedimentation Handbook: Design and Management of Dams, Reservoirs and Watersheds for Sustainable Use. McGraw-Hill Book Co., New York.

Nearing, M., F. F. Pruski, and M. R. O'Neal. 2004. Expected climate change impacts on soil erosion rates: A review. Journal of Soil and Water Conservation **59**:43-50.

Nunes, J. P., and M. A. Nearing. 2011. Modelling impacts ofcliamtic change: case studies using the new generation of erosion models. Pages 289-312 *in* R. P. C. Morgan and M. A. Nearing, editors. Handbook of Erosion Modeling. Blackwell Publishing Ltd., New York.

Pinson, A. O., B. E. Baker, P. Boyd, R. Grandpre, K. D. White, and M. Jonas. 2016. USACE Reservoir Sedimentation in the Context of Climate Change. USACE Civil Works Technical Series (CWTS) 2016-05 (August 2016).

Pinson, A. O., J. R. Lee, and D. J. Gallegos. 2012. Climate Change Associated Sediment Yield Changes on the Rio Grande in New Mexico: Specific Sediment Evaluation for Cochiti Dam and Lake (Revised). U.S. Army Corps of Engineers Climate Change Pilot Study.

Renard, K., G. Foster, G. Weesies, D. McCool, and D. Yoder. 1997. Predicting soil erosion by water. A guide to conservation planning with the Revised Universal Soil Loss Equation (RUSLE). U.S. Department of Agriculture, Agriculture Handbook No. 703.

Renard, K., and J. R. Freimund. 1994. Using monthly precipitation data to estimate the R-factor in the revised USLE. Journal of Hydrology **157**:287-306.

Renard, K. G., D. C. Yoder, D. T. Lightle, and S. M. Dabney. 2011. Universal Soil Loss Equation and Revised Universal Soil Loss Equation. Pages 137-167 *in* R. P. C. Morgan and M. A. Nearing, editors. Handbook of Erosion Modeling. Blackwell Publishing Ltd., New York.

Risse, L. M., M. Nearing, A. D. Nicks, and J. M. Laflen. 1993. Error assessment in the Universal Soil Loss Equation. Soil Science Society of America Journal **57**:825-833.

Sauerborn, P., A. Klein, J. Botschek, and A. Skowronek. 1999. Future rainfall erosivity derived from large-scale climate models--methods and scenarios for a humid region. Geoderma **93**:269-276.

Segura, C., G. Sun, S. McNulty, and Y. Zhang. 2014. Potential impacts of climate change on soil erosion vulnerability across the conterminous United States. Journal of Soil and Water Conservation **69**:171-181.

Serpa, D., J. P. Nunes, J. Santos, E. Sampaio, R. Jacinto, S. Veiga, J. C. Lima, M. Moreira, J. Corte-Real, J. J. Keizer, and N. Abrantes. 2015. Impacts of climate and land use changes on the hydrological and erosion processes of two contrasting Mediterranean catchments. Science of The Total Environment **538**:64-77.

Sleeter, B. M., T. L. Sohl, M. A. Bouchard, R. R. Reker, C. E. Soulard, W. Acevedo, G. E. Griffith, R. R. Sleeter, R. F. Auch, K. L. Sayler, S. Prisley, and Z. Zhu. 2012. Scenarios of land use and land cover change in the conterminous United States: Utilizing the special report on emission scenarios at ecoregional scales. Global Environmental Change **22**:869-914.

Sohl, T. L., R. Reker, M. Bouchard, K. Sayler, J. Dornbierer, S. Wika, R. Quenzer, and A. Friesz. 2016. Modeled historical land use and land cover for the conterminous United States. Journal of Land Use Science **DOI: 10.1080/1747423X.2016.1147619**.

Sohl, T. L., K. L. Sayler, M. A. Bouchard, R. R. Reker, A. M. Friesz, S. L. Bennett, B. M. Sleeter, R. R. Sleeter, T. S. Wilson, M. Knuppe, and T. Van Hofwegen. 2014. Spatially explicit modeling of 1992 to 2100 land cover and forest stand age for the conterminous United States. Ecological Applications **24**:1015-1036, **DOI: 1010.1890/1013-1245.1011.**

Trimble, S. W., and P. Crosson. 2000. U.S. Soil Erosion Rates--Myth and Reality. Science **289**:248-250.

U.S. Army Corps of Engineers (USACE). 1995. Engineer Manual (EM) 1110-2-4000, Sedimentation Investigations of Rivers and Reservoirs.

U.S. Army Corps of Engineers (USACE). 1997. Engineer Manual (EM) 1110-2-1420, Hydrologic Engineering Requirements for Reservoirs.

U.S. Army Corps of Engineers (USACE). 2018. Enhancing Reservoir Sedimentation Information for Climate Preparedness and Resilience. Page URL: https://maps.crrel.usace.army.mil/projects/rcc/portal.html.

U.S. Geological Survey. 2016. USGS National Hydrography Dataset (NHD) Downloadable Data Collection - National Geospatial Data Asset (NGDA) National Hydrography Dataset (NHD). Page URL: http://nhd.usgs.gov.

Wischmeier, W., and D. Smith. 1978. Predicting rainfall erosion losses: a guide to conservation planning. U.S. Department of Agriculture, Agriculture Handbook No. 537, online at https://www.ars.usda.gov/SP2UserFiles/ad_hoc/36021500USLEDatabase/AH_537.pdf , accessed 30 June 2016.

Wolock, D. M. 1997. STATSGO soil characteristics for the conterminous United States. USGS Open-File Report 97-656, online at https://water.usgs.gov/GIS/metadata/usgswrd/XML/muid.xml.

Yang, D., S. Kanae, T. Oki, T. Koike, and K. Musiake. 2003. Global potential soil erosion with reference to land use and climate changes. Hydrological Processes **17**:2913-2928.

Zhu, Z. e., B. Bergamaschi, R. Bernknopf, D. Clow, D. Dye, S. Faulkner, W. Forney, R. Gleason, T. Hawbaker, J. Liu, S. Liu, S. Prisley, B. Reed, M. Reeves, M. Rollins, B. Sleeter, T. Sohl,

S. Stackpoole, S. Stehman, R. Striegl, A. Wein, and Z. Zhu. 2010. A method for assessing carbon stocks, carbon sequestration, and greenhouse-gas fluxes in ecosystems of the United States under present conditions and future scenarios:. U.S. Geological Survey Scientific Investigations Report 2010–5233:188.

Appendix: Data and Methodology

The datasets used in this study are listed in Table 2.

Table 2. Datasets used in this study.

Dataset	Source	Variable Used In
Livneh 1/16 degree monthly precipitation dataset	Livneh et al. (2013)	Precipitation for estimating erosivity (R) in the calculation of the historical SDR for each watershed
Downscaled CMIP3 and CMIP5 Climate and Hydrology Projections	Bureau of Reclamation (2013)	Precipitation for estimating erosivity (R) in calculation of future watershed soil loss
USGS LandCarbon Land Cover datasets (modeled future and back-\casted)	Sohl et al. (2014), Sohl et al. (2016)	Calculation of C-factor for the RUSLE: Historical soil loss estimate for each reservoir used the raster associated with the mean of the period of sediment survey record (except for Chatfield whose mean POR is 1993 and the 1992 dataset was used) Future soil loss estimate used the 1992 baseline land cover raster for the historical period, and the rasters for 2050 A2, 2050 B1, 2085 A2 and 2095 B1 for the future land cover corresponding to the RCP 8.5 and 4.5 mean future condition for the periods 2035-2064 and 2070 to 2099, respectively.
90 m Shuttle Radar Topography Mission (SRTM) elevation data	Farr et al. (2007)	Elevation data for calculation of the LS-factor
USDA STATSGO 1km gridded dataset	Foster et al. (1981), Wolock (1997)	K-factor
USACE Reservoir Sedimentation Information Data Portal	U.S. Army Corps of Engineers (USACE) (2018)	Capacity loss data used in the calculation of observed SDR and SY

Contributing watersheds for each reservoir were defined as the watershed upstream of that reservoir. Upstream reservoirs that captured a large fraction of the watershed were assumed to have reservoir trap efficiencies approaching 100%, and their watershed areas were subtracted from the watershed area of the reservoir of interest.

Soil loss encompasses losses due to rill and inter-rill erosion (Wischmeier and Smith 1978, Renard et al. 1997). Because of its importance to agricultural productivity, soil loss is well-characterized at both small and large spatial scales (Yang et al. 2003, de Vente and Poesen 2005, Segura et al. 2014). For this study, soil loss is estimated using the Revised Universal Soil Loss Equation (RUSLE) (Renard et al. 1997). The RUSLE accounts for precipitation, slope, soil susceptibility to erosion, and land cover within the watershed, but not for the transport of this sediment by channel flows (Trimble and Crosson 2000). Although originally developed to model soil erosion from agricultural fields (Wischmeier and Smith 1978, Renard et al. 1997), the RUSLE has been found to give acceptable first-order estimates for changes in soil erosion at larger geographic scales and monthly or annual time steps (Arnoldus 1980, Renard and Freimund 1994, Fernandez et al. 2003, Yang et al. 2003, Nearing et al. 2004, Segura et al. 2014). Its simple structure has made it practical for use in continent-scale erosion studies using gridded satellite and climate model data. The underlying data model has been found to be more

effective at predicting long-term average annual values rather than erosion due to individual storm events (Risse et al. 1993)

RUSLE computes average annual soil loss as (Wischmeier and Smith 1978, Renard et al. 1997):

$$A = R*K*LS*C*P ,$$

where A is the average annual soil loss (t ha^{-1} y^{-1}), R is the rainfall/runoff erosivity (MJ mm ha^{-1} h^{-1} $year^{-1}$), K is the USDA soil erodibility factor (t ha h ha^{-1} MJ^{-1} mm^{-1}), LS is the slope length and steepness factor (unitless), C is the cover management factor (vegetation cover, unitless), and P is the erosion control practice (unitless, assumed =1 for landscape-level studies). Data for each factor was resampled to match the resolution of the 90-m DEM, A was calculated for each grid cell, and then summed across all the cells in each watershed to produce an average annual soil loss for the watershed.

Erosivity (R) in the original RUSLE formulation is the average 30 minute storm intensity calculated from field observations of precipitation events (Wischmeier and Smith 1978, Renard et al. 1997). Monthly precipitation data can be used to estimate R where rainfall data are not available (Renard and Freimund 1994), and may result in a small overestimate of R (Risse et al. 1993). Use of monthly climate data to estimate future changes in R using climate model data (Sauerborn et al. 1999) can be done using the modified Fournier index, F (Fournier 1960, Arnoldus 1980):

$$F = \frac{\sum_{j=1}^{12} P_j^2}{\sum_{j=1}^{12} P_j}$$

where P_j is the monthly rainfall depth for the calendar month j, and months with higher precipitation totals result in greater rates of erosion (contribute more to the total than if the rainfall were spread out). The index weights more heavily months with higher precipitation totals on the assumption that higher precipitation correlates with higher erosivity. An improved fit between F and isoerodent values was obtained by Biasuitti and Seager (2015) through the use of a linear model that maps gridded values obtained from historic precipitation data to observed isoerodent values. The modified Fournier Index calibrated using the linear equation $R= \alpha F+ \beta$, and the local values for α and β developed by Biasutti and Seager (2015) are used to compute R.

For the calculation of the watershed-specific SDR, the Livneh 1/16 degree gridded monthly historical precipitation dataset (Livneh et al. 2013) was used to calculate R for the period of the observed capacity loss for each reservoir. To calculate future changes in soil loss, R was calculated using the average monthly precipitation for hydrologic unit code 4 (HUC4) watersheds in CONUS for the period 1950-2099. These data were obtained from the Downscaled CMIP5 Climate and Hydrology Projections archive (Bureau of Reclamation 2013) for the full ensemble of CMIP5 climate models for two future emissions scenarios: Relative Concentration Pathways (RCPs) 4.5 and 8.5. These data have been downscaled using the bias correction, spatial disaggregation (BCSD) method.

C-factor depends on both canopy cover and duff thickness, and Wischmeier and Smith (1978) provide ranges for various cover types. C-factor is estimated from the USGS Land Carbon Land Cover dataset (https://landcover-modeling.cr.usgs.gov/projects.php) (Zhu et al. 2010). This dataset provides both observed historic conditions, modeled historic back to 1938 (Sohl et al. 2016) and future land use (Sohl et al. 2014) based on economic projections and expert assessment. The modeled historic land cover data for the year in the middle of the period of

record was used in estimating watershed SDRs. For the projected change in SY with climate change analysis, the baseline 1992 data was used for the baseline condition, and files for the epoch midpoints (2050, 2085) for the A2 (high emissions) and B1 (low emissions) SRES CMIP3 scenarios were used. C-factor values are mapped to the land cover categories as shown in Table 2.

Table 3. C-factor values for Land Carbon Land Cover classes.

Code	Name	C-factor
1	Water	0
2	Developed	0.02
3	Mechanically-disturbed National Forests	0.45
4	Mechanically disturbed other public land	0.45
5	Mechanically disturbed private land	0.45
6	Mining	0.45
7	Barren	0.3
8	Deciduous forest	0.003
9	Evergreen forest	0.003
10	Mixed forest	0.003
11	Grassland	0.05
12	Shrubland	0.06
13	Cropland	0.09
14	Hay/pasture land	0.02
15	Herbaceous wetland	0.0006
16	Woody wetland	0.0003
17	Perennial ice/snow	0

The climate scenarios driving changes in land use (SRES B1, A2) and changes in erosivity (RCP4.5, 8.5) are from different generations of IPCC climate models. While this is not ideal, a practical alternative was not available. Over the 21st Century, the radiative forcing under the RCP 4.5 and SRES B1 scenarios are very similar, while that of the SRES A2 scenario parallels, but is systematically lower than the forcing in the RCP 8.5 scenario (Collins et al. 2013). The SRES A1FI scenario might have been a better match with RCP 8.5, but it is not used in the USGS Land Carbon Land Cover dataset. In this paper, the phrase “high emissions scenario” is used to refer to either RCP 8.5 or A2 scenario data; likewise the phrase “low emissions scenario” is used to refer to either RCP 4.5 or B1 scenario data.

The combined length (L) and slope (S) factor measures the impact of relief and slope angle on erosion. The LS factor calculation used the SRSTM 90-m digital elevation gridded datasets (Farr et al. 2007). Calculation of the LS-factor follows the unit stream power approach (Mitasova et al. 1996a, Mitasova et al. 1996b):

$$LS = (m+1)\left(\frac{\lambda}{22.13}\right)^{m}\left(\frac{Sin\ \theta}{0.0896}\right)^{1.3} \ ,$$

where λ=flow accumulation contributed by upstream cells, and θ = slope angle. Researchers working with 30-m gridded data have suggested that the limit of cells draining into a given cell could conservatively be set at four, giving a maximum distance over which flow can accumulate of 120 m (Fernandez et al. 2003). Sensitivity tests were conducted comparing unlimited upstream flow accumulation with schemes that limit flow accumulation to a maximum of 4 grid cells, or approximately 360 m in a 90 m DEM, equivalent to the maximum field size of 1000 ft in the original model (Wischmeier and Smith 1978). However, the model performed better when no limits were placed on the number of upstream contributing cells (data not shown).

The exponent *m* is the ratio of rill to inter-rill erosion (Renard et al. 2011) for each grid cell in the model:

m= β /(1+ β), where,

$$\beta = \frac{\frac{sin\ \theta}{0.0896}}{3*(((sin\theta)^{0.8})+0.56)} \ ,$$

where θ = slope angle.

Soil K-factor is a measure of soil cohesion, and therefore the ease with which rainsplash and runoff are able to detach and transport sediment. K-factor was obtained from the USDA STATSGO 1 km gridded soils dataset (Foster et al. 1981, Wolock 1997).

Soil P-factor, representing modifications to agricultural fields to reduce surface erosion, was set to 1 (no conservation treatment) indicating that such efforts are not typically undertaken at the landscape scale and the model is designed to represent an undeveloped condition (Linard et al. 2014).

Finally, the sediment delivery ratio (SDR) is that fraction of eroded sediment in a watershed that reaches a given reservoir (Julien 2010):

$$SDR=SY/A$$

SDR for the period of sediment accumulation in reservoirs was determined using the observed sediment yield and modeled gross soil loss from the contributing watershed using the RUSLE model with the R factor calculated for the period of record of sediment loss using the Livneh monthly precipitation dataset and the Land Carbon land cover dataset for the midpoint of the period of record for sediment loss.

Reservoir Sediment Management: Building a Legacy of Sustainable Water Storage Reservoirs

Timothy Randle, Bureau of Reclamation, Denver, CO, trandle@usbr.gov
Greg Morris, Gregory Morris Consultants
Michael Whelan, Anchor QEA, L.L.C.
Bryan Baker, U.S. Army Corps of Engineers
George Annandale, George W. Annandale, Consultant
Rollin Hotchkiss, Brigham Young University
Paul Boyd, U.S. Army Corps of Engineers
J. Toby Minear, Cooperative Institute for Research in Environmental Sciences
Stan Ekren, Great Lakes Dredge & Dock Company
Kent Collins, Bureau of Reclamation
Mustafa Altinakar, University of Mississippi
Jon Fripp, USDA-Natural Resource Conservation Service
Meg Jonas, U.S. Army Corps of Engineers (retired)
Kyle Juracek, U.S. Geological Survey
Sean Kimbrel, Bureau of Reclamation
Matt Kondolf, University of California, Berkeley
Doug Raitt, Denver Water
Frank Weirich, University of Iowa
Darrell Eidson, U.S. Army Corps of Engineers
John Shelley, U.S. Army Corps of Engineers
Rene Vermeeren, U.S. Army Corps of Engineers
David Wegner, Woolpert Engineering
Peter Nelson, Colorado State University
Kevin Jensen, McMillen Jacobs Associates
Desirée Tullos, Oregon State University

Introduction

This extended abstract is a summary of a larger paper by the National Reservoir Sedimentation and Sustainability Team written by the same authors.

The United States economy and welfare depends on a continuous and reliable system of water supply and infrastructure for municipal, industrial, agricultural, flood control, and hydropower uses. These water systems are also important for recreational and environmental management, and even aquifer recharge. Water storage reservoirs are essential to regulate highly variable river flows, making water available whenever needed, creating a singularly important, but often unseen foundation for modern society. The 90,000 dams and reservoirs (National Inventory on Dams, 2017) constitute a critical component of the country's water infrastructure. There are perhaps more than a million additional dams that are too small to be included in the national inventory.

The vast majority of the nation's water storage reservoirs were constructed decades ago, and since construction, they have been trapping the sediment eroded from the land surface and carried downstream by rivers (Morris and Fan, 1998). The downstream transport of sediment is particularly evident during floods, when waters run turbid with eroded soil. In most reservoirs, this sediment consists of clay, silt, sand, and gravel particles (Morris and Fan, 1998; Randle and Greimann, 2006; and Morris et al., 2007).

Without active management, the continual accumulation of sediments will eventually displace the storage volume in a reservoir, rendering it useless for capturing and storing water. However, sedimentation impacts will occur long before the reservoir has lost nearly all of its water storage capacity and include: reduction in the reliability of water supply, burial of dam outlets and intakes for water supply and power production, damage to hydropower and pumping equipment, burial of boat ramps or marinas, navigation impairment, reduction in the surface area for lake recreation, increased flood stage upstream, downstream channel degradation, and other environmental impacts.

In addition to the financial and environmental burden facing future generations as they decommission legacy infrastructure, replacement sites for most dams and reservoirs are not readily available. The most appropriate dam sites have already been utilized, and they are losing their storage capacity. Removal and storage of large volumes of sediment on land, while technically feasible, can be costly, and there typically isn't room to sustainably store inflowing sediments. Fortunately, multiple measures are available to manage sediment, to help ensure the long-term viability of reservoirs while minimizing the difficulty and cost of maintaining the nation's water resources.

Sustainable Sediment Management Planning

The general strategies for sustainable reservoir sediment management are graphically illustrated in Figure 1. Based on Kondolf et al., 2014 and Sumi et al., 2017, these strategies include sediment yield reduction from the upstream watershed (shown in green, e.g., landslide stabilization and check dams), routing the inflowing sediments through or around the reservoir (shown in yellow, e.g., sediment bypassing and pass through), removing or redistributing reservoir sediment deposits (shown in turquoise, e.g., mechanical excavation and hydraulic dredging), and adaptive strategies to better cope with reservoir sedimentation, or a combination of these strategies. A more detailed list of sediment management methods under each of these general strategies is presented in Figure 2 (Morris, 2015). For optimum performance, more than one type of strategy or method may be needed, either in sequence or simultaneously.

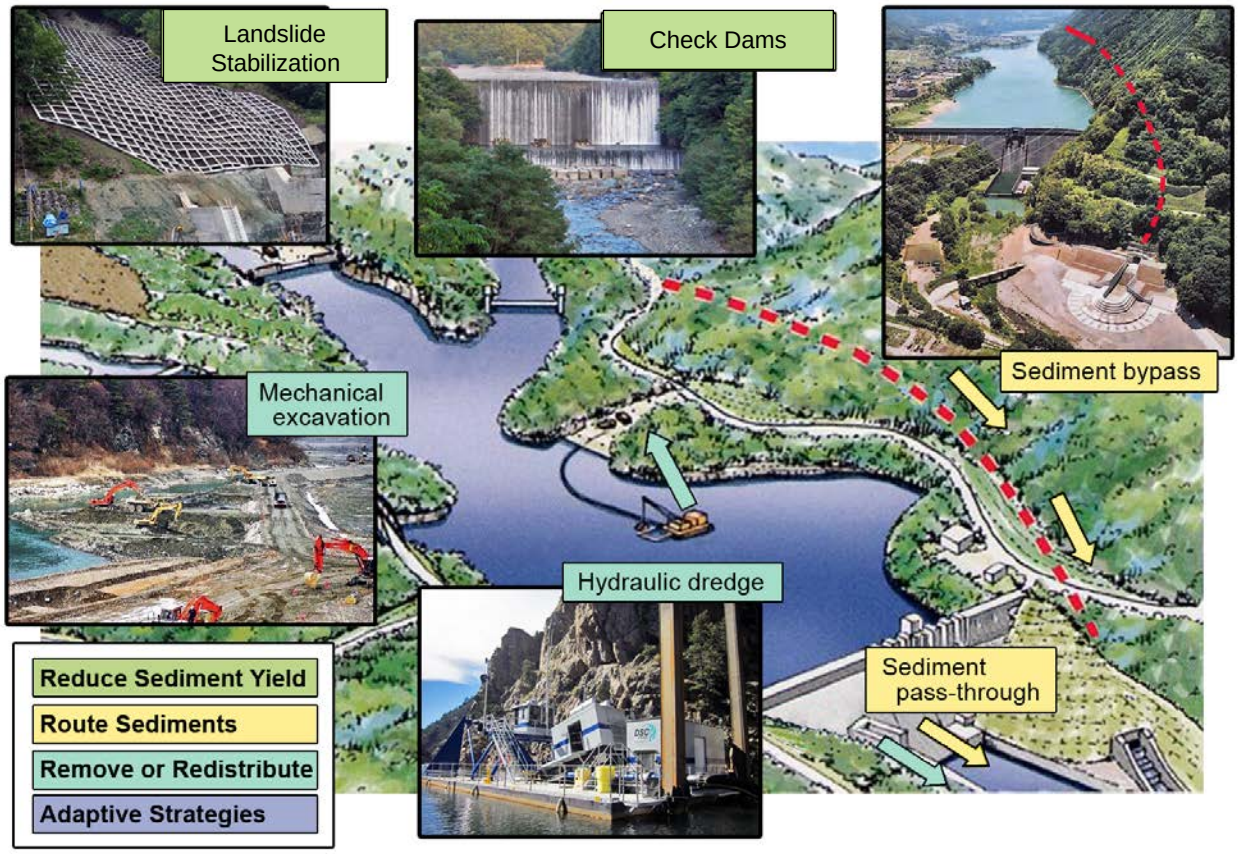

Figure 1. The range of reservoir sedimentation management strategies include the reduction of sediment yield from the upstream watershed, routing the inflowing sediments through or around the reservoir, removing sedimentation from the reservoir or redistributing sediments within the reservoir, and adaptive strategies to better cope with reservoir sedimentation (modified from Sumi et al., 2017). Adaptive strategies can use a combination of the above-mentioned methods and alternative reservoir operations to manage sediment.

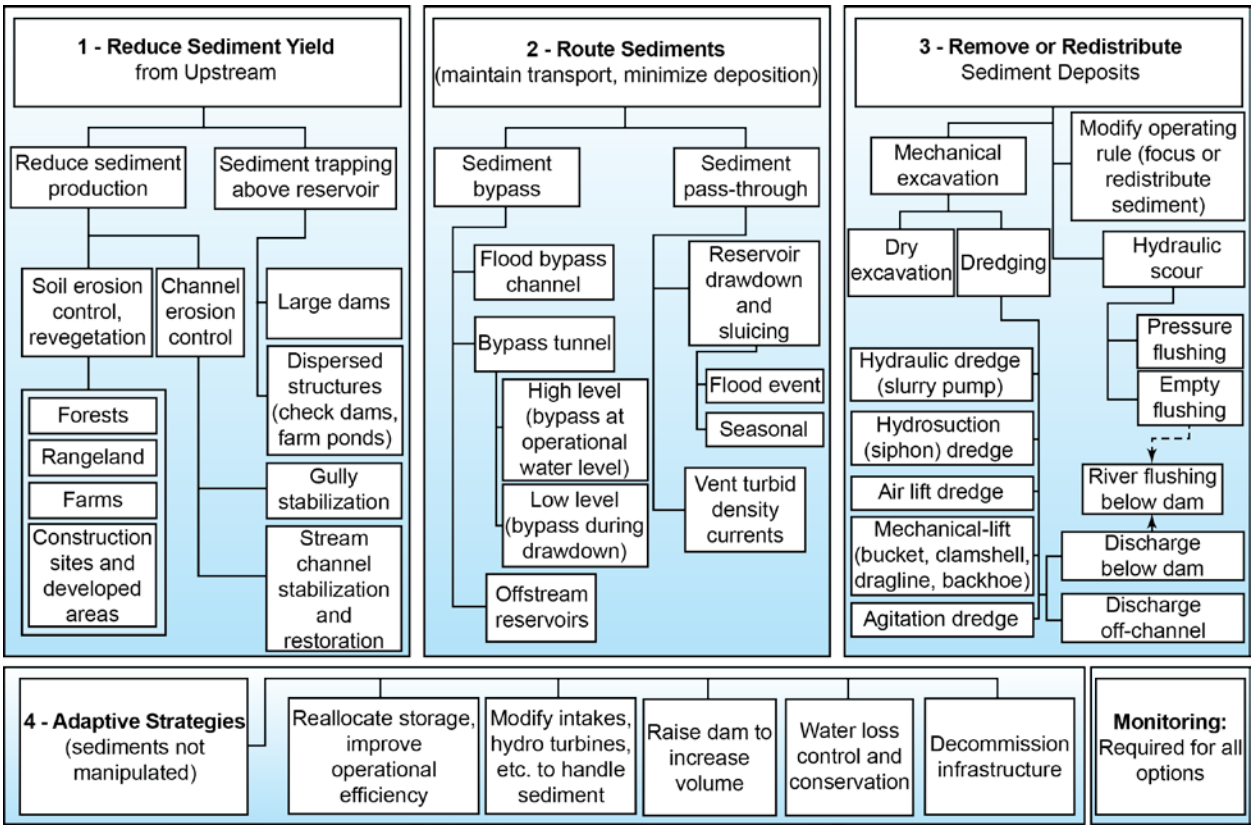

Figure 2. Classification of methods to manage reservoir sedimentation (Morris, 2015).

Conclusions and Recommendations

The present practice of allowing the nation's reservoirs to continually fill with sediment over time is not sustainable. Once the benefits of a reservoir have been lost to sedimentation, dam removal is often the eventual outcome and can be expensive for large sedimentation volumes. Even after dam removal, significant quantities of sediment may remain in the reservoir and render the area unsuitable for future generations to use for water storage.

Plans to periodically monitor reservoir sedimentation need to be formulated and implemented at each reservoir to document the remaining storage capacity and estimate when important dam and reservoir facilities will be impacted.

Long-term reservoir sediment-management plans need to be formulated for each reservoir. These management plans should include either the implementation of sustainable sediment-management practices or the eventual retirement of the reservoir. A prudent, long-term sustainable goal for reservoir management is to pass inflowing sediments to the downstream channel each year in a quantity similar to the mass or volume of sediments entering the reservoir and, to the extent possible, with similar timing. Reservoir operations and environmental permitting laws and regulations may need to be modified. Ultimately, with carefully planned sediment management, downstream habitats and infrastructure may benefit from restored sediment continuity. Allowing inflowing reservoir sediments to pass downstream restores natural

sediment processes and improves conditions for dependent habitat. Reservoir sediments should be allowed to pass downstream by manipulating reservoir operations; installing new gates, bypass channels, or tunnels; and mechanically or hydraulically transporting the sediment.

The sustainable management of reservoir sedimentation may seem expensive, but the sediment management costs need to be compared with the costs of eventually losing the reservoir benefits and the costs of removing the dam and reservoir.

References

Kondolf, G.M.; Gao, Y; Annandale, G.W.; Morris, G.L.; Jiang, E.; Zhang, J.; Cao, Y.; Carling, P.; Fu, K.; Guo, Q.; Hotchkiss, R.; Peteuil, C.; Sumi, T.; Wang, H.W.; Wang, Z.; Wei, Z.; Wu, B.; Wu, C.; and Yang, C.T. (2014). "Sustainable sediment management in reservoirs and regulated rivers: Experiences from five continents." Earth's Future, 2, doi:10.1002/2013EF000184.

Morris, Gregory L. and Fan, Jiahua. 1998. *Reservoir Sedimentation Handbook*, McGraw-Hill Book Co., New York, New York, https://reservoirsedimentation.com/.

Morris, G.L., G. Annandale, and R. Hotchkiss (2007). "Reservoir Sedimentation," *In*: *ASCE Manuals and Reports on Engineering Practice No. 110, Sedimentation Engineering, Processes, measurements, Modeling, and Practice*, García, M.H. editor, American Society of Civil Engineers, Reston, VA, Chapter 12, pp 579 to 612.

National Inventory of Dams (2017). https://catalog.data.gov/dataset/national-inventory-of-dams, accessed December 4, 2018.

Randle, T.J. and B. Greimann (2006). "Chapter 2, Erosion and Reservoir Sedimentation" in *Erosion and Sedimentation Manual*. U.S. Department of the Interior, Bureau of Reclamation, Denver, CO, 94 pp.

Sumi T., S. Kantoush, T. Esmaeili, and G. Ock (2017). "Chapter 14, Reservoir Sediment Flushing and Replenishment Below Dams: Insights from Japanese Case Studies", Gravel-Bed Rivers: Processes and Disasters, First Edition. Edited by D. Tsutsumi and J. Laronne. © 2017 John Wiley and Sons Ltd. https://doi.org/10.1002/9781118971437.ch14

Surrogate Streamgage, Snowmelt, and Sedimentation Rates to Provide Alternatives for a High Hazard Dam Rehabilitation Conceptual Design

Nathaniel Todea, former United States Department of Agriculture - Natural Resources Conservation Service, Hydraulic Engineer, Salt Lake City, Utah, current United States Bureau of Reclamation, Hydraulic Engineer, ntodea@usbr.gov

Abstract

As part of the Santaquin Debris Basin Dam Rehabilitation Environmental Assessment (EA), the Natural Resources Conservation Service undertook a sedimentation study and principal spillway hydrograph (PSH) study to determine storage needs to provide 50 to 100 years of dam life and set the auxiliary spillway elevation to not activate until the 100-year, 10-day snowmelt event occurs. This sedimentation study is the basis for all hydraulic routing and pool capacity calculations to determine the life of the dam. Furthermore, the PSH is used to set routing elevations after the 10 day draw down concerning stability/integrity design hydrographs as well as with dam scenarios for the 2-to 500-year flood frequency for the economic analyses portion of the EA.

Construction of the dam was accomplished in 1955 through the authority of the Watershed Protection and Flood Protection Act, Public Law 566 (PL-566). Santaquin Debris Basin is located on the Southern Wasatch Front and western edge of the Rocky Mountain physiographic provide in the Summit Creek watershed just upstream of the Santaquin City, Utah. The normally empty debris basin is a small, approximately 85-acre-foot reservoir fed by a 19.25 square-mile watershed, with an average elevation near 7,200 feet above mean sea level, varying from approximately 5,200 - 9,400 - in elevation.

Surrogate bedload sedimentation rates from the RiverMorph FlowSed sediment module were used to determine annual sediment rates and was compared to various sedimentation methods that include Automated Geospatial Watershed Assessment tool with Soil Watershed Assessment Tool (SWAT), Rangeland Hydrology Erosion (RHEM), Pacific Southwest Inter-Agency Committee (PSIAC) and a Utah comprehensive USDA study (Bridges 1973).

The results of the study show an average 1.056 acre- feet per year (0.07 acre-feet per square mile (af/mi^2/yr) sediment yield) of material is deposited in Santaquin Debris Basin. The compilation of sediment yield rates ranged from 0.07 to 0.86 af/mi^2/yr, with most values ranging near or below 0.14 af/mi^2/yr. The 1954 design sediment yield was either calculated to be 0.12 to 0.18 af/mi^2/yr depending on interpretation. Bridge's 1973 map can provide initial estimates and is a gross over estimates for sediment yield in this case. The RHEM is not optimally suited for these environmental conditions but provides another overall relative comparison against other methodologies. Pairing of results from RiverMorph FlowSed with bedload and suspended sediment and using the Hotchkiss and Hinton (2015) HydroServer Lite – Bedload Database provide final estimates of sediment deposition and is the lowest number evaluated in the sediment portion of the study.

The 19.25 mi^2 contributing area is a high elevation snowmelt dominated system that has a partially complete stream gage record but is inadequate to use to derive snowmelt runoff estimates. Snowmelt runoff rates are being used to determine which flows activate the principal spillway and auxiliary spillway. Computations based on the limited gage data from the contributing area and surrogate gages near were compared to surrounding gages to derive the 2- to 500-year 10-day, and 1-day snowmelt runoff. Finally, a Franson Engineering (2013) study that produced similar runoff ratios for the 10-day 1-day snowmelt runoff was used to determine the snowmelt ratios. This compared well to using surrogate data from an adjacent watershed to address data gaps and extend the Summit Creek daily data.

Introduction

The United States Department of Agriculture Natural Resources Conservation Service (NRCS) Earth Dams and Reservoir Technical Note Number 60 (TR-60) (NRCS, 2005) requires determination of a sediment storage and routing of the principal spillway hydrograph (PSH) to start the routing elevation for design storms for low, significant, and high hazard dams that have storage-acre feet and height-feet greater than 3,000. Sediment storage can be anywhere between 50 years to 100 years of the anticipated design, per NRCS program requirements (NRCS, 2009). The PSH is determined using precipitation and runoff amounts. The sediment pool elevation/storage, one parameter, is used to route the PSH. The PSH is used to set the elevation of an earther auxiliary spillway, to allow less frequency use of the auxiliary spillway.

The Santaquin Debris Basin was initially built as a pilot dam for the United States Department of Agriculture Soil Conservation Service (SCS, now NRCS) in 1955 and is now under review for redesign to be brought to current NRCS and Utah Dam Safety design standards, under the NRCS Dam Rehabilitation Program. This paper reviews and discusses multiple methods to calculate sedimentation rates and sediment storage into the basin to develop design alternatives. Additionally, a site-specific study was undertaken to determine the starting elevation required design storms using a snowmelt runoff PSH.

A sedimentation study (Todea, 2015) and a PSH study (Todea, 2017) were developed to support the analyses and evaluation portion of the Plan Environmental Assessment for the Santaquin Debris Basin (NRCS, 2009). These studies form the basis of this paper and will be reference throughout.

Sedimentation Study

The original dam plans allowed for 84 ac-ft of sediment accumulation in a 125 ac-ft pool for the 40-year design life (SCS1954). This rate indicates the sediment detention portion of the basin will fill in 40 years at an average rate of 2.1 ac-ft/yr. The original Santaquin debris basin watershed size was calculated as 23.3 mi^2, which is 4.8 mi^2 larger than the newest delineation (USGS, 2017g). When back calculating with a sediment trap efficiency of 75%, the annual total sediment deposition in the reservoir would be 2.1 ac-feet per year deposition, or a sediment yield of 0.12 ac-ft/mi^2/yr. Sediment deposition measurements were not used due to periodic dredging of the basin.

This study assesses the accuracy of the 0.12 ac-ft/mi^2/yr sediment yield calculated from data from the original dam design (SCS 1954) to suggest the appropriate sediment yield to use for planning and design of the Santaquin Debris Basin rehabilitation.

Methods

Bridges 1973 Sedimentation Map: The Bridges (1973) map entitled “Estimated Sediment Yield Rates for the State of Utah” has considerable referenced data sources as part of the map, including: 1) Great Basin Upper Colorado and Lower Colorado Regions, Comprehensive Framework Study, Appendices VIII, Water Management, June 1971, Pacific Southwest Inter-Agency Committee/Water Resources Council; 2) Utah State soils map and soil descriptions; 3) Reservoir surveys by NRCS and USBR; 4) Suspended load measurements by USGS, USBR and NRCS; 5) Watershed studies by SCS/NRCS, and General knowledge of the state from regular NRCS program work. Bridges notes “Do not use these rates to determine sediment yields at specific sites”. Large variations in sediment rates may occur within the delineated areas”. However, with this information the Bridge’s 1973 sedimentation maps does produce good and realistic results and should be used only for “first cut” comparative purposes.

Rangeland Hydrology Erosion Model: The Rangeland Hydrology Erosion Model estimates erosion, runoff, and sediment delivery volumes and rates for individual precipitation events and hillslopes (Nearing et al. 2011) and is used in this study to calculate these parameters for the Santaquin watershed. Precipitation data were pulled from the RHEM list of available stations that best matched the upper Santaquin watershed. The Pine View Dam (426869) weather station has an annual average precipitation

of 30.54 in (WRCC 2017). Soil surface texture types were compiled from Soil Survey Geographic Database (SSURGO; NRCS, 2017c) for input to RHEM. For input into the RHEM model the hillslope was considered uniform.

RiverMorph FlowSed: RiverMorph FlowSed (Rosgen 2006a) was used to determine annual bedload and suspended sediment using a defined period within the stream gage records. The Rosgen Pagosa rating curves as part of FlowSed were applied with both good and poor conditions for bedload and suspended sediment. This resulted in four scenarios. After reviewing bedload studies from the Hotchkiss and Hinton (2015) bedload database it was determined to use a bedload of 0.41 lbs. /sec during bankfull flow. Table 1 shows the results of collection sites from the Hotchkiss and Hinton (2015) database. These sites were chosen due to similarly to the Santaquin site regarding drainage area, bed material, and stream classification. Figure 1 shows normalized bankfull discharges with corresponding measured bedload.

Table 1. Bedload collection sites information from the bedload database used for comparative purposes (Hotchkiss and Hinton 2015)

Location	State	Drainage Area (mi^2)	Average Slope (m/m)	Surface Note	Bankfull Discharge (cfs)	Stream Classification / Note
St. Louis Creek Site 3	CO	20.9	0.019	Pebble	162.1	Good
Blackmare Creek	ID	17.8	0.0299	Bulk Core	167.0	B3
Fourth of July Creek	ID	17.1	0.0202	Pebble Count	137.0	B4c
Wolf Creek at Bridge	CO	18.0	0.0163	Pebble Count	280.0	B4

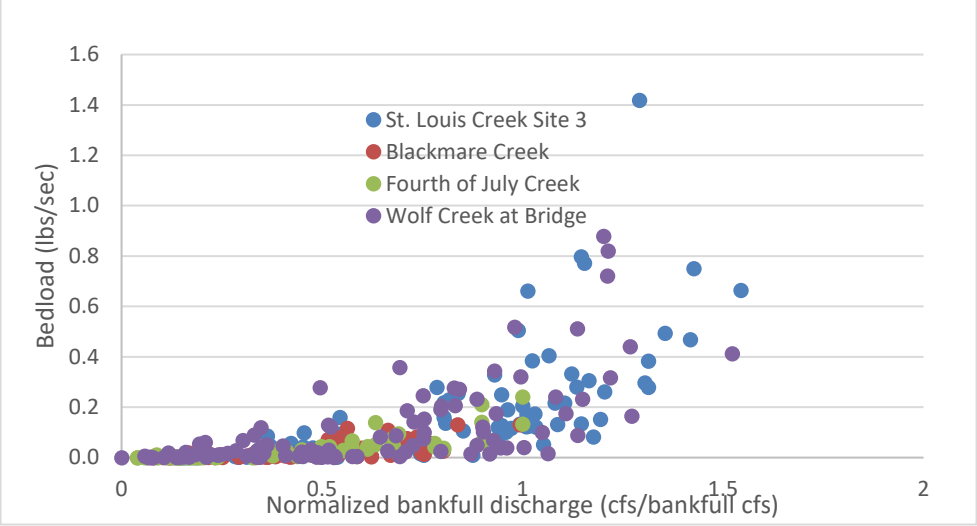

Figure 1. Normalized bankfull discharge of selected bedload measurements (Hotchkiss and Hinton, 2015)

The Tibble Fork sedimentation and bedload study (Todea and Hasenyager, 2012) was taken into consideration for analysis in the RiverMorph FlowSed. The Todea and Hasenyager (2012) study results using the DH48 depth-integrated sampler showed a low Total Suspended Sediment (TSS) of 58 mg/l for the bankfull discharge. The new accretion layer only showed 3.8 mg that settled in 1 hour. This Todea and Hasenyager TSS study result is considered comparable to the Santaquin Watershed.

Flow duration curves for Payson Creek above Diversions (USGS 10147500, 2017c) were generated in RiverMorph using. Although there is a stream gage (USGS 10147000, 2017f) located in the Santaquin watershed, the peaks and period or record is considered unrepresentative of possible flows; see comparison in Figure 2. The flow frequency curve was made dimensionless and the study area bankfull was applied to the dimensionless data in RiverMorph FlowSed.

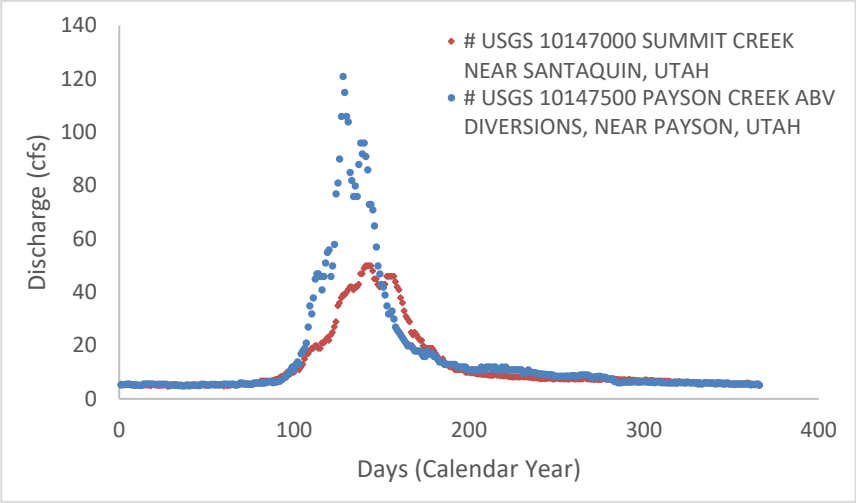

Figure 2. Comparison of USGS Summit (USGS, 2017f) and Payson Gages (USGS, 2017c)

Automated Geospatial Watershed Assessment-Soil and Water Assessment Tool and Kinematic Runoff and Erosion Model (AGWA): The Automated Geospatial Watershed Assessment (AGWA;Burns et al., 2007) Soil and Water Assessment Tool (SWAT) was used. The SWAT model was used to determine average annual sedimentation rates contributing to the Santaquin Debris Basin. The AGWA SWAT model uses the following data sources. SSURGO (NRCS, 2017c) data to characterize soil properties, precipitation data from the Payson SNOTEL site (NRCS, 2017a), and 5 meter auto-correlated digital elevation models (AGRC, 2007a) to calculate hydrological characteristics were used for the SWAT model. The hydraulic geometry relationships from sites in central and southern Arizona (Moody et al., 2003) were selected, as they best correlate to width and depth ratios of channel cross sections collected in the field. Runoff curve numbers were determined using the 2011 National Land Cover Dataset (USDA-EROS-DC, 2001) and SSURGO data (NRCS, 2017c), cover was determined visually, and interception, percent impervious, and roughness were estimated during field visits.

Sedimentation Results

The Bridge sediment map, McMillen PSIAC, and AGWA all have comparable results, whereas comparison to RHEM and RiverMorph FlowSed shows that these methods calculate a lower bound estimate. The left side of Table 2 shows gross sediment yield calculations transformed to net deposition in the debris basin with an applied trap efficiency of 75%. The right side of Table 2 are methods that start with net deposition in the reservoir that are later transformed to gross sediment yield using a trap efficiency of 50 percent.

Table 2. Sediment yields transformed to sediment yield and deposition into Santaquin debris basin

	Net Deposition				*Sediment Yield*		
	Bridges	RHEM Sandy Loam	McMillen PSAIC	AGWA	125 acre feet 40 years	84 acre feet 40 years	SLF original
Sediment Yield (ac- ft/mi^2)	0.35	0.1	0.64	0.86	0.18	0.12	0.15
Sediment Yield (ac- ft/yr)	6.74	1.93	12.32	16.56	3.44	2.31	2.83
Sediment deposited into Reservoir (ac/yr) @ 75% trap efficiency	5.05	1.44	9.24	12.42	2.58	1.73	2.12

RiverMorph FlowSed analysis included an average scenario without including aggradation or trap efficiencies, resulting in 1.056 ac-ft/yr of deposition. Multiple rating curves and bedload and suspended sediment rates were calculated. The calculated annual sediment deposition rate is 1.056 ac-ft/yr under conditions of 0.07 af/mi^2/yr and 75% trap efficiency, table 3.

Table 3. FlowSed sediment input rates with annual sediment deposition to the Santaquin Debris Basin

Pagosa Bedload Rating Curve	Pagosa Suspended Sediment Rating Curve	Bedload / Suspended Result Tons	Bedload + Suspended Sediment (Tons)	Bedload and Suspended Sediment (ac-ft/yr) @ 1.35 tons/cubic yards
good/fair	good/fair	447 / 731	1178	0.562
good/fair	poor	447 2285	2732	1.303
poor	poor	966 / 2285	3251	1.550
poor	good/fair	966 / 731	1697	0.809
			Mean	1.056

Sedimentation Decision

The RiverMorph FlowSed provides the lowest result when compared to other methods analyzed in this study. The original study (SCS 1954) sediment yield is 0.12. The new updated sediment yield rate of 0.07 ac-ft/mi^2, yields a sediment deposition rate of 1.056 ac-ft/yr to Santaquin Debris Basin. The RiverMorph FlowSed model likely provides the most accurate results due to realistic inputs, upper bedload considerations (0.41 lbs./sec), and larger more conservative flows from the Payson Creek above Diversion stream gage. This sedimentation rate is recommended for planning purposes.

PSH Snowmelt

A typical rain 100-year, 10-day rain PSH and a TR60 100-year, 10-day snowmelt runoff volume were initially modelled. The snow melt runoff volume controlled. TR60 (2005) snowmelt runoff volume for this study area for the 100-year, 10-day runoff volume value is 3.0 inches and the ratio of volumes of runoff volume (Q1/Q10) is 0.3 for a 100- year, 1-day runoff volume of 0.9 inches. This number when compared to estimated 100-year events seemed to be an outlier. TR60 does say in the hydrology section under Precipitation and runoff amounts beneath Principal spillway “A special study may show that local streamflow records can be used directly or regionalized to develop design runoff volumes.” Using this language a special study was conducted. The National Engineering Handbook (NEH) Section 4 Chapter 21 (NRCS, 1972) states “No standard NRCS procedure exists for regional analysis of runoff volumes for varying frequencies and durations”, thus motivating the present study.

It should be noted TR-60 contains only regional representations (NRCS 2005), and the analyses required for the Santaquin site necessitate more localized data. Therefore, this study presents the 100-year, 1-day and 100-year, 10-day runoff values derived from local snowmelt-induced stream gage data using surrogate gage data.

Methods

Multiple methods were used to provide runoff verification estimates, including an overview of gages, SNOTEL data, and studies in the areas. The Franson Civil Engineering (Franson 2013) was used to provide surrogate stream gage results for the Summit Stream Gage. This Franson study provided data to derive the 100-year, 1-day, and 10-day runoff values for the snowmelt volume. The long duration data set was also used to provide return intervals for both the 1 day and 10 day. The Utah SNOTEL Staff Report (Julander and Clayton, 2017) provides a base for early snowmelt in the lower Santaquin watershed but provides little snowmelt runoff for the larger, upper 100-year 1-day 10-day snowmelt runoff; and takes into consideration elevation and aspect-facing slopes. Next, a rain-on-snowmelt event was used to provide possible alternatives for this type of event. The results of all estimates were then compared to the TR60 PSH rain and snowmelt events.

Assessment of potential surrogate stream gages and SNOTEL Data: A previous study determined average daily flows from 1927-2010 for the Summit Creek stream gage in the Santaquin watershed (Franson 2013). A total of six stream gages and one snow telemetry (SNOTEL) site were examined (Figures 3-4) in comparison to this Summit Creek gage. The assessment of stream gage data showed anomalously low values at the Summit Creek site compared to other nearby stream gages. Therefore, additional datasets were assessed. The Payson SNOTEL site has the longest record in the proximal area, spanning 1980 to 2018 (NRCS 2017a), and is located in the watershed adjacent to the Santaquin Debris Basin. Although the Spanish Fork stream gage does not directly contribute to the Santaquin watershed, this gage was used as a surrogate to compare the overall runoff volume trend and 10-day aggregations of runoff volumes at stream gages and to compare with stream gages or the snow water equivalent (SWE) from the Payson SNOTEL site.

The Spanish Fork gage and Payson SNOTEL site were used to compare stream gages used in this study and their overall applicability to the Santaquin Debris Basin watershed (Figure 3). Overall, the stream gage data peaks and runoff volumes parallel or mimic the Spanish Fork gage or Payson SNOTEL runoff volume data (Figure 4).

The Payson and Summit 10-day accumulated average daily values match well, concerning occurrences of peaks and lows of daily data (Figure 4). However, the periods of record do not continuously overlap. The early 1910s data from Summit Creek gage have six years of representation. Payson gage does not start recording until 1948. Summit gage has a lack of data from 1917 to 1954. There are only eight years of overlapping datasets from 1955 to 1962. It appears that a possible crucial, high positive spike period that the Payson gage covers in the early 1950s is not covered in the Summit gage data. The timing of the highs and lows for the Payson and Summit gages coincide with those of the Spanish Fork gage. The Nebo gage runoff volume values are lower than the Payson, Summit, and Sixth Water runoff volume values (Figure 4). The data at the Nebo site do, however, correlate with the Spanish Fork site high and low runoff volume values.

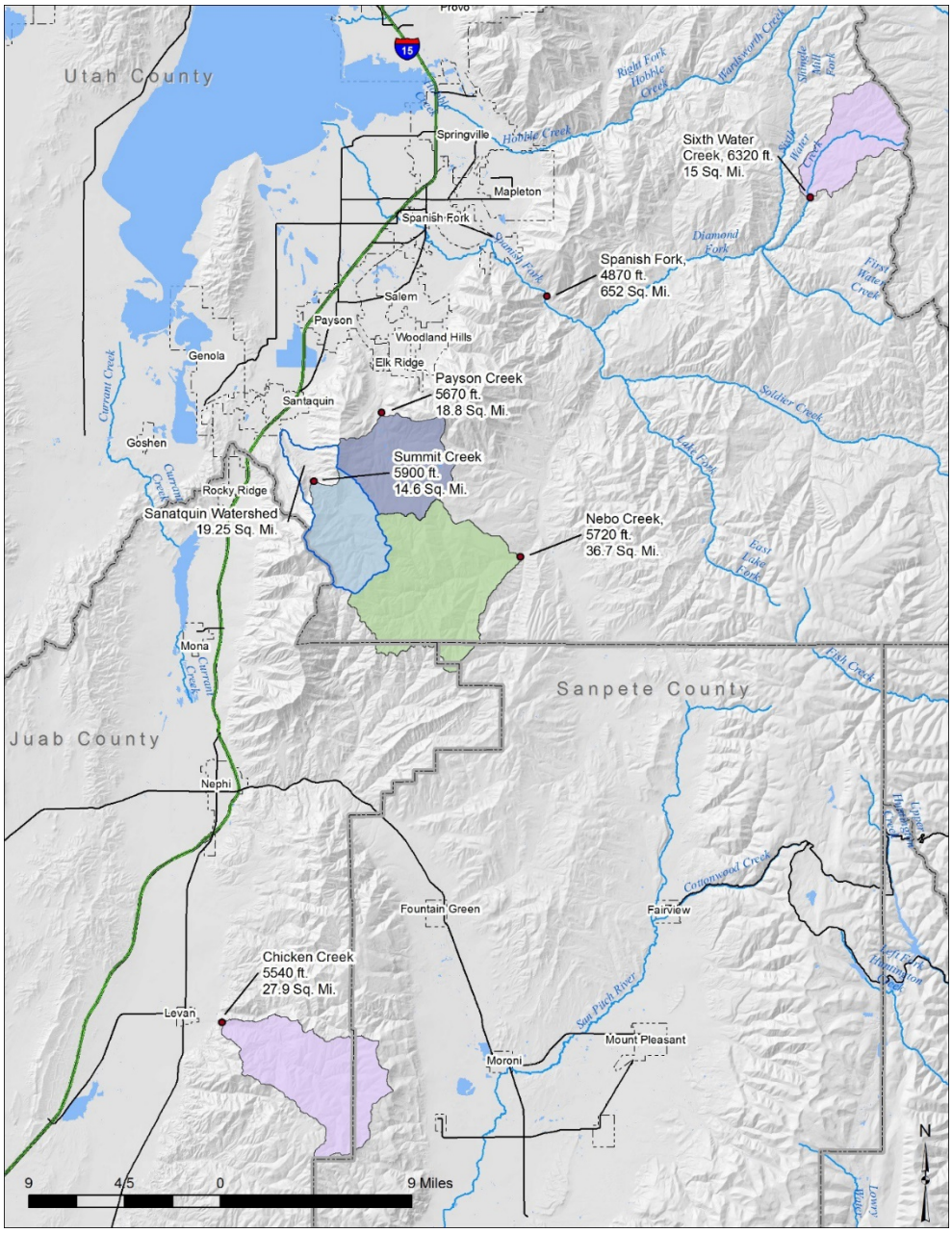

Figure 3. Location of stream gages (USGS 2017a-f) and SNOTEL site (NRCS 2017a) used in study. Base map derived from 5m auto-correlated DEM from 1m GSD NAIP (AGRC 2007a). All). All shapefiles from USGS (USGS 2017a-g) and AGRC (AGRC 2005, 2007a, 2007b, 2017a, 2017b)

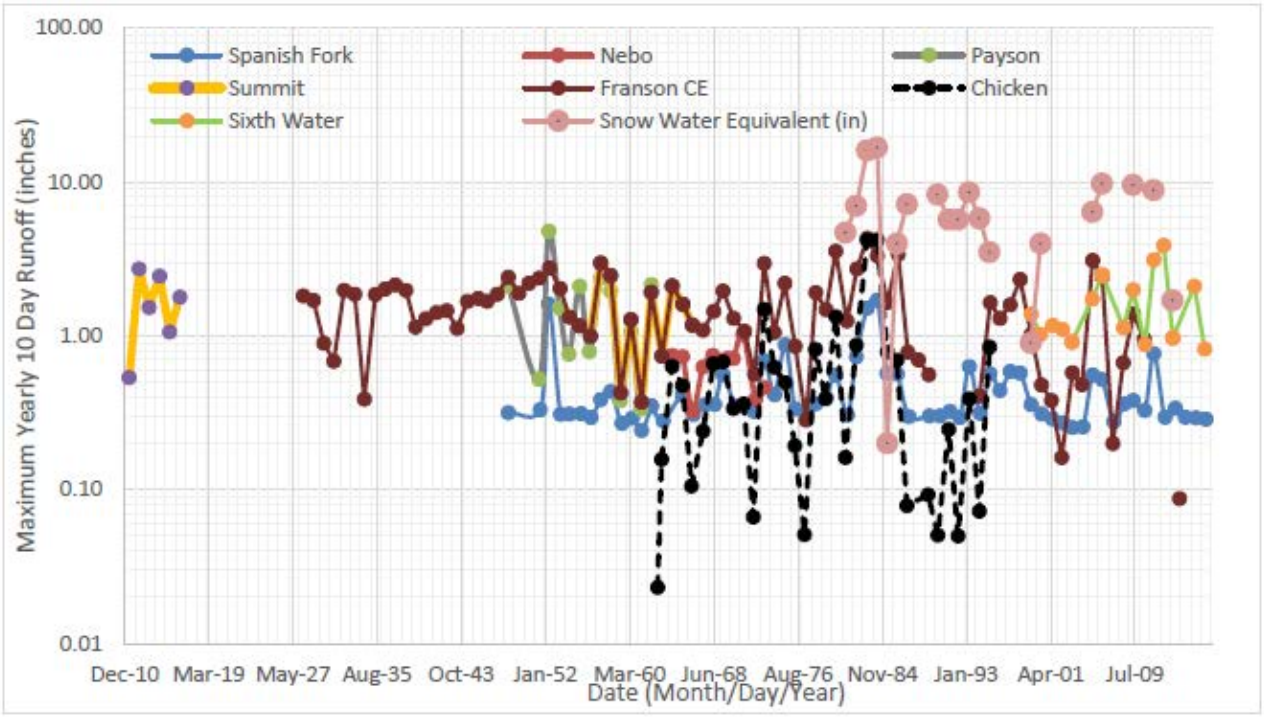

Figure 4. Largest 10-day runoff volumes for SNOTEL (NRCS 2017a) and stream gages (USGS 2017a-f)

Most of the stream gages assessed indicate that the watersheds are snowmelt-driven systems, with the exceptions of a few events at the Sixth Water and Nebo stream gages, See Table 4 for the number of peaks that occur during spring runoff period. Most peaks occurred in April, May, June, and a few in early July (WRCC 2017). Of the 18 years of maximum 10-day runoff volumes at the Sixth Water stream gage, three values were determined to be non-snowmelt events that occurred in late July, October, and November. Of the 10 years of maximum 10-day runoff volumes at the Nebo stream gage, only one year (1969) had a peak maximum 10-day outside of the April, May, and July period.

Table 4. Maximum 10-day flows and non-snowmelt flows for at stream gage sites

USGS Gage	No. of 10-days / non-snowmelt peaks	Area (mi^2)	CSM @ 100-year	Elevation (ft)
Sixth Water	18/3	15.0	22.0[1]	6320
Summit	18/0	14.6	18.6	5900
Nebo	10/1	36.7	18.9	5720
Payson	15/0	18.8	37.0	5670
Chicken Creek	41/0	27.9	31.5	5540

Table 4 shows the number of maximum 10-day flows and non-snowmelt 10-day flows for each site. To normalize the watersheds and determine outliers, the watersheds are compared using a cfs/mi^2 (CSM) approach, with cfs values from Kenney et al. (2007). Chicken Creek and Payson gages show the highest CSM at the 100-year return interval, at 31.5 and 37.00, respectively (Table 4). The Sixth Water, Summit, and Nebo gages have a CSM of approximately 20.0 at the 100-year return interval. Some noticeable differences are that the Nebo gage has the largest contributing area, and the Sixth Water gage is located at the highest elevation (Table 4).

In most cases, spring snowmelt runoff peaks occurred from mid-April to early June. Figure 5 shows the date of snowmelt starting peak daily flows for the five stream gages analyzed in this report for their period of record.

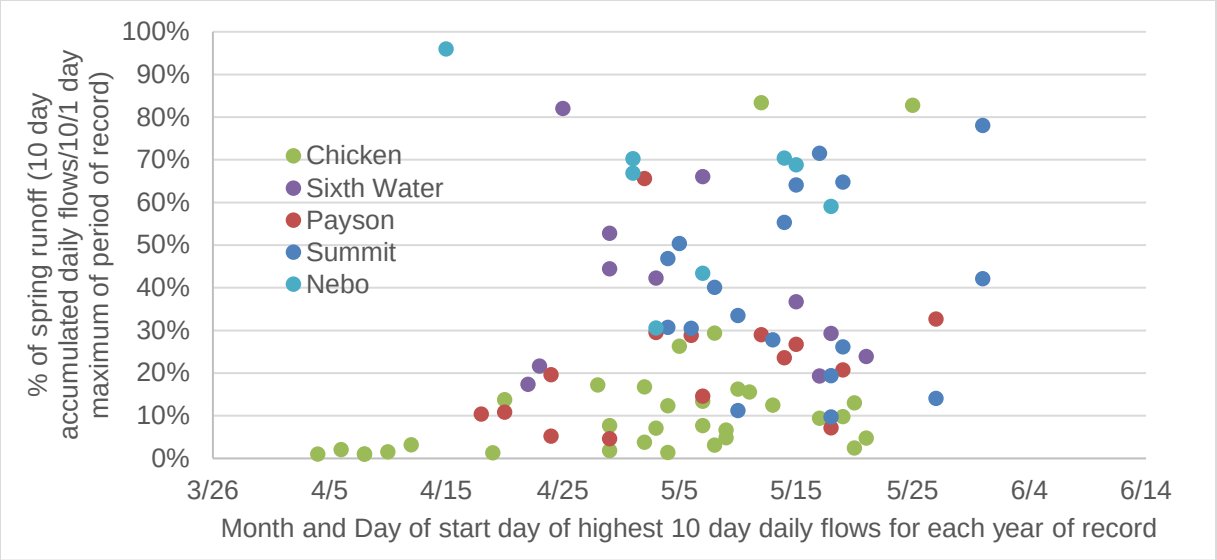

Figure 5. Beginning peaks of selected gages of the largest 10-day snowmelt period

Using Franson study to derive surrogate 10-day flows

The Summit gage is believed to be an under-representation of possible 100-year, 1-day and 100-year, 10-day snowmelt runoff volume values when initially comparing datasets from other nearby stream gages, and the Summit gage does not capture some critical periods of the hydrologic record. The next closest gage, the Payson gage, is an over-representation of possible 100-year, 1-day and 100-year, 10-day snowmelt runoff volume values, showing a CSM higher than the others. According to Franson (2013), the Payson gage has a low R-value for surrogate incorporating to substitute and develop daily flows for the Summit gage. The Franson (2013) study, which uses the Summit Creek gage, Salt Creek gage, and American Fork gage, was used to develop the 100-year, 1-day and 100-year, 10-day runoff volume values. and the 2-year runoff volume values was used in a rain-on-snow scenario.

To develop the 100-year, 1-day and 10-day discharge values, the daily data from the Franson (2013) largest 1-day and 10-day accumulated discharge values for each year were used to develop a Log Pearson III distribution. Table 5 shows the resulting quartiles from the largest 1-day and 10-day accumulated daily flows for each year for the period available.

Table 5. Minimum, maximum, and 1st, 2nd and 3rd quartiles for the 1-day daily and accumulate 10-day flow and runoff volumes from the Franson (2013) dataset.

	10-day accumulated daily flow (cfs)	10-day accumulated runoff volume (in)	1-day mean daily flow (cfs)	10-day mean daily runoff volume (in)
Minimum	64	0.16	10	0.03
1st Quartile	363	0.92	45	0.11
2nd Quartile	573	1.46	73	0.19
3rd Quartile	785	2.00	92	0.23
Maximum	1695	4.32	263	0.67

Return flow frequencies were generated using the 10-day daily accumulated average discharges and largest average 1-day daily flow (Table 6). Table 6 also shows the transformation from the discharge to runoff volumes, cfs to inches, for the 14.6 mi^2 watershed.

Table 6. Franson (2013) derived 1-day and 10-day accumulated daily flow return intervals and 1-day and 10-day transformed runoff values

Recurrence (years)	Discharge 10-day (cfs)	Discharge 1-day (cfs)	Runoff 10-day (inches)	Runoff 1-day (inches)
1000	2,343	312	5.97	0.79
500	2,207	288	5.62	0.73
200	2,009	255	5.12	0.65
100	1,843	230	4.69	0.59
50	1,661	203	4.23	0.52
25	1,463	176	3.73	0.45
20	1,395	167	3.55	0.43
10	1,170	139	2.98	0.35
5	920	109	2.34	0.28
2	532	65	1.36	0.17

Transformation from runoff at Summit Stream gage to the Debris Basin

The Summit watershed faces in a north direction slightly orientated to the west. Figure 6 shows the area in question and specifically the Summit gage and Santaquin Debris Basin contributing areas, emphasizing that the lower portion of the basin is more exposed than the upper portion. The difference between the areas (4.65 mi^2) between the Summit gage and the Santaquin Debris Basin needs to be transposed from the gage to debris basin or not is in question.

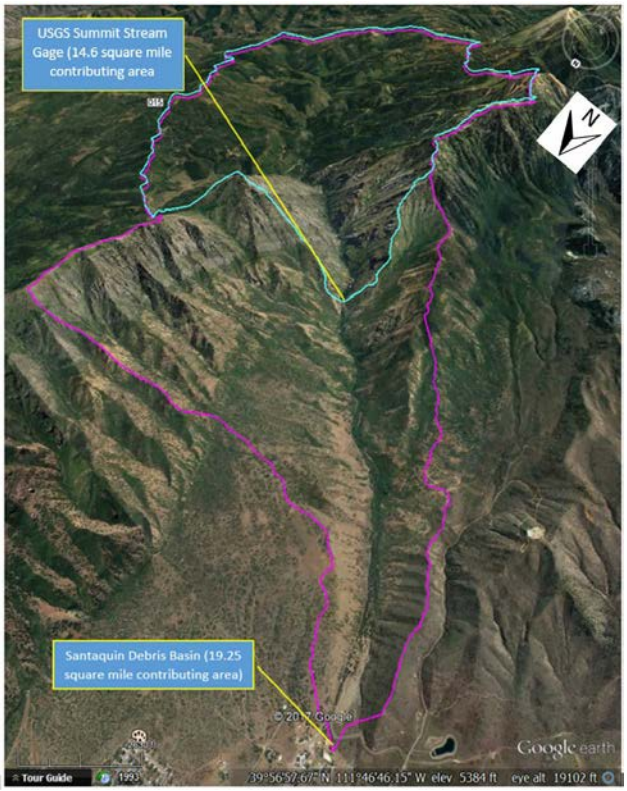

Figure 6. Contributing areas of the Summit stream gage and Santaquin Debris Basin.

Julander and Clayton (2017) state that only 16% of the watershed area (0.75 mi^2) contributes the annual peak snowmelt runoff. Therefore, 25% of the runoff volume from the upper section should be more than

sufficient to -account- for the lower 4.65 mi² section between the Summit gage and the Santaquin Debris Basin. This being the case, the 100-year, 10-day runoff volume of 4.69 inches at the Summit gage derived from the Franson (2013) study and applying 25% to the runoff volume at the gage to the area below the gage to the debris basin will have a total runoff volume of 3.84 inches for the 100-year, 10-day. and the 100-year, 1- day runoff volume is 0.48 in. Tables 7 show calculations for both the 100-year, 10-day and 100-year, 1-day runoff volume for the 2- year to 1000- year return intervals.

Table 7. 100-year, 10-day and 1-day runoff accounting for ¼ the runoff volume for the unaccounted area between Summit gage and Santaquin Debris Basin.

Return Interval	10-day, 1-day runoff volumes at 14.6 mi² (in)	10-day, 1-day runoff volume (25% of 10-day runoff volume) at 4.65 mi² (in)	10-day, 1-day runoff volume at 19.25 Mi² (in)
1000	5.97, 0.79	1.49, 0.20	4.89, 0.65*
500	5.62, 0.73	1.41, 0.18	4.6, 0.60
200	5.12, 0.65	1.28, 0.16	4.19, 0.53
100	4.69, 0.59	1.17, 0.15	3.84, 0.48
50	4.23, 0.52	1.06, 0.13	3.46, 0.43
25	3.73, 0.45	0.93, 0.11	3.05, 0.37
20	3.55, 0.43	0.89, 0.11	2.91, 0.35
10	2.98, 0.35	0.75, 0.09	2.44, 0.29
5	2.34, 0.28	0.59, 0.07	1.92, 0.23
2	1.36, 0.17	0.34, 0.04	1.11, 0.14

A 100-year, 1-day and 100-year, 10-day rain-on-snow scenario was analyzed to make certain that the 100-year, 1-day and 100-year, 10-day snowmelt were not underestimated. The 100-year, 1-day and 100-year, 10-day precipitation events were taken from NOAA Atlas 14 (NOAA, 2011) and 100-year, 24-hour and 100-year, 10-day grids from the NOAA Precipitation Frequency Data Server (PFDS; 2017). A weighted analysis over the entire Santaquin watershed to derived mean precipitation. This produced a 100-year, 1-day precipitation of 3.37 inches and a 100-year, 10-day precipitation of 7.72 inches.

Data from Table 4 and Table 6 contribute to base flow calculations for rain-on-snow scenarios. The three methods for 2-year base flow calculation result in 65 cfs, 0.17 inches runoff volume, and 3.37 CSM for a 19.25 mi² watershed (Table 9). The 2-year base flow is calculated in three methods as Table 8 has the 1-day and 10-day rainfall totals from the 2-1000-year return intervals with the 2-year derived runoff volume to be used a base flow for the rain-on-snow scenarios

Table 8. Rain-on-snow scenario using the high 10-day flows overall average and 2-year runoff volume scenario.

	1-day rain (in)	10-day rain (in)	2-year derived runoff volume (Franson, 2013) (in)
1000	4.43	10.4	0.17
500	4.11	9.54	0.17
200	3.7	8.46	0.17
100	3.38	7.68	0.17
50	3.08	6.92	0.17
25	2.77	6.18	0.17
10	2.38	5.25	0.17
5	2.09	4.56	0.17
2	1.73	3.73	0.17

TR60 PSH rain-snowmelt runoff, surrogate PSH snowmelt runoff and rain on snow scenarios

There are four scenarios in Table 9. Two scenarios are customary PSH scenarios as explicitly defined by TR60 (NRCS 2005). Rain-on-snow events were modelled using the 2-year runoff volume (derived from Franson (2013) study) and NOAA Atlas 14 10-day rainfall value (Table 9). The last scenario shows the Franson (2013) study results for the runoff volume at the Summit gage and transformation from the Summit gage to Santaquin Debris Basin, using Utah SNOTEL's Report (Julander and Jordan, 2017) up for the area (Tables 7). The scenarios and nomenclature used are below:

Scenario 1. Using the Franson data with 25% of the upper watershed applied to the lower watershed below the Summit gage. $Franson_{25\%belowgage}$
Scenario 2. The TR60 derived values for comparative purposes. $TR60\text{-}PSH_{snowmelt}$
Scenario 3. Rain 100-year, 1-day and 100-year, 10-day. $TR60\text{-}PSH_{rain}$
Scenario 4. Rain-on-snow, using Franson data to derive 2-year runoff volume base flow with the 100-year, 1-day and 100-year, 10-day precipitation. $TR60Rain_{rain\text{-}on\text{-}snow\text{-}NOAA\ 2\ year}$
Table 9 outlines the results of the SITES software runs and an auxiliary spillway elevation required for the existing condition.

Table 9. Results with pertinent 100-year, 1-day and 100-year, 10-day runoff volume information with auxiliary spillway required height for the existing condition.

Scenario/Run	*100-year, 10-day Runoff volume (inches)*	*100-year, 1-day Runoff volume (inches)*	*Inflow Peak(cfs)*	*Volume (acre feet)*	*Auxiliary Elevation above MSL (feet)*	*2-year base flow as both cfs and runoff*
1/ $Franson_{25\%belowgage}$	3.84	0.48	304.2	158.4	5195.25	
2/ $TR60\text{-}PSH_{snowmelt}$	3.0	0.90	1309.8	564	5231.95	
3/ $TR60\text{-}PSH_{rainNOAA}$	7.68	3.38	586.6	92.4	5188.92	
4/ $TR60Rain_{rain\text{-}on\text{-}snow\text{-}NOAA\ 2\ year}$	7.68	3.38	651.7	130.5	5192.69	65 cfs / 0.17 inches

PSH Decisions and Discussion

The basis of this study is that the Summit gage daily flows are not representative or plausible for the 100-year, 1-day and 100-year, 10-day discharges to set the auxiliary spillway height for the Santaquin Debris Basin. The Franson study (2013) provides insight and average daily replicated record from 1927-2010, excluding six years of data. The Franson study (2013) was used to derive the 100-year, 1-day and 100-year, 10-day snowmelt runoff volume events. The Franson-derived data can provide one of the recommended values to derive frequency intervals and runoff volume values. A rain-on-snow scenario with the 2-year base flow was analyzed to provide a level of confidence in Franson-derived 100-year, 1-day and 100-year, 10-day runoff volume values for comparative purposes.

The derived data using the TR60 snowmelt (NRCS 2005) to determine runoff volume values are high based on the stream gage data in the area, and therefore considered not representative. The PSH rainfall event is the lower bound event concerning volume and auxiliary elevation height, and the TR60 snowmelt derived values results in the upper bound. This was all done to create a defensible and justifiable estimate and to provide an upper and lower bound.

Conclusions

Multiple sedimentation methods were analyzed and compared to the original 1954 sediment deposition as part of this study. Methods such as the RHEM, PSAIC and the 1973 Bridges map provide a quick reference to a possible range of sediment values but provide little confidence in actual range of possible values. The AGWA SWAT method is more data intensive but resulted in a high value. The question I

would ask is "does two or three methods justify due diligence." Although a sediment rate is documented and justified, it is known that these values are an average, but fires, high intense storms, and drought (non-typical year(s)) could result in a large sediment load or none. Using a system of averages does seem to work and looking at multiple methods does have value to document your decision support. Access to the Hotchkiss and Hinton bedload database, multiple software (HEC RAS, FlowSED, GIS) data, and the surrounding stream gage data facilitates derivation of multiple results to estimate runoff and support these estimates.

The PSH is routed upon the sediment pool. The existing auxiliary spillway is undersized and currently causes an induced flooding scenario. The height of the existing auxiliary spillway from a PSH standpoint is set at the lower elevation, meaning that the auxiliary spillway will be active at smaller events. Ideas and concepts have included not activating the auxiliary spillway until the 500-year event. This will mean a limited capacity secondary spillway will need to be activated and limited to a possible 500-year event, possibly using the existing auxiliary spillway as a secondary principal spillway. The PSH is to set the auxiliary spillway elevation, but this in only true for earthen spillways. In this case this study has showed that both the TR60 rain and snowmelt runoff volume PSH are extreme events. These scenarios may not be appropriate runs to set the height of the auxiliary spillway. Due diligence warrants to have the PSH 100-year, 10-day snowmelt runoff volume modelled to assure that the auxiliary spillways route this event as anticipated. TR60 currently has wording to include a special study. In this case it is not a special study but a site-specific study. Perhaps future TR60 wording should include the wording "to conduct a site-specific study and have different criteria between a site specific and special study." Else a new TR60 snowmelt runoff volumes should be generated to provide the level of detail needed to not need a site specific study.

References

Bridges, B.L. 1973. Map: "Estimated sediment yield for the State of Utah". Erosion and Sedimentation, Western U.S. Water Plan, prepared by SCS.

Burns, I.S., Scott, S.N., Levick, L.R., Semmens, D.J., Miller, S.N., Hernandez, M., Goodrich, D.C., and Kepner, W.G. 2007. Automated Geospatial Watershed Assessment 2.0 (AGWA 2.0) – A GIS-Based Hydrologic Modeling Tool: Documentation and User Manual; U.S. Department of Agriculture, Agricultural Research Service.

Franson Civil Engineering (Franson CE). 2013. Summit Creek Water Management Project – Hydrology Report. American Fork, Utah

Hotchkiss, R. and Hinton, D. 2015. "HydroServer Lite – Bedload Database." http://www.worldwater.byu.edu/interactive/app/application/config/installations/, Brigham Young University, Provo, Utah. (Updated regularly.)

Jensen, D. T., Bingham, G. E, Ashcroft, G. L., Malek, E., McCurdy, G. D., and McDougal, W. K. 1990. "Precipitation Pattern Analysis Uinta Basin – Wasatch Front WRE 340AL." Office of the State Climatologist Utah State University, Logan, Utah

Julander, Randall and Clayton, Jordan, 2017, Summit Creek Hydrologic Analyses. United Stated Department of Agriculture, Natural Resources Conservation Service (NRCS)

Kenney, T.A., Wilkowske, C.D., and Wright, S.J., 2007. "Methods for estimating magnitude and frequency of peak flows for natural streams in Utah", U.S. Geological Survey Scientific Investigations Report 2007-5158, 28 p.

Moody, Tom, Wirtanen, Mark, and Yard, Stephanie N. 2003. "Regional Relationships for Bankfull Stage in Natural Channels of the Arid Southwest". Natural Channel Design, INC. Flagstaff, Arizona.

National Ocean and Atmospheric Administration (NOAA). 2011, NOAA Atlas 14 – Precipitation-Frequency Atlas of the United States, Volume 1, Version 5.0: Semiarid Southwest (Arizona, Southeast California, Nevada, New Mexico, Utah).

National Ocean and Atmospheric Administration. 2017. Precipitation Frequency Data Server (PFDS), accessed July, 2017.

Nearing M.A., Wei H., Stone J.J., Pierson F.B., Spaeth K.E., Weltz M.A., and Flanagan D.C. 2011. "A rangeland hydrology and erosion model". Transaction of American Society of Agricultural and Biological Engineers 54:1-8.

RIVERMorph, LLC. 2008. Rivermorph User's Manual Version 4.3. Louisville, Kentucky, 40223.

Rosgen, D.L. 2006a. "FlowSed/PowerSed – Prediction Models for Suspended and Bedload Transport". Proceeding from the 8th Joint Federal Interagency Conference, Reno, Nevada.

Rosgen, D.L. 2006b. Watershed Assessment of River Stability and Sediment Supply (WARSSS). Wildland Hydrology, Fort Collins, Colorado.

Todea, Nathaniel. 2015. NRCS Utah Santaquin Sediment Study Memo Santaquin Debris Basin, Dam Rehabilitation. United States Department of Agriculture, Natural Resources Conservation Service, Salt Lake City, Utah.

Todea, Nathaniel. 2017. NRCS Utah Snowmelt Based Principal Spillway Hydrograph Development Report – Santaquin Debris Basin, Dam Rehabilitation. United States Department of Agriculture, Natural Resources Conservation Service, Salt Lake City, Utah.

Todea, Nathaniel and Hasenyager, Candice. 2012. Integration of Time Series data with Geospatial Data for Tibble Fork Reservoir Sedimentation Study. American Water Resources Association Spring Speciality Conference, Geographic Information System and Water Resources VII, New Orleans, Louisiana, March 26-28.

United Stated Department of Agriculture, Natural Resources Conservation Service (NRCS). 1972. Design Hydrographs. National Engineering Handbook, Part 630, Chapter 21. Washington, DC.

United Stated Department of Agriculture, Natural Resources Conservation Service (NRCS). 2005. Earth Dams and Reservoirs, Technical Release 60, https://directives.sc.egov.usda.gov/OpenNonWebContent.aspx?content=24937.wba.

United Stated Department of Agriculture, Natural Resources Conservation Service (NRCS). 2009. National Watershed Program Manual, https://directives.sc.egov.usda.gov/viewerFS.aspx?hid=36702

United Stated Department of Agriculture, Natural Resources Conservation Service (NRCS). 2017a. SNOTEL Site: Payson R.S., https://wcc.sc.egov.usda.gov/nwcc/site?sitenum=686, Date last accessed: October 2016.

United Stated Department of Agriculture, Natural Resources Conservation Service (NRCS). 2017b. Excel Spreadsheet FreqCurves_ver306.xlsm, https://www.nrcs.usda.gov/wps/portal/nrcs/detailfull/national/water/manage/hydrology/?cid=stelprdb1042910

United Stated Department of Agriculture, Natural Resources Conservation Service (NRCS). 2017c. Soil Survey Geographic (SSURGO) Database. Available online at 32TUhttp://sdmdataaccess.nrcs.usda.gov/U32T. Accessed [2017].

United States Department of Agriculture Soil Conservation Service (USDA-SCS). 1954. Workplan Santaquin Canyon Watershed Protection Project Utah, Salt Lake City, Utah.

United States Department of Agriculture Soil Conservation Service (USDA-SCS). 1975. Procedure, sediment storage requirements for reservoirs. Engineering Division Tech. Release No. 12.

United States Geological Survey (USGS). 2017a. USGS 10219200 CHICKEN CREEK NEAR LEVAN, UT, https://waterdata.usgs.gov/nwis/dv/?referred_module=sw&site_no=10219200, Date accessed: October 2016.

United States Geological Survey (USGS). 2017b. USGS 10148400 NEBO CREEK NEAR THISTLE,UTAH, https://waterdata.usgs.gov/nwis/inventory/?site_no=10148400&agency_cd=USGS/, Date accessed: October 2016.

United States Geological Survey (USGS). 2017c. USGS 10147500 PAYSON CREEK ABV DIVERSIONS, NEAR PAYSON, UTAH, https://waterdata.usgs.gov/nwis/dv/?referred_module=sw&site_no=10147500, Date last accessed: October 2016.

United States Geological Survey (USGS). 2017d. USGS 10149000 SIXTH WATER CRK AB SYAR NR SPRINGVILLE, UT, https://waterdata.usgs.gov/nwis/uv?site_no=10149000, Date accessed: October 2016.

United States Geological Survey (USGS). 2017e. USGS 10150500 SPANISH FORK AT CASTILLA, UT, https://waterdata.usgs.gov/nwis/uv?site_no=10150500, Date accessed: October 2016.

United States Geological Survey (USGS). 2017f. USGS 10147000 SUMMIT CREEK NEAR SANTAQUIN,UTAH, https://waterdata.usgs.gov/nwis/dv/?referred_module=sw&site_no=10147000, Date last accessed: October 2016.

United States Geological Service (USGS) StreamStats. 2017g. StreamStats watershed [shapefile]. https://water.usgs.gov/osw/streamstats/ssonline.html

United States Geological Survey Earth Resources Observation System Data Center (USGS-EROS-DC). 2001. National Land Cover Dataset. Sioux Falls, South Dakota.
Utah Automated Geographic Reference Center (AGRC). 2005. AGRC Municipalities [shapefile]. https://gis.utah.gov/
Utah Automated Geographic Reference Center (AGRC). 2007a. AGRC 5 m Auto-correlated DEM from 1m GSD NAIP. https://gis.utah.gov/
Utah Automated Geographic Reference Center (AGRC). 2007b. AGRC The National Hydrography Dataset (NHD) [shapefile]. https://gis.utah.gov/
Utah Automated Geographic Reference Center (AGRC). 2017a. Road Centerlines [shapefile]. https://gis.utah.gov/
Utah Automated Geographic Reference Center (AGRC). 2017b. AGRC Shaded Relief [ArcGIS Image Service]. https://gis.utah.gov/
Western Regional Climate Center (WRCC). 2017. CLIMATE OF UTAH. 2215 Raggio Parkway, Reno, NV access 2017 at http://www.wrcc.dri.edu/narratives/UTAH.htm

Understanding the Environmental Parameters that Influence Reservoir Sedimentation

Melissa A. Foster, Geomorphologist, U.S. Bureau of Reclamation, Denver, Colorado, mfoster@usbr.gov
Blair Greimann, Hydraulic Engineer, U.S. Bureau of Reclamation, Denver, Colorado, bgreimann@usbr.gov
Vince Benoit, Engineering Technician, U.S. Bureau of Reclamation, Denver, Colorado, vbenoit@usbr.gov

Abstract

Water resource management in the western U.S. is reliant upon aging reservoirs for critical storage and flood mitigation. Sediment accumulation can limit resource availability and storage and also reduce dam safety. A better understanding of reservoir sedimentation rates will improve the projections for water reliability, delivery, and availability, as well as enable better reservoir-management planning for storage and power generation. Reservoir surveys provide an estimate of reservoir sedimentation through time, but can be cost-prohibitive, and in some cases, the pre-dam surveys lack the necessary quality to accurately determine sedimentation rates.

Our work seeks to establish how modern sedimentation rates are influenced by various environmental parameters. We are constraining historical and modern sedimentation rates with the Reservoir Sedimentation Information (RSI) database, which the US Bureau of Reclamation and US Army Corps of Engineers (USACE) are close to completing. The database contains all reservoirs within USACE and Reclamation management that have been surveyed; the database reports estimates of reservoir sedimentation based on the initial topographic surveys, or where applicable, subsequent re-surveys. There are over 350 reservoirs with at least two surveys, enabling a calculation of reservoir sedimentation. Our initial analysis will focus on 74 Reclamation reservoirs with calculated sedimentation rates, which we hope to expand to the USACE reservoirs.

Potential environmental parameters of interest include rock and soil type, climate zone, latitude, elevation, relief, mean annual precipitation and temperature, mean basin slope, land use, vegetation cover, and long term (millennial scale) drainage-basin erosion rates. We will compare measured sedimentation rates with environmental parameters, using both bivariate and multiple regression analyses. Our goal is to develop a series of regression equations that may be used as an estimate of sedimentation rates in un-surveyed reservoirs. A previous study found that long term drainage-basin erosion rates were best-explained by environmental parameters when combined in multiple regression analyses and that mean basin slope was the most powerful regressor (Portenga and Bierman, 2011). Long-term drainage basin erosion rates can be calculated from ^{10}Be measurements in quartz river sands, if quartz is well-distributed in a watershed. The concentration of ^{10}Be in sediment indicates the amount of time it takes to exhume and transport rocks from hillslopes, and therefore indicates drainage-basin erosion rates over timescales of 10^3-10^4 years (e.g., Brown et al., 1995; Granger and Schaller, 2014). It is unknown as to whether modern drainage-basin erosion rates can be explained by similar environmental parameters, and if so, whether this signal will be recorded in reservoir sedimentation.

We conducted preliminary analyses comparing sediment yield rates with elevation and contributing drainage area from 10-m digital elevation models (DEMs; https://viewer.nationalmap.gov/), mean annual precipitation and temperature over 1981-2010 (30-yr Normals from PRISM Climate Group, http://prism.oregonstate.edu/normals/), and latitude. Of these analyses, contributing drainage area yielded the strongest bivariate correlation (R^2=0.12); Figure 1) while other parameters did not demonstrate a bivariate correlation (R^2 values <0.04; Figure 2). Other researchers have found that sediment yield rate correlates with drainage area (e.g., Chow, 1964); the correlation we present here updates a 1982 analysis by Reclamation (Strand and Pemberton, 1982; see also Figure 1). We plan to improve upon our calculation of contributing drainage area by applying a weighting factor to represent how drainage area has changed over time due to the emplacement of upstream dams. Our presentation will cover the available data in the RSI database, as well as the results from ongoing regression analyses.

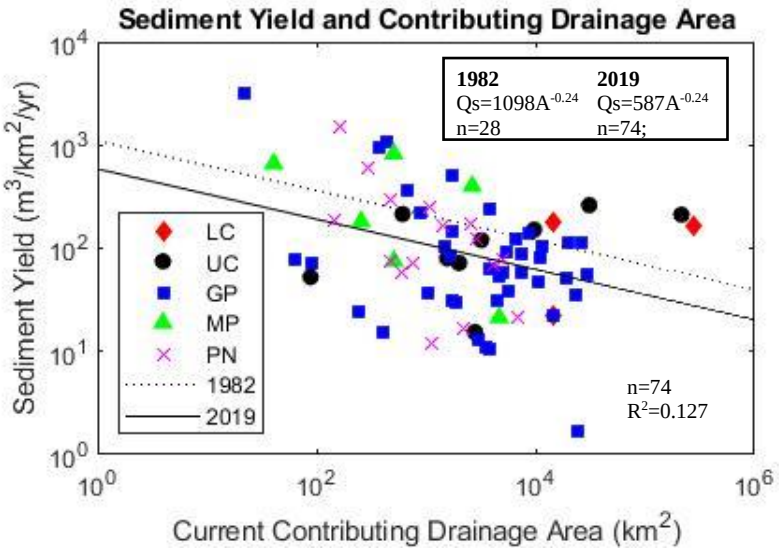

Figure 1. Correlation between drainage area and sediment yield rate. The best fit line is shown in black; the best fit line based on 1982 data analysis is shown in the dotted line. The data are also divided into Reclamation's regional groups: LC= Lower Colorado, UC= Upper Colorado, GP= Great Plains, MP= Mid-Pacific, PN= Pacific Northwest.

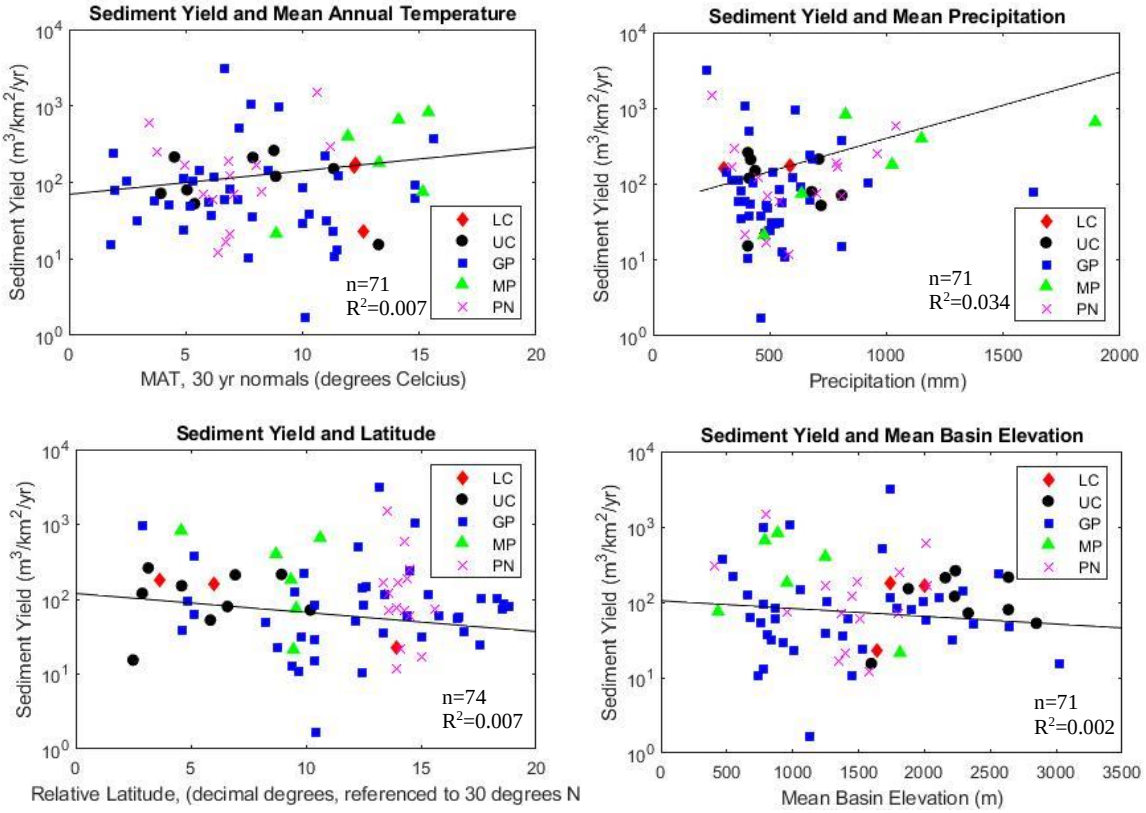

Figure 2. Correlations between mean annual temperature, mean annual precipitation, latitude, mean basin elevation, and sediment yield rate. Best fit lines are shown in black. The data are also divided into Reclamation's regional groups: LC= Lower Colorado, UC= Upper Colorado, GP= Great Plains, MP= Mid-Pacific, PN= Pacific Northwest.

Reference

Brown, E.T., Stallard, R.F., Larsen, M.C., Raisbeck, G.M., Yiou, F., 1995. Denudation rates determined from the accumulation of in situ-produced ^{10}Be in the Luquillo Experimental Forest, Puerto Rico. Earth Planet. Sci. Lett. 129 (1-4), 193-202. *http://dx.doi.org/10.1016/0012-821X(94)00249-X*.

Chow, Ven Te, 1964, Handbook of Applied Hydrology, McGraw-Hill, New York, NY.

Granger, D.E., Schaller, M., 2014. Cosmogenic nuclides and erosion at the watershed scale. Elements 10 (5), 369-373. *http://dx.doi.org/10.2113/gselements.10.5.369*.

Portenga, E.W., Bierman, P.R., 2011. Understanding Earth's eroding surface with ^{10}Be. GSA Today 21 (8), 4-10. http://dx.doi.org/10.1130/G111A.1.

Strand, R.I., Pemberton, E.L., 1982, Reservoir Sedimentation. Technical Guideline for Bureau of Reclamation, Sedimentation and River Hydraulics Section, Division of Planning Technical Services Engineering and Research Center, Bureau of Reclamation, Denver, Colorado, October 1982.

Sediment Properties

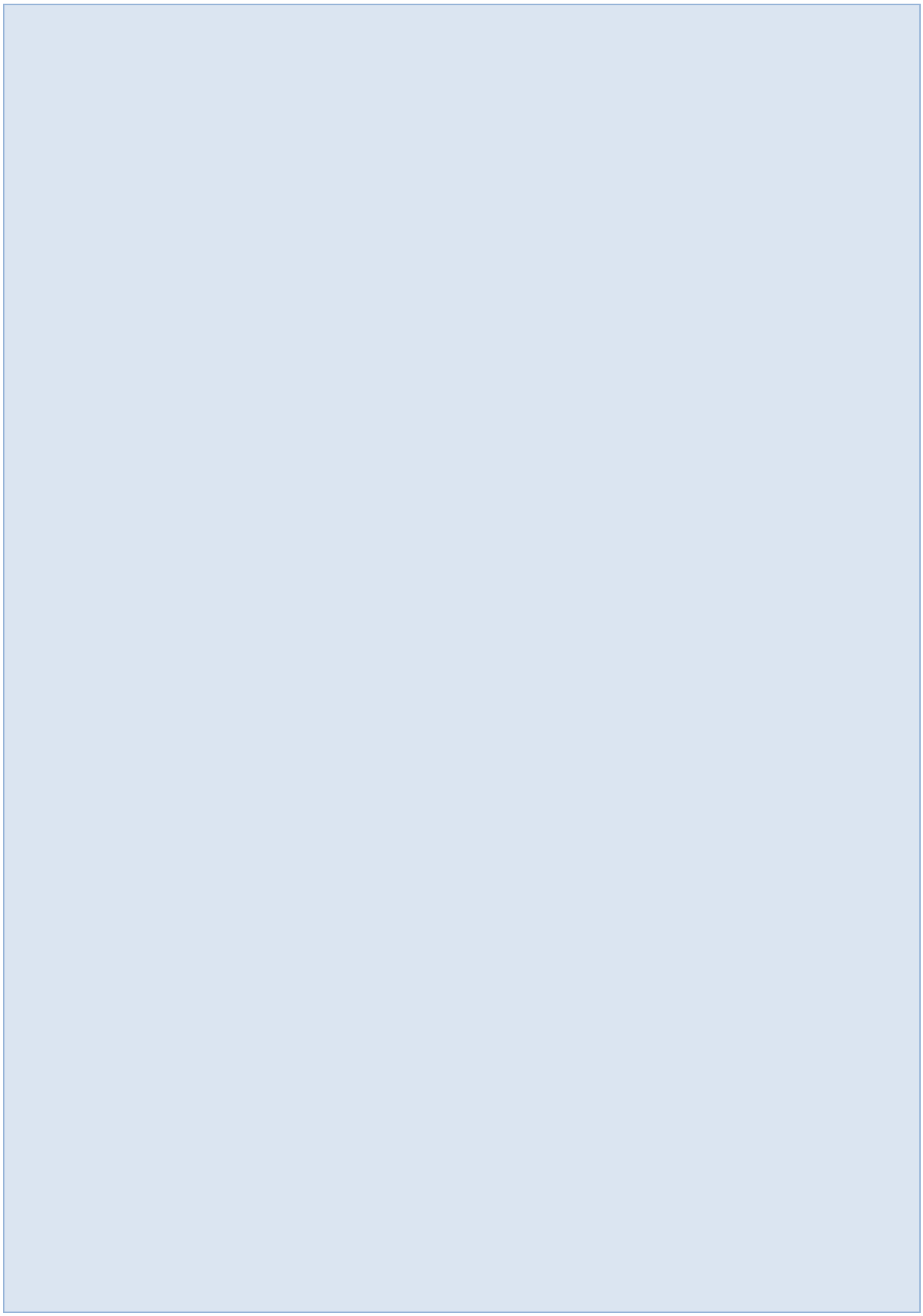

Assessing the Precision and Accuracy of Particle-Size Analysis with a Laboratory Laser-Diffraction Analyzer

Katherine Norton, Physical Science Technician, U.S. Geological Survey Cascades Volcano Observatory, Vancouver, Wash., knorton@usgs.gov

Introduction

The purpose of this study is to assess the precision and accuracy of laboratory laser-diffraction particle-size distribution (PSD) analysis in support of an effort to formally adopt the method for routine use in U.S. Geological Survey (USGS) sediment laboratories. USGS sediment laboratories analyze the PSD of sediment in support of a wide variety of sediment-transport and water-quality studies from around the United States (US).

The precision of the PSD for a sample can be assessed through replicate measurements, with typical quality control (QC) standards in USGS sediment laboratories requiring that the PSD results from primary and replicate sub-samples differ by no more than five percent finer to meet standards for acceptability (Shreve and Downs 2005). Precision defined in this way captures the combined uncertainty of the subsampling, preparation, and PSD analysis methods used in the analysis.

The International Standards Organization (ISO) defines precision for laser-diffraction analysis in terms of repeatability and reproducibility. To isolate the uncertainty associated with the laser-diffraction PSD analysis method, the ISO standard for laser-diffraction analysis requires the assessment of the coefficient of variation (CV) of the 10th, 50th, and 90th percentile diameters (d_{10}, d_{50}, d_{90}) among at least three repeated measurements of the same material (instrument repeatability) or at least three separate subsamples of the same bulk material (method repeatability) (ISO 13320:2009 6.4). The method used in this study adopts this definition of precision for QC of laser-diffraction PSD analysis.

The ISO standard also calls for method reproducibility checks using the same assessment technique (ISO 13320:2009 6.4). Method reproducibility checks by the ISO definition require multiple measurements of separate subsamples of the same bulk material by different operators using similar instruments (ISO 13320:2009 3.1). Because only one instrument and one operator were available for this study, reproducibility was assessed by measuring separate subsamples of the same bulk material over time.

Instrument accuracy for laboratory laser-diffraction analysis is assessed through the measurement of mixtures of spherical glass beads (ISO 13320:2009 6.5). According to the ISO standard, the best practice is to use nationally-traceable certified reference materials with well-known optical properties and a d_{90}/d_{10} ratio of at least 1.5 (ISO 13320:2009 6.5). The current protocol requires the measurement of traceable glass bead reference materials as part of the QC for the analysis.

Laboratory laser-diffraction results are reported in terms of the *laser-diffraction diameter*, which is the diameter of a spherical particle that produces the same light scattering pattern as the target particle, using a given optical model. The optical model requires the real and imaginary components of the refractive index (RI) of the particles in the sample as parameters. By this definition, an instrument that has verified accuracy for spherical particles of a known RI produces accurate results.

PSD results produced by laser-diffraction analysis are reported in terms of the percent by volume of sediment in a sample that occurs in various user-defined size classes. This contrasts with sieve and sedimentation methods, which are based on the percent by mass of sediment that is measured in user-defined size classes. Mass-based and volume-based particle-size analysis results can be used interchangeably as long as the particles in each size class have the same average density within a sample.

Different PSD analysis methods use different definitions of the "diameter" of irregularly-shaped particles (Inter-Agency Committee on Water Resources, Subcommittee on Sedimentation, 1957). Consequently, the PSD produced by one method cannot be directly compared to the results from a different PSD method unless the particles are spherical and any other assumptions required by both methods are met. Previous studies of inter-method comparability between laser-diffraction and other PSD analysis methods have mostly concluded that inter-method calibrations are possible for some populations of particles, but that there is no scientific basis for developing universal inter-method calibration functions between laser-diffraction and any other PSD analysis method (Kowlenko and Babuin 2013; Roberson and Weltje 2014). The unpredictable inter-method comparability between laser-diffraction and other PSD analysis methods limits the ability to test the accuracy of the particle sizes measured in laser-diffraction PSD analysis to testing with artificial spherical particles.

Because the purpose of the current protocol is to measure naturally-occurring sediment, a further definition of accuracy has been adopted that allows the laser-diffraction instrument to be tested with geologic materials. Accuracy in this context is extended to include the capacity of a PSD analysis to correctly measure PSD for mixtures of reference materials, each component of which has a well-known PSD for the target method. Under this definition of accuracy, the target of measurement is not the diameter of the particles, but rather the proportion of the sample composed of particles that fall into user-specified diameter ranges. The same method is used to define the accuracy targets and to perform the performance tests. Testing accuracy by this definition demonstrates whether a PSD analysis method is internally consistent without reference to other PSD analysis methods.

Methods

A single-wavelength Beckman-Coulter LS13320 particle-size analyzer with the Aqueous Liquid Module (ALM) attachment was tested with 1) vendor-supplied reference materials 2) NIST-traceable polydisperse glass bead standards 3) mixtures of commercially-available glass beads 4) mixtures of sands (<1 mm to >0.063 mm) and fines (<0.063 mm). Any use of trade, firm, or product names is for descriptive purposes only and does not imply endorsement by the U.S. Government.

Two vendor-supplied reference materials were measured: G15 (Beckman-Coulter), a garnet sample with a mean diameter of approximately 15 microns (μm), and GB500 (Beckman-

Coulter), a population of glass beads with a mean diameter of approximately 500µm. The vendor-supplied reference materials were prepared and analyzed according to the instructions provided by the vendor. The results from the LS13320 were compared to the defined targets for mean and standard deviation of the PSD supplied by the vendor.

Three NIST-traceable polydisperse glass bead reference materials were measured: Whitehouse Scientific 3–30µm (PS204), 50–350µm (PS227), and 150–650µm (PS237) standards. All three materials met the ISO requirements for use as an accuracy verification material for laser-diffraction analysis (ISO 13320:2009 6.5).

The 3–30µm material was suspended in a 1:100 solution of chemical dispersant (Guy 1969, p. 29) and de-ionized water (DI). The suspension was physically dispersed for 10–12 seconds with a sonic probe (Sonic Materials Vibra Cell VC375, power level 6, 90% duty cycle).

The coarser two materials (PS227, PS237) were split into two subsamples using a vane splitter (Rickly Hydrological Hydrolgical #505-001). The prepared material was introduced to the ALM and analyzed for three 30-second or 60-second runs following the instructions in the LS13320 user manual (Beckman-Coulter, 2011). The choice of 30-second or 60-second runs was made to explore whether differences in the results were observed based on run duration. The repeatability of each analysis was assessed according to the ISO method (ISO 13320:2009 6.4) using the instrument software. The LS13320 software was used to produce the geometric d_x values for the average of the three runs under both the glass optical model (RI: real component 1.5, imaginary component 0) and the Fraunhofer model (RI: real component 0, imaginary component 1). The Fraunhofer model is known to be inaccurate for particles finer than about 50µm for transparent particles and about 2µm for opaque particles (ISO 13320:2009 Annex A), however for most naturally-occurring sediment the RI is unknown, so the Fraunhofer model is used to provide a uniform basis for comparison with other results. The measured d_x values were compared to the target values on the Certificate of Analysis for the reference material. The control limits for the target values were the 95%CI times 1.03 or 1.04 as specified in ISO 1320:2009 6.5.

Internal reference materials (IRMs) of monodisperse commercially-available glass beads and geologic materials were created by measuring replicate subsamples of each IRM in the LS13320 under a variety of analysis conditions (e.g. run duration, pump speed, dilution). Three size ranges of glass beads were used: Polysciences 30–50 microns (Catalog #18901), 150–210 microns (Catalog #05483), and 210–250 microns (Catalog #18902). Six geologic materials were created by dry-sieving material contained in a bag of "Play Sand" (Quickrete, sourced from a local home improvement center) at standard phi intervals (2.0mm, 1.0mm, 0.5mm, 0.250mm, 0.125mm, 0.063mm). The sands were washed and oven-dried at 103°C after dry-sieving; the fines were oven-dried at 103°C after dry-sieving. A second population of fines was dry-sieved from a bed-material sample that had been collected in a stormwater settling basin in California. The fines from the settling basin were finer than the Quickrete fines based on a sedigraph analysis. The settling basin fines are referred to as 'Clayey' fines and the Quickrete fines are referred to as 'Silty' fines. The proportions of the reference materials used in each test mixture are given in Table 1 and Table 2.

At least six scoop subsamples were taken of each IRM. The size of the scoop was sufficient to produce the target 8 to 12 percent obscuration in the LS13320 (Beckman-Coulter, 2011), and varied by the size of the particles (Norton, 2019). The fines were suspended and dispersed as

described above for the polydisperse glass beads, but with 30 seconds of sonication. The subsamples were introduced to the ALM and analyzed according to the instructions in the LS13320 user's manual (Beckman-Coulter, 2011). The volume percent of each subsample that fell into each of the 92 size bins measured by the LS13320 was computed based on the Fraunhofer optical model. The mean and standard deviation of the volume percent in each size bin was computed among all the subsamples of each IRM.

Table 1. Percent by mass of each of three glass bead (GB) internal reference materials (Polysciences) used to construct mixtures for accuracy testing of the laboratory laser-diffraction analysis

Mixture	210–250µm	150–210µm	30–50µm
GB-A	20	0	80
GB-B	24	52	24
GB-C	50	50	0
GB-D	5	95	0
GB-E	75	25	0

Table 2. Percent by mass of each of six sediment (SED) internal reference materials used to construct mixtures for accuracy testing of the laboratory laser-diffraction analysis.

Mixture	500–1000µm	250–500µm	125–250µm	63–125µm	Silty Fines	Clayey Fines
SED-A	20	30	20	20	10	0
SED-B	0	10	20	20	0	50
SED-C	39	0	50	0	0	11
SED-D	0	0	0	0	80	20
SED-E	0	0	0	0	50	50
SED-F	0	0	0	0	20	80

Test mixtures of the IRMs were prepared by combining known masses of the individual IRMs to construct test samples with well-known expected PSD results from laser-diffraction analysis. For SED-A, SED-B, and SED-C, two separate test samples were prepared with identical proportions of the IRMs but different total mass. The expected volume percent in each size bin was computed as:

$$p_e = \sum_{i=1}^{n} \frac{m_i}{m} p_i \tag{1}$$

where p_e was the expected volume percent in a single size bin measured by the LS13320, n was the number of IRMs used to construct the test sample, m_i was the mass of a single IRM within the test sample in grams, m was the total mass of the test sample in grams, and p_i was the mean volume percent in the target size bin for the IRM. Using the mass-based weighted average to compute an expected volume percent depended on the assumption that there was no systematic difference in density among the IRMs that were used to construct a test sample.

The standard deviation of the replicate tests of each IRM was used to compute a standard deviation of the expected volume percent for each size bin using standard methods for propagation of uncertainty:

$$\sigma_{pe} = \sqrt{\sum_{i=1}^{n} \frac{m_i}{m} {\sigma_{p(i)}}^2} \quad (2)$$

where σ_{pe} was the standard deviation of the expected volume percent in a single size bin measured by the LS13320, $\sigma_{p(i)}$ was the standard deviation of the volume percent in the target size bin for the IRM, and other symbols were as described above.

The test samples were subsampled, prepared, and analyzed in the LS13320. When sands and fines were included in the same mixture, the fines were separated from the sand by sieving, and each fraction was subsampled and analyzed separately in the LS13320. The sand fractions were subsampled using the vane splitter. The fines were subsampled by either scoop subsampling or aliquot subsampling. Three 60-second runs on the LS13320 were measured at the target 8 to 12 percent obscuration for each subsample (Beckman-Coulter 2011). Other details of the handling and run conditions are documented in Norton (2019). The test results were checked for quality standards, including instrument repeatability and obscuration. The whole-sample volume percent finer was computed according to Equation 1, using the observed mass of sand and fines in the sample. This method of combining results from separate laser-diffraction analysis of multiple fractions in a sample was similar to that used by the USGS Coastal and Marine Geology Laboratory in Santa Cruz, Calif. (Penscil Inc., 2011). Observed results for the volume percent in each size bin from the LS13320 were compared to the expected volume percent to investigate the accuracy of the laser-diffraction PSD analysis for geologic materials.

Results

Vendor-Supplied Reference Materials

The LS13320 produced results for vendor-supplied reference materials that fell within the targets identified by the vendor (Table 1). The passing results indicate that the instrument was installed correctly and was operated in accordance with the instructions provided by the vendor.

Table 3. Results from analysis of two vendor-supplied reference materials in a Beckman-Coulter LS13320 with Aqueous Liquid Module attachment.

Material	Analysis Date	Test statistic	Expected Value (µm)	Control Limits (µm)	Observed Value (µm)	Pass/ Fail
G15	8/10/2017	Mean	14.4	±1.8	14.54	Pass
		St.Dev.	6.17	±2.25	6.383	Pass
GB500	8/10/2017	D10	518	±25.9	518.1	Pass
		D50	578	±17.3	577.9	Pass
		D90	645	±32.2	644.6	Pass
G15	3/12/2018	Mean	14.4	±1.8	14.80	Pass
		St.Dev.	6.17	±2.25	6.519	Pass
G15	3/28/2018	Mean	14.4	±1.8	14.60	Pass

		St.Dev.	6.17	±2.25	6.371	Pass
GB500	8/10/2017	D10	518	±25.9	518.5	Pass
		D50	578	±17.3	577.5	Pass
		D90	645	±32.2	643.1	Pass
G15	5/21/2018	Mean	14.4	±1.8	14.60	Pass
		St.Dev.	6.17	±2.25	6.446	Pass

NIST-Traceable Polydisperse Glass Bead Reference Materials

Tests of the NIST-traceable polydisperse glass bead reference materials demonstrated that the laser-diffraction analysis met the ISO standards for precision, as measured by the repeatability and reproducibility. All the tests except for one passed the ISO instrument repeatability test for the CV of the d_{10}, d_{50}, and d_{90} values among the 3 runs in each set (ISO 13320:2009 6.4, Norton, 2019). Similarly, the method repeatability among 3 to 8 replicate measurements of each reference material was excellent, with the CV of the d_{10}, d_{50}, and d_{90} falling within the ISO standards for all but the finest size reported for the finest standard (Table 4, Table 5, Table 6). Details of the analysis conditions and the results from individual tests can be found in the data release that accompanies this report (Norton, 2019).

The LS13320 results for the 3–30um NIST-traceable polydisperse glass beads fell within the certified targets for all but the d_{90} when the glass optical model was used (Table 4). When the Fraunhofer model was used, the d_{10} and d_{25} results were lower than the control limits (Table 4).

Table 4. Results from analysis of a 3–30um NIST-traceable polydisperse glass bead reference material (Whitehouse Scientific PS205). The control limits for the expected results were computed based on the standards outlined in ISO 13320:2009 6.5

[d_x: the particle size at which x percent of the total sediment volume in the sample occurs in particles of a smaller size than the Dx value; St.Dev.: Standard Deviation; Fraun.: Fraunhofer; CV: Coefficient of Variation]

Percentile Diameter	**d_{10}**	**d_{25}**	**d_{50}**	**d_{75}**	**d_{90}**
Lower Control Limit (µm)	8.25	10.28	12.55	15.33	18.84
Upper Control Limit (µm)	10.03	11.76	14.51	17.71	21.84
Observed dx (µm), Glass Optical Model Mean of n=3 replicate tests	8.848	10.70	13.26	16.75	21.88
Observed dx (µm), Glass Optical Model St. Dev. of n=3 replicate tests	0.121	0.18	0.14	0.21	0.58
CV (St. Dev./Mean), Glass Optical Model	1.4%	1.1%	1.1%	1.3%	2.7%
Observed dx (µm), Fraun. Optical Model Mean of n=3 replicate tests	1.803[a]	9.363	13.11	17.04	20.72
Observed dx (µm), Fraun. Optical Model St. Dev. of n=3 replicate tests	0.269	0.148	0.21	0.31	0.56
CV (St. Dev./Mean), Fraun.Optical Model	14.9%	1.6%	1.6%	1.8%	2.7%

[a] Only two replicate tests were used for the d_{10} value because one test did not pass the quality check for instrument repeatability of the d_{10} value.

The LS13320 results for the 50–350um and 150–650um NIST-traceable polydisperse glass beads fell within the certified targets for some of the d_x values (Table 5, Table 6). However, the LS13320 consistently measured the d_{25}, d_{50}, and d_{75} values as coarser than the upper control

limit for the 50–350µm standard (Table 5). Similarly, the LS13320 consistently measured the d_{10}, d_{50}, d_{75}, and d_{90} values as coarser than the upper control limit for the 150–650µm standard (Table 6). The excellent reproducibility of the results across a range of conditions (Norton, 2019) indicated that the readings were unlikely to be due to variations in handling, subsampling, or analysis conditions.

Table 5. Results from analysis of a 50–350um NIST-traceable polydisperse glass bead reference material (Whitehouse Scientific PS227). The control limits for the expected results have been computed based on the standards outlined in ISO 13320:2009 6.5

[d_x: the particle size at which x percent of the total sediment volume in the sample occurs in particles of a smaller size than the Dx value; St.Dev.: Standard Deviation; Fraun.: Fraunhofer; CV: Coefficient of Variation]

Percentile Diameter	**d_{10}**	**d_{25}**	**d_{50}**	**d_{75}**	**d_{90}**
Lower Control Limit (µm)	90.05	117.3	147.9	185.3	232.5
Upper Control Limit (µm)	97.35	119.7	153.7	195.2	245.1
Observed dx (µm), Glass Optical Model Mean of n=8 replicate tests	97.98	122.9	157.4	197.1	237.7
Observed dx (µm), Glass Optical Model St. Dev. of n=8 replicate tests	0.53	0.5	0.5	0.6	0.8
CV (St. Dev./Mean), Glass Optical Model	0.5%	0.4%	0.3%	0.3%	0.4%
Observed dx (µm), Fraun. Optical Model Mean of n=8 replicate tests	97.31	123.8	157.9	197.2	236.9
Observed dx (µm), Fraun. Optical Model St. Dev. of n=8 replicate tests	0.60	0.5	0.5	0.6	0.8
CV (St. Dev./Mean), Fraun Optical Model	0.6%	0.4%	0.3%	0.3%	0.4%

Table 6. Results from analysis of a 150–650µm NIST-traceable polydisperse glass bead reference material (Whitehouse Scientific PS237). The control limits for the expected results have been computed based on the standards outlined in ISO 13320:2009 6.5

[d_x: the particle size at which x percent of the total sediment volume in the sample occurs in particles of a smaller size than the Dx value; St.Dev.: Standard Deviation; Fraun.: Fraunhofer; CV: Coefficient of Variation]

Percentile Diameter	**d_{10}**	**d_{25}**	**d_{50}**	**d_{75}**	**d_{90}**
Lower Control Limit (µm)	239.9	301.3	356.9	419.4	508.3
Upper Control Limit (µm)	248.1	310.7	368.3	428.6	545.7
Observed dx (µm), Glass Optical Model Mean of n=3 replicate tests	253.1	303.4	371.4	458.0	561.3
Observed dx (µm), Glass Optical Model St. Dev. of n=3 replicate tests	1.3	1.0	1.5	3.5	6.1
CV (St. Dev./Mean), Glass Optical Model	0.5%	0.3%	0.4%	0.8%	1.1%
Observed dx (µm), Fraun. Optical Model Mean of n=3 replicate tests	253.1	303.4	371.4	458.1	561.4
Observed dx (µm), Fraun. Optical Model St. Dev. of n=3 replicate tests	1.2	1.0	1.5	3.5	6.1
CV (St. Dev./Mean), Fraun Optical Model	0.5%	0.3%	0.4%	0.8%	1.1%

Internal Reference Materials

Tests of the IRMs demonstrated that the laser-diffraction analysis with the LS13320 met the ISO standards for repeatability and reproducibility. The instrument repeatability was checked using the ISO standards (ISO 13320:2009 6.4); only two out of 74 tests had a CV of the d_{10}, d_{50}, or d_{90} that was larger than the ISO target of <3% for the d_{50} and <5% for the d_{10} and d_{90}. (Norton, 2019). When the d_x values are less than 10µm, the targets can be doubled (ISO 13320:2009 6.4.2). Similarly, the reproducibility among 4 to 6 replicate measurements of each reference material was excellent, with the CV of the d_{10}, d_{50}, and d_{90} among the replicate tests falling within the ISO standards (Table 7). Details of the analysis conditions and the results from individual tests are documented in Norton (2019).

Table 7. Reproducibility of the d_{10}, d_{50}, and d_{90} computed from a laser-diffraction PSD analysis among n replicate subsamples of a mixture of internal reference materials. Details of the composition of the mixtures can be found in Table 1 and Table 2. All values were computed using the Fraunhofer optical model.

[S/F: (S)and or (F)ines, the fraction analyzed in the LS13320; Hv: Heavy; Lt: Light; d_x: the particle size at which x percent of the total sediment volume in the sample occurs in particles of a smaller size than the Dx value; St.Dev.: Standard Deviation; CV: Coefficient of Variation]

Mixture	S/F	n	Mean d_{10} µm	St. Dev. d_{10} µm	CV d_{10} %	Mean d_{50} µm	St. Dev. d_{50} µm	CV d_{50} %	Mean d_{90} µm	St. Dev. $D9_0$ µm	CV d_{90} %
GB-A	All	4	39.97	0.05	0.1	46.89	0.11	0.2	228.4	1.1	0.5
GB-B	All	4	44.12	0.15	0.3	178.0	0.5	0.3	230.4	0.4	0.2
GB-C	All	4	155.6	1.0	0.6	202.2	0.6	0.3	254.2	0.5	0.2
GB-D	All	4	146.9	0.6	0.4	179.3	0.3	0.1	211.5	0.4	0.2
GB-E	All	4	173.6	0.8	0.5	217.7	0.3	0.1	253.3	0.3	0.1
SED-A Hv	S	6	133.3	0.9	0.7	411.8	8.7	2.1	880.0	22.3	2.5
SED-A Hv	F	4	3.420	0.165	4.8	28.38	0.55	1.9	69.99	1.56	2.2
SED-A Lt	S	6	136.5	2.3	1.7	429.6	10.3	2.4	871.8	1.2	2.1
SED-A Lt	F	6	3.854	0.253	6.6	27.96	1.17	3.9	70.44	18.00	1.8
SED-B Hv	S	6	105.3	0.4	0.4	215.4	2.2	1.0	489.4	3.7	0.8
SED-B Hv	F	5	1.056	0.005	0.5	7.133	0.140	2.0	35.79	0.84	2.3
SED-B Lt	S	5	105.2	1.0	1.0	539.6	1.6	0.7	516.6	3.3	0.6
SED-B Lt	F	4	1.048	0.010	0.9	7.869	0.114	1.6	36.12	0.76	2.1
SED-C Hv	S	6	191.5	1.0	0.5	571.2	10.0	1.7	1028	7	0.6
SED-C Hv	F	4	1.085	0.007	0.6	7.571	0.068	0.9	36.77	0.32	0.9
SED-C Lt	S	6	188.6	2.0	1.1	220.3	30.6	5.7	1021	12	1.2
SED-C Lt	F	4	1.093	0.012	1.1	7.122	0.071	0.9	36.82	0.24	0.7
SED-D	All	4	1.120	0.004	0.3	8.418	0.06	0.7	41.93	0.52	1.2
SED-E	All	4	1.242	0.004	0.3	12.41	0.06	0.5	51.56	0.25	0.5
SED-F	All	4	1.580	0.008	0.5	18.48	0.08	0.4	58.95	0.16	0.3

The difference between the observed volume percent and the expected volume percent in each size class was greater for coarser sizes than for finer sizes for both the glass bead IRMs and the sediment IRMs (Figure 1, Figure 2). The glass bead IRMs did not show a consistent pattern of reading coarser or finer than the expected value for the sand-sized size classes (Figure 1). Rather, the deviation from the expected value varied depending on the test mixture (Figure 1).

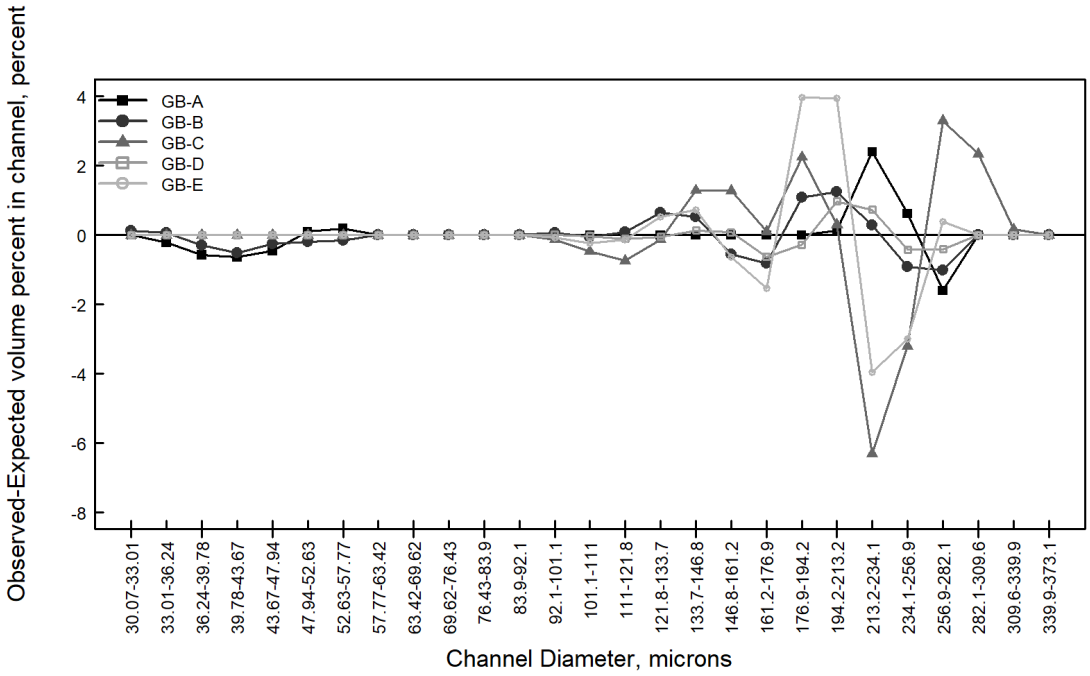

Figure 2: Difference between the mean observed volume percent and the expected volume percent in each size class for n=4 replicate subsamples of mixtures of internal reference materials prepared from commercially-available glass beads. The composition of each mixture is given in Table 2. Channels outside the range of the sizes of the beads are omitted for visual clarity; no sediment was detected in any of the omitted channels.

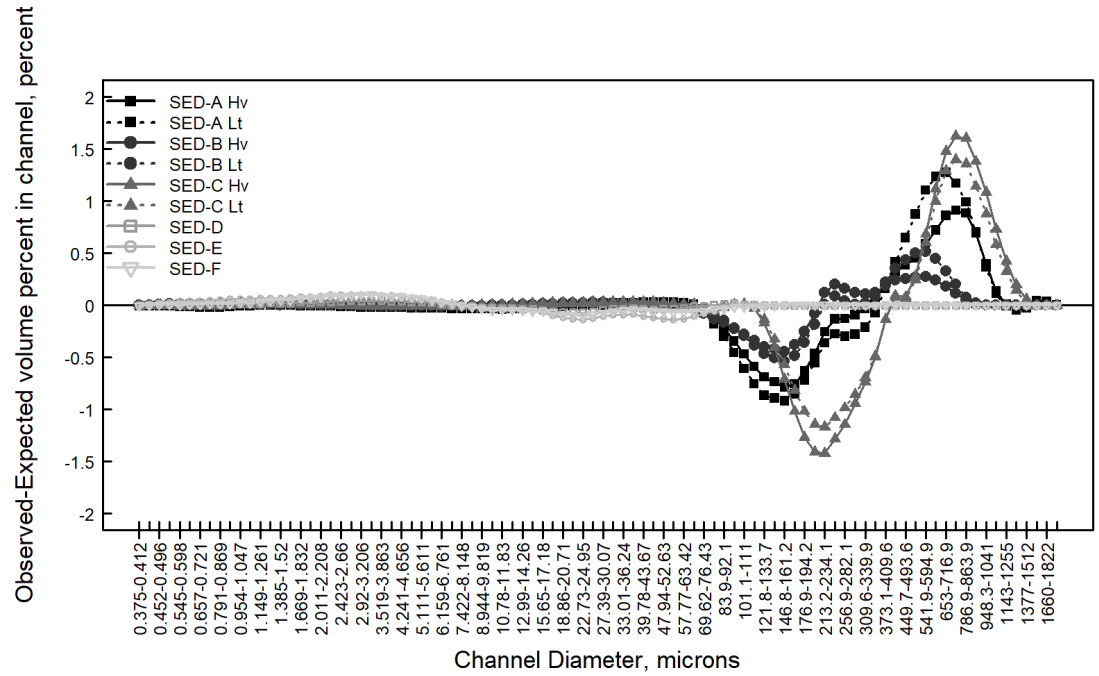

Figure 1: Difference between the mean observed volume percent and the expected volume percent in each size class for mixtures of internal reference materials prepared from commercially-available play sand. The composition of each mixture is given in Table 2.

For the sediment IRMs, the sand PSD measured in the LS13320 was shifted coarse relative to the expected values (Figure 2). In contrast, the difference between the observed and expected values for the fines was very low (Figure 2). The pattern of coarse-shift for the sands was very similar between the heavy (Hv) and light (Lt) test samples for each of the three mixtures that had two test samples (SED-A, SED-B, SED-C, Figure 2).

Discussion and Conclusions

The laser-diffraction PSD method in this study is precise because it is both repeatable and reproducible. As with any PSD analysis, variation in sample handling can affect the reproducibility of the results. However, the laser-diffraction PSD analysis in this study was reproducible under normal variation in sample handling methods for a single operator in a single laboratory over time.

The observation that laser-diffraction PSD analysis has excellent precision agreed with findings from other studies. Kuchenbecer et.al. (2012) conducted an inter-laboratory study with 31 European labs and found that all were able to meet (or exceed) the ISO method repeatability targets for well-prepared subsamples of three different reference materials. For well-prepared subsamples, the method repeatability of a laser-diffraction analysis can be better than other particle size analysis methods, including the sedigraph (Goossens, 2008; Roberson and Weltje, 2014), the pipet (Beuselinck and others, 1998), and dry sieving (Blott and Pye, 2006). When the results of the laser-diffraction PSD analysis are combined with results from a different method (for example, sieving material too coarse to analyze with laser diffraction), the uncertainty of the combined PSD is dominated by the uncertainty on the least-certain method used for a sample.

The accuracy of the laser-diffraction PSD method in this study was verified for fines. The accuracy of the physical sizing of spherical particles with known optical properties was verified by the tests of the 3–30μm NIST-traceable glass bead standard (Table 4). Further, the accuracy of the observed proportions of different mixtures of fine IRMs was verified by the fact that there was a negligible difference between the observed and expected volume percent in each size class for these test mixtures (Figure 2, SED-D, SED-E, SED-F). While this test cannot verify that results from this laser-diffraction analysis method will match fine PSD results from other methods, it does indicate that the method used to analyze fines in this study is internally consistent.

Knowing that the laser-diffraction PSD analysis method used in this study can correctly detect proportions of mixtures of fines suggests that the method can be used to measure PSDs that can be compared among each other, and further suggests that the method could likely be used to calibrate results to other fine PSD analysis results if an inter-method comparison is required. Careful investigation of the RI of various populations of sediment particles could improve the accuracy of laser-diffraction PSD results by allowing a Mie optical model to be used to compute the results. Such studies would be methodologically challenging, however, and would still require further calibration to relate the laser-diffraction PSD results to the PSD results from sedimentation methods, which have direct hydraulic interpretability for sediment transport studies.

The accuracy of the laser-diffraction PSD analysis method used in this study was not verified for sand. This finding agrees with other observations. Blott and Pye (2006) found that an LS230 (Beckman-Coulter) over-reported the proportion of the coarse component of mixtures of ballotini (glass beads) in the sand size range. They observed that the LS230 may have been over-fitting log-normal distributions to a variety of data sets (Blott and Pye, 2006). The inversion of a light-scattering signal to a PSD is a complex mathematical operation and requires some constraints to produce viable results; however, over-constraint can lead to inaccurately wide PSD results (ISO 13320:2009 Annex A.10). Each model of laser-diffraction PSD instrument and software algorithm likely uses different constraints. The details of the LS13320 algorithm are proprietary, but it is possible that the software is using constraints that produce reasonable-looking, but sometimes inaccurate, PSD results in the coarser size ranges.

Because each laser-diffraction instrument model has different a physical configuration and uses different software algorithms, the findings in this study are not generalizable across all makes and models of laser-diffraction instruments. Particle shape and surface roughness alter the light-scattering pattern produced by natural particles compared to spherical particles (ISO 13302:2009 Annex A). Each instrument make and model is affected differently by irregular-shaped particles and handles the interpretation of the observed light scattering pattern differently, leading to weak expectations of reproducibility of laser diffraction results across different instrument makes and models. Kuchenbecer et. al. (2012) found clear differences among different makes and models of laboratory laser-diffraction instruments in their inter-laboratory study, but also observed good reproducibility among different laboratories using the same make and model laser-diffraction instrument. The techniques used in this study to assess the precision and accuracy of a laboratory laser-diffraction PSD method using a single instrument in a single laboratory can be used by other operators in other laboratories with other instruments to conduct laboratory-specific quality assessments for laser-diffraction analysis.

Further work is needed to evaluate how to incorporate laser-diffraction PSD analysis into the workflow for sediment studies at the USGS and beyond. For fines, laser-diffraction PSD analysis dramatically expands the range of sediment samples for which PSD information can be obtained because the laser-diffraction method typically requires only 0.1–0.3 grams of fines for a reproducible PSD analysis (Norton, 2019). A typical sedimentation method such as the pipet method requires a minimum of 0.8 grams (Guy 1969). For sands, the LS13320 records 37 channels for particles 63–2000µm. A similar quarter-phi sieve analysis records 21 size classes. Thus, the laser-diffraction PSD analysis for sands produces higher resolution results than traditional sand analysis methods. The higher resolution should lead to greater precision on d_x values for the sand fraction than a sieve analysis can produce.

The promise of laser-diffraction PSD analysis will likely best be realized through the use of sediment-population-specific calibrations between laser-diffraction results and results produced by other methods. Determining how to produce, verify, document, and use such calibrations in fluvial sediment projects is likely a next step in incorporating laser-diffraction PSD into the sediment project workflow.

Acknowledgments

The author wishes to thank the Federal Interagency Sedimentation Project (2018), the USGS Office of Surface Water (2016), and the USGS Office of Quality Assurance for Water Quality Activities (2016) for their generous support of this work.

The author further wishes to thank Michael Torresan and Angela Tan of the USGS Coastal and Marine Geology Sediment Lab in Santa Cruz, Calif.; Anthony Preistas of the US Army Corps of Engineers Engineer Research Development Center in Vicksburg, MS; and Scott Wright, Mat Marineu, and Joan Lopez of the USGS California Water Science Center in Sacramento, Calif. for sharing details of their existing methods of conducting laser-diffraction PSD analysis.

References

Beckman-Coulter, 2011, Instructions for Use: LS 13 320 Laser Diffraction Particle Size Analyzer: Brea, Calif., Beckman-Coulter, 246 p.

Blott, S.J. and Pye, K., 2006, Particle size distribution analysis of sand-sized particles by laser diffraction: an experimental investigation of instrument sensitivity and the effects of particle shape: Sedimentology, 53, 671-685.

Guy, H.P., 1969, Laboratory Theory and Methods for Sediment Analysis: Techniques of Water Resources Investigations of the United States Geological Survey, Book 5, Chapter 1, 58 p.

Inter-Agency Committee on Water Resources, Subcommittee on Sedimentation, 1957, Some Fundamentals of Particle Size Analysis: Report No. 12 in A Study of Methods Used in Measurement and Analysis of Loads in Streams, accessed January 15, 2017, at https://water.usgs.gov/fisp/docs/Report_12.pdf.

International Standards Organization (ISO), 2009, Standard 13320:2009(E) Particle Size Analysis—Laser Diffraction Methods.

Kowalenko, C.G. and Babuin, D., 2013, Inherent factors limiting the use of laser diffraction for determining particle size distributions of soil and related samples: Geoderma, 193-194, 22-28.

Kuchenbecker, P., Gemeinert, M., and Rabe, T., 2012, Inter-laboratory study of particle size distribution measurements by laser diffraction: Particles and Particle Systems Characterization, 29, 304-310.

Norton, K., 2019. Results from Precision and Accuracy Testing of a Laboratory Laser-Diffraction Analyzer: U.S. Geological Survey data release, https://doi.org/10.5066/P9D93GTQ.

Penscil Inc., 2011, pcSDSZ: Sediment Size Analysis Software for Windows Operation Manual Version 1.70, prepared for USGS Coastal and Marine Geology, 127 p.

Roberson, S. and Weltje, G.J., 2014, Inter-instrument comparison of particle-size analysers: Sedimentology, 61, 1157-1174.

Shreve, E.A., Downs, A.C., 2005, Quality Assurance Plan for the Analysis of Fluvial Sediment by the U.S. Geological Survey Kentucky Water Science Center Sediment Laboratory: U.S. Geological Survey Open File Report 2005-1230, 28 p.

Capturing Lead-Contaminated Sediment from a River Using a Side Channel Trap

Joseph B. Collum, Hydraulic Engineer, U.S. Army Corps of Engineers, St. Louis, Missouri, joseph.b.collum@usace.army.mil

Introduction

The Southeast Missouri Lead District was the world leader in lead production for nearly 100 years, until the early 1970's. During and since that time, mine waste material was introduced into the Big River watershed and transported downstream, primarily by flood flows. In 2017, a 10,000 cubic yard side channel was excavated in Southeast Missouri, adjacent to the Big River, in an attempt to capture legacy mine sediment during flood flows. The concept of a side channel trap is illustrated in Figure 1. This trap is a component of a plan to reduce the downstream migration of mine waste material in the Big River watershed (U.S. Army Corps of Engineers 2018).

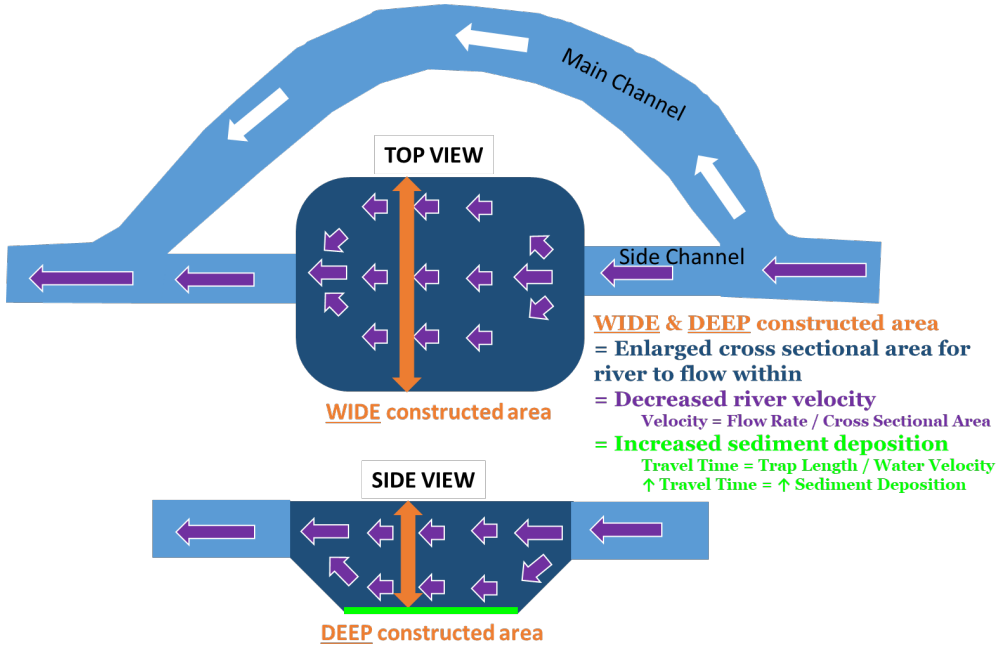

Figure 1. Conceptual overview of side channel trap function.

Site Selection and Analysis Process

Site Selection

There are various methods for trapping or collecting sediment from a river. One common method is dredging, which can be expensive, ecologically intrusive, and geomorphically risky. The passive side channel trap is not a new concept, but varying economics, hydrology, site conditions, and environmental factors mean that this method for collecting and removing sediment from a river is not often the most feasible or appropriate choice. A similar effort was implemented elsewhere in the watershed, but it focused on the removal of sediment from

behind a low-water bridge/dam, and from a downstream point bar (Martin and Pavlowsky 2010). As such, careful consideration was placed on selecting a suitable location to build this trap. While no perfect site exists, site access and hydrogeomorphic context strongly influenced the selection of this site.

Access: Side channel sediment traps are not well-documented; there is little literature that discusses geomorphic, hydrologic, environmental, construction, maintenance, and sizing considerations for a side channel trap. This project serves as a good opportunity to document some of these considerations. Therefore, in an effort to make monitoring and studying this site as easy and inexpensive as practicable, the site was placed within a thousand feet of a road to improve access and reduce haul and maintenance costs. Adequate staging area provided the contractor with good maneuverability during construction and subsequent maintenance. Finally, the landowner understood the implications of allowing a trap to be built on their property: the trap would need to be monitored and maintained.

Hydrogeomorphology: The site is located on a sand and gravel bar that was formed in a remnant channel dating back to 1937 (Pavlowsky and Owen 2013). Since this historic channel is now covered by deposited sediment, it was assumed that the river would be capable of naturally filling an excavated portion of the bar with new material similar to the in-situ material. Mature vegetation on the bar indicated that the bar has not experienced rapid aggradation or degradation during recent flood flows. Additionally, there was enough space for entrance and exit structures to be constructed far enough from the main channel to reduce the likelihood of adverse geomorphic effects on the main channel.

Analysis

The three primary components analyzed at this site include hydrology, hydraulics, and bed material transport. These components all directly affected the details of the trap design. By combining these three components, the trap was designed to target a specific range of sediment sizes during a specific range of flows.

Hydrology: The Big River is a free-flowing gravel-bed river with no significant man-made impoundments. Daily flow trends at this site are derived from the Big River at Richwoods gage data (USGS Gage 07018100), which is located 6 miles downstream of the trap. A flow duration analysis was conducted on this data using HEC-SSP, a statistical software package produced by the U.S. Army Corps of Engineers. The results of this analysis indicate that flows greater than 9,000 cubic feet per second (cfs) occur for a less than <1% of the time; while flows between 650 cfs and 5,000 cfs occur 23% of the time; and 76% of the time, flows are less than 650 cfs (Figure 2). Additionally, HEC-SSP computed that a flow of 5,000 cfs has an annual exceedance probability (AEP) of approximately 90% (also referred to as 1.1-year flow).

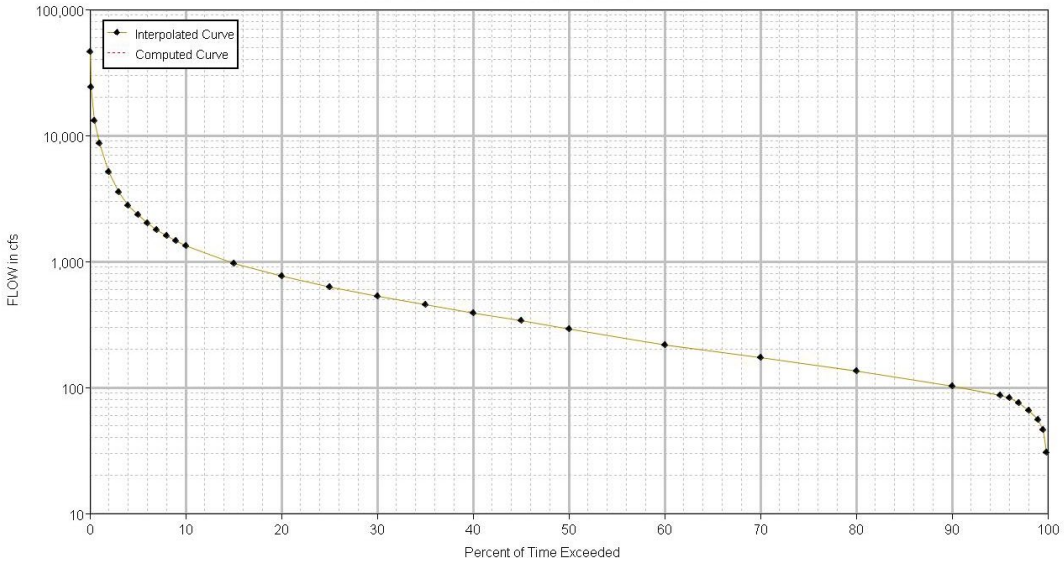

Figure 2. Flow duration analysis

Hydraulics: HEC-RAS, a numerical river hydraulics software package, was used to compute the estimated water velocity and predict the behavior of the trap at various flows. According to the 2D model, water begins to inundate the trap at 650 cfs. The velocity within the trap is near-zero (dark blue) at the design flow of 5,000 cfs (Figure 3). Near-zero velocity is desirable to allow finer sediment fractions deposit within the trap.

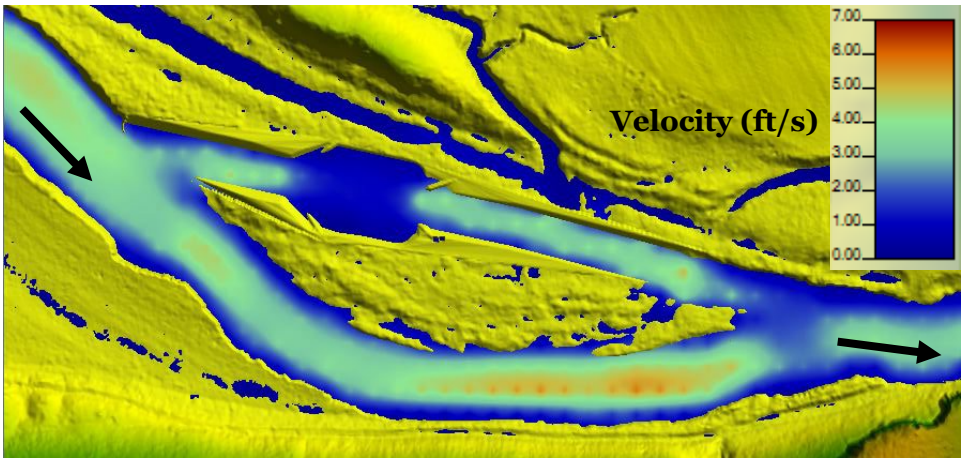

Figure 3. 2D HEC-RAS model of side channel trap at 5,000 cfs

Bed Material Transport: Bedload Assessment for Gravel-bed Streams (BAGS) implements six bedload transport equations developed for gravel-bed rivers (Pitlick et al. 2009). The Wilcock-Crowe equation was used to estimate bedload transport capacity in a nearby reach using flow exceedance probabilities (Figure 2), sediment grain size data, energy slope, and cross section data (Pitlick et al. 2009). All of the variables required for this calculation were acquired previously. Sediment samples were not acquired at this specific site, but two independent

measurements of D_{50} near this river reach range from 1.1 mm to 4.1 mm. This wide range, and the lack of site-specific data, highlights the imprecision of estimating bedload transport.

Since BAGS calculates the maximum bedload transport capacity of the river reach, a reduction factor was applied in order to estimate the actual amount of sediment that would be deposited inside of the trap, which is situated in a constructed side-channel. After the reduction factors were applied, the trap was estimated to fill at an average rate of 900 cubic yards per year, which would fill the entire excavation within about 11 years.

Sediment transport calculations are notoriously complicated and inexact, and the actual sediment transport can vary considerably from calculations and averages. The BAGS analysis calculates theoretical maximum transport capacity, but sediment supply varies. This is why it is important to closely monitor the site after construction.

Monitoring

Multiple flood flow events occurred within six months of construction. Stage data is continuously recorded at the Big River at Richwoods gage (USGS Gage 07018100). A rating curve was used to convert the stage to discharge, and the discharge data was input into Microsoft Excel to create a custom flow-duration curve (Figure 4). Between 2/1/2018 and 5/15/2018, the trap was inundated by flows exceeding 650 cfs for approximately 1,300 hours (54 days). Four distinct flow events exceeded 4,000 cfs. The design flow of 5,000 cfs was exceeded for approximately 150 hours (six days).

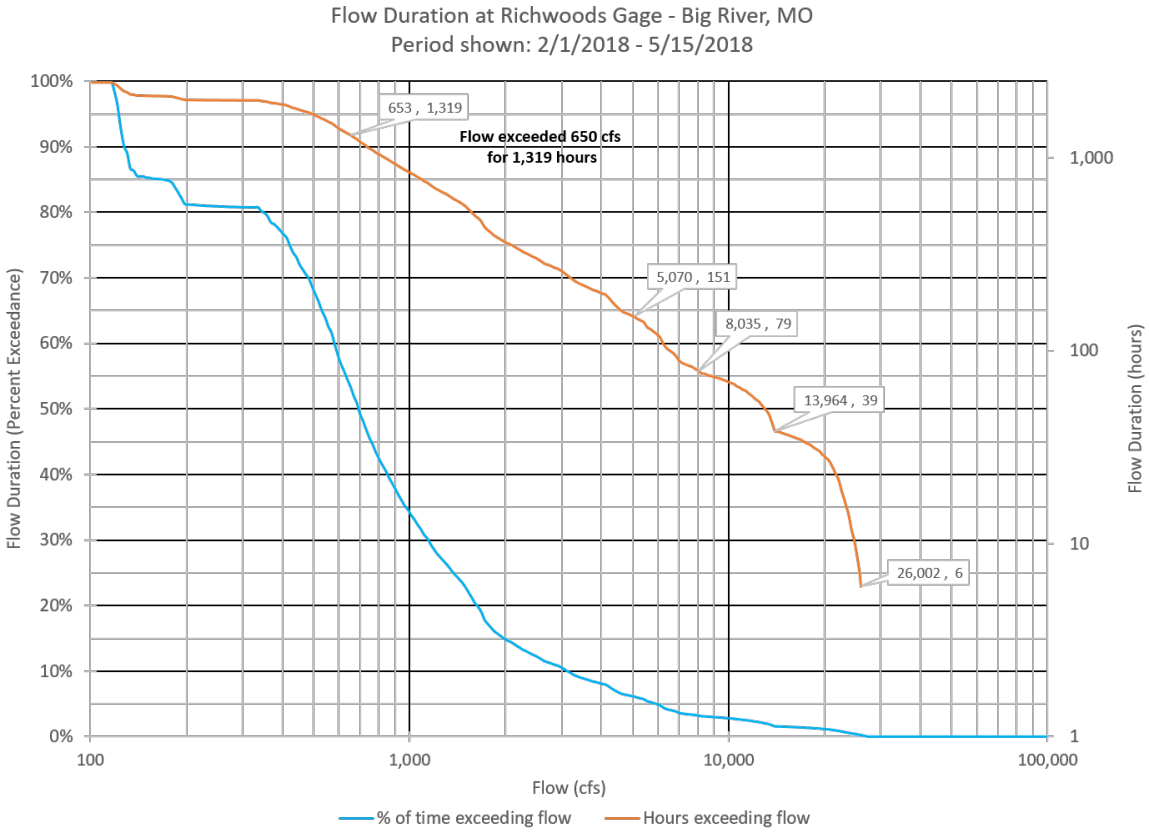

Figure 4. Flow duration on Big River at Richwoods Gage (USGS 07018100) from 2/1/2018 – 5/15/2018

These flood flows transported and deposited a significant amount of coarse sediment (small gravel through coarse sand) at the upstream entrance to the trap, as highlighted in Figure 5 within the red dashed line. This deposition is significant because it increased the elevation of the entrance channel by a few feet, which increases the flow at which the trap begins to inundate. This increase in entrance elevation reduces the amount of coarse sediment that can enter the trap in the future, which reduces the grain size that is targeted by this trap. In other words, the river provided an example design for permanent inlet modifications at this site.

Figure 5. Deposition of coarse sediment at the upstream entrance to trap; during low water (Pics: J.Collum)

Finer sediment deposited within the trap, as shown in Figure 6 within the red dashed line. Samples elsewhere in the watershed have indicated that the finer sediment fraction contains more mine waste than the coarser sediment fraction. Discrete measurements of deposited sediment have not yet been taken. Some scour was noted at the transition of the excavated entrance channel and the armored (undisturbed) gravel bar. Minor scour is visible along the right bank of the trap, as shown in Figure 6 within the yellow dashed line, as the site did not have a chance to vegetate before experiencing flood flows. While the HEC-RAS model shows near-zero velocity in the trap at 5,000 cfs, elevated velocity and/or turbulence along the bank of the trap is occurring at some flows, as evidenced by this scour.

Figure 6. Deposition of fine sediment within trap; during low water (Pic: J.Collum)

Geomorphic changes have not yet been observed on the main channel of the Big River, but a monitoring plan has been outlined to detect subtle changes in plan and profile of the main channel. This plan includes repeated cross sections and visual analysis by comparing photographs from set perspectives.

Conclusions and Recommendations

This trap has successfully captured sediment from the Big River. It is not yet clear if the estimated fill rate of 900 cy per year is accurate, since the trap has only been in place since late 2017. The entrance condition at this site changed almost immediately after construction due freshly deposited sediment from spring flows (Figure 5 and Figure 6). Once the trap has filled, it can be excavated, sampled, and resurveyed to verify the fill rate and determine the proportion of mine waste material. In addition, the sediment samples, quantity, and flow statistics can be used to assess the accuracy of the bed material transport calculations and predictions. Future monitoring efforts at this site should also involve a visual inspection of the main channel near the site to determine if any major geomorphic adjustments are taking place.

Planners and designers should anticipate physical adjustments that are likely to happen to the site over its lifespan (e.g. the deposition of fine and coarse sediment, localized scour, and settling of entrance and exit structures.) These anticipated changes should influence the design team in their attempt to design a versatile configuration that can function even after the site has adjusted. Part of this effort involves closely monitoring the post-construction site and being ready to use contingency funding to assess and address physical adjustments to the site.

Depending on the configuration of the site, it may be beneficial to include flood-resistant vegetation spanning the width of the trap to increase roughness, especially when design flows are exceeded. Vegetation can be used on the banks of the trap to minimize undesirable scour that may occur during flood flows. Entrance and exit channels should be properly designed to resist scour as well, especially in areas where there is a transition in roughness, such as between the constructed channel and the armored channel or bar.

References

Martin, D. and Pavlowsky, R. 2010. “Big River borrow pit monitoring project,” Ozarks Environmental and Water Resources Institute, Missouri State University, OEWRI EDR-10-003.

Pavlowsky, R. T., and Owen, M. R. 2013. “Historic channel change maps for the Big River system in St. Francois, Washington, and Jefferson Counties, Missouri,” Ozarks Environmental and Water Resources Institute, Missouri State University, OEWRI EDR-13-001.

Pitlick, J., Cui, Y., and Wilcock, P. 2009. “Manual for computing bed load transport using BAGS (Bedload Assessment for Gravel-bed Streams) software,” U.S. Department of Agriculture, Forest Service, General Technical Report RMRS-GTR-223.

U.S. Army Corps of Engineers. 2018. “St. Louis Riverfront - Meramec River basin ecosystem restoration feasibility study with integrated environmental assessment,” *Draft*.

Wilcock, P. and Crowe, J. 2003. “Surface-based transport model for mixed-size sediment,” Journal of Hydraulic Engineering, ASCE, 129(2):120-128.

Wilcock, P., Pitlick, J., and Cui, Y. 2009. “Sediment transport primer estimating bed-material transport in gravel-bed rivers,” U.S. Department of Agriculture, Forest Service, General Technical Report RMRS-GTR-226.

Through Ice Bed Material Sampling to Determine Main Channel Bed Material Gradation on a Large Seasonably Turbid River

Ryan Kilgren, Water Resources Engineer, Tetra Tech, Inc., Eugene, OR, Ryan.Kilgren@TetraTech.com
Bill Fullerton, Discipline Leader, Hydraulics and Hydrology, Tetra Tech, Inc., Seattle, Washington, Bill.Fullerton@TetraTech.com
Renee Vandermause, Project Engineer, Tetra Tech, Inc., San Juan, Puerto Rico, Renee.Vandermause@TetraTech.com

Extended Abstract

River morphological studies depend on knowledge of main channel bed material gradations. Field efforts focused on assessing bed materials are highly challenging when presented with large scale rivers having deep, swift, and typically turbid glacially supplied seasonal flows. The high turbidities from glacial runoff and the associated fine particle mobilization precludes the application of standard visual sampling techniques for much of the year, and swift and deep flow greatly restricts the use of other sampling techniques, such as by dredge samplers. The Susitna River, located in Alaska, has all the traits associated with a river posing difficulty for geomorphic field assessment.

The glacially sourced headwaters of the Susitna River supply highly turbid flow during the open-water period, generally occurring between mid-May and mid-October. An example of the highly turbid flow conditions is shown in Figure 1, in which the instrumentation cable is obscured by the relatively shallow turbid water. The ice-cover period persists during the remainder of the year and the river receives a substantially lower amount of glacial inflow due to freezing conditions in the headwaters. Because of the lower glacial inflow during the ice-cover period, the turbidities within the Susitna River can be up to 100 times less than during the open-water period. An example of the less turbid and clearer water conditions during the ice-cover period is shown in Figure 2, which is a still frame image extracted from the through ice methods described by this extended abstract.

As part of a larger geomorphic study effort on the Susitna River, transported bed material was characterized at bar head locations using surface and subsurface sampling during relatively lower flow portions of the open-water period. To understand the presence of coarser bed material vertical layers and longitudinal deposits (i.e. armor layers and lag deposits), a method was needed to investigate the main channel bed materials. A methodology was developed to collect samples during the ice-cover period, taking advantage of low turbidities and low flows. The developed method consisted of lowering underwater cameras through augered holes in river ice to obtain images of the channel bed, rectifying the underwater images to remove distortion, and measuring bed material particles observed in the rectified images.

Image rectification was achieved by calibrating the underwater camera by taking underwater images of a 0.15-meter square calibration grid submerged in a quiescent pool. The calibration

grid images were then analyzed using photogrammetric techniques and software to measure the distance between grid points for each of the images obtained at different camera heights above the calibration grid, and the camera focal length and distortion parameters were computed.

Images of the studied channel bed were collected at over 20 locations along 400-kilometers of the Susitna River during the ice-covered period. Sample transect locations were planned and then adjusted during the field assessment. Following sample transect location determination, exploratory holes were augered along the transect to determine the lateral extent of flow beneath the river ice. The depth of the flow was then measured to determine the number of sample holes needed for each transect, with the goal of measuring approximately 100 surficial bed material particles from each transect. The sample holes locations were then laid out and snow was cleared from those locations to assist with augering. The underwater camera, mounted to an adjustable pole, was then lowered through the holes with flowing water and not completely frozen to the bed, until the base of the pole reached the river bed. The camera mounting position on the adjustable pole was varied based on the depth of flow, ice thickness, and the size of the bed material observed in initial images. The underwater camera was operated in video mode for the bed image acquisition to take advantage of the camera's automated low-light adjustment. Once the pole was on the river bed, it was positioned vertically and held in place for a minimum of 10 seconds to ensure that multiple video frames were available for post-processing extraction of still frame images for bed material gradation analysis. Each sample hole video was inspected to ensure adequate scene illumination and mounting position based on the bed material size. Adjustments and repeated imaging were performed if warranted. Examples of sample videos are viewable at https://youtu.be/v79bMJv4Vfs or by using the QR code provided in Figure 3.

After the field work, a still frame image of the bed material was extracted for each sample hole video. The extracted still frame images were then rectified, using the developed calibration parameters to remove camera lens distortion. Figure 4 shows an example of an unrectified extracted still frame image and Figure 5 shows an example of a rectified still frame image. Repeatable particle count methods were determined and used with standardized digital sampling grids established with GIS software to count individual bed material particles measured on each photograph. Approximately 100 particles were measured at each sample transect to develop grain size distributions in each 0.4 phi size bin. The effort demonstrated a practical technique to collect bed material samples within the main channel of rivers with challenging field work conditions. The results are compared with open-water period obtained bar head sample locations in Figure 6.

Figure 1. Typical high turbidity conditions for glacially supplied rivers during the open-water period.

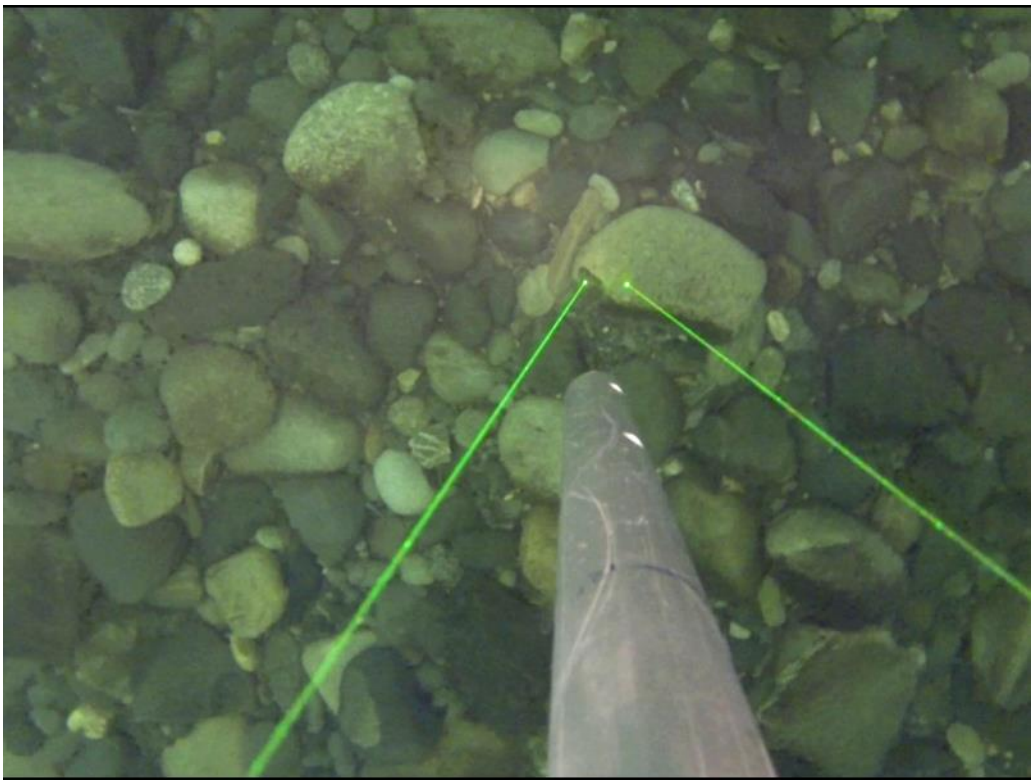

Figure 2. Typical low turbidity during ice-cover period. Freezing conditions in headwaters reduces glacial input.

Figure 3. QR code link to example through ice bed imaging sample video

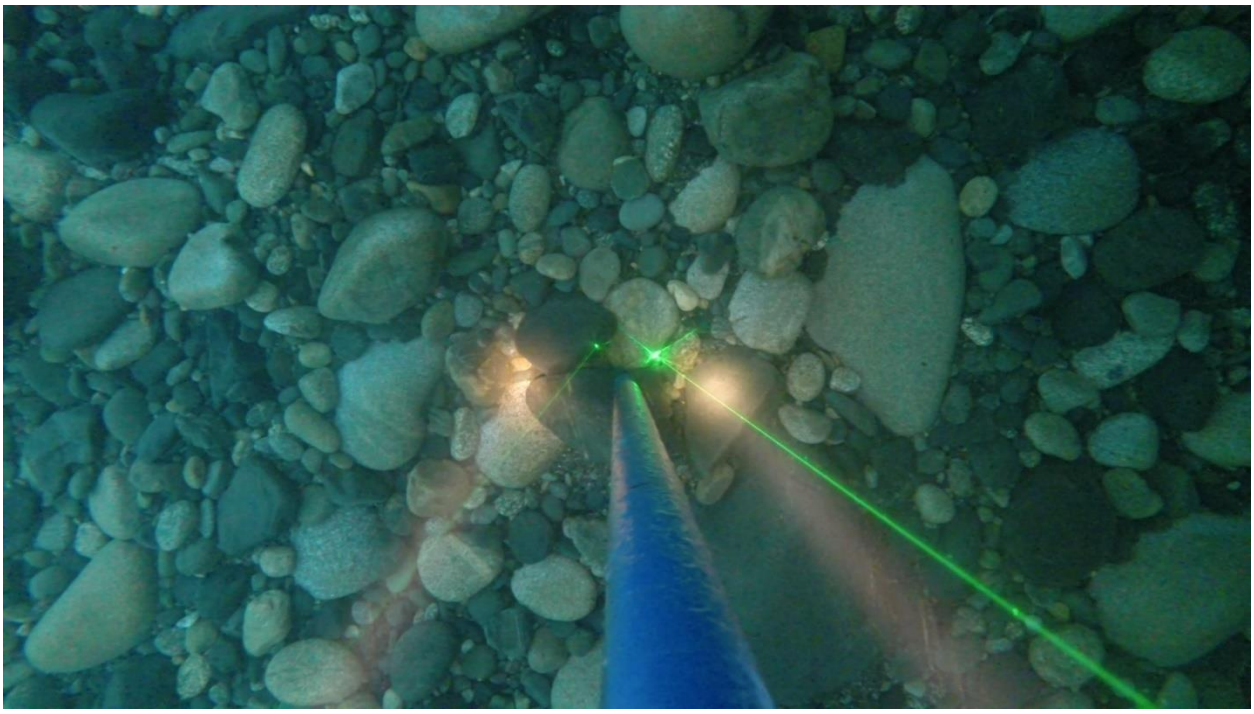

Figure 4. Unrectified example still frame image extracted from through ice bed image sample video

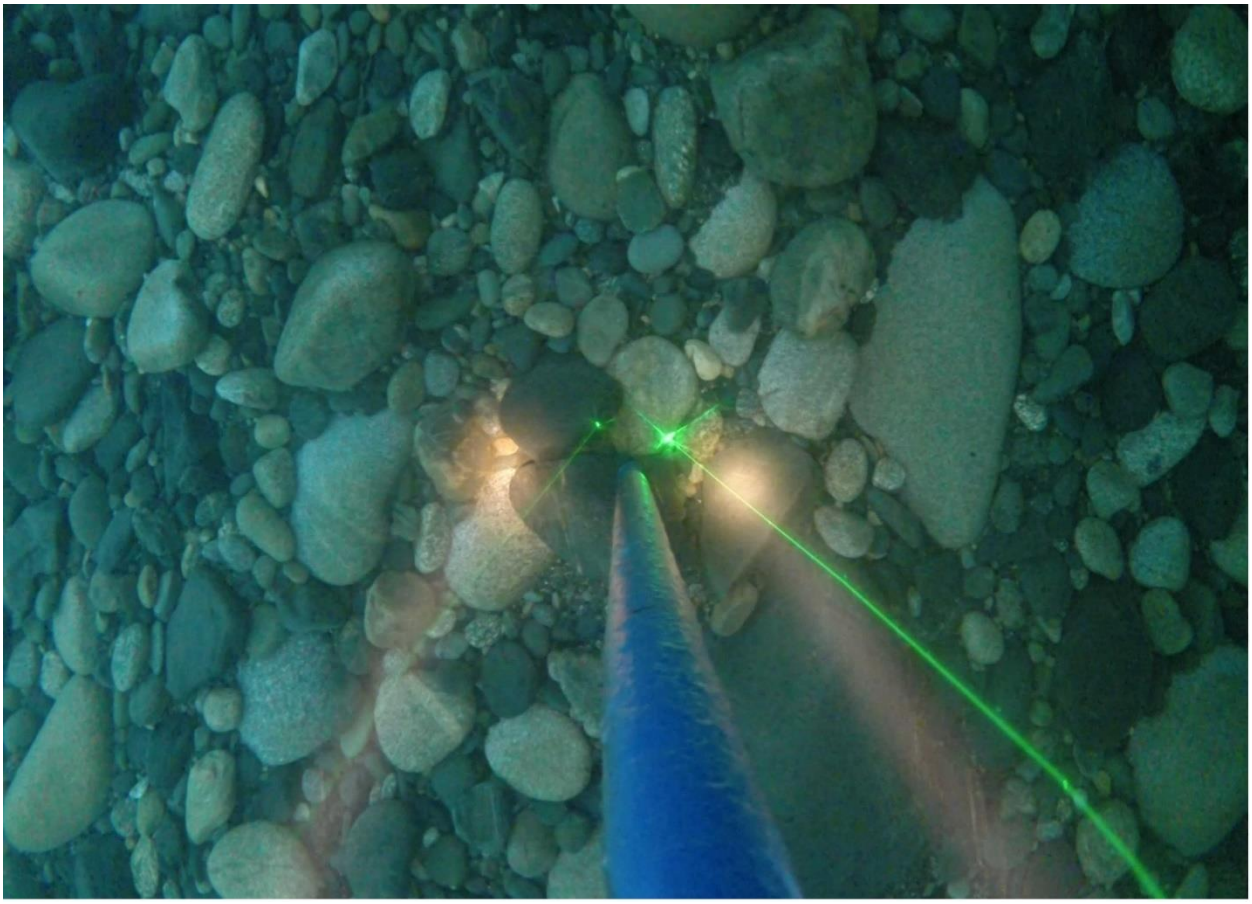

Figure 5. Rectified example still frame image extracted from through ice bed image sample video

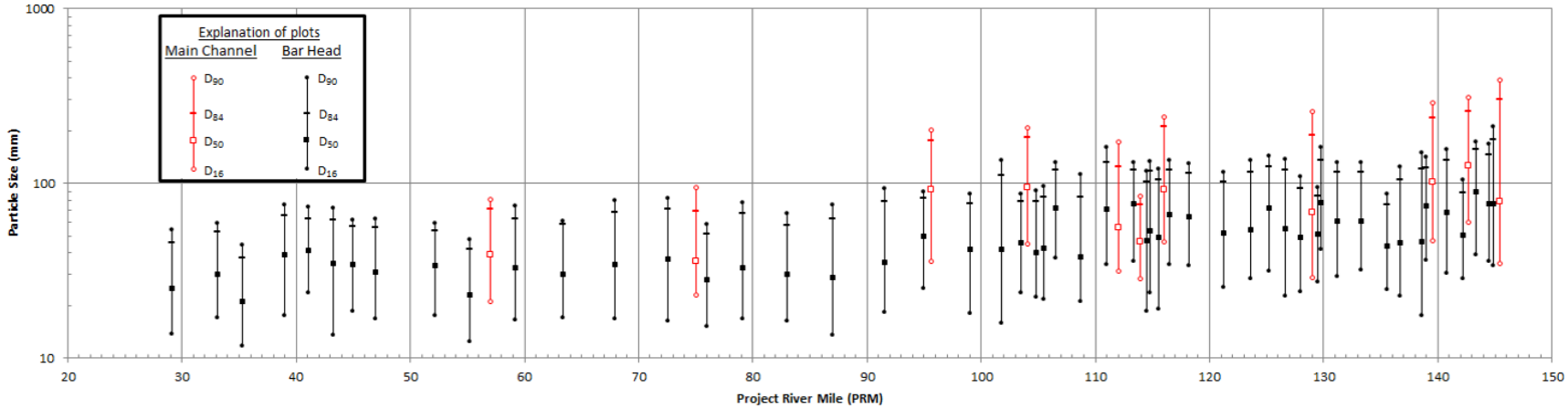

Figure 6. Comparison of ice-cover period through-ice bed image and open-water period bar head sample grain size analyses results.